Site characterization of the highest-priority geologic formations for CO_2 storage in Wyoming

Final Report to U.S. Department of Energy

Reporting Period Start Date: December 8, 2009
Reporting Period End Date: December 7, 2013

Principal Author: Ronald C. Surdam - Principal Investigator

Contributing Authors
Ramsey Bentley
Erin Campbell-Stone
Shanna Dahl
Allory Deiss
Yuri Ganshin
Zunsheng Jiao
John Kaszuba
Subhashis Mallick
Fred McLaughlin
James Myers
Scott Quillinan

Date Report was issued: December 2013

DOE Award Number: DE-FE0002142

Carbon Management Institute
University of Wyoming
2020 Grand Avenue, Suite 500
Laramie, WY 82072

Baker Hughes, Inc.
P.O. Box 200415
Houston, TX 77216

DISCLAIMER*

This report was prepared as an account of work sponsored by an agency of the United States Government. Neither the United States Government nor any agency thereof, nor any of their employees, makes any warranty, express or implied, or assumes any legal liability or responsibility for the accuracy, completeness, or usefulness of any information, apparatus, product, or process disclosed, or represents that its use would not infringe privately owned rights. Reference herein to any specific commercial product, process, or service by trade name, trademark, manufacturer, or otherwise does not necessarily constitute or imply its endorsement, recommendation, or favoring by the United States Government or any agency thereof. The views and opinions of authors expressed herein do not necessarily state or reflect those of the United States Government or any agency thereof.

ABSTRACT

This study, funded by U.S. Department of Energy National Energy Technology Laboratory award DE-FE0002142 along with the state of Wyoming, uses outcrop and core observations, a diverse electric log suite, a VSP survey, in-bore testing (DST, injection tests, and fluid sampling), a variety of rock/fluid analyses, and a wide range of seismic attributes derived from a 3-D seismic survey to thoroughly characterize the highest-potential storage reservoirs and confining layers at the premier CO_2 geological storage site in Wyoming. An accurate site characterization was essential to assessing the following critical aspects of the storage site: (1) more accurately estimate the CO_2 reservoir storage capacity (Madison Limestone and Weber Sandstone at the Rock Springs Uplift (RSU)), (2) evaluate the distribution, long-term integrity, and permanence of the confining layers, (3) manage CO_2 injection pressures by removing formation fluids (brine production/treatment), and (4) evaluate potential utilization of the stored CO_2.

To obtain accurate CO_2 storage capacities, it was necessary to determine the spatial heterogeneity of the petrophysical properties for two storage reservoirs (Madison Limestone and Weber Sandstone). As part of this study, researchers built a realistic 3-D geological property model of the two reservoir intervals by combining lithofacies/petrophysical analyses with seismic attribute computations and mapping. This approach, along with outstanding correlations between laboratory-measured porosity and permeability, sonic velocity and log porosity, and acoustic impedance and density porosity, resulted in realistic dynamic fluid-flow assessments yielding greatly improved CO_2 storage capacity estimates.

Both the Paleozoic and Mesozoic stratigraphic sections within the RSU contain a multitude of truly outstanding confining layers. The micritic limestone in the upper Madison Formation (CO_2 sealing capacities are 6,900ft to 20,000ft), the Amsden Formation (CO_2 sealing capacity is 7,700ft), and the Dinwoody Formation (CO_2 sealing capacity is 5,000ft to 17,000ft) are all truly outstanding confining layers. The sealing quality of these confining layers explains the trapping of helium (0.6% of the gas phase) at both the LaBarge Platform and the Rock Springs Uplift in southwestern Wyoming.

It has been obvious since early in the Wyoming Carbon Underground Storage Program (WY-CUSP) that pressure management in the form of formation fluid production/treatment would be essential in any injection/storage scenario. Without brine production during CO_2 injection/storage, performance assessments suggest that pressure will quickly exceed fracture pressures, or that the brines will migrate outside the boundaries of the storage domain. The U.W. Carbon Management Institute (CMI) has designed a brine production/treatment strategy that includes utilization of the elevated temperature and pressure to power the treatment of brine to recover potable water and metals such as lithium. The brines have elevated concentrations of various metals, particularly lithium (90 mg/L–100 mg/L). This strategy will convert the economic penalty of pressure management during CO_2 storage via brine production/treatment into a source of revenue.

Utilization of CO_2 is a vital aspect of any CCUS strategy, so the potential for EOR, ECBM, EGR, and CO_2 fracking have been integrated into the design of a commercial-scale geological CO_2 storage facility at the Rock Springs Uplift, Wyoming. In addition, CMI has explored advantages to Wyoming of deploying innovative, multiple-resource development strategies, including geological CO_2 storage, designed to foster the sustainability of the state's energy and environmental resources. This approach relies on synergistic relationships

among resource elements to increase the efficiency of development, minimize environmental degradation, and sustain long-term resource use.

Overcoming the four major hurdles to CCUS activities at the Rock Springs Uplift: (1) improving the estimates of CO_2 storage capacity of the reservoirs, (2) establishing long-term integrity and permanence of confining layers, (3) designing a profitable strategy for pressure management, and (4) evaluating the utilization of stored CO_2 for Enhanced Oil Recovery (EOR), EGR, ECBM, and fracking applications, has greatly enhanced the Carbon Capture Utilization and Sequestration (CCUS) potential in Wyoming and elsewhere.

The ultimate mission of the WY-CUSP program managed by the U.W. Carbon Management Institute – delivery of a thoroughly characterized, certified commercial CO_2 storage site in Wyoming that could be used as a surge tank for CO_2 utilization – has been accomplished.

TABLE OF CONTENTS

Abstract 3

Executive Summary 7

CO_2 Storage 8

Confining Layer Integrity/Permanence 13

Pressure Management 16

CO_2 Utilization 19

On-Going Work 22

Summary 22

Lessons Learned 22

Report Details 24

Introduction 24

Reservoir Storage Capacity 26

Borehole Catalog Development and Risk Assessment 28

Stratigraphic Test Well 46

Vertical Seismic Profiling (VSP) Survey 50

Acquire a 3-D Seismic Survey 65

Detailed Geological Analysis 73

Methodology and Approach 81

Determination of Confining Layer Integrity and Permanence 101

Regional Study Site Geologic Structural Characterization 112

Pressure Management 116

CO_2 Storage Utilization 135

Deliverables Issues and Milestones 140

Conclusions 144

Graphical Materials 145
Figures 145
Tables 151
References 152
Bibliography 157
List of Acronyms and Abbreviations 159
Appendix A: VSP Supplemental Data 162
Appendix B: Brine Permeability Report 204
Appendix C: Lithium Concentration from Core Samples 252
Appendix D: Madison Core Description 254
Appendix E: Mercury Injection Capillary Testing 257
Appendix F: Routine Core Analysis 351
Appendix G: Triaxial Shear Test Final Report and Summary 369
Appendix H: Weber Core Description 392
Appendix I: XRD Diagrams 405
Appendix J: XRF Data 416
Appendix K: Water Quality Data 419
Appendix L: Microseismic Monitoring Report 425
Appendix M: Final Drilling Report 479
Appendix N: Mini-Drill Stem Test and Vertical Interference Test 582

EXECUTIVE SUMMARY

This study (WY-CUSP), funded by U.S. Department of Energy National Energy Technology Laboratory, award number DE-FE0002142 and the State of Wyoming, was originally organized around seven tasks and a scope of work that focused on the acquisition of a 3-D seismic survey, design and completion of a stratigraphic test well, and a risk assessment and design of a commercial-scale geological CO_2 storage site at the Rock Springs Uplift, Wyoming. Preliminary work on all of the originally-proposed seven tasks quickly suggested that acquisition of a more robust set of databases directed specifically at the targeted study area were imperative if the main project objective was to be achieved: generation of a detailed characterization of two deep saline aquifers at the premier potential geological CO_2 storage site in Wyoming and design of a commercial-scale CO_2 storage facility complete with formation fluid production/treatment essential for pressure management during CO_2 injection at the Rock Springs Uplift. Once the 3-D seismic survey was completed and the initial seismic attribute volumes were created, the early observations and initial interpretations from the stratigraphic test well were made, and the preliminary CO_2 injection numerical simulations were complete, the essential new robust databases were assembled and continually improved upon at each step of the project. In subsequent work, WY-CUSP investigators had access to both outcrop and core observations, a diverse electric log suite, a VSP survey, in-bore testing (DST, injection tests, and fluid sampling), a variety of rock/fluid analyses, and a wide range of seismic attributes derived from a custom-designed and reprocessed 3-D seismic survey. All information was combined to thoroughly characterize the highest-potential storage reservoirs and confining layers at the premier CO_2 geological storage site in Wyoming. An accurate site characterization was absolutely essential to assessing the following critical aspects of the storage site: (1) more accurately estimate the CO_2 reservoir storage capacity, (2) evaluate long-term integrity and permanence of the confining layers, (3) manage injection pressures and brine production, and (4) integrate CO_2 utilization into carbon storage strategies.

CO_2 Storage Capacity

To obtain accurate CO_2 storage capacities, it was necessary to accomplish the following four tasks.

1. Inventory and prioritize potential storage reservoir intervals and CO_2 storage sites in Wyoming, using outcrop and regional well data to select the most outstanding targets for characterization studies (**Fig. 1**). This task was completed by inventorying and prioritizing all potential storage sites and reservoirs with preference given to thickness and petrophysical properties of reservoirs (special emphasis was given to known hydrocarbon reservoirs) and structural closure and integrity of storage sites.

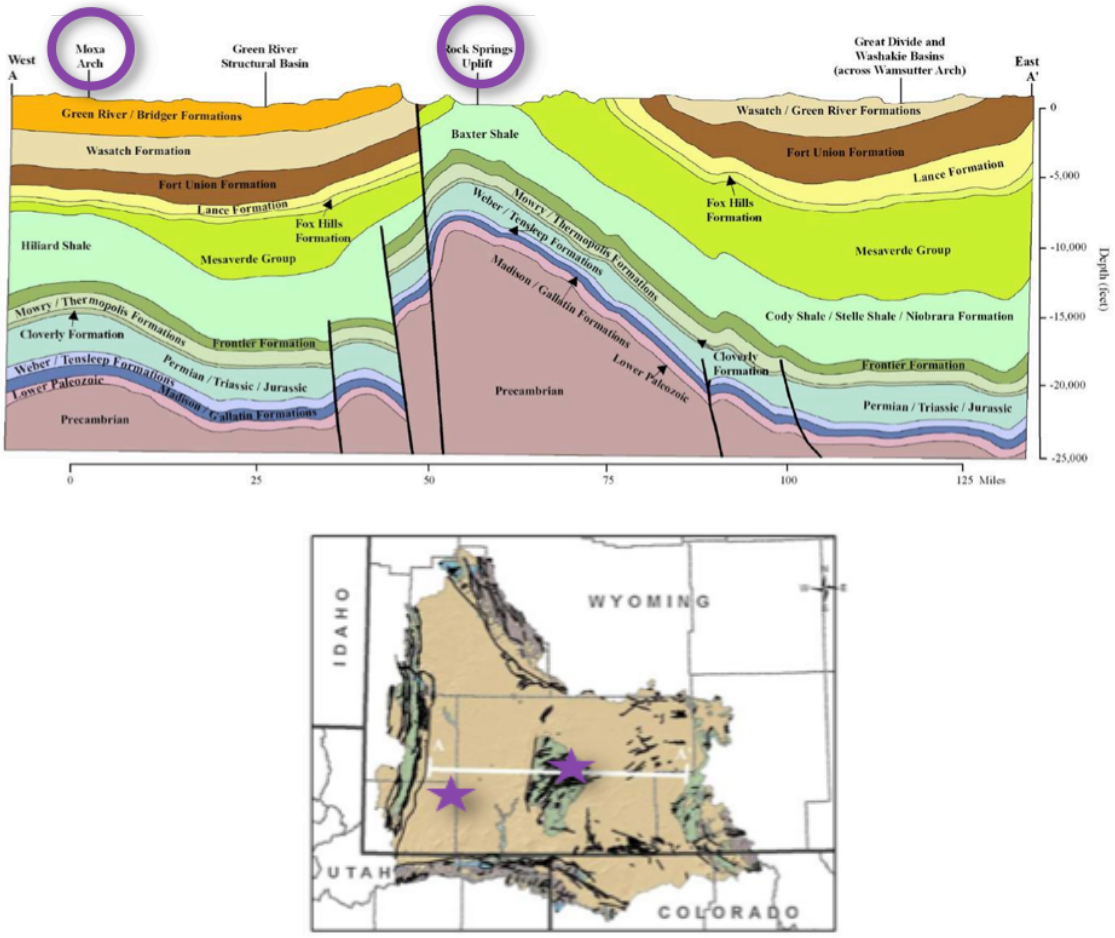


Fig.1. Map and cross section of two premier CO_2 storage sites in Wyoming

2. Acquire robust databases for the target storage domains and adjacent areas. Recommended data sources included a 3-D seismic survey with customized processing, and a stratigraphic test well designed to provide a diverse log suite, cores, a VSP survey, in-bore testing (DST, injection, and rock property testing), and a variety of rock/fluid sampling (**Fig. 2**).

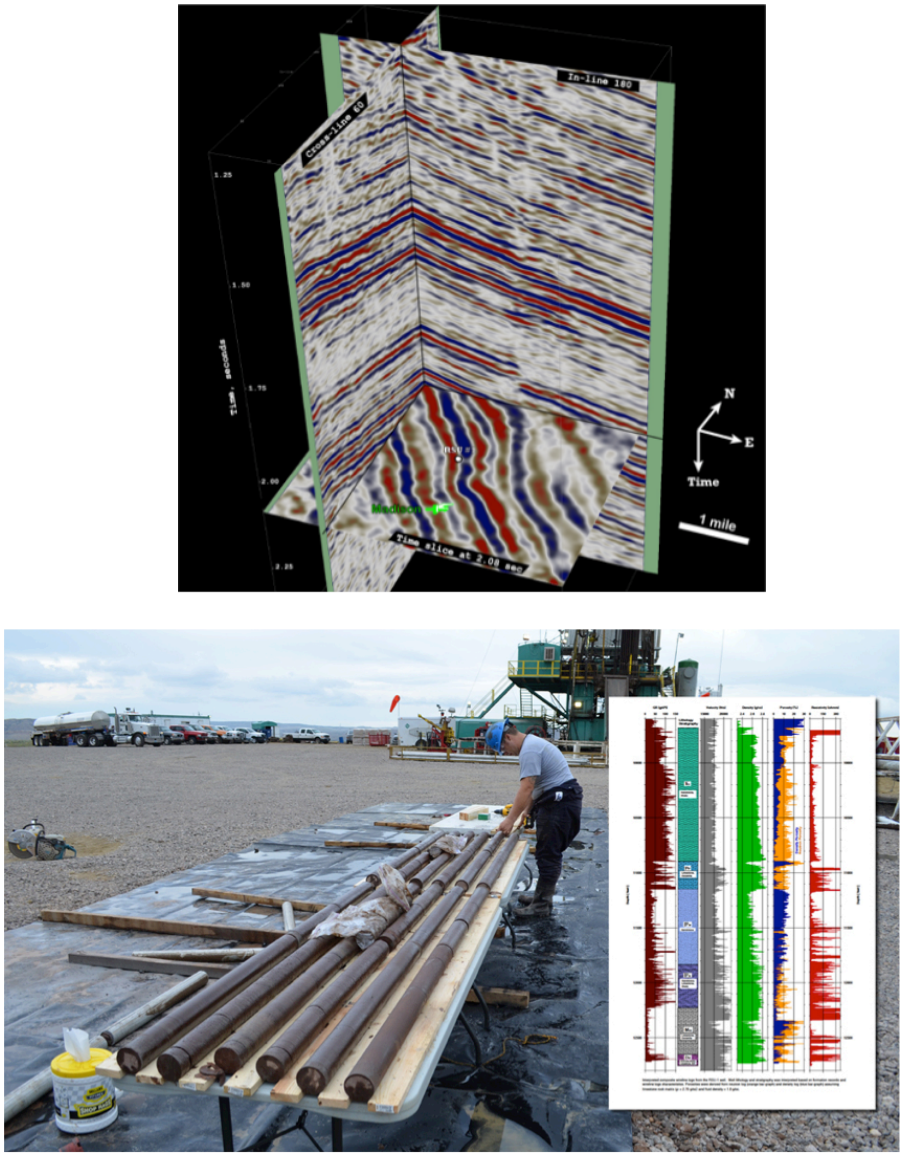


Fig. 2. Top, results from the 3-D seismic survey, core from the stratigraphic test well, and bottom, a well log suite from the WY-CUSP study site at the Rock Springs Uplift.

3. Construct realistic 3-D geological/petrophysical property models of targeted storage reservoirs and associated confining layers. Property models were constructed by combining lithofacies/petrophysical analyses with seismic attribute computations and mapping (calibrated with laboratory measurements, sonic and log porosity, and acoustic impedance and density porosity (**Figs. 3a, 3b**). This procedure allowed for petrophysical properties to be extrapolated away from the stratigraphic test well out into the 3-D seismic volume so that stratal slices could be cut parallel to bedding within the reservoir and confining layers (**Fig. 4**).

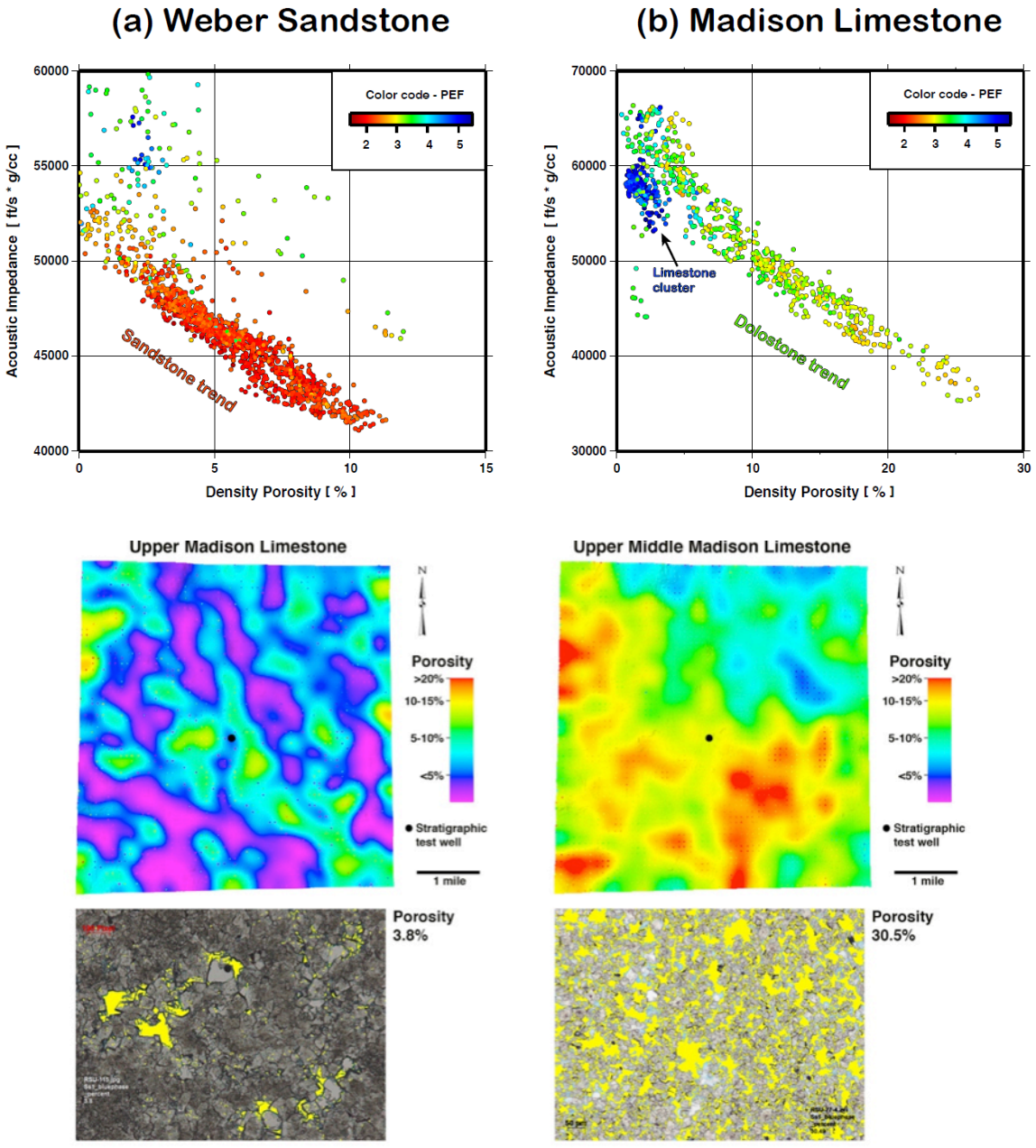


Fig. 3. (a) Acoustic impedance versus density porosity for the Madison Limestone and Weber Sandstone. (b) The upper two diagrams represent stratal slices through the Upper and Middle Madison Limestone showing the variability of reservoir properties within the formation. The lower two diagrams are thin section photographs and illustrate the extreme differences in porosity within the Madison Limestone.

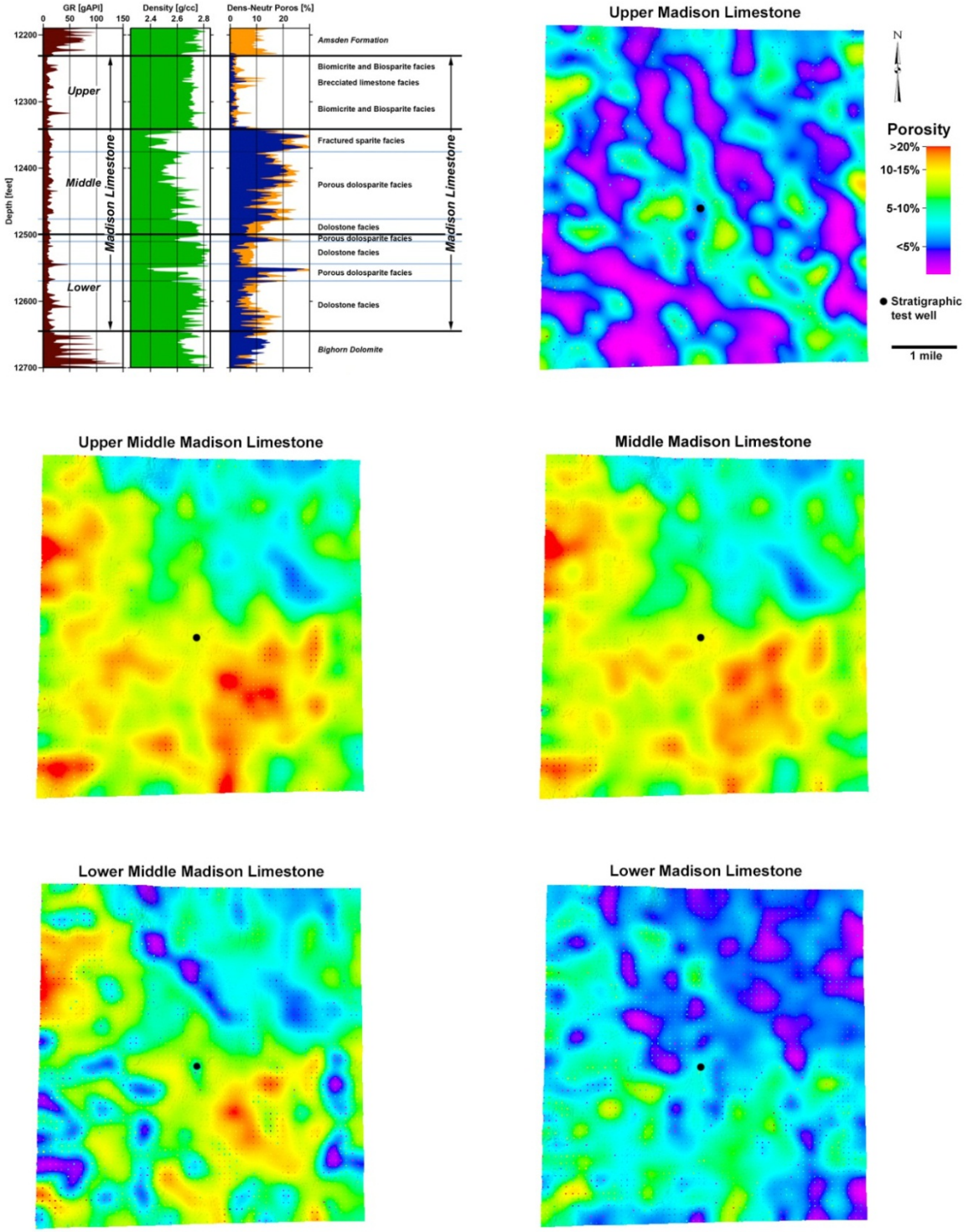


Fig. 4. Stratal slices parallel to bedding showing the distribution of porosity in the Upper Madison, upper Middle Madison, Middle Madison, and lower Madison Limestone. The GR, density, and density porosity from the log suite at the stratigraphic test well (RSU #1) is shown at the upper left for reference. Each of the stratal slices shown is approximately 5 mi x 5 mi.

4. Export these more realistic 3-D property models (porosity, permeability, and lithofacies models, especially petrophysical heterogeneity of reservoir intervals) to numerical simulations for performance assessments (**Fig. 5**). A diverse set of CO_2 injection/storage scenarios was evaluated to determine the optimum CO_2 storage capacity for the target storage reservoir and the regional storage domain (**Fig. 5**).

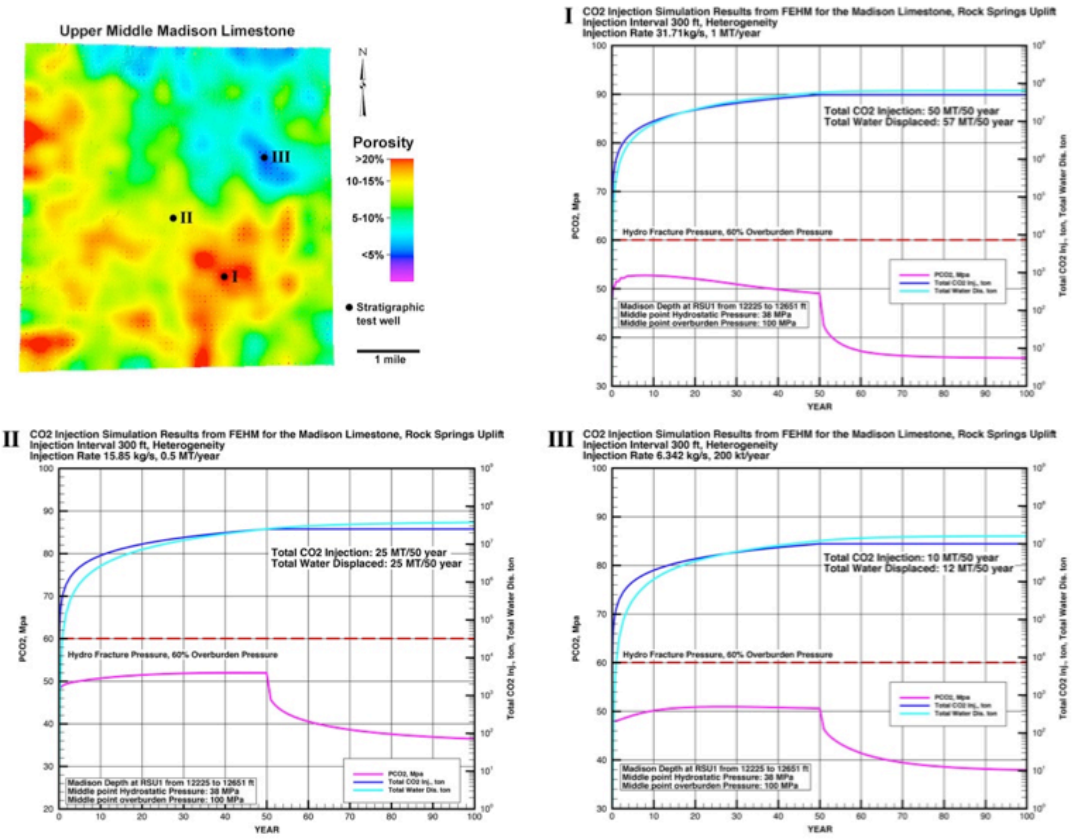


Fig. 5. Numerical simulations of three CO_2 injection scenarios representing three different locations within the best reservoir interval in the Madison Limestone: the Upper Middle Madison.

Applying the diagnostic protocol for CO_2 sequestration suggested by the DOE for the FutureGen project, the storage capacity of the Weber and Madison formations on the RSU was estimated at 26 Gt. In contrast, using the technique developed by the WY-CUSP team in the ARRA/DOE site characterization project described above, the storage capacity of the Weber and Madison formations on the RSU was estimated at 14 Gt to 17 Gt.

The WY-CUSP CO_2 storage capacity estimates are based on realistic 3-D reservoir property models that capture the petrophysical heterogeneity of the storage interval. The basis for these property models was the correlation of seismic attributes (acoustic impedance) from the 3-D seismic survey with density porosity profiles from the well log suite (calibrated by laboratory and core measurement analyses) from the stratigraphic test well (RSU #1). To determine CO_2 storage capacity, these realistic 3-D property models were used in both the FEHM and Eclipse numerical simulators to estimate more reliable CO_2 storage capacity values. The CO_2 storage capacity value derived for the storage domain in this study was extrapolated to the entire Rock Springs Uplift to obtain the estimates described above (14Gt – 17Gt storage capacity for the RSU).

In addition, results from performance assessments generated by the numerical simulations, allows the spatial aspects of the CO_2 plumes, at specific locations in the storage area, to be evaluated (**Fig. 5**). Determination of the evolving plume geometry with injection history allows estimates of injected CO_2 plume boundaries and the required CO_2 storage domain for a specific CO_2 injection/storage scenario.

Confining Layer Integrity/Permanence

To evaluate long-term integrity and permanence of the confining layers, it was essential to complete the following three tasks.

1. Select potential confining layers for petrographic evaluation and laboratory analyses for capillary properties (displacement pressures and CO_2 sealing capacity) and rock strength (**Fig. 6**).

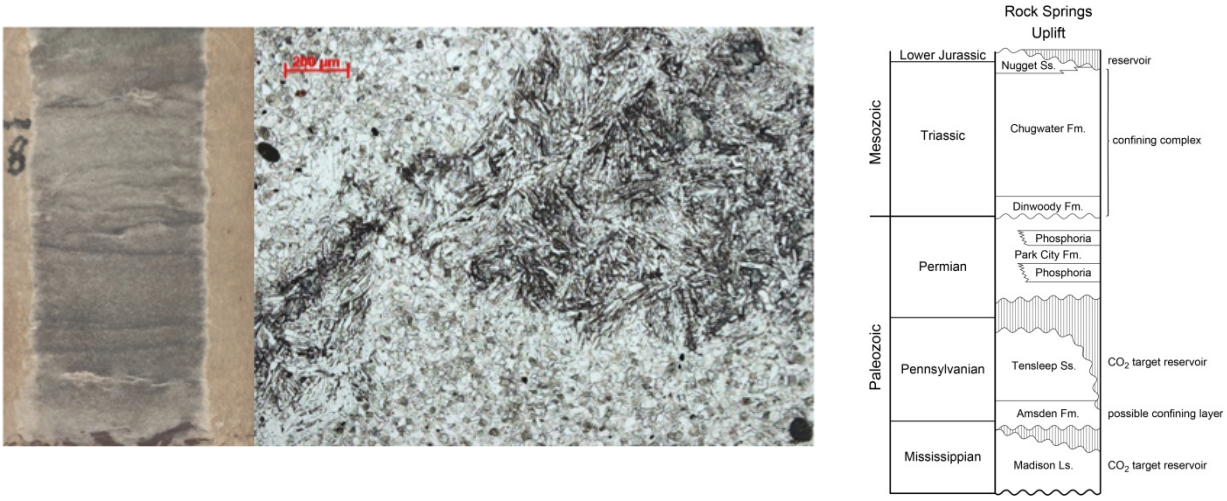


Fig. 6. Thin section and core photograph of an outstanding confining layer capable of trapping helium in the Dinwoody formation (left). Modified stratigraphic column of the Rock Springs Uplift identifying confining layers and target CO_2 storage reservoirs (right). Modified from Love, Christiansen, and VerPloeg (1993).

2. Analyze the differences in dissolved gas compositions, rock/fluid inclusion volatiles, and isotopic compositions of reservoir units separated by confining layers (**Fig. 7**).

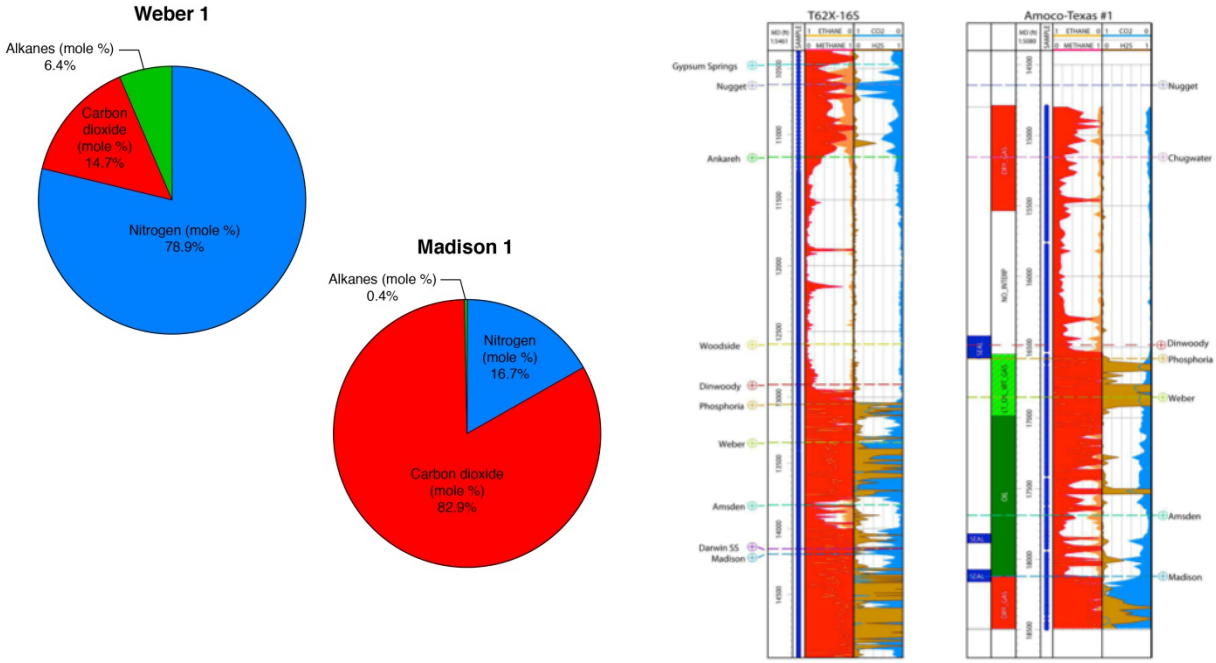


Fig. 7. Pie charts showing dissolved gas composition of the Weber and Madison formation fluids (left). The substantial differences in composition suggest that the Madison and Weber formation fluids are not in communication. Right, fluid inclusion compositions for wells from the Moxa Arch and Rock Springs Uplift (Campbell-Stone et.al. (2010)). In both cases the Triassic units have acted as hydrocarbon seals above the Madison and Weber formations.

3. Use seismic attributes such as semblance coherency, instantaneous phase, curvature, dip azimuth, dip magnitude, and energy-normalized amplitude gradient to evaluate confining layer continuity (spatial distribution, scale, and structural setting) (**Fig. 8**).

Results from these three tasks demonstrated that the assemblage of confining layers in the stratigraphic interval containing the Paleozoic reservoir rocks on the Rock Springs Uplift is characterized by integrity and permanence (world-class seals). As a consequence, both on the Moxa Arch and Rock Springs Uplift, this assemblage of confining layers has trapped helium over millions of years (helium constitutes 0.6% of the volatile phase at both sites (**Fig. 7**).

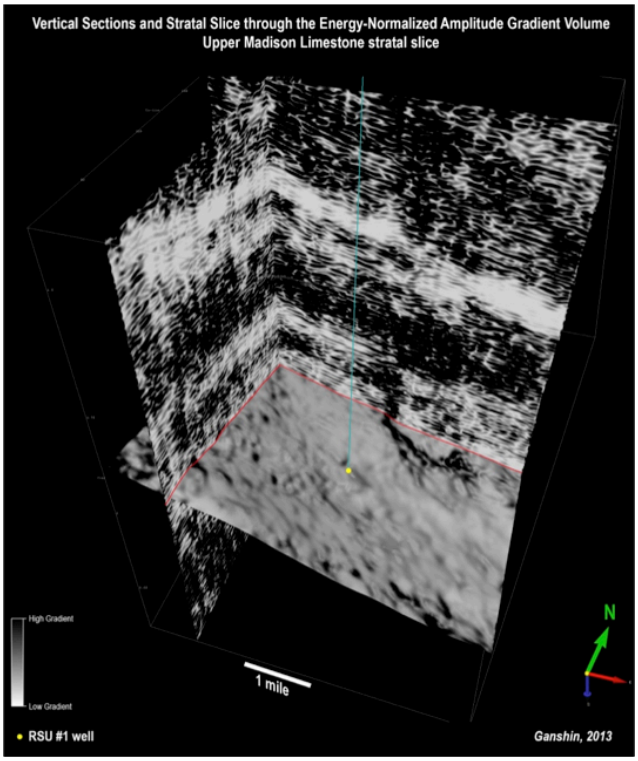


Fig. 8. Vertical sections and stratal slice through the 3-D seismic volume. The homogenous nature of the Upper Madison suggests that this interval has continuous confining integrity.

Pressure Management

To estimate the need for pressure management during CCUS projects on the RSU, the following three tasks were completed.

1. Evaluate a range of CO_2 injection/storage scenarios for target reservoir intervals using numerical simulation techniques (performance assessments) (**Fig. 9**).

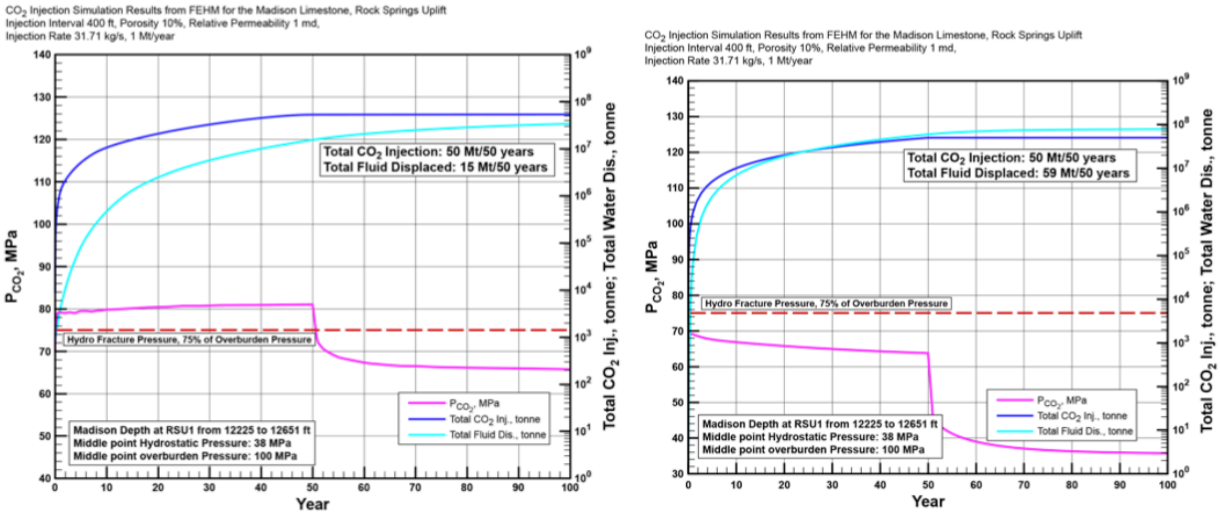


Fig. 9. Output from numerical simulations of two CO_2 injection scenarios. The left panel shows a scenario in which only a small amount of formation fluid is produced during CO_2 injection, while the right panel shows a scenario in which the volume of formation fluid is produced equals the volume of CO_2 injection (1:1 ration). Note that in the left panel, CO_2 injection causes the pressure to rapidly approach fracture pressure.

2. If pressure management is required to maintain the integrity of the storage domain, or to ensure domain boundaries, evaluate the plume boundaries, volume, and rate of formation fluid removal necessary for low-risk storage (**Fig. 10**).

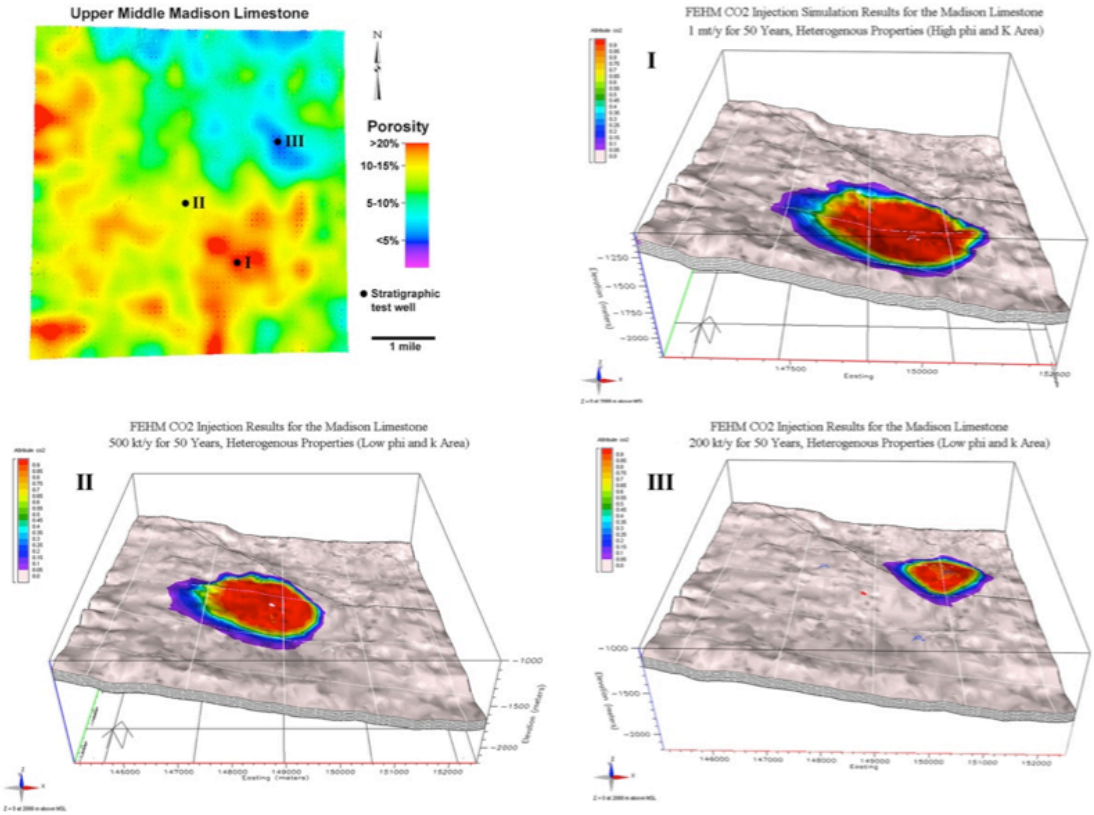


Fig. 10. Diagram showing the size of the CO_2 plume resulting from CO_2 injection into the Madison Limestone from CO_2 injection at three locations in the study area (upper left panel).

3. If formation fluid production is required during CO_2 injection/storage, design a treatment plan that converts the economic penalty of pressure management during CO_2 injection/storage via brine production/treatment into a source of revenue (**Fig. 11**).

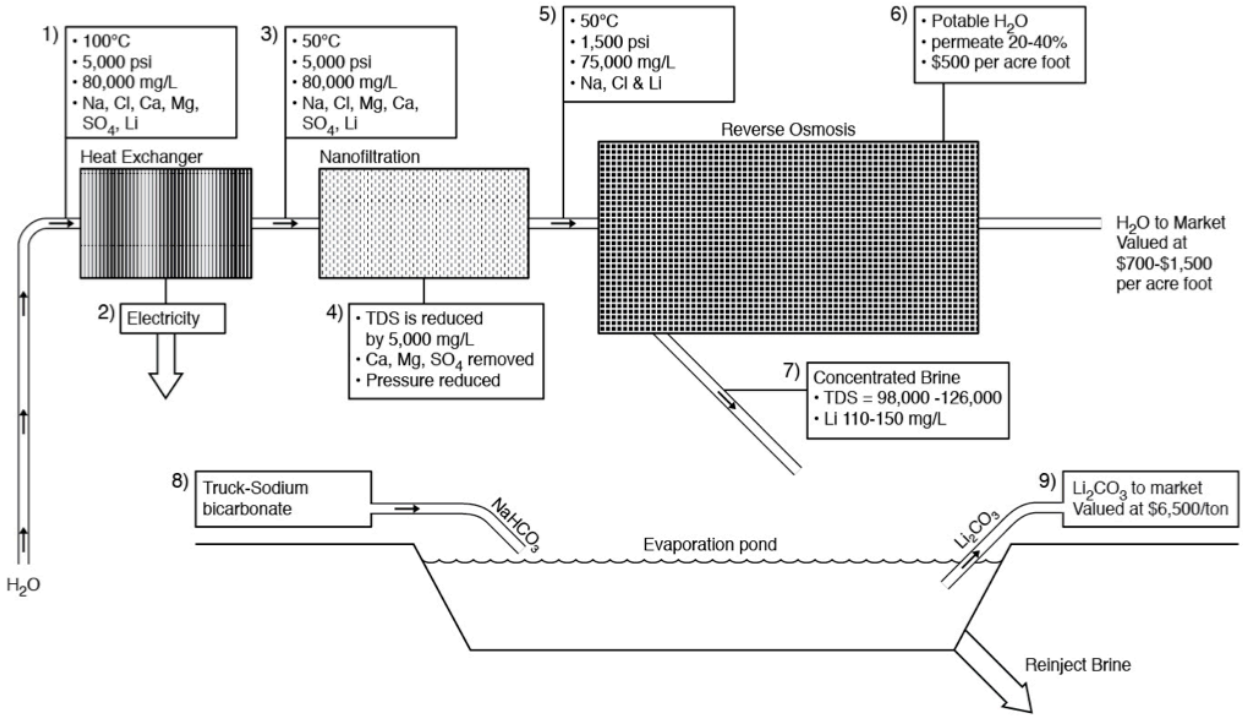


Fig. 11. Schematic diagram of proposed formation fluid treatment resulting from CO_2 injection into the Madison and Weber formations on the Rock Springs Uplift. Potable water and metals are produced from the fluid, and residual brines are re-injected.

It has been obvious since early in the WY-CUSP program that pressure management in the form of formation fluid removal (production/treatment) would be essential in any injection/storage scenario envisioned for the RSU. Without brine production during CO_2 injection/storage, performance assessments all suggest that pressure will quickly exceed fracture pressures, or that brines will migrate outside the boundaries of the storage domain. The CMI has designed a brine production/treatment strategy that includes utilization of the elevated temperature and pressure to power the treatment of brine to recover potable water and metals such as lithium. The brines recovered from the Madison and Weber formations on the RSU have elevated concentrations of various metals, particularly lithium (90mg/L–100 mg/L). This strategy converts the economic penalty of pressure management during CO_2 storage via brine production/treatment into a source of revenue.

CO_2 Utilization

To survey the potential for CO_2 utilization at the RSU, the following four tasks were completed.

1. Determine the potential CO_2 sources and sinks for CO_2 utilization in Wyoming (**Fig. 12**).

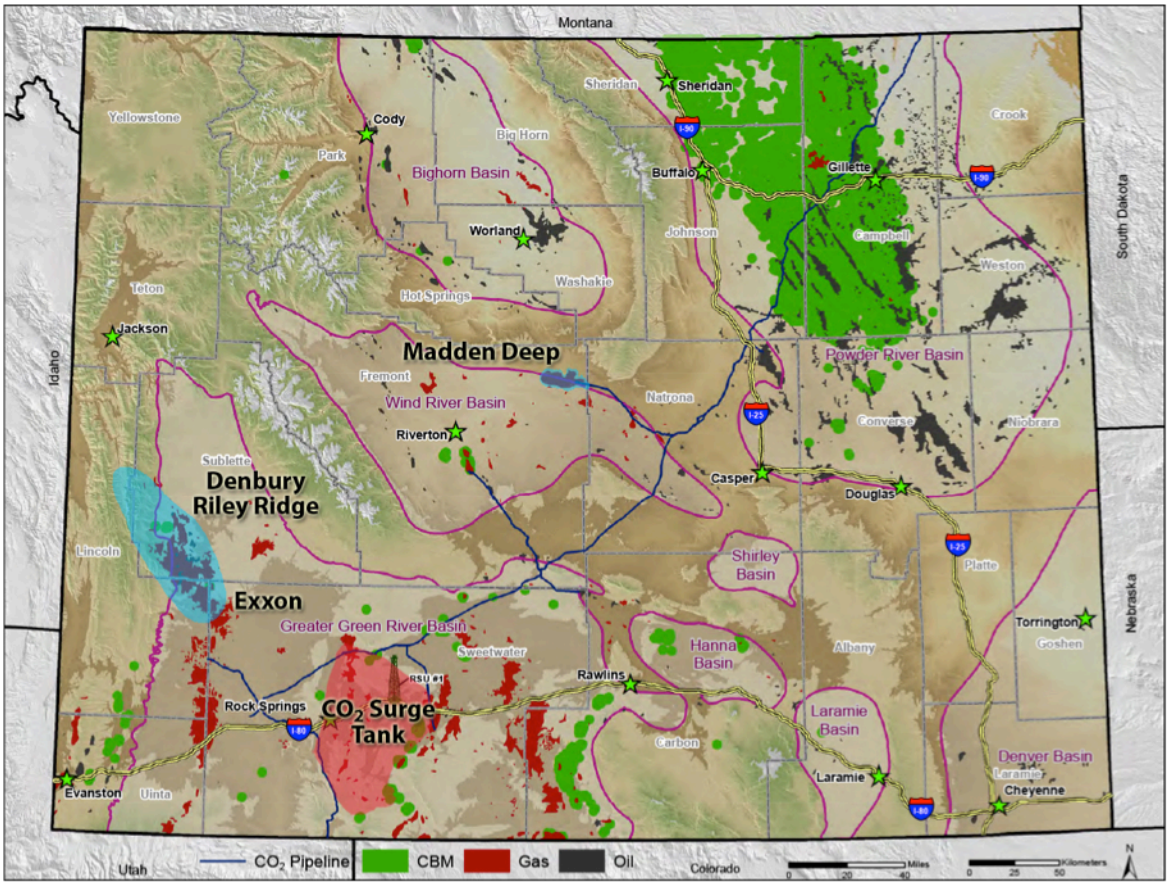


Fig.12. Map showing the location of the EOR targets (black), CO_2 pipelines (blue), CO_2 production sites (blue), and position of the Rock Springs Uplift as a regional surge tank for CO_2 and EOR projects.

2. Map depleted oil fields in Wyoming that have potential as EOR targets based on permeability, oil saturation, anomalous pressures, reservoir heterogeneity, and distance to CO_2 sources (**Fig.13**).

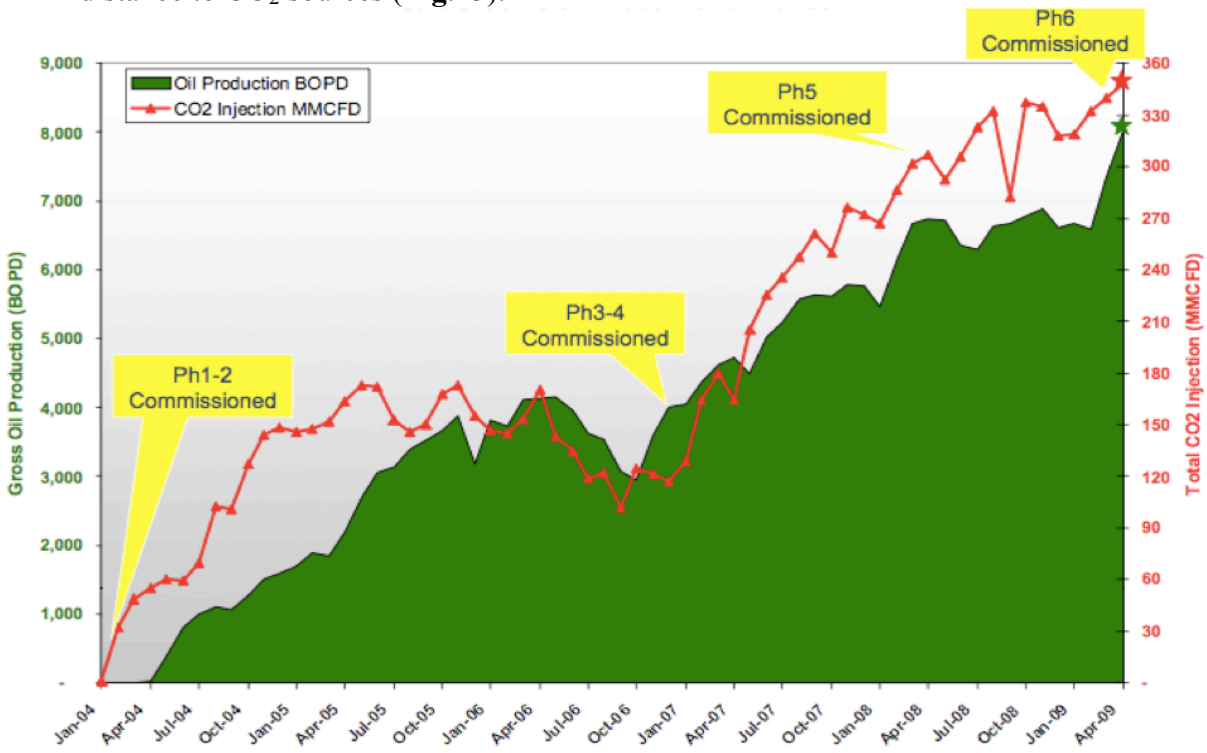


Fig. 13. Example of CO_2 flooding and stranded oil recovery at the Salt Creek Oil Field.

3. Design multiple resource development plans, including CO_2 storage, as synergistic systems that increase efficiency of development, minimize environmental footprints, and sustain and stabilize long-term resource utilization (**Fig.14**).

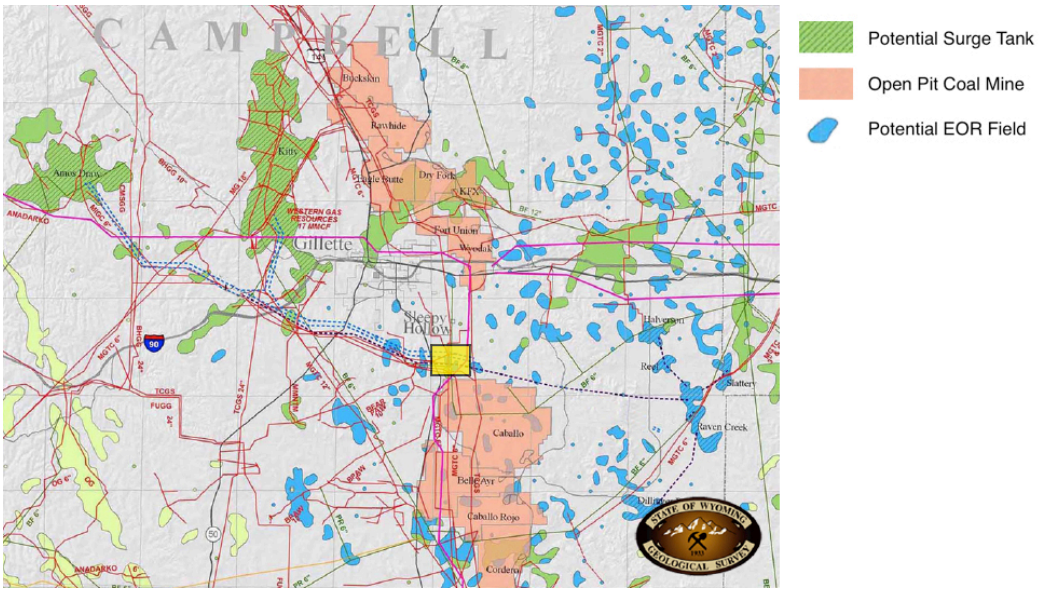


Fig. 14. Example of a potential integrated schematic strategy for resource development in the PRB. This type of strategy more efficiently and effectively recovers energy resources by exploiting synergistic relationships among resources, thereby increasing substantially. The yellow box is the location of a potential coal-to-chemical plant, the one element of this plan not yet deployed in the PRB.

4. Explore other uses of CO_2, including enhanced coal bed methane (ECBM), enhanced gas recovery (EGR), and utilization of CO_2 in fracking applications.

The energy and mineral industries in southwestern Wyoming emit 30 Mt of CO_2 annually (half of Wyoming's total CO_2 emissions from stationary sources). The RSU is ideally suited to serve as a surge tank for EOR projects and other CO_2 utilizations, such as fracking and ECBM in Wyoming. At present, Wyoming has a critical shortage of CO_2 for EOR projects and other CO_2 utilizations. The state has at least 2 billion barrels of stranded oil that could be recovered with anthropogenic CO_2 stored in a surge tank at the Rock Springs Uplift. If stranded oil in the residual oil zone (ROZ) of the depleted oil fields is included, the oil resource that could be recovered by CO_2 flooding may be as large as 4 billion barrels.

On-Going Work

It should be noted that CMI has a second financial assistance agreement with DOE (DE-FE0009202) that is focused on determining the integrity, continuity and permanence of confining layers within the entire Rock Springs Uplift (~2,000 mi^2). This work is a continuation of work on fluid-flow barriers initiated in this project. The work transition between the two agreements has been mutually beneficial and supportive. It is within the supportive framework that some of the conclusions described in this final report are supported by the findings of the ongoing work in the second, continuing DOE project listed above. Specific examples of this mutual support include, but are not limited to seismic survey re-processing and additional laboratory analyses.

Summary

Overcoming the four major hurdles to CCUS activities at the Rock Springs Uplift: (1) improving the estimates of CO_2 storage capacity of the reservoirs, (2) establishing long-term integrity and permanence of confining layers, (3) designing a profitable strategy for pressure management, and (4) evaluating CO_2 utilization, has greatly enhanced the CCUS potential in Wyoming and elsewhere.

The ultimate mission of the WY-CUSP program managed by the CMI – delivery of a certified commercial CO_2 storage site in Wyoming that could be used as a surge tank for CO_2 utilization – has been accomplished.

Lessons learned

The following list of lessons learned during the course of the WY-CUSP program may be useful to others who initiate geological CO_2 storage characterization studies.

1. To obtain more accurate characterizations of CO_2 storage sites, it is imperative to reduce geological uncertainty as much as possible.

2. Typically, geological uncertainty is a function of data availability.

3. To reduce characterization uncertainty, a strategy to obtain more robust and focused databases is essential.

4. A 3-D seismic survey and stratigraphic test well should be considered as sources of vital information for most CO_2 storage characterization studies.

5. The initial seismic survey should be reprocessed to remove acquisition footprints and to improve signal-to-noise ratios as much as possible.

6. The performance and evaluation of a VSP survey in the stratigraphic test well are essential to allow surface seismic and well observations to be correlated accurately.

7. As much data as possible should be retrieved from the stratigraphic test well (core from targeted reservoirs and confining layers, VSP survey, DSTs, injectivity tests, complete electric log suite, rock strength tests, fluid samples, mud and gas logs); these data sources will result in a plethora of observations, analyses, insights, evaluations, interpretations, and new avenues of investigation.

8. One of the most valuable tools in the WY-CUSP study was the correlation of seismic attributes and log/core observations and analyses. These correlations allowed petrophysical parameters to be extrapolated to areas at a distance from the wellbore, so that the spatial heterogeneity of the properties within the reservoir/seal system could be included in a variety of evaluations.

9. The concurrent use of both research and commercially available numerical simulators made it possible to obtain performance assessments for a wide range of CO_2 injection/storage scenarios.

10. Using the performance assessments derived from the numerical simulators, it is possible to define the most significant barriers to a high-quality characterization product.

11. The WY-CUSP program found that it was very informative to consider geological CO_2 storage as an integral component of an energy/environmental resource development system.

12. In drilling and acquiring seismic surveys, it is necessary to have extremely competent industrial partners – the WY-CUSP drilling operator (Baker Hughes) and drilling contractor (True Drilling) did a superb job and the RSU #1 well was completed effectively, efficiently, and without serious problems.

13. A highly competent attorney, with permitting experience, must be a member of the team in order to avoid excessive delays in all phases of the project.

14. The two most significant disappointments in the project were related to the EM survey (lack of incisive results) and geophones (problems with hanging a string of geophones at 12,000-ft depth).

15. In Wyoming, weather must always be considered when scheduling outside activities (drilling, coring, logging, testing, and shooting seismic surveys). Attempting these activities in snow, wind, and freezing temperatures increases the level of difficulty, and may cause failure.

REPORT DETAILS

Introduction

The WY-CUSP program at the University of Wyoming Carbon Management Institute (CMI) is one of ten geological CO_2 storage site characterization projects selected for award in September 2009 by the U.S. DOE Office of Fossil Energy's National Energy Technology Laboratory. The objective of the program was to increase scientific understanding of the potential of promising geological formations to safely and permanently store CO_2.

After an extensive inventory and prioritization of potential geological CO_2 storage sites in Wyoming, the Rock Springs Uplift emerged as the state's premier potential storage site, and the Madison Limestone and Weber Sandstone were identified as the highest-priority storage reservoirs.

The decision to focus on the RSU was based on the following factors: thickness and petrophysical properties of the reservoir interval, presence of outstanding confining layers, presence of four-way closure and 10,000 ft of structural closure on the uplift, recent formation of the structure (~43 million years before present; Surdam and Jiao, 2007), proximity to sources of half of Wyoming's CO_2 emissions, and distribution of both brines and potable water in the aquifers (8,000 ft of stratigraphic separation).

The CMI team revisited and substantially improved the understanding of the depositional environment of the reservoirs and sealing lithologies, and structural framework of the RSU, especially with respect to the burial history of both the Weber and Madison Formations. This improved understanding was facilitated in part by the new data that provided new insights into earlier evaluations. This work proved to be especially useful because there were aspects of the depositional setting and burial/uplift history that left indelible imprints on the petrophysical properties of the reservoir intervals and confining layers. As a consequence of this emphasis on the sedimentological and burial/ uplift history of the stratigraphic section at the RSU, it was possible to better understand the following aspects of the potential storage site: (1) diagenetic evolution of both reservoir intervals and the confining layers, (2) implications of the maximum burial and relatively recent uplift (dynamic thermal framework) on determination of the timing of petrophysical parameter evolution, (3) importance of organic maturation and thermal sulfate reduction on porosity and permeability distribution, and (4) relationship between burial history and aquifer formation and communication. Importantly, this work placed important constraints on subsequent work directed toward geological CO_2 storage capacity, confining layer continuity, and evaluations such as property models of reservoir intervals and confining layers on the RSU.

In addition to available regional data, particularly data at the Wyoming Oil and Gas Conservation Commission (WOGCC), a new robust database for the RSU compiled from observations, interpretations, analyses, and evaluations of a 5 mi x 5-mi 3-D seismic survey and a 12,810-ft-deep stratigraphic test well has provided the CMI team with a wealth of data. These resultant databases have allowed the CMI team to accomplish the objectives of the WY-CUSP program and more. Most importantly, they have resulted in a thorough characterization of a premier geological CO_2 storage site in the Rocky Mountain region.

The new data available to the CMI team includes 916 ft of core through the Madison and Weber storage reservoirs and the Dinwoody confining layer, including digital imaging and continuous visual documentation (grain size, mineralogy, facies distribution, and porosity), along with cuttings from the rest of the Paleozoic and Mesozoic stratigraphic sections. An extensive wire-line log suite (GR, sonic velocity, density, resistivity, neutron, and mud logs) was obtained from the well, as a vertical seismic profile (VSP), DSTs, fluid samples from two separate sampling efforts separated by one year, injectivity and rock strength testing, and rock samples. These data provided the team with a plethora of

observations, analyses, insights, evaluations, interpretations, and new avenues of investigation all directed at reducing the uncertainty that has plagued previous attempts at characterizing geological CO_2 storage sites.

The other major data asset available was the 3-D seismic survey encompassing the area surrounding the stratigraphic test well. In order to remove acquisition footprints and improve the signal-to-noise ratio, the original processed 3-D seismic survey volume underwent highly successful custom reprocessing. The custom reprocessing greatly improved the seismic velocity knowledge. Seismic velocity was derived from pre-stack data, and all of the other seismic attributes were derived from the stacked volume. The VSP log from the stratigraphic test well was absolutely essential to the study, for it allowed the CMI team to correlate data from surface seismic with geological observations and analyses from the well. As a result, it was possible to extrapolate observations from the well into the 3-D seismic volume. This ability was necessary to reduce uncertainty with regard to petrophysical properties of the storage reservoirs and confining layers at a distance from the stratigraphic test well.

The newly generated robust database and improved understanding of the regional burial/uplift, diagenetic and structural frameworks allowed the CMI team to accomplish a rarely achieved result – a thorough characterization of an outstanding geological CO_2 storage site. This result was a product of the team's ability to overcome the following four important barriers to establishing a commercial-scale geological CO_2 storage site: (1) generating accurate reservoir CO_2 storage capacity, (2) determining confining layer integrity and permanence, (3) designing pressure management strategies, and (4) evaluating potential uses of stored CO_2.

Once these barriers were overcome, the delivery of a certified commercial geological CO_2 storage site to Wyoming became a reality. The remainder of this report will trace the efforts leading to the thorough characterization of the premier CO_2 storage site in Wyoming – a characterization that provides future operators with essential knowledge required to obtain the permits necessary to construct a commercial-scale CO_2 storage facility on the Rock Springs Uplift, Wyoming.

Reservoir Storage Capacity

Inventory and prioritize storage reservoir intervals and CO_2 storage sites

The process of inventory and prioritization of potential reservoir rock intervals and high capacity storage reservoir sites was based on the following characteristics: (1) reservoir rock of sufficient area and thickness (capacity), with sufficient porosity (unit capacity, percentage of voids) and permeability (deliverability) to accommodate substantial amounts of CO_2; (2) a fluid trap, a geologic setting in which the reservoir-rock fluids are trapped by adjacent nearly impermeable rock units and sealing faults; (3) reservoir conditions of temperature, pressure, and rock/fluid chemistry that allow the reservoir to accept large amounts of CO_2 without incurring damage; (4) water quality in the reservoir of more than 10,000 ppm total dissolved solids, as prescribed by the Safe Drinking Water Act Underground Sources of Drinking Water (USDW) criterion, (groundwater containing less than 10,000 ppm total dissolved solids (TDS) may be suitable for development as drinking water and therefore must be protected).

The best examples of reservoir quality rock intervals and storage sites fitting these criteria were the state's hydrocarbon reservoirs, sites with proven fluid storage capacity. Two hydrocarbon producing formations stood out as particularly suitable; the Pennsylvanian Weber/Tensleep Sandstone and the Mississippian Madison Limestone. Both were proven fluid storage units statewide, especially in southwest Wyoming where several large geologic structures containing the two formations presented opportunities for large-scale storage reservoir development. These structures included the Moxa Arch and the RSU; with the latter chosen as the location of the WY-CUSP project. These structures hold the two formations in deep, isolated environments, with formation water TDS well above 10,000 ppm. Numerous oil and gas accumulations occur in both formations in the Greater Green River Basin. In particular, on the northern end of the Moxa Arch, the Madison is host to one of the largest accumulations of CO_2, methane, and helium in the world.

A suitable CO_2 storage site also needed to fulfill other practical criteria, including proximity to a source of CO_2, a location that offered good access and a reasonable level of regulatory permission. The chosen drill site on the northeastern flank of the RSU offered these attributes. The Jim Bridger coal-fired power plant, the single largest source of CO_2 in the state, was located within 2 mi of the site. The location, on State of Wyoming owned surface and mineral estate, provided easier regulatory permitting than is sometimes required, and the site is easily accessed by an available coal mine haul road that was optimal for moving drilling equipment.

Building a robust database

Assemble available regional data

Several databases were created in order to better assess the region surrounding the site chosen for the RSU #1. Excel databases were created including all oil and gas wells that penetrated either the Weber or the Madison on the RSU and in the immediate surrounding area, formation tops picked for each well using mainly online well logs were also included. Digitized logs were purchased for several wells and these proved highly useful in creating cross-sections across the uplift and over the proposed well site. This, along with formation thicknesses derived from the well database, allowed for predicting depths to formations that would be encountered while drilling the RSU #1. Additional information was gathered on all oil and gas fields in the area and on all deep, wildcat wells that had been drilled. The information included formation porosities, permeabilities, pressure regimes, production numbers, and gas and fluid compositions. Data for these databases came primarily from the WOGCC website, a subscription to IHS Energy Online, Wyoming Geologic Association Oil and Gas Symposium publications, and in-house well field data at the WSGS.

CMI cataloged the groundwater wells within the entire township surrounding the RSU #1, which is located in Section 16, near the township center. A major concern in long-term carbon capture and sequestration (CCS) is the potential for leakage, or a breach in the reservoir confining unit, and the resulting risk of contamination of groundwater aquifers. It is therefore important to catalog and describe the baseline groundwater quality of associated aquifers and active groundwater wells at potential CCS sites. An inventory was completed of all groundwater wells within the 36mi^2 (93km^2) township, Township 20 North, Range 101 West (T20N, R101W), surrounding the study area in section 16 (sec. 16) and expanded to include all the drinking water wells in the seven adjacent townships**.** In addition to the well inventory, a literature search was conducted to identify and characterize hydrogeologic units – aquifers and confining units – on the RSU. Finally, fresh water zones were identified and catalogued during drilling of the RSU #1. These measures can be used as an example of providing groundwater data to inform a CO_2 reservoir/site characterization.

The results of this investigation found that groundwater use in the study area is sparse. Only four groundwater permits for drinking water wells were identified in the study area and these were located more than 3 mi from the proposed site of CO_2 injection. However, 120 permits were identified for monitoring wells within the study area. Many of the monitoring well permits indicate that they have geological and water quality data associated with their records, some of which predates portions of the industrial activity that they were to monitor, thus creating a robust baseline for water quality in the study area.

Eight distinct designated hydrogeologic units (aquifers or confining units) overlie the potential CCS Paleozoic reservoirs at the study site (Bartos and Hallberg 2010): from top to bottom the Mesaverde aquifer, Baxter-Mowry confining unit, Cloverly aquifer, Morrison confining unit, Sundance aquifer, Gypsum Spring confining unit, Nugget aquifer, and Chugwater-Dinwoody confining unit. Below these units are the Weber/Tensleep aquifer, Amsden confining unit, and Madison aquifer.

Two intervals of fresh water were identified in the Ericson sandstone during the completion of the RSU #1 well. On the basis of an extensive literary search and petrophysical data from the RSU #1 well, we conclude that no other stratigraphic intervals are favorable for future groundwater development. It is important to note that several major confining units were identified within the stratigraphic column of the study area. Among these are the thick, regionally extensive Baxter-Mowry confining unit and the Chugwater-Dinwoody confining unit. The presence of these major hydrogeologic divides in addition to the several other confining units implies that there is little, if any, groundwater communication between aquifers within the RSU.

From this investigation we conclude that sequestering CO_2 in the Tensleep-Weber and Madison aquifers on the RSU poses no perceptible threat to current groundwater use and resources.

Borehole catalog development and risk assessment for southwest Wyoming

The main focus for borehole catalog development and risk assessment for southwest Wyoming were to: (1) review EPA/WDEQ CCS permit requirements relative to boreholes; (2) design, build, test and refine the borehole catalog relational database structure; (3) catalog boreholes in probable area of review (AOR); (4) identify boreholes penetrating potential reservoirs and their seals; (5) catalog construction of penetrating boreholes; (6) assess penetrating borehole geospatial locations; and (7) perform borehole risk assessment. The main results were: (1) development of a standardized set of GIS and field procedures for assembling an AOR artificial penetration database, (the well catalog), to meet Class VI well permitting requirements; (2) creation of a well catalog for the RSU; (3) assessment of borehole spatial error recorded WOGCC well locations; and (4) assignment of a preliminary CO_2 leakage risk level to boreholes in the AOR.

Well Catalog Assembly Procedures

Any industrial activity in a developed nation is subject to a variety of laws and the regulations used to enforce them. CCS projects will be no exception. At various stages of a CCS project, different laws and agencies will be relevant. Arguably the most significant and untested constraint is the Class VI regulation of the EPA's Underground Injection Control (UIC) program (**Fig.15**).

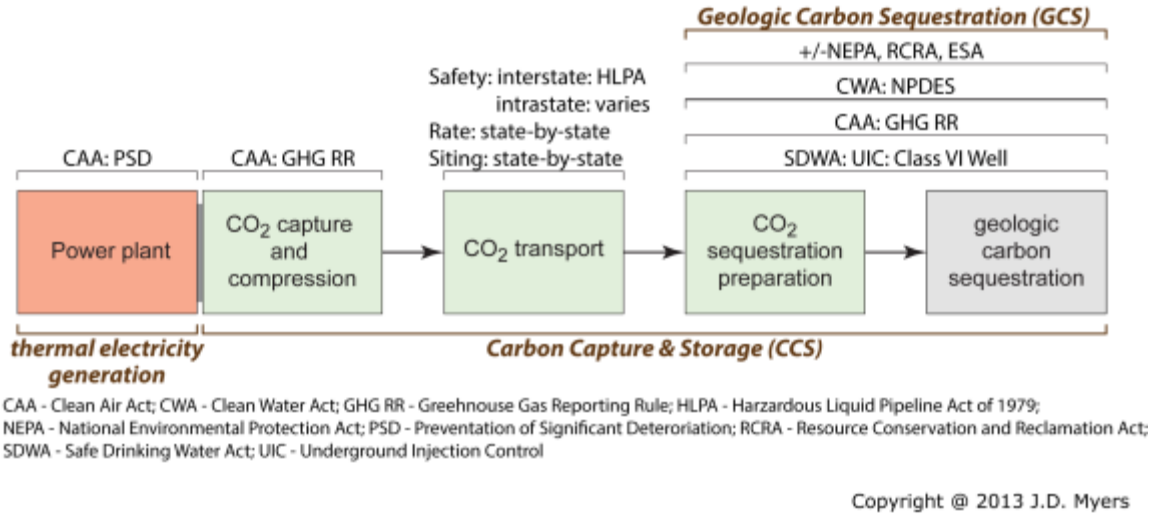


Fig.15. Timeline of a hypothetical CCS project with the environmental laws applicable to each project stage.

Discussions of how carbon capture and storage would fit in the UIC program began in 2005 with a series of technical workshops on the various aspects of carbon capture and storage for a variety of stakeholders (**Fig. 16**). By 2005, EPA had concluded from these discussions that CO_2 injection wells would not be adequately covered by any of the existing UIC well classes. Therefore in 2007, the agency announced its intention to create a new well class strictly for the underground injection of carbon dioxide for the express purpose of long-term storage. The Class VI draft rule was published in the Federal Register on July 25, 2008. Public hearings were then held at different cities across the country and there were calls for public input. The final rule was published on December 6, 2010 and immediately became effective. At this time, the rule is administered only by the EPA, although numerous states have indicated their intention of applying primacy over the new UIC well class.

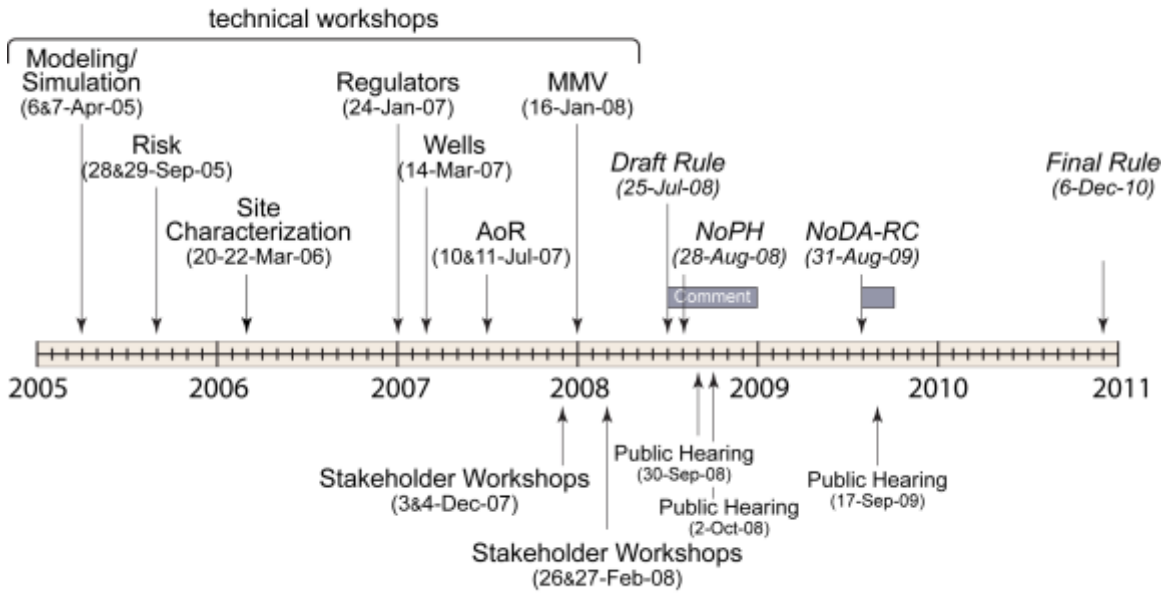


Fig. 16. Timeline with the major events in the development of EPA's Class VI well regulation. The process involved a wide variety of stakeholders. Abbreviations: NoPH – Notice of Public Hearing; NoDA-RC – Notice of Data Availability and Request for Comment. (Myers, 2013).

The Class VI well class is defined in sections 40 DFR, parts 124, 144, 145, 146, and 147 of the Code of Federal Regulations (Myers, 2013). A new section of the code, 40 CFR Part 146 Subpart H contains the primary elements of the new well class. New requirements pertaining to the well catalog are: more extensive permitting requirements, strict site characterization, expanded corrective action for artificial penetrations that could be conduits for CO_2 leakage, new injection well construction requirements, additional pre-injection activities, limitations on injection well operation, emphasis on injection well mechanical integrity, expanded testing and monitoring, additional financial responsibilities, and expanded recordkeeping and reporting requirements among other changes. Many of these new components of the UIC Class VI well class have guided the development of the well catalog and the information it manages.

To assist federal and state UIC program directors as well as injection well owners and operators, EPA published a series of guidance documents. These include: Geologic Sequestration of Carbon Dioxide: Underground Injection Control (UIC) Program Class VI Well Testing and Monitoring Guidance; Geologic Sequestration of Carbon Dioxide: Underground Injection Control (UIC) Program Class VI Well Project Plan Development Guidance; Geologic Sequestration of Carbon Dioxide: Underground Injection Control (UIC) Program Class VI Well Construction Guidance; Geological Sequestration of Carbon Dioxide: Underground Injection Control (UIC) Class VI Program: Financial Responsibility Guidance; Research and Analysis in Support of UIC Class VI Program: Financial Responsibility Requirements and Guidance; Geological Sequestration of Carbon Dioxide: Underground Injection Control (UIC) Class VI Well Site Characterization Guidance; and Geological Sequestration of Carbon Dioxide: Underground Injection Control (UIC) Class VI Well Area of Review and Corrective Action Guidance. These documents were consulted frequently during the development of the well catalog.

In developing the well catalog, two important, new aspects of the Class VI well were considered (**Fig. 17**). These factors were the diverse nature of the stakeholders that are likely to engage in a CCS project and the long timeframe anticipated for such projects (Myers and Kirkwood, 2012). Given the emerging legal and regulatory regimes for GCS, any GIS application developed for the permitting of GCS projects must be capable of serving the needs of a diverse range of stakeholders for timelines of varying duration. One key point is, however, that most of these timelines are very long (**Fig. 17**) and will span multiple changes in project staffing, regulatory regimes, and economic environments. Thus, the well catalog must function as a means of institutional memory.

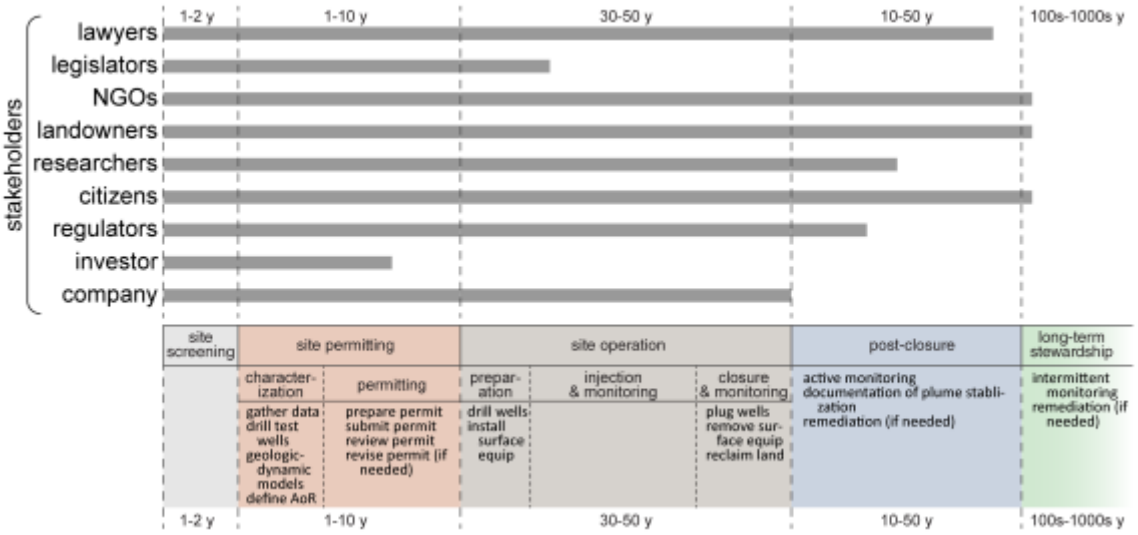


Fig. 17. Types of stakeholders with potential interest in Class VI permitting and the likely duration for each (Myers and Kirkwood, 2012).

Given the unique nature of CCS projects, a properly designed, implemented and maintained GIS geodatabase must meet the diverse suite of needs a GCS project will face. The database must serve both internal and external stakeholders through a combination of direct and indirect Web access (**Fig. 18**). The full suite of GIS tools will be crucial in creating the necessary application. The application must be stable and robust and will have to handle the technological changes likely over a project lifetime effortlessly. As an initial step in developing such an application, the well catalog has been designed and implemented as a GIS geodatabase that should fulfill the needs of a GCS project through the initial permitting stage. The software application uses a variety of GIS tools that make the application useable in the office, field, and on the Web (**Fig. 18**). It employs robust and cutting edge data management tools that are built into a relational database foundation.

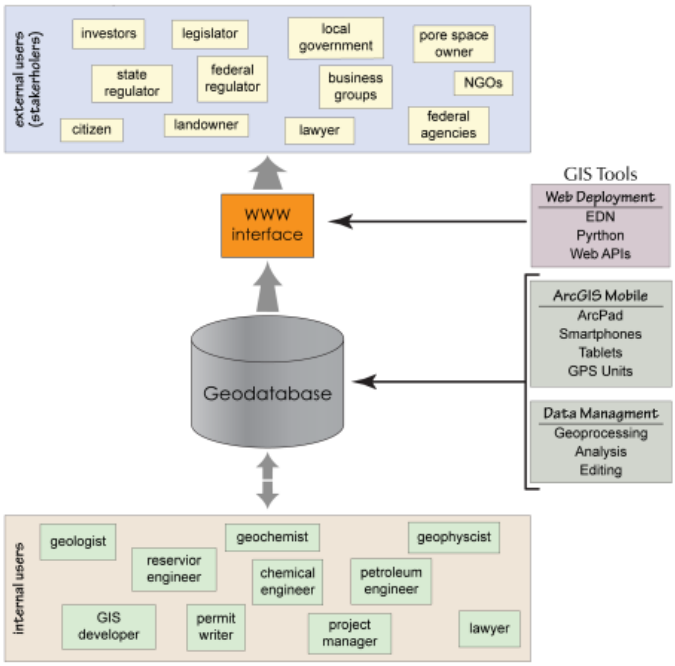


Fig. 18. Relation of different CCS stakeholders to well catalog and major technological tools used to create it. (Myers and Kirkwood, 2012).

The producures for well catalog creation have been refined and tested by creating three different well catalogs for different oil/gas fields in Wyoming (Kirkwood and Myers, 2012). Although a major first step in designing a first version (ver. 1.0) of a well catalog, there are several important components of the data base that require further development. Additional design formulation revolves primarily around defining how well construction and plugging information will be included in future versions of the well catalog. Both of these well parameters are critical in assigning well CO_2 leakage risk.

Rock Springs Uplift Well Catalog

An AOR with a 10 mi radius was established centered on the location of the stratigraphic test well (lat: 41.71261; long: -108.79482). A one-mile buffer encircling this AOR was also defined. Statewide data for active and abandoned oil and gas wells were downloaded from the WOGCC (**Fig. 19**). This data set was screened to remove all wells outside the AOR and its buffer. The initial WOGCC download revealed that 262 wells of different types, e.g. oil, gas, injection, etc., that fell in this area. Up until May 31, 2011, three updates from the WOGCC were to update the well catalog for recent drilling activity. The last update before the milestone date was April 28th, 2011. The data file downloaded from the WOGCC had 42 data columns including: API #, total depth, well class, longitude, latitude, status, status date, bottom formation, section, township, land type, county, etc.

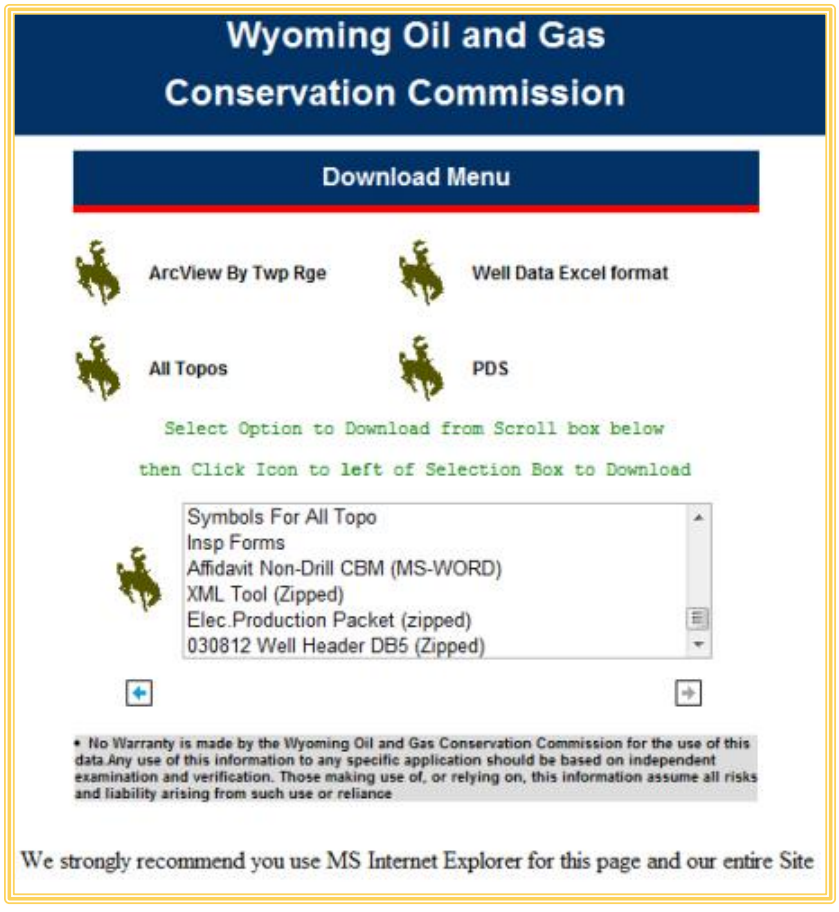


Fig. 19. Screen capture of Wyoming oil and gas download from the Wyoming Oil and Gas Conservation Commission (WOGCC) (Kirkwood and Myers. 2012).

All data columns from the WOGCC download files were imported into a GIS geodatabase (**Fig. 20**). In addition to a well layer, the geodatabase has layers for: township/range, quarter-quarter sections, roads, land ownership, the UW seismic survey and 2009 air photos for the region. Each new WOGCC download is imported into this file after a

check to determine what changes there might have been made to the data set since the last download.

County	DESC
001	Albany
003	Big Horn
005	Campbell
007	Carbon
009	Converse
011	Crook
013	Fremont
015	Goshen
017	Hot Springs
019	Johnson
021	Laramie
023	Lincoln
025	Natrona
027	Niobrara
029	Park
031	Platte
033	Sheridan
035	Sublette
037	Sweetwater
039	Teton
041	Uinta
043	Washakie
045	Weston

Well_STATUS	DESC
AI	Active Injector
AP	Permit to Drill/Active Permit
DH	Dry Hole
DP	Drilling or Drilled Permit
DR	Dormant
EP	Expired Permit
FL	Flowing
GL	Gas Lift
NI	Notice of Intent to Abandon
NO	Denied or Cancelled
NR	No Report
PA	Permanently Abandoned
PG	Producing Gas Well
PH	Pumping Hydraulic
PL	Plunger Lift
PO	Producing Oil Well
PR	Pumping Rods
PS	Pumping Submersible
SI	Shut - In
SO	Suspended Operations
SP	Well Spudded
SR	Subsequent Report of Abandonment
TA	Temporarily Abandoned
UNK	Unknown
WP	Waiting on Approval

WELL_CLASS	DESC
O	Oil
G	Gas
C	Condensate
I	Injector
S	Source
AP	Active
D	Disposal
M	Monitor
MW	Monitor
ST	Strat Test
GS	Gas Storage
05	Class 5 (WDEQ)
01	Class 1 (WDEQ)
NA	Not Applicable

LAND_TYPE	DESC
10	Federal/Unknown
11	Federal/Federal
13	Federal/Fee
14	Federal/State
20	Patented
23	Fee/Fee
30	Fee
31	Fee/Federal
34	Fee/State
36	Fee/Tribal
40	State
41	State/Federal
43	State/Fee
46	State/Tribal
60	Tribal
63	Tribal/State

Fig. 20. Some of the geodatabase tables showing the fields from the WOGCC well download that are incorporated in the well catalog (Kirkwood and Myers, 2012).

In addition to the data discussed above, APDs (application to drill) sundries, well logs and well records were downloaded and added to the geodatabase for the 262 wells that occur in the footprint of the AOR and buffer. This geodatabase was the foundation for the fieldwork that was conducted in the summer of 2011 to 2013.

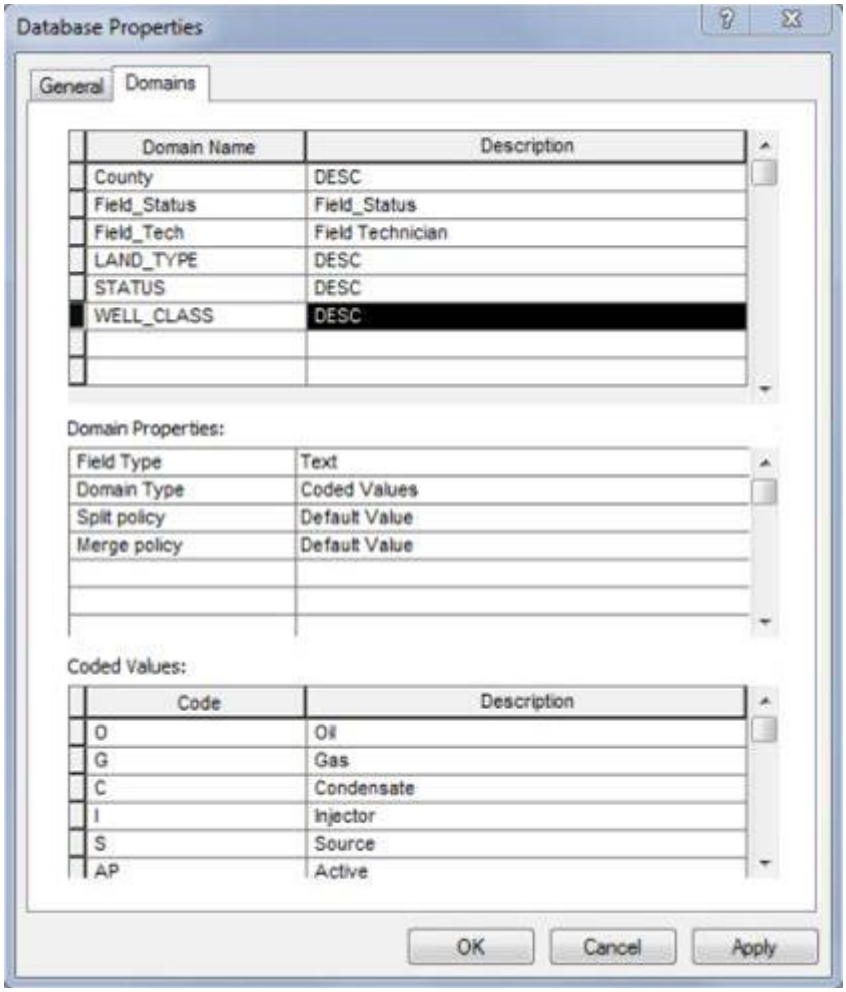


Fig. 21. Screen capture illustrating data fields and types in three of the well catalog's data tables (Kirkwood and Myers, 2012).

The Rock Springs Uplift well catalog is a freestanding database that contains all of the data mentioned previously. A graphical user interface allows access to a well's records by simply clicking on the well symbol (**Fig. 22**). The final well catalog contains 269 wells, all with updated spatial locations. Each well is documented by three photographs. To facilitate revisiting a particular field site, each well also has track logs showing the route by which the well was reached during this project. In the AOR, three wells were found that were not in the WOGCC download. In the WOGCC database, the status of these wells is listed as expired permit. Thus, the WOGCC catalogs them as not having been drilled, a status which the field evidence contradicts.

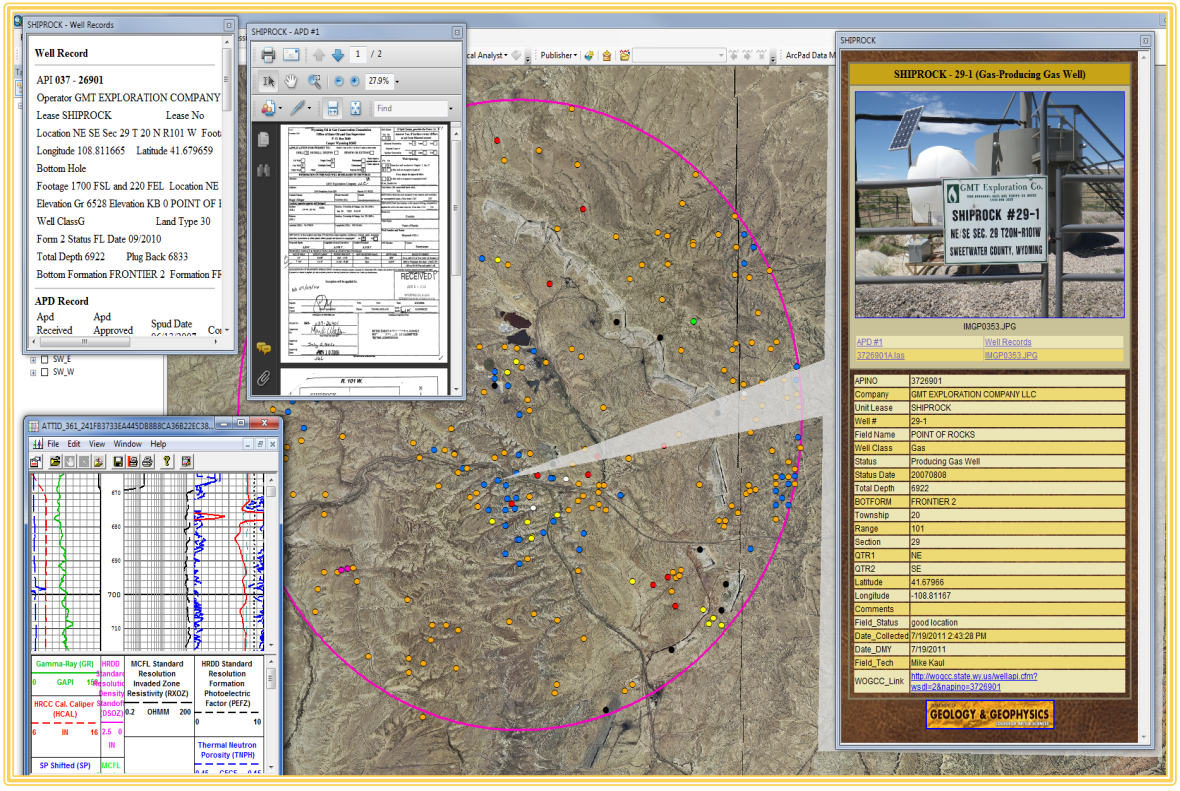


Fig. 22. Screen capture of the RSU well catalog user interface (Kirkwood and Myers, 2012; Myers and Kirkwood, 2012).

Borehole Spatial Error

The proper selection of a sequestration site is critically dependent upon accurate and realistic geologic and fluid models of the subsurface and the identification of competent seals and likely reservoir formations. Artificial penetrations, i.e. wells (cased penetrations), boreholes (uncased penetrations), and even mines, play a critical role in the formulation of such models. In particular, they provide the only direct data on the subsurface strata, e.g. cores, logs, cuttings, are useful in assessing a project's long-term potential for leakage, and factor into injection and monitoring plans. Specifically, a penetration is a source of information about the geologic formations intersected, e.g. rocks, mineralogy, textures, fractures, porosity, permeability, etc., and formation fluids, e.g. brines, gas, oil, water. This information is critical in constructing static geologic and dynamic fluid models of the sequestration site.

A key parameter in accurately modeling the subsurface is the spatial location of the wells used to construct these models. If penetrations are marked by significant spatial error, then leakage assessment could be significantly impacted. Accordingly, this project accessed the spatial error associated with oil and gas well locations as recorded by the WOGCC's online database.

Oil and gas wells in the WOGCC database are characterized by three independent spatial descriptions: a legal location, footages, and longitude/latitude. Ideally, these three spatial descriptions should be internally consistent. Accordingly, each spatial location was checked for internal consistency. Well location is described legally by the tier and range system down to the quarter-quarter section. When plotted, a well should fall in the correct tier, range, township, section, and quarter. Using ArcGIS Model Builder Tool, a procedure was developed to check for internal consistency in the legal description of a well (**Fig. 23**).

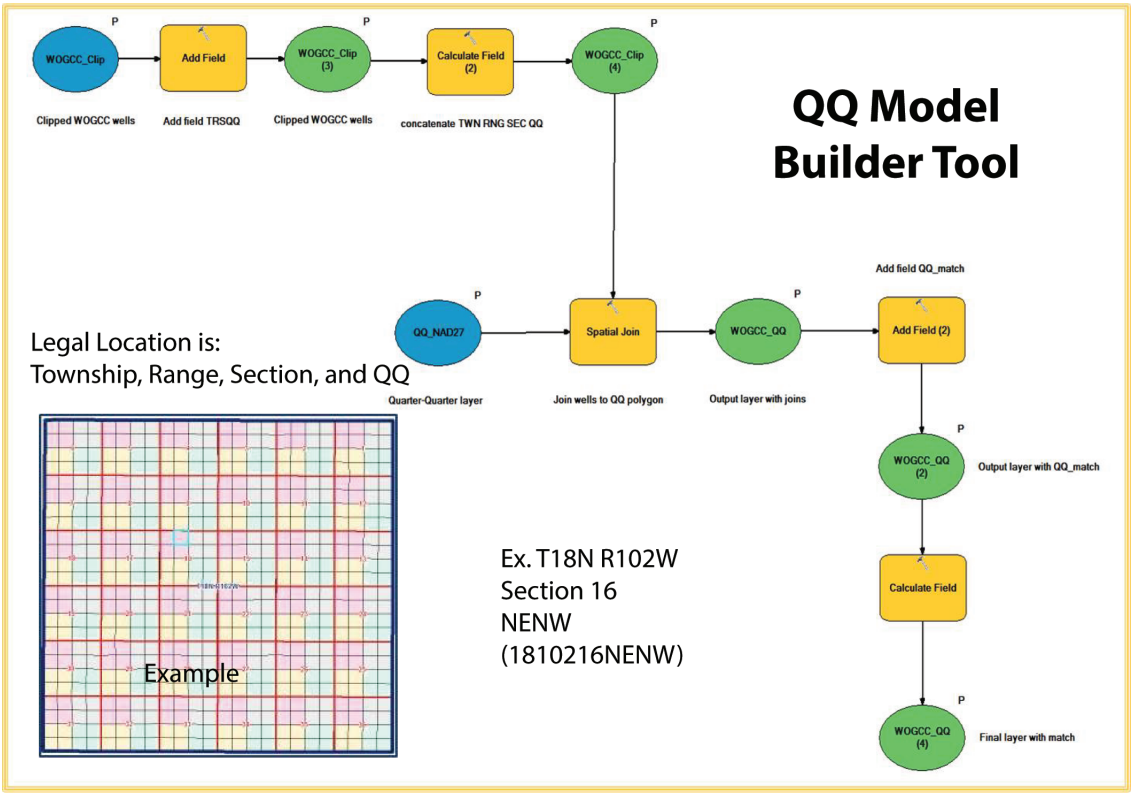


Fig. 23. Flow sequence for testing quarter-quarter location as constructed using AcrGIS Model Builder tool (Kirkwood and Myers, 2012).

Applications for Permit to Drill (APD) also identify oil and gas well location by footage. Footages are denoted as easterly and westerly and are the distance in feet from section lines (**Fig. 24**). Using a GIS tool, footages were converted to longitude and latitude and compared against the quarter-quarter and longitude/latitude data.

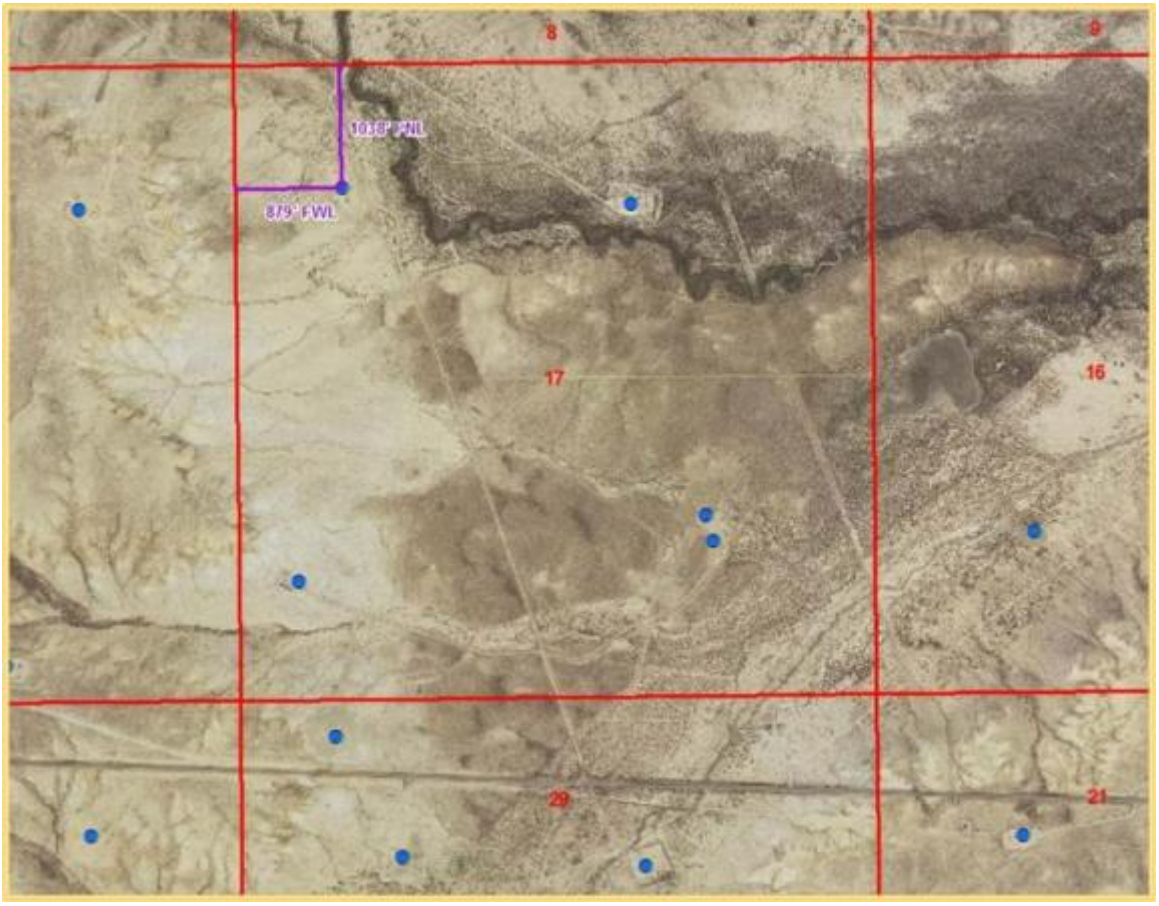


Fig. 24. Procedure for checking consistency of WOGCC well locations based on footages (Kirkwood and Myers, 2012).

As another check on location, well locations were plotted on recent air photos of the Rock Springs Uplift area (**Fig. 25**). Because this region is quite arid, well pads remain visible for several decades. Thus, wells were assessed to determine if they fell on a recognizable well pad.

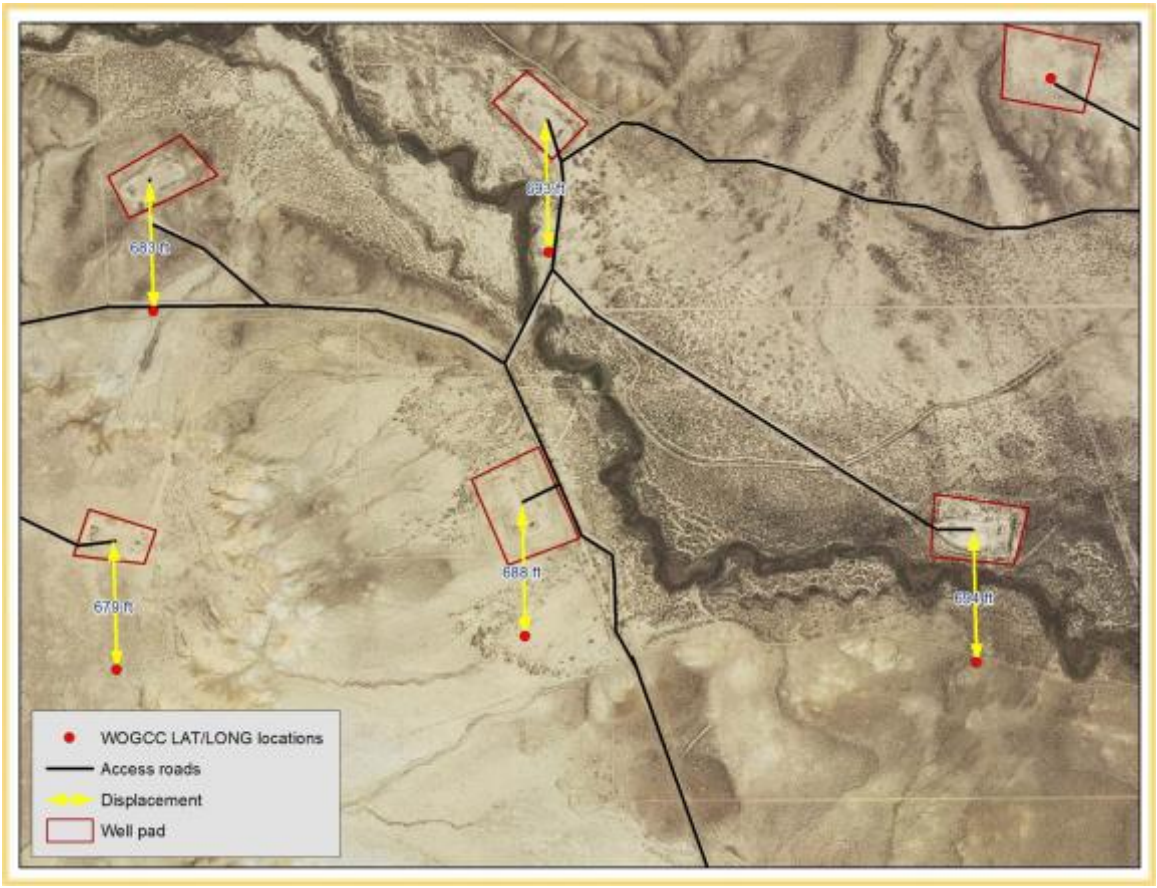


Fig. 25. Aerial photos were used to determine if plotted well locations fall on observable well pads (Kirkwood and Myers, 2012).

As a final test of spatial location, well longitudes and latitudes (assumed referenced to NAD 27) were field verified using GPS. For fieldwork, well data was electronically checked out from the geodatabase in ArcMap and converted to ArcPad. The information was loaded onto a Trimble YUMA tablet (**Fig. 26**). In the In the field each well was visited and the wellhead located using a Trimble Pathfinder GPS, which has an accuracy of 7.5 inches. All wells GPSed in the field were also documented with photographs either of the well placard (active wells) or the stinger (permanently abandoned wells, (**Fig. 27**). After each field session, data was checked back into the geodatabase along with associated photos. Spatially compared field-verified latitude/longitude co-ordinates were then checked against the recorded WOGCC latitude/longitude for each well in the AOR.

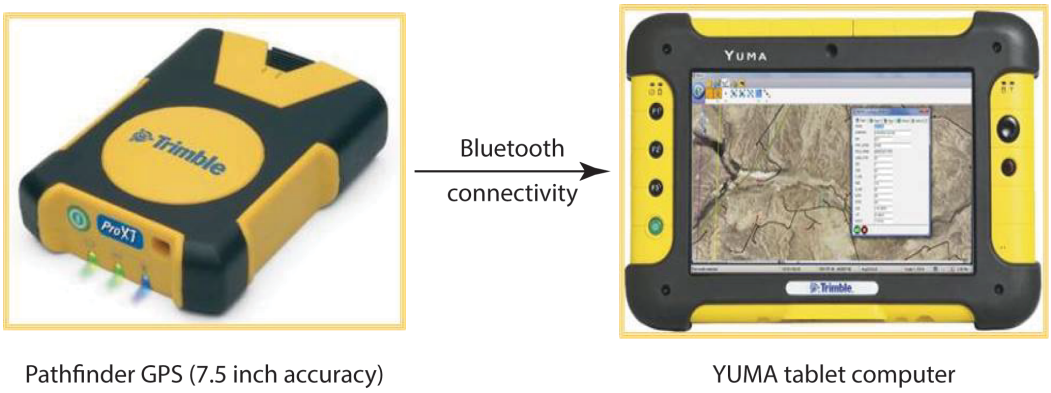


Fig. 26. Well locations were verified in the field using a Pathfinder GPS unit and a YUMA tablet computer (Kirkwood and Myers, 2012).

(a) (b)



Photographs: Robert Kirkwood

Fig. 27. Each well site GPS-verified in the field was photographed for documentation and the resultant photos added to the well catalog. (a) For producing or shut-in wells, the well placard and oil field equipment were documented. (b) At permanently abandoned well sites, the stingers were photographed for the well catalog.

The RSU well catalog contains the original WOGCC well locations in addition to updated field-verified locations. To graphically illustrate the error in spatial location associated with a well, a displacement line connecting the original WOGCC location to the field-verified location was calculating for every well in the catalog and stored in the database. Displacement lines can be viewed by clicking on an individual well. The largest displacement was 27,300 ft. Excluding this well, the average displacement recorded in the catalog is 513 ft. The well dataset has 50 wells that are displaced over a 100 ft. Extrapolating to the entire WOGCC dataset, these findings suggest about 20% of the well locations in the WOGCC data set are mislocated. This well database will not be able to be maintained and updated once all the DOE funds are spent.

Preliminary Leakage Risk

The artificial penetrations, primarily oil and gas wells, which intersect the target injection formation of a CCS project or lie above it represent potential leakage pathways for injected CO_2. Consequently, a major permitting requirement of a Class VI well is the evaluation of the potential for CO_2 leakage from every artificial penetration in the AOR (Myers, 2013). If a well is deemed likely to allow CO_2 to escape, it must be remediated before a site construction or operating permit can be issued. Many factors determine the likelihood of a leak from an oil and gas well. Two factors that influence risk, i.e. surface accumulation of carbon dioxide, and well abandonment regulatory requirements, were explicitly investigated during this project (Nelson, 2013). In addition a preliminary graphical protocol for assigning individual well risk based on multicriteria analysis was developed.

A unique feature of CO_2 is that it is heavier than air, which means given the correct topography carbon dioxide escaping from a leaking well might accumulate on the surface (Myers et al., 2011). Such accumulations of CO_2 will represent hazards to humans as well as animals. Oil and gas wells are located in a multitude of terrain types. For example, in a single oil and gas play, the surface location of wells can lie on ridges, in plains, or in valleys. The well location is important in identifying potential risk, especially with regards to accumulation of leaking CO_2. Valleys, or depressions, naturally tend to accumulate CO_2 due to stratification and density differences relative to ambient air. CO_2 leaking at high enough rates might accumulate in depressions at sufficient levels to produce hazardous conditions for plants, animals, and humans. Accordingly, a simple GIS algorithm has been created to identify wells located in depressions that are at risk of accumulating CO_2 (Nelson, 2013). This algorithm assigns the level of accumulation risk to individual wells on a scale of 1 to 8 with 8 the highest risk (**Fig. 28**). The procedure uses easily accessible digital elevation models (DEM) and well spatial locations.

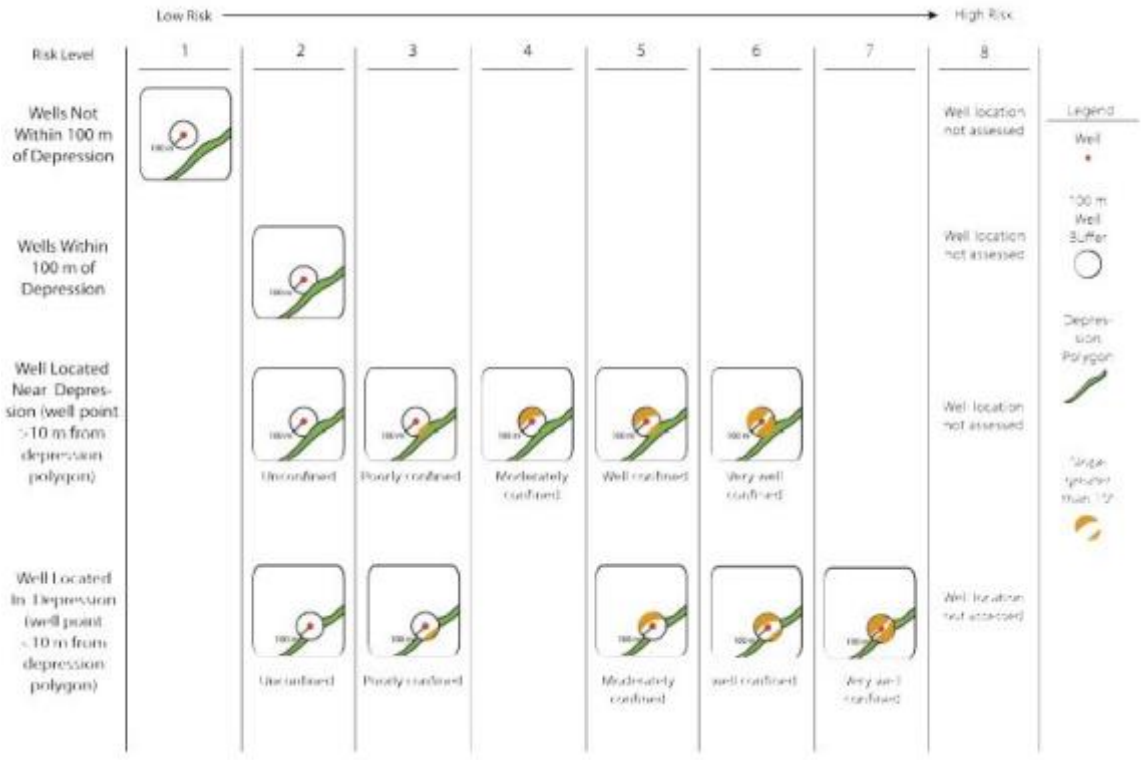


Fig. 28. Risk matrix for surface accumulation of carbon dioxide leaking from an abandoned oil and gas well (Nelson, 2013).

Because of their lack of monitoring, abandoned wells pose a significantly higher risk of undetected CO_2 leakage than producing wells. Thus, the integrity of their plugging jobs becomes paramount in the determining their likelihood of leaking. The nature of the plugging is mandated by the regulatory regime in place at the time the well was abandoned. In the 150 years of oil and gas operations of Wyoming, the plugging requirements for permanently abandoning an oil and gas well have changed markedly (**Fig. 29**). Depending upon the nature of the plugging requirements, different levels of leakage risk have been assigned to wells abandoned at different times in the past.

Dates Abandoned	Responsible regulatory body in Wyoming	Written rule?	Cement used?	Cementing standards	Leakage Risk
1883 - 1933	No regulatory oversight	No	Unknown	• No written cementing standard • Stumps, logs, and animal carcasses sometimes used to plug holes • Mud laden fluid used for plugging	6
1933 - 1951	State Mineral Supervisor	Yes	Most state agencies require cement plugs	Plug placement and length not defined, but operators required to report location and depth of plugs in SRA	5
1951 – 1962	WOGCC	No	Probably, however, no regulation to prohibit plugging by other materials	API published cementing standards and classes of cement	5
1962 – 1976	WOGCC	Yes	Likely, regulation states that no other materials other than those normally involved in plugging may be used	Cement circulation method for plugging in widespread use	4
1976 – 1982	WOGCC	Yes	Yes	• Plugged in a manner to protect drinking water sources • Displacement method of cementing common practice, which is still used today • Cementing records from third party must be kept and transmitted to Supervisor	3
1982 - 1998	WOGCC	Yes	Yes	Specific well plugging instructions including length and intervals	2 or 5*
1998 - Present	WOGCC	Yes	Yes	Job log and cement verification report required from plugging contractor	1

Fig. 29. Risk levels assigned to the different regulatory requires for oil and gas plugging in Wyoming (Nelson, 2013).

The potential for leakage of CO_2 through a pre-existing artificial penetration is a function of a wide variety of factors. These parameters fall into a number of different categories. For example, there are factors describing the well bore's location and penetration, how it was constructed, its status, and, if abandoned, how it was ultimately plugged. Thus, a thorough assessment of well leakage potential must include all these diverse parameters. A wide variety of computational and quantitative procedures have been developed to make decisions when faced with multiple, but competing inputs.

To address the need to convey risk assessments, a complex endeavor, to the general public in an honest and effective manner, a preliminary graphical leakage risk matrix (GLRM) has been developed for assessing individual well leakage risk (**Fig. 30**). The parameters found to be most important in assigning leakage risk were separated into two classes – general and locale-specific. The general class is applicable to all sequestration projects regardless of location (left side of **Fig. 30**). In this class are: well penetration, well location, well status, well construction, cementing and plugging procedures, artificial and natural connectivity, surface CO_2 accumulation potential, and surface infrastructure proximity. Each of these parameters was assigned a weighting factor and a numerical constant that normalized all risk parameters to the same quantitative scale. For the second (locale-specific) class of parameters (right side on **Fig. 30**), only a single parameter has been identified for Wyoming thus far – well abandonment date (Nelson, 2013). The contribution from all these risk factors are summed to produce a cumulative leakage risk for each well and displayed on the right-hand side of the GLRM (**Fig. 30**). With this graphical and somewhat simplistic risk assessment mechanism, it is hoped that the risk level of wells located on a landowner's property or near it can be conveyed in a simple, effective, and transparent, but realistic manner.

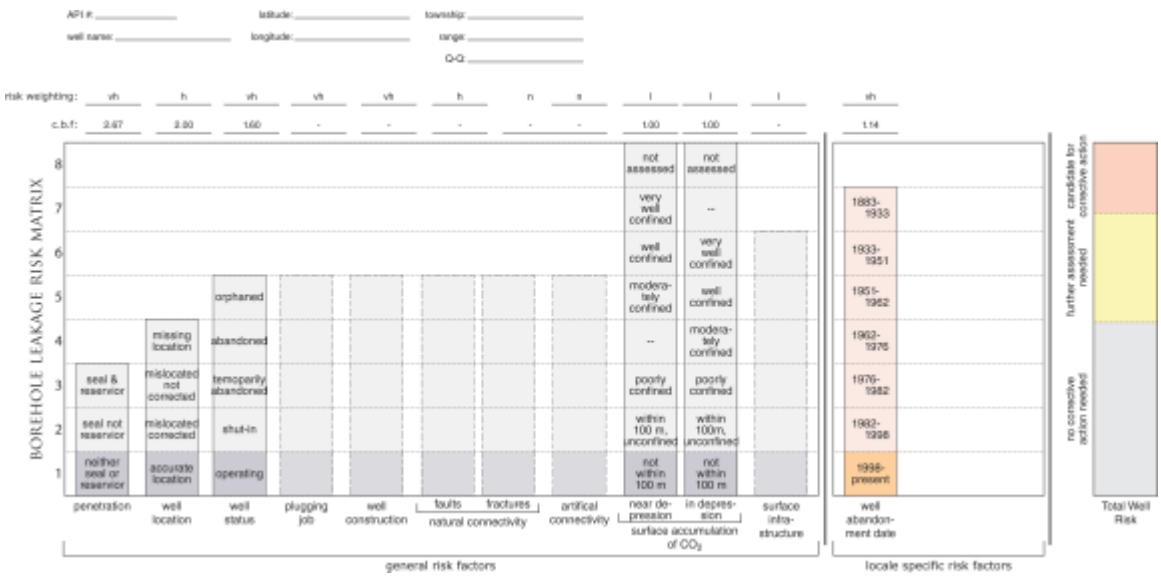


Fig. 30. Preliminary well risk assessment diagram for Class VI well permiting using a graphical form of multcriteria risk assessment.

A major permitting requirement of a Class VI well is the evaluation of the potential for CO_2 leakage from every artificial penetration in the AOR (Myers, 2013). If a well is deemed likely to allow CO_2 to escape, it must be remediated before a site construction or operating permit can be issued.

Within the RSU AOR, 185 wells are permanently abandoned (**Fig. 31**). Of these wells, thirteen have no recorded abandonment date and are assigned the highest level of risk, i.e. 6 (Nelson, 2013). Twenty-three wells abandoned between 1933 and 1962 are assigned a risk level of 5. An additional 100 wells fall in the 3-4 risk categories and only seventeen wells abandoned since 1998 have risk levels of 1.

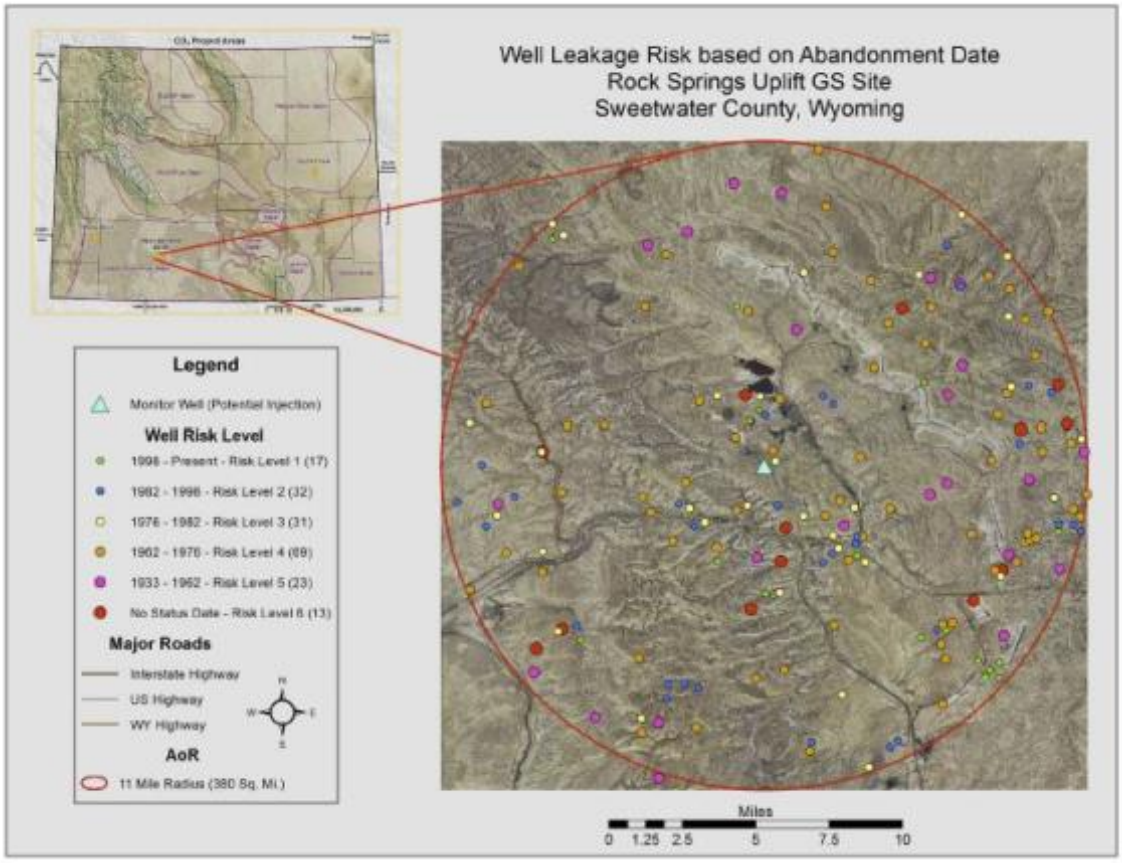


Fig. 31. Leakage risk assigned based on data of well abandonment and plugging (Nelson, 2013).

Within the RSU AOR, there are 156 (out of 269 total) wells with elevated risk of surface accumulation of leaking carbon dioxide due to their proximity to surface depressions (**Fig. 32**; Nelson, 2013). A closer examination of the near topography reveals that for most of these wells the elevated risk is, in fact, small. Most of the elevated risk wells (108) lack a confining system for actually trapping the released CO_2. Eight wells were deemed to be at very high risk for surface accumulation of CO_2 and should be monitored throughout the lifetime of a sequestration project. Two wells are assigned the highest level of risk and would require additional assessment to determine if they would require remediation (Nelson, 2013).

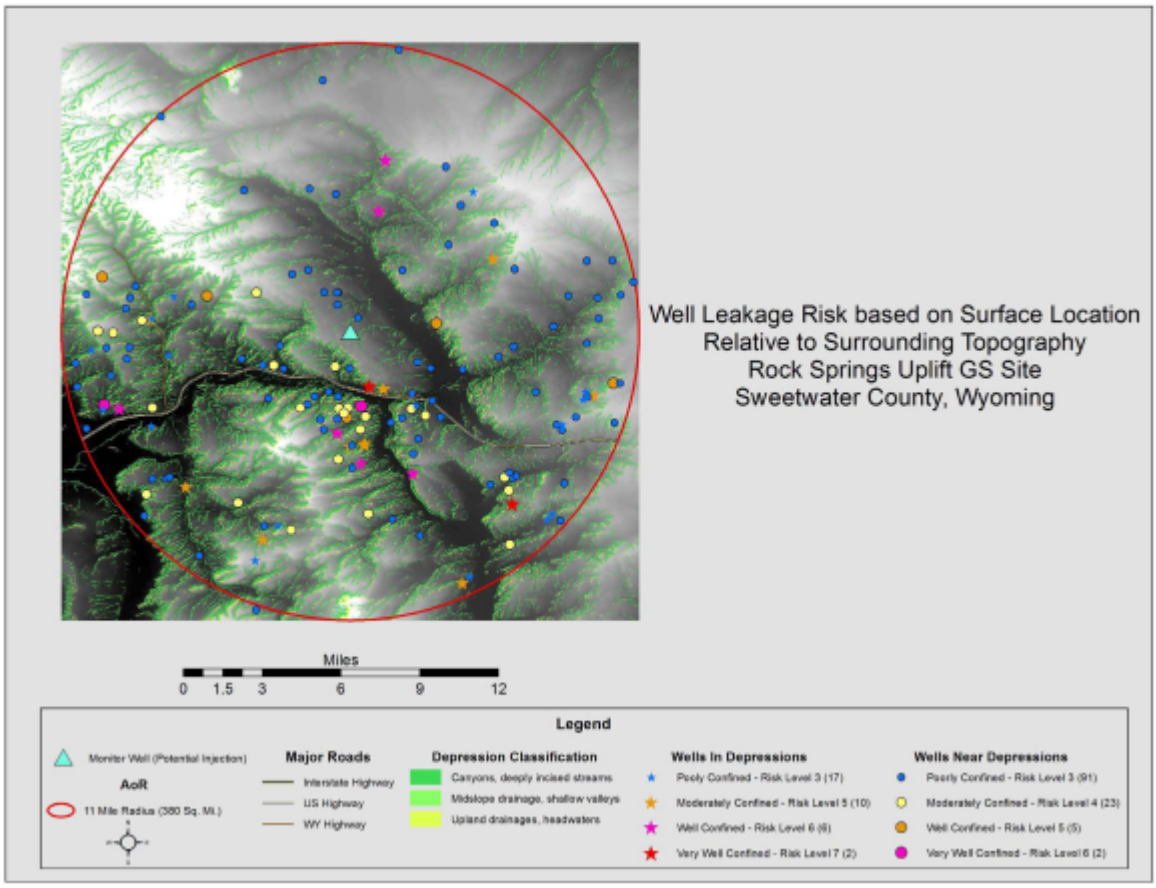


Fig. 32. Results of the surface accumulation tests for the Rock Springs Uplift AOR (Nelson, 2013).

Given its present state of development, the well catalog provides the data required to evaluate only a subset of the risk factors currently identified by the graphic well risk matrix (**Fig. 30**). Thus, a cumulative leakage risk level calculated from well penetration, well location, well status, surface CO_2 accumulation, and well abandonment data can be calculated for each well in the RSU AOR.

Incorporating the other important factors in the risk assessment matrix will require further development of the well catalog and data management practices. In particular, it will require the addition of new data fields and types to manage information about well construction, cementing and plugging, and surface infrastructure proximity. Additional catalog development will have to also be coordinated with geologists to assess the geomechanical behavior of the reservoir and seal units.

The completion of a Class VI well permit requires the compilation of a large amount of varied data about all artificial penetrations in the area of review. In regions where there has been significant previous oil and gas activity, the data management issues raised by this large required data set are significant. In the first case, the management of this amount of data is difficult and will require special procedures that must be robust enough to maintain

functionality across project staff changes and technological advances. In addition, the types of data required by the Class VI regulations are often not available. Many of the types of data needed for well leakage risk assessment are not collected by the relevant agency in Wyoming, i.e. the WOGCC, or is simply missing. Without such information, the only prudent course of action is to assign wells with insufficient information to the highest risk level. This assessment, in turn, will probably force regulators to require remediation of the well, a costly activity. At present, the stringent requirements of a Class VI permit would appear to preclude significant sequestration activity in historic oil and gas plays except for enhanced oil and gas recovery (EOR/EGR) achieved via CO_2 injection wells permitted under less-stringent EPA Class II requirements. Given that many in industry, government, and academia see CO_2-EOR/EGR as the path to a large-scale, commercial CCS industry, the current Class VI regulation may add an additional and significant barrier to large-scale CCS deployment.

Stratigraphic test well

Baker Hughes test well summation

Baker Hughes, Inc. was responsible for managing and constructing drilling of the University of Wyoming RSU #1 well during 2011 to 2013 to investigate the feasibility of long-term storage of CO_2 within the Madison and Weber formations of the RSU. RSU #1 was spudded on June 13th, 2011 with a total drilling process time of 79 days. The drilling rig was released on August 30th, 2011 after drilling to TD / PBTD (plug back total depth) 12,810ft/12,747ft, final logging, and setting a liner across the zones of interest. The well was temporarily abandoned.

After initial drilling of the well, intervention performed on RSU #1 was broken into three phases. The main objectives for phase one—post initial drilling—was perforating selected intervals, recovering formation fluid samples from the Madison formation and the Weber formation, and performing limited injection tests on both the Madison and Weber formations. Utilizing a work-over this operation began on November 13, 2012 and ended on December 21, 2012.

The objective of phase two was to equip RSU #1 with the capability of monitoring potential seismic activity due to future CO_2 injection in the vicinity of the well bore by deploying a permanent geophone array (micro-seismic sonde) within the top part of the 3½" liner. Surface interface data recording equipment was intended to be installed and fenced adjacent to the wellhead for the purposes of long term micro seismic monitoring, recording, and data collection. This operation using a coil-tubing unit started on December 27, 2012 and was suspended on December 29, 2012. While performing the operation it was observed that the array used to set the geophones would not test and no signals were detected at surface and it was decided to secure the well and send the array for repairs. It was determined that there was a manufacturing defect that allowed fluid to enter the main chamber of the geophones. Once a detailed investigation of the array failure was finished, and repairs were done, the operation was planned for the first week of April 2013.

Continuation of the second phase successfully began on April 3, 2013 with well cleanup and logging. The geophone array was then lowered, set, and cemented in place. At that point it was determined that 30 of 42 geophone data channels were non-functional after cementing. Within two weeks all geophone channels were non-functional. This second string of phones was not removed, and the coil and cable were cut above the cement and removed from the well bore. It is not known why the second string failed. Operations concluded on April 8, 2013 when surface recording equipment was installed and the area was fenced.

As a result of analog geophone failure, Baker Hughes and CMI met to discuss a third phase for RSU #1. To meet the DOE geophone milestone, it was decided to create a micro-seismic baseline utilizing digital geophones. Digital geophones were deployed in four different zones for 36 hours of continual monitoring in each zone. The 36-hour period was an arbitrary number chosen to produce a representative background noise measurement. The objective was to assess seismic noise levels at 4 different depths in the well and identify, locate, and characterize any detected seismicity. During this monitoring period for background noise, there was no microseismicity. Once monitoring reached completion, the well was plugged and abandoned.

The third phase was not originally planned creating the necessity for unique operations to sever the un-cemented portion of the tubing and Kevlar geophone cable to allow for correct monitoring to take place.

The third phase of operations began on August 26, 2013 and ended on October 2, 2013 with a total operating time of 23 days. Once this phase reached completion, RSU #1 was permanently abandoned with 4 cement plugs. The existing fence was removed, an abandonment well monument was set in place, and the reclamation of the site was scheduled for spring, after the winter thaw.

Diverse Log Suite

A very diverse and robust log suite was retrieved from the RSU #1, in large part due to our collaboration with Baker Hughes, who provided their expertise and latest available logging tools and products. Logs run on the RSU #1 included the following Baker Hughes products: X-Multipole Array Acoustilog, High Definition Induction Log, Compensated Z-Densilog, Compensated Neutron Log, Gamma Ray Log, Caliper Log, Earth Imager/CBIL (Circumferential Borehole Imaging Log), and a TVD (Total Vertical Depth) Log. Also run was a Zero Offset Vertical Seismic Profile (VSP), and a Reservoir Characterization Instrument (RCI) with Mini-DST/VIT Analysis. Decollement Consulting Inc. provided mudlogging services, including a mudlog and a complete well data summary and geologic report.

In order to create a microseismic baseline as described in the previous section, Baker Hughes (under its subsidiary Magnitude) reentered the well with Sercel Maxiwave tools. Over a seven-day period, four different zones were monitored as a surface vibrator source—used to orient the geophones down hole—was triggered and a signal was received by each of the geophones. The source was located approximately 975 m to the northwest of the well. Had any microseismic events been detected, knowing the orientation of the digital tools would have allowed for the location of those events. Results were interpreted to show no microseismic events occurring in the well area during the testing. The zones selected by CMI personnel were two sandstone zones and two shale zones in the Upper Cretaceous Blair Formation and the Baxter Shale. Following this testing the RSU #1 was permanently plugged and abandoned.

Core observations

Approximately 916' (280 m) of core was recovered from RSU #1 (**Table 1**). The recovery plan focused on extracting core from targeted reservoir and associated sealing formations, specifically the lower Triassic Dinwoody, the Permian-Pennsylvanian Weber Sandstone, the Permian-Mississippian Amsden Formation, and the Mississippian Madison Limestone. The well depth and intervals to be cored were determined by integrating regional geologic data, mainly petrophysical logs, to the study site. However, deep regional data was sparse and thicknesses and lithologic character of geologic units are naturally diverse. Therefore, the preliminary core recovery plan served as a template to define desired depth intervals. Exact coring intervals were most often determined at the well site as drilling progressed by University of Wyoming and Baker Hughes geologists.

Core Intervals	**Depth Ranges**		**Recovery (ft.)**	**Recovery (m.)**
#1 Triassic	10,600	10,690	89.2	27.2
#2 Weber	11,169	11,170	0.5	0.2
#3 Weber	11,185	11,275	93.4	28.5
#4 Weber	11,275	11,348	69.25	21.1
#5 Weber	11,348	11,468	123.4	37.6
#6 Weber	11,468	11,508	39.5	12.0
#7 Weber	11,520	11,597	77.25	23.5
#8 Weber	11,597	11,625	28	8.5
#9 Weber	11,701	11,793	91	27.7
#10 Amsden/Madison	12,169	12,257	88.25	26.9
#11 Madison	12,301	12,393	92	28.0
#12 Madison	12,393	12,477	84.5	25.8
#13 Madison	12,477	12,511	17	5.2
#14 Madison	12,511	12,532	19.5	5.9
#15 Madison	12,532	12,536	4	1.2
Total			916.75	279.4

Table 1. Total core recovery, intervals, and depths from RSU #1.

Using regional and well-site data to determine exact coring depths was the best possible procedure, though it was not devoid of error. At the RSU #1 study site, portions of the lower Triassic were recovered, though they are likely correlative to members of the lower Triassic Chugwater group. There was limited regional data regarding the depths and thicknesses of Lower Triassic formations and formation tops did not provide clear seismic reflectors. As a result our research team did not risk drilling through these formations and chose to make a conservative choice for this interval. While core recovered from the lower Triassic was not lithologically representative of the targeted formation, later analysis proved it has effective sealing characteristics; the thickness and lateral continuity of the formation makes it a lower risk seal. This data was used to populate seismic and geologic models, resulting in a successful characterization of lower Triassic sealing formations.

Due to an experienced drilling team and lack of difficulties during recovery, a significant amount of core was retrieved above what was originally anticipated. Once core was recovered it was wrapped, labeled, logged and shipped to the CMI. At CMI, the core was cleaned of drilling mud, slabbed, and photographed in both plain and ultraviolet light. Photos of the core and well-bore cuttings were uploaded to PetroArc International CORSystem 1.3 core analysis software. This allowed researchers to view and define core at high definitions remotely. Macroscopic core descriptions of lithology and visible porosity were completed at CMI's offices in Laramie, Wyoming and focused primarily on the reservoirs (these tables can be found in the **Appendix**). From these descriptions, multiple lithologic units within each reservoir were characterized.

Core analysis of the Weber Sandstone identified two members: an upper, eolian member at a depth of 11,530ft to 11,160ft (3,514.3m to 3,401.5m) deep and a lower mixed-marine member that spans from 11,810ft to 11,530ft (3,599.7m to 3,514.3m).

The upper member is defined by three facies: (1) cross-bedded eolian sandstones characterized by fine to very fine quartz sandstone, (2) bioturbated fine quartz sandstones, and (3) homogeneous quartz sandstones indicative of interdune deposits. Sedimentary features of the upper unit include fine to very fine grain size distribution with good to excellent sorting, bimodal grain distribution, cross bedding, disturbed bedding, and the extended quartz cementation. Oil stains were present at the top of formation. Core analysis, coupled with petrophysical data suggests the upper unit has the greatest porosity and that the porosity generally increases upwards (a trend confirmed by porosity and density logs). The lower mixed-marine interval is defined by three facies: (1) carbonate beds with micritic limestone, fine-grained dolostones, and coarser-grained clastic carbonates, (2) fine to very fine quartz sandstone, often cross-bedded, and (3) bioturbated fine-grain quartz sandstones. Dominant sedimentary structures of the sandstones are cross bedding and bioturbation. Definitive sedimentary structures of the carbonates are laminations in the micritic limestone.

Core analysis of the Madison limestone identified upper and lower lithologies; an upper limestone (12,225ft to 12,350ft (3,726.2m to 3,764.3m)) and a lower dolostone (12,350ft to 12,650ft (3,764.3m to 3855.7m)). The limestone is comprised of multiple facies including micritic to biomicritic limestones, minor clastic carbonates, and carbonate breccias. Brecciated intervals are cemented with calcite and contain claystones and abundant pyrite. The dolostone is comprised of several facies including biomicrite, biolithites, biosparites. There is abundant evidence of porosity such as vugs, grain-dominated porosity, and larger-scale dissolution and fracture zones. Similar to the Weber eolian unit, porosity increases towards the top of the dolostone unit (a trend confirmed by porosity and density logs).

Retrieved core proved to be an integral part of this study. Without the core, the fine-scale model of geologic and reservoir heterogeneity would have been impossible to complete. Core analysis provided the basis for:

- characterizing porosity types and distribution
- defining permeable zones and character
- defining local and regional geologic heterogeneity
- extrapolating fine-scale geologic data to the seismic area
- identifying zones for geochemical analysis
- defining mechanical integrity
- defining sealing capacities
- correlating the geochemistry of formation fluids and associated reservoir rocks
- populating the geologic injection simulation model
- defining the geologic processes that created, destroyed, or maintained the best reservoir characteristics.

Vertical Seismic Profiling (VSP) Survey

A Vertical Seismic Profile (VSP) is generated by placing a seismic energy source at the surface and lowering receivers into a borehole. This type of survey enables calibration of surface seismic data recorded in time-domain to the borehole geology directly, since in VSP we know both *depth* and *time* to seismic reflections. With VSP, geoscientists can rely on accurate, detailed physical measurements rather than on assumptions, predictions, speculations, or synthetic calculations.

VSP Data Acquisition

Baker Hughes, Inc., Houston, Texas, conducted a zero-offset VSP in the RSU #1 well. The objectives of the VSP Survey were to:

- provide time-depth information and subsurface velocity function.
- generate VSP corridor stack to tie vertical seismic with the 3-D surface seismic.

At the time of the survey, the well was drilled to a depth of 12,810ft and was cased to 9,750ft. All measured depths are referenced to the kelly bushing (KB) elevation of 6,860ft above Mean Sea Level (MSL). The ground elevation at the wellhead is 6,841.2ft above MSL. The source used for the VSP survey was two LRS-315 seismic vibrators positioned 285ft from the wellhead at 6,837ft elevation above MSL. A 12-s, linear upsweep, with 8Hz to 80Hz frequency range was used for seismic wave generation. A two-level, three-component ASR receiver tool was used to record the seismic wavefield. The depth range of recording was 500ft–12,800ft below KB. Data was gathered at 76 down-hole receiver stations. There were 360 files recorded during the survey. The time length of the correlated output data was 6s with a 2ms sampling rate.

VSP Data Processing

The Baker Hughes processing team processed the seismic data acquired in the well through the following steps.

Editing and Stacking The three-component data was format-converted and referenced to the elevation of the source. The down-hole geophone traces for each depth level were edited as necessary and then stacked using a median summation technique. The stacked record was arranged according to increasing depth, and the first arrival times were picked. A time/depth curve was computed from the first break times. The accuracy of the depth sensor was checked by comparing the first arrival times during the *down* and *up* runs of the tool.

Velocity Computations The observed first arrival times at all depth levels were converted to vertical times, and then referenced to the Seismic Reference Datum (SRD = 7,500ft above MSL), using a correction velocity of 9,000ft/sc. These time-depth pairs were then used as

input data for final velocity computations, which gave *average, RMS*, and *interval* velocities. (**Appendix A - VSP Supplemental Data Plate 1**)

Acoustic Log Calibration The VSP-derived velocity function was calibrated with the acoustic log over the 1,780ft–12,717ft measured depth interval below KB. (At each depth level the time difference (drift) between the VSP times and the acoustic times are computed. The drift time is added to all acoustic log values over the calibration interval. This effectively shifts the acoustic log to match the VSP-generated velocity values.)

Synthetic Seismogram An acoustic impedance log was computed by multiplying the calibrated acoustic log by the density log. A reflectivity series, showing primaries only (without transmission-loss effects), was derived from the acoustic impedance log. The reflectivity series was then convolved with a seismic wavelet to produce a synthetic seismogram. The synthetic seismograms, having different frequency content and polarity, are shown in **Appendix A – VSP Supplemental Data Plate 2**.

Wavefield Separation VSP wavefields consist of a superposition of the downward and upward traveling (or simply downgoing and upgoing) wavetrains. Both the downgoing and upgoing wavetrains are useful, but need to be separated before they can be studied and utilized. In this study, the wavefields were separated using a median filter. The downgoing and residual upgoing wavefields are shown, respectively, **Appendix A – VSP Supplemental Data - panels 2 and 4 of Plate 3**. The unwanted wave modes left in the dataset after the wavefield separation was removed by applying a seven-point median filter and zero-phase 10–80-Hz bandpass filter. The upgoing wavefield at two-way time and the enhanced upwaves are displayed, respectively, in **Appendix A – VSP Supplemental Data - panels 5 and 6 of Plate 3**.

Downwave Deconvolution The VSP downwave deconvolution shapes the input source wavelet to zero phase and collapses upcoming multiple reflections generated above the depth of the deepest receiver. A 400-ms trace-by-trace deconvolution operator was computed and then applied to the downgoing and upgoing wavefields followed by a zero phase 10HZ–80Hz bandpass filter. The deconvolved downgoing and upgoing wavefields are shown respectively in **Appendix A – VSP Supplemental Data - panels 3 and 7 of Plate 3**.

Corridor Window and Corridor Stack The basic computed product of the VSP is known as a *corridor stack*, which in appearance resembles a synthetic seismogram. In reality it is a vastly superior well correlation tool, because it contains actual seismic reflections comparable with the surface seismic data. In this study, a narrow time window was designed to include only primary events with similar reflection character on enhanced deconvolved upwaves. The data that lies outside the stacking corridor was muted (**Appendix A – VSP Supplemental Data - panel 9 of Plate 3**). The resultant muted traces were then stacked to one trace, called a *VSP corridor stack trace*. This stacked trace is repeated eight times for visual clarity and represents the seismic response at the RSU #1 wellbore. The 10HZ–80Hz filtered corridor stack, with normal and reverse polarity, is shown, respectively, **Appendix A – VSP Supplemental Data - panels 10 and 11 of Plate 3**.

L-Plot Correlation Display An L-Plot correlation display ties together the depth domain and time domain properties of the VSP with well-log data and synthetic seismograms. The VSP deconvolved upwaves are displayed with linear depth-of-trace spacing. Well-log data displayed in the depth domain are plotted above the upwaves panel using the same depth scale. In this way, the reflection events can be directly correlated in the depth domain with the well-log data (**Appendix A – VSP Supplemental Data - Plate 4).** In addition to the depth-domain data, time-domain synthetic seismograms and well logs converted to time domain are also displayed using the same time scale as that of the deconvolved upwaves. This allows time domain event correlation between the well-generated data and VSP data (**Appendix A – VSP Supplemental Data - Plate 4**).

Interpolated Time-Depth Table The most basic information that we want from the VSP is a seismic time-to-depth relationship. This information was acquired by just picking the first-breaking energy of the direct arrivals. The time-interpolated results (with 2-ms sample rate) are presented in tabular form in **Appendix A – VSP Supplemental Data - Plate 5** for the two depth-reference points – the seismic reference datum and the kelly bushing of RSU #1.

Comparison of VSP and Surface Seismic (CMP) Data

The deconvolved and enhanced upgoing events show that the VSP wavefield separation and processing has been fairly successful. The seismic reflections corresponding to the major stratigraphic intervals are continuous across all traces (**Appendix A – VSP Supplemental Data - panel 8 - Plate 3**). One can easily determine the time of the geologic interface that created the upgoing event by following the characteristic feature of this event up to its intersection with the time axis.

One of the main reasons for acquiring VSP data is to improve the analysis of CMP reflection data. In order to accomplish this objective there should be reasonable correlation between the two data sets. **Fig. 33** illustrates the surface P-wave reflection seismic data with the VSP inserted at the tie point (RSU #1). The overall reflectivity trends of the surface reflection data and VSP data match well. The reflectivity is moderate within the interlayered sand and shale Cretaceous and Jurassic strata and very low within the shale-rich strata of the underlying Triassic formations (**Fig. 33**). The top and base of the major sealing horizon is obvious on the CMP data and the VSP; the relative amplitudes are also comparable (1.83s–1.97s time interval in the VSP panel on **Fig. 33**). Going down in time, the reflectivity increases considerably within the carbonate-rich units of the Paleozoic Phosphoria, Weber, and Madison formations. At the RSU #1 well location, the top of the Weber Sandstone corresponds to a seismic trough at 2.0s two-way traveltime (TWTT). The Madison Limestone is imaged with a reflection just below 2.1s TWTT (**Fig. 33**). The seismic trough at a TWTT of 2.13s at the well location corresponds to the low-impedance middle Madison unit.

The higher frequency content of the VSP data is evident. The prestack VSP traces (VSP panel on **Fig. 33**) show a series of distinct reflections just above and below the Triassic shales, whereas the same reflections on CMP data are overlapping and complex. This difference in frequency content allows for laterally continuous features to be better resolved in CMP data than in VSP data.

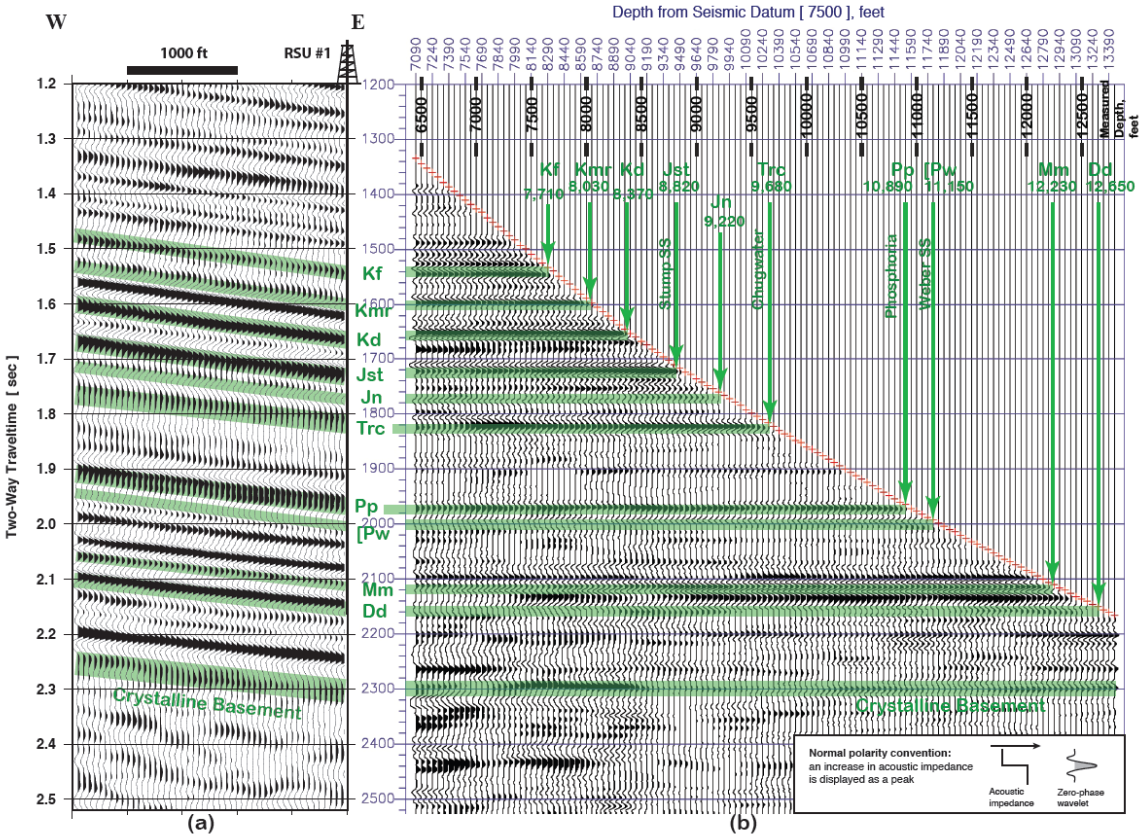


Fig. 33. (**a**) Interpreted west–east profile through the PSTM seismic volume with the RSU #1 well located on the east side. (**b**) upgoing (reflected) VSP wavefield displayed at the same time (vertical) scale as the surface seismic. Green highlights the interpreted seismic reflections

Comparison of VSP and Well Data (Geologic Property Modeling)
Forward modeling was used to gain insights into the geometrical and physical relationships between seismic reflection amplitude and rock/reservoir properties derived from the well logs and core. The modeling was limited to the one-dimensional case along the test well-bore axis within a depth interval that includes the major deep saline aquifers (10,500ft–12,700ft below KB). The density and velocity values used in the modeling are based loosely on physical properties of the major target reservoir rocks (the Weber and Madison Formations) and confining units. The perturbed geologic models were convolved with seismic wavelet (10Hz–80-Hz band pass) to produce simple, zero-offset acoustic models of the expected seismic response. These acoustic responses were further compared with the VSP stacked trace using a basic cross-correlation technique. Pearson's cross correlation coefficient was used as a criterion to validate the match between the modeled and observed data. The modeling iteration was stopped after obtaining a fairly strong ($r = 0.86$) correlation coefficient between the synthetic response and VSP trace. For comparison, the starting model values (original velocity/density logs) produce a synthetic trace that correlates moderately with the observed VSP trace ($r = 0.69$). The resultant geologic property model contains estimates of reservoir thickness, porosity, and permeability. The tabulated property model and the corresponding synthetic trace, as well as the wireline log data and the VSP trace, are displayed in **Appendix A – VSP Supplemental Data - Plate 6**.

In-bore testing

Baker Hughes, Inc. deployed their Atlas Reservoir Characterization Instrument (RCI) in RSU #1. The RCI tool utilizes a straddle packer configuration1 in combination with an observation probe. One mini-drill stem test (Mini-DST) was performed in the Weber Sandstone at a depth of 11,398.53ft and along with a Mini-DST and vertical interference test (VIT) performed in the Madison Limestone at a depth of 12,361.57ft below land surface. There was no vertical communication in the Weber Sandstone at the probe depths and consequently only a Mini-DST could be performed.

A vertical interference test is a pressure transient test in which pressure is monitored at the observation probe above and area of fluid production. This test helps to determine the degree of vertical permeability with in the reservoir. The mini-drill stem test is used to determine the types of fluids in the formation and horizontal permeability.

To predict pressure and rate response during pressure testing, it is necessary to make assumptions as to the nature of the formation and the fluids therein. For the packer configuration, an analytical model for a partially completed well with storage and skin is used. The partially penetrating well model with homogenous reservoir behavior assumes uniform reservoir thickness (***h***), and porosity (ϕ) with the well completed over a limited section (***hw***), in the middle of the zone. Permeability anisotropy is included in the model as defined by the horizontal permeability, ***kxy***, and vertical permeability, ***kz***. A diagram of the tool and the flow model is shown below in **Fig. 34**.

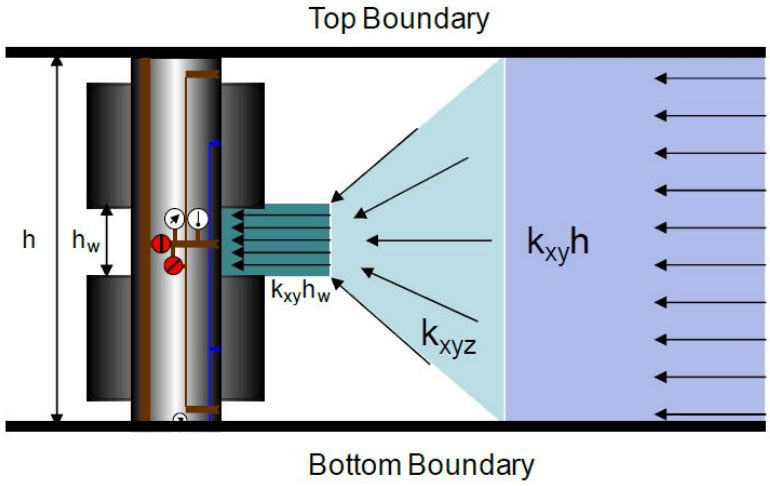


Fig. 34. Expected flow regimes. Reservoir thickness (h), perforated zone (h_w), radial flow ($k_{xy}h_w$), spherical flow (k_{xyz}), radial Flow ($k_{zy}h$)

The straddle packer configuration consists of two inflatable packers that are set in the borehole isolating the section of the formation to be tested. The distance between the packers is 3.28ft. The fluid inlet port is placed approximately 2.19ft from the bottom of the isolated section. The packer elements are inflated with filtered mud – the mud is filtered by drawing-in borehole mud through large area filters that are fitted in the six-tank carrier. The mud is filtered to prevent plugging of the sample lines within the tool. An observation probe is included above the SP to assess connectivity and estimate the vertical permeability between the straddle packer and the location of the probe. The observation probe is located 6.50ft above the center of the straddle packer. Both the straddle packer and the single probe modules have their own quartz pressure gauges and measure the pressure disturbance in the formation around the vicinity of their respective locations.

Mini-DST pressure data was imported into the analytical well test software "Interpret-2010" along with the fluid rate, fluid properties and reservoir/wellbore parameters to analyze the pressure transient data from the build-up tests.

A total of 163.61L of fluid was pumped using the large-volume pump (500cc/stroke) during the VIT operation. A flow rate of 11.6cc/s was obtained prior to the final shut-in. The maximum pressure drawdown at the SP probe during the final flow period was 82 psi. A total of 213L of fluid was pumped using the large-volume pump (500cc/stroke) during the Mini-DST operation. A flow rate of 11.6cc/s was obtained prior to the final shut-in. The maximum pressure drawdown at the SP during the final flow period was 507 psi.

During the pressure drawdown and build-up periods in the VIT at the SP interval, corresponding pressure disturbances were observed at the OP. This indicates that there is good vertical communication between the SP and the OP within the 6.5ft. However in the Mini-DST interval, the pre-tests at several locations with the observation probe were tight indicating no reservoir communication at the probe depths. Consequently, the OP was not used and only a Mini-DST was conducted.

For both the VIT and the Mini-DST a partially penetrating wellbore model in a homogeneous infinite acting reservoir was used. The VIT results indicate a horizontal permeability value of 4.16mD, a vertical permeability of 0.48mD, a radius of investigation of 74 ft and a model calculated initial pressure of 5312.47 psi. The results of the Mini-DST indicate a horizontal permeability value of 1.73, a vertical permeability of 0.41mD, a radius of investigation of 159.00ft and a model calculated initial pressure of 4860.35 psi.

TEST	h	$k_{xy}.h$	k_{xy}	k_z	r_{inv}	P*	P_{wf}	PI
	ft	mD.ft	mD	mD	Ft	psia	psia	B/D/psi
VIT	60	249.6	4.16	0.48	74	5312.47	5264.80	0.090
Mini-DST	30	52.02	1.73	0.41	159	4860.35	4349.82	0.012

Table 2. Summary of results for the vertical interference test and mini-drill stem tests. Horizontal permeability (***Kxy***), vertical permeability (***Kz***), radius of investigation (r_{inv}), average pressure (P*), and measured productivity index (PI)

Mechanical integrity and step rate injection testing

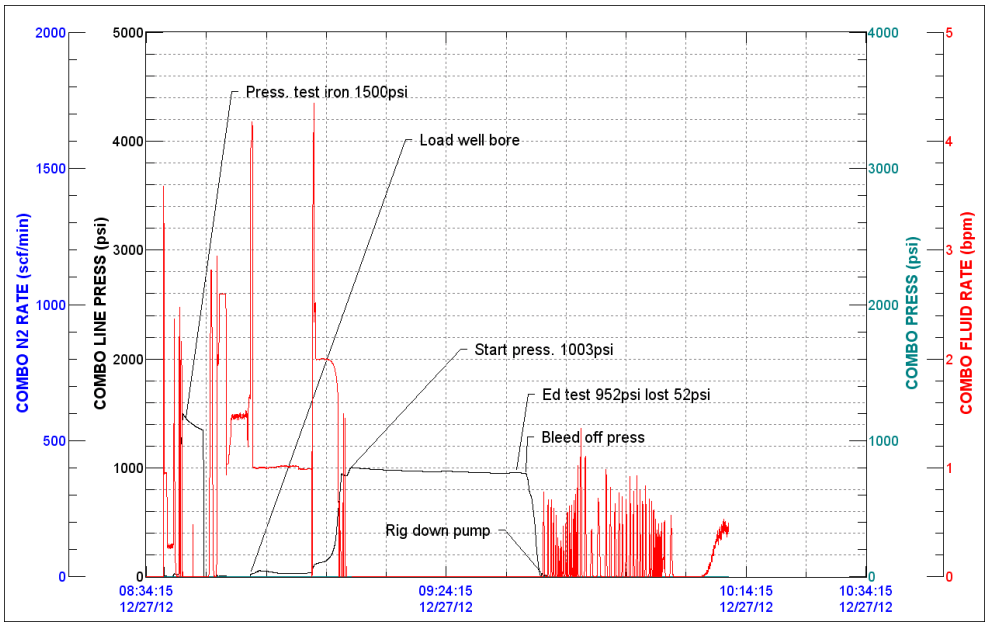


Fig. 35. Graphical results of the mechanical integrity test

Mechanical integrity of the well and cement bonding of the long string casing were determined as part of the mechanical integrity test. The mechanical integrity test had two goals. The first was to demonstrate the absence of leaks through the packer, tubing, casing and wellhead. The second goal of the mechanical integrity test is to demonstrate the absence of fluid movement behind the casing above the top most perforation.

Prior to injection the casing-tubing annulus of the well must best be tested to 0.25 psi/ft multiplied by the true vertical depth to the top of the packer and the inner casing. A successful test shows no more than 10% change after 30 minutes. During the first part of the mechanical integrity test in RSU #1, the wellhead was pressured to 1,003 psi. After 30 minutes the pressure dropped 52 psi. The results of this test are illustrated in **Fig. 35**. The success of the second goal of the mechanical integrity test is determined by a radioactive tracer test or a by using a temperature log after injection tests. Temperature logs were run in RSU #1 directly after performing the step rate injection test to ensure that there was no fluid movement behind the casing.

A step rate test is conducted by increasing the injection pressure in stages while measuring the intake rate of injected fluids. A sharp increase of intake can indicate formation fracturing. Step rate injection tests were attempted on each of the target formations; however, the test was unsuccessful in the Weber Sandstone due to pressure losses in the well bore. The results of the step rate test calculated a fracture pressure gradient of 0.84 psi/ft. The fracture pressure gradient was found to within the estimated range of the models and can be used to develop a safe CO2 injection strategy.

Rock/fluid samples

Core plugs and cuttings from RSU #1 were used for various analyses. Specific tests and samples are listed below. Results for all analyses, including sampled locations, are presented in the **Appendix**.

- Routine permeability and porosity evaluation
- Thin sections, stained for porosity, and often for calcite and ferroan carbonates
- Mercury capillary displacement pressure analysis
- X-ray diffraction analysis
- X-ray fluorescence analysis
- Absolute brine permeability analysis
- Triaxial shear analysis
- Brinell hardness testing
- Stable isotopic analysis of carbonates
- Total organic carbon, organic type characterization and source rock analysis
- IC-PMS

In addition to the analyzed core samples, drilling mud was collected on-site and analyzed to compare to water samples.

Formation Fluid Sampling

For this project the Wyoming Department of Environmental Quality (WDEQ) issued a Class I UIC permit (#12-257) for the University of Wyoming to operate well RSU #1 for the purpose of completing injectivity testing. In accordance with this permit the baseline water quality had to be characterized and classified prior to injection. The analytical work required for permitting is described in the Wyoming Water Quality Rules and Regulations (WQRR Chapter 8, Table 1).

Two sets of formation fluid samples were collected from the target reservoirs to provide the regulatory required baseline data to classify and characterize the groundwater within the reservoirs. In addition, these data were used to investigate brine evolution and the hydraulic confinement of the reservoirs. Geochemical analyses were then used in creation of a geochemical model to further predict fluid-rock interactions in the reservoir.Methods

Water samples were collected on August 27th, 2011 from the wellbore using the Baker Hughes Atlas RCI tool. The RCI tool maintained formation pressure of the samples. Samples were then transferred to two laboratories for analyses, Energy Labs in Casper, Wyoming and Core labs in Broussard, Louisiana. A second set of samples was collected in December 2012 using a bailer. Samples were collected for measurement of minor and major elements, radionuclides, organic acids, volatile organics, organic characteristics and flash gas compositions using the methods described by Brown et al. (1970). The results of these analyses are presented in the **Appendix**. Thermodynamic calculations from the pressurized samples were computed using Geochem Workbench (Bethke 1996).

Geophysical Characterization

Prestack waveform inversion (PWI): a wave equation was developed based on methodology for inverting prestack seismic data for subsurface elastic properties. The methodology is an improved version of the waveform inversion using genetic algorithm (GA) that was previously developed by Mallick (1995, 1999). In this new version, two levels of parallelization are implemented that leads to an extremely fast computation of the in a high-performance computing environment and is therefore applicable for inverting three dimensional (3-D) data volumes. The methodology starts with a random population of subsurface earth models specified within a given search window and uses the evolution theory to iteratively modify the models until the synthetic data predicted by the model matches with the observation within reasonably accepted limit as specified by the user.

Typically, amplitude-variation-with-offset/angle (AVO/AVA) is the state-of-the-art in the oil and gas industry for prestack inversion. Such an AVO/AVA method assumes that the reflection amplitudes on the recorded seismic data are proportional to plane P-wave reflection coefficients without any contamination from other wave modes. In the past, Mallick (2007) demonstrated that this inherent assumption of AVO/AVA is valid for small angles only and they fail to duplicate reality for large angles (typically more than 30°). While this demonstration used synthetic modeling studies, there was no direct comparison between PWI and AVO/AVA on real seismic data. Recently, Adhikari et al. (2013) and Pafeng et al. (2013) demonstrated the superiority of PWI over AVO/AVA on RSU seismic data and results of these works are shown below in **Fig. 36-38**.

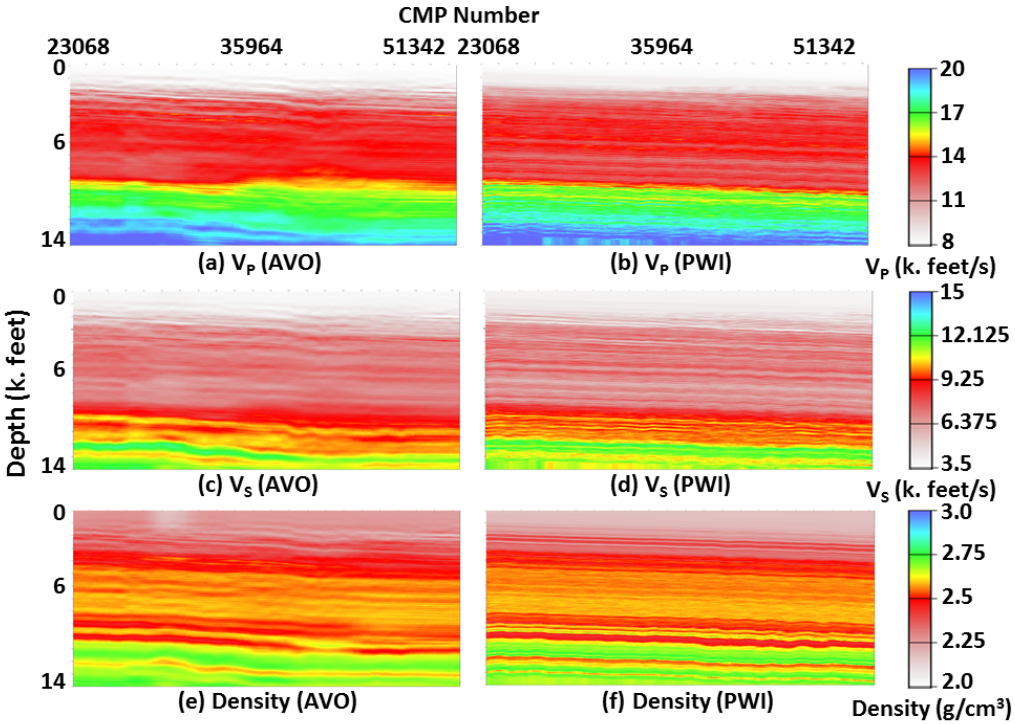


Fig. 36. Comparison between the AVO/AVA inversion and PWI on real seismic data from RSU. (a), (b) inverted P-wave velocity (V_P), (c), (d) inverted S-wave velocity (V_S) , and (e), (f) inverted density. The depths shown are with respect to the seismic datum (7,500ft).

Inverted V_P, V_S, and density, shown in **Fig. 36** by both inversions are similar, but PWI is clearly of much higher resolution than the AVO/AVA. In **Fig. 37**, the Poisson's ratio computed from the inverted V_P and V_S from both inversions are displayed. In addition, some major formation tops, interpreted from the RSU #1 data are also shown. The Poisson's ratio display with identified formation tops demonstrates the superiority of PWI over AVO/AVA

inversion. For example, the Baxter and Frontier formations are not clear on the AVO/AVA, but they are on the PWI. The Mowry formation is barely visible on the AVO/AVA, but it is clear on the PWI. Nugget, Dinwoody, Weber, and Madison formations are more consistent with the RSU geology on the PWI result than they are in the AVO/AVA. Additionally, many other formations such as the Phosphoria A and B in between the Weber and Madison, different formations in between Baxter and Frontier, and even above Baxter, etc., could be identified in the PWI, but not the in the AVO/AVA. The superiority of PWI is further verified in **Fig. 38** where the real RSU stacked data are compared with the synthetic stacked data computed using both AVO/AVA and PWI models. To compute the synthetic stacks shown in **Fig. 38(a) and (c),** prestack seismic gathers were first computed using the respective models for exactly the same range offsets as they are on the real data. These gathers were then corrected for the normal moveout (NMO) using their respective V_P models and stacked. Notice that the synthetic stacked data computed using the PWI model duplicated the real data almost exactly, but AVO/AVA did not except for the shallow part. In view of these results, we believe that the future for reservoir characterization and monitoring must be PWI, not AVO/AVA, which is the current state-of-the-art.

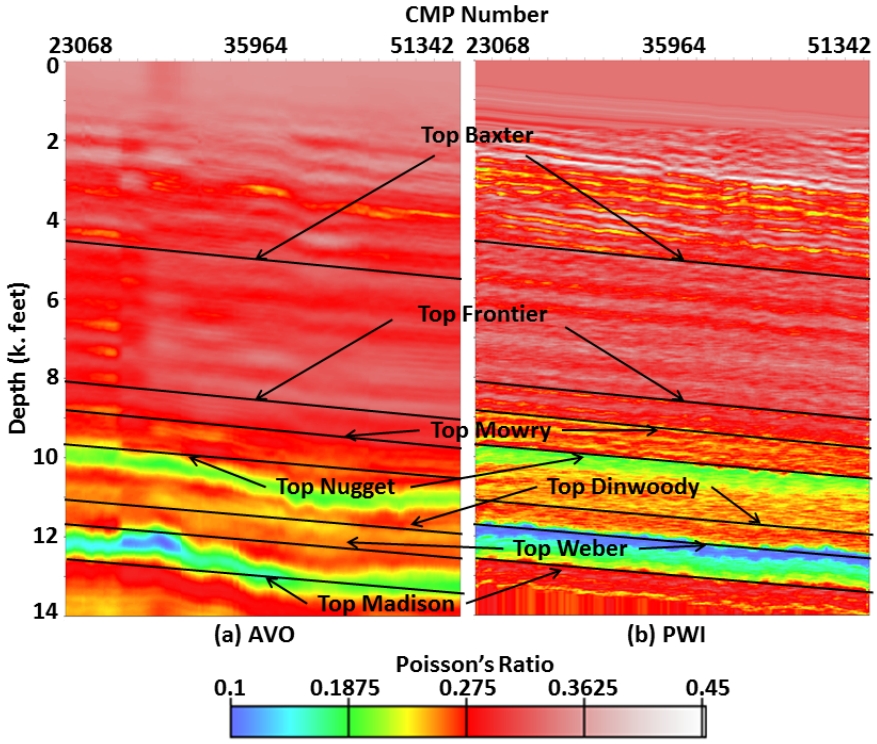


Fig. 37. Computed Poisson's ratio from (a) AVO inversion and (b) PWI. The depths are with respect to the seismic datum (7,500ft).

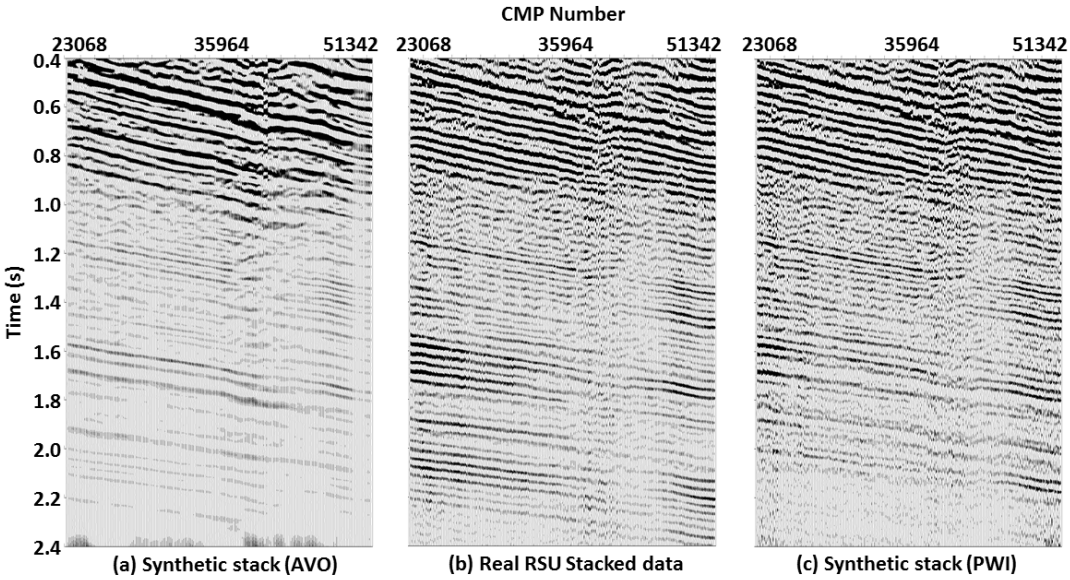


Fig. 38. (a) Synthetic stacked data computed using the AVO inverted model. (b) Real RSU stacked data. (c) Same as (a) but computed using the PWI model.

Note that the PWI and AVO/AVA examples shown above are for a single (vertical) component data only. While a multicomponent (3-D/3-C) seismic data at RSU was acquired, the horizontal components were not processed, as it was not originally included in the project. An anisotropic PWI method for multicomponent seismic data was developed under a separately funded DOE project. Such a multicomponent inversion requires optimization of multiple objectives, one for each data component. These multiple objectives are typically handled by defining a single objective given as a weighted sum of different objectives (Mallick, 2000; Chang and McMechan, 2009) and sometimes with additional regularization terms (Du and McGregor, 2010; Karaulis et al., 2012), which is then followed by a single objective method. Although such an approach gave good results on synthetic data (Mallick, 2000; Chang and McMechan, 2009); Padhi and Mallick (2013a, b) pointed out some fundamental drawbacks of such an approach. All multiobjective problems are nonlinear with nonunique solutions, known as the Pareto-optimal solutions, none of which could be considered better than the other (Deb et al., 2002). Defining multiple such objectives as a single one can provide only a single solution out of the entire Pareto-optimal set, which could be biased by the choice of the individual weights. The entire Pareto-set could be obtained by changing weights and inverting repeatedly, but it is too cumbersome and computationally inefficient (Padhi and Mallick, 2013b). A more efficient approach would be to treat the entire set of objectives as a vector and simultaneously invert them all. Padhi and Mallick (2013a, b) used such an approach using a fast-nondominated sorting genetic algorithm or NSGA-II (Deb et al., 2002) to successfully invert two component (primary or P-P and mode-converted or P-SV) synthetic seismic data for the simplest type of anisotropy known as the transverse isotropy with a vertical symmetry axis (VTI). Li and Mallick (2013) extended the work of Padhi and Mallick (2013a, b) further to invert 3C seismic data along two azimuths (i.e., for a total of six objectives) for more general forms of anisotropy such as transverse isotropy with a horizontal symmetry axis (HTI) and orthorhombic (ORT) media.

EM Inversion: Although seismic methods are commonly used in reservoir characterization, the sensitivity of seismic data to reservoir pore fluids is increasingly poor at deeper depths. Therefore, having access to another independent geophysical measurement in addition to seismic is helpful. Over the past years, electromagnetic (EM) data has drawn much attention to the oil and gas industry as one of the key tools for reservoir monitoring (Alumbaugh and Morrison, 1995; Constable and Cox, 1996). In view of this, EM data using both circular

electric dipole (CED) and horizontal electric dipole (HED) source has been acquired in the RSU area. Because the resolution of EM is much less than that of the seismic (Harris and MacGregor, 2006), EM data have been traditionally used in the past to derive low frequency models for velocities or impedances to be used as a low frequency trend for seismic inversion: EM data are first inverted for resistivity, then resistivity is inverted for velocity, and the so-obtained velocity model is then used as a prior model for seismic inversion. In spite of its low resolution, it must be noted that EM data are sensitive to the fluid effect in gas reservoirs. On the other side, seismic data depend on the elastic contrast at the interface between two different layers, where the elastic contrast depends on changes in porosity, lithology and fluid saturations.

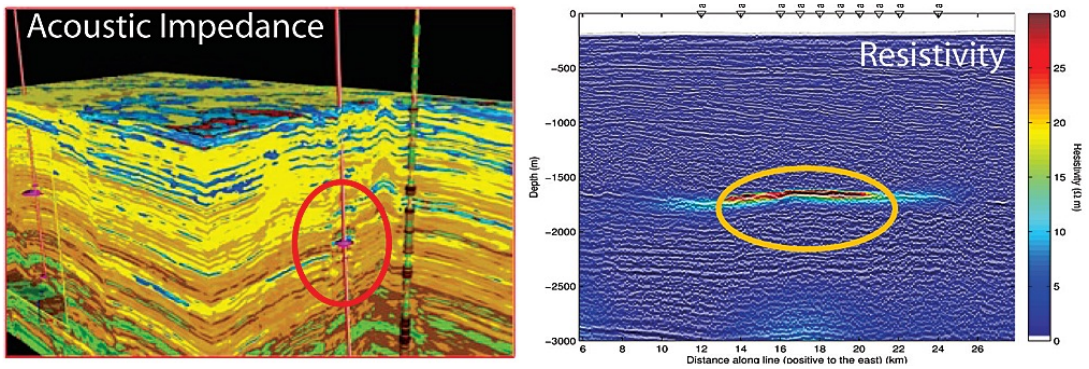


Fig. 39: Comparison between inverted seismic impedance and inverted EM resistivity (MacGregor, 2012).The reservoir interval is marked in both.

Even though the resolution of seismic data is higher than that of the EM, the fluid signature is generally hard to detect from seismic data, especially at deeper depths when the change in elastic response due to saturation changes is not large. This is demonstrated in **Fig. 39** where inverted seismic impedance is compared with the inverted resistivity. Note from **Fig. 39** that while the fluid signature in the acoustic impedance is subtle, it is much clear in the resistivity section. Thus, to overcome the dichotomy between high fluid sensitivity and low resolution of EM data and low fluid sensitivity and high resolution of the seismic, a joint inversion of both to derive seismic properties and resistivity and use them together for estimating rock properties and fluid saturation is desirable. Such a joint inversion could potentially provide a better constraint on the porosity and fluid saturation compared to using the seismic or the EM data alone. **Fig. 40** shows a preliminary study on combining EM with seismic data in predicting porosity and water saturation. In **Fig. 40**, Raymer function (Raymer et al., 1980) and Archie's law (Archie, 1942) was first used to calibrate and predict the V_P and resistivity form the porosity and water saturation over the reservoir interval. After successful calibration (**Fig. 40a-b**), the established relations were used in a least square inversion scheme to predict porosity and water saturation directly from V_P and resistivity (**Fig. 40c**).

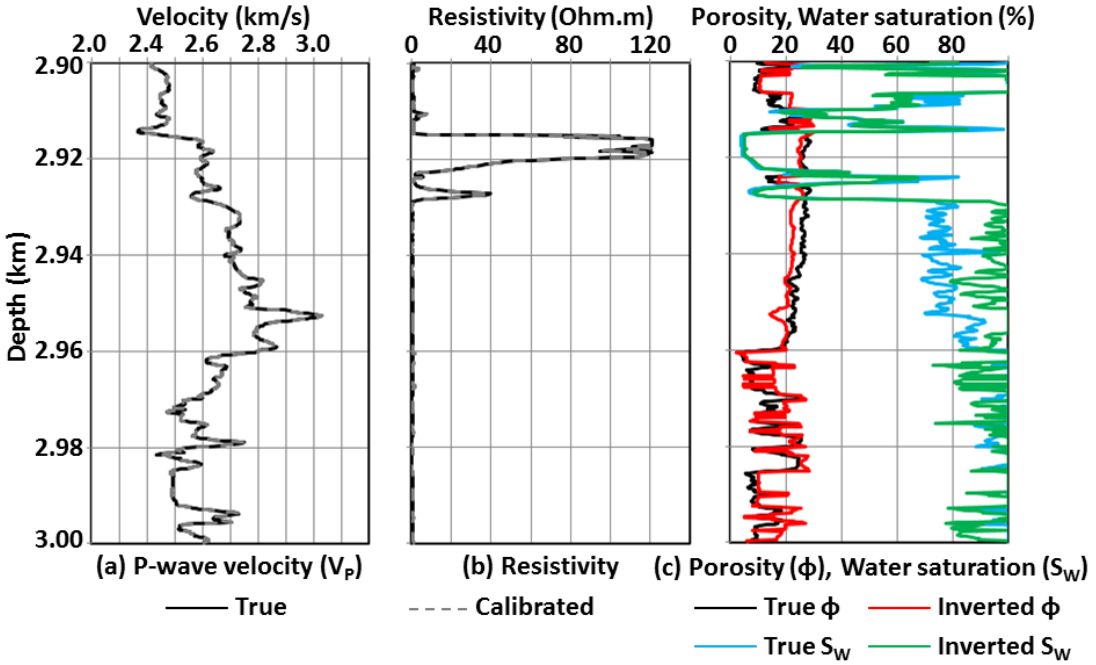


Fig. 40: Feasibility of combining seismic with EM in reservoir property prediction. (a)-(b) Measured and calibrated V_P and resistivity over the reservoir interval. (c) Inverted porosity and water saturation compared with their true values.

Although demonstrated using log data over the reservoir interval, it is obvious from **Fig. 40** that if sonic and resistivity logs are calibrated at well locations, velocities and resistivity from seismic and EM inversion could be used to predict porosity and water saturation over a 3-D volume. Similar to multicomponent seismic problems, such an inversion will also be nonlinear with non-unique solutions. However, to the multi-objective method developed by Padhi and Mallick (2013a, b) and Li and Mallick (2013), it is straightforward to add EM as an additional component. Although such a joint seismic and EM inversion was an objective of the original project, here we were only able to demonstrate the feasibility of such an inversion.

By developing a wave equation based PWI methodology and applying it on the RSU seismic data, not only has it been demonstrated as a difference over a traditional AVO/AVA inversion, currently used in practice, but were also successful in obtaining a detailed subsurface elastic earth model for the RSU area. If RSU is used for future CO_2 sequestration experiments, this elastic model would be vital to the reservoir fluid flow and geomechanical analysis. Another point to be noted about PWI is unlike AVO/AVA, which requires low-frequency background model from other sources such as well-logs and local/regional geology to be supplied to inversion, PWI extracts a broad-band model and does not require the low-frequency trend (Mallick, 1999). Strong dependence on the low-frequency background trend is the primary reason to force repeatability between time-lapse seismic surveys using different cross-equalization methods (Rickett and Lumley, 2001; Atmutlaq and Margrave, 2013). However, if PWI is used instead of AVO/AVA for time-lapse studies, the requirement of repeatability between surveys could be potentially eliminated, which will make the time-lapse analysis a real powerful tool. Additionally, by developing a multi-objective inversion methodology, we have introduced a new method of combining different data into a single inversion such that seismic could be easily inverted jointly with EM and possibly other types of data. This capability is also vital to the future of subsurface characterization and time-lapse monitoring.

Acquire a 3-D seismic survey

The Jim Bridger 3-D and 3-C is a wide-azimuth seismic data set acquired in Sweetwater County, southwestern Wyoming, using vibroseis as a source and three-component digital sensors covering an area of about 25 mi^2. The survey was designed as a baseline study for possible CO_2 injection and was acquired by Geokinetics Service Co., Houston, Texas, during November 2010. The cross-spread shooting method used for data acquisition implies multiple perpendicular source and receiver lines (**Fig. 41**).

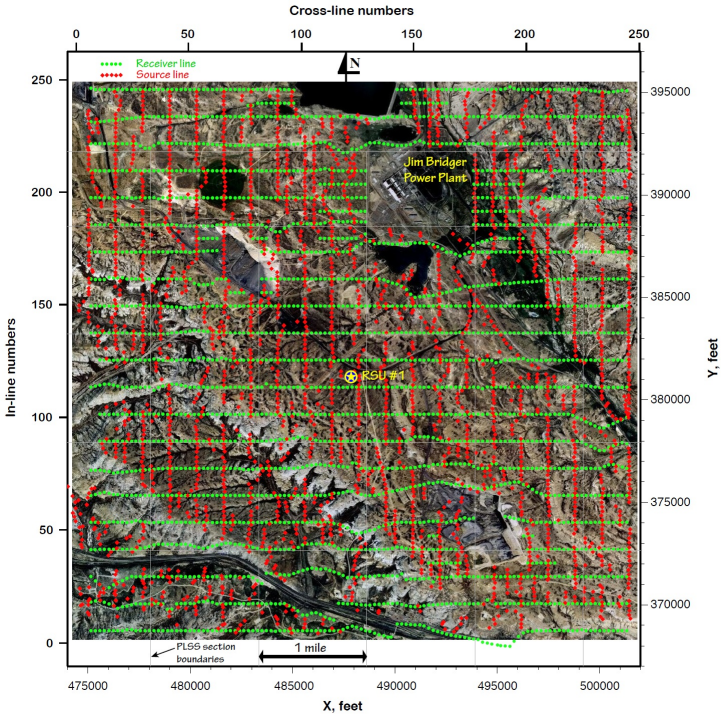


Fig. 41. Jim Bridger 3-D seismic survey. Source (shotpoint) and receiver layout overlying infrared satellite image

The CMP bin, 110ft in both the X and Y directions, is less than one-quarter the minimum wavelength (λ_{min} = 500ft) and ensures that the data is not spatially biased. The final CMP fold map, **Fig. 42a**, shows a maximum fold of 48× at the center of the survey. The middle part of the survey area is characterized by a maximum offset (source-to-farthest-receiver distance) of 19,800ft, which is adequate for imaging geologic targets in 10,000ft–15,000ft depth range. CMP fold coverage and source-to-receiver offset distributions are the most important survey design parameters that affect reflected signal strength and allow lithology/fluid predictions to be made. A rectangular area (3×3 mi) centered on RSU #1 is shown in **Fig. 42b**. This area is characterized by the maximum and most uniform CMP-fold and maximum-offset distributions, enabling the most favorable conditions for seismic imaging of the subsurface geology. The work presented here will concern only compressional (P-wave) data recorded on the vertical component. **Table 3** summarizes the survey design details.

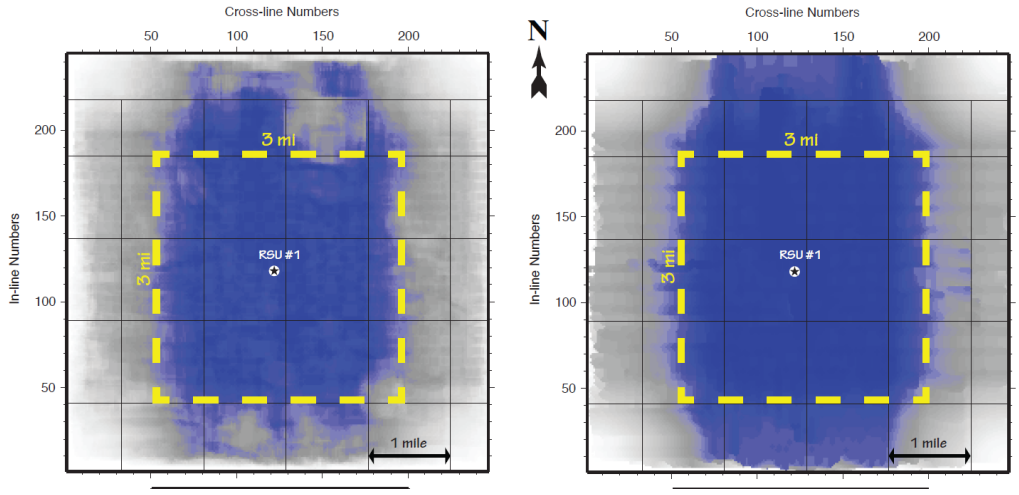


Fig. 42. Jim Bridger 3-D seismic survey. (**a**) CMP fold coverage map and (**b**) maximum source-receiver offset map. The dashed rectangle (3×3 mi) centered around the RSU #1 well, outlines seismic image area where the data is most reliable

Record length; Sample rate	6s, 2ms
Geophone type	SVSM 3-component digital sensor
Total geophone stations	2,514
Total source points	2,541
Number of live receiver lines	18 (144 live stations per line)
Receiver group and source interval	220ft
Receiver and source line spacing	1,320ft
Maximum source to receiver offset	19,800ft
Survey size	25.16 mi^2
Source type	I/O AVH IV Vibroseis, 4 over flag
Sweep parameters	Linear 6Hz–110Hz
Sweep tapers	Linear 300ms–300ms

Table 3. Survey acquisition details

Importance of custom processing

An orthogonal shooting scheme used by Geokinetics tends to create a non-uniform distribution of offsets, a pattern that is not related to geologic variations and may "leak" into the data, creating an artificial *acquisition footprint*. Regularly oriented gaps in the source and receiver lines due to surface conditions (power plant, ponds, cliffs, roads) (**Fig. 41**) may also introduce acquisition artifacts into the data. Geokinetics did the basic preprocessing of the reflection seismic data that was aimed on data conditioning for velocity analyses and reliable stacked volume generation. The quality of the resultant pre-stack time-migrated (PSTM) amplitude volume is illustrated in **Fig. 43**. Strong and coherent reflections in the time range 1.4s to 2.2s correspond to geologic interfaces in the depth range approximately from 7,000ft to 13,000ft below the ground surface at the RSU #1 location. This means that the structure of the targeted reservoir and sealing stratigraphic units can be imaged with the reflected P-waves. However, an isochrone slice at 2.08s two-way travel time (horizontal section, **Fig. 43**) clearly demonstrates the acquisition footprint (grid of east-west and north-south stripes) present in the stacked amplitude volume. As is seen in **Fig. 43**, the acquisition footprint intensifies northeast from the test well, in the areas with the largest gaps in the shooting scheme (**Fig. 41**). The seismic data quality deteriorates in the areas corresponding to rough topography and the power plant facilities. The removal routine of the Geokinetics processing flow didn't remove the footprint completely, thus leaving a potential problem for the subsequent data interpretation.

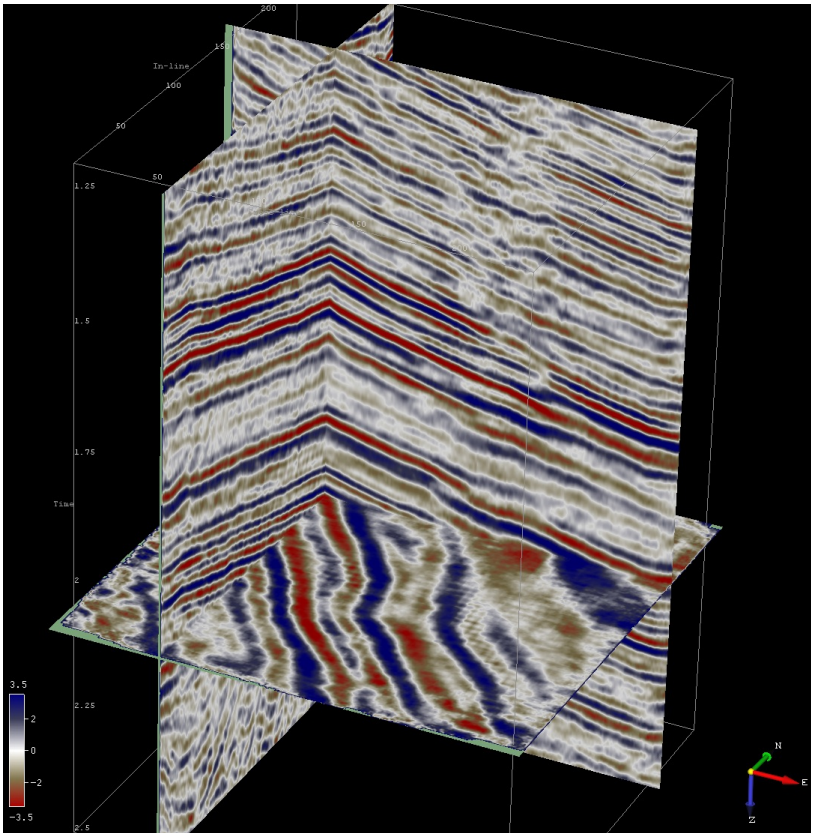


Fig. 43. 3-D seismic amplitude volume displayed in three orthogonal slices. Note an overall northeast dip of reflectors and acquisition footprint pattern in the time slice (regular grid of stripes trending south-north and east-west). Approximate location of RSU #1 is shown on the time slice is shown

Considering the importance of seismic attribute analysis for characterization of reservoir and seal properties, it was decided to re-process seismic data at Echo Geophysical Corporation, Denver, Colorado. The purpose of custom processing was twofold, (1) pre-stack data interpolation and re-binning to minimize gaps and acquisition footprint and (2) broadening frequency bandwidth to enhance vertical resolution.

Another aspect of custom seismic data processing for WY-CUSP is related to the importance of porosity/permeability estimation away from RSU #1. With extremely sparse well control within the study area, seismic data appears to be the major source of rock physics information necessary for geological modeling. Hence, it implies additional requirements to the data quality used for indirect porosity/permeability estimation, and first of all, to seismic P-wave velocities. An automatic velocity analyses routine, specially designed at CMI, was applied at each common-depth-point (CDP) location and resulted in a high-density interval-velocity volume. This velocity volume served as the basis for 3-D geologic modeling, reservoir flow simulation, and time-to-depth conversion.

Seismic attribute analysis

The specific objective was to apply selected seismic attributes to aid in quantifying the reservoir properties and lateral continuity of CO_2 sequestration targets. More than a dozen seismic attributes were systematically tested and found that curvature, interval velocity, acoustic impedance, iso-frequency amplitude, and mean frequency were particularly useful in mapping structural trends, performing seismic facies analysis, and imaging porosity distributions within the target horizons. Locating impermeable barriers to flow as well as assessing the integrity of confining layers was also within the scope of the research. The attempt to not overwhelm the study was made by calculating seismic attributes that lack geologic significance or have no clear physical meaning. Thus, the foremost criterion for selecting attributes was a physical basis of correlation between properties measured in the well bore and the core. For example, interval velocity has a physical correlation with porosity: as velocity increases, porosity typically decreases. Therefore, the scope of this study comprised only the few attributes discussed below. Another reason in a more detailed description of the following attributes, is that they were designed at CMI specifically for the needs of WY-CUSP.

Mean Frequency The mean frequency, actually the weighted mean frequency, is derived from a spectrally decomposed seismic trace (generated through a Fourier Transform in this study). The weighted mean is similar to the arithmetic mean, and is used in situations where instead of each sample frequency contributing equally to the final average, some frequencies contribute more than others. The degree of contribution (weight) is defined by the spectral amplitude value. In the digital signal processing literature the weighted mean frequency is often termed the spectral centroid frequency (or simply the centroid frequency) because it indicates the location of the "center of mass" of the spectrum. Formally, the weighted mean frequency F of a set of frequencies $\{f_1, f_2, \ldots, f_n\}$ with weights $\{a_1, a_2, \ldots, a_n\}$ is the quantity

$$F = \frac{\sum_1^n a_i f_i}{\sum_1^n a_i}. \qquad \textbf{(Eq. 1)}$$

Spectral Decomposition The spectral decomposition algorithm, used in this study for several attribute computations, is based on a Short Time Fourier Transform (STFT). The general Fourier Transform relates a waveform (a function of time) to its spectrum (a function of frequency). If the time band of the waveform is multiplied by a constant, then the bandwidth of the spectrum is divided by the same constant. This property is an expression of the Heisenberg uncertainty principle with respect to seismic processing. Simply speaking, if one wants to gain better resolution in time, he must pay for it with resolution reduction in the frequency domain. The spectral decomposition software used in this study implements STFT by choosing frequency-domain windows as opposed to time-domain windows. STFT can be seen as the filtering of a signal through a set of fixed bandwidth band-pass filters whose center frequencies are distributed uniformly along the frequency axis. To bypass the Heisenberg uncertainty principle, we implemented a sort of multi-resolution STFT by

combining (or averaging) individual spectrograms with different time-frequency resolutions. The *spectral amplitude attribute* that is often referred to in this study is the iso-frequency magnitude resulting from spectral decomposition. This attribute is always computed normalized to the maximum magnitude value.

Velocity Attribute The velocity attribute was derived from stacking-velocity analysis applied to prestack CMP gathers. High-density, high-resolution interval velocity volume was calculated using an automated routine that performed velocity analysis at every time sample and at every CMP location. For the homogeneous earth with planar interface, the travel-time curve of the reflections for various offsets between source and receiver is conventionally calculated using:

$$t^2 = t_0^2 + \frac{x^2}{v_{stack}^2}. \qquad \textbf{(Eq. 2)}$$

At every CMP gather (with source-receiver offsets x) and every time sample t_0, a velocity spectrum is calculated for a set of trial stacking velocities v_{stack} using semblance as a coherency measure. The semblance value reflects how well the model path corresponding to the trial velocity v_{stack} fits the actual trajectory of reflected signals in the data. The semblance *S*, as defined by Neidell and Taner (1971), is given by the equation:

$$S = \frac{\sum[\sum a(t,x)]^2}{N \sum\sum a(t,x)^2}. \qquad \textbf{(Eq. 3)}$$

The inner sums in this equation are over N traces having various offsets x, while the outer sums correspond to time smoothing with the operator centered at time index t. Semblance is maximized when the values $a(t,x)$ do not vary with index x. Time smoothing is necessary to increase semblance stability for coherent events located close to zero-crossings. Within the computer code, the velocity spectrum is estimated with relatively few trial velocities (25 in this study) and is fitted to a Gaussian curve,

$$f(x) = b + pe^{(-0.5(x-c)/w)^2}, \qquad \textbf{(Eq. 4)}$$

where $b, p, c,$ and w represent the *base* (semblance shift), *peak* (peak semblance value), *central point* (central or mean velocity value), and *width* (velocity standard deviation) of the Gaussian distribution, respectively. A velocity distribution fitted with the Gaussian formula enables precise and unambiguous estimation of the peak semblance value and the corresponding stacking velocity. When computation over the trace samples (t_{0i}) is complete, the resultant stacking velocity function is smoothed with an operator whose size is proportional to the time t_0 and velocity standard deviation (parameter w in the Gaussian curve equation) at that time. The smoothed stacking velocity function is further processed using Dix's formula (1955) to produce interval velocities that can be readily interpreted in terms of lithology, pore-fluid or porosity variations.

Acoustic Impedance (AI) Acoustic impedance (the product of the rock density and velocity) is a basic physical property of rocks that is commonly calculated from corresponding density and sonic well logs. AI has the benefit over seismic reflectivity data in that it is a layer property that can be directly related to lithology and to changes due to fluid production/injection. A problem arises when the well-log data is not adequate to image the targeted subsurface. Additionally, reservoir heterogeneity may require more control than from existing well locations alone: in this case (including this study), an acoustic impedance volume can be created through inversion of the P-wave seismic volume. The inversion scheme followed an approach known as *synthetic sonic log* section (volume) generation, described first by Lindseth (1979). In outline, the inversion operations included (1) computation of an approximate reflection coefficient sequence using post-stack seismic amplitude volume, (2) inversion of the reflection coefficients to band-limited, high-frequency velocity coefficients, and (3) use of (2) to modulate low-frequency velocity components, obtained from high-density reflection velocity analysis, to produce synthetic sonic logs. If the subsurface density distribution is known (or estimated), it can be incorporated in this scheme to produce synthetic acoustic impedance logs. In this study, the accuracy of the inverted synthetic volumes was verified by comparing them with the corresponding logs from RSU #1. The P-wave *synthetic sonic log attribute* obtained in this study combines the features of stacked amplitude and interval velocity volumes. Namely, it derives its volumetric property (rather than an interface property) from the interval velocity field, and it derives better resolution from the amplitude volume. Inverted data, a layer property, is a more intuitive tool that allows one to tie lithology and fluid presence to seismic data.

Seismic Coherency Seismic coherency is a measure of the consistency of seismic reflections. In other words, it quantifies the similarity in appearance and shape of seismic waveforms from trace to trace. Where events are similar, coherency is high. Low-coherent, discontinuous reflections may be caused by variation in structure, stratigraphy, lithology, porosity, and pore fluids. The semblance-based coherence attribute estimation in this study was performed on post-stack amplitude data. The basic algorithm of coherency estimation can be summarized as follows: for each point in a 3-D seismic volume, compare the waveform of adjacent traces over a short vertical window. At the same time, uniformly tilted strata should not affect the coherency computation. This was accomplished in the following steps. First, for each volume sample, a small reflection surface (3×3 horizontal samples) is identified around the central sample. The surface coordinates at trace intersections are calculated by finding the maximum cross-correlation value over a vertical analysis window between the central trace and each surrounding trace. A parabolic fitting technique is used for precise time shift (tilt) identification that corresponds to the maximum value of the cross-correlation between the discrete trace samples. The inter-trace tilt effect is removed and the semblance value is calculated using **Eq. 3** for the spline-interpolated trace samples. For the coherence attribute calculation, the inner sums in the semblance equation (**Eq. 3**) are over N tilt-corrected traces x, while the outer sums correspond to time smoothing with the operator centered at time index t. As with semblance-based velocity analysis, time smoothing is necessary to increase semblance stability for coherent events located close to zero-crossings.

Curvature Attribute In a general sense the seismic curvature attribute is a measure of how deformed a reflecting surface is at a particular location. The more deformed the surface, the larger its curvature. With respect to geometry, curvature is defined as the reciprocal of the radius of curvature, and correspondingly, belongs to the geometrical category of attributes. The suite of curvature attributes utilized in this study, comprises dip magnitude, dip azimuth, maximum and minimum, and strike and dip curvatures. Analysis of these attributes can help remove the effects of regional dip and emphasizes small-scale features such as tight folds, faults, karst, and fractures.

The estimation of volumetric curvature attributes is performed in three stages. First, for each volume sample, a small reflection surface (3×3 horizontal samples) is identified around the central sample. The surface Z-positions are calculated by finding the maximum cross-correlation value over a vertical analysis window between the central trace and each surrounding trace. A parabolic fitting technique is used for precise time shift (tilt) identification that corresponds to the maximum value of the cross-correlation between the discrete trace samples. Next, a least-squares quadratic surface $Z(X, Y)$ is fitted to the data within the analysis range. Finally, the set of curvature attributes is computed from the coefficients of the quadratic surface using traditional differential geometry (Roberts 2001). At any point of the surface, the curvature (positive or negative) can be measured at any azimuth. One of these azimuths will yield the largest curvature. This curvature is named the *maximum curvature* and the curvature at the orthogonal azimuth is named the *minimum curvature*. The *maximum* and *minimum curvature* attributes are very effective at delimiting faults and fault geometries, with maximum curvature corresponding to the up-thrown (positive) side of a fault. The curvature attribute extracted in the direction of maximum dip is named the *dip curvature*, while the one extracted in the orthogonal direction (along strike) gives us the *strike curvature*. The last two attributes can be especially useful in examining the local surface morphology and interconnectivity that can help explain buoyancy-driven processes and fluid migration pathways. The curvature attributes described above are lateral second-order derivatives of structural relief components of the seismic time- (or depth)-of-reflection events. This is what makes them so sensitive to subtle structural variations. In contrast, the *dip magnitude* and *dip azimuth* are derived using first-order derivatives, which allows using them as regional structural trend indicators.

Permeability Attribute Permeability and porosity are key parameters in reservoir flow simulation. When an impedance-porosity transform is available, as for the Weber Sandstone and Madison Limestone units, porosity can be inferred from acoustic impedance. However, the permeability that necessarily has to be supplied in reservoir modeling seems to be the most elusive of reservoir properties and remains extremely uncertain. In this study, a spectral decomposition technique was used to derive a relative qualitative attribute from seismic data. Based on theoretical predictions for vuggy, dual-porosity carbonate rocks, the normal-incident P-wave reflection should produce low-frequency amplitude resonance for highly permeable reservoir rocks. Correspondingly, a permeability attribute was designed that is proportional to the difference between the low-frequency spectral amplitude component along the middle Madison reflection horizon and the high-frequency component, and is scaled by the sum of the two components. The resultant permeability attribute maps reveal an extended area of increased permeability south and southwest of the RSU #1 well (**Fig. 44).**

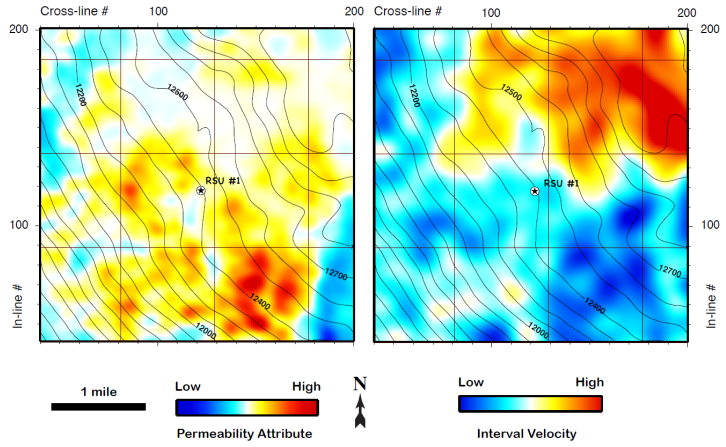


Fig. 44. Color-coded permeability attribute (left panel) and interval velocity (right panel) maps calculated on top of the Middle Madison horizon. Note that high-permeability area southeast from RSU #1 correlates with low-velocity zone. Labeled structure contour lines represent depth (feet) below KB at the RSU #1

Based on Core observations, petrography, rock/fluid compositions, and structural framework (burial/thermal history), interpret the diagenetic history, particularly those aspects that affect reservoir/seal performance.

Detailed geological analysis

Porosity types and evolution

As described earlier, porosity was macroscopically observed in portions of the cored intervals of the Weber and Madison formations. Thin sections were recovered from porous zones and impregnated with blue epoxy for porosity evaluation. Porous zones were generally limited to two lithofacies; eolian sands and massive homogenous sands (interdune). Petrographic porosity was analyzed using Leica's Axiovision 4.8 software, and was shown to vary from 0% and 17% (**Fig. 45**). In eolian sands, porosity distribution is heterogeneous; zones of high porosity are typically found within the largest grains (**Fig. 46**). Within interdune sands, porosity distribution is more homogenous (**Fig. 47**). Most Weber porosity is primary, though minor secondary dissolution was responsible for some post-burial porosity enhancement through mineral dissolution (**Fig. 48**). Porosity in the Weber is generally lower than primary depositional porosity due to pressure solution and cementation (**Fig. 49**). Quartz overgrowths and cementation have had the largest negative impact on porosity in the Weber, and in some places have completely replaced pore space.

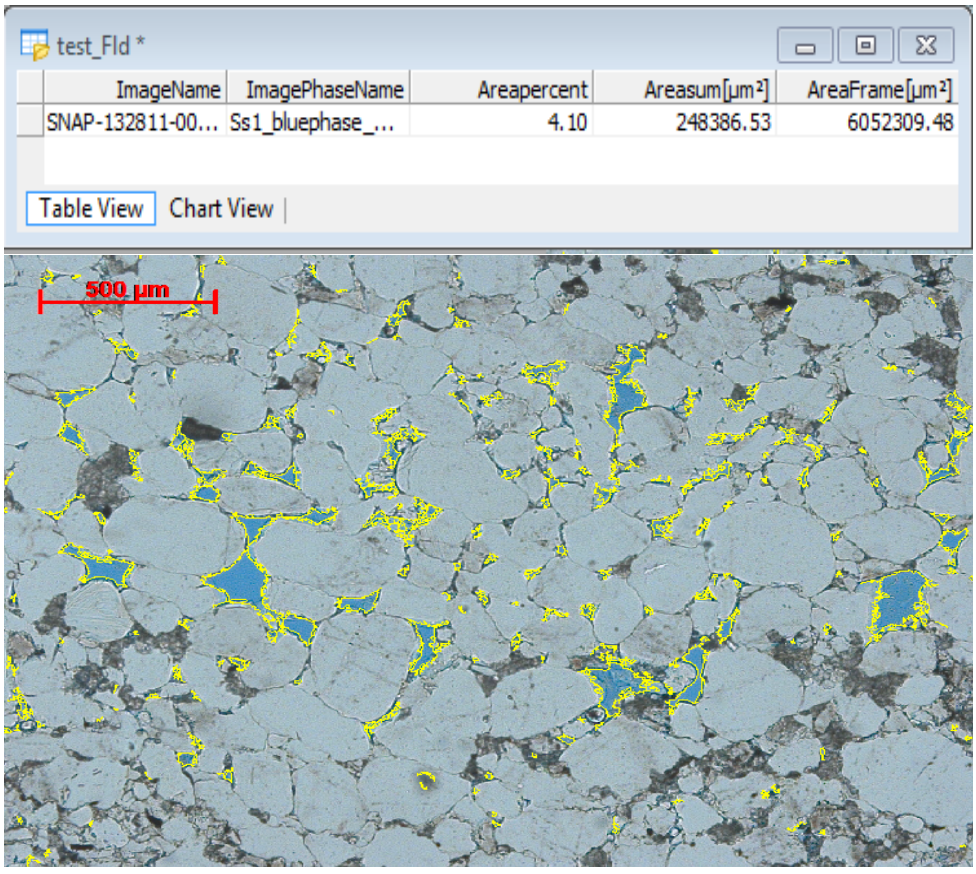


Fig. 45. Example of petrographic porosity analyses on eolian Weber sands. Note bimodal grains and their influence on porosity (in blue, highlighted yellow by software).

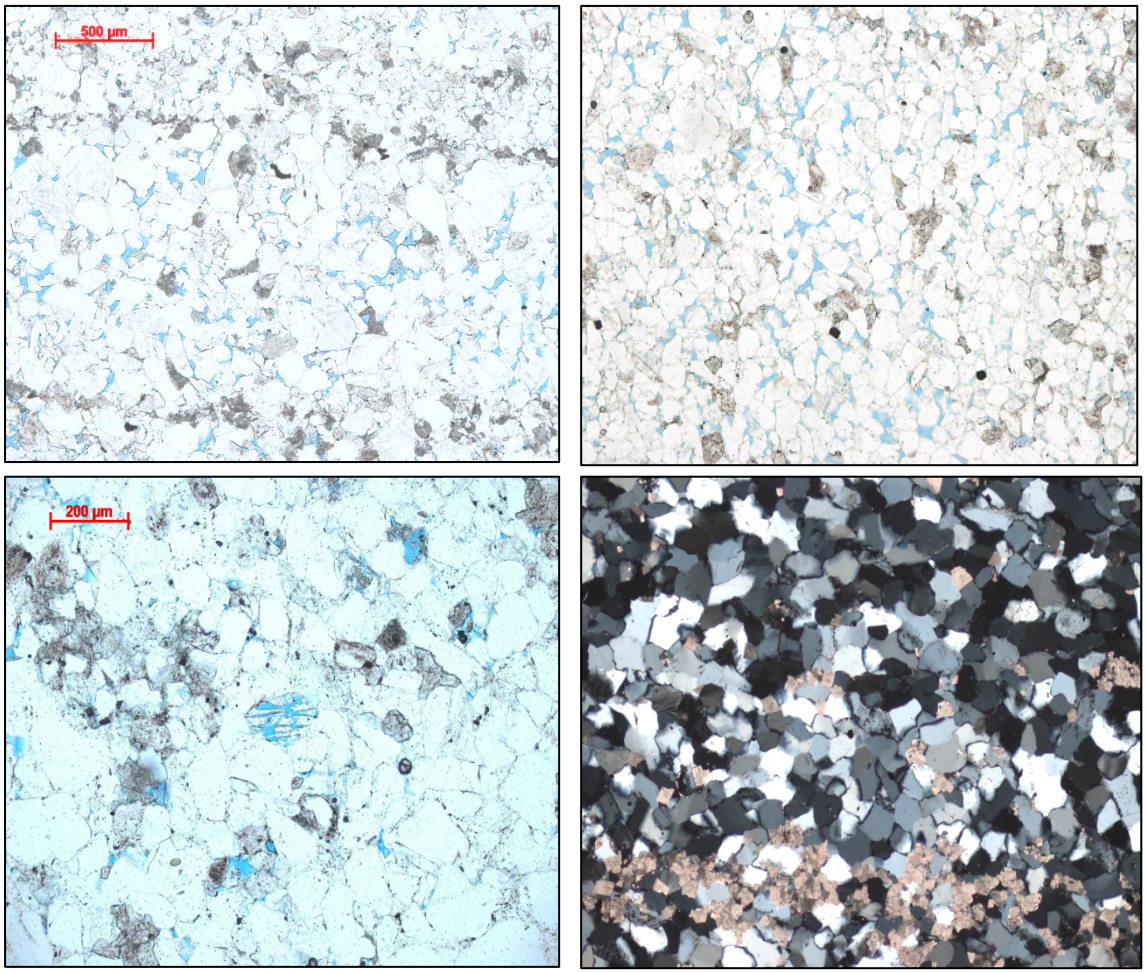


Fig. 46-49. Clockwise from top left: **Fig. 46**, eolian sands. Note largest pore space associated with biggest grains; **Fig. 47**, massive, interdune sands with well-spaced porosity; **Fig. 48**, dissolving feldspar, center, has enhanced secondary porosity; **Fig. 49**, pressure solution of quartz grains has overgrown or infiltrated primary porosity. Note carbonate cement at the bottom of the slide.

Two types were identified in Madison dolostones; intergranular porosity is identified in biolithites and moldic/vuggy porosity is associated with biomicrites. Petrographic porosity of intergranular zones is uniform, with the exception of small zones of anhydrite cement, and averaged 12% (**Fig. 50**). The porosity of moldic/vuggy zones was highly irregular, and varied from <1% to over >50% petrographic porosity (**Fig. 51**). The pore space of moldic/vuggy porosity zones commonly contains secondary minerals (quartz, anhydrite, and calcite) that decrease the overall porosity (**Fig. 51**). Two processes were identified that created pore space in Madison dolostones.

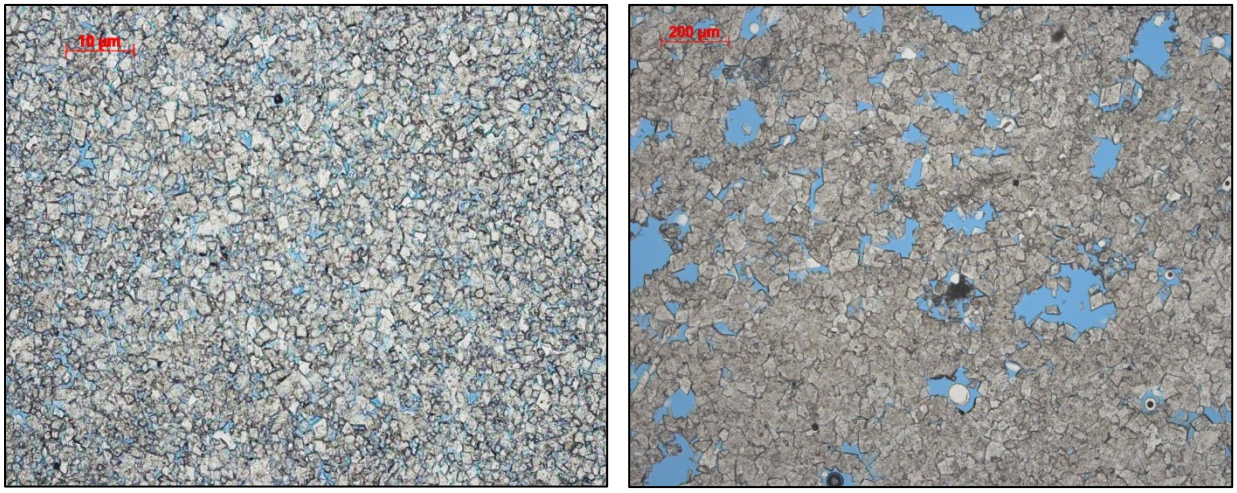


Fig. 50-51. **Fig. 50**. (on left) identifies intergranular porosity zone; **Fig 51**. (on right) identifies moldic/vuggy porosity zone

Stable isotopic compositions of Madison dolostones indicate dolomitization occurred in near-surface, hypersaline evaporative fluids (**Fig. 52**). Therefore, intergranular porosity formed at or near surface and has been retained. The dolostone matrix of moldic/vuggy porosity zones also formed at the onset of burial history, enveloping calcitic shells, organic matter, and anhydrite crystals. These later dissolved post-burial.

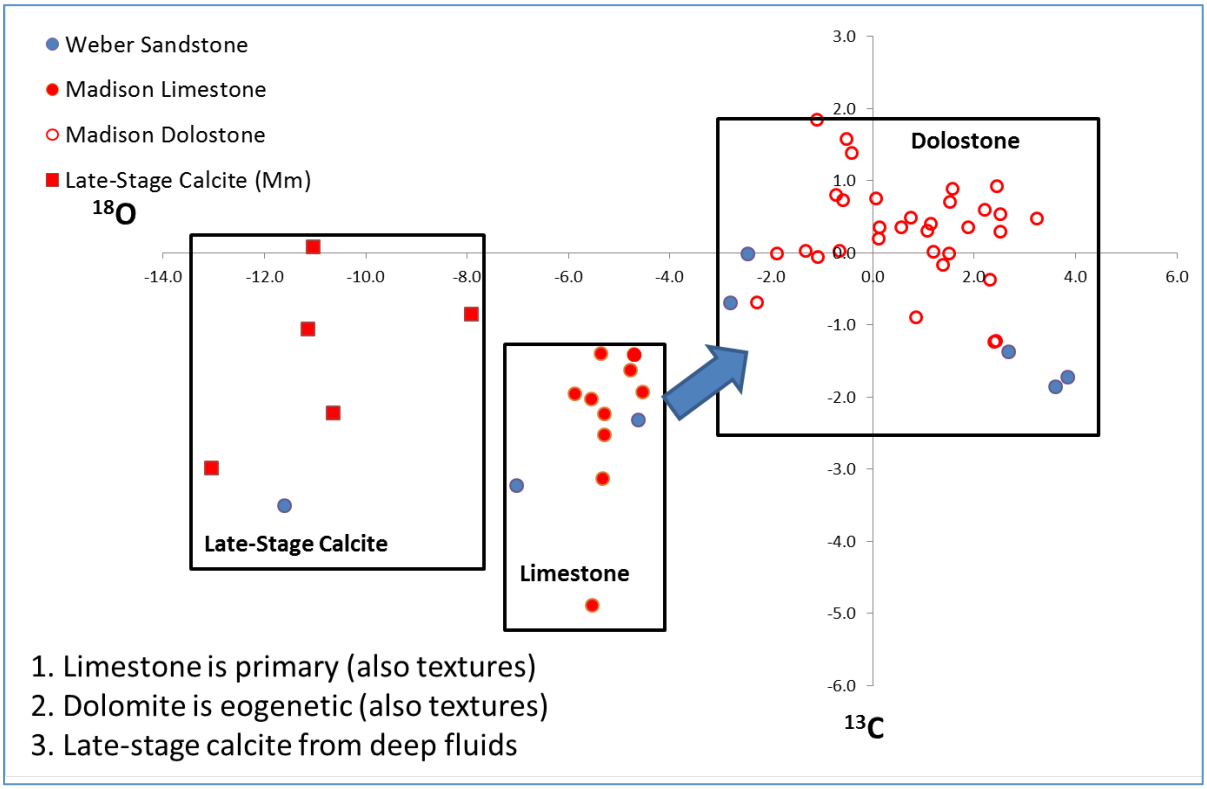


Fig. 52: Stable isotopic analysis of Madison and Weber carbonates. The enrichment between limestone and dolostone (highlighted by blue arrow) indicates dolomitization under hypersaline fluid conditions. This is also noted in several Weber samples. Late-stage calcite as veins and fracture fill indicates higher temperature, deep burial fluid conditions.

Porosity and permeability of core samples were measured by Intertek Laboratories in Houston, Texas (**Appendix)**. Intervals in both formations were shown to have storage space greater than 5% in the best zones, and a high degree of porosity/permeability heterogeneity (**Appendix**). The Madison was identified as having the best porosity and permeability (**Fig. 53**). Permeability varied by porosity type (**Fig. 53**). Dolostone with intergranular porosity has measured permeability that ranges from 0.001 mD to 82.6 mD (12 samples). Total measured porosity in intergranular zones ranges from 0.3% to 22.4%. The measured permeability in moldic/vuggy zones ranges from 0.001 mD to 2,245 mD and averages 75.7 mD. The maximum value, 2,245 mD, is potentially an outlier: removing that datum results in a range from 0.001 mD to 176.0 mD and an average of 22.7 mD. Porosity in the moldic/vuggy zones ranges from 0.3% to 19.8% and averages 13.1%. Pore size within vuggy/moldic zones is variable, and pores as large as 2,500 µm are observed (**Fig. 54**).

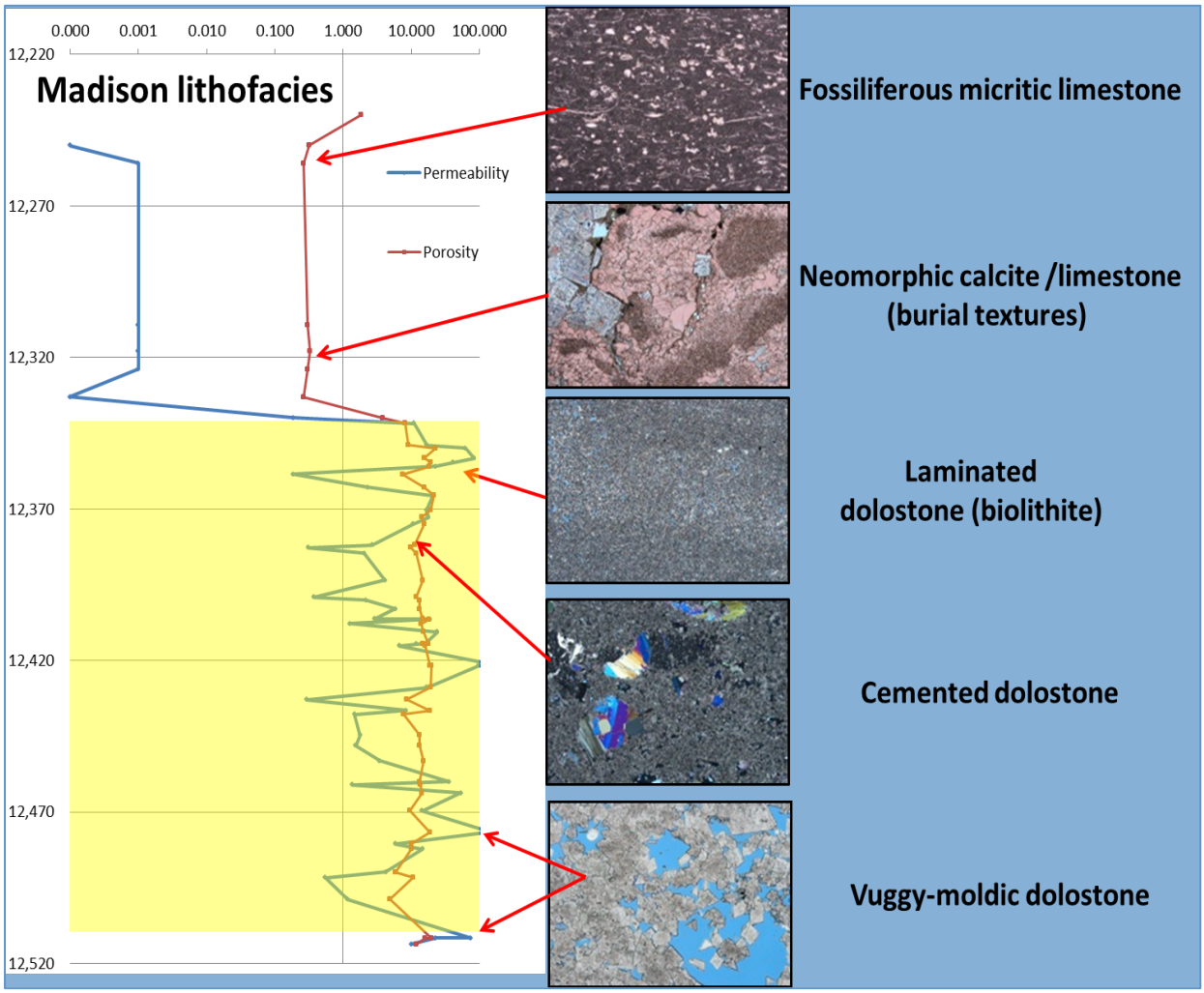


Fig. 53. Measured permeability and porosity of the Madison with associated lithofacies. Potential reservoir zone highlighted in yellow.

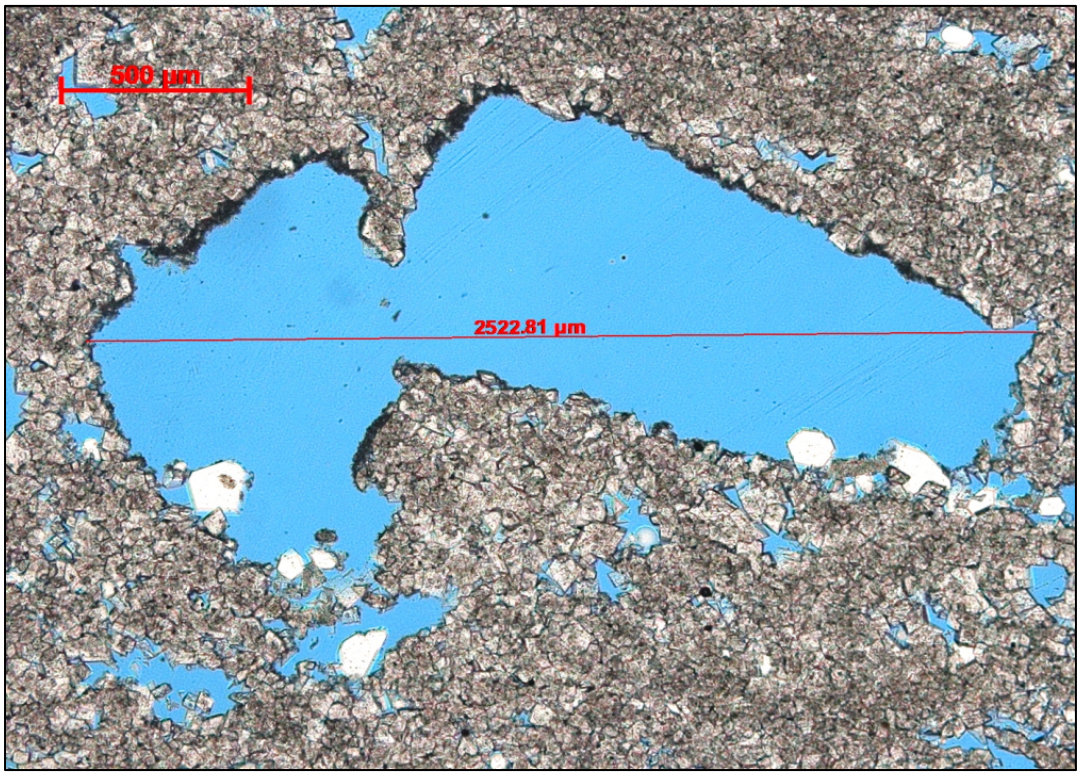


Fig. 54. Massive dissolution pore in Madison dolostone.

The highest permeability in the Weber is measured in the eolian facies (**Fig. 55**). The measured permeability through this section ranges from 0.001 mD to 13.8 mD and averages 2.7 mD (30 samples). The porosity ranges from 1.7% to 8.8% and averages 6.3% (30 samples). Pore size within the Weber is mostly uniform, though dissolution of reactive minerals has resulted in anomalously large pores (> 400 µ). Drill stem tests, described earlier, identified vertical anisotropy.

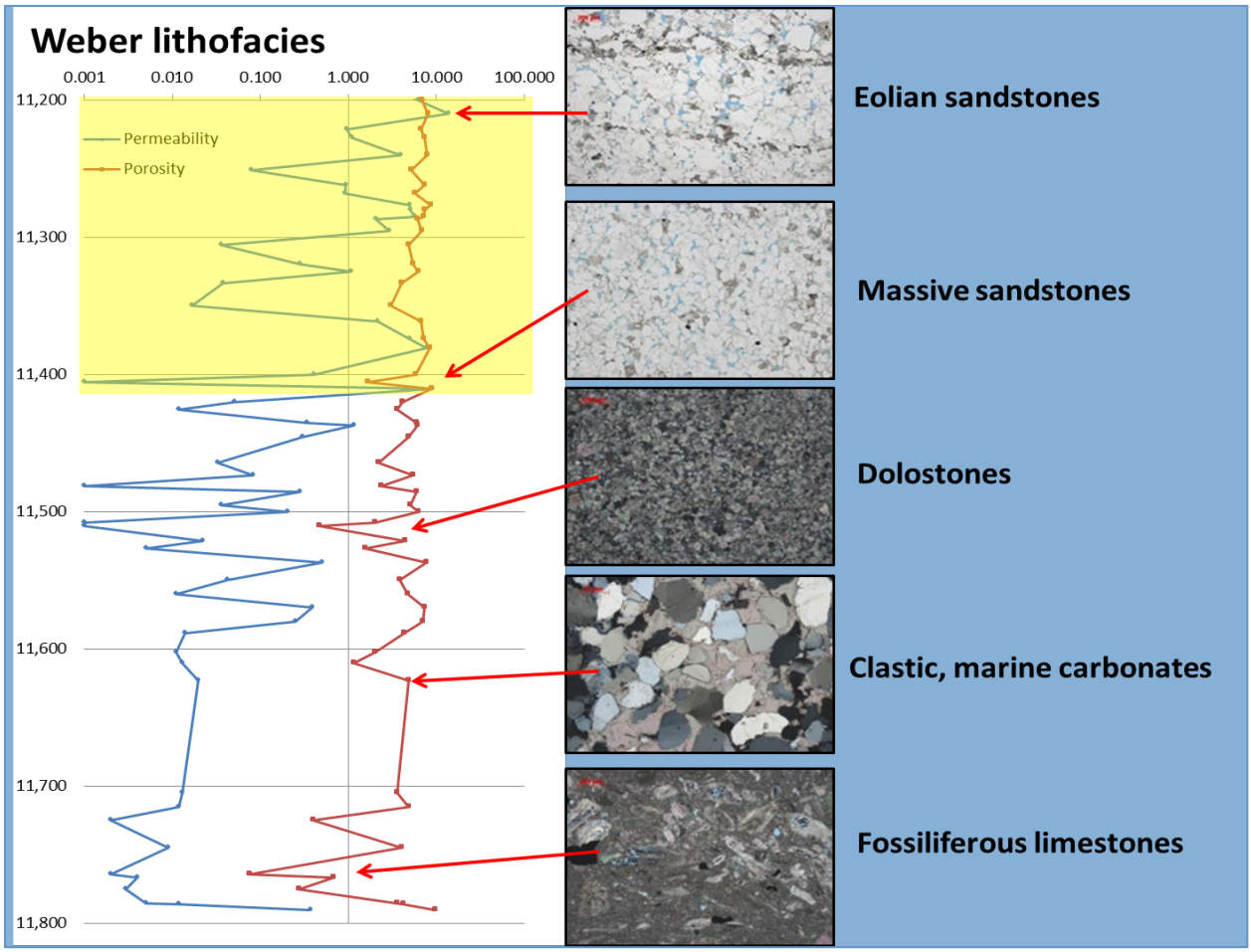


Fig. 55: Measured porosity and permeability of the Weber Sandstone associated with lithofacies. Potential reservoir zone highlighted in yellow.

Porosity and permeability analysis shows that both the Weber and Madison have CO_2 storage potential. However, the Madison has higher porosity and permeability and would be the preferential target for injection.

Diagenesis and Burial History

The burial and geochemical history of the RSU#1 well site was modeled using Petromod® 12 software. The burial history reconstruction was used to generate 1-D site profile models using a constant heat-flow of 25mW/m2 from 500m.y.b.p., to 25m.y.b.p. after which the heat flow was increased to 55mW/m2. These models were correlated to geochemical and diagenetic alteration of reservoirs and seals observed in petrographic and isotopic data. At the study site, maximum burial of targeted reservoirs and seals was greater than 8,000m in the late Eocene and maximum temperatures were greater than 150˚C (**Fig. 56**). This was followed by geologically-rapid uplift and denudation (**Fig. 56**). A complex burial history resulted in extensive diagenesis and geochemical alteration, all of which affected the storage and sealing capabilities of targeted formations.

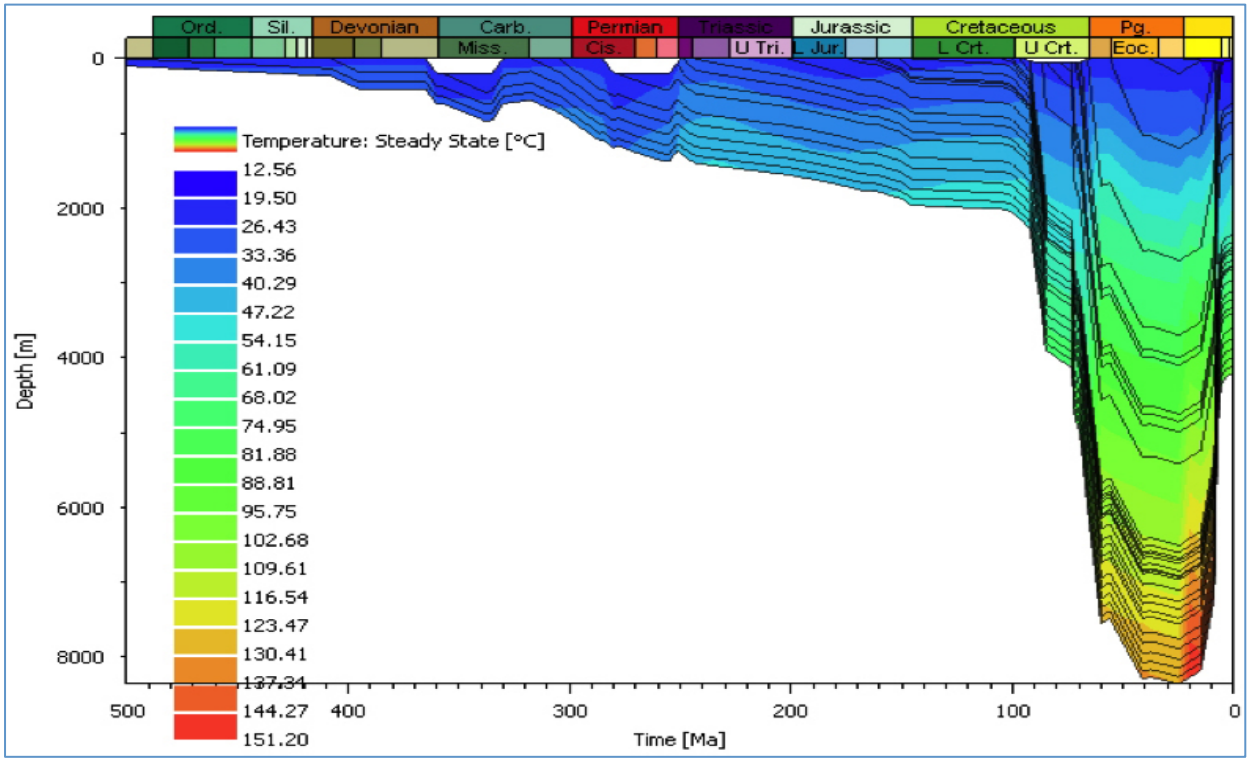


Fig. 56. 1-D burial and thermal history of the RSU#1 well site.

Diagenetic alteration at the study site can be divided into four stages; early burial, deep burial, maximum burial, and exhumation. Early burial diagenesis includes hypersaline dolomitization and evaporite deposition. Early dolomitization of the Madison created porosity. In the Weber, early dolomitization of pinstriped lamellae created internal baffles, resulting in vertical anisotropy (lateral k > vertical k). A similar anisotropic response is noted in intergranular porosity zones in the Madison. Widespread evaporite precipitation resulted in diminished porosity in the Weber and Madison reservoirs. In sealing lithologies, early burial diagenesis supplied pore-filling evaporitic cements to the lower Triassic section. Early dolomitization in Amsden carbonates resulted in complete cementation. Deep burial diagenesis is defined by pressure solution, extraneous fluid migration, thermochemical sulfate reduction, cementation, and secondary dissolution. These processes resulted in a net loss of porosity in the Weber, and an increase of porosity in the Madison. Deep burial diagenesis resulted in net total porosity losses in both sealing lithologies. Maximum burial is delineated by continued pressure solution and cementation, which generally resulted in porosity losses in all formations. Exhumation diagenesis is defined by vein and fracture fill, as well as late-stage mineral precipitation. While both processes negatively impacted porosity, vein and fracture fill negated the permeability of sealing formations, increasing sealing capabilities. In addition to altering formation characteristics, diagenesis and burial history affected the geochemical evolution of formation brines. Diagenesis at the study site was instrumental in the creation or negation of reservoir and seal capacities.

Construction of realistic 3-D geological petrophysical models

Using comprehensive regional and site specific geologic, structural, geochemical, log suites, core, and seismic data, a field-scale heterogeneous reservoir model of the geological CO_2 storage site in the RSU is presented. This model is used to evaluate uncertainty in two critical GCS performance metrics: storage capacity and well injectivity. First a description of the implementation of heterogeneities in porosity and permeability model of the reservoirs will be presented based on analysis results from log suites, cores, and 3-D seismic data. Then realistic evaluations of permeability and porosity are generated for each of the geologic units including storage targets in the Mid-Late Pennsylvanian Weber Sandstone and the Mississippian Madison Limestone, sealing formations in the Early-Pennsylvanian Amsden, Triassic Dinwoody, Chugwater, and more. These heterogenetic property fields then are used to simulate non-isothermal CO_2 injection for 50 years to evaluate the geological CO_2 storage capacity and injectivity utilizing various injection scenarios for the targeted reservoirs in the Madison Limestone and Weber Sandstone.

Methodology and **A**pproach

This study utilizes a multidisciplinary, integration approach to characterize the heterogeneities of the porosity and permeability for targeted storage reservoirs and containment formations. The high vertical resolution core measurement data and petrophysical log data are used to calibrate and generate the reservoir heterogeneity property model based on the seismic attribute analyses results from the newly acquired 3-D seismic survey. The steps were (1) litho-facies are determined for each formation based on the detailed core descriptions and petrographic observations; (2) selected core samples from each litho-facies are measured for porosities and permeabilities under the in situ conditions; (3) log porosity is calibrated with the laboratory measured core porosities; (4) relationship between the porosity and acoustic velocity is derived from all available logs for each formations; (5) 3-D porosity distribution of the modeling domain is populated using the interval velocity volume of the 3-D seismic survey, and the function between the porosity and acoustic velocity derive from the well logs; (6) once spatial distributions of porosity in the modeling domain had been acquired, permeability spatial distributions were obtained on

the basis of empirical correlation between porosity and permeability; (7) numerical simulations of CO_2 injection into the Weber Sandstone and Madison Limestone using both homogeneity and heterogeneity reservoir properties were conducted with a finite element multiphase flow simulator, FEHM (Zyvoloski et al., 1997).

Establish reservoir heterogeneity through correlation of seismic attributes with well log parameters and core observations

Core measured porosity

Routine core analysis was conducted on 128 core plug samples from the reservoir strata Weber Sandstone and Madison Limestone, and from the containment strata in the Dinwoody/Red Peak Formation and Amsden Formation from RSU #1. All tests were conducted by Intertek Westport Technology Center and following core analysis procedures specified in API RP40 Method Recommended Practices for Core Analysis (1988).

The porosity shows significant variations within the targeted reservoirs of the Weber Sandstone and Madison Limestone (**Fig. 57**). Porosities in the Weber Sandstone samples range from 0.7% to 8.2% under the reservoir net confining stress (NCS) condition, and densities range from 2.63g/cm^3 to 2.7 g/cm^3. The variations of the porosity distribution in the Weber Sandstone are clearly affected by the deposition environments. The Weber Sandstone is composed of both clastic and carbonate deposits (Love et al., 1993), that can be divided into an upper eonian facies, and lower, shallow, warm epicontinental marine facies. The micrite limestone and quartz sandstone in the lower marine facies are very tight, and the porosity is less than 5%. The massive quartz sandstone in the upper eolian facies has a relatively higher porosity up to 10%. For the Madison Limestone samples, the porosities range from 0.3% to 19% under the reservoir NCS condition, and densities range from 2.7g/cm^3 to 2.87g/cm^3 (**Fig. 57**). The porosity and permeability of the Madison Limestone is mainly controlled by the following factors: (1) dolomitization (2) dissolution associated with karst developments on a regional unconformity, (3) large scale fracturing, and (4) dissolution of foram shells or minerals in the matrix.

The porosities of the containment formation (Dinwoody) formation are less than 1%, and average density is 2.7g/cm^3. The porosity differences between the 5.5Mpa NCS and reservoir NCS are small in the Weber Sandstone and Dinwoody/Red Peak Formation, less than 1%, but significant in the Madison Limestone. The porosity difference of some Madison Limestone samples is larger than 5% (from 14% under the reservoir NCS to 19% under the 5.5Mpa NCS). The significant porosity difference of the Madison Limestone under the 5.5Mpa NCS and reservoir NCS (over 34.5Mpa) may be the result of two factors, higher porosity, and mineral compositions. The porosities measured from several samples of the Madison Limestone are larger than 20%. These porosities are mostly secondary porosity resulting from either the karst development or fracture development.

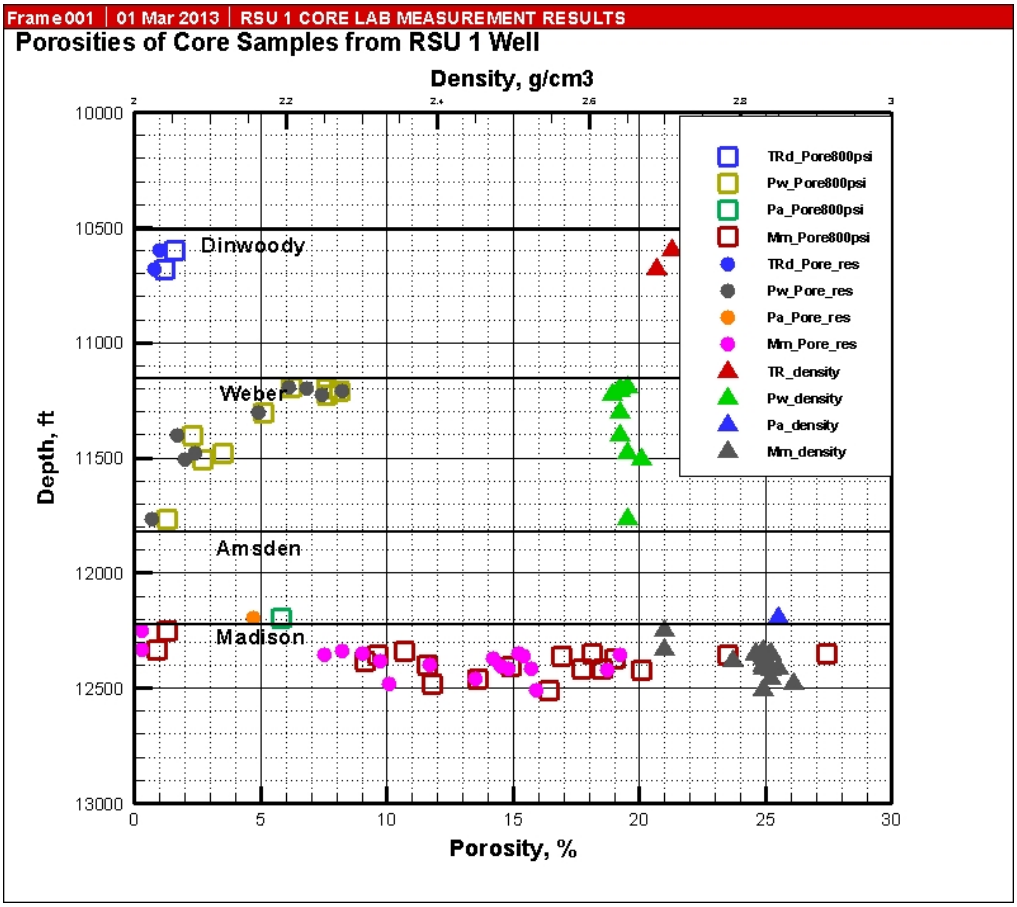


Fig. 57. The plot of the porosity and density versus depth for the CO_2 storage targeted reservoirs Weber Sandstone and Madison Limestone, and containment strata the Dinwoody Formation and Amsden Formation. Both porosities measured under 5.5Mpa NCS and reservoir NCS are shown.

Fig. 58 shows the air and Klinkenberg permeability variations in both targeted reservoirs and containment formations under 5.5Mpa NCS and reservoir NCS. Klinkenberg permeability of the Weber Sandstone under the reservoir condition (34.5Mpa) ranges from 0md to 12.9md. The higher permeability (> 1md) mainly occurs at the upper portion of the Weber Sandstone. For Madison Limestone, the Klinkenberg permeability under reservoir NCS (38Mpa) ranges from 0md to 16.8md. Several higher permeabilities (up to 183md) were measured from the Madison Limestone within the karst or fractured sections. The lower permeability samples are more sensitive to the effects of net confining stress. Klinkenberg permeability under the reservoir NCS can be two orders of magnitude lower than permeabilities under the 5.5Mpa NCS.

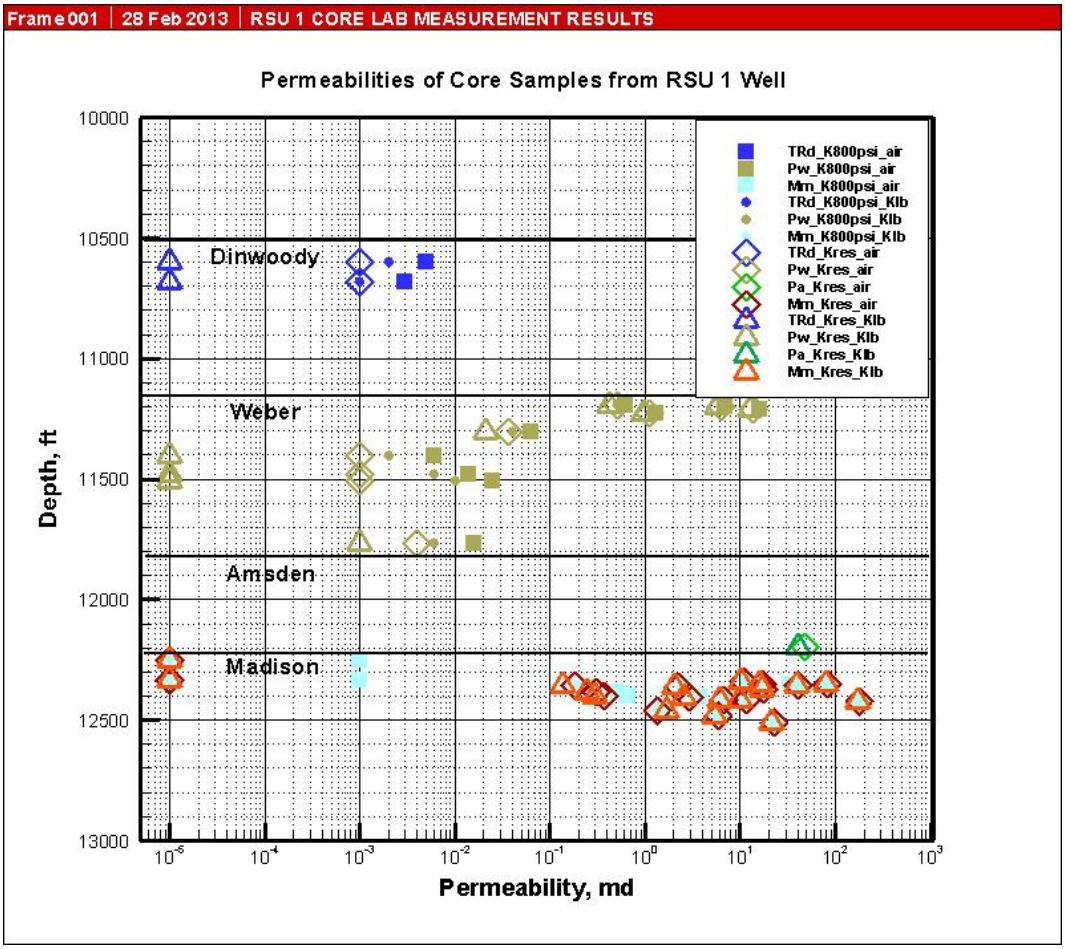


Fig. 58. Showing the air and Klinkenberg permeability variations in both targeted reservoirs and containment formations under 5.5Mpa NCS and reservoir NCS.

Log porosity and core porosity

To have confidence in log evaluations, the porosity calculated from logs should agree with those derived from the core measurements. Porosity is classified as total porosity and effective porosity. Total porosity may be defined as all the pore space containing fluids (water, oil or gas), whether or not the fluids are mobile. This pore space includes any hydrocarbon fluids, mobile water, capillary bound water and clay-bound water**.** Effective porosity is the total porosity less the fraction of the pore space occupied by capillary bound water and clay-bound water. Because it is not possible to measure effective porosities in a reliable and repeatable manner, calibration with core analyses is best achieved by estimating total porosities from logs and comparing these with measured total porosities from core plugs.

The most common way to calculate total porosity is using the density log corrected for lithology and fluid density. Formation bulk density is a function of matrix density, porosity, and fluid density in the pores. To determine the density porosity from the bulk density log, the matrix density, and fluid density in the pores must be known. Based on the results of Laboratory core measurements from RSU #1, densities of 2.7g/cm^3 for the Dinwoody Formation, 2.64g/cm^3 for the Weber Sandstone, 2.70g/cm^3 for limestone in the Madison Limestone, and 2.84g/cm^3 for dolostone in the Madison Limestone are used for the porosity estimation from the bulk density log in this study. The porosity also can be calculated from the neutron log.

The cross plots of the Laboratory measured porosities under reservoir conditions with log derived porosity show that the neutron porosity overestimates the porosity of the carbonate rocks and carbonaceous shale, whereas the density porosity underestimates the porosity of the carbonate rocks (**Fig. 59**). As indicated by George Asquith and Charles Gibson (1982), true porosity could be calculated from combining neutron porosity and density porosity logs using the root mean square formula (gas-bearing formation) or mathematic mean formula (oil and water bearing formations). The heavy magenta line shown on the **Fig. 60** represents the total porosity estimated from the neutron and density porosity log from the RSU #1 well. These neutron-density porosities match well with the core measured porosity (**Fig. 61**).

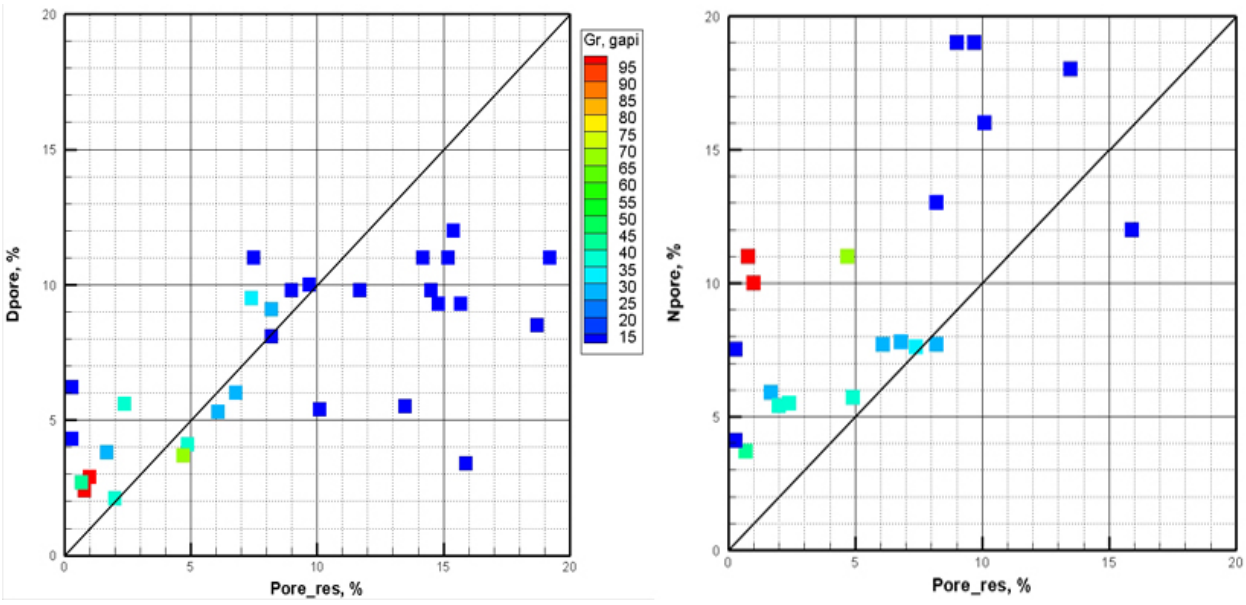


Fig. 59. Cross plot of the laboratory measured porosity at reservoir conditions with the log derived bulk density porosity (A) and neutron porosity (B).

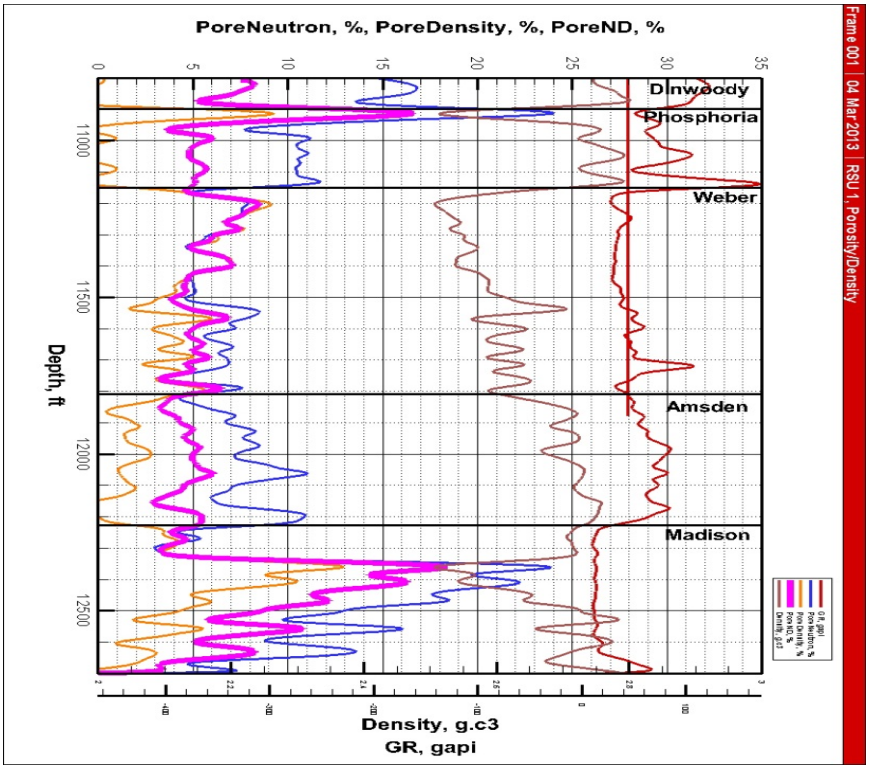


Fig. 60. Plots of the gamma ray, bulk density, neutron porosity, density porosity for the Dinwoody Formation, Phosphoria formation, Weber Sandstone, Amsden formation and Madison Limestone from RSU #1. The heavy magenta line is neutron-density porosity calculated from neutron and density porosity and is used to establish the function between the porosity and sonic velocity.

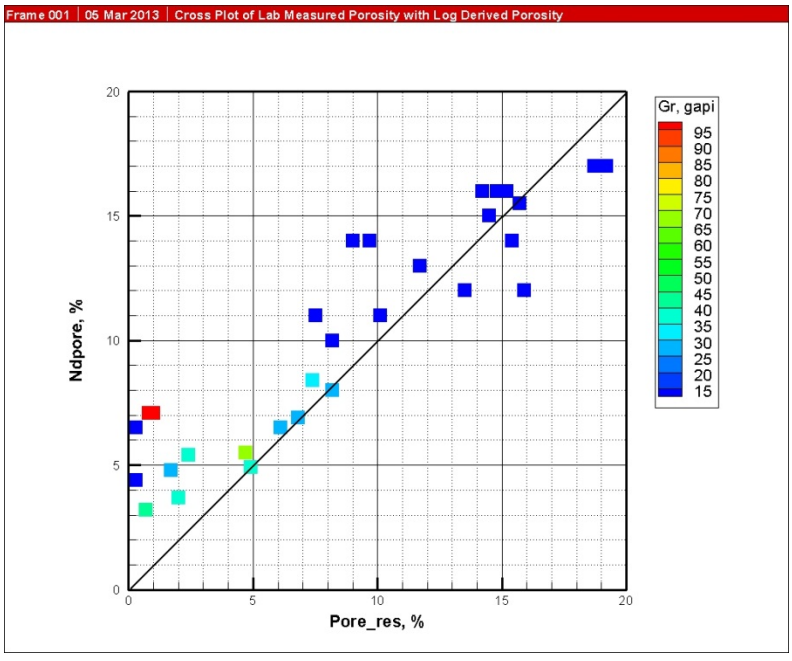


Fig. 61. Cross plot of the laboratory-measured porosity at reservoir conditions with the log derived neutron-density porosity.

Sonic Velocity and Neutron-density porosity

On the basis of the vertical resolution of the borehole data used here, the vertical heterogeneities are more fully captured than the horizontal heterogeneities. In order to characterize the spatial distributions of the heterogeneous properties of the targeted reservoirs and containment strata, seismic attributes needed to be correlated with the core and log derived properties. Using log suite from RSU #1, the relationships of the neutron-density porosity and sonic velocity were established for the Cretaceous Mowry Shale and Muddy Sandstone, the Jurassic Morrison Formation, Entrada Sandstone, Carmel Formation, and Nugget Sandstone, Triassic Chugwater Formation, Red Peak Formation, and Dinwoody Formation, the Permian Phosphoria Formation, Pennsylvanian Weber Sandstone and Amsden Formation, the Mississppian Madison Limestone and the Devonian Darby Formation.

The depositional environment of the Weber Sandstone is characterized by near shore eolian and shallow marine environments, these facies changes (sand dune and inter dune) within the Weber Sandstone cause significant variation of rock porosity. **Fig. 62a** shows the sonic velocity and neutron-density porosity variations of the Weber Sandstone in RSU #1. The relationship between the sonic velocity and neutron-density porosity for the Weber Sandstone is shown on **Fig. 62b**. The higher porosities falling off the function line are from samples with secondary micro fractures porosities. The neutron-density porosities of the Weber Sandstone in RSU #1 range from 2% to 10% with mean 5% (**Fig. 62a**).

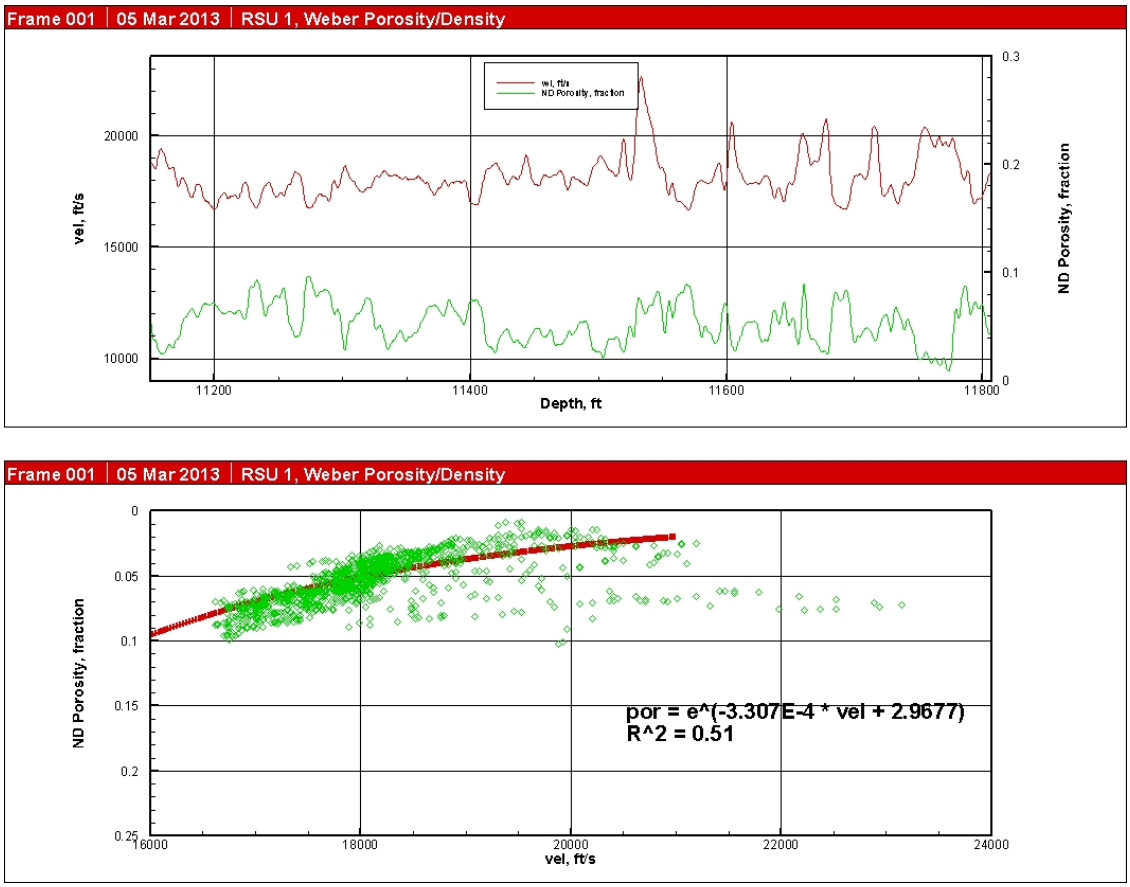


Fig. 62. (**a**) The smoothed sonic velocity and neutron-density porosity of change through the Weber Sandstone in RSU #1. (**b**) The relationship between the sonic velocity and neutron-density porosity for the Weber Sandstone is derived from the cross plot.

Fig. 63a shows the sonic velocity and neutron-density porosity variations of the Madison Limestone in RSU #1. The relationship between the sonic velocity and neutron-density porosity for the Madison Limestone is shown on **Fig. 63b**. The neutron-density porosities from well logs of the Madison Limestone in RSU #1 range from 1% to 18% with mean 7% (**Fig. 63a**).

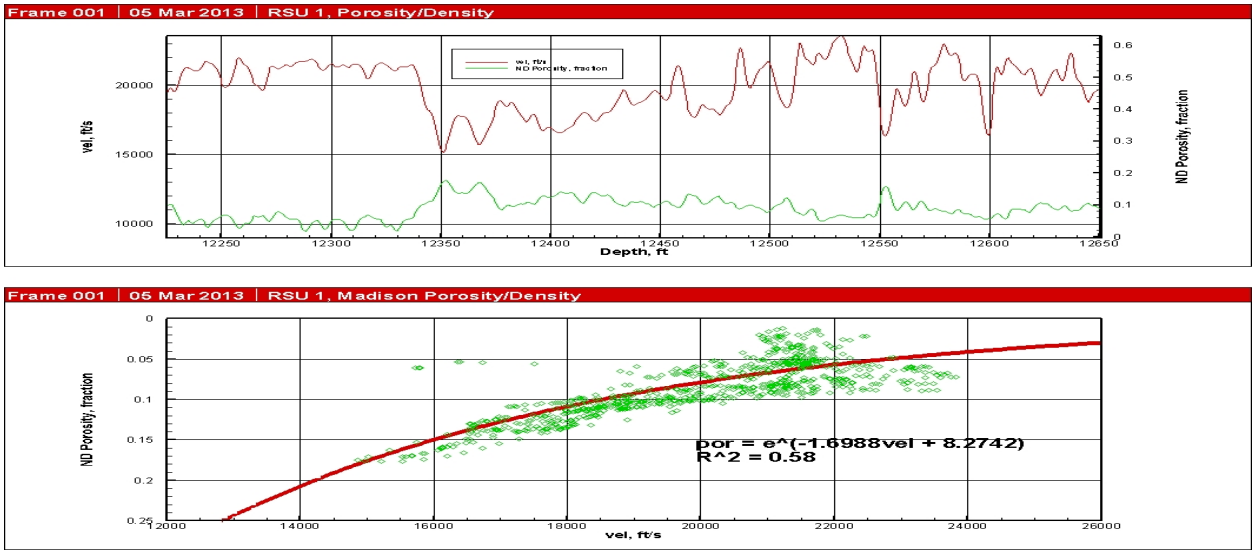


Fig. 63. (**a**) The smoothed sonic velocity and neutron-density porosity change through the Madison Limestone in the RSU #1. (**b**) The relationship between the sonic velocity and neutron-density porosity for the Madison Limestone is derived from the cross plot.

Using the sonic velocity and neutron-density porosity functions established for each formation, a 3-D porosity volume for the CO_2 injection simulation domain was generated from the Jim Bridger 3-D interval velocity volume. The distributions of porosities derived from seismic interval velocities for the CO_2 storage targeted reservoirs Weber Sandstone and Madison Limestone are shown on **Fig. 64** and **Fig. 65**. The porosities derived from seismic interval velocity for the Weber Sandstone range from 2% to 13% with a mean of 5% within the modeling domain (**Fig. 64a**). The porosities derived from seismic interval velocity for the Madison Limestone ranges from 7% to 18% with a mean of 11% within the modeling domain (**Fig. 64b**). The porosities of both Weber Sandstone and Madison Limestone show significant heterogeneity. The porosities of the Madison Limestone derived from seismic interval velocities show a clear bi-modal distribution (**Fig. 64b**).

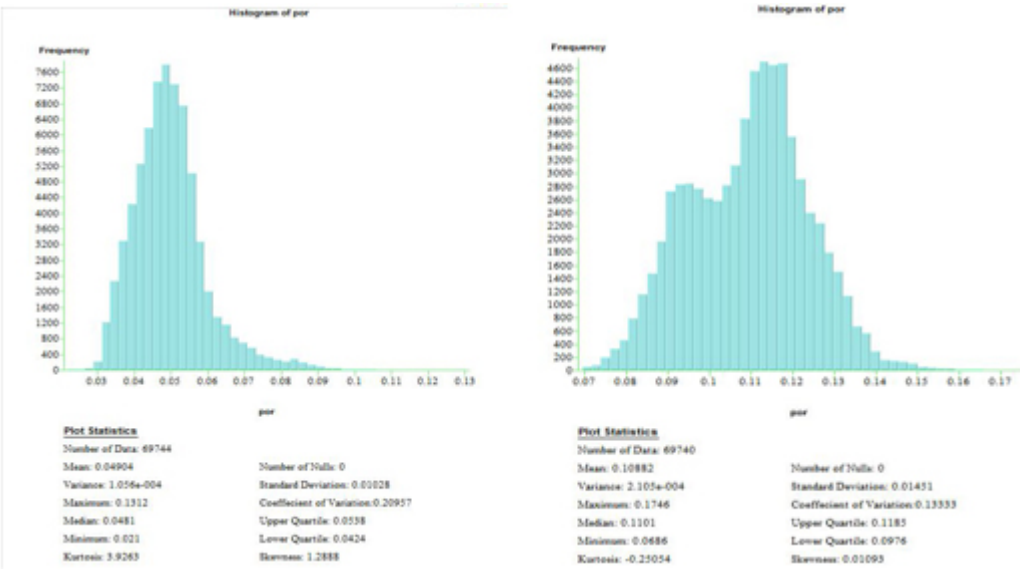


Fig. 64. (**a**) The histograms show the porosity distributions of the targeted storage reservoirs Weber Sandstone and (**b**) Madison Limestone within the 3-D simulation domain.

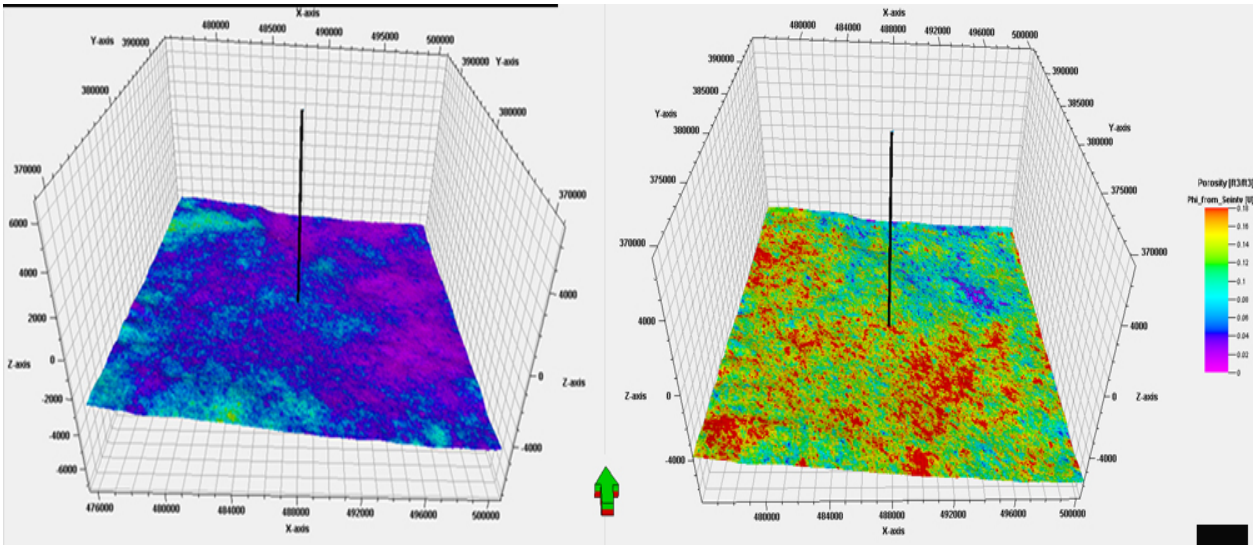


Fig. 65. The porosities derived from the seismic interval velocities for the Weber Sandstone and the Madison Limestone show significant heterogenetic characteristics in the geological CO_2 storage domain.

Permeability and porosity

The permeability parameters are mapped from porosity by applying empirical correlations between porosity and permeability.

Three sets of porosity/permeability data measured on the Weber/Tensleep Sandstone samples from RSU #1 and adjacent area were collected in this study (Fox et al., 1975, Bowker and Jackson, 1989, and CMI, 2013). The cross plot of porosity and permeability for the Weber/Tensleep Sandstone samples is shown on **Fig. 66**. The measured permeability from the RSU #1 core sample ranges from 0md to 10md. With the mean porosity of 0.5md, the permeabilities derived from 3 sets of the porosity data are fairly close, but with high porosity, the permeability can be an order higher from different data sets. For example, with the same porosity of 10%, the derived permeability is 0.6md from the Fox 1975 dataset and 1.05md from CMI 2013 dataset. The Weber Sandstone at RSU #1 typically has a higher permeability when compared to the Weber/Tensleep Sandstone in other areas. An exponential function was derived by utilizing a least squares curve fitting to the CMI 2013 core measured porosity-permeability dataset.

$$K = e^{(1.02 * \text{porosity} - 7.51)}, \qquad \textbf{Eq. 5}$$

The regression correlation has a correlation coefficient of $R^2 = 0.86$. The permeability volume of the modeling domain was derived from the porosity volume using the above exponential function. The permeabilities within the modeling domain range from 0.01md to 10md with a mean 0.3md for the Weber Sandstone. **Fig. 67** shows the distribution of the derived permeabities from 0md to 1md, which accounts for the permeabilities with 98% of the simulation cells (67,615 of 69,147 cells) in the Weber Sandstone in the modeling domain.

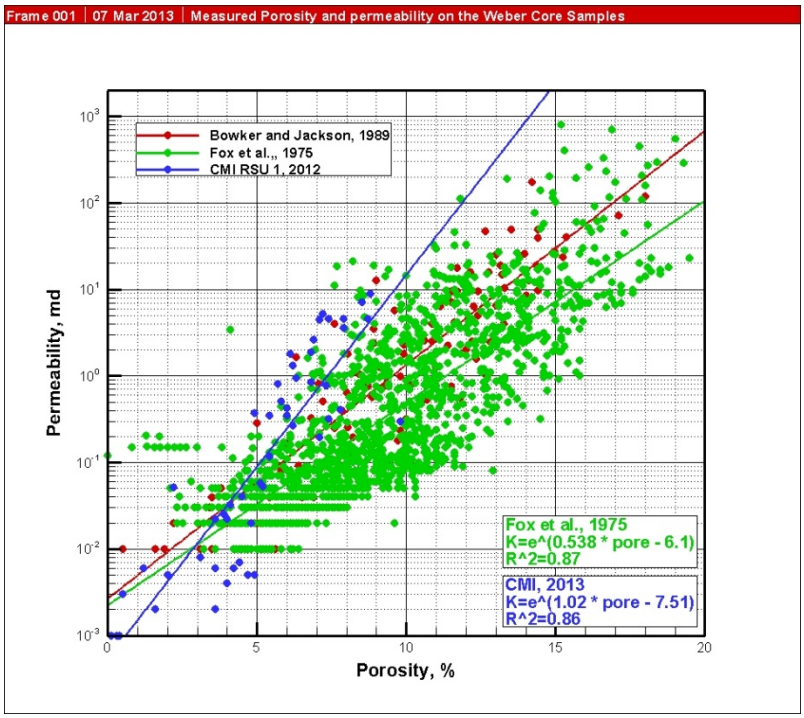


Fig. 66. Plot of the permeability versus porosity for the Weber Sandstone in the RSU and vicinity area. All porosity and permeability data are laboratory measurements on the core samples.

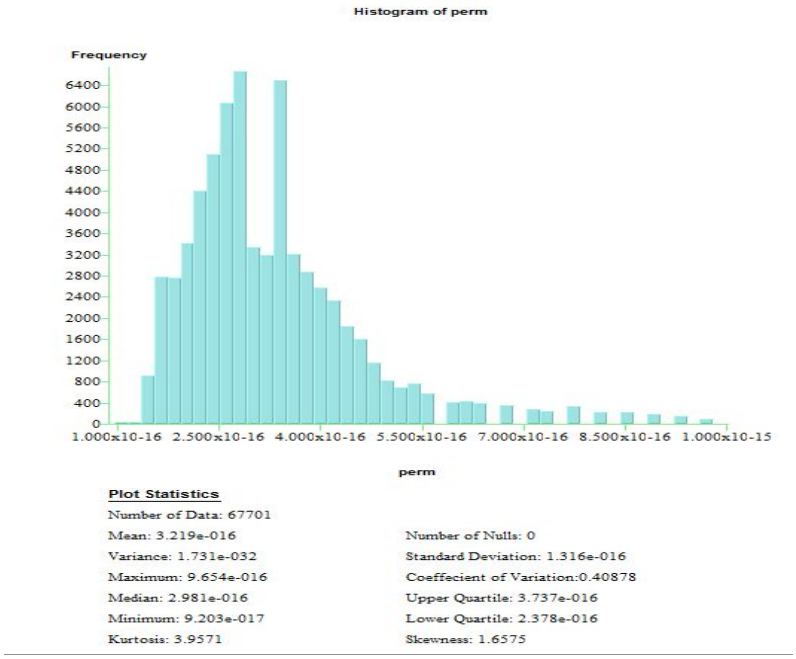


Fig. 67. The dominated permeability distribution of the Weber Sandstone in the modeling domain**.**

For the Madison Limestone, two sets of porosity/permeability data from RSU #1 and the surrounding areas were available in this study (Ehrenberg, 2006, and CMI, 2013). The cross plot of porosity and permeability for the Madison Limestone samples is shown on **Fig. 68**. The two sets of measured data have similar trends for the relationship between the porosity and permeability. The permeabilities of RSU #1 core samples range from 0.001md to 200md. An exponential function was derived by applying least squares curve fitting on the CMI 2013 core measured porosity-permeability dataset.

$$K = e^{(0.291 * \text{porosity} - 2.09)}, \qquad \textbf{Eq. 6}$$

The regression correlation has a correlation coefficient of $R^2 = 0.72$. The permeability volume of the modeling domain was derived from the porosity volume by applying the above function. **Fig. 69** shows distribution of the derived permeabilities of the Madison Limestone in the modeling domain. The permeabilities within the modeling domain range from 0.01md to 20md with a mean 3md. The permeability of the Madison Limestone in the RSU is characterized by a bi-modal distribution. The higher porosity and permeability are mainly a result of karstification, leaching and micro fracture developments.

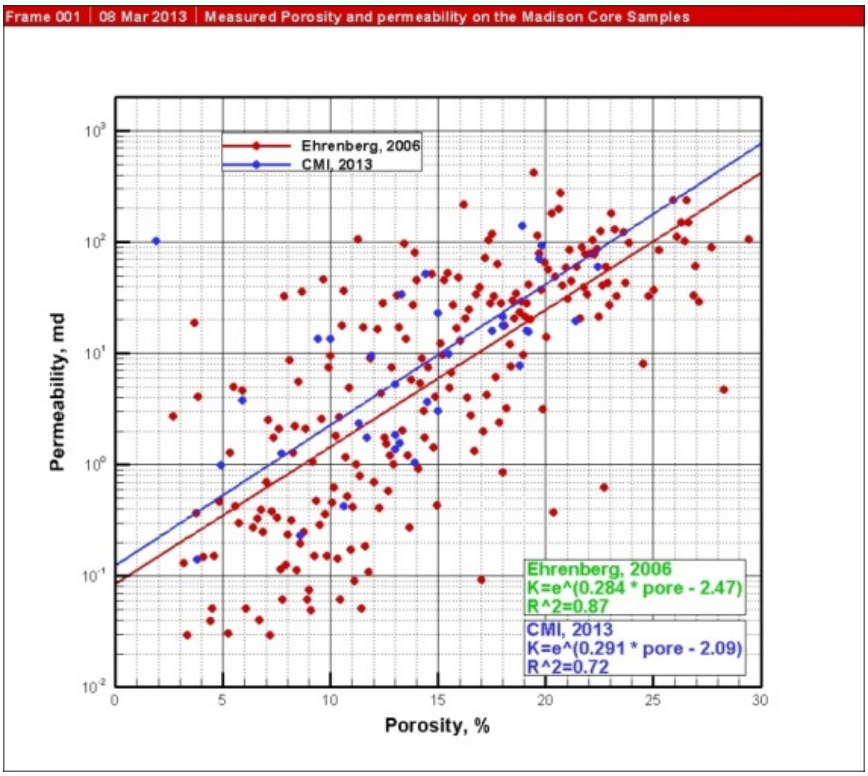


Fig. 68. Plot of the permeability versus porosity for the Madison Limestone in the RSU and surrounding area. All porosity and permeability data are laboratory measurements on the core samples.

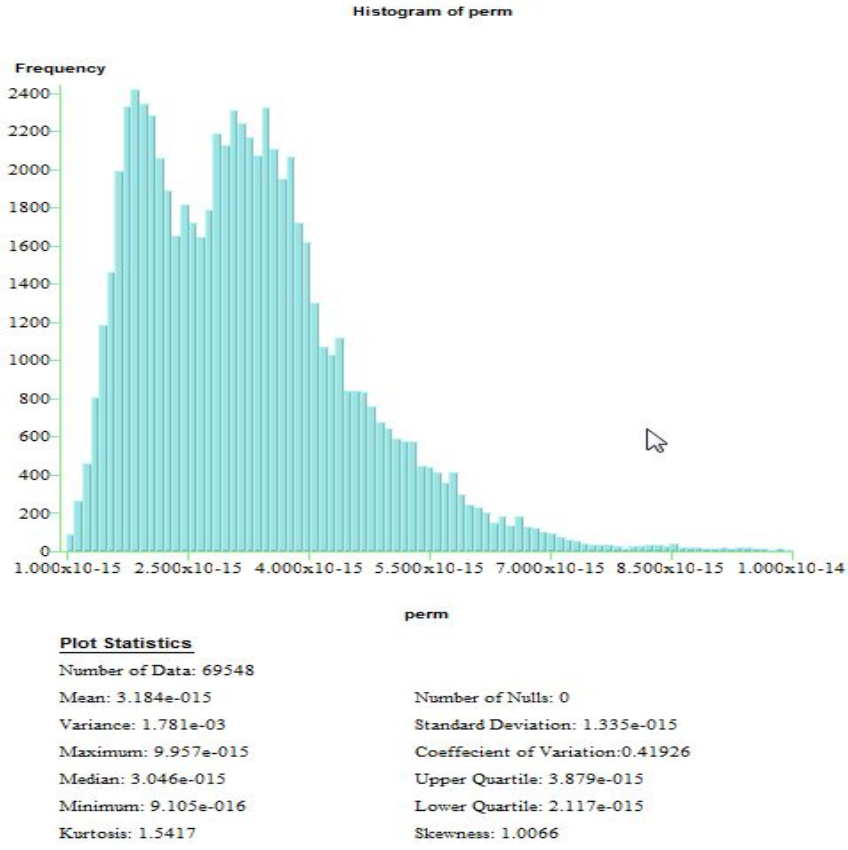


Fig.69. The permeability distribution of the Madison Limestone in the modeling domain. The permeability of the Madison Limestone is characterized by bi-modal distribution.

The primary containment formations for geological CO_2 storage in the RSU are Amsden, Dinwoody, Red Peak, and Chugwater formations. The Cretaceous shale section, over 1,500m thick, can serve as a secondary sealing sequence. The lithologies of these containment formations are siliceous shale, mudstone, and carbonaceous shale. The permeability of the shale and mudstone is a complex function of porosity, clay content, effective stress and diagenesis (Yang and Aplin, 2010). Because of the difficulty in the Laboratory measurements, high quality data of porosity and permeability for shale and mudstone is relatively rare (Neuzil, 1994). A simple linear regression relationship cannot capture a realistic relationship between porosity and permeability, particularly from measurement data from the Dinwoody/Red Peak, and Amsden cores collected in this study. In light of this complexity, an empirical correlation (Yang and Aplin, 2010) was used to compute the permeability of the sealing-rocks with an assumption of clay content of 25%.

$$\ln k = -69.59 - 26.79C + 44.07C0.5 + (-53.61 - 80.03C + 132.78C0.5)e + (86.61 + 81.91C - 163.61C0.5)e0.5 \quad (12) \qquad \textbf{Eq. 7}$$

where $e = \theta/(1-\theta)$, e is void ratio, and θ is porosity, k is vertical permeability in unit of m^2, and C is clay content in percent.

Fig. 70 shows the permeability distributions of the Dinwoody Formation and Chugwater Formation are derived from the 3-D porosity volume and are used in the RSU CO_2 injection simulations.

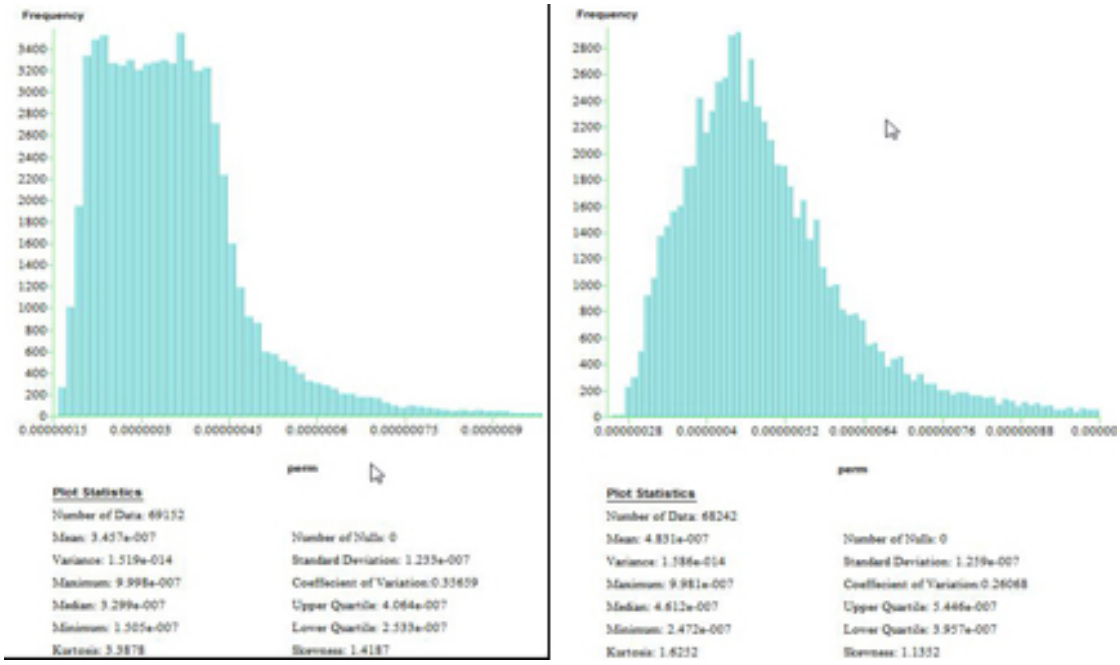


Fig. 70. The histograms show the permeability distribution of the containment formations (a) Dinwoody and (b) Chugwater in the RSU geological CO_2 storage domain.

Permeabilities for all reservoir rocks are prescribed as isotropic. For the sealing rocks, the Dinwoody and Chugwater formations are prescribed as anisotropic with a ratio of 10 (horizontal permeability is 1 order larger than vertical one).

Combined with geological setting, well log suites, and detailed 3-D seismic attribute analyses, the spatial heterogeneities both in the vertical and horizontal direction within the modeling domains are fairly captured. The spatial heterogeneities for porosity and permeability are then incorporated into the 3-D modeling domain to simulate supercritical CO_2 storage processes with injection of CO_2 for 50 years and observation for an additional 50 years after injection ceased using the FEHM simulator.

Export realistic 3-D petrophysical property models to numerical simulation

Generate the computation mesh

The geological structural model is located one mile south of the JBPP, and consists of a block that is 8km x 8km in map view, with the elevation extending from sea-level to 3,600m below sea-level (**Fig. 71**). Following the logic and methodology outlined in Miller et al. (2007), a computational hydrostratigraphic model that maintains sharp material interfaces between the units of interest was generated from the geological structural model. In this model, the Voronoi volume elements are aligned to follow the curvature of the unit interfaces and do not stair-step in the manner of a traditional finite element grid. This alignment allows a more accurate calculation of CO_2 moving along the caprock in the up-dip direction. Grid spacing is 150m in the X and Y directions, and variable in the vertical direction.

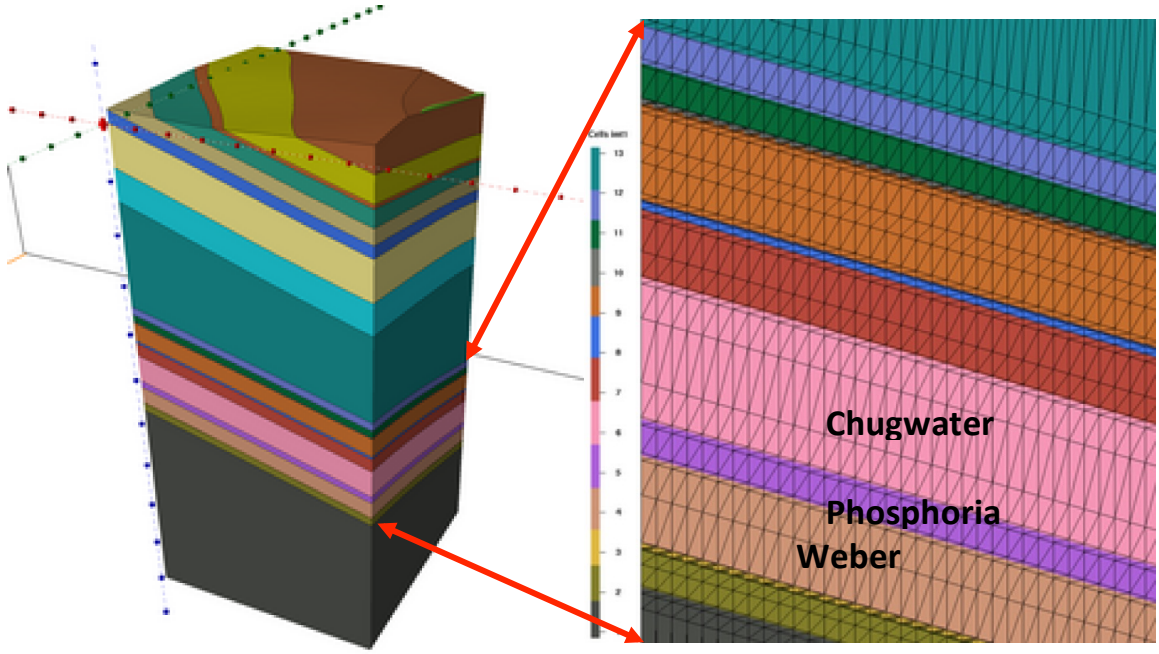


Fig. 71. (**a**) Cross-section of the hydrostratigraphic model showing the map view location of the JBPP. (**b**) Zoomed in view of the numerical mesh in the region of interest for injection into the Weber sandstone. Grid spacing in B is 200m in the horizontal direction.

Numerical model setup

The simulation domain is 8km (x) × 8km (y) × 3.6km (z) and is discretized into 291,954 tetrahedral nodes with horizontal spacing of 150m and 37.5m near the injection well. The variable vertical resolution was reduced to 37.5m in order to capture relative small vertical correlation lengths in the Chugwater, Phosphoria, Weber, Amsden, Madison, and Darby formations. The formations are inclined to the southeast with an angle of 5° and an azimuth of 130°. The domain implicitly includes 2km overburden rock above its top. The CO_2 injected into the Weber sandstone and Madison Limestone is assumed to be a fixed temperature (45◦C) and constant injecting pressures of 18.5MPa at the wellhead. The maximum injection pressure at the penetrated reservoirs is limited to below 65% of lithostatic pressures, and is comparable with the maximum sustainable injection pressure estimated by Rutqvist et al. (2007), who analyzed coupled fluid flow and geomechanical fault-slip under conditions of hypothetical compression and extension stress. The important parameters used in these simulations are listed in **Table 4**.

Table 4. Parameters used for CO_2 injection simulation in the Weber Sandstone and Madison Limestone.

Parameters	Symbol	Unit	Values	
			Weber	Madison
Saline aquifer effective permeability	k	m2	Hete	Hete
Saline aquifer effective Porosity	ø	%	Hete	Hete
Saline aquifer thickness	b	m	200	130
Saline aquifer salinity	s	%	11	8
Saline aquifer thermal conductivity	λ_m	W/Km	3.3	3.3
Saline aquifer initial fluid pressure	P_{inf}	MPa	31–40	34-43
Maximum Temperature difference	T	◦C	22	22
Brine viscosity	μ_w	Pa s	1.33×10^{-4}	1.33×10^{-4}
Brine density	ρ_w	kg/m3	1,100	1,100
CO_2 fluid viscosity	μ_{co2}	Pa s	5.8×10^{-5}	$5.8\text{x}10^{-5}$
CO_2 fluid density	ρ_{co2}	kg/m3	700	700
Brine compressibility	c_w	Pa−1	3.5×10^{-10}	3.5×10^{-10}
CO_2 fluid compressibility	c_{co2}	Pa−1	1.0×10^{-9}	1.0×10^{-9}
Pore compressibility	cp	Pa−1	4.5×10^{-10}	4.5×10^{-10}
Injection time	t	Year	50	50
Specific storage	S_s	–	5×10^{-6}	5×10^{-6}
Injection rate	Q	kg/s	constant	constant
Gravitational acceleration	g	m/s2	9.8	9.8
Residual water saturation	S_{wr}	%	10	10
Maximum water saturation	S_{ws}	%	90	90
Residual CO_2 saturation	S_{CO2r}	%	10	10
Maximum CO_2 saturation	S_{CO2s}	%	90	90
Brine thermal expansion	λf	K−1	0.001	0.001
Brine specific heat capacity	C_{pf}	J/kg K	4.2×10^{3}	4.2×10^{3}

The bottom of the simulation domain is a no flow boundary. For all simulations, the down-dip sides (east and north sides) of the domain were closed to avoid the impact on the mineral resources, whereas the up-dip sides (south and west sides) were open for the reservoir fluids to flow freely out of the simulation area. Due to the buoyancy, the injected CO_2 will move up-dip. Constant temperatures are held at the top (55.6°C) and bottom (147.7°C) of the domain, which is equivalent to a specified geothermal gradient of 25.6°C /km (1.7°F/100 ft), and average surface temperature 4.4°C (40°F). The fixed side boundaries are used to estimate the amount of water that must be produced to ensure that the injection site does not impact surrounding parcels of land. Hydrostatic pressure and temperature fields are used as initial conditions for all simulations in this study. Initial CO_2 fractions in injection well nodes are set at zero. This simulation incorporates the CO_2 density model (Duan et al., 2008) and solubility model of CO_2 in brine (Duan et al., 2006) into the CO_2 transport modeling. Combined with thermodynamic updating, the density, viscosity, solubility of CO_2 in brine are simulated with changing temperature and pressure.

Carbon dioxide injection simulation

Simulations of CO_2 injection are run on the Los Alamos National Laboratory multiphase porous flow simulator (Finite Element Heat and Mass transfer code, or FEHM) (Zyvoloski et al., 1988). The CO_2 equations of state are built into a lookup table that can capture the transition from supercritical fluid to liquid/gas across the region of discontinuous derivatives. Solubility of CO_2 in brine is determined using the model of Duan and Sun, 2003 and Stauffer et al., 2009.

Initial conditions for the domain include a geothermal gradient of 25.6°C/km with a bottom temperature of 147.7°C and a top temperature of 55.6°C, and a hydrostatic pressure gradient ranging from 20MPa at top of the domain (sea-level, depth at 2,160m) to 56MPa at the bottom of the domain (depth 5.600m). Further simplifying assumptions for the 3-D injection calculations are that thermal conductivity of the rocks is constant at 0.5W/(mK), rock density is constant at 2650kg/m^3, and heat capacity is constant at 1000J/(kg K). Capillary pressure effects are ignored; brine TDS are assigned to be 100,000 ppm for the Weber Sandstone and Madison Limestone, and are constant at 90,000 ppm for the rest of the formations, and water viscosity is calculated independently of brine content or dissolved CO_2. Initial dissolved CO_2 concentration was set at zero, as a bounding calculation. The formation test report data from the region suggest that the in-situ concentration of dissolved CO_2 in the Weber Sandstone and Madison Limestone brines may be greater than zero. Even though the regional test data show that the Weber Sandstone and Madison Limestone brines may have dissolved CO_2 in the brines, no CO_2 was measured in the sample from the stratigraphic test well. During CO_2 injection, the simulator allows for the possibility of CO_2 dissolution in water. The open boundaries (up-dip west and south boundaries of modeling domain) are essential conditions to create accommodation spaces and to prevent the reservoir pressure elevating too high to reach the fracture pressure of the sealing formations.

Perform a series of CO_2 injection-formation fluid production scenarios to optimize CO_2 storage capacity

Injection into the Weber Sandstone

An artificial well was created using a location of section 16, Township 20 north, and Range 101 West. The thickness of the Weber Sandstone at this location is 200m. There are a total of 27 nodes within the Weber Sandstone in this well, and 16 nodes within the Weber Sandstone were used for injection. In the homogeneous property case, the reservoir petrophysical properties were held constant. The porosity of the Weber Sandstone was assigned to 10%, and the permeability to 1md. The permeability for confining layers of the Amsden below and

the Dinwoody, Chugwater above are assigned to be 0.01md. A series of injection simulations for the Weber Sandstone were performed (injection rates of 0.5Mt/year, 1Mt/year, and 1.5Mt/year).

The results, presented in this section, are based on simulations that span 50 years of injection into one well that was completed in the Weber sandstone with 50 years of observation after the injection ceased. Fifty years of injection is chosen to simulate CO_2 storage corresponding to a typical lifetime of a coal-fired power plant in North America.

The injection rate of 1Mt/year, 0.75Mt/year, 0.5Mt/year, and 0.3Mt/year were tried using a heterogeneous reservoir property model described in previous sections, but the injection rate is limited to 0.3Mt/year for the 50-year injection period. The other three higher injection rates caused the simulation to stop early in the simulation due to serious convergent errors or excessive reservoir pressure elevations. It is concluded that heterogeneities within the porosity and permeability distributions in the Weber Sandstone have a significant effect on the CO_2 injection rates.

Injection into the Madison Limestone

The same artificial injection well located in the section 16, Township 20 north, and Range 101 West was used for the CO_2 injection simulations for the Madison Limestone with homogeneous reservoir property. There are total 16 nodes within the Madison Limestone interval in this well, and 12 nodes were used for CO_2 injection. The thickness of the Madison Limestone at this location is 120m. For the homogeneous property case, the porosity of the Madison Limestone was assigned as 10%, and the permeability as 1md. The permeability for confining layers of the Amsden the Dinwoody, Chugwater above are assigned to be 0.01md. Like the case for the Weber Sandstone previously described, a series of injection simulations for the Madison Limestone were performed at various injection rates (injection rates of 0.5Mt/year, 1Mt/year, and 1.5Mt/year).

The reservoir-property heterogeneities of the Madison Limestone are obvious in the RSU modeling domain. The porosities within the modeling domain range from less than 1% to over 20%, and permeabilities range from 0.001md to over 100md. Three wells located in the higher, medium, lower reservoir quality areas were chosen to evaluate the injectivity and storage capacity of the Madison Limestone along with various injection rates in the modeling domain (**Figure 72**). The characteristics of the reservoir heterogeneity were discussed in more detail on page 82 under “Establish reservoir heterogeneity through correlation seismic attributes with well log parameters and core observations.”

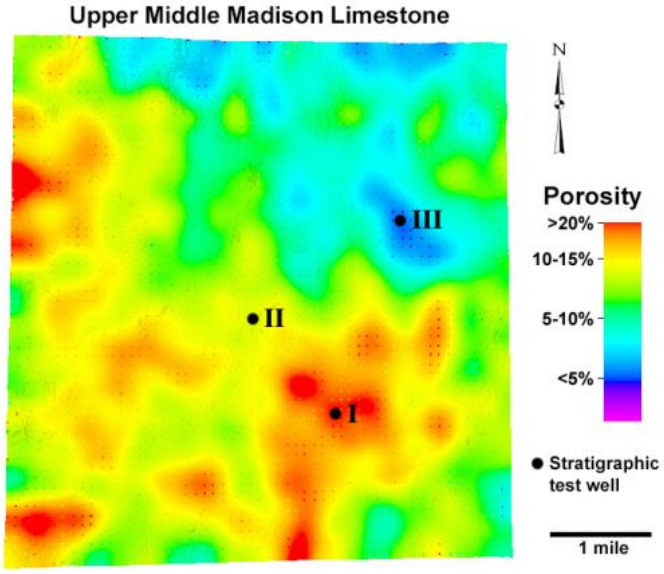


Fig.72. The porosity distribution of the Upper-Middle Madison Limestone within the storage domain. Three wells located in the higher, medium, lower reservoir quality areas are chosen to evaluate the injectivity and storage capacity of the Madison Limestone in the RSU geological CO_2 storage site.

Laboratory measurement of containment-mineralization and brine

Read full report in Appendix

Reactivity of Madison Limestone in water saturated supercritical CO_2

Injected carbon dioxide is stored at multiple scales in porous media, from the pore-level as a residual phase to large scales as macroscopic accumulations by the injection site, under the caprock and at reservoir internal capillary pressure barriers. These carbon dioxide saturation zones create regions across which the full spectrum of mutual CO_2-H_2O solubility may occur. Most studies assume that geochemical reaction is restricted to rocks and carbon dioxide-saturated formation waters, but this paradigm ignores injection of anhydrous carbon dioxide against brine.

A series of laboratory experiments was performed to evaluate the reactivity of the common reservoir mineral dolomite with water-saturated supercritical carbon dioxide. Experiments were conducted at reservoir conditions (55°C and 110°C, 25 MPa) and elevated temperature (220°C, 25 MPa) for approximately 96 hours and 164 hours (4 days and 7 days). Dolomite dissolves and new carbonate mineral precipitates by reaction with water-saturated supercritical carbon dioxide. Dolomite does not react with anhydrous supercritical carbon dioxide. Temperature and reaction time control the composition, morphology, and extent of formation of new carbonate minerals.

Mineral dissolution and re-precipitation due to reaction with water-saturated carbon dioxide may affect the contact line between phases, the carbon dioxide contact angle, and the relative permeability and permeability distribution of the reservoir. These changes influence fundamental properties of hysteresis of drainage and imbibition cycles, rock wettability, and capillary pressure. The efficacy of physical carbon dioxide trapping mechanisms, integrity of caprock, and injectivity of a carbon dioxide storage reservoir may be affected.

Reactivity of caprock in water-saturated supercritical carbon dioxide and carbon dioxide-saturated brine

Experiments were conducted to evaluate the reactivity of carbonate reservoir and shale caprock in both H_2O-saturated CO_2 and in CO_2-saturated brine for the potential CCS reservoir on the RSU. Experiments were conducted on cuttings of Madison Limestone from RSU #1. The nature of these cuttings was such that the experiments failed to yield useable data for this report. Suitable samples of caprock of the Rock Spring Uplift were unavailable at the time this study was implemented. Instead, two shales that represent the spectrum of shale caprock compositions, from silicate-rich to carbonate rich, were evaluated.

These results are also broadly applicable to understanding the reactivity of silicate-rich reservoir rock (e.g., Weber Sandstone) and carbonate-rich reservoir rock (Madison Limestone). Enhanced carbonate and silicate dissolution occurs in response to injection of supercritical CO_2. Re-precipitation of carbonates and silicates buffer the pH and alter the textures of the shale. Anhydrite precipitation may occur in response to injection of supercritical CO_2, which possibly will decrease the porosity and permeability of the shale and enhance its sealing characteristics. Clay dissolution/precipitation likely occurs and the compositional/structural changes likely affect the porosity, permeability, and wettability of the shale and possibly the large-scale basinal properties.

Rate of Mineralization

Assuming dissolution rates equal precipitation rates, the rate of carbonate mineralization in carbonate-rich rocks is 1.1×10^{-4} mol calcite m^{-2} of pore space s^{-1} (3.6×10^{2} kg calcite m^{-2} of pore space $year^{-1}$). Mineralization only takes place after the immiscible supercritical CO_2 phase dissolves into the brine. No carbonate mineralization rate can be calculated for silicate-rich rocks on the time frame of the laboratory experiments. By inference, this rate must be much less than the rate calculated for the carbonate-rich rocks. Data and analysis is presented in Part II of this report.

Dissolution rate of CO_2 into brine

A minimum CO_2 dissolution rate of 2.5×10^{-3} CO_2 mol m^{-2} pore space s^{-1} (3.5×10^{3} kg CO_2 m^{-2} pore space $year^{-1}$) was determined for silica-rich mudstone and, by inference, sandstones such as the Weber Sandstone. A minimum CO_2 dissolution rate of 4.7×10^{-4} mol CO_2 m^{-2} pore space s^{-1} (6.5×10^{2} kg CO_2 m^{-2} pore space $year^{-1}$) was determined for carbonate-rich mudstone and, by inference, carbonates rocks such as the Madison Limestone.

Determination of Confining Layer Integrity and Permanence
Select potential confining layers for petrographic and laboratory analyses

Determination of Confining Layer Integrity

Selecting potential sealing lithologies

As outlined earlier, core was extracted from three potential sealing lithologies; the lower Triassic section, the Pennsylvanian/Mississippian Amsden Formation, and the limestone lithofacies of the Mississippian Madison Limestone. These units were evaluated for potential sealing capacity, pore character, lithology, and regional lithologic continuity.

Lower Triassic section

Approximately 90ft (27m) of core was recovered from the lower Triassic section (**Table 1**). Thin section analysis identified lithology that is dominantly hematite-stained siltstone with shale, mudstone, evaporite, clastic grains of quartz and feldspar, heavy accessory minerals, ooids, glauconite, intraclasts of mudstone and limestone, replacive dolomite, and abundant calcite and anhydrite cement (**Fig. 73**). This suggests deposition in a shallow, evaporative, oxidizing marine environment. Post-burial diagenetic alteration includes the formation of potassic clays and secondary cements of anhydrite and calcite. Multiple zones within the core are pale green to white, indicating burial-related reduction of hematite. Petrographic analysis shows that primary pore space was filled by cementation, and that burial diagenesis resulted in clay formation. This enhances overall sealing capabilities.

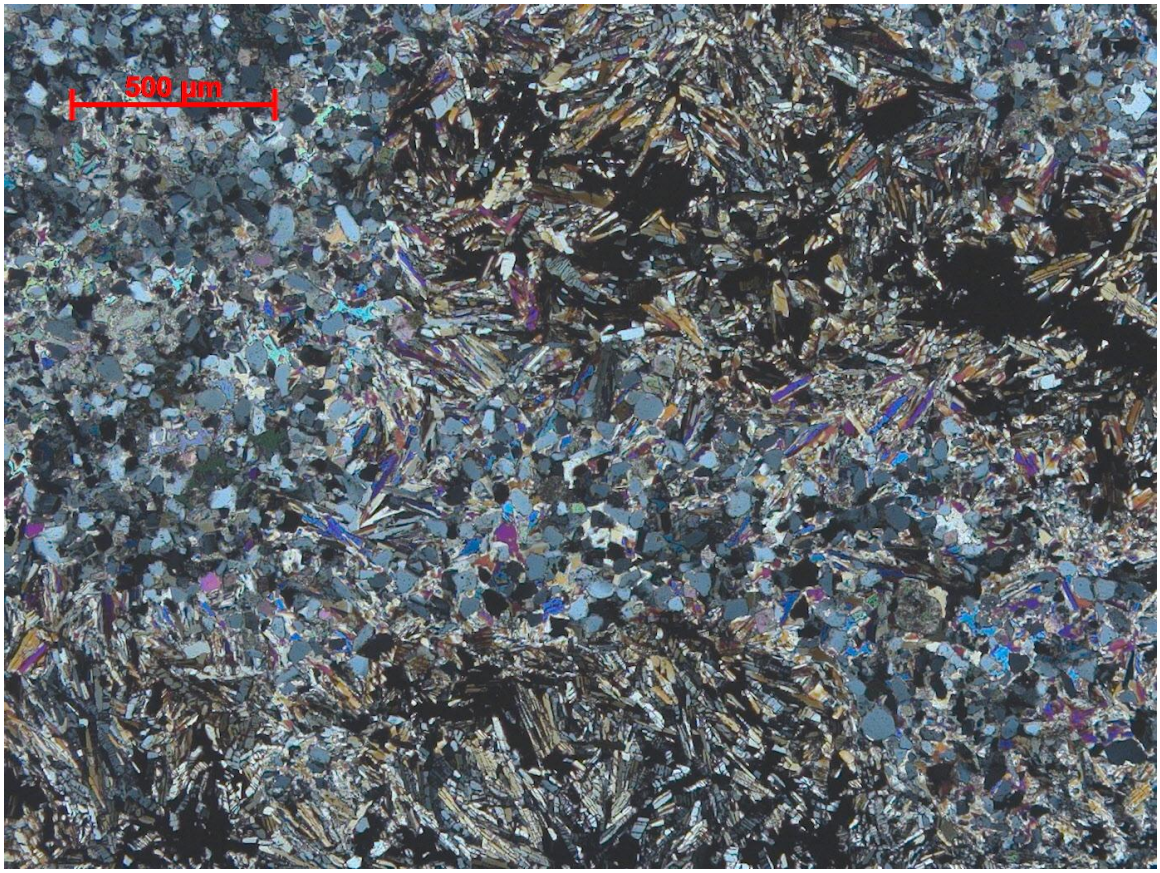


Fig. 73: Lower Triassic siltstone with nodules of evaporite (hematite and halite) and calcite cement.

Further core analysis for porosity, permeability, and mercury capillary displacement pressure was implemented. Porosity ranges from 0.62% to 1.4%, and permeability is less than 0.001mD (reservoir conditions) (**Table 5, 6**). Pore throat radii are < 2 μ, ranging between 0.001 μ and 1.6 μ (**Table 6**). Displacement pressures, calculated from mercury capillary injection tests, range between 939 psi and 2,718 psi (6,474 kPa and 18,740 kPa) (**Table 6**). Column height calculations for the lower Triassic seal result in heights from 300ft to 1900ft., based on the work of Chiquet et al. (2007) and Daniel and Kaldi (2008). The contact angle of super critical CO_2 is not currently understood, which results in the wide range of possible values, as well as possible overestimation of the column height. Also, these calculations are based on only four samples from the seal, and may not fully represent the lithologic variation. The effect of supercritical CO_2 on the fluid entry into pore throats has not been characterized, so column height calculations contain some uncertainties.

Sample No.	Sample Depth		Permeability				Porosity		Density
			800 psi NCS		Reservoir NCS		800 NCS	Res. NCS	
			Air	Klinkenberg	Air	Klinkenberg	Porosity	Porosity	
	(ft)	(m)	(mD)		(mD)		(percent)		(g/cm^3)
Lower Triassic section									
1	10,601.9	3,231.5	0.005	0.002	0.001	0.000	1.64	1.00	2.71
120	10636.3	3,241.9	0.11	0.075	0.001	0.000	1.79	0.62	2.73
125	10671.8	3,252.8	0.01	0.005	0.001	0.000	2.54	1.43	2.67
18	10,682.1	3,255.9	0.003	0.001	0.001	0.000	1.24	0.79	2.69
Amsden Formation									
186	12170.3	3,709.5	0.016	0.008	< 0.001	< 0.001	2.05	0.59	2.68
190	12198.95	3,718.2	0.159	0.21	0.028	0.045	3.62	2.04	2.80
195	12215.6	3,723.3	0.183	0.129	< 0.001	< 0.001	2.90	1.27	2.64
199	12224.6	3,726.1	0.002	< 0.001	< 0.001	<0.001	4.98	2.58	2.83

Table 5: Porosity and permeability measurements of core samples from sealing lithologies

Sample ID	Interval Depth (ft)	Helium Porosity (%)	Formation ID	Sample Type	Grain Density g/cc	Mercury/Air Displacement Pressure (psi)	Pore Throat Distribution			Swanson	
							Micropores < 0.1 micron (%PV)	Intermediate 0.1-3 micron (%PV)	Macropores > 3 micron (%PV)	Brine Permeability (mD)	Air Permeability (mD)
1	10601.9	1.01	Triassic	Core Plug	2.71	939.71	90.15	9.84	0.000	0.000	0.000
4	10605.8	ND	Triassic	Core Plug	ND	1,140.44	82.09	17.90	0.000	0.000	0.000
16	10656.4	ND	Triassic	Core Plug	ND	2,718.73	54.80	45.19	0.000	0.000	0.000
18	10682.1	0.99	Triassic	Core Plug	2.69	1,521.42	86.79	13.20	0.000	0.000	0.000
53	12197.4	4.95	Amsden	Core Plug	2.64	1,381.10	83.32	16.67	0.000	0.001	0.005
187	12178.1	ND	Amsden	Core Plug	2.91	No Injection	0.000	0.000	0.000	0.000	0.000
200	12227.3	ND	Amsden	Core Plug	2.85	No Injection	0.000	0.000	0.000	0.000	0.000
59	12250.0	0.42	Madison	Core Plug	2.63	1253.69	100.00	0.000	0.000	0.000	0.000
206	12301.1	ND	Madison	Core Plug	2.74	No Injection	0.000	0.000	0.000	0.000	0.000
214	12333.9	ND	Madison	Core Plug	2.83	3630.11	100.00	0.000	0.000	0.000	0.000

Table 6: Mercury injection capillary pressure analysis and pore throat distribution of sealing lithologies

Low measured porosity, permeability, and pore throat radii are ideal properties of seals. Confining properties are attributable to both deposition and diagenetic alteration. Primary depositional features that augment sealing characteristics of the siltstone include fine-grained impermeable shale, mudstone, intraclasts of mudstone and carbonate, and anhydrite. Post-burial diagenetic alteration of fluids and minerals also enhanced the holding capacity of the siltstone, specifically through the precipitation of secondary cements and oriented potassic phyllosilicates. The ductility of these rocks also makes them less likely to fracture, further enhancing its sealing efficiency.

The Amsden Formation

Approximately 56ft (17m) of core was recovered from the base of the Amsden Formation (**Table 1**). Thin section analysis indicates the Amsden is composed primarily of shaly carbonates and clastic beds, and also contains collapse breccia, dolomite, limestone, mudstone, shale, clastic carbonate, evaporites, heavy accessory minerals, minor bimodal sands with glauconite, and intraclasts of mudstone, sandstone and carbonates (**Fig. 74**). Deposition likely took place in a fluctuating marine environment, with episodes of subaerial exposure. Diagenesis was pervasive; aside from remnant beds of fossiliferous limestone, much of the formation has been diagenetically altered or recrystallized.

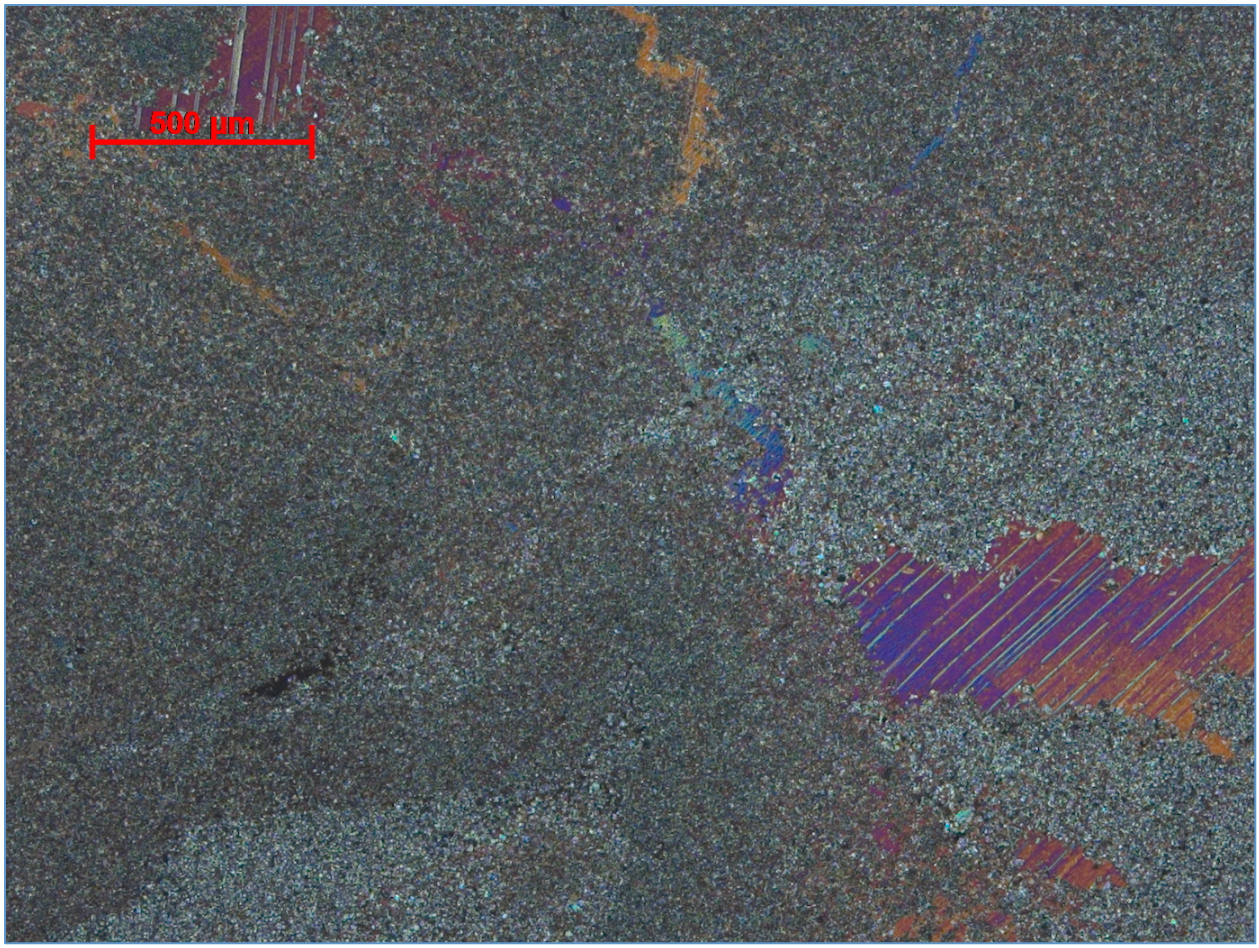


Fig. 74: Siliceous carbonate of the Amsden Formation.

Core was analyzed for porosity, permeability, and mercury capillary displacement pressure. The measured porosity ranges from 0.59% to 4.6%, and permeability ranges from < 0.001mD to 0.005mD (reservoir conditions) (**Tables 5, 6**). Pore throat radii were <3 μ, ranging between 0.008 μ and 2.5 μ (**Table 6**). Displacement pressures, calculated from mercury capillary injection tests, range between 1,381 psi to greater than 20,000 psi (9,521 kPa and 137,895 kPa) (**Table 6**). Analyzed displacement pressures indicate that the Amsden Formation can contain a gas column in lower reservoirs.

The low measured porosity, permeability, and pore throat radii of the Amsden are ideal properties for seals. Confining properties can be attributed to diagenetic alteration and fine-grained nature of primary depositional clasts. Unlike Madison dolostones, Amsden dolostones are largely devoid of pore space. There is evidence of pre-existent moldic, vuggy, channel, and vein porosity, but most pore-space has been filled with cements. Clastic lithofacies in the Amsden are heavily cemented with diagenetic clay, silica, or carbonate, and have low porosity.

The Upper Limestone Unit of the Madison Limestone

Approximately 74ft (23m) of core was recovered from the upper limestone unit in the Madison (**Table 1**). Petrographic analysis identifies multiple facies including limestone, minor mudstone and clastic carbonate, and collapse breccias. Core recovered from the well site is composed primarily of biomicrites and biosparites (**Fig. 75**). It contains post-depositional textures and minerals such as bioturbation, silica cement, stylolites, pyrite, and mineralized veins. Deposition commenced in a prograding, shallow marine environment with periods of subaerial exposure. Many of the textures observed in the limestone facies are primary, as diagenesis was limited to vug-, mold-, and vein-filling cement, sulfate reduction, and pressure solution.

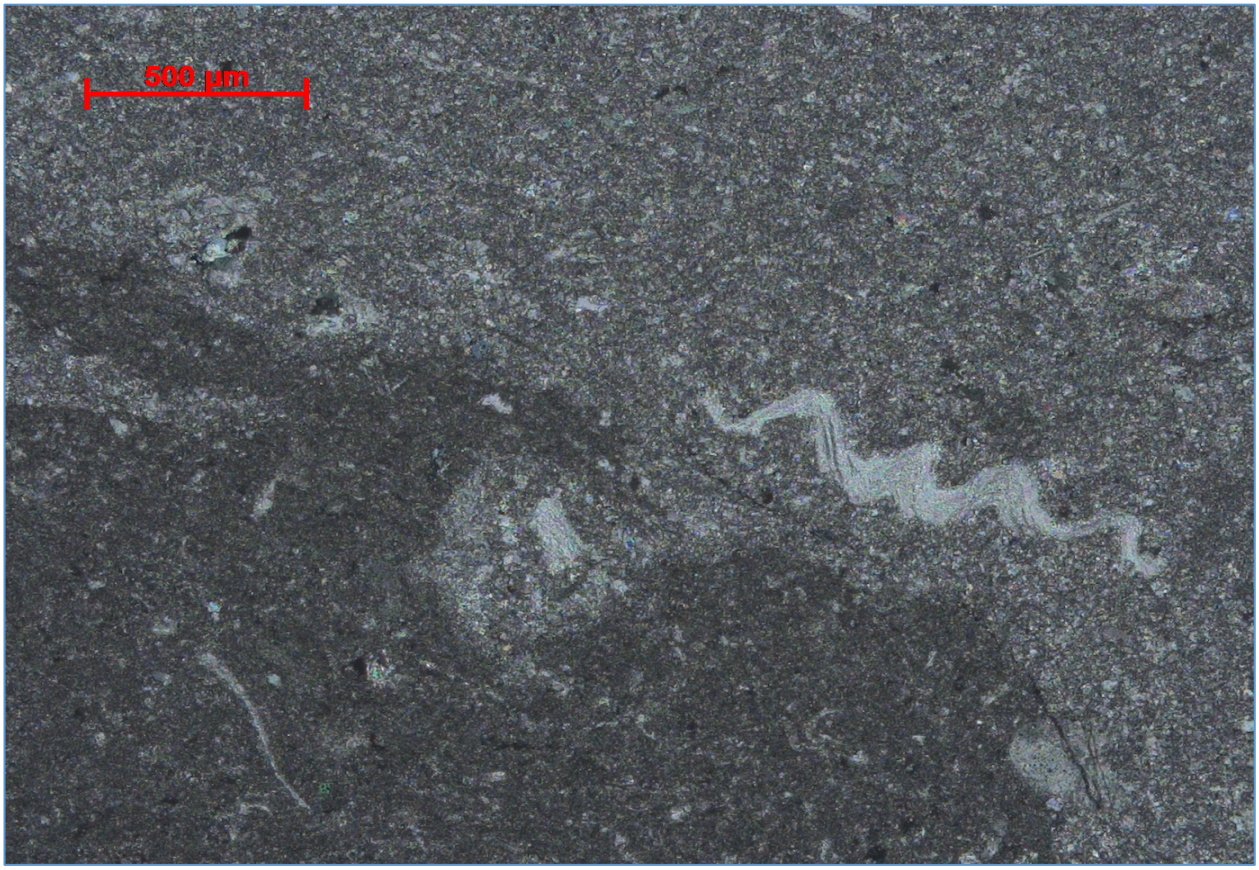


Fig. 75: Biomicrite in the Madison Limestone. This thin section was taken less than 10cm from the porous dolostone unit.

Core was analyzed for porosity, permeability, and mercury capillary displacement pressure. The measured porosity ranges from 0.2% to 0.42%, and permeability is <0.001mD (reservoir conditions) (**Tables 5, 6**). Pore throat radii are <0.3 µ, ranging between 0.05 µ and 0.25 µ (**Table 6**). Displacement pressures, measured by mercury capillary injection, range between 1,253 psi and greater than 20,000 psi (8,639 kPa and 137, 895 kPa) (**Table 6**). Analyzed displacement pressures indicate that the upper limestone can contain a gas column in lower reservoirs.

The low measured porosity, permeability, and pore throat radii of the upper limestone unit are ideal properties of seals. These confining properties are attributable to deposition and minor diagenetic cementation. Fine-grained depositional micrites, primary carbonate textures that compose most of the core, generally lack porosity. The molds and vugs in biomicrites are filled with diagenetic cements of silica and calcite, as are veins and fractures.

Regional Seal Lithology Correlation

Well logs from regional hydrocarbon fields across the RSU were correlated with the RSU#1 well log suite. The goal was to determine the lateral extent and lithologic heterogeneity of seal lithologies. Petrophysical data from adjacent fields including the North Baxter Basin Field, the Table Rock Field, and the Brady Field indicate that the lower Triassic section and the Amsden Formation are lithologically similar and may be laterally continuous across the RSU. The confining properties of these units are proven in the aforementioned fields, where they effectively trap hydrocarbons and CO_2. Oil field data also identifies the upper limestone unit of the Madison as an effective seal in portions of the Greater Green River Basin, though it is missing in other portions of the basin (WOGCC 2013).

Summary of Confining Layer Integrity

Of the three studied confining layers, all were shown to contain the capability to effectively seal the targeted reservoirs. Calculated CO_2 column heights from the lower Triassic unit, which recorded the lowest displacement pressures, indicate the capacity to retain a gas column in underlying reservoirs. Petrographic analysis, correlated to measured displacement pressures and porosity character, indicates sealing capacity is related to a combination of original depositional environment, mineral character, and diagenetic alteration. Of the three units, the Amsden has the greatest overall holding capacity. However, all three confining layers could successfully retain a full CO_2 gas column injected in either the Weber or the Madison reservoirs. This study concludes that there are multiple, competent seals at the study site and these formations are laterally extensive across the RSU.

Establish Dissolved gas composition for the targeted reservoir intervals

The composition of dissolved gases in Weber and Madison formation fluids is unique to each formation (**Appendix – Water Quality Data, pg. 441, Fig. 76**). Though the total abundance of gas in both formations is dominated by three species – nitrogen, carbon dioxides, and alkanes – the concentrations are markedly different (**Appendix – Water Quality Data, pg. 441, Fig. 76**). Nitrogen is the dominant gas species (approximately 79%) in fluids from the Weber Sandstone, followed by carbon dioxide (approximately 15%) and alkanes, mostly methane and hexane (approximately 6%). Carbon dioxide is the dominant gas species (approximately 83%) in fluids from the Madison Limestone, followed by nitrogen (approximately 17%) and a minor alkane component (<1%).

The dissimilarities of gases within formation fluids suggest that the reservoirs are not mixing as the evolution of fluid and gases within each reservoir is distinct. These data, along with the water chemistry analysis, suggests that the Weber and Madison formation fluids are isolated and injected CO_2 is not likely to migrate between reservoirs.

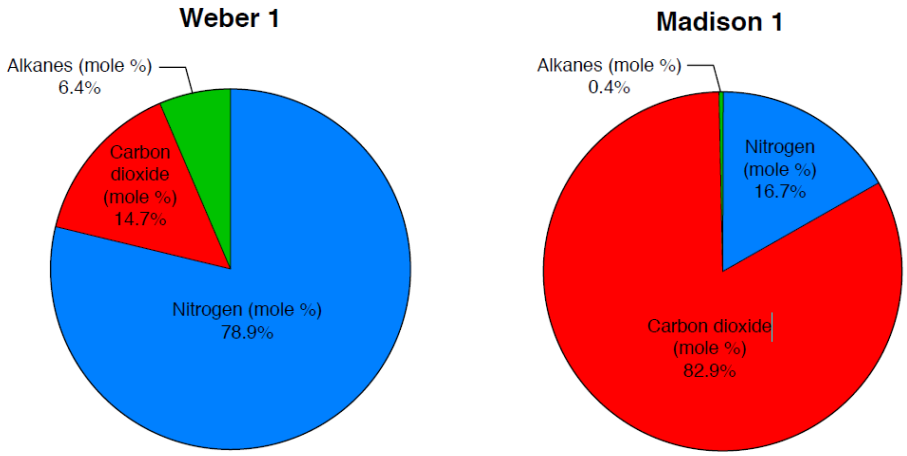


Fig. 76. Dissolved gas compositions

Evaluate confining layer continuity using seismic attributes

Any lithology can serve as a seal for sequestration purposes. The only requirement is that minimum displacement pressure of the lithologic unit comprising the sealing surface be greater than the buoyancy pressure of the injected CO_2 column in the reservoir rock. Even a few inches of ordinary clay shale are theoretically adequate to trap very large column heights of injected gas. Unfortunately, there is a low probability that a zone only a few inches thick could be continuous, unbroken, and maintain stable lithic character over a sizable reservoir. The benefits of a very thick seal are that it provides many layers of contingent sealing beds and a larger probability that a sealing surface will actually be distributed over an entire prospect.

About a 1000 ft thick confining shale interval within the Chugwater and Dinwoody Formations is characterized by increased impedance values and relatively homogeneous appearance (**Fig. 77**). This allows interpretation of these shales as low-porosity, thick, and laterally continuous.

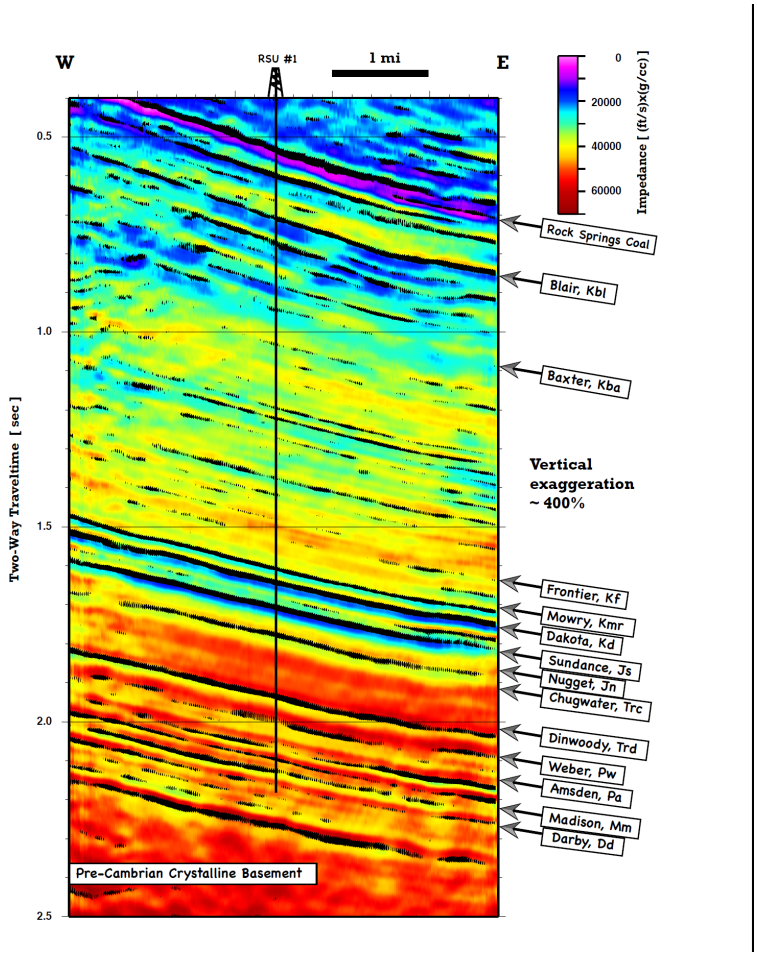


Fig. 77. Interpreted west–east profile through the acoustic impedance volume at RSU #1. The color-coded impedance image is co-rendered with seismic amplitude section

Faulting and fracturing can act as fluid flow barriers creating compartmentalization when they are shale filled or hydrothermally altered. In other situations, the faults and fractures that cause heterogeneity can act as a fluid-flow conduit. Thus, it becomes imperative to understand these features and map their distribution in the study area. Efforts are directed at the Middle Madison chert reservoirs that have been diagenetically altered through hydrothermal processes. Typically for a karsted carbonate region, the chert horizons display an irregular, heterogeneous surface. Sinkholes, cockpit karsts, frying-pan valleys, and collapse systems are some of the features that are generally associated with Paleozoic karsted carbonate regions (Elebiju et al, 2011). Most of these features exhibit polygonal shapes that may result from subaerial karst processes, cavern collapse, hydrothermal alteration and dissolution, faulting, or a combination of these processes.

Seismic coherency is a measure of the consistency of a seismic reflection. Where events are continuous, coherency is high. But where events are terminated either by faulting or stratigraphy, there is a lack of continuity, which is clearly evident as dark areas on coherency displays. Coherence, curvature, and amplitude gradient attributes computed from the seismic data facilitate mapping of karst features and associated fracture patterns.

In this study, volumetric seismic attributes such as amplitude gradient attribute and semblance-based coherence were used to better characterize subtle features such as collapse features and fracturing within the Triassic and Pennsylvanian confining layers. **Fig. 78a** shows an overall high continuity of reflections within the major reservoir rocks and confining layers. However, on the corresponding coherency section shown in **Fig. 78b**, the faults show up very clearly. The interpreted faults are more readily apparent where the coherence is mapped over the interpreted horizons (red arrowheads in **Fig. 79**). A joint interpretation of vertical sections together with the stratal (horizon) slices makes spatial interpretation a simpler task. Thus, an orthogonal system of faults northeast of RSU #1 was identified in the coherence data (**Fig. 78b and 79a**).

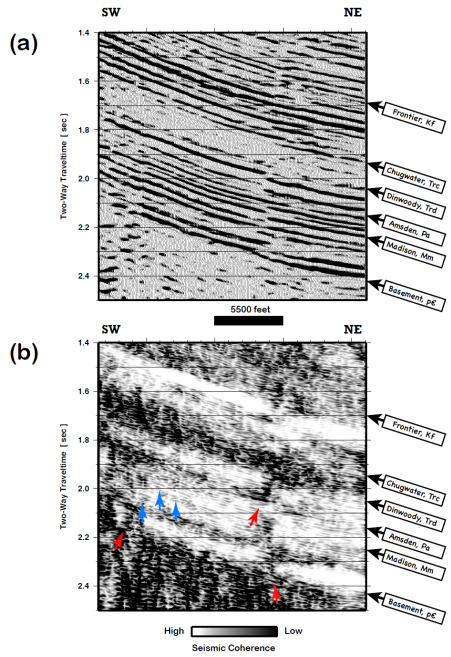


Fig. 78. Interpreted southwest-northeast profile through seismic amplitude volume (**a**) and corresponding coherency section (**b**). Seismic amplitude variations (**a**) are presented with conventional variable area wiggle trace display method, while coherency (**b**) is shown in shades of gray-scale. The red arrowheads indicate basement-involved faults. The blue arrowheads point at near-vertical features that we interpret as dissolution pipes.

The coherence horizon slice on top of the Middle Madison horizon exhibit an overall high continuity southwest of RSU #1 (the up-dip direction). There are only a few isolated dark areas that do not form any trend (**Fig. 79a**). However, at the Dinwoody level, the presence of isometric incoherent features become more dominant, especially about one mile south and southwest of RSU #1 (**Fig. 79b**). The evidence presented in **Fig. 79** suggests that the low-coherence, oval-in-shape planforms originate at or above the Middle Madison chert horizon. Correspondingly, we interpret these features as dissolution pipes or collapse features. Dissolution pipes form by dissolution of rock units at depth to produce subsurface cavities that promote instability in the overburden leading to collapse. They are thus likely to occur in areas of evaporate or carbonate karst. Seismically the pipes produce near-vertical zones lacking reflection's continuity (in the section views), and isolated, low-coherent planforms in map view (Cartwright et al, 2007).

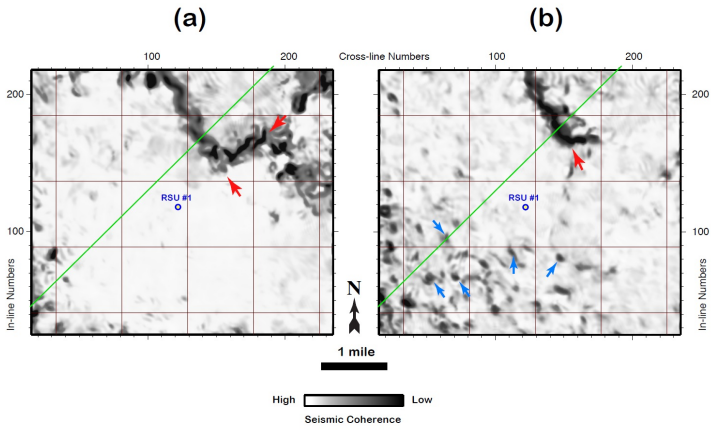


Fig. 79. Interpreted stratal slices through seismic coherency volume: (**a**) at the Middle Madison stratigraphic level, (**b**) at the Dinwoody level. Seismic coherency variations are displayed in shades of gray-scale. Note an orthogonal system of faults (red arrowheads) northeast of RSU #1 (**a**), and oval dark planforms southwest of the well along the sealing horizon (blue arrowheads in (**b**)) that are interpreted as dissolution pipes (karst collapse features). The green lines on both panels show location for vertical sections in **Fig. 77**.

Regional and Study Site Geologic Structural Characterization

RSU and study site fault characterization

Analysis of faults exposed at the surface of the RSU was achieved through field data collected on the orientation of fractures and faults at the surface. These data were plotted on stereonets and used to make rose diagrams and dip frequency plots. The subsurface interpretation utilized well log and seismic data, which were used to create structure contour maps, isopach maps, and cross sections.

Faults exposed at the surface of the RSU have been documented on several geologic maps of the area. These features change direction across the uplift and are interpreted to be influenced by oblique slip near the main thrust fault. The primary structural mechanism affecting these faults on the east flank, near the proposed injection site, is outer arc extension. Outer arc extension results from the flexure of the arching layer, and is not expected to reach great depths. This interpretation was based on over 1000 fracture measurements across the RSU, which indicate dominant N-S hinge-parallel extension, and NNW extension localized on the western flank. This interpretation is corroborated by seismic data, which show no offset of layers at depth with observed surface faults (**Fig. 80**).

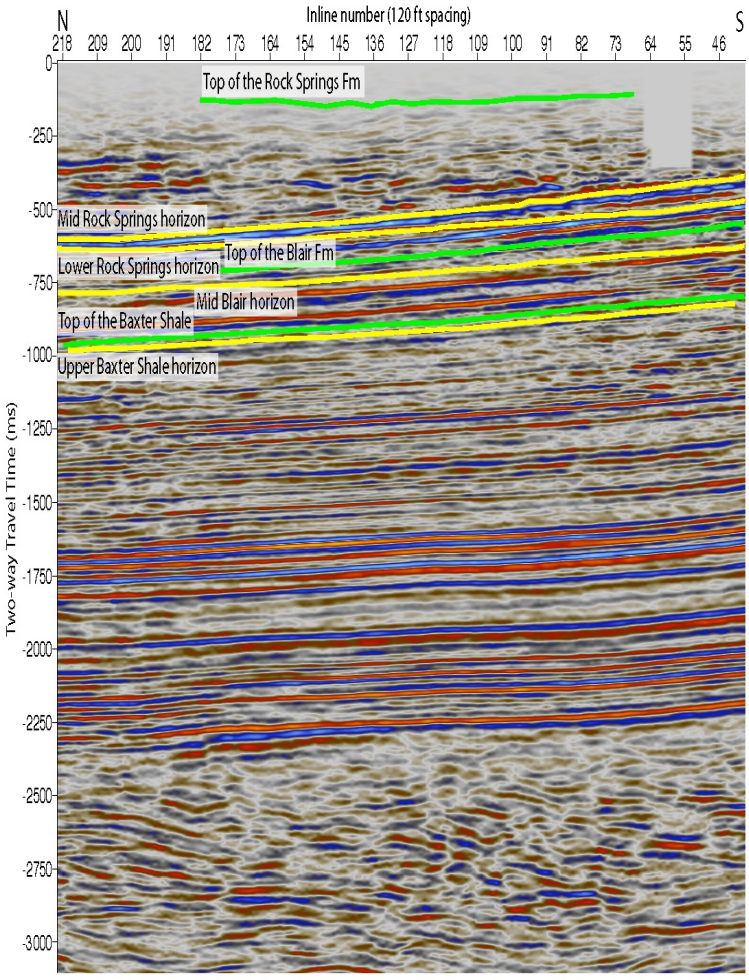


Fig. 80. Interpretation of crossline though seismic data over RSU. Crossline was chosen to intersect faults mapped at the surface; no fault offset is seen at depth. From the MS thesis of Bridget Garnier, in prep.

Isopach maps created from well tops on each surface show slight possible fault offset, but are also affected by thickness changes due to transgressions and regressions, as well as shoreline and delta movement. The Rock Springs and Blair formations show possible active faulting during deposition (**Fig. 81**).

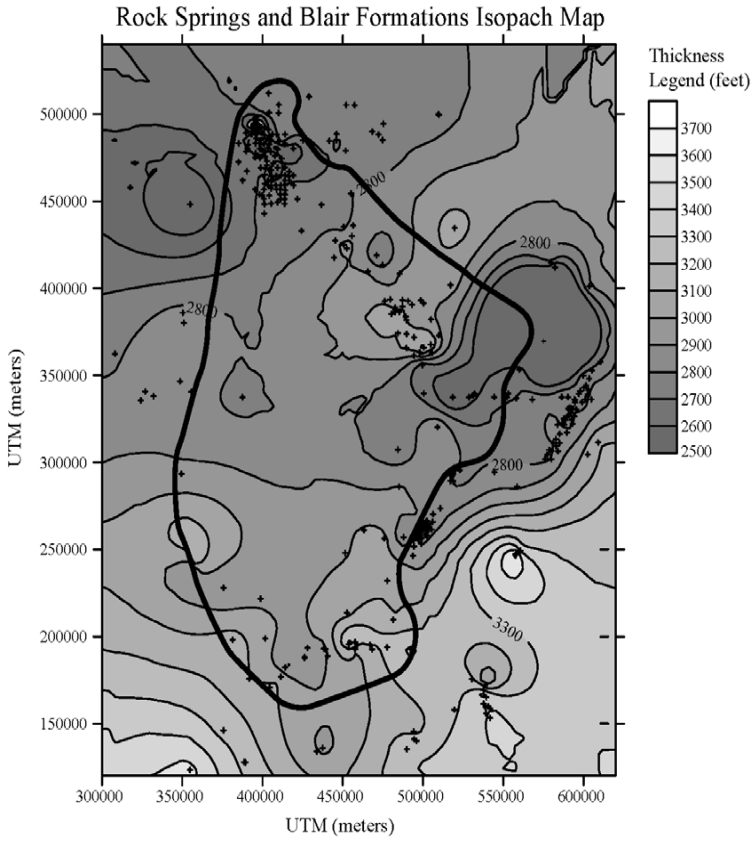


Fig. 81. Isopach map of the Rock Springs and Blair formations (100ft contour intervals). Black dots indicate location of data points. From the MS thesis of Bridget Garnier, in prep.

The faults exposed at the surface on the eastern flank of the uplift are determined to be formed primarily due to outer arc extension, with minor contribution from gravitational collapse. Faults on the western flank also show a component of oblique slip from the blind thrust. These faults are not imaged in seismic data to depths beyond Cretaceous units. This suggests that the faults are unlikely to compromise the Triassic confining system.

Study site stress fields and geomechanical analyses

Fracture and geomechanical analysis of the injection zones were conducted through interpretation of well logs, image logs, fracture documentation in core, triaxial tests on core samples, Brinell Hardness tests on core samples, pore pressure tests, step rate injection tests, well temperature profiles, and micro-frac tests.

The dominant direction of unfilled subsurface fractures at the location of RSU #1 is ENE-WSW, correlative to the direction of regional structural features. The Weber and Madison formations are under-pressured, and the stress state is transitional between strike-slip and normal faulting (**Fig. 82**). With very little pore pressure increase (1000 psi in the Weber, 1500 psi in the Madison), the fractures will become critically stressed and hydraulically conductive in the ENE-WSW direction (**Fig. 82).** Higher injection pressures will cause a wider range of fracture orientations to become permeable.

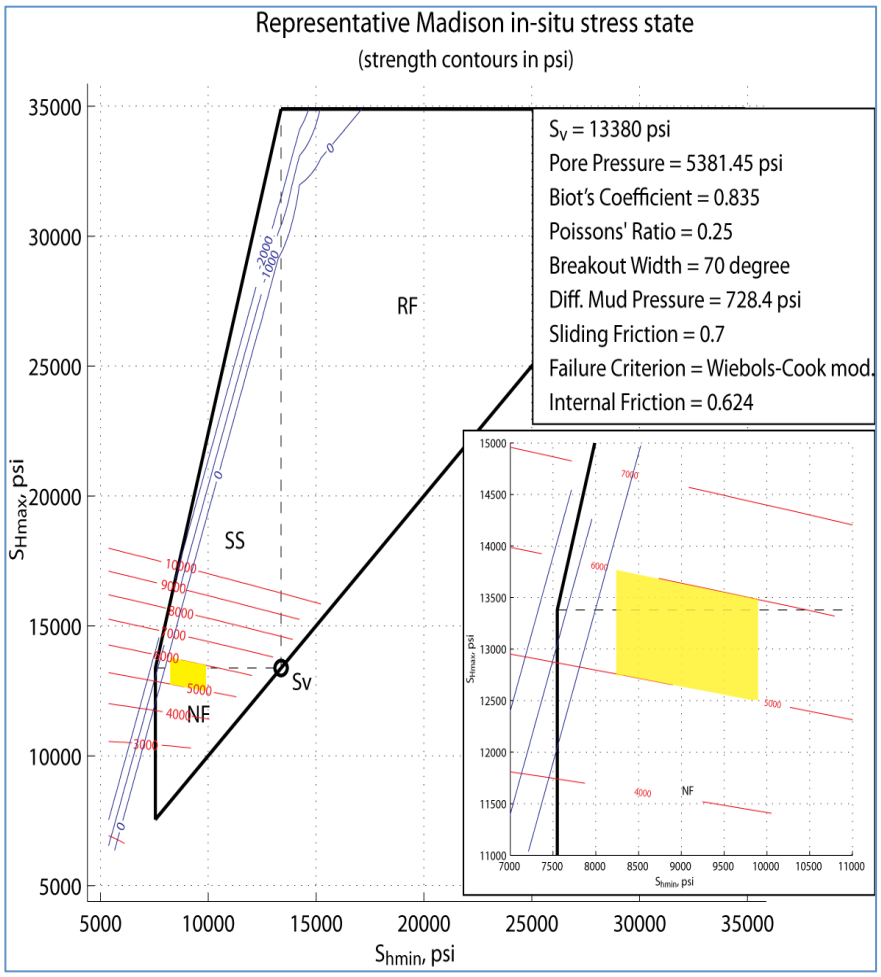


Fig. 82. Stress polygon and associated strength contours for the most likely stress state in the Madison. From the MS thesis of Luke Shafer (2013).

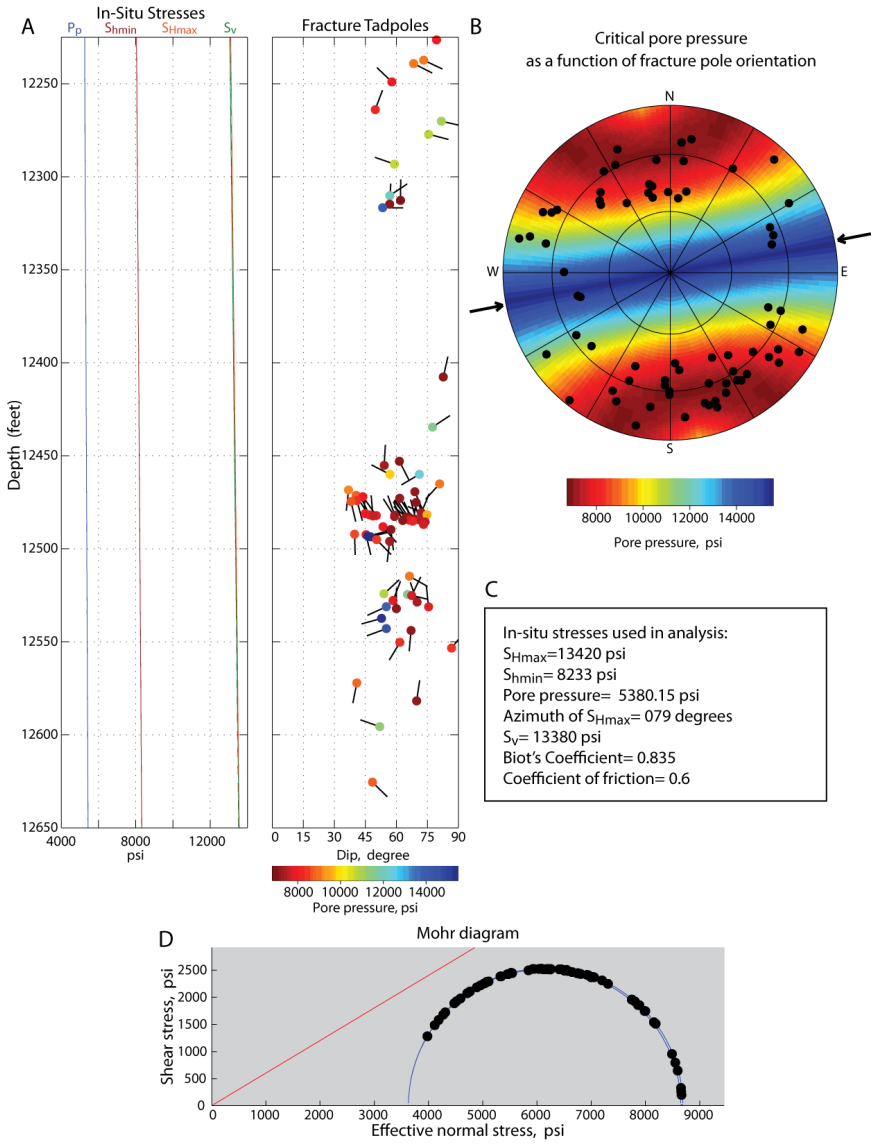


Fig. 83. (**a**) Most likely in-situ stresses in the Madison formation plotted relative to depth (left) and fracture tadpoles colored with respect to critical pore pressure (right). (**b**) Poles to Madison fractures plotted on a stereonet colored with respect to critical pore pressure. (**c**) Geomechanical parameters used in this analysis. (**d**) 3-D Mohr diagram with listed stresses used to construct Mohr circles and poles to fractures plotted as points. From MS thesis by Luke Shafer (2013).

Faults mapped at the surface of the RSU most likely do not pose a threat to the Triassic confining system. The fracture system in the reservoir indicates preferential permeability in the ENE-WSW direction. With injection of CO_2, the range of orientation of permeable fractures will increase.

Pressure management

Evaluate a range of potential CO_2 injection/storage scenarios for targeted reservoir intervals using numerical simulation techniques

Inject to the Weber Sandstone with homogeneous petrophysical properties

The simulation for the 1.0Mt/year of injection rate scenario at 10% of porosity, and 1md of relative permeability had pressures that remained well below hydro-fracture; 66Mt of pore fluids were displaced over the 50-year injection period to maintain the reservoir pressure below the hydro-fracture pressure. The reservoir pressure elevated quickly when the injection started, but kept below the hydro-fracture pressure throughout the duration of the injection. After the injection ceased, the reservoir pressure returned to original pressure within 10 years (**Fig. 84**). The injection rate of 1.5Mt/year resulted in elevating the reservoir pressure to fracture pressures early in the simulation.

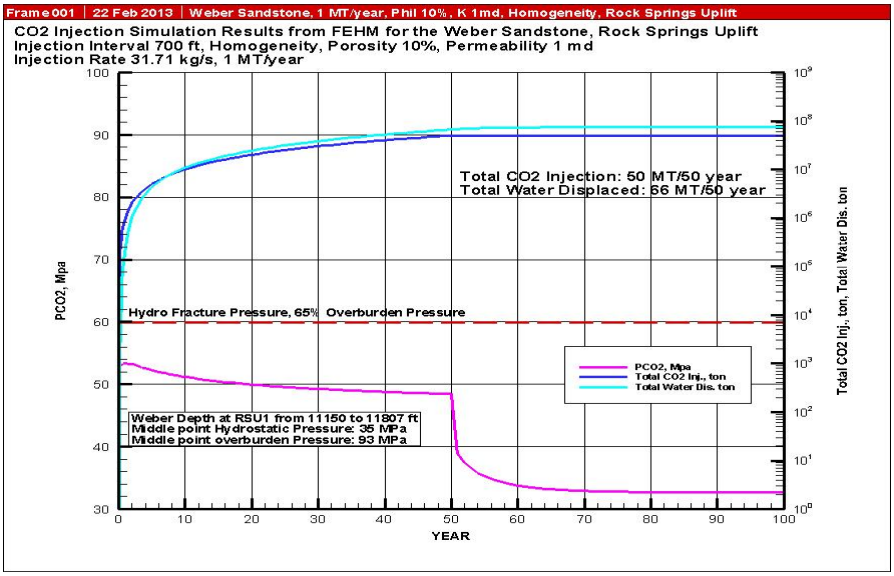


Fig. 84. FEHM CO_2 injection simulation results for the Weber Sandston, RSU. The simulation is for a homogeneous reservoir petrophysical conditions with 10% of porosity and 1md of relative permeability. The injection rate of 31.71kg/s is constant for 50 years, then the injection ceased, and the simulation continued to run for another 50 years without CO_2 injection.

Inject to the Weber Sandstone with heterogeneous properties

Injection rates of 1Mt/year, 0.5Mt/year, and 0.3Mt/year were run for the Weber Sandstone with heterogeneous petrophysical properties. However, only 0.3Mt/year case could be completed without exceeding the fracture gradient. With an injection rate of 0.3Mt/year, 15Mt CO_2 could be stored within the Weber Sandstone. In order to keep the reservoir pressure below the hydro fracture, 19Mt of formation water must be removed in same 50-year period (**Fig. 85**). The pressure changes are not uniformly distributed, and mainly occur around the injection well and at down dip directions where the boundaries are closed. There is no pressure elevation at the up dip directions where the boundaries are opened for the fluid flow moving out of the storage domain (**Fig. 86**).

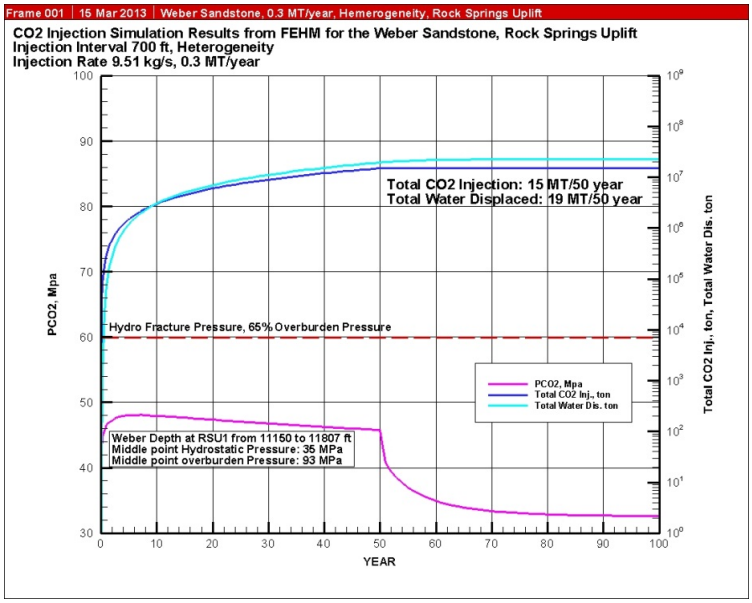


Fig. 85. FEHM CO_2 injection simulation results for the Weber Sandstone, RSU. The simulations are setup for a heterogeneous reservoir properties. The injection rate of 9.51kg/s is constant for 50 years, then the injection ceased, and the simulation continued to run for other 50 years without CO_2 injection.

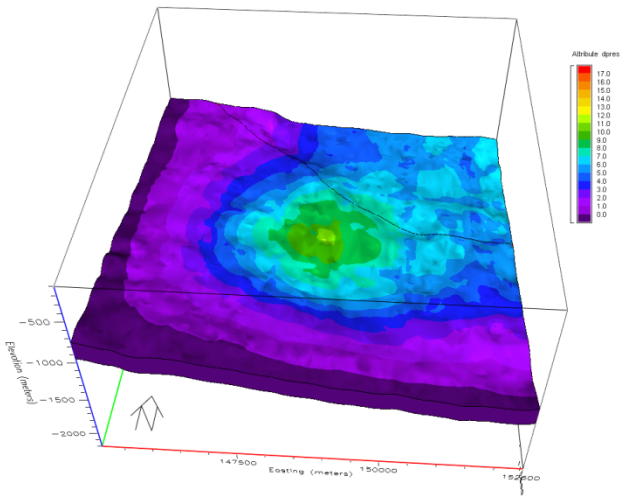


Fig. 86. The pressure changes of the Weber storage reservoir at the end of the CO_2 injection. The delta pressures are different between the reservoir hydrostatic pressure and the reservoir pressure at the end of 50-year injection.

The Madison Limestone with homogeneous properties

A series of injection simulations for the Madison Limestone were performed (injection rates of 0.5Mt/year, 1Mt/year, and 1.5Mt/year) with homogenous reservoir properties. The simulation for 1.0Mt/year, 10% porosity, and 1md of relative permeability had reservoir pressures that remained below hydro-fracture pressure (70% of the overburden pressure). The reservoir pressure elevated quickly when the injection started, then leveled off until the injection ceased at the beginning of 51st year; with a total of 59Mt of pore fluids displaced over the 50-year injection period in order to maintain the reservoir pressure below the hydro-fracture pressure. After the injection ceased, the reservoir pressure returned to original pressure within 10 years (**Fig. 87**). An injection rate of 1.5 Mt/year caused the reservoir pressure to exceed fracture pressure and stopped the simulation.

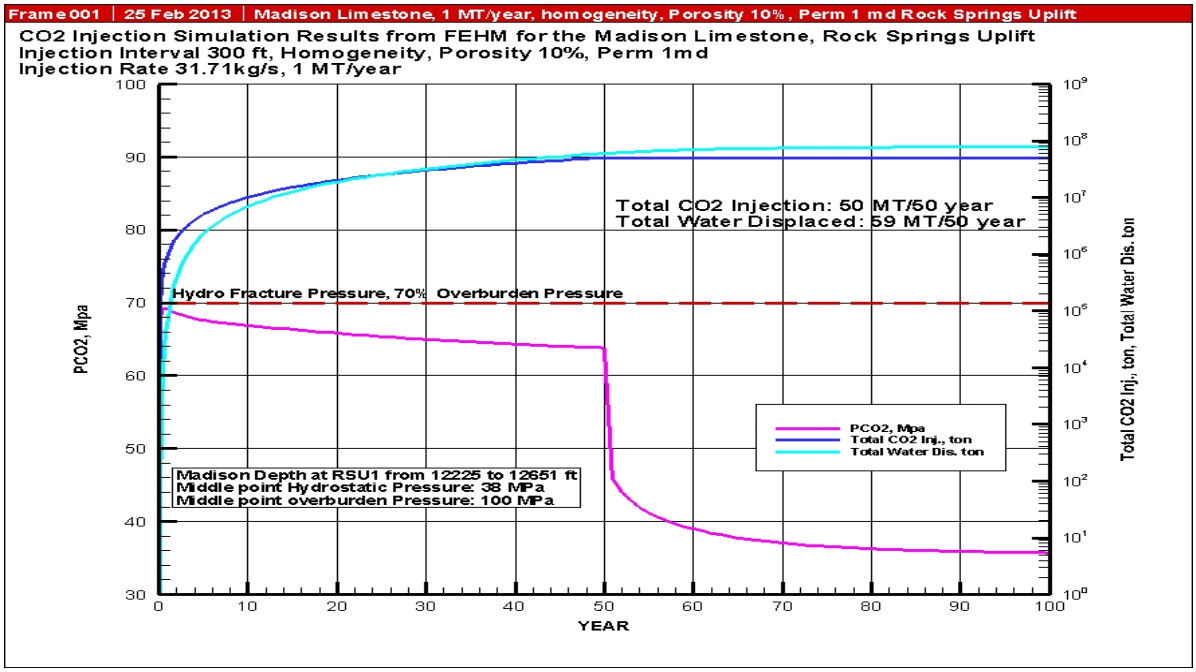


Fig. 87. FEHM CO_2 injection simulation results for the Madison Limestone, RSU. The simulation was setup for a homogeneous reservoir petrophysical conditions with 10% of porosity and 1md of relative permeability. The injection rate of 31.71kg/s is constant for 50 years, then the injection ceased, and the simulation still ran for another 50 years without CO_2 injection.

The Madison Limestone with heterogeneous properties

A series of injection scenarios for heterogeneous reservoir properties (High, medium, and low) (**Fig.72**), were run for the Madison Limestone. For the higher reservoir quality case, the fluid-pressure field reaches a quasi-steady state by four years after injection, and then decreases gradually. However, pressures in the medium and lower reservoir quality cases evolve gradually over the 50 years. Fluid pressure raises mainly in the injection horizon, with increased pressure of 1MPa–17 MPa in the Madison Limestone. For all three locations, the formation water must be displaced to create accommodation space and to keep the reservoir pressure below the hydro fracture pressure. Also for all injection scenarios, the reservoir pressure increases rapidly at the start of injection, and quickly attenuates to the reservoir hydrostatic pressure within 10 years after the injection ceases. The injectivity and storage capacities are much different between higher, medium, and lower reservoir quality areas. At the higher reservoir quality area, 50 Mt CO_2 could be injected and safely stored in the Madison Limestone during a 50-year period with injection rate of 31.71kg/s and 57Mt of formation water displaced (**Fig. 88b,** Well I). For the medium reservoir quality area, in order to keep the reservoir pressure below the hydro fractural pressure, only 25Mt CO_2 could be injected and safely stored in the Madison Limestone during a 50 year period with an injection rate of 15.85kg/s and 25Mt formation water displaced (**Fig. 88c**, Well II). Whereas at the lower reservoir quality area, only 10Mt CO_2 could be injected and safely stored in the Madison Limestone during a 50 year period with injection rate of 6.34kg/s and 12 Mt of formation water displaced (**Fig. 88d**, Well III). For all cases, the amounts of displaced fluid are on the same order as the amounts of the injected CO_2 in to the reservoirs.

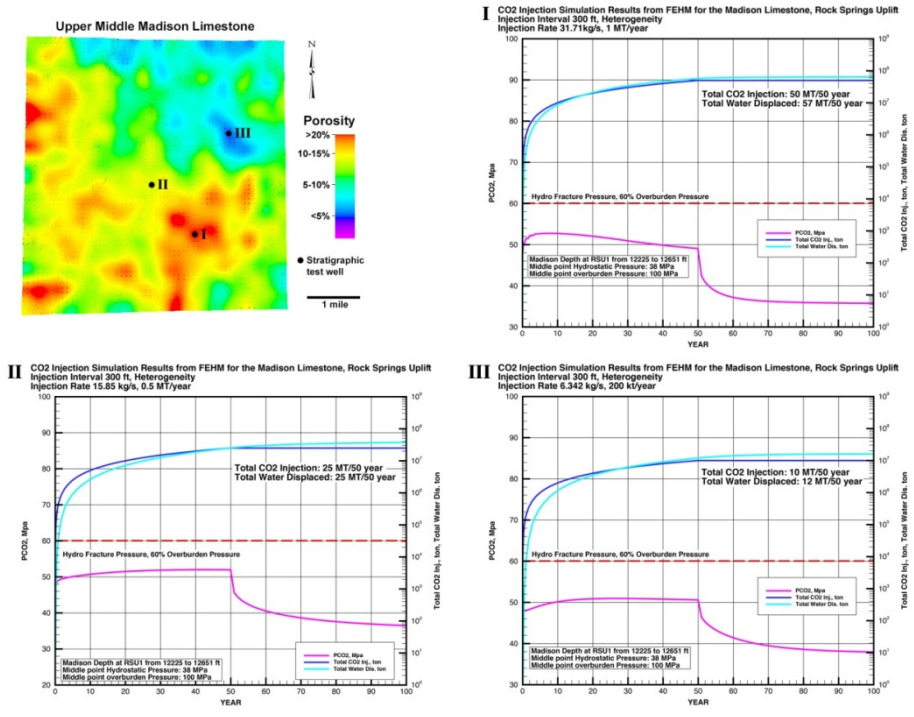


Fig. 88. FEHM CO_2 injection simulation results for the Madison Limestone, RSU. The simulations are setup for a reservoir with heterogeneous petrophysical. The injection rates of 31.71 kg/s, 15.85 kg/s, and 6.34 are constant for 50 years of injection at the Wells in the higher, medium, and lower reservoir quality areas, respectively. The injections continue for 50 years, then cease with the simulations continued to run for other 50 years without CO_2 injection.

Determine the CO_2 plume geometry, volume, and the rate of displaced fluid removal required to lower storage risks for each CO_2 injection/storage scenario.

The Weber Sandstone with homogeneous properties

Fig. 89 is an incline view of the injected CO_2 plume for the targeted Weber Sandstone after 50 years of injection of 1Mt/year with homogeneous reservoir properties. After 50 years of injection, the CO_2 plume has moved across the formation boundary of the Weber Sandstone into the Phosphoria Formation above and the Amsden Formation, and the Madison Limestone below. The map view of the plume with 1Mt CO_2 injection rate after 50 years of injection at a single well injection is nearly a circle with radio of 1,600m, covering an area of 8km^2 (**Fig. 90**).

The storage capacity of the Weber Sandstone for the entire RSU is estimated by assuming that the 3-D simulation domain in this study is a representative element of the whole structure. Therefore, once the volume of the CO_2 plume in the simulation domain (V_{plume}) and the volume of the Weber Sandstone in the whole RSU (V_{RSU}) are known, a simple approximation of the storage capacity (C) can be calculated by following equation:

$$C = V_{RSU} * V_{plume} \times M_{CO2} \quad (14) \qquad \textbf{Eq. 7}$$

where M_{CO2} is the average mass of CO_2 injected into saline aquifers in the simulation domain for 50 years. The assumption is that the distribution of the homogeneous reservoir properties is the same as the prescribed for the simulation domain.

The CO_2 plume with saturations from 0.05% to 0.9% used a space of 1.2km^3. The total volume of the Weber Sandstone above depth of 5,000m within the RSU is 412km^3. Therefore, if all Weber Sandstone is used for the storage in the RSU, its storage capacity could be 17Gt of CO_2.

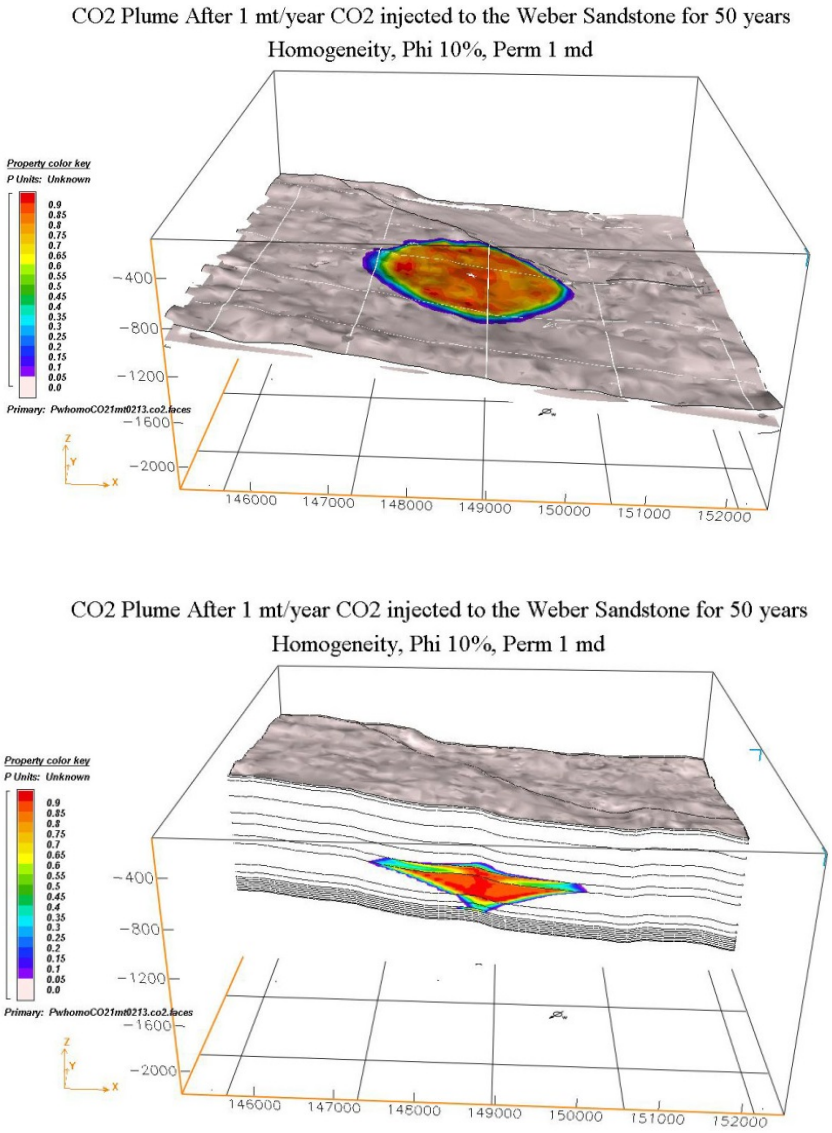


Fig. 89. The CO_2 plume distribution based on results from the FEHM simulator for the Weber Sandstone after 50 years of injection within the 3-D seismic survey area, RSU. The simulation used an injection interval of 210m, homogenous porosity (10%) and relative permeability (1md), and an injection rate of 1Mt/year in a single injection well. The up-dip boundary is opened to imitate displaced fluid production. After 50 years of CO_2 injection with a constant injection rate of 31.7kg/s, the simulation continued for 50 years to let reservoir pressure dissipate and to monitor further CO_2 migration. (**a**) Incline view; **(b**) An east-west cross section.

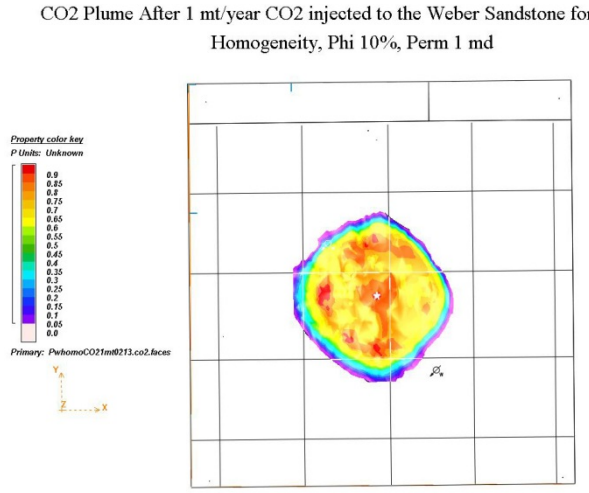


Fig. 90. A map view of the CO_2 plume distribution on the top of the Weber Sandstone after 1MT of CO_2 per year after 50 years of injection within the Jim Bridger 3-D seismic survey area, RSU. The plume at the top of the Weber Sandstone is nearly circular with a radius of 1,600m. The white five-pointed star is the location of injection well.

The Weber Sandstone with heterogeneous properties

Fig. 91 is an incline view and cross section of the injected CO_2 plume for the targeted Weber Sandstone after 50 years of injection at a rate of 0.3Mt/year with the heterogeneous reservoir property model. After 50 year of injection, the CO_2 plume remained within the Weber Sandstone reservoir. The CO_2 plume after 50 years of injection in a single injection well is irregular, covering an area of 10km^2 (**Fig.91**). Unlike the CO_2 distributions in the plume with the homogeneous case, the CO_2 distributions in the plume for the heterogeneous case have a patchy pattern. This patch pattern is mainly a result of the heterogeneous porosity and permeability distributions. Large variations in the total amount of CO_2 stored over 50 years are caused by differences of porosity and permeability fields for the Weber Sandstone.

The CO_2 plume with saturations from 0.05% to 0.9% used a space of 0.65km^3. The total volume of the Weber Sandstone above a depth of 5,000m within the RSU is 412km^3. Therefore, if all Weber Sandstone is used for the storage in the RSU, its storage capacity could be 9.5Gt of CO_2. Note that the assumption here is that the distributions of the heterogeneous reservoir properties of the RSU are assumed to be the same as those prescribe for the simulation domain.

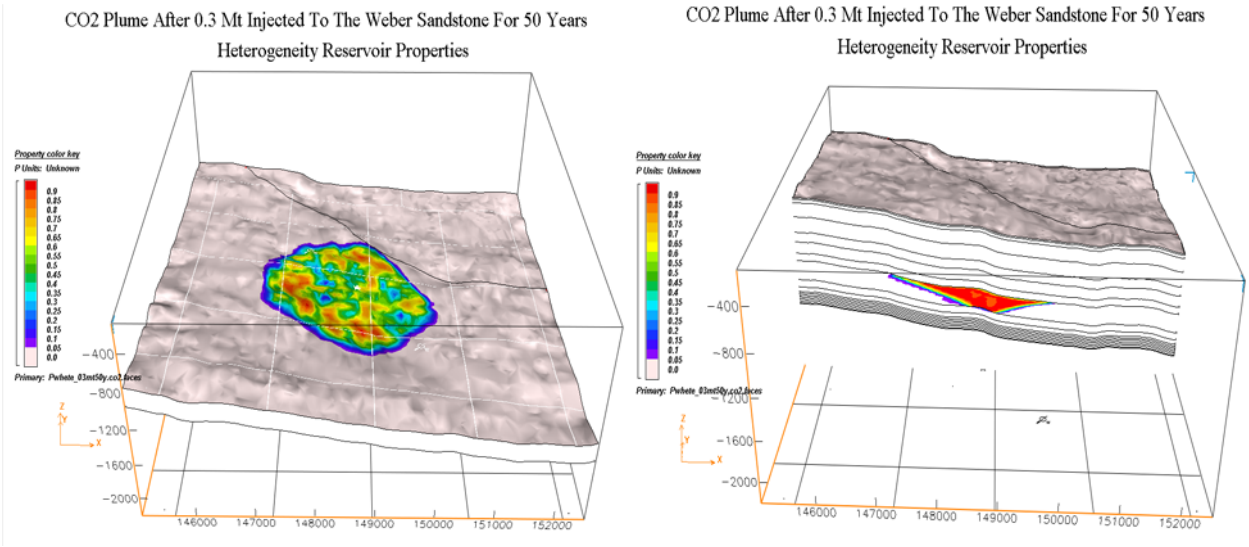


Fig. 91. The incline view (**a**) and cross section of the CO_2 plume in the Weber Sandstone are for 15 Mt CO_2 injected into the reservoir over a 50 year injection period.

The Madison Limestone with homogeneous property

Fig. 92a, b are an incline view and cross section of the injected CO_2 plume for the targeted Madison Limestone after 50 years of injection at a rate of 1Mt/year. After 50 years of injection, the CO_2 plume crossed the formation boundary of the Madison Limestone into the overlying Amsden Formation. The plume for 1Mt CO_2/year of injection rate, after 50-year injection at a single well injection is nearly a circle with radius of 1,950m, covering an area of 12km^2 (**Fig. 93**). The CO_2 plume after 50 years of a single well injection with saturations from 0.05% to 0.9% used a space of 1.23km^3 within the Madison Limestone. The total volume of the Madison above depth of 5,000m within the RSU is 179km^3. Therefore, if all Madison Limestone is used for the storage, its storage capacity could be 7Gt of CO_2.

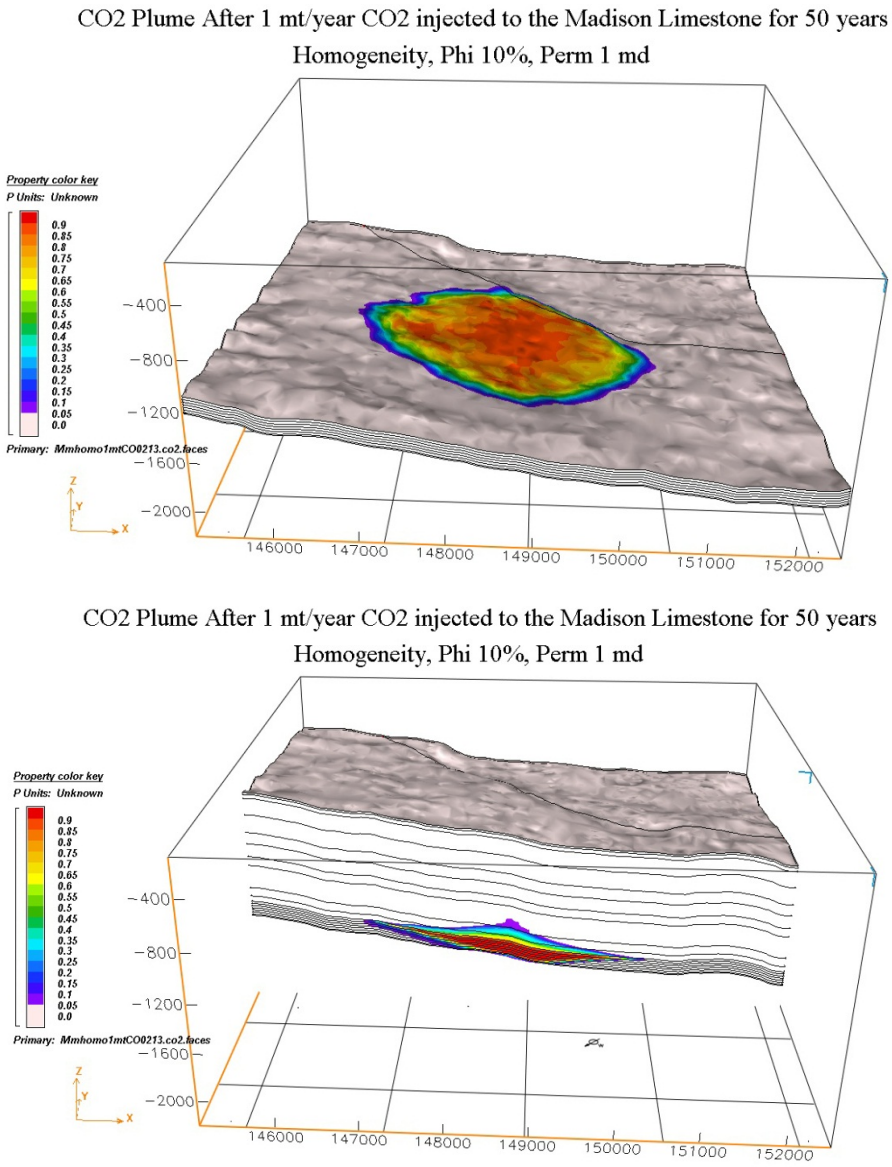


Fig. 92. The CO_2 plume distribution for the Madison Limestone after 50 years of injection within the 3-D seismic survey area, RSU. The simulation used an injection interval of 121m, homogenous porosity (10%) and relative permeability (1md), and an injection rate of 1Mt/year in a single injection well. The up-dip boundary is opened to imitate displaced fluid production. (a) Incline view; (b) An east-west cross section.

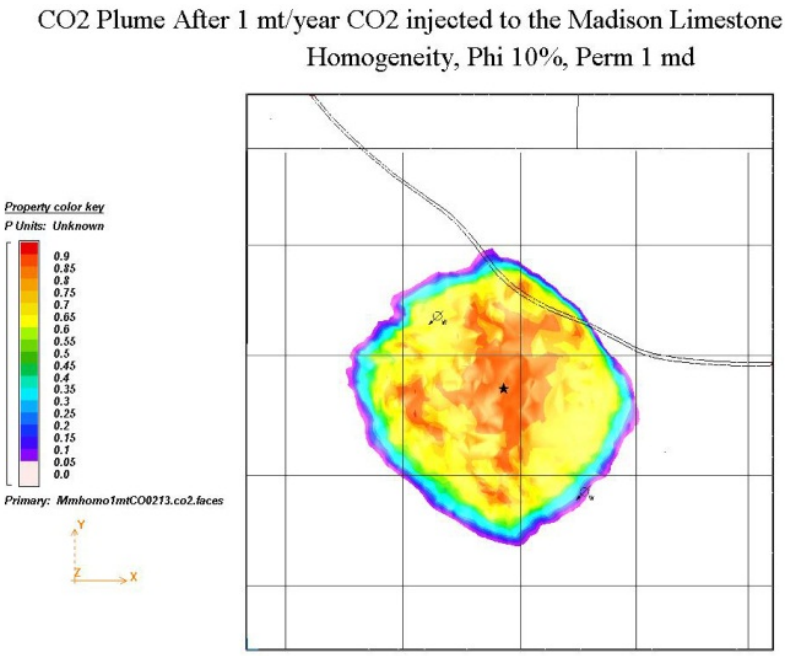


Fig.93. A map view of the CO_2 plume distribution on the top of the Madison after 1MT/yr of CO_2, 50 years of injection within the 3-D seismic survey area, RSU. The plume on the top of the Madison Limestone is nearly circular with a radius of 1,950m. The black five-pointed star is the location of the injection well.

The Madison Limestone with heterogeneous petrophysical property

The plumes of injected CO_2 are much different among the three areas where the injection wells were located (**Fig. 94**). In contrast, the results are different from the homogeneous reservoir conditions. In this case, the CO_2 plumes on the plane at the top of the Madison Limestone exhibit an irregular shape and spread to the up dip directions, through a relatively higher porosity and permeability zones toward up-dip open boundary (**Fig. 95 and 96**). As expected, all the CO_2 plume distributions show some expansion at the plume top because of buoyancy driven spreading along the lower permeability units above (the Amsden Formation). No part of the supercritical CO_2 plumes has crossed the domain boundaries in 50 years of injection.

Concurrent with the pressure increase at the start of injection, the CO_2 plumes begin to grow and migrate. At the end of 50 years of injection, the supercritical CO_2 plumes expand away from the injection wells with a preferential flow toward the up-dip open boundary drains. The CO_2 plumes do not grow uniformly in either the horizontal or vertical directions due to heterogeneity, pressure interference, and the inclination of the formations. In the vertical profiles, the CO_2 plume migrates far away from the injection well and develops a long narrow front near the top of the Madison Limestone.

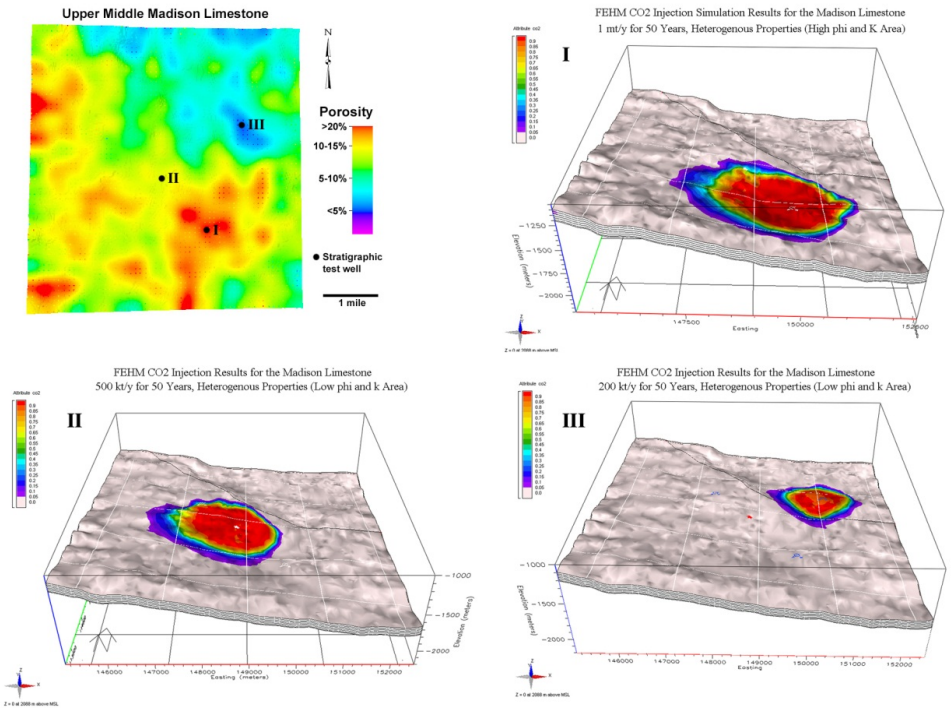


Fig. 94. The CO_2 plume distribution on the Madison Limestone with a heterogeneous reservoir after 50 years of injection within the 3-D seismic survey area, RSU. (**b**) The simulation used an injection interval of 400ft, and injection rates of 1Mt/year in a single injection well in the higher reservoir quality case (**c**), 0.5Mt/year in the medium reservoir quality case (**d**), and 0.2Mt/year in the lower reservoir quality case.

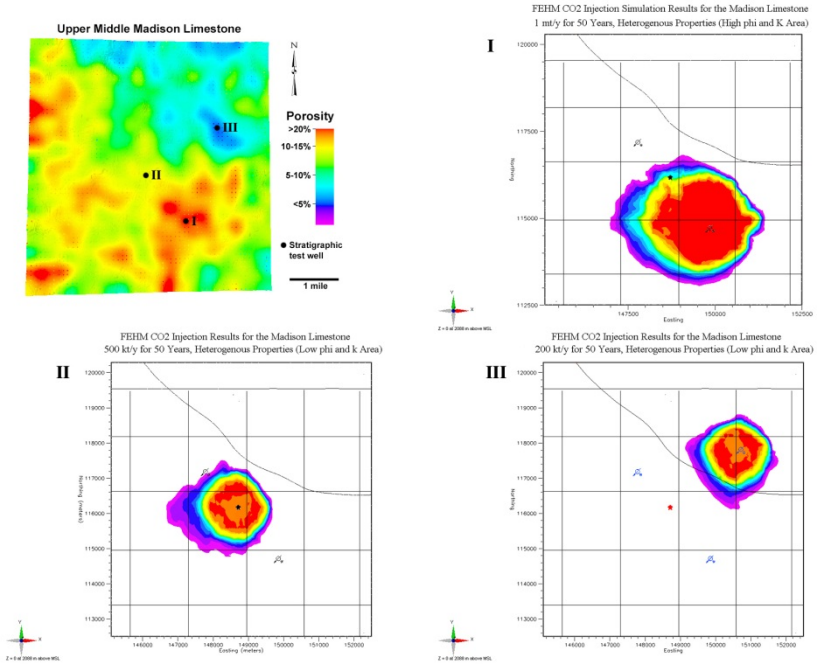


Fig. 95. The map view of CO_2 plume distribution on the Madison Limestone with a heterogeneous reservoir after 50 years of injection for the RSU modeling domain. The injection rates of (**b**) 1Mt/year in a single injection well in the higher reservoir quality case, (**c**) 0.5Mt/year in the medium reservoir quality case, (**d**) and 0.2Mt/year in the lower reservoir quality case.

Fig. 96 shows the three cross sections from the higher, medium, and lower reservoir property simulation cases. All injected CO_2 are kept in the Madison Limestone reservoir. The injected CO_2 migrates much farther up dip because of the buoyancy.

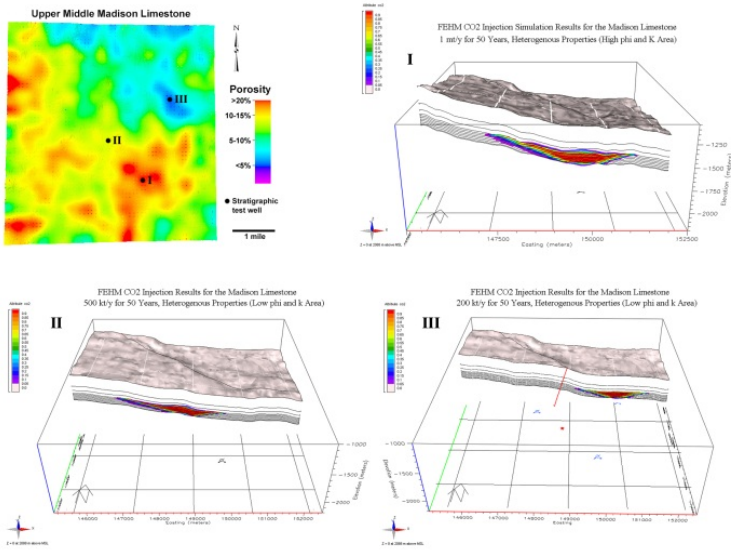


Fig. 96. The cross sections of CO_2 plume distribution on the Madison Limestone with a heterogeneous reservoir after 50 years of injection for the RSU modeling domain. The injection rates of (**b**) 1Mt/year in a single injection well in the higher reservoir quality area (**c**), 0.5Mt/year in the medium reservoir quality area **(d)**, and 0.2Mt/year in the lower reservoir quality area.

Large variations in the total amount of CO_2 stored over 50 years are caused by differences in porosity and permeability fields for the Madison Limestone. Because no CO_2 leaks into the overlying the Amsden Formation were observed in the simulations, the storage capacity was defined as equal to the amount of CO_2 injected over 50 years for each simulation. Using the same equation described in previous sections, the storage capacity of the Madison Limestone for the entire RSU is estimated by assuming that the 3-D simulation domain is a representative element for the whole RSU. The volumes of CO_2 plume are 1.1km^3 for the higher reservoir quality case, 0.642km^3 for the medium reservoir quality case, and 0.337km^3 for the lower reservoir quality case. The volume 179km^3 of the Madison Limestone above depth of 5,000m in the whole RSU is calculated from the RSU geological structural model constructed using the EarthVision geospatial modeling software. For the higher reservoir quality case, the Madison Limestone in the RSU could store 8Mt of CO_2. For the medium reservoir quality case, the Madison Limestone could store 7Mt of CO_2, whereas for the lower reservoir quality case, the Madison Limestone only could store 5Mt of CO_2.

Reducing uncertainty in evaluations of geological CO_2 storage site scenarios requires a robust database that allows an accurate reconstruction of the targeted storage rock/fluid volume, especially with respect to spatial heterogeneity. The results relied on a generalized regional database to populate a homogenous rock/fluid volume based on average reservoir properties; this approach yielded general insights into injection/storage characteristics but lacked specificity, resulting in performance assessments plagued by substantial uncertainty. To move from idealistic, highly generalized assessments to realistic, lower risk of the RSU storage capacity and injectivity assessments, it was necessary to acquire high-resolution data specific to the storage site of interest.

The integration of the 3-D seismic and well log data, along with visual observations from the core, has substantially reduced the uncertainty attached to performance assessments and risk analysis for the RSU site characterization project (WY-CUSP). As the new data from laboratory analyses, experimental determinations, and test evaluations became available and were integrated into the RSU property models, uncertainty, particularly with respect to reservoir property heterogeneity was reduced further. This study establishes an exemplary strategy for dealing with CO_2 storage projects in relatively deep saline aquifers in the Rocky Mountain region. **Table 7** shows how the CO_2 storage capacity and injectivity assessments of the Jim Bridger 5mi x 5mi simulation domain are affected significantly by the quality of the utilized database used. From a static volumetric approach using the regional geological data to a dynamic numerical simulation approach using more realistic reservoir data, the CO_2 storage of the Weber Sandstone within a 5mi x 5mi simulation domain reduced from 503Mt to 33Mt; the Madison Limestone reduced from 290Mt to 270Mt.

			Static Volumetric Approach[1]	*Dynamic Numerical Simulation*[2] *Homogenous Reservoir Model*			*Dynamic Numerical Simulation*[2] *Heterogeneous Reservoir Model*		
Formation	Area, km^2	Thickness, m	Storage Capacity, Mt	Injection Rate, Mt/y	Storage Capacity, Mt	Injection Wells	Injection Rate, Mt/y	Storage Capacity, Mt	Injection Wells
Weber	64	210	503	1.0	350	7	0.3	33	7
Madison	64	120	290	1.0	305	6	1.0	270	6

1 – USGS Open File Report 2009-1035
2 – FEHM, Los Alomos National Laboratory

Table 7. Comparison of CO_2 storage capacity utilizing 3 different technologies – 5mi x5mi storage domain.

The reservoir heterogeneity has a significant effect on the geological CO_2 injectivity and storage capacity of the targeted saline aquifers. Applying the diagnostic protocol for the CO_2 sequestration suggested by DOE for the FutureGen project, the CO_2 storage capacity of the Weber Sandstone in the RSU was estimated to be 18Gt (Surdam and Jiao, 1997). Applying the volumetric approach proposed by the USGS, the CO_2 storage capacity of the Weber Sandstone was estimated to be 9Gt with the probability density ranging from 2.4Gt to 20Gt. Using the FEHM multiflow numerical simulator, the CO_2 storage capacity of the Weber Sandstone was estimated to be 17Gt based on the homogeneous reservoir property (porosity 10%, and permeability 1md), and to be 33Mt within the 5mi x 5mi modeling domain (**Table 7**), and 9.5Gt for the whole RSU structure based on the heterogeneous reservoir property. This capacity is based on the assumption that the distribution of the heterogeneous reservoir properties is the same as prescribed for the simulation domain in the study area. However, the reservoir characterization conducted in this study revealed that only approximately 25% of the Weber Sandstone is suitable for the CO_2 storage. Then, the CO_2 storage capacity of the Weber Sandstone in the RSU can be lowered to 2.4Gt. The 2.1GW of JBPP located a mile from the simulation injection well emits 15Mt of CO_2 annually. Therefore, the Weber Sandstone reservoir in the RSU is capable of storing the CO_2 emitted from JBPP for 160 years.

For the Madison Limestone reservoir in the RSU, the geological CO_2 storage capacity was estimated to be 8Gt using the protocol of the FutureGen project suggested by the DOE. Using the USGS volumetric approach, the probability density of the CO_2 storage capacity of the Madison Limestone ranges from 1.6Gt to 14Gt, with a mean of 6.5Gt. Using the FEHM multiflow numerical simulator, the CO_2 storage capacity of the Madison Limestone was estimated to be 7Gt based on the homogeneous reservoir properties (porosity 10%, and permeability 1md). Based on the heterogeneous reservoir properties, the CO_2 storage capacity of the Madison Limestone in the RSU area was estimated to be 8Gt for the higher reservoir quality case, 7Gt for the medium reservoir quality case, and 5Gt for the lower reservoir quality case. Using the result from the CO_2 injection simulation for the medium reservoir quality case, the Madison Limestone could store the amount of CO_2 emitted from the JBPP for 460 years.

Well injectivity is highly dependent on the local permeability distribution in the storage formation. The areas and intervals with higher quality reservoirs are critical for establishing a successful commercial-scale geological CO_2 storage project. Choosing the higher quality reservoir initially could substantially reduce the project cost and significantly increase the CO_2 injectivity and storage capacity. For the upper portions of the middle Madison Limestone and selected intervals in the Weber Sandstone with higher quality reservoirs, the injection rate can be as high as 1Mt/yr, where at the lower quality reservoir section, the injection rate could be lower than 0.3Mt/yr.

Formation brine production around the perimeter of the storage site is necessary to keep formation pressure below the hydro fractural pressure, and reduce associated leakage, decrease seismic risks, and create the accommodation space to enhance storage capacity for CO_2 storage. The average ratio of the amount of injected CO_2 to the produced brine is 1.14. This ratio indicates that for an industrial-scale injection with limited impacts on neighboring pore space, nearly as much brine must be produced as CO_2 is injected.

CO_2 leakage from the storage formations into the overlying rocks is related to connectivity of high-permeability layers. Leakage from the Madison limestone into the Amsden Formation above appears to be limited. However, migration from the Weber into the Phosphoria is relatively high. This result implies that the Phosphoria should be considered as a secondary storage unit and not as a cap-rock. Importantly no injected CO_2 migrated into the primary cap rocks within the Dinwoody formation.

Document the composition of produced brines

Brines from both formations are sodium-chloride-type with measured total dissolved solids concentrations of 89,000mg/L – 109,000mg/L from the Weber Sandstone and 75,000mg/L – 95,000mg/L from the Madison Limestone. The brine densities are calculated to be 1.06g/cm^3 (Weber) and 1.05g/cm^3 (Madison). Ionic strength ranges from 1.77molal – 2.03molal (Weber) and from 1.44molal – 1.61molal (Madison). Brine temperatures range from 92° C (Weber) to 95°C (Madison), with a formation pressure of 4,800 psi (Weber) and 5,900 psi (Madison).

Study site brines exceed the standards for TDS using USEPA maximum contaminant standards. In addition, MCLs are exceeded with respect to chloride, fluoride, sulfate, aluminum, barium, iron, lead, manganese, and gross beta.

Formation fluids were analyzed for 63 volatile organic compounds (**Appendix – Water Quality Data, pg. 441, Fig. 76**). The first sample set (August, 2011) detected six volatile organic compounds in both the Weber and the Madison. This increased to fourteen in the second round of sampling (December, 2012). With exception of BTEX compounds, then when a VOC was detected a similar concentration was measured in both reservoirs. This indicates that some VOC's were likely introduced upon reentry of the wellbore (**Appendix –**

Water Quality Data, pg. 441, Fig. 76). Benzene, toluene, xylenes were not detected in the first round of sampling but were measured in the second round. Concentrations were much higher in the Weber. Ethylbenzene was found in equal concentrations in both formations in the first sample set (20 µg/L), but more than doubled in the Weber in the second round (50 µg/L).

Based on these analyses, the WDEQ classified the groundwater as Class VI groundwater within 1,320ft of the RSU #1 wellbore in both the Weber and Madison formations. According to the Wyoming Water Quality Rules and Regulations (Ch. 8) of the State Class VI groundwater is defined as "unusable, or unsuitable for use", due to high TDS concentrations, excessive contamination or to excessive depth

Differences in fluid compositions between sample sets

It is important to note the molar ratios of Br-Na-Cl record a noticeable decrease between the first and the second sample sets, mostly due to decreases in concentrations of Na and Cl (**Appendix – Water Quality Data, pg. 441, Fig. 76**). The differences of solute concentrations between the two samples could be attributable to several factors. The first set of samples was maintained at reservoir pressures by capture cylinders, whereas the second set was collected using a wireline bailer and pressure was not maintained. The second sampling methods could have led to the precipitation of some solutes.

The first set of samples collected had very low concentrations of H_2S (Madison 29mg/L, Weber 0.04 mg/L). The second set of samples measured a much higher concentration of H_2S (Madison 87 mg/L, Weber 127 mg/L). Interestingly, the sulfate concentrations decreased between the first and second sample set (**Appendix – Water Quality Data, pg. 441, Fig. 76**). This suggests that fluid circulated during drilling, completion and work over of the well-introduced sulfate reducing bacteria (SRB). SRB ingest sulphate and organic acids and generate H_2S. Mixing these waters with highly saline reservoir fluids could sour the reservoir in these mixing zones (Ligthelm et al. 1991). Another possibility is that work within the wellbore oxidized sulfide-bearing minerals, such as pyrite. Increases in Fe concentrations observed between sample sets support this theory. Though it is uncertain which process or combination generated the H_2S, if targeted reservoirs and associated fluids are sensitive to redox reactions or non-native fluids, fluids injected during CCS will have to be closely monitored to avoid the possibility of degrading the reservoir and formation fluids.

It is also advisable to carefully design the downhole data collection program, particularly with regards to alteration of formation fluids or the potential for borehole-adjacent reservoir degradation. While it is foolhardy to omit collection of all downhole data, identifying the most invasive tests and the potential consequences associated with testing should be carefully considered.

Design a brine treatment plan that converts the economic penalty of pressure management during CO_2 injection via brine production/treatment into a source of revenue (recovery of potable water and metals)

Fluid analysis from RSU #1 measured TDS concentrations ranging from 80,000mg/L to 100,000mg/L. Research has shown that the lower range of these waters could be treated with standard RO with low recovery, ~10% (Aines et al. 2010). By combining multistage RO or adding nanofiltration membranes at the front end of RO treatment, makes the treatment of these waters probable (Aines et al. 2010; Bourcier et al. 2011).

In conventional applications (treatment of sea water), much of the cost of the procedure is the energy required to pressurize the treatment system. Pressures of 700 psi–1200 psi are needed to create the reverse osmotic pressure gradient between the saline and fresh water (Fritzmann et al. 2007). Reverse osmosis is limited by the maximum pressure difference that the membrane spacers can withstand without collapsing and causing the membrane to become impermeable (Matsurra 2001). The current limit for commercially available membrane spacers is 1,200 psi (Bourcier 2011); presently the membrane itself can withstand higher pressures. Higher-pressure membranes have been developed for osmotic pressures of 1,500 psi (Baker 2004) but have not been demonstrated commercially. This is likely due to the large amount of energy required to pressurize seawater to above 1,200 psi; thus, seawater treatment is not economical at 1,500 psi.

However, in treating displaced fluids, pressure is an asset rather than a problem because the fluid arrives at the membrane pressurized (the in-situ formation fluids in the Weber/Madison formations on the RSU come in at 4,800 psi–5,900 psi). The energy needed to drive the RO process would be harvested directly from the pressure of the formation. Consequently, treating these produced fluids would cost half as much as treating seawater with RO (Aines at al. 2010). Estimated recovery for the RSU brines is approximately 10% using osmotic pressures of 1,200 psi, but could exceed 20% by incorporating nanofiltration and increasing osmotic pressure to 1,500 psi (Aines et al. 2010, Bourcier et al. 2011).

Nanofiltration membranes resemble RO membranes but discriminate against larger-molecular-weight ions and divalent ions due to larger pore sizes and a surface charge on the membrane. Hilal et al. (2004) suggest that nanofiltration membranes reject >90% of the divalent ions while letting monovalent ions pass. Nanofiltration is used to partially lower the salinity of the brine in order to increase the efficiency of the RO process and is especially attractive in fluids that have a hardness of >10,000mg/L. Though RSU brines are relatively soft (2,000mg/L to 5,000mg/L), the nanofiltration phase could be utilized as a pressure-reduction step, decreasing scaling potential in the RO process by removing Ca, Mg, and SO_4, and lastly to begin the separation process for potential mineral recovery.

The temperature of the brines provides another means for a further energy/cost reduction benefit of treating formation brines compared to seawater. The brines of the RSU have a measured temperature of 92°C to 100°C. Modern binary power generating units have demonstrated success with temperatures as low as 73°C (Green and Nix 2006). Geothermal heat recovered from produced brine could generate enough electricity to defray the cost of water treatment, and perhaps, to sell an excess. Aines et al. (2010) report that the lifetime of RO membranes is greatest when fluid temperatures range between 40°C and 50°C. Thus RSU brines would need to undergo a cooling phase prior to treatment; it simply makes sense to harvest that heat via a heat exchanger for electricity generation.

Fig. 97 illustrates a potential course of operations for the water treatment of RSU brines. First, the water is produced from the formation, arriving to the surface at about 100°C, 5,000 psi, and 80,000mg/L TDS, a strongly sodium-chloride brine, with lesser amounts of Ca, Mg, and SO_4. The first step in the operation is a geothermal heat exchanger: this step not only harvests thermal energy for electricity generation, but also decreases the temperature of the

brine to optimize the RO treatment. Next, the brine is passed through a nanofiltration membrane, and as a result the overall TDS is reduced to about 75,000mg/L, pressure is reduced to 1,500 psi, and more than 90% of the calcium, magnesium, and sulfate are removed. Removing the divalent ions greatly reduces the risk of mineral scale during RO treatment, also effectively lowering the magnesium-to-lithium ratio. The feed is now ready for RO treatment. The permeate from the RO process is estimated to be 20% to 40% of the original feed stream while 60% to 80% is further concentrated in the brine. The permeate water is ready to be sold to market. The TDS concentration of the residual brine is expected to increase from 75,000mg/L to 98,000mg/L–126,000mg/L**.** By concentrating the brine, the lithium concentration is also increased from 95mg/L to 110mg/L–150mg/L along with other recoverable constituents. The residual brine is then moved to evaporation ponds for mineral recovery. The last step is to dispose of any remaining brine back into the original formation.

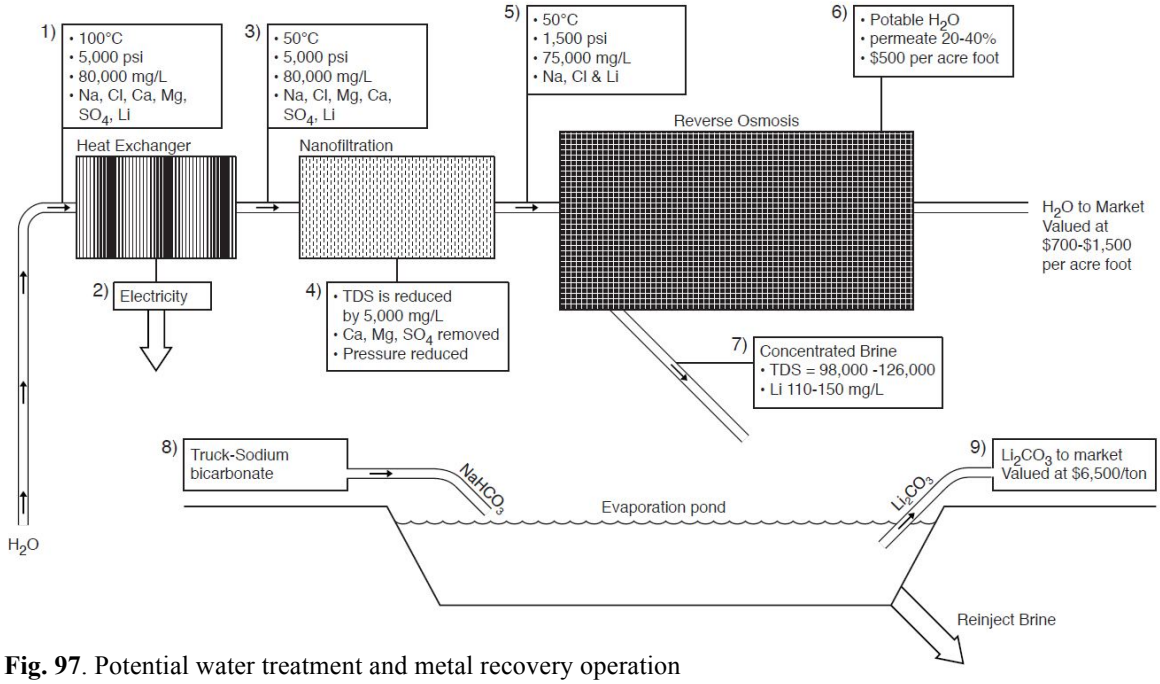


Fig. 97. Potential water treatment and metal recovery operation

Value added products

A treatment scenario, as described above, produces value-added products: fresh water, electricity, and metals. In arid Wyoming, the need and demand for potable water is very high: local coal-to-power and coal-to-chemical plants, agriculture operations, hydraulic fracturing water, residential users, and downstream users in the Colorado River drainage, among others, all require increasing amounts of water. Bourcier et al. (2011) suggest that treatment cost for reservoir pressure driven RO with 20% recovery might range between US$450 to US$600 per acre-ft of permeate. Agriculture users in some areas of the Colorado River drainage pay more than US$700 per acre-ft. Therefore it is conceivable that the sale of fresh water to market could in fact cover the cost of treating the produced fluid.

Treating these formation fluids at a reverse osmosis treatment plant, or other desalination facility, would yield approximately 10,000 acre-ft of portable water per year, which could be used by an adjacent power plant; by the community of Rock Springs, Wyoming; as replacement water in the Upper Colorado river drainage; or perhaps by communities along the Colorado Front Range. The feasibility of such a large-scale desalination endeavor is demonstrated by desalination projects in Israel, where desalination plants produce 2 million barrels of potable water per day –13% of the country's annual water consumption (water-technology.net 2012).

Geological CO_2 sequestration on the scale required by a large power plant – on the RSU or elsewhere in the Rocky Mountain region – will require displaced fluid management. Work at the WSGS and CMI suggests an integrated CO_2 sequestration/fluid production/fluid treatment strategy to accomplish CO_2 sequestration on the RSU: carbon is sequestered on a commercial scale at depth while displaced fluids are produced and treated at the surface. The volume of treated water produced as a result of this strategy represents a valuable commodity in arid southwestern Wyoming.

Formation fluids from the Weber and Madison formations contain potentially recoverable concentrations of salts and metals: lithium (90mg/L to 100mg/L), boron (60mg/L to 120mg/L), potassium (1,940mg/L to 4,210mg/L), sodium (27,900mg/L to 40,700mg/L) chloride (50,300mg/L to 60,900mg/L). In sufficient volume, fluids with these elevated constituent concentrations could support a successful and profitable recovery industry. In fact, recovery of metals from the residual brine may not only pay for the displaced-fluid treatment, but may create a significant profit center. Finally, even the heat contained in the produced brine (100°C–130°C) is valuable, as process heat or as a heat exchange source for steam generation.

The proposed integrated strategy may be expensive, but there is presently no viable alternative in Rocky Mountain basins. Finally, it is important to realize that this proposed strategy will be a test of the whole idea of CO_2 sequestration: if commercial-scale geological CO_2 sequestration cannot be accomplished on the RSU, it probably cannot be accomplished anywhere in the Rocky Mountain region.

CO_2 Storage Utilization

Construct integrated CO_2 source/sink strategies to optimize CO_2 utilization.
The multiple resource development approach optimizes the assemblage of energy/environmental resources in a given area as a synergistic system, rather than as a collection of disparate parts. This type of approach relies on synergistic relationships between the targeted natural resources to increase the efficiency of development, minimize environmental degradation, sustain long-term resource use, and maximize revenue to the state and to energy industries. Most importantly, all of this resource development can be accomplished without significantly increasing the industrial footprint in the basin.

The resources available in a given area present the opportunity to utilize this approach. In Wyoming, the Powder River Basin (PRB) has the following key resource elements that lend themselves to an integrated development strategy: abundant coal resources and mines, and the opportunity to build coal-to-chemical plants capable of capturing CO_2 (to be located at mine-mouth sites); a significant source of water (groundwater produced during coalbed methane development); nearby CO_2 storage sites (depleted, Cretaceous compartmentalized gas fields); and multiple Pennsylvanian oil fields highly suitable for enhanced oil recovery (EOR) utilizing CO_2, with ultimate storage potential afterwards. These elements are close in proximity geographically within the central PRB.

Similarly, the WYCUSP/RSU CO_2 storage site is optimally located within the GGRB and would offer a similar integrated multiple-resource development strategy. The key resource elements available in the RSU area that would power an integrated development strategy include: abundant coal resources and mines, and the opportunity to build coal-to-chemical plants capable of capturing CO_2 (to be located at mine-mouth sites); a large source of anthropogenic CO_2 from the JBPP; close proximity to the primary CO_2 pipeline in Wyoming, currently providing CO_2 for five different EOR projects; and the WYCUSP/RSU CO_2 storage site/surge tank. Development of the RSU CO_2 storage resource would involve the integration of several resources in and of itself. CO_2 injection would necessitate production of brine, brine that contains an extractable lithium resource. This highly saline produced water is also very warm; the heat (steam) would help to provide electricity to a reverse osmosis desalination plant, with an end product of fresh water, which is of increasing monetary value.

These energy development plans focus on the future synchronous development of resources. The examples used to illustrate the approach are based on the confluence of a set of natural resources in the two basins, but the approach itself is flexible and could be tailored to fit other Wyoming and many Rocky Mountain basins. This approach emphasizes synergistic relationships among resource elements in order to optimize the effective and efficient exploitation of energy resources while minimizing environmental degradation. The fundamental idea is that it is more effective and efficient to develop a set of resource elements together systematically rather than separately.

Relationship between RSU storage and EOR

The RSU storage site is centrally located near the highest concentration of anthropogenic CO_2 emissions in the State of Wyoming. The GRB is host to the largest coal fired power plant in the state, the Jim Bridger Power Plant, four trona mines and processing facilities, and a number of oil and gas related pipeline compressor stations and gas plants.Also, it is less than 20mi from the primary CO_2 pipeline corridor leading from ExxonMobil's Shute Creek facility. From this facility, ExxonMobil sells approximately 6.4Mt of naturally occurring CO_2 for use at five different EOR projects in Colorado and Wyoming. Production of the CO_2 is from the LaBarge Anticline, one of the world's largest CO_2 reservoirs. Denbury Resources is in the process of developing gas processing facilities and a 20" pipeline from this field area, and will utilize the same pipeline corridor. Capacity of Denbury's pipeline would be on the order of 13-14Mt/yr, and the CO_2 is to be transported to the PRB and north into Montana for use in EOR projects. This places the RSU storage site in a strategic location for integration into rapidly emerging CO_2 EOR projects in Wyoming. This integration of capture and storage would be essential to the success of a carbon capture program, and it would more easily facilitate large-scale EOR development scenarios.

The UW Enhanced Oil Recovery Institute (EORI) estimates that 4.0 to 8.0 billion barrels of recoverable oil remain in production zones and residual oil zones within Wyoming's depleted oil fields. Use of CO_2 flooding technology would be integral to recovering this oil.

No.	Co.	Facility	Facility code	CO_2 kt/yr
1	18	Amazon-Congo	CS	41
2	6	Arlington	CS	41
3	10	Beaver Creek	GP	43
4	9	Bentonite Performance Minerals	IP	43
5	21	Osage	PP	220
6	3	Bpe Prairie Dog Booster	PP	27
7	10	Burlington Resources Lost Cabin	GP	784
8	23	Big Piney	CS	63
9	10	Bird Canyon	CS	119
10	17	Bison Treating Facility	RF	47
11	16	Bolster	CS	28
12	17	Bombsite/Nichols	CS	52
13	23	Bridger	CS	173
14	6	CIG Station 5660 Rawlins	CS	66
15	5	CIG Station 5670 Laramie	CS	44
16	6	CIG Station 5690 Muddy Gap	CS	26
17	19	Carter Creek	GP	59
18	2	Cheyenne Plant	GP	337
19	13	Dave Johnston	PP	5,436
20	16	Deer Gulch-Falcon	CS	31
21	6	Doty Mountain	CS	26
22	13	Douglas	GP	47
23	19	East Painter Facility	CS	59
24	6	Echo Springs	GP	290

No.	Co.	Facility	Facility code	CO_2 kt/yr
25	6	Eight Mile Lake	CS	51
26	11	Encore Energy Partners	IP	74
27	4	FMC Westvaco	TM	1,609
28	4	Frewen Lake	CS	51
29	23	Falcon	CS	74
30	16	Fletcher-Terhune	CS	48
31	16	Flying Creek/ Bridge Draw	CS	63
32	2	Frontier Refining	RF	531
33	4	General Chemical	TM	1,631
34	9	Georgia Pacific Corporation	TM	32
35	17	Hilight-Reno Junction	GP	89
36	16	Indian Creek-Crow	CS	38
37	16	Jameson-Kessler	CS	31
38	16	JAQ	CS	40
39	4	Jim Bridger	PP	14,768
40	19	KRGT Co. - Coyote Creek	CS	40
41	12	KRGT Co. - Muddy Creek	CS	232
42	23	Labarge	CS	53
43	8	Laramie River Station	PP	13,358
44	17	Little Thunder-Stratus	CS	26
45	16	Luke-Gus	CS	32
46	23	Luman	CS	44
47	4	Merit Energy Co Brady	GP	49
48	5	Mountain Cement Co.	IP	272

No.	Co.	Facility	Facility code	CO_2 kt/yr
49	17	Malibu-Surfer	CS	29
50	13	Medicine Bow Treatment Facility	IP	59
51	12	Moxa North	CS	34
52	12	Moxa South	CS	34
53	12	Northwest Pipeline - Muddy Creek	CS	28
54	12	Naughton	PP	5,337
55	17	Neil Simpson	PP	306
56	17	Neil Simpson II	PP	816
57	17	Newport-Laguna	CS	32
58	4	OCI Wyoming	TM	763
59	12	Opal	GP	492
60	4	P4 Production	IP	203
61	4	Patrick Draw	GP	126
62	23	Paradise	CS	97
63	16	Perla	CS	35
64	23	Pinedale Complex	GP	80
65	12	Pioneer Cryogenic Plant	IP	35
66	16	Pumpkin-Bruno	CS	45
67	4	QEP Field Services Blacks Fork	GP	63
68	4	Questar Rock Springs Complex	GP	72
69	3	Rucki 15	CS	37
70	16	River-Nile	CS	43
71	12	Roberson	CS	42
72	12	Shute Creek Facility	GP	1,169
73	19	Silver Eagle Refining	RF	30

No.	Co.	Facility	Facility Code	CO_2 kt/yr
74	4	Simplot Phosphates	IP	41
75	1	Sinclair Casper Refining Co.	RF	225
76	6	Sinclair Oil Corporation	RF	944
77	4	Solvay Chemicals, Inc.	TM	1,112
78	6	Sun Dog	CS	38
79	9	The Western Sugar Cooperative	IP	36
80	16	Tex-Dallas	CS	53
81	13	Thunder Creek Gas Services Buckshot	GP	41
82	16	Thunder Creek	CS	58
83	17	Thunder Creek Gas Services Mtg.	CS	39
84	5	UW Central Energy Plant	PP	50
85	4	WGR Operating Granger	GP	69
86	13	WIC Station 7950 Douglas	GP	85
87	11	Wyoming Lime Producers	IP	162
88	21	Wyoming Refining Co.	RF	120
89	20	Wyoming Sugar Co.	IP	26
90	4	Wamsutter	CS	97
91	7	Western Sugar Cooperative	IP	92
92	16	Westwind-Astra	CS	37
93	16	Whiskey Draw-Jack Daniels	CS	70
94	17	Wygen I	PP	744
95	17	Wygen II	PP	871
96	17	Wygen III	PP	568
97	17	Wyodak	PP	2,902
		Total		**59,825**

Facility

Map code	Facility type	Facility code
-1	Gas processing plant	GP
-2	Compressor station	CS
-3	Coal fired power plant	PP
-4	Trona mine	TM
-5	Refinery	RF
-6	Industrial plant	IP

Stationary CO_2 emissions by basin

Basin	CO_2 kt/yr
Bighorn	298
Denver	960
Greater Green River	23,829
Hanna	<1
Laramie	365
Powder River	13,170
Shirley	<1
Wind River	827
subtotal	39,449
Extrabasinal	20,376
Total	59,825

County codes

Code	County
1	Natrona
2	Laramie
3	Sheridan
4	Sweetwater
5	Albany
6	Carbon
7	Goshen
8	Crook
8	Platte
9	Big Horn
10	Fremont
11	Park

Code	County
12	Lincoln
13	Converse
14	Niobrara
15	Hot Springs
16	Johnson
17	Campbell
19	Uinta
20	Washakie
21	Weston
22	Teton
23	Sublette

CO_2 emmisions (kt/yr)

- 0 - 100
- 100 - 500
- 500 - 1,000
- 1,000 - 5,000
- 5,000 - 15,000

Explanation

- RSU #1
- 11-3 [map No.] - [Facility code] Facility
- City
- CO_2 pipeline
- EOR CO_2 flood field
- Energy basin*
- CO_2 producing field
- Prospective CO_2 producing field
- County boundary

*Basin outlines from De Bruin 2007

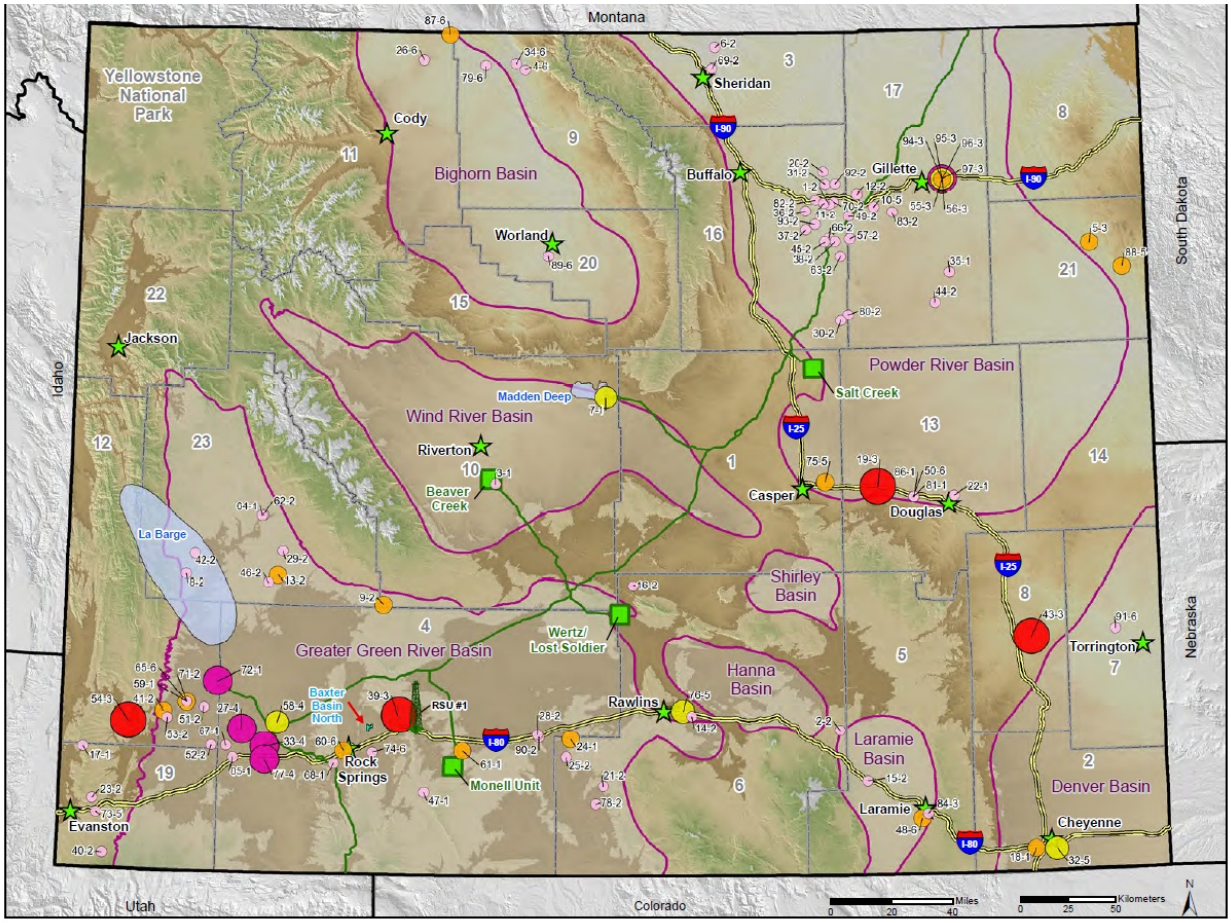


Fig. 98 (a) (b) – Major stationary anthropogenic sources of emitted CO_2 in Wyoming, CO_2 source fields, CO_2 pipelines, CO_2 EOR fields and the RSU #1 location.

Design multiple resource development plans that emphasize synergistic relationships that increase efficiency of development minimize environmental footprints, and sustain and stabilize long-term resource utilization

CO_2 storage utilization in designing strategies for the sustainable development of energy resources

Northeastern Wyoming's PRB offers a rare opportunity to illustrate the advantages of deploying an innovative, multiple-resource development strategy designed to foster the sustainability of energy and environmental resources. The multiple resource development plan advocated here is based on considering the assemblage of energy/environmental resources in a given basin as a synergistic system, rather than a collection of disparate parts. This new approach increases the efficiency of development, minimizes its environmental footprint, sustains and stabilizes long-term resource use, and maximizes revenue.

The key resource elements required to employ an integrated development strategy for any Wyoming Laramide Basin are as follows:

- Coal resources and mines (large coal reserves)
- Significant source of water (groundwater produced during the course of coalbed methane development, or deep basin bringes)
- Mine-mouth coal-to-chemical plants capable of capturing CO_2
- Nearby CO_2 storage/surge tank sites (depleted, compartmentalized gas fields)
- Depleted oil fields with substantial stranded oil suitable for enhanced oil recovery
- Final CO_2 storage in both depleted gas fields and depleted oil fields (doubling of the geological CO_2 storage capacity)

By developing this suite of resource elements as a system, it is possible to optimize the benefits to the energy industry while maximizing both the sustainability of energy resource development and state and federal revenue. This suggested resource development strategy can be accomplished within the existing regulatory framework, and without significantly increasing the industrial footprint in the basin. This approach would provide a more effective, efficient, and sustainable approach to energy development by accomplishing the following:

- providing added value products (diesel, gasoline, syngas, methanol, and others);
- monetizing the CO_2 captured at coal conversion facilities;
- protecting the coal extraction industry;
- recovering stranded oil;
- monetizing otherwise wasted resources (coalbed methane produced water);
- doubling CO_2 storage capacity by utilizing depleted oil/gas reservoirs; and
- reversing the regional trend of energy-related job loss.

Wyoming, with more than 4 billion barrels of stranded oil, is currently experiencing a critical shortage of CO_2. The capture and storage of CO_2 in surge tanks near EOR targets is essential to oil recovery. Otherwise, tertiary oil recovery will remain dependent on construction of new gas processing plants and long pipelines. In the systematic approach, a contentious problem associated with the development of one resource becomes part of a useful solution in the development of another (**Fig. 99**).

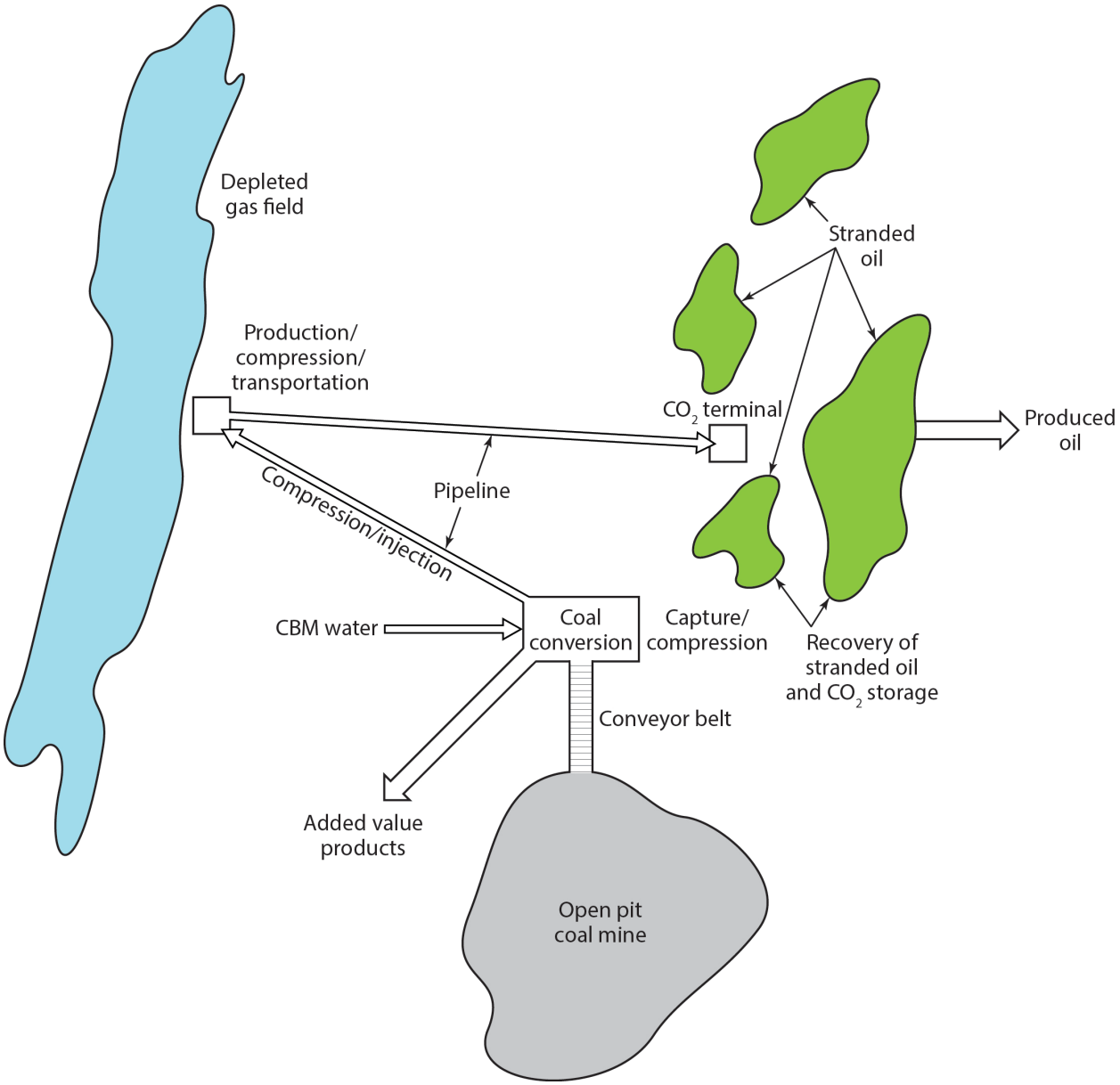


Fig. 99. Schematic diagram of sustainable energy development made possible by the convergence of resource elements in the Powder River Basin, Wyoming. All of the resource elements of this convergence can occur in an area with a 3 to 5 mile radius. Using the integrated resource development scheme illustrated in this diagram it will be possible to increase the lives of the open-pit coal mines and depleted oil fields, utilize the depleted, compartmentalized gas fields as surge tanks for EOR projects, and eliminate the presently wasted CBM water and future CO_2 emissions associated with coal conversion. At the termination of CO_2 flooding the depleted oil field can be utilized for CO_2 storage. The only resource element missing is the deployment of a coal conversion industry in the Powder River Basin. All of the resource development illustrated in this diagram can be implement with only a minimal increase in environmental degradation.

Deliverables Issues and Milestones

All of the deliverables listed in the original and subsequent WY-CUSP proposals to DOE have been completed (**Table 8**). The scope of the funded project included a series of issues to be addressed (**Table 9**). All of these and a multitude of other issues were addressed and completed during the progress of the WY-CUSP Program. In addition, the work on the WY-CUSP Program included a series of milestones that marked the progress of the DOE funded CMI work at the University of Wyoming (**Table 10 and 11**). Table 10 correlates the Milestones to the original tasks and to the FOA or ARRA segments of the funding, whereas **Table 10** references the planned completion date and actual completion date of the milestone. Both **Table 10 and 11** list the required validation of the project milestone. There is only one subtask of the study (subtask 3.5: development of an inversion methodology for EM data) that remains incomplete and the work to complete this subtask is in progress (i.e., UW collaboration with Oklahoma State University) and should be complete in the spring of 2014.

Deliverables	**Completed**
Design and plan a sub-commercial CO_2 storage facility.	x
Research and identify commercial sources of CO_2.	x
Design and utilize comparisons of FEHM and Eclipse numerical simulations utilizing data obtained from the stratigraphic test well on the Rock Springs Uplift.	x
Design an efficient customized displaced water treatment facility.	x
Design and acquire 3-D/3-C seismic data and other geophysical surveys of the RSU.	x
Design and complete a stratigraphic test well.	x
Acquire a complete well log suite.	x
Design and complete the stratigraphic test well as a monitoring well.	x
Design additional injection, monitoring, production and demonstration wells for the RSU.	x
Complete detailed risk assessments and design commercial-scale sequestration projects for both sites.	x

Table 8. Deliverables for WY-CUSP project.

Issues to address	Addressed
Regional significance Sink accommodates CO_2 from regional sources	X
Capacity estimates (site) Estimated capacity to +/- 30%	X
Injectivity (site) Significant storage and adequate seals to protect USDW	X
Containment (stratigraphic) Effectiveness of seals	X
Containment (brine) Dissolution rate of CO_2 into brine	X
Containment (mineralization) Rate of mineralization	X
Leakage pathways Impacts of faults, fractures, wells	X
Site selection Tools needed to select site	X
Risk assessment Determine and rank potential risks	X
Well bore management Identify risk and mitigation strategy for wells in area	X
Produced water management Volumes and uses	X

Table 9. Issues to address for WY-CUSP.

Task	M1 Name	Milestone Description	Required by FOA	Required by ARRA	Planned Completion Date (original)	Planned Completion Date (revised)	Actual Completion Date	Validation/Notes
1.1	**FOA Milestone 1**	Updated Project Management Plan	*		3/1/2010	3/1/2010	12/17/2009	Milestones and dates were finalized in the PMP on 12/17/2009
1.5	**FOA Milestone 2**	Document links between project and RCSP and NATCARB	*		3/1/2010	3/1/2010	1/28/2010	The project team met with Dr. Tim Carr (Laramie; 1/28/2010) to establish a protocol for data transfer from WY-CUSP to NATCARB
1.4	**HQ-ARRA Milestone 1**	Hold Project Kickoff Meeting		*	3/31/2010	3/31/2010	2/4/2010	A kickoff presentation was made at the NETL-PGH facility on 02/04/2010
1.4	**FOA Milestone 3**	Submit site characterization plan	*		4/1/2010	4/1/2010	3/31/2010	A complete site characterization plan was submitted on 3/31/2010
1.4	**FOA Milestone 4**	Notification to Project Manager that reservoir data collection has been initiated	*		6/1/2010	6/1/2010	6/152010	E-mail from PI to NETL project manager dated June 15, 2010
5.1	**HQ-ARRA Milestone 2**	Begin collection of formation information from geologic surveys and private vendors		*	6/30/2010	6/30/2010	6/30/2010	Collected stratigraphic and lithologic characterization information, oil and natural gas information, rock samples, water quality information, and seismic data from multiple reference sources, including: - USGS - Rocky Mountain Geological Association - Wyoming Geological Association - American Association of Petroleum Geologists - Wyoming Oil and Gas Conservation Commission - IHS Energy on-line - Anadarko - Wyoming State Geological Survey - Personal communications.
1.4	**FOA Milestone 5**	Notification to Project Manager that subcontractors have been identified for drilling/field service operations	*		9/1/2010	9/1/2010	6/30/2010	Geokinetics has been chosen to design and complete the 3-D seismic survey over the potential CO2 storage area (i.e., area of review) on the Rock Springs Uplift. EMTEK (USA) has been selected to provide the UW characterization project with the electromagnetic data acquisition and processing. Baker Hughes, Inc. has been chosen to design and drill the stratigraphic test well.
1.3	**HQ-ARRA Milestone 3**	Semi-Annual Progress Report on data availability and field contractors		*	9/30/2010	9/30/2010	7/30/2010	The Quarterly Report for the period ending ending 6/30/10 was submitted to FITS@NETL.DOE.GOV on 7/30/10
2.1	**Finalize well design and budget**	Finalize well design and budget			10/31/2010	11/29/2010	11/29/2010	Comespondence form UW on 12/09/10 suggested that both UW and Baker Hughes had signed the drilling contract for the stratigraphic test well on 11/29/10
1.4	**FOA Milestone 6**	Notification to Project Manager that field service operations have begun at project site	*		12/1/2010	12/1/2010	12/10/2010	Geokinetics has completed 3-D seismic survey and Emtek is mobilizing for the electromagnetic survey at the field site.
1.5	**HQ-ARRA Milestone 4**	Establish database links to NATCARB and Regional Partnerships		*	12/31/2010	12/31/2010	12/13/2010	The project website URL has been supplied to the appropriate personnel responsible for the NATCARB database. The project team has ensured the functionality of all other links to the database.
1.3	**FOA Milestone 7**	Annual progress report submitted	*		1/8/2011	1/8/2011	1/7/2011	The Quarterly progress report covering the period ending December 31, 2010 will be used for this purpose. This report is due on 1/31/10 and was sent on January 7, 2011.
1.4	**FOA Milestone 8**	Notification to Project Manager that activities to populate database with geologic characterization data has begun	*		2/1/2011	2/1/2011	1/5/2011	A remote FTP Server has been created for Carbon Management Institute and WY-CUSP to serve as a database for the geologic, geomechanical, geophysical, and petrophysical characterization data. The FTP server will allow all project teams to access data and add data in a secure environment.
1.2	**HQ-ARRA Milestone 5**	Yearly Review Meeting attended		*	3/31/2011	3/31/2011	10/7/2010	The Yearly review meeting for this project was held in conjunction with the 2010 Annual Meeting of the DOE Regional Carbon Sequestration Partnerships. A presentation on Project DE-FE0002142 was made on October 7, 2010
2.3		Begin installation of monitoring well in Rock Springs Uplift (RSU)			5/31/2011	5/31/2011	4/27/2011	Drilling of the stratigraphic test/monitoring well was begun on April 24, 2011 with a small "top-hole" rig. A 16-inch conductor was set to 120 feet at the prepared drill site. By April 27, 2011, the well was drilled, cased, and cemented to a depth of 2,000 feet while awaiting the arrival of a deep-hole rig. The deep-hole rig began drilling on June 15, 2011
1.4	**FOA Milestone 9**	Notification to Project Manager that characterization wells have been drilled	*		3/1/2011	9/30/2011	8/30/2011	The site characterization well reached its total depth of 12,810 ft on 8/21/11. It was cased and cemented on August 30, 2011. The only remaining activity with the well is to install geophones for long-term microseismic monitoring, and to perform additional geophysical tests to identify the proper location of the geophones. The expected completion date of this work is 9/30/2012.
1.4	**FOA Milestone 10**	Notification to Project Manager that well logging has been completed	*		3/1/2011	9/30/2011	8/26/2011	The driller's report dated 8/26/2011 stated that all logging in the site characterization well had been completed. The University of Wyoming Project Manager stated that logging had been completed as of 09/06/2011.
4.3	**Catalog boreholes**	Catalog boreholes in potential area of review (AOR)			9/1/2011	9/30/2011	5/31/2011	Data were downloaded and entered into a GIS geodatabase from WOGCC including 262 different types of wells.
1.3	**FOA Milestone 11**	2nd Annual progress report submitted	*		1/8/2012	1/31/2012	1/6/2012	The Quarterly progress report covering the period ending December 31, 2011 will be used for this purpose. The report was submitted on January 6, 2012
5.2	**Core descriptions**	Complete core descriptions			8/31/2011	3/31/2012	3/9/2012	The core (912 total ft) is described and sample locations have been chosen for thin sections, rock strength tests and entry pressure tests.
1.2	**HQ-ARRA Milestone 6**	Yearly Review Meeting attended		*	3/31/2012	3/31/2012	11/16/2011	The project PI presented the results of the project at the DOE Carbon Storage Program Infrastructure Review Meeting, Pittsburgh, PA, November 16, 2011
	HQ-ARRA Milestone 7	HQ Milestone: Complete at least one major field activity such as well drilling, 2-D or 3-D seismic survey, or well logging		*	3/31/2012	3/31/2012	8/30/2011	3 major field activities were completed by 3/31/12: 3-D seismic survey (11/30/10); Electromagnetic Survey (2/28/11); and drilling/logging/casing of stratigraphic test well in Rock Springs Uplift (8/30/11)
	HQ-ARRA Milestone 8	Semi-annual report (i.e. Quarterly Report ending June 30, 2012) on project activities summarizing major milestones and costs for the project			9/30/2012	9/30/2012	7/27/2012	The Quarterly Report for the period ending June 30, 2012 is the functional equivalent of a semi-annual report. The report was delivered to NETL (FITS) on July 27, 2012
1.4	**FOA Milestone 12**	Notification to Project Manager that activities on the lessons learned document on site characterization have been initiated	*		11/1/2012	11/1/2012	10/24/2012	Notification that data and activities to date are being compiled in a lessons learned document was received by the NETL Project Manager on October 24, 2012. New information will continue to be added as the project nears completion.
6.2	**Formation fluid samples**	Complete analysis of formation fluid samples			3/1/2011	12/31/2012	11/15/2011	The final suite of tests to be performed on these samples has been completed. External laboratories provided the analyses to the University of Wyoming. Interpretation has been and will continue to be provided in the quarterly and annual reports.
1.7	Catalog of commercial CO2 sources	Develop catalog of commercial CO2 sources for potential sequestration in RSU area			12/31/2011	12/31/2012	12/12/2012	The catalog has been completed and includes a map of natural and anthropogenic sources of CO2. This information will be included in the next quarterly report.
2.3	**Install RSU Well**	Complete installation of monitoring well in Rock Springs Uplift (RSU)			8/31/2011	5/31/2013	4/8/2013	Geophones have been hung and monitoring has begun.
3.4, 3.5	**Seismic and EM inversion**	Complete 3-D/3-C and EM inversion on synthetic data			12/1/2011	11/30/2013		The seismic inversion has been completed utilizing a hybrid inversion strategy. The EM Inversion milestone continues to be behind due to lack of personnel. Milestone deadline has been changed.
1.8	Compare FEHM and Eclipse	Complete comparisons of FEHM and Eclipse numerical simulations utilizing data obtained from the RSU area			10/31/2012	4/30/2013	4/8/2013	Comparison of FEHM and Eclipse has been completed. Report will be attached to next quarterly report.
7.3	**3-D geologic model**	Complete 3-D geologic model			6/30/2012	6/30/2013	6/1/2013	The 3-D geologic model was completed at the beginning of June 2013. The results will be included in the next quarterly report.
1.9	Design water treatment facility.	Complete design of displaced water treatment facility.			10/31/2012	6/30/2013	4/30/2013	The water treatment facility has been designed including steps for the extraction of the lithium resource that was discovered. This was completed the end of April 2013.
1.4		Complete major field activity such as drilling or seismic survey at the site	*					

Key:	
	Milestones required by DOE for sequestration site characterization projects
	Project Milestones from original Project Management Plan
	Project Milestones added after Modification 003

		HQ Milestone: Complete at least one major field activity such as well drilling, 2-D or 3-D seismic survey, or well logging	3/31/2012					
		HQ Milestone: Complete at least one major field activity such as well drilling, 2-D or 3-D seismic survey, or well logging	6/30/2012					

Table 10. FOA milestone completion log

Milestone	Planned Completion Date	Actual Completion Date	Validation
FOA Milestone: Updated Project Management Plan	3/31/10	03/31/10	Revised PMP Sent to NETL PM via E-mail
HQ Milestone: Kick-off Meeting Held	3/31/10	02/04/10	Presentation provided to NETL on 2/4/10
FOA Milestone: Submit Site Characterization Plan	4/1/10	03/31/10	Site Characterization Plan Sent to NETL 3/31/10
FOA Milestone: Notification to Project Manager that reservoir data collection has been initiated	6/1/10	06/01/10	Milestone report sent to NETL 6/14/10
HQ Milestone: Begin collection of formation information from geologic surveys and private vendors	6/30/10	06/01/10	Collected stratigraphic and lithologic characterization information, oil and natural gas information, rock samples, water quality information, and seismic data from multiple reference sources, including: - USGS - Rocky Mountain Geological Association - Wyoming Geological Association - American Association of Petroleum Geologists - Wyoming Oil and Gas Conservation Commission - IHS Energy on-line - Anadarko - Wyoming State Geological Survey - Personal communications.
FOA Milestone: Notification to Project Manager that subcontractors have been identified for drilling/field service operations	9/1/10	06/30/10	Geokinetics has been chosen to design and complete the 3-D seismic survey over the potential CO2 storage area (i.e., area of review) on the Rock Springs Uplift. EMTEK (USA) has been selected to provide the UW characterization project with the electromagnetic data acquisition and processing. Baker Hughes, Inc. has been chosen to design and drill the stratigraphic test well.
HQ Milestone: Semi-Annual Progress Report on data availability and field contractors	9/30/10	07/30/10	The Quarterly Report for the period ending 6/30/10 was submitted to FITS@NETL.DOE.GOV on 7/30/10
FOA Milestone: Notification to Project Manager that field service operations have begun at the project site	12/1/10	12/10/10	Geokinetics has completed 3-D seismic survey and Emtek is mobilizing for the electromagnetic survey at the field site.
HQ Milestone: Establish database links to NATCARB and Regional Partnerships	12/31/10	12/13/10	The project website URL has been supplied to the appropriate personnel responsible for the NATCARB database. The project team has ensured the functionality of all other links to the database.
FOA Milestone: Notification to Project Manager that activities to populate database with geologic characterization data has begun	2/1/11	01/05/11	A remote FTP Server has been created for CMI and WY-CUSP to serve as a database for the geologic, geomechanical, geophysical, and petrophysical characterization data. The FTP server will allow all project teams to access data and add data in a secure environment.
FOA Milestone: Notification to Project Manager that characterization wells have been drilled	3/1/11	08/21/11	The planned completion date of this milestone must be postponed because the well will not be completed by 3/31/11. The revised completion is 9/30/2011
FOA Milestone: Notification to Project Manager that well logging has been completed	3/1/11	09/06/11	The planned completion date of this milestone must be postponed because the well will not be completed by 3/31/11. The revised completion is 9/30/2011
HQ Milestone: Annual Review Meeting attended	3/31/11	10/07/10	The Yearly review meeting for this project was held in conjunction with the 2010 Annual meeting of the DOE Regional Carbon Sequestration Partnerships. Presentation on Project DE-FE0002142 was made on October 7, 2010.
Complete major field activities, such as drilling or seismic surveys at several characterization sites	6/30/11	Note: This milestone was met collectively by all projects. No one project was held accountable to the milestone. Completed 8/21/11	University of Wyoming and its subcontractor Baker Hughes completed drilling the "top hole" of the site characterization well in the Rock Springs Uplift in Sweetwater County, Wyoming in May 2011. The first ~2000 ft. of hole was completed with an air-drilling rig. Drilling resumed in mid-June with a deep-hole rig to complete the full-hole depth (~14,000 ft). Two other major field activities were completed during the quarter including a 3-D seismic survey over the project site and an electromagnetic (EM) survey over the same area covered by the 3-D seismic survey.
HQ Milestone: Semi-Annual Progress Report (i.e. Quarterly Report ending June 30, 2011)	9/30/11	07/29/11	The Quarterly Progress Report for the Period Ending June 30, 2011 was received by NETL on 7/29/11
HQ Milestone: Yearly Review Meeting of all recipients; opportunities for information exchange and collaboration	12/31/2011	11/17/11	Participated in the "Carbon Storage Program Infrastructure Annual Review Meeting" held in Pittsburgh on November 15-17, 2011.
HQ Milestone: Complete at least one major field activity such as well drilling, 2-D or 3-D seismic survey, or well logging	3/31/2012	Note: This milestone was met collectively by all projects. No one project was held accountable to the milestone.	The planned completion date of this milestone has been postponed to 3/31/2013 as the EM is delayed due to a change n personnel
HQ Milestone: Complete at least one major field activity such as well drilling, 2-D or 3-D seismic survey, or well logging	6/30/2012	Note: This milestone was met collectively by all projects. No one project was held accountable to the milestone.	The planned completion date for this milestone has changed as there has been a delay in getting all of the date due to the delay from the well.
HQ Milestone: Semi-annual report (i.e. Quarterly Report ending June 30, 2012) on project activities summarizing major milestones and costs for the project 9/30/2012	09/30/12	07/31/12	Report was submitted to DOE, July 2012.
FOA Milestone: Notification to Project Manager that activities on the lessons learned document on site characterization have been initiated	11/1/12	10/24/12	Notification that data and activities to date are being compiled in a lessons learned document was received by the NETL Project Manager on 10/24/12. New information will continue to be added as the project nears completion.
HQ Milestone: Make data set from one site characterization project publicly available.	12/31/12	Note: This milestone was met collectively by all projects. No one project was held accountable to the milestone.	
HQ Milestone: Complete one major field activity to collect additional characterization data from well drilling, 2-D or 3-D seismic surveys, or well logging/testing.	03/31/13	Note: This milestone was met collectively by all projects. No one project was held accountable to the milestone.	
HQ Milestone: Complete, at a minimum, planning for one major field activity, such as well drilling, 2-D or 3-D seismic surveys, or well logging/testing.	06/30/13	Note: This milestone was met collectively by all projects. No one project was held accountable to the milestone.	
HQ Milestone: Yearly Review Meeting of active projects; opportunities for information exchange and collaboration	09/30/13	08/22/13	Attended annual meeting in Pittsburgh in August

Table 11. Project milestone completion log

CONCLUSIONS

The Wyoming Carbon Underground Storage Project (WY-CUSP), funded by the U.S. Department of Energy and the State of Wyoming, and managed by the University of Wyoming Carbon Management Institute (CMI), ended in December 2013. Results from the WY-CUSP CO_2 storage site characterization program have produced numerous scientific articles, presentations at professional meetings, new scientific discoveries, and a first of its kind book titled *Geological CO_2 storage characterization – the key to deploying clean fossil energy technology* (Springer-Verlag publication date December 2013). The WY-CUSP program has brought CMI to the forefront of geological CO_2 storage research, and also international recognition as a leader in geological CO_2 storage characterization. During the WY-CUSP program, CMI has acquired the expertise and experience required to excel at applied research directed at many of the state's most important energy/environmental problems.

In completing the WY-CUSP program, the team at CMI has thoroughly characterized the geological CO_2 storage potential of the Rock Springs Uplift. This work has provided the state with a legitimate commercial-scale geological CO_2 storage site. If and when the federal government requires that anthropogenic CO_2 be captured and stored, Wyoming will be prepared with a certified CO_2 storage site. It is important to note that stationary sources in Wyoming presently emit approximately 60Mt of CO_2 annually, and half these emissions come from industrial facilities in the southwestern part of the state. The RSU CO_2 storage site is ideally situated at the geographic center of half of Wyoming's industrial CO_2 emissions. The results of the WY-CUSP program will provide operators in Wyoming with information that is essential to obtaining the permits required to construct commercial-scale CO_2 storage facilities on the Rock Springs Uplift. As such, the CMI team has accomplished the ultimate WY-CUSP mission: delivery to Wyoming of a thoroughly characterized, certified geological CO_2 storage site that can be used as a surge tank for CO_2 utilization.

GRAPHICAL MATERIALS LIST(S)

Figures

Fig.1. Map and cross section of two premier CO_2 storage sites in Wyoming

Fig. 2. Top, results from the 3-D seismic survey, core from the stratigraphic test well, and bottom, a well log suite from the WY-CUSP study site at the Rock Springs Uplift.

Fig. 3. (a) Acoustic impedance versus density porosity for the Madison Limestone and Weber Sandstone. (b) The upper two diagrams represent stratal slices through the Upper and Middle Madison Limestone showing the variability of reservoir properties within the formation. The lower two diagrams are thin section photographs and illustrate the extreme differences in porosity within the Madison Limestone.

Fig. 4. Stratal slices parallel to bedding showing the distribution of porosity in the Upper Madison, upper Middle Madison, Middle Madison, lower Madison Limestone. The GR, density, and density porosity from the log suite at the stratigraphic test well (RSU #1) is shown at the upper left for reference. Each of the stratal slices shown is approximately 5 mi x 5 mi.

Fig. 5. Numerical simulations of three CO2 injection scenarios representing three different locations within the best reservoir interval in the Madison Limestone: the Upper Middle Madison.

Fig. 6. Thin section and core photograph of an outstanding confining layer capable of trapping helium in the Dinwoody formation (left). Modified stratigraphic column of the Rock Springs Uplift identifying confining layers and target CO_2 storage reservoirs (right). Modified from Love, Christiansen, and VerPloeg (1993)

Fig. 7. Pie charts showing dissolved gas composition of the Weber and Madison formation fluids (left). The substantial differences in composition suggest that the Madison and Weber formation fluids are not in communication. Fluid inclusion compositions for wells from the Moxa Arch and Rock Springs Uplift (right: from Campbell-Stone et.al. (2010)). In both cases the Triassic units have acted as hydrocarbon seals above the Madison and Weber formations.

Fig. 8. Vertical sections and stratal slice through the 3-D seismic volume. The homogenous nature of the Upper Madison suggests that this interval has continuous confining integrity.

Fig. 9. Output from numerical simulations of two CO_2 injection scenarios. The left panel shows a scenario in which only a small amount of formation fluid is produced during CO_2 injection, while the right panel shows a scenario in which the volume of formation fluid is produced equals the volume of CO_2 injection (1:1 ration). Note that in the left panel, CO_2 injection causes the pressure to rapidly approach fracture pressure.

Fig. 10. Diagram showing the size of the CO_2 plume resulting from CO_2 injection into the Madison Limestone from CO_2 injection at three locations in the study area (upper left panel).

Fig. 11. Schematic diagram of proposed formation fluid treatment resulting from CO_2 injection into the Madison and Weber formations on the Rock Springs Uplift. Potable water and metals are produced from the fluid, and residual brines are re-injected.

Fig.12. Map showing the location of the EOR targets (black), CO_2 pipelines (blue), CO_2 production sites (blue), and position of the Rock Springs Uplift as a regional surge tank for CO_2 and EOR projects.

Fig. 13. Example of CO_2 flooding and stranded oil recovery at the Salt Creek Oil Field.

Fig. 14. Example of a potential integrated schematic strategy for resource development in the PRB. This type of strategy more efficiently and effectively recovers energy resources by exploiting synergistic relationships among resources, thereby increasing substantially. The yellow box is the location of a potential coal-to-chemical plant, the one element of this plan not yet been deployed in the PRB.

Fig.15: Timeline of a hypothetical CCS project with the environmental laws applicable to each project stage.

Fig. 16: Timeline with the major events in the development of EPA's Class VI well regulation. The process involved a wide variety of stakeholders. Abbreviations: NoPH – Notice of Public Hearing; NoDA-RC – Notice of Data Availability and Request for Comment. (Myers, 2013).

Fig. 17. Types of stakeholders with potential interest in Class VI permitting and the likely duration for each (Myers and Kirkwood, 2012).

Fig. 18. Relation of different CCS stakeholders to well catalog and major technological tools used to create it (Myers and Kirkwood, 2012).

Fig. 19. Screen capture of Wyoming oil and gas download from the Wyoming Oil and Gas Conservation Commission (WOGCC) (Kirkwood and Myers. 2012).

Fig. 20. Some of the geodatabase tables showing the fields from the WOGCC well download that are incorporated in the well catalog (Kirkwood and Myers, 2012).

Fig. 21. Screen capture illustrating data fields and types in three of the well catalog's data tables (Kirkwood and Myers, 2012).

Fig. 22. Screen capture of the RSU well catalog user interface (Kirkwood and Myers, 2012; Myers and Kirkwood, 2012).

Fig. 23. Flow sequence for testing quarter-quarter location as constructed using AcrGIS Model Builder tool (Kirkwood and Myers, 2012).

Fig. 24. Procedure for checking consistency of WOGCC well locations based on footages (Kirkwood & Myers, 2012).

Fig. 25. Aerial photos were used to determine if plotted well locations fall on observable well pads (Kirkwood and Myers, 2012).

Fig. 26. Well locations were verified in the field using a Pathfinder GPS unit and a YUMA tablet computer (Kirkwood and Myers, 2012).

Fig. 27. Each well site GPS-verified in the field was photographed for documentation and the resultant photos added to the well catalog. (a) For producing or shut-in wells, the well placad and oil field equipment was documented. (b) At permanently abandoned well sites, the stingers were photographed for the well catalog.

Fig. 28. Risk matric for surface accumulation of carbon dioxide leaking from an abandoned oil and gas well (Nelson, 2013).

Fig. 29. Risk levels assigned to the different regulatory requires for oil and gas plugging in Wyoming (Nelson, 2013).

Fig. 30. Preliminary well risk assessment diagram for Class VI well permiting using a graphical form of multcriteria risk assessment.

Fig. 31. Leakage risk assigned based on data of well abandonment and plugging (Nelson, 2013).

Fig. 32. Results of the surface accumulation tests for the Rock Springs Uplift AOR (Nelson, 2013).

Fig. 33. (**a**) Interpreted west–east profile through the PSTM seismic volume with the RSU #1 well located on the east side. (**b**) upgoing (reflected) VSP wavefield displayed at the same time (vertical) scale as the surface seismic. Green highlights the interpreted seismic reflections

Fig. 34. Straddle packer schematic and expected flow regimes

Fig. 35. Graphical results of the mechanical integrity test

Fig. 36. Comparison between the AVO/AVA inversion and PWI on real seismic data from RSU. (a), (b) inverted P-wave velocity (V_P), (c), (d) inverted S-wave velocity (V_S) , and (e), (f) inverted density. The depths shown are with respect to the seismic datum (7,500 ft).

Fig. 37. Computed Poisson's ratio from (a) AVO inversion and (b) PWI. The depths are with respect to the seismic datum (7,500 ft).

Fig. 38. (a) Synthetic stacked data computed using the AVO inverted model. (b) Real RSU stacked data. (c) Same as (a) but computed using the PWI model.

Fig. 39: Comparison between inverted seismic impedance and inverted EM resistivity (from MacGregor, 2012).The reservoir interval is marked in both.

Fig. 40: Feasibility of combining seismic with EM in reservoir property prediction. (a)-(b) Measured and calibrated V_P and resistivity over the reservoir interval. (c) Inverted porosity and water saturation compared with their true values.

Fig. 41. Jim Bridger 3-D seismic survey. Source (shotpoint) and receiver layout overlying infrared satellite image

Fig. 42. Jim Bridger 3-D seismic survey. (**a**) CMP fold coverage map and (**b**) maximum source-receiver offset map. The dashed rectangle (3×3 mi) centered around the RSU #1 well, outlines seismic image area where the data is most reliable

Fig. 43. 3-D seismic amplitude volume displayed in three orthogonal slices. Note an overall northeast dip of reflectors and acquisition footprint pattern in the time slice (regular grid of stripes trending south-north and east-west). Approximate location of RSU #1 is shown on the time slice is shown

Fig. 44. Color-coded permeability attribute (left panel) and interval velocity (right panel) maps calculated on top of the Middle Madison horizon. Note that high-permeability area southeast from RSU #1 correlates with low-velocity zone. Labeled structure contour lines represent depth (feet) below KB at the RSU #1

Fig. 45. Example of petrographic porosity analyses on eolian Weber sands. Note bimodal grains and their influence on porosity (in blue, highlighted yellow by software).

Fig. 46-49. Clockwise from top left: **Fig. 46**, eolian sands. Note largest pore space associated with biggest grains; **Fig. 47**, massive, interdune sands with well-spaced porosity; **Fig. 48**, dissolving feldspar, center, has enhanced secondary porosity; **Fig. 49**, pressure solution of quartz grains has overgrown or infiltrated primary porosity. Note carbonate cement at the bottom of the slide.

Fig. 50-51. **Fig. 50**. (on left) identifies intergranular porosity zone; **Fig 51**. (on right) identifies moldic/vuggy porosity zone

Fig. 52: Stable isotopic analysis of Madison and Weber carbonates. The enrichment between limestone and dolostone indicates dolomitization under near-surface hypersaline fluid conditions. This is also noted in several Weber samples. Late-stage calcite as veins and fracture fill indicates higher temperature, deep burial fluid conditions.

Fig. 53. Measured permeability and porosity of the Madison with associated lithofacies. Potential reservoir zone highlighted in yellow.

Fig. 54. Massive dissolution pore in Madison dolostone.

Fig. 55: Measured porosity and permeability of the Weber Sandstone associated with lithofacies. Potential reservoir zone highlighted in yellow.

Fig. 56. 1-D burial and thermal history of the RSU#1 well site.

Fig. 57. The plot of the porosity and density versus depth for the CO_2 storage targeted reservoirs Weber Sandstone and Madison Limestone, and containment strata the Dinwoody Formation and Amsden Formation. Both porosities measured under 5.5Mpa NCS and reservoir NCS are shown.

Fig. 58. Showing the air and Klinkenberg permeability variations in both targeted reservoirs and containment formations under 5.5Mpa NCS and reservoir NCS.

Fig. 59. Cross plot of the laboratory measured porosity at reservoir conditions with the log derived bulk density porosity (A) and neutron porosity (B).

Fig. 60. Plots of the gamma ray, bulk density, neutron porosity, density porosity for the Dinwoody Formation, Phosphoria formation, Weber Sandstone, Amsden formation and Madison Limestone from RSU #1. The heavy magenta line is neutron-density porosity calculated from neutron and density porosity and is used to establish the function between the porosity and sonic velocity.

Fig. 61. Cross plot of the laboratory-measured porosity at reservoir conditions with the log derived neutron-density porosity.

Fig. 62. (**a**) The smoothed sonic velocity and neutron-density porosity of change through the Weber Sandstone in RSU #1. (**b**) The relationship between the sonic velocity and neutron-density porosity for the Weber Sandstone is derived from the cross plot.

Fig. 63. (**a**) The smoothed sonic velocity and neutron-density porosity change through the Madison Limestone in the RSU #1. (**b**) The relationship between the sonic velocity and neutron-density porosity for the Madison Limestone is derived from the cross plot.

Fig. 64. (**a**) The histograms show the porosity distributions of the targeted storage reservoirs Weber Sandstone and (**b**) Madison Limestone within the Jim Bridger 3-D simulation domain.

Fig. 65. The porosities derived from the seismic interval velocities for the Weber Sandstone and the Madison Limestone show significant heterogenetic characteristics in the geological CO_2 storage domain.

Fig. 66. Plot of the permeability versus porosity for the Weber Sandstone in the RSU and vicinity area. All porosity and permeability data are laboratory measurements on the core samples.

Fig. 67. The dominated permeability distribution of the Weber Sandstone in the Jim Bridger modeling domain**.**

Fig. 68. Plot of the permeability versus porosity for the Madison Limestone in the RSU and surrounding area. All porosity and permeability data are laboratory measurements on the core samples.

Fig.69. The permeability distribution of the Madison Limestone in the Jim Bridger modeling domain. The permeability of the Madison Limestone is characterized by bi-modal distribution.

Fig. 70. The histograms show the permeability distribution of the containment formations (**a**) Dinwoody and (**b**) Chugwater in the RSU geological CO_2 storage domain.

Fig. 71. (**a**) Cross-section of the hydrostratigraphic model showing the map view location of the JBPP. (**b**) Zoomed in view of the numerical mesh in the region of interest for injection into the Weber sandstone. Grid spacing in B is 200m in the horizontal direction.

Fig.72. The porosity distribution of the Upper-Middle Madison Limestone within the Jim Bridger storage domain. Three wells located in the higher, medium, lower reservoir quality areas are chosen to evaluate the injectivity and storage capacity of the Madison Limestone in the RSU geological CO_2 storage site.

Fig. 73: Lower Triassic siltstone with nodules of evaporite (hematite and halite) and calcite cement.

Fig. 74: Siliceous carbonate of the Amsden Formation.

Fig. 75: Biomicrite in the Madison Limestone. This thin section was taken less than 10cm from the porous dolostone unit.

Fig. 76. Dissolved gas compositions

Fig. 77. Interpreted west–east profile through the acoustic impedance volume at RSU #1. The color-coded impedance image is co-rendered with seismic amplitude section

Fig. 78. Interpreted southwest-northeast profile through seismic amplitude volume (**a**) and corresponding coherency section (**b**). Seismic amplitude variations (**a**) are presented with conventional variable area wiggle trace display method, while coherency (**b**) is shown in shades of gray-scale. The red arrowheads indicate basement-involved faults. The blue arrowheads point at near-vertical features that we interpret as dissolution pipes.

Fig. 79. Interpreted stratal slices through seismic coherency volume: (**a**) at the Middle Madison stratigraphic level, (**b**) at the Dinwoody level. Seismic coherency variations are displayed in shades of gray-scale. Note an orthogonal system of faults (red arrowheads) northeast of RSU #1 (**a**), and oval dark planforms southwest of the well along the sealing horizon (blue arrowheads in (**b**)) that are interpreted as dissolution pipes (karst collapse features). The green lines on both panels show location for vertical sections in **Fig. 77**.

Fig. 80. Interpretation of crossline though seismic data over RSU. Crossline was chosen to intersect faults mapped at the surface; no fault offset is seen at depth. From the MS thesis of Bridget Garnier, in prep

Fig. 81. Isopach map of the Rock Springs and Blair formations (100ft contour intervals). Black dots indicate location of data points. From the MS thesis of Bridget Garnier, in prep.

Fig. 82. Stress polygon and associated strength contours for the most likely stress state in the Madison. From the MS thesis of Luke Shafer (2013).

Fig. 83. (**a**) Most likely in-situ stresses in the Madison formation plotted relative to depth (left) and fracture tadpoles colored with respect to critical pore pressure (right). (**b**) Poles to Madison fractures plotted on a stereonet colored with respect to critical pore pressure. (**c**) Geomechanical parameters used in this analysis. (**d**) 3-D Mohr diagram with listed stresses used to construct Mohr circles and poles to fractures plotted as points. From MS thesis by Luke Shafer (2013).

Fig. 84. FEHM CO_2 injection simulation results for the Weber Sandston, RSU. The simulation is for a homogeneous reservoir petrophysical conditions with 10% of porosity and 1md of relative permeability. The injection rate of 31.71kg/s is constant for 50 years, then the injection ceased, and the simulation continued to run for another 50 years without CO_2 injection.

Fig. 85. FEHM CO_2 injection simulation results for the Weber Sandstone, RSU. The simulations are setup for a heterogeneous reservoir properties. The injection rate of 9.51kg/s is constant for 50 years, then the injection ceased, and the simulation continued to run for other 50 years without CO_2 injection.

Fig. 86. The pressure changes of the Weber storage reservoir at the end of the CO_2 injection. The delta pressures are different between the reservoir hydrostatic pressure and the reservoir pressure at the end of 50 year injection.

Fig. 87. FEHM CO_2 injection simulation results for the Madison Limestone, RSU. The simulation was setup for a homogeneous reservoir petrophysical conditions with 10% of porosity and 1md of relative permeability. The injection rate of 31.71kg/s is constant for 50 years, then the injection ceased, and the simulation still ran for another 50 years without CO_2 injection.

Fig. 88. FEHM CO_2 injection simulation results for the Madison Limestone, RSU. The simulations are setup for a reservoir with heterogeneous petrophysical. The injection rates of 31.71 kg/s, 15.85 kg/s, and 6.34 are constant for 50 years of injection at the Wells in the higher, medium, and lower reservoir quality areas, respectively. The injections continue for 50 years, then cease with the simulations continued to run for other 50 years without CO_2 injection.

Fig. 89. The CO_2 plume distribution based on results from the FEHM simulator for the Weber Sandstone after 50 years of injection within the Jim Bridger 3-D seismic survey area, RSU. The simulation used an injection interval of 210m, homogenous porosity (10%) and relative permeability (1md), and an injection rate of 1Mt/year in a single injection well. The up-dip boundary is opened to imitate displaced fluid production. After 50 years of CO_2 injection with a constant injection rate of 31.7kg/s, the simulation continued for 50 years to let reservoir pressure dissipate and to monitor further CO_2 migration. (**a**) Incline view; **(b**) An east-west cross section.

Fig. 90. A map view of the CO_2 plume distribution on the top of the Weber Sandstone after 1MT of CO_2 per year after 50 years of injection within the Jim Bridger 3-D seismic survey area, RSU. The plume at the top of the Weber Sandstone is nearly a circular with a radius of 1,600m. The white five-pointed star is the location of injection well.

Fig. 91. The incline view (**a**) and cross section of the CO_2 plume in the Weber Sandstone are for 15 Mt CO_2 injected into the reservoir over a 50 year injection period.

Fig. 92. The CO_2 plume distribution for the Madison Limestone after 50 years of injection within the Jim Bridger 3-D seismic survey area, RSU. The simulation used an injection interval of 121m, homogenous porosity (10%) and relative permeability (1md), and an injection rate of 1Mt/year in a single injection well. The up-dip boundary is opened to imitate displaced fluid production. (**a**) Incline view; (**b**) An east-west cross section.

Fig.93. A map view of the CO_2 plume distribution on the top of the Madison after 1MT/yr of CO_2, 50 years of injection within the Jim Bridger 3-D seismic survey area, RSU. The plume on the top of the Madison Limestone is nearly a circular with a radius of 1,950m. The black five-pointed star is the location of the injection well.

Fig. 94. The CO_2 plume distribution on the Madison Limestone with a heterogeneous reservoir after 50 years of injection within the Jim Bridger 3-D seismic survey area, RSU. (**b**) The simulation used an injection interval of 400ft, and injection rates of 1Mt/year in a single injection well in the higher reservoir quality case (**c**), 0.5Mt/year in the medium reservoir quality case (**d**), and 0.2Mt/year in the lower reservoir quality case.

Fig. 95. The map view of CO_2 plume distribution on the Madison Limestone with a heterogeneous reservoir after 50 years of injection for the RSU modeling domain. The injection rates of (**b**) 1Mt/year in a single injection well in the higher reservoir quality case, (**c**) 0.5Mt/year in the medium reservoir quality case, (**d**) and 0.2Mt/year in the lower reservoir quality case.

Fig. 96. The cross sections of CO_2 plume distribution on the Madison Limestone with a heterogeneous reservoir after 50 years of injection for the RSU modeling domain. The injection rates of (**b**) 1Mt/year in a single injection well in the higher reservoir quality area (**c**), 0.5Mt/year in the medium reservoir quality area **(d**), and 0.2Mt/year in the lower reservoir quality area.

Fig. 97. Potential water treatment and metal recovery operation.

Fig. 98 (**a**) (**b**) – Major stationary anthropogenic sources of emitted CO_2 in Wyoming, CO_2 source fields, CO_2 pipelines, CO_2 EOR fields and the RSU #1 location.

Fig. 99. Schematic diagram of sustainable energy development made possible by the convergence of resource elements in the Powder River Basin, Wyoming. All of the resource elements of this convergence can occur in an area with a 3 to 5 mile radius. Using the integrated resource development scheme illustrated in this diagram it will be possible to increase the lives of the open-pit coal mines and depleted oil fields, utilize the depleted, compartmentalized gas fields as surge tanks for EOR projects, and eliminate the presently wasted CBM water and future CO_2 emissions associated with coal conversion. At the termination of CO_2 flooding the depleted oil field can be utilized for CO_2 storage. The only resource element missing is the deployment of a coal conversion industry in the Powder River Basin. All of the resource development illustrated in this diagram can be implement with only a minimal increase in environmental degradation.

Tables

Table 1. Total core recovery, intervals, and depths from the RSU#1 well.

Table 2. Summary of results for the vertical interference test and mini-drill stem tests. Horizontal permeability (***Kxy***), vertical permeability (***Kz***), radius of investigation (r_{inv}), average pressure (P*****), and measured productivity index (PI)

Table 3. Survey acquisition details

Table 4. Parameters used for CO_2 injection simulation in the Weber Sandstone and Madison Limestone.

Table 5: Porosity and permeability measurements of core samples from sealing lithologies

Table 6: Mercury injection capillary pressure analysis and pore throat distribution of sealing lithologies

Table 7. Comparison of CO_2 storage capacity utilizing 3 different technologies – 5mi x5mi storage domain.

Table 8. Deliverables for WY-CUSP project.

Table 9. Issues to address for WY-CUSP

Table 10. FOA milestone completion log

Table 11. Project milestone completion log

REFERENCES

Adhikari S., Pafeng J., & Mallick S. (2013). Subsurface model prediction using a neural network- A real data example from the Rock-springs uplift. *Wyoming: SEG Technical Program Expanded Abstracts, 32, 3154-3158.*

Aines R., Wolery T., & Bourcier W. (2010). Fresh water generation from aquifer-pressured carbon storage. *Ninth annual conference on carbon capture and sequestration, Pittsburgh, Pennsylvania*

Alumbaugh D. L., & Morrison H. F. (1995). Theoretical and practical considerations for crosswell electromagnetic tomography assuming a cylindrical geometry. *Geophysics, 60, 846-870.*

Ambrose W. A., Lakshminarasimhan S., Holtz M. H., Núñez-López V., Hovorka S. D., & Duncan I. (2008). "Geologic factors controlling CO_2 storage capacity and permanence: case studies based on experience with heterogeneity in oil and gas reservoirs applied to CO_2 storage," *Environmental Geology* (Vol. 54, pp. 1649-1633).

Archie G. E. (1942). The electrical resistivity log as an aid in determining some reservoir characteristics. *Transactions of the AIME, 146, 54-62*.

Almutlaq M. K., & Margrave G. F. (2013). Surface-consistent matching filters for time-lapse seismic processing. *Geophysics, 78, M29-M41*.

A. P. Institute (1998). *Recommended Practices for Core Analysis (2 ed).*

Asquith G., & Gibson C. (1982). "Basic well log analysis for geologists," *American Association of Petroleum Geologist, Tulsa, Oklahoma, USA*.

Bachu S., & Adams J. J. (2003). "Sequestration of CO_2 in geological media in response to climate change: capacity of deep saline aquifers to sequester CO_2 in solution," *Energy Conversion and Management*. (Vol. 44, pp. 3151-3175).

Bachu S., Bonijolyb D., Bradshaw J., Burruss S., Hollowaye N. P., & Christensen *et al.* (2007). "CO_2 storage capacity estimation: Methodology and gaps," *International Journal of Greenhouse Gas Control,* (Vol. 1, pp. 430-443).

Baker R. W. (2004). Membrane technology and applications *(2nd ed.).* Wiley, Chichester

Bartos T. T., & Hallberg L. (2010). Chapter 5, Groundwater and hydrogeologic units. In: Copeland D, Ewald E (eds) Available groundwater determination technical memorandum, Green River Basin Water Plan II. *Report to the Wyoming Water Development Commission by the Wyoming State Geological Survey et al., p. 5-1 – 5-94*.

Bethke C. M. (1996). Geochemical reaction modeling: concepts and applications. *Oxford University Press*

Bourcier W. L., Wolery T. J., Wolfe T., Haussmann, Buscheck T. A., & Aines R. D. (2011). A preliminary cost and engineering estimate for desalinating produced formation water associated with carbon dioxide capture and storage. *International Journal of Greenhouse Gas Control 5:1319–1328*

Bowker K. A., & Jackson W. D. (1989). The Weber Sandstone at Rangely Field, Colorado. *Rocky Mountain Association of Geologists, pp. 65-80+310-311.*

Bradshaw W., & Holzapfel C. (2007). .Genetic response to rapid climate change: it's seasonal timing that matters. *Molecular Ecology,* (Vol. 17, pp. 157-166).

Brown E. M., Skuogstad W., & Fishman M. J. (1970). Methods for collection and analysis of water samples for dissolved minerals and gases, laboratory analysis. *U.S.Geological Survey Technical Water Resource Investigation 5(C1).*

Campbell-Stone E., Lynds R., Frost C., Becker T. P., & Deim B. (2010). The Wyoming Carbon Underground Storage Project: geologic characterization of the Moxa Arch and Rock Springs Uplift. *Energy Procedia 4: p. 4656-4663.*

Cartwright J., Huuse M., & Aplin A. (2007). Seal bypass systems. *AAPG Bulletin*. (Vol. 91, no. 8, pp. 1141-1166).

Chang H., & McMechan G. (2009). 3-D 3-C full-wavefield elastic inversion for estimating anisotropic parameters: A feasibility study with synthetic data. *Geophysics, 74, WCC159-WCC175*.

Chiquet P., Broseta D., & Thibeau S. (2007). Wettability alteration of caprock minerals by carbon dioxide. *Geofluids*. (Vol. 7, p. 112-122).

Constable S., & Cox C. S. (1996). Marine controlled source electromagnetic sounding 2. The PEGASUS experiment. *Journal of Geophysical Research, 101, B3, 5519-5530*.

CSLF Task Force (2008). Comparison between methodologies recommended for estimation of CO_2 storage capacity in geological media. *Phase III report, by CSLF(Carbon Sequestration Leadership Forum) Task Force on CO_2 Storage Capacity Estimation and the USDOE capacity and Fairways Subgroup of the Regional Carbon Sequestration Partnerships Program.*

Daniel R. F., & Kaldi J. G. (2008) Evaluating Seal Capacity of Caprocks and Intraformational Barriers for the Geosequestration of CO_2, in Proceedings. *PESA Eastern Australian Basins Symposium III, Sydney, p. 475 – 484.*

Deb K., Pratap A., Agarwal S., & Meyarivan T. (2002). A fast and elitist multi-objective genetic algorithm: NSGA-II. *IEEE Transaction on Evolutionary Computation, 6(2), 181-197.*

Dix C. H. (1955). Seismic velocities from surface measurements. *Geophysics 20:68–86.*

Du Z., & MacGregor L. M. (2010). Reservoir characterization from joint inversion of marine CSEM and seismic AVA data using Genetic Algorithms: a case study based on the Luva gas field. *SEG Technical Program Expanded Abstracts, 29, 737-741.*

Duan Z., Hu J., Li D., & Mao S. (2008). Densities of the CO_2–H_2O and CO_2–H_2O–NaCl Systems Up to 647K and 100MPa. *Energy Fuels.* (Vol. 22, pp. 1666-1674).

Duan Z., & Sun R. (2003). An improved model calculating CO_2 solubility in pure water and aqueous NaCl solutions from 273 to 533 K and from 0 to 2,000 bar. *Chemical Geology.*(Vol. 193, pp. 257-271).

Duan Z., Sun R., Zhu C., & Chou I. M. (2006). An improved model for the calculation of CO_2 solubility in aqueous solutions containing Na+, K+, Ca2+, Mg2+, Cl−, and SO42−. *Marine Chemistry.* (Vol. 98, pp. 131-139).

Ehrenberg S. N., Eberli G. P., Keramati M., & Moallemi S. A. (2006). Porosity-permeability relationships in interlayered limestone-dolostone reservoirs. *The American Association of Petroleum Geologists*. (Vol. 90, pp. 91-114).

Elebiju O., Matson S., Keller G., Randy, & Marfurt K. J. (2011). Integrated geophysical studies of the basement structures, the Mississippi chert, and the Arbuckle Group of Osage County region, Oklahoma. *AAPG Bulletin*. (Vol. 95, no. 3, pp. 371-393).

Fox J. E., Lambert P. W., Mast R. F., Nuss N. W., & Rein R. D. (1975). Porosity Variation in the Tensleep and its Equivalent the Weber Sandstone, Western Wyoming: A Log and Petrographic Analysis. Presented at the Symposium on *Deep Drilling Frontiers in the Central Rocky Mountains*.

Green B., & Nix R. G. (2006) Geothermal – the energy under our feet, geothermal resource estimates for the United States. *National Renewable Energy Laboratory Technical Report NREL/TP-840-40665.*

Harris P., & MacGregor L. (2006). Determination of reservoir properties from the integration of CSEM, seismic, and well-log data. *First Break, 25, 53–59.*

Hilal N., Al-Zoubi H., Darwish N. A., Mohammed A. W., & Arabi M. A. (2004) A comprehensive review of nanofiltration membranes: treatment, pretreatment, modeling, and atomic force microscopy. *Desalination 170:281–308*

Juanes R., MacMinn C. W., & Szulczewski M. L. (2010). The Footprint of the CO_2 Plume during Carbon Dioxide Storage in Saline Aquifers: Storage Efficiency for Capillary Trapping at the Basin Scale. *Transport in Porous Media.* (Vol. 82, pp. 19-30).

Karaulis M., Revil A., Zhang J., & Werkema D. D. (2012). Time-lapse joint inversion of crosswell DC resistivity and seismic data. *A numerical investigation: Geophysics, 77, D141-D157.*

Keating E. H., Hakala J. A., Viswanathana H., Capoc R., Stewart B., Gardiner J.*, et al.* (2011) The challenge of predicting groundwater quality impacts in a CO_2 leakage scenario: Results from field, laboratory, and modeling studies at a natural analog site in New Mexico, USA. *Energy Procedia.* (Vol. 1, pp. 3239–3245).

Kirkwood R., & Myers J. D. (2012). Using GIS to Advance Geological Carbon Sequestration. *2012 ERSI International Users Conference, July 23-27, 2012, San Diego, CA*.

Li T., & Mallick S. (2013). Prestack waveform inversion of four-component, two-azimuth surface seismic data for orthorhombic elastic media parameters using a nondominated sorting genetic algorithm. *SEG Technical Program Expanded Abstracts, 32, 3283-3287.*

Ligthelm R. B., de Boer R. B., & Brint J. F. (1991). Reservoir souring: sn analytical model for H_2S generations and transportations in an oil reservoir owing to bacterial activity. *Society of Petroleum Engineers SPE23141, p. 369–378.*

Lindseth R. O. (1979). Synthetic sonic logs – a process for stratigraphic interpretation. *Geophysics 44:3–26*

Love J., Christiansen, & Verploeg A. (1993). Fifth anniversary field conference Wyoming Geological Association Guidebook. *Guidebook: Wyoming Geological Association, Jubilee Anniversary Field Conference. Casper, Wyoming, p. 3.*

Mallick S. (1995). Model-based inversion of amplitude-variations-with-offset data using a genetic algorithm. *Geophysics, 60, 939-954.*

Mallick S. (1999). Some practical aspects of prestack waveform inversion using a genetic algorithm: an example from the east Texas Woodbine gas sand. *Geophysics, 64, 326–336.*

Mallick S. (2000). Prestack waveform inversion of multicomponent seismic data. *SEG Technical Program Expanded Abstracts, 19, 2273-2276.*

Mallick S. (2007). Amplitude-variation-with-offset, elastic impedance, and prestack waveform inversion, a modeling study. *Geophysics, 72, C1-C7.*

Matsuura T. (2001) Progress in membrane science and technology for seawater desalination – a review. *Desalination 134:47–54.*

Miller S. D., Marandino C., & Saltzman E. S. (2010). Ship-based measurement of air-sea CO_2 exchange by eddy covariance. *Journal of Geophysical Research-Atmospheres.* (Vol. 115, p. D02304).

Miller T. A., Vessilinov V. V., Stauffer P. H., Birdsell K. H., & Gable C. W. (2007). Integreation of geologic frameworks in meshing and setup of computational hydrogeologic models, Pajarito Plateay, New Mexico. *New Mexico Geological Society Guide Book, 58th Field Conference, Geology of the Jemez Mountains Region III.*

Myers J. D. (2013). A Guide to geologic carbon sequestration – Science, technology, and regulatory framework. *Wyoming State Geological Survey Technical Memorandum No. 4, 197 p.,* http://www.wsgs.uwyo.edu/research/energy/co2.aspx.

Myers J. D., & Kirkwood R. (2012). Using GIS to Advance Geological Carbon Sequestration. *2012 ERSI International Users Conference, July 23-27, 2012, San Diego, CA.*

Myers J. D., Kirkwood R., & Buss A.R. (2011). An Overview of Wyoming's Efforts to Create CCS Legal and Regulatory Frameworks. *Tenth Annual Conference on Carbon Capture and Sequestration, May 2-5, 2011, Pittsburgh, PA.*

Neidell N. S., & Taner M. T. (1971). Semblance and other coherency measures for multichannel data. *Geophysics 36:482–497.*

Nelson J. D. (2013). Assessment Tools for Assigning Leakage Risk to Individual Wells at a Geologic Sequestration Site in Wyoming. *M.S. Thesis, University of Wyoming, 198 pp.*

Neuzil C. E. (1994). How permeable are clays and shales? *Water Resources Research.* (Vol. 30, pp. 145-150).

Padhi A., & Mallick S. (2013a). Accurate estimation of density from the inversion of multicomponent prestack seismic waveform data using a nondominated sorting genetic algorithm. *The Leading Edge, 32, 94-98.*

Padhi A., & Mallick S. (2013b). Multicomponent prestack seismic waveform inversion in transversely isotropic media using a nondominated sorting genetic algorithm. *Geophysical Journal International (in press).*

Pafeng J., Adhikari S., & Mallick S. (2013). Prediction of a three-dimensional model volume ahead of the drill-bit using a hybrid seismic inversion- A real data example. *SEG Technical Program Expanded Abstracts, 32, 3108-3112.*

Raymer L. L., Hunt E. R., & Gardner J. S. (1980). An improved sonic transit time-to-porosity transform: Transactions of the Society of Professional Well log Analysts. *21st Annual Logging Symposium, Paper P.*

Rickett J. E., & Lumley D. E. (2001). Cross-equalization data processing for time-lapse seismic reservoir monitoring: A case study from the Gulf of Mexico. *Geophysics, 66, 1015-1025.*

Roberts A. (2001). Curvature attributes and their application to 3-D interpreted horizons. *First Break 19:85–99*

Rutqvist J., Birkholzer J., Cappa F., & Tsang C. F. (2007). Estimating maximum sustainable injection pressure during geological sequestration of CO2 using coupled fluid flow and geomechanical fault-slip analysis. *Energy Conversion and Management.* (Vol. 48, pp. 1798-1807).

Shafer L. R. (2013). Assessing injection zone fracture permeability through identification of critically stressed fracture orientations at the Rock Springs Uplift CO_2 sequestration site, SW Wyoming. *MS Thesis, University of Wyoming, 111 p.*

Socolow R., Hotinski R., Greenblatt J. B., & Pacala S. (2004). Solving the climate problem - Technologies available to curb CO_2 emissions. *Environment.* (Vol. 46, pp. 8-19).

Stauffer P. H., Surdam R. C, Jiao Z., Miller T. A., & Bentley R. D. (2009). Combining geologic data and numerical modeling to improve estimates of the CO_2 sequestration potential of the Rock Springs Uplift, Wyoming. *Energy Procedia.* (Vol. 1, pp. 2717-2724).

Surdam R. C., & Jiao Z. (2007). The Rock Springs Uplift: An outstanding geological CO_2 sequestration site in southwest Wyoming. *Wyoming State Geological Survey.*

Surdam R. C., Jiao Z. S., & Heasler H. P. (1997) Anomalously Pressured Gas Compartments in Cretaceous Rocks of the Laramide Basins of Wyoming: A New Class of Hydrocarbon Accumulation. *AAPG Memoir 67: Seals, Traps, and the Petroleum System*, *ed. AAPG, pp. 199-222.*

U.S. Department of Energy. (2009). Monitoring, verification, and account of CO_2 sotred in deep geologic formations. *DOE Document: DOE/NETL-311/081508.* http://www.netl.doe.gov/technologies/carbon_seq/refshelf/MVA_Document. Pdf.

Water-technology.net (2012) Ashkelon, Israel. *Net Resources International.* www.water-technology.net/projects/israel. *Accessed January, 2013*

WOGCC. (2013) Wyoming Oil and Gas Conservation Commission. *Casper.* http://wogcc.state.wy.us/. *Accessed 2009–2013 (Sect. 5.2).*

Yang Y., & Aplin A. C. (2010). A permeability–porosity relationship for mudstones. *Marine and Petroleum Geology.* (Vol. 27, pp. 1692-1697).

Zhou Q. L., Birkholzer J. T., Tsang C. F., & Rutqvist J. (2008). A method for quick assessment of CO_2 storage capacity in closed and semi-closed saline formations. *International Journal of Greenhouse Gas Control.* (Vol. 2, pp. 626-639).

Zyvoloski G., Dash Z., & Kelkar S. (1988). FEHM: Finite element heat and mass transfer code. *Los Alamos National Lab., NM (USA).*

Zyvoloski G., Robinson B., Dash Z., & Trease L. (1997). Users manual for the FEHM application--A finite-element heat-and mass-transfer code. *Los Alamos National Lab., NM (United States).*

BIBLIOGRAPHY

Bachu S., Gunter W. D., & Perkins E. H. (1994, April). Aquifer Disposal of Co2 - Hydrodynamic and Mineral Trapping. *Energy Conversion and Management.* (Vol. 35, pp. 269-279).

Benson S. M., & Cole D. R. (2008). CO2 Sequestration in Deep Sedimentary Formations. *Elements.* (Vol. 4, pp. 325-331).

Bickle M. J. (2009, December). Geological carbon storage. *Nature Geoscience.* (Vol. 2, pp. 815-818).

Brennan S. T., Burruss R. C., Merrill M. D., Freeman P. A., & Ruppert L. F. (2010). A Probabilistic Assessment Methodology for the Evaluation of Geologic Carbon Dioxide Storage. *U.S. Geological Survey*. U.S. Department of the Interior.

Burruss R. C., Brennan S. T., Freeman P. A., Merrill M. D., Ruppert L. F., & Becker M. F. *et al.* (2009). Development of a Probabilistic Assessment Methodology for Evaluation of Carbon Dioxide Storage. *U.S. Geological Survey*.

Celia M. A., & Nordbotten J. M. (2009, September-October). Practical modeling approaches for geological storage of carbon dioxide. *Ground Water.* (Vol. 47, pp. 627-38).

Clarey K, Bartos T, Copeland D, Hallberg L, Clark M, Thompson M. (2010). Available groundwater determination-Technical Memorandum. *WWDC Green River Basin Water Plan II–Groundwater study, Level I (2007–2009)*.

Duan ZH, Sun R. (2006, August-September). A model to predict phase equilibrium of CH4 and CO2 clathrate hydrate in aqueous electrolyte solutions. *American Mineralogist.* (Vol. 91, pp. 1346-1354).

Field CB, Raupach MR. (2004). Global Carbon Cycle : Integrating Humans, Climate, and the Natural World. *Covelo, CA, USA: Island Press*.

Friedmann SJ. (2003, March). Storing carbon in Earth. *Geotimes*. (Vol. 48, pp. 16-20).

Greenblatt JB, Sarmiento JL. (2004). Variability and climate feedback mechanisms in ocean uptake of CO2. The global carbon cycle: integrating humans, climate, and the natural world, F. C. B and R. M. R, Eds., ed. *Washington: Island Press*, p. 526.

Han WS, Stillman GA, Lu M, Lu CA, McPherson BJ, Park E. (2010, July 23). Evaluation of potential nonisothermal processes and heat transport during CO2 sequestration. *Journal of Geophysical Research-Solid Earth*. (Vol. 115, p. B7209).

Hein JR. (2002). Life cycle of the Phosphoria Formation: from deposition to the post-mining environment. *1 ed. Boston: Elsevier*.

IPCC. (2005). *Carbon Dioxide Capture and Storage*.

Jiao ZS, Surdam RC. (1997). Characteristics of Anomalously Pressured Cretaceous Shales in the Laramide Basins of Wyoming. *AAPG Memoir 67: Seals, Traps, and the Petroleum System*. *ed: AAPG, pp. 243-253.*

Kwicklisa EM, Wolfsberga AV, Stauffera PH, Walvoordb MA, Sullyc MJ. (2006). Multiphase, Multicomponent Parameter Estimation for Liquid and Vapor Fluxes in Deep Arid Systems Using Hydrologic Data and Natural Environmental Tracers. *Vadose Zone Journal*. (Vol. 5, pp. 934-950).

N. E. T. Laboratory. (2007). *Carbon Sequestration Atlas of the U.S. and Canada*. http://www.netl.doe.gov/technologies/carbon_seq/refshelf/atlas/index.html

Piper DZ, Link PK. (2002, July). An upwelling model for the Phosphoria sea: A Permian, ocean-margin sea in the northwest United States. *Aapg Bulletin*. (Vol. 86, pp. 1217-123).

Pruess K, Muller N. (2009, March 3). Formation dry-out from CO2 injection into saline aquifers. Effects of solids precipitation and their mitigation. *Water Resources Research*. (Vol. 45, p. W03402).

Stauffer P, Stein J, Travis B. (2003). The Correct Form of the Energy Balance for Fully Coupled Thermodynamics in Liquid Water. *Report LA-UR-03-155. Los Alamos National Laboratory*. *Los Alamos, New Mexico.*

Stauffer PH, Vrugt JA, Turin HJ, Gable CW, Soll WE. (2009, May). Untangling Diffusion from Advection in Unsaturated Porous Media: Experimental Data, Modeling, and Parameter Uncertainty. *Vadose Zone Journal*. (Vol. 8, pp. 510-522).

Surdam RC. (1997). A New Paradigm for Gas Exploration in Anomalously Pressured: Tight Gas Sand. Rocky Mountain Laramide Basins. *MEMOIRS-AMERICAN ASSOCIATION OF PETROLEUM GEOLOGISTS, pp. 283-298.*

Surdam RC, Jiao Z, Stauffer P, Miller T. (2009). An integrated strategy for carbon management combining geological CO2 sequestration, displaced fluid production, and water treatment. *Wyoming State Geological Survey*.

Sweeney JJ, Burnham AK. (1990). Evaluation of a simple model of vitrinite reflectance based on chemical Kinetic. *American Association of Petroleum Geologists Bulletin, 74:1559–1570.*

WOGCC. (2003). Wyoming Oil and Gas Conservation Commission, Casper.

http://wogcc.state.wy.us. Accessed 2009–2013 (Sect. 5.2)

LIST OF ACRONYMS AND ABBREVIATIONS

DST:	drill stem test
CO2:	Carbon dioxide
3-D:	Three-dimensional space
RSU:	Rock Springs Uplift
WY-CUSP:	Wyoming Carbon Underground Storage Program
DOE:	Department of Energy
Mg/L:	Milligrams per Liter
CCUS:	Carbon Capture Utilization and Sequestration
EOR:	Enhanced Oil Recovery
ECBM:	Enhanced Coal-Bed Methane
EGR:	Exhaust Gas Recirculation
CMI:	Carbon Management Institute
VSP:	vertical seismic profile
USDW:	Underground Source of Drinking Water
FEHM:	Finite Element Heat and Mass GR
ROZ:	Residual Oil Zone
PRB:	Powder River Basin
EM:	Electron Microscope
WOGCC:	Wyoming Oil and Gas Conservation Commission
GGRB:	Greater green river basin
TDS:	Total Dissolved Solids
RSU #1:	well site
HIS:	Hyperspectral Imaging Spectroscopy
WSGS:	Wyoming State Geological Survey
EPA:	Environmental Protection Agency
WDEQ:	Wyoming Department of Environmental Quality
AOR:	Accumulated Operating Results
GIS:	Geographic Information System
GPS:	Global Positioning System
UIC:	Underground Injection Control
APDS:	application to drill sundries
DEM:	digital elevation models
NIMBY:	Not in my back yard
GLRM:	graphical leakage risk matrix
NOPH:	Notice Of Public Hearing
MSL:	Mean Sea Level
ASR:	Aquifer Storage and Recovery
KB:	Kelly bushing
SRD:	Seismic Reference Datum
RMS:	Records Management System
CMP:	Connection Management Protocol
P-WAVE:	Seismic reflection wave
VIT:	Virtual Information Technology
SP:	Straddle packer
OP:	Observation probe
NoDA-RC:	Notice of Data Availability and Request for Comment
WDEQ:	Wyoming Department of Environmental Quality
WQRR:	Wyoming Water Quality Rules and Regulations

TD:	total depth
PBTD:	Plug back total depth
AVO:	amplitude-variation-with-offset
AVA:	amplitude-variation-with-angle
CED:	circular electric dipole
HED:	horizontal electric dipole
CDP:	common-depth-point
STFT:	Short Time Fourier Transform
GCS:	geological CO_2 storage project
NCS:	net confining stress
JBPP:	Jim Bridger Power Plant
PRB:	Powder River Basin

APPENDICES

APPENDIX A: VSP SUPPLEMENTAL DATA

Plate 1

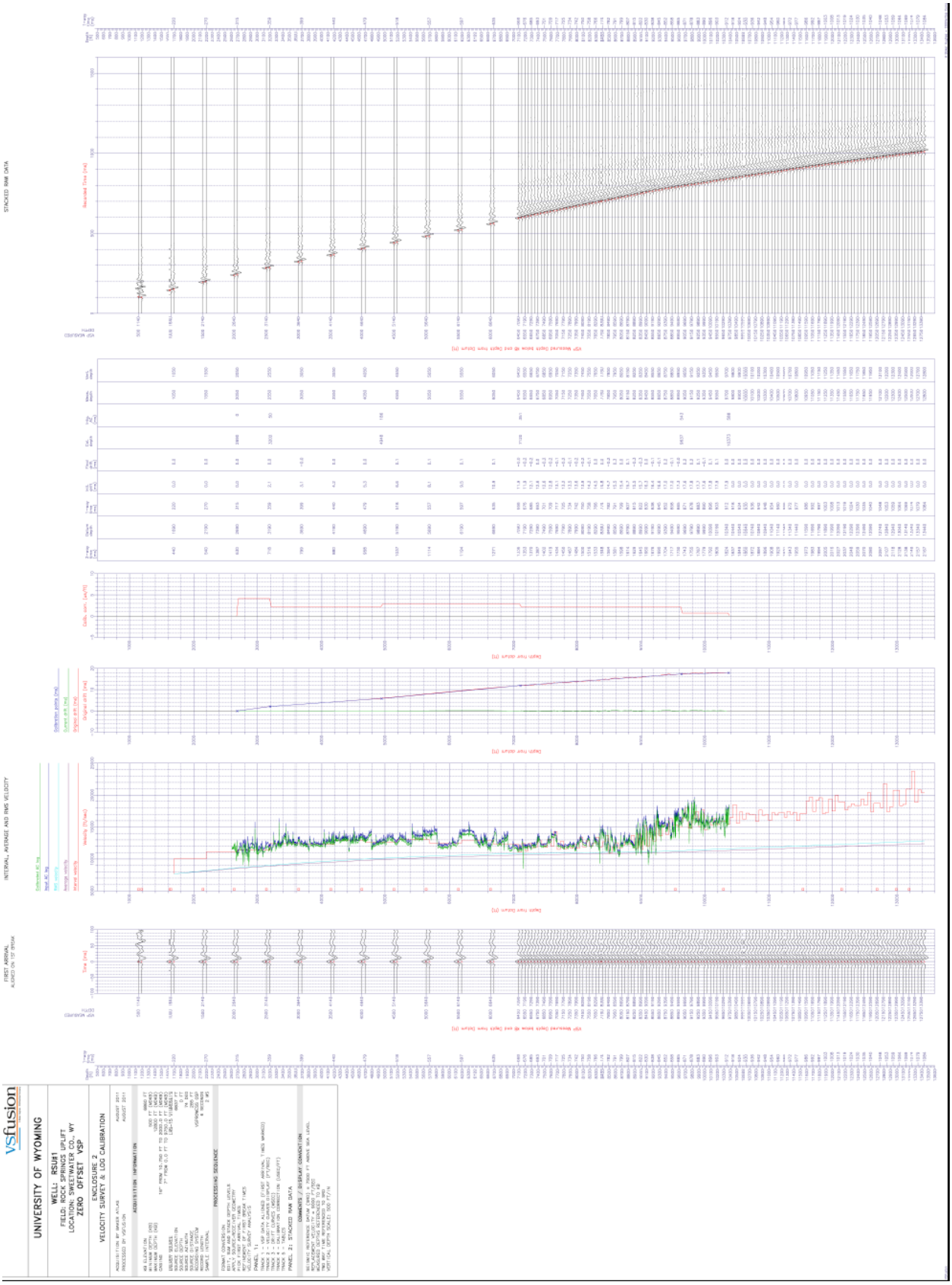

UNIVERSITY OF WYOMING
WELL: RSU#1
FIELD: ROCK SPRINGS UPLIFT
LOCATION: SWEETWATER CO., WY
ZERO OFFSET VSP
ENCLOSURE 2
VELOCITY SURVEY & LOG CALIBRATION
STACKED RAW DATA
INTERVAL, AVERAGE AND RMS VELOCITY
FIRST ARRIVAL

Plate 2

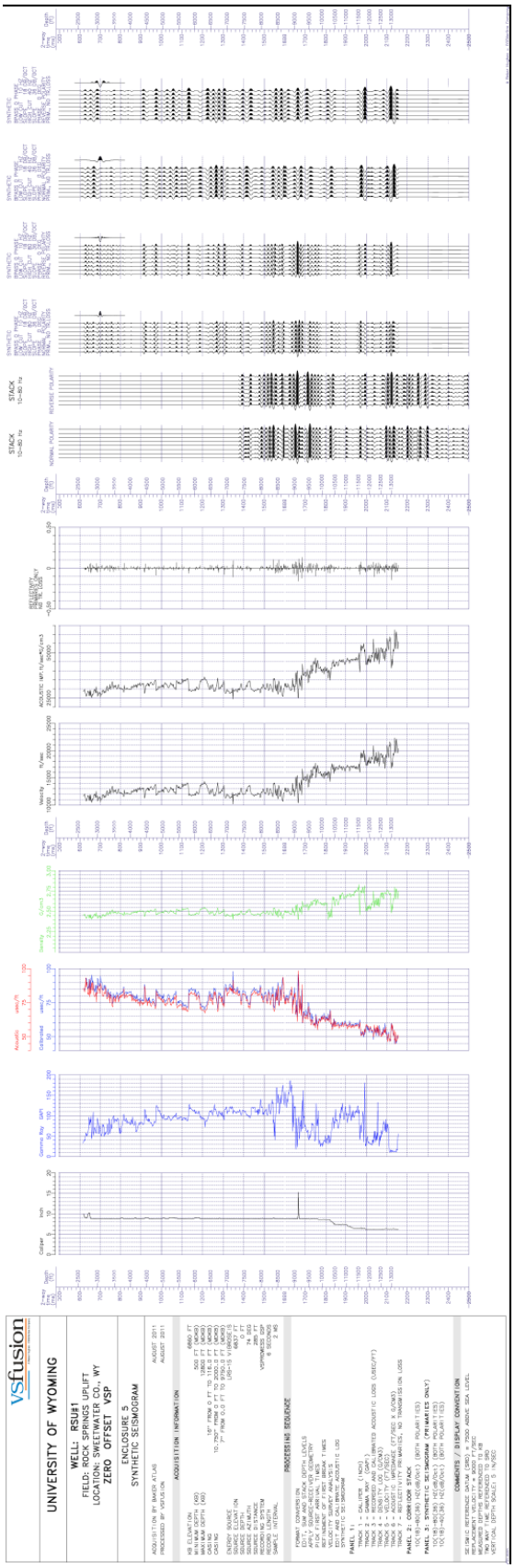


Plate 3

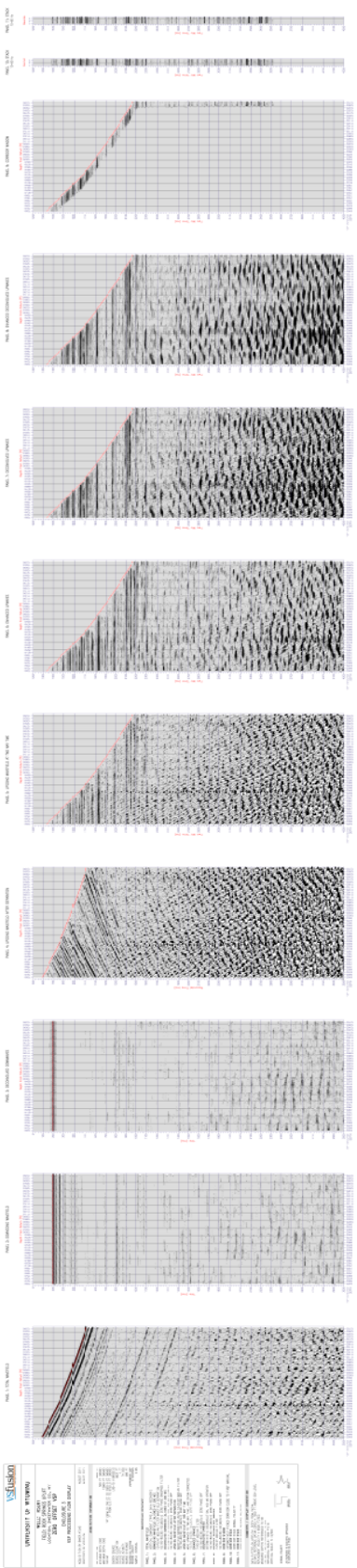


Plate 4

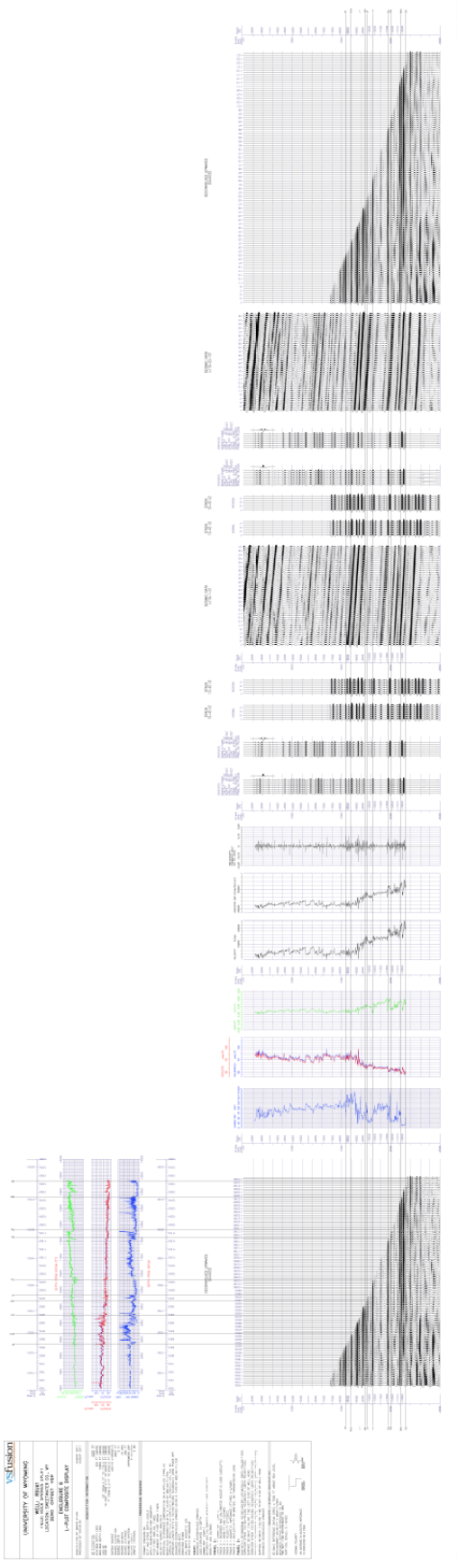


Plate 5

TIME [msec]	DEPTH reference [feet]	
	Seis_Datum	KB_RSU#1
0.0	0.0	-640.0
2.0	7.7	-632.3
4.0	15.4	-624.6
6.0	23.0	-617.0
8.0	30.7	-609.3
10.0	38.4	-601.6
12.0	46.1	-593.9
14.0	53.8	-586.2
16.0	61.4	-578.6
18.0	69.1	-570.9
20.0	76.8	-563.2
22.0	84.5	-555.5
24.0	92.2	-547.8
26.0	99.8	-540.2
28.0	107.5	-532.5
30.0	115.2	-524.8
32.0	122.9	-517.1
34.0	130.6	-509.4
36.0	138.2	-501.8
38.0	145.9	-494.1
40.0	153.6	-486.4
42.0	161.3	-478.7
44.0	169.0	-471.0
46.0	176.6	-463.4
48.0	184.3	-455.7
50.0	192.0	-448.0
52.0	199.7	-440.3
54.0	207.4	-432.6
56.0	215.0	-425.0
58.0	222.7	-417.3
60.0	230.4	-409.6
62.0	238.1	-401.9
64.0	245.8	-394.2
66.0	253.4	-386.6

TIME [msec]	DEPTH reference [feet]	
	Seis_Datum	KB_RSU#1
68.0	261.1	-378.9
70.0	268.8	-371.2
72.0	276.5	-363.5
74.0	284.2	-355.8
76.0	291.8	-348.2
78.0	299.5	-340.5
80.0	307.2	-332.8
82.0	314.9	-325.1
84.0	322.6	-317.4
86.0	330.2	-309.8
88.0	337.9	-302.1
90.0	345.6	-294.4
92.0	353.3	-286.7
94.0	361.0	-279.0
98.0	376.3	-263.7
100.0	384.0	-256.0
102.0	391.7	-248.3
104.0	399.4	-240.6
106.0	407.0	-233.0
108.0	414.7	-225.3
110.0	422.4	-217.6
112.0	430.1	-209.9
114.0	437.8	-202.2
116.0	445.4	-194.6
118.0	453.1	-186.9
120.0	460.8	-179.2
122.0	468.5	-171.5
124.0	476.2	-163.8
126.0	483.8	-156.2
128.0	491.5	-148.5
130.0	499.2	-140.8
132.0	506.9	-133.1
134.0	514.6	-125.4
136.0	522.2	-117.8
138.0	529.9	-110.1
140.0	537.6	-102.4

TIME [msec]	DEPTH reference [feet]	
	Seis_Datum	KB_RSU#1
142.0	545.3	-94.7
144.0	553.0	-87.0
146.0	560.6	-79.4
148.0	568.3	-71.7
150.0	576.0	-64.0
152.0	583.7	-56.3
154.0	591.4	-48.6
156.0	599.0	-41.0
158.0	606.7	-33.3
160.0	614.4	-25.6
162.0	622.1	-17.9
164.0	629.8	-10.2
166.0	637.4	-2.6
168.0	645.1	5.1
170.0	652.8	12.8
172.0	660.5	20.5
174.0	668.2	28.2
176.0	675.8	35.8
178.0	683.5	43.5
180.0	691.2	51.2
182.0	698.9	58.9
184.0	706.6	66.6
186.0	714.2	74.2
188.0	721.9	81.9
190.0	729.6	89.6
192.0	737.3	97.3
194.0	745.0	105.0
196.0	752.6	112.6
198.0	760.3	120.3
200.0	768.0	128.0
202.0	775.7	135.7
204.0	783.4	143.4
206.0	791.0	151.0
208.0	798.7	158.7
210.0	806.4	166.4
212.0	814.1	174.1

TIME [msec]	DEPTH reference [feet]	
	Seis_Datum	KB_RSU#1
214.0	822.0	181.5
216.0	829.4	189.4
218.0	837.1	197.1
220.0	844.8	204.8
222.0	852.5	212.5
224.0	860.2	220.2
226.0	867.8	227.8
228.0	875.5	235.5
230.0	883.2	243.2
232.0	890.9	250.9
234.0	898.6	258.6
236.0	906.2	266.2
238.0	913.9	273.9
240.0	921.6	281.6
242.0	929.3	289.3
244.0	937.0	297.0
246.0	944.6	304.6
248.0	952.3	312.3
250.0	960.0	320.0
252.0	967.7	327.7
254.0	975.4	335.4
256.0	983.0	343.0
258.0	990.7	350.7
260.0	998.4	358.4
262.0	1006.1	366.1
264.0	1013.8	373.8
266.0	1021.4	381.4
268.0	1029.1	389.1
270.0	1036.8	396.8
272.0	1044.5	404.5
274.0	1052.2	412.2
276.0	1059.8	419.8
278.0	1067.5	427.5
280.0	1075.2	435.2
282.0	1082.9	442.9
284.0	1090.6	450.6

TIME [msec]	DEPTH reference [feet]	
	Seis_Datum	KB_RSU#1
286.0	1098.2	458.2
288.0	1105.9	465.9
290.0	1113.6	473.6
292.0	1121.3	481.3
294.0	1129.0	489.0
296.0	1136.6	496.6
298.0	1144.3	504.3
300.0	1152.0	512.0
302.0	1159.7	519.7
304.0	1167.4	527.4
306.0	1175.0	535.0
308.0	1182.7	542.7
310.0	1190.4	550.4
312.0	1198.1	558.1
314.0	1205.8	565.8
316.0	1213.4	573.4
318.0	1221.1	581.1
320.0	1228.8	588.8
322.0	1236.5	596.5
324.0	1244.2	604.2
326.0	1251.8	611.8
328.0	1259.5	619.5
330.0	1267.2	627.2
332.0	1274.9	634.9
334.0	1282.5	642.5
336.0	1290.2	650.2
338.0	1297.9	657.9
340.0	1305.6	665.6
342.0	1313.3	673.3
344.0	1320.9	680.9
346.0	1328.6	688.6
348.0	1336.3	696.3
350.0	1344.0	704.0
352.0	1351.7	711.7
354.0	1359.3	719.3
356.0	1367.0	727.0

TIME [msec]	DEPTH reference [feet]	
	Seis_Datum	KB_RSU#1
358.0	1374.7	734.7
360.0	1382.4	742.4
362.0	1390.1	750.1
364.0	1397.7	757.7
366.0	1405.4	765.4
368.0	1413.1	773.1
370.0	1420.8	780.8
372.0	1428.5	788.5
374.0	1436.1	796.1
376.0	1443.8	803.8
378.0	1451.5	811.5
380.0	1459.2	819.2
382.0	1466.9	826.9
384.0	1474.5	834.5
386.0	1482.2	842.2
388.0	1489.9	849.9
390.0	1497.6	857.6
392.0	1505.3	865.3
394.0	1512.9	872.9
396.0	1520.6	880.6
398.0	1528.3	888.3
400.0	1536.0	896.0
402.0	1543.7	903.7
404.0	1551.3	911.3
406.0	1559.0	919.0
408.0	1566.7	926.7
410.0	1574.4	934.4
412.0	1582.1	942.1
414.0	1589.7	949.7
416.0	1597.4	957.4
418.0	1605.1	965.1
420.0	1612.8	972.8
422.0	1620.5	980.5
424.0	1628.1	988.1
426.0	1635.8	995.8
428.0	1643.5	1003.5

TIME [msec]	DEPTH reference [feet]	
	Seis_Datum	KB_RSU#1
430.0	1651.2	1011.2
432.0	1658.9	1018.9
434.0	1666.5	1026.5
436.0	1674.2	1034.2
438.0	1681.9	1041.9
440.0	1689.6	1049.6
442.0	1699.5	1059.5
444.0	1709.5	1069.5
446.0	1719.5	1079.5
448.0	1729.6	1089.6
450.0	1739.6	1099.6
452.0	1749.6	1109.6
454.0	1759.6	1119.6
456.0	1769.7	1129.7
458.0	1779.7	1139.7
460.0	1789.7	1149.7
462.0	1799.7	1159.7
464.0	1809.8	1169.8
466.0	1819.8	1179.8
468.0	1829.8	1189.8
470.0	1839.8	1199.8
472.0	1849.9	1209.9
474.0	1859.9	1219.9
476.0	1869.9	1229.9
478.0	1879.9	1239.9
480.0	1890.0	1250.0
482.0	1900.0	1260.0
484.0	1910.0	1270.0
486.0	1920.1	1280.1
488.0	1930.1	1290.1
490.0	1940.1	1300.1
492.0	1950.1	1310.1
494.0	1960.2	1320.2
496.0	1970.2	1330.2
498.0	1980.2	1340.2
500.0	1990.2	1350.2

TIME [msec]	DEPTH reference [feet]	
	Seis_Datum	KB_RSU#1
502.0	2000.3	1360.3
504.0	2010.3	1370.3
506.0	2020.3	1380.3
508.0	2030.3	1390.3
510.0	2040.4	1400.4
512.0	2050.4	1410.4
514.0	2060.4	1420.4
516.0	2070.4	1430.4
518.0	2080.5	1440.5
520.0	2090.5	1450.5
522.0	2100.5	1460.5
524.0	2110.5	1470.5
526.0	2120.6	1480.6
528.0	2130.6	1490.6
530.0	2140.6	1500.6
532.0	2150.6	1510.6
534.0	2160.7	1520.7
536.0	2170.7	1530.7
538.0	2180.7	1540.7
540.0	2190.8	1550.8
542.0	2201.8	1561.8
544.0	2212.8	1572.8
546.0	2223.8	1583.8
548.0	2234.8	1594.8
550.0	2245.8	1605.8
552.0	2256.8	1616.8
554.0	2267.8	1627.8
556.0	2278.8	1638.8
558.0	2289.8	1649.8
560.0	2300.8	1660.8
562.0	2311.7	1671.7
564.0	2322.7	1682.7
566.0	2333.7	1693.7
568.0	2344.7	1704.7
570.0	2355.0	1715.0
572.0	2366.7	1726.7

TIME [msec]	DEPTH reference [feet]	
	Seis_Datum	KB_RSU#1
574.0	2377.7	1737.7
576.0	2388.7	1748.7
578.0	2399.7	1759.7
580.0	2410.7	1770.7
582.0	2421.7	1781.7
584.0	2432.7	1792.7
586.0	2443.7	1803.7
588.0	2454.7	1814.7
590.0	2465.7	1825.7
592.0	2476.6	1836.6
594.0	2487.6	1847.6
596.0	2498.6	1858.6
598.0	2509.6	1869.6
600.0	2520.6	1880.6
602.0	2531.6	1891.6
604.0	2542.6	1902.6
606.0	2553.6	1913.6
608.0	2564.6	1924.6
610.0	2575.6	1935.6
612.0	2586.6	1946.6
614.0	2597.6	1957.6
616.0	2608.6	1968.6
618.0	2620.3	1980.3
620.0	2632.0	1992.0
622.0	2644.1	2004.1
624.0	2655.9	2015.9
626.0	2667.3	2027.3
628.0	2678.0	2038.0
630.0	2689.5	2049.5
632.0	2700.2	2060.2
634.0	2711.1	2071.1
636.0	2722.2	2082.2
638.0	2733.9	2093.9
640.0	2745.5	2105.5
642.0	2757.3	2117.3
644.0	2768.4	2128.4

TIME [msec]	DEPTH reference [feet]	
	Seis_Datum	KB_RSU#1
646.0	2778.7	2138.7
648.0	2790.7	2150.7
650.0	2801.7	2161.7
652.0	2813.3	2173.3
654.0	2824.8	2184.8
656.0	2835.5	2195.5
658.0	2846.3	2206.3
660.0	2857.6	2217.6
662.0	2868.2	2228.2
664.0	2879.1	2239.1
666.0	2890.4	2250.4
668.0	2902.1	2262.1
670.0	2914.0	2274.0
672.0	2926.0	2286.0
674.0	2937.7	2297.7
676.0	2949.3	2309.3
678.0	2961.0	2321.0
680.0	2973.5	2333.5
682.0	2985.0	2345.0
684.0	2996.6	2356.6
686.0	3007.7	2367.7
688.0	3018.6	2378.6
690.0	3029.7	2389.7
692.0	3041.0	2401.0
694.0	3052.2	2412.2
696.0	3063.8	2423.8
698.0	3075.3	2435.3
700.0	3086.0	2446.0
702.0	3097.1	2457.1
704.0	3108.1	2468.1
706.0	3119.3	2479.3
708.0	3130.7	2490.7
710.0	3142.6	2502.6
712.0	3154.4	2514.4
714.0	3166.3	2526.3
716.0	3177.9	2537.9

TIME [msec]	DEPTH reference [feet]	
	Seis_Datum	KB_RSU#1
718.0	3189.4	2549.4
720.0	3201.0	2561.0
722.0	3212.9	2572.9
724.0	3224.1	2584.1
726.0	3235.7	2595.7
728.0	3247.6	2607.6
730.0	3260.1	2620.1
732.0	3272.6	2632.6
734.0	3284.9	2644.9
736.0	3296.6	2656.6
738.0	3308.5	2668.5
740.0	3320.8	2680.8
742.0	3333.0	2693.0
744.0	3346.0	2706.0
746.0	3358.0	2718.0
748.0	3370.1	2730.1
750.0	3382.5	2742.5
752.0	3394.9	2754.9
754.0	3407.5	2767.5
756.0	3420.7	2780.7
758.0	3434.2	2794.2
760.0	3447.7	2807.7
762.0	3460.1	2820.1
764.0	3472.4	2832.4
766.0	3485.3	2845.3
768.0	3497.9	2857.9
770.0	3510.4	2870.4
772.0	3523.0	2883.0
774.0	3535.3	2895.3
776.0	3547.7	2907.7
778.0	3560.6	2920.6
780.0	3573.1	2933.1
782.0	3585.4	2945.4
784.0	3597.6	2957.6
786.0	3609.7	2969.7
788.0	3621.9	2981.9

TIME [msec]	DEPTH reference [feet]	
	Seis_Datum	KB_RSU#1
790.0	3634.4	2994.4
792.0	3647.3	3007.3
794.0	3660.0	3020.0
796.0	3672.2	3032.2
798.0	3684.7	3044.7
800.0	3696.8	3056.8
802.0	3709.1	3069.1
804.0	3721.1	3081.1
806.0	3733.3	3093.3
808.0	3745.7	3105.7
810.0	3758.0	3118.0
812.0	3769.7	3129.7
814.0	3781.8	3141.8
816.0	3793.6	3153.6
818.0	3805.0	3165.0
820.0	3817.4	3177.4
822.0	3829.8	3189.8
824.0	3842.0	3202.0
826.0	3854.1	3214.1
828.0	3866.2	3226.2
830.0	3878.2	3238.2
832.0	3890.5	3250.5
834.0	3902.7	3262.7
836.0	3914.9	3274.9
838.0	3927.0	3287.0
840.0	3939.2	3299.2
842.0	3951.3	3311.3
844.0	3963.4	3323.4
846.0	3975.4	3335.4
848.0	3987.4	3347.4
850.0	3999.6	3359.6
852.0	4011.6	3371.6
854.0	4023.9	3383.9
856.0	4036.4	3396.4
858.0	4049.1	3409.1
860.0	4061.2	3421.2

TIME [msec]	DEPTH reference [feet]	
	Seis_Datum	KB_RSU#1
862.0	4073.6	3433.6
864.0	4086.2	3446.2
866.0	4098.8	3458.8
868.0	4111.5	3471.5
870.0	4124.2	3484.2
872.0	4136.7	3496.7
874.0	4149.3	3509.3
876.0	4162.2	3522.2
878.0	4174.8	3534.8
880.0	4187.6	3547.6
882.0	4200.2	3560.2
884.0	4212.7	3572.7
886.0	4225.8	3585.8
888.0	4238.9	3598.9
890.0	4251.8	3611.8
892.0	4264.7	3624.7
894.0	4277.6	3637.6
896.0	4291.0	3651.0
898.0	4303.7	3663.7
900.0	4316.4	3676.4
902.0	4329.3	3689.3
904.0	4342.4	3702.4
906.0	4355.3	3715.3
908.0	4368.6	3728.6
910.0	4381.6	3741.6
912.0	4394.7	3754.7
914.0	4407.6	3767.6
916.0	4420.7	3780.7
918.0	4432.1	3792.1
920.0	4443.4	3803.4
922.0	4455.4	3815.4
924.0	4468.3	3828.3
926.0	4480.9	3840.9
928.0	4493.7	3853.7
930.0	4507.0	3867.0
932.0	4519.9	3879.9

TIME [msec]	DEPTH reference [feet]	
	Seis_Datum	KB_RSU#1
934.0	4532.7	3892.7
936.0	4545.7	3905.7
938.0	4558.6	3918.6
940.0	4571.5	3931.5
942.0	4584.1	3944.1
944.0	4597.1	3957.1
946.0	4610.2	3970.2
948.0	4623.5	3983.5
950.0	4636.9	3996.9
952.0	4650.3	4010.3
954.0	4663.4	4023.4
956.0	4676.5	4036.5
958.0	4689.4	4049.4
960.0	4702.2	4062.2
962.0	4715.2	4075.2
964.0	4728.2	4088.2
966.0	4741.3	4101.3
968.0	4754.8	4114.8
970.0	4768.5	4128.5
972.0	4782.3	4142.3
974.0	4795.3	4155.3
976.0	4806.9	4166.9
978.0	4818.9	4178.9
980.0	4831.1	4191.1
982.0	4843.1	4203.1
984.0	4855.2	4215.2
986.0	4867.7	4227.7
988.0	4880.0	4240.0
990.0	4892.3	4252.3
992.0	4904.6	4264.6
994.0	4917.1	4277.1
996.0	4929.7	4289.7
998.0	4942.2	4302.2
1000.0	4954.6	4314.6
1002.0	4967.1	4327.1
1004.0	4979.7	4339.7

TIME [msec]	DEPTH reference [feet]	
	Seis_Datum	KB_RSU#1
1006.0	4992.5	4352.5
1008.0	5005.2	4365.2
1010.0	5017.7	4377.7
1012.0	5030.2	4390.2
1014.0	5043.2	4403.2
1016.0	5056.3	4416.3
1018.0	5069.5	4429.5
1020.0	5082.7	4442.7
1022.0	5095.7	4455.7
1024.0	5108.7	4468.7
1026.0	5121.7	4481.7
1028.0	5134.7	4494.7
1030.0	5147.4	4507.4
1032.0	5159.9	4519.9
1034.0	5172.2	4532.2
1036.0	5184.7	4544.7
1038.0	5197.0	4557.0
1040.0	5209.7	4569.7
1042.0	5222.5	4582.5
1044.0	5235.6	4595.6
1046.0	5248.7	4608.7
1048.0	5261.9	4621.9
1050.0	5274.9	4634.9
1052.0	5287.9	4647.9
1054.0	5300.7	4660.7
1056.0	5313.5	4673.5
1058.0	5326.4	4686.4
1060.0	5339.0	4699.0
1062.0	5351.3	4711.3
1064.0	5363.5	4723.5
1066.0	5376.0	4736.0
1068.0	5388.3	4748.3
1070.0	5400.5	4760.5
1072.0	5412.5	4772.5
1074.0	5425.7	4785.7
1076.0	5439.2	4799.2

TIME [msec]	DEPTH reference [feet]	
	Seis_Datum	KB_RSU#1
1078.0	5452.7	4812.7
1080.0	5466.1	4826.1
1082.0	5479.4	4839.4
1084.0	5492.6	4852.6
1086.0	5505.8	4865.8
1088.0	5519.1	4879.1
1090.0	5532.2	4892.2
1092.0	5545.3	4905.3
1094.0	5558.4	4918.4
1096.0	5571.6	4931.6
1098.0	5584.7	4944.7
1100.0	5598.3	4958.3
1102.0	5612.1	4972.1
1104.0	5625.9	4985.9
1106.0	5639.5	4999.5
1108.0	5653.0	5013.0
1110.0	5666.7	5026.7
1112.0	5680.4	5040.4
1114.0	5694.2	5054.2
1116.0	5707.9	5067.9
1118.0	5721.3	5081.3
1120.0	5735.2	5095.2
1122.0	5749.0	5109.0
1124.0	5762.8	5122.8
1126.0	5776.8	5136.8
1128.0	5790.9	5150.9
1130.0	5804.8	5164.8
1132.0	5818.1	5178.1
1134.0	5829.9	5189.9
1136.0	5841.8	5201.8
1138.0	5853.8	5213.8
1140.0	5865.6	5225.6
1142.0	5877.4	5237.4
1144.0	5889.2	5249.2
1146.0	5900.9	5260.9
1148.0	5912.6	5272.6

TIME [msec]	DEPTH reference [feet]	
	Seis_Datum	KB_RSU#1
1150.0	5924.5	5284.5
1152.0	5936.3	5296.3
1154.0	5948.2	5308.2
1156.0	5960.0	5320.0
1158.0	5971.9	5331.9
1160.0	5983.6	5343.6
1162.0	5995.5	5355.5
1164.0	6007.6	5367.6
1166.0	6019.6	5379.6
1168.0	6031.5	5391.5
1170.0	6044.0	5403.0
1172.0	6056.2	5416.2
1174.0	6068.5	5428.5
1176.0	6080.7	5440.7
1178.0	6093.0	5453.0
1180.0	6105.0	5465.0
1182.0	6117.1	5477.1
1184.0	6129.4	5489.4
1186.0	6141.8	5501.8
1188.0	6154.9	5514.9
1190.0	6168.6	5528.6
1192.0	6182.0	5542.0
1194.0	6195.5	5555.5
1196.0	6209.4	5569.4
1198.0	6223.3	5583.3
1200.0	6237.1	5597.1
1202.0	6251.0	5611.0
1204.0	6264.8	5624.8
1206.0	6278.7	5638.7
1208.0	6292.6	5652.6
1210.0	6306.7	5666.7
1212.0	6320.9	5680.9
1214.0	6334.8	5694.8
1216.0	6348.7	5708.7
1218.0	6362.5	5722.5
1220.0	6376.2	5736.2

TIME [msec]	DEPTH reference [feet]	
	Seis_Datum	KB_RSU#1
1222.0	6389.8	5749.8
1224.0	6402.9	5762.9
1226.0	6416.0	5776.0
1228.0	6429.0	5789.0
1230.0	6441.5	5801.5
1232.0	6453.7	5813.7
1234.0	6465.8	5825.8
1236.0	6477.7	5837.7
1238.0	6490.3	5850.3
1240.0	6502.9	5862.9
1242.0	6515.3	5875.3
1244.0	6527.5	5887.5
1246.0	6539.8	5899.8
1248.0	6552.8	5912.8
1250.0	6565.9	5925.9
1252.0	6578.4	5938.4
1254.0	6590.6	5950.6
1256.0	6602.4	5962.4
1258.0	6614.1	5974.1
1260.0	6626.1	5986.1
1262.0	6637.8	5997.8
1264.0	6649.6	6009.6
1266.0	6661.9	6021.9
1268.0	6674.4	6034.4
1270.0	6687.2	6047.2
1272.0	6700.4	6060.4
1274.0	6714.5	6074.5
1276.0	6728.4	6088.4
1278.0	6741.1	6101.1
1280.0	6753.2	6113.2
1282.0	6765.3	6125.3
1284.0	6777.6	6137.6
1286.0	6790.0	6150.0
1288.0	6802.3	6162.3
1290.0	6815.0	6174.0
1292.0	6827.3	6187.3

TIME [msec]	DEPTH reference [feet]	
	Seis_Datum	KB_RSU#1
1294.0	6840.0	6200.0
1296.0	6852.2	6212.2
1298.0	6865.3	6225.3
1300.0	6878.5	6238.5
1302.0	6891.4	6251.4
1304.0	6904.8	6264.8
1306.0	6917.7	6277.7
1308.0	6929.4	6289.4
1310.0	6940.8	6300.8
1312.0	6952.2	6312.2
1314.0	6963.4	6323.4
1316.0	6974.8	6334.8
1318.0	6986.5	6346.5
1320.0	6998.6	6358.6
1322.0	7010.5	6370.5
1324.0	7022.2	6382.2
1326.0	7034.0	6394.0
1328.0	7045.7	6405.7
1330.0	7057.3	6417.3
1332.0	7068.5	6428.5
1334.0	7080.0	6440.0
1336.0	7091.2	6451.2
1338.0	7102.8	6462.8
1340.0	7114.1	6474.1
1342.0	7125.7	6485.7
1344.0	7137.2	6497.2
1346.0	7148.8	6508.8
1348.0	7160.6	6520.6
1350.0	7171.4	6531.4
1352.0	7183.2	6543.2
1354.0	7195.0	6555.0
1356.0	7206.9	6566.9
1358.0	7218.7	6578.7
1360.0	7230.4	6590.4
1362.0	7242.4	6602.4
1364.0	7254.3	6614.3

TIME [msec]	DEPTH reference [feet]	
	Seis_Datum	KB_RSU#1
1366.0	7266.3	6626.3
1368.0	7278.0	6638.0
1370.0	7289.5	6649.5
1372.0	7301.4	6661.4
1374.0	7313.6	6673.6
1376.0	7325.6	6685.6
1378.0	7337.7	6697.7
1380.0	7349.7	6709.7
1382.0	7361.6	6721.6
1384.0	7373.9	6733.9
1386.0	7386.6	6746.6
1388.0	7399.9	6759.9
1390.0	7412.9	6772.9
1392.0	7425.6	6785.6
1394.0	7437.7	6797.7
1396.0	7449.7	6809.7
1398.0	7461.7	6821.7
1400.0	7473.6	6833.6
1402.0	7485.6	6845.6
1404.0	7497.6	6857.6
1406.0	7509.6	6869.6
1408.0	7521.6	6881.6
1410.0	7537.0	6894.0
1412.0	7546.2	6906.2
1414.0	7558.9	6918.9
1416.0	7571.6	6931.6
1418.0	7584.2	6944.2
1420.0	7596.9	6956.9
1422.0	7610.4	6970.4
1424.0	7623.9	6983.9
1426.0	7637.3	6997.3
1428.0	7650.7	7010.7
1430.0	7664.5	7024.5
1432.0	7677.6	7037.6
1434.0	7690.4	7050.4
1436.0	7702.5	7062.5

TIME [msec]	DEPTH reference [feet]	
	Seis_Datum	KB_RSU#1
1438.0	7714.6	7074.6
1440.0	7726.5	7086.5
1442.0	7738.6	7098.6
1444.0	7750.5	7110.5
1446.0	7762.4	7122.4
1448.0	7774.2	7134.2
1450.0	7786.0	7146.0
1452.0	7797.6	7157.6
1454.0	7809.3	7169.3
1456.0	7821.3	7181.3
1458.0	7833.2	7193.2
1460.0	7845.0	7205.0
1462.0	7856.8	7216.8
1464.0	7868.7	7228.7
1466.0	7880.6	7240.6
1468.0	7892.8	7252.8
1470.0	7904.9	7264.9
1472.0	7916.8	7276.8
1474.0	7928.8	7288.8
1476.0	7940.9	7300.9
1478.0	7952.9	7312.9
1480.0	7964.7	7324.7
1482.0	7976.0	7336.0
1484.0	7987.5	7347.5
1486.0	7999.6	7359.6
1488.0	8012.1	7372.1
1490.0	8024.3	7384.3
1492.0	8036.8	7396.8
1494.0	8049.6	7409.6
1496.0	8062.5	7422.5
1498.0	8075.4	7435.4
1500.0	8087.9	7447.9
1502.0	8100.2	7460.2
1504.0	8112.4	7472.4
1506.0	8124.5	7484.5
1508.0	8136.7	7496.7

TIME [msec]	DEPTH reference [feet]	
	Seis_Datum	KB_RSU#1
1510.0	8148.8	7508.8
1512.0	8161.5	7521.5
1514.0	8174.6	7534.6
1516.0	8187.6	7547.6
1518.0	8200.3	7560.3
1520.0	8212.4	7572.4
1522.0	8224.2	7584.2
1524.0	8236.2	7596.2
1526.0	8248.3	7608.3
1528.0	8260.9	7620.9
1530.0	8273.0	7633.0
1532.0	8286.9	7646.9
1534.0	8299.5	7659.5
1536.0	8311.9	7671.9
1538.0	8323.9	7683.9
1540.0	8336.2	7696.2
1542.0	8348.1	7708.1
1544.0	8360.3	7720.3
1546.0	8374.1	7734.1
1548.0	8388.2	7748.2
1550.0	8402.3	7762.3
1552.0	8416.0	7776.0
1554.0	8428.8	7788.8
1556.0	8441.0	7801.0
1558.0	8453.7	7813.7
1560.0	8465.3	7825.3
1562.0	8477.8	7837.8
1564.0	8490.4	7850.4
1566.0	8502.1	7862.1
1568.0	8513.3	7873.3
1570.0	8526.0	7886.0
1572.0	8539.4	7899.4
1574.0	8552.3	7912.3
1576.0	8564.3	7924.3
1578.0	8575.9	7935.9
1580.0	8587.4	7947.4

TIME [msec]	DEPTH reference [feet]	
	Seis_Datum	KB_RSU#1
1582.0	8600.2	7960.2
1584.0	8612.7	7972.7
1586.0	8624.5	7984.5
1588.0	8635.7	7995.7
1590.0	8646.7	8006.7
1592.0	8657.1	8017.1
1594.0	8668.1	8028.1
1596.0	8680.5	8040.5
1598.0	8692.6	8052.6
1600.0	8704.6	8064.6
1602.0	8716.8	8076.8
1604.0	8729.8	8089.8
1606.0	8742.9	8102.9
1608.0	8755.4	8115.4
1610.0	8767.8	8127.8
1612.0	8780.4	8140.4
1614.0	8792.9	8152.9
1616.0	8805.8	8165.8
1618.0	8818.8	8178.8
1620.0	8831.3	8191.3
1622.0	8843.7	8203.7
1624.0	8856.1	8216.1
1626.0	8868.2	8228.2
1628.0	8880.1	8240.1
1630.0	8892.0	8252.0
1632.0	8904.1	8264.1
1634.0	8915.4	8275.4
1636.0	8928.0	8288.0
1638.0	8942.5	8302.5
1640.0	8955.2	8315.2
1642.0	8967.7	8327.7
1644.0	8981.0	8341.0
1646.0	8992.8	8352.8
1648.0	9005.2	8365.2
1650.0	9018.0	8378.0
1652.0	9031.5	8391.5

TIME [msec]	DEPTH reference [feet]	
	Seis_Datum	KB_RSU#1
1654.0	9045.9	8405.9
1656.0	9059.9	8419.9
1658.0	9073.3	8433.3
1660.0	9089.0	8449.0
1662.0	9103.4	8463.4
1664.0	9115.8	8475.8
1666.0	9125.8	8485.8
1668.0	9136.7	8496.7
1670.0	9151.1	8511.1
1672.0	9165.5	8525.5
1674.0	9177.6	8537.6
1676.0	9191.5	8551.5
1678.0	9204.6	8564.6
1680.0	9219.4	8579.4
1682.0	9232.9	8592.9
1684.0	9243.9	8603.9
1686.0	9260.0	8620.0
1688.0	9275.9	8635.9
1690.0	9291.1	8651.1
1692.0	9305.7	8665.7
1694.0	9320.0	8680.0
1696.0	9335.2	8695.2
1698.0	9350.3	8710.3
1700.0	9365.3	8725.3
1702.0	9380.6	8740.6
1704.0	9395.4	8755.4
1706.0	9410.0	8770.0
1708.0	9424.7	8784.7
1710.0	9440.0	8800.0
1712.0	9455.3	8815.3
1714.0	9469.0	8829.0
1716.0	9482.4	8842.4
1718.0	9496.4	8856.4
1720.0	9511.0	8871.0
1722.0	9525.4	8885.4
1724.0	9541.1	8901.1

TIME [msec]	DEPTH reference [feet]	
	Seis_Datum	KB_RSU#1
1726.0	9556.5	8916.5
1728.0	9572.9	8932.9
1730.0	9589.3	8949.3
1732.0	9604.7	8964.7
1734.0	9620.3	8980.3
1736.0	9636.0	8996.0
1738.0	9652.3	9012.3
1740.0	9669.2	9029.2
1742.0	9686.0	9046.0
1744.0	9702.9	9062.9
1746.0	9719.2	9079.2
1748.0	9736.6	9096.6
1750.0	9752.9	9112.9
1752.0	9768.1	9128.1
1754.0	9783.8	9143.8
1756.0	9800.4	9160.4
1758.0	9817.1	9177.1
1760.0	9834.9	9194.9
1762.0	9851.0	9211.0
1764.0	9867.4	9227.4
1766.0	9883.5	9243.5
1768.0	9899.1	9259.1
1770.0	9916.0	9276.0
1772.0	9931.0	9291.0
1774.0	9947.1	9307.1
1776.0	9962.9	9322.9
1778.0	9978.2	9338.2
1780.0	9994.0	9354.0
1782.0	10009.1	9369.1
1784.0	10024.8	9384.8
1786.0	10040.4	9400.4
1788.0	10056.1	9416.1
1790.0	10071.3	9431.3
1792.0	10086.5	9446.5
1794.0	10102.3	9462.3
1796.0	10118.5	9478.5

TIME [msec]	DEPTH reference [feet]	
	Seis_Datum	KB_RSU#1
1798.0	10134.3	9494.3
1800.0	10149.7	9509.7
1802.0	10165.3	9525.3
1804.0	10181.0	9541.0
1806.0	10196.9	9556.9
1808.0	10212.5	9572.5
1810.0	10228.3	9588.3
1812.0	10244.2	9604.2
1814.0	10259.2	9619.2
1816.0	10275.3	9635.3
1818.0	10291.5	9651.5
1820.0	10306.5	9666.5
1822.0	10320.9	9680.9
1824.0	10337.5	9697.5
1826.0	10353.9	9713.9
1828.0	10370.6	9730.6
1830.0	10388.3	9748.3
1832.0	10405.8	9765.8
1834.0	10422.0	9782.0
1836.0	10439.0	9799.0
1838.0	10455.9	9815.9
1840.0	10471.5	9831.5
1842.0	10488.7	9848.7
1844.0	10505.0	9865.0
1846.0	10521.0	9881.0
1848.0	10538.0	9898.0
1850.0	10554.8	9914.8
1852.0	10571.7	9931.7
1854.0	10588.7	9948.7
1856.0	10605.5	9965.5
1858.0	10622.0	9982.0
1860.0	10638.5	9998.5
1862.0	10655.4	10015.4
1864.0	10672.8	10032.8
1866.0	10690.1	10050.1
1868.0	10707.0	10067.0

TIME [msec]	DEPTH reference [feet]	
	Seis_Datum	KB_RSU#1
1870.0	10724.0	10084.0
1872.0	10740.8	10100.8
1874.0	10757.6	10117.6
1876.0	10774.3	10134.3
1878.0	10791.2	10151.2
1880.0	10808.1	10168.1
1882.0	10825.1	10185.1
1884.0	10841.3	10201.3
1886.0	10857.8	10217.8
1888.0	10874.8	10234.8
1890.0	10891.0	10252.0
1892.0	10908.7	10268.7
1894.0	10925.4	10285.4
1896.0	10941.9	10301.9
1898.0	10958.2	10318.2
1900.0	10974.6	10334.6
1902.0	10991.5	10351.5
1904.0	11008.4	10368.4
1906.0	11025.0	10385.0
1908.0	11042.6	10402.6
1910.0	11059.7	10419.7
1912.0	11076.9	10436.9
1914.0	11093.7	10453.7
1916.0	11110.7	10470.7
1918.0	11127.9	10487.9
1920.0	11144.2	10504.2
1922.0	11160.8	10520.8
1924.0	11177.7	10537.7
1926.0	11194.8	10554.8
1928.0	11212.1	10572.1
1930.0	11228.9	10588.9
1932.0	11246.0	10606.0
1934.0	11263.2	10623.2
1936.0	11279.9	10639.9
1938.0	11296.8	10656.8
1940.0	11314.0	10674.0

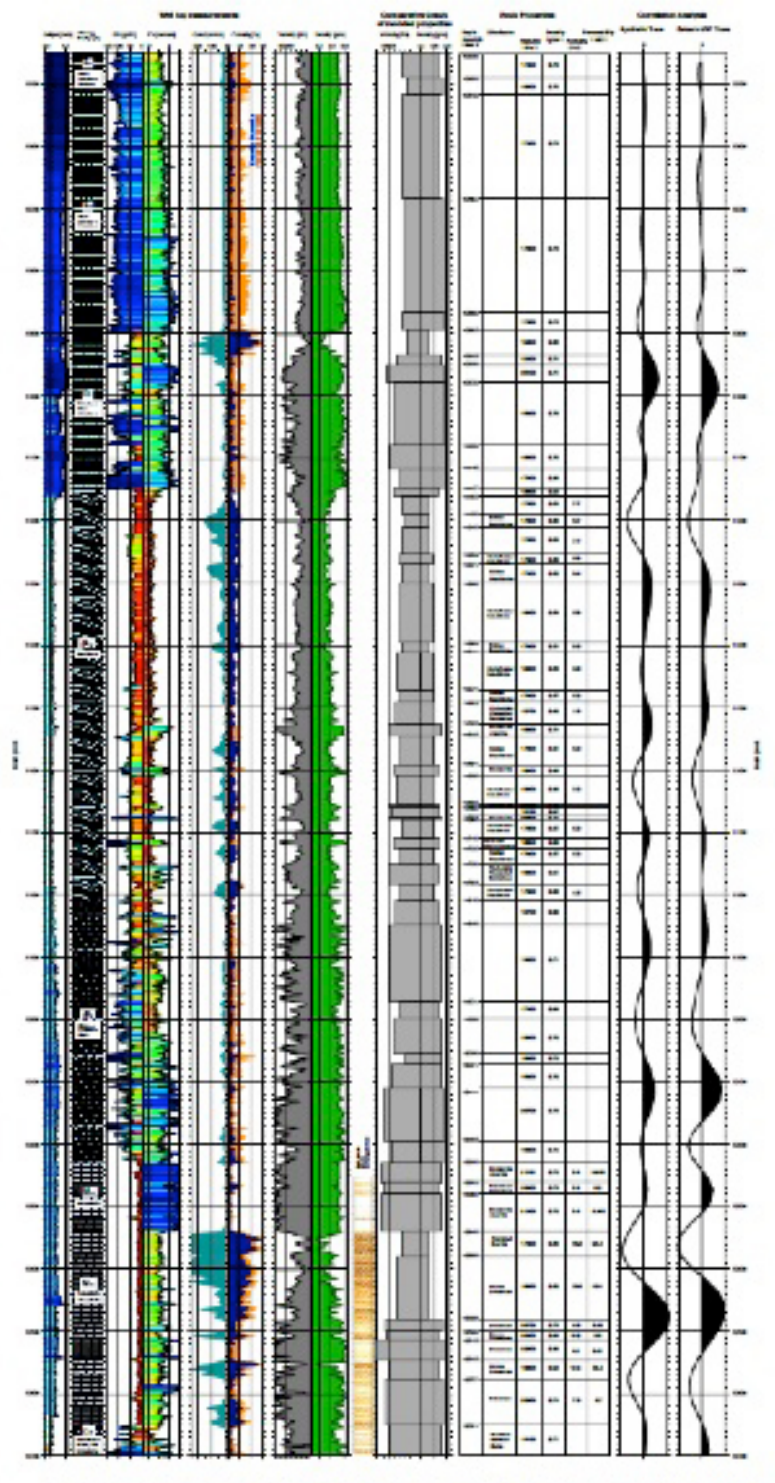
TIME [msec]	DEPTH reference [feet]	
	Seis_Datum	KB_RSU#1
1942.0	11331.2	10691.2
1944.0	11348.2	10708.2
1946.0	11365.0	10725.0
1948.0	11382.0	10742.0
1950.0	11398.6	10758.6
1952.0	11415.6	10775.6
1954.0	11432.5	10792.5
1956.0	11449.4	10809.4
1958.0	11466.0	10826.0
1960.0	11482.7	10842.7
1962.0	11499.4	10859.4
1964.0	11516.6	10876.6
1966.0	11534.1	10894.1
1968.0	11550.8	10910.8
1970.0	11567.0	10927.0
1972.0	11584.6	10944.6
1974.0	11603.6	10963.6
1976.0	11622.8	10982.8
1978.0	11641.6	11001.6
1980.0	11660.8	11020.8
1982.0	11680.1	11040.1
1984.0	11698.9	11058.9
1986.0	11718.2	11078.2
1988.0	11738.1	11098.1
1990.0	11757.8	11117.8
1992.0	11776.1	11136.1
1994.0	11794.7	11154.7
1996.0	11813.8	11173.8
1998.0	11831.6	11191.6
2000.0	11848.7	11208.7
2002.0	11866.2	11226.2
2004.0	11883.5	11243.5
2006.0	11901.2	11261.2
2008.0	11918.9	11278.9
2010.0	11936.0	11296.0
2012.0	11954.8	11314.8

TIME [msec]	DEPTH reference [feet]	
	Seis_Datum	KB_RSU#1
2014.0	11973.1	11333.1
2016.0	11991.9	11351.9
2018.0	12009.8	11369.8
2020.0	12027.6	11387.6
2022.0	12045.3	11405.3
2024.0	12063.8	11423.8
2026.0	12082.4	11442.4
2028.0	12101.1	11461.1
2030.0	12119.6	11479.6
2032.0	12138.1	11498.1
2034.0	12157.3	11517.3
2036.0	12177.6	11537.6
2038.0	12196.9	11556.9
2040.0	12214.2	11574.2
2042.0	12232.5	11592.5
2044.0	12251.6	11611.6
2046.0	12269.9	11629.9
2048.0	12287.8	11647.8
2050.0	12306.9	11666.9
2052.0	12326.0	11686.0
2054.0	12343.5	11703.5
2056.0	12362.6	11722.6
2058.0	12380.2	11740.2
2060.0	12399.5	11759.5
2062.0	12419.0	11779.0
2064.0	12436.7	11796.7
2066.0	12454.7	11814.7
2068.0	12473.0	11833.0
2070.0	12492.0	11852.0
2072.0	12511.6	11871.6
2074.0	12530.8	11890.8
2076.0	12550.2	11910.2
2078.0	12568.6	11928.6
2080.0	12587.6	11947.6
2082.0	12606.7	11966.7
2084.0	12624.3	11984.3

TIME [msec]	DEPTH reference [feet]	
	Seis_Datum	KB_RSU#1
2086.0	12642.5	12002.5
2088.0	12661.2	12021.2
2090.0	12679.0	12039.0
2092.0	12697.6	12057.6
2094.0	12714.8	12074.8
2096.0	12733.1	12093.1
2098.0	12752.1	12112.1
2100.0	12771.4	12131.4
2102.0	12791.3	12151.3
2104.0	12812.5	12172.5
2106.0	12832.1	12192.1
2108.0	12850.9	12210.9
2110.0	12870.2	12230.2
2112.0	12891.1	12251.1
2114.0	12911.7	12271.7
2116.0	12933.3	12293.3
2118.0	12954.7	12314.7
2120.0	12975.9	12335.9
2122.0	12993.8	12353.8
2124.0	13010.6	12370.6
2126.0	13028.9	12388.9
2128.0	13046.0	12406.0
2130.0	13064.0	12424.0
2132.0	13082.7	12442.7
2134.0	13102.5	12462.5
2136.0	13120.9	12480.9
2138.0	13141.9	12501.9
2140.0	13162.7	12522.7
2142.0	13185.2	12545.2
2144.0	13204.0	12564.0
2146.0	13225.3	12585.3
2148.0	13246.9	12606.9
2150.0	13267.8	12627.8
2152.0	13288.4	12648.4
2154.0	13307.9	12667.9
2156.0	13328.4	12688.4

TIME [msec]	DEPTH reference [feet]	
	Seis_Datum	KB_RSU#1
2158.0	13348.5	12708.5
2160.0	13367.9	12727.9
2162.0	13387.2	12747.2
2164.0	13407.4	12767.4
2166.0	13427.8	12787.8

Plate 6



Interpreted open-hole wireline logs from the RSU-1 well. Well lithology and stratigraphy was interpreted based on formation records and wireline logs characteristics. Porosities were derived from neutron log (orange bar-graph) and density log (blue bar-graph) assuming sandstone rock matrix (ρ = 2.67 g/cc) for the shallow depth interval (above 12231 ft), limestone rock matrix (ρ = 2.74 g/cc, 12231-12337 ft depth interval), and dolostone rock matrix (ρ = 2.87 g/cc, below 12337 ft). Fluid density = 1.1 g/cc for the whole logged interval. Acoustic porosity was calculated assuming sandstone rock matrix (Vp=19,500 ft/sec) for the shallow depth interval (above 9752 ft), and limestone rock matrix (Vp=23,200 ft/sec) for the deeper (below 9753 ft) portion of the well. Fluid velocity = 5,250 ft/sec for the whole logged interval. Sonic P-wave velocities (gray bar-graph in Velocity panel) are overlaid with interval velocities obtained from VSP measurements (black solid line)

Available Plugs and Powder

Samples

Sample #	Depth (ft)	Depth (m)
1	10601.9	3231.5
4	10605.9	3232.7
5	10607.0	3233.0
6	10610.0	3233.9
7	10619.5	3236.8
8	10619.7	3236.9
10	10621.4	3237.4
13	10627.6	3239.3
119	10628.0	3239.4
15	10629.3	3239.8
120	10636.3	3241.9
122	10649.1	3245.8
172	10649.1	3245.8
16	10656.4	3248.1
123	10659.2	3248.9
124	10662.9	3250.0
125	10671.8	3252.8
126	10676.4	3254.2
18	10682.1	3255.9
22	11194.1	3412.0
127	11197.7	3413.1
23	11200.1	3413.8
128	11200.2	3413.8
24V	11201.0	3414.1
130	11221.0	3420.2
27	11227.1	3422.0
131	11227.2	3422.1
132	11240.0	3426.0
133	11251.2	3429.4
134	11262.0	3432.7
135	11268.0	3434.5
136	11276.6	3437.1
138	11285.0	3439.7
139	11286.6	3440.1
140	11293.1	3442.1
141	11295.0	3442.7
142	11300.0	3444.2
28	11305.5	3445.9

Sample #	Depth (ft)	Depth (m)
143	11319.5	3450.2
144	11325.1	3451.9
145	11333.5	3454.5
146	11350.0	3459.5
147	11361.0	3462.8
148	11374.0	3466.8
150	11400.0	3474.7
30	11405.3	3476.3
152	11420.0	3480.8
153	11425.4	3482.5
154	11434.9	3485.4
156	11445.2	3488.5
157	11464.5	3494.4
158	11473.6	3497.1
32	11481.2	3499.5
159	11485.4	3500.7
160	11495.0	3503.7
161	11500.0	3505.2
33	11508.0	3507.6
162	11510.0	3508.2
163	11521.0	3511.6
164	11526.7	3513.3
116	11537.0	3516.5
35V	11547.1	3519.6
165	11549.9	3520.4
167	11569.9	3526.5
168	11580.0	3529.6
169	11588.5	3532.2
170	11602.3	3536.4
38V	11615.9	3540.5
172	11622.8	3542.6
173	11705.0	3567.7
174	11715.1	3570.8
40V	11718.5	3571.8
41V	11720.1	3572.3
175	11725.0	3573.8
177	11735.4	3576.9
176	11745.0	3579.9
180	11764.2	3585.7
45	11766.8	3586.5

Sample #	Depth (ft)	Depth (m)
181	11775.0	3589.0
182	11785.0	3592.1
183	11786.0	3592.4
184	11790.0	3593.6
185	11791.7	3594.1
48V	12169.8	3709.3
186	12170.0	3709.4
51	12183.1	3713.4
188	12188.1	3714.9
189	12196.8	3717.6
53	12197.4	3717.8
54V	12199.0	3718.3
191	12204.5	3719.9
193	12209.6	3721.5
194	12214.4	3722.9
195	12215.6	3723.3
197	12221.1	3725.0
198	12223.0	3725.6
199	12224.6	3726.1
201	12240.0	3730.8
203	12243.7	3731.9
58V	12247.0	3732.9
204	12249.8	3733.7
205	12255.9	3735.6
208	12309.3	3751.9
209	12313.3	3753.1
210	12318.0	3754.5
212	12323.8	3756.3
62V	12327.0	3757.3
63	12333.0	3759.1
215	12339.9	3761.2
216	12343.1	3762.2
72	12348.9	3763.9
218	12349.9	3764.2
77	12353.2	3765.2
79	12354.7	3765.7
219	12355.9	3766.1
83	12358.5	3766.9
220	12360.8	3767.6
86	12362.8	3768.2

Sample #	Depth (ft)	Depth (m)
222	12370.4	3770.5
89	12372.7	3771.2
223	12375.0	3771.9
93	12380.0	3773.4
224	12381.9	3774.0
94	12382.7	3774.3
225	12384.6	3774.8
227	12393.5	3777.5
99	12399.0	3779.2
228	12400.0	3779.5
229	12403.0	3780.4
102	12406.2	3781.4
230	12406.4	3781.5
231	12407.8	3781.9
232	12410.6	3782.7
233	12414.4	3783.9
104	12414.5	3783.9
106	12415.1	3784.1
234	12417.7	3784.9
107	12421.5	3786.1
236	12428.9	3788.3
237	12432.8	3789.5
238	12436.4	3790.6
239	12437.7	3791.0
240	12444.6	3793.1
242	12448.1	3794.2
243	12453.0	3795.7
245	12460.0	3797.8
108	12461.0	3798.1
109	12463.1	3798.7
246	12463.7	3798.9
247	12469.5	3800.7
110	12480.5	3804.1
249	12482.2	3804.6
250	12485.5	3805.6
251	12489.8	3806.9
252	12491.7	3807.5
253	12498.9	3809.6
112	12511.6	3813.5
117	12513.5	3814.1

Sample #	Depth (ft)	Depth (m)
118	12514.7	3814.5

Powder

196	12218.65
211	12218.65
180	11764.15
RSU-12	10,633.80
RSU-14	10,645.50
RSU-17	10,680.0
RSU-21	11,169.30
RSU-25	11,209.0
RSU-36	11,570.00
RSU-39	11,620.0
RSU-42	11,720.0
RSU-44	11,763.3
RSU-47	11,788.1
RSU-49	12,174.40
RSU-50	12,174.40
RSU-52	12,187.30
RSU-56	12,219.15
RSU-57	12,233.0
RSU-65	12,336.90
RSU-68	12,343.44
RSU-87	12,365.64
RSU-88	12,371.0
RSU-90	12,374.53
RSU-91	12,377.65
RSU-96	12,385.05
RSU-97	12,393.32
RSU-98	12,398.50
RSU-101	12,403.38
RSU-105	12,414.55
RSU-CV	12355.7

Appendix B: Brine Permeability Report

Brine Permeability Report

Final Report to U.S. Department of Energy

Task 6: Laboratory measurement of containment-mineralization and brine.

PI: Dr. John Kaszuba
coPI: Dr. Vladimir Alvarado

Executive Summary

This Final Report is divided into several parts, each discussing a component of Task 6 activities.

Part I. Subtask 6.1 Containment-mineralization. Reactivity of Madison Limestone in water-saturated supercritical carbon dioxide

Carbon dioxide injection in porous reservoirs is the basis for carbon capture and storage. Injected carbon dioxide is stored at multiple scales in porous media, from the pore-level as a residual phase to large scales as macroscopic accumulations by the injection site, under the caprock and at reservoir internal capillary pressure barriers. These carbon dioxide saturation zones create regions across which the full spectrum of mutual CO_2-H_2O solubility may occur. Most studies assume that geochemical reaction is restricted to rocks and carbon dioxide-saturated formation waters, but this paradigm ignores injection of anhydrous carbon dioxide against brine.

A series of laboratory experiments was performed to evaluate the reactivity of the common reservoir mineral dolomite with water-saturated supercritical carbon dioxide. Experiments were conducted at reservoir conditions (55 and 110°C, 25 MPa) and elevated temperature (220°C, 25 MPa) for approximately 96 and 164 hours (4 and 7 days). Dolomite dissolves and new carbonate mineral precipitates by reaction with water-saturated supercritical carbon dioxide. Dolomite does not react with anhydrous supercritical carbon dioxide. Temperature and reaction time control the composition, morphology, and extent of formation of new carbonate minerals.

Mineral dissolution and re-precipitation due to reaction with water-saturated carbon dioxide may affect the contact line between phases, the carbon dioxide contact angle, and the relative permeability and permeability distribution of the reservoir. These changes influence fundamental properties of hysteresis of drainage and imbibition cycles, rock wettability, and capillary pressure. The efficacy of physical carbon dioxide trapping mechanisms, integrity of caprock, and injectivity of a carbon dioxide storage reservoir may be affected.

This work has produced a manuscript authored by the following: Xiuyu Wang (Department of Geology and Geophysics), Vladimir Alvarado (Department of Chemical and Petroleum Engineering), Norbert Swoboda-Colberg (Department of Geology and Geophysics), and John P. Kaszuba (Department of Geology and Geophysics and School of Energy Resources).

Part II. Subtask 6.1 Containment-mineralization. Reactivity of caprock in water-saturated supercritical carbon dioxide and carbon dioxide-saturated brine

The purpose of this study is to conduct experiments to evaluate the reactivity of carbonate reservoir and shale caprock in both H_2O-saturated CO_2 and in CO_2-saturated brine for the potential CCS reservoir on the Rock Springs Uplift. Experiments were conducted on cuttings of Madison Limestone from RSU #1. The nature of these cuttings was such that the experiments failed to yield useable data for this report. Suitable samples of caprock of the Rock Spring Uplift were unavailable at the time this study was implemented. Instead, two shales that represent the spectrum of shale caprock compositions, from silicate-rich to carbonate rich, were evaluated. These results are also broadly applicable to understanding the reactivity of silicate-rich reservoir rock (e.g., Weber Sandstone) and carbonate-rich reservoir rock (Madison Limestone). Enhanced carbonate and silicate dissolution occurs in response to injection of supercritical CO_2. Re-precipitation of carbonates and silicates buffer the pH and alter the textures of the shale. Anhydrite precipitation may occur in response to injection of supercritical CO_2, which possibly will decrease the porosity and permeability of the shale and enhance its sealing characteristics. Clay dissolution/precipitation likely occurs and the compositional/structural changes likely affect the porosity, permeability, and wettability of the shale and possibly the large-scale basinal properties.

Part III. Subtask 6.1 Containment-mineralization. Capillary pressure. To be provided in a separate document.

Part IV. Subtask 6.1 Containment-mineralization. Rate of Mineralization. Assuming dissolution rates equal precipitation rates, the rate of carbonate mineralization in carbonate-rich rocks is 1.1×10^{-4} mol calcite m^{-2} of pore space s^{-1} (3.6×10^{2} kg calcite m^{-2} of pore space $year^{-1}$). Mineralization only takes place after the immiscible supercritical CO_2 phase dissolves into the brine. No carbonate mineralization rate can be calculated for silicate-rich rocks on the time frame of the laboratory experiments. By inference, this rate must be much less than the rate calculated for the carbonate-rich rocks. Data and analysis is presented in Part II of this report.

Part V. Subtask 6.2 Containment-brine. Analyze fluids collected from target reservoir formations in Task 2. Tabulated data and interpretation provided by S. Quillinan in a separate document.

Part VI. Subtask 6.2 Containment-brine. Dissolution rate of CO_2 into brine. A minimum CO_2 dissolution rate of 2.5×10^{-3} CO_2 mol m^{-2} pore space s^{-1} (3.5×10^{3} kg CO_2 m^{-2} pore space $year^{-1}$)
was determined for silica-rich mudstone and, by inference, sandstones such as the Weber Sandstone. A minimum CO_2 dissolution rate of 4.7×10^{-4} mol CO_2 m^{-2} pore space s^{-1} (6.5×10^{2} kg CO_2 m^{-2} pore space $year^{-1}$) was determined for carbonate-rich mudstone and, by inference, carbonate rocks such as the Madison Limestone. Detailed analysis is presented in Part II of this report.

Part I. Subtask 6.1 Containment-mineralization. Reactivity of Madison Limestone in water-saturated supercritical carbon dioxide

1 Introduction

Deep saline formations [1] such as the Madison Formation as well as depleted oil and gas reservoirs [10-13] are leading targets for Carbon Capture and Storage (CCS) reservoirs (Figure 1). Injection of carbon dioxide is also used to enhance oil or gas recovery (CO_2-EOR or CO_2-EGR) in hydrocarbon reservoirs (Figure 2). Four trapping and storage mechanisms are widely discussed in the CCS literature: structural, residual (also known as capillary trapping), hydrodynamic and mineral trapping [14]. Carbon dioxide can become a residual phase in two- and three-phase flow due to capillary action. As carbon dioxide is injected into a reservoir, anhydrous or "dry" carbon dioxide moves through the porous media and displaces resident fluids as a non-wetting phase. Capillary effects such as snap-off [15] can leave some of the carbon dioxide behind as disconnected droplets. In addition, internal heterogeneities in the formation can trap carbon dioxide at saturations well above its residual value [16, 17]. Water drainage and rewetting (or imbibition) are impacted by the advancing and receding contact angles, respectively, which contribute to multiphase flow hysteresis [18]. This hysteresis plays a very important role in residual trapping [16-19]. In the absence of significant hysteresis, little capillary trapping occurs, but local capillary trapping offers a mechanism for high saturation of carbon dioxide in the reservoir [16, 20].

During the injection period in CCS (and similarly CO_2-EOR), water (or hydrocarbon) displacement is piston-like, mostly controlled by viscous forces. This creates a near-wellbore region, on the order of several meters [15, 21], where dry-out occurs. Deeper into the formation, or in post-injection scenarios, carbon dioxide rises due to buoyancy. The saturation distribution of carbon dioxide transitions from the desiccation or dryout zones in the near-wellbore area, a few meters from the injection site, to trapped carbon dioxide. Thus, carbon dioxide injection creates regions across which the full spectrum of mutual CO_2-H_2O solubility may occur (Figure 1). Dry supercritical carbon dioxide exists at the injection-well nearby area, as a result of dry-out, whereas CO_2-saturated and -undersaturated formation waters exist at the displacement front. H_2O-saturated and -undersaturated or "wet" supercritical carbon dioxide can exist between these two chemical extremes, toward the cap rock due to buoyancy forces [15, 16] and at the CO_2-H_2O front.

Carbon dioxide can act as a wetting fluid [18] potentially leading to mixed-wettability [22]. In this scenario, different mineral surfaces are exposed to different fluids, namely either water or CO_2. The reactivity of carbon dioxide with mineral surfaces will depend on its distribution in the pore space. In contrast, most geochemical and reservoir models assume mineral surface reactivity with carbonic acid [e.g., 23, 24]. Experimental laboratory studies that evaluate fluid-rock and fluid-mineral interactions relevant to CCS and EOR scenarios traditionally focus on reactions among minerals and aqueous solutions [e.g., 25-29]. These studies are performed at conditions corresponding to CO_2-saturated and -undersaturated formation waters at the displacement front. More recently, experimental studies have begun to evaluate the reactivity of silicate and hydroxide minerals with wet supercritical carbon dioxide [30-40]. These studies agree that silicate and hydroxide minerals react with wet supercritical carbon dioxide and form carbonate minerals. Regnault et al. [41] also evaluated the reactivity of portlandite and dolomite with wet supercritical carbon dioxide but only reported results for portlandite. Not surprisingly, portlandite is highly reactive with wet supercritical carbon dioxide. Clearly it is important to understand the interactions take place between rocks and wet supercritical carbon dioxide in CCS, CO_2-EOR, and CO_2-EGR reservoirs.

In this study we investigate the reactivity of Madison Limestone with wet (H_2O-saturated) supercritical carbon dioxide in laboratory experiments. Laboratory experiments were performed using the mineral dolomite as a surrogate for Madison Limestone. Experiments were conducted at 55 and 110°C, temperatures characteristic of reservoir conditions such as those found in the Rocks Springs Uplift. We also performed experiments at 220°C to accelerate reaction rates and enhance the likelihood for results at realistic laboratory time scales. Our study qualitatively evaluates dolomite reactivity in H_2O-saturated carbon dioxide; quantitative assessment of reaction mechanisms and kinetics are beyond the scope of this study. This study demonstrates that dolomite in the Madison Limestone is reactive in H_2O-saturated supercritical carbon dioxide and explores implications for this reactivity with respect to CCS, CO_2-EOR, and CO_2-EGR in carbonate-bearing formations and hydrocarbon reservoirs.

2 Experimental Methods

2.1 Approach and Design

Our approach was to conduct experiments that react the mineral dolomite, a surrogate for Madison Limestone, with H_2O-saturated supercritical carbon dioxide (Figure 3). Recent experimental work demonstrates mineral reactivity with H_2O-undersaturated supercritical carbon dioxide [30-40]; thus dolomite reactivity in H_2O-undersaturated supercritical carbon dioxide presents a potentially fruitful avenue of investigation. However, evaluating these complexities will require additional experiments and is beyond the scope of this investigation. Therefore, for this study, maintaining water saturation was a key aspect. Water is consumed if, for example, carbonate minerals such as nesquehonite, dypingite, and hydromagnesite precipitate. To ensure water saturation of supercritical carbon dioxide for the duration of each experiment we added de-ionized water to the bottom of the reaction chamber in an amount greater than needed for saturation (Table 1). The mass of water needed to saturate supercritical carbon dioxide at the temperature and pressure conditions of each experiment was determined using equations of state for carbon dioxide [42].

The presence of liquid water in the reaction chamber presents the possibility of dolomite reaction as an artifact of the experimental procedure. Splashing water onto the dolomite, for example, could take place while injecting carbon dioxide. Our design and procedures (Section 2.3) were implemented to ensure that dolomite and bulk water remained physically separated during the experiment. As one check on our methods, one experiment was repeated using an alternative method of introducing water into the reaction chamber. As a second check on our methods, aqueous samples were withdrawn from each ongoing experiment and after terminating each experiment. This method check assumes that the chemistry of the water sampled from the bottom of the reactor will change if water splashes onto and drains from the dolomite during the course of the experiment or if dolomite powders are washed off of dolomite fragments and into the water reservoir. Thus our design provides sufficient water in the bottom of the reactor for sampling purposes while simultaneously minimizing the amount of water to avoid splashing it onto the dolomite.

2.2 Apparatus and Materials

The experimental apparatus consists of a pressurized reaction chamber and furnace (Figure 3). The experimental design places de-ionized water in the bottom of the reaction chamber and supercritical carbon dioxide with a grade of 99.95% in the top. A sample holder constructed of gold mesh and wire secures the sample above the water and in the carbon dioxide. The mesh is 99.9% pure gold and possesses a nominal aperture of 0.25 mm.

Research grade dolomite ($CaMg(CO_3)_2$) was purchased from Ward Scientific (#49 V 1557, Selasvann, Norway). The mineral composition was determined by inductively coupled plasma optical emission spectrometer (ICP-OES) after digestion with hydrochloric acid. The ratio of calcium to magnesium is about 1.3 and the ratio of magnesium to iron ranges from 4.4 to 4.5 (Figure 4). The dolomite is not uniform in composition because it contains veinlets of calcite. Use of heterogeneous dolomite does not allow us to determine quantitative reaction parameters for these experiments but does approximate natural field conditions more closely.

Dolomite was prepared for the experiments in two different ways. In the first method, dolomite fragments were stored in a container and permitted to accumulate dolomite powder on mineral surfaces due to abrasion among the fragments. The advantage of this method is that dolomite reactive surface area and the resulting kinetic rates increase, enhancing reactivity at laboratory time scales. The disadvantages are that we do not have rigorous control on the distribution of the powders on mineral surfaces and that we cannot quantify the reactive surface area of the powders. Another disadvantage is that the mineralogy of the powders varies because, as described in the previous paragraph, their dolomite source is not homogeneous. All but one of the experiments was conducted using dolomite prepared in this manner. In the alternate preparation method, dolomite was cleansed of all powders. To accomplish this, dolomite fragments were rinsed with and sonicated in de-ionized water for 30 minutes, rinsed with de-ionized water three times, rinsed with methanol, dried overnight in a hood, and dried overnight in an oven at 110°C. This method allows us to evaluate whether the use of mineral powders induced artifacts into our experiments. SEM images of dolomite prepared using this method are presented in Figure 5.

2.3 Procedures

De-ionized water was first placed at the bottom of the reaction vessel (Figure 3). The gold mesh containing 1 g of dolomite fragments (approximately 3 mm in diameter) was emplaced and the reactor sealed. To avoid generating steam that could have reacted with dolomite, the reactor was pressurized to about 5 MPa before heating. Pressurization was accomplished by injecting carbon dioxide through the port at the top of the reactor (Figure 3) using a syringe pump at a low flow rate (5 ml/min). The reactor was subsequently heated to the predetermined temperature of the experiment. Carbon dioxide was again injected until the final pressure of 25 MPa was reached.

To evaluate our procedures, one experiment was performed using a different method of adding water into the reaction chamber. In this experiment (Experiment #4, Table 1), dolomite was sealed in the reactor without water. Carbon dioxide was injected to a pressure of 5 MPa, then water was injected at a flow rate of 5 ml/min into the bottom of the reactor through the sampling tube (Figure 3). The furnace was subsequently heated to 220°C. Additional carbon dioxide was then injected until the pressure reached 25 MPa.

The mass of water placed in the reactor at the beginning of each experiment ranged from 23 to 37 g. The mole fraction of water relative to carbon dioxide in the reactor at the beginning of the experiment was equal to or less than 0.5 (Table 1). The temperature of each experiment was maintained to within 0.2°C and the pressure to within 0.7 MPa.

Aqueous samples were withdrawn from ongoing experiments using the sampling tube that extends to the deepest portion of the reactor (Figure 3). About 1 ml of solution was first collected and discarded to rinse the sampling tube and fill it with fresh fluid. The pH was subsequently determined on samples cooled to 25°C and depressurized to 0.1 MPa using a Thermo Scientific Orion 4 Star pH meter and Ross micro electrode. Samples for cation analysis were filtered using a 0.45 μm filter and diluted 10x. To prevent mineral precipitation, the samples for cation analysis were acidified to pH 2 using trace metal grade nitric acid and stored at about 5°C prior to analysis. Cations were analyzed with an ARL 3410+ ICP-OES. Mineral precipitants were not observed in any of the fluid samples. At the conclusion of each experiment the reacted dolomite was recovered, weighed, and dried in air prior to analysis. Recovered minerals were analyzed using optical microscopy, scanning electron microscopy (SEM), and energy dispersive spectra (EDS). Mineral growth in the experiments was insufficient for analysis by X-ray diffraction (XRD) or electron probe microanalysis (EPMA).

3 Results

Experiments reacting dolomite with H_2O-saturated supercritical carbon dioxide were performed at 25 MPa, 55°C and 220°C for approximately 96 and 164 hours (approximately 4 and 7 days) (Table 1). A control experiment that reacted dolomite with anhydrous supercritical carbon dioxide for 272 hours (Experiment #1) was performed at an intermediate temperature of 110°C. Dolomite fragments containing dolomite powder on mineral surfaces were used in this experiment. No evidence of dolomite dissolution or mineral growth was observed in this experiment (Figure 6).

SEM and EDS analysis of dolomite reacted with H_2O-saturated supercritical carbon dioxide at 55°C for 93 and 164 hours (Experiments #2 and #5, respectively) are shown in Figure 7. Dolomite fragments containing dolomite powder on mineral surfaces were used in these two experiments. At the conclusion of both experiments, dolomite fragments exhibit edges of cleavage planes that are no longer straight and smooth but are rounded and rough due to dissolution. Dolomite powders are no longer present on mineral surfaces. A new carbonate mineral exhibiting irregular morphology precipitated on dolomite surfaces. Crystals of this morphology are not present on unreacted dolomite (Figure 5a) or on the dolomite reacted with anhydrous supercritical carbon dioxide (Figure 6a). EDS spectra suggest that this carbonate mineral contains magnesium, calcium, and iron in relative proportions consistent with dolomite. Iron may be more abundant compared to the unreacted dolomite, however, the EDS spectra are not conclusive. New mineral growth covers a larger area of the dolomite in the 164-hour experiment compared to the 93-hour experiment. The absence of quench morphology of the new crystals and the greater extent of mineral growth as a function of reaction time suggest that mineral growth took place during the experiment and is not an artifact of the quenching process.

The results of SEM and EDS analysis of dolomite reacted with H_2O-saturated supercritical carbon dioxide at 220°C for 94 and 162 hours (Experiments #3 and #6, respectively) are shown in Figure 8. Dolomite fragments containing dolomite powder on mineral surfaces were also used in these two experiments. Dolomite powders are no longer present on mineral surfaces at the conclusion of both experiments. Two new minerals grew on dolomite surfaces, one exhibiting platelet morphology and a second of rhombohedral carbonate crystals (Figure 8). Crystals exhibiting these morphologies are not present on unreacted dolomite (Figure 5a) or on the dolomite reacted with anhydrous supercritical carbon dioxide (Figure 6a). The rhombohedral carbonates are euhedral crystals ranging in size from 1 to 5 or more microns. EDS spectra suggest that these rhombohedral carbonate minerals contain magnesium, calcium, and iron in relative proportions consistent with dolomite. Iron may again be more abundant compared to the original dolomite, however the EDS spectra are not conclusive.

An additional experiment reacted dolomite with H_2O-saturated supercritical carbon dioxide at 220°C for 90 hours (Experiment #4). This is the experiment in which water was introduced into the reaction chamber by an alternate method (Section 2.3). Dolomite fragments containing dolomite powder on mineral surfaces were also used in this experiment. Dolomite powders are no longer present on mineral surfaces at the conclusion of both experiments. Two new minerals grew on dolomite surfaces, one exhibiting platelet morphology and a second of rhombohedral carbonate crystals. These are the same morphologies as observed in experiments performed at 220°C with water sealed in the bottom of the reaction chamber at the beginning of the experiment (Experiments #3 and #6, compare Figure 8 (a) to (c) and (g) to (i)). The growth of crystals with similar morphology in these experiments provides confidence that the liquid water reservoir remains physically separated from the dolomite during the experiment.

Dolomite fragments cleansed of mineral powders (Section 2.1) reacted with H_2O-saturated supercritical carbon dioxide at 220°C in one experiment (Experiment #7). Cleavage planes became more abundant and prominent in dolomite fragments (compare Figure 5a to Figure 5b). Two new minerals grew on dolomite surfaces. Newly-formed rhombohedral carbonate crystals range from a submicron scale to 1 to 3 microns in size (Figure 10). Submicron platelets of new crystal growth are also evident (Figure 9 (a) and (b)), but the crystals could not be identified by morphology or by EDS spectra. Neither morphology is present on unreacted dolomite (Figures 5b) or on the dolomite reacted with anhydrous supercritical carbon dioxide (Figure 6a). New crystal growth covers a much larger proportion of mineral surfaces compared to experiments that reacted dolomite fragments containing dolomite powder on mineral surfaces. EDS spectra collected from the large rhombohedral carbonates suggests that these crystals may contain more iron compared to the unreacted dolomite.

The analytical results reported in Table 1 are for aqueous samples collected immediately prior to terminating each experiment. We do not report bicarbonate analyses because the immiscible supercritical carbon dioxide present throughout the experiment maintains carbon dioxide saturation in the water. Except for pH, the de-ionized water analysis and the analysis of the water samples collected from each experiment are similar. These relationships suggest that dolomite and bulk water did not directly interact with each other and that dolomite powder was not washed off of dolomite fragments during the experiments. In fact, several experiments were rejected because water sampled from these experiments contained elevated cation concentrations relative to the de-ionized water used in the reaction chamber, indicating that dolomite and water had interacted with each other.

4 Discussion

Computer simulations of carbon dioxide storage in deep saline aquifers focus on trapping mechanisms and processes involving the reservoir and CO_2-saturated formation waters [e.g., 15-17, 21]. Studies such as these implicitly assume that all reactions take place in the water-rock environment or conclude that injected carbon dioxide does not react directly with minerals. Our results demonstrate that chemical reaction takes place between dolomite and H_2O-saturated supercritical carbon dioxide. Dolomite fragments exhibit dissolution textures and dolomite powders are no longer present on mineral surfaces. A new carbonate mineral precipitated in the experiments performed at reservoir temperatures (55 to 110°C); this mineral growth covers a larger area in a longer-running experiment. Experiments performed at higher temperatures of 220°C produced both platelets and rhombohedral carbonates. New crystal growth covered an even larger proportion of mineral surfaces of dolomite cleansed of powders, likely due to relaxation of the lattice strain produced by the cleaning process. No net mineralization occurred in these experiments because cations provided for carbonate precipitation can only be derived from dissolution of the original dolomite. However, the fact that reaction even takes place between dolomite and carbon dioxide suggests that regions within CCS, CO_2-EOR, and CO_2-EGR reservoirs that are believed to be non-reactive are in fact susceptible to chemical reaction.

Our findings are consistent with recent studies that have determined that silicate and hydroxide minerals react with wet supercritical carbon dioxide [30-40]. A thin film of water (a few nm thick) develops on the surface of minerals in contact with H_2O-undersaturated as well as H_2O-saturated supercritical carbon dioxide [33, 35]. In addition, dolomite has been found to exhibit hydrophilic surfaces [43] under mixed [44] or oil wet [45] conditions. Water composition [46, 47] and temperature [45] can turn oil-wet carbonate into a more hydrophilic surface. Oil wettability is usually associated with the presence of organic material in the depositional environment [44]. Despite the overall neutral or oil wet condition, dolomite often contains water-wet surfaces. Hydrophilic surfaces always develop a precursor nanoscale wetting film ahead of the contact line. Surface roughness offers capillary traps that enhance the formation of liquid films that can be at equilibrium with saturated phases [48]. In this sense, we expected the existence of water films on dolomite in our experiments. We speculate that these films can lead to new mineral growth. However, we currently lack the molecular-scale data needed to conclusively make this determination.

Our findings are also consistent with recent studies that have determined the reactivity of minerals with anhydrous supercritical carbon dioxide. In one study, montmorillinite loses interlayer water when exposed to anhydrous supercritical carbon dioxide, depending on the initial hydration state of the clay [39]. In a second pair of studies, montmorillinite expands due to carbon dioxide migration into the interlayer [34, 38]. In contrast, anhydrous supercritical carbon dioxide does not react with minerals that lack the expandable/collapsible interlayer spacing of swelling clays, including forsterite [32, 33, 35], kaolinite [34], brucite [36, 40], and, as we demonstrate, dolomite.

The reaction of minerals and wet supercritical carbon dioxide potentially holds several implications for CCS, CO_2-EOR, and CO_2-EGR fluid-rock systems. Mineral dissolution and re-precipitation may redistribute the porous matrix of the reservoir. This process can impact multi-phase flow of the reservoir by changing the dynamics of the contact line between phases and, therefore, changing hysteresis of drainage and imbibition cycles. Previous modeling results show weak hysteresis effects or changes of relative permeability [49]. However, the experimental conditions that were simulated neglect the impact of wet carbon dioxide reacting with mineral surfaces. Since the carbon dioxide saturation distribution arises from multiscale phenomena and a multitude of reactive conditions, wettability alteration as well as surface roughness may vary significantly between surfaces reacted with CO_2-saturated formation waters and those reacted with wet carbon dioxide. New growth on mineral surfaces may also change the carbon dioxide contact angle, consequently altering wettability of rock and capillary pressure, which in turn can affect physical carbon dioxide trapping mechanisms. Wettability alteration, leading to lower water wettability in clastic rocks, has been demonstrated through contact angle measurements [50, 51]. This process is particularly important for the ability of the caprock to act as barrier against carbon dioxide migration.

In CO_2-EOR and CO_2-EGR, reaction of carbonate rock with wet supercritical carbon dioxide may affect the three-phase mixing zone and the efficiency of the recovery process. This may occur by modifying phase mobility through changes in relative permeability [52]. Reaction of carbonate rock with wet supercritical carbon dioxide may possibly change the permeability of the reservoir by redistributing minerals, if precipitation-dissolution events occur at pore throats. These events will be regulated by the state of saturation of carbon dioxide as it displaces brine or in regions highly saturated with carbon dioxide, as well as by the mutual solubility of phases and capillary pressure. Since carbon dioxide acts as a good solvent for crude oil, regions of very low oil saturation are possible and the interplay of wettability alteration and multiphase flow hysteresis can lead to regions of high carbon dioxide saturation, even in cases of three-phase flow displacement. We speculate that mixed wettability can be significantly affected by drying of water-wet films and direct contact of surfaces by water-loaded carbon dioxide. The change of permeability, as well as capillary pressure and relative permeability, will affect the injection rate (injectivity) and oil production rate during CO_2-EOR. Carbon dioxide can also become more mobile in a CCS reservoir as the result of wettability alteration, thus affecting carbon dioxide storage capacity in these reservoirs.

Reaction with wet supercritical carbon dioxide may also affect the caprocks that seal CCS, CO_2-EOR, and CO_2-EGR reservoirs. Mineral reactions in the caprock that produce negative volume changes may yield zone of higher permeability and subsequent release of carbon dioxide. Alternatively, mineral reactions producing positive volume changes may lead to reduced porosity and permeability and enhance the sealing characteristics of the caprock. Both of these scenarios illustrate the richness of geochemical complexity previously unexamined. Secure storage of carbon dioxide in a CCS, CO_2-EOR, or CO_2-EGR scenario must account for these potential reactions.

5 Conclusions

The reactivity of dolomite with H_2O-saturated supercritical carbon dioxide was studied at reservoir conditions (55 to 110°C, 25 MPa) and elevated temperature (220°C, 25 MPa) for reaction times of approximately 96 and 164 hours (approximately 4 days and 7 days). Dolomite does not react with anhydrous supercritical carbon dioxide. Dolomite dissolves and carbonate minerals precipitate by reaction with H_2O-saturated supercritical carbon dioxide. Temperature and reaction time control the composition, morphology, and extent of formation of new carbonate minerals. Crystals with irregular morphology precipitate at 55°C; crystal platelets and rhombohedral dolomite precipitate at 220°C.

Mineral dissolution and re-precipitation due to reaction with H_2O-saturated supercritical carbon dioxide may affect the dynamics of the contact line between phases, the carbon dioxide contact angle, and the relative permeability and permeability distribution of the reservoir. Changes to these fundamental properties may in turn influence hysteresis of drainage and imbibition cycles, wettability of rock, and capillary pressure. On a larger scale, the efficacy of physical carbon dioxide trapping mechanisms, integrity of caprock, and injectivity of a carbon dioxide storage reservoir such as the Madison Limestone, as well as the injectivity and oil production rate of an EOR operation, may be affected.

References

[1] S. Bachu. Sequestration of CO_2 in geological media: Criteria and approach for site selection in response to climate change. Energy Convers Mgmt. 41 (2000) 953-70.
[2] J. Gale, N.P. Christensen, A. Cutler, T.A. Torp. Demonstrating the potential for geological storage of CO_2: The Sleipner and GESTCO Projects. Environ Geosci. 8 (2001) 160-5.
[3] W.S. Han, B.J. McPherson. Optimizing geologic CO_2 sequestration by injection in deep saline formations below oil reservoirs. Energy Convers Mgmt. 50 (2009) 2570-82.
[4] D. Gerard, E.J. Wilson. Environmental bonds and the challenge of long-term carbon sequestration. J Environ Manage. 90 (2009) 1097-105.
[5] N. Voltattorni, A. Sciarra, G. Caramanna, D. Cinti, L. Pizzino, F. Quattrocchi. Gas geochemistry of natural analogues for the studies of geological CO_2 sequestration. Appl Geochem. 24 (2009) 1339-46.
[6] A. Schreiber, P. Zapp, P. Markewitz, S. Vögele. Environmental analysis of a German strategy for carbon capture and storage of coal power plants. Energy Policy. 38 (2010) 7873-83.
[7] J.C. Moore, S. Jevrejeva, A. Grinsted. Efficacy of geoengineering to limit 21st century sea-level rise. Proc Natl Acad Sci USA. 107 (2010) 15699-703.
[8] F. Yang, B.J. Bai, D.Z. Tang, S. Dunn-Norman, D. Wronkiewicz. Characteristics of CO_2 sequestration in saline aquifers. Petrol Sci. 7 (2010) 83-92.
[9] R. Shukla, P. Ranjith, A. Haque, X. Choi. A review of studies on CO_2 sequestration and caprock integrity. Fuel. 89 (2010) 2651-64.
[10] K. Jessen, A.R. Kovscek, F.M. Orr. Increasing CO_2 storage in oil recovery. Energy Convers Mgmt. 46 (2005) 293-311.
[11] A.R. Kovscek, M.D. Cakici. Geologic storage of carbon dioxide and enhanced oil recovery. II. Cooptimization of storage and recovery. Energy Convers Mgmt. 46 (2005) 1941-56.
[12] A.R. Kovscek, Y. Wang. Geologic storage of carbon dioxide and enhanced oil recovery. I. Uncertainty quantification employing a streamline based proxy for reservoir flow simulation. Energy Convers Mgmt. 46 (2005) 1920-40.
[13] Y.Q. Zhang, C.M. Oldenburg, S. Finsterle, G.S. Bodvarsson. System-level modeling for economic evaluation of geological CO_2 storage in gas reservoirs. Energy Convers Mgmt. 48 (2007) 1827-33.
[14] S. Bachu, W.D. Gunter, E.H. Perkins. Aquifer disposal of CO_2: Hydrodynamic and mineral trapping. Energy Convers Mgmt. 35 (1994) 269-79.
[15] K. Pruess, N. Muller. Formation dry-out from CO_2 injection into saline aquifers: 1. Effects of solids precipitation and their mitigation. Water Resour Res. 45 (2009).
[16] H. Behzadi, V. Alvarado, S. Mallick. CO_2 saturation, distribution and seismic response in two-dimensional permeability model. Environ Sci Technol. 45 (2011) 9435-41.
[17] S.C.M. Krevor, R. Pini, B.X. Li, S.M. Benson. Capillary heterogeneity trapping of CO_2 in a sandstone rock at reservoir conditions. Geop Res Lett. 38 (2011).
[18] C.H. Pentland, R. El-Maghraby, S. Iglauer, M.J. Blunt. Measurements of the capillary trapping of super-critical carbon dioxide in Berea sandstone. Geop Res Lett. 38 (2011).
[19] E.J. Spiteri, R. Juanes, M.J. Blunt, F.M. Orr. A new model of trapping and relative permeability hysteresis for all wettability characteristics. SPE J. 13 (2008) 277-88.
[20] E. Saadatpoor, S.L. Bryant, K. Sepehrnoori. New trapping mechanism in carbon sequestration. Transp Porous Media. 82 (2010) 3-17.

[21] L. André, P. Audigane, M. Azaroual, A. Menjoz. Numerical modeling of fluid-rock chemical interactions at the supercritical CO_2-liquid interface during CO_2 injection into a

carbonate reservoir, the Dogger aquifer (Paris Basin, France). Energy Convers Mgmt. 48 (2007) 1782-97.
[22] N.R. Morrow, G. Mason. Recovery of oil by spontaneous imbibition. Current Opinion in Colloid & Interface Science. 6 (2001) 321-37.
[23] V.T.H. Pham, P. Lu, P. Aagaard, C. Zhu, H. Hellevang. On the potential of CO_2-water-rock interactions for CO_2 storage using a modified kinetic model. Int J Greenhouse Gas Control. 5 (2011) 1002-15.
[24] C. Noiriel, L. Luquot, B. Made, L. Raimbault, P. Gouze, J. van der Lee. Changes in reactive surface area during limestone dissolution: An experimental and modelling study. Chem Geol. 265 (2009) 160-70.
[25] J.P. Kaszuba, D.R. Janecky, M.G. Snow. Carbon dioxide reaction processes in a model brine aquifer at 200^{o}C and 200 bars: Implications for geologic sequestration of carbon. Appl Geochem. 18 (2003) 1065-80.
[26] S.J. Gerdemann, W.K. O'Connor, D.C. Dahlin, L.R. Penner, H. Rush. Ex situ aqueous mineral carbonation. Environ Sci Technol. 41 (2007) 2587-93.
[27] D.L. Newell, J.P. Kaszuba, H.S. Viswanathan, R.J. Pawar, T. Carpenter. Significance of carbonate buffers in natural waters reacting with supercritical CO_2 - Implications for monitoring, measuring and verification (MMV) of geologic carbon sequestration. Geop Res Lett. 35 (2008) doi: 10.1029/2008GL035615.
[28] B. Garcia, V. Beaumont, E. Perfetti, V. Rouchon, D. Blanchet, P. Oger, et al. Experiments and geochemical modelling of CO_2 sequestration by olivine: Potential, quantification. Appl Geochem. 25 (2010) 1383-96.
[29] S. Fischer, A. Liebscher, M. Wandrey. CO_2-brine-rock interaction -- First results of long-term exposure experiments at in situ P-T conditions of the Ketzin CO_2 reservoir. Chemie der Erde - Geochemistry. 70 (2010) 155-64.
[30] H. Lin, T. Fujii, R. Takisawa, T. Takahashi, T. Hashida. Experimental evaluation of interactions in supercritical CO_2/water/rock minerals system under geologic CO_2 sequestration conditions. Journal of Materials Science. 43 (2008) 2307-15.
[31] B.P. McGrail, H.T. Schaef, V.A. Glezakou, L.X. Dang, A.T. Owen. Water reactivity in the liquid and supercritical CO_2 phase: Has half the story been neglected? Energy Procedia. 1 (2009) 3415-9.
[32] J.H. Kwak, J.Z. Hu, D.W. Hoyt, J.A. Sears, C.M. Wang, K.M. Rosso, et al. Metal carbonation of forsterite in supercritical CO_2 and H_2O using solid state ^{29}Si, ^{13}C NMR spectroscopy. J Phys Chem C. 114 (2010) 4126-34.
[33] J.H. Kwak, J.Z. Hu, R.V.F. Turcu, K.M. Rosso, E.S. Ilton, C. Wang, et al. The role of H_2O in the carbonation of forsterite in supercritical CO_2. Int J Greenhouse Gas Control. 5 (2011) 1081-92.
[34] J.S. Loring, H.T. Schaef, R.V.F. Turcu, C.J. Thompson, Q.R.S. Miller, P.F. Martin, et al. In situ molecular spectroscopic evidence for CO_2 intercalation into montmorillonite in supercritical carbon dioxide. Langmuir. 28 (2012) 7125-8.
[35] J.S. Loring, C.J. Thompson, Z. Wang, A.G. Joly, D.S. Sklarew, H.T. Schaef, et al. In situ infrared spectroscopic study of forsterite carbonation in wet supercritical CO_2. Environ Sci Technol. 45 (2011) 6204-10.
[36] J.S. Loring, C.J. Thompson, C. Zhang, Z. Wang, H.T. Schaef, K.M. Rosso. In situ infrared spectroscopic study of brucite carbonation in dry to water-saturated supercritical carbon dioxide. Journal of Physical Chemistry A. 116 (2012) 4768-77.
[37] N.N. Yang, X.N. Yang. Molecular simulation of swelling and structure for Na-Wyoming montmorillonite in supercritical CO_2. Molecular Simulation. 37 (2011) 1063-70.
[38] E.S. Ilton, H.T. Schaef, O. Qafoku, K.M. Rosso, A.R. Felmy. In situ x-ray diffraction study of Na^+ saturated montmorillonite exposed to variably wet super critical CO_2. Environ Sci Technol. 46 (2012) 4241-8.

[39] H.T. Schaef, E.S. Ilton, O. Qafoku, P.F. Martin, A.R. Felmy, K.M. Rosso. In situ XRD study of Ca^{2+} saturated montmorillonite (STX-1) exposed to anhydrous and wet supercritical carbon dioxide. Int J Greenhouse Gas Control. 6 (2012) 220-9.
[40] H.T. Schaef, C.F. Windisch, B.P. McGrail, P.F. Martin, K.M. Rosso. Brucite $Mg(OH_2)$ carbonation in wet supercritical CO_2: An in situ high pressure X-ray diffraction study. Geochim Cosmochim Acta. 75 (2011) 7458-71.
[41] O. Regnault, V. Lagneau, H. Catalette, H. Schneider. Experimental study of pure mineral phases/supercritical CO_2 reactivity. Implications for geological CO_2 sequestration. C R Geosci. 337 (2005) 1331-9.
[42] S. Takenouchi, G.C. Kennedy. The binary system H_2O-CO_2 at high temperatures and pressures. Am J Sci. 262 (1964) 1055-74.
[43] N. Gence. Wetting behavior of magnesite and dolomite surfaces. Applied Surface Science. 252 (2006) 3744-50.
[44] I. Matyasik, G. Leśniak, P. Such, Z. Mikołajweski. Mixed wetted carbonate reservoir: origins of mixed wettability and affecting reservoir properties. Annales Societatis Geologorum Poloniae. 80 (2010) 115-22.
[45] B.S. Sola, F. Rashidi. Experimental study of hot water injection into low-permeability carbonate rocks. Energy & Fuels. 22 (2008) 2353-61.
[46] S. Strand, T. Austad, T. Puntervold, E.J. Hognesen, M. Olsen, S.M.F. Barstad. "Smart Water" for oil recovery from fractured limestone: A preliminary study. Energy & Fuels. 22 (2008) 3126-33.
[47] A. RezaeiDoust, T. Puntervold, S. Strand, T. Austad. Smart water as wettability modifier in carbonate and sandstone: A discussion of similarities/differences in the chemical mechanisms. Energy & Fuels. 23 (2009) 4479-85.
[48] P.-G.d. Gennes, F. Brochard-Wyart, D. Quéré. Capillarity and Wetting Phenomena: Drops, Bubbles, Pearls, Waves. Springer Science+Business Media, Inc., New York, NY USA, 2004.
[49] G. Radilla, M. Kacem, J.M. Lombard, M. Fourar. Transport properties of Lavoux Limestone at various stages of CO_2-like acid-rock alteration. Oil & Gas Science and Technology-Revue D Ifp Energies Nouvelles. 65 (2010) 557-63.
[50] P. Chiquet, D. Broseta, S. Thibeau. Wettability alteration of caprock minerals by carbon dioxide. Geofluids. 7 (2007) 112-22.
[51] P. Chiquet, J.L. Daridon, D. Broseta, S. Thibeau. CO_2/water interfacial tensions under pressure and temperature conditions of CO_2 geological storage. Energy Convers Mgmt. 48 (2007) 736-44.
[52] H. Behzadi, V. Alvarado. Impact of three-phase relative permeability model on recovery in mixed media: Miscibility, IFT, and hysteresis issues. Energy & Fuels. 24 (2010) 5765-72.

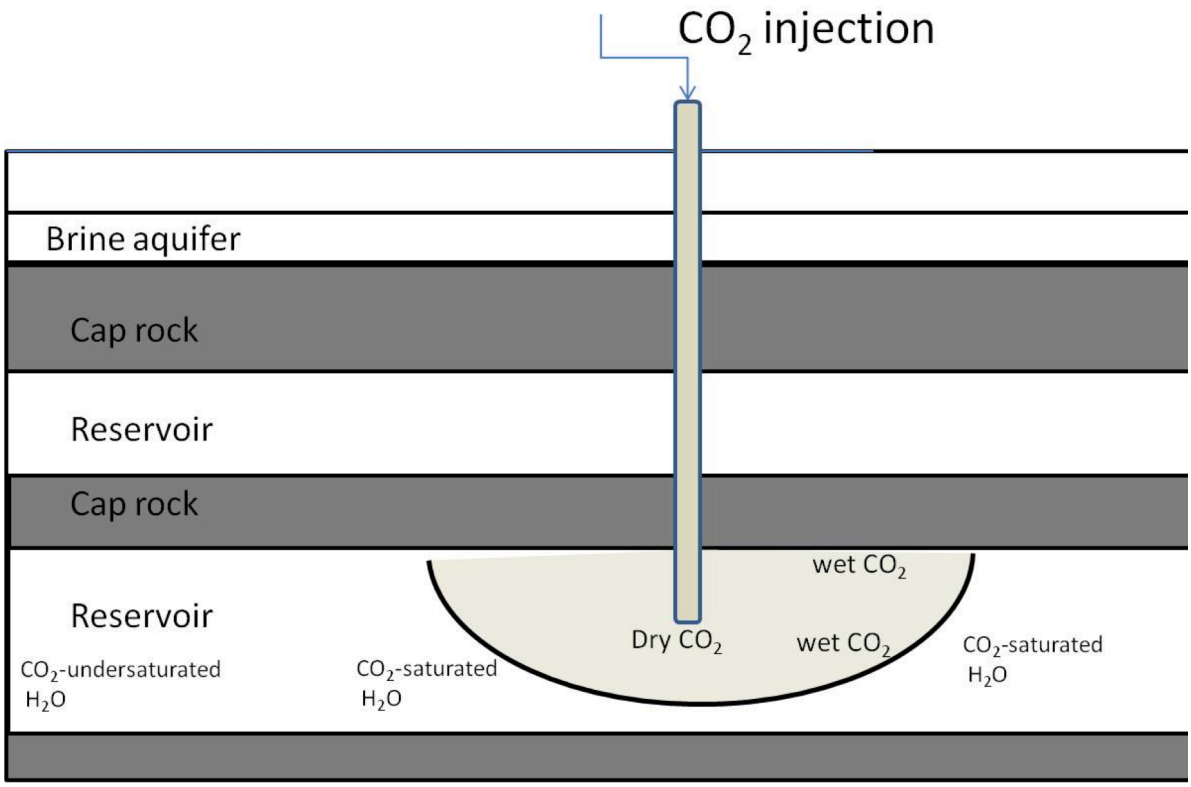


Figure 1. Schematic diagram of CCS scenario in a saline aquifer. Injection of carbon dioxide creates regions across which the full spectrum of mutual CO_2-H_2O solubility may occur. Anhydrous supercritical carbon dioxide occurs at the injection well; CO_2-saturated and -undersaturated formation waters occur at the displacement front. H_2O-saturated and -undersaturated or "wet" supercritical carbon dioxide can exist between these two extremes, toward the cap rock and at the CO_2-H_2O front.

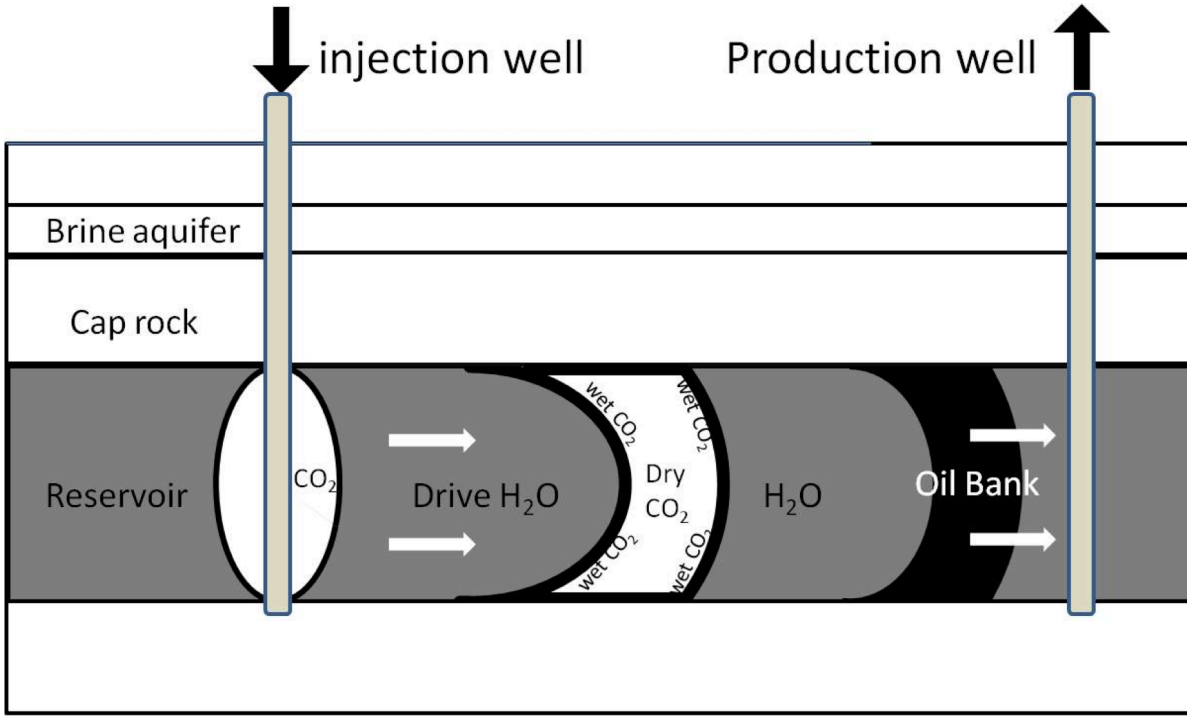


Figure 2. Schematic diagram of CO_2 injection and enhance oil recovery (modified from http://www.fe.doe.gov/programs/oilgas/eor/). As described in Figure 1, injection of carbon dioxide creates regions across which the full spectrum of mutual CO_2-H_2O solubility may occur (Figures 1 and 2). This is only schematic and does not show the mixing zone between carbon dioxide and water. In reality, gravitational ascencion of carbon dioxide and water slumping will take place as the mixing zone between fluids destabilizes. The successive fluid slugs create multiphase flow hysteresis that traps both water and carbon dioxide, leading to formation of oil banks and enhanced recovery.

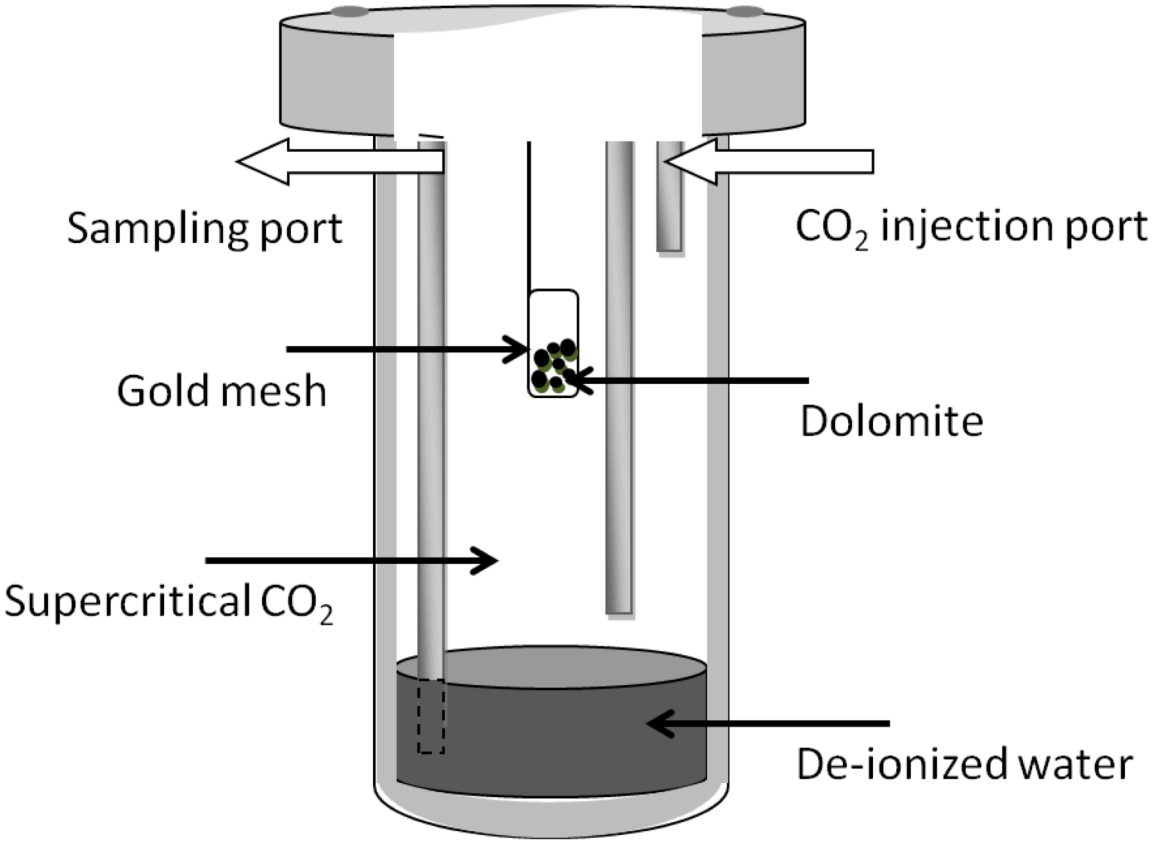


Figure 3. Schematic diagram of experimental apparatus and design. The reaction chamber is a 300-cm^3 customized bolted closure reactor manufactured by Autoclave Engineers. The reaction chamber and its multiple tubing inlets and outlets are constructed of Hastelloy C-276.

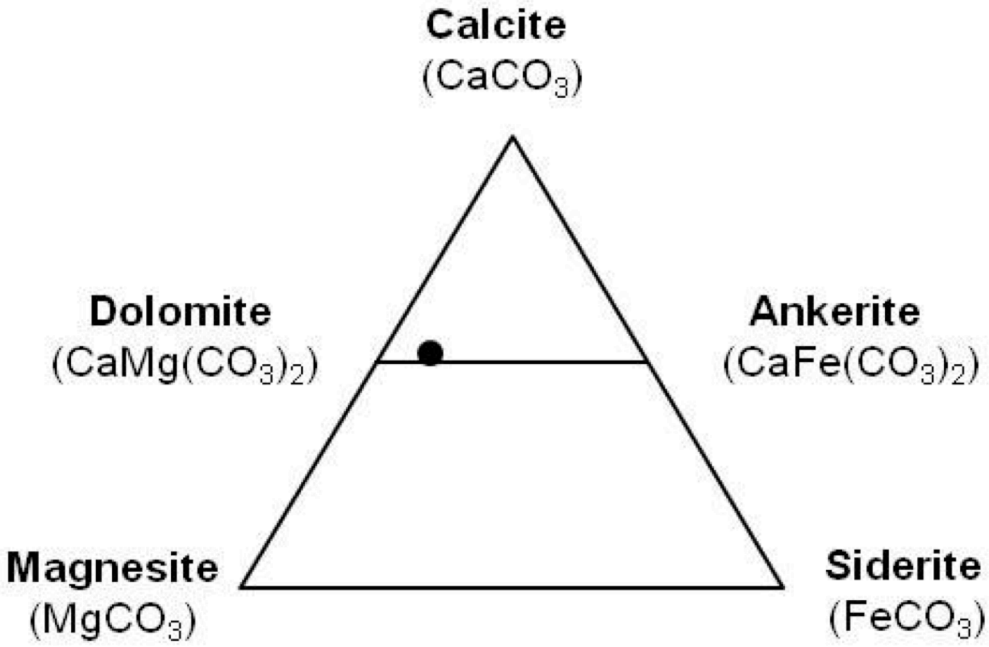


Figure 4. Ternary diagram illustrating composition of dolomite (in mole %) used in the experiments.

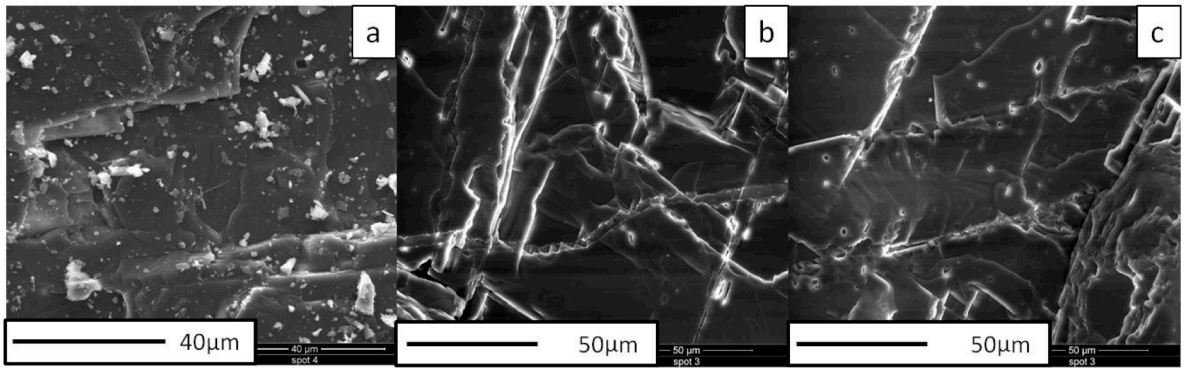


Figure 5. Secondary electron SEM micrographs of unreacted dolomite. (a) Dolomite fragments containing dolomite powder on mineral surfaces; (b) Dolomite cleansed of mineral powders.

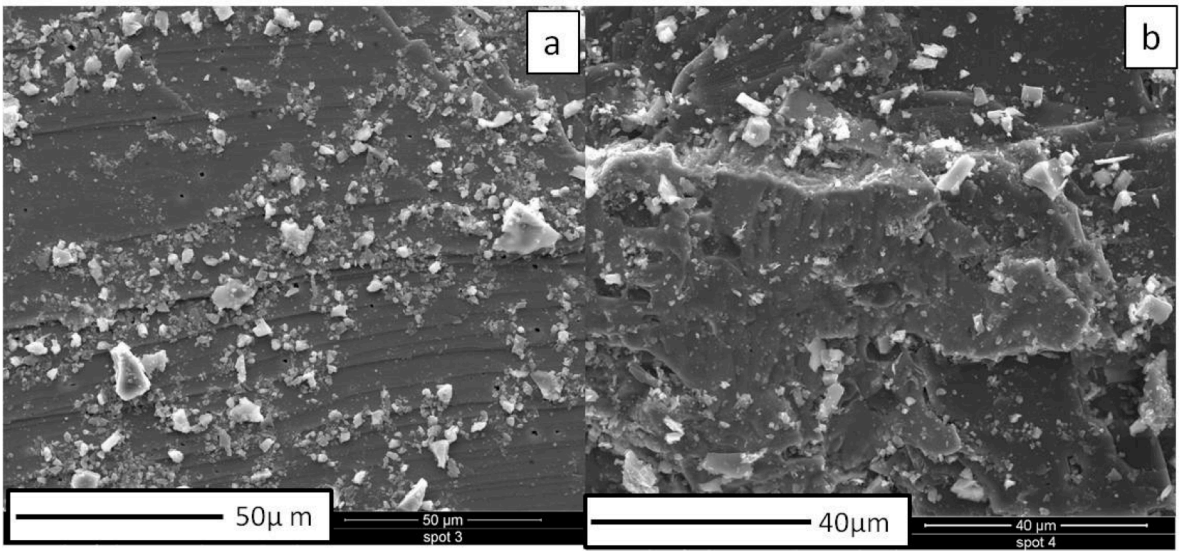


Figure 6. Secondary electron SEM micrographs of (a) dolomite after reaction with anhydrous carbon dioxide at 110°C and 272 hours. No evidence of dolomite dissolution or mineral growth was observed in this experiment. (b) Unreacted dolomite.

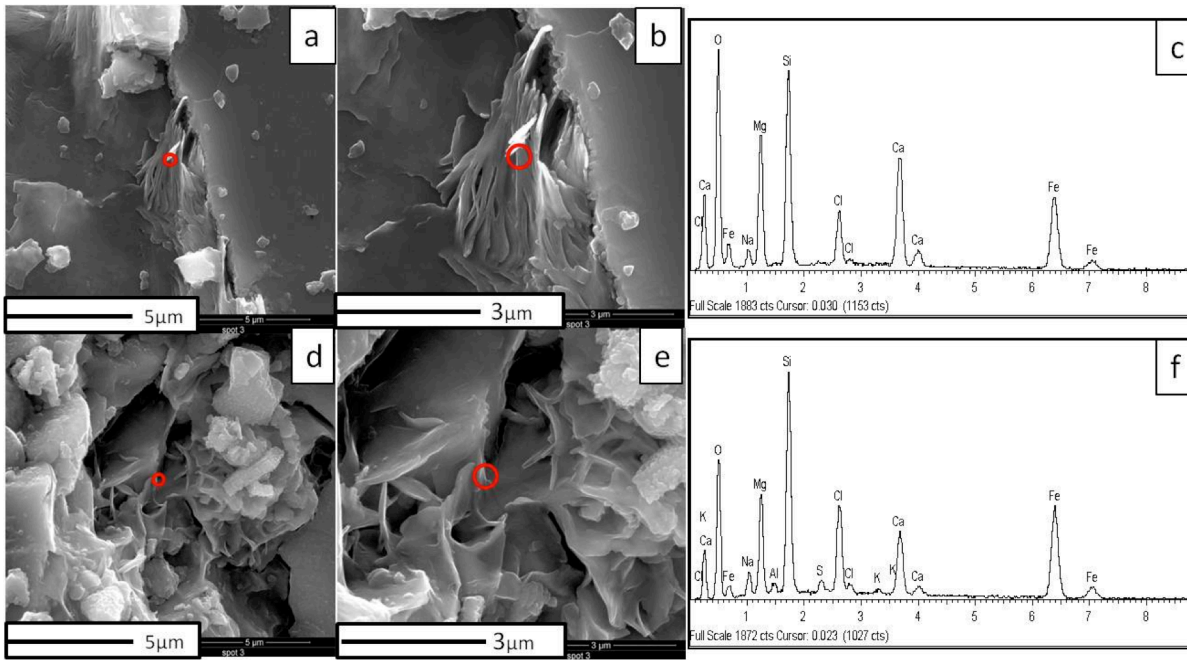


Figure 7. Secondary electron SEM micrographs and EDS spectra of dolomite reacted with H_2O-saturated supercritical carbon dioxide at 55°C. Dolomite used in these experiments contained powder on mineral surfaces. (a to c) Reaction for 93 hours (Experiment #2 in Table 1). (d to f) Reaction for 164 hours (Experiment #5 in Table 1). New mineral growth exhibiting irregular morphology is observed. EDS spectra are consistent with this mineral being recrystallized dolomite. New mineral growth covers a larger area of the dolomite in the 164-hour experiment compared to the 93-hour experiment.

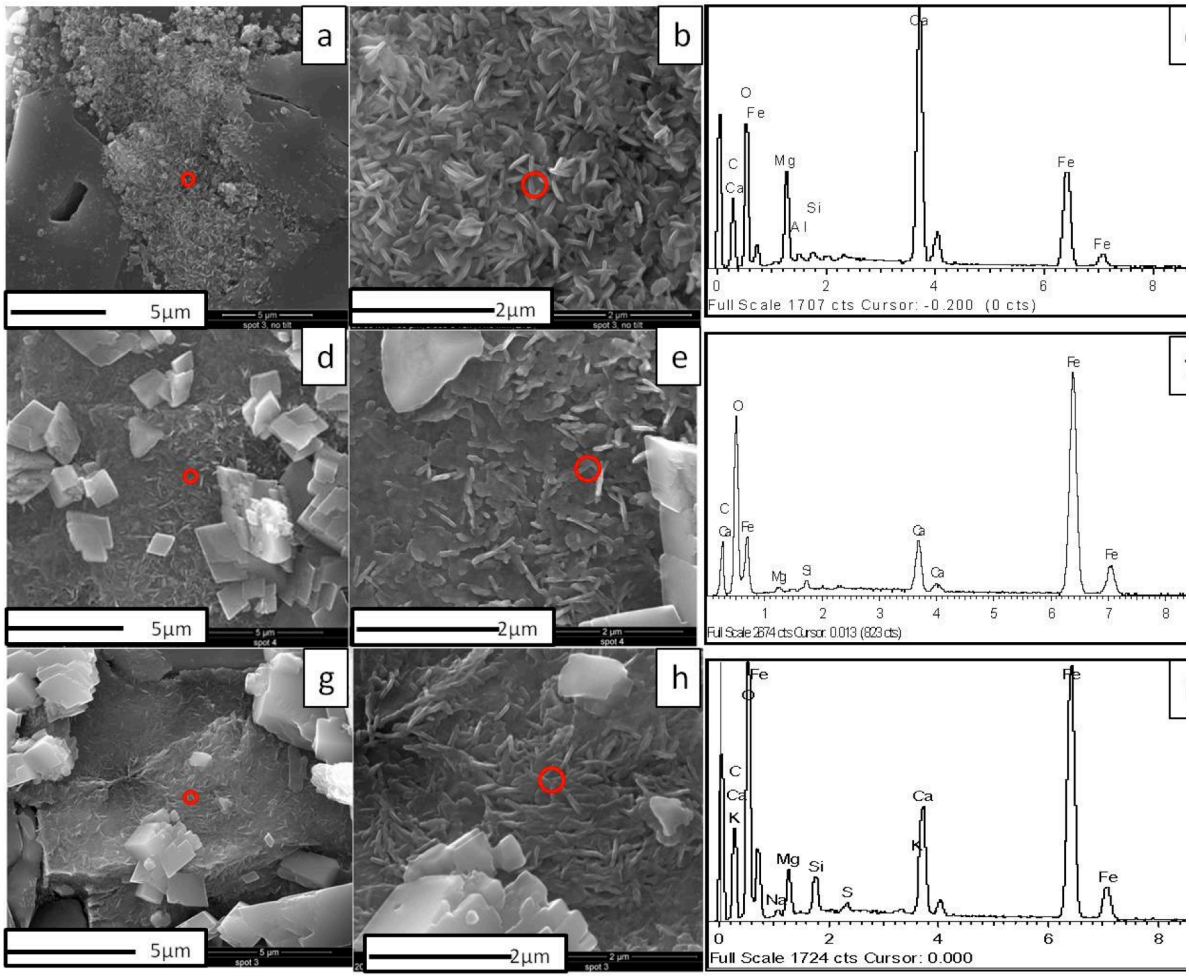


Figure 8. Secondary electron SEM micrographs and EDS spectra of dolomite reacted with H_2O-saturated supercritical carbon dioxide at 220°C. Dolomite used in these experiments contained powder on mineral surfaces. (a to c) Reaction for 94 hours, standard method of adding de-ionized water to the bottom of the reaction chamber before sealing the reactor was employed (Experiment #3 in Table 1). (d to f) Reaction for 162 hours, de-ionized water added by standard method (Experiment #6 in Table 1). (g to i) Reaction for 90 hours, de-ionized water added to bottom of reactor after sealing the reactor (Experiment #4 in Table 1). Two types of new mineral growth are observed, one exhibiting platelet morphology and a second of rhombohedral carbonate crystals. EDS spectra of rhombohedral carbonate minerals are consistent with recrystallized dolomite. Iron may be more abundant compared to unreacted dolomite, however the EDS spectra are not conclusive. Rhombohedral carbonate crystals depicted in (g) and (h) are out of the field of view in (a) and (b).

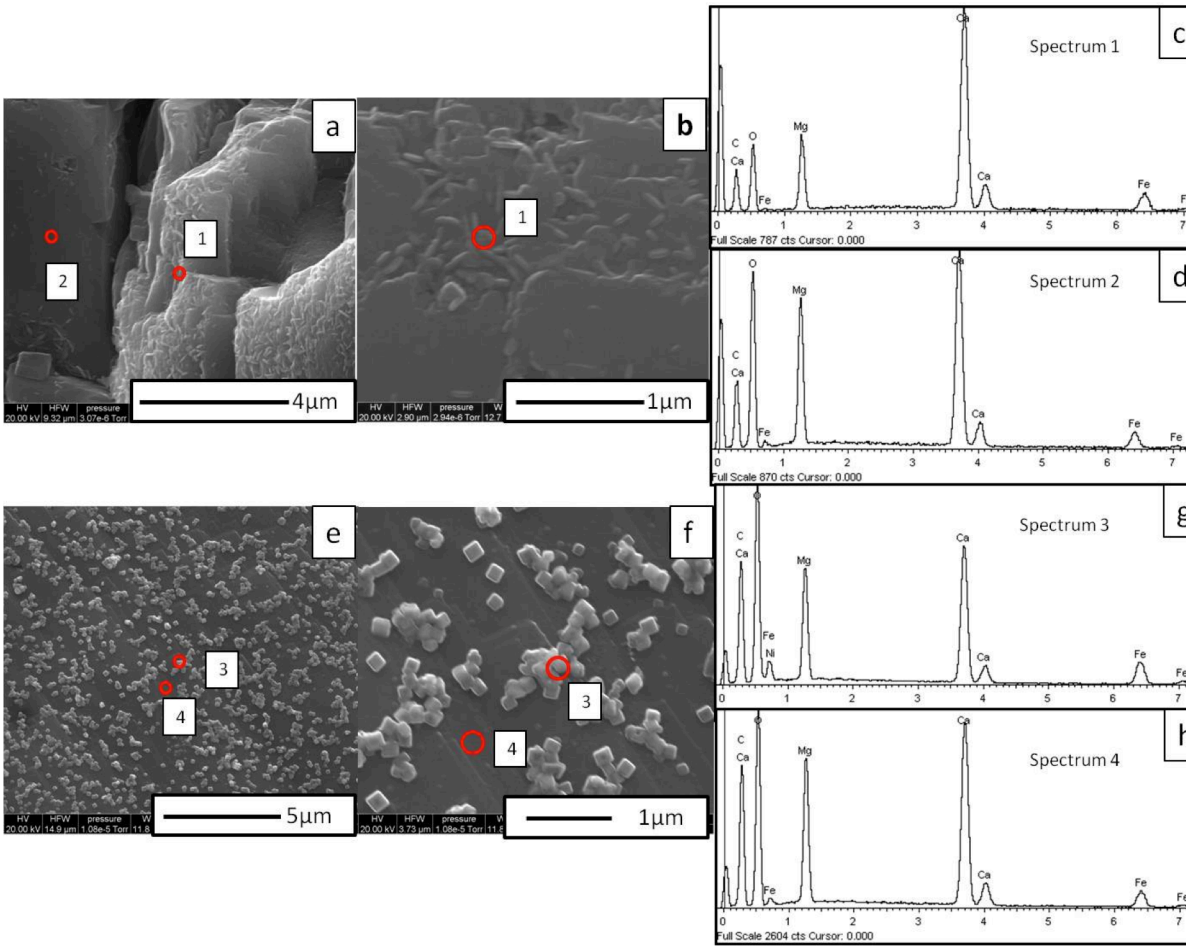


Figure 9. Secondary electron SEM micrographs and EDS spectra of dolomite reacted with H_2O-saturated supercritical carbon dioxide at 220°C. Dolomite used in this experiment was cleansed of mineral powders. Two types of new mineral growth are observed, submicron scale platelets (a and b) and submicron scale rhombohedral carbonate crystals (not pictured). New crystal growth in this experiment covers a much larger proportion of mineral surfaces compared to experiments that reacted dolomite containing dolomite powder on mineral surfaces.

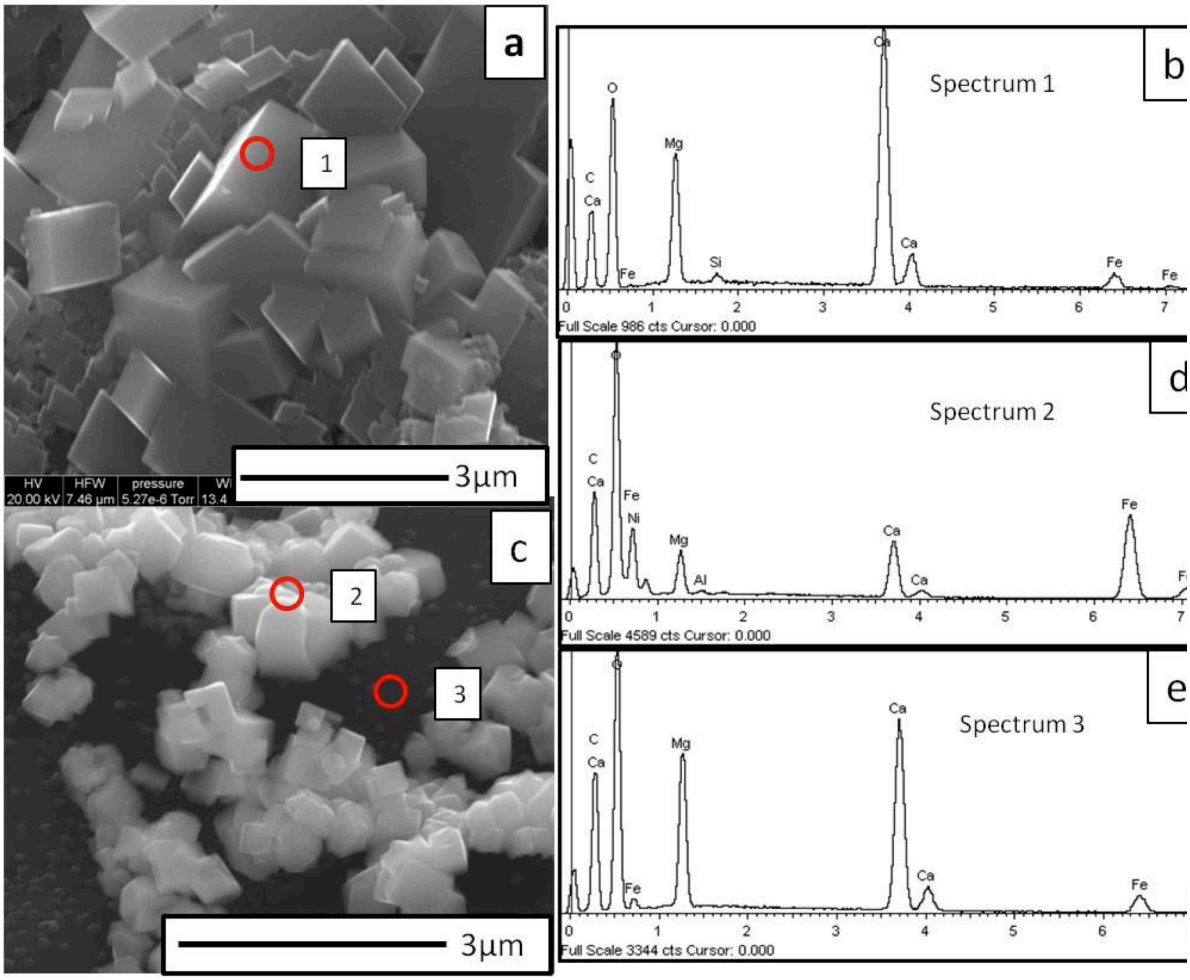


Figure 10. Secondary electron SEM micrographs and EDS spectra of dolomite reacted with H_2O-saturated supercritical carbon dioxide at 220°C. Dolomite used in this experiment was cleansed of mineral powders. (a) Dolomite rhombohedrons. (b) EDS spectra of point 1 in (a) is consistent with this mineral being recrystallized dolomite.

Table 1. Summary for the experiments performed and major cation analysis of water samples (in millimole/kg)

#	T (°C)	Information regarding H_2O	Dolomite starting material	Time (hours)	X_{H2O} in reactor at beginning of experiment	pH[a]	Ca	Mn	Fe	Mg	Na	Comment
		de-ionized H_2O	---			6.8	0.2155	0.0002	0.0002	0.1198	0.0873	Composition of H_2O added to reactor control experiment
1	110	anhydrous CO_2	fragments + powder	272	0	---	---	---	---	---	---	
2	55	H_2O added before reactor is sealed (standard method)	fragments + powder	93	0.24	4.9	0.1339	0.0006	0.0064	0.0596	0.1014	---
3	220	H_2O added by standard method	fragments + powder	94	0.49	4.4	0.5888	0.0129	0.0122	0.0271	0.1048	---
4	220	H_2O injected after reactor is sealed	fragments + powder	90	0.5	4.2	NA[b]	NA	NA	NA	NA	---
5	55	H_2O added by standard method	fragments + powder	164	0.24	4.7	0.1137	0.0043	0.0154	0.0668	0.0619	---
6	220	H_2O added by standard method	fragments + powder	162	0.44	4.7	0.0097	0.0009	<0.00013	<0.00052	<0.00147	---
7	220	H_2O added by standard method	fragments, no powder	94	0.48	4.6	0.067	0.0043	0.0012	<0.00157	0.2103	sonicate dolomite 30 minutes

[a]pH measured on samples cooled to 25°C and depressurized to 0.1 MPa

[b]not availablesample container leaked

Part II. Subtask 6.1 Containment-mineralization. Reactivity of carbonate reservoir and caprock in water-saturated supercritical carbon dioxide and carbon dioxide-saturated brine

Part IV. Subtask 6.1 Containment-mineralization. Rate of Mineralization.

Part VI. Subtask 6.2 Containment-brine. Dissolution rate of CO_2 into brine.

1. Introduction

After CO_2 is injected in aquifers and hydrocarbon reservoirs during CO_2 geological storage operations, a significant fraction of the injected gas will tend to rise up and accumulate in the reservoir beneath the caprock due to buoyancy. The reaction among CO_2, brine, and rock can lead to changes of reservoir and caprock properties, such as porosity and permeability. Regnault et al. (2005) found from their experimental study that reactions between minerals and supercritical CO_2 might degrade the caprock sealing capacity by possible creation of shortcuts and increased porosity. Xu et al. (2004) developed a conceptual model of CO_2 injection in bedded sandstone-shale sequences using hydrogeologic properties and mineral compositions commonly encountered in Gulf Coast sediments and found that the addition of CO_2 as secondary carbonates results in decreased porosity, while the leaching of chemical constituents from the interior of the shale causes slightly increased porosity (Xu et al., 2004). The impact of CO_2 injection on the caprock at Sleipner in Norway was investigated by reactive transport modeling; a slight decrease of porosity in the lower few meters of the formation was predicted (Gaus et al., 2005). One of the critical factors that control the efficiency of caprock is the so-called capillary entry pressure, which is proportional to water/acid gas interfacial tension and phase contact angle (i.e. wettability of caprock minerals). A careful analysis of the available literature on breakthrough pressure measurements in caprock samples confirms wettability alteration by dense CO_2 both in shale and in evaporite caprocks (Shah et al., 2008; Xu et al., 2004).

The purpose of this study is to conduct experiments to evaluate the reactivity of carbonate reservoir and shale caprock in both H_2O-saturated CO_2 and in CO_2-saturated brine for the potential CCS reservoir on the Rock Springs Uplift. Experiments were conducted on cuttings of Madison Limestone from RSU #1. The nature of these cuttings was such that the experiments failed to yield useable data for this report. Suitable samples of Dinwoody Formation, a caprock on the Rock Spring Uplift, were unavailable at the time this study was implemented. Instead, shale caprock from other carbon sequestration sites, the Marine Shale of the Tuscaloosa Group (henceforth referred to as the Marine Tuscaloosa Shale) and the Gothic Shale, were used. Together these two shales represent the spectrum of shale compositions, from silica-rich to carbonate rich, which occur within the Dinwoody Formation. Given the mineralogy of both of these rocks, the results can also be used to understand the reactivity of Madison Limestone and Weber Sandstone in the RSU #1. The reactivity of both shales was evaluated in H_2O-saturated CO_2 and in CO_2-saturated brine (Table 1). The Marine Tuscaloosa Shale is a silica-rich mudstone containing quartz, micas, feldspar, chlorite, kaolinite, and illite with trace calcite and ~ 0.73 wt% total organic carbon (TOC) (Heath et al., 2011). The Gothic Shale is a carbonate-rich mudstone composed of calcite, dolomite, quartz, and mica in a dominantly clay matrix. It also contains pyrite and 2.2 to 4.4 wt% TOC. Griffith et al. (2011) further details the composition, listing calcite/dolomite cements, plagioclase feldspar, siderite, pyrite, clay-sized quartz, illite-smectite, chlorite, chlorite-smectite, muscovite, illite, and fracture-filling anhydrite and halite. Cantrell et al. (2012) performed semi-quantification of X-ray diffraction (XRD) analysis of Gothic shale samples and identified quartz (25%), calcite (37%), dolomite (9%), pyrite (7%) and montmorillonite (22%) as major mineral phases.

2. Experimental and Modeling Approach

The experimental apparatus is the same as described in Section 2 of Part I of this report. Synthetic brines were used in the experiments (Table 2). These brines were calculated to be in equilibrium with the respective shales through the use of a geochemical code (the Geochemist's Workbench). The initial brine composition was calculated to be in equilibrium, or as close as possible, to the minerals used in the experiments. This strategy is used to minimize experimental artifacts that may develop due to reaction between the minerals and brine prior to injection of CO_2. This strategy emulates natural conditions in which formation waters approach equilibrium with the host rock. The ionic strength of the respective brines were matched to the natural formation waters by using appropriate amounts of sodium chloride.

Brine was periodically sampled from all of the experiments on a logarithmic time scale and subsequently analyzed (Tables 3 and 4). The minerals and quenched brine were also analyzed after the experiments were terminated. To prevent mineral precipitation, the samples for cation analysis were acidified to pH 2 using trace metal grade nitric acid. Dissolved major cations were determined by inductively coupled plasma optical emission spectroscopy (ICP-OES), dissolved minor and trace cations by inductively coupled plasma mass spectroscopy (ICP-MS), and dissolved anions by ion chromatography. The pH was determined on brine samples cooled to 25°C and depressurized to 0.1 MPa using an Orion pH meter and Ross microelectrode. Total dissolved inorganic carbon (as carbon dioxide) was determined for in-situ conditions by analyzing a sample of brine plus exsolved gas collected in a glass gas-tight syringe. The analysis was performed using coulometric titration (Huffmann, 1977). Total dissolved inorganic carbon (as carbon dioxide) was also determined on degassed brine samples cooled to 25°C and depressurized to 0.1 MPa. Mineral precipitants were not observed in any of the brine samples. Analytical results, including charge balance and analytical uncertainties, are reported in Tables 3 and 4. Minerals were analyzed using optical microscopy, high resolution field emission scanning electron microscopy (FE-SEM), energy dispersive spectra (EDS), and X-ray diffraction (XRD).

In this study, different reservoir profiles were investigated by experimental designs in which shale samples were positioned within CO_2-saturated brine (bottom of the reactor vessel) and H_2O-saturated CO_2 (top of the reactor vessel). The former represents CO_2-saturated formation waters at the CO_2 displacement front whereas the latter represents "wet" supercritical carbon dioxide can exist both toward the cap rock due to buoyancy forces and at the CO_2-H_2O front (see Part I). The reaction temperature was selected to be 160^{o}C, a value greater than temperatures naturally found in the respective reservoirs (55-70˚C). The temperature was chosen to accelerate kinetics, but geochemical calculations suggest that the water-rock interactions are the same as those predicted at lower in-situ temperatures. This approach is used in similar studies (Gunter et al., 1997; Credoz et al., 2009; Alemu et al., 2011). The targeted pressure of 15 MPa was attained in 3 steps. First, before turning on the heating unit, the reactor is pressurized to about 5 MPa as a leak check. In the second step, the heating unit is turned on and the temperature of the reactor is allowed to reach a predetermined value. Lastly, CO_2 or argon (for baseline experiments) is injected continuously until the pressure reaches 15 MPa. The total mass of injected CO_2 or argon is recorded.

In the experiments reacting shale with CO_2-saturated brine (Figure 1a), five grams of shale were emplaced at the bottom of the reaction vessel followed by 270 grams of brine (in the case of injecting CO_2) or 299 gr of brine (in the case of injecting argon for a baseline experiment).

The experiments reacting shale with H_2O-saturated brine (Figure 1b) are similar in approach to the dolomite experiments described in Part I. A total of 1.85 grams of shale are placed in gold mesh that is folded to a cup shape and hung from the top of the reactor with a 0.5 mm diameter gold wire. A total of 80 grams of brine is introduced, an amount sufficient to saturate the overlying supercritical CO_2 while leaving sufficient H_2O in the bottom of the reactor for sampling purposes. The temperature and pressure is attained by the same procedure as previously described for the other design. In addition to providing a leak check, initially pressurizing the reactor to 5 MPa also avoids the splashing of water from the bottom of the reactor onto the shale.

Geochemical calculations were performed using The Geochemist's Workbench version 9.0.05 (Bethke and Yeakel, 2013) and the b-dot extended form of the Debye-Huckel equation. The thermo.dat thermodynamic database was chosen due to its internal consistency. Geochemical data from samples collected during the experiments was used to determine saturation states of the waters and activities of minerals and aqueous complexes. Additionally, the in situ pH was calculated using the method of Newell et al. (2008). The results of the calculations were used to construct reaction paths and elucidate the geochemical changes occurring in the solid and fluid phases.

Neutrons passing through a rock sample will scatter from interfaces of geologic materials at angles that contain information about the length scales of features such as pores in the rock. Small angle neutron scattering (SANS) data contains statistical information about features and structures in the rock at length scales from ~1 nm to 700 nm. Using established modeling approaches, SANS data provides information about the topology and architecture of pore networks (Navarre-Sitchler et al., 2013). SANS experiments performed on cuttings from the Madison Limestone experiments failed to provide useable results. Although SANS experiments on shale caprock are beyond the scope of this study, our on going collaborations (Katherine Mouzakis, Alexis K. Navarre-Sitchler, and John McCray at the Colorado School of Mines; Gernot Rother and Jose Leo Banuelos at Oak Ridge National Laboratory) permitted SANS analysis of the shales. The SANS data herein represents their efforts, as funded by another project, working with shales that were reacted in UW laboratories for this project. SANS data were collected at the High Flux Isotope Reactor facility at Oak Ridge National Laboratory on the General Purpose SANS (CG-2) and Bio SANS (CG-3) beamlines. SANS results from the two shales, silica-rich to carbonate rich, yield information on the reactivity of the caprock in the RSU #1. These results also yield insight into the reactivity of Madison Limestone and Weber Sandstone.

3. Results and Discussion

3.1. pH, Carbonation, and Rate of Mineral Precipitation

The calculated in situ pH values are listed in Tables 3 and 4 and illustrated in Figure 2. After pressurization with supercritical CO_2, pH decreases to a value of ~3.5 for the Gothic Shale-Brine-supercritical CO_2 experiment and ~4 for the Marine Tuscaloosa Shale Brine-supercritical CO_2 experiment. These pH values are too low for carbonate to mineralize, as confirmed by saturation state calculations. The pH of the Marine Tuscaloosa Shale Brine-supercritical CO_2 experiment remains constant throughout the experiment. The pH of the Gothic Shale-Brine-supercritical CO_2 experiment increases to a value of ~4 during the course of the experiment, but this pH is still too low to mineralize carbonate. Saturation state calculations confirm this as well. Thus, as long as an immiscible supercritical CO2 phase is present, mineral carbonation will not take place.

The pH in the Marine Tuscaloosa Shale Brine-supercritical CO_2 experiment remains constant, as controlled by the immiscible supercritical CO_2 phase that is present, because silicates predominate and little to no carbonate minerals are present to buffer pH. The pH gradually increases in the Gothic Shale-Brine-supercritical CO_2 experiment due to buffering, mainly from the dissolving carbonates. Increasing activities of Ca^{2+} and Mg^{2+} (Table 4) that correlate with decreasing pH are indicative of calcite and dolomite dissolving and contributing their cations to the aqueous fluid. The changing activities of the divalent cations are correlative with each other. Using the pH increase/carbonate mineral dissolution as a guide to mineral precipitation, assuming dissolution rates equal precipitation rates, indicates that the rate of carbonate mineralization once the immiscible supercritical CO_2 phase dissolves into the brine hosted by the carbonate-rich shale, equals 1.13×10^{-4} mol calcite m^{-2} of pore space s^{-1} (3.6×10^{2} kg calcite m^{-2} of pore space $year^{-1}$). With no discernable pH change in the Marine Tuscaloosa Shale Brine-supercritical CO_2 experiment, no mineralization rate can be calculated for this silicate-rich rock. By inference, the rate of carbonate mineralization in silicate-rich rocks must be much less than the rate calculated for the carbonate-rich rocks.

The carbonate dissolution and precipitation can affect the sealing properties of the caprock and porosity of the reservoir rock. Dissolution can increase the porosity and permeability of the shale (Liu et al., 2012). Conversely, precipitation and redistribution of carbonate cements may fortify defects in shale, and by analogy in carbonate reservoir, possibly even preferentially precipitating and clogging leaks due to the associated decrease in pCO_2 at the leakage pathways (Harvey et al., 2013). This process is significant as it may represent the potential for long-term mineral trapping of CO_2 as stable carbonates.

Anhydrite is thermodynamically stable for the entirety of the Gothic Shale-brine experiment whereas anhydrite undergoes dissolution-precipitation reactions in the Gothic Shale-brine-supercritical CO_2 experiment. This result is consistent with the findings of Kohler et al. (2009). This behavior is controlled by the availability of Ca^{2+} in the brine, which in turn is predominantly controlled by the dissolution of calcite and dolomite, which exhibit dissolution behavior opposite to that of anhydrite (common ion effect). Anhydrite precipitation would potentially reduce the permeability and porosity (Kupecz et al., 1997), which would be beneficial to caprock but deleterious to reservoir rock in carbon sequestration and utilization scenarios.

3.2. Interlayer Cation Exchange

In addition to dissolution of components of the framework of clays, the interlayer cations are susceptible to exchange reactions, which are enhanced when pH decreases (Shao et al., 2010) due to CO_2 dissolution into the aqueous phase. It is likely that interlayer cation exchange reaction contributed to controlling the relative proportions of divalent cations released into the brine during carbonate dissolution. The correlative relationship between divalent cation activity minima in the fluid and monovalent cation activity maxima is illustrated in Tables 3a and 4a. It likely represents interlayer exchange due to the increased Ca^{+2} and Mg^{+2} abundances in the brine due to carbonate dissolution. These higher charged ions are more strongly attracted to the negatively charged clay structures and preferentially displace the monovalent cations. In non-expandable clays, the intercalation of larger ions may lead to structural defects, such as crack and bulge formation (Hu et al., 2013). Additionally, intercalation of larger hydrated cations in smectites change the swelling properties of the clay (Ferrage et al., 2005), which in turn will affect shale porosity, permeability, and wetting properties (Ilton et al., 2012; Schaef et al., 2012).

3.3 Dissolution Rate of CO_2 into Brine

The solubility of CO_2 in waters reacted with the silica-rich mudstone (Marine Tuscaloosa Shale) is 0.47 mol/kg according to an equation of state that is widely used in the geochemical community (Duan et al. 2006). In the experiment, 0.46 mol/kg CO_2 was measured in the sample collected 24 hours after the experiment began (Table 3a). Therefore, CO_2 saturation was achieved within 24 hours (or less). This yields a minimum CO_2 dissolution rate of $2.5x10^{-3}$ CO_2 mol m^{-2} pore space s^{-1} ($3.5x10^3$ kg CO_2 m^{-2} pore space $year^{-1}$) for the silica-rich mudstone and, by inference, sandstones such as the Weber Sandstone. The solubility of CO_2 in waters reacted with the carbonate-rich mudstone (Gothic Shale) is 0.56 mol/kg according to the CO_2 equation of state (Duan et al. 2006). In the experiment, 0.52 mol/kg CO_2 was measured in the sample collected 146 hours after the experiment began (Table 4a). This value is sufficiently close to the predicted value that we consider the experiment to be saturated with CO_2. This yields a minimum CO_2 dissolution rate of $4.7x10^{-4}$ mol CO_2 m^{-2} pore space s^{-1} ($6.5x10^2$ kg CO_2 m^{-2} pore space $year^{-1}$) for the carbonate-rich mudstone and, by inference, carbonate rocks such as the Madison Limestone. Differences in these rates is partly due to the different brine compositions (ionic strength of 2.1 mol/kg for the silica-rich shale and 2.5 mol/kg for the carbonate-rich shale) but largely due to the different mineralogies of the two shales.

3.4 Porosity Changes

In unreacted samples of Gothic Shale and Marine Tuscaloosa Shale, < 10 nm pores dominant the pore size distribution as calculated from SANS data. Total and connected porosity in the unreacted Gothic Shale are 4.21% and 1.53%, respectively. Brine-reacted samples have total and connected porosities higher than the unreacted samples (5.64% and 2.55%, respectively). Thus, despite little visible evidence of porosity generation in the brine-reacted Gothic Shale, porosity did increase. Unconnected porosity increased slightly in the CO_2-reacted samples (0.04%) indicating potential precipitation and blocking of pore throats. The total porosity in the CO_2-reacted samples is the same as the brine-reacted sample but the connected porosity is lower. This behavior can be attributed to a combination of a greater degree of mineral dissolution. The net effect of combined mineral dissolution and precipitation is little change in total porosity but decreased connected porosity. Pore size distributions in the Gothic Shale samples also show that porosity increase in the < 10 nm length-scale is approximately the same in the CO_2- and brine-reacted samples. However, porosity in the 100-1000 nm size pores increases more in the brine-reacted than in the CO_2-reacted samples. Thus, while the total porosity would suggest that the CO_2-reacted experiment produced the same results as the control, the pore size distribution data show the difference in how that porosity was generated between the two experiments.

Unlike the Gothic Shale samples, the CO_2-reacted Marine Tuscaloosa total porosity is higher than the brine-reacted and unreacted total porosity. The SANS calculated porosity of the unreacted Marine Tuscalooa is 3.22% which increased to 3.75% during the CO_2-reacted experiment and decreased slightly to 3.16% during the brine-reacted experiment. The connected porosity in the brine-reacted samples is higher (2.18%) than both the unreacted (1.1%) and CO_2-reacted (0.65%) samples, and the connected porosity is lowest in the CO_2-reacted samples. The pore size distributions are very similar and show an increase in porosity at length scales < ~50 nm and decreased porosity at length scales > ~50 nm compared to the unreacted samples. The porosity in pores < ~ 50 nm is higher in the CO_2-reacted than the brine-reacted samples, which may be responsible for the overall higher total porosity.

4. Conclusions

The following results are concluded from this investigation:

1) Enhanced carbonate and silicate dissolution occurs when supercritical CO_2 reacts with the shale and brine compared to the baseline experiment. Re-precipitation of carbonates and silicates buffer the pH and change the mineralogy and textures of the shale.
2) Anhydrite precipitates in response to injection of supercritical CO_2, which possibly will decrease the porosity and permeability of the shale.
3) Clay dissolution/precipitation likely occurs and the compositional/structural changes likely affect the porosity, permeability, and wettability of the shale and possibly the large-scale basinal properties.
4) Using pH and carbonate mineral dissolution data, and assuming dissolution rates equal precipitation rates, the rate of carbonate mineralization in carbonate-rich rocks is $1.1x10^{-4}$ mol calcite m^{-2} of pore space s^{-1} ($3.6x10^{2}$ kg calcite m^{-2} of pore space $year^{-1}$). Mineralization only takes place after the immiscible supercritical CO_2 phase dissolves into the brine. No carbonate mineralization rate can be calculated for silicate-rich rocks on the time frame of the laboratory experiments. By inference, this rate must be much less than the rate calculated for the carbonate-rich rocks.
5) A minimum CO_2 dissolution rate of $2.5x10^{-3}$ mol CO_2 m^{-2} pore space s^{-1} ($3.5x10^{3}$ kg CO_2 m^{-2} pore space $year^{-1}$) was determined for silica-rich mudstone and, by inference, sandstones such as the Weber Sandstone. A minimum CO_2 dissolution rate of $4.7x10^{-4}$ mol CO_2 m^{-2} pore space s^{-1} ($6.5x10^{2}$ kg CO_2 m^{-2} pore space $year^{-1}$) was determined for carbonate-rich mudstone and, by inference, carbonate rocks such as the Madison Limestone.
6) Total porosity and pore connectivity increased in both the brine-reacted and CO_2-reacted samples of Gothic Shale. In contrast, total porosity did not change but connected porosity increased in the brine-reacted Marine Tuscaloosa Shale samples while the total porosity increased and connected porosity decreased in the CO_2-reacted Marine Tuscaloosa Shale samples. Carbonate-rich shale caprocks (and by analogy carbonate reservoirs) may be more susceptible to long-term loss of sealing capacity (but greater porosity and hence storage in carbonate reservoirs) with geochemical reaction as carbonate mineral solubility is sensitive to pH changes and kinetic dissolution rates are fast, resulting in increased pore connectivity and median pore size.

References

Alemu, B. L., P. Aagaard, I. A. Munz, and E. Skurtveit, 2011, Caprock interaction with CO2: A laboratory study of reactivity of shale with supercritical CO2 and brine: Applied Geochemistry, v. 26, p. 1975-1989.

Bethke, C.M., Yeakel, S., 2013. The Geochemist's Workbench Release 9.0: Reaction Modeling Guide Aqueous Solutions, LLC, Champaign, Illinois, p. 130.

Cantrell, K.J., Thompson, C.J., Shao, H., Jung, H.B., Zhong, L., Um, W., 2012. FY 12 ARRA-NRAP Report – Studies to Support Risk Assessment of Geologic Carbon Sequestration Pacific Northwest National Laboratory, USA.

Ferrage, E., Lanson, B., Sakharov, B.A., Drits, V.A., 2005. Investigation of smectite hydration properties by modeling experimental X-ray diffraction patterns: Part I. Montmorillonite hydration properties. American Mineralogist 90, 1358-1374.

Gaus, I., M. Azaroual, and I. Czernichowski-Lauriol, 2005, Reactive transport modelling of the impact of CO2 injection on the clayey cap rock at Sleipner (North Sea): Chemical Geology, v. 217, p. 319-337.

Griffith, C.A., Dzombak, D.A., Lowry, G.V., 2011. Physical and chemical characteristics of potential seal strata in regions considered for demonstrating geological saline CO2 sequestration. Environmental Earth Sciences 64, 925-948.

Harvey, O.R., Qafoku, N.P., Cantrell, K.J., Lee, G., Amonette, J.E., Brown, C.F., 2013. Geochemical Implications of Gas Leakage associated with Geologic CO2 Storage-A Qualitative Review. Environmental Science & Technology 47, 23-36.

Heath, J.E., Dewers, T.A., McPherson, B.J.O.L., Petrusak, R., Chidsey, T.C., Jr., Rinehart, A.J., Mozley, P.S., 2011. Pore networks in continental and marine mudstones: Characteristics and controls on sealing behavior. Geosphere 7, 429-454.

Helgeson, H.C., 1968. Evaluation of Irreversible Reactions in Geochemical Processes Involving Minerals and Aqueous Solutions .I. Thermodynamic Relations. Geochimica Et Cosmochimica Acta 32, 853-&.

Helgeson, H.C., Garrels, R.M., Mackenzi.Ft, 1969. Evaluation of Irreversible Reactions in Geochemical Processes Involving Minerals and Aqueous Solutions .2. Applications. Geochimica Et Cosmochimica Acta 33, 455-&.

Hu, Y., Ray, J.R., Jun, Y.-S., 2013. Na+, Ca2+, and Mg2+ in Brines Affect Supercritical CO2-Brine-Biotite Interactions: Ion Exchange, Biotite Dissolution, and Illite Precipitation. Environmental Science & Technology 47, 191-197.

Ilton, E.S., Schaef, H.T., Qafoku, O., Rosso, K.M., Felmy, A.R., 2012. In Situ X-ray Diffraction Study of Na+ Saturated Montmorillonite Exposed to Variably Wet Super Critical CO2. Environmental Science & Technology 46.

Kang, S. M., 2011, Carbon dioxide storage capacity of Barnett shale.

Karamalidis, A.K., Torres, S.G., Hakala, J.A., Shao, H., Cantrell, K.J., Carroll, S., 2013. Trace Metal Source Terms in Carbon Sequestration Environments. Environmental Science & Technology 47, 322-329.

Kharaka, Y.K., Cole, D.R., Hovorka, S.D., Gunter, W.D., Knauss, K.G., Freifeld, B.M., 2006. Gas-water-rock interactions in Frio Formation following CO2 injection: Implications for the storage of greenhouse gases in sedimentary basins. Geology 34, 577-580.

Kohler, E., Parra, T., Vidal, O., 2009. Clayey Cap-Rock Behavior in H2O-CO2 Media at Low Pressure and Temperature Conditions: An Experimental Approach. Clays and Clay Minerals 57, 616-637.

Kupecz, J.A., Gluyas, J.G., Bloch, S., 1997. Reservoir quality prediction in sandstones and carbonates. AAPG Memoir 69, VII-XXIV.

Kwak, J. H., J. Z. Hu, R. V. F. Turcu, K. M. Rosso, E. S. Ilton, C. Wang, J. A. Sears, M. H. Engelhard, A. R. Felmy, and D. W. Hoyt, 2011, The role of H2O in the carbonation of forsterite in supercritical CO2: International Journal of Greenhouse Gas Control, v. 5, p. 1081-1092.

Langmuir, D., 1997. Aqueous Environmental Geochemistry. Prentice Hall.

Lin, H., T. Fujii, R. Takisawa, T. Takahashi, and T. Hashida, 2008, Experimental evaluation of interactions in supercritical CO_2/water/rock minerals system under geologic CO_2 sequestration conditions: Journal of Materials Science, v. 43, p. 2307-2315.

Litynski, J. T., S. Plasynski, H. G. McIlvried, C. Mahoney, and R. D. Srivastava, 2008, The United States Department of Energy's Regional Carbon Sequestration Partnerships Program Validation Phase: Environment International, v. 34, p. 127-138.

Liu, F., Lu, P., Griffith, C., Hedges, S.W., Soong, Y., Hellevang, H., Zhu, C., 2012. CO2-brine-caprock interaction: Reactivity experiments on Eau Claire shale and a review of relevant literature. International Journal of Greenhouse Gas Control 7.

Liu, K., 2005, Upper Cretaceous sequence stratigraphy, sealevel fluctuations and oceanic anoxic events 2 and 3, northeastern Gulf of Mexico, v. 2, p. 147-166.

Long, D.T., Angino, E.E., 1982. The Mobilization of Selected Trace-Metals from Shales by Aqueous-Solutions - Effects Of Temperature and Ionic-Strength. Economic Geology 77, 646-652.

Loring, J. S., C. J. Thompson, Z. Wang, A. G. Joly, D. S. Sklarew, H. T. Schaef, E. S. Ilton, K. M. Rosso, and A. R. Felmy, 2011, In Situ Infrared Spectroscopic Study of Forsterite Carbonation in Wet Supercritical CO2: Environmental Science & Technology, v. 45, p. 6204-6210.

Loucks, R. G., R. M. Reed, S. C. Ruppel, and D. M. Jarvie, 2009, Morphology, Genesis, and Distribution of Nanometer-Scale Pores in Siliceous Mudstones of the Mississippian Barnett Shale: Journal of Sedimentary Research, v. 79, p. 848-861.

Montes-Hernandez, G., Pironon, J., 2009. Hematite and iron carbonate precipitation-coexistence at the iron-montmorillonite-salt solution-CO2 interfaces under high gas pressure at 150 degrees C. Applied Clay Science 45, 194-200.

Montes-Hernandez, G., Pironon, J., Villieras, F., 2006. Synthesis of a red iron oxide/montmorillonite pigment in a CO2-rich brine solution. Journal of Colloid and Interface Science 303, 472-476.

Moore, D.M., Reynolds, R.C., 1989. X-Ray Diffraction and the Identification and Analysis of Clay Minerals. Oxford University Press, New York, NY.

Mouzakis, K., Navarre-Stichler, A.K., Rother, G., Banuelos, J.L., Wang, X., Kaszuba, J., McCray, J., 2013. Laboratory Investigation of Caprock Reactivity under Carbon Sequestration Conditions. in prep.

Newell, D.L., Kaszuba, J.P., Viswanathan, H.S., Pawar, R.J., Carpenter, T., 2008. Significance of carbonate buffers in natural waters reacting with supercritical CO2: Implications for monitoring,

measuring and verification (MMV) of geologic carbon sequestration. Geophysical Research Letters 35.

Potter, P. E., J. B. Maynard, and P. J. Depetris, 2005, Mud and mudstones—Introduction and overview: New York, Springer.

Regnault, O., V. Lagneau, H. Catalette, and H. Schneider, 2005, Étude expérimentale de la réactivité du CO2 supercritique vis-à-vis de phases minérales pures. Implications pour la séquestration géologique de CO2: Comptes Rendus Geoscience, v. 337, p. 1331-1339.

Rempel, K.U., Liebscher, A., Heinrich, W., Schettler, G., 2011. An experimental investigation of trace element dissolution in carbon dioxide: Applications to the geological storage of CO2. Chemical Geology 289.

Schaef, H.T., Ilton, E.S., Qafoku, O., Martin, P.F., Felmy, A.R., Rosso, K.M., 2012. In situ XRD study of Ca2+ saturated montmorillonite (STX-1) exposed to anhydrous and wet supercritical carbon dioxide. International Journal of Greenhouse Gas Control 6.

Schleicher, A.M., van der Pluijm, B.A., Warr, L.N., 2012. Chlorite-smectite clay minerals and fault behavior: New evidence from the San Andreas Fault Observatory at Depth (SAFOD) core. Lithosphere 4, 209-220.

Shah, V., D. Broseta, G. Mouronval, and F. Montel, 2008, Water/acid gas interfacial tensions and their impact on acid gas geological storage: International Journal of Greenhouse Gas Control, v. 2, p. 594-604.

Shao, H., Ray, J.R., Jun, Y.-S., 2010. Dissolution and Precipitation of Clay Minerals under Geologic CO2 Sequestration Conditions: CO2-Brine-Phlogopite Interactions. Environmental Science & Technology 44, 5999-6005.

Shukla, R., P. Ranjith, A. Haque, and X. Choi, 2010, A review of studies on CO_2 sequestration and caprock integrity: Fuel, v. 89, p. 2651-2664.

Siirila, E.R., Navarre-Sitchler, A.K., Maxwell, R.M., McCray, J.E., 2012. A quantitative methodology to assess the risks to human health from CO2 leakage into groundwater. Advances in Water Resources 36, 146-164.

Weiss, A., Amstutz, G.C., 1966. Ion-exchange reactions on clay minerals and cation selective membrane properties as possible mechanisms of economic metal concentration. Mineralium Deposita 1, 60-66.

Xu, T., J. A. Apps, and K. Pruess, 2004, Mineral Sequestration of Carbon Dixoide in a Sandstone-Shale System.

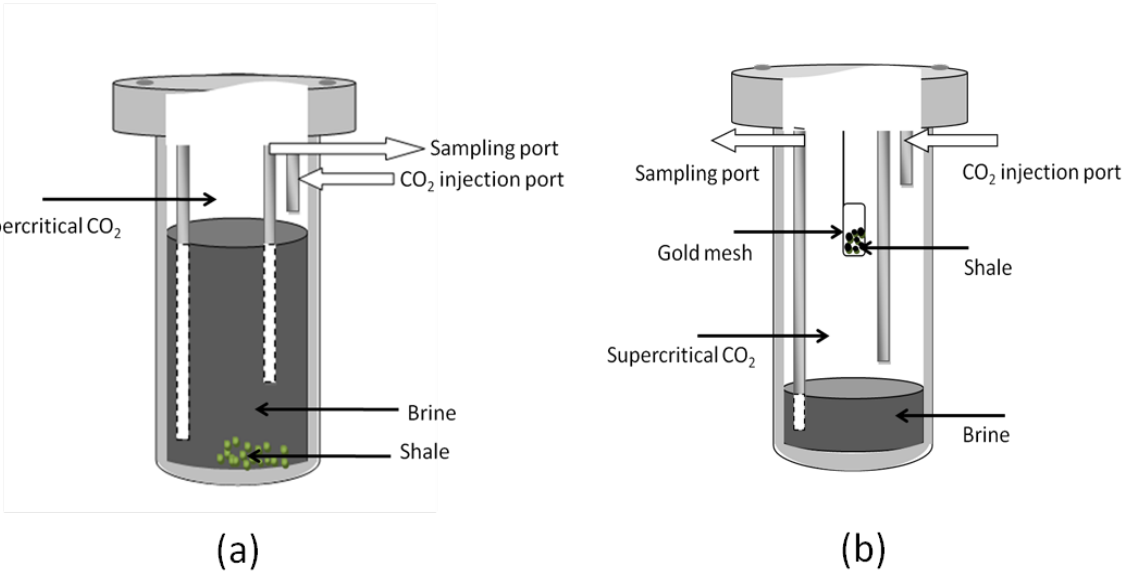


Figure 1. Schematic diagram of experimental apparatus and design. The internal volume of the apparatus is 300 cm^3 and the cross sectional area, as required for determining CO2 dissolution rates, is 0.046 mm.

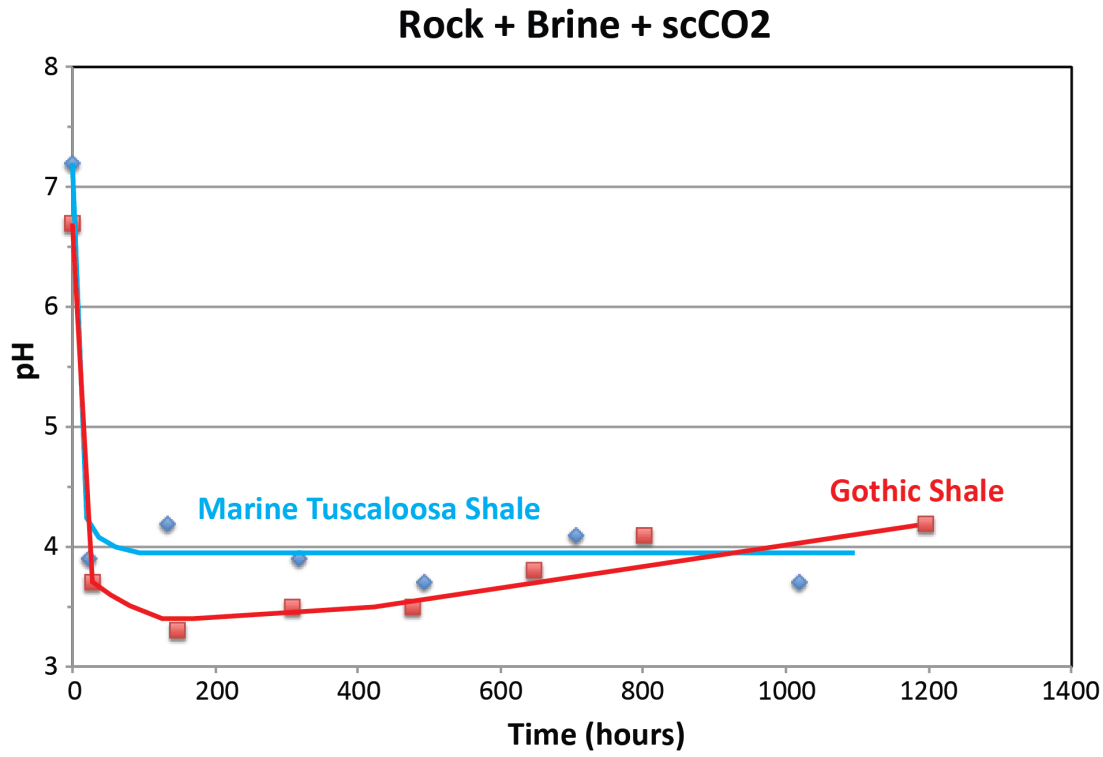


Figure 2. Calculated in situ pH for shale-brine-supercritical CO_2 experiments.

Table 1. Summary of experiments

Description	Time (hours)	Shale (grams)	Brine (grams)	CO_2 (grams)	Brine (mole fraction)
Marine Tuscaloosa Shale in brine, supercritical CO_2 headspace	1045	5	270	32.82	0.95
Marine Tuscaloosa Shale in brine, Ar headspace	864	5	299	0	1.00
Marine Tuscaloosa Shale in water-saturated supercritical CO_2	627	1.85	80	71.43	0.73
Gothic Shale in brine, supercritical CO_2 headspace	1197	5	270	34.65	0.95
Gothic Shale in brine, Ar headspace	820	5	299	0	1.00
Gothic Shale in water-saturated supercritical CO_2	497	1.85	80	77.11	0.72

Table 2. Brine composition (millimole per kilogram unless otherwise noted)

	Marine Tuscaloosa Shale	Gothic Shale
Ca	340	1190
Mg	6.76	29.90
SO_4	2.49	0.08
Fe	0.0030	0.0402
CO_3^{2-}	19.60	0.15
Al	0.0001	0.0007
SiO_2(aq)	1.33	1.62
K	69.00	4.72
Na	2644	172
Cl	3362	2616
TDS (mg/L)	21440	19202
Ionic strength (mol/kg)	2.07	2.53

Table 3a. Aqueous geochemistry (mmol/kg unless otherwise noted), Marine Tuscaloosa Shale in brine, supercritical CO_2 headspace.

Hours	pH (STD)	pH (in-situ)	SiO_2(aq)	Mn	Fe	Mg	Ca	Na	K	Cl	SO_4	ΣCO2	charge balance (%)
0	7.2	na	0.8	0.0	0.0	7.1	336.1	2942.1	75.4	3865.5	2.6	0.067	4.3
24.0	5.0	3.9	1.6	0.1	0.1	6.8	332.5	2701.8	45.3	3790.4	3.0	455.6	9.8
133.3	5.0	4.2	1.8	0.1	0.2	7.1	335.6	2705.0	68.9	3835.1	2.5	191.6	9.9
316.5	5.0	3.9	1.7	0.1	0.4	6.2	276.6	2400.0	61.6	2767.2	1.9	418.8	-9.3
492.5	5.1	3.7	2.0	0.1	0.5	6.7	297.1	2560.6	65.2	3410.8	1.9	152.3	5.3
705.8	5.0	4.1	2.1	0.1	0.7	7.3	332.9	2531.9	71.2	3607.6	1.7	414.5	9.0
1017.5	5.2	3.7	1.8	0.1	0.8	7.2	333.5	2528.1	67.7	3605.1	1.8	214.6	9.1
1044.5 Q	5.1	na	1.6	0.1	0.8	7.2	326.1	2552.7	65.4	3587.0	2.0	16.8	8.5
uncertainty	±0.1	±0.1	±0.03	0	±0.003	±0.5	±4.5	±2.4	±0.6	±14	±0.1	±6%	na

na = not available
Q denotes sample collected after experiment was terminated

Table 3b. Aqueous geochemistry (mmol/kg unless otherwise noted), Marine Tuscaloosa Shale in brine, Ar headspace.

Hours	pH (STD)	pH (in-situ)	SiO_2(aq)	Mn	Fe	Mg	Ca	Na	K	Cl	SO_4	ΣCO2	charge balance (%)
0	7.1	na	0.8	0.0	0.0	6.0	325.2	2798.1	67.8	3342.0	2.5	0.27	5.4
24.0	5.7	5.1	0.8	0.1	0.0	5.8	280.6	2501.1	64.8	3375.6	2.9	0.29	7.2
186.9	5.5	5.3	1.2	0.1	0.6	6.5	346.0	2691.2	74.0	3506.7	2.6	1.02	1.1
354.2	5.4	4.9	1.2	0.1	0.4	6.0	300.7	2531.6	64.0	3441.9	2.4	1.16	6.9
576.3	5.6	5.5	1.3	0.1	0.1	6.6	326.8	2707.1	67.3	3693.2	2.3	0.88	6.9
698.0	5.9	5.4	1.1	0.1	0.0	5.6	272.4	2600.0	54.2	3590.4	2.4	1.03	10.7
861.0	5.5	5.2	1.4	0.1	0.4	6.5	320.7	2584.1	66.9	3631.4	2.3	0.96	9.1
864.0Q	5.6	na	1.3	0.1	0.0	6.3	315.8	2516.4	60.8	3677.5	2.3	0.24	12.5
uncertainty	±0.1	±0.1	±0.03	0	±0.003	±0.5	±4.5	±2.4	±0.6	±14	±0.1	±6%	na

na = not available
Q denotes sample collected after experiment was terminated

Table 4a. Aqueous geochemistry (mmol/kg unless otherwise noted), Gothic Shale in brine, supercritical CO_2 headspace

Hours	pH (STD)	pH (in-situ)	SiO_2(aq)	Mn	Fe	Mg	Ca	Na	K	Cl	SO_4	ΣCO2	charge balance (%)
0	6.7	na	0.9	0.0	0.0	29.1	1346.2	194.3	4.9	2956.4	2.7	0.73	0.4
28	5.1	3.7	1.8	0.1	0.3	32.3	1305.2	181.5	5.7	3130.3	0.8	275.6	8.6
146	4.8	3.3	1.9	0.1	0.3	33.1	1281.7	173.2	5.9	3040.8	0.9	520.4	7.7
308	4.9	3.5	2.0	0.1	0.6	35.9	1249.2	185.3	5.9	2885.9	0.9	464.7	4.3
477	4.9	3.5	2.0	0.1	0.9	34.6	1234.3	185.5	4.6	2894.3	0.8	411.1	5.7
646	5.3	3.8	2.0	0.1	0.8	32.2	1134.4	165.2	4.6	2912.4	0.9	422.4	14.1
801	5.2	4.1	2.2	0.1	1.7	34.9	1224.1	180.2	5.2	2880.2	0.9	199.7	6.1
1195	5.4	4.2	2.3	0.1	1.1	37.3	1322.6	190.8	5.3	3157.4	1.0	300.8	7.6
1197Q	5.2	na	3.0	0.1	1.3	43.6	1631.2	225.1	6.3	3056.5	1.1	0.50	17.2
uncertainty	±0.1	±0.1	±0.05	0	±0.02	±0.3	±5.1	±34	±5.2	±50	±0.1	±6%	na

na = not available
Q denotes sample collected after experiment was terminated

Table 4b. Aqueous geochemistry (mmol/kg unless otherwise noted), Gothic Shale in brine, Ar headspace

Hours	pH (STD)	pH (in-situ)	SiO_2(aq)	Mn	Fe	Mg	Ca	Na	K	Cl	SO_4	ΣCO2	charge balance (%)
0	6.8	na	0.0	0.0	0.0	30.6	1351.3	193.0	4.3	2902.2	0.1	0.08	2.0
32.6	6.0	2.9	1.3	0.0	0.1	28.8	1135.3	154.6	4.0	2932.8	0.8	0.44	15.2
149.7	6.0	2.9	2.0	0.0	0.6	34.9	1194.6	259.5	6.2	2943.3	0.8	0.60	7.4
342.6	6.0	2.9	2.8	0.0	0.2	36.0	1189.5	273.1	6.1	2956.6	0.8	0.93	7.7
483.0	5.7	2.9	3.4	0.1	0.0	37.6	1217.0	191.3	5.7	3212.7	1.0	0.99	15.8
820.2	6.0	2.9	3.0	0.0	0.0	37.7	1215.5	182.0	9.6	2894.0	1.0	1.06	6.8
822.6Q	5.7	na	2.9	0.0	0.0	36.1	1163.9	184.1	5.0	2746.9	0.9	0.76	5.8
uncertainty	±0.1	±0.1	±0.05	0	±0.02	±0.3	±5.1	±34	±5.2	±50	±0.1	±6%	na

na = not available
Q denotes sample collected after experiment was terminated

ROUTINE CORE ANALYSIS

University of Wyoming

Well: RSU #1

FINAL REPORT

Prepared for

University of Wyoming

By

Intertek Westport Technology Center
6700 Portwest Drive
Houston, Texas 77024
(713) 479-8400 (Phone)
(713) 864-9357 (Fax)
www.westport1.com

November 12, 2012

Project No.: WTC-12-002873

TABLE 1. TEST SELECTION AND INVENTORY

Project No.:	WTC-12-002873
Company	University of Wyoming
Well Location:	,

			Tests Selected			
Sample ID	**Net Confining Stress**	**Formation**	**Routine Core Analysis Density**	**Absolute Brine Permeability**	**CO_2 - Brine Relative Permeability**	**Mercury Injection Cap Pressure**
26	4370	Weber Sandstone	X	x		x
27	4370	Weber Sandstone	X	x		x
45	4370	Weber Sandstone	X	x		x
72	4900	Madison Carbonate	X	x		x
79	4900	Madison Carbonate	X	x		x
99	4900	Madison Carbonate	X	x		x
106	4900	Madison Carbonate	X	x		x
110	4900	Madison Carbonate	X	x		x

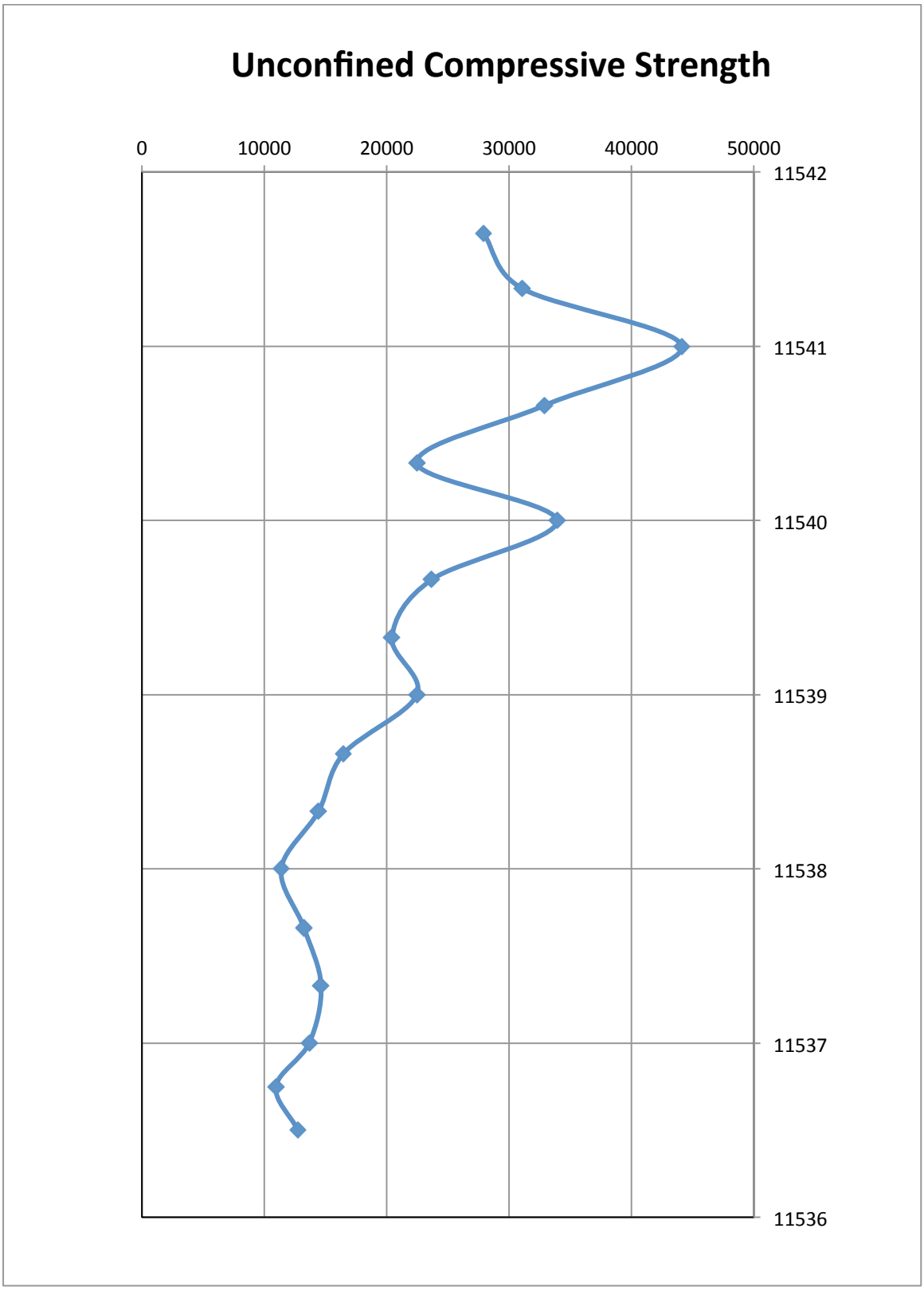
TABLE 2. ROUTINE CORE PROPERTIES

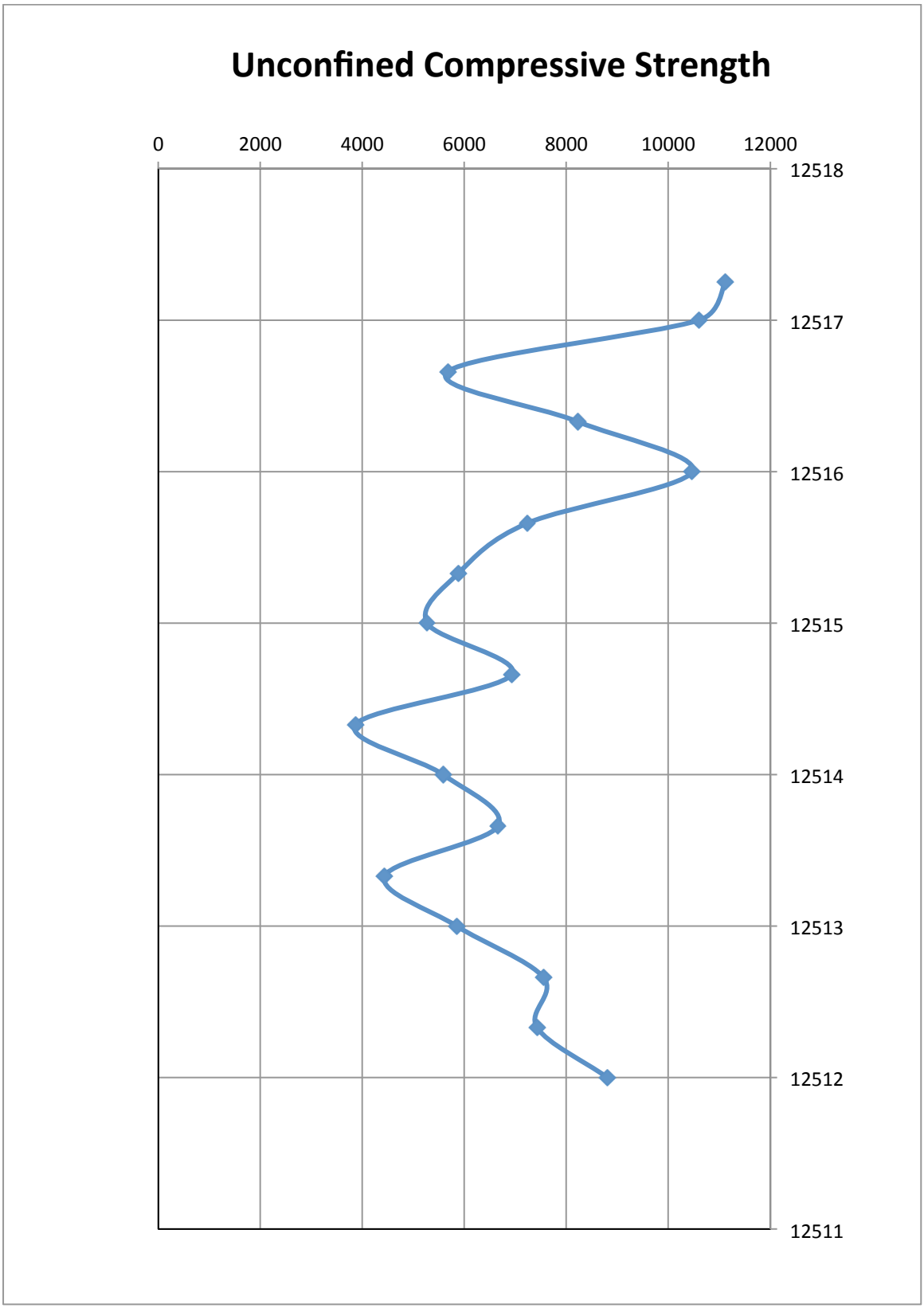
Sample ID	Sample Dimensions		Permeability			Res. NCS Porosity	Grain Density	Lithologic Description
	Length	Diameter	Reservoir NCS					
			to Air	Klinkenberg	Brine			
	(cm)	(cm)	(mD)				(g/cm^3)	
Weber Sandstone								
26	4.61	2.48	12.9	12.9	6.67	8.2	2.64	Sst wht, f-m grn, calc, dolo, py
27	4.40	2.48	1.12	0.969	0.99	7.4	2.63	Sst wht, f-m grn, calc, py
45	3.73	2.47	0.004	0.001	0.000	0.7	2.65	Sst wht, f-m grn, calc, py
Madison Carbonate								
72	4.37	2.46	6.63	6.06	11.2	15.7	2.85	Ls- wht, dolo, org, py, frac
79	2.73	2.47	82.6	80.1	26.6	15.2	2.82	Ls- wht, f xln, org, vugs
99	3.65	2.50	0.372	0.292	0.272	11.7	2.84	Ls- wht, f xln, org, dolo, vugs
106	4.77	2.47	2.87	2.59	1.92	14.5	2.83	Ls- wht, f xln, org, dolo, vugs
110	4.83	2.47	1.35	1.68	0.573	13.5	2.84	Ls- wht, f xln, org, dolo, vugs

Brinell Hardness Test

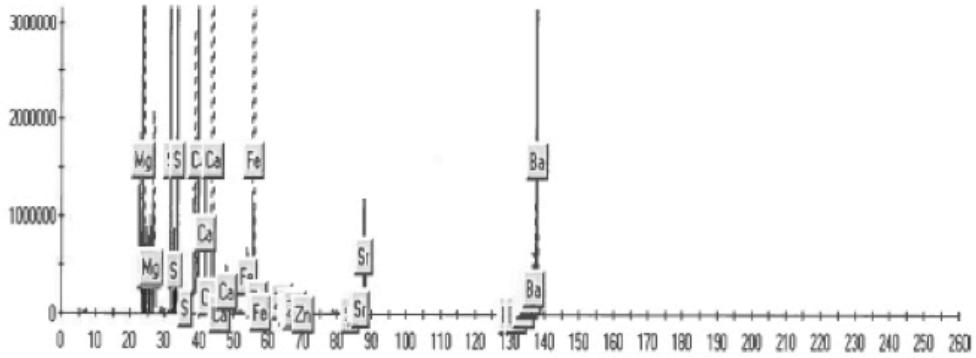
Company	**University of Wyoming**	Date	**2/25/13**
Well Name	**RSU #1**	Job No.	**120536**
Field Name		Saturation Fluid	**None**
Location		Rock Type	

Sample Number	Depth (ft)	BH (kg/mm^2)	UCS (psi)
FD1	11536.50	13.11	12759.68
FD1	11536.75	10.81	10950.66
FD1	11537.00	14.27	13665.44
FD1	11537.33	15.51	14639.21
FD1	11537.66	13.73	13245.54
FD1	11538.00	11.36	11382.95
FD1	11538.33	15.24	14431.14
FD1	11538.66	17.83	16465.05
FD1	11539.00	25.47	22464.21
FD1	11539.33	22.88	20431.23
FD1	11539.66	27.02	23676.16
FD1	11540.00	40.04	33899.08
FD1	11540.33	25.47	22464.21
FD1	11540.66	38.77	32897.54
FD1	11541.00	53.04	44100.64
FD1	11541.33	36.46	31091.81
FD1	11541.65	32.39	27892.44
FD2	12512.00	8.08	8809.69
FD2	12512.33	6.32	7425.86
FD2	12512.66	6.48	7552.09
FD2	12513.00	4.31	5848.17
FD2	12513.33	2.51	4438.94
FD2	12513.66	5.34	6658.03
FD2	12514.00	3.97	5581.47
FD2	12514.33	1.78	3865.44
FD2	12514.66	5.68	6924.98
FD2	12515.00	3.57	5269.42
FD2	12515.33	4.36	5886.07
FD2	12515.66	6.08	7237.80
FD2	12516.00	10.19	10465.88
FD2	12516.33	7.33	8221.18
FD2	12516.66	4.09	5674.34
FD2	12517.00	10.37	10605.40
FD2	12517.25	11.02	11116.44


Unconfined Compressive Strength
0
10000
20000
30000
40000
50000
11542
11541
11540
11539
11538
11537
11536


Unconfined Compressive Strength
0
2000
4000
6000
8000
10000
12000
12518
12517
12516
12515
12514
12513
12512
12511

Drilling Mud Geochemistry



Indium (In), Holmium (Ho), Gold (Au), Bismuth (Bi) are 50ppb internal standards used to verify, response factors across the mass range. Chloride is not scanned by this method.

As scanned the major constituents (approximate)

Sulfur	0.4 -0.8 % by Wt
Iron	0.1 % by Wt
Calcium	2-3% by Wt
Barium	0.5 - 1.0% by Wt

As scanned the trace constituents (approximate)

Magnesium	1000 ppm
Zinc	80-100 ppm
Strontium	100-200 ppm

Appendix C: Lithium Concentration from Core Samples

Fred McLaughlin
University of Wyoming
2020 East Grand Ave, Suite 500
Laramie, WY. 82070

Date: June 26, 2012
Request Number: 30550
Date Received:6-4-12
Matrix: Pulverized Core
Method: 3052/6020

REPORT OF ANALYSIS

Lab Number	Sample ID:	Total Lithium, ug/g
N4007	RSU-21	0.265
N4008	RSU-25	0.782
N4009	RSU-36	0.52
N4010	RSU-39	0.535
N4011	RSU-43	0.397
N4012	RSU-44	4.74
N4013	RSU-47	0.191
N4014	RSU-57	2.9
N4015	RSU-81	1.37
N4016	RSU-91	< 0.01
N4017	RSU-97	< 0.01
N4018	RSU-101	< 0.01
N4019	RSU-105	4.69

Monte L. Ellis
Laboratory Manager

WYOMING ANALYTICAL LABORATORIES, INC.
1660 Harrison St. Wallaramie@wal-lab.com (307) 742-7995
Laramie, WY 82070 Fax: (307) 721-8956

Appendix D: Madison Core Description

Top Depth	Facies	Visible Porosity	
12236.3	0	0	
12246	0	0	
12247	2	0	
12253.5	5	0	
12256	6	0	
12257	0	0	
12307.7	5	0	
12310.6	2	0	
12317.5	5	0	
12318.5	7	0	
12319.5	5	0	
12320.6	0	0	
12326.3	3	0	
12328.9	1	0	
12329.5	0	0	
12331.3			boxes taken to NER
12421.9	8	1	
12423	8	1	
12423.8	10	2	
12437	8	0	
12441	5	0	
12442	8	2	
12443	10	1	
12446.8	9	1	
12447.2	10	2	
12453	8	1	
12454.6	10	2	
12458.2	9	2	
12459	10	2	
12465.4	9	1	
12466.2	10	0	
12466.7	9	1	
12468.6	9	1	
12470.6	10	2	
12473.1	10	0	
12473.5	10	2	
12476.7	9	1	
12477.2	10	2	
12478.6	10	2	
12479.6	9	1	
12484.4	10	2	
12488.5	10	1	
12491.2	8	0	
12492.8	10	1	
12492.9			
12495.72	9	0	box 160 at NER
12501			
12511	9	1	
12514.8	8	0	
12518.5	10	1	
12519.9	8	0	
12522	11	1	
12522.2	10	1	
12525.25	5	0	
12532			

Facies	
0	calc. mudstone
1	wackestone
2	interbedded mudstone/wackestone
3	packstone
4	grainstone
5	breccia
6	silty/muddy limestone
7	silic. mudstone
8	dolomite mudstone
9	dol wackestone
10	dol packstone
11	dol grainstone

Porosity	
0	none
1	some
2	high

Top Depth	Facies	Visible Porosity
12229.8	0	0
12239.5	0	0
12240.5	2	0
12247	5	0
12249.5	6	0
12250.5	0	0
12301.2	5	0
12304.1	2	0
12311	5	0
12312	7	0
12313	5	0
12314.1	0	0
12319.8	3	0
12322.4	1	0
12323	0	0
12324.8		
12415.4	8	1
12416.5	8	1
12417.3	10	2
12430.5	8	0
12434.5	5	0
12435.5	8	2
12436.5	10	1
12440.3	9	1
12440.7	10	2
12446.5	8	1
12448.1	10	2
12451.7	9	2
12452.5	10	2
12458.9	9	1
12459.7	10	0
12460.2	9	1
12462.1	9	1
12464.1	10	2
12466.6	10	0
12467	10	2
12470.2	9	1
12470.7	10	2
12472.1	10	2
12473.1	9	1
12477.9	10	2
12482	10	1
12484.7	8	0
12486.3	10	1
12486.4		
12489.22	9	0
12494.5		
12504.5	9	1
12508.3	8	0
12512	10	1
12513.4	8	0
12515.5	11	1
12515.7	10	1
12518.75	5	0
12525.5		

Appendix E: Mercury Injection Capillary Testing

MERCURY INJECTION CAPILLARY PRESSURE

UNIVERSITY OF WYOMING
WELL: RSU#1
SAMPLE: PLUGS AND CUTTINGS

FINAL REPORT

Prepared for

UNIVERSITY OF WYOMING

By

Intertek Westport Technology Center
6700 Portwest Drive
Houston, Texas 77024
(713) 479-8400 (Phone)
(713) 864-9357 (Fax)
www.westport1.com

April 16, 2013

Project No.: WTC-13-003568

II - MICP - RSU#1 WELL

TABLE OF CONTENTS II - i

RESULTS AND DISCUSSION II - 1

SUMMARY II - 2

APPENDICES

APPENDIX 1 - MERCURY INJECTION RESULT OF SAMPLE # 176 APPENDIX 1 - i
APPENDIX 2 - MERCURY INJECTION RESULT OF SAMPLE # 187 APPENDIX 2 - i
APPENDIX 3 - MERCURY INJECTION RESULT OF SAMPLE # 200 APPENDIX 3 - i
APPENDIX 4 - MERCURY INJECTION RESULT OF SAMPLE # 206 APPENDIX 4 - i
APPENDIX 5 - MERCURY INJECTION RESULT OF SAMPLE # 214 APPENDIX 5 - i
APPENDIX 6 - MERCURY INJECTION RESULT OF SAMPLE # B1 APPENDIX 6 - i
APPENDIX 7 - MERCURY INJECTION RESULT OF SAMPLE # B2 APPENDIX 7 - i
APPENDIX 8 - MERCURY INJECTION RESULT OF SAMPLE # 53 APPENDIX 8 - i
APPENDIX 9 - MERCURY INJECTION RESULT OF SAMPLE # G1 APPENDIX 9 - i
APPENDIX 10 - MERCURY INJECTION RESULT OF SAMPLE # M1 APPENDIX 10 - i
APPENDIX 11 - MERCURY INJECTION RESULT OF SAMPLE # M2 APPENDIX 11 - i
APPENDIX 12 - MERCURY INJECTION RESULT OF SAMPLE # PH1 APPENDIX 12 - i
APPENDIX 13 - MERCURY INJECTION RESULT OF SAMPLE # PH2 APPENDIX 13 - i

RESULTS AND DISCUSSION

Mercury injection capillary pressure measurements were made on five plugs and eight cutting samples.

The endtrims were placed in a Micromeretics Autopore IV porosimeter, under a 50 micron vacuum and injected with mercury at about 121 TO 122 increasing capillary pressure steps until 60,000 psi was achieved.

Results are summarized in the Summary. Detailed mercury injection capillary pressure results are shown in appendices. There was no injection for the plug Samples 176, 187, 200, 206 and 214. There was some intrusion volume as a result of fractures only.

SUMMARY

Sample ID	Interval Depth (ft)	Formation ID	Helium Porosity (%)	Grain Density g/cc	Mercury/Air Displacement Pressure (psi)	Pore Throat Distribution			Swanson	
						Micropores < 0.1 micron (%PV)	Intermediate 0.1-3 micron (%PV)	Macropores > 3 micron (%PV)	Brine Permeability (mD)	Air Permeability (mD)
176	11725.9	Weber 1	NA	2.70	No Injection	0.000	0.000	0.000	0.000	0.002
187	12178.1	Amsden 1	NA	2.91	No Injection	0.000	0.000	0.000	0.000	0.000
200	12227.3	Amsden 2	NA	2.85	No Injection	0.000	0.000	0.000	0.000	0.000
206	Unknown	Unknown	NA	2.74	No Injection	0.000	0.000	0.000	0.000	0.000
214	12333.9	Madison 1	NA	2.83	No Injection	0.000	0.000	0.000	0.000	0.000
B1	6300-6330	Baxter 1	NA	2.59	354.277	83.604	16.396	0.000	0.003	0.022
B2	7680-7710	Baxter 2	NA	2.57	217.251	76.340	23.660	0.000	0.006	0.040
B3	7590-7620	Baxter 3	NA	2.49	430.624	85.288	14.712	0.000	0.003	0.018
G1	9190-9200	Gypsum Springs 1	NA	2.59	429.616	88.278	11.722	0.000	0.003	0.023
M1	8130-8160	Mowry 1	NA	2.51	264.285	77.692	22.308	0.000	0.004	0.026
M2	8220-8250	Mowry 2	NA	2.50	473.679	89.438	10.562	0.000	0.002	0.013
PH1	11040-11050	Phosphoria 1	NA	2.71	239.449	69.770	30.230	0.000	0.024	0.121
PH2	11140-11150	Phosphoria 2	NA	2.65	194.398	67.981	32.019	0.000	0.020	0.105

APPENDIX 1 - MICP - SAMPLE 176

TABLE OF CONTENTS i

LIST OF TABLES

TABLE 1-1. MERCURY INJECTION DATA SUMMARY FOR SAMPLE ID 176 1
TABLE 1-2. MERCURY INJECTION DATA FOR SAMPLE ID 176 2

TABLE 1-1. MERCURY INJECTION DATA SUMMARY FOR SAMPLE ID 176

Sample Info and Properties	
Depth:	11725.9 ft
Well:	RSU#1
Formation:	Weber 1
Porosity:	NA % @ 800 psi
Air Permeability:	NA md @ 800 psi
Klink. Permeability:	NA md @ 800 psi
Grain Density:	2.70 g/cm3

Mercury Injection Data	
IFT (σ):	485 dynes/cm
Contact angle (θ):	130 degrees
σcosθ Hg/air:	367.7 dynes/cm
σcosθ Air/brine:	72 dynes/cm
Total Pore Area:	0.000 m^2/g
Hg Porosity:	0.00 %
Corr. Hg Porosity:	0.00 %

Height Computation	
Water - Oil Reservoir System	
Res. Oil Grad:	0.360 psi/ft
Res. Wtr. Gradient:	0.470 psi/ft
σcosθ reservoir:	10.0 dynes/cm
Conversion Factor "C":	0.247 ft/psi

Computations	
Displacement Pressure (Pd)	
Mercury/Air:	NA psi
Air/Brine Equiv:	NA psi
Equiv. Height:	NA ft
Pr Throat Rad:	NA microns
Pore Radius Distributions	
Mean (arithmetic):	NA microns
Mean (geometric):	NA microns
Mean (harmonic):	NA microns
Micropores - Pore throat radius < .1 micron:	NA % PV
Intermediate - Pore throat radius .1<r<3 micron:	NA % PV
Macropores - Pore throat radius > 3 micron:	NA % PV
Swanson Parameter[1]	
(Sb/Pc)max:	NA
Kbrine Swanson:	0.000 md
Kair Swanson:	0.000 md

TABLE 1-2. MERCURY INJECTION DATA FOR SAMPLE ID 176

Hg/air Pres. psi	Equivalent Air/brine Pres. psi	Height above Free Wtr. ft.	Pore radius Aperture microns	Hg Volume Injected cm3	Hg Sat. Pore Volume %	1-Hg Sat. Pore Volume %	Hg Porosity Injected %
0.5	0.11	0.13	167.5121	0.0000	0.0000	100.0	0.0000
0.6	0.11	0.14	154.6600	0.0041	1.8206	98.2	0.0772
0.6	0.13	0.16	140.4573	0.0073	5.0622	94.9	0.1374
0.7	0.14	0.17	128.9800	0.0073	8.3039	91.7	0.1374
0.8	0.15	0.19	117.2291	0.0084	12.0339	88.0	0.1582
0.8	0.17	0.21	106.7533	0.0092	16.1192	83.9	0.1732
0.9	0.18	0.23	97.2406	0.0094	20.2934	79.7	0.1770
1.0	0.20	0.25	88.6083	0.0071	23.4684	76.5	0.1346
1.1	0.22	0.28	80.6148	0.0080	27.0208	73.0	0.1506
1.2	0.24	0.30	73.6275	0.0075	30.3513	69.6	0.1412
1.4	0.26	0.33	66.9317	0.0059	32.9712	67.0	0.1111
1.5	0.29	0.37	60.9896	0.0054	35.3691	64.6	0.1017
1.6	0.32	0.40	55.5069	0.0060	38.0556	61.9	0.1139
1.8	0.35	0.44	50.5139	0.0046	40.1205	59.9	0.0876
2.0	0.4	0.49	45.9341	0.0042	42.0077	58.0	0.0800
2.2	0.4	0.53	41.8209	0.0039	43.7618	56.2	0.0744
2.4	0.5	0.59	38.0697	0.0034	45.2938	54.7	0.0650
2.6	0.5	0.65	34.6459	0.0036	46.8924	53.1	0.0678
2.9	0.6	0.71	31.5135	0.0036	48.5132	51.5	0.0687
3.2	0.6	0.78	28.6829	0.0035	50.0674	49.9	0.0659
3.5	0.7	0.86	26.0829	0.0031	51.4661	48.5	0.0593
3.8	0.7	0.94	23.7237	0.0023	52.5097	47.5	0.0442
4.2	0.8	1.04	21.5403	0.0023	53.5310	46.5	0.0433
4.6	0.9	1.14	19.5709	0.0020	54.4413	45.6	0.0386
5.1	1.0	1.26	17.7641	0.0019	55.2850	44.7	0.0358
5.6	1.1	1.39	16.1307	0.0029	56.5728	43.4	0.0546
6.2	1.2	1.53	14.6546	0.0021	57.5053	42.5	0.0395
6.8	1.3	1.68	13.3054	0.0018	58.3268	41.7	0.0348
7.5	1.5	1.85	12.0840	0.0015	59.0151	41.0	0.0292
8.2	1.6	2.04	10.9731	0.0017	59.7700	40.2	0.0320
9.1	1.8	2.24	9.9602	0.0030	61.1244	38.9	0.0574
10.0	2.0	2.47	9.0466	0.0018	61.9237	38.1	0.0339
11.0	2.2	2.72	8.2132	0.0017	62.6786	37.3	0.0320
12.1	2.4	3.00	7.4598	0.0016	63.4113	36.6	0.0311
13.3	2.6	3.3	6.7744	0.0016	64.1217	35.9	0.0301
14.7	2.9	3.6	6.1519	0.0011	64.6324	35.4	0.0217
16.2	3.2	4.0	5.5866	0.0013	65.2097	34.8	0.0245
17.8	3.5	4.4	5.0731	0.0013	65.7870	34.2	0.0245
19.6	3.8	4.9	4.6041	0.0013	66.3642	33.6	0.0245
21.7	4.2	5.4	4.1721	0.0012	66.8971	33.1	0.0226
23.9	4.7	5.9	3.7890	0.0013	67.4786	32.5	0.0247
26.3	5.1	6.5	3.4417	0.0013	68.0733	31.9	0.0252
28.9	5.7	7.2	3.1240	0.0013	68.6614	31.3	0.0249
31.9	6.2	7.9	2.8368	0.0016	69.3666	30.6	0.0299
35.1	6.9	8.7	2.5759	0.0013	69.9373	30.1	0.0242
38.7	7.6	9.6	2.3358	0.0012	70.4773	29.5	0.0229
42.9	8.4	10.6	2.1089	0.0012	71.0173	29.0	0.0229
48.1	9.4	11.9	1.8796	0.0012	71.5647	28.4	0.0232
53.0	10.4	13.1	1.7061	0.0013	72.1339	27.9	0.0241
59.6	11.7	14.7	1.5173	0.0026	73.2949	26.7	0.0492
65.4	12.8	16.2	1.3825	0.0020	74.1651	25.8	0.0369
72.6	14.2	18.0	1.2455	0.0008	74.5331	25.5	0.0156
80.3	15.7	19.8	1.1267	0.0010	74.9995	25.0	0.0198
88.3	17.3	21.8	1.0242	0.0007	75.3187	24.7	0.0135
98.5	19.3	24.4	0.9181	0.0007	75.6518	24.3	0.0141
108.2	21.2	26.7	0.8359	0.0006	75.9202	24.1	0.0114
120.0	23.5	29.7	0.7538	0.0008	76.2881	23.7	0.0156
132.6	26.0	32.8	0.6821	0.0007	76.5817	23.4	0.0124
146.6	28.7	36.2	0.6170	0.0007	76.8818	23.1	0.0127

TABLE 1-2. MERCURY INJECTION DATA FOR SAMPLE ID 176 - CONTINUED

Hg/air Pres. psi	Equivalent Air/brine Pres. psi	Height above Free Wtr. ft.	Pore radius Aperture microns	Hg Volume Injected cm3	Hg Sat. Pore Volume %	1-Hg Sat. Pore Volume %	Hg Porosity Injected %
161.5	31.6	40	0.5598	0.0010	77.3084	22.7	0.0181
178.8	35.0	44	0.5058	0.0007	77.6396	22.4	0.0140
197.0	38.6	49	0.4591	0.0009	78.0322	22.0	0.0166
217.2	42.5	54	0.4163	0.0008	78.3689	21.6	0.0143
239.4	46.9	59	0.3778	0.0013	78.9306	21.1	0.0238
263.7	52	65	0.3430	0.0009	79.3341	20.7	0.0171
291.5	57	72	0.3102	0.0009	79.7216	20.3	0.0164
321.4	63	79	0.2813	0.0012	80.2716	19.7	0.0233
354.2	69	88	0.2553	0.0014	80.8748	19.1	0.0256
390.6	76	97	0.2315	0.0010	81.3166	18.7	0.0187
431.1	84	107	0.2098	0.0014	81.9558	18.0	0.0271
475.1	93	117	0.1903	0.0017	82.7151	17.3	0.0322
523.0	102	129	0.1729	0.0019	83.5411	16.5	0.0350
576.5	113	143	0.1569	0.0016	84.2524	15.7	0.0302
635.4	124	157	0.1423	0.0021	85.2024	14.8	0.0403
700.3	137	173	0.1291	0.0017	85.9666	14.0	0.0324
772.3	151	191	0.1171	0.0026	87.1396	12.9	0.0497
851.3	167	210	0.1062	0.0018	87.9194	12.1	0.0331
937.4	184	232	0.0965	0.0016	88.6241	11.4	0.0299
1034.0	202	256	0.0875	0.0017	89.3772	10.6	0.0319
1138.3	223	281	0.0794	0.0017	90.1153	9.9	0.0313
1253.7	245	310	0.0721	0.0018	90.9060	9.1	0.0335
1381.4	271	342	0.0655	0.0013	91.4802	8.5	0.0243
1521.5	298	376	0.0594	0.0015	92.1547	7.8	0.0286
1675.6	328	414	0.0540	0.0016	92.8597	7.1	0.0299
1846.9	362	457	0.0490	0.0011	93.3666	6.6	0.0215
2033.6	398	503	0.0445	0.0009	93.7609	6.2	0.0167
2240.0	439	554	0.0404	0.0015	94.4261	5.6	0.0282
2466.8	483	610	0.0367	0.0010	94.8786	5.1	0.0192
2717.8	532	672	0.0333	0.0010	95.3191	4.7	0.0187
2993.2	586	740	0.0302	0.0011	95.7984	4.2	0.0203
3296.4	645	815	0.0274	0.0010	96.2441	3.8	0.0189
3632.0	711	898	0.0249	0.0004	96.4158	3.6	0.0073
3999.1	783	989	0.0226	0.0012	96.9399	3.1	0.0222
4406.0	863	1089	0.0205	0.0010	97.3853	2.6	0.0189
4844.3	949	1198	0.0187	0.0009	97.7698	2.2	0.0163
5338.0	1045	1320	0.0169	0.0004	97.9647	2.0	0.0083
5879.8	1151	1454	0.0154	0.0010	98.4024	1.6	0.0186
6475.8	1268	1601	0.0140	0.0007	98.7073	1.3	0.0129
7132.9	1397	1764	0.0127	0.0006	98.9901	1.0	0.0120
7857.3	1539	1943	0.0115	0.0007	99.3076	0.7	0.0135
8658.8	1695	2141	0.0104	0.0007	99.5992	0.4	0.0124
9538.0	1868	2358	0.0095	0.0002	99.6752	0.3	0.0032
10510.7	2058	2599	0.0086	0.0007	100.0000	0.0	0.0138
11576.7	2267	2862	0.0078	0.0000	100.0000	0.0	0.0000
12757.0	2498	3154	0.0071	0.0000	100.0000	0.0	0.0000
14048.4	2751	3473	0.0064	0.0000	100.0000	0.0	0.0000
15479.0	3031	3827	0.0058	0.0000	100.0000	0.0	0.0000
17052.5	3339	4216	0.0053	0.0000	100.0000	0.0	0.0000
18784.8	3678	4644	0.0048	0.0000	100.0000	0.0	0.0000
20699.3	4053	5118	0.0044	0.0000	100.0000	0.0	0.0000
22811.1	4467	5640	0.0040	0.0000	100.0000	0.0	0.0000
25130.1	4921	6213	0.0036	0.0000	100.0000	0.0	0.0000
27682.3	5420	6844	0.0033	0.0000	100.0000	0.0	0.0000
30495.1	5971	7539	0.0030	0.0000	100.0000	0.0	0.0000
33589.2	6577	8304	0.0027	0.0000	100.0000	0.0	0.0000
36995.3	7244	9147	0.0024	0.0000	100.0000	0.0	0.0000
40737.6	7977	10072	0.0022	0.0000	100.0000	0.0	0.0000
44856.3	8783	11090	0.0020	0.0000	100.0000	0.0	0.0000
49353.8	11740	14825	0.0015	0.0000	100.0000	0.0	0.0000

APPENDIX 2 - MICP - SAMPLE 187

TABLE OF CONTENTS i

LIST OF TABLES

TABLE 2-1. MERCURY INJECTION DATA SUMMARY FOR SAMPLE ID 187 1
TABLE 2-2. MERCURY INJECTION DATA FOR SAMPLE ID 187 2

TABLE 2-1. MERCURY INJECTION DATA SUMMARY FOR SAMPLE ID 187

Sample Info and Properties	
Depth:	12178.1 ft
Well:	RSU#1
Formation:	Amsden 1
Porosity:	NA % @ 800 psi
Air Permeability:	NA md @ 800 psi
Klink. Permeability:	NA md @ 800 psi
Grain Density:	2.91 g/cm3

Mercury Injection Data	
IFT (σ):	485 dynes/cm
Contact angle (θ):	130 degrees
σcosθ Hg/air:	367.7 dynes/cm
σcosθ Air/brine:	72 dynes/cm
Total Pore Area:	0.000 m^2/g
Hg Porosity:	0.00 %
Corr. Hg Porosity:	0.00 %

Height Computation	
Water - Oil Reservoir System	
Res. Oil Grad:	0.360 psi/ft
Res. Wtr. Gradient:	0.470 psi/ft
σcosθ reservoir:	10.0 dynes/cm
Conversion Factor "C":	0.247 ft/psi

Computations	
Displacement Pressure (Pd)	
Mercury/Air:	NA psi
Air/Brine Equiv:	NA psi
Equiv. Height:	NA ft
Pr Throat Rad:	NA microns
Pore Radius Distributions	
Mean (arithmetic):	NA microns
Mean (geometric):	NA microns
Mean (harmonic):	NA microns
Micropores - Pore throat radius < .1 micron:	NA % PV
Intermediate - Pore throat radius .1<r<3 micron:	NA % PV
Macropores - Pore throat radius > 3 micron:	NA % PV
Swanson Parameter[1]	
(Sb/Pc)max:	NA
Kbrine Swanson:	0.000 md
Kair Swanson:	0.000 md

TABLE 2-2. MERCURY INJECTION DATA FOR SAMPLE ID 187

Hg/air Pres. psi	Equivalent Air/brine Pres. psi	Height above Free Wtr. ft.	Pore radius Aperture microns	Hg Volume Injected cm3	Hg Sat. Pore Volume %	1-Hg Sat. Pore Volume %	Hg Porosity Injected %
0.5	0.11	0.13	167.5121	0.0000	0.0000	100.0	0.0000
0.6	0.11	0.14	154.6600	0.0016	1.4498	98.6	0.0265
0.6	0.13	0.16	140.4573	0.0025	3.7129	96.3	0.0413
0.7	0.14	0.17	128.9800	0.0028	6.2943	93.7	0.0472
0.8	0.15	0.19	117.2291	0.0032	9.1939	90.8	0.0530
0.8	0.17	0.21	106.7533	0.0034	12.3411	87.7	0.0575
0.9	0.18	0.23	97.2406	0.0028	14.8517	85.1	0.0459
1.0	0.20	0.25	88.6083	0.0030	17.5746	82.4	0.0497
1.1	0.22	0.28	80.6148	0.0025	19.8730	80.1	0.0420
1.2	0.24	0.30	73.6275	0.0026	22.2423	77.8	0.0433
1.4	0.26	0.33	66.9317	0.0024	24.4347	75.6	0.0401
1.5	0.29	0.37	60.9896	0.0023	26.5563	73.4	0.0388
1.6	0.32	0.40	55.5069	0.0023	28.6780	71.3	0.0388
1.8	0.35	0.44	50.5139	0.0049	33.1335	66.9	0.0814
2.0	0.4	0.49	45.9341	0.0051	37.7659	62.2	0.0846
2.2	0.4	0.53	41.8209	0.0050	42.2921	57.7	0.0827
2.4	0.5	0.59	38.0697	0.0058	47.6317	52.4	0.0976
2.6	0.5	0.65	34.6459	0.0060	53.1480	46.9	0.1008
2.9	0.6	0.71	31.5135	0.0086	60.9982	39.0	0.1434
3.2	0.6	0.78	28.6829	0.0049	65.4538	34.5	0.0814
3.5	0.7	0.86	26.0829	0.0049	69.9093	30.1	0.0814
3.8	0.7	0.94	23.7237	0.0034	73.0564	26.9	0.0575
4.2	0.8	1.04	21.5403	0.0029	75.7085	24.3	0.0485
4.6	0.9	1.14	19.5709	0.0023	77.7948	22.2	0.0381
5.1	1.0	1.26	17.7641	0.0020	79.6336	20.4	0.0336
5.6	1.1	1.39	16.1307	0.0017	81.1542	18.8	0.0278
6.2	1.2	1.53	14.6546	0.0012	82.2504	17.7	0.0200
6.8	1.3	1.68	13.3054	0.0010	83.1698	16.8	0.0168
7.5	1.5	1.85	12.0840	0.0007	83.8416	16.2	0.0123
8.2	1.6	2.04	10.9731	0.0006	84.4074	15.6	0.0103
9.1	1.8	2.24	9.9602	0.0006	84.9732	15.0	0.0103
10.0	2.0	2.47	9.0466	0.0006	85.5390	14.5	0.0103
11.0	2.2	2.72	8.2132	0.0007	86.1401	13.9	0.0110
12.1	2.4	3.00	7.4598	0.0006	86.7059	13.3	0.0103
13.3	2.6	3.3	6.7744	0.0005	87.1656	12.8	0.0084
14.7	2.9	3.6	6.1519	0.0006	87.6960	12.3	0.0097
16.2	3.2	4.0	5.5866	0.0006	88.2264	11.8	0.0097
17.8	3.5	4.4	5.0731	0.0006	88.7568	11.2	0.0097
19.6	3.8	4.9	4.6041	0.0006	89.2873	10.7	0.0097
21.7	4.2	5.4	4.1721	0.0007	89.8884	10.1	0.0110
23.9	4.7	5.9	3.7890	0.0005	90.3481	9.7	0.0084
26.3	5.1	6.5	3.4417	0.0006	90.8785	9.1	0.0097
28.9	5.7	7.2	3.1240	0.0003	91.1339	8.9	0.0047
31.9	6.2	7.9	2.8368	0.0003	91.3900	8.6	0.0047
35.1	6.9	8.7	2.5759	0.0003	91.6448	8.4	0.0047
38.7	7.6	9.6	2.3359	0.0003	91.9008	8.1	0.0047
42.9	8.4	10.6	2.1091	0.0003	92.1558	7.8	0.0047
48.1	9.4	11.9	1.8796	0.0003	92.4118	7.6	0.0047
53.0	10.4	13.1	1.7061	0.0003	92.6668	7.3	0.0047
59.6	11.7	14.7	1.5173	0.0004	93.0229	7.0	0.0065
65.4	12.8	16.2	1.3825	0.0007	93.6453	6.4	0.0114
72.6	14.2	18.0	1.2455	0.0002	93.8001	6.2	0.0028
80.3	15.7	19.8	1.1266	0.0003	94.0948	5.9	0.0054
88.3	17.3	21.8	1.0241	0.0002	94.2871	5.7	0.0035
98.5	19.3	24.4	0.9181	0.0002	94.5134	5.5	0.0041
108.2	21.2	26.7	0.8358	0.0003	94.7881	5.2	0.0050
120.1	23.5	29.7	0.7527	0.0002	94.9702	5.0	0.0033
132.6	26.0	32.8	0.6821	0.0003	95.2566	4.7	0.0052
146.6	28.7	36.2	0.6170	0.0001	95.3129	4.7	0.0010

TABLE 2-2. MERCURY INJECTION DATA FOR SAMPLE ID 187 - CONTINUED

Hg/air Pres. psi	Equivalent Air/brine Pres. psi	Height above Free Wtr. ft.	Pore radius Aperture microns	Hg Volume Injected cm3	Hg Sat. Pore Volume %	1-Hg Sat. Pore Volume %	Hg Porosity Injected %
161.5	31.6	40	0.5598	0.0002	95.5052	4.5	0.0035
178.8	35.0	44	0.5058	0.0002	95.7157	4.3	0.0038
197.0	38.6	49	0.4591	0.0003	95.9757	4.0	0.0047
217.2	42.5	54	0.4163	0.0002	96.1478	3.9	0.0031
239.4	46.9	59	0.3778	0.0002	96.2994	3.7	0.0028
263.7	52	65	0.3430	0.0001	96.3970	3.6	0.0018
291.5	57	72	0.3102	0.0002	96.5918	3.4	0.0036
321.5	63	79	0.2813	0.0001	96.6700	3.3	0.0014
354.2	69	88	0.2553	0.0001	96.7489	3.3	0.0014
390.6	76	97	0.2315	0.0000	96.7489	3.3	0.0000
431.1	84	107	0.2098	0.0001	96.8184	3.2	0.0013
475.2	93	117	0.1903	0.0001	96.9342	3.1	0.0021
523.1	102	129	0.1729	0.0000	96.9667	3.0	0.0006
576.6	113	143	0.1568	0.0003	97.2165	2.8	0.0046
635.5	124	157	0.1423	0.0002	97.4002	2.6	0.0034
700.4	137	173	0.1291	0.0001	97.5096	2.5	0.0020
772.3	151	191	0.1171	0.0002	97.6991	2.3	0.0035
851.4	167	210	0.1062	0.0001	97.7938	2.2	0.0017
937.4	184	232	0.0965	0.0000	97.7938	2.2	0.0000
1034.1	202	256	0.0875	0.0001	97.8758	2.1	0.0015
1138.4	223	281	0.0794	0.0001	97.9981	2.0	0.0022
1253.8	246	310	0.0721	0.0001	98.0757	1.9	0.0014
1381.5	271	342	0.0655	0.0001	98.1796	1.8	0.0019
1521.6	298	376	0.0594	0.0001	98.2853	1.7	0.0019
1675.6	328	414	0.0540	0.0001	98.3565	1.6	0.0013
1847.0	362	457	0.0490	0.0000	98.3781	1.6	0.0004
2033.7	398	503	0.0445	0.0001	98.4420	1.6	0.0012
2240.1	439	554	0.0404	0.0000	98.4822	1.5	0.0007
2466.9	483	610	0.0367	0.0001	98.5777	1.4	0.0017
2717.9	532	672	0.0333	0.0000	98.6149	1.4	0.0007
2993.3	586	740	0.0302	0.0000	98.6527	1.3	0.0007
3296.5	645	815	0.0274	0.0001	98.7464	1.3	0.0017
3632.1	711	898	0.0249	0.0000	98.7758	1.2	0.0005
3999.2	783	989	0.0226	0.0001	98.8427	1.2	0.0012
4406.1	863	1089	0.0205	0.0000	98.8427	1.2	0.0000
4844.8	949	1198	0.0187	0.0001	98.9165	1.1	0.0013
5338.2	1045	1320	0.0169	0.0001	98.9761	1.0	0.0011
5879.9	1151	1454	0.0154	0.0001	99.0788	0.9	0.0019
6475.9	1268	1601	0.0140	0.0000	99.0788	0.9	0.0000
7133.0	1397	1764	0.0127	0.0000	99.1193	0.9	0.0007
7857.4	1539	1943	0.0115	0.0000	99.1549	0.8	0.0007
8658.9	1696	2141	0.0104	0.0001	99.2276	0.8	0.0013
9538.1	1868	2358	0.0095	0.0001	99.2903	0.7	0.0011
10510.9	2058	2599	0.0086	0.0002	99.4408	0.6	0.0027
11576.9	2267	2862	0.0078	0.0000	99.4408	0.6	0.0000
12757.1	2498	3154	0.0071	0.0002	99.6101	0.4	0.0031
14048.5	2751	3473	0.0064	0.0000	99.6101	0.4	0.0000
15479.1	3031	3827	0.0058	0.0001	99.7020	0.3	0.0017
17052.6	3339	4216	0.0053	0.0001	99.7840	0.2	0.0015
18784.9	3678	4644	0.0048	0.0000	99.7840	0.2	0.0000
20699.4	4053	5118	0.0044	0.0002	100.0000	0.0	0.0039
22811.2	4467	5640	0.0040	0.0000	100.0000	0.0	0.0000
25130.2	4921	6213	0.0036	0.0000	100.0000	0.0	0.0000
27682.4	5421	6844	0.0033	0.0000	100.0000	0.0	0.0000
30495.2	5971	7540	0.0030	0.0000	100.0000	0.0	0.0000
33589.3	6577	8304	0.0027	0.0000	100.0000	0.0	0.0000
36995.4	7244	9147	0.0024	0.0000	100.0000	0.0	0.0000
40737.7	7977	10072	0.0022	0.0000	100.0000	0.0	0.0000
44856.4	8783	11090	0.0020	0.0000	100.0000	0.0	0.0000
59955.9	11740	14825	0.0015	0.0000	100.0000	0.0	0.0000

APPENDIX 3 - MICP - WELL RSU#1 SAMPLE 200

TABLE OF CONTENTS i

LIST OF TABLES

TABLE 3-1. MERCURY INJECTION DATA SUMMARY FOR SAMPLE 200 1
TABLE 3-2. MERCURY INJECTION DATA FOR SAMPLE 200 2

TABLE 3-1. MERCURY INJECTION DATA SUMMARY FOR SAMPLE 200

Sample Info and Properties	
Depth:	12227.30 ft
Well:	RSU#1
Formation:	Amsden 2
Porosity:	NA %
Air Permeability:	NA md
Klink. Permeability:	NA md
Grain Density:	2.85 g/cm3

Mercury Injection Data	
IFT (σ):	485 dynes/cm
Contact angle (θ):	130 degrees
σcosθ Hg/air:	367.7 dynes/cm
σcosθ Air/brine:	72 dynes/cm
Total Pore Area:	0.000 m^2/g
Hg Porosity:	0.00 %
Corr. Hg Porosity:	0.00 %

Height Computation	
Water - Oil Reservoir System	
Res. Oil Grad:	0.360 psi/ft
Res. Wtr. Gradient:	0.470 psi/ft
σcosθ reservoir:	10.0 dynes/cm
Conversion Factor "C":	0.247 ft/psi

Computations	
Displacement Pressure (Pd)	
Mercury/Air:	NA psi
Air/Brine Equiv:	NA psi
Equiv. Height:	NA ft
Pr Throat Rad:	NA microns
Pore Radius Distributions	
Mean (arithmetic):	NA microns
Mean (geometric):	NA microns
Mean (harmonic):	NA microns
Micropores - Pore throat radius < .1 micron:	NA % PV
Intermediate - Pore throat radius .1<r<3 micron:	NA % PV
Macropores - Pore throat radius > 3 micron:	NA % PV
Swanson Parameter[1]	
(Sb/Pc)max:	NA
Klorine Swanson:	0.000 md
Kair Swanson:	0.000 md

TABLE 3-2. MERCURY INJECTION DATA FOR SAMPLE 200

Hg/air Pres. psi	Equivalent Air/brine Pres. psi	Height above Free Wtr. ft.	Pore radius Aperture microns	Hg Volume Injected cm3	Hg Sat. Pore Volume %	1-Hg Sat. Pore Volume %	Hg Porosity Injected %
0.5	0.11	0.13	167.8718	0.0000	0.0000	100.0	0.0000
0.6	0.11	0.14	155.4802	0.0015	1.9114	98.1	0.0333
0.6	0.13	0.16	141.4372	0.0019	4.2544	95.7	0.0408
0.7	0.14	0.17	128.8083	0.0020	6.7824	93.2	0.0440
0.8	0.15	0.19	117.2969	0.0016	8.8172	91.2	0.0354
0.8	0.17	0.21	106.8835	0.0015	10.7286	89.3	0.0333
0.9	0.18	0.23	97.2601	0.0016	12.7016	87.3	0.0343
1.0	0.20	0.25	88.7937	0.0016	14.6747	85.3	0.0343
1.1	0.22	0.28	80.8227	0.0032	18.6825	81.3	0.0697
1.2	0.24	0.30	73.7219	0.0046	24.3551	75.6	0.0987
1.4	0.26	0.33	66.9724	0.0074	33.4805	66.5	0.1588
1.5	0.29	0.37	60.9697	0.0074	42.6676	57.3	0.1599
1.6	0.32	0.40	55.5140	0.0032	46.6138	53.4	0.0687
1.8	0.35	0.44	50.5551	0.0028	50.0667	49.9	0.0601
2.0	0.4	0.49	46.0033	0.0014	51.7931	48.2	0.0300
2.2	0.4	0.53	41.8519	0.0012	53.3346	46.7	0.0268
2.4	0.5	0.59	38.0902	0.0010	54.6294	45.4	0.0225
2.6	0.5	0.65	34.6524	0.0013	56.2942	43.7	0.0290
2.9	0.6	0.71	31.5331	0.0015	58.2056	41.8	0.0333
3.2	0.6	0.78	28.6870	0.0019	60.6102	39.4	0.0418
3.5	0.7	0.86	26.0920	0.0024	63.5699	36.4	0.0515
3.8	0.7	0.94	23.7360	0.0021	66.2212	33.8	0.0461
4.2	0.8	1.04	21.5442	0.0014	67.9476	32.1	0.0300
4.6	0.9	1.14	19.5741	0.0012	69.4891	30.5	0.0268
5.1	1.0	1.26	17.7752	0.0010	70.7222	29.3	0.0215
5.6	1.1	1.39	16.1383	0.0010	71.9554	28.0	0.0215
6.2	1.2	1.53	14.6549	0.0018	74.2191	25.8	0.0394
6.8	1.3	1.68	13.3028	0.0030	77.9363	22.1	0.0647
7.5	1.5	1.85	12.0845	0.0017	80.0327	20.0	0.0365
8.2	1.6	2.04	10.9695	0.0015	81.8824	18.1	0.0322
9.1	1.8	2.24	9.9661	0.0010	83.1156	16.9	0.0215
10.0	2.0	2.47	9.0481	0.0012	84.5954	15.4	0.0257
11.0	2.2	2.72	8.2172	0.0011	85.9519	14.0	0.0236
12.1	2.4	3.00	7.4606	0.0008	87.0001	13.0	0.0182
13.3	2.6	3.3	6.7742	0.0009	88.1099	11.9	0.0193
14.7	2.9	3.6	6.1520	0.0007	88.9731	11.0	0.0150
16.2	3.2	4.0	5.5861	0.0005	89.6514	10.3	0.0118
17.8	3.5	4.4	5.0726	0.0013	91.3162	8.7	0.0290
19.6	3.8	4.9	4.6053	0.0006	92.1177	7.9	0.0139
21.7	4.2	5.4	4.1728	0.0006	92.8576	7.1	0.0129
23.9	4.7	5.9	3.7883	0.0006	93.5975	6.4	0.0129
26.3	5.1	6.5	3.4407	0.0005	94.2141	5.8	0.0107
28.9	5.7	7.2	3.1246	0.0005	94.8307	5.2	0.0107
31.9	6.2	7.9	2.8371	0.0005	95.4473	4.6	0.0107
35.1	6.9	8.7	2.5759	0.0005	96.0639	3.9	0.0107
37.4	7.3	9.2	2.4201	0.0000	96.0639	3.9	0.0000
38.5	7.5	9.5	2.3512	0.0000	96.0639	3.9	0.0000
42.8	8.4	10.6	2.1153	0.0000	96.0639	3.9	0.0000
48.0	9.4	11.9	1.8855	0.0000	96.0639	3.9	0.0000
53.4	10.5	13.2	1.6943	0.0000	96.0660	3.9	0.0000
58.8	11.5	14.5	1.5387	0.0001	96.1594	3.8	0.0016
65.5	12.8	16.2	1.3811	0.0001	96.2513	3.7	0.0016
72.4	14.2	17.9	1.2490	0.0001	96.3217	3.7	0.0012
80.5	15.8	19.9	1.1230	0.0002	96.5463	3.5	0.0039
89.0	17.4	22.0	1.0158	0.0002	96.8005	3.2	0.0044
98.1	19.2	24.2	0.9222	0.0002	97.0114	3.0	0.0037
108.4	21.2	26.8	0.8344	0.0001	97.1723	2.8	0.0028
120.9	23.7	29.9	0.7479	0.0001	97.2840	2.7	0.0019
132.3	25.9	32.7	0.6836	0.0003	97.6119	2.4	0.0057

TABLE 3-2. MERCURY INJECTION DATA FOR SAMPLE 200 - CONTINUED

Hg/air Pres. psi	Equivalent Air/brine Pres. psi	Height above Free Wtr. ft.	Pore radius Aperture microns	Hg Volume Injected cm3	Hg Sat. Pore Volume %	1-Hg Sat. Pore Volume %	Hg Porosity Injected %
146.3	28.6	36	0.6181	0.0000	97.6119	2.4	0.0000
161.7	31.7	40	0.5592	0.0000	97.6335	2.4	0.0004
179.1	35.1	44	0.5049	0.0001	97.7966	2.2	0.0028
197.6	38.7	49	0.4577	0.0001	97.8639	2.1	0.0012
218.0	42.7	54	0.4149	0.0002	98.1128	1.9	0.0043
240.1	47	59	0.3766	0.0001	98.2325	1.8	0.0021
264.2	52	65	0.3423	0.0001	98.3304	1.7	0.0017
291.2	57	72	0.3105	0.0000	98.3892	1.6	0.0010
321.4	63	79	0.2813	0.0000	98.4180	1.6	0.0005
354.2	69	88	0.2553	0.0002	98.6808	1.3	0.0046
390.6	76	97	0.2315	0.0000	98.6808	1.3	0.0000
430.6	84	106	0.2100	0.0000	98.6808	1.3	0.0000
474.6	93	117	0.1906	0.0001	98.7752	1.2	0.0016
523.2	102	129	0.1728	0.0001	98.9241	1.1	0.0026
576.7	113	143	0.1568	0.0000	98.9241	1.1	0.0000
636.3	125	157	0.1421	0.0001	99.0293	1.0	0.0018
700.5	137	173	0.1291	0.0000	99.0879	0.9	0.0010
772.5	151	191	0.1171	0.0001	99.2718	0.7	0.0032
850.3	167	210	0.1064	0.0001	99.4243	0.6	0.0027
938.1	184	232	0.0964	0.0002	99.6118	0.4	0.0033
1033.4	202	255	0.0875	0.0000	99.6118	0.4	0.0000
1138.5	223	281	0.0794	0.0000	99.6164	0.4	0.0001
1254.4	246	310	0.0721	0.0000	99.6296	0.4	0.0002
1381.4	270	342	0.0655	0.0000	99.6794	0.3	0.0009
1521.5	298	376	0.0594	0.0000	99.6857	0.3	0.0001
1675.7	328	414	0.0540	0.0002	99.9709	0.0	0.0050
1846.4	362	456	0.0490	0.0000	100.0000	0.0	0.0005
2033.8	398	503	0.0445	0.0000	100.0000	0.0	0.0000
2240.3	439	554	0.0404	0.0000	100.0000	0.0	0.0000
2467.8	483	610	0.0366	0.0000	100.0000	0.0	0.0000
2718.3	532	672	0.0333	0.0000	100.0000	0.0	0.0000
2993.6	586	740	0.0302	0.0000	100.0000	0.0	0.0000
3295.2	645	815	0.0274	0.0000	100.0000	0.0	0.0000
3631.4	711	898	0.0249	0.0000	100.0000	0.0	0.0000
4000.4	783	989	0.0226	0.0000	100.0000	0.0	0.0000
4406.0	863	1089	0.0205	0.0000	100.0000	0.0	0.0000
4845.6	949	1198	0.0187	0.0000	100.0000	0.0	0.0000
5337.8	1045	1320	0.0169	0.0000	100.0000	0.0	0.0000
5881.0	1152	1454	0.0154	0.0000	100.0000	0.0	0.0000
6472.2	1267	1600	0.0140	0.0000	100.0000	0.0	0.0000
7133.4	1397	1764	0.0127	0.0000	100.0000	0.0	0.0000
7861.9	1539	1944	0.0115	0.0000	100.0000	0.0	0.0000
8660.8	1696	2141	0.0104	0.0000	100.0000	0.0	0.0000
9540.8	1868	2359	0.0095	0.0000	100.0000	0.0	0.0000
10510.5	2058	2599	0.0086	0.0000	100.0000	0.0	0.0000
11579.0	2267	2863	0.0078	0.0000	100.0000	0.0	0.0000
12753.1	2497	3153	0.0071	0.0000	100.0000	0.0	0.0000
14045.2	2750	3472	0.0064	0.0000	100.0000	0.0	0.0000
15479.4	3031	3827	0.0058	0.0000	100.0000	0.0	0.0000
17046.9	3338	4215	0.0053	0.0000	100.0000	0.0	0.0000
18785.4	3678	4644	0.0048	0.0000	100.0000	0.0	0.0000
20701.1	4053	5118	0.0044	0.0000	100.0000	0.0	0.0000
22811.3	4467	5640	0.0040	0.0000	100.0000	0.0	0.0000
25131.3	4921	6213	0.0036	0.0000	100.0000	0.0	0.0000
27682.4	5421	6844	0.0033	0.0000	100.0000	0.0	0.0000
30493.2	5971	7539	0.0030	0.0000	100.0000	0.0	0.0000
33589.3	6577	8304	0.0027	0.0000	100.0000	0.0	0.0000
36994.8	7244	9146	0.0024	0.0000	100.0000	0.0	0.0000
40736.2	7977	10071	0.0022	0.0000	100.0000	0.0	0.0000
59954.7	11740	14825	0.0015	0.0000	100.0000	0.0	0.0000

APPENDIX 4 - MICP - WELL RSU#1 SAMPLE 206

TABLE OF CONTENTS i

LIST OF TABLES

TABLE 4-1. MERCURY INJECTION DATA SUMMARY FOR SAMPLE 206 1
TABLE 4-2. MERCURY INJECTION DATA FOR SAMPLE 206 2

TABLE 4-1. MERCURY INJECTION DATA SUMMARY FOR SAMPLE 206

Sample Info and Properties	
Depth:	NA ft
Well:	RSU#1
Formation:	NA
Porosity:	NA %
Air Permeability:	NA md
Klink. Permeability:	NA md
Grain Density:	2.74 g/cm3

Mercury Injection Data	
IFT (σ):	485 dynes/cm
Contact angle (θ):	130 degrees
σcosθ Hg/air:	367.7 dynes/cm
σcosθ Air/brine:	72 dynes/cm
Total Pore Area:	0.000 m^2/g
Hg Porosity:	0.00 %
Corr. Hg Porosity:	0.00 %

Height Computation	
Water - Oil Reservoir System	
Res. Oil Grad:	0.360 psi/ft
Res. Wtr. Gradient:	0.470 psi/ft
σcosθ reservoir:	10.0 dynes/cm
Conversion Factor "C":	0.247 ft/psi

Computations	
Displacement Pressure (Pd)	
Mercury/Air:	NA psi
Air/Brine Equiv:	NA psi
Equiv. Height:	NA ft
Pr Throat Rad:	NA microns
Pore Radius Distributions	
Mean (arithmetic):	NA microns
Mean (geometric):	NA microns
Mean (harmonic):	NA microns
Micropores - Pore throat radius < .1 micron:	NA % PV
Intermediate - Pore throat radius .1<r<3 micron:	NA % PV
Macropores - Pore throat radius > 3 micron:	NA % PV
Swanson Parameter[1]	
(Sb/Pc)max:	NA
Kbrine Swanson:	0.000 md
Kair Swanson:	0.000 md

TABLE 4-2. MERCURY INJECTION DATA FOR SAMPLE 206

Hg/air Pres. psi	Equivalent Air/brine Pres. psi	Height above Free Wtr. ft.	Pore radius Aperture microns	Hg Volume Injected cm3	Hg Sat. Pore Volume %	1-Hg Sat. Pore Volume %	Hg Porosity Injected %
0.5	0.11	0.13	167.8718	0.0000	0.0000	100.0	0.0000
0.6	0.11	0.14	155.4802	0.0014	6.0914	93.9	0.0347
0.6	0.13	0.16	141.4372	0.0036	21.5160	78.5	0.0879
0.7	0.14	0.17	128.8083	0.0023	31.2612	68.7	0.0555
0.8	0.15	0.19	117.2969	0.0020	39.5939	60.4	0.0475
0.8	0.17	0.21	106.8835	0.0016	46.1929	53.8	0.0376
0.9	0.18	0.23	97.2601	0.0014	52.2843	47.7	0.0347
1.0	0.20	0.25	88.7937	0.0012	57.3604	42.6	0.0289
1.1	0.22	0.28	80.8227	0.0011	61.9289	38.1	0.0260
1.2	0.24	0.30	73.7219	0.0008	65.4822	34.5	0.0202
1.4	0.26	0.33	66.9724	0.0008	69.0355	31.0	0.0202
1.5	0.29	0.37	60.9697	0.0006	71.5736	28.4	0.0145
1.6	0.32	0.40	55.5140	0.0005	73.6041	26.4	0.0116
1.8	0.35	0.44	50.5551	0.0005	75.5410	24.5	0.0110
2.0	0.4	0.49	46.0033	0.0003	76.6498	23.4	0.0063
2.2	0.4	0.53	41.8519	0.0002	77.6650	22.3	0.0058
2.4	0.5	0.59	38.0902	0.0003	79.1255	20.9	0.0083
2.6	0.5	0.65	34.6524	0.0003	80.2030	19.8	0.0061
2.9	0.6	0.71	31.5331	0.0002	80.9333	19.1	0.0042
3.2	0.6	0.78	28.6870	0.0001	81.4721	18.5	0.0031
3.5	0.7	0.86	26.0920	0.0001	81.9797	18.0	0.0029
3.8	0.7	0.94	23.7360	0.0001	82.4873	17.5	0.0029
4.2	0.8	1.04	21.5442	0.0002	83.2487	16.8	0.0043
4.6	0.9	1.14	19.5741	0.0002	84.2640	15.7	0.0058
5.1	1.0	1.26	17.7752	0.0001	84.5178	15.5	0.0014
5.6	1.1	1.39	16.1383	0.0002	85.2792	14.7	0.0043
6.2	1.2	1.53	14.6549	0.0001	85.5330	14.5	0.0014
6.8	1.3	1.68	13.3028	0.0002	86.2944	13.7	0.0043
7.5	1.5	1.85	12.0845	0.0001	86.8020	13.2	0.0029
8.2	1.6	2.04	10.9695	0.0002	87.5635	12.4	0.0043
9.1	1.8	2.24	9.9661	0.0001	88.0711	11.9	0.0029
10.0	2.0	2.47	9.0481	0.0001	88.5787	11.4	0.0029
11.0	2.2	2.72	8.2172	0.0001	89.0863	10.9	0.0029
12.1	2.4	3.00	7.4606	0.0002	89.8477	10.2	0.0043
13.3	2.6	3.3	6.7742	0.0002	90.6091	9.4	0.0043
14.7	2.9	3.6	6.1520	0.0001	91.1168	8.9	0.0029
16.2	3.2	4.0	5.5861	0.0002	91.8782	8.1	0.0043
17.8	3.5	4.4	5.0726	0.0001	92.3858	7.6	0.0029
19.6	3.8	4.9	4.6053	0.0002	93.1784	6.8	0.0045
21.7	4.2	5.4	4.1728	0.0002	94.1624	5.8	0.0056
23.9	4.7	5.9	3.7883	0.0003	95.4315	4.6	0.0072
26.3	5.1	6.5	3.4407	0.0003	96.8920	3.1	0.0083
28.9	5.7	7.2	3.1246	0.0002	97.7157	2.3	0.0047
31.9	6.2	7.9	2.8371	0.0002	98.7310	1.3	0.0058
35.1	6.9	8.7	2.5759	0.0003	100.0000	0.0	0.0072
37.5	7.3	9.3	2.4100	0.0000	100.0000	0.0	0.0000
38.6	7.6	9.5	2.3417	0.0000	100.0000	0.0	0.0000
42.9	8.4	10.6	2.1076	0.0000	100.0000	0.0	0.0000
48.1	9.4	11.9	1.8793	0.0000	100.0000	0.0	0.0000
53.5	10.5	13.2	1.6894	0.0000	100.0000	0.0	0.0000
58.9	11.5	14.6	1.5346	0.0000	100.0000	0.0	0.0000
65.6	12.9	16.2	1.3777	0.0000	100.0000	0.0	0.0000
72.6	14.2	17.9	1.2463	0.0000	100.0000	0.0	0.0000
80.7	15.8	19.9	1.1208	0.0000	100.0000	0.0	0.0000
89.2	17.5	22.0	1.0140	0.0000	100.0000	0.0	0.0000
98.2	19.2	24.3	0.9207	0.0000	100.0000	0.0	0.0000
108.5	21.3	26.8	0.8332	0.0000	100.0000	0.0	0.0000
121.1	23.7	29.9	0.7469	0.0000	100.0000	0.0	0.0000
132.5	25.9	32.7	0.6827	0.0000	100.0000	0.0	0.0000

TABLE 4-2. MERCURY INJECTION DATA FOR SAMPLE 206 - CONTINUED

Hg/air Pres. psi	Equivalent Air/brine Pres. psi	Height above Free Wtr. ft.	Pore radius Aperture microns	Hg Volume Injected cm3	Hg Sat. Pore Volume %	1-Hg Sat. Pore Volume %	Hg Porosity Injected %
146.5	28.7	36	0.6174	0.0000	100.0000	0.0	0.0000
161.9	31.7	40	0.5586	0.0000	100.0000	0.0	0.0000
179.3	35.1	44	0.5044	0.0000	100.0000	0.0	0.0000
197.8	38.7	49	0.4573	0.0000	100.0000	0.0	0.0000
218.1	42.7	54	0.4146	0.0000	100.0000	0.0	0.0000
240.3	47	59	0.3764	0.0000	100.0000	0.0	0.0000
264.3	52	65	0.3421	0.0000	100.0000	0.0	0.0000
291.4	57	72	0.3104	0.0000	100.0000	0.0	0.0000
321.6	63	80	0.2812	0.0000	100.0000	0.0	0.0000
354.3	69	88	0.2552	0.0000	100.0000	0.0	0.0000
390.8	77	97	0.2314	0.0000	100.0000	0.0	0.0000
430.8	84	107	0.2099	0.0000	100.0000	0.0	0.0000
474.7	93	117	0.1905	0.0000	100.0000	0.0	0.0000
523.4	102	129	0.1728	0.0000	100.0000	0.0	0.0000
576.9	113	143	0.1568	0.0000	100.0000	0.0	0.0000
636.5	125	157	0.1421	0.0000	100.0000	0.0	0.0000
700.7	137	173	0.1291	0.0000	100.0000	0.0	0.0000
772.7	151	191	0.1170	0.0000	100.0000	0.0	0.0000
850.5	167	210	0.1063	0.0000	100.0000	0.0	0.0000
938.2	184	232	0.0964	0.0000	100.0000	0.0	0.0000
1033.6	202	256	0.0875	0.0000	100.0000	0.0	0.0000
1138.6	223	282	0.0794	0.0000	100.0000	0.0	0.0000
1254.6	246	310	0.0721	0.0000	100.0000	0.0	0.0000
1381.6	271	342	0.0655	0.0000	100.0000	0.0	0.0000
1521.6	298	376	0.0594	0.0000	100.0000	0.0	0.0000
1675.9	328	414	0.0540	0.0000	100.0000	0.0	0.0000
1846.5	362	457	0.0490	0.0000	100.0000	0.0	0.0000
2033.9	398	503	0.0445	0.0000	100.0000	0.0	0.0000
2240.5	439	554	0.0404	0.0000	100.0000	0.0	0.0000
2467.9	483	610	0.0366	0.0000	100.0000	0.0	0.0000
2718.5	532	672	0.0333	0.0000	100.0000	0.0	0.0000
2993.7	586	740	0.0302	0.0000	100.0000	0.0	0.0000
3295.3	645	815	0.0274	0.0000	100.0000	0.0	0.0000
3631.6	711	898	0.0249	0.0000	100.0000	0.0	0.0000
4000.6	783	989	0.0226	0.0000	100.0000	0.0	0.0000
4406.2	863	1089	0.0205	0.0000	100.0000	0.0	0.0000
4845.8	949	1198	0.0187	0.0000	100.0000	0.0	0.0000
5338.0	1045	1320	0.0169	0.0000	100.0000	0.0	0.0000
5881.2	1152	1454	0.0154	0.0000	100.0000	0.0	0.0000
6472.4	1267	1600	0.0140	0.0000	100.0000	0.0	0.0000
7133.5	1397	1764	0.0127	0.0000	100.0000	0.0	0.0000
7862.1	1539	1944	0.0115	0.0000	100.0000	0.0	0.0000
8661.0	1696	2141	0.0104	0.0000	100.0000	0.0	0.0000
9541.0	1868	2359	0.0095	0.0000	100.0000	0.0	0.0000
10510.7	2058	2599	0.0086	0.0000	100.0000	0.0	0.0000
11579.2	2267	2863	0.0078	0.0000	100.0000	0.0	0.0000
12753.3	2497	3153	0.0071	0.0000	100.0000	0.0	0.0000
14045.4	2750	3473	0.0064	0.0000	100.0000	0.0	0.0000
15479.6	3031	3827	0.0058	0.0000	100.0000	0.0	0.0000
17047.1	3338	4215	0.0053	0.0000	100.0000	0.0	0.0000
18785.5	3678	4644	0.0048	0.0000	100.0000	0.0	0.0000
20701.2	4054	5118	0.0044	0.0000	100.0000	0.0	0.0000
22811.5	4467	5640	0.0040	0.0000	100.0000	0.0	0.0000
25131.5	4921	6213	0.0036	0.0000	100.0000	0.0	0.0000
27682.6	5421	6844	0.0033	0.0000	100.0000	0.0	0.0000
30493.4	5971	7539	0.0030	0.0000	100.0000	0.0	0.0000
33589.5	6577	8305	0.0027	0.0000	100.0000	0.0	0.0000
36995.0	7244	9147	0.0024	0.0000	100.0000	0.0	0.0000
40736.4	7977	10072	0.0022	0.0000	100.0000	0.0	0.0000
59954.9	11740	14825	0.0015	0.0000	100.0000	0.0	0.0000

APPENDIX 5 - MICP - WELL RSU#1 SAMPLE 214

TABLE OF CONTENTS i

LIST OF TABLES

TABLE 5-1. MERCURY INJECTION DATA SUMMARY FOR SAMPLE 214 1
TABLE 5-2. MERCURY INJECTION DATA FOR SAMPLE 214 2

TABLE 5-1. MERCURY INJECTION DATA SUMMARY FOR SAMPLE 214

Sample Info and Properties	
Depth:	12333.90 ft
Well:	RSU#1
Formation:	Madison 1
Porosity:	6.55 %
Air Permeability:	NA md
Klink. Permeability:	NA md
Grain Density:	2.83 g/cm3

Mercury Injection Data	
IFT (σ):	485 dynes/cm
Contact angle (θ):	130 degrees
σcosθ Hg/air:	367.7 dynes/cm
σcosθ Air/brine:	72 dynes/cm
Total Pore Area:	0.000 m^2/g
Hg Porosity:	0.00 %
Corr. Hg Porosity:	0.00 %

Height Computation	
Water - Oil Reservoir System	
Res. Oil Grad:	0.360 psi/ft
Res. Wtr. Gradient:	0.470 psi/ft
σcosθ reservoir:	10.0 dynes/cm
Conversion Factor "C":	0.247 ft/psi

Computations	
Displacement Pressure (Pd)	
Mercury/Air:	NA psi
Air/Brine Equiv:	NA psi
Equiv. Height:	NA ft
Pr Throat Rad:	NA microns
Pore Radius Distributions	
Mean (arithmetic):	NA microns
Mean (geometric):	NA microns
Mean (harmonic):	NA microns
Micropores - Pore throat radius < .1 micron:	NA % PV
Intermediate - Pore throat radius .1<r<3 micron:	NA % PV
Macropores - Pore throat radius > 3 micron:	NA % PV
Swanson Parameter[1]	
(Sb/Pc)max:	NA
Kbrine Swanson:	0.000 md
Kair Swanson:	0.000 md

TABLE 5-2. MERCURY INJECTION DATA FOR SAMPLE 214

Hg/air Pres. psi	Equivalent Air/brine Pres. psi	Height above Free Wtr. ft.	Pore radius Aperture microns	Hg Volume Injected cm3	Hg Sat. Pore Volume %	1-Hg Sat. Pore Volume %	Hg Porosity Injected %
0.5	0.11	0.13	168.0543	0.0000	0.0000	100.0	0.0000
0.6	0.11	0.14	155.4830	0.0012	2.0383	98.0	0.0189
0.6	0.13	0.16	141.3817	0.0024	6.1148	93.9	0.0379
0.7	0.14	0.17	128.8308	0.0034	11.9747	88.0	0.0544
0.8	0.15	0.19	117.1782	0.0040	18.8539	81.1	0.0639
0.8	0.17	0.21	106.9825	0.0043	26.1576	73.8	0.0678
0.9	0.18	0.23	97.4389	0.0054	35.4147	64.6	0.0860
1.0	0.20	0.25	88.7103	0.0068	47.0497	53.0	0.1081
1.1	0.22	0.28	80.8658	0.0052	55.9671	44.0	0.0828
1.2	0.24	0.30	73.7264	0.0046	63.7804	36.2	0.0726
1.4	0.26	0.33	66.9817	0.0023	67.7720	32.2	0.0371
1.5	0.29	0.37	61.0244	0.0016	70.5746	29.4	0.0260
1.6	0.32	0.40	55.5873	0.0014	73.0375	27.0	0.0229
1.8	0.35	0.44	50.5263	0.0010	74.7360	25.3	0.0158
2.0	0.4	0.49	46.0020	0.0006	75.8401	24.2	0.0103
2.2	0.4	0.53	41.8663	0.0006	76.9441	23.1	0.0103
2.4	0.5	0.59	38.0765	0.0006	77.9632	22.0	0.0095
2.6	0.5	0.65	34.6568	0.0003	78.4728	21.5	0.0047
2.9	0.6	0.71	31.5233	0.0003	78.9824	21.0	0.0047
3.2	0.6	0.78	28.6793	0.0001	79.2371	20.8	0.0024
3.5	0.7	0.86	26.0956	0.0003	79.7467	20.3	0.0047
3.8	0.7	0.94	23.7391	0.0002	80.0864	19.9	0.0032
4.2	0.8	1.04	21.5480	0.0001	80.2563	19.7	0.0016
4.6	0.9	1.14	19.5762	0.0000	80.2563	19.7	0.0000
5.1	1.0	1.26	17.7774	0.0000	80.3412	19.7	0.0008
5.6	1.1	1.39	16.1421	0.0002	80.7658	19.2	0.0039
6.2	1.2	1.53	14.6564	0.0000	80.8508	19.1	0.0008
6.8	1.3	1.68	13.3012	0.0000	80.8508	19.1	0.0000
7.5	1.5	1.85	12.0844	0.0000	80.8508	19.1	0.0000
8.2	1.6	2.04	10.9724	0.0000	80.8508	19.1	0.0000
9.1	1.8	2.24	9.9615	0.0000	80.8508	19.1	0.0000
10.0	2.0	2.47	9.0462	0.0000	80.8508	19.1	0.0000
11.0	2.2	2.72	8.2157	0.0001	81.0206	19.0	0.0016
12.1	2.4	3.00	7.4613	0.0000	81.0206	19.0	0.0000
13.3	2.6	3.3	6.7744	0.0000	81.0206	19.0	0.0000
14.7	2.9	3.6	6.1509	0.0000	81.0206	19.0	0.0000
16.2	3.2	4.0	5.5830	0.0000	81.0206	19.0	0.0000
17.8	3.5	4.4	5.0735	0.0000	81.0206	19.0	0.0000
19.6	3.8	4.9	4.6052	0.0000	81.0206	19.0	0.0000
21.7	4.2	5.4	4.1706	0.0000	81.0206	19.0	0.0000
23.9	4.7	5.9	3.7886	0.0000	81.0206	19.0	0.0000
26.3	5.1	6.5	3.4406	0.0000	81.0206	19.0	0.0000
29.0	5.7	7.2	3.1237	0.0000	81.0206	19.0	0.0000
31.9	6.2	7.9	2.8372	0.0062	91.5516	8.4	0.0978
35.1	6.9	8.7	2.5754	0.0003	92.0612	7.9	0.0047
37.1	7.3	9.2	2.4399	0.0000	92.1108	7.9	0.0005
38.6	7.6	9.6	2.3410	0.0001	92.3363	7.7	0.0021
43.5	8.5	10.8	2.0775	0.0000	92.4157	7.6	0.0007
47.6	9.3	11.8	1.9006	0.0000	92.4157	7.6	0.0000
52.9	10.4	13.1	1.7091	0.0001	92.5699	7.4	0.0014
59.1	11.6	14.6	1.5307	0.0000	92.6507	7.3	0.0008
64.8	12.7	16.0	1.3951	0.0000	92.7267	7.3	0.0007
72.4	14.2	17.9	1.2498	0.0000	92.7267	7.3	0.0000
79.5	15.6	19.7	1.1375	0.0000	92.7267	7.3	0.0000
89.7	17.6	22.2	1.0079	0.0000	92.7267	7.3	0.0000
97.3	19.1	24.1	0.9295	0.0000	92.7267	7.3	0.0000
109.0	21.3	26.9	0.8298	0.0000	92.8073	7.2	0.0007
120.7	23.6	29.8	0.7494	0.0001	92.9697	7.0	0.0015
132.9	26.0	32.9	0.6802	0.0000	92.9697	7.0	0.0000

TABLE 5-2. MERCURY INJECTION DATA FOR SAMPLE 214 - CONTINUED

Hg/air Pres. psi	Equivalent Air/brine Pres. psi	Height above Free Wtr. ft.	Pore radius Aperture microns	Hg Volume Injected cm3	Hg Sat. Pore Volume %	1-Hg Sat. Pore Volume %	Hg Porosity Injected %
146.7	28.7	36	0.6166	0.0000	92.9697	7.0	0.0000
162.1	31.7	40	0.5578	0.0000	92.9697	7.0	0.0000
178.3	34.9	44	0.5073	0.0000	92.9697	7.0	0.0000
197.0	38.6	49	0.4591	0.0000	92.9697	7.0	0.0000
217.6	42.6	54	0.4156	0.0000	92.9697	7.0	0.0000
239.8	47	59	0.3770	0.0000	92.9697	7.0	0.0000
264.5	52	65	0.3419	0.0000	92.9697	7.0	0.0000
291.5	57	72	0.3102	0.0000	92.9697	7.0	0.0000
321.3	63	79	0.2815	0.0000	92.9697	7.0	0.0000
355.0	70	88	0.2548	0.0000	92.9697	7.0	0.0000
390.4	76	97	0.2316	0.0000	92.9697	7.0	0.0000
430.2	84	106	0.2102	0.0000	92.9697	7.0	0.0000
474.9	93	117	0.1904	0.0000	92.9697	7.0	0.0000
524.0	103	130	0.1726	0.0000	92.9697	7.0	0.0000
576.7	113	143	0.1568	0.0000	92.9697	7.0	0.0000
635.3	124	157	0.1423	0.0000	92.9697	7.0	0.0000
700.7	137	173	0.1291	0.0002	93.2543	6.7	0.0026
772.9	151	191	0.1170	0.0001	93.4075	6.6	0.0014
851.0	167	210	0.1063	0.0000	93.4075	6.6	0.0000
937.5	184	232	0.0965	0.0000	93.4075	6.6	0.0000
1034.5	203	256	0.0874	0.0000	93.4075	6.6	0.0000
1138.2	223	281	0.0794	0.0000	93.4075	6.6	0.0000
1253.7	245	310	0.0721	0.0000	93.4075	6.6	0.0000
1381.1	270	341	0.0655	0.0000	93.4075	6.6	0.0000
1521.3	298	376	0.0594	0.0000	93.4075	6.6	0.0000
1675.7	328	414	0.0540	0.0000	93.4454	6.6	0.0004
1846.4	362	456	0.0490	0.0000	93.5304	6.5	0.0008
2033.8	398	503	0.0445	0.0001	93.6638	6.3	0.0012
2239.8	439	554	0.0404	0.0000	93.6638	6.3	0.0000
2467.4	483	610	0.0367	0.0000	93.6638	6.3	0.0000
2717.4	532	672	0.0333	0.0000	93.6638	6.3	0.0000
2992.4	586	740	0.0302	0.0000	93.6951	6.3	0.0003
3296.1	645	815	0.0274	0.0002	94.0356	6.0	0.0032
3630.1	711	897	0.0249	0.0000	94.1036	5.9	0.0006
4000.5	783	989	0.0226	0.0003	94.6554	5.3	0.0051
4404.2	862	1089	0.0205	0.0003	95.2424	4.8	0.0055
4845.7	949	1198	0.0187	0.0005	96.0689	3.9	0.0077
5337.7	1045	1320	0.0169	0.0007	97.2372	2.8	0.0109
5877.6	1151	1453	0.0154	0.0006	98.2068	1.8	0.0090
6473.9	1268	1601	0.0140	0.0002	98.5461	1.5	0.0032
7135.2	1397	1764	0.0127	0.0007	99.7507	0.2	0.0112
7859.0	1539	1943	0.0115	0.0000	99.7507	0.2	0.0000
8658.3	1695	2141	0.0104	0.0001	100.0000	0.0	0.0023
9540.8	1868	2359	0.0095	0.0000	100.0000	0.0	0.0000
10512.6	2058	2599	0.0086	0.0000	100.0000	0.0	0.0000
11580.2	2268	2863	0.0078	0.0000	100.0000	0.0	0.0000
12753.6	2497	3153	0.0071	0.0000	100.0000	0.0	0.0000
14050.4	2751	3474	0.0064	0.0000	100.0000	0.0	0.0000
15480.5	3031	3827	0.0058	0.0000	100.0000	0.0	0.0000
17052.6	3339	4216	0.0053	0.0000	100.0000	0.0	0.0000
18783.2	3678	4644	0.0048	0.0000	100.0000	0.0	0.0000
20698.3	4053	5117	0.0044	0.0000	100.0000	0.0	0.0000
22810.8	4467	5640	0.0040	0.0000	100.0000	0.0	0.0000
25131.1	4921	6213	0.0036	0.0000	100.0000	0.0	0.0000
27683.1	5421	6844	0.0033	0.0000	100.0000	0.0	0.0000
30492.4	5971	7539	0.0030	0.0000	100.0000	0.0	0.0000
33588.9	6577	8304	0.0027	0.0000	100.0000	0.0	0.0000
36998.0	7245	9147	0.0024	0.0000	100.0000	0.0	0.0000
40738.8	7977	10072	0.0022	0.0000	100.0000	0.0	0.0000
59956.0	11740	14825	0.0015	0.0000	100.0000	0.0	0.0000

APPENDIX 6 - MICP - WELL RSU#1 SAMPLE B1

TABLE OF CONTENTS

i

LIST OF TABLES

TABLE 6-1. MERCURY INJECTION DATA SUMMARY FOR SAMPLE B1 1
TABLE 6-2. MERCURY INJECTION DATA FOR SAMPLE B1 2

LIST OF FIGURES

FIGURE 6-1. MERCURY INJECTION CAPILLARY PRESSURE FOR SAMPLE B1 4
FIGURE 6-2. PORE THROAT DISTRIBUTION FOR SAMPLE B1 5

TABLE 6-1. MERCURY INJECTION DATA SUMMARY FOR SAMPLE B1

Sample Info and Properties	
Depth:	6300-6330 ft
Well:	RSU#1
Formation:	Baxter 1
Porosity:	NA %
Air Permeability:	NA md
Klink. Permeability:	NA md
Grain Density:	2.59 g/cm3

Mercury Injection Data	
IFT (σ):	485 dynes/cm
Contact angle (θ):	130 degrees
σcosθ Hg/air:	367.7 dynes/cm
σcosθ Air/brine:	72 dynes/cm
Total Pore Area:	9.486 m^2/g
Hg Porosity:	34.31 %
Corr. Hg Porosity:	15.43 %

Height Computation	
Water - Oil Reservoir System	
Res. Oil Grad:	0.360 psi/ft
Res. Wtr. Gradient:	0.470 psi/ft
σcosθ reservoir:	10.0 dynes/cm
Conversion Factor "C":	0.247 ft/psi

Computations	
Displacement Pressure (Pd)	
Mercury/Air:	354.28 psi
Air/Brine Equiv:	69.37 psi
Equiv. Height:	87.59 ft
Pr Throat Rad:	0.301 microns
Pore Radius Distributions	
Mean (arithmetic):	0.051 microns
Mean (geometric):	0.029 microns
Mean (harmonic):	0.015 microns
Micropores - Pore throat radius < .1 micron:	83.604 % PV
Intermediate - Pore throat radius .1<r<3 micron:	16.396 % PV
Macropores - Pore throat radius > 3 micron:	0.000 % PV
Swanson Parameter[1]	
(Sb/Pc)max:	0.003
Kbrine Swanson:	0.003 md
Kair Swanson:	0.022 md

TABLE 6-2. MERCURY INJECTION DATA FOR SAMPLE B1

Hg/air Pres. psi	Equivalent Air/brine Pres. psi	Height above Free Wtr. ft.	Pore radius Aperture microns	Hg Volume Injected cm3	Hg Sat. Pore Volume %	1-Hg Sat. Pore Volume %	Hg Porosity Injected %
0.5	0.11	0.13	167.8718	0.0000	0.0000	100.0	0.0000
0.6	0.11	0.14	155.4802	0.0000	0.0000	100.0	0.0000
0.6	0.13	0.16	141.4372	0.0000	0.0000	100.0	0.0000
0.7	0.14	0.17	128.8083	0.0000	0.0000	100.0	0.0000
0.8	0.15	0.19	117.2969	0.0000	0.0000	100.0	0.0000
0.8	0.17	0.21	106.8835	0.0000	0.0000	100.0	0.0000
0.9	0.18	0.23	97.2601	0.0000	0.0000	100.0	0.0000
1.0	0.20	0.25	88.7937	0.0000	0.0000	100.0	0.0000
1.1	0.22	0.28	80.8227	0.0000	0.0000	100.0	0.0000
1.2	0.24	0.30	73.7219	0.0000	0.0000	100.0	0.0000
1.4	0.26	0.33	66.9724	0.0000	0.0000	100.0	0.0000
1.5	0.29	0.37	60.9697	0.0000	0.0000	100.0	0.0000
1.6	0.32	0.40	55.5140	0.0000	0.0000	100.0	0.0000
1.8	0.35	0.44	50.5551	0.0000	0.0000	100.0	0.0000
2.0	0.4	0.49	46.0033	0.0000	0.0000	100.0	0.0000
2.2	0.4	0.53	41.8519	0.0000	0.0000	100.0	0.0000
2.4	0.5	0.59	38.0902	0.0000	0.0000	100.0	0.0000
2.6	0.5	0.65	34.6524	0.0000	0.0000	100.0	0.0000
2.9	0.6	0.71	31.5331	0.0000	0.0000	100.0	0.0000
3.2	0.6	0.78	28.6870	0.0000	0.0000	100.0	0.0000
3.5	0.7	0.86	26.0920	0.0000	0.0000	100.0	0.0000
3.8	0.7	0.94	23.7360	0.0000	0.0000	100.0	0.0000
4.2	0.8	1.04	21.5442	0.0000	0.0000	100.0	0.0000
4.6	0.9	1.14	19.5741	0.0000	0.0000	100.0	0.0000
5.1	1.0	1.26	17.7752	0.0000	0.0000	100.0	0.0000
5.6	1.1	1.39	16.1383	0.0000	0.0000	100.0	0.0000
6.2	1.2	1.53	14.6549	0.0000	0.0000	100.0	0.0000
6.8	1.3	1.68	13.3028	0.0000	0.0000	100.0	0.0000
7.5	1.5	1.85	12.0845	0.0000	0.0000	100.0	0.0000
8.2	1.6	2.04	10.9695	0.0000	0.0000	100.0	0.0000
9.1	1.8	2.24	9.9661	0.0000	0.0000	100.0	0.0000
10.0	2.0	2.47	9.0481	0.0000	0.0000	100.0	0.0000
11.0	2.2	2.72	8.2172	0.0000	0.0000	100.0	0.0000
12.1	2.4	3.00	7.4606	0.0000	0.0000	100.0	0.0000
13.3	2.6	3.3	6.7742	0.0000	0.0000	100.0	0.0000
14.7	2.9	3.6	6.1520	0.0000	0.0000	100.0	0.0000
16.2	3.2	4.0	5.5861	0.0000	0.0000	100.0	0.0000
17.8	3.5	4.4	5.0726	0.0000	0.0000	100.0	0.0000
19.6	3.8	4.9	4.6053	0.0000	0.0000	100.0	0.0000
21.7	4.2	5.4	4.1728	0.0000	0.0000	100.0	0.0000
23.9	4.7	5.9	3.7883	0.0000	0.0000	100.0	0.0000
26.3	5.1	6.5	3.4407	0.0000	0.0000	100.0	0.0000
28.9	5.7	7.2	3.1246	0.0000	0.0000	100.0	0.0000
31.9	6.2	7.9	2.8371	0.0000	0.0000	100.0	0.0000
35.1	6.9	8.7	2.5759	0.0000	0.0000	100.0	0.0000
35.1	6.9	8.7	2.5745	0.0000	0.0000	100.0	0.0000
39.4	7.7	9.7	2.2958	0.0000	0.0000	100.0	0.0000
43.7	8.6	10.8	2.0685	0.0000	0.0000	100.0	0.0000
49.0	9.6	12.1	1.8449	0.0000	0.0000	100.0	0.0000
53.4	10.5	13.2	1.6926	0.0000	0.0000	100.0	0.0000
59.1	11.6	14.6	1.5309	0.0000	0.0000	100.0	0.0000
66.0	12.9	16.3	1.3699	0.0000	0.0000	100.0	0.0000
72.4	14.2	17.9	1.2483	0.0000	0.0000	100.0	0.0000
80.4	15.8	19.9	1.1242	0.0000	0.0000	100.0	0.0000
88.2	17.3	21.8	1.0256	0.0000	0.0000	100.0	0.0000
98.7	19.3	24.4	0.9164	0.0000	0.0000	100.0	0.0000
108.6	21.3	26.8	0.8328	0.0000	0.0000	100.0	0.0000
119.8	23.5	29.6	0.7547	0.0000	0.0000	100.0	0.0000
133.1	26.1	32.9	0.6795	0.0000	0.0000	100.0	0.0000

TABLE 6-2. MERCURY INJECTION DATA FOR SAMPLE B1 - CONTINUED

Hg/air Pres. psi	Equivalent Air/brine Pres. psi	Height above Free Wtr. ft.	Pore radius Aperture microns	Hg Volume Injected cm3	Hg Sat. Pore Volume %	1-Hg Sat. Pore Volume %	Hg Porosity Injected %
146.7	28.7	36	0.6163	0.0000	0.0000	100.0	0.0000
161.6	31.6	40	0.5597	0.0000	0.0000	100.0	0.0000
178.1	34.9	44	0.5077	0.0000	0.0000	100.0	0.0000
196.9	38.6	49	0.4592	0.0000	0.0000	100.0	0.0000
217.1	42.5	54	0.4166	0.0000	0.0000	100.0	0.0000
240.1	47	59	0.3767	0.0000	0.0000	100.0	0.0000
264.9	52	65	0.3414	0.0000	0.0000	100.0	0.0000
291.9	57	72	0.3098	0.0000	0.0000	100.0	0.0000
321.0	63	79	0.2818	0.0000	0.0000	100.0	0.0000
354.3	69	88	0.2553	0.0020	1.2034	98.8	0.1857
394.2	77	97	0.2294	0.0023	2.5577	97.4	0.2090
430.9	84	107	0.2099	0.0020	3.7701	96.2	0.1871
476.5	93	118	0.1898	0.0025	5.2451	94.8	0.2276
524.2	103	130	0.1725	0.0024	6.6811	93.3	0.2216
576.9	113	143	0.1568	0.0027	8.2807	91.7	0.2468
635.0	124	157	0.1424	0.0030	10.0544	89.9	0.2737
700.6	137	173	0.1291	0.0030	11.8498	88.2	0.2771
771.7	151	191	0.1172	0.0033	13.7795	86.2	0.2978
850.2	166	210	0.1064	0.0034	15.8223	84.2	0.3152
937.8	184	232	0.0964	0.0036	17.9784	82.0	0.3327
1033.9	202	256	0.0875	0.0037	20.1884	79.8	0.3411
1139.1	223	282	0.0794	0.0038	22.4363	77.6	0.3469
1253.7	245	310	0.0721	0.0040	24.8366	75.2	0.3704
1381.2	270	341	0.0655	0.0042	27.3531	72.6	0.3884
1521.1	298	376	0.0595	0.0043	29.9230	70.1	0.3966
1676.3	328	414	0.0539	0.0044	32.5581	67.4	0.4067
1846.0	361	456	0.0490	0.0046	35.3090	64.7	0.4245
2033.8	398	503	0.0445	0.0048	38.1532	61.8	0.4389
2239.9	439	554	0.0404	0.0049	41.0370	59.0	0.4450
2467.8	483	610	0.0366	0.0048	43.8942	56.1	0.4409
2716.8	532	672	0.0333	0.0049	46.7978	53.2	0.4481
2993.1	586	740	0.0302	0.0050	49.7858	50.2	0.4611
3297.3	646	815	0.0274	0.0049	52.7059	47.3	0.4506
3631.0	711	898	0.0249	0.0050	55.6512	44.3	0.4545
4000.2	783	989	0.0226	0.0049	58.5634	41.4	0.4494
4405.3	863	1089	0.0205	0.0048	61.4256	38.6	0.4417
4845.9	949	1198	0.0187	0.0059	64.9456	35.1	0.5432
5338.0	1045	1320	0.0169	0.0045	67.5967	32.4	0.4091
5879.6	1151	1454	0.0154	0.0042	70.0846	29.9	0.3839
6474.8	1268	1601	0.0140	0.0043	72.6089	27.4	0.3896
7134.8	1397	1764	0.0127	0.0039	74.9388	25.1	0.3596
7861.3	1539	1944	0.0115	0.0043	77.5004	22.5	0.3953
8658.4	1695	2141	0.0104	0.0047	80.3036	19.7	0.4326
9540.6	1868	2359	0.0095	0.0030	82.0816	17.9	0.2744
10508.8	2058	2598	0.0086	0.0032	83.9938	16.0	0.2951
11576.3	2267	2862	0.0078	0.0032	85.9215	14.1	0.2975
12753.1	2497	3153	0.0071	0.0030	87.7138	12.3	0.2766
14049.0	2751	3473	0.0064	0.0029	89.4415	10.6	0.2666
15478.4	3031	3827	0.0058	0.0025	90.9388	9.1	0.2311
17050.0	3339	4215	0.0053	0.0011	91.5807	8.4	0.0991
18786.4	3679	4645	0.0048	0.0024	93.0042	7.0	0.2197
20700.1	4053	5118	0.0044	0.0026	94.5328	5.5	0.2359
22811.8	4467	5640	0.0040	0.0016	95.4878	4.5	0.1474
25130.9	4921	6213	0.0036	0.0012	96.2130	3.8	0.1119
27682.9	5421	6844	0.0033	0.0013	96.9767	3.0	0.1179
30492.7	5971	7539	0.0030	0.0009	97.5269	2.5	0.0849
33587.7	6577	8304	0.0027	0.0018	98.6125	1.4	0.1675
36995.7	7244	9147	0.0024	0.0008	99.1059	0.9	0.0761
40736.6	7977	10072	0.0022	0.0005	99.4267	0.6	0.0495
59952.5	11739	14822	0.0015	0.0000	100.0000	0.0	0.0000

FIGURE 6-1. MERCURY INJECTION CAPILLARY PRESSURE FOR SAMPLE B1

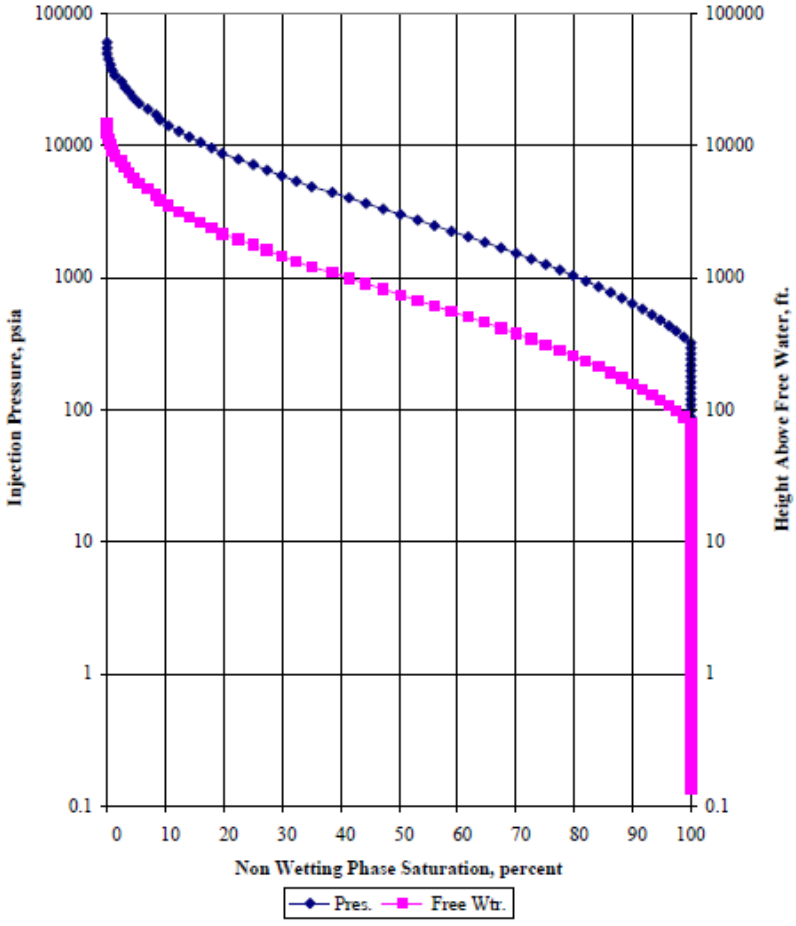
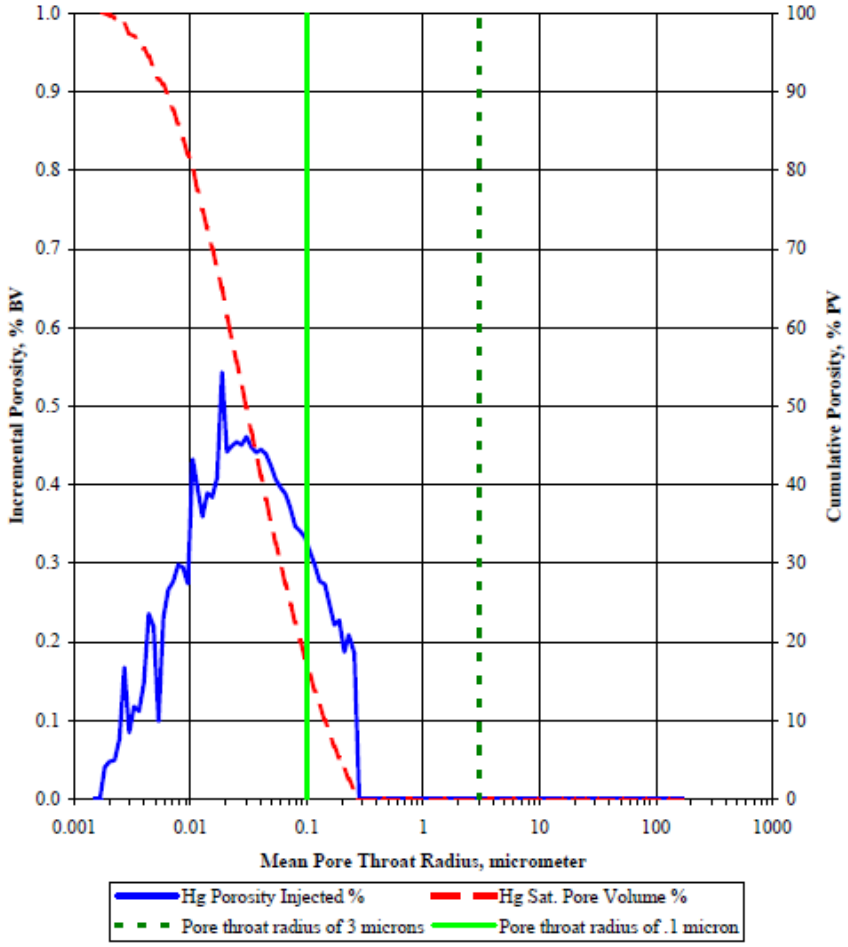


FIGURE 6-2. PORE THROAT DISTRIBUTION FOR SAMPLE B1



APPENDIX 7 - MICP - WELL RSU#1 SAMPLE B2

TABLE OF CONTENTS i

LIST OF TABLES

TABLE 7-1. MERCURY INJECTION DATA SUMMARY FOR SAMPLE B2 1
TABLE 7-2. MERCURY INJECTION DATA FOR SAMPLE B2 2

LIST OF FIGURES

FIGURE 7-1. MERCURY INJECTION CAPILLARY PRESSURE FOR SAMPLE B2 4
FIGURE 7-2. PORE THROAT DISTRIBUTION FOR SAMPLE B2 5

TABLE 7-1. MERCURY INJECTION DATA SUMMARY FOR SAMPLE B2

Sample Info and Properties	
Depth:	7680-7710 ft
Well:	RSU#1
Formation:	Baxter 2
Porosity:	NA %
Air Permeability:	NA md
Klink. Permeability:	NA md
Grain Density:	2.57 g/cm3

Mercury Injection Data	
IFT (σ):	485 dynes/cm
Contact angle (θ):	130 degrees
σcosθ Hg/air:	367.7 dynes/cm
σcosθ Air/brine:	72 dynes/cm
Total Pore Area:	8.917 m^2/g
Hg Porosity:	31.72 %
Corr. Hg Porosity:	15.46 %

Height Computation	
Water - Oil Reservoir System	
Res. Oil Grad:	0.360 psi/ft
Res. Wtr. Gradient:	0.470 psi/ft
σcosθ reservoir:	10.0 dynes/cm
Conversion Factor "C":	0.247 ft/psi

Computations	
Displacement Pressure (Pd)	
Mercury/Air:	217.25 psi
Air/Brine Equiv:	42.54 psi
Equiv. Height:	53.71 ft
Pr Throat Rad:	0.491 microns
Pore Radius Distributions	
Mean (arithmetic):	0.072 microns
Mean (geometric):	0.034 microns
Mean (harmonic):	0.015 microns
Micropores - Pore throat radius < .1 micron:	76.340 % PV
Intermediate - Pore throat radius .1<r<3 micron:	23.660 % PV
Macropores - Pore throat radius > 3 micron:	0.000 % PV
Swanson Parameter[1]	
(Sb/Pc)max:	0.004
Kbrine Swanson:	0.006 md
Kair Swanson:	0.040 md

TABLE 7-2. MERCURY INJECTION DATA FOR SAMPLE B2

Hg/air Pres. psi	Equivalent Air/brine Pres. psi	Height above Free Wtr. ft.	Pore radius Aperture microns	Hg Volume Injected cm3	Hg Sat. Pore Volume %	1-Hg Sat. Pore Volume %	Hg Porosity Injected %
0.5	0.11	0.13	167.9140	0.0000	0.0000	100.0	0.0000
0.6	0.11	0.14	154.8548	0.0000	0.0000	100.0	0.0000
0.6	0.13	0.16	140.8627	0.0000	0.0000	100.0	0.0000
0.7	0.14	0.17	128.9401	0.0000	0.0000	100.0	0.0000
0.8	0.15	0.19	117.4390	0.0000	0.0000	100.0	0.0000
0.8	0.17	0.21	106.8874	0.0000	0.0000	100.0	0.0000
0.9	0.18	0.23	97.4692	0.0000	0.0000	100.0	0.0000
1.0	0.20	0.25	88.6457	0.0000	0.0000	100.0	0.0000
1.1	0.22	0.28	80.8470	0.0000	0.0000	100.0	0.0000
1.2	0.24	0.30	73.6394	0.0000	0.0000	100.0	0.0000
1.4	0.26	0.33	66.9694	0.0000	0.0000	100.0	0.0000
1.5	0.29	0.37	60.9653	0.0000	0.0000	100.0	0.0000
1.6	0.32	0.40	55.5277	0.0000	0.0000	100.0	0.0000
1.8	0.35	0.44	50.5560	0.0000	0.0000	100.0	0.0000
2.0	0.4	0.49	45.9691	0.0000	0.0000	100.0	0.0000
2.2	0.4	0.53	41.8716	0.0000	0.0000	100.0	0.0000
2.4	0.5	0.59	38.0773	0.0000	0.0000	100.0	0.0000
2.6	0.5	0.65	34.6586	0.0000	0.0000	100.0	0.0000
2.9	0.6	0.71	31.5180	0.0000	0.0000	100.0	0.0000
3.2	0.6	0.78	28.6954	0.0000	0.0000	100.0	0.0000
3.5	0.7	0.86	26.0862	0.0000	0.0000	100.0	0.0000
3.8	0.7	0.94	23.7259	0.0000	0.0000	100.0	0.0000
4.2	0.8	1.04	21.5529	0.0000	0.0000	100.0	0.0000
4.6	0.9	1.14	19.5789	0.0000	0.0000	100.0	0.0000
5.1	1.0	1.26	17.7716	0.0000	0.0000	100.0	0.0000
5.6	1.1	1.39	16.1388	0.0000	0.0000	100.0	0.0000
6.2	1.2	1.53	14.6549	0.0000	0.0000	100.0	0.0000
6.8	1.3	1.68	13.3049	0.0000	0.0000	100.0	0.0000
7.5	1.5	1.85	12.0862	0.0000	0.0000	100.0	0.0000
8.2	1.6	2.04	10.9699	0.0000	0.0000	100.0	0.0000
9.1	1.8	2.24	9.9621	0.0000	0.0000	100.0	0.0000
10.0	2.0	2.47	9.0467	0.0000	0.0000	100.0	0.0000
11.0	2.2	2.72	8.2154	0.0000	0.0000	100.0	0.0000
12.1	2.4	3.00	7.4605	0.0000	0.0000	100.0	0.0000
13.3	2.6	3.3	6.7750	0.0000	0.0000	100.0	0.0000
14.7	2.9	3.6	6.1500	0.0000	0.0000	100.0	0.0000
16.2	3.2	4.0	5.5867	0.0000	0.0000	100.0	0.0000
17.8	3.5	4.4	5.0734	0.0000	0.0000	100.0	0.0000
19.7	3.9	4.9	4.5936	0.0000	0.0000	100.0	0.0000
21.7	4.2	5.4	4.1716	0.0000	0.0000	100.0	0.0000
23.9	4.7	5.9	3.7889	0.0000	0.0000	100.0	0.0000
26.3	5.1	6.5	3.4406	0.0000	0.0000	100.0	0.0000
28.9	5.7	7.2	3.1254	0.0000	0.0000	100.0	0.0000
31.9	6.2	7.9	2.8371	0.0000	0.0000	100.0	0.0000
35.1	6.9	8.7	2.5738	0.0000	0.0000	100.0	0.0000
36.6	7.2	9.0	2.4717	0.0000	0.0000	100.0	0.0000
38.3	7.5	9.5	2.3610	0.0000	0.0000	100.0	0.0000
43.4	8.5	10.7	2.0857	0.0000	0.0000	100.0	0.0000
47.9	9.4	11.8	1.8877	0.0000	0.0000	100.0	0.0000
54.2	10.6	13.4	1.6694	0.0000	0.0000	100.0	0.0000
59.5	11.6	14.7	1.5207	0.0000	0.0000	100.0	0.0000
65.5	12.8	16.2	1.3797	0.0000	0.0000	100.0	0.0000
72.3	14.2	17.9	1.2511	0.0000	0.0000	100.0	0.0000
79.6	15.6	19.7	1.1366	0.0000	0.0000	100.0	0.0000
88.1	17.2	21.8	1.0265	0.0000	0.0000	100.0	0.0000
98.3	19.3	24.3	0.9195	0.0000	0.0000	100.0	0.0000
109.1	21.4	27.0	0.8292	0.0000	0.0000	100.0	0.0000
120.0	23.5	29.7	0.7538	0.0000	0.0000	100.0	0.0000
132.8	26.0	32.8	0.6807	0.0000	0.0000	100.0	0.0000

TABLE 7-2. MERCURY INJECTION DATA FOR SAMPLE B2 - CONTINUED

Hg/air Pres. psi	Equivalent Air/brine Pres. psi	Height above Free Wtr. ft.	Pore radius Aperture microns	Hg Volume Injected cm3	Hg Sat. Pore Volume %	1-Hg Sat. Pore Volume %	Hg Porosity Injected %
146.3	28.7	36	0.6180	0.0000	0.0000	100.0	0.0000
162.1	31.7	40	0.5580	0.0000	0.0000	100.0	0.0000
178.6	35.0	44	0.5064	0.0000	0.0000	100.0	0.0000
197.3	38.6	49	0.4584	0.0000	0.0000	100.0	0.0000
217.3	42.5	54	0.4163	0.0015	1.0330	99.0	0.1598
239.6	47	59	0.3774	0.0016	2.1312	97.9	0.1698
264.0	52	65	0.3426	0.0018	3.3640	96.6	0.1907
291.8	57	72	0.3099	0.0020	4.7480	95.3	0.2140
321.5	63	79	0.2813	0.0020	6.1370	93.9	0.2148
354.0	69	88	0.2555	0.0019	7.4755	92.5	0.2070
390.5	76	97	0.2316	0.0022	8.9683	91.0	0.2309
430.9	84	107	0.2099	0.0024	10.5956	89.4	0.2517
474.6	93	117	0.1905	0.0024	12.2751	87.7	0.2597
523.4	102	129	0.1728	0.0027	14.1540	85.8	0.2906
576.9	113	143	0.1567	0.0027	16.0225	84.0	0.2890
635.8	124	157	0.1422	0.0026	17.7829	82.2	0.2722
700.2	137	173	0.1292	0.0025	19.4997	80.5	0.2655
772.2	151	191	0.1171	0.0024	21.1828	78.8	0.2603
850.8	167	210	0.1063	0.0028	23.0852	76.9	0.2942
938.0	184	232	0.0964	0.0031	25.2054	74.8	0.3279
1033.2	202	255	0.0875	0.0030	27.2604	72.7	0.3178
1137.8	223	281	0.0795	0.0030	29.3495	70.7	0.3231
1254.8	246	310	0.0721	0.0032	31.5634	68.4	0.3424
1382.3	271	342	0.0654	0.0031	33.6873	66.3	0.3285
1521.6	298	376	0.0594	0.0034	36.0257	64.0	0.3616
1676.0	328	414	0.0540	0.0033	38.3190	61.7	0.3547
1845.8	361	456	0.0490	0.0033	40.5686	59.4	0.3479
2034.2	398	503	0.0445	0.0033	42.8428	57.2	0.3517
2240.2	439	554	0.0404	0.0036	45.3366	54.7	0.3857
2467.4	483	610	0.0367	0.0036	47.8166	52.2	0.3835
2717.2	532	672	0.0333	0.0036	50.3186	49.7	0.3869
2993.2	586	740	0.0302	0.0037	52.8768	47.1	0.3956
3296.5	645	815	0.0274	0.0038	55.4641	44.5	0.4001
3630.2	711	898	0.0249	0.0038	58.0603	41.9	0.4015
4000.3	783	989	0.0226	0.0038	60.6848	39.3	0.4059
4405.7	863	1089	0.0205	0.0039	63.3376	36.7	0.4103
4846.3	949	1198	0.0187	0.0049	66.6938	33.3	0.5190
5336.6	1045	1319	0.0169	0.0037	69.2646	30.7	0.3976
5877.6	1151	1453	0.0154	0.0038	71.8691	28.1	0.4028
6476.1	1268	1601	0.0140	0.0035	74.2873	25.7	0.3740
7133.2	1397	1764	0.0127	0.0034	76.6434	23.4	0.3644
7858.4	1539	1943	0.0115	0.0033	78.8799	21.1	0.3459
8660.7	1696	2141	0.0104	0.0030	80.9671	19.0	0.3228
9539.9	1868	2359	0.0095	0.0028	82.9072	17.1	0.3000
10510.8	2058	2599	0.0086	0.0028	84.8641	15.1	0.3026
11579.1	2267	2863	0.0078	0.0026	86.6493	13.4	0.2761
12755.9	2498	3154	0.0071	0.0024	88.3253	11.7	0.2592
14052.0	2752	3474	0.0064	0.0013	89.2512	10.7	0.1432
15477.7	3031	3827	0.0058	0.0023	90.8218	9.2	0.2429
17051.7	3339	4216	0.0053	0.0019	92.1209	7.9	0.2009
18785.1	3678	4644	0.0048	0.0017	93.2924	6.7	0.1812
20700.0	4053	5118	0.0044	0.0015	94.2991	5.7	0.1557
22811.3	4467	5640	0.0040	0.0013	95.1737	4.8	0.1353
25130.5	4921	6213	0.0036	0.0013	96.0600	3.9	0.1371
27683.7	5421	6844	0.0033	0.0008	96.6337	3.4	0.0887
30494.0	5971	7539	0.0030	0.0012	97.4555	2.5	0.1271
33587.9	6577	8304	0.0027	0.0012	98.2629	1.7	0.1249
36995.2	7244	9147	0.0024	0.0010	98.9310	1.1	0.1033
40737.2	7977	10072	0.0022	0.0007	99.4253	0.6	0.0764
59955.7	11740	14825	0.0015	0.0000	100.0000	0.0	0.0000

FIGURE 7-1. MERCURY INJECTION CAPILLARY PRESSURE FOR SAMPLE B2

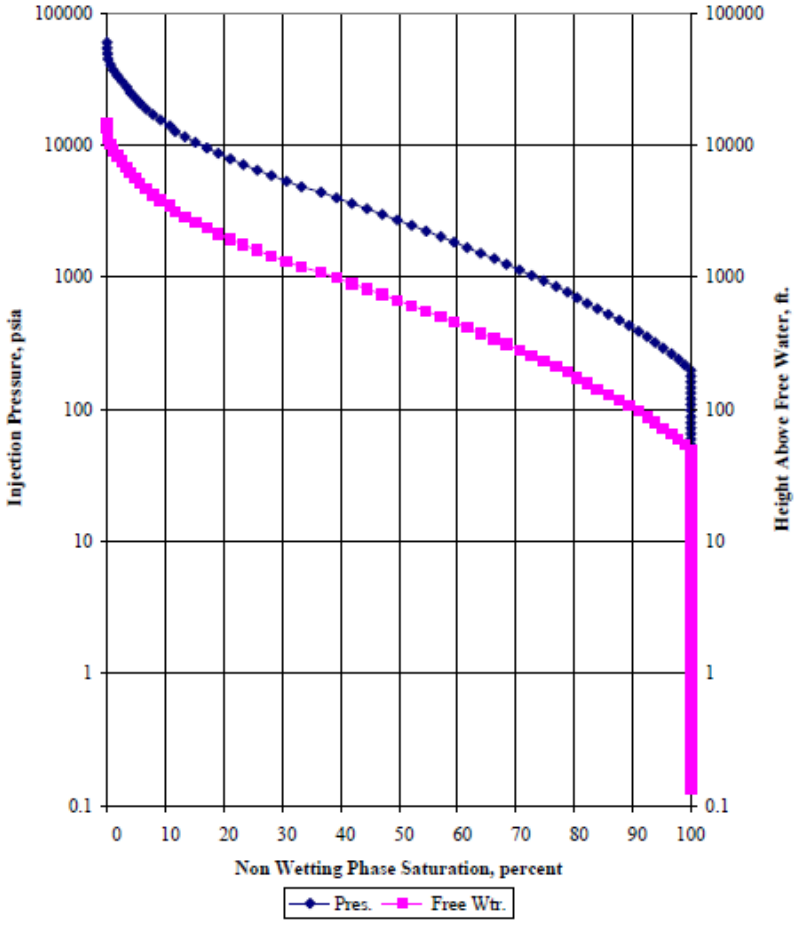
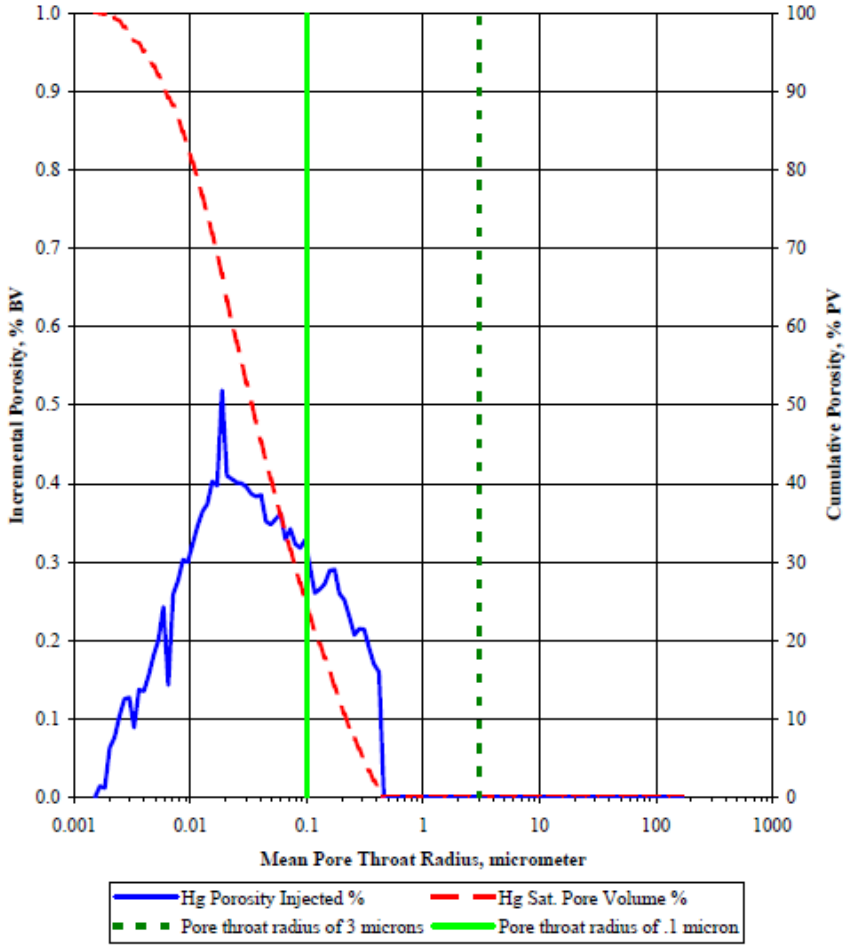


FIGURE 7-2. PORE THROAT DISTRIBUTION FOR SAMPLE B2



APPENDIX 8 - MICP - SAMPLE B3

TABLE OF CONTENTS i

LIST OF TABLES

TABLE 8-1. MERCURY INJECTION DATA SUMMARY FOR SAMPLE ID B3 1
TABLE 8-2. MERCURY INJECTION DATA FOR SAMPLE ID B3 2

LIST OF FIGURES

FIGURE 8-1. MERCURY INJECTION CAPILLARY PRESSURE FOR SAMPLE ID B3 4
FIGURE 8-2. PORE THROAT DISTRIBUTION FOR SAMPLE ID B3 5

TABLE 8-1. MERCURY INJECTION DATA SUMMARY FOR SAMPLE ID B3

Sample Info and Properties	
Depth:	7590-7620 ft
Well:	RSU#1
Formation:	Baxter 3
Porosity:	NA % @ 800 psi
Air Permeability:	NA md @ 800 psi
Klink. Permeability:	NA md @ 800 psi
Grain Density:	2.49 g/cm3

Mercury Injection Data	
IFT (σ):	485 dynes/cm
Contact angle (θ):	130 degrees
σcosθ Hg/air:	367.7 dynes/cm
σcosθ Air/brine:	72 dynes/cm
Total Pore Area:	10.564 m^2/g
Hg Porosity:	48.27 %
Corr. Hg Porosity:	15.23 %

Height Computation	
Water - Oil Reservoir System	
Res. Oil Grad:	0.360 psi/ft
Res. Wtr. Gradient:	0.470 psi/ft
σcosθ reservoir:	10.0 dynes/cm
Conversion Factor "C":	0.247 ft/psi

Computations	
Displacement Pressure (Pd)	
Mercury/Air:	430.62 psi
Air/Brine Equiv:	84.32 psi
Equiv. Height:	106.47 ft
Pr Throat Rad:	0.248 microns
Pore Radius Distributions	
Mean (arithmetic):	0.046 microns
Mean (geometric):	0.026 microns
Mean (harmonic):	0.013 microns
Micropores - Pore throat radius < .1 micron:	85.288 % PV
Intermediate - Pore throat radius .1<r<3 micron:	14.712 % PV
Macropores - Pore throat radius > 3 micron:	0.000 % PV
Swanson Parameter[1]	
(Sb/Pc)max:	0.003
Kbrine Swanson:	0.003 md
Kair Swanson:	0.018 md

TABLE 8-2. MERCURY INJECTION DATA FOR SAMPLE ID B3

Hg/air Pres. psi	Equivalent Air/brine Pres. psi	Height above Free Wtr. ft.	Pore radius Aperture microns	Hg Volume Injected cm3	Hg Sat. Pore Volume %	1-Hg Sat. Pore Volume %	Hg Porosity Injected %
0.5	0.10	0.13	168.7755	0.0000	0.0000	100.0	0.0000
0.6	0.11	0.14	156.2039	0.0000	0.0000	100.0	0.0000
0.6	0.12	0.16	142.1512	0.0000	0.0000	100.0	0.0000
0.7	0.14	0.17	129.2740	0.0000	0.0000	100.0	0.0000
0.8	0.15	0.19	118.0059	0.0000	0.0000	100.0	0.0000
0.8	0.17	0.21	107.3126	0.0000	0.0000	100.0	0.0000
0.9	0.18	0.23	97.6510	0.0000	0.0000	100.0	0.0000
1.0	0.20	0.25	88.9044	0.0000	0.0000	100.0	0.0000
1.1	0.22	0.28	81.0479	0.0000	0.0000	100.0	0.0000
1.2	0.24	0.30	73.8036	0.0000	0.0000	100.0	0.0000
1.3	0.26	0.33	67.1108	0.0000	0.0000	100.0	0.0000
1.5	0.29	0.37	61.1101	0.0000	0.0000	100.0	0.0000
1.6	0.32	0.40	55.6241	0.0000	0.0000	100.0	0.0000
1.8	0.35	0.44	50.6387	0.0000	0.0000	100.0	0.0000
2.0	0.4	0.49	46.0471	0.0000	0.0000	100.0	0.0000
2.2	0.4	0.53	41.9009	0.0000	0.0000	100.0	0.0000
2.4	0.5	0.59	38.1219	0.0000	0.0000	100.0	0.0000
2.6	0.5	0.64	34.6934	0.0000	0.0000	100.0	0.0000
2.9	0.6	0.71	31.5448	0.0000	0.0000	100.0	0.0000
3.1	0.6	0.78	28.7203	0.0000	0.0000	100.0	0.0000
3.5	0.7	0.86	26.1179	0.0000	0.0000	100.0	0.0000
3.8	0.7	0.94	23.7429	0.0000	0.0000	100.0	0.0000
4.2	0.8	1.04	21.5776	0.0000	0.0000	100.0	0.0000
4.6	0.9	1.14	19.5899	0.0000	0.0000	100.0	0.0000
5.1	1.0	1.26	17.7831	0.0000	0.0000	100.0	0.0000
5.6	1.1	1.38	16.1498	0.0000	0.0000	100.0	0.0000
6.2	1.2	1.53	14.6608	0.0000	0.0000	100.0	0.0000
6.8	1.3	1.68	13.3071	0.0000	0.0000	100.0	0.0000
7.5	1.5	1.85	12.0870	0.0000	0.0000	100.0	0.0000
8.2	1.6	2.04	10.9727	0.0000	0.0000	100.0	0.0000
9.1	1.8	2.24	9.9708	0.0000	0.0000	100.0	0.0000
10.0	2.0	2.47	9.0500	0.0000	0.0000	100.0	0.0000
11.0	2.2	2.72	8.2186	0.0000	0.0000	100.0	0.0000
12.1	2.4	3.00	7.4624	0.0000	0.0000	100.0	0.0000
13.3	2.6	3.3	6.7752	0.0000	0.0000	100.0	0.0000
14.7	2.9	3.6	6.1524	0.0000	0.0000	100.0	0.0000
16.2	3.2	4.0	5.5867	0.0000	0.0000	100.0	0.0000
17.8	3.5	4.4	5.0715	0.0000	0.0000	100.0	0.0000
19.6	3.8	4.9	4.6059	0.0000	0.0000	100.0	0.0000
21.7	4.2	5.4	4.1731	0.0000	0.0000	100.0	0.0000
23.9	4.7	5.9	3.7892	0.0000	0.0000	100.0	0.0000
26.3	5.1	6.5	3.4411	0.0000	0.0000	100.0	0.0000
28.9	5.7	7.2	3.1255	0.0000	0.0000	100.0	0.0000
31.9	6.2	7.9	2.8373	0.0000	0.0000	100.0	0.0000
35.1	6.9	8.7	2.5735	0.0000	0.0000	100.0	0.0000
38.7	7.6	9.6	2.3374	0.0000	0.0000	100.0	0.0000
43.4	8.5	10.7	2.0816	0.0000	0.0000	100.0	0.0000
47.9	9.4	11.8	1.8889	0.0000	0.0000	100.0	0.0000
53.4	10.5	13.2	1.6924	0.0000	0.0000	100.0	0.0000
58.5	11.5	14.5	1.5457	0.0000	0.0000	100.0	0.0000
65.6	12.8	16.2	1.3796	0.0000	0.0000	100.0	0.0000
72.1	14.1	17.8	1.2541	0.0000	0.0000	100.0	0.0000
79.3	15.5	19.6	1.1404	0.0000	0.0000	100.0	0.0000
89.0	17.4	22.0	1.0165	0.0000	0.0000	100.0	0.0000
98.3	19.2	24.3	0.9199	0.0000	0.0000	100.0	0.0000
108.6	21.3	26.8	0.8330	0.0000	0.0000	100.0	0.0000
120.4	23.6	29.8	0.7510	0.0000	0.0000	100.0	0.0000
132.8	26.0	32.8	0.6809	0.0000	0.0000	100.0	0.0000
146.0	28.6	36.1	0.6194	0.0000	0.0000	100.0	0.0000

TABLE 8-2. MERCURY INJECTION DATA FOR SAMPLE ID B3 - CONTINUED

Hg/air Pres. psi	Equivalent Air/brine Pres. psi	Height above Free Wtr. ft.	Pore radius Aperture microns	Hg Volume Injected cm3	Hg Sat. Pore Volume %	1-Hg Sat. Pore Volume %	Hg Porosity Injected %
161.5	31.6	40	0.5598	0.0000	0.0000	100.0	0.0000
178.5	35.0	44	0.5066	0.0000	0.0000	100.0	0.0000
196.5	38.5	49	0.4601	0.0000	0.0000	100.0	0.0000
216.0	42.3	53	0.4187	0.0000	0.0000	100.0	0.0000
239.7	46.9	59	0.3773	0.0000	0.0000	100.0	0.0000
264.5	52	65	0.3419	0.0000	0.0000	100.0	0.0000
291.8	57	72	0.3099	0.0000	0.0000	100.0	0.0000
321.6	63	80	0.2812	0.0000	0.0000	100.0	0.0000
359.2	70	89	0.2518	0.0000	0.0000	100.0	0.0000
391.0	77	97	0.2313	0.0000	0.0000	100.0	0.0000
430.6	84	106	0.2100	0.0022	1.4787	98.5	0.2253
474.9	93	117	0.1904	0.0023	3.0334	97.0	0.2368
523.6	103	129	0.1727	0.0025	4.6845	95.3	0.2515
576.9	113	143	0.1567	0.0025	6.3866	93.6	0.2593
635.5	124	157	0.1423	0.0026	8.1464	91.9	0.2681
700.1	137	173	0.1292	0.0028	10.0137	90.0	0.2844
772.2	151	191	0.1171	0.0028	11.8981	88.1	0.2871
850.7	167	210	0.1063	0.0029	13.8574	86.1	0.2985
937.4	184	232	0.0965	0.0031	15.9125	84.1	0.3131
1033.2	202	255	0.0875	0.0031	18.0064	82.0	0.3190
1139.2	223	282	0.0794	0.0033	20.2061	79.8	0.3351
1253.7	245	310	0.0721	0.0034	22.4845	77.5	0.3471
1380.8	270	341	0.0655	0.0034	24.7800	75.2	0.3497
1521.4	298	376	0.0594	0.0036	27.1960	72.8	0.3680
1675.7	328	414	0.0540	0.0038	29.7271	70.3	0.3856
1846.0	361	456	0.0490	0.0038	32.2783	67.7	0.3886
2033.4	398	503	0.0445	0.0039	34.8761	65.1	0.3957
2240.2	439	554	0.0404	0.0040	37.5821	62.4	0.4122
2467.4	483	610	0.0367	0.0041	40.3435	59.7	0.4207
2717.7	532	672	0.0333	0.0042	43.1410	56.9	0.4261
2993.5	586	740	0.0302	0.0043	45.9856	54.0	0.4333
3295.7	645	815	0.0274	0.0044	48.9325	51.1	0.4489
3630.9	711	898	0.0249	0.0043	51.8275	48.2	0.4410
3999.6	783	989	0.0226	0.0045	54.8105	45.2	0.4544
4405.9	863	1089	0.0205	0.0052	58.3083	41.7	0.5328
4847.0	949	1198	0.0187	0.0054	61.9080	38.1	0.5483
5336.5	1045	1319	0.0169	0.0042	64.6912	35.3	0.4240
5880.8	1152	1454	0.0154	0.0042	67.4732	32.5	0.4238
6476.4	1268	1601	0.0140	0.0038	70.0029	30.0	0.3853
7133.6	1397	1764	0.0127	0.0040	72.6998	27.3	0.4108
7860.4	1539	1943	0.0115	0.0037	75.1619	24.8	0.3751
8659.8	1696	2141	0.0104	0.0031	77.2601	22.7	0.3196
9538.3	1868	2358	0.0095	0.0037	79.7078	20.3	0.3729
10506.8	2057	2598	0.0086	0.0030	81.6935	18.3	0.3025
11575.3	2267	2862	0.0078	0.0031	83.7692	16.2	0.3162
12755.1	2498	3154	0.0071	0.0027	85.5606	14.4	0.2729
14051.1	2751	3474	0.0064	0.0027	87.3634	12.6	0.2746
15480.2	3031	3827	0.0058	0.0023	88.9312	11.1	0.2388
17050.7	3339	4216	0.0053	0.0022	90.4103	9.6	0.2253
18783.1	3678	4644	0.0048	0.0020	91.7790	8.2	0.2085
20697.9	4053	5117	0.0044	0.0018	92.9669	7.0	0.1810
22811.2	4467	5640	0.0040	0.0017	94.1352	5.9	0.1780
25130.8	4921	6213	0.0036	0.0009	94.7217	5.3	0.0893
27683.8	5421	6844	0.0033	0.0028	96.5815	3.4	0.2833
30492.0	5971	7539	0.0030	0.0001	96.6508	3.3	0.0106
33588.6	6577	8304	0.0027	0.0006	97.0664	2.9	0.0633
36996.6	7244	9147	0.0024	0.0015	98.0855	1.9	0.1552
40738.9	7977	10072	0.0022	0.0007	98.5577	1.4	0.0719
44860.5	8784	11091	0.0020	0.0009	99.1454	0.9	0.0895
5995.7.0	11740	14824	0.0015	0.0000	100.0000	0.0	0.0000

FIGURE 8-1. MERCURY INJECTION CAPILLARY PRESSURE FOR SAMPLE ID B3

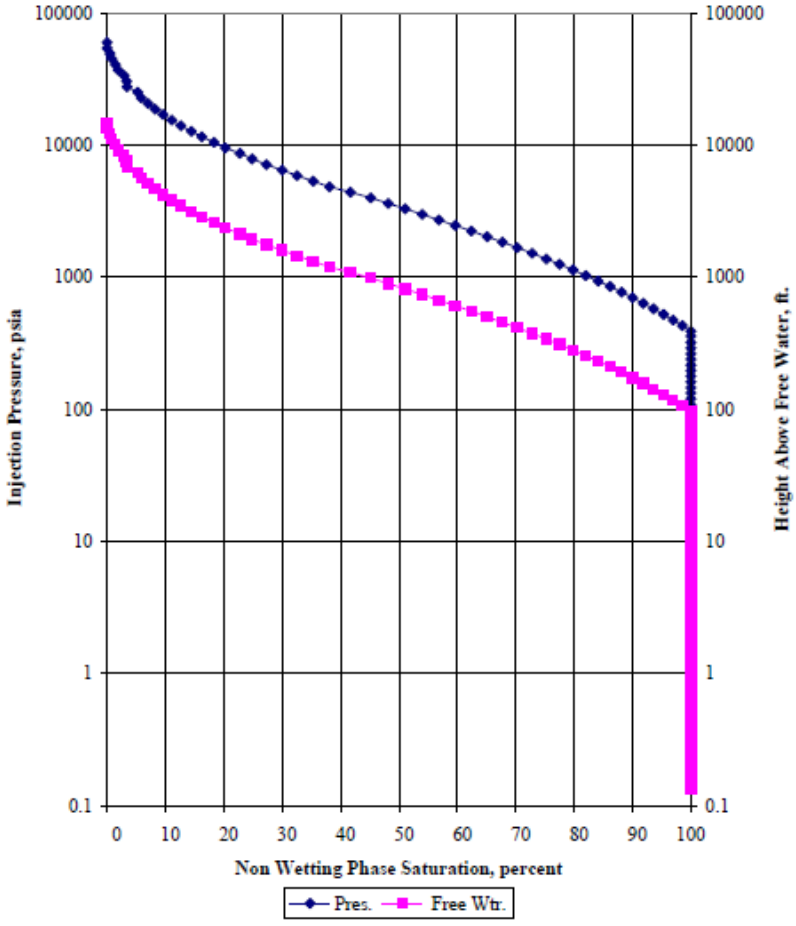
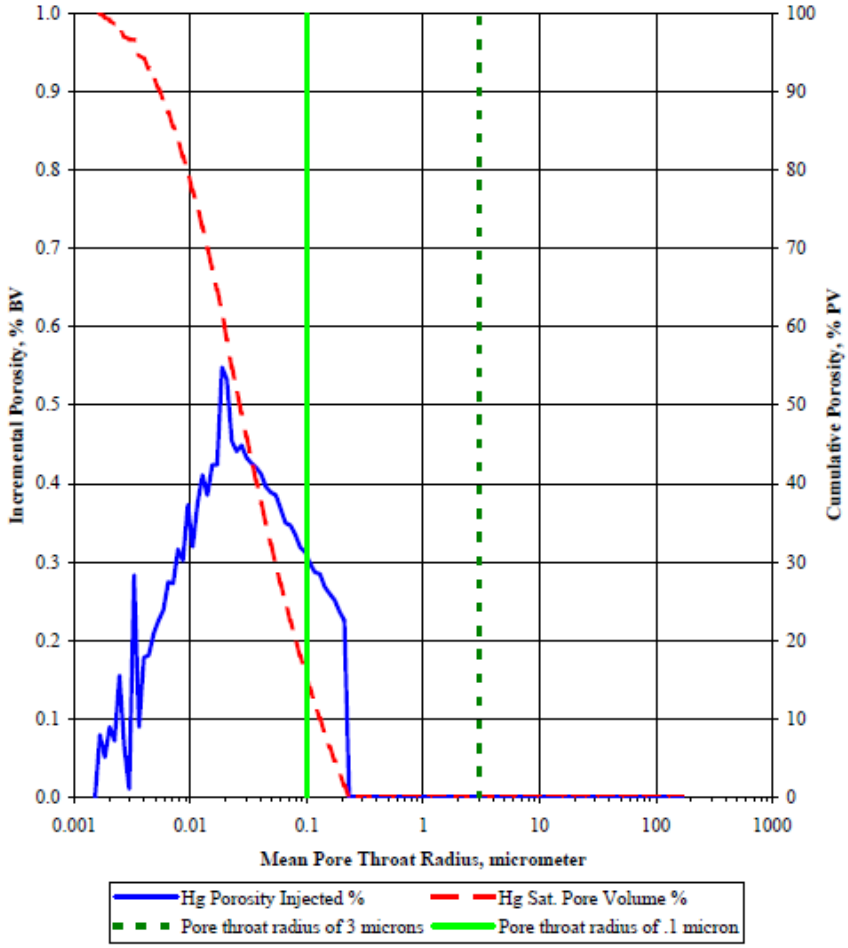


FIGURE 8-2. PORE THROAT DISTRIBUTION FOR SAMPLE ID B3



APPENDIX 9 - MICP - WELL RSU#1 SAMPLE G1

TABLE OF CONTENTS i

LIST OF TABLES

TABLE 9-1. MERCURY INJECTION DATA SUMMARY FOR SAMPLE G1 1
TABLE 9-2. MERCURY INJECTION DATA FOR SAMPLE G1 2

LIST OF FIGURES

FIGURE 9-1. MERCURY INJECTION CAPILLARY PRESSURE FOR SAMPLE G1 4
FIGURE 9-2. PORE THROAT DISTRIBUTION FOR SAMPLE G1 5

TABLE 9-1. MERCURY INJECTION DATA SUMMARY FOR SAMPLE G1

Sample Info and Properties	
Depth:	9190-9200 ft
Well:	RSU#1
Formation:	Gypsum Springs 1
Porosity:	NA %
Air Permeability:	NA md
Klink. Permeability:	NA md
Grain Density:	2.59 g/cm3

Mercury Injection Data	
IFT (σ):	485 dynes/cm
Contact angle (θ):	130 degrees
σcosθ Hg/air:	367.7 dynes/cm
σcosθ Air/brine:	72 dynes/cm
Total Pore Area:	11.932 m^2/g
Hg Porosity:	37.21 %
Corr. Hg Porosity:	19.13 %

Height Computation	
Water - Oil Reservoir System	
Res. Oil Grad:	0.360 psi/ft
Res. Wtr. Gradient:	0.470 psi/ft
σcosθ reservoir:	10.0 dynes/cm
Conversion Factor "C":	0.247 ft/psi

Computations	
Displacement Pressure (Pd)	
Mercury/Air:	429.62 psi
Air/Brine Equiv:	84.12 psi
Equiv. Height:	106.22 ft
Pr Throat Rad:	0.248 microns
Pore Radius Distributions	
Mean (arithmetic):	0.043 microns
Mean (geometric):	0.026 microns
Mean (harmonic):	0.015 microns
Micropores - Pore throat radius < .1 micron:	88.278 % PV
Intermediate - Pore throat radius .1<r<3 micron:	11.722 % PV
Macropores - Pore throat radius > 3 micron:	0.000 % PV
Swanson Parameter[1]	
(Sb/Pc)max:	0.003
Kbrine Swanson:	0.003 md
Kair Swanson:	0.023 md

TABLE 9-2. MERCURY INJECTION DATA FOR SAMPLE G1

Hg/air Pres. psi	Equivalent Air/brine Pres. psi	Height above Free Wtr. ft.	Pore radius Aperture microns	Hg Volume Injected cm3	Hg Sat. Pore Volume %	1-Hg Sat. Pore Volume %	Hg Porosity Injected %
0.5	0.11	0.13	168.0543	0.0000	0.0000	100.0	0.0000
0.6	0.11	0.14	155.4830	0.0000	0.0000	100.0	0.0000
0.6	0.13	0.16	141.3817	0.0000	0.0000	100.0	0.0000
0.7	0.14	0.17	128.8308	0.0000	0.0000	100.0	0.0000
0.8	0.15	0.19	117.1782	0.0000	0.0000	100.0	0.0000
0.8	0.17	0.21	106.9825	0.0000	0.0000	100.0	0.0000
0.9	0.18	0.23	97.4389	0.0000	0.0000	100.0	0.0000
1.0	0.20	0.25	88.7103	0.0000	0.0000	100.0	0.0000
1.1	0.22	0.28	80.8658	0.0000	0.0000	100.0	0.0000
1.2	0.24	0.30	73.7264	0.0000	0.0000	100.0	0.0000
1.4	0.26	0.33	66.9817	0.0000	0.0000	100.0	0.0000
1.5	0.29	0.37	61.0244	0.0000	0.0000	100.0	0.0000
1.6	0.32	0.40	55.5873	0.0000	0.0000	100.0	0.0000
1.8	0.35	0.44	50.5263	0.0000	0.0000	100.0	0.0000
2.0	0.4	0.49	46.0020	0.0000	0.0000	100.0	0.0000
2.2	0.4	0.53	41.8663	0.0000	0.0000	100.0	0.0000
2.4	0.5	0.59	38.0765	0.0000	0.0000	100.0	0.0000
2.6	0.5	0.65	34.6568	0.0000	0.0000	100.0	0.0000
2.9	0.6	0.71	31.5233	0.0000	0.0000	100.0	0.0000
3.2	0.6	0.78	28.6793	0.0000	0.0000	100.0	0.0000
3.5	0.7	0.86	26.0956	0.0000	0.0000	100.0	0.0000
3.8	0.7	0.94	23.7391	0.0000	0.0000	100.0	0.0000
4.2	0.8	1.04	21.5480	0.0000	0.0000	100.0	0.0000
4.6	0.9	1.14	19.5762	0.0000	0.0000	100.0	0.0000
5.1	1.0	1.26	17.7774	0.0000	0.0000	100.0	0.0000
5.6	1.1	1.39	16.1421	0.0000	0.0000	100.0	0.0000
6.2	1.2	1.53	14.6564	0.0000	0.0000	100.0	0.0000
6.8	1.3	1.68	13.3012	0.0000	0.0000	100.0	0.0000
7.5	1.5	1.85	12.0844	0.0000	0.0000	100.0	0.0000
8.2	1.6	2.04	10.9724	0.0000	0.0000	100.0	0.0000
9.1	1.8	2.24	9.9615	0.0000	0.0000	100.0	0.0000
10.0	2.0	2.47	9.0462	0.0000	0.0000	100.0	0.0000
11.0	2.2	2.72	8.2157	0.0000	0.0000	100.0	0.0000
12.1	2.4	3.00	7.4613	0.0000	0.0000	100.0	0.0000
13.3	2.6	3.3	6.7744	0.0000	0.0000	100.0	0.0000
14.7	2.9	3.6	6.1509	0.0000	0.0000	100.0	0.0000
16.2	3.2	4.0	5.5830	0.0000	0.0000	100.0	0.0000
17.8	3.5	4.4	5.0735	0.0000	0.0000	100.0	0.0000
19.6	3.8	4.9	4.6052	0.0000	0.0000	100.0	0.0000
21.7	4.2	5.4	4.1706	0.0000	0.0000	100.0	0.0000
23.9	4.7	5.9	3.7886	0.0000	0.0000	100.0	0.0000
26.3	5.1	6.5	3.4406	0.0000	0.0000	100.0	0.0000
29.0	5.7	7.2	3.1237	0.0000	0.0000	100.0	0.0000
31.9	6.2	7.9	2.8372	0.0000	0.0000	100.0	0.0000
35.1	6.9	8.7	2.5754	0.0000	0.0000	100.0	0.0000
36.6	7.2	9.0	2.4733	0.0000	0.0000	100.0	0.0000
38.1	7.5	9.4	2.3717	0.0000	0.0000	100.0	0.0000
43.0	8.4	10.6	2.1017	0.0000	0.0000	100.0	0.0000
47.1	9.2	11.6	1.9209	0.0000	0.0000	100.0	0.0000
52.4	10.3	13.0	1.7256	0.0000	0.0000	100.0	0.0000
58.6	11.5	14.5	1.5439	0.0000	0.0000	100.0	0.0000
64.3	12.6	15.9	1.4061	0.0000	0.0000	100.0	0.0000
71.8	14.1	17.8	1.2587	0.0000	0.0000	100.0	0.0000
79.0	15.5	19.5	1.1449	0.0000	0.0000	100.0	0.0000
89.2	17.5	22.1	1.0138	0.0000	0.0000	100.0	0.0000
96.8	18.9	23.9	0.9345	0.0000	0.0000	100.0	0.0000
108.5	21.2	26.8	0.8338	0.0000	0.0000	100.0	0.0000
120.1	23.5	29.7	0.7528	0.0000	0.0000	100.0	0.0000
132.4	25.9	32.7	0.6830	0.0000	0.0000	100.0	0.0000

TABLE 9-2. MERCURY INJECTION DATA FOR SAMPLE G1 - CONTINUED

Hg/air Pres. psi	Equivalent Air/brine Pres. psi	Height above Free Wtr. ft.	Pore radius Aperture microns	Hg Volume Injected cm3	Hg Sat. Pore Volume %	1-Hg Sat. Pore Volume %	Hg Porosity Injected %
146.1	28.6	36	0.6188	0.0000	0.0000	100.0	0.0000
161.6	31.6	40	0.5597	0.0000	0.0000	100.0	0.0000
177.7	34.8	44	0.5088	0.0000	0.0000	100.0	0.0000
196.4	38.5	49	0.4604	0.0000	0.0000	100.0	0.0000
217.0	42.5	54	0.4167	0.0000	0.0000	100.0	0.0000
239.3	47	59	0.3779	0.0000	0.0000	100.0	0.0000
263.9	52	65	0.3426	0.0000	0.0000	100.0	0.0000
290.9	57	72	0.3108	0.0000	0.0000	100.0	0.0000
320.7	63	79	0.2820	0.0000	0.0000	100.0	0.0000
354.4	69	88	0.2552	0.0000	0.0000	100.0	0.0000
389.8	76	96	0.2320	0.0000	0.0000	100.0	0.0000
429.6	84	106	0.2105	0.0024	1.2082	98.8	0.2312
474.3	93	117	0.1907	0.0024	2.4403	97.6	0.2358
523.4	102	129	0.1728	0.0026	3.7720	96.2	0.2548
576.0	113	142	0.1570	0.0026	5.0989	94.9	0.2539
634.7	124	157	0.1425	0.0027	6.4848	93.5	0.2652
700.0	137	173	0.1292	0.0031	8.0653	91.9	0.3024
772.2	151	191	0.1171	0.0030	9.6097	90.4	0.2955
850.3	167	210	0.1063	0.0034	11.3239	88.7	0.3280
936.8	183	232	0.0965	0.0038	13.2604	86.7	0.3705
1033.7	202	256	0.0875	0.0039	15.2623	84.7	0.3830
1137.5	223	281	0.0795	0.0042	17.3829	82.6	0.4058
1253.0	245	310	0.0722	0.0046	19.7171	80.3	0.4466
1380.4	270	341	0.0655	0.0047	22.1171	77.9	0.4592
1520.5	298	376	0.0595	0.0051	24.6823	75.3	0.4908
1674.9	328	414	0.0540	0.0055	27.4747	72.5	0.5343
1845.5	361	456	0.0490	0.0056	30.3379	69.7	0.5478
2032.9	398	503	0.0445	0.0061	33.4325	66.6	0.5921
2238.9	438	554	0.0404	0.0061	36.5435	63.5	0.5952
2466.5	483	610	0.0367	0.0064	39.7955	60.2	0.6222
2716.4	532	672	0.0333	0.0062	42.9404	57.1	0.6017
2991.4	586	740	0.0302	0.0068	46.4082	53.6	0.6635
3295.1	645	815	0.0274	0.0067	49.8018	50.2	0.6493
3629.1	711	897	0.0249	0.0068	53.2482	46.8	0.6594
3999.4	783	989	0.0226	0.0065	56.5237	43.5	0.6267
4403.2	862	1089	0.0205	0.0062	59.6819	40.3	0.6043
4844.6	949	1198	0.0187	0.0079	63.6892	36.3	0.7667
5336.6	1045	1319	0.0169	0.0063	66.8939	33.1	0.6132
5876.5	1151	1453	0.0154	0.0058	69.8440	30.2	0.5644
6472.7	1267	1600	0.0140	0.0057	72.7530	27.2	0.5566
7134.0	1397	1764	0.0127	0.0053	75.4300	24.6	0.5122
7857.8	1539	1943	0.0115	0.0052	78.0656	21.9	0.5043
8657.1	1695	2140	0.0104	0.0049	80.5461	19.5	0.4746
9539.5	1868	2359	0.0095	0.0045	82.8226	17.2	0.4356
10511.4	2058	2599	0.0086	0.0042	84.9369	15.1	0.4045
11578.9	2267	2863	0.0078	0.0038	86.8431	13.2	0.3647
12752.3	2497	3153	0.0071	0.0037	88.7288	11.3	0.3608
14049.1	2751	3473	0.0064	0.0031	90.2878	9.7	0.2983
15479.2	3031	3827	0.0058	0.0028	91.6952	8.3	0.2693
17051.3	3339	4216	0.0053	0.0028	93.1244	6.9	0.2735
18781.8	3678	4644	0.0048	0.0025	94.3818	5.6	0.2406
20697.0	4053	5117	0.0044	0.0021	95.4347	4.6	0.2015
22809.5	4466	5639	0.0040	0.0021	96.5018	3.5	0.2042
25129.7	4921	6213	0.0036	0.0018	97.4050	2.6	0.1728
27681.8	5420	6844	0.0033	0.0013	98.0589	1.9	0.1251
30491.0	5970	7538	0.0030	0.0009	98.5321	1.5	0.0905
33587.5	6577	8304	0.0027	0.0009	99.0040	1.0	0.0903
36996.6	7244	9147	0.0024	0.0006	99.3249	0.7	0.0614
40737.4	7977	10072	0.0022	0.0005	99.6017	0.4	0.0530
59954.5	11740	14825	0.0015	0.0000	100.0000	0.0	0.0000

FIGURE 9-1. MERCURY INJECTION CAPILLARY PRESSURE FOR SAMPLE G1

9

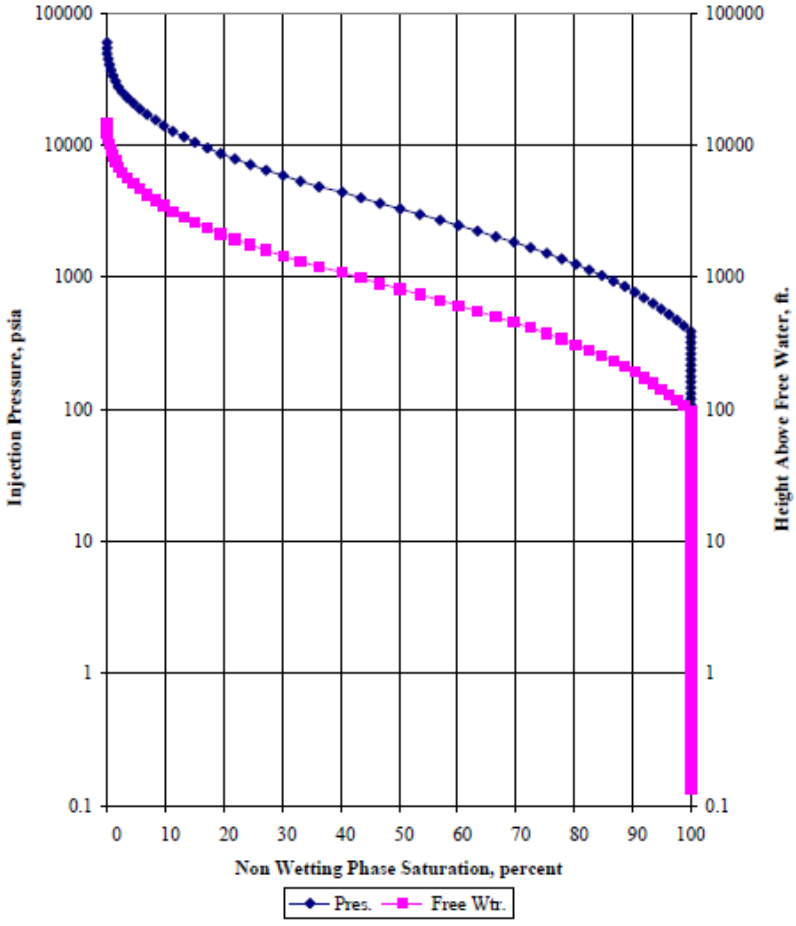
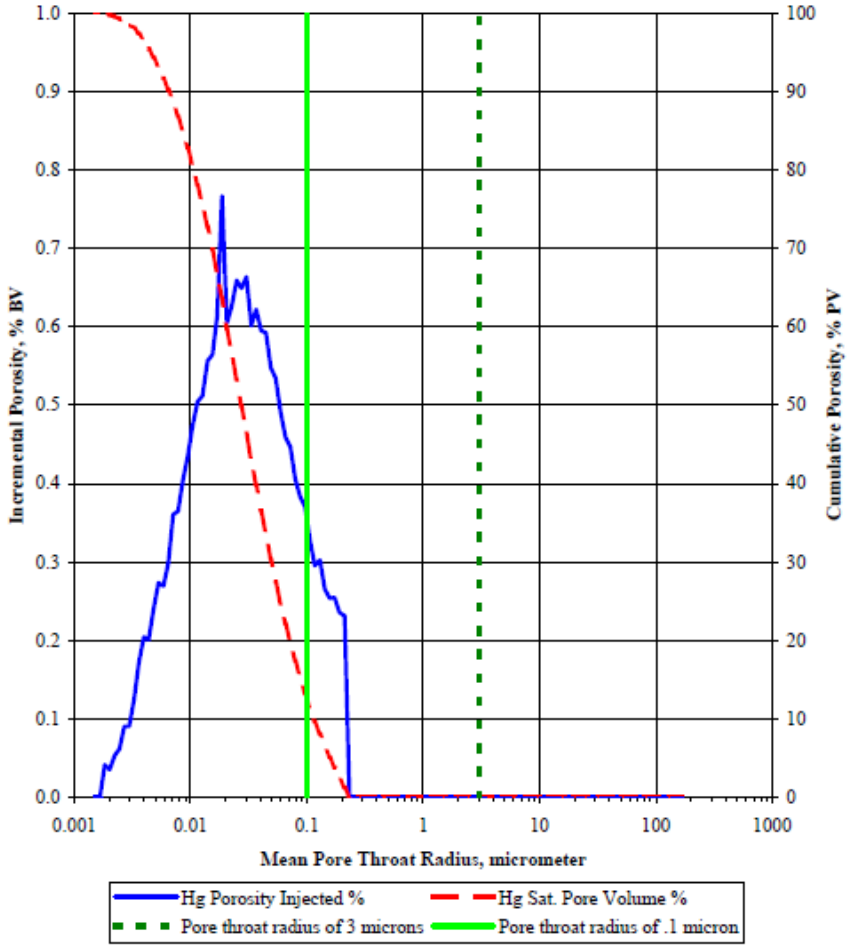


FIGURE 9-2. PORE THROAT DISTRIBUTION FOR SAMPLE G1



APPENDIX 10 - MICP - SAMPLE M1

TABLE OF CONTENTS i

LIST OF TABLES
TABLE 10-1. MERCURY INJECTION DATA SUMMARY FOR SAMPLE ID M1 1
TABLE 10-2. MERCURY INJECTION DATA FOR SAMPLE ID M1 2

LIST OF FIGURES
FIGURE 10-1. MERCURY INJECTION CAPILLARY PRESSURE FOR SAMPLE ID M1 4
FIGURE 10-2. PORE THROAT DISTRIBUTION FOR SAMPLE ID M1 5

TABLE 10-1. MERCURY INJECTION DATA SUMMARY FOR SAMPLE ID M1

Sample Info and Properties	
Depth:	8130-8160 ft
Well:	RSU#1
Formation:	Mowry 1
Porosity:	NA % @ 800 psi
Air Permeability:	NA md @ 800 psi
Klink. Permeability:	NA md @ 800 psi
Grain Density:	2.51 g/cm3

Mercury Injection Data	
IFT (σ):	485 dynes/cm
Contact angle (θ):	130 degrees
σcosθ Hg/air:	367.7 dynes/cm
σcosθ Air/brine:	72 dynes/cm
Total Pore Area:	5.971 m^2/g
Hg Porosity:	38.14 %
Corr. Hg Porosity:	12.74 %

Height Computation	
Water - Oil Reservoir System	
Res. Oil Grad:	0.360 psi/ft
Res. Wtr. Gradient:	0.470 psi/ft
σcosθ reservoir:	10.0 dynes/cm
Conversion Factor "C":	0.247 ft/psi

Computations	
Displacement Pressure (Pd)	
Mercury/Air:	264.28 psi
Air/Brine Equiv:	51.75 psi
Equiv. Height:	65.34 ft
Pr Throat Rad:	0.403 microns
Pore Radius Distributions	
Mean (arithmetic):	0.069 microns
Mean (geometric):	0.037 microns
Mean (harmonic):	0.019 microns
Micropores - Pore throat radius < .1 micron:	77.692 % PV
Intermediate - Pore throat radius .1<r<3 micron:	22.308 % PV
Macropores - Pore throat radius > 3 micron:	0.000 % PV
Swanson Parameter[1]	
(Sb/Pc)max:	0.003
Kbrine Swanson:	0.004 md
Kair Swanson:	0.026 md

TABLE 10-2. MERCURY INJECTION DATA FOR SAMPLE ID M1

Hg/air Pres. psi	Equivalent Air/brine Pres. psi	Height above Free Wtr. ft.	Pore radius Aperture microns	Hg Volume Injected cm3	Hg Sat. Pore Volume %	1-Hg Sat. Pore Volume %	Hg Porosity Injected %
0.5	0.10	0.13	169.5136	0.0000	0.0000	100.0	0.0000
0.6	0.11	0.14	156.4327	0.0000	0.0000	100.0	0.0000
0.6	0.12	0.16	141.9218	0.0000	0.0000	100.0	0.0000
0.7	0.14	0.17	129.5040	0.0000	0.0000	100.0	0.0000
0.8	0.15	0.19	117.9952	0.0000	0.0000	100.0	0.0000
0.8	0.16	0.21	107.3506	0.0000	0.0000	100.0	0.0000
0.9	0.18	0.23	97.7890	0.0000	0.0000	100.0	0.0000
1.0	0.20	0.25	89.1217	0.0000	0.0000	100.0	0.0000
1.1	0.22	0.28	81.0301	0.0000	0.0000	100.0	0.0000
1.2	0.24	0.30	73.9228	0.0000	0.0000	100.0	0.0000
1.3	0.26	0.33	67.1775	0.0000	0.0000	100.0	0.0000
1.5	0.29	0.37	61.1721	0.0000	0.0000	100.0	0.0000
1.6	0.32	0.40	55.6623	0.0000	0.0000	100.0	0.0000
1.8	0.35	0.44	50.6258	0.0000	0.0000	100.0	0.0000
2.0	0.4	0.49	46.0914	0.0000	0.0000	100.0	0.0000
2.2	0.4	0.53	41.9431	0.0000	0.0000	100.0	0.0000
2.4	0.5	0.59	38.1642	0.0000	0.0000	100.0	0.0000
2.6	0.5	0.64	34.7007	0.0000	0.0000	100.0	0.0000
2.9	0.6	0.71	31.5702	0.0000	0.0000	100.0	0.0000
3.1	0.6	0.78	28.7335	0.0000	0.0000	100.0	0.0000
3.5	0.7	0.86	26.1261	0.0000	0.0000	100.0	0.0000
3.8	0.7	0.94	23.7571	0.0000	0.0000	100.0	0.0000
4.2	0.8	1.04	21.5651	0.0000	0.0000	100.0	0.0000
4.6	0.9	1.14	19.5946	0.0000	0.0000	100.0	0.0000
5.1	1.0	1.26	17.7836	0.0000	0.0000	100.0	0.0000
5.6	1.1	1.38	16.1472	0.0000	0.0000	100.0	0.0000
6.2	1.2	1.52	14.6658	0.0000	0.0000	100.0	0.0000
6.8	1.3	1.68	13.3128	0.0000	0.0000	100.0	0.0000
7.5	1.5	1.85	12.0886	0.0000	0.0000	100.0	0.0000
8.2	1.6	2.04	10.9749	0.0000	0.0000	100.0	0.0000
9.1	1.8	2.24	9.9667	0.0000	0.0000	100.0	0.0000
10.0	2.0	2.47	9.0520	0.0000	0.0000	100.0	0.0000
11.0	2.2	2.72	8.2195	0.0000	0.0000	100.0	0.0000
12.1	2.4	3.00	7.4613	0.0000	0.0000	100.0	0.0000
13.3	2.6	3.3	6.7766	0.0000	0.0000	100.0	0.0000
14.7	2.9	3.6	6.1538	0.0000	0.0000	100.0	0.0000
16.2	3.2	4.0	5.5877	0.0000	0.0000	100.0	0.0000
17.8	3.5	4.4	5.0739	0.0000	0.0000	100.0	0.0000
19.7	3.9	4.9	4.5944	0.0000	0.0000	100.0	0.0000
21.7	4.2	5.4	4.1723	0.0000	0.0000	100.0	0.0000
23.9	4.7	5.9	3.7912	0.0000	0.0000	100.0	0.0000
26.3	5.1	6.5	3.4415	0.0000	0.0000	100.0	0.0000
28.9	5.7	7.2	3.1243	0.0000	0.0000	100.0	0.0000
31.9	6.2	7.9	2.8372	0.0000	0.0000	100.0	0.0000
35.1	6.9	8.7	2.5757	0.0000	0.0000	100.0	0.0000
39.2	7.7	9.7	2.3081	0.0000	0.0000	100.0	0.0000
42.9	8.4	10.6	2.1099	0.0000	0.0000	100.0	0.0000
47.9	9.4	11.8	1.8878	0.0000	0.0000	100.0	0.0000
52.8	10.3	13.0	1.7142	0.0000	0.0000	100.0	0.0000
59.4	11.6	14.7	1.5235	0.0000	0.0000	100.0	0.0000
64.9	12.7	16.0	1.3934	0.0000	0.0000	100.0	0.0000
72.4	14.2	17.9	1.2494	0.0000	0.0000	100.0	0.0000
81.7	16.0	20.2	1.1066	0.0000	0.0000	100.0	0.0000
87.8	17.2	21.7	1.0300	0.0000	0.0000	100.0	0.0000
98.3	19.2	24.3	0.9203	0.0000	0.0000	100.0	0.0000
107.6	21.1	26.6	0.8402	0.0000	0.0000	100.0	0.0000
119.6	23.4	29.6	0.7559	0.0000	0.0000	100.0	0.0000
133.7	26.2	33.1	0.6762	0.0000	0.0000	100.0	0.0000
146.5	28.7	36.2	0.6172	0.0000	0.0000	100.0	0.0000

TABLE 10-2. MERCURY INJECTION DATA FOR SAMPLE ID M1 - CONTINUED

Hg/air Pres. psi	Equivalent Air/brine Pres. psi	Height above Free Wtr. ft.	Pore radius Aperture microns	Hg Volume Injected cm3	Hg Sat. Pore Volume %	1-Hg Sat. Pore Volume %	Hg Porosity Injected %
161.7	31.7	40	0.5591	0.0000	0.0000	100.0	0.0000
178.5	35.0	44	0.5065	0.0000	0.0000	100.0	0.0000
197.1	38.6	49	0.4587	0.0000	0.0000	100.0	0.0000
217.5	42.6	54	0.4158	0.0000	0.0000	100.0	0.0000
239.5	46.9	59	0.3776	0.0000	0.0000	100.0	0.0000
264.3	52	65	0.3422	0.0017	1.3514	98.6	0.1722
291.1	57	72	0.3107	0.0018	2.7751	97.2	0.1814
321.7	63	80	0.2811	0.0018	4.2074	95.8	0.1825
355.0	70	88	0.2547	0.0018	5.6669	94.3	0.1860
393.1	77	97	0.2300	0.0022	7.4415	92.6	0.2261
431.2	84	107	0.2097	0.0018	8.8890	91.1	0.1845
474.9	93	117	0.1904	0.0022	10.6554	89.3	0.2251
525.4	103	130	0.1721	0.0023	12.4769	87.5	0.2321
576.9	113	143	0.1568	0.0022	14.2378	85.8	0.2244
635.8	125	157	0.1422	0.0018	15.6550	84.3	0.1806
701.0	137	173	0.1290	0.0025	17.6380	82.4	0.2527
771.9	151	191	0.1171	0.0030	20.0168	80.0	0.3031
851.4	167	210	0.1062	0.0028	22.2492	77.8	0.2845
938.2	184	232	0.0964	0.0028	24.4706	75.5	0.2831
1033.8	202	256	0.0875	0.0029	26.8175	73.2	0.2991
1139.2	223	282	0.0794	0.0032	29.4065	70.6	0.3299
1253.8	246	310	0.0721	0.0032	31.9645	68.0	0.3260
1380.9	270	341	0.0655	0.0035	34.7557	65.2	0.3557
1521.6	298	376	0.0594	0.0035	37.5487	62.5	0.3559
1676.2	328	414	0.0540	0.0036	40.4397	59.6	0.3684
1846.4	362	456	0.0490	0.0036	43.3613	56.6	0.3723
2033.3	398	503	0.0445	0.0038	46.4133	53.6	0.3889
2240.3	439	554	0.0404	0.0038	49.4569	50.5	0.3878
2467.2	483	610	0.0367	0.0036	52.3290	47.7	0.3660
2717.6	532	672	0.0333	0.0038	55.3613	44.6	0.3864
2993.2	586	740	0.0302	0.0039	58.4895	41.5	0.3986
3297.7	646	815	0.0274	0.0039	61.6064	38.4	0.3972
3631.2	711	898	0.0249	0.0036	64.4952	35.5	0.3681
4000.0	783	989	0.0226	0.0036	67.3751	32.6	0.3670
4405.7	863	1089	0.0205	0.0033	70.0489	30.0	0.3407
4846.1	949	1198	0.0187	0.0039	73.1929	26.8	0.4006
5337.5	1045	1320	0.0169	0.0031	75.6613	24.3	0.3145
5879.2	1151	1454	0.0154	0.0026	77.7885	22.2	0.2711
6475.1	1268	1601	0.0140	0.0026	79.8699	20.1	0.2652
7133.3	1397	1764	0.0127	0.0025	81.8692	18.1	0.2548
7858.2	1539	1943	0.0115	0.0024	83.7708	16.2	0.2423
8660.0	1696	2141	0.0104	0.0023	85.6126	14.4	0.2347
9539.9	1868	2359	0.0095	0.0017	87.0009	13.0	0.1769
10507.9	2058	2598	0.0086	0.0018	88.4887	11.5	0.1896
11576.2	2267	2862	0.0078	0.0020	90.0952	9.9	0.2047
12755.7	2498	3154	0.0071	0.0016	91.3557	8.6	0.1606
14052.4	2752	3474	0.0064	0.0015	92.5561	7.4	0.1530
15481.7	3031	3828	0.0058	0.0013	93.6351	6.4	0.1375
17052.3	3339	4216	0.0053	0.0012	94.6263	5.4	0.1263
18784.7	3678	4644	0.0048	0.0009	95.3657	4.6	0.0942
20700.7	4053	5118	0.0044	0.0010	96.1713	3.8	0.1027
22811.5	4467	5640	0.0040	0.0010	97.0122	3.0	0.1072
25130.9	4921	6213	0.0036	0.0010	97.8327	2.2	0.1045
27683.3	5421	6844	0.0033	0.0005	98.2485	1.8	0.0530
30493.2	5971	7539	0.0030	0.0006	98.7139	1.3	0.0593
33589.2	6577	8304	0.0027	0.0006	99.1810	0.8	0.0595
36996.4	7244	9147	0.0024	0.0006	99.6355	0.4	0.0579
40738.8	7977	10072	0.0022	0.0000	99.6355	0.4	0.0000
44858.1	8784	11091	0.0020	0.0001	99.7287	0.3	0.0119
49946.2	11758	14821	0.0015	0.0005	100.0000	0.0	0.0471

FIGURE 10-1. MERCURY INJECTION CAPILLARY PRESSURE FOR SAMPLE ID M1

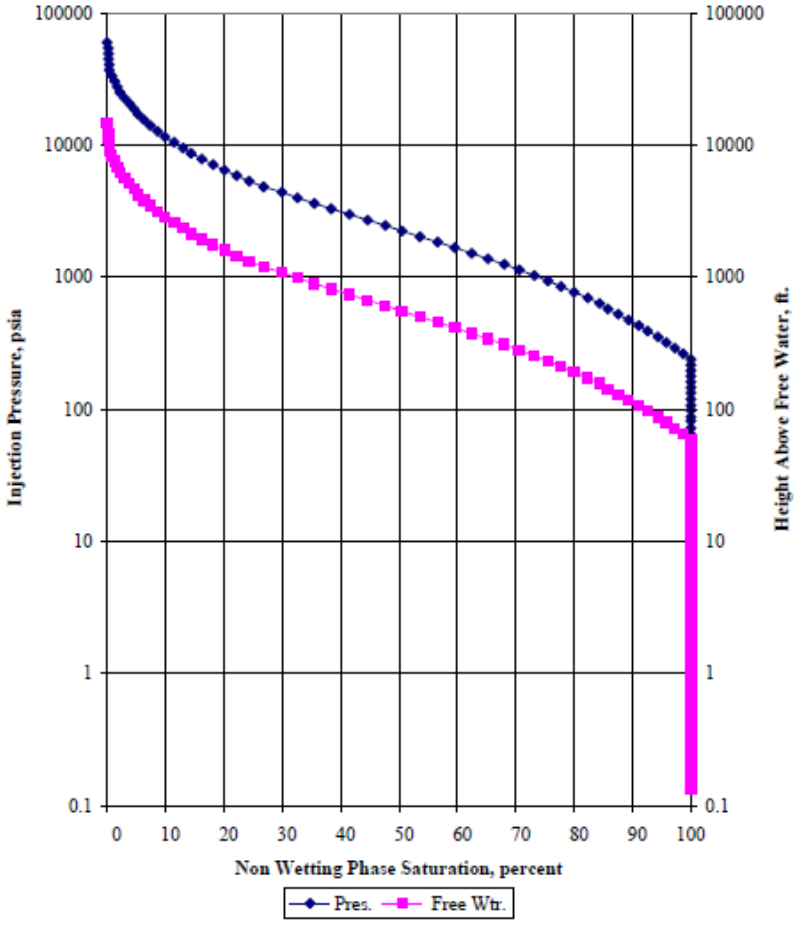
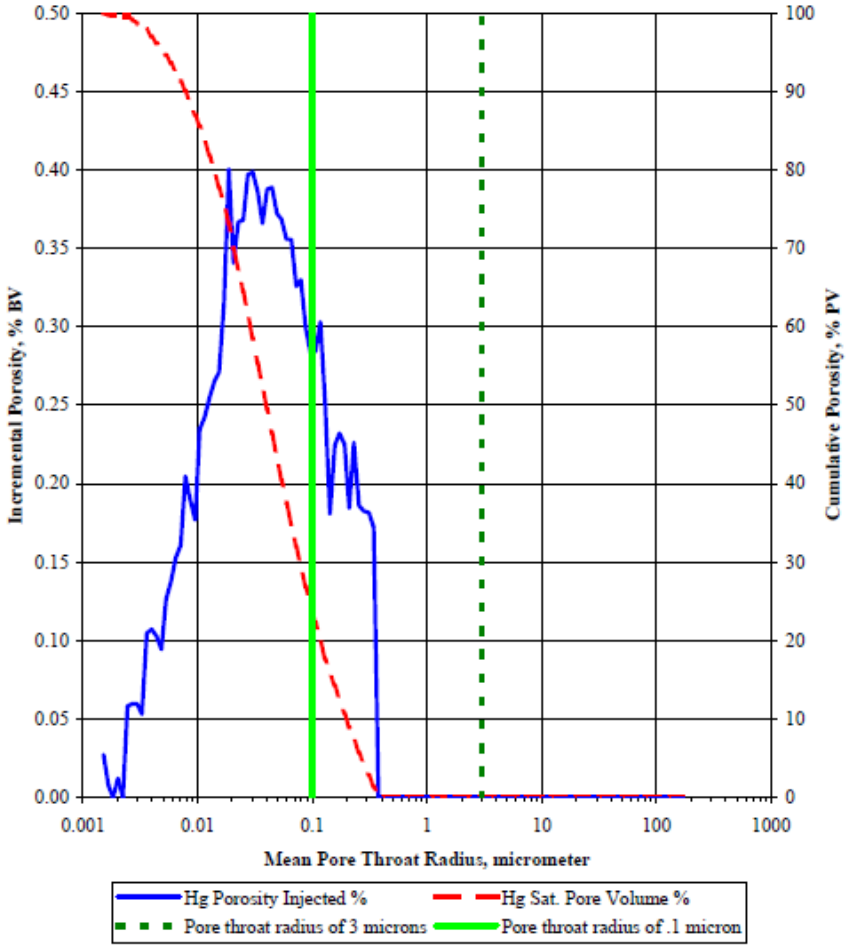


FIGURE 10-2. PORE THROAT DISTRIBUTION FOR SAMPLE ID M1



APPENDIX 11 - MICP - SAMPLE M2

TABLE OF CONTENTS i

LIST OF TABLES
TABLE 11-1. MERCURY INJECTION DATA SUMMARY FOR SAMPLE ID M2 1
TABLE 11-2. MERCURY INJECTION DATA FOR SAMPLE ID M2 2

LIST OF FIGURES
FIGURE 11-1. MERCURY INJECTION CAPILLARY PRESSURE FOR SAMPLE ID M2 4
FIGURE 11-2. PORE THROAT DISTRIBUTION FOR SAMPLE ID M2 5

TABLE 11-1. MERCURY INJECTION DATA SUMMARY FOR SAMPLE ID M2

Sample Info and Properties	
Depth:	8220-8250 ft
Well:	RSU#1
Formation:	Mowry 2
Porosity:	NA % @ 800 psi
Air Permeability:	NA md @ 800 psi
Klink. Permeability:	NA md @ 800 psi
Grain Density:	2.50 g/cm3

Mercury Injection Data	
IFT (σ):	485 dynes/cm
Contact angle (θ):	130 degrees
σcosθ Hg/air:	367.7 dynes/cm
σcosθ Air/brine:	72 dynes/cm
Total Pore Area:	11.765 m^2/g
Hg Porosity:	36.32 %
Corr. Hg Porosity:	15.25 %

Height Computation	
Water - Oil Reservoir System	
Res. Oil Grad:	0.360 psi/ft
Res. Wtr. Gradient:	0.470 psi/ft
σcosθ reservoir:	10.0 dynes/cm
Conversion Factor "C":	0.247 ft/psi

Computations	
Displacement Pressure (Pd)	
Mercury/Air:	473.68 psi
Air/Brine Equiv:	92.75 psi
Equiv. Height:	117.11 ft
Pr Throat Rad:	0.225 microns
Pore Radius Distributions	
Mean (arithmetic):	0.039 microns
Mean (geometric):	0.022 microns
Mean (harmonic):	0.012 microns
Micropores - Pore throat radius < .1 micron:	89.438 % PV
Intermediate - Pore throat radius .1<r<3 micron:	10.562 % PV
Macropores - Pore throat radius > 3 micron:	0.000 % PV
Swanson Parameter[1]	
(Sb/Pc)max:	0.002
Kbrine Swanson:	0.002 md
Kair Swanson:	0.013 md

TABLE 11-2. MERCURY INJECTION DATA FOR SAMPLE ID M2

Hg/air Pres. psi	Equivalent Air/brine Pres. psi	Height above Free Wtr. ft.	Pore radius Aperture microns	Hg Volume Injected cm3	Hg Sat. Pore Volume %	1-Hg Sat. Pore Volume %	Hg Porosity Injected %
0.5	0.10	0.13	169.5136	0.0000	0.0000	100.0	0.0000
0.6	0.11	0.14	156.4327	0.0000	0.0000	100.0	0.0000
0.6	0.12	0.16	141.9218	0.0000	0.0000	100.0	0.0000
0.7	0.14	0.17	129.5040	0.0000	0.0000	100.0	0.0000
0.8	0.15	0.19	117.9952	0.0000	0.0000	100.0	0.0000
0.8	0.16	0.21	107.3506	0.0000	0.0000	100.0	0.0000
0.9	0.18	0.23	97.7890	0.0000	0.0000	100.0	0.0000
1.0	0.20	0.25	89.1217	0.0000	0.0000	100.0	0.0000
1.1	0.22	0.28	81.0301	0.0000	0.0000	100.0	0.0000
1.2	0.24	0.30	73.9228	0.0000	0.0000	100.0	0.0000
1.3	0.26	0.33	67.1775	0.0000	0.0000	100.0	0.0000
1.5	0.29	0.37	61.1721	0.0000	0.0000	100.0	0.0000
1.6	0.32	0.40	55.6623	0.0000	0.0000	100.0	0.0000
1.8	0.35	0.44	50.6258	0.0000	0.0000	100.0	0.0000
2.0	0.4	0.49	46.0914	0.0000	0.0000	100.0	0.0000
2.2	0.4	0.53	41.9431	0.0000	0.0000	100.0	0.0000
2.4	0.5	0.59	38.1642	0.0000	0.0000	100.0	0.0000
2.6	0.5	0.64	34.7007	0.0000	0.0000	100.0	0.0000
2.9	0.6	0.71	31.5702	0.0000	0.0000	100.0	0.0000
3.1	0.6	0.78	28.7335	0.0000	0.0000	100.0	0.0000
3.5	0.7	0.86	26.1261	0.0000	0.0000	100.0	0.0000
3.8	0.7	0.94	23.7571	0.0000	0.0000	100.0	0.0000
4.2	0.8	1.04	21.5651	0.0000	0.0000	100.0	0.0000
4.6	0.9	1.14	19.5946	0.0000	0.0000	100.0	0.0000
5.1	1.0	1.26	17.7836	0.0000	0.0000	100.0	0.0000
5.6	1.1	1.38	16.1472	0.0000	0.0000	100.0	0.0000
6.2	1.2	1.52	14.6658	0.0000	0.0000	100.0	0.0000
6.8	1.3	1.68	13.3128	0.0000	0.0000	100.0	0.0000
7.5	1.5	1.85	12.0886	0.0000	0.0000	100.0	0.0000
8.2	1.6	2.04	10.9749	0.0000	0.0000	100.0	0.0000
9.1	1.8	2.24	9.9667	0.0000	0.0000	100.0	0.0000
10.0	2.0	2.47	9.0520	0.0000	0.0000	100.0	0.0000
11.0	2.2	2.72	8.2195	0.0000	0.0000	100.0	0.0000
12.1	2.4	3.00	7.4613	0.0000	0.0000	100.0	0.0000
13.3	2.6	3.3	6.7766	0.0000	0.0000	100.0	0.0000
14.7	2.9	3.6	6.1538	0.0000	0.0000	100.0	0.0000
16.2	3.2	4.0	5.5877	0.0000	0.0000	100.0	0.0000
17.8	3.5	4.4	5.0739	0.0000	0.0000	100.0	0.0000
19.7	3.9	4.9	4.5944	0.0000	0.0000	100.0	0.0000
21.7	4.2	5.4	4.1723	0.0000	0.0000	100.0	0.0000
23.9	4.7	5.9	3.7912	0.0000	0.0000	100.0	0.0000
26.3	5.1	6.5	3.4415	0.0000	0.0000	100.0	0.0000
28.9	5.7	7.2	3.1243	0.0000	0.0000	100.0	0.0000
31.9	6.2	7.9	2.8372	0.0000	0.0000	100.0	0.0000
35.1	6.9	8.7	2.5757	0.0000	0.0000	100.0	0.0000
38.2	7.5	9.4	2.3682	0.0000	0.0000	100.0	0.0000
41.9	8.2	10.3	2.1605	0.0000	0.0000	100.0	0.0000
46.9	9.2	11.6	1.9285	0.0000	0.0000	100.0	0.0000
51.7	10.1	12.8	1.7480	0.0000	0.0000	100.0	0.0000
58.3	11.4	14.4	1.5504	0.0000	0.0000	100.0	0.0000
63.9	12.5	15.8	1.4161	0.0000	0.0000	100.0	0.0000
71.3	14.0	17.6	1.2678	0.0000	0.0000	100.0	0.0000
80.7	15.8	19.9	1.1212	0.0000	0.0000	100.0	0.0000
86.7	17.0	21.4	1.0428	0.0000	0.0000	100.0	0.0000
97.2	19.0	24.0	0.9305	0.0000	0.0000	100.0	0.0000
106.5	20.9	26.3	0.8488	0.0000	0.0000	100.0	0.0000
118.5	23.2	29.3	0.7629	0.0000	0.0000	100.0	0.0000
132.6	26.0	32.8	0.6818	0.0000	0.0000	100.0	0.0000
145.4	28.5	35.9	0.6220	0.0000	0.0000	100.0	0.0000

TABLE 11-2. MERCURY INJECTION DATA FOR SAMPLE ID M2 - CONTINUED

Hg/air Pres. psi	Equivalent Air/brine Pres. psi	Height above Free Wtr. ft.	Pore radius Aperture microns	Hg Volume Injected cm3	Hg Sat. Pore Volume %	1-Hg Sat. Pore Volume %	Hg Porosity Injected %
160.6	31.4	40	0.5631	0.0000	0.0000	100.0	0.0000
177.4	34.7	44	0.5098	0.0000	0.0000	100.0	0.0000
196.0	38.4	48	0.4614	0.0000	0.0000	100.0	0.0000
216.3	42.4	53	0.4180	0.0000	0.0000	100.0	0.0000
238.3	46.7	59	0.3795	0.0000	0.0000	100.0	0.0000
263.1	52	65	0.3437	0.0000	0.0000	100.0	0.0000
289.9	57	72	0.3120	0.0000	0.0000	100.0	0.0000
320.5	63	79	0.2822	0.0000	0.0000	100.0	0.0000
353.8	69	87	0.2556	0.0000	0.0000	100.0	0.0000
391.9	77	97	0.2307	0.0000	0.0000	100.0	0.0000
429.9	84	106	0.2103	0.0000	0.0000	100.0	0.0000
473.7	93	117	0.1909	0.0018	1.2663	98.7	0.1931
524.1	103	130	0.1725	0.0019	2.5702	97.4	0.1988
575.6	113	142	0.1571	0.0019	3.9225	96.1	0.2062
634.6	124	157	0.1425	0.0020	5.3108	94.7	0.2117
699.7	137	173	0.1292	0.0021	6.7637	93.2	0.2215
770.6	151	191	0.1173	0.0022	8.2680	91.7	0.2294
850.1	166	210	0.1064	0.0023	9.8587	90.1	0.2425
936.9	183	232	0.0965	0.0024	11.5631	88.4	0.2599
1032.4	202	255	0.0876	0.0025	13.3345	86.7	0.2701
1137.8	223	281	0.0795	0.0028	15.2779	84.7	0.2963
1252.4	245	310	0.0722	0.0028	17.2614	82.7	0.3024
1379.5	270	341	0.0656	0.0031	19.4306	80.6	0.3308
1520.1	298	376	0.0595	0.0033	21.7326	78.3	0.3510
1674.7	328	414	0.0540	0.0035	24.1454	75.9	0.3679
1844.9	361	456	0.0490	0.0038	26.7954	73.2	0.4041
2031.8	398	502	0.0445	0.0039	29.5207	70.5	0.4155
2238.7	438	553	0.0404	0.0041	32.4103	67.6	0.4406
2465.6	483	610	0.0367	0.0043	35.3789	64.6	0.4526
2716.0	532	671	0.0333	0.0045	38.5031	61.5	0.4764
2991.5	586	740	0.0302	0.0046	41.6803	58.3	0.4844
3296.0	645	815	0.0274	0.0046	44.9133	55.1	0.4930
3629.5	711	897	0.0249	0.0046	48.1496	51.9	0.4935
3998.2	783	989	0.0226	0.0046	51.3781	48.6	0.4923
4403.9	862	1089	0.0205	0.0045	54.5327	45.5	0.4810
4844.2	949	1198	0.0187	0.0057	58.4861	41.5	0.6028
5335.6	1045	1319	0.0169	0.0042	61.4451	38.6	0.4512
5877.2	1151	1453	0.0154	0.0041	64.2757	35.7	0.4316
6473.1	1268	1600	0.0140	0.0039	66.9774	33.0	0.4119
7131.3	1396	1763	0.0127	0.0037	69.5875	30.4	0.3980
7856.2	1538	1942	0.0115	0.0035	72.0358	28.0	0.3733
8658.0	1695	2141	0.0104	0.0033	74.3533	25.6	0.3534
9537.8	1868	2358	0.0095	0.0032	76.6031	23.4	0.3430
10505.8	2057	2597	0.0086	0.0030	78.6933	21.3	0.3187
11574.0	2266	2862	0.0078	0.0029	80.7280	19.3	0.3102
12753.5	2497	3153	0.0071	0.0026	82.5663	17.4	0.2803
14050.2	2751	3474	0.0064	0.0026	84.3544	15.6	0.2726
15479.5	3031	3827	0.0058	0.0025	86.0837	13.9	0.2637
17050.0	3339	4215	0.0053	0.0024	87.7282	12.3	0.2507
18782.5	3678	4644	0.0048	0.0023	89.3153	10.7	0.2420
20698.5	4053	5117	0.0044	0.0022	90.8410	9.2	0.2326
22809.2	4466	5639	0.0040	0.0021	92.3048	7.7	0.2232
25128.6	4920	6213	0.0036	0.0020	93.6650	6.3	0.2074
27681.0	5420	6844	0.0033	0.0019	94.9888	5.0	0.2018
30490.8	5970	7538	0.0030	0.0016	96.1285	3.9	0.1738
33586.9	6577	8304	0.0027	0.0015	97.1844	2.8	0.1610
36994.0	7244	9146	0.0024	0.0011	97.9817	2.0	0.1216
40736.4	7977	10072	0.0022	0.0010	98.6738	1.3	0.1055
44855.7	8783	11090	0.0020	0.0007	99.1916	0.8	0.0789
59946.2	11738	14821	0.0015	0.0002	100.0000	0.0	0.0160

FIGURE 11-1. MERCURY INJECTION CAPILLARY PRESSURE FOR SAMPLE ID M2

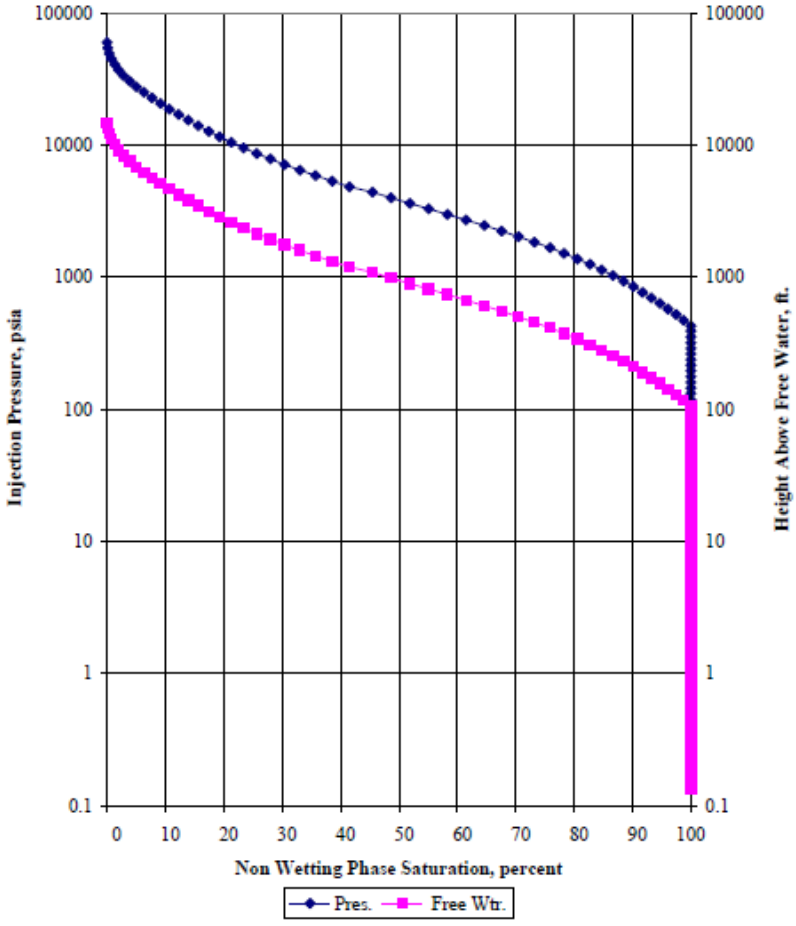
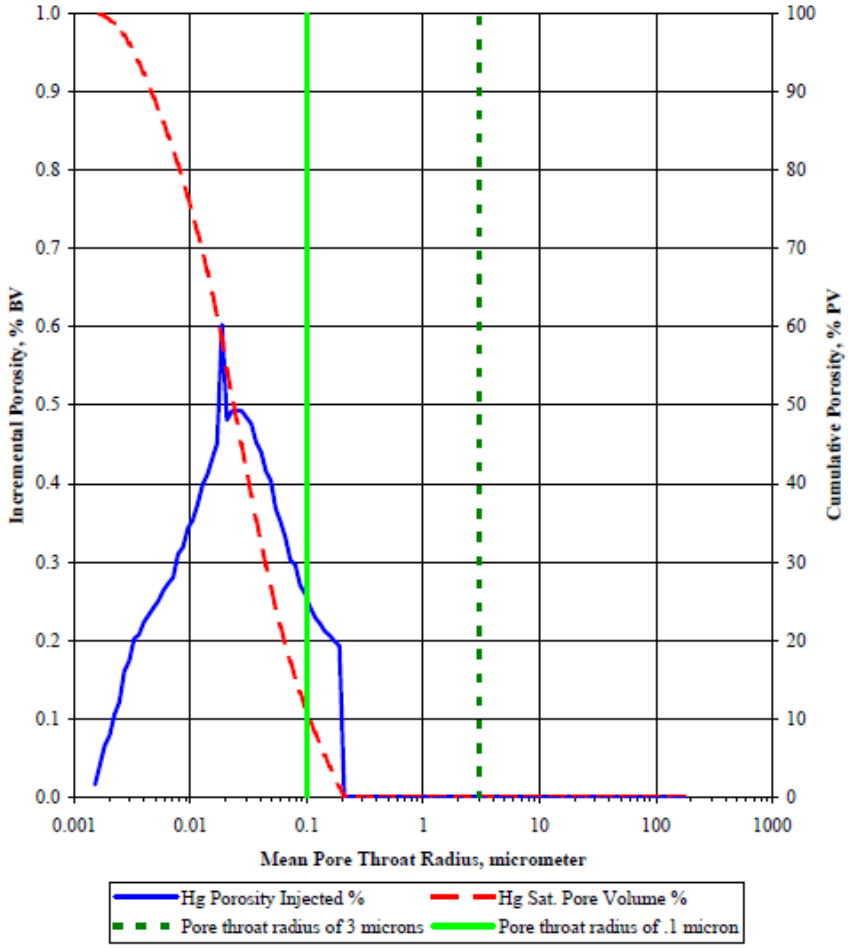


FIGURE 11-2. PORE THROAT DISTRIBUTION FOR SAMPLE ID M2



APPENDIX 12 - MICP - SAMPLE PH1

TABLE OF CONTENTS i

LIST OF TABLES
TABLE 12-1. MERCURY INJECTION DATA SUMMARY FOR SAMPLE ID PH1 1
TABLE 12-2. MERCURY INJECTION DATA FOR SAMPLE ID PH1 2

LIST OF FIGURES
FIGURE 12-1. MERCURY INJECTION CAPILLARY PRESSURE FOR SAMPLE ID PH1 4
FIGURE 12-2. PORE THROAT DISTRIBUTION FOR SAMPLE ID PH1 5

TABLE 12-1. MERCURY INJECTION DATA SUMMARY FOR SAMPLE ID PH1

Sample Info and Properties		Computations	
Depth:	11040-11050 ft	**Displacement Pressure (Pd)**	
Well:	RSU#1	Mercury/Air:	239.45 psi
Formation:	Phosphoria 1	Air/Brine Equiv:	46.89 psi
Porosity:	NA % @ 800 psi	Equiv. Height:	59.20 ft
Air Permeability:	NA md @ 800 psi	Pr Throat Rad:	0.445 microns
Klink. Permeability:	NA md @ 800 psi	**Pore Radius Distributions**	
Grain Density:	2.71 g/cm3	Mean (arithmetic):	0.086 microns
Mercury Injection Data		Mean (geometric):	0.053 microns
IFT (σ):	485 dynes/cm	Mean (harmonic):	0.029 microns
Contact angle (θ):	130 degrees	Micropores - Pore throat radius < .1 micron:	69.770 % PV
σcosθ Hg/air:	367.7 dynes/cm	Intermediate - Pore throat radius .1<r<3 micron:	30.230 % PV
σcosθ Air/brine:	72 dynes/cm	Macropores - Pore throat radius > 3 micron:	0.000 % PV
Total Pore Area:	7.379 m^2/g	**Swanson Parameter**[1]	
Hg Porosity:	44.31 %	(Sb/Pc)max:	0.008
Corr. Hg Porosity:	23.29 %	Kbrine Swanson:	0.024 md
Height Computation		Kair Swanson:	0.121 md
Water - Oil Reservoir System			
Res. Oil Grad:	0.360 psi/ft		
Res. Wtr. Gradient:	0.470 psi/ft		
σcosθ reservoir:	10.0 dynes/cm		
Conversion Factor "C":	0.247 ft/psi		

TABLE 12-2. MERCURY INJECTION DATA FOR SAMPLE ID PH1

Hg/air Pres. psi	Equivalent Air/brine Pres. psi	Height above Free Wtr. ft.	Pore radius Aperture microns	Hg Volume Injected cm3	Hg Sat. Pore Volume %	1-Hg Sat. Pore Volume %	Hg Porosity Injected %
0.5	0.10	0.13	168.6967	0.0000	0.0000	100.0	0.0000
0.6	0.11	0.14	156.0125	0.0000	0.0000	100.0	0.0000
0.6	0.12	0.16	141.7853	0.0000	0.0000	100.0	0.0000
0.7	0.14	0.17	129.3142	0.0000	0.0000	100.0	0.0000
0.8	0.15	0.19	117.9334	0.0000	0.0000	100.0	0.0000
0.8	0.16	0.21	107.3785	0.0000	0.0000	100.0	0.0000
0.9	0.18	0.23	97.6841	0.0000	0.0000	100.0	0.0000
1.0	0.20	0.25	88.9491	0.0000	0.0000	100.0	0.0000
1.1	0.22	0.28	81.1229	0.0000	0.0000	100.0	0.0000
1.2	0.24	0.30	73.8446	0.0000	0.0000	100.0	0.0000
1.3	0.26	0.33	67.2030	0.0000	0.0000	100.0	0.0000
1.5	0.29	0.37	61.0867	0.0000	0.0000	100.0	0.0000
1.6	0.32	0.40	55.6423	0.0000	0.0000	100.0	0.0000
1.8	0.35	0.44	50.6512	0.0000	0.0000	100.0	0.0000
2.0	0.4	0.49	46.0798	0.0000	0.0000	100.0	0.0000
2.2	0.4	0.53	41.9373	0.0000	0.0000	100.0	0.0000
2.4	0.5	0.59	38.1266	0.0000	0.0000	100.0	0.0000
2.6	0.5	0.64	34.6922	0.0000	0.0000	100.0	0.0000
2.9	0.6	0.71	31.5608	0.0000	0.0000	100.0	0.0000
3.1	0.6	0.78	28.7121	0.0000	0.0000	100.0	0.0000
3.5	0.7	0.86	26.1218	0.0000	0.0000	100.0	0.0000
3.8	0.7	0.94	23.7570	0.0000	0.0000	100.0	0.0000
4.2	0.8	1.04	21.5647	0.0000	0.0000	100.0	0.0000
4.6	0.9	1.14	19.5935	0.0000	0.0000	100.0	0.0000
5.1	1.0	1.26	17.7843	0.0000	0.0000	100.0	0.0000
5.6	1.1	1.38	16.1530	0.0000	0.0000	100.0	0.0000
6.2	1.2	1.52	14.6662	0.0000	0.0000	100.0	0.0000
6.8	1.3	1.68	13.3112	0.0000	0.0000	100.0	0.0000
7.5	1.5	1.85	12.0883	0.0000	0.0000	100.0	0.0000
8.2	1.6	2.04	10.9799	0.0000	0.0000	100.0	0.0000
9.1	1.8	2.24	9.9691	0.0000	0.0000	100.0	0.0000
10.0	2.0	2.47	9.0507	0.0000	0.0000	100.0	0.0000
11.0	2.2	2.72	8.2182	0.0000	0.0000	100.0	0.0000
12.1	2.4	3.00	7.4623	0.0000	0.0000	100.0	0.0000
13.3	2.6	3.3	6.7769	0.0000	0.0000	100.0	0.0000
14.7	2.9	3.6	6.1528	0.0000	0.0000	100.0	0.0000
16.2	3.2	4.0	5.5875	0.0000	0.0000	100.0	0.0000
17.8	3.5	4.4	5.0735	0.0000	0.0000	100.0	0.0000
19.6	3.8	4.9	4.6048	0.0000	0.0000	100.0	0.0000
21.7	4.2	5.4	4.1716	0.0000	0.0000	100.0	0.0000
23.9	4.7	5.9	3.7889	0.0000	0.0000	100.0	0.0000
26.3	5.1	6.5	3.4419	0.0000	0.0000	100.0	0.0000
28.9	5.7	7.2	3.1249	0.0000	0.0000	100.0	0.0000
31.9	6.2	7.9	2.8373	0.0000	0.0000	100.0	0.0000
35.1	6.9	8.7	2.5737	0.0000	0.0000	100.0	0.0000
38.5	7.5	9.5	2.3503	0.0000	0.0000	100.0	0.0000
42.5	8.3	10.5	2.1264	0.0000	0.0000	100.0	0.0000
47.6	9.3	11.8	1.9017	0.0000	0.0000	100.0	0.0000
53.2	10.4	13.2	1.6996	0.0000	0.0000	100.0	0.0000
59.0	11.6	14.6	1.5328	0.0000	0.0000	100.0	0.0000
65.2	12.8	16.1	1.3862	0.0000	0.0000	100.0	0.0000
71.2	13.9	17.6	1.2694	0.0000	0.0000	100.0	0.0000
80.3	15.7	19.9	1.1262	0.0000	0.0000	100.0	0.0000
88.0	17.2	21.8	1.0271	0.0000	0.0000	100.0	0.0000
98.3	19.2	24.3	0.9202	0.0000	0.0000	100.0	0.0000
108.5	21.2	26.8	0.8338	0.0000	0.0000	100.0	0.0000
120.1	23.5	29.7	0.7527	0.0000	0.0000	100.0	0.0000
132.3	25.9	32.7	0.6836	0.0000	0.0000	100.0	0.0000
146.2	28.6	36.2	0.6184	0.0000	0.0000	100.0	0.0000

TABLE 12-2. MERCURY INJECTION DATA FOR SAMPLE ID PH1 - CONTINUED

Hg/air Pres. psi	Equivalent Air/brine Pres. psi	Height above Free Wtr. ft.	Pore radius Aperture microns	Hg Volume Injected cm3	Hg Sat. Pore Volume %	1-Hg Sat. Pore Volume %	Hg Porosity Injected %
161.8	31.7	40	0.5590	0.0000	0.0000	100.0	0.0000
178.6	35.0	44	0.5064	0.0000	0.0000	100.0	0.0000
195.5	38.3	48	0.4625	0.0000	0.0000	100.0	0.0000
217.7	42.6	54	0.4153	0.0000	0.0000	100.0	0.0000
239.4	46.9	59	0.3777	0.0026	1.1225	98.9	0.2614
264.6	52	65	0.3418	0.0032	2.5128	97.5	0.3238
291.4	57	72	0.3104	0.0031	3.8629	96.1	0.3144
321.7	63	80	0.2811	0.0035	5.3724	94.6	0.3515
354.5	69	88	0.2551	0.0037	6.9816	93.0	0.3748
391.0	77	97	0.2313	0.0047	9.0247	91.0	0.4758
430.6	84	106	0.2100	0.0043	10.8987	89.1	0.4364
476.9	93	118	0.1896	0.0061	13.5516	86.4	0.6178
523.4	102	129	0.1728	0.0049	15.6797	84.3	0.4956
576.6	113	143	0.1568	0.0061	18.3103	81.7	0.6126
635.2	124	157	0.1424	0.0068	21.2677	78.7	0.6887
700.6	137	173	0.1291	0.0067	24.1568	75.8	0.6728
771.7	151	191	0.1172	0.0071	27.2219	72.8	0.7138
851.4	167	210	0.1062	0.0069	30.2304	69.8	0.7006
938.1	184	232	0.0964	0.0074	33.4192	66.6	0.7426
1033.7	202	256	0.0875	0.0074	36.6368	63.4	0.7493
1138.0	223	281	0.0795	0.0077	39.9582	60.0	0.7735
1254.4	246	310	0.0721	0.0075	43.2140	56.8	0.7582
1381.4	270	342	0.0655	0.0077	46.5649	53.4	0.7804
1521.8	298	376	0.0594	0.0077	49.8964	50.1	0.7759
1676.7	328	415	0.0539	0.0076	53.1939	46.8	0.7679
1845.9	361	456	0.0490	0.0074	56.4138	43.6	0.7499
2034.4	398	503	0.0445	0.0075	59.6569	40.3	0.7553
2240.4	439	554	0.0404	0.0072	62.7556	37.2	0.7216
2467.7	483	610	0.0366	0.0070	65.7703	34.2	0.7021
2717.9	532	672	0.0333	0.0068	68.7005	31.3	0.6824
2993.6	586	740	0.0302	0.0063	71.4410	28.6	0.6382
3297.3	646	815	0.0274	0.0062	74.1278	25.9	0.6257
3631.3	711	898	0.0249	0.0058	76.6358	23.4	0.5841
4000.1	783	989	0.0226	0.0054	78.9774	21.0	0.5453
4406.7	863	1089	0.0205	0.0051	81.1868	18.8	0.5145
4845.4	949	1198	0.0187	0.0057	83.6539	16.3	0.5745
5336.4	1045	1319	0.0169	0.0044	85.5720	14.4	0.4467
5876.3	1151	1453	0.0154	0.0037	87.1770	12.8	0.3738
6472.6	1267	1600	0.0140	0.0037	88.8000	11.2	0.3780
7134.7	1397	1764	0.0127	0.0033	90.2387	9.8	0.3351
7861.2	1539	1944	0.0115	0.0029	91.5064	8.5	0.2952
8659.5	1696	2141	0.0104	0.0027	92.6680	7.3	0.2705
9539.5	1868	2358	0.0095	0.0024	93.6993	6.3	0.2402
10510.9	2058	2599	0.0086	0.0023	94.7005	5.3	0.2332
11576.2	2267	2862	0.0078	0.0017	95.4234	4.6	0.1683
12754.0	2497	3153	0.0071	0.0019	96.2544	3.7	0.1935
14047.7	2751	3473	0.0064	0.0017	96.9719	3.0	0.1671
15479.7	3031	3827	0.0058	0.0014	97.5964	2.4	0.1454
17048.5	3338	4215	0.0053	0.0013	98.1590	1.8	0.1310
18784.7	3678	4644	0.0048	0.0015	98.7895	1.2	0.1468
20700.7	4053	5118	0.0044	0.0010	99.2164	0.8	0.0994
22810.7	4467	5640	0.0040	0.0002	99.3240	0.7	0.0251
25130.3	4921	6213	0.0036	0.0002	99.3890	0.6	0.0151
27683.5	5421	6844	0.0033	0.0001	99.4362	0.6	0.0110
30493.5	5971	7539	0.0030	0.0010	99.8732	0.1	0.1018
33587.3	6577	8304	0.0027	0.0000	99.8732	0.1	0.0000
36992.3	7244	9146	0.0024	0.0003	100.0000	0.0	0.0295
40732.7	7976	10071	0.0022	0.0000	100.0000	0.0	0.0000
44855.5	8783	11090	0.0020	0.0000	100.0000	0.0	0.0000
59952.6	11739	14822	0.0015	0.0000	100.0000	0.0	0.0000

FIGURE 12-1. MERCURY INJECTION CAPILLARY PRESSURE FOR SAMPLE ID PH1

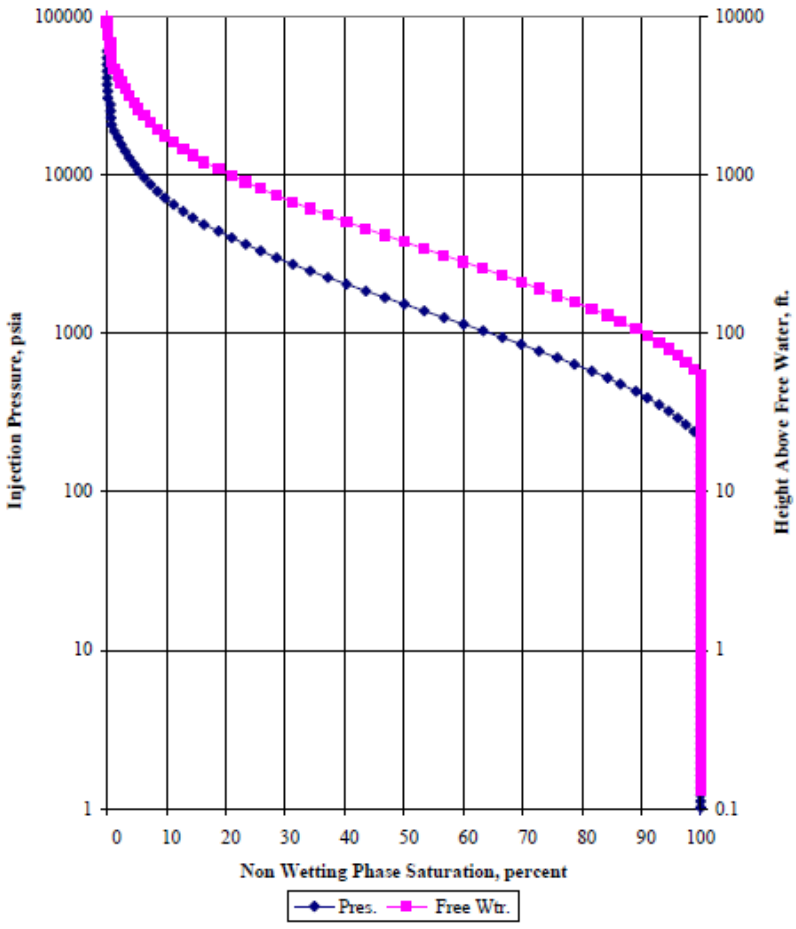
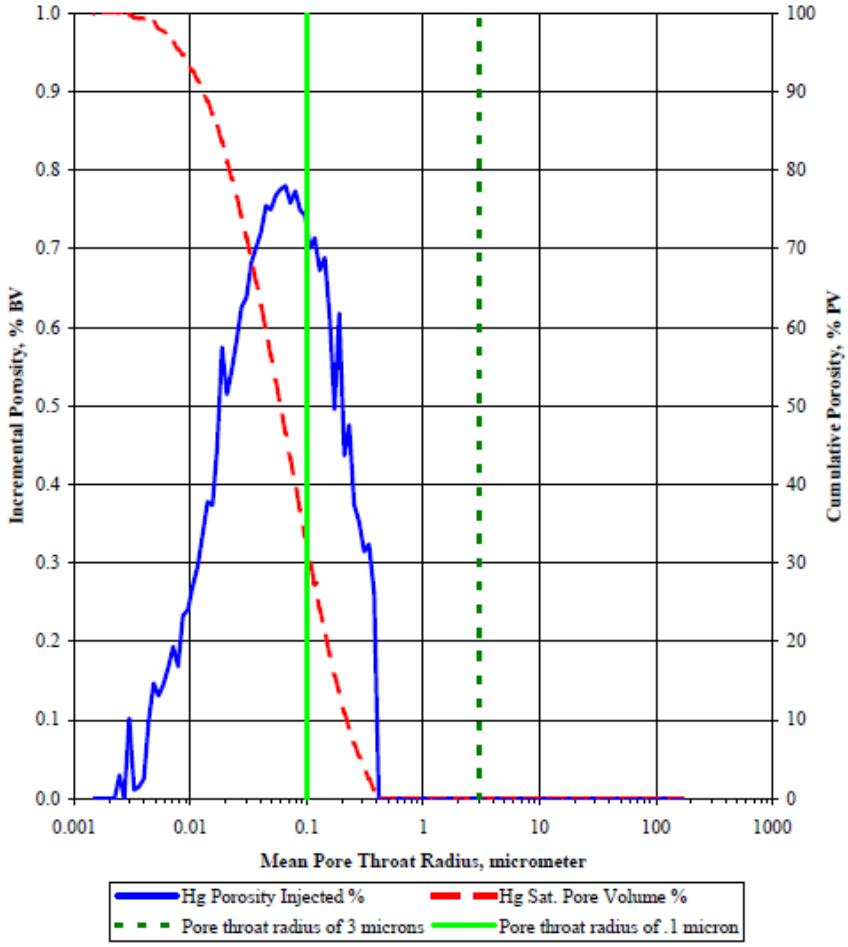


FIGURE 12-2. PORE THROAT DISTRIBUTION FOR SAMPLE ID PH1



APPENDIX 13 - MICP - SAMPLE PH2

TABLE OF CONTENTS i

LIST OF TABLES
TABLE 13-1. MERCURY INJECTION DATA SUMMARY FOR SAMPLE ID PH2 1
TABLE 13-2. MERCURY INJECTION DATA FOR SAMPLE ID PH2 2

LIST OF FIGURES
FIGURE 13-1. MERCURY INJECTION CAPILLARY PRESSURE FOR SAMPLE ID PH2 4
FIGURE 13-2. PORE THROAT DISTRIBUTION FOR SAMPLE ID PH2 5

TABLE 13-1. MERCURY INJECTION DATA SUMMARY FOR SAMPLE ID PH2

Sample Info and Properties		Computations	
Depth:	11140-11150 ft	**Displacement Pressure (Pd)**	
Well:	RSU#1	Mercury/Air:	194.40 psi
Formation:	Phosphoria 2	Air/Brine Equiv:	38.07 psi
Porosity:	NA % @ 800 psi	Equiv. Height:	48.06 ft
Air Permeability:	NA md @ 800 psi	Pr Throat Rad:	0.549 microns
Klink. Permeability:	NA md @ 800 psi	**Pore Radius Distributions**	
Grain Density:	2.65 g/cm3	Mean (arithmetic):	0.098 microns
Mercury Injection Data		Mean (geometric):	0.054 microns
IFT (σ):	485 dynes/cm	Mean (harmonic):	0.029 microns
Contact angle (θ):	130 degrees	Micropores - Pore throat radius < .1 micron:	67.981 % PV
σcosθ Hg/air:	367.7 dynes/cm	Intermediate - Pore throat radius .1<r<3 micron:	32.019 % PV
σcosθ Air/brine:	72 dynes/cm	Macropores - Pore throat radius > 3 micron:	0.000 % PV
Total Pore Area:	6.087 m^2/g	**Swanson Parameter**[1]	
Hg Porosity:	37.95 %	(Sb/Pc)max:	0.008
Corr. Hg Porosity:	19.71 %	Klorine Swanson:	0.020 md
Height Computation		Kair Swanson:	0.105 md
Water - Oil Reservoir System			
Res. Oil Grad:	0.360 psi/ft		
Res. Wtr. Gradient:	0.470 psi/ft		
σcosθ reservoir:	10.0 dynes/cm		
Conversion Factor "C":	0.247 ft/psi		

TABLE 13-2. MERCURY INJECTION DATA FOR SAMPLE ID PH2

Hg/air Pres. psi	Equivalent Air/brine Pres. psi	Height above Free Wtr. ft.	Pore radius Aperture microns	Hg Volume Injected cm3	Hg Sat. Pore Volume %	1-Hg Sat. Pore Volume %	Hg Porosity Injected %
0.5	0.10	0.13	168.6967	0.0000	0.0000	100.0	0.0000
0.6	0.11	0.14	156.0125	0.0000	0.0000	100.0	0.0000
0.6	0.12	0.16	141.7853	0.0000	0.0000	100.0	0.0000
0.7	0.14	0.17	129.3142	0.0000	0.0000	100.0	0.0000
0.8	0.15	0.19	117.9334	0.0000	0.0000	100.0	0.0000
0.8	0.16	0.21	107.3785	0.0000	0.0000	100.0	0.0000
0.9	0.18	0.23	97.6841	0.0000	0.0000	100.0	0.0000
1.0	0.20	0.25	88.9491	0.0000	0.0000	100.0	0.0000
1.1	0.22	0.28	81.1229	0.0000	0.0000	100.0	0.0000
1.2	0.24	0.30	73.8446	0.0000	0.0000	100.0	0.0000
1.3	0.26	0.33	67.2030	0.0000	0.0000	100.0	0.0000
1.5	0.29	0.37	61.0867	0.0000	0.0000	100.0	0.0000
1.6	0.32	0.40	55.6423	0.0000	0.0000	100.0	0.0000
1.8	0.35	0.44	50.6512	0.0000	0.0000	100.0	0.0000
2.0	0.4	0.49	46.0798	0.0000	0.0000	100.0	0.0000
2.2	0.4	0.53	41.9373	0.0000	0.0000	100.0	0.0000
2.4	0.5	0.59	38.1266	0.0000	0.0000	100.0	0.0000
2.6	0.5	0.64	34.6922	0.0000	0.0000	100.0	0.0000
2.9	0.6	0.71	31.5608	0.0000	0.0000	100.0	0.0000
3.1	0.6	0.78	28.7121	0.0000	0.0000	100.0	0.0000
3.5	0.7	0.86	26.1218	0.0000	0.0000	100.0	0.0000
3.8	0.7	0.94	23.7570	0.0000	0.0000	100.0	0.0000
4.2	0.8	1.04	21.5647	0.0000	0.0000	100.0	0.0000
4.6	0.9	1.14	19.5935	0.0000	0.0000	100.0	0.0000
5.1	1.0	1.26	17.7843	0.0000	0.0000	100.0	0.0000
5.6	1.1	1.38	16.1530	0.0000	0.0000	100.0	0.0000
6.2	1.2	1.52	14.6662	0.0000	0.0000	100.0	0.0000
6.8	1.3	1.68	13.3112	0.0000	0.0000	100.0	0.0000
7.5	1.5	1.85	12.0883	0.0000	0.0000	100.0	0.0000
8.2	1.6	2.04	10.9799	0.0000	0.0000	100.0	0.0000
9.1	1.8	2.24	9.9691	0.0000	0.0000	100.0	0.0000
10.0	2.0	2.47	9.0507	0.0000	0.0000	100.0	0.0000
11.0	2.2	2.72	8.2182	0.0000	0.0000	100.0	0.0000
12.1	2.4	3.00	7.4623	0.0000	0.0000	100.0	0.0000
13.3	2.6	3.3	6.7769	0.0000	0.0000	100.0	0.0000
14.7	2.9	3.6	6.1528	0.0000	0.0000	100.0	0.0000
16.2	3.2	4.0	5.5875	0.0000	0.0000	100.0	0.0000
17.8	3.5	4.4	5.0735	0.0000	0.0000	100.0	0.0000
19.6	3.8	4.9	4.6048	0.0000	0.0000	100.0	0.0000
21.7	4.2	5.4	4.1716	0.0000	0.0000	100.0	0.0000
23.9	4.7	5.9	3.7889	0.0000	0.0000	100.0	0.0000
26.3	5.1	6.5	3.4419	0.0000	0.0000	100.0	0.0000
28.9	5.7	7.2	3.1249	0.0000	0.0000	100.0	0.0000
31.9	6.2	7.9	2.8373	0.0000	0.0000	100.0	0.0000
35.1	6.9	8.7	2.5737	0.0000	0.0000	100.0	0.0000
37.5	7.3	9.3	2.4106	0.0000	0.0000	100.0	0.0000
41.6	8.1	10.3	2.1759	0.0000	0.0000	100.0	0.0000
46.6	9.1	11.5	1.9414	0.0000	0.0000	100.0	0.0000
52.2	10.2	12.9	1.7313	0.0000	0.0000	100.0	0.0000
58.0	11.4	14.3	1.5588	0.0000	0.0000	100.0	0.0000
64.2	12.6	15.9	1.4077	0.0000	0.0000	100.0	0.0000
70.2	13.8	17.4	1.2875	0.0000	0.0000	100.0	0.0000
79.3	15.5	19.6	1.1406	0.0000	0.0000	100.0	0.0000
87.0	17.0	21.5	1.0392	0.0000	0.0000	100.0	0.0000
97.2	19.0	24.0	0.9300	0.0000	0.0000	100.0	0.0000
107.4	21.0	26.6	0.8420	0.0000	0.0000	100.0	0.0000
119.1	23.3	29.4	0.7594	0.0000	0.0000	100.0	0.0000
131.2	25.7	32.4	0.6892	0.0000	0.0000	100.0	0.0000
145.1	28.4	35.9	0.6230	0.0000	0.0000	100.0	0.0000

TABLE 13-2. MERCURY INJECTION DATA FOR SAMPLE ID PH2 - CONTINUED

Hg/air Pres. psi	Equivalent Air/brine Pres. psi	Height above Free Wtr. ft.	Pore radius Aperture microns	Hg Volume Injected cm3	Hg Sat. Pore Volume %	1-Hg Sat. Pore Volume %	Hg Porosity Injected %
160.7	31.5	40	0.5628	0.0000	0.0000	100.0	0.0000
177.5	34.7	44	0.5096	0.0000	0.0000	100.0	0.0000
194.4	38.1	48	0.4652	0.0027	1.4601	98.5	0.2877
216.6	42.4	54	0.4176	0.0028	2.9790	97.0	0.2993
238.3	46.7	59	0.3795	0.0028	4.4986	95.5	0.2994
263.4	52	65	0.3433	0.0032	6.2251	93.8	0.3402
290.1	57	72	0.3117	0.0032	7.9602	92.0	0.3419
320.4	63	79	0.2822	0.0031	9.6785	90.3	0.3386
353.2	69	87	0.2560	0.0035	11.5743	88.4	0.3736
389.7	76	96	0.2320	0.0036	13.5592	86.4	0.3911
429.3	84	106	0.2107	0.0037	15.5852	84.4	0.3992
475.5	93	118	0.1902	0.0043	17.9401	82.1	0.4640
522.1	102	129	0.1732	0.0035	19.8707	80.1	0.3804
575.2	113	142	0.1572	0.0041	22.1132	77.9	0.4419
633.8	124	157	0.1427	0.0045	24.5596	75.4	0.4821
699.2	137	173	0.1293	0.0041	26.7856	73.2	0.4387
770.3	151	190	0.1174	0.0050	29.5096	70.5	0.5368
849.9	166	210	0.1064	0.0046	32.0189	68.0	0.4945
936.6	183	232	0.0966	0.0049	34.6958	65.3	0.5275
1032.1	202	255	0.0876	0.0050	37.4437	62.6	0.5415
1136.5	223	281	0.0796	0.0051	40.2454	59.8	0.5521
1252.8	245	310	0.0722	0.0052	43.0800	56.9	0.5586
1379.8	270	341	0.0655	0.0053	45.9757	54.0	0.5706
1520.2	298	376	0.0595	0.0053	48.8662	51.1	0.5696
1675.0	328	414	0.0540	0.0053	51.7669	48.2	0.5716
1844.2	361	456	0.0490	0.0053	54.6474	45.4	0.5676
2032.6	398	503	0.0445	0.0052	57.5085	42.5	0.5638
2238.7	438	553	0.0404	0.0052	60.3316	39.7	0.5563
2465.9	483	610	0.0367	0.0051	63.1379	36.9	0.5530
2716.1	532	672	0.0333	0.0049	65.8311	34.2	0.5307
2991.8	586	740	0.0302	0.0048	68.4515	31.5	0.5164
3295.4	645	815	0.0274	0.0047	71.0235	29.0	0.5068
3629.4	711	897	0.0249	0.0045	73.4779	26.5	0.4837
3998.1	783	988	0.0226	0.0043	75.8493	24.2	0.4673
4404.7	862	1089	0.0205	0.0041	78.0851	21.9	0.4406
4843.4	948	1197	0.0187	0.0050	80.8388	19.2	0.5426
5334.4	1045	1319	0.0170	0.0038	82.9175	17.1	0.4096
5874.3	1150	1452	0.0154	0.0035	84.8466	15.2	0.3801
6470.5	1267	1600	0.0140	0.0034	86.7172	13.3	0.3686
7132.6	1397	1763	0.0127	0.0033	88.5296	11.5	0.3572
7859.1	1539	1943	0.0115	0.0031	90.2368	9.8	0.3364
8657.4	1695	2140	0.0104	0.0029	91.8352	8.2	0.3150
9537.3	1868	2358	0.0095	0.0028	93.3421	6.7	0.2969
10508.7	2058	2598	0.0086	0.0026	94.7693	5.2	0.2812
11573.9	2266	2861	0.0078	0.0023	96.0431	4.0	0.2510
12751.7	2497	3153	0.0071	0.0020	97.1618	2.8	0.2205
14045.4	2750	3473	0.0064	0.0017	98.1003	1.9	0.1849
15477.5	3031	3827	0.0058	0.0013	98.7936	1.2	0.1366
17046.2	3338	4214	0.0053	0.0008	99.2475	0.8	0.0894
18782.4	3678	4644	0.0048	0.0006	99.5793	0.4	0.0654
20698.4	4053	5117	0.0044	0.0004	99.8073	0.2	0.0449
22808.5	4466	5639	0.0040	0.0002	99.9069	0.1	0.0196
25128.0	4920	6213	0.0036	0.0002	100.0000	0.0	0.0183
27681.2	5420	6844	0.0033	0.0000	100.0000	0.0	0.0000
30491.2	5971	7539	0.0030	0.0000	100.0000	0.0	0.0000
33585.0	6576	8303	0.0027	0.0000	100.0000	0.0	0.0000
36990.1	7243	9145	0.0024	0.0000	100.0000	0.0	0.0000
40730.5	7975	10070	0.0022	0.0000	100.0000	0.0	0.0000
44853.2	8783	11089	0.0020	0.0000	100.0000	0.0	0.0000
49390.4	11739	14822	0.0015	0.0000	100.0000	0.0	0.0000

FIGURE 13-1. MERCURY INJECTION CAPILLARY PRESSURE FOR SAMPLE ID PH2

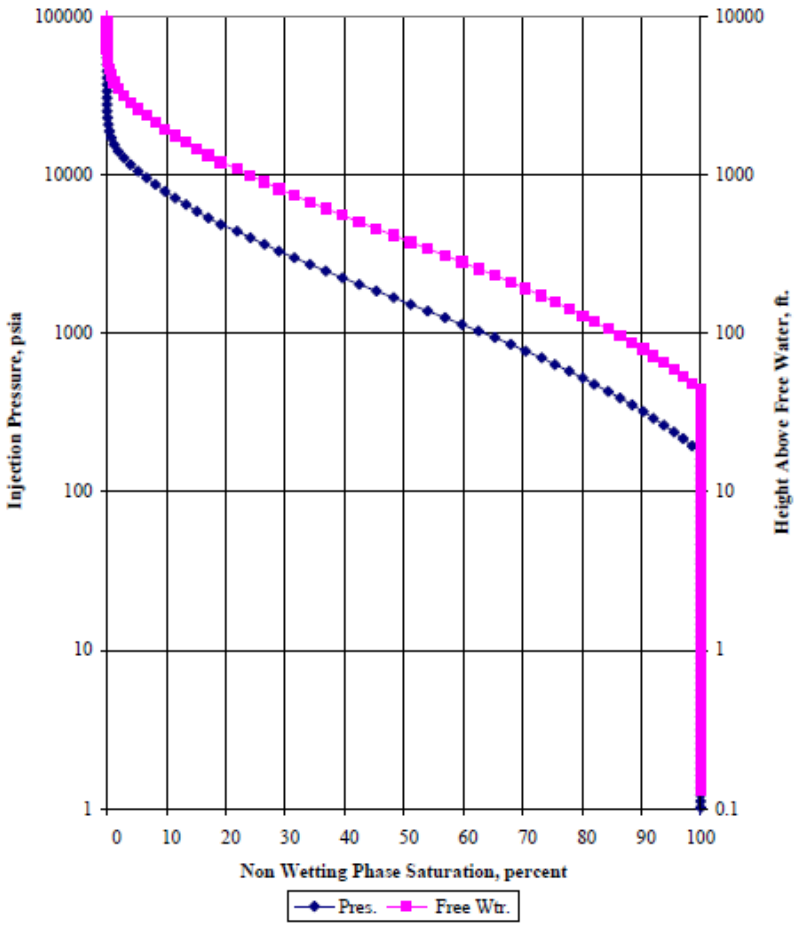
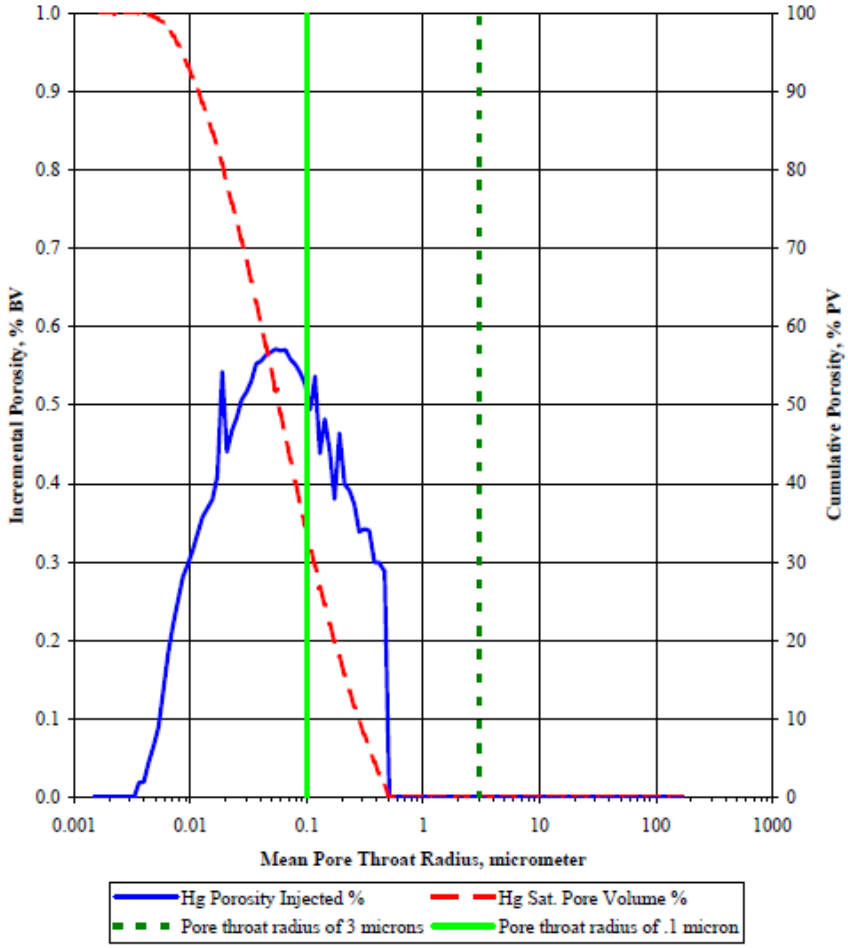


FIGURE 13-2. PORE THROAT DISTRIBUTION FOR SAMPLE ID PH2



Company: Univ. of Wyoming
Well: RSU #1
File: WTC-12-2873

Sample ID: 18
Depth, ft:
Permeability to Air, md: 0.003
Calculated Permeability to Air, md: 0.000
Helium Porosity, percent: 1.2
Mercury Porosity, %. 0.85
Mercury Pore Volume: 0.027
Helium Pore Volume: 0.039
Entry Pressure 1521.419

Injection Pressure (Absolute), psia	Non-Wetting Phase Saturation			Wetting Phase Saturation, fraction	Pore Throat Radius, microns	Leverett "J" Function	Capillary Pressure			Height Above Free Water	
	Incremental percent	Normalized Incremental percent	Cumulative percent				Gas/Water psi	Gas/Oil psi	Oil/water psi	Gas/Water feet	Oil/Water feet
0.5356	0.00	0.00	0.00	100.00	199.0943	0.00	0.09	0.03	0.04	0.26	1.13
0.5800	0.00	0.00	0.00	100.00	183.8469	0.00	0.10	0.03	0.05	0.28	1.23
0.6385	0.00	0.00	0.00	100.00	166.9872	0.00	0.11	0.04	0.05	0.31	1.35
0.6999	0.00	0.00	0.00	100.00	152.3489	0.00	0.12	0.04	0.06	0.33	1.48
0.7685	0.00	0.00	0.00	100.00	138.7452	0.00	0.13	0.04	0.06	0.37	1.63
0.8442	0.00	0.00	0.00	100.00	126.2991	0.00	0.14	0.05	0.07	0.40	1.79
0.9253	0.00	0.00	0.00	100.00	115.2317	0.00	0.16	0.05	0.08	0.44	1.96
1.0175	0.00	0.00	0.00	100.00	104.7914	0.00	0.17	0.06	0.08	0.49	2.15
1.1172	0.00	0.00	0.00	100.00	95.4400	0.00	0.19	0.06	0.09	0.53	2.36
1.2278	0.00	0.00	0.00	100.00	86.8455	0.00	0.21	0.07	0.10	0.59	2.60
1.3471	0.00	0.00	0.00	100.00	79.1513	0.00	0.23	0.08	0.11	0.64	2.85
1.4813	0.00	0.00	0.00	100.00	71.9841	0.00	0.25	0.08	0.12	0.71	3.14
1.6257	0.00	0.00	0.00	100.00	65.5886	0.00	0.28	0.09	0.14	0.78	3.44
1.7889	0.00	0.00	0.00	100.00	59.6047	0.00	0.31	0.10	0.15	0.86	3.79
1.9640	0.00	0.00	0.00	100.00	54.2904	0.00	0.34	0.11	0.16	0.94	4.16
2.1593	0.00	0.00	0.00	100.00	49.3795	0.00	0.37	0.12	0.18	1.03	4.57
2.3726	0.00	0.00	0.00	100.00	44.9404	0.00	0.41	0.14	0.20	1.14	5.02
2.6080	0.00	0.00	0.00	100.00	40.8849	0.00	0.45	0.15	0.22	1.25	5.52
2.8686	0.00	0.00	0.00	100.00	37.1708	0.00	0.49	0.16	0.24	1.37	6.07
3.1506	0.00	0.00	0.00	100.00	33.8437	0.00	0.54	0.18	0.26	1.51	6.67
3.4652	0.00	0.00	0.00	100.00	30.7704	0.00	0.59	0.20	0.29	1.66	7.34
3.8103	0.00	0.00	0.00	100.00	27.9841	0.01	0.65	0.22	0.32	1.82	8.07
4.1933	0.00	0.00	0.00	100.00	25.4278	0.01	0.72	0.24	0.35	2.01	8.88
4.6177	0.00	0.00	0.00	100.00	23.0910	0.01	0.79	0.26	0.38	2.21	9.77
5.0845	0.00	0.00	0.00	100.00	20.9711	0.01	0.87	0.29	0.42	2.43	10.76
5.6025	0.00	0.00	0.00	100.00	19.0322	0.01	0.96	0.32	0.47	2.68	11.86
6.1715	0.00	0.00	0.00	100.00	17.2774	0.01	1.06	0.35	0.51	2.95	13.06
6.7941	0.00	0.00	0.00	100.00	15.6940	0.01	1.16	0.39	0.57	3.25	14.38
7.4812	0.00	0.00	0.00	100.00	14.2526	0.01	1.28	0.43	0.62	3.58	15.84
8.2419	0.00	0.00	0.00	100.00	12.9372	0.01	1.41	0.47	0.69	3.94	17.45
9.0751	0.00	0.00	0.00	100.00	11.7494	0.01	1.56	0.52	0.76	4.34	19.21
9.9930	0.00	0.00	0.00	100.00	10.6701	0.01	1.71	0.57	0.83	4.78	21.15
11.0041	0.00	0.00	0.00	100.00	9.6897	0.01	1.89	0.63	0.92	5.26	23.29
12.1199	0.00	0.00	0.00	100.00	8.7977	0.02	2.08	0.69	1.01	5.80	25.66
13.3436	0.00	0.00	0.00	100.00	7.9909	0.02	2.29	0.76	1.11	6.38	28.25
14.6975	0.00	0.00	0.00	100.00	7.2547	0.02	2.52	0.84	1.22	7.03	31.11
16.1848	0.00	0.00	0.00	100.00	6.5881	0.02	2.77	0.92	1.35	7.74	34.26
17.8243	0.00	0.00	0.00	100.00	5.9821	0.02	3.06	1.02	1.49	8.53	37.73
19.6833	0.00	0.00	0.00	100.00	5.4171	0.03	3.37	1.12	1.64	9.42	41.67
21.6755	0.00	0.00	0.00	100.00	4.9192	0.03	3.72	1.24	1.81	10.37	45.88
23.8661	0.00	0.00	0.00	100.00	4.4677	0.03	4.09	1.36	1.99	11.42	50.52
26.2814	0.00	0.00	0.00	100.00	4.0571	0.04	4.51	1.50	2.19	12.57	55.63
28.9378	0.00	0.00	0.00	100.00	3.6847	0.04	4.96	1.65	2.41	13.85	61.25
31.8733	0.00	0.00	0.00	100.00	3.3453	0.04	5.46	1.82	2.66	15.25	67.47
35.1085	0.00	0.00	0.00	100.00	3.0371	0.05	6.02	2.01	2.93	16.80	74.32
36.1746	0.00	0.00	0.00	100.00	2.9476	0.05	6.20	2.07	3.01	17.31	76.57
41.2210	0.00	0.00	0.00	100.00	2.5867	0.06	7.07	2.36	3.44	19.72	87.26
42.4912	0.00	0.00	0.00	100.00	2.5094	0.06	7.28	2.43	3.54	20.33	89.94
48.3010	0.00	0.00	0.00	100.00	2.2076	0.06	8.28	2.76	4.02	23.11	102.24
53.0647	0.00	0.00	0.00	100.00	2.0094	0.07	9.10	3.03	4.42	25.39	112.33
59.0792	0.00	0.00	0.00	100.00	1.8048	0.08	10.13	3.38	4.92	28.27	125.06
65.4939	0.00	0.00	0.00	100.00	1.6280	0.09	11.23	3.74	5.46	31.34	138.64
73.0552	0.00	0.00	0.00	100.00	1.4595	0.10	12.52	4.17	6.09	34.95	154.64
80.8393	0.00	0.00	0.00	100.00	1.3190	0.11	13.86	4.62	6.74	38.68	171.12
88.3361	0.00	0.00	0.00	100.00	1.2071	0.12	15.14	5.05	7.36	42.26	186.99
98.3263	0.00	0.00	0.00	100.00	1.0844	0.13	16.86	5.62	8.19	47.04	208.13
107.8995	0.00	0.00	0.00	100.00	0.9882	0.14	18.50	6.17	8.99	51.62	228.40
120.1296	0.00	0.00	0.00	100.00	0.8876	0.16	20.59	6.86	10.01	57.48	254.29
132.1945	0.00	0.00	0.00	100.00	0.8066	0.18	22.66	7.55	11.02	63.25	279.83
146.3208	0.00	0.00	0.00	100.00	0.7287	0.20	25.08	8.36	12.19	70.01	309.73
161.8420	0.00	0.00	0.00	100.00	0.6588	0.22	27.74	9.25	13.49	77.43	342.58
178.2241	0.00	0.00	0.00	100.00	0.5983	0.24	30.55	10.18	14.85	85.27	377.26
196.8313	0.00	0.00	0.00	100.00	0.5417	0.26	33.74	11.25	16.40	94.17	416.65
217.7201	0.00	0.00	0.00	100.00	0.4897	0.29	37.32	12.44	18.14	104.17	460.86
240.3571	0.00	0.00	0.00	100.00	0.4436	0.32	41.20	13.73	20.03	115.00	508.78
264.5117	0.00	0.00	0.00	100.00	0.4031	0.35	45.34	15.11	22.04	126.55	559.91
291.4342	0.00	0.00	0.00	100.00	0.3659	0.39	49.96	16.65	24.29	139.43	616.90
321.3529	0.00	0.00	0.00	100.00	0.3318	0.43	55.09	18.36	26.78	153.75	680.23
354.1289	0.00	0.00	0.00	100.00	0.3011	0.47	60.71	20.24	29.51	169.43	749.61
391.1703	0.00	0.00	0.00	100.00	0.2726	0.52	67.06	22.35	32.60	187.15	828.02
430.8433	0.00	0.00	0.00	100.00	0.2475	0.58	73.86	24.62	35.90	206.13	912.00
474.7763	0.00	0.00	0.00	100.00	0.2246	0.63	81.39	27.13	39.56	227.15	1004.99
523.2123	0.00	0.00	0.00	100.00	0.2038	0.70	89.69	29.90	43.60	250.33	1107.52
576.9897	0.00	0.00	0.00	100.00	0.1848	0.77	98.91	32.97	48.08	276.06	1221.36
635.6848	0.00	0.00	0.00	100.00	0.1677	0.85	108.97	36.32	52.97	304.14	1345.60
700.6454	0.00	0.00	0.00	100.00	0.1522	0.94	120.11	40.04	58.39	335.22	1483.11
772.2783	0.00	0.00	0.00	100.00	0.1381	1.03	132.39	44.13	64.35	369.49	1634.74
851.3761	0.00	0.00	0.00	100.00	0.1252	1.14	145.95	48.65	70.95	407.34	1802.17
937.6433	0.00	0.00	0.00	100.00	0.1137	1.25	160.74	53.58	78.14	448.61	1984.78
1033.5782	0.00	0.00	0.00	100.00	0.1032	1.38	177.18	59.06	86.13	494.51	2187.85
1137.9362	0.00	0.00	0.00	100.00	0.0937	1.52	195.07	65.02	94.83	544.44	2408.76
1253.0435	0.00	0.00	0.00	100.00	0.0851	1.67	214.80	71.60	104.42	599.51	2652.41
1381.0278	0.00	0.00	0.00	100.00	0.0772	1.84	236.74	78.91	115.08	660.74	2923.33
1521.4187	2.22	0.44	2.22	97.78	0.0701	2.03	260.81	86.94	126.78	727.91	3220.50
1675.5696	2.83	0.56	5.05	94.95	0.0636	2.24	287.23	95.74	139.63	801.67	3546.81
1845.6757	3.01	0.59	8.06	91.94	0.0578	2.46	316.39	105.46	153.80	883.05	3906.88
2033.5968	3.16	0.62	11.23	88.77	0.0524	2.72	348.61	116.20	169.46	972.96	4304.67
2239.9856	2.98	0.58	14.20	85.80	0.0476	2.99	383.99	128.00	186.66	1071.71	4741.55
2467.3975	4.13	0.81	18.33	81.67	0.0432	3.29	422.97	140.99	205.61	1180.51	5222.93
2717.6853	3.73	0.73	22.06	77.94	0.0392	3.63	465.88	155.29	226.47	1300.26	5752.73
2992.9438	3.72	0.73	25.78	74.22	0.0356	4.00	513.06	171.02	249.41	1431.96	6335.39
3295.4351	4.08	0.80	29.86	70.14	0.0324	4.40	564.92	188.31	274.61	1576.68	6975.70
3631.1350	4.09	0.80	33.95	66.05	0.0294	4.85	622.47	207.49	302.59	1737.30	7686.30
4000.1035	4.50	0.88	38.45	61.55	0.0267	5.34	685.72	228.57	333.33	1913.83	8467.32
4399.0884	5.04	0.99	43.49	56.51	0.0242	5.87	754.11	251.37	366.58	2104.72	9311.88
4844.8032	5.10	1.00	48.59	51.41	0.0220	6.47	830.52	276.84	403.72	2317.97	10255.36
5337.7744	4.66	0.91	53.25	46.75	0.0200	7.13	915.03	305.01	444.80	2553.83	11298.87
5881.0239	5.01	0.98	58.25	41.75	0.0181	7.85	1008.15	336.05	490.07	2813.74	12448.81
6477.2456	3.59	0.70	61.84	38.16	0.0165	8.65	1110.36	370.12	539.76	3099.00	13710.88
7134.2490	3.44	0.68	65.29	34.71	0.0149	9.53	1222.98	407.66	594.51	3413.34	15101.61
7859.8921	2.62	0.51	67.91	32.09	0.0136	10.50	1347.38	449.13	654.98	3760.52	16637.63
8658.8096	2.04	0.40	69.95	30.05	0.0123	11.56	1484.33	494.78	721.55	4142.76	18328.76
9540.8369	2.01	0.39	71.96	28.04	0.0112	12.74	1635.53	545.18	795.05	4564.76	20195.81
10510.8027	0.99	0.19	72.95	27.05	0.0101	14.04	1801.81	600.60	875.88	5028.83	22249.01
11579.7461	1.79	0.35	74.75	25.25	0.0092	15.46	1985.05	661.68	964.96	5540.26	24511.73
12755.3135	2.51	0.49	77.26	22.74	0.0084	17.03	2186.57	728.86	1062.92	6102.70	27000.14
14051.1426	1.42	0.28	78.68	21.32	0.0076	18.76	2408.71	802.90	1170.90	6722.69	29743.12
15480.8340	1.49	0.29	80.17	19.83	0.0069	20.67	2653.79	884.60	1290.04	7406.71	32769.46
17053.5430	1.44	0.28	81.61	18.39	0.0063	22.77	2923.39	974.46	1421.09	8159.17	36098.53
18784.6504	1.26	0.25	82.87	17.13	0.0057	25.08	3220.15	1073.38	1565.35	8987.40	39762.89
20699.5781	1.92	0.38	84.79	15.21	0.0052	27.64	3548.41	1182.80	1724.92	9903.59	43816.37
22810.8965	0.96	0.19	85.76	14.24	0.0047	30.46	3910.35	1303.45	1900.86	10913.74	48285.56
25130.7520	0.36	0.07	86.12	13.88	0.0042	33.56	4308.03	1436.01	2094.18	12023.66	53196.17
27683.3887	1.59	0.31	87.71	12.29	0.0039	36.97	4745.61	1581.87	2306.89	13244.95	58599.53
30494.3184	3.11	0.61	90.82	9.18	0.0035	40.72	5227.47	1742.49	2541.13	14589.83	64549.64
33589.6914	1.89	0.37	92.71	7.29	0.0032	44.85	5758.10	1919.37	2799.07	16070.79	71101.85
36996.8477	1.37	0.27	94.08	5.92	0.0029	49.40	6342.17	2114.06	3083.00	17700.92	78314.03
40739.0547	0.55	0.11	94.63	5.37	0.0026	54.40	6983.67	2327.89	3394.84	19491.36	86235.45
44863.3477	1.01	0.20	95.64	4.36	0.0024	59.91	7690.68	2563.56	3738.52	21464.60	94965.65
49413.9414	0.67	0.13	96.31	3.69	0.0022	65.98	8470.76	2823.59	4117.73	23641.81	104598.24
54432.6992	3.03	0.60	99.35	0.65	0.0020	72.68	9331.10	3110.37	4535.95	26043.00	115221.82
59956.6172	0.65	0.13	100.00	0.00	0.0018	80.06	10278.03	3426.01	4996.27	28685.89	126914.72

Company: Univ. of Wyoming
Well: RSU #1
File: WTC-12-2873

Sample ID: 4
Depth, ft:
Permeability to Air, md:
Calculated Permeability to Air, md: 0.000
Helium Porosity, percent: 1.6
Mercury Porosity, %. 1.50
Mercury Pore Volume: 0.019
Helium Pore Volume: 0.062
Entry Pressure 1140.440

Incremental Pore Volume cc	Injection Pressure (Absolute), psia	Non-Wetting Phase Saturation			Wetting Phase Saturation, fraction	Pore Throat Radius, microns	Leverett "J" Function	Capillary Pressure			Height Above Free Water	
		Incremental percent	Normalized Incremental percent	Cumulative percent				Gas/Water psi	Gas/Oil psi	Oil/water psi	Gas/Water feet	Oil/Water feet
0.0000	0.5352	0.00	0.00	0.00	100.00	199.2387	0.00	0.09	0.03	0.04	0.26	1.13
0.0000	0.5799	0.00	0.00	0.00	100.00	183.8683	0.00	0.10	0.03	0.05	0.28	1.23
0.0000	0.6377	0.00	0.00	0.00	100.00	167.2137	0.00	0.11	0.04	0.05	0.31	1.35
0.0000	0.6989	0.00	0.00	0.00	100.00	152.5720	0.00	0.12	0.04	0.06	0.33	1.48
0.0000	0.7669	0.00	0.00	0.00	100.00	139.0312	0.00	0.13	0.04	0.06	0.37	1.62
0.0000	0.8445	0.00	0.00	0.00	100.00	126.2605	0.00	0.14	0.05	0.07	0.40	1.79
0.0000	0.9262	0.00	0.00	0.00	100.00	115.1199	0.00	0.16	0.05	0.08	0.44	1.96
0.0000	1.0156	0.00	0.00	0.00	100.00	104.9870	0.00	0.17	0.06	0.08	0.49	2.15
0.0000	1.1143	0.00	0.00	0.00	100.00	95.6911	0.00	0.19	0.06	0.09	0.53	2.36
0.0000	1.2274	0.00	0.00	0.00	100.00	86.8719	0.00	0.21	0.07	0.10	0.59	2.60
0.0000	1.3483	0.00	0.00	0.00	100.00	79.0840	0.00	0.23	0.08	0.11	0.65	2.85
0.0000	1.4802	0.00	0.00	0.00	100.00	72.0369	0.00	0.25	0.08	0.12	0.71	3.13
0.0000	1.6250	0.00	0.00	0.00	100.00	65.6162	0.00	0.28	0.09	0.14	0.78	3.44
0.0000	1.7869	0.00	0.00	0.00	100.00	59.6727	0.00	0.31	0.10	0.15	0.85	3.78
0.0000	1.9630	0.00	0.00	0.00	100.00	54.3179	0.00	0.34	0.11	0.16	0.94	4.16
0.0000	2.1578	0.00	0.00	0.00	100.00	49.4150	0.00	0.37	0.12	0.18	1.03	4.57
0.0000	2.3729	0.00	0.00	0.00	100.00	44.9349	0.00	0.41	0.14	0.20	1.14	5.02
0.0000	2.6068	0.00	0.00	0.00	100.00	40.9028	0.00	0.45	0.15	0.22	1.25	5.52
0.0000	2.8650	0.00	0.00	0.00	100.00	37.2177	0.00	0.49	0.16	0.24	1.37	6.06
0.0000	3.1506	0.00	0.00	0.00	100.00	33.8439	0.00	0.54	0.18	0.26	1.51	6.67
0.0000	3.4656	0.00	0.00	0.00	100.00	30.7669	0.01	0.59	0.20	0.29	1.66	7.34
0.0000	3.8079	0.00	0.00	0.00	100.00	28.0017	0.01	0.65	0.22	0.32	1.82	8.06
0.0000	4.1922	0.00	0.00	0.00	100.00	25.4345	0.01	0.72	0.24	0.35	2.01	8.87
0.0000	4.6171	0.00	0.00	0.00	100.00	23.0937	0.01	0.79	0.26	0.38	2.21	9.77
0.0000	5.0855	0.00	0.00	0.00	100.00	20.9667	0.01	0.87	0.29	0.42	2.43	10.76
0.0000	5.5993	0.00	0.00	0.00	100.00	19.0429	0.01	0.96	0.32	0.47	2.68	11.85
0.0000	6.1673	0.00	0.00	0.00	100.00	17.2891	0.01	1.06	0.35	0.51	2.95	13.05
0.0000	6.7957	0.00	0.00	0.00	100.00	15.6904	0.01	1.16	0.39	0.57	3.25	14.38
0.0000	7.4796	0.00	0.00	0.00	100.00	14.2557	0.01	1.28	0.43	0.62	3.58	15.83
0.0000	8.2378	0.00	0.00	0.00	100.00	12.9437	0.01	1.41	0.47	0.69	3.94	17.44
0.0000	9.0756	0.00	0.00	0.00	100.00	11.7487	0.01	1.56	0.52	0.76	4.34	19.21
0.0000	9.9940	0.00	0.00	0.00	100.00	10.6691	0.02	1.71	0.57	0.83	4.78	21.15
0.0000	11.0046	0.00	0.00	0.00	100.00	9.6893	0.02	1.89	0.63	0.92	5.27	23.29
0.0000	12.1192	0.00	0.00	0.00	100.00	8.7982	0.02	2.08	0.69	1.01	5.80	25.65
0.0000	13.3441	0.00	0.00	0.00	100.00	7.9906	0.02	2.29	0.76	1.11	6.38	28.25
0.0000	14.6949	0.00	0.00	0.00	100.00	7.2561	0.02	2.52	0.84	1.22	7.03	31.11
0.0000	16.1835	0.00	0.00	0.00	100.00	6.5886	0.02	2.77	0.92	1.35	7.74	34.26
0.0000	17.8302	0.00	0.00	0.00	100.00	5.9801	0.03	3.06	1.02	1.49	8.53	37.74
0.0000	19.6329	0.00	0.00	0.00	100.00	5.4310	0.03	3.37	1.12	1.64	9.39	41.56
0.0000	21.6700	0.00	0.00	0.00	100.00	4.9205	0.03	3.71	1.24	1.81	10.37	45.87
0.0000	23.8688	0.00	0.00	0.00	100.00	4.4672	0.04	4.09	1.36	1.99	11.42	50.52
0.0000	26.2740	0.00	0.00	0.00	100.00	4.0583	0.04	4.50	1.50	2.19	12.57	55.62
0.0000	28.9385	0.00	0.00	0.00	100.00	3.6846	0.04	4.96	1.65	2.41	13.85	61.26
0.0000	31.8714	0.00	0.00	0.00	100.00	3.3455	0.05	5.46	1.82	2.66	15.25	67.46
0.0000	35.1074	0.00	0.00	0.00	100.00	3.0372	0.05	6.02	2.01	2.93	16.80	74.31
0.0000	39.5611	0.00	0.00	0.00	100.00	2.6952	0.06	6.78	2.26	3.30	18.93	83.74
0.0000	44.1790	0.00	0.00	0.00	100.00	2.4135	0.07	7.57	2.52	3.68	21.14	93.52
0.0000	48.6312	0.00	0.00	0.00	100.00	2.1926	0.07	8.34	2.78	4.05	23.27	102.94
0.0000	54.1606	0.00	0.00	0.00	100.00	1.9687	0.08	9.28	3.09	4.51	25.91	114.65
0.0000	60.2937	0.00	0.00	0.00	100.00	1.7685	0.09	10.34	3.45	5.02	28.85	127.63
0.0000	66.5167	0.00	0.00	0.00	100.00	1.6030	0.10	11.40	3.80	5.54	31.82	140.80
0.0000	74.0928	0.00	0.00	0.00	100.00	1.4391	0.11	12.70	4.23	6.17	35.45	156.84
0.0000	81.6187	0.00	0.00	0.00	100.00	1.3064	0.12	13.99	4.66	6.80	39.05	172.77
0.0000	89.8993	0.00	0.00	0.00	100.00	1.1861	0.14	15.41	5.14	7.49	43.01	190.30
0.0000	99.4968	0.00	0.00	0.00	100.00	1.0717	0.15	17.06	5.69	8.29	47.60	210.61
0.0000	109.4868	0.00	0.00	0.00	100.00	0.9739	0.17	18.77	6.26	9.12	52.38	231.76
0.0000	121.1962	0.00	0.00	0.00	100.00	0.8798	0.18	20.78	6.93	10.10	57.99	256.55
0.0000	134.0772	0.00	0.00	0.00	100.00	0.7953	0.20	22.98	7.66	11.17	64.15	283.81
0.0000	147.8989	0.00	0.00	0.00	100.00	0.7209	0.22	25.35	8.45	12.32	70.76	313.07
0.0000	162.4138	0.00	0.00	0.00	100.00	0.6565	0.25	27.84	9.28	13.53	77.71	343.79
0.0000	180.2541	0.00	0.00	0.00	100.00	0.5915	0.27	30.90	10.30	15.02	86.24	381.56
0.0000	198.3603	0.00	0.00	0.00	100.00	0.5375	0.30	34.00	11.33	16.53	94.90	419.88
0.0000	218.6184	0.00	0.00	0.00	100.00	0.4877	0.33	37.48	12.49	18.22	104.60	462.77
0.0000	241.1820	0.00	0.00	0.00	100.00	0.4421	0.37	41.34	13.78	20.10	115.39	510.53
0.0000	266.0117	0.00	0.00	0.00	100.00	0.4008	0.40	45.60	15.20	22.17	127.27	563.09
0.0000	292.8062	0.00	0.00	0.00	100.00	0.3642	0.44	50.19	16.73	24.40	140.09	619.81
0.0000	323.1558	0.00	0.00	0.00	100.00	0.3300	0.49	55.40	18.47	26.93	154.61	684.05
0.0000	355.8335	0.00	0.00	0.00	100.00	0.2998	0.54	60.96	20.32	29.64	170.15	752.80
0.0000	392.5961	0.00	0.00	0.00	100.00	0.2716	0.60	67.30	22.43	32.72	187.84	831.04
0.0000	432.2816	0.00	0.00	0.00	100.00	0.2467	0.66	74.10	24.70	36.02	206.82	915.04
0.0000	475.9541	0.00	0.00	0.00	100.00	0.2240	0.72	81.59	27.20	39.66	227.72	1007.49
0.0000	524.9880	0.00	0.00	0.00	100.00	0.2031	0.80	90.00	30.00	43.75	251.18	1111.28
0.0000	578.1315	0.00	0.00	0.00	100.00	0.1844	0.88	99.11	33.04	48.18	276.60	1223.77
0.0000	637.7979	0.00	0.00	0.00	100.00	0.1672	0.97	109.33	36.44	53.15	305.15	1350.08
0.0000	701.8077	0.00	0.00	0.00	100.00	0.1519	1.06	120.31	40.10	58.48	335.78	1485.57
0.0000	773.4885	0.00	0.00	0.00	100.00	0.1379	1.17	132.59	44.20	64.46	370.07	1637.30
0.0000	852.6705	0.00	0.00	0.00	100.00	0.1251	1.29	146.17	48.72	71.05	407.96	1804.91
0.0000	939.7095	0.00	0.00	0.00	100.00	0.1135	1.42	161.09	53.70	78.31	449.60	1989.15
0.0000	1034.8668	0.00	0.00	0.00	100.00	0.1030	1.57	177.40	59.13	86.24	495.13	2190.58
0.0000	1140.4404	0.00	0.00	0.00	100.00	0.0935	1.73	195.50	65.17	95.03	545.64	2414.06
0.0000	1255.2491	0.00	0.00	0.00	100.00	0.0849	1.90	215.18	71.73	104.60	600.57	2657.08
0.0006	1383.1692	3.11	0.64	3.11	96.89	0.0771	2.10	237.11	79.04	115.26	661.77	2927.86
0.0002	1523.1829	1.29	0.27	4.40	95.60	0.0700	2.31	261.11	87.04	126.93	728.76	3224.24
0.0002	1677.2303	1.19	0.24	5.59	94.41	0.0636	2.54	287.52	95.84	139.77	802.46	3550.32
0.0003	1848.0651	1.32	0.27	6.91	93.09	0.0577	2.80	316.80	105.60	154.00	884.20	3911.94
0.0003	2036.1731	1.47	0.30	8.37	91.63	0.0524	3.09	349.05	116.35	169.68	974.19	4310.12
0.0003	2242.0073	1.35	0.28	9.72	90.28	0.0476	3.40	384.33	128.11	186.83	1072.68	4745.83
0.0003	2469.1345	1.48	0.30	11.20	88.80	0.0432	3.74	423.27	141.09	205.76	1181.34	5226.60
0.0003	2718.7278	1.68	0.35	12.88	87.12	0.0392	4.12	466.06	155.35	226.56	1300.76	5754.94
0.0003	2994.6660	1.71	0.35	14.59	85.41	0.0356	4.54	513.36	171.12	249.55	1432.78	6339.04
0.0003	3298.2808	1.81	0.37	16.39	83.61	0.0323	5.00	565.41	188.47	274.85	1578.04	6981.72
0.0004	3631.5916	1.96	0.41	18.36	81.64	0.0294	5.50	622.54	207.51	302.63	1737.51	7687.27
0.0004	4001.6211	2.06	0.43	20.42	79.58	0.0266	6.07	685.98	228.66	333.46	1914.55	8470.53
0.0005	4400.7041	2.56	0.53	22.98	77.02	0.0242	6.67	754.39	251.46	366.72	2105.49	9315.30
0.0005	4847.1104	2.42	0.50	25.40	74.60	0.0220	7.35	830.91	276.97	403.92	2319.07	10260.25
0.0004	5338.8242	2.27	0.47	27.67	72.33	0.0200	8.09	915.21	305.07	444.89	2554.33	11301.09
0.0004	5880.4819	1.91	0.39	29.58	70.42	0.0181	8.91	1008.06	336.02	490.03	2813.48	12447.66
0.0004	6474.8027	1.97	0.41	31.55	68.45	0.0165	9.81	1109.94	369.98	539.55	3097.83	13705.71
0.0004	7135.7119	1.84	0.38	33.38	66.62	0.0149	10.82	1223.24	407.75	594.63	3414.04	15104.70
0.0003	7860.8657	1.71	0.35	35.09	64.91	0.0136	11.91	1347.54	449.18	655.06	3760.98	16639.69
0.0004	8661.2998	1.86	0.38	36.96	63.04	0.0123	13.13	1484.76	494.92	721.76	4143.95	18334.03
0.0004	9543.1553	1.84	0.38	38.80	61.20	0.0112	14.46	1635.93	545.31	795.24	4565.87	20200.72
0.0004	10510.1396	2.05	0.42	40.85	59.15	0.0101	15.93	1801.70	600.57	875.82	5028.51	22247.61
0.0004	11577.5059	2.11	0.44	42.97	57.03	0.0092	17.55	1984.67	661.56	964.77	5539.19	24506.98
0.0004	12756.2148	2.15	0.44	45.12	54.88	0.0084	19.33	2186.73	728.91	1062.99	6103.14	27002.05
0.0005	14052.1982	2.40	0.49	47.52	52.48	0.0076	21.30	2408.89	802.96	1170.99	6723.19	29745.35
0.0005	15480.8477	2.52	0.52	50.03	49.97	0.0069	23.46	2653.80	884.60	1290.04	7406.72	32769.48
0.0005	17053.7637	2.77	0.57	52.80	47.20	0.0063	25.85	2923.43	974.48	1421.11	8159.27	36099.00
0.0006	18782.1738	3.05	0.63	55.85	44.15	0.0057	28.47	3219.72	1073.24	1565.14	8986.22	39757.65
0.0006	20698.1934	3.11	0.64	58.96	41.04	0.0052	31.37	3548.18	1182.73	1724.81	9902.93	43813.44
0.0007	22812.6484	3.52	0.73	62.48	37.52	0.0047	34.58	3910.65	1303.55	1901.01	10914.58	48289.26
0.0004	25130.6563	2.06	0.43	64.54	35.46	0.0042	38.09	4308.01	1436.00	2094.17	12023.61	53195.97
0.0007	27683.9023	3.69	0.76	68.23	31.77	0.0039	41.96	4745.70	1581.90	2306.94	13245.20	58600.62
0.0006	30494.0859	3.36	0.69	71.59	28.41	0.0035	46.22	5227.43	1742.48	2541.11	14589.71	64549.15
0.0007	33589.6523	3.37	0.70	74.96	25.04	0.0032	50.91	5758.09	1919.36	2799.07	16070.77	71101.77
0.0007	36997.6953	3.67	0.76	78.63	21.37	0.0029	56.08	6342.31	2114.10	3083.07	17701.33	78315.83
0.0008	40739.7266	3.91	0.81	82.54	17.46	0.0026	61.75	6983.79	2327.93	3394.90	19491.68	86236.87
0.0008	44861.8203	4.02	0.83	86.57	13.43	0.0024	68.00	7690.41	2563.47	3738.40	21463.87	94962.42
0.0008	49413.2109	4.08	0.84	90.65	9.35	0.0022	74.89	8470.63	2823.54	4117.67	23641.46	104596.69
0.0009	54432.4844	4.85	1.00	95.49	4.51	0.0020	82.50	9331.06	3110.35	4535.93	26042.90	115221.37
0.0009	59959.2188	4.51	0.93	100.00	0.00	0.0018	90.88	10278.48	3426.16	4996.48	28687.13	126920.23

Company: Univ. of Wyoming
Well: RSU #1
File: WTC-12-2873

Sample ID: 16
Depth, ft:
Permeability to Air, md:
Calculated Permeability to Air, md: 0.000
Helium Porosity, percent:
Mercury Porosity, %. 0.04
Mercury Pore Volume: 0.002
Helium Pore Volume: 0.045
Entry Pressure 2718.728

Injection Pressure (Absolute), psia	Non-Wetting Phase Saturation			Wetting Phase Saturation, fraction	Pore Throat Radius, microns	Leverett "J" Function	Capillary Pressure			Height Above Free Water	
	Incremental percent	Normalized Incremental percent	Cumulative percent				Gas/Water psi	Gas/Oil psi	Oil/water psi	Gas/Water feet	Oil/Water feet
0.5352	0.00	0.00	0.00	100.00	199.2387	0.00	0.09	0.03	0.04	0.26	1.13
0.5799	0.00	0.00	0.00	100.00	183.8683	0.00	0.10	0.03	0.05	0.28	1.23
0.6377	0.00	0.00	0.00	100.00	167.2137	0.00	0.11	0.04	0.05	0.31	1.35
0.6989	0.00	0.00	0.00	100.00	152.5720	0.00	0.12	0.04	0.06	0.33	1.48
0.7669	0.00	0.00	0.00	100.00	139.0312	0.00	0.13	0.04	0.06	0.37	1.62
0.8445	0.00	0.00	0.00	100.00	126.2605	0.00	0.14	0.05	0.07	0.40	1.79
0.9262	0.00	0.00	0.00	100.00	115.1199	0.00	0.16	0.05	0.08	0.44	1.96
1.0156	0.00	0.00	0.00	100.00	104.9870	0.00	0.17	0.06	0.08	0.49	2.15
1.1143	0.00	0.00	0.00	100.00	95.6911	0.00	0.19	0.06	0.09	0.53	2.36
1.2274	0.00	0.00	0.00	100.00	86.8719	0.00	0.21	0.07	0.10	0.59	2.60
1.3483	0.00	0.00	0.00	100.00	79.0840	0.00	0.23	0.08	0.11	0.65	2.85
1.4802	0.00	0.00	0.00	100.00	72.0369	0.00	0.25	0.08	0.12	0.71	3.13
1.6250	0.00	0.00	0.00	100.00	65.6162	0.00	0.28	0.09	0.14	0.78	3.44
1.7869	0.00	0.00	0.00	100.00	59.6727	0.00	0.31	0.10	0.15	0.85	3.78
1.9630	0.00	0.00	0.00	100.00	54.3179	0.00	0.34	0.11	0.16	0.94	4.16
2.1578	0.00	0.00	0.00	100.00	49.4150	0.00	0.37	0.12	0.18	1.03	4.57
2.3729	0.00	0.00	0.00	100.00	44.9349	0.00	0.41	0.14	0.20	1.14	5.02
2.6068	0.00	0.00	0.00	100.00	40.9028	0.00	0.45	0.15	0.22	1.25	5.52
2.8650	0.00	0.00	0.00	100.00	37.2177	0.00	0.49	0.16	0.24	1.37	6.06
3.1506	0.00	0.00	0.00	100.00	33.8439	0.00	0.54	0.18	0.26	1.51	6.67
3.4656	0.00	0.00	0.00	100.00	30.7669	0.00	0.59	0.20	0.29	1.66	7.34
3.8079	0.00	0.00	0.00	100.00	28.0017	0.00	0.65	0.22	0.32	1.82	8.06
4.1922	0.00	0.00	0.00	100.00	25.4345	0.00	0.72	0.24	0.35	2.01	8.87
4.6171	0.00	0.00	0.00	100.00	23.0937	0.00	0.79	0.26	0.38	2.21	9.77
5.0855	0.00	0.00	0.00	100.00	20.9667	0.00	0.87	0.29	0.42	2.43	10.76
5.5993	0.00	0.00	0.00	100.00	19.0429	0.00	0.96	0.32	0.47	2.68	11.85
6.1673	0.00	0.00	0.00	100.00	17.2891	0.00	1.06	0.35	0.51	2.95	13.05
6.7957	0.00	0.00	0.00	100.00	15.6904	0.00	1.16	0.39	0.57	3.25	14.38
7.4796	0.00	0.00	0.00	100.00	14.2557	0.00	1.28	0.43	0.62	3.58	15.83
8.2378	0.00	0.00	0.00	100.00	12.9437	0.00	1.41	0.47	0.69	3.94	17.44
9.0756	0.00	0.00	0.00	100.00	11.7487	0.00	1.56	0.52	0.76	4.34	19.21
9.9940	0.00	0.00	0.00	100.00	10.6691	0.00	1.71	0.57	0.83	4.78	21.15
11.0046	0.00	0.00	0.00	100.00	9.6893	0.00	1.89	0.63	0.92	5.27	23.29
12.1192	0.00	0.00	0.00	100.00	8.7982	0.00	2.08	0.69	1.01	5.80	25.65
13.3441	0.00	0.00	0.00	100.00	7.9906	0.00	2.29	0.76	1.11	6.38	28.25
14.6949	0.00	0.00	0.00	100.00	7.2561	0.00	2.52	0.84	1.22	7.03	31.11
16.1835	0.00	0.00	0.00	100.00	6.5886	0.00	2.77	0.92	1.35	7.74	34.26
17.8302	0.00	0.00	0.00	100.00	5.9801	0.00	3.06	1.02	1.49	8.53	37.74
19.6329	0.00	0.00	0.00	100.00	5.4310	0.00	3.37	1.12	1.64	9.39	41.56
21.6700	0.00	0.00	0.00	100.00	4.9205	0.00	3.71	1.24	1.81	10.37	45.87
23.8688	0.00	0.00	0.00	100.00	4.4672	0.00	4.09	1.36	1.99	11.42	50.52
26.2740	0.00	0.00	0.00	100.00	4.0583	0.00	4.50	1.50	2.19	12.57	55.62
28.9385	0.00	0.00	0.00	100.00	3.6846	0.00	4.96	1.65	2.41	13.85	61.26
31.8714	0.00	0.00	0.00	100.00	3.3455	0.00	5.46	1.82	2.66	15.25	67.46
35.1074	0.00	0.00	0.00	100.00	3.0372	0.00	6.02	2.01	2.93	16.80	74.31
39.5611	0.00	0.00	0.00	100.00	2.6952	0.00	6.78	2.26	3.30	18.93	83.74
44.1790	0.00	0.00	0.00	100.00	2.4135	0.00	7.57	2.52	3.68	21.14	93.52
48.6312	0.00	0.00	0.00	100.00	2.1926	0.00	8.34	2.78	4.05	23.27	102.94
54.1606	0.00	0.00	0.00	100.00	1.9687	0.00	9.28	3.09	4.51	25.91	114.65
60.2937	0.00	0.00	0.00	100.00	1.7685	0.00	10.34	3.45	5.02	28.85	127.63
66.5167	0.00	0.00	0.00	100.00	1.6030	0.00	11.40	3.80	5.54	31.82	140.80
74.0928	0.00	0.00	0.00	100.00	1.4391	0.00	12.70	4.23	6.17	35.45	156.84
81.6187	0.00	0.00	0.00	100.00	1.3064	0.00	13.99	4.66	6.80	39.05	172.77
89.8993	0.00	0.00	0.00	100.00	1.1861	0.00	15.41	5.14	7.49	43.01	190.30
99.4968	0.00	0.00	0.00	100.00	1.0717	0.00	17.06	5.69	8.29	47.60	210.61
109.4868	0.00	0.00	0.00	100.00	0.9739	0.00	18.77	6.26	9.12	52.38	231.76
121.1962	0.00	0.00	0.00	100.00	0.8798	0.00	20.78	6.93	10.10	57.99	256.55
134.0772	0.00	0.00	0.00	100.00	0.7953	0.00	22.98	7.66	11.17	64.15	283.81
147.8989	0.00	0.00	0.00	100.00	0.7209	0.00	25.35	8.45	12.32	70.76	313.07
162.4138	0.00	0.00	0.00	100.00	0.6565	0.00	27.84	9.28	13.53	77.71	343.79
180.2541	0.00	0.00	0.00	100.00	0.5915	0.00	30.90	10.30	15.02	86.24	381.56
198.3603	0.00	0.00	0.00	100.00	0.5375	0.00	34.00	11.33	16.53	94.90	419.88
218.6184	0.00	0.00	0.00	100.00	0.4877	0.00	37.48	12.49	18.22	104.60	462.77
241.1820	0.00	0.00	0.00	100.00	0.4421	0.00	41.34	13.78	20.10	115.39	510.53
266.0117	0.00	0.00	0.00	100.00	0.4008	0.00	45.60	15.20	22.17	127.27	563.09
292.8062	0.00	0.00	0.00	100.00	0.3642	0.00	50.19	16.73	24.40	140.09	619.81
323.1558	0.00	0.00	0.00	100.00	0.3300	0.00	55.40	18.47	26.93	154.61	684.05
355.6335	0.00	0.00	0.00	100.00	0.2998	0.00	60.96	20.32	29.64	170.15	752.80
392.5961	0.00	0.00	0.00	100.00	0.2716	0.00	67.30	22.43	32.72	187.84	831.04
432.2816	0.00	0.00	0.00	100.00	0.2467	0.00	74.10	24.70	36.02	206.82	915.04
475.9541	0.00	0.00	0.00	100.00	0.2240	0.00	81.59	27.20	39.66	227.72	1007.49
524.9880	0.00	0.00	0.00	100.00	0.2031	0.00	90.00	30.00	43.75	251.18	1111.28
578.1315	0.00	0.00	0.00	100.00	0.1844	0.00	99.11	33.04	48.18	276.60	1223.77
637.7979	0.00	0.00	0.00	100.00	0.1672	0.00	109.33	36.44	53.15	305.15	1350.08
701.8077	0.00	0.00	0.00	100.00	0.1519	0.00	120.31	40.10	58.48	335.78	1485.57
773.4885	0.00	0.00	0.00	100.00	0.1379	0.00	132.59	44.20	64.46	370.07	1637.30
852.6705	0.00	0.00	0.00	100.00	0.1251	0.00	146.17	48.72	71.05	407.96	1804.91
939.7095	0.00	0.00	0.00	100.00	0.1135	0.00	161.09	53.70	78.31	449.60	1989.15
1034.8668	0.00	0.00	0.00	100.00	0.1030	0.00	177.40	59.13	86.24	495.13	2190.58
1140.4404	0.00	0.00	0.00	100.00	0.0935	0.00	195.50	65.17	95.03	545.64	2414.06
1255.2491	0.00	0.00	0.00	100.00	0.0849	0.00	215.18	71.73	104.60	600.57	2657.08
1383.1692	0.00	0.00	0.00	100.00	0.0771	0.00	237.11	79.04	115.26	661.77	2927.86
1523.1829	0.00	0.00	0.00	100.00	0.0700	0.00	261.11	87.04	126.93	728.76	3224.24
1677.2303	0.00	0.00	0.00	100.00	0.0636	0.00	287.52	95.84	139.77	802.46	3550.32
1848.0651	0.00	0.00	0.00	100.00	0.0577	0.00	316.80	105.60	154.00	884.20	3911.94
2036.1731	0.00	0.00	0.00	100.00	0.0524	0.00	349.05	116.35	169.68	974.19	4310.12
2242.0073	0.00	0.00	0.00	100.00	0.0476	0.00	384.33	128.11	186.83	1072.68	4745.83
2469.1345	0.00	0.00	0.00	100.00	0.0432	0.00	423.27	141.09	205.76	1181.34	5226.60
2718.7278	0.00	0.00	0.00	100.00	0.0392	0.00	466.06	155.35	226.56	1300.76	5754.94
2994.6660	25.06	0.96	25.06	74.94	0.0356	0.00	513.36	171.12	249.55	1432.78	6339.04
3298.2808	8.76	0.33	33.83	66.17	0.0323	0.00	565.41	188.47	274.85	1578.04	6981.72
3631.5916	26.22	1.00	60.05	39.95	0.0294	0.00	622.54	207.51	302.63	1737.51	7687.27
4001.6211	2.12	0.08	62.17	37.83	0.0266	0.00	685.98	228.66	333.46	1914.55	8470.53
4400.7041	8.25	0.31	70.42	29.58	0.0242	0.00	754.39	251.46	366.72	2105.49	9315.30
4847.1104	7.09	0.27	77.51	22.49	0.0220	0.00	830.91	276.97	403.92	2319.07	10260.25
5338.8242	6.12	0.23	83.63	16.37	0.0200	0.00	915.21	305.07	444.89	2554.33	11301.09
5880.4819	1.97	0.07	85.60	14.40	0.0181	0.00	1008.06	336.02	490.03	2813.48	12447.66
6474.8027	2.71	0.10	88.30	11.70	0.0165	0.00	1109.94	369.98	539.55	3097.83	13705.71
7135.7119	1.02	0.04	89.32	10.68	0.0149	0.00	1223.24	407.75	594.63	3414.04	15104.70
7860.8657	5.77	0.22	95.10	4.90	0.0136	0.00	1347.54	449.18	655.06	3760.98	16639.69
8661.2998	4.90	0.19	100.00	0.00	0.0123	0.00	1484.76	494.92	721.76	4143.95	18334.03
9543.1553	0.00	0.00	100.00	0.00	0.0112	0.00	1635.93	545.31	795.24	4565.87	20200.72
10510.1396	0.00	0.00	100.00	0.00	0.0101	0.00	1801.70	600.57	875.82	5028.51	22247.61
11577.5059	0.00	0.00	100.00	0.00	0.0092	0.00	1984.67	661.56	964.77	5539.19	24506.98
12756.2148	0.00	0.00	100.00	0.00	0.0084	0.00	2186.73	728.91	1062.99	6103.14	27002.05
14052.1982	0.00	0.00	100.00	0.00	0.0076	0.00	2408.89	802.96	1170.99	6723.19	29745.35
15480.8477	0.00	0.00	100.00	0.00	0.0069	0.00	2653.80	884.60	1290.04	7406.72	32769.48
17053.7637	0.00	0.00	100.00	0.00	0.0063	0.00	2923.43	974.48	1421.11	8159.27	36099.00
18782.1738	0.00	0.00	100.00	0.00	0.0057	0.00	3219.72	1073.24	1565.14	8986.22	39757.65
20698.1934	0.00	0.00	100.00	0.00	0.0052	0.00	3548.18	1182.73	1724.81	9902.93	43813.44
22812.6484	0.00	0.00	100.00	0.00	0.0047	0.00	3910.65	1303.55	1901.01	10914.58	48289.26
25130.6563	0.00	0.00	100.00	0.00	0.0042	0.00	4308.01	1436.00	2094.17	12023.61	53195.97
27683.9023	0.00	0.00	100.00	0.00	0.0039	0.00	4745.70	1581.90	2306.94	13245.20	58600.62
30494.0859	0.00	0.00	100.00	0.00	0.0035	0.00	5227.43	1742.48	2541.11	14589.71	64549.15
33589.6523	0.00	0.00	100.00	0.00	0.0032	0.00	5758.09	1919.36	2799.07	16070.77	71101.77
36997.6953	0.00	0.00	100.00	0.00	0.0029	0.00	6342.31	2114.10	3083.07	17701.33	78315.83
40739.7266	0.00	0.00	100.00	0.00	0.0026	0.00	6983.79	2327.93	3394.90	19491.68	86236.87
44861.8203	0.00	0.00	100.00	0.00	0.0024	0.00	7690.41	2563.47	3738.40	21463.87	94962.42
49413.2109	0.00	0.00	100.00	0.00	0.0022	0.00	8470.63	2823.54	4117.67	23641.46	104596.69
54432.4844	0.00	0.00	100.00	0.00	0.0020	0.00	9331.06	3110.35	4535.93	26042.90	115221.37
59959.2188	0.00	0.00	100.00	0.00	0.0018	0.00	10278.48	3426.16	4996.48	28687.13	126920.23

Company: Univ. of Wyoming
Well: RSU #1
File: WTC-12-2873

Sample ID: 18
Depth, ft:
Permeability to Air, md: 0.003
Calculated Permeability to Air, md: 0.000
Helium Porosity, percent: 1.2
Mercury Porosity, %. 0.85
Mercury Pore Volume: 0.027
Helium Pore Volume: 0.039
Entry Pressure 1521.419

Injection Pressure (Absolute), psia	Non-Wetting Phase Saturation			Wetting Phase Saturation, fraction	Pore Throat Radius, microns	Leverett "J" Function	Capillary Pressure			Height Above Free Water	
	Incremental percent	Normalized Incremental percent	Cumulative percent				Gas/Water psi	Gas/Oil psi	Oil/water psi	Gas/Water feet	Oil/Water feet
0.5356	0.00	0.00	0.00	100.00	199.0943	0.00	0.09	0.03	0.04	0.26	1.13
0.5800	0.00	0.00	0.00	100.00	183.8469	0.00	0.10	0.03	0.05	0.28	1.23
0.6385	0.00	0.00	0.00	100.00	166.9872	0.00	0.11	0.04	0.05	0.31	1.35
0.6999	0.00	0.00	0.00	100.00	152.3489	0.00	0.12	0.04	0.06	0.33	1.48
0.7685	0.00	0.00	0.00	100.00	138.7452	0.00	0.13	0.04	0.06	0.37	1.63
0.8442	0.00	0.00	0.00	100.00	126.2991	0.00	0.14	0.05	0.07	0.40	1.79
0.9253	0.00	0.00	0.00	100.00	115.2317	0.00	0.16	0.05	0.08	0.44	1.96
1.0175	0.00	0.00	0.00	100.00	104.7914	0.00	0.17	0.06	0.08	0.49	2.15
1.1172	0.00	0.00	0.00	100.00	95.4400	0.00	0.19	0.06	0.09	0.53	2.36
1.2278	0.00	0.00	0.00	100.00	86.8455	0.00	0.21	0.07	0.10	0.59	2.60
1.3471	0.00	0.00	0.00	100.00	79.1513	0.00	0.23	0.08	0.11	0.64	2.85
1.4813	0.00	0.00	0.00	100.00	71.9841	0.00	0.25	0.08	0.12	0.71	3.14
1.6257	0.00	0.00	0.00	100.00	65.5886	0.00	0.28	0.09	0.14	0.78	3.44
1.7889	0.00	0.00	0.00	100.00	59.6047	0.00	0.31	0.10	0.15	0.86	3.79
1.9640	0.00	0.00	0.00	100.00	54.2904	0.00	0.34	0.11	0.16	0.94	4.16
2.1593	0.00	0.00	0.00	100.00	49.3795	0.00	0.37	0.12	0.18	1.03	4.57
2.3726	0.00	0.00	0.00	100.00	44.9404	0.00	0.41	0.14	0.20	1.14	5.02
2.6080	0.00	0.00	0.00	100.00	40.8849	0.00	0.45	0.15	0.22	1.25	5.52
2.8686	0.00	0.00	0.00	100.00	37.1708	0.00	0.49	0.16	0.24	1.37	6.07
3.1506	0.00	0.00	0.00	100.00	33.8437	0.00	0.54	0.18	0.26	1.51	6.67
3.4652	0.00	0.00	0.00	100.00	30.7704	0.00	0.59	0.20	0.29	1.66	7.34
3.8103	0.00	0.00	0.00	100.00	27.9841	0.01	0.65	0.22	0.32	1.82	8.07
4.1933	0.00	0.00	0.00	100.00	25.4278	0.01	0.72	0.24	0.35	2.01	8.88
4.6177	0.00	0.00	0.00	100.00	23.0910	0.01	0.79	0.26	0.38	2.21	9.77
5.0845	0.00	0.00	0.00	100.00	20.9711	0.01	0.87	0.29	0.42	2.43	10.76
5.6025	0.00	0.00	0.00	100.00	19.0322	0.01	0.96	0.32	0.47	2.68	11.86
6.1715	0.00	0.00	0.00	100.00	17.2774	0.01	1.06	0.35	0.51	2.95	13.06
6.7941	0.00	0.00	0.00	100.00	15.6940	0.01	1.16	0.39	0.57	3.25	14.38
7.4812	0.00	0.00	0.00	100.00	14.2526	0.01	1.28	0.43	0.62	3.58	15.84
8.2419	0.00	0.00	0.00	100.00	12.9372	0.01	1.41	0.47	0.69	3.94	17.45
9.0751	0.00	0.00	0.00	100.00	11.7494	0.01	1.56	0.52	0.76	4.34	19.21
9.9930	0.00	0.00	0.00	100.00	10.6701	0.01	1.71	0.57	0.83	4.78	21.15
11.0041	0.00	0.00	0.00	100.00	9.6897	0.01	1.89	0.63	0.92	5.26	23.29
12.1199	0.00	0.00	0.00	100.00	8.7977	0.02	2.08	0.69	1.01	5.80	25.66
13.3436	0.00	0.00	0.00	100.00	7.9909	0.02	2.29	0.76	1.11	6.38	28.25
14.6975	0.00	0.00	0.00	100.00	7.2547	0.02	2.52	0.84	1.22	7.03	31.11
16.1848	0.00	0.00	0.00	100.00	6.5881	0.02	2.77	0.92	1.35	7.74	34.26
17.8243	0.00	0.00	0.00	100.00	5.9821	0.02	3.06	1.02	1.49	8.53	37.73
19.6833	0.00	0.00	0.00	100.00	5.4171	0.03	3.37	1.12	1.64	9.42	41.67
21.6755	0.00	0.00	0.00	100.00	4.9192	0.03	3.72	1.24	1.81	10.37	45.88
23.8661	0.00	0.00	0.00	100.00	4.4677	0.03	4.09	1.36	1.99	11.42	50.52
26.2814	0.00	0.00	0.00	100.00	4.0571	0.04	4.51	1.50	2.19	12.57	55.63
28.9378	0.00	0.00	0.00	100.00	3.6847	0.04	4.96	1.65	2.41	13.85	61.25
31.8733	0.00	0.00	0.00	100.00	3.3453	0.04	5.46	1.82	2.66	15.25	67.47
35.1085	0.00	0.00	0.00	100.00	3.0371	0.05	6.02	2.01	2.93	16.80	74.32
36.1746	0.00	0.00	0.00	100.00	2.9476	0.05	6.20	2.07	3.01	17.31	76.57
41.2210	0.00	0.00	0.00	100.00	2.5867	0.06	7.07	2.36	3.44	19.72	87.26
42.4912	0.00	0.00	0.00	100.00	2.5094	0.06	7.28	2.43	3.54	20.33	89.94
48.3010	0.00	0.00	0.00	100.00	2.2076	0.06	8.28	2.76	4.02	23.11	102.24
53.0647	0.00	0.00	0.00	100.00	2.0094	0.07	9.10	3.03	4.42	25.39	112.33
59.0792	0.00	0.00	0.00	100.00	1.8048	0.08	10.13	3.38	4.92	28.27	125.06
65.4939	0.00	0.00	0.00	100.00	1.6280	0.09	11.23	3.74	5.46	31.34	138.64
73.0552	0.00	0.00	0.00	100.00	1.4595	0.10	12.52	4.17	6.09	34.95	154.64
80.8393	0.00	0.00	0.00	100.00	1.3190	0.11	13.86	4.62	6.74	38.68	171.12
88.3361	0.00	0.00	0.00	100.00	1.2071	0.12	15.14	5.05	7.36	42.26	186.99
98.3263	0.00	0.00	0.00	100.00	1.0844	0.13	16.86	5.62	8.19	47.04	208.13
107.8995	0.00	0.00	0.00	100.00	0.9882	0.14	18.50	6.17	8.99	51.62	228.40
120.1296	0.00	0.00	0.00	100.00	0.8876	0.16	20.59	6.86	10.01	57.48	254.29
132.1945	0.00	0.00	0.00	100.00	0.8066	0.18	22.66	7.55	11.02	63.25	279.83
146.3208	0.00	0.00	0.00	100.00	0.7287	0.20	25.08	8.36	12.19	70.01	309.73
161.8420	0.00	0.00	0.00	100.00	0.6588	0.22	27.74	9.25	13.49	77.43	342.58
178.2241	0.00	0.00	0.00	100.00	0.5983	0.24	30.55	10.18	14.85	85.27	377.26
196.8313	0.00	0.00	0.00	100.00	0.5417	0.26	33.74	11.25	16.40	94.17	416.65
217.7201	0.00	0.00	0.00	100.00	0.4897	0.29	37.32	12.44	18.14	104.17	460.86
240.3571	0.00	0.00	0.00	100.00	0.4436	0.32	41.20	13.73	20.03	115.00	508.78
264.5117	0.00	0.00	0.00	100.00	0.4031	0.35	45.34	15.11	22.04	126.55	559.91
291.4342	0.00	0.00	0.00	100.00	0.3659	0.39	49.96	16.65	24.29	139.43	616.90
321.3529	0.00	0.00	0.00	100.00	0.3318	0.43	55.09	18.36	26.78	153.75	680.23
354.1289	0.00	0.00	0.00	100.00	0.3011	0.47	60.71	20.24	29.51	169.43	749.61
391.1703	0.00	0.00	0.00	100.00	0.2726	0.52	67.06	22.35	32.60	187.15	828.02
430.8433	0.00	0.00	0.00	100.00	0.2475	0.58	73.86	24.62	35.90	206.13	912.00
474.7763	0.00	0.00	0.00	100.00	0.2246	0.63	81.39	27.13	39.56	227.15	1004.99
523.2123	0.00	0.00	0.00	100.00	0.2038	0.70	89.69	29.90	43.60	250.33	1107.52
576.9897	0.00	0.00	0.00	100.00	0.1848	0.77	98.91	32.97	48.08	276.06	1221.36
635.6848	0.00	0.00	0.00	100.00	0.1677	0.85	108.97	36.32	52.97	304.14	1345.60
700.6454	0.00	0.00	0.00	100.00	0.1522	0.94	120.11	40.04	58.39	335.22	1483.11
772.2783	0.00	0.00	0.00	100.00	0.1381	1.03	132.39	44.13	64.35	369.49	1634.74
851.3761	0.00	0.00	0.00	100.00	0.1252	1.14	145.95	48.65	70.95	407.34	1802.17
937.6433	0.00	0.00	0.00	100.00	0.1137	1.25	160.74	53.58	78.14	448.61	1984.78
1033.5782	0.00	0.00	0.00	100.00	0.1032	1.38	177.18	59.06	86.13	494.51	2187.85
1137.9362	0.00	0.00	0.00	100.00	0.0937	1.52	195.07	65.02	94.83	544.44	2408.76
1253.0435	0.00	0.00	0.00	100.00	0.0851	1.67	214.80	71.60	104.42	599.51	2652.41
1381.0278	0.00	0.00	0.00	100.00	0.0772	1.84	236.74	78.91	115.08	660.74	2923.33
1521.4187	2.22	0.44	2.22	97.78	0.0701	2.03	260.81	86.94	126.78	727.91	3220.50
1675.5696	2.83	0.56	5.05	94.95	0.0636	2.24	287.23	95.74	139.63	801.67	3546.81
1845.6757	3.01	0.59	8.06	91.94	0.0578	2.46	316.39	105.46	153.80	883.05	3906.88
2033.5968	3.16	0.62	11.23	88.77	0.0524	2.72	348.61	116.20	169.46	972.96	4304.67
2239.9856	2.98	0.58	14.20	85.80	0.0476	2.99	383.99	128.00	186.66	1071.71	4741.55
2467.3975	4.13	0.81	18.33	81.67	0.0432	3.29	422.97	140.99	205.61	1180.51	5222.93
2717.6853	3.73	0.73	22.06	77.94	0.0392	3.63	465.88	155.29	226.47	1300.26	5752.73
2992.9438	3.72	0.73	25.78	74.22	0.0356	4.00	513.06	171.02	249.41	1431.96	6335.39
3295.4351	4.08	0.80	29.86	70.14	0.0324	4.40	564.92	188.31	274.61	1576.68	6975.70
3631.1350	4.09	0.80	33.95	66.05	0.0294	4.85	622.47	207.49	302.59	1737.30	7686.30
4000.1035	4.50	0.88	38.45	61.55	0.0267	5.34	685.72	228.57	333.33	1913.83	8467.32
4399.0884	5.04	0.99	43.49	56.51	0.0242	5.87	754.11	251.37	366.58	2104.72	9311.88
4844.8032	5.10	1.00	48.59	51.41	0.0220	6.47	830.52	276.84	403.72	2317.97	10255.36
5337.7744	4.66	0.91	53.25	46.75	0.0200	7.13	915.03	305.01	444.80	2553.83	11298.87
5881.0239	5.01	0.98	58.25	41.75	0.0181	7.85	1008.15	336.05	490.07	2813.74	12448.81
6477.2456	3.59	0.70	61.84	38.16	0.0165	8.65	1110.36	370.12	539.76	3099.00	13710.88
7134.2490	3.44	0.68	65.29	34.71	0.0149	9.53	1222.98	407.66	594.51	3413.34	15101.61
7859.8921	2.62	0.51	67.91	32.09	0.0136	10.50	1347.38	449.13	654.98	3760.52	16637.63
8658.8096	2.04	0.40	69.95	30.05	0.0123	11.56	1484.33	494.78	721.55	4142.76	18328.76
9540.8369	2.01	0.39	71.96	28.04	0.0112	12.74	1635.53	545.18	795.05	4564.76	20195.81
10510.8027	0.99	0.19	72.95	27.05	0.0101	14.04	1801.81	600.60	875.88	5028.83	22249.01
11579.7461	1.79	0.35	74.75	25.25	0.0092	15.46	1985.05	661.68	964.96	5540.26	24511.73
12755.3135	2.51	0.49	77.26	22.74	0.0084	17.03	2186.57	728.86	1062.92	6102.70	27000.14
14051.1426	1.42	0.28	78.68	21.32	0.0076	18.76	2408.71	802.90	1170.90	6722.69	29743.12
15480.8340	1.49	0.29	80.17	19.83	0.0069	20.67	2653.79	884.60	1290.04	7406.71	32769.46
17053.5430	1.44	0.28	81.61	18.39	0.0063	22.77	2923.39	974.46	1421.09	8159.17	36098.53
18784.6504	1.26	0.25	82.87	17.13	0.0057	25.08	3220.15	1073.38	1565.35	8987.40	39762.89
20699.5781	1.92	0.38	84.79	15.21	0.0052	27.64	3548.41	1182.80	1724.92	9903.59	43816.37
22810.8965	0.96	0.19	85.76	14.24	0.0047	30.46	3910.35	1303.45	1900.86	10913.74	48285.56
25130.7520	0.36	0.07	86.12	13.88	0.0042	33.56	4308.03	1436.01	2094.18	12023.66	53196.17
27683.3887	1.59	0.31	87.71	12.29	0.0039	36.97	4745.61	1581.87	2306.89	13244.95	58599.53
30494.3184	3.11	0.61	90.82	9.18	0.0035	40.72	5227.47	1742.49	2541.13	14589.83	64549.64
33589.6914	1.89	0.37	92.71	7.29	0.0032	44.85	5758.10	1919.37	2799.07	16070.79	71101.85
36996.8477	1.37	0.27	94.08	5.92	0.0029	49.40	6342.17	2114.06	3083.00	17700.92	78314.03
40739.0547	0.55	0.11	94.63	5.37	0.0026	54.40	6983.67	2327.89	3394.84	19491.36	86235.45
44863.3477	1.01	0.20	95.64	4.36	0.0024	59.91	7690.68	2563.56	3738.52	21464.60	94965.65
49413.9414	0.67	0.13	96.31	3.69	0.0022	65.98	8470.76	2823.59	4117.73	23641.81	104598.24
54432.6992	3.03	0.60	99.35	0.65	0.0020	72.68	9331.10	3110.37	4535.95	26043.00	115221.82
59956.6172	0.65	0.13	100.00	0.00	0.0018	80.06	10278.03	3426.01	4996.27	28685.89	126914.72

Company: Univ. of Wyoming
Well: RSU #1
File: WTC-12-2873

Sample ID: 26
Depth, ft:
Permeability to Air, md: 15.829
Calculated Permeability to Air, md: 0.752
Helium Porosity, percent: 8.1
Mercury Porosity, %. 6.43
Mercury Pore Volume: 0.554
Helium Pore Volume: 0.702
Entry Pressure 7.480

Injection Pressure (Absolute), psia	Non-Wetting Phase Saturation			Wetting Phase Saturation, fraction	Pore Throat Radius, microns	Leverett "J" Function	Capillary Pressure			Height Above Free Water	
	Incremental percent	Normalized Incremental percent	Cumulative percent				Gas/Water psi	Gas/Oil psi	Oil/water psi	Gas/Water feet	Oil/Water feet
0.5352	0.00	0.00	0.00	100.00	199.2387	0.02	0.09	0.03	0.04	0.26	1.13
0.5799	0.00	0.00	0.00	100.00	183.8683	0.02	0.10	0.03	0.05	0.28	1.23
0.6377	0.00	0.00	0.00	100.00	167.2137	0.02	0.11	0.04	0.05	0.31	1.35
0.6989	0.00	0.00	0.00	100.00	152.5720	0.03	0.12	0.04	0.06	0.33	1.48
0.7669	0.00	0.00	0.00	100.00	139.0312	0.03	0.13	0.04	0.06	0.37	1.62
0.8445	0.00	0.00	0.00	100.00	126.2605	0.03	0.14	0.05	0.07	0.40	1.79
0.9262	0.00	0.00	0.00	100.00	115.1199	0.04	0.16	0.05	0.08	0.44	1.96
1.0156	0.00	0.00	0.00	100.00	104.9870	0.04	0.17	0.06	0.08	0.49	2.15
1.1143	0.00	0.00	0.00	100.00	95.6911	0.04	0.19	0.06	0.09	0.53	2.36
1.2274	0.00	0.00	0.00	100.00	86.8719	0.05	0.21	0.07	0.10	0.59	2.60
1.3483	0.00	0.00	0.00	100.00	79.0840	0.05	0.23	0.08	0.11	0.65	2.85
1.4802	0.00	0.00	0.00	100.00	72.0369	0.06	0.25	0.08	0.12	0.71	3.13
1.6250	0.00	0.00	0.00	100.00	65.6162	0.06	0.28	0.09	0.14	0.78	3.44
1.7869	0.00	0.00	0.00	100.00	59.6727	0.07	0.31	0.10	0.15	0.85	3.78
1.9630	0.00	0.00	0.00	100.00	54.3179	0.07	0.34	0.11	0.16	0.94	4.16
2.1578	0.00	0.00	0.00	100.00	49.4150	0.08	0.37	0.12	0.18	1.03	4.57
2.3729	0.00	0.00	0.00	100.00	44.9349	0.09	0.41	0.14	0.20	1.14	5.02
2.6068	0.00	0.00	0.00	100.00	40.9028	0.10	0.45	0.15	0.22	1.25	5.52
2.8650	0.00	0.00	0.00	100.00	37.2177	0.11	0.49	0.16	0.24	1.37	6.06
3.1506	0.00	0.00	0.00	100.00	33.8439	0.12	0.54	0.18	0.26	1.51	6.67
3.4656	0.00	0.00	0.00	100.00	30.7669	0.13	0.59	0.20	0.29	1.66	7.34
3.8079	0.00	0.00	0.00	100.00	28.0017	0.14	0.65	0.22	0.32	1.82	8.06
4.1922	0.00	0.00	0.00	100.00	25.4345	0.16	0.72	0.24	0.35	2.01	8.87
4.6171	0.00	0.00	0.00	100.00	23.0937	0.18	0.79	0.26	0.38	2.21	9.77
5.0855	0.00	0.00	0.00	100.00	20.9667	0.19	0.87	0.29	0.42	2.43	10.76
5.5993	0.00	0.00	0.00	100.00	19.0429	0.21	0.96	0.32	0.47	2.68	11.85
6.1673	0.00	0.00	0.00	100.00	17.2891	0.23	1.06	0.35	0.51	2.95	13.05
6.7957	0.00	0.00	0.00	100.00	15.6904	0.26	1.16	0.39	0.57	3.25	14.38
7.4796	0.00	0.00	0.00	100.00	14.2557	0.28	1.28	0.43	0.62	3.58	15.83
8.2378	0.67	0.15	0.67	99.33	12.9437	0.31	1.41	0.47	0.69	3.94	17.44
9.0756	0.69	0.16	1.37	98.63	11.7487	0.35	1.56	0.52	0.76	4.34	19.21
9.9940	2.00	0.45	3.36	96.64	10.6691	0.38	1.71	0.57	0.83	4.78	21.15
11.0046	2.22	0.50	5.59	94.41	9.6893	0.42	1.89	0.63	0.92	5.27	23.29
12.1192	2.51	0.57	8.10	91.90	8.7982	0.46	2.08	0.69	1.01	5.80	25.65
13.3441	2.31	0.52	10.41	89.59	7.9906	0.51	2.29	0.76	1.11	6.38	28.25
14.6949	2.20	0.50	12.61	87.39	7.2561	0.56	2.52	0.84	1.22	7.03	31.11
16.1835	2.60	0.59	15.21	84.79	6.5886	0.62	2.77	0.92	1.35	7.74	34.26
17.8302	3.62	0.82	18.83	81.17	5.9801	0.68	3.06	1.02	1.49	8.53	37.74
19.6329	3.38	0.76	22.21	77.79	5.4310	0.75	3.37	1.12	1.64	9.39	41.56
21.6700	3.61	0.82	25.82	74.18	4.9205	0.82	3.71	1.24	1.81	10.37	45.87
23.8688	3.46	0.78	29.28	70.72	4.4672	0.91	4.09	1.36	1.99	11.42	50.52
26.2740	3.85	0.87	33.13	66.87	4.0583	1.00	4.50	1.50	2.19	12.57	55.62
28.9385	3.66	0.83	36.79	63.21	3.6846	1.10	4.96	1.65	2.41	13.85	61.26
31.8714	4.42	1.00	41.21	58.79	3.3455	1.21	5.46	1.82	2.66	15.25	67.46
35.1074	3.63	0.82	44.84	55.16	3.0372	1.33	6.02	2.01	2.93	16.80	74.31
38.9052	1.11	0.25	45.95	54.05	2.7407	1.48	6.67	2.22	3.24	18.61	82.35
43.4761	2.16	0.49	48.11	51.89	2.4525	1.65	7.45	2.48	3.62	20.80	92.03
47.8618	3.10	0.70	51.21	48.79	2.2278	1.82	8.20	2.73	3.99	22.90	101.31
53.3049	3.99	0.90	55.20	44.80	2.0003	2.03	9.14	3.05	4.44	25.50	112.83
59.3617	3.55	0.80	58.75	41.25	1.7962	2.26	10.18	3.39	4.95	28.40	125.66
65.5198	3.04	0.69	61.79	38.21	1.6274	2.49	11.23	3.74	5.46	31.35	138.69
73.0281	3.16	0.71	64.94	35.06	1.4601	2.78	12.52	4.17	6.09	34.94	154.58
80.5032	2.39	0.54	67.33	32.67	1.3245	3.06	13.80	4.60	6.71	38.52	170.41
88.7423	1.97	0.45	69.30	30.70	1.2015	3.37	15.21	5.07	7.40	42.46	187.85
98.2987	1.95	0.44	71.25	28.75	1.0847	3.74	16.85	5.62	8.19	47.03	208.08
108.2572	1.52	0.34	72.77	27.23	0.9849	4.12	18.56	6.19	9.02	51.80	229.16
119.9333	1.60	0.36	74.37	25.63	0.8891	4.56	20.56	6.85	9.99	57.38	253.87
132.7855	1.42	0.32	75.79	24.21	0.8030	5.05	22.76	7.59	11.07	63.53	281.08
146.5818	1.26	0.29	77.05	22.95	0.7274	5.57	25.13	8.38	12.21	70.13	310.28
161.0736	1.16	0.26	78.21	21.79	0.6620	6.12	27.61	9.20	13.42	77.06	340.96
178.8901	1.22	0.28	79.43	20.57	0.5960	6.80	30.67	10.22	14.91	85.59	378.67
196.9759	1.06	0.24	80.49	19.51	0.5413	7.49	33.77	11.26	16.41	94.24	416.95
217.2134	1.07	0.24	81.56	18.44	0.4909	8.26	37.24	12.41	18.10	103.92	459.79
239.7571	1.06	0.24	82.63	17.37	0.4447	9.12	41.10	13.70	19.98	114.71	507.51
264.5668	1.08	0.24	83.70	16.30	0.4030	10.06	45.35	15.12	22.05	126.58	560.03
291.3423	1.06	0.24	84.76	15.24	0.3660	11.08	49.94	16.65	24.28	139.39	616.71
321.6731	1.06	0.24	85.82	14.18	0.3315	12.23	55.14	18.38	26.81	153.90	680.91
354.1331	1.04	0.24	86.86	13.14	0.3011	13.46	60.71	20.24	29.51	169.43	749.62
391.0799	0.96	0.22	87.82	12.18	0.2726	14.87	67.04	22.35	32.59	187.11	827.83
430.7494	0.99	0.22	88.81	11.19	0.2475	16.38	73.84	24.61	35.89	206.09	911.80
474.4078	0.94	0.21	89.75	10.25	0.2248	18.04	81.33	27.11	39.53	226.98	1004.21
523.4287	0.92	0.21	90.67	9.33	0.2037	19.90	89.73	29.91	43.62	250.43	1107.98
576.5605	0.88	0.20	91.55	8.45	0.1849	21.92	98.84	32.95	48.05	275.85	1220.45
636.2176	0.81	0.18	92.36	7.64	0.1676	24.19	109.06	36.35	53.02	304.39	1346.73
700.2200	0.76	0.17	93.12	6.88	0.1523	26.62	120.03	40.01	58.35	335.02	1482.21
771.8953	0.72	0.16	93.84	6.16	0.1381	29.35	132.32	44.11	64.32	369.31	1633.93
851.0745	0.65	0.15	94.49	5.51	0.1253	32.36	145.90	48.63	70.92	407.19	1801.53
938.1125	0.60	0.14	95.09	4.91	0.1137	35.67	160.82	53.61	78.17	448.83	1985.77
1033.2709	0.55	0.12	95.64	4.36	0.1032	39.29	177.13	59.04	86.10	494.36	2187.20
1138.8477	0.53	0.12	96.17	3.83	0.0936	43.30	195.23	65.08	94.90	544.87	2410.69
1253.6621	0.47	0.11	96.64	3.36	0.0851	47.66	214.91	71.64	104.47	599.81	2653.72
1381.5898	0.43	0.10	97.07	2.93	0.0772	52.53	236.84	78.95	115.13	661.01	2924.52
1521.6145	0.38	0.09	97.44	2.56	0.0701	57.85	260.84	86.95	126.80	728.01	3220.92
1675.6742	0.35	0.08	97.79	2.21	0.0636	63.71	287.25	95.75	139.64	801.72	3547.03
1846.5245	0.32	0.07	98.11	1.89	0.0577	70.21	316.54	105.51	153.87	883.46	3908.68
2034.6504	0.28	0.06	98.39	1.61	0.0524	77.36	348.79	116.26	169.55	973.47	4306.90
2240.5051	0.26	0.06	98.65	1.35	0.0476	85.18	384.08	128.03	186.70	1071.96	4742.65
2467.6555	0.22	0.05	98.87	1.13	0.0432	93.82	423.02	141.01	205.63	1180.64	5223.47
2717.2747	0.19	0.04	99.06	0.94	0.0392	103.31	465.81	155.27	226.43	1300.06	5751.86
2993.2415	0.19	0.04	99.25	0.75	0.0356	113.80	513.11	171.04	249.43	1432.10	6336.02
3296.8865	0.16	0.04	99.41	0.59	0.0323	125.35	565.17	188.39	274.73	1577.38	6978.77
3630.2280	0.14	0.03	99.55	0.45	0.0294	138.02	622.31	207.44	302.51	1736.86	7684.38
4000.2905	0.12	0.03	99.67	0.33	0.0267	152.09	685.75	228.58	333.35	1913.92	8467.72
4399.4092	0.12	0.03	99.79	0.21	0.0242	167.27	754.17	251.39	366.61	2104.87	9312.56
4845.8496	0.07	0.02	99.85	0.15	0.0220	184.24	830.70	276.90	403.81	2318.47	10257.58
5337.5942	0.07	0.01	99.92	0.08	0.0200	202.94	914.99	305.00	444.79	2553.74	11298.49
5879.2822	0.04	0.01	99.96	0.04	0.0181	223.53	1007.85	335.95	489.93	2812.91	12445.12
6473.6323	0.03	0.01	99.99	0.01	0.0165	246.13	1109.74	369.91	539.46	3097.27	13703.23
7134.5713	0.01	0.00	100.00	0.00	0.0149	271.26	1223.04	407.68	594.53	3413.49	15102.29
7859.7549	0.00	0.00	100.00	0.00	0.0136	298.83	1347.35	449.12	654.96	3760.45	16637.34
8660.2188	0.00	0.00	100.00	0.00	0.0123	329.26	1484.57	494.86	721.67	4143.43	18331.74
9542.1035	0.00	0.00	100.00	0.00	0.0112	362.79	1635.75	545.25	795.16	4565.36	20198.49
10509.1162	0.00	0.00	100.00	0.00	0.0101	399.56	1801.52	600.51	875.74	5028.02	22245.44
11576.5117	0.00	0.00	100.00	0.00	0.0092	440.14	1984.50	661.50	964.69	5538.71	24504.88
12755.2461	0.00	0.00	100.00	0.00	0.0084	484.96	2186.56	728.85	1062.91	6102.67	27000.00
14051.2559	0.00	0.00	100.00	0.00	0.0076	534.23	2408.73	802.91	1170.91	6722.74	29743.36
15479.9297	0.00	0.00	100.00	0.00	0.0069	588.55	2653.64	884.55	1289.96	7406.28	32767.54
17052.8672	0.00	0.00	100.00	0.00	0.0063	648.35	2923.28	974.43	1421.04	8158.84	36097.10
18781.2988	0.00	0.00	100.00	0.00	0.0057	714.07	3219.57	1073.19	1565.07	8985.80	39755.80
20697.3379	0.00	0.00	100.00	0.00	0.0052	786.92	3548.03	1182.68	1724.74	9902.52	43811.63
22811.8125	0.00	0.00	100.00	0.00	0.0047	867.31	3910.50	1303.50	1900.94	10914.18	48287.49
25129.8359	0.00	0.00	100.00	0.00	0.0042	955.44	4307.87	1435.96	2094.10	12023.22	53194.23
27683.0957	0.00	0.00	100.00	0.00	0.0039	1052.52	4745.56	1581.85	2306.87	13244.81	58598.91
30493.2969	0.00	0.00	100.00	0.00	0.0035	1159.36	5227.30	1742.43	2541.05	14589.34	64547.47
33588.8750	0.00	0.00	100.00	0.00	0.0032	1277.06	5757.96	1919.32	2799.01	16070.40	71100.12
36996.9297	0.00	0.00	100.00	0.00	0.0029	1406.63	6342.18	2114.06	3083.00	17700.96	78314.21
40738.9727	0.00	0.00	100.00	0.00	0.0026	1548.90	6983.66	2327.89	3394.83	19491.32	86235.27
44861.0742	0.00	0.00	100.00	0.00	0.0024	1705.63	7690.29	2563.43	3738.33	21463.52	94960.84
49412.4609	0.00	0.00	100.00	0.00	0.0022	1878.67	8470.51	2823.50	4117.61	23641.10	104595.10
54431.7344	0.00	0.00	100.00	0.00	0.0020	2069.50	9330.93	3110.31	4535.87	26042.54	115219.78
59958.4609	0.00	0.00	100.00	0.00	0.0018	2279.63	10278.35	3426.12	4996.42	28686.77	126918.62

Company: Univ. of Wyoming
Well: RSU #1
File: WTC-12-2873

Sample ID: 27
Depth, ft:
Permeability to Air, md: 1.305
Calculated Permeability to Air, md: 0.197
Helium Porosity, percent: 7.6
Mercury Porosity, %. 6.45
Mercury Pore Volume: 0.550
Helium Pore Volume: 0.652
Entry Pressure 35.109

Injection Pressure (Absolute), psia	Non-Wetting Phase Saturation			Wetting Phase Saturation, fraction	Pore Throat Radius, microns	Leverett "J" Function	Capillary Pressure			Height Above Free Water	
	Incremental percent	Normalized Incremental percent	Cumulative percent				Gas/Water psi	Gas/Oil psi	Oil/water psi	Gas/Water feet	Oil/Water feet
0.5354	0.00	0.00	0.00	100.00	199.1687	0.01	0.09	0.03	0.04	0.26	1.13
0.5792	0.00	0.00	0.00	100.00	184.1060	0.01	0.10	0.03	0.05	0.28	1.23
0.6385	0.00	0.00	0.00	100.00	167.0045	0.01	0.11	0.04	0.05	0.31	1.35
0.7001	0.00	0.00	0.00	100.00	152.3041	0.01	0.12	0.04	0.06	0.33	1.48
0.7683	0.00	0.00	0.00	100.00	138.7882	0.01	0.13	0.04	0.06	0.37	1.63
0.8452	0.00	0.00	0.00	100.00	126.1496	0.01	0.14	0.05	0.07	0.40	1.79
0.9262	0.00	0.00	0.00	100.00	115.1218	0.01	0.16	0.05	0.08	0.44	1.96
1.0160	0.00	0.00	0.00	100.00	104.9427	0.01	0.17	0.06	0.08	0.49	2.15
1.1150	0.00	0.00	0.00	100.00	95.6295	0.01	0.19	0.06	0.09	0.53	2.36
1.2272	0.00	0.00	0.00	100.00	86.8850	0.01	0.21	0.07	0.10	0.59	2.60
1.3487	0.00	0.00	0.00	100.00	79.0584	0.02	0.23	0.08	0.11	0.65	2.85
1.4807	0.00	0.00	0.00	100.00	72.0125	0.02	0.25	0.08	0.12	0.71	3.13
1.6253	0.00	0.00	0.00	100.00	65.6060	0.02	0.28	0.09	0.14	0.78	3.44
1.7874	0.00	0.00	0.00	100.00	59.6562	0.02	0.31	0.10	0.15	0.86	3.78
1.9645	0.00	0.00	0.00	100.00	54.2775	0.02	0.34	0.11	0.16	0.94	4.16
2.1591	0.00	0.00	0.00	100.00	49.3848	0.02	0.37	0.12	0.18	1.03	4.57
2.3730	0.00	0.00	0.00	100.00	44.9335	0.03	0.41	0.14	0.20	1.14	5.02
2.6065	0.00	0.00	0.00	100.00	40.9087	0.03	0.45	0.15	0.22	1.25	5.52
2.8666	0.00	0.00	0.00	100.00	37.1970	0.03	0.49	0.16	0.24	1.37	6.07
3.1503	0.00	0.00	0.00	100.00	33.8466	0.04	0.54	0.18	0.26	1.51	6.67
3.4651	0.00	0.00	0.00	100.00	30.7721	0.04	0.59	0.20	0.29	1.66	7.33
3.8106	0.00	0.00	0.00	100.00	27.9818	0.04	0.65	0.22	0.32	1.82	8.07
4.1922	0.00	0.00	0.00	100.00	25.4348	0.05	0.72	0.24	0.35	2.01	8.87
4.6168	0.00	0.00	0.00	100.00	23.0953	0.05	0.79	0.26	0.38	2.21	9.77
5.0870	0.00	0.00	0.00	100.00	20.9608	0.06	0.87	0.29	0.42	2.43	10.77
5.6025	0.00	0.00	0.00	100.00	19.0320	0.06	0.96	0.32	0.47	2.68	11.86
6.1697	0.00	0.00	0.00	100.00	17.2824	0.07	1.06	0.35	0.51	2.95	13.06
6.7928	0.00	0.00	0.00	100.00	15.6971	0.08	1.16	0.39	0.57	3.25	14.38
7.4826	0.00	0.00	0.00	100.00	14.2500	0.08	1.28	0.43	0.62	3.58	15.84
8.2372	0.00	0.00	0.00	100.00	12.9446	0.09	1.41	0.47	0.69	3.94	17.44
9.0749	0.00	0.00	0.00	100.00	11.7496	0.10	1.56	0.52	0.76	4.34	19.21
9.9902	0.00	0.00	0.00	100.00	10.6731	0.11	1.71	0.57	0.83	4.78	21.15
11.0065	0.00	0.00	0.00	100.00	9.6876	0.12	1.89	0.63	0.92	5.27	23.30
12.1218	0.00	0.00	0.00	100.00	8.7963	0.14	2.08	0.69	1.01	5.80	25.66
13.3479	0.00	0.00	0.00	100.00	7.9883	0.15	2.29	0.76	1.11	6.39	28.25
14.6976	0.00	0.00	0.00	100.00	7.2547	0.17	2.52	0.84	1.22	7.03	31.11
16.1853	0.00	0.00	0.00	100.00	6.5879	0.18	2.77	0.92	1.35	7.74	34.26
17.8299	0.00	0.00	0.00	100.00	5.9802	0.20	3.06	1.02	1.49	8.53	37.74
19.6407	0.00	0.00	0.00	100.00	5.4289	0.22	3.37	1.12	1.64	9.40	41.58
21.6743	0.00	0.00	0.00	100.00	4.9195	0.24	3.72	1.24	1.81	10.37	45.88
23.8732	0.00	0.00	0.00	100.00	4.4664	0.27	4.09	1.36	1.99	11.42	50.53
26.2779	0.00	0.00	0.00	100.00	4.0577	0.30	4.50	1.50	2.19	12.57	55.62
28.9407	0.00	0.00	0.00	100.00	3.6843	0.33	4.96	1.65	2.41	13.85	61.26
31.8770	0.00	0.00	0.00	100.00	3.3450	0.36	5.46	1.82	2.66	15.25	67.48
35.1093	0.00	0.00	0.00	100.00	3.0370	0.39	6.02	2.01	2.93	16.80	74.32
39.9273	1.80	0.20	1.80	98.20	2.6705	0.45	6.84	2.28	3.33	19.10	84.52
43.6446	2.98	0.33	4.78	95.22	2.4431	0.49	7.48	2.49	3.64	20.88	92.39
48.3742	5.31	0.60	10.10	89.90	2.2042	0.54	8.29	2.76	4.03	23.14	102.40
53.5692	6.52	0.73	16.61	83.39	1.9905	0.60	9.18	3.06	4.46	25.63	113.39
59.3143	7.21	0.81	23.83	76.17	1.7977	0.67	10.17	3.39	4.94	28.38	125.56
65.8604	8.92	1.00	32.75	67.25	1.6190	0.74	11.29	3.76	5.49	31.51	139.41
72.3873	8.62	0.97	41.37	58.63	1.4730	0.81	12.41	4.14	6.03	34.63	153.23
81.2101	8.05	0.90	49.42	50.58	1.3130	0.91	13.92	4.64	6.77	38.85	171.90
89.7029	5.83	0.65	55.25	44.75	1.1887	1.01	15.38	5.13	7.48	42.92	189.88
98.3633	3.91	0.44	59.17	40.83	1.0840	1.11	16.86	5.62	8.20	47.06	208.21
108.8537	3.59	0.40	62.76	37.24	0.9795	1.22	18.66	6.22	9.07	52.08	230.42
119.4338	2.82	0.32	65.58	34.42	0.8928	1.34	20.47	6.82	9.95	57.14	252.81
132.7056	2.61	0.28	68.09	31.91	0.8035	1.49	22.75	7.58	11.06	63.49	280.91
145.8998	2.05	0.23	70.13	29.87	0.7308	1.64	25.01	8.34	12.16	69.80	308.84
161.5621	1.97	0.22	72.11	27.89	0.6600	1.82	27.70	9.23	13.46	77.30	341.99
178.6671	1.81	0.20	73.91	26.09	0.5968	2.01	30.63	10.21	14.89	85.48	378.20
197.1837	1.65	0.18	75.56	24.44	0.5407	2.22	33.80	11.27	16.43	94.34	417.39
217.6849	1.58	0.18	77.14	22.86	0.4898	2.45	37.32	12.44	18.14	104.15	460.79
239.8529	1.41	0.16	78.54	21.46	0.4446	2.69	41.12	13.71	19.99	114.76	507.71
264.5090	1.33	0.15	79.87	20.13	0.4031	2.97	45.34	15.11	22.04	126.55	559.91
291.3293	1.24	0.14	81.11	18.89	0.3660	3.27	49.94	16.65	24.28	139.38	616.68
321.3036	1.17	0.13	82.29	17.71	0.3319	3.61	55.08	18.36	26.77	153.73	680.13
354.1250	1.12	0.13	83.41	16.59	0.3011	3.98	60.71	20.24	29.51	169.43	749.60
391.2323	1.06	0.12	84.47	15.53	0.2725	4.40	67.07	22.36	32.60	187.18	828.15
430.5778	0.99	0.11	85.46	14.54	0.2476	4.84	73.81	24.60	35.88	206.01	911.44
474.3749	0.96	0.11	86.43	13.57	0.2248	5.33	81.32	27.11	39.53	226.96	1004.15
523.2623	0.95	0.11	87.38	12.62	0.2038	5.88	89.70	29.90	43.60	250.35	1107.63
577.5435	0.93	0.10	88.30	11.70	0.1846	6.49	99.01	33.00	48.13	276.32	1222.53
635.8544	0.91	0.10	89.21	10.79	0.1677	7.14	109.00	36.33	52.99	304.22	1345.96
700.8451	0.88	0.10	90.09	9.91	0.1521	7.87	120.14	40.05	58.40	335.32	1483.53
772.3495	0.87	0.10	90.97	9.03	0.1381	8.68	132.40	44.13	64.36	369.53	1634.89
851.0815	0.84	0.09	91.81	8.19	0.1253	9.56	145.90	48.63	70.92	407.19	1801.55
937.9417	0.80	0.09	92.61	7.39	0.1137	10.54	160.79	53.60	78.16	448.75	1985.41
1033.3047	0.77	0.09	93.38	6.62	0.1032	11.61	177.13	59.04	86.11	494.38	2187.27
1138.9978	0.73	0.08	94.11	5.89	0.0936	12.80	195.25	65.08	94.91	544.95	2411.00
1253.7845	0.65	0.07	94.76	5.24	0.0850	14.09	214.93	71.64	104.48	599.87	2653.98
1381.4462	0.64	0.07	95.40	4.60	0.0772	15.52	236.81	78.94	115.12	660.94	2924.21
1521.9127	0.56	0.06	95.96	4.04	0.0701	17.10	260.89	86.96	126.82	728.15	3221.55
1675.2698	0.55	0.06	96.51	3.49	0.0636	18.82	287.18	95.73	139.60	801.52	3546.17
1845.7423	0.46	0.05	96.96	3.04	0.0578	20.74	316.41	105.47	153.81	883.08	3907.02
2034.2457	0.43	0.05	97.39	2.61	0.0524	22.85	348.72	116.24	169.52	973.27	4306.04
2239.9619	0.39	0.04	97.78	2.22	0.0476	25.17	383.98	127.99	186.66	1071.70	4741.50
2467.8535	0.35	0.04	98.13	1.87	0.0432	27.73	423.05	141.02	205.65	1180.73	5223.89
2717.5322	0.32	0.04	98.45	1.55	0.0392	30.53	465.85	155.28	226.46	1300.19	5752.41
2993.1672	0.26	0.03	98.71	1.29	0.0356	33.63	513.10	171.03	249.42	1432.06	6335.86
3295.8245	0.26	0.03	98.97	1.03	0.0324	37.03	564.99	188.33	274.65	1576.87	6976.52
3631.4031	0.21	0.02	99.17	0.83	0.0294	40.80	622.51	207.50	302.61	1737.42	7686.87
4000.3652	0.19	0.02	99.37	0.63	0.0267	44.94	685.76	228.59	333.36	1913.95	8467.88
4399.8638	0.19	0.02	99.55	0.45	0.0242	49.43	754.24	251.41	366.65	2105.09	9313.53
4844.9048	0.14	0.02	99.70	0.30	0.0220	54.43	830.54	276.85	403.73	2318.02	10255.58
5337.7480	0.11	0.01	99.81	0.19	0.0200	59.97	915.02	305.01	444.80	2553.81	11298.82
5878.7344	0.08	0.01	99.89	0.11	0.0181	66.05	1007.76	335.92	489.88	2812.65	12443.96
6475.9790	0.07	0.01	99.96	0.04	0.0165	72.76	1110.14	370.05	539.65	3098.39	13708.20
7133.1162	0.03	0.00	99.98	0.02	0.0149	80.14	1222.79	407.60	594.41	3412.80	15099.21
7858.2471	0.02	0.00	100.00	0.00	0.0136	88.29	1347.10	449.03	654.84	3759.73	16634.15
8656.8477	0.00	0.00	100.00	0.00	0.0123	97.26	1484.00	494.67	721.39	4141.82	18324.61
9543.5967	0.00	0.00	100.00	0.00	0.0112	107.22	1636.01	545.34	795.28	4566.08	20201.66
10512.0293	0.00	0.00	100.00	0.00	0.0101	118.10	1802.02	600.67	875.98	5029.42	22251.61
11578.6592	0.00	0.00	100.00	0.00	0.0092	130.09	1984.87	661.62	964.87	5539.74	24509.43
12754.9189	0.00	0.00	100.00	0.00	0.0084	143.30	2186.51	728.84	1062.88	6102.52	26999.30
14050.6934	0.00	0.00	100.00	0.00	0.0076	157.86	2408.63	802.88	1170.86	6722.47	29742.17
15478.6445	0.00	0.00	100.00	0.00	0.0069	173.90	2653.42	884.47	1289.86	7405.67	32764.82
17050.7441	0.00	0.00	100.00	0.00	0.0063	191.56	2922.92	974.31	1420.86	8157.83	36092.60
18784.0684	0.00	0.00	100.00	0.00	0.0057	211.04	3220.05	1073.35	1565.30	8987.13	39761.66
20699.8203	0.00	0.00	100.00	0.00	0.0052	232.56	3548.46	1182.82	1724.94	9903.71	43816.88
22810.9199	0.00	0.00	100.00	0.00	0.0047	256.28	3910.35	1303.45	1900.86	10913.75	48285.60
25130.2832	0.00	0.00	100.00	0.00	0.0042	282.34	4307.95	1435.98	2094.14	12023.44	53195.18
27683.1309	0.00	0.00	100.00	0.00	0.0039	311.02	4745.57	1581.86	2306.87	13244.83	58598.98
30494.4375	0.00	0.00	100.00	0.00	0.0035	342.60	5227.49	1742.50	2541.14	14589.88	64549.89
33587.5625	0.00	0.00	100.00	0.00	0.0032	377.35	5757.73	1919.24	2798.90	16069.77	71097.34
36993.2656	0.00	0.00	100.00	0.00	0.0029	415.62	6341.55	2113.85	3082.70	17699.21	78306.45
40735.7305	0.00	0.00	100.00	0.00	0.0026	457.66	6983.10	2327.70	3394.56	19489.77	86228.41
44858.5859	0.00	0.00	100.00	0.00	0.0024	503.98	7689.86	2563.29	3738.13	21462.32	94955.57
49411.7461	0.00	0.00	100.00	0.00	0.0022	555.14	8470.38	2823.46	4117.55	23640.76	104593.59
54431.4648	0.00	0.00	100.00	0.00	0.0020	611.53	9330.89	3110.30	4535.85	26042.41	115219.21
59957.7148	0.00	0.00	100.00	0.00	0.0018	673.62	10278.22	3426.07	4996.36	28686.41	126917.04

Company: Univ. of Wyoming
Well: RSU #1
File: WTC-12-2873

Sample ID: 45
Depth, ft:
Permeability to Air, md: 0.016
Calculated Permeability to Air, md: 0.000
Helium Porosity, percent: 1.3
Mercury Porosity, %. 0.58
Mercury Pore Volume: 0.073
Helium Pore Volume: 0.162
Entry Pressure 1034.229

Injection Pressure (Absolute), psia	Non-Wetting Phase Saturation			Wetting Phase Saturation, fraction	Pore Throat Radius, microns	Leverett "J" Function	Capillary Pressure			Height Above Free Water	
	Incremental percent	Normalized Incremental percent	Cumulative percent				Gas/Water psi	Gas/Oil psi	Oil/water psi	Gas/Water feet	Oil/Water feet
0.5363	0.00	0.00	0.00	100.00	198.8062	0.00	0.09	0.03	0.04	0.26	1.14
0.5804	0.00	0.00	0.00	100.00	183.7240	0.00	0.10	0.03	0.05	0.28	1.23
0.6375	0.00	0.00	0.00	100.00	167.2584	0.00	0.11	0.04	0.05	0.31	1.35
0.6989	0.00	0.00	0.00	100.00	152.5537	0.00	0.12	0.04	0.06	0.33	1.48
0.7704	0.00	0.00	0.00	100.00	138.4075	0.00	0.13	0.04	0.06	0.37	1.63
0.8429	0.00	0.00	0.00	100.00	126.5062	0.00	0.14	0.05	0.07	0.40	1.78
0.9264	0.00	0.00	0.00	100.00	115.1028	0.00	0.16	0.05	0.08	0.44	1.96
1.0178	0.00	0.00	0.00	100.00	104.7646	0.00	0.17	0.06	0.08	0.49	2.15
1.1164	0.00	0.00	0.00	100.00	95.5112	0.00	0.19	0.06	0.09	0.53	2.36
1.2258	0.00	0.00	0.00	100.00	86.9874	0.00	0.21	0.07	0.10	0.59	2.59
1.3483	0.00	0.00	0.00	100.00	79.0842	0.00	0.23	0.08	0.11	0.65	2.85
1.4805	0.00	0.00	0.00	100.00	72.0200	0.00	0.25	0.08	0.12	0.71	3.13
1.6254	0.00	0.00	0.00	100.00	65.6009	0.00	0.28	0.09	0.14	0.78	3.44
1.7871	0.00	0.00	0.00	100.00	59.6641	0.01	0.31	0.10	0.15	0.86	3.78
1.9659	0.00	0.00	0.00	100.00	54.2390	0.01	0.34	0.11	0.16	0.94	4.16
2.1580	0.00	0.00	0.00	100.00	49.4108	0.01	0.37	0.12	0.18	1.03	4.57
2.3736	0.00	0.00	0.00	100.00	44.9228	0.01	0.41	0.14	0.20	1.14	5.02
2.6077	0.00	0.00	0.00	100.00	40.8895	0.01	0.45	0.15	0.22	1.25	5.52
2.8685	0.00	0.00	0.00	100.00	37.1716	0.01	0.49	0.16	0.24	1.37	6.07
3.1514	0.00	0.00	0.00	100.00	33.8351	0.01	0.54	0.18	0.26	1.51	6.67
3.4636	0.00	0.00	0.00	100.00	30.7853	0.01	0.59	0.20	0.29	1.66	7.33
3.8090	0.00	0.00	0.00	100.00	27.9934	0.01	0.65	0.22	0.32	1.82	8.06
4.1926	0.00	0.00	0.00	100.00	25.4319	0.01	0.72	0.24	0.35	2.01	8.87
4.6182	0.00	0.00	0.00	100.00	23.0883	0.01	0.79	0.26	0.38	2.21	9.78
5.0862	0.00	0.00	0.00	100.00	20.9641	0.02	0.87	0.29	0.42	2.43	10.77
5.6023	0.00	0.00	0.00	100.00	19.0328	0.02	0.96	0.32	0.47	2.68	11.86
6.1687	0.00	0.00	0.00	100.00	17.2850	0.02	1.06	0.35	0.51	2.95	13.06
6.7939	0.00	0.00	0.00	100.00	15.6944	0.02	1.16	0.39	0.57	3.25	14.38
7.4818	0.00	0.00	0.00	100.00	14.2516	0.02	1.28	0.43	0.62	3.58	15.84
8.2414	0.00	0.00	0.00	100.00	12.9380	0.02	1.41	0.47	0.69	3.94	17.45
9.0728	0.00	0.00	0.00	100.00	11.7524	0.03	1.56	0.52	0.76	4.34	19.21
9.9895	0.00	0.00	0.00	100.00	10.6739	0.03	1.71	0.57	0.83	4.78	21.15
11.0062	0.00	0.00	0.00	100.00	9.6879	0.03	1.89	0.63	0.92	5.27	23.30
12.1209	0.00	0.00	0.00	100.00	8.7969	0.04	2.08	0.69	1.01	5.80	25.66
13.3486	0.00	0.00	0.00	100.00	7.9879	0.04	2.29	0.76	1.11	6.39	28.26
14.7008	0.00	0.00	0.00	100.00	7.2531	0.04	2.52	0.84	1.23	7.03	31.12
16.1888	0.00	0.00	0.00	100.00	6.5865	0.05	2.78	0.93	1.35	7.75	34.27
17.8254	0.00	0.00	0.00	100.00	5.9818	0.05	3.06	1.02	1.49	8.53	37.73
19.6402	0.00	0.00	0.00	100.00	5.4290	0.06	3.37	1.12	1.64	9.40	41.57
21.6718	0.00	0.00	0.00	100.00	4.9201	0.07	3.72	1.24	1.81	10.37	45.87
23.8690	0.00	0.00	0.00	100.00	4.4672	0.07	4.09	1.36	1.99	11.42	50.53
26.2803	0.00	0.00	0.00	100.00	4.0573	0.08	4.51	1.50	2.19	12.57	55.63
28.9410	0.00	0.00	0.00	100.00	3.6843	0.09	4.96	1.65	2.41	13.85	61.26
31.8726	0.00	0.00	0.00	100.00	3.3454	0.10	5.46	1.82	2.66	15.25	67.47
35.1110	0.00	0.00	0.00	100.00	3.0369	0.11	6.02	2.01	2.93	16.80	74.32
39.1075	0.00	0.00	0.00	100.00	2.7265	0.12	6.70	2.23	3.26	18.71	82.78
43.4978	0.00	0.00	0.00	100.00	2.4513	0.13	7.46	2.49	3.62	20.81	92.08
48.6901	0.00	0.00	0.00	100.00	2.1899	0.15	8.35	2.78	4.06	23.30	103.07
54.7548	0.00	0.00	0.00	100.00	1.9474	0.17	9.39	3.13	4.56	26.20	115.90
59.9849	0.00	0.00	0.00	100.00	1.7776	0.18	10.28	3.43	5.00	28.70	126.97
66.8569	0.00	0.00	0.00	100.00	1.5949	0.20	11.46	3.82	5.57	31.99	141.52
73.6458	0.00	0.00	0.00	100.00	1.4478	0.22	12.62	4.21	6.14	35.24	155.89
81.0770	0.00	0.00	0.00	100.00	1.3151	0.25	13.90	4.63	6.76	38.79	171.62
88.9465	0.00	0.00	0.00	100.00	1.1988	0.27	15.25	5.08	7.41	42.56	188.28
99.3140	0.00	0.00	0.00	100.00	1.0736	0.30	17.02	5.67	8.28	47.52	210.23
109.5986	0.00	0.00	0.00	100.00	0.9729	0.33	18.79	6.26	9.13	52.44	232.00
120.7695	0.00	0.00	0.00	100.00	0.8829	0.37	20.70	6.90	10.06	57.78	255.64
133.1482	0.00	0.00	0.00	100.00	0.8008	0.40	22.82	7.61	11.10	63.70	281.84
147.2706	0.00	0.00	0.00	100.00	0.7240	0.45	25.25	8.42	12.27	70.46	311.74
162.6728	0.00	0.00	0.00	100.00	0.6555	0.49	27.89	9.30	13.56	77.83	344.34
179.3994	0.00	0.00	0.00	100.00	0.5944	0.54	30.75	10.25	14.95	85.83	379.75
196.9750	0.00	0.00	0.00	100.00	0.5413	0.60	33.77	11.26	16.41	94.24	416.95
218.4099	0.00	0.00	0.00	100.00	0.4882	0.66	37.44	12.48	18.20	104.50	462.32
240.8033	0.00	0.00	0.00	100.00	0.4428	0.73	41.28	13.76	20.07	115.21	509.73
265.2698	0.00	0.00	0.00	100.00	0.4020	0.80	45.47	15.16	22.11	126.92	561.52
292.8863	0.00	0.00	0.00	100.00	0.3641	0.89	50.21	16.74	24.41	140.13	619.97
322.1875	0.00	0.00	0.00	100.00	0.3309	0.98	55.23	18.41	26.85	154.15	682.00
355.3599	0.00	0.00	0.00	100.00	0.3001	1.08	60.92	20.31	29.61	170.02	752.22
392.2375	0.00	0.00	0.00	100.00	0.2718	1.19	67.24	22.41	32.69	187.66	830.28
432.1140	0.00	0.00	0.00	100.00	0.2468	1.31	74.07	24.69	36.01	206.74	914.69
476.1000	0.00	0.00	0.00	100.00	0.2240	1.44	81.62	27.21	39.67	227.79	1007.80
524.0073	0.00	0.00	0.00	100.00	0.2035	1.59	89.83	29.94	43.67	250.71	1109.21
578.2725	0.00	0.00	0.00	100.00	0.1844	1.75	99.13	33.04	48.19	276.67	1224.07
636.9202	0.00	0.00	0.00	100.00	0.1674	1.93	109.18	36.39	53.08	304.73	1348.22
702.3174	0.00	0.00	0.00	100.00	0.1518	2.13	120.39	40.13	58.53	336.02	1486.65
773.7386	0.00	0.00	0.00	100.00	0.1378	2.34	132.64	44.21	64.48	370.19	1637.83
851.4498	0.00	0.00	0.00	100.00	0.1252	2.58	145.96	48.65	70.95	407.37	1802.33
938.9796	0.00	0.00	0.00	100.00	0.1136	2.85	160.96	53.65	78.25	449.25	1987.61
1034.2294	3.48	0.25	3.48	96.52	0.1031	3.13	177.29	59.10	86.18	494.82	2189.23
1139.3657	6.19	0.45	9.67	90.33	0.0936	3.45	195.32	65.11	94.94	545.12	2411.78
1254.1642	8.26	0.60	17.92	82.08	0.0850	3.80	214.99	71.66	104.51	600.05	2654.78
1382.2800	11.06	0.81	28.98	71.02	0.0771	4.19	236.96	78.99	115.19	661.34	2925.98
1522.1940	12.95	0.95	41.94	58.06	0.0700	4.61	260.94	86.98	126.85	728.28	3222.14
1676.2396	13.65	1.00	55.59	44.41	0.0636	5.08	287.35	95.78	139.68	801.99	3548.22
1846.0220	12.05	0.88	67.63	32.37	0.0578	5.59	316.45	105.48	153.83	883.22	3907.61
2033.6848	8.53	0.63	76.17	23.83	0.0524	6.16	348.62	116.21	169.47	973.00	4304.85
2241.4023	4.48	0.33	80.65	19.35	0.0476	6.79	384.23	128.08	186.78	1072.39	4744.55
2467.8767	3.08	0.23	83.73	16.27	0.0432	7.48	423.05	141.02	205.65	1180.74	5223.94
2718.5227	2.61	0.19	86.33	13.67	0.0392	8.24	466.02	155.34	226.54	1300.66	5754.50
2993.4038	2.24	0.16	88.57	11.43	0.0356	9.07	513.14	171.05	249.44	1432.18	6336.36
3297.0869	1.92	0.14	90.49	9.51	0.0323	9.99	565.20	188.40	274.75	1577.47	6979.19
3632.0881	1.61	0.12	92.10	7.90	0.0294	11.00	622.63	207.54	302.67	1737.75	7688.32
4001.1111	1.38	0.10	93.49	6.51	0.0266	12.12	685.89	228.63	333.42	1914.31	8469.46
4400.1108	1.39	0.10	94.87	5.13	0.0242	13.33	754.29	251.43	366.67	2105.21	9314.05
4846.4028	1.02	0.07	95.89	4.11	0.0220	14.68	830.79	276.93	403.86	2318.73	10258.75
5338.2729	0.88	0.06	96.77	3.23	0.0200	16.17	915.11	305.04	444.85	2554.07	11299.93
5879.7319	0.73	0.05	97.50	2.50	0.0181	17.82	1007.93	335.98	489.97	2813.12	12446.07
6474.6196	0.60	0.04	98.10	1.90	0.0165	19.62	1109.91	369.97	539.54	3097.74	13705.32
7135.2490	0.52	0.04	98.62	1.38	0.0149	21.62	1223.16	407.72	594.59	3413.82	15103.72
7864.4424	0.45	0.03	99.07	0.93	0.0136	23.83	1348.16	449.39	655.35	3762.70	16647.26
8662.3271	0.32	0.02	99.39	0.61	0.0123	26.25	1484.94	494.98	721.84	4144.44	18336.21
9539.7119	0.31	0.02	99.70	0.30	0.0112	28.90	1635.34	545.11	794.96	4564.22	20193.43
10513.4072	0.19	0.01	99.88	0.12	0.0101	31.85	1802.26	600.75	876.10	5030.08	22254.53
11579.6650	0.10	0.01	99.98	0.02	0.0092	35.09	1985.04	661.68	964.95	5540.22	24511.56
12757.2158	0.02	0.00	100.00	0.00	0.0084	38.65	2186.90	728.97	1063.08	6103.61	27004.17
14052.4990	0.00	0.00	100.00	0.00	0.0076	42.58	2408.94	802.98	1171.01	6723.33	29745.99
15477.9766	0.00	0.00	100.00	0.00	0.0069	46.90	2653.30	884.43	1289.80	7405.35	32763.41
17050.8242	0.00	0.00	100.00	0.00	0.0063	51.66	2922.93	974.31	1420.87	8157.87	36092.77
18783.1348	0.00	0.00	100.00	0.00	0.0057	56.91	3219.89	1073.30	1565.22	8986.68	39759.69
20701.6348	0.00	0.00	100.00	0.00	0.0052	62.72	3548.77	1182.92	1725.10	9904.57	43820.72
22812.2266	0.00	0.00	100.00	0.00	0.0047	69.12	3910.57	1303.52	1900.97	10914.37	48288.37
25130.9902	0.00	0.00	100.00	0.00	0.0042	76.14	4308.07	1436.02	2094.20	12023.77	53196.67
27683.9746	0.00	0.00	100.00	0.00	0.0039	83.88	4745.71	1581.90	2306.94	13245.23	58600.77
30494.4258	0.00	0.00	100.00	0.00	0.0035	92.40	5227.49	1742.50	2541.14	14589.88	64549.86
33588.9648	0.00	0.00	100.00	0.00	0.0032	101.77	5757.97	1919.32	2799.01	16070.44	71100.31
36996.8672	0.00	0.00	100.00	0.00	0.0029	112.10	6342.17	2114.06	3083.00	17700.93	78314.08
40740.3008	0.00	0.00	100.00	0.00	0.0026	123.44	6983.89	2327.96	3394.94	19491.96	86238.09
44861.8633	0.00	0.00	100.00	0.00	0.0024	135.93	7690.42	2563.47	3738.40	21463.89	94962.51
49412.6523	0.00	0.00	100.00	0.00	0.0022	149.72	8470.54	2823.51	4117.62	23641.19	104595.51
54433.9766	0.00	0.00	100.00	0.00	0.0020	164.93	9331.32	3110.44	4536.06	26043.61	115224.53
59957.5273	0.00	0.00	100.00	0.00	0.0018	181.67	10278.19	3426.06	4996.34	28686.32	126916.65

Company: Univ. of Wyoming
Well: RSU #1
File: WTC-12-2873

Sample ID: 53f
Depth, ft:
Permeability to Air, md: 1098.894
Calculated Permeability to Air, md: 0.000
Helium Porosity, percent: 5.8
Mercury Porosity, %. 3.06
Mercury Pore Volume: 0.169
Helium Pore Volume: 0.318
Entry Pressure 1381.100

Injection Pressure (Absolute), psia	Non-Wetting Phase Saturation			Wetting Phase Saturation, fraction	Pore Throat Radius, microns	Leverett "J" Function	Capillary Pressure			Height Above Free Water	
	Incremental percent	Normalized Incremental percent	Cumulative percent				Gas/Water psi	Gas/Oil psi	Oil/water psi	Gas/Water feet	Oil/Water feet
0.5357	0.00	0.00	0.00	100.00	199.0328	0.20	0.09	0.03	0.04	0.26	1.13
0.5788	0.00	0.00	0.00	100.00	184.2194	0.22	0.10	0.03	0.05	0.28	1.23
0.6383	0.00	0.00	0.00	100.00	167.0361	0.24	0.11	0.04	0.05	0.31	1.35
0.7006	0.00	0.00	0.00	100.00	152.1922	0.26	0.12	0.04	0.06	0.34	1.48
0.7689	0.00	0.00	0.00	100.00	138.6672	0.29	0.13	0.04	0.06	0.37	1.63
0.8448	0.00	0.00	0.00	100.00	126.2173	0.32	0.14	0.05	0.07	0.40	1.79
0.9270	0.00	0.00	0.00	100.00	115.0200	0.35	0.16	0.05	0.08	0.44	1.96
1.0171	0.00	0.00	0.00	100.00	104.8340	0.38	0.17	0.06	0.08	0.49	2.15
1.1157	0.00	0.00	0.00	100.00	95.5671	0.42	0.19	0.06	0.09	0.53	2.36
1.2272	0.00	0.00	0.00	100.00	86.8849	0.46	0.21	0.07	0.10	0.59	2.60
1.3483	0.00	0.00	0.00	100.00	79.0822	0.51	0.23	0.08	0.11	0.65	2.85
1.4803	0.00	0.00	0.00	100.00	72.0327	0.56	0.25	0.08	0.12	0.71	3.13
1.6259	0.00	0.00	0.00	100.00	65.5811	0.61	0.28	0.09	0.14	0.78	3.44
1.7878	0.00	0.00	0.00	100.00	59.6413	0.67	0.31	0.10	0.15	0.86	3.78
1.9652	0.00	0.00	0.00	100.00	54.2567	0.74	0.34	0.11	0.16	0.94	4.16
2.1586	0.00	0.00	0.00	100.00	49.3971	0.81	0.37	0.12	0.18	1.03	4.57
2.3722	0.00	0.00	0.00	100.00	44.9485	0.89	0.41	0.14	0.20	1.13	5.02
2.6079	0.00	0.00	0.00	100.00	40.8862	0.98	0.45	0.15	0.22	1.25	5.52
2.8675	0.00	0.00	0.00	100.00	37.1848	1.08	0.49	0.16	0.24	1.37	6.07
3.1517	0.00	0.00	0.00	100.00	33.8316	1.18	0.54	0.18	0.26	1.51	6.67
3.4655	0.00	0.00	0.00	100.00	30.7684	1.30	0.59	0.20	0.29	1.66	7.34
3.8089	0.00	0.00	0.00	100.00	27.9941	1.43	0.65	0.22	0.32	1.82	8.06
4.1926	0.00	0.00	0.00	100.00	25.4321	1.57	0.72	0.24	0.35	2.01	8.87
4.6170	0.00	0.00	0.00	100.00	23.0944	1.73	0.79	0.26	0.38	2.21	9.77
5.0842	0.00	0.00	0.00	100.00	20.9721	1.91	0.87	0.29	0.42	2.43	10.76
5.5995	0.00	0.00	0.00	100.00	19.0422	2.10	0.96	0.32	0.47	2.68	11.85
6.1684	0.00	0.00	0.00	100.00	17.2860	2.32	1.06	0.35	0.51	2.95	13.06
6.7926	0.00	0.00	0.00	100.00	15.6975	2.55	1.16	0.39	0.57	3.25	14.38
7.4812	0.00	0.00	0.00	100.00	14.2526	2.81	1.28	0.43	0.62	3.58	15.84
8.2407	0.00	0.00	0.00	100.00	12.9390	3.10	1.41	0.47	0.69	3.94	17.44
9.0758	0.00	0.00	0.00	100.00	11.7484	3.41	1.56	0.52	0.76	4.34	19.21
9.9911	0.00	0.00	0.00	100.00	10.6722	3.75	1.71	0.57	0.83	4.78	21.15
11.0013	0.00	0.00	0.00	100.00	9.6922	4.13	1.89	0.63	0.92	5.26	23.29
12.1220	0.00	0.00	0.00	100.00	8.7962	4.55	2.08	0.69	1.01	5.80	25.66
13.3493	0.00	0.00	0.00	100.00	7.9875	5.01	2.29	0.76	1.11	6.39	28.26
14.7004	0.00	0.00	0.00	100.00	7.2533	5.52	2.52	0.84	1.23	7.03	31.12
16.1887	0.00	0.00	0.00	100.00	6.5865	6.08	2.78	0.93	1.35	7.75	34.27
17.8287	0.00	0.00	0.00	100.00	5.9806	6.70	3.06	1.02	1.49	8.53	37.74
19.6393	0.00	0.00	0.00	100.00	5.4293	7.38	3.37	1.12	1.64	9.40	41.57
21.6718	0.00	0.00	0.00	100.00	4.9201	8.14	3.72	1.24	1.81	10.37	45.87
23.8733	0.00	0.00	0.00	100.00	4.4664	8.97	4.09	1.36	1.99	11.42	50.53
26.2859	0.00	0.00	0.00	100.00	4.0564	9.87	4.51	1.50	2.19	12.58	55.64
28.9421	0.00	0.00	0.00	100.00	3.6841	10.87	4.96	1.65	2.41	13.85	61.26
31.8749	0.00	0.00	0.00	100.00	3.3452	11.97	5.46	1.82	2.66	15.25	67.47
35.1049	0.00	0.00	0.00	100.00	3.0374	13.19	6.02	2.01	2.93	16.80	74.31
37.8821	0.00	0.00	0.00	100.00	2.8147	14.23	6.49	2.16	3.16	18.12	80.19
38.5032	0.00	0.00	0.00	100.00	2.7693	14.46	6.60	2.20	3.21	18.42	81.50
43.2761	0.00	0.00	0.00	100.00	2.4639	16.26	7.42	2.47	3.61	20.71	91.61
47.5051	0.00	0.00	0.00	100.00	2.2445	17.85	8.14	2.71	3.96	22.73	100.56
53.6037	0.00	0.00	0.00	100.00	1.9892	20.14	9.19	3.06	4.47	25.65	113.47
58.7179	0.00	0.00	0.00	100.00	1.8159	22.06	10.07	3.36	4.89	28.09	124.29
64.6152	0.00	0.00	0.00	100.00	1.6502	24.27	11.08	3.69	5.38	30.91	136.78
72.2718	0.00	0.00	0.00	100.00	1.4754	27.15	12.39	4.13	6.02	34.58	152.98
80.4077	0.00	0.00	0.00	100.00	1.3261	30.21	13.78	4.59	6.70	38.47	170.21
88.3833	0.00	0.00	0.00	100.00	1.2064	33.20	15.15	5.05	7.37	42.29	187.09
98.2151	0.00	0.00	0.00	100.00	1.0856	36.89	16.84	5.61	8.18	46.99	207.90
108.7818	0.00	0.00	0.00	100.00	0.9802	40.86	18.65	6.22	9.06	52.05	230.27
119.0390	0.00	0.00	0.00	100.00	0.8957	44.72	20.41	6.80	9.92	56.95	251.98
131.9496	0.00	0.00	0.00	100.00	0.8081	49.57	22.62	7.54	11.00	63.13	279.31
147.0065	0.00	0.00	0.00	100.00	0.7253	55.22	25.20	8.40	12.25	70.33	311.18
161.4652	0.00	0.00	0.00	100.00	0.6604	60.66	27.68	9.23	13.46	77.25	341.79
178.2363	0.00	0.00	0.00	100.00	0.5982	66.96	30.55	10.18	14.85	85.28	377.29
196.6220	0.00	0.00	0.00	100.00	0.5423	73.86	33.71	11.24	16.38	94.07	416.20
217.3671	0.00	0.00	0.00	100.00	0.4905	81.65	37.26	12.42	18.11	104.00	460.12
240.1552	0.00	0.00	0.00	100.00	0.4440	90.22	41.17	13.72	20.01	114.90	508.35
263.9091	0.00	0.00	0.00	100.00	0.4040	99.14	45.24	15.08	21.99	126.27	558.64
291.5862	0.00	0.00	0.00	100.00	0.3657	109.54	49.99	16.66	24.30	139.51	617.22
321.3016	0.00	0.00	0.00	100.00	0.3319	120.70	55.08	18.36	26.77	153.72	680.12
354.1620	0.00	0.00	0.00	100.00	0.3011	133.04	60.71	20.24	29.51	169.45	749.68
391.0832	0.00	0.00	0.00	100.00	0.2726	146.91	67.04	22.35	32.59	187.11	827.84
430.0919	0.00	0.00	0.00	100.00	0.2479	161.57	73.73	24.58	35.84	205.77	910.41
474.6470	0.00	0.00	0.00	100.00	0.2246	178.30	81.37	27.12	39.55	227.09	1004.72
523.2661	0.00	0.00	0.00	100.00	0.2038	196.57	89.70	29.90	43.60	250.35	1107.64
577.0566	0.00	0.00	0.00	100.00	0.1848	216.77	98.92	32.97	48.09	276.09	1221.50
636.1764	0.00	0.00	0.00	100.00	0.1676	238.98	109.06	36.35	53.01	304.37	1346.64
700.2621	0.00	0.00	0.00	100.00	0.1523	263.06	120.04	40.01	58.35	335.04	1482.30
772.7280	0.00	0.00	0.00	100.00	0.1380	290.28	132.46	44.15	64.39	369.71	1635.69
850.4719	0.00	0.00	0.00	100.00	0.1254	319.48	145.79	48.60	70.87	406.90	1800.26
938.0883	0.00	0.00	0.00	100.00	0.1137	352.40	160.81	53.60	78.17	448.82	1985.72
1034.0851	0.00	0.00	0.00	100.00	0.1031	388.46	177.27	59.09	86.17	494.75	2188.93
1138.1780	0.00	0.00	0.00	100.00	0.0937	427.56	195.11	65.04	94.85	544.55	2409.27
1253.4078	0.00	0.00	0.00	100.00	0.0851	470.85	214.86	71.62	104.45	599.69	2653.18
1381.1001	3.75	0.40	3.75	96.25	0.0772	518.82	236.75	78.92	115.09	660.78	2923.48
1520.9843	4.89	0.52	8.63	91.37	0.0701	571.36	260.73	86.91	126.75	727.71	3219.58
1675.5369	5.82	0.61	14.45	85.55	0.0636	629.42	287.23	95.74	139.62	801.65	3546.74
1845.8069	7.11	0.75	21.56	78.44	0.0578	693.38	316.42	105.47	153.81	883.12	3907.16
2034.0188	8.17	0.86	29.72	70.28	0.0524	764.09	348.68	116.23	169.50	973.16	4305.56
2239.7280	8.99	0.95	38.71	61.29	0.0476	841.36	383.94	127.98	186.64	1071.58	4741.00
2466.4978	9.48	1.00	48.19	51.81	0.0432	926.55	422.82	140.94	205.54	1180.08	5221.02
2717.0029	9.34	0.99	57.53	42.47	0.0392	1020.65	465.76	155.25	226.41	1299.93	5751.29
2993.5479	8.91	0.94	66.44	33.56	0.0356	1124.54	513.17	171.06	249.46	1432.25	6336.67
3295.3799	7.70	0.81	74.15	25.85	0.0324	1237.92	564.91	188.30	274.61	1576.65	6975.58
3631.2625	6.78	0.71	80.92	19.08	0.0294	1364.10	622.49	207.50	302.60	1737.36	7686.57
3999.6838	4.82	0.51	85.74	14.26	0.0267	1502.50	685.64	228.55	333.30	1913.63	8466.43
4399.1025	4.41	0.47	90.15	9.85	0.0242	1652.54	754.11	251.37	366.58	2104.72	9311.91
4844.8906	3.32	0.35	93.47	6.53	0.0220	1820.00	830.53	276.84	403.73	2318.01	10255.55
5338.1763	2.67	0.28	96.14	3.86	0.0200	2005.31	915.09	305.03	444.84	2554.02	11299.72
5879.1484	1.64	0.17	97.78	2.22	0.0181	2208.52	1007.83	335.94	489.92	2812.84	12444.84
6477.7095	1.07	0.11	98.86	1.14	0.0165	2433.38	1110.44	370.15	539.80	3099.22	13711.86
7134.1191	0.54	0.06	99.40	0.60	0.0149	2679.96	1222.96	407.65	594.50	3413.28	15101.33
7859.3716	0.32	0.03	99.72	0.28	0.0136	2952.40	1347.29	449.10	654.93	3760.27	16636.53
8656.3047	0.19	0.02	99.91	0.09	0.0123	3251.77	1483.90	494.63	721.34	4141.56	18323.46
9542.6416	0.07	0.01	99.98	0.02	0.0112	3584.73	1635.84	545.28	795.20	4565.62	20199.63
10511.5156	0.02	0.00	100.00	0.00	0.0101	3948.69	1801.93	600.64	875.94	5029.17	22250.52
11579.6260	0.00	0.00	100.00	0.00	0.0092	4349.93	1985.03	661.68	964.95	5540.20	24511.47
12757.7646	0.00	0.00	100.00	0.00	0.0084	4792.50	2186.99	729.00	1063.12	6103.88	27005.33
14049.5840	0.00	0.00	100.00	0.00	0.0076	5277.78	2408.44	802.81	1170.77	6721.94	29739.82
15479.3389	0.00	0.00	100.00	0.00	0.0069	5814.87	2653.54	884.51	1289.91	7406.00	32766.29
17049.7012	0.00	0.00	100.00	0.00	0.0063	6404.78	2922.74	974.25	1420.77	8157.33	36090.40
18788.1543	0.00	0.00	100.00	0.00	0.0057	7057.84	3220.75	1073.58	1565.64	8989.08	39770.31
20700.1328	0.00	0.00	100.00	0.00	0.0052	7776.08	3548.51	1182.84	1724.97	9903.86	43817.54
22810.7676	0.00	0.00	100.00	0.00	0.0047	8568.95	3910.32	1303.44	1900.85	10913.68	48285.28
25130.6016	0.00	0.00	100.00	0.00	0.0042	9440.41	4308.00	1436.00	2094.17	12023.59	53195.85
27682.6191	0.00	0.00	100.00	0.00	0.0039	10399.08	4745.48	1581.83	2306.83	13244.59	58597.90
30493.1035	0.00	0.00	100.00	0.00	0.0035	11454.85	5227.26	1742.42	2541.03	14589.24	64547.07
33588.1953	0.00	0.00	100.00	0.00	0.0032	12617.53	5757.84	1919.28	2798.95	16070.07	71098.68
36996.3672	0.00	0.00	100.00	0.00	0.0029	13897.82	6342.08	2114.03	3082.96	17700.69	78313.02
40737.5078	0.00	0.00	100.00	0.00	0.0026	15303.20	6983.41	2327.80	3394.71	19490.62	86232.17
44862.0469	0.00	0.00	100.00	0.00	0.0024	16852.60	7690.45	2563.48	3738.41	21463.98	94962.90
49412.8359	0.00	0.00	100.00	0.00	0.0022	18562.12	8470.57	2823.52	4117.64	23641.28	104595.90
54435.1992	0.00	0.00	100.00	0.00	0.0020	20448.79	9331.53	3110.51	4536.16	26044.20	115227.12
59953.4844	0.00	0.00	100.00	0.00	0.0018	22521.75	10277.50	3425.83	4996.00	28684.39	126908.09

Company: Univ. of Wyoming
Well: RSU #1
File: WTC-12-2873

Sample ID: 59
Depth, ft:
Permeability to Air, md: 0.001
Calculated Permeability to Air, md: 0.000
Helium Porosity, percent: 1.3
Mercury Porosity, %. 0.66
Mercury Pore Volume: 0.079
Helium Pore Volume: 0.159
Entry Pressure 1253.697

Injection Pressure (Absolute), psia	Non-Wetting Phase Saturation			Wetting Phase Saturation, fraction	Pore Throat Radius, microns	Leverett "J" Function	Capillary Pressure			Height Above Free Water	
	Incremental percent	Normalized Incremental percent	Cumulative percent				Gas/Water psi	Gas/Oil psi	Oil/water psi	Gas/Water feet	Oil/Water feet
0.5364	0.00	0.00	0.00	100.00	198.7807	0.00	0.09	0.03	0.04	0.26	1.14
0.5802	0.00	0.00	0.00	100.00	183.7722	0.00	0.10	0.03	0.05	0.28	1.23
0.6381	0.00	0.00	0.00	100.00	167.1033	0.00	0.11	0.04	0.05	0.31	1.35
0.7000	0.00	0.00	0.00	100.00	152.3319	0.00	0.12	0.04	0.06	0.33	1.48
0.7697	0.00	0.00	0.00	100.00	138.5354	0.00	0.13	0.04	0.06	0.37	1.63
0.8437	0.00	0.00	0.00	100.00	126.3804	0.00	0.14	0.05	0.07	0.40	1.79
0.9274	0.00	0.00	0.00	100.00	114.9744	0.00	0.16	0.05	0.08	0.44	1.96
1.0168	0.00	0.00	0.00	100.00	104.8682	0.00	0.17	0.06	0.08	0.49	2.15
1.1171	0.00	0.00	0.00	100.00	95.4500	0.00	0.19	0.06	0.09	0.53	2.36
1.2270	0.00	0.00	0.00	100.00	86.8994	0.00	0.21	0.07	0.10	0.59	2.60
1.3488	0.00	0.00	0.00	100.00	79.0505	0.00	0.23	0.08	0.11	0.65	2.86
1.4822	0.00	0.00	0.00	100.00	71.9389	0.00	0.25	0.08	0.12	0.71	3.14
1.6259	0.00	0.00	0.00	100.00	65.5794	0.00	0.28	0.09	0.14	0.78	3.44
1.7877	0.00	0.00	0.00	100.00	59.6440	0.00	0.31	0.10	0.15	0.86	3.78
1.9651	0.00	0.00	0.00	100.00	54.2600	0.00	0.34	0.11	0.16	0.94	4.16
2.1601	0.00	0.00	0.00	100.00	49.3623	0.00	0.37	0.12	0.18	1.03	4.57
2.3727	0.00	0.00	0.00	100.00	44.9385	0.00	0.41	0.14	0.20	1.14	5.02
2.6078	0.00	0.00	0.00	100.00	40.8871	0.00	0.45	0.15	0.22	1.25	5.52
2.8680	0.00	0.00	0.00	100.00	37.1786	0.00	0.49	0.16	0.24	1.37	6.07
3.1514	0.00	0.00	0.00	100.00	33.8344	0.00	0.54	0.18	0.26	1.51	6.67
3.4646	0.00	0.00	0.00	100.00	30.7757	0.00	0.59	0.20	0.29	1.66	7.33
3.8102	0.00	0.00	0.00	100.00	27.9849	0.00	0.65	0.22	0.32	1.82	8.07
4.1933	0.00	0.00	0.00	100.00	25.4279	0.00	0.72	0.24	0.35	2.01	8.88
4.6196	0.00	0.00	0.00	100.00	23.0816	0.00	0.79	0.26	0.38	2.21	9.78
5.0865	0.00	0.00	0.00	100.00	20.9628	0.00	0.87	0.29	0.42	2.43	10.77
5.6018	0.00	0.00	0.00	100.00	19.0344	0.00	0.96	0.32	0.47	2.68	11.86
6.1696	0.00	0.00	0.00	100.00	17.2826	0.00	1.06	0.35	0.51	2.95	13.06
6.7956	0.00	0.00	0.00	100.00	15.6907	0.01	1.16	0.39	0.57	3.25	14.38
7.4832	0.00	0.00	0.00	100.00	14.2488	0.01	1.28	0.43	0.62	3.58	15.84
8.2428	0.00	0.00	0.00	100.00	12.9358	0.01	1.41	0.47	0.69	3.94	17.45
9.0742	0.00	0.00	0.00	100.00	11.7506	0.01	1.56	0.52	0.76	4.34	19.21
9.9938	0.00	0.00	0.00	100.00	10.6694	0.01	1.71	0.57	0.83	4.78	21.15
11.0077	0.00	0.00	0.00	100.00	9.6865	0.01	1.89	0.63	0.92	5.27	23.30
12.1231	0.00	0.00	0.00	100.00	8.7954	0.01	2.08	0.69	1.01	5.80	25.66
13.3500	0.00	0.00	0.00	100.00	7.9870	0.01	2.29	0.76	1.11	6.39	28.26
14.7004	0.00	0.00	0.00	100.00	7.2533	0.01	2.52	0.84	1.23	7.03	31.12
16.1856	0.00	0.00	0.00	100.00	6.5878	0.01	2.77	0.92	1.35	7.74	34.26
17.8342	0.00	0.00	0.00	100.00	5.9788	0.01	3.06	1.02	1.49	8.53	37.75
19.6874	0.00	0.00	0.00	100.00	5.4160	0.01	3.37	1.12	1.64	9.42	41.67
21.6808	0.00	0.00	0.00	100.00	4.9180	0.02	3.72	1.24	1.81	10.37	45.89
23.8692	0.00	0.00	0.00	100.00	4.4671	0.02	4.09	1.36	1.99	11.42	50.53
26.2850	0.00	0.00	0.00	100.00	4.0566	0.02	4.51	1.50	2.19	12.58	55.64
28.9390	0.00	0.00	0.00	100.00	3.6845	0.02	4.96	1.65	2.41	13.85	61.26
31.8748	0.00	0.00	0.00	100.00	3.3452	0.02	5.46	1.82	2.66	15.25	67.47
35.1054	0.00	0.00	0.00	100.00	3.0373	0.03	6.02	2.01	2.93	16.80	74.31
36.1477	0.00	0.00	0.00	100.00	2.9498	0.03	6.20	2.07	3.01	17.29	76.52
40.4593	0.00	0.00	0.00	100.00	2.6354	0.03	6.94	2.31	3.37	19.36	85.64
43.0006	0.00	0.00	0.00	100.00	2.4797	0.03	7.37	2.46	3.58	20.57	91.02
48.2146	0.00	0.00	0.00	100.00	2.2115	0.04	8.27	2.76	4.02	23.07	102.06
53.6427	0.00	0.00	0.00	100.00	1.9877	0.04	9.20	3.07	4.47	25.67	113.55
59.5535	0.00	0.00	0.00	100.00	1.7904	0.04	10.21	3.40	4.96	28.49	126.06
65.6902	0.00	0.00	0.00	100.00	1.6232	0.05	11.26	3.75	5.47	31.43	139.05
72.4286	0.00	0.00	0.00	100.00	1.4722	0.05	12.42	4.14	6.04	34.65	153.32
80.8237	0.00	0.00	0.00	100.00	1.3193	0.06	13.86	4.62	6.74	38.67	171.09
89.3388	0.00	0.00	0.00	100.00	1.1935	0.07	15.31	5.10	7.44	42.74	189.11
98.2831	0.00	0.00	0.00	100.00	1.0849	0.07	16.85	5.62	8.19	47.02	208.04
108.7323	0.00	0.00	0.00	100.00	0.9806	0.08	18.64	6.21	9.06	52.02	230.16
120.4742	0.00	0.00	0.00	100.00	0.8851	0.09	20.65	6.88	10.04	57.64	255.02
133.1754	0.00	0.00	0.00	100.00	0.8007	0.10	22.83	7.61	11.10	63.72	281.90
146.7234	0.00	0.00	0.00	100.00	0.7267	0.11	25.15	8.38	12.23	70.20	310.58
161.5269	0.00	0.00	0.00	100.00	0.6601	0.12	27.69	9.23	13.46	77.28	341.92
178.2077	0.00	0.00	0.00	100.00	0.5983	0.13	30.55	10.18	14.85	85.26	377.23
197.3941	0.00	0.00	0.00	100.00	0.5402	0.15	33.84	11.28	16.45	94.44	417.84
217.4978	0.00	0.00	0.00	100.00	0.4902	0.16	37.28	12.43	18.12	104.06	460.39
239.6662	0.00	0.00	0.00	100.00	0.4449	0.18	41.08	13.69	19.97	114.67	507.32
264.1389	0.00	0.00	0.00	100.00	0.4037	0.20	45.28	15.09	22.01	126.38	559.12
291.7165	0.00	0.00	0.00	100.00	0.3655	0.22	50.01	16.67	24.31	139.57	617.50
321.7311	0.00	0.00	0.00	100.00	0.3314	0.24	55.15	18.38	26.81	153.93	681.03
354.0869	0.00	0.00	0.00	100.00	0.3011	0.26	60.70	20.23	29.51	169.41	749.52
390.7027	0.00	0.00	0.00	100.00	0.2729	0.29	66.98	22.33	32.56	186.93	827.03
431.0890	0.00	0.00	0.00	100.00	0.2473	0.32	73.90	24.63	35.92	206.25	912.52
474.6847	0.00	0.00	0.00	100.00	0.2246	0.35	81.37	27.12	39.56	227.11	1004.80
522.8869	0.00	0.00	0.00	100.00	0.2039	0.39	89.64	29.88	43.57	250.17	1106.83
577.5081	0.00	0.00	0.00	100.00	0.1846	0.43	99.00	33.00	48.12	276.31	1222.46
635.9944	0.00	0.00	0.00	100.00	0.1677	0.47	109.03	36.34	53.00	304.29	1346.26
700.5488	0.00	0.00	0.00	100.00	0.1522	0.52	120.09	40.03	58.38	335.17	1482.90
772.3849	0.00	0.00	0.00	100.00	0.1380	0.58	132.41	44.14	64.36	369.54	1634.97
851.1096	0.00	0.00	0.00	100.00	0.1253	0.63	145.90	48.63	70.92	407.21	1801.61
937.9198	0.00	0.00	0.00	100.00	0.1137	0.70	160.78	53.59	78.16	448.74	1985.37
1033.5359	0.00	0.00	0.00	100.00	0.1032	0.77	177.17	59.06	86.13	494.49	2187.76
1138.6312	0.00	0.00	0.00	100.00	0.0936	0.85	195.19	65.06	94.88	544.77	2410.23
1253.6970	5.42	0.52	5.42	94.58	0.0851	0.93	214.91	71.64	104.47	599.82	2653.80
1380.9058	9.04	0.87	14.46	85.54	0.0772	1.03	236.72	78.91	115.07	660.69	2923.07
1521.3964	10.34	1.00	24.80	75.20	0.0701	1.13	260.80	86.93	126.78	727.90	3220.46
1675.6682	7.22	0.70	32.02	67.98	0.0636	1.25	287.25	95.75	139.64	801.71	3547.01
1846.2622	6.35	0.61	38.37	61.63	0.0578	1.38	316.49	105.50	153.85	883.33	3908.12
2033.1974	4.98	0.48	43.35	56.65	0.0524	1.51	348.54	116.18	169.43	972.77	4303.82
2240.5217	5.81	0.56	49.16	50.84	0.0476	1.67	384.08	128.03	186.71	1071.96	4742.68
2465.8982	4.68	0.45	53.84	46.16	0.0432	1.84	422.72	140.91	205.49	1179.79	5219.75
2717.2192	3.77	0.36	57.61	42.39	0.0392	2.02	465.80	155.27	226.43	1300.04	5751.74
2992.7810	3.55	0.34	61.16	38.84	0.0356	2.23	513.04	171.01	249.39	1431.88	6335.05
3296.5315	3.28	0.32	64.43	35.57	0.0323	2.46	565.11	188.37	274.70	1577.21	6978.02
3629.8569	2.66	0.26	67.09	32.91	0.0294	2.70	622.25	207.42	302.48	1736.68	7683.59
3999.3840	2.56	0.25	69.66	30.34	0.0267	2.98	685.59	228.53	333.27	1913.48	8465.80
4399.5449	2.61	0.25	72.27	27.73	0.0242	3.28	754.19	251.40	366.62	2104.94	9312.85
4846.2056	2.76	0.27	75.02	24.98	0.0220	3.61	830.76	276.92	403.84	2318.64	10258.33
5337.3003	2.07	0.20	77.09	22.91	0.0200	3.98	914.94	304.98	444.76	2553.60	11297.87
5876.0420	2.00	0.19	79.09	20.91	0.0181	4.38	1007.30	335.77	489.66	2811.36	12438.26
6476.6787	1.92	0.19	81.01	18.99	0.0165	4.83	1110.26	370.09	539.71	3098.73	13709.68
7131.4688	1.35	0.13	82.36	17.64	0.0150	5.31	1222.51	407.50	594.27	3412.01	15095.72
7858.7202	1.45	0.14	83.82	16.18	0.0136	5.86	1347.18	449.06	654.88	3759.96	16635.15
8660.6855	1.87	0.18	85.69	14.31	0.0123	6.45	1484.65	494.88	721.71	4143.65	18332.73
9539.5957	1.31	0.13	87.00	13.00	0.0112	7.11	1635.32	545.11	794.95	4564.16	20193.19
10510.7002	1.23	0.12	88.23	11.77	0.0101	7.83	1801.79	600.60	875.87	5028.78	22248.80
11577.6113	0.91	0.09	89.14	10.86	0.0092	8.63	1984.69	661.56	964.78	5539.24	24507.21
12755.7168	0.67	0.06	89.80	10.20	0.0084	9.50	2186.64	728.88	1062.95	6102.90	27000.99
14054.4990	0.62	0.06	90.42	9.58	0.0076	10.47	2409.29	803.10	1171.18	6724.29	29750.22
15481.1689	0.62	0.06	91.03	8.97	0.0069	11.54	2653.85	884.62	1290.07	7406.87	32770.16
17054.0566	0.49	0.05	91.53	8.47	0.0063	12.71	2923.48	974.49	1421.14	8159.41	36099.62
18783.9219	0.42	0.04	91.95	8.05	0.0057	14.00	3220.02	1073.34	1565.29	8987.06	39761.35
20699.9844	0.49	0.05	92.44	7.56	0.0052	15.42	3548.48	1182.83	1724.96	9903.78	43817.23
22811.8906	0.59	0.06	93.03	6.97	0.0047	17.00	3910.52	1303.51	1900.95	10914.21	48287.66
25130.9141	1.38	0.13	94.41	5.59	0.0042	18.73	4308.05	1436.02	2094.19	12023.74	53196.51
27682.7500	0.74	0.07	95.15	4.85	0.0039	20.63	4745.50	1581.83	2306.84	13244.65	58598.18
30492.5645	0.76	0.07	95.91	4.09	0.0035	22.72	5227.17	1742.39	2540.99	14588.99	64545.92
33587.3242	0.71	0.07	96.63	3.37	0.0032	25.03	5757.69	1919.23	2798.88	16069.66	71096.84
36996.3555	0.64	0.06	97.27	2.73	0.0029	27.57	6342.08	2114.03	3082.96	17700.69	78312.99
40738.5117	0.49	0.05	97.76	2.24	0.0026	30.35	6983.58	2327.86	3394.80	19491.10	86234.30
44862.5039	0.67	0.06	98.42	1.58	0.0024	33.43	7690.53	2563.51	3738.45	21464.20	94963.87
49412.9258	0.52	0.05	98.94	1.06	0.0022	36.82	8470.59	2823.53	4117.65	23641.32	104596.09
54431.2969	0.54	0.05	99.48	0.52	0.0020	40.56	9330.86	3110.29	4535.83	26042.33	115218.86
59957.9180	0.52	0.05	100.00	0.00	0.0018	44.68	10278.26	3426.09	4996.37	28686.51	126917.47

Company: Univ. of Wyoming
Well: RSU #1
File: WTC-12-2873

Sample ID: 72
Depth, ft:
Permeability to Air, md: 33.067
Calculated Permeability to Air, md: 1.958
Helium Porosity, percent: 18.1
Mercury Porosity, %. 16.96
Mercury Pore Volume: 0.651
Helium Pore Volume: 0.647
Entry Pressure 21.677

Injection Pressure (Absolute), psia	Non-Wetting Phase Saturation			Wetting Phase Saturation, fraction	Pore Throat Radius, microns	Leverett "J" Function	Capillary Pressure			Height Above Free Water	
	Incremental percent	Normalized Incremental percent	Cumulative percent				Gas/Water psi	Gas/Oil psi	Oil/water psi	Gas/Water feet	Oil/Water feet
0.5368	0.00	0.00	0.00	100.00	198.6477	0.02	0.09	0.03	0.04	0.26	1.14
0.5805	0.00	0.00	0.00	100.00	183.6910	0.02	0.10	0.03	0.05	0.28	1.23
0.6378	0.00	0.00	0.00	100.00	167.1906	0.02	0.11	0.04	0.05	0.31	1.35
0.7002	0.00	0.00	0.00	100.00	152.2724	0.03	0.12	0.04	0.06	0.34	1.48
0.7697	0.00	0.00	0.00	100.00	138.5358	0.03	0.13	0.04	0.06	0.37	1.63
0.8437	0.00	0.00	0.00	100.00	126.3865	0.03	0.14	0.05	0.07	0.40	1.79
0.9272	0.00	0.00	0.00	100.00	114.9948	0.03	0.16	0.05	0.08	0.44	1.96
1.0182	0.00	0.00	0.00	100.00	104.7253	0.04	0.17	0.06	0.08	0.49	2.16
1.1164	0.00	0.00	0.00	100.00	95.5067	0.04	0.19	0.06	0.09	0.53	2.36
1.2269	0.00	0.00	0.00	100.00	86.9051	0.05	0.21	0.07	0.10	0.59	2.60
1.3488	0.00	0.00	0.00	100.00	79.0543	0.05	0.23	0.08	0.11	0.65	2.86
1.4805	0.00	0.00	0.00	100.00	72.0192	0.05	0.25	0.08	0.12	0.71	3.13
1.6270	0.00	0.00	0.00	100.00	65.5363	0.06	0.28	0.09	0.14	0.78	3.44
1.7879	0.00	0.00	0.00	100.00	59.6378	0.07	0.31	0.10	0.15	0.86	3.78
1.9657	0.00	0.00	0.00	100.00	54.2442	0.07	0.34	0.11	0.16	0.94	4.16
2.1586	0.00	0.00	0.00	100.00	49.3954	0.08	0.37	0.12	0.18	1.03	4.57
2.3744	0.00	0.00	0.00	100.00	44.9075	0.09	0.41	0.14	0.20	1.14	5.03
2.6070	0.00	0.00	0.00	100.00	40.9009	0.10	0.45	0.15	0.22	1.25	5.52
2.8683	0.00	0.00	0.00	100.00	37.1742	0.11	0.49	0.16	0.24	1.37	6.07
3.1518	0.00	0.00	0.00	100.00	33.8306	0.12	0.54	0.18	0.26	1.51	6.67
3.4648	0.00	0.00	0.00	100.00	30.7747	0.13	0.59	0.20	0.29	1.66	7.33
3.8100	0.00	0.00	0.00	100.00	27.9861	0.14	0.65	0.22	0.32	1.82	8.06
4.1943	0.00	0.00	0.00	100.00	25.4218	0.15	0.72	0.24	0.35	2.01	8.88
4.6181	0.00	0.00	0.00	100.00	23.0889	0.17	0.79	0.26	0.38	2.21	9.78
5.0864	0.00	0.00	0.00	100.00	20.9632	0.19	0.87	0.29	0.42	2.43	10.77
5.6012	0.00	0.00	0.00	100.00	19.0365	0.21	0.96	0.32	0.47	2.68	11.86
6.1714	0.00	0.00	0.00	100.00	17.2777	0.23	1.06	0.35	0.51	2.95	13.06
6.7944	0.00	0.00	0.00	100.00	15.6933	0.25	1.16	0.39	0.57	3.25	14.38
7.4834	0.00	0.00	0.00	100.00	14.2485	0.28	1.28	0.43	0.62	3.58	15.84
8.2388	0.00	0.00	0.00	100.00	12.9420	0.30	1.41	0.47	0.69	3.94	17.44
9.0759	0.00	0.00	0.00	100.00	11.7484	0.33	1.56	0.52	0.76	4.34	19.21
9.9885	0.00	0.00	0.00	100.00	10.6750	0.37	1.71	0.57	0.83	4.78	21.14
11.0061	0.00	0.00	0.00	100.00	9.6879	0.41	1.89	0.63	0.92	5.27	23.30
12.1228	0.00	0.00	0.00	100.00	8.7956	0.45	2.08	0.69	1.01	5.80	25.66
13.3498	0.00	0.00	0.00	100.00	7.9871	0.49	2.29	0.76	1.11	6.39	28.26
14.6966	0.00	0.00	0.00	100.00	7.2552	0.54	2.52	0.84	1.22	7.03	31.11
16.1877	0.00	0.00	0.00	100.00	6.5869	0.60	2.77	0.92	1.35	7.74	34.27
17.8320	0.00	0.00	0.00	100.00	5.9795	0.66	3.06	1.02	1.49	8.53	37.75
19.6404	0.00	0.00	0.00	100.00	5.4290	0.72	3.37	1.12	1.64	9.40	41.57
21.6768	0.00	0.00	0.00	100.00	4.9189	0.80	3.72	1.24	1.81	10.37	45.88
23.8698	0.19	0.02	0.19	99.81	4.4670	0.88	4.09	1.36	1.99	11.42	50.53
26.2805	0.43	0.04	0.62	99.38	4.0573	0.97	4.51	1.50	2.19	12.57	55.63
28.9394	1.05	0.10	1.67	98.33	3.6845	1.07	4.96	1.65	2.41	13.85	61.26
31.8752	1.71	0.17	3.38	96.62	3.3451	1.17	5.46	1.82	2.66	15.25	67.47
35.1056	2.15	0.21	5.53	94.47	3.0373	1.29	6.02	2.01	2.93	16.80	74.31
35.1061	1.65	0.16	7.18	92.82	3.0373	1.29	6.02	2.01	2.93	16.80	74.31
39.8015	3.64	0.36	10.82	89.18	2.6790	1.46	6.82	2.27	3.32	19.04	84.25
43.6042	6.07	0.59	16.89	83.11	2.4453	1.60	7.47	2.49	3.63	20.86	92.30
48.0060	8.21	0.80	25.10	74.90	2.2211	1.77	8.23	2.74	4.00	22.97	101.62
53.9044	10.25	1.00	35.34	64.66	1.9781	1.98	9.24	3.08	4.49	25.79	114.10
59.5657	8.89	0.87	44.24	55.76	1.7901	2.19	10.21	3.40	4.96	28.50	126.09
65.9065	8.25	0.81	52.49	47.51	1.6179	2.43	11.30	3.77	5.49	31.53	139.51
72.9484	7.99	0.78	60.48	39.52	1.4617	2.68	12.51	4.17	6.08	34.90	154.42
80.7343	6.63	0.65	67.10	32.90	1.3207	2.97	13.84	4.61	6.73	38.63	170.90
89.0889	5.72	0.56	72.82	27.18	1.1969	3.28	15.27	5.09	7.42	42.62	188.58
98.6420	4.87	0.47	77.69	22.31	1.0809	3.63	16.91	5.64	8.22	47.19	208.80
108.5355	3.85	0.38	81.54	18.46	0.9824	3.99	18.61	6.20	9.04	51.93	229.75
120.0761	3.11	0.30	84.64	15.36	0.8880	4.42	20.58	6.86	10.01	57.45	254.17
132.4460	2.47	0.24	87.12	12.88	0.8051	4.87	22.70	7.57	11.04	63.37	280.36
146.3664	2.02	0.20	89.14	10.86	0.7285	5.39	25.09	8.36	12.20	70.03	309.82
161.4751	1.65	0.16	90.79	9.21	0.6603	5.94	27.68	9.23	13.46	77.26	341.81
178.5818	1.34	0.13	92.12	7.88	0.5971	6.57	30.61	10.20	14.88	85.44	378.02
197.1656	1.09	0.11	93.21	6.79	0.5408	7.26	33.80	11.27	16.43	94.33	417.36
217.1623	0.91	0.09	94.12	5.88	0.4910	7.99	37.23	12.41	18.10	103.90	459.68
239.5329	0.77	0.08	94.90	5.10	0.4451	8.82	41.06	13.69	19.96	114.60	507.04
264.3886	0.70	0.07	95.60	4.40	0.4033	9.73	45.32	15.11	22.03	126.50	559.65
291.1785	0.47	0.05	96.07	3.93	0.3662	10.72	49.92	16.64	24.26	139.31	616.36
321.5706	0.47	0.05	96.54	3.46	0.3316	11.83	55.13	18.38	26.80	153.85	680.69
354.8169	0.37	0.04	96.91	3.09	0.3005	13.06	60.82	20.27	29.57	169.76	751.07
390.3492	0.37	0.04	97.28	2.72	0.2732	14.37	66.92	22.31	32.53	186.76	826.28
430.9375	0.29	0.03	97.57	2.43	0.2474	15.86	73.87	24.62	35.91	206.18	912.20
475.3603	0.25	0.02	97.82	2.18	0.2243	17.49	81.49	27.16	39.61	227.43	1006.23
522.9943	0.22	0.02	98.04	1.96	0.2039	19.25	89.65	29.88	43.58	250.22	1107.06
577.0852	0.20	0.02	98.24	1.76	0.1848	21.24	98.93	32.98	48.09	276.10	1221.56
635.6159	0.16	0.02	98.40	1.60	0.1678	23.39	108.96	36.32	52.97	304.11	1345.46
701.2309	0.15	0.01	98.55	1.45	0.1521	25.81	120.21	40.07	58.43	335.50	1484.35
771.7952	0.14	0.01	98.69	1.31	0.1382	28.40	132.30	44.10	64.31	369.26	1633.72
851.5499	0.13	0.01	98.82	1.18	0.1252	31.34	145.98	48.66	70.96	407.42	1802.54
937.8317	0.10	0.01	98.92	1.08	0.1137	34.51	160.77	53.59	78.15	448.70	1985.18
1033.2689	0.11	0.01	99.03	0.97	0.1032	38.03	177.13	59.04	86.10	494.36	2187.20
1138.3497	0.10	0.01	99.13	0.87	0.0937	41.89	195.14	65.05	94.86	544.64	2409.63
1253.4832	0.08	0.01	99.22	0.78	0.0851	46.13	214.88	71.63	104.45	599.72	2653.34
1381.1880	0.08	0.01	99.30	0.70	0.0772	50.83	236.77	78.92	115.10	660.82	2923.67
1521.3820	0.07	0.01	99.37	0.63	0.0701	55.99	260.80	86.93	126.78	727.90	3220.42
1675.9579	0.08	0.01	99.46	0.54	0.0636	61.68	287.30	95.77	139.66	801.85	3547.63
1845.7971	0.08	0.01	99.53	0.47	0.0578	67.93	316.41	105.47	153.81	883.11	3907.14
2033.9001	0.04	0.00	99.58	0.42	0.0524	74.85	348.66	116.22	169.49	973.11	4305.31
2240.2178	0.08	0.01	99.65	0.35	0.0476	82.45	384.03	128.01	186.68	1071.82	4742.04
2468.0957	0.07	0.01	99.72	0.28	0.0432	90.83	423.09	141.03	205.67	1180.85	5224.41
2717.2593	0.05	0.00	99.77	0.23	0.0392	100.00	465.80	155.27	226.43	1300.06	5751.83
2992.4834	0.05	0.00	99.82	0.18	0.0356	110.13	512.98	170.99	249.37	1431.74	6334.42
3295.8430	0.04	0.00	99.86	0.14	0.0324	121.30	564.99	188.33	274.65	1576.88	6976.56
3631.1396	0.05	0.01	99.92	0.08	0.0294	133.63	622.47	207.49	302.59	1737.30	7686.31
3999.5608	0.03	0.00	99.95	0.05	0.0267	147.19	685.62	228.54	333.29	1913.57	8466.17
4397.9697	0.03	0.00	99.97	0.03	0.0242	161.86	753.92	251.31	366.49	2104.18	9309.52
4845.4507	0.00	0.00	99.98	0.02	0.0220	178.32	830.63	276.88	403.78	2318.28	10256.73
5337.5728	0.02	0.00	100.00	0.00	0.0200	196.44	914.99	305.00	444.79	2553.73	11298.45
5878.0884	0.00	0.00	100.00	0.00	0.0181	216.33	1007.65	335.88	489.83	2812.34	12442.60
6477.0015	0.00	0.00	100.00	0.00	0.0165	238.37	1110.32	370.11	539.74	3098.88	13710.36
7133.4990	0.00	0.00	100.00	0.00	0.0149	262.53	1222.86	407.62	594.44	3412.98	15100.02
7858.6719	0.00	0.00	100.00	0.00	0.0136	289.22	1347.17	449.06	654.87	3759.94	16635.05
8661.4990	0.00	0.00	100.00	0.00	0.0123	318.76	1484.79	494.93	721.77	4144.04	18334.45
9535.8037	0.00	0.00	100.00	0.00	0.0112	350.94	1634.67	544.89	794.63	4562.35	20185.16
10510.7070	0.00	0.00	100.00	0.00	0.0101	386.82	1801.79	600.60	875.87	5028.79	22248.81
11577.8740	0.00	0.00	100.00	0.00	0.0092	426.09	1984.73	661.58	964.80	5539.37	24507.76
12755.7568	0.00	0.00	100.00	0.00	0.0084	469.44	2186.65	728.88	1062.95	6102.92	27001.08
14049.7402	0.00	0.00	100.00	0.00	0.0076	517.07	2408.47	802.82	1170.78	6722.02	29740.15
15477.2080	0.00	0.00	100.00	0.00	0.0069	569.60	2653.17	884.39	1289.74	7404.98	32761.78
17046.1367	0.00	0.00	100.00	0.00	0.0063	627.34	2922.13	974.04	1420.48	8155.82	36082.85
18785.4375	0.00	0.00	100.00	0.00	0.0057	691.35	3220.28	1073.43	1565.42	8987.78	39764.56
20697.7246	0.00	0.00	100.00	0.00	0.0052	761.73	3548.10	1182.70	1724.77	9902.70	43812.44
22810.9355	0.00	0.00	100.00	0.00	0.0047	839.50	3910.35	1303.45	1900.87	10913.76	48285.64
25130.3242	0.00	0.00	100.00	0.00	0.0042	924.86	4307.95	1435.98	2094.14	12023.45	53195.26
27683.8203	0.00	0.00	100.00	0.00	0.0039	1018.83	4745.68	1581.89	2306.93	13245.16	58600.44
30492.6348	0.00	0.00	100.00	0.00	0.0035	1122.20	5227.18	1742.39	2540.99	14589.02	64546.07
33587.7344	0.00	0.00	100.00	0.00	0.0032	1236.11	5757.76	1919.25	2798.91	16069.85	71097.71
36995.3047	0.00	0.00	100.00	0.00	0.0029	1361.52	6341.90	2113.97	3082.87	17700.18	78310.77
40737.3789	0.00	0.00	100.00	0.00	0.0026	1499.24	6983.38	2327.79	3394.70	19490.56	86231.90
44858.6484	0.00	0.00	100.00	0.00	0.0024	1650.91	7689.87	2563.29	3738.13	21462.35	94955.70
49413.1406	0.00	0.00	100.00	0.00	0.0022	1818.53	8470.62	2823.54	4117.66	23641.42	104596.54
54432.8516	0.00	0.00	100.00	0.00	0.0020	2003.26	9331.12	3110.37	4535.96	26043.08	115222.15

Company: Univ. of Wyoming
Well: RSU #1
File: WTC-12-2873

Sample ID: 99
Depth, ft:
Permeability to Air, md: 0.666
Calculated Permeability to Air, md: 0.444
Helium Porosity, percent: 11.6
Mercury Porosity, %. 10.81
Mercury Pore Volume: 1.005
Helium Pore Volume: 1.230
Entry Pressure 36.642

Injection Pressure (Absolute), psia	Non-Wetting Phase Saturation			Wetting Phase Saturation, fraction	Pore Throat Radius, microns	Leverett "J" Function	Capillary Pressure			Height Above Free Water	
	Incremental percent	Normalized Incremental percent	Cumulative percent				Gas/Water psi	Gas/Oil psi	Oil/water psi	Gas/Water feet	Oil/Water feet
0.5364	0.00	0.00	0.00	100.00	198.7807	0.00	0.09	0.03	0.04	0.26	1.14
0.5802	0.00	0.00	0.00	100.00	183.7722	0.00	0.10	0.03	0.05	0.28	1.23
0.6381	0.00	0.00	0.00	100.00	167.1033	0.00	0.11	0.04	0.05	0.31	1.35
0.7000	0.00	0.00	0.00	100.00	152.3319	0.00	0.12	0.04	0.06	0.33	1.48
0.7697	0.00	0.00	0.00	100.00	138.5354	0.01	0.13	0.04	0.06	0.37	1.63
0.8437	0.00	0.00	0.00	100.00	126.3804	0.01	0.14	0.05	0.07	0.40	1.79
0.9274	0.00	0.00	0.00	100.00	114.9744	0.01	0.16	0.05	0.08	0.44	1.96
1.0168	0.00	0.00	0.00	100.00	104.8682	0.01	0.17	0.06	0.08	0.49	2.15
1.1171	0.00	0.00	0.00	100.00	95.4500	0.01	0.19	0.06	0.09	0.53	2.36
1.2270	0.00	0.00	0.00	100.00	86.8994	0.01	0.21	0.07	0.10	0.59	2.60
1.3488	0.00	0.00	0.00	100.00	79.0505	0.01	0.23	0.08	0.11	0.65	2.86
1.4822	0.00	0.00	0.00	100.00	71.9389	0.01	0.25	0.08	0.12	0.71	3.14
1.6259	0.00	0.00	0.00	100.00	65.5794	0.01	0.28	0.09	0.14	0.78	3.44
1.7877	0.00	0.00	0.00	100.00	59.6440	0.01	0.31	0.10	0.15	0.86	3.78
1.9651	0.00	0.00	0.00	100.00	54.2600	0.01	0.34	0.11	0.16	0.94	4.16
2.1601	0.00	0.00	0.00	100.00	49.3623	0.01	0.37	0.12	0.18	1.03	4.57
2.3727	0.00	0.00	0.00	100.00	44.9385	0.02	0.41	0.14	0.20	1.14	5.02
2.6078	0.00	0.00	0.00	100.00	40.8871	0.02	0.45	0.15	0.22	1.25	5.52
2.8680	0.00	0.00	0.00	100.00	37.1786	0.02	0.49	0.16	0.24	1.37	6.07
3.1514	0.00	0.00	0.00	100.00	33.8344	0.02	0.54	0.18	0.26	1.51	6.67
3.4646	0.00	0.00	0.00	100.00	30.7757	0.02	0.59	0.20	0.29	1.66	7.33
3.8102	0.00	0.00	0.00	100.00	27.9849	0.02	0.65	0.22	0.32	1.82	8.07
4.1933	0.00	0.00	0.00	100.00	25.4279	0.03	0.72	0.24	0.35	2.01	8.88
4.6196	0.00	0.00	0.00	100.00	23.0816	0.03	0.79	0.26	0.38	2.21	9.78
5.0865	0.00	0.00	0.00	100.00	20.9628	0.03	0.87	0.29	0.42	2.43	10.77
5.6018	0.00	0.00	0.00	100.00	19.0344	0.04	0.96	0.32	0.47	2.68	11.86
6.1696	0.00	0.00	0.00	100.00	17.2826	0.04	1.06	0.35	0.51	2.95	13.06
6.7956	0.00	0.00	0.00	100.00	15.6907	0.04	1.16	0.39	0.57	3.25	14.38
7.4832	0.00	0.00	0.00	100.00	14.2488	0.05	1.28	0.43	0.62	3.58	15.84
8.2428	0.00	0.00	0.00	100.00	12.9358	0.05	1.41	0.47	0.69	3.94	17.45
9.0742	0.00	0.00	0.00	100.00	11.7506	0.06	1.56	0.52	0.76	4.34	19.21
9.9938	0.00	0.00	0.00	100.00	10.6694	0.07	1.71	0.57	0.83	4.78	21.15
11.0077	0.00	0.00	0.00	100.00	9.6865	0.07	1.89	0.63	0.92	5.27	23.30
12.1231	0.00	0.00	0.00	100.00	8.7954	0.08	2.08	0.69	1.01	5.80	25.66
13.3500	0.00	0.00	0.00	100.00	7.9870	0.09	2.29	0.76	1.11	6.39	28.26
14.7004	0.00	0.00	0.00	100.00	7.2533	0.10	2.52	0.84	1.23	7.03	31.12
16.1856	0.00	0.00	0.00	100.00	6.5878	0.11	2.77	0.92	1.35	7.74	34.26
17.8342	0.00	0.00	0.00	100.00	5.9788	0.12	3.06	1.02	1.49	8.53	37.75
19.6874	0.00	0.00	0.00	100.00	5.4160	0.13	3.37	1.12	1.64	9.42	41.67
21.6808	0.00	0.00	0.00	100.00	4.9180	0.14	3.72	1.24	1.81	10.37	45.89
23.8692	0.00	0.00	0.00	100.00	4.4671	0.16	4.09	1.36	1.99	11.42	50.53
26.2850	0.00	0.00	0.00	100.00	4.0566	0.17	4.51	1.50	2.19	12.58	55.64
28.9390	0.00	0.00	0.00	100.00	3.6845	0.19	4.96	1.65	2.41	13.85	61.26
31.8748	0.00	0.00	0.00	100.00	3.3452	0.21	5.46	1.82	2.66	15.25	67.47
35.1054	0.00	0.00	0.00	100.00	3.0373	0.23	6.02	2.01	2.93	16.80	74.31
36.6419	0.84	0.10	0.84	99.16	2.9100	0.24	6.28	2.09	3.05	17.53	77.56
40.9267	1.08	0.12	1.92	98.08	2.6053	0.27	7.02	2.34	3.41	19.58	86.63
43.4249	1.78	0.20	3.70	96.30	2.4554	0.28	7.44	2.48	3.62	20.78	91.92
48.5600	3.33	0.38	7.03	92.97	2.1958	0.32	8.32	2.77	4.05	23.23	102.79
53.8752	4.72	0.54	11.75	88.25	1.9791	0.35	9.24	3.08	4.49	25.78	114.04
59.6321	6.38	0.73	18.14	81.86	1.7881	0.39	10.22	3.41	4.97	28.53	126.23
65.5819	7.76	0.89	25.89	74.11	1.6259	0.43	11.24	3.75	5.47	31.38	138.82
72.1090	8.73	1.00	34.62	65.38	1.4787	0.47	12.36	4.12	6.01	34.50	152.64
80.2941	8.69	0.99	43.31	56.69	1.3280	0.52	13.76	4.59	6.69	38.42	169.96
88.6227	7.72	0.88	51.03	48.97	1.2032	0.58	15.19	5.06	7.39	42.40	187.59
97.4441	5.10	0.58	56.13	43.87	1.0942	0.63	16.70	5.57	8.12	46.62	206.27
107.8040	3.72	0.43	59.85	40.15	0.9891	0.70	18.48	6.16	8.98	51.58	228.20
119.4692	3.20	0.37	63.05	36.95	0.8925	0.78	20.48	6.83	9.96	57.16	252.89
132.1000	2.95	0.34	66.00	34.00	0.8072	0.86	22.65	7.55	11.01	63.20	279.63
145.5798	2.85	0.33	68.84	31.16	0.7324	0.95	24.96	8.32	12.13	69.65	308.16
160.3207	2.60	0.30	71.44	28.56	0.6651	1.04	27.48	9.16	13.36	76.70	339.36
176.9416	2.49	0.28	73.93	26.07	0.6026	1.15	30.33	10.11	14.74	84.66	374.55
196.0723	2.35	0.27	76.28	23.72	0.5438	1.28	33.61	11.20	16.34	93.81	415.04
216.1256	2.09	0.24	78.37	21.63	0.4934	1.41	37.05	12.35	18.01	103.40	457.49
238.2497	1.86	0.21	80.23	19.77	0.4475	1.55	40.84	13.61	19.85	113.99	504.32
262.6808	1.73	0.20	81.96	18.04	0.4059	1.71	45.03	15.01	21.89	125.68	556.04
290.2208	1.57	0.18	83.53	16.47	0.3674	1.89	49.75	16.58	24.18	138.85	614.33
320.2021	1.43	0.16	84.96	15.04	0.3330	2.08	54.89	18.30	26.68	153.20	677.80
352.5275	1.27	0.15	86.23	13.77	0.3025	2.29	60.43	20.14	29.38	168.66	746.22
389.1134	1.20	0.14	87.43	12.57	0.2740	2.53	66.70	22.23	32.43	186.17	823.67
429.4755	1.07	0.12	88.50	11.50	0.2483	2.80	73.62	24.54	35.79	205.48	909.10
473.0487	0.97	0.11	89.46	10.54	0.2254	3.08	81.09	27.03	39.42	226.33	1001.34
521.2316	0.87	0.10	90.34	9.66	0.2046	3.39	89.35	29.78	43.43	249.38	1103.33
575.8339	0.81	0.09	91.14	8.86	0.1852	3.75	98.71	32.90	47.99	275.50	1218.91
634.3048	0.71	0.08	91.85	8.15	0.1681	4.13	108.74	36.25	52.86	303.48	1342.68
698.8447	0.64	0.07	92.49	7.51	0.1526	4.55	119.80	39.93	58.24	334.36	1479.30
770.6677	0.58	0.07	93.07	6.93	0.1384	5.02	132.11	44.04	64.22	368.72	1631.33
849.3803	0.53	0.06	93.60	6.40	0.1255	5.53	145.60	48.53	70.78	406.38	1797.95
936.1800	0.48	0.05	94.08	5.92	0.1139	6.09	160.48	53.49	78.01	447.91	1981.68
1031.7861	0.44	0.05	94.51	5.49	0.1033	6.72	176.87	58.96	85.98	493.65	2184.06
1136.8715	0.41	0.05	94.92	5.08	0.0938	7.40	194.89	64.96	94.74	543.93	2406.50
1251.9277	0.38	0.04	95.30	4.70	0.0852	8.15	214.61	71.54	104.32	598.98	2650.05
1379.1276	0.38	0.04	95.68	4.32	0.0773	8.98	236.42	78.81	114.92	659.84	2919.30
1519.6084	0.37	0.04	96.05	3.95	0.0702	9.89	260.50	86.83	126.63	727.05	3216.67
1673.8701	0.37	0.04	96.41	3.59	0.0637	10.90	286.94	95.65	139.49	800.85	3543.21
1844.4530	0.37	0.04	96.78	3.22	0.0578	12.01	316.18	105.39	153.70	882.47	3904.29
2031.3777	0.38	0.04	97.17	2.83	0.0525	13.22	348.23	116.08	169.28	971.90	4299.97
2238.6904	0.39	0.04	97.56	2.44	0.0476	14.57	383.77	127.92	186.55	1071.09	4738.81
2464.0552	0.38	0.04	97.94	2.06	0.0433	16.04	422.40	140.80	205.33	1178.91	5215.85
2715.3635	0.38	0.04	98.32	1.68	0.0393	17.68	465.48	155.16	226.27	1299.15	5747.82
2990.9133	0.35	0.04	98.67	1.33	0.0357	19.47	512.72	170.91	249.24	1430.98	6331.09
3294.6526	0.31	0.04	98.98	1.02	0.0324	21.45	564.78	188.26	274.55	1576.31	6974.04
3627.9668	0.26	0.03	99.25	0.75	0.0294	23.62	621.92	207.31	302.32	1735.78	7679.59
3997.4832	0.22	0.02	99.46	0.54	0.0267	26.02	685.27	228.42	333.12	1912.57	8461.78
4397.6318	0.21	0.02	99.67	0.33	0.0242	28.63	753.86	251.29	366.46	2104.02	9308.80
4844.2822	0.14	0.02	99.81	0.19	0.0220	31.54	830.43	276.81	403.68	2317.72	10254.26
5335.3677	0.09	0.01	99.90	0.10	0.0200	34.73	914.61	304.87	444.60	2552.68	11293.78
5874.0991	0.06	0.01	99.96	0.04	0.0182	38.24	1006.96	335.65	489.50	2810.43	12434.15
6474.7261	0.03	0.00	100.00	0.00	0.0165	42.15	1109.93	369.98	539.55	3097.79	13705.54
7129.5059	0.00	0.00	100.00	0.00	0.0150	46.41	1222.17	407.39	594.11	3411.07	15091.57
7856.7461	0.00	0.00	100.00	0.00	0.0136	51.15	1346.84	448.95	654.71	3759.01	16630.97
8658.6982	0.00	0.00	100.00	0.00	0.0123	56.37	1484.31	494.77	721.54	4142.70	18328.52
9537.5957	0.00	0.00	100.00	0.00	0.0112	62.09	1634.98	544.99	794.78	4563.21	20188.95
10508.6865	0.00	0.00	100.00	0.00	0.0101	68.41	1801.45	600.48	875.70	5027.82	22244.53
11575.5830	0.00	0.00	100.00	0.00	0.0092	75.36	1984.34	661.45	964.61	5538.27	24502.91
12753.6719	0.00	0.00	100.00	0.00	0.0084	83.03	2186.29	728.76	1062.78	6101.92	26996.66
14052.4355	0.00	0.00	100.00	0.00	0.0076	91.48	2408.93	802.98	1171.01	6723.30	29745.86
15479.0840	0.00	0.00	100.00	0.00	0.0069	100.77	2653.49	884.50	1289.89	7405.88	32765.75
17051.9492	0.00	0.00	100.00	0.00	0.0063	111.01	2923.12	974.37	1420.96	8158.40	36095.15
18781.7910	0.00	0.00	100.00	0.00	0.0057	122.27	3219.66	1073.22	1565.11	8986.04	39756.84
20697.8262	0.00	0.00	100.00	0.00	0.0052	134.74	3548.11	1182.70	1724.78	9902.75	43812.66
22809.7012	0.00	0.00	100.00	0.00	0.0047	148.49	3910.14	1303.38	1900.76	10913.17	48283.02
25128.6934	0.00	0.00	100.00	0.00	0.0042	163.59	4307.67	1435.89	2094.01	12022.67	53191.81
27680.4961	0.00	0.00	100.00	0.00	0.0039	180.20	4745.11	1581.70	2306.65	13243.57	58593.41
30490.2715	0.00	0.00	100.00	0.00	0.0035	198.49	5226.78	1742.26	2540.80	14587.89	64541.07
33584.9844	0.00	0.00	100.00	0.00	0.0032	218.64	5757.29	1919.10	2798.68	16068.54	71091.88
36993.9688	0.00	0.00	100.00	0.00	0.0029	240.83	6341.67	2113.89	3082.76	17699.55	78307.94
40736.0703	0.00	0.00	100.00	0.00	0.0026	265.19	6983.16	2327.72	3394.59	19489.93	86229.13
44860.0039	0.00	0.00	100.00	0.00	0.0024	292.03	7690.10	2563.37	3738.24	21463.00	94958.57
49410.3555	0.00	0.00	100.00	0.00	0.0022	321.66	8470.14	2823.38	4117.43	23640.09	104590.65
54428.6563	0.00	0.00	100.00	0.00	0.0020	354.33	9330.40	3110.13	4535.61	26041.07	115213.27
59955.1914	0.00	0.00	100.00	0.00	0.0018	390.30	10277.79	3425.93	4996.15	28685.21	126911.70

Company: Univ. of Wyoming
Well: RSU #1
File: WTC-12-2873

Sample ID: 79
Depth, ft:
Permeability to Air, md: 42.288
Calculated Permeability to Air, md: 6.484
Helium Porosity, percent: 23.5
Mercury Porosity, %. 22.41
Mercury Pore Volume: 1.853
Helium Pore Volume: 1.932
Entry Pressure 35.106

Injection Pressure (Absolute), psia	Non-Wetting Phase Saturation			Wetting Phase Saturation, fraction	Pore Throat Radius, microns	Leverett "J" Function	Capillary Pressure			Height Above Free Water	
	Incremental percent	Normalized Incremental percent	Cumulative percent				Gas/Water psi	Gas/Oil psi	Oil/water psi	Gas/Water feet	Oil/Water feet
0.5358	0.00	0.00	0.00	100.00	199.0116	0.02	0.09	0.03	0.04	0.26	1.13
0.5804	0.00	0.00	0.00	100.00	183.7199	0.02	0.10	0.03	0.05	0.28	1.23
0.6378	0.00	0.00	0.00	100.00	167.1688	0.02	0.11	0.04	0.05	0.31	1.35
0.7010	0.00	0.00	0.00	100.00	152.1119	0.03	0.12	0.04	0.06	0.34	1.48
0.7694	0.00	0.00	0.00	100.00	138.5867	0.03	0.13	0.04	0.06	0.37	1.63
0.8448	0.00	0.00	0.00	100.00	126.2108	0.03	0.14	0.05	0.07	0.40	1.79
0.9277	0.00	0.00	0.00	100.00	114.9357	0.03	0.16	0.05	0.08	0.44	1.96
1.0171	0.00	0.00	0.00	100.00	104.8302	0.04	0.17	0.06	0.08	0.49	2.15
1.1170	0.00	0.00	0.00	100.00	95.4618	0.04	0.19	0.06	0.09	0.53	2.36
1.2279	0.00	0.00	0.00	100.00	86.8377	0.04	0.21	0.07	0.10	0.59	2.60
1.3487	0.00	0.00	0.00	100.00	79.0575	0.05	0.23	0.08	0.11	0.65	2.85
1.4816	0.00	0.00	0.00	100.00	71.9697	0.05	0.25	0.08	0.12	0.71	3.14
1.6260	0.00	0.00	0.00	100.00	65.5775	0.06	0.28	0.09	0.14	0.78	3.44
1.7878	0.00	0.00	0.00	100.00	59.6412	0.07	0.31	0.10	0.15	0.86	3.78
1.9648	0.00	0.00	0.00	100.00	54.2700	0.07	0.34	0.11	0.16	0.94	4.16
2.1589	0.00	0.00	0.00	100.00	49.3901	0.08	0.37	0.12	0.18	1.03	4.57
2.3735	0.00	0.00	0.00	100.00	44.9247	0.09	0.41	0.14	0.20	1.14	5.02
2.6079	0.00	0.00	0.00	100.00	40.8867	0.10	0.45	0.15	0.22	1.25	5.52
2.8665	0.00	0.00	0.00	100.00	37.1978	0.10	0.49	0.16	0.24	1.37	6.07
3.1512	0.00	0.00	0.00	100.00	33.8365	0.12	0.54	0.18	0.26	1.51	6.67
3.4649	0.00	0.00	0.00	100.00	30.7732	0.13	0.59	0.20	0.29	1.66	7.33
3.8090	0.00	0.00	0.00	100.00	27.9936	0.14	0.65	0.22	0.32	1.82	8.06
4.1934	0.00	0.00	0.00	100.00	25.4274	0.15	0.72	0.24	0.35	2.01	8.88
4.6183	0.00	0.00	0.00	100.00	23.0878	0.17	0.79	0.26	0.38	2.21	9.78
5.0859	0.00	0.00	0.00	100.00	20.9654	0.19	0.87	0.29	0.42	2.43	10.77
5.6012	0.00	0.00	0.00	100.00	19.0365	0.20	0.96	0.32	0.47	2.68	11.86
6.1700	0.00	0.00	0.00	100.00	17.2816	0.23	1.06	0.35	0.51	2.95	13.06
6.7931	0.00	0.00	0.00	100.00	15.6963	0.25	1.16	0.39	0.57	3.25	14.38
7.4823	0.00	0.00	0.00	100.00	14.2506	0.27	1.28	0.43	0.62	3.58	15.84
8.2401	0.00	0.00	0.00	100.00	12.9401	0.30	1.41	0.47	0.69	3.94	17.44
9.0762	0.00	0.00	0.00	100.00	11.7480	0.33	1.56	0.52	0.76	4.34	19.21
9.9912	0.00	0.00	0.00	100.00	10.6721	0.36	1.71	0.57	0.83	4.78	21.15
11.0067	0.00	0.00	0.00	100.00	9.6874	0.40	1.89	0.63	0.92	5.27	23.30
12.1197	0.00	0.00	0.00	100.00	8.7978	0.44	2.08	0.69	1.01	5.80	25.65
13.3457	0.00	0.00	0.00	100.00	7.9896	0.49	2.29	0.76	1.11	6.39	28.25
14.7034	0.00	0.00	0.00	100.00	7.2519	0.54	2.52	0.84	1.23	7.03	31.12
16.1874	0.00	0.00	0.00	100.00	6.5870	0.59	2.77	0.92	1.35	7.74	34.27
17.8293	0.00	0.00	0.00	100.00	5.9804	0.65	3.06	1.02	1.49	8.53	37.74
19.6421	0.00	0.00	0.00	100.00	5.4285	0.72	3.37	1.12	1.64	9.40	41.58
21.6739	0.00	0.00	0.00	100.00	4.9196	0.79	3.72	1.24	1.81	10.37	45.88
23.8731	0.00	0.00	0.00	100.00	4.4664	0.87	4.09	1.36	1.99	11.42	50.53
26.2780	0.00	0.00	0.00	100.00	4.0577	0.96	4.50	1.50	2.19	12.57	55.62
28.9375	0.00	0.00	0.00	100.00	3.6847	1.06	4.96	1.65	2.41	13.84	61.25
31.8658	0.00	0.00	0.00	100.00	3.3461	1.16	5.46	1.82	2.66	15.25	67.45
35.1056	1.98	0.08	1.98	98.02	3.0373	1.28	6.02	2.01	2.93	16.80	74.31
36.6332	1.40	0.06	3.39	96.61	2.9107	1.34	6.28	2.09	3.05	17.53	77.54
39.4086	3.30	0.13	6.69	93.31	2.7057	1.44	6.76	2.25	3.28	18.85	83.42
43.2975	11.23	0.46	17.91	82.09	2.4627	1.58	7.42	2.47	3.61	20.72	91.65
48.6190	19.80	0.81	37.71	62.29	2.1931	1.77	8.33	2.78	4.05	23.26	102.92
54.2253	24.45	1.00	62.16	37.84	1.9664	1.98	9.30	3.10	4.52	25.94	114.78
59.6753	10.44	0.43	72.60	27.40	1.7868	2.18	10.23	3.41	4.97	28.55	126.32
65.7411	6.28	0.26	78.89	21.11	1.6219	2.40	11.27	3.76	5.48	31.45	139.16
73.0857	4.48	0.18	83.37	16.63	1.4589	2.67	12.53	4.18	6.09	34.97	154.71
80.4532	3.31	0.14	86.68	13.32	1.3253	2.94	13.79	4.60	6.70	38.49	170.30
89.2285	2.64	0.11	89.33	10.67	1.1950	3.26	15.30	5.10	7.44	42.69	188.88
98.3528	1.87	0.08	91.20	8.80	1.0841	3.59	16.86	5.62	8.20	47.06	208.19
108.3039	1.55	0.06	92.75	7.25	0.9845	3.95	18.57	6.19	9.03	51.82	229.26
120.2861	1.26	0.05	94.01	5.99	0.8864	4.39	20.62	6.87	10.02	57.55	254.62
132.6746	0.94	0.04	94.96	5.04	0.8037	4.84	22.74	7.58	11.06	63.48	280.84
146.3766	0.78	0.03	95.74	4.26	0.7284	5.34	25.09	8.36	12.20	70.03	309.85
161.4751	0.64	0.03	96.38	3.62	0.6603	5.89	27.68	9.23	13.46	77.26	341.81
178.0299	0.51	0.02	96.89	3.11	0.5969	6.52	30.62	10.21	14.89	85.46	378.12
196.3456	0.41	0.02	97.30	2.70	0.5431	7.17	33.66	11.22	16.36	93.94	415.62
217.4840	0.35	0.01	97.65	2.35	0.4903	7.94	37.28	12.43	18.12	104.05	460.36
239.4883	0.29	0.01	97.94	2.06	0.4452	8.74	41.05	13.68	19.96	114.58	506.94
264.4721	0.24	0.01	98.18	1.82	0.4032	9.65	45.34	15.11	22.04	126.54	559.83
291.7997	0.21	0.01	98.39	1.61	0.3654	10.65	50.02	16.67	24.32	139.61	617.67
321.3738	0.17	0.01	98.56	1.44	0.3318	11.73	55.09	18.36	26.78	153.76	680.28
354.5191	0.14	0.01	98.70	1.30	0.3008	12.94	60.77	20.26	29.54	169.62	750.44
390.6251	0.13	0.01	98.83	1.17	0.2730	14.26	66.96	22.32	32.55	186.89	826.87
430.4330	0.11	0.00	98.94	1.06	0.2477	15.71	73.79	24.60	35.87	205.94	911.13
474.3568	0.10	0.00	99.04	0.96	0.2248	17.31	81.32	27.11	39.53	226.95	1004.11
523.2463	0.08	0.00	99.11	0.89	0.2038	19.10	89.70	29.90	43.60	250.34	1107.60
576.7112	0.06	0.00	99.18	0.82	0.1849	21.05	98.86	32.95	48.06	275.92	1220.77
635.9993	0.07	0.00	99.24	0.76	0.1677	23.21	109.03	36.34	53.00	304.29	1346.27
700.7429	0.06	0.00	99.30	0.70	0.1522	25.58	120.12	40.04	58.39	335.27	1483.32
772.4998	0.05	0.00	99.35	0.65	0.1380	28.20	132.43	44.14	64.37	369.60	1635.21
851.0416	0.06	0.00	99.41	0.59	0.1253	31.06	145.89	48.63	70.92	407.18	1801.46
937.6114	0.03	0.00	99.45	0.55	0.1137	34.22	160.73	53.58	78.13	448.59	1984.71
1033.8719	0.06	0.00	99.51	0.49	0.1031	37.74	177.23	59.08	86.15	494.65	2188.48
1138.5439	0.05	0.00	99.56	0.44	0.0937	41.56	195.17	65.06	94.88	544.73	2410.04
1253.5789	0.04	0.00	99.60	0.40	0.0851	45.76	214.89	71.63	104.46	599.77	2653.55
1381.2491	0.04	0.00	99.64	0.36	0.0772	50.42	236.78	78.93	115.10	660.85	2923.79
1522.0068	0.04	0.00	99.68	0.32	0.0701	55.56	260.91	86.97	126.83	728.20	3221.75
1675.9232	0.04	0.00	99.73	0.27	0.0636	61.17	287.29	95.76	139.66	801.84	3547.55
1845.9939	0.05	0.00	99.77	0.23	0.0578	67.38	316.45	105.48	153.83	883.20	3907.56
2033.4264	0.04	0.00	99.81	0.19	0.0524	74.22	348.58	116.19	169.45	972.88	4304.31
2240.6099	0.04	0.00	99.85	0.15	0.0476	81.79	384.10	128.03	186.71	1072.01	4742.87
2467.8179	0.03	0.00	99.88	0.12	0.0432	90.08	423.04	141.01	205.65	1180.71	5223.82
2717.5176	0.03	0.00	99.91	0.09	0.0392	99.19	465.85	155.28	226.45	1300.18	5752.38
2993.5588	0.03	0.00	99.94	0.06	0.0356	109.27	513.17	171.06	249.46	1432.25	6336.69
3296.5569	0.02	0.00	99.96	0.04	0.0323	120.33	565.11	188.37	274.71	1577.22	6978.07
3630.8533	0.02	0.00	99.98	0.02	0.0294	132.53	622.42	207.47	302.56	1737.16	7685.70
4000.2715	0.01	0.00	99.99	0.01	0.0267	146.01	685.74	228.58	333.35	1913.91	8467.68
4398.6948	0.01	0.00	100.00	0.00	0.0242	160.56	754.04	251.35	366.55	2104.53	9311.05
4846.5503	0.00	0.00	100.00	0.00	0.0220	176.91	830.82	276.94	403.87	2318.80	10259.06
5337.5879	0.00	0.00	100.00	0.00	0.0200	194.83	914.99	305.00	444.79	2553.74	11298.48
5880.1777	0.00	0.00	100.00	0.00	0.0181	214.63	1008.01	336.00	490.00	2813.34	12447.02
6476.8135	0.00	0.00	100.00	0.00	0.0165	236.41	1110.28	370.09	539.72	3098.79	13709.96
7133.9966	0.00	0.00	100.00	0.00	0.0149	260.40	1222.94	407.65	594.49	3413.22	15101.07
7861.1030	0.00	0.00	100.00	0.00	0.0136	286.94	1347.59	449.20	655.08	3761.10	16640.19
8660.5850	0.00	0.00	100.00	0.00	0.0123	316.12	1484.64	494.88	721.70	4143.61	18332.52
9541.7344	0.00	0.00	100.00	0.00	0.0112	348.29	1635.69	545.23	795.13	4565.19	20197.71
10511.6904	0.00	0.00	100.00	0.00	0.0101	383.69	1801.96	600.65	875.95	5029.26	22250.89
11581.6396	0.00	0.00	100.00	0.00	0.0092	422.74	1985.38	661.79	965.11	5541.17	24515.74
12755.3145	0.00	0.00	100.00	0.00	0.0084	465.58	2186.57	728.86	1062.92	6102.70	27000.14
14051.7314	0.00	0.00	100.00	0.00	0.0076	512.91	2408.81	802.94	1170.95	6722.97	29744.37
15481.9814	0.00	0.00	100.00	0.00	0.0069	565.11	2653.99	884.66	1290.13	7407.26	32771.88
17051.3242	0.00	0.00	100.00	0.00	0.0063	622.39	2923.01	974.34	1420.91	8158.11	36093.83
18782.8984	0.00	0.00	100.00	0.00	0.0057	685.60	3219.85	1073.28	1565.20	8986.57	39759.19
20700.4355	0.00	0.00	100.00	0.00	0.0052	755.59	3548.56	1182.85	1725.00	9904.00	43818.18
22811.2617	0.00	0.00	100.00	0.00	0.0047	832.64	3910.41	1303.47	1900.89	10913.91	48286.33
25130.6953	0.00	0.00	100.00	0.00	0.0042	917.30	4308.02	1436.01	2094.17	12023.63	53196.05
27683.2324	0.00	0.00	100.00	0.00	0.0039	1010.47	4745.58	1581.86	2306.88	13244.88	58599.20
30493.5879	0.00	0.00	100.00	0.00	0.0035	1113.05	5227.35	1742.45	2541.07	14589.48	64548.09
33589.0938	0.00	0.00	100.00	0.00	0.0032	1226.04	5757.99	1919.33	2799.02	16070.50	71100.58
36995.7109	0.00	0.00	100.00	0.00	0.0029	1350.39	6341.97	2113.99	3082.90	17700.38	78311.63
40736.7734	0.00	0.00	100.00	0.00	0.0026	1486.94	6983.28	2327.76	3394.65	19490.27	86230.62
44860.6797	0.00	0.00	100.00	0.00	0.0024	1637.47	7690.22	2563.41	3738.30	21463.33	94960.00
49411.9883	0.00	0.00	100.00	0.00	0.0022	1803.60	8470.42	2823.47	4117.57	23640.87	104594.10
54433.8984	0.00	0.00	100.00	0.00	0.0020	1986.91	9331.30	3110.43	4536.05	26043.58	115224.36
59953.6250	0.00	0.00	100.00	0.00	0.0018	2188.38	10277.52	3425.84	4996.02	28684.46	126908.39

Company: Univ. of Wyoming
Well: RSU #1
File: WTC-12-2873

Sample ID: 106
Depth, ft:
Permeability to Air, md: 7.494
Calculated Permeability to Air, md: 2.811
Helium Porosity, percent: 18.5
Mercury Porosity, %: 12.92
Mercury Pore Volume: 0.682
Helium Pore Volume: 0.792
Entry Pressure 9.074

Injection Pressure (Absolute), psia	Non-Wetting Phase Saturation			Wetting Phase Saturation, fraction	Pore Throat Radius, microns	Leverett "J" Function	Capillary Pressure			Height Above Free Water	
	Incremental percent	Normalized Incremental percent	Cumulative percent				Gas/Water psi	Gas/Oil psi	Oil/water psi	Gas/Water feet	Oil/Water feet
0.5358	0.00	0.00	0.00	100.00	199.0180	0.01	0.09	0.03	0.04	0.26	1.13
0.5807	0.00	0.00	0.00	100.00	183.6246	0.01	0.10	0.03	0.05	0.28	1.23
0.6385	0.00	0.00	0.00	100.00	167.0067	0.01	0.11	0.04	0.05	0.31	1.35
0.6997	0.00	0.00	0.00	100.00	152.3948	0.01	0.12	0.04	0.06	0.33	1.48
0.7706	0.00	0.00	0.00	100.00	138.3611	0.01	0.13	0.04	0.06	0.37	1.63
0.8442	0.00	0.00	0.00	100.00	126.3104	0.01	0.14	0.05	0.07	0.40	1.79
0.9258	0.00	0.00	0.00	100.00	115.1676	0.02	0.16	0.05	0.08	0.44	1.96
1.0165	0.00	0.00	0.00	100.00	104.8912	0.02	0.17	0.06	0.08	0.49	2.15
1.1150	0.00	0.00	0.00	100.00	95.6291	0.02	0.19	0.06	0.09	0.53	2.36
1.2270	0.00	0.00	0.00	100.00	86.9027	0.02	0.21	0.07	0.10	0.59	2.60
1.3477	0.00	0.00	0.00	100.00	79.1163	0.02	0.23	0.08	0.11	0.64	2.85
1.4797	0.00	0.00	0.00	100.00	72.0575	0.03	0.25	0.08	0.12	0.71	3.13
1.6272	0.00	0.00	0.00	100.00	65.5280	0.03	0.28	0.09	0.14	0.78	3.44
1.7883	0.00	0.00	0.00	100.00	59.6245	0.03	0.31	0.10	0.15	0.86	3.79
1.9656	0.00	0.00	0.00	100.00	54.2475	0.03	0.34	0.11	0.16	0.94	4.16
2.1588	0.00	0.00	0.00	100.00	49.3916	0.04	0.37	0.12	0.18	1.03	4.57
2.3740	0.00	0.00	0.00	100.00	44.9140	0.04	0.41	0.14	0.20	1.14	5.03
2.6074	0.00	0.00	0.00	100.00	40.8943	0.05	0.45	0.15	0.22	1.25	5.52
2.8662	0.00	0.00	0.00	100.00	37.2021	0.05	0.49	0.16	0.24	1.37	6.07
3.1515	0.00	0.00	0.00	100.00	33.8342	0.05	0.54	0.18	0.26	1.51	6.67
3.4641	0.00	0.00	0.00	100.00	30.7806	0.06	0.59	0.20	0.29	1.66	7.33
3.8098	0.00	0.00	0.00	100.00	27.9874	0.07	0.65	0.22	0.32	1.82	8.06
4.1943	0.00	0.00	0.00	100.00	25.4219	0.07	0.72	0.24	0.35	2.01	8.88
4.6179	0.00	0.00	0.00	100.00	23.0897	0.08	0.79	0.26	0.38	2.21	9.78
5.0868	0.00	0.00	0.00	100.00	20.9614	0.09	0.87	0.29	0.42	2.43	10.77
5.6016	0.00	0.00	0.00	100.00	19.0352	0.10	0.96	0.32	0.47	2.68	11.86
6.1664	0.00	0.00	0.00	100.00	17.2916	0.11	1.06	0.35	0.51	2.95	13.05
6.7939	0.00	0.00	0.00	100.00	15.6944	0.12	1.16	0.39	0.57	3.25	14.38
7.4812	0.00	0.00	0.00	100.00	14.2526	0.13	1.28	0.43	0.62	3.58	15.84
8.2433	0.00	0.00	0.00	100.00	12.9350	0.14	1.41	0.47	0.69	3.94	17.45
9.0743	0.85	0.20	0.85	99.15	11.7504	0.16	1.56	0.52	0.76	4.34	19.21
9.9896	3.98	0.94	4.83	95.17	10.6738	0.17	1.71	0.57	0.83	4.78	21.15
11.0065	3.02	0.71	7.85	92.15	9.6876	0.19	1.89	0.63	0.92	5.27	23.30
12.1191	2.85	0.67	10.70	89.30	8.7982	0.21	2.08	0.69	1.01	5.80	25.65
13.3499	3.48	0.82	14.18	85.82	7.9871	0.23	2.29	0.76	1.11	6.39	28.26
14.6984	2.26	0.53	16.44	83.56	7.2543	0.25	2.52	0.84	1.22	7.03	31.11
16.1884	1.81	0.43	18.25	81.75	6.5866	0.28	2.78	0.93	1.35	7.75	34.27
17.8268	4.20	0.99	22.45	77.55	5.9813	0.31	3.06	1.02	1.49	8.53	37.74
19.6414	2.19	0.52	24.64	75.36	5.4287	0.34	3.37	1.12	1.64	9.40	41.58
21.6814	4.24	1.00	28.88	71.12	4.9179	0.38	3.72	1.24	1.81	10.37	45.89
23.8714	2.27	0.54	31.15	68.85	4.4667	0.41	4.09	1.36	1.99	11.42	50.53
26.2833	3.59	0.85	34.74	65.26	4.0568	0.46	4.51	1.50	2.19	12.58	55.64
28.9385	3.77	0.89	38.51	61.49	3.6846	0.50	4.96	1.65	2.41	13.85	61.26
31.8745	3.53	0.83	42.04	57.96	3.3452	0.55	5.46	1.82	2.66	15.25	67.47
35.1048	2.83	0.67	44.87	55.13	3.0374	0.61	6.02	2.01	2.93	16.80	74.31
37.7002	2.87	0.68	47.74	52.26	2.8283	0.65	6.46	2.15	3.14	18.04	79.80
39.4625	1.20	0.28	48.94	51.06	2.7020	0.68	6.76	2.25	3.29	18.88	83.53
43.6218	1.77	0.42	50.71	49.29	2.4443	0.76	7.48	2.49	3.64	20.87	92.34
47.9422	1.95	0.46	52.66	47.34	2.2241	0.83	8.22	2.74	4.00	22.94	101.48
53.4790	2.06	0.49	54.72	45.28	1.9938	0.93	9.17	3.06	4.46	25.59	113.20
60.2545	2.26	0.53	56.98	43.02	1.7696	1.04	10.33	3.44	5.02	28.83	127.55
65.0843	1.61	0.38	58.59	41.41	1.6383	1.13	11.16	3.72	5.42	31.14	137.77
72.5332	2.16	0.51	60.75	39.25	1.4700	1.26	12.43	4.14	6.04	34.70	153.54
80.4058	2.42	0.57	63.17	36.83	1.3261	1.39	13.78	4.59	6.70	38.47	170.20
90.0802	2.28	0.54	65.45	34.55	1.1837	1.56	15.44	5.15	7.51	43.10	190.68
97.9108	1.99	0.47	67.44	32.56	1.0890	1.70	16.78	5.59	8.16	46.84	207.26
109.2221	2.06	0.49	69.50	30.50	0.9762	1.89	18.72	6.24	9.10	52.26	231.20
120.2531	1.75	0.41	71.25	28.75	0.8867	2.08	20.61	6.87	10.02	57.53	254.55
132.5602	1.57	0.37	72.82	27.18	0.8044	2.30	22.72	7.57	11.05	63.42	280.60
146.3804	1.58	0.37	74.40	25.60	0.7284	2.53	25.09	8.36	12.20	70.03	309.85
162.2707	1.10	0.26	75.49	24.51	0.6571	2.81	27.82	9.27	13.52	77.64	343.49
178.3436	1.07	0.25	76.57	23.43	0.5979	3.09	30.57	10.19	14.86	85.33	377.51
197.0404	0.93	0.22	77.49	22.51	0.5411	3.41	33.78	11.26	16.42	94.27	417.09
217.3175	0.97	0.23	78.46	21.54	0.4907	3.76	37.25	12.42	18.11	103.97	460.01
239.5400	0.85	0.20	79.31	20.69	0.4451	4.15	41.06	13.69	19.96	114.61	507.05
264.1708	0.80	0.19	80.11	19.89	0.4036	4.57	45.29	15.10	22.01	126.39	559.19
291.3585	0.95	0.22	81.06	18.94	0.3660	5.05	49.95	16.65	24.28	139.40	616.74
321.3762	0.84	0.20	81.90	18.10	0.3318	5.56	55.09	18.36	26.78	153.76	680.28
354.2317	0.72	0.17	82.62	17.38	0.3010	6.13	60.72	20.24	29.52	169.48	749.83
390.2401	0.62	0.15	83.23	16.77	0.2732	6.76	66.90	22.30	32.52	186.71	826.05
431.1652	0.64	0.15	83.87	16.13	0.2473	7.47	73.91	24.64	35.93	206.29	912.68
474.9195	0.58	0.14	84.45	15.55	0.2245	8.22	81.41	27.14	39.58	227.22	1005.30
523.0961	0.56	0.13	85.00	15.00	0.2038	9.06	89.67	29.89	43.59	250.27	1107.28
577.0939	0.60	0.14	85.60	14.40	0.1848	9.99	98.93	32.98	48.09	276.11	1221.58
635.5620	0.59	0.14	86.20	13.80	0.1678	11.01	108.95	36.32	52.96	304.08	1345.34
700.4777	0.56	0.13	86.76	13.24	0.1522	12.13	120.08	40.03	58.37	335.14	1482.75
771.2505	0.59	0.14	87.35	12.65	0.1383	13.35	132.21	44.07	64.27	369.00	1632.56
851.1367	0.62	0.15	87.97	12.03	0.1253	14.74	145.91	48.64	70.93	407.22	1801.67
937.5867	0.69	0.16	88.66	11.34	0.1137	16.24	160.73	53.58	78.13	448.58	1984.66
1034.1561	0.75	0.18	89.41	10.59	0.1031	17.91	177.28	59.09	86.18	494.79	2189.08
1139.3365	0.85	0.20	90.27	9.73	0.0936	19.73	195.31	65.10	94.94	545.11	2411.72
1253.7026	0.91	0.22	91.18	8.82	0.0850	21.71	214.92	71.64	104.47	599.83	2653.81
1381.3760	1.01	0.24	92.19	7.81	0.0772	23.92	236.80	78.93	115.11	660.91	2924.06
1521.4857	1.09	0.26	93.28	6.72	0.0701	26.35	260.82	86.94	126.79	727.95	3220.64
1675.8857	1.13	0.27	94.41	5.59	0.0636	29.02	287.29	95.76	139.65	801.82	3547.47
1846.2195	1.10	0.26	95.51	4.49	0.0578	31.97	316.49	105.50	153.85	883.31	3908.03
2033.5057	1.01	0.24	96.53	3.47	0.0524	35.21	348.59	116.20	169.45	972.92	4304.48
2240.1006	0.95	0.22	97.47	2.53	0.0476	38.79	384.01	128.00	186.67	1071.76	4741.79
2467.0156	0.74	0.17	98.21	1.79	0.0432	42.72	422.91	140.97	205.58	1180.33	5222.12
2717.9841	0.60	0.14	98.81	1.19	0.0392	47.06	465.93	155.31	226.49	1300.40	5753.36
2993.6619	0.47	0.11	99.29	0.71	0.0356	51.84	513.19	171.06	249.47	1432.30	6336.91
3296.4963	0.23	0.06	99.52	0.48	0.0323	57.08	565.10	188.37	274.70	1577.19	6977.94
3629.5542	0.19	0.04	99.71	0.29	0.0294	62.85	622.19	207.40	302.46	1736.54	7682.95
4000.3447	0.14	0.03	99.84	0.16	0.0267	69.27	685.76	228.59	333.35	1913.94	8467.83
4398.8877	0.11	0.03	99.95	0.05	0.0242	76.17	754.08	251.36	366.57	2104.62	9311.46
4845.0903	0.03	0.01	99.97	0.03	0.0220	83.90	830.57	276.86	403.75	2318.10	10255.97
5338.0820	0.03	0.01	100.00	0.00	0.0200	92.43	915.08	305.03	444.83	2553.97	11299.52
5876.6729	0.00	0.00	100.00	0.00	0.0181	101.76	1007.41	335.80	489.71	2811.66	12439.60
6477.3667	0.00	0.00	100.00	0.00	0.0165	112.16	1110.38	370.13	539.77	3099.06	13711.13
7133.9697	0.00	0.00	100.00	0.00	0.0149	123.53	1222.94	407.65	594.48	3413.21	15101.01
7863.4414	0.00	0.00	100.00	0.00	0.0136	136.16	1347.99	449.33	655.27	3762.22	16645.14
8660.3916	0.00	0.00	100.00	0.00	0.0123	149.96	1484.60	494.87	721.68	4143.51	18332.11
9536.6191	0.00	0.00	100.00	0.00	0.0112	165.14	1634.81	544.94	794.70	4562.74	20186.89
10509.9180	0.00	0.00	100.00	0.00	0.0101	181.99	1801.66	600.55	875.81	5028.41	22247.14
11580.3467	0.00	0.00	100.00	0.00	0.0092	200.52	1985.16	661.72	965.01	5540.55	24513.00
12754.0332	0.00	0.00	100.00	0.00	0.0084	220.85	2186.35	728.78	1062.81	6102.09	26997.43
14051.5479	0.00	0.00	100.00	0.00	0.0076	243.32	2408.78	802.93	1170.93	6722.88	29743.98
15480.0732	0.00	0.00	100.00	0.00	0.0069	268.05	2653.66	884.55	1289.98	7406.35	32767.85
17052.9785	0.00	0.00	100.00	0.00	0.0063	295.29	2923.30	974.43	1421.05	8158.90	36097.33
18781.7676	0.00	0.00	100.00	0.00	0.0057	325.22	3219.65	1073.22	1565.11	8986.03	39756.79
20698.2285	0.00	0.00	100.00	0.00	0.0052	358.41	3548.18	1182.73	1724.81	9902.94	43813.51
22811.8027	0.00	0.00	100.00	0.00	0.0047	395.01	3910.50	1303.50	1900.94	10914.17	48287.47
25131.0254	0.00	0.00	100.00	0.00	0.0042	435.17	4308.07	1436.02	2094.20	12023.79	53196.75
27682.9824	0.00	0.00	100.00	0.00	0.0039	479.36	4745.54	1581.85	2306.86	13244.76	58598.67
30493.5840	0.00	0.00	100.00	0.00	0.0035	528.03	5227.35	1742.45	2541.07	14589.47	64548.08
33589.3867	0.00	0.00	100.00	0.00	0.0032	581.63	5758.04	1919.35	2799.05	16070.64	71101.20
36996.6406	0.00	0.00	100.00	0.00	0.0029	640.63	6342.13	2114.04	3082.98	17700.82	78313.60
40738.8242	0.00	0.00	100.00	0.00	0.0026	705.43	6983.63	2327.88	3394.82	19491.25	86234.96
44861.4063	0.00	0.00	100.00	0.00	0.0024	776.82	7690.34	2563.45	3738.36	21463.67	94961.54
49411.5469	0.00	0.00	100.00	0.00	0.0022	855.61	8470.35	2823.45	4117.53	23640.66	104593.17
54434.5625	0.00	0.00	100.00	0.00	0.0020	942.59	9331.42	3110.47	4536.11	26043.89	115225.77
59955.5430	0.00	0.00	100.00	0.00	0.0018	1038.19	10277.85	3425.95	4996.18	28685.37	126912.45

Company: Univ. of Wyoming
Well: RSU #1
File: WTC-12-2873

Sample ID: 110
Depth, ft:
Permeability to Air, md: 6.357
Calculated Permeability to Air, md: 6.810
Helium Porosity, percent: 11.8
Mercury Porosity, %. 9.08
Mercury Pore Volume: 0.801
Helium Pore Volume: 1.040
Entry Pressure 5.086

Injection Pressure (Absolute), psia	Non-Wetting Phase Saturation			Wetting Phase Saturation, fraction	Pore Throat Radius, microns	Leverett "J" Function	Capillary Pressure			Height Above Free Water	
	Incremental percent	Normalized Incremental percent	Cumulative percent				Gas/Water psi	Gas/Oil psi	Oil/water psi	Gas/Water feet	Oil/Water feet
0.5363	0.00	0.00	0.00	100.00	198.8062	0.01	0.09	0.03	0.04	0.26	1.14
0.5804	0.00	0.00	0.00	100.00	183.7240	0.01	0.10	0.03	0.05	0.28	1.23
0.6375	0.00	0.00	0.00	100.00	167.2584	0.01	0.11	0.04	0.05	0.31	1.35
0.6989	0.00	0.00	0.00	100.00	152.5537	0.01	0.12	0.04	0.06	0.33	1.48
0.7704	0.00	0.00	0.00	100.00	138.4075	0.02	0.13	0.04	0.06	0.37	1.63
0.8429	0.00	0.00	0.00	100.00	126.5062	0.02	0.14	0.05	0.07	0.40	1.78
0.9264	0.00	0.00	0.00	100.00	115.1028	0.02	0.16	0.05	0.08	0.44	1.96
1.0178	0.00	0.00	0.00	100.00	104.7646	0.02	0.17	0.06	0.08	0.49	2.15
1.1164	0.00	0.00	0.00	100.00	95.5112	0.02	0.19	0.06	0.09	0.53	2.36
1.2258	0.00	0.00	0.00	100.00	86.9874	0.02	0.21	0.07	0.10	0.59	2.59
1.3483	0.00	0.00	0.00	100.00	79.0842	0.03	0.23	0.08	0.11	0.65	2.85
1.4805	0.00	0.00	0.00	100.00	72.0200	0.03	0.25	0.08	0.12	0.71	3.13
1.6254	0.00	0.00	0.00	100.00	65.6009	0.03	0.28	0.09	0.14	0.78	3.44
1.7871	0.00	0.00	0.00	100.00	59.6641	0.04	0.31	0.10	0.15	0.86	3.78
1.9659	0.00	0.00	0.00	100.00	54.2390	0.04	0.34	0.11	0.16	0.94	4.16
2.1580	0.00	0.00	0.00	100.00	49.4108	0.04	0.37	0.12	0.18	1.03	4.57
2.3736	0.00	0.00	0.00	100.00	44.9228	0.05	0.41	0.14	0.20	1.14	5.02
2.6077	0.00	0.00	0.00	100.00	40.8895	0.05	0.45	0.15	0.22	1.25	5.52
2.8685	0.00	0.00	0.00	100.00	37.1716	0.06	0.49	0.16	0.24	1.37	6.07
3.1514	0.00	0.00	0.00	100.00	33.8351	0.06	0.54	0.18	0.26	1.51	6.67
3.4636	0.00	0.00	0.00	100.00	30.7853	0.07	0.59	0.20	0.29	1.66	7.33
3.8090	0.00	0.00	0.00	100.00	27.9934	0.08	0.65	0.22	0.32	1.82	8.06
4.1926	0.00	0.00	0.00	100.00	25.4319	0.08	0.72	0.24	0.35	2.01	8.87
4.6182	0.00	0.00	0.00	100.00	23.0883	0.09	0.79	0.26	0.38	2.21	9.78
5.0862	0.00	0.00	0.00	100.00	20.9641	0.10	0.87	0.29	0.42	2.43	10.77
5.6023	2.21	0.36	2.21	97.79	19.0328	0.11	0.96	0.32	0.47	2.68	11.86
6.1687	2.01	0.33	4.22	95.78	17.2850	0.12	1.06	0.35	0.51	2.95	13.06
6.7939	2.18	0.36	6.40	93.60	15.6944	0.14	1.16	0.39	0.57	3.25	14.38
7.4818	4.88	0.80	11.27	88.73	14.2516	0.15	1.28	0.43	0.62	3.58	15.84
8.2414	5.35	0.87	16.62	83.38	12.9380	0.16	1.41	0.47	0.69	3.94	17.45
9.0728	4.27	0.70	20.89	79.11	11.7524	0.18	1.56	0.52	0.76	4.34	19.21
9.9895	6.13	1.00	27.02	72.98	10.6739	0.20	1.71	0.57	0.83	4.78	21.15
11.0062	6.05	0.99	33.07	66.93	9.6879	0.22	1.89	0.63	0.92	5.27	23.30
12.1209	3.91	0.64	36.98	63.02	8.7969	0.24	2.08	0.69	1.01	5.80	25.66
13.3486	4.20	0.69	41.17	58.83	7.9879	0.27	2.29	0.76	1.11	6.39	28.26
14.7008	3.58	0.58	44.75	55.25	7.2531	0.29	2.52	0.84	1.23	7.03	31.12
16.1888	2.81	0.46	47.57	52.43	6.5865	0.32	2.78	0.93	1.35	7.75	34.27
17.8254	3.35	0.55	50.92	49.08	5.9818	0.36	3.06	1.02	1.49	8.53	37.73
19.6402	2.42	0.40	53.34	46.66	5.4290	0.39	3.37	1.12	1.64	9.40	41.57
21.6718	3.39	0.55	56.73	43.27	4.9201	0.43	3.72	1.24	1.81	10.37	45.87
23.8690	1.49	0.24	58.22	41.78	4.4672	0.48	4.09	1.36	1.99	11.42	50.53
26.2803	1.34	0.22	59.57	40.43	4.0573	0.52	4.51	1.50	2.19	12.57	55.63
28.9410	2.02	0.33	61.58	38.42	3.6843	0.58	4.96	1.65	2.41	13.85	61.26
31.8726	1.69	0.28	63.28	36.72	3.3454	0.64	5.46	1.82	2.66	15.25	67.47
35.1110	0.84	0.14	64.12	35.88	3.0369	0.70	6.02	2.01	2.93	16.80	74.32
38.2753	1.62	0.26	65.74	34.26	2.7858	0.76	6.56	2.19	3.19	18.31	81.02
42.6641	0.73	0.12	66.47	33.53	2.4992	0.85	7.31	2.44	3.56	20.41	90.31
47.8549	1.02	0.17	67.49	32.51	2.2281	0.96	8.20	2.73	3.99	22.90	101.30
53.9115	1.10	0.18	68.59	31.41	1.9778	1.08	9.24	3.08	4.49	25.79	114.12
59.1221	0.84	0.14	69.43	30.57	1.8035	1.18	10.13	3.38	4.93	28.29	125.15
65.9672	0.95	0.15	70.37	29.63	1.6164	1.32	11.31	3.77	5.50	31.56	139.64
72.7319	0.51	0.08	70.88	29.12	1.4660	1.45	12.47	4.16	6.06	34.80	153.96
80.1363	0.67	0.11	71.55	28.45	1.3306	1.60	13.74	4.58	6.68	38.34	169.63
87.9913	0.86	0.14	72.41	27.59	1.2118	1.76	15.08	5.03	7.33	42.10	186.26
98.3417	1.02	0.17	73.43	26.57	1.0842	1.96	16.86	5.62	8.19	47.05	208.17
108.6190	0.52	0.08	73.95	26.05	0.9817	2.17	18.62	6.21	9.05	51.97	229.92
119.7799	0.67	0.11	74.63	25.37	0.8902	2.39	20.53	6.84	9.98	57.31	253.55
132.1468	0.75	0.12	75.37	24.63	0.8069	2.64	22.65	7.55	11.01	63.22	279.73
146.2578	0.81	0.13	76.19	23.81	0.7290	2.92	25.07	8.36	12.19	69.98	309.59
161.6524	0.60	0.10	76.79	23.21	0.6596	3.23	27.71	9.24	13.47	77.34	342.18
178.3701	0.66	0.11	77.44	22.56	0.5978	3.56	30.58	10.19	14.86	85.34	377.57
195.9382	0.58	0.10	78.03	21.97	0.5442	3.91	33.59	11.20	16.33	93.75	414.76
217.3640	0.72	0.12	78.75	21.25	0.4905	4.34	37.26	12.42	18.11	104.00	460.11
239.7501	0.63	0.10	79.38	20.62	0.4447	4.79	41.10	13.70	19.98	114.71	507.50
264.2076	0.73	0.12	80.10	19.90	0.4036	5.27	45.29	15.10	22.02	126.41	559.27
291.8115	0.96	0.16	81.07	18.93	0.3654	5.83	50.02	16.67	24.32	139.62	617.70
321.0982	1.05	0.17	82.12	17.88	0.3321	6.41	55.04	18.35	26.76	153.63	679.69
354.2567	1.06	0.17	83.18	16.82	0.3010	7.07	60.73	20.24	29.52	169.49	749.88
391.1198	1.14	0.19	84.32	15.68	0.2726	7.81	67.05	22.35	32.59	187.13	827.91
430.9823	1.14	0.19	85.46	14.54	0.2474	8.60	73.88	24.63	35.91	206.20	912.29
474.9503	1.34	0.22	86.80	13.20	0.2245	9.48	81.42	27.14	39.58	227.24	1005.36
522.8466	1.04	0.17	87.84	12.16	0.2039	10.44	89.63	29.88	43.57	250.15	1106.75
577.1121	0.53	0.09	88.37	11.63	0.1848	11.52	98.93	32.98	48.09	276.12	1221.62
635.7598	0.62	0.10	88.99	11.01	0.1677	12.69	108.98	36.33	52.98	304.18	1345.76
701.1567	0.68	0.11	89.67	10.33	0.1521	14.00	120.20	40.07	58.43	335.46	1484.19
772.5809	0.63	0.10	90.30	9.70	0.1380	15.42	132.44	44.15	64.38	369.64	1635.38
850.3015	0.44	0.07	90.74	9.26	0.1254	16.97	145.76	48.59	70.86	406.82	1799.90
937.8461	0.50	0.08	91.23	8.77	0.1137	18.72	160.77	53.59	78.15	448.71	1985.21
1033.1191	0.57	0.09	91.81	8.19	0.1032	20.62	177.10	59.03	86.09	494.29	2186.88
1138.2944	0.63	0.10	92.44	7.56	0.0937	22.72	195.13	65.04	94.86	544.61	2409.51
1253.1471	0.72	0.12	93.16	6.84	0.0851	25.01	214.82	71.61	104.43	599.56	2652.63
1381.3394	0.78	0.13	93.94	6.06	0.0772	27.57	236.80	78.93	115.11	660.89	2923.99
1521.3446	0.82	0.13	94.76	5.24	0.0701	30.37	260.80	86.93	126.78	727.88	3220.35
1675.4850	0.94	0.15	95.70	4.30	0.0636	33.45	287.22	95.74	139.62	801.63	3546.63
1845.3507	0.84	0.14	96.53	3.47	0.0578	36.84	316.34	105.45	153.78	882.90	3906.19
2033.0690	0.78	0.13	97.31	2.69	0.0524	40.58	348.52	116.17	169.42	972.71	4303.55
2240.8098	0.71	0.12	98.03	1.97	0.0476	44.73	384.13	128.04	186.73	1072.10	4743.29
2467.2986	0.57	0.09	98.60	1.40	0.0432	49.25	422.96	140.99	205.60	1180.46	5222.72
2717.9568	0.47	0.08	99.07	0.93	0.0392	54.26	465.92	155.31	226.49	1300.39	5753.31
2992.8503	0.32	0.05	99.39	0.61	0.0356	59.74	513.05	171.02	249.40	1431.91	6335.19
3296.5452	0.22	0.04	99.61	0.39	0.0323	65.80	565.11	188.37	274.71	1577.21	6978.05
3631.5569	0.13	0.02	99.74	0.26	0.0294	72.49	622.54	207.51	302.62	1737.50	7687.19
4000.5898	0.09	0.01	99.83	0.17	0.0267	79.86	685.80	228.60	333.37	1914.06	8468.35
4399.5996	0.09	0.01	99.92	0.08	0.0242	87.82	754.20	251.40	366.62	2104.96	9312.97
4845.8989	0.03	0.00	99.95	0.05	0.0220	96.73	830.71	276.90	403.82	2318.49	10257.68
5337.7759	0.04	0.01	99.98	0.02	0.0200	106.55	915.03	305.01	444.80	2553.83	11298.88
5879.2402	0.02	0.00	100.00	0.00	0.0181	117.36	1007.85	335.95	489.93	2812.89	12445.03
6474.1338	0.00	0.00	100.00	0.00	0.0165	129.23	1109.83	369.94	539.50	3097.51	13704.29
7134.7676	0.00	0.00	100.00	0.00	0.0149	142.42	1223.07	407.69	594.55	3413.59	15102.70
7863.9658	0.00	0.00	100.00	0.00	0.0136	156.98	1348.08	449.36	655.31	3762.47	16646.25
8661.4854	0.00	0.00	100.00	0.00	0.0123	172.90	1484.79	494.93	721.77	4144.04	18334.42
9539.2451	0.00	0.00	100.00	0.00	0.0112	190.42	1635.26	545.09	794.92	4564.00	20192.44
10512.9443	0.00	0.00	100.00	0.00	0.0101	209.86	1802.18	600.73	876.06	5029.86	22253.55
11579.2070	0.00	0.00	100.00	0.00	0.0092	231.14	1984.96	661.65	964.91	5540.00	24510.59
12756.7607	0.00	0.00	100.00	0.00	0.0084	254.65	2186.82	728.94	1063.04	6103.40	27003.20
14052.0479	0.00	0.00	100.00	0.00	0.0076	280.50	2408.87	802.96	1170.98	6723.12	29745.04
15477.5273	0.00	0.00	100.00	0.00	0.0069	308.96	2653.23	884.41	1289.76	7405.13	32762.46
17050.3770	0.00	0.00	100.00	0.00	0.0063	340.35	2922.85	974.28	1420.83	8157.65	36091.83
18782.6875	0.00	0.00	100.00	0.00	0.0057	374.93	3219.81	1073.27	1565.19	8986.47	39758.74
20701.1875	0.00	0.00	100.00	0.00	0.0052	413.23	3548.69	1182.90	1725.06	9904.36	43819.77
22811.7773	0.00	0.00	100.00	0.00	0.0047	455.36	3910.50	1303.50	1900.94	10914.16	48287.42
25130.5352	0.00	0.00	100.00	0.00	0.0042	501.65	4307.99	1436.00	2094.16	12023.56	53195.71
27683.5137	0.00	0.00	100.00	0.00	0.0039	552.61	4745.63	1581.88	2306.90	13245.01	58599.79
30493.9531	0.00	0.00	100.00	0.00	0.0035	608.71	5227.41	1742.47	2541.10	14589.65	64548.86
33588.4766	0.00	0.00	100.00	0.00	0.0032	670.48	5757.89	1919.30	2798.97	16070.21	71099.28
36996.3672	0.00	0.00	100.00	0.00	0.0029	738.51	6342.08	2114.03	3082.96	17700.69	78313.02
40739.7773	0.00	0.00	100.00	0.00	0.0026	813.24	6983.80	2327.93	3394.90	19491.71	86236.98
44861.3125	0.00	0.00	100.00	0.00	0.0024	895.51	7690.33	2563.44	3738.35	21463.63	94961.34
49412.0742	0.00	0.00	100.00	0.00	0.0022	986.35	8470.44	2823.48	4117.57	23640.91	104594.29
54433.3672	0.00	0.00	100.00	0.00	0.0020	1086.58	9331.21	3110.40	4536.01	26043.32	115223.24
59956.8789	0.00	0.00	100.00	0.00	0.0018	1196.84	10278.08	3426.03	4996.29	28686.01	126915.27

Recovered Core

Core Intervals	Depths		Recovery (ft.)
#1 Triassic	10600	10690	89.2
#2 Weber	11169	11170	0.5
#3 Weber	11185	11275	93.4
#4 Weber	11275	11348	69.25
#5 Weber	11348	11468	123.4
#6 Weber	11468	11508	39.5
#7 Weber	11520	11597	77.25
#8 Weber	11597	11625	28
#9 Weber	11701	11793	91
#10 Amsden/Madison	12169	12257	88.25
#11 Madison	12301	12393	92
#12 Madison	12393	12477	84.5
#13 Madison	12477	12511	17
#14 Madison	12511	12532	19.5
#15 Madison	12532	12536	4
Total			916.75

Rock Evaluations

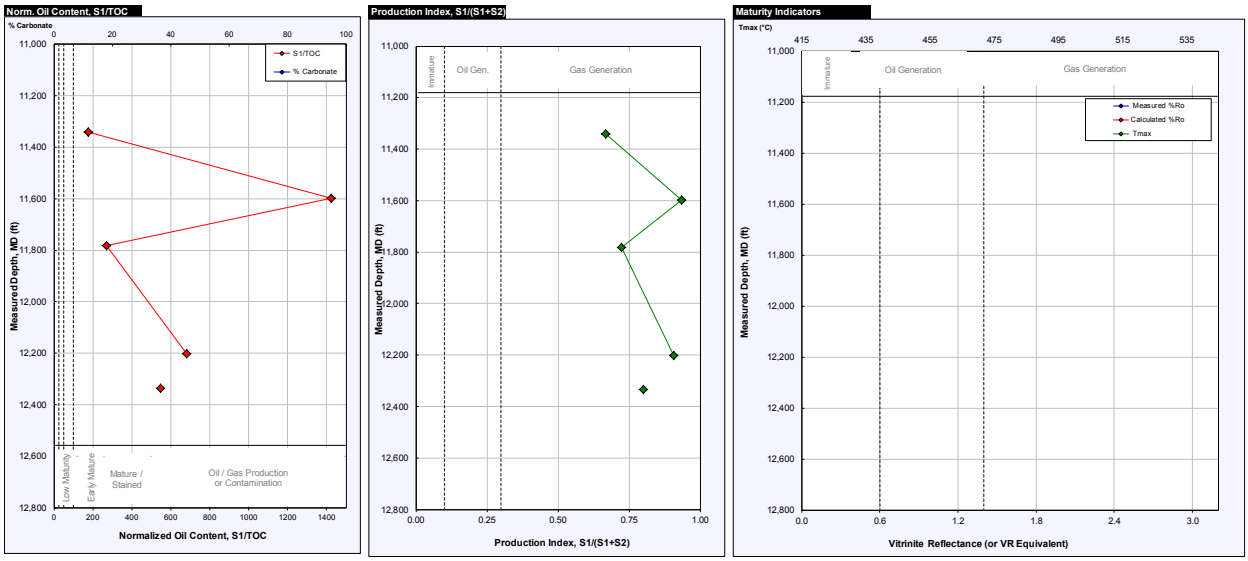
Data

Core Laboratories																					Job # 120536G - RSU #1,
Sample ID										**Source Rock Analyses**											
Project / Sample ID	Rock ID	Job #	County	State	Formation Name	Upper Depth (ft)	Lower Depth (ft)	Median Depth (ft)	Sample Type	Percent Carbonate (wt%)	Leco TOC (wt% HC)	Rock-Eval S1 (mg HC/g)	Rock-Eval S2 (mg HC/g)	Rock-Eval S3 (mg CO2/g)	Tmax (°C)	Measured %Ro (Vitrinite Refl.)	Calculated %Ro (RE TMAX)	Hydrogen Index (S2x100/TOC)	Oxygen Index (S3x100/TOC)	S2/S3 Conc. (mg HC/mg CO2)	S1/TOC Norm. Oil Content	Production Index (S1/(S1+S2)	Experimental Notations
ROOR-120447-001	29	120536G - RSU #1	Sweetwater	WY		11,340.05		11,340.05			0.07	0.12	0.06	0.02	0		-7.16	88	29	3	177	0.67	
ROOR-120447-002	37	120536G - RSU #1	Sweetwater	WY		11,597.05		11,597.05			0.09	1.29	0.09	0.14	0		-7.16	99	155	1	1,424	0.93	
ROOR-120447-003	46	120536G - RSU #1	Sweetwater	WY		11,782.05		11,782.05			0.05	0.13	0.05	0.04	0		-7.16	104	83	1	270	0.72	
ROOR-120447-004	55	120536G - RSU #1	Sweetwater	WY		12,203.00		12,203.00			0.10	0.68	0.07	0.19	0		-7.16	70	190	0	681	0.91	
ROOR-120447-005	60	120536G - RSU #1	Sweetwater	WY		12,309.10		12,309.10			0.06												
ROOR-120447-006	61	120536G - RSU #1	Sweetwater	WY		12,324.00		12,324.00			0.04												
ROOR-120447-007	64	120536G - RSU #1	Sweetwater	WY		12,335.25		12,335.25			0.04	0.20	0.05	0.03	0		-7.16	137	82	2	546	0.80	
ROOR-120447-008	66	120536G - RSU #1	Sweetwater	WY		12,339.10		12,339.10			0.11												
ROOR-120447-009	89	120536G - RSU #1	Sweetwater	WY		12,345.70		12,345.70			0.48												
ROOR-120447-010	76	120536G - RSU #1	Sweetwater	WY		12,350.20		12,350.20			0.08												
ROOR-120447-011	92	120536G - RSU #1	Sweetwater	WY		12,379.85		12,379.85			0.09												
ROOR-120447-012	103	120536G - RSU #1	Sweetwater	WY		12,411.52		12,411.52			0.28												
ROOR-120447-013	111	120536G - RSU #1	Sweetwater	WY		12,495.30		12,495.30			0.09												
												(amount of HC @ 300C)	(amount of HC @ 550C)	CO2 from organics									

Data provided by Geomark Research Ltd. using LECO TOC and Rock-Eval 2

Source Potential Logs

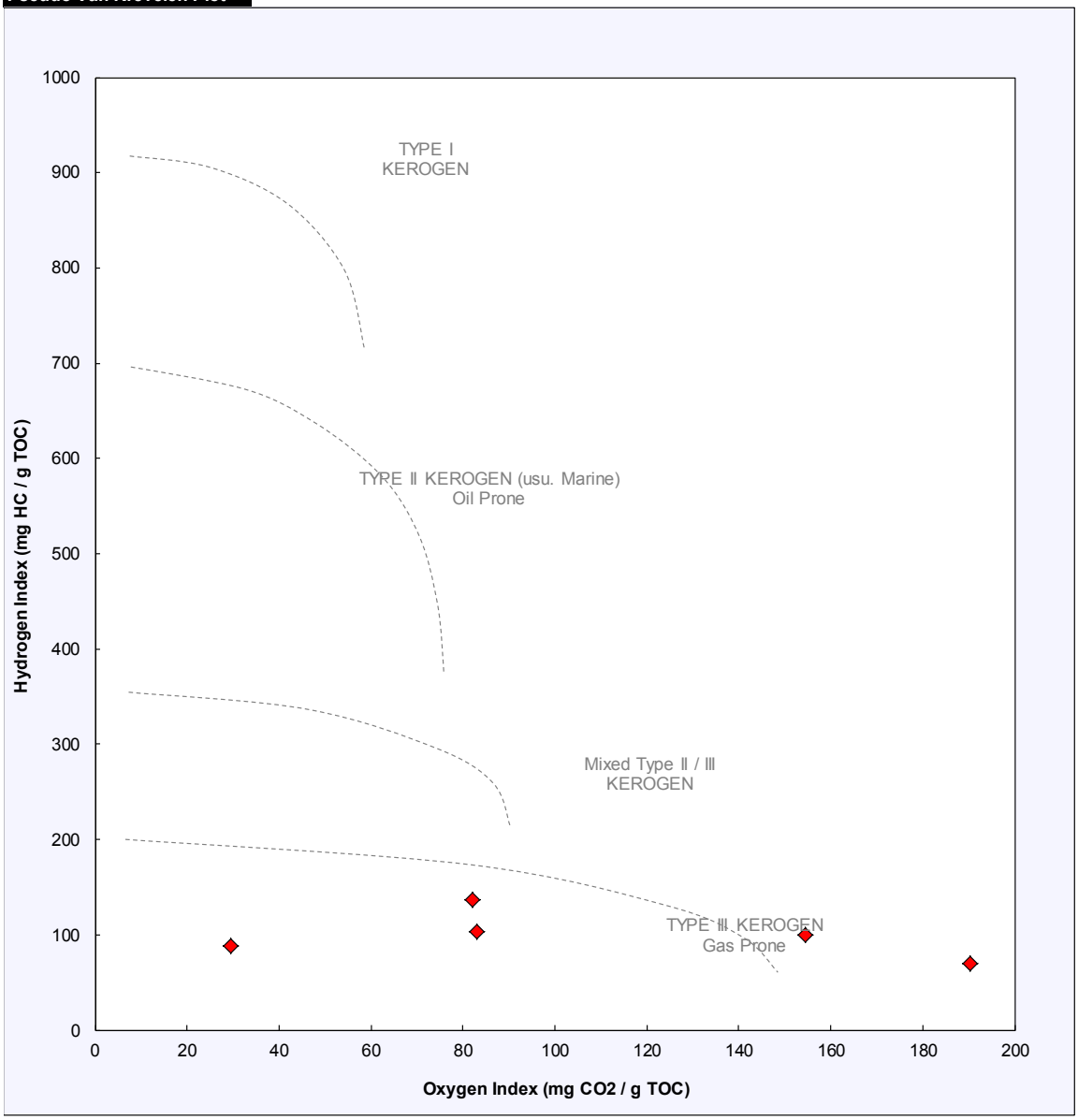
HC Indicator and Maturity Logs



Pseudo Van Krevelen Plot

Core Laboratories	Job # 120536G - RSU #1,

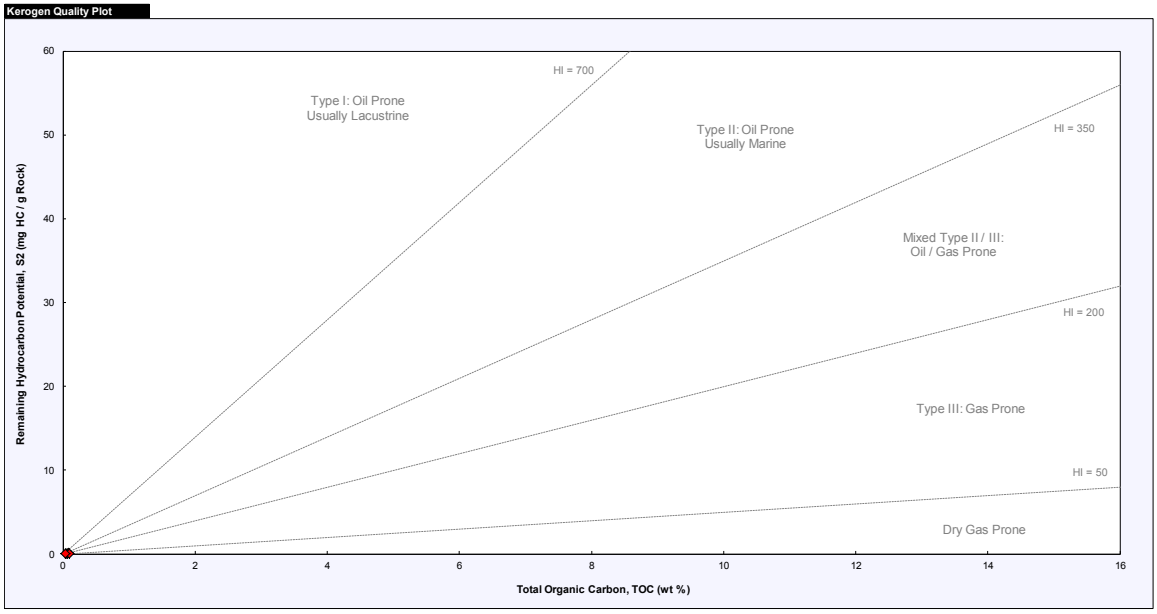
Pseudo Van Krevelen Plot



Kerogen Quality Plot

Core Laboratories	Job # 120536G - RSU #1,

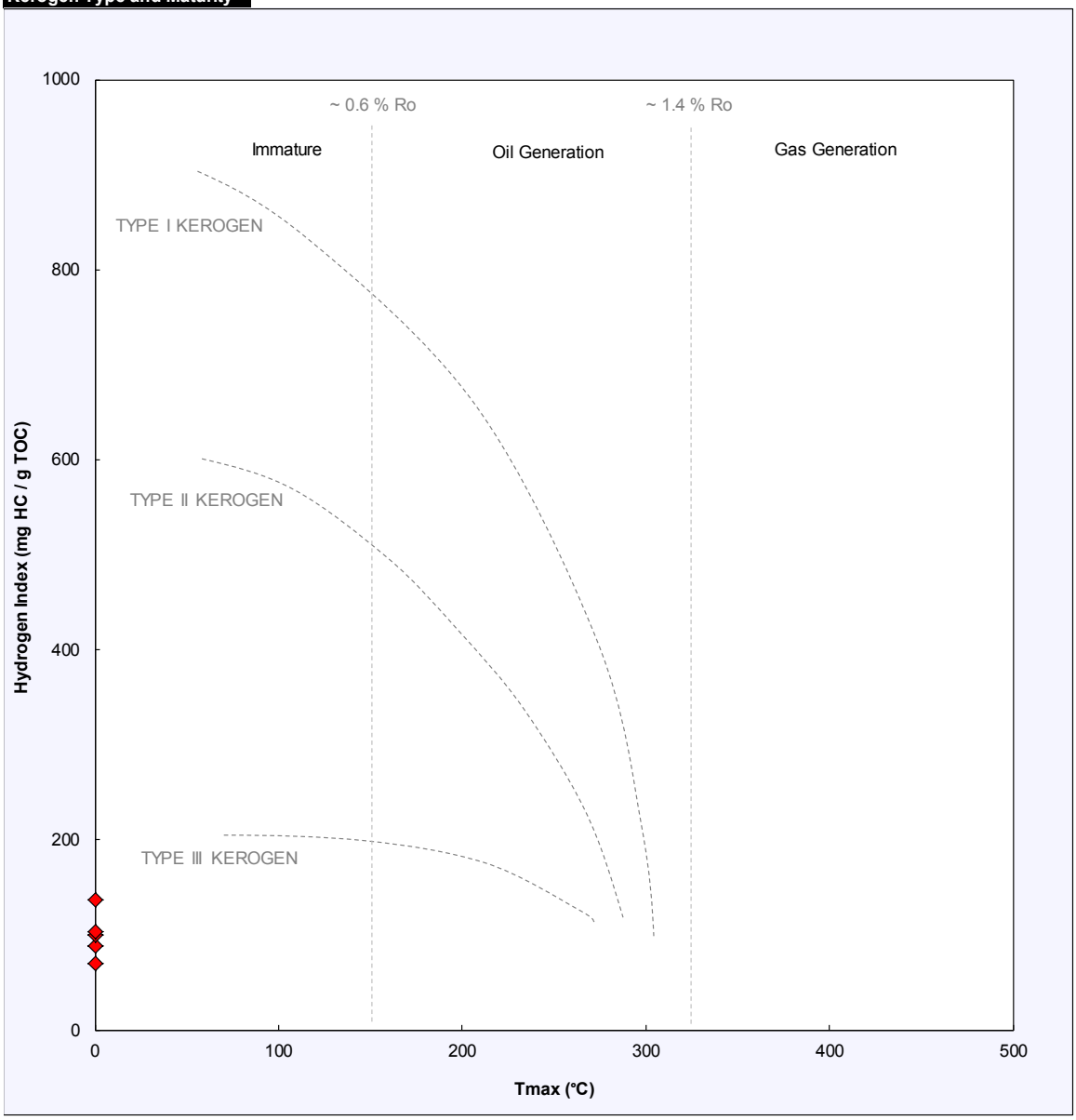
Kerogen Quality Plot



Kerogen Type and Maturity

Core Laboratories	Job # 120536G - RSU #1,

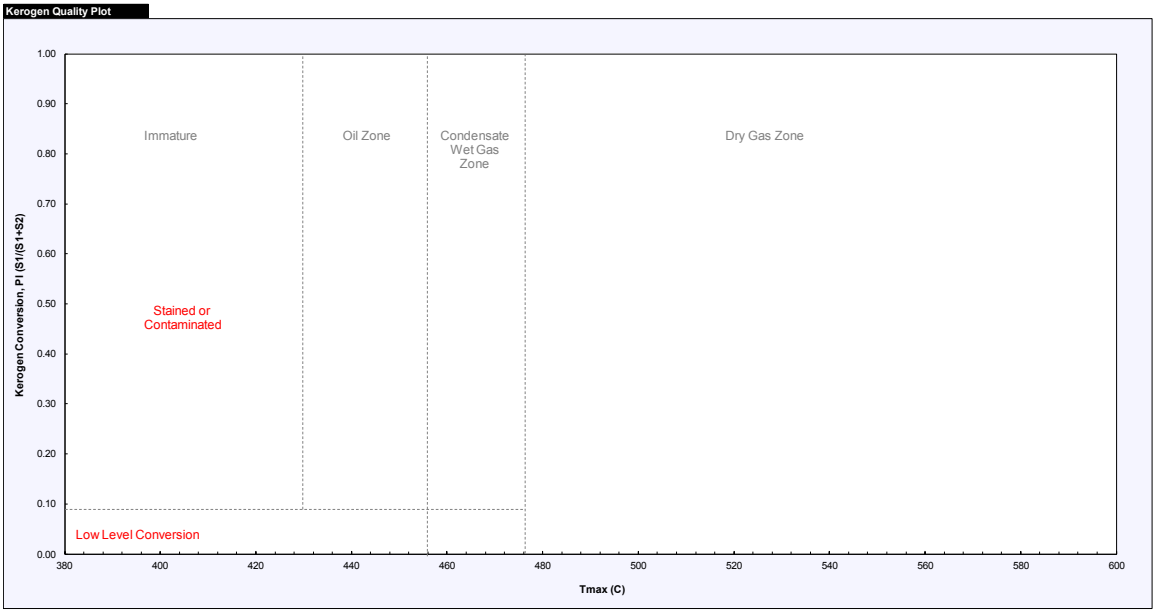
Kerogen Type and Maturity



Kerogen Conversion and Maturity

Core Laboratories	Job # 120536G - RSU #1,

Kerogen Quality Plot



Appendix F: Routine Core Analysis – Report #1

ROUTINE CORE ANALYSIS

University of Wyoming

Well: RSU #1

F I N A L R E P O R T

Prepared for

University of Wyoming

By

Intertek Westport Technology Center
6700 Portwest Drive
Houston, Texas 77024
(713) 479-8400 (Phone)
(713) 864-9357 (Fax)
www.westport1.com

September 25, 2012

Project No.: WTC-12-002873

ROUTINE CORE ANALYSIS - Well: RSU #1

TABLE OF CONTENTS i

RESULTS AND DISCUSSION 1

LIST OF TABLES

TABLE 1. TEST SELECTION AND INVENTORY 2

TABLE 2. ROUTINE CORE PROPERTIES 3

RESULTS AND DISCUSSION

Routine core analysis was conducted on thirty core plug samples obtained from multiple formations from the RSU #1 well.

All testing was conducted following core analysis procedures specified in API RP40 method, Recommended Practices for Core Analysis (1998).

The samples were extracted of hydrocarbons and brine using soxhlet techiques. A chloroform/methanol azeotrope was used as the extracting solvent. The samples were dried to stable weights in a convection oven at 180^{o} F. After stable weights were attained, the samples were transferred to airtight containers and allowed to cool to room temperature before dry weights were taken.

Direct grain volume measurements were made using a small volume helium porosimeter, utilizing Boyle's Law principle of gas expansion. Apparent grain density was calculated from dry weight and grain volume. Pore volume and permeability measurements were made with the samples mounted in a rubber-sleeved, hydrostatically loaded overburden cell. The samples were tested at 800 psig and a calculated reservior net confining stress. Boyle's Law principle, using helium as the gas medium, was employed to determine pore volume. Unsteady-state Klinkenberg permeability was measured after each pore volume measurement. Permeability to air was calculated using form the unsteady-state flow data.

The sample inventory and assigned analyses are provided in Table 1. The routine core properties are summarized in Table 2.

The permeability-porosity relationship is shown in Figure 1.

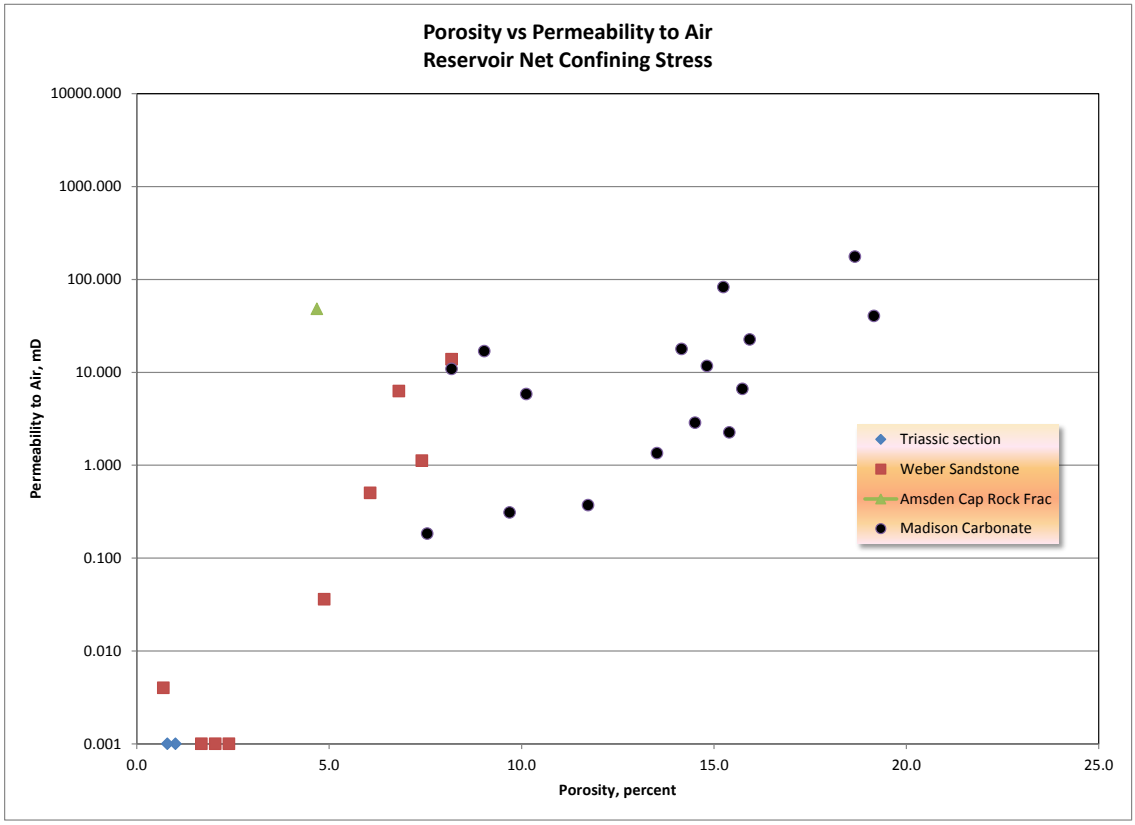
TABLE 1. TEST SELECTION AND INVENTORY

Project No.:	WTC-12-002873
Company	University of Wyoming
Well Location:	,

			Tests Selected			
Sample ID	**Net Confining Stress**	**Formation**	**Routine Core Analysis Density**	**Absolute Brine Permeability**	**CO_2 - Brine Relative Permeability**	**Mercury Injection Cap Pressure**
1	4175	Dinwoody Cap Rock	X			**x**
18	4175	Dinwoody Cap Rock	X			**x**
22	4370	Weber Sandstone	X			
23	4370	Weber Sandstone	X		**x**	
26	4370	Weber Sandstone	X	**x**		**x**
27	4370	Weber Sandstone	X	**x**		**x**
28	4370	Weber Sandstone	X			
30	4370	Weber Sandstone	X			
32	4370	Weber Sandstone	X			
33	4370	Weber Sandstone	X		**x**	
45	4370	Weber Sandstone	X	**x**		**x**
53	4515	Amsden Cap Rock	X			**x**
59	4900	Madison Carbonate	X			**x**
63	4900	Madison Carbonate	X			
67	4900	Madison Carbonate	X			
72	4900	Madison Carbonate	X	**x**		**x**
77	4900	Madison Carbonate	X		**x**	
79	4900	Madison Carbonate	X	**x**		**x**
83	4900	Madison Carbonate	X			
86	4900	Madison Carbonate	X			
89	4900	Madison Carbonate	X			
94	4900	Madison Carbonate	X		**x**	
99	4900	Madison Carbonate	X	**x**		**x**
102	4900	Madison Carbonate	X			
104	4900	Madison Carbonate	X			
106	4900	Madison Carbonate	X	**x**		**x**
107	4900	Madison Carbonate	X			
108	4900	Madison Carbonate	X			
110	4900	Madison Carbonate	X	**x**		**x**
112	4900	Madison Carbonate	X			

TABLE 2. ROUTINE CORE PROPERTIES

Sample ID	Sample Dimensions		Permeability				Porosity		Grain Density	Depth	Lithologic Description
			800 psi NCS		Reservoir NCS		800 NCS	Res. NCS			
	Length	Diameter	to Air	Klinkenberg	to Air	Klinkenberg	Porosity	Porosity			
	(cm)	(cm)	(mD)		(mD)		(percent)		(g/cm^3)		
Triassic section											
1	3.99	2.48	0.005	0.002	0.001	0.000	1.6	1.0	2.71		Sst rd f g dol calc mica sid
18	3.19	2.48	0.003	0.001	0.001	0.000	1.2	0.8	2.69		Sst rd f g dol calc mica sid
Weber Sandstone											
22	4.33	2.48	0.616	0.514	0.504	0.415	6.2	6.1	2.65	11194.10	Sst wht, f-m grn, calc, py, org, frac
23	3.98	2.48	6.94	6.36	6.28	5.73	7.6	6.8	2.64	11200.05	Sst wht, f-m grn, calc, py
26	4.61	2.48	15.8	14.9	13.8	12.9	8.1	8.2	2.64	11209.90	Sst wht, f-m grn, calc, dolo, py
27	4.40	2.48	1.31	1.15	1.12	0.969	7.6	7.4	2.63	11227.05	Sst wht, f-m grn, calc, py
28	4.30	2.48	0.063	0.040	0.036	0.021	5.1	4.9	2.64	11305.50	Sst wht, f-m grn, calc, py, org
30	2.87	2.48	0.006	0.002	0.001	0.000	2.3	1.7	2.64	11405.30	Sst wht, f-m grn, calc, py, org
32	4.34	2.48	0.014	0.006	0.001	0.000	3.5	2.4	2.65	11481.20	Ls- wht, org, py, frac
33	4.36	2.46	0.025	0.010	0.001	0.000	2.7	2.0	2.67	11507.95	Sst wht, f-m grn, calc, py, org, vugs, frac
45	3.73	2.47	0.016	0.006	0.004	0.001	1.3	0.7	2.65	11766.80	Sst wht, f-m grn, calc, py
Amsden Cap Rock Frac											
53	4.00	2.45	1099.	1083.	48.3	41.3	5.8	4.7	2.85		Dol wht, org, py, vugs
Madison Carbonate											
59	2.35	2.45	0.001	0.000	0.000	0.000	1.3	0.3	2.70	12250.00	Ls- wht, dolo, org, py
63	4.11	2.47	0.001	0.000	0.000	0.000	0.9	0.3	2.70	12333.00	Ls- wht, dolo, org, py
67	4.84	2.47	12.3	11.5	10.9	10.2	10.7	8.2	2.83	12341.75	Ls- wht, dolo, org, py, vugs
72	4.37	2.46	33.1	31.7	16.9	15.9	18.1	9.0	2.84	12348.85	Ls- wht, dolo, org, py, frac
77	4.34	2.46	87.1	84.6	82.6	80.1	27.4	15.2	2.82	12353.15	Ls- wht, dolo, sid
79	2.73	2.47	42.3	40.7	40.4	38.8	23.5	19.2	2.82	12354.65	Ls- wht, f xln, org, vugs
83	4.83	2.48	0.255	0.194	0.183	0.135	9.6	7.5	2.84	12358.50	Ls- wht, f xln, dolo, py, coal seam
86	3.00	2.46	2.620	2.360	2.250	2.01	16.9	15.4	2.83	12362.80	Ls- wht, f xln, org
89	3.94	2.47	18.7	17.7	17.800	16.8	19.0	14.2	2.83	12372.70	Ls- wht, f xln, org, foss
94	3.64	2.46	0.504	0.408	0.309	0.241	9.1	9.7	2.79	12382.74	Ls- wht, f xln, org
99	3.65	2.50	0.666	0.552	0.372	0.292	11.6	11.7	2.83	12399.00	Ls- wht, f xln, org, dolo, vugs
102	4.45	2.47	3.75	3.42	2.87	2.59	14.9	14.5	2.83	12406.19	Ls- wht, f xln, org, dolo, vugs
104	3.52	2.47	11.8	11.0	11.7	9.94	17.7	14.8	2.83	12414.50	Ls- wht, f xln, org, dolo, vugs
106	4.77	2.47	7.49	6.88	6.63	6.06	18.5	15.7	2.85	12415.08	Ls- wht, f xln, org, dolo, vugs
107	4.10	2.48	183.	178.	176.	173.	20.1	18.7	2.84	12421.52	Ls- wht, f xln, org, dolo, vugs
108	4.79	2.47	1.56	1.36	1.35	1.68	13.6	13.5	2.84	12461.00	Ls- wht, f xln, org, dolo, vugs, org
110	4.83	2.47	6.36	5.82	5.84	5.34	11.8	10.1	2.87	12480.50	Ls- wht, f xln, org, dolo, vugs
112	4.73	2.46	24.6	23.4	22.6	21.4	16.4	15.9	2.83	12511.6	Ls- wht, f xln, org, dolo


Porosity vs Permeability to Air
Reservoir Net Confining Stress
10000.000
1000.000
100.000
10.000
1.000
0.100
0.010
0.001
Permeability to Air, mD
0.0
5.0
10.0
15.0
20.0
25.0
Porosity, percent
Triassic section
Weber Sandstone
Amsden Cap Rock Frac
Madison Carbonate

Routine Core Analysis – Report 2

ROUTINE CORE ANALYSIS

University of Wyoming

Well: RSU #1

F I N A L R E P O R T

Prepared for

University of Wyoming

By

Intertek Westport Technology Center
6700 Portwest Drive
Houston, Texas 77024
(713) 479-8400 (Phone)
(713) 864-9357 (Fax)
www.westport1.com

September 25, 2012

Project No.: WTC-12-002873

ROUTINE CORE ANALYSIS - Well: RSU #1

TABLE OF CONTENTS i

RESULTS AND DISCUSSION 1

LIST OF TABLES

TABLE 1. TEST SELECTION AND INVENTORY 2

TABLE 2. ROUTINE CORE PROPERTIES 3

RESULTS AND DISCUSSION

Routine core analysis was conducted on thirty core plug samples obtained from multiple formations from the RSU #1 well.

All testing was conducted following core analysis procedures specified in API RP40 method, Recommended Practices for Core Analysis (1998).

The samples were extracted of hydrocarbons and brine using soxhlet techiques. A chloroform/methanol azeotrope was used as the extracting solvent. The samples were dried to stable weights in a convection oven at 180^{o} F. After stable weights were attained, the samples were transferred to airtight containers and allowed to cool to room temperature before dry weights were taken.

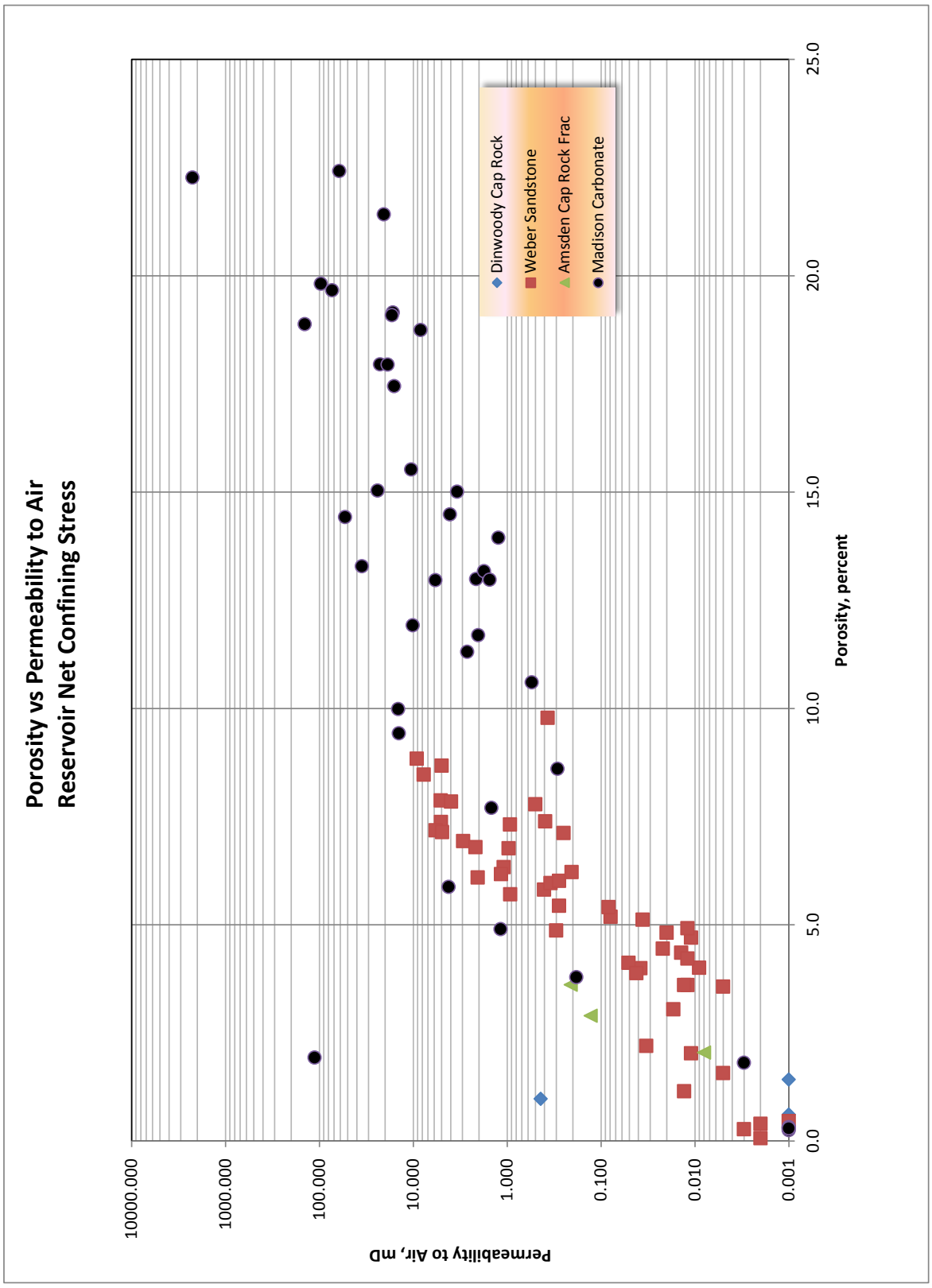
Direct grain volume measurements were made using a small volume helium porosimeter, utilizing Boyle's Law principle of gas expansion. Apparent grain density was calculated from dry weight and grain volume. Pore volume and permeability measurements were made with the samples mounted in a rubber-sleeved, hydrostatically loaded overburden cell. The samples were tested at 800 psig and a calculated reservior net confining stress. Boyle's Law principle, using helium as the gas medium, was employed to determine pore volume. Unsteady-state Klinkenberg permeability was measured after each pore volume measurement. Permeability to air was calculated using form the unsteady-state flow data.

The sample inventory and assigned analyses are provided in Table 1. The routine core properties are summarized in Table 2.

The permeability-porosity relationship is shown in Figure 1.

TABLE 2. ROUTINE CORE PROPERTIES

Sample ID	Sample Depth / Length	Permeability: 800 psi NCS to Air	Permeability: 800 psi NCS Klinkenberg	Permeability: Reservoir NCS to Air	Permeability: Reservoir NCS Klinkenberg	Porosity: 800 NCS Porosity	Porosity: Res. NCS Porosity	Grain Density	Comments
	(ft)	(mD)		(mD)		(percent)		(g/cm³)	
Dinwoody Cap Rock									
120	10636.30	0.110	0.075	0.001	0.000	1.8	0.6	2.73	Fractured
122	10649.10	235.533	229.866	0.438	0.342	2.2	1.0	2.71	Fractured
125	10671.80	0.010	0.005	0.001	0.000	2.5	1.4	2.67	
Weber Sandstone									
127	11197.70	5.569	5.061	5.082	4.601	8.5	7.9	2.61	
130	11221.00	1.115	0.938	0.966	0.837	7.4	6.8	2.60	
132	11240.00	4.362	3.924	3.951	3.538	8.7	7.9	2.60	Chipped
133	11251.20	0.108	0.077	0.079	0.053	5.8	5.2	2.61	
134	11262.00	1.056	0.883	0.933	0.777	8.0	7.3	2.60	
135	11268.00	1.067	0.930	0.925	0.802	6.3	5.7	2.61	
136	11276.60	5.370	4.874	4.986	4.512	9.3	8.7	2.59	
137	11280.30	5.368	4.872	5.080	4.600	8.0	7.4	2.61	
138	11285.00	6.370	5.821	5.775	5.257	7.5	7.2	2.62	
139	11286.55	2.235	1.943	2.053	1.777	6.8	6.1	2.60	
141	11295.00	3.175	2.813	2.941	2.596	7.5	6.9	2.61	
143	11319.50	0.431	0.348	0.280	0.350	6.2	5.4	2.61	
144	11325.05	1.259	1.108	1.089	0.951	6.9	6.3	2.61	
145	11333.50	0.076	0.049	0.038	0.022	5.4	4.0	2.60	Irregular
146	11350.00	0.036	0.020	0.017	0.008	4.1	3.1	2.62	Chipped
147	11361.00	2.327	2.024	2.175	1.886	7.2	6.8	2.61	
148	11374.00	5.249	4.754	4.940	4.463	7.4	7.1	2.62	
149	11380.70	8.255	7.610	7.720	7.100	9.1	8.5	2.60	
150	11400.00	0.462	0.568	0.405	0.502	6.5	5.8	2.63	
151	11410.00	9.763	9.055	9.190	8.802	9.2	8.8	2.61	
152	11420.00	0.074	0.048	0.051	0.032	4.7	4.1	2.61	
153	11425.40	0.026	0.044	0.012	0.022	4.7	3.6	2.62	
154	11434.90	0.454	0.545	0.344	0.421	7.4	6.0	2.60	
155	11437.15	1.458	1.635	1.159	1.313	6.9	6.2	2.62	
156	11445.20	0.377	0.458	0.300	0.370	6.0	4.9	2.60	
157	11464.45	0.070	0.102	0.033	0.052	3.0	2.2	2.71	
158	11473.55	0.150	0.202	0.083	0.118	5.8	5.4	2.64	
159	11485.35	0.386	0.474	0.280	0.351	6.7	6.0	2.61	
160	11495.00	0.091	0.131	0.036	0.057	5.7	5.1	2.63	
161	11500.00	0.328	0.266	0.206	0.266	7.0	6.2	2.63	
162	11510.00	0.001	0.003	0.001	0.003	2.1	0.5	2.62	
163	11521.00	0.059	0.093	0.022	0.040	5.1	4.5	2.64	
164	11526.70	0.026	0.014	0.005	0.002	2.0	1.6	2.74	
116	11537.00	1.258	1.056	0.502	0.406	8.7	7.8	2.81	
165	11549.90	0.116	0.080	0.042	0.025	4.7	3.9	2.77	
166	11560.00	0.042	0.024	0.011	0.005	5.3	4.7	2.63	
167	11569.90	0.532	0.436	0.393	0.316	8.1	7.4	2.64	
168	11580.00	0.380	0.302	0.251	0.195	8.1	7.1	2.62	
169	11588.45	0.083	0.050	0.014	0.007	5.2	4.4	2.63	
170	11602.30	0.069	0.043	0.011	0.005	2.8	2.0	2.79	
171	11610.50	0.067	0.043	0.013	0.006	1.9	1.2	2.79	
172	11622.80	0.087	0.056	0.020	0.020	5.6	4.8	2.63	
173	11705.00	0.031	0.017	0.013	0.006	4.3	3.6	2.63	
174	11715.10	0.040	0.022	0.012	0.005	6.4	4.9	2.65	
175	11725.00	0.007	0.002	0.002	0.001	1.2	0.4	2.72	
178	11745.00	0.058	0.033	0.009	0.004	4.9	4.0	2.65	
180	11764.15	0.009	0.004	0.002	0.001	0.8	0.1	2.69	
181	11775.00	0.004	0.001	0.003	0.001	1.4	0.3	2.66	
182	11785.00	0.019	0.009	0.005	0.002	3.9	3.6	2.76	
183	11786.00	0.062	0.039	0.012	0.006	5.1	4.2	2.78	
184	11790.00	0.738	0.618	0.371	0.296	10.8	9.8	2.73	
Amsden Cap Rock Frac									
186	12170.30	0.016	0.008	< .001	< .001	2.1	0.6	2.68	
190	12198.95	0.159	0.210	0.028	0.045	3.6	2.0	2.80	
195	12215.60	0.183	0.129	< .001	< .001	2.9	1.3	2.64	
199	12224.60	0.002	0.000	< .001	< .001	5.0	2.6	2.83	
Madison Carbonate									
201	12240.00	0.043	0.026	0.003	0.001	2.9	1.8	2.69	
205	12255.90	0.013	0.006	0.001	0.000	1.0	0.3	2.69	
207	12304.60	596.313	588.053	112.602	101.459	3.7	1.9	2.68	Fractured
208	12309.30	0.008	0.003	0.001	0.	1.3	0.3	2.68	
210	12318.00	0.012	0.005	0.001	0.	1.3	0.3	2.68	
212	12323.80	0.003	0.001	0.001	0.	0.5	0.3	2.68	
215	12339.85	0.871	0.753	0.183	0.139	5.6	3.8	2.81	Chipped
218	12349.90	63.398	61.351	61.449	59.438	22.8	22.4	2.81	
219	12355.90	23.745	22.572	22.576	21.44	18.5	18.0	2.80	
221	12365.50	21.513	20.407	20.639	19.551	22.2	21.4	2.81	
222	12370.40	17.582	16.603	16.544	15.595	20.1	19.2	2.80	
223	12375.00	11.256	10.491	10.524	9.796	16.2	15.5	2.81	
224	12381.85	2.903	2.563	2.666	2.343	12.1	11.3	2.83	
225	12384.60	2.235	1.944	2.03	1.756	12.5	11.7	2.83	
227	12393.45	4.503	4.057	4.076	3.655	15.3	14.5	2.84	
228	12400.00	3.058	2.705	2.141	1.858	14.2	13.0	2.79	
229	12402.95	15.68	14.752	5.822	5.299	14.0	13.0	2.83	
230	12406.40	20.722	19.633	18.711	17.683	19.7	18.0	2.82	
231	12407.80	1.491	1.263	1.242	1.044	14.8	13.9	2.81	
232	12410.55	27.847	26.545	23.946	22.754	16.2	15.0	2.80	
233	12414.35	21.06	21.060	15.990	15.990	18.7	17.5	2.79	
235	12421.70	105.955	103.216	96.296	93.674	20.8	19.8	2.81	
236	12428.90	18.635	17.611	16.847	15.880	20.1	19.1	2.81	
237	12432.80	0.421	0.340	0.291	0.228	9.4	8.6	2.85	
238	12436.40	9.193	8.503	8.377	7.728	19.3	18.8	2.82	
239	12437.70	5.534	5.025	1.470	1.244	8.6	7.7	2.82	
240	12444.60	2.389	2.134	1.763	1.559	14.0	13.2	2.81	
242	12448.10	1.996	1.780	1.535	1.359	13.9	13.0	2.81	
243	12453.00	4.102	3.677	3.414	3.033	16.1	15.0	2.83	
245	12460.00	37.713	36.177	35.290	33.806	14.6	13.3	2.80	
246	12463.65	57.243	55.299	53.123	51.263	15.7	14.4	2.79	
247	12469.50	15.331	14.411	14.255	13.369	10.6	9.4	2.80	
248	12476.50	149.503	146.216	142.933	139.740	19.8	18.9	2.77	
249	12482.15	15.35	14.410	14.470	13.559	11.1	10.0	2.79	
250	12485.50	2225.937	2161.201	2245.793	2180.514	23.4	22.3	2.79	
251	12489.75	4.982	4.509	4.194	3.766	6.2	5.9	2.81	
252	12491.65	1.387	1.087	0.546	0.419	12.3	10.6	2.80	
253	12498.85	1.608	1.370	1.175	0.980	6.0	4.9	2.80	
254	12511.50	77.224	74.898	73.122	70.883	20.7	19.7	2.80	
117	12513.50	13.413	12.566	10.137	9.416	12.8	11.9	2.81	


Porosity vs Permeability to Air
Reservoir Net Confining Stress
Permeability to Air, mD
10000.000
1000.000
100.000
10.000
1.000
0.100
0.010
0.001
0.0
5.0
10.0
15.0
20.0
25.0
Porosity, percent
Dinwoody Cap Rock
Weber Sandstone
Amsden Cap Rock Frac
Madison Carbonate

Stable Isotope Analysis

Sample ID	Depth (feet)	Formation	$\delta^{13}C$ (‰ VDB)	$\delta^{18}O$ (‰ VSMOW)
RSU-03	10603.2	Triassic	1.5	-7.0
RSU-12	10633.8	Triassic	1.4	-5.4
RSU-14	10645.5	Triassic	0.4	-6.7
RSU-17	10680.05	Triassic	-0.1	-5.4
RSU-21	11169.2	Weber	-3.5	-11.6
RSU-25	11209.05	Weber	-1.9	3.6
RSU-36	11570	Weber	-1.4	2.7
RSU-39	11620	Weber	0.0	-2.5
RSU-42	11720	Weber	-1.7	3.8
RSU-43	11726.4	Weber	-3.2	-7.0
RSU-44	11763.3	Weber	-2.3	-4.6
RSU-47	11788.1	Weber	-0.7	-2.8
RSU-49	12174.45	Amsden	-2.6	-6.4
RSU-50	12178.45	Amsden	-3.2	-4.2
RSU-52	12187.3	Amsden	-2.5	-5.6
RSU-56	12219.15	Amsden	-1.5	-3.8
RSU-M-01	12,227.90	Madison	0.7	-1.3
RSU-57	12233	Madison	0.4	-0.2
RSU-M-02	12,241.35	Madison	-2.5	-5.3
RSU-M-03	12,243.70	Madison	-2.2	-5.3
RSU-M-04	12,249.80	Madison	-2.0	-5.6
RSU-M-05	12,304.70	Madison	-1.6	-4.8
RSU-CV-01	12,307.80	Madison	-2.2	-10.6
RSU-M-06	12,314.75	Madison	-1.9	-4.5
RSU-M-07	12,323.80	Madison	-1.4	-5.4
RSU-M-08	12,329.20	Madison	-1.9	-5.9
RSU-M-09	12,333.00	Madison	-3.1	-5.3
RSU-68	12336.75	Madison	-0.9	0.8
RSU-65	12336.75	Madison	-4.9	-5.5
RSU-M-10	12,343.00	Madison	-1.2	2.4
RSU-75	12350	Madison	-0.7	-2.3
RSU-CV-02	12,354.85	Madison	-1.1	-11.1
RSU-CV	12355.7	Madison	-3.0	-13.0
RSU-81	12356.7	Madison	0.0	-1.9
RSU-M-11	12,360.70	Madison	-1.4	-4.7

Sample ID	Depth (feet)	Formation	$\delta^{13}C$ (‰ VDB)	$\delta^{18}O$ (‰ VSMOW)
RSU-87	12365.6	Madison	0.8	-0.7
RSU-88	12371.05	Madison	0.4	0.1
RSU-90	12374.5	Madison	-0.2	1.4
RSU-91	12377.65	Madison	0.0	-1.3
RSU-CV-03	12,383.50	Madison	-0.9	-7.9
RSU-96	12385.06	Madison	0.5	0.7
RSU-97	12393.32	Madison	0.7	-0.6
RSU-98	12398.5	Madison	0.4	1.1
RSU-101	12403.38	Madison	0.0	1.5
RSU-M-12	12,406.40	Madison	0.4	1.9
RSU-105	12414.55	Madison	-1.2	2.4
RSU-M-14	12,421.10	Madison	-0.4	2.3
RSU-M-15	12,429.00	Madison	0.5	3.2
RSU-M-16	12,432.80	Madison	0.7	1.5
RSU-M-17	12,438.00	Madison	0.0	-1.1
RSU-M-18	12,446.00	Madison	0.9	2.4
RSU-M-19	12,453.00	Madison	0.9	1.6
RSU-M-20	12,457.40	Madison	0.5	2.5
RSU-M-21	12,463.90	Madison	0.6	2.2
RSU-M-22	12,468.80	Madison	0.0	-0.7
RSU-M-23	12,476.60	Madison	1.4	-0.4
RSU-M-24	12,482.20	Madison	0.3	2.5
RSU-M-25	12,489.00	Madison	0.3	1.1
RSU-M-26	12,491.80	Madison	0.4	0.5
RSU-M-27	12,499.20	Madison	0.2	0.1
RSU-M-28	12,511.40	Madison	1.9	-1.1
RSU-CV-04	12,511.70	Madison	0.1	-11.0
RSU-M-29	12,513.50	Madison	1.6	-0.5
RSU-M-30	12,519.50	Madison	0.8	0.1
RSU-M-31	12,535.00	Madison	0.0	1.2

Results quantitative - ProTrace

Seq.	Sample name (1-60)	Application or Instrument monitor or Calibration update	Initial weight (g)	Final weight (g)	Sc Sc (ppm)	TiO2 Ti (ppm)	V V (ppm)	Cr Cr (ppm)	Mn Mn (ppm)	Co Co (ppm)	Ni Ni (ppm)	Cu Cu (ppm)
1	RSU-3	Pe ProTrace	4.03	4.99	<d.l.	8010.5	61.1	75.7	542.0	<d.l.	29.3	14.3
2	RSU-12	P(ProTrace	4.01	5.04	<d.l.	5488.7	46.9	42.6	526.2	<d.l.	21.1	15.2
3	RSU-14	P(ProTrace	4.01	5.01	<d.l.	4899.5	35.3	36.2	416.6	<d.l.	17.3	10.3
4	RSU-17	P(ProTrace	4.04	5	<d.l.	6976.3	63.8	52.7	523.1	<d.l.	27.5	14.1
5	RSU-21	P(ProTrace	3.99	5.02	<d.l.	307.6	<d.l.	14.9	24.3	<d.l.	4.4	<d.l.
6	RSU-25	P(ProTrace	4.03	5.03	<d.l.	1952.7	11.5	34.4	36.3	<d.l.	7.3	2.9
7	RSU-36	P(ProTrace	4.01	5.02	<d.l.	782.7	<d.l.	13.7	59.5	<d.l.	3.9	<d.l.
8	RSU-39	P(ProTrace	4.01	5.01	<d.l.	739.3	8.5	22.9	61.3	<d.l.	3.9	<d.l.
9	RSU-42	P(ProTrace	3.99	5.03	<d.l.	1444.7	46.4	43.1	202.9	<d.l.	17.9	<d.l.
10	RSU-43	P(ProTrace	4	5	<d.l.	6423.2	1069.2	1702.1	39.9	12.3	558.3	131.7
11	RSU-44	P(ProTrace	4.02	5.04	<d.l.	510.0	12.9	22.3	201.3	<d.l.	23.2	4.3
12	RSU-47	P(ProTrace	4.03	5.05	<d.l.	315.4	<d.l.	30.3	140.7	<d.l.	<d.l.	<d.l.
13	RSU-49	P(ProTrace	3.98	5.02	<d.l.	80.0	<d.l.	11.1	60.1	<d.l.	<d.l.	<d.l.
14	RSU-50	P(ProTrace	4.02	5	12.0	8579.0	56.6	100.5	32.1	<d.l.	31.2	5.0
15	RSU-52	P(ProTrace	3.99	5.24	<d.l.	453.1	<d.l.	10.6	85.3	<d.l.	<d.l.	<d.l.
16	RSU-56	P(ProTrace	4.03	5.02	<d.l.	3492.3	43.4	40.5	77.0	<d.l.	16.3	<d.l.
17	RSU-57	P(ProTrace	4.02	5.01	<d.l.	72.8	<d.l.	8.9	1297.0	15.3	20.0	<d.l.
18	RSU-65	P(ProTrace	4.03	5.02	<d.l.	50.0	<d.l.	7.8	39.1	<d.l.	<d.l.	<d.l.
19	RSU-68	P(ProTrace	3.99	4.98	<d.l.	63.3	<d.l.	21.9	173.9	<d.l.	13.5	<d.l.
20	RSU-75	P(ProTrace	4.01	5	<d.l.	117.3	11.1	14.3	101.2	<d.l.	11.0	<d.l.
21	RSU-CV	P ProTrace	4.02	5	<d.l.	<d.l.	<d.l.	<d.l.	270.8	<d.l.	<d.l.	<d.l.
22	RSU-81	P(ProTrace	3.99	5.01	<d.l.	129.8	<d.l.	17.5	67.7	<d.l.	7.5	<d.l.
23	RSU-87	P(ProTrace	4.01	5.02	<d.l.	424.5	12.1	21.4	65.2	<d.l.	7.2	<d.l.
24	RSU-88	P(ProTrace	4	5	<d.l.	248.8	<d.l.	18.4	111.8	<d.l.	9.5	<d.l.
25	RSU-90	P(ProTrace	4	5.03	<d.l.	106.8	<d.l.	11.8	118.0	<d.l.	10.2	<d.l.
26	RSU-91	P(ProTrace	4	5.02	<d.l.	62.5	<d.l.	10.2	87.7	<d.l.	8.1	<d.l.
27	RSU-96	P(ProTrace	3.99	4.99	<d.l.	162.9	<d.l.	14.0	175.7	<d.l.	9.2	<d.l.
28	RSU-97	P(ProTrace	4.01	5.01	<d.l.	174.3	<d.l.	11.5	203.4	<d.l.	7.3	<d.l.
29	RSU-98	P(ProTrace	4.01	5.02	<d.l.	102.2	<d.l.	9.6	100.7	<d.l.	7.5	<d.l.
30	RSU-101	P ProTrace	4.01	5.02	<d.l.	85.7	<d.l.	6.3	111.4	<d.l.	7.7	<d.l.
31	RSU-105	P ProTrace	4	5.03	<d.l.	50.2	<d.l.	5.9	111.5	<d.l.	5.8	<d.l.
				det. Lim.	12.0	21.5	8.5	5.7	10.2	12.0	3.9	1.7

Results quantitative - ProTrace

Seq.	Sample name (1-60)				Application or Instrument monitor or Calibration update	Zn Zn (ppm)	Ga Ga (ppm)	Ge Ge (ppm)	As As (ppm)	Se Se (ppm)	Br Br (ppm)	Rb Rb (ppm)	Sr Sr (ppm)	Y Y (ppm)	Zr Zr (ppm)	Nb Nb (ppm)	Mo Mo (ppm)	Ag Ag (ppm)
1	RSU-3	Pellet	nsc	RSU-Fre	ProTrace	54.2	14.7	<d.l.	44.7	8.9	7.2	79.9	118.3	29.5	331.3	12.1	<d.l.	18.3
2	RSU-12	Pellet	nsc	RSU-Fre	ProTrace	47.2	11.9	<d.l.	43.0	9.8	7.4	65.0	491.5	21.1	182.5	7.8	<d.l.	23.8
3	RSU-14	Pellet	nsc	RSU-Fre	ProTrace	29.3	9.7	<d.l.	44.4	9.1	7.5	53.5	589.0	16.5	196.1	7.0	<d.l.	17.0
4	RSU-17	Pellet	nsc	RSU-Fre	ProTrace	47.9	14.2	<d.l.	42.1	8.4	6.3	82.2	268.1	25.0	315.1	11.2	<d.l.	14.3
5	RSU-21	Pellet	nsc	RSU-Fre	ProTrace	<d.l.	2.7	<d.l.	31.4	7.3	5.8	11.8	28.6	<d.l.	37.6	<d.l.	2.2	15.0
6	RSU-25	Pellet	nsc	RSU-Fre	ProTrace	2.9	3.6	<d.l.	33.5	8.8	8.6	36.0	47.1	5.7	338.5	2.5	1.3	12.9
7	RSU-36	Pellet	nsc	RSU-Fre	ProTrace	<d.l.	3.1	<d.l.	30.6	6.6	7.1	29.7	44.6	2.4	169.6	<d.l.	<d.l.	13.5
8	RSU-39	Pellet	nsc	RSU-Fre	ProTrace	2.2	2.3	<d.l.	33.2	7.5	7.6	22.7	30.1	2.3	166.5	<d.l.	<d.l.	19.2
9	RSU-42	Pellet	nsc	RSU-Fre	ProTrace	162.8	3.7	<d.l.	45.2	10.4	8.6	18.9	80.4	7.7	43.8	<d.l.	1.3	20.0
10	RSU-43	Pellet	nsc	RSU-Fre	ProTrace	1640.0	20.1	<d.l.	73.1	23.1	8.4	172.4	348.7	110.2	274.8	9.1	21.0	25.2
11	RSU-44	Pellet	nsc	RSU-Fre	ProTrace	85.6	3.4	<d.l.	65.8	12.3	11.1	9.0	312.2	10.9	2.8	<d.l.	2.7	24.8
12	RSU-47	Pellet	nsc	RSU-Fre	ProTrace	2.2	2.0	<d.l.	35.1	7.1	6.7	8.1	22.4	<d.l.	43.1	<d.l.	<d.l.	16.7
13	RSU-49	Pellet	nsc	RSU-Fre	ProTrace	3.9	2.8	<d.l.	62.9	12.6	10.5	2.1	186.9	<d.l.	<d.l.	<d.l.	<d.l.	28.0
14	RSU-50	Pellet	nsc	RSU-Fre	ProTrace	35.5	16.8	<d.l.	41.7	8.4	6.2	201.5	191.3	22.8	392.7	12.3	<d.l.	21.0
15	RSU-52	Pellet	nsc	RSU-Fre	ProTrace	2.6	2.4	<d.l.	56.8	10.5	9.6	4.5	148.5	<d.l.	11.8	<d.l.	<d.l.	22.6
16	RSU-56	Pellet	nsc	RSU-Fre	ProTrace	10.4	7.4	<d.l.	56.9	11.0	9.5	48.0	60.2	5.6	37.1	2.4	<d.l.	22.2
17	RSU-57	Pellet	nsc	RSU-Fre	ProTrace	33.8	2.3	<d.l.	41.5	9.1	11.9	2.3	126.4	<d.l.	<d.l.	<d.l.	<d.l.	13.5
18	RSU-65	Pellet	nsc	RSU-Fre	ProTrace	5.9	3.0	<d.l.	64.7	11.8	11.4	<d.l.	30.1	<d.l.	<d.l.	<d.l.	<d.l.	23.2
19	RSU-68	Pellet	nsc	RSU-Fre	ProTrace	55.0	2.1	<d.l.	38.4	7.8	8.5	1.6	50.0	2.2	<d.l.	<d.l.	<d.l.	17.7
20	RSU-75	Pellet	nsc	RSU-Fre	ProTrace	23.0	2.2	<d.l.	44.6	8.3	13.4	4.9	39.1	2.2	<d.l.	<d.l.	<d.l.	15.1
21	RSU-CV	Pellet	nsc	RSU-Fr	ProTrace	<d.l.	2.8	<d.l.	54.7	12.2	12.0	<d.l.	70.1	<d.l.	<d.l.	<d.l.	<d.l.	17.6
22	RSU-81	Pellet	nsc	RSU-Fre	ProTrace	20.0	2.3	<d.l.	43.7	9.1	11.5	3.0	93.5	3.3	<d.l.	<d.l.	<d.l.	10.8
23	RSU-87	Pellet	nsc	RSU-Fre	ProTrace	13.4	1.5	<d.l.	42.4	8.5	18.0	5.7	48.2	2.0	4.4	<d.l.	2.6	17.5
24	RSU-88	Pellet	nsc	RSU-Fre	ProTrace	10.4	1.8	<d.l.	41.4	9.0	9.7	4.2	45.0	2.0	2.5	<d.l.	<d.l.	19.3
25	RSU-90	Pellet	nsc	RSU-Fre	ProTrace	12.3	2.2	<d.l.	42.9	7.9	8.6	5.3	130.4	2.0	<d.l.	<d.l.	<d.l.	17.8
26	RSU-91	Pellet	nsc	RSU-Fre	ProTrace	23.4	<d.l.	<d.l.	47.8	11.1	10.3	4.6	795.9	3.7	<d.l.	<d.l.	<d.l.	22.2
27	RSU-96	Pellet	nsc	RSU-Fre	ProTrace	7.5	2.1	<d.l.	40.9	9.0	8.3	6.0	39.4	2.2	1.5	<d.l.	<d.l.	17.9
28	RSU-97	Pellet	nsc	RSU-Fre	ProTrace	5.4	2.3	<d.l.	40.0	8.5	9.7	5.1	271.4	<d.l.	<d.l.	<d.l.	<d.l.	18.6
29	RSU-98	Pellet	nsc	RSU-Fre	ProTrace	12.2	1.9	<d.l.	39.0	8.2	9.2	4.4	902.6	<d.l.	<d.l.	<d.l.	1.4	21.0
30	RSU-101	Pellet	nsc	RSU-Fr	ProTrace	9.1	2.0	<d.l.	36.9	8.2	9.7	2.6	33.1	<d.l.	<d.l.	<d.l.	<d.l.	12.9
31	RSU-105	Pellet	nsc	RSU-Fr	ProTrace	2.9	1.7	<d.l.	46.3	8.9	11.7	1.6	39.0	1.8	<d.l.	<d.l.	<d.l.	16.3
1.3				1.4	1.5	10.9	2.4	1.8	1.4	1.0	1.7	1.5	1.6	1.3	9.5			

Results quantitative - ProTrace

Seq.	Sample name (1-60)				Application or Instrument monitor or Calibration update	Initial weight (g)	Final weight (g)	Cd Cd (ppm)	Sn Sn (ppm)	Sb Sb (ppm)	Te Te (ppm)	I I (ppm)	Cs Cs (ppm)	Ba Ba (ppm)	La La (ppm)	Ce Ce (ppm)	Nd Nd (ppm)	Sm Sm (ppm)	Yb Yb (ppm)	Hf Hf (ppm)	Ta Ta (ppm)	W W (ppm)	Tl Tl (ppm)	Pb Pb (ppm)	Bi Bi (ppm)	Th Th (ppm)	U U (ppm)
1	RSU-3	Pellet	nsc	RSU-Fre	ProTrace	4.03	4.99	16.8	<d.l.	<d.l.	<d.l.	<d.l.	<d.l.	368.9	36.3	69.7	36.5	<d.l.	<d.l.	<d.l.	<d.l.	5.3	14.9	18.9	15.4	9.1	<d.l.
2	RSU-12	Pellet	nsc	RSU-Fre	ProTrace	4.01	5.04	14.5	<d.l.	<d.l.	<d.l.	<d.l.	<d.l.	474.8	30.7	<d.l.	<d.l.	<d.l.	<d.l.	<d.l.	<d.l.	4.7	17.0	10.7	16.9	5.7	<d.l.
3	RSU-14	Pellet	nsc	RSU-Fre	ProTrace	4.01	5.01	11.1	<d.l.	<d.l.	9.8	<d.l.	<d.l.	245.1	<d.l.	<d.l.	<d.l.	<d.l.	<d.l.	<d.l.	<d.l.	<d.l.	20.2	12.3	17.2	<d.l.	<d.l.
4	RSU-17	Pellet	nsc	RSU-Fre	ProTrace	4.04	5	15.4	<d.l.	<d.l.	<d.l.	<d.l.	<d.l.	340.1	34.3	51.0	25.7	<d.l.	<d.l.	<d.l.	<d.l.	4.9	16.1	19.0	16.5	7.0	<d.l.
5	RSU-21	Pellet	nsc	RSU-Fre	ProTrace	3.99	5.02	12.4	<d.l.	<d.l.	<d.l.	<d.l.	<d.l.	86.2	<d.l.	<d.l.	<d.l.	<d.l.	<d.l.	<d.l.	<d.l.	11.6	12.2	7.2	11.6	<d.l.	<d.l.
6	RSU-25	Pellet	nsc	RSU-Fre	ProTrace	4.03	5.03	10.1	<d.l.	<d.l.	<d.l.	<d.l.	<d.l.	350.0	<d.l.	<d.l.	<d.l.	<d.l.	<d.l.	<d.l.	<d.l.	10.1	14.5	17.5	10.9	<d.l.	<d.l.
7	RSU-36	Pellet	nsc	RSU-Fre	ProTrace	4.01	5.02	10.6	<d.l.	<d.l.	9.1	<d.l.	<d.l.	223.6	<d.l.	<d.l.	<d.l.	<d.l.	<d.l.	<d.l.	<d.l.	7.9	13.1	9.1	9.3	<d.l.	<d.l.
8	RSU-39	Pellet	nsc	RSU-Fre	ProTrace	4.01	5.01	18.1	<d.l.	<d.l.	<d.l.	<d.l.	<d.l.	183.1	<d.l.	<d.l.	<d.l.	<d.l.	<d.l.	<d.l.	<d.l.	10.1	14.5	8.3	10.7	<d.l.	<d.l.
9	RSU-42	Pellet	nsc	RSU-Fre	ProTrace	3.99	5.03	14.3	<d.l.	<d.l.	<d.l.	<d.l.	<d.l.	55.5	<d.l.	<d.l.	<d.l.	<d.l.	<d.l.	<d.l.	<d.l.	<d.l.	19.1	18.7	16.5	<d.l.	<d.l.
10	RSU-43	Pellet	nsc	RSU-Fre	ProTrace	4	5	40.2	<d.l.	<d.l.	<d.l.	<d.l.	47.3	300.2	102.3	135.8	50.8	<d.l.	<d.l.	<d.l.	<d.l.	<d.l.	23.2	137.2	17.9	8.4	81.2
11	RSU-44	Pellet	nsc	RSU-Fre	ProTrace	4.02	5.04	16.4	<d.l.	<d.l.	11.0	<d.l.	<d.l.	55.4	<d.l.	<d.l.	<d.l.	<d.l.	<d.l.	<d.l.	<d.l.	<d.l.	29.4	10.8	24.8	<d.l.	<d.l.
12	RSU-47	Pellet	nsc	RSU-Fre	ProTrace	4.03	5.05	11.9	<d.l.	<d.l.	9.9	<d.l.	<d.l.	38.0	<d.l.	<d.l.	<d.l.	<d.l.	<d.l.	<d.l.	<d.l.	6.1	15.1	6.3	12.8	<d.l.	<d.l.
13	RSU-49	Pellet	nsc	RSU-Fre	ProTrace	3.98	5.02	15.2	<d.l.	<d.l.	<d.l.	<d.l.	<d.l.	40.3	<d.l.	<d.l.	<d.l.	<d.l.	<d.l.	<d.l.	<d.l.	6.3	29.6	8.6	23.6	<d.l.	<d.l.
14	RSU-50	Pellet	nsc	RSU-Fre	ProTrace	4.02	5	14.8	<d.l.	<d.l.	<d.l.	<d.l.	31.5	112.7	28.8	74.9	37.1	<d.l.	<d.l.	<d.l.	<d.l.	4.5	17.6	12.1	14.5	9.7	<d.l.
15	RSU-52	Pellet	nsc	RSU-Fre	ProTrace	3.99	5.24	14.2	<d.l.	<d.l.	<d.l.	<d.l.	<d.l.	28.7	<d.l.	<d.l.	<d.l.	<d.l.	<d.l.	<d.l.	<d.l.	5.2	25.8	6.0	21.7	<d.l.	<d.l.
16	RSU-56	Pellet	nsc	RSU-Fre	ProTrace	4.03	5.02	12.2	<d.l.	<d.l.	19.9	<d.l.	<d.l.	99.7	<d.l.	<d.l.	<d.l.	<d.l.	<d.l.	<d.l.	<d.l.	5.5	25.0	6.1	22.5	<d.l.	<d.l.
17	RSU-57	Pellet	nsc	RSU-Fre	ProTrace	4.02	5.01	<d.l.	<d.l.	<d.l.	<d.l.	<d.l.	<d.l.	31.8	<d.l.	<d.l.	<d.l.	<d.l.	<d.l.	<d.l.	<d.l.	4.4	20.2	8.3	15.4	<d.l.	<d.l.
18	RSU-65	Pellet	nsc	RSU-Fre	ProTrace	4.03	5.02	12.0	<d.l.	<d.l.	<d.l.	<d.l.	<d.l.	39.7	<d.l.	<d.l.	<d.l.	<d.l.	<d.l.	<d.l.	<d.l.	5.1	30.7	8.6	25.1	<d.l.	<d.l.
19	RSU-68	Pellet	nsc	RSU-Fre	ProTrace	3.99	4.98	11.3	<d.l.	<d.l.	13.8	<d.l.	<d.l.	<d.l.	<d.l.	<d.l.	<d.l.	<d.l.	<d.l.	<d.l.	<d.l.	<d.l.	18.0	8.2	14.1	<d.l.	<d.l.
20	RSU-75	Pellet	nsc	RSU-Fre	ProTrace	4.01	5	<d.l.	<d.l.	<d.l.	<d.l.	<d.l.	19.7	<d.l.	<d.l.	<d.l.	<d.l.	<d.l.	<d.l.	<d.l.	<d.l.	7.2	19.5	6.4	15.9	<d.l.	<d.l.
21	RSU-CV	Pellet	nsc	RSU-Fr	ProTrace	4.02	5	<d.l.	<d.l.	<d.l.	12.6	<d.l.	<d.l.	50.2	<d.l.	<d.l.	<d.l.	<d.l.	<d.l.	<d.l.	<d.l.	<d.l.	26.0	4.1	24.0	<d.l.	<d.l.
22	RSU-81	Pellet	nsc	RSU-Fre	ProTrace	3.99	5.01	<d.l.	<d.l.	<d.l.	<d.l.	<d.l.	<d.l.	<d.l.	<d.l.	<d.l.	<d.l.	<d.l.	<d.l.	<d.l.	<d.l.	5.1	16.9	6.0	17.1	<d.l.	<d.l.
23	RSU-87	Pellet	nsc	RSU-Fre	ProTrace	4.01	5.02	13.9	<d.l.	<d.l.	<d.l.	<d.l.	<d.l.	<d.l.	<d.l.	<d.l.	<d.l.	<d.l.	<d.l.	<d.l.	<d.l.	4.1	17.6	8.1	14.3	<d.l.	<d.l.
24	RSU-88	Pellet	nsc	RSU-Fre	ProTrace	4	5	14.5	<d.l.	<d.l.	10.3	<d.l.	<d.l.	<d.l.	<d.l.	<d.l.	<d.l.	<d.l.	<d.l.	<d.l.	<d.l.	4.2	18.4	6.3	15.8	<d.l.	<d.l.
25	RSU-90	Pellet	nsc	RSU-Fre	ProTrace	4	5.03	14.1	<d.l.	<d.l.	<d.l.	<d.l.	<d.l.	<d.l.	<d.l.	<d.l.	<d.l.	<d.l.	<d.l.	<d.l.	<d.l.	<d.l.	18.0	6.0	14.9	<d.l.	<d.l.
26	RSU-91	Pellet	nsc	RSU-Fre	ProTrace	4	5.02	18.7	<d.l.	<d.l.	<d.l.	<d.l.	<d.l.	<d.l.	<d.l.	<d.l.	<d.l.	<d.l.	<d.l.	<d.l.	<d.l.	4.1	19.4	4.3	21.9	<d.l.	<d.l.
27	RSU-96	Pellet	nsc	RSU-Fre	ProTrace	3.99	4.99	12.9	<d.l.	<d.l.	<d.l.	<d.l.	<d.l.	<d.l.	<d.l.	<d.l.	<d.l.	<d.l.	<d.l.	<d.l.	<d.l.	<d.l.	17.4	5.4	14.4	<d.l.	<d.l.
28	RSU-97	Pellet	nsc	RSU-Fre	ProTrace	4.01	5.01	9.8	<d.l.	<d.l.	<d.l.	<d.l.	<d.l.	<d.l.	<d.l.	<d.l.	<d.l.	<d.l.	<d.l.	<d.l.	<d.l.	4.2	17.7	5.1	15.5	<d.l.	<d.l.
29	RSU-98	Pellet	nsc	RSU-Fre	ProTrace	4.01	5.02	15.8	<d.l.	<d.l.	<d.l.	<d.l.	<d.l.	<d.l.	<d.l.	<d.l.	<d.l.	<d.l.	<d.l.	<d.l.	<d.l.	4.2	14.0	4.0	16.7	<d.l.	<d.l.
30	RSU-101	Pellet	nsc	RSU-Fr	ProTrace	4.01	5.02	<d.l.	<d.l.	<d.l.	<d.l.	<d.l.	<d.l.	<d.l.	<d.l.	<d.l.	<d.l.	<d.l.	<d.l.	<d.l.	<d.l.	<d.l.	16.6	5.8	14.7	<d.l.	<d.l.
31	RSU-105	Pellet	nsc	RSU-Fr	ProTrace	4	5.03	10.4	<d.l.	<d.l.	<d.l.	<d.l.	<d.l.	<d.l.	<d.l.	<d.l.	<d.l.	<d.l.	<d.l.	<d.l.	<d.l.	<d.l.	18.6	7.4	17.2	<d.l.	<d.l.
							det. Lim.	9.8	6.4	11.7	9.1	10.9	18.3	24.0	28.8	49.4	25.7	21.2	6.6	9.3	4.7	4.1	4.4	3.8	4.5	5.2	3.5

Appendix G: Triaxial Shear Test Final Report and Summary

ADVANCED CORE ANALYSIS STUDY

University of Wyoming
RSU #1 Well
Sweetwater County, Wyoming

FINAL REPORT

Submitted to:

University of Wyoming

June 6, 2012

Performed by:

Core Laboratories
Petroleum Services Division
6316 Windfern
Houston, Texas 77040

HOU-120536

The analytical results, opinions, or interpretations contained in this report are based upon information and material supplied by the client for whose exclusive and confidential use this report has been made. The analytical results, opinions, or interpretations expressed represent the best judgement of Core Laboratories. Core Laboratories, however, makes no warranty or representation, express or implied, of any type, and expressly disclaims same as to the productivity, proper operations, or profitableness of any oil, gas, coal, or other mineral, property, well, or sand in connection with which such report is used or relied upon for any reason whatsoever. This report shall not be reproduced, in whole or in part, without the written approval of Core Laboratories.

University of Wyoming
RSU #1 Well
Sweetwater County, Wyoming

Table of Contents

Summary of Results

Test Schedule Summary

Geomechanical Analysis

Laboratory Procedures

Triaxial Compressive Strength

Acoustic Velocity

SUMMARY OF RESULTS

The Houston Advanced Technology Center of Core Laboratories received seven (7) 1-inch core plug samples for geomechanical analysis of the RSU #1 well. The sample material was from the depths of 10602.60 to 12512.00 feet.

Geomechanical Analysis

Triaxial Compressive Strength and Acoustic Velocity

In a triaxial test, the sample dimensions are accurately measured using two Linear Variable Displacement Transducers (LVDT). One LVDT measures changes in sample circumference and one LVDT measures changes in sample length as a function of applied stress. The applied stress is calculated based on measurements of applied load using a calibrated pressure gauge to measure the applied pressure. Each sample was tested at a single net confining stress, as listed in the table below.

The triaxial compressive strength tests are commonly used to simulate the in-situ stress conditions of the reservoirs and provide compressive strength and static values of elastic constants: Young's modulus and Poisson's ratio. Young's modulus is the slope of a line when axial stress is plotted against axial strain. An important property of linear-elastic material is the ability to expand in a lateral direction when the load is applied on the material in a vertical direction. This ability to expand laterally is expressed by Poisson's ratio, which is defined by the ratio of lateral expansion to vertical contraction. Poisson's ratio is a critical parameter in determining formation stress and consequently influences fracture height and width.

The Triaxial testing, at the listed net confining stresses, including Young's modulus and Poisson's ratio, is summarized in the table below.

Triaxial Compressive Strength

Sample Number	Depth (ft)	Confining Pressure (psi)	Compressive Strength (psi)	Young's Modulus (10^6 psi)	Poisson's Ratio
2V	10602.60	2490	49378	7.96	0.17
11V	10630.70	2490	38504	6.11	0.20
19V	10683.25	2490	41146	5.04	0.19
31V	11417.25	2490	61867	8.23	0.16
34V	11521.35	2490	72048	9.56	0.19
95V	12384.00	2490	36400	6.91	0.26
113V	12512.00	2490	12870	2.62	0.29

Acoustic velocity measurements were performed on the samples using the pulse transmission technique at the same net confining stresses as shown in the triaxial tests and at varied axial pressures. The acoustic velocities ranged from 16744 to 18933 ft/sec for the compressional waves and from 8916 to 11637 ft/sec for the shear waves at the highest axial pressure tested. Dynamic Young's moduli ranged from 6.91 x 10^6 psi to 11.38 x 10^6 psi while the dynamic Poisson's ratios ranged from 0.14 to 0.30. The stress-strain curves for each Triaxial test and acoustic velocity measurements are presented together with sample dimensions and experimental conditions later in this report.

TEST SCHEDULE SUMMARY

Company: **University of Wyoming** File: **HOU-120536**
Well: **RSU #1**
Location: **Sweetwater County, Wyoming**

Sample Number	Depth, feet	Triaxial Compressive Strength	Acoustic Velocity
2V	10602.60	X	X
11V	10630.70	X	X
19V	10683.25	X	X
31V	11417.25	X	X
34V	11521.35	X	X
95V	12384.00	X	X
113V	12512.00	X	X



Geomechanical Analysis

Triaxial Compressive Strength
Acoustic Velocity

LABORATORY PROCEDURES

Single-stage Triaxial Compressive Strength

1. Sample length, diameter and mass were measured and recorded. The samples were tested as received.
2. The samples were inserted into rubber jackets and a radial Linear Variable Displacement Transducer (LVDT) was placed around the lateral surface of each sample.
3. Each sample was mounted between pistons with ports on the contacting surfaces for controlling pore pressure.
4. The entire assembly was mounted in a pressure vessel that allows application of confining pressure and axial stress. The top piston extends through the top of the pressure vessel enabling the application of axial load.
5. The pressure vessel was then loaded into a computer-controlled load frame where another LVDT is attached for axial strain measurements.
6. The pressure system was inspected for leaks, then confining and axial pressures were increased at the same rate to initial triaxial test conditions.
7. After confining and axial pressure reached the net confining pressure, both pressures were held constant and until both axial and radial strain were constant. All pressure, stress and strain data were recorded.
8. The test was terminated upon attaining the desired level of axial stress or after sample failure. Axial stress was reduced to the hydrostatic condition. Axial and confining pressures were reduced to zero simultaneously.

Triaxial Data Analysis

Deviatory stresses are plotted against both axial strain ε_L (= $\Delta L/L_o$) and radial strain ε_R (= $\Delta R/R_o$). Deviatory stress (σ_d) is defined as the difference between the total axial stress and the confining pressure. Since all the tests were conducted under compressive stresses, compressive stress and contraction (shortening) are considered positive. Accordingly, positive axial strain indicates a shortening of the sample and negative radial strain indicates an increase in the sample diameter during deformation.

The compressive strength is defined as the maximum principal stress (σ_1) achieved during testing, however, the deviatory stresses (σ_1 – Pc) are plotted in the stress-strain curves. Static Young's modulus is determined by taking the slope of the linear elastic part of the curve, plotted on σ_d vs. ε_L space. Static Poisson's ratio (= $-\Delta\varepsilon_R/\Delta\varepsilon_L$) is also determined in a similar way by taking the ratio of the slope of the axial curve to the slope of the radial curve.

Acoustic Velocities and Dynamic Elastic Parameters

The pulse transmission technique of velocity measurements was used with 1MHz frequency for P-waves and S-waves. The accuracy of velocity measurements is about 1%. Dynamic elastic parameters (bulk modulus, Young's modulus, shear modulus, and Poisson's ratio) were calculated using compressional-wave and shear-wave velocities (Vp and Vs, respectively) and the bulk density of the sample, based on the linear elastic theory.

TRIAXIAL COMPRESSIVE TEST RESULTS

Company:	**University of Wyoming**	Date:	**May, 2012**
Well:	**RSU #1**	File:	**HOU-120536**
		Saturation Fluid:	**As Received**

Triaxial Static Young's Modulus, Poisson's Ratio and Compressive Strength

Sample Number	Depth (ft)	Confining Pressure (psi)	Bulk Density (g/cm^3)	Compressive Strength (psi)	Young's Modulus (10^6 psi)	Poisson's Ratio
2V	10602.60	2490	2.69	49378	7.96	0.17
11V	10630.70	2490	2.78	38504	6.11	0.20
19V	10683.25	2490	2.65	41146	5.04	0.19
31V	11417.25	2490	2.48	61867	8.23	0.16
34V	11521.35	2490	2.56	72048	9.56	0.19
95V	12384.00	2490	2.53	36400	6.91	0.26
113V	12512.00	2490	2.48	12870	2.62	0.29

ACOUSTIC VELOCITIES AND DYNAMIC ELASTIC PARAMETERS

Company: **University of Wyoming**
Well: **RSU #1**

Date: **May, 2012**
File: **HOU-120536**
Saturation Fluid: **As Received**

Acoustic Velocities and Dynamic Moduli at Triaxial Stress Conditions

Sample Number	Depth (ft)	Confining Pressure (psi)	Axial Pressure (psi)	Bulk Density (g/cm^3)	Acoustic Velocity				Dynamic Elastic Parameters			
					Compressional		Shear		Bulk Modulus ($x10^6$ psi)	Young's Modulus ($x10^6$ psi)	Shear Modulus ($x10^6$ psi)	Poisson's Ratio
					ft/sec	µs/ft	ft/sec	µs/ft				
2V	10602.60	2490	2490	2.69	17307	57.8	10886	91.9	5.13	10.07	4.29	0.17
		2490	25000	2.69	18391	54.4	11249	88.9	6.14	11.01	4.58	0.20
11V	10630.70	2490	2490	2.78	18149	55.1	11051	90.5	6.24	11.02	4.57	0.21
		2490	19000	2.78	18590	53.8	11175	89.5	6.70	11.38	4.68	0.22
19V	10683.25	2490	2490	2.65	16141	62.0	10016	99.8	4.52	8.50	3.58	0.19
		2490	20000	2.65	16914	59.1	10197	98.1	5.26	9.01	3.71	0.21
31V	11417.25	2490	2490	2.48	17754	56.3	11547	86.6	4.59	10.10	4.46	0.13
		2490	30000	2.48	17990	55.6	11637	85.9	4.78	10.32	4.53	0.14
34V	11521.35	2490	2490	2.56	17911	55.8	11361	88.0	5.13	10.36	4.45	0.16
		2490	36000	2.56	18494	54.1	11414	87.6	5.81	10.72	4.49	0.19
95V	12384.00	2490	2490	2.53	18350	54.50	10479	95.43	6.50	9.43	3.75	0.26
		2490	18000	2.53	18933	52.82	10536	94.92	7.19	9.67	3.79	0.28
113V	12512.00	2490	2490	2.48	16162	61.87	8875	112.67	5.21	6.75	2.63	0.28
		2490	7000	2.48	16744	59.72	8916	112.15	5.82	6.91	2.65	0.30

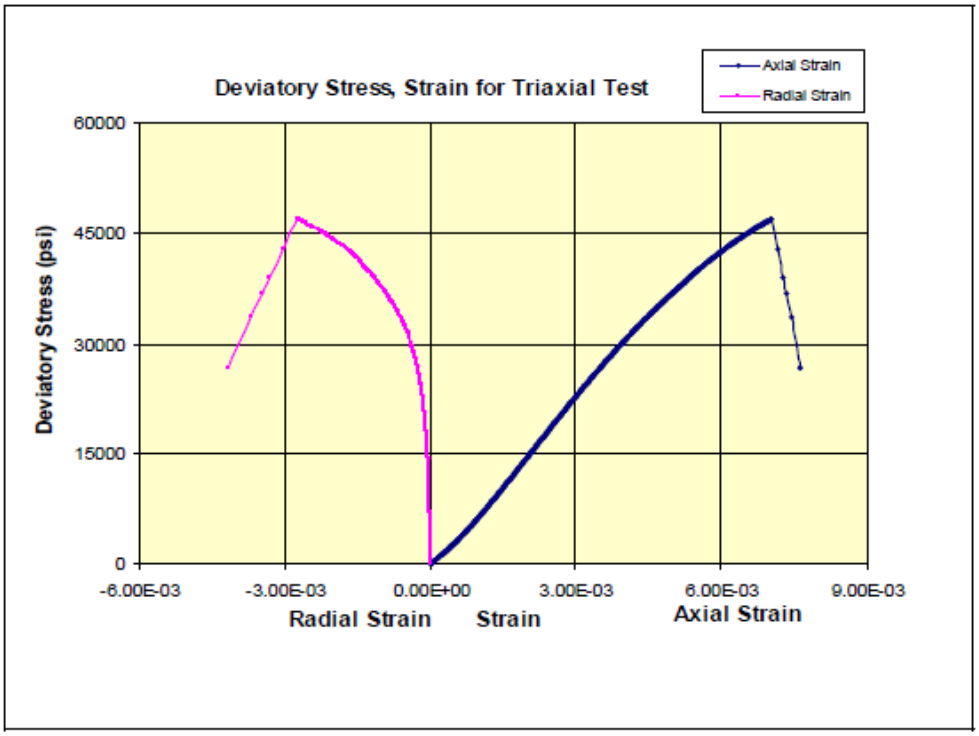
Core Laboratories

7

Results of Triaxial Test

Company: **University of Wyoming**
Well: **RSU #1**

Date: **May, 2012**
File: **HOU-120536**
Saturation Fluid: **As Received**



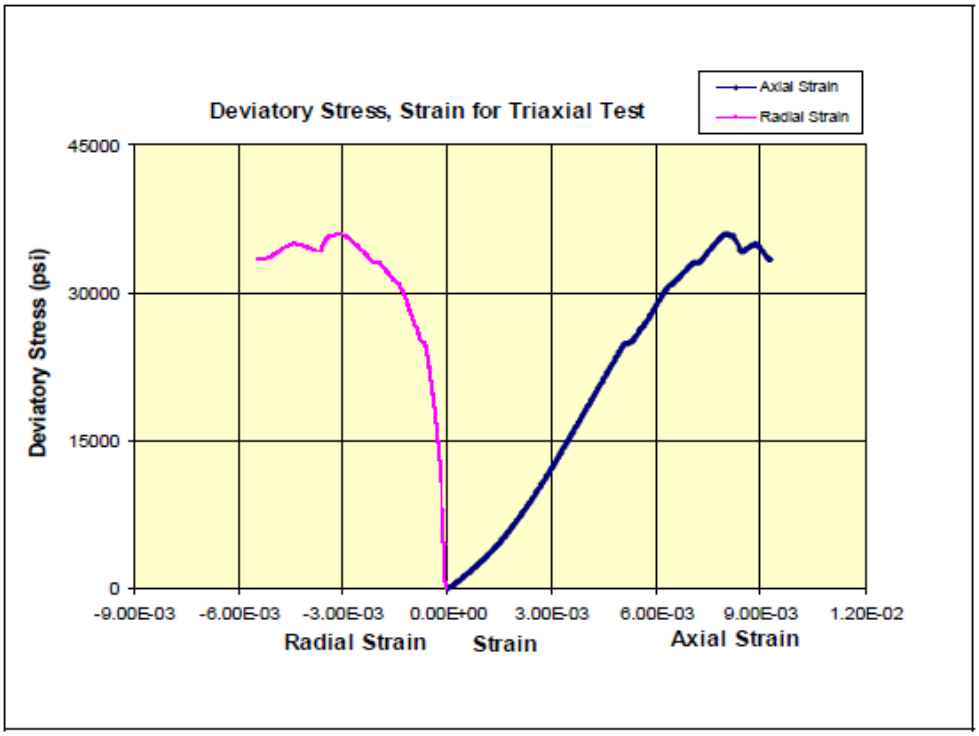
Sample	2V
Depth (ft)	10602.60
Diameter (in)	0.9689
Length (in)	1.6199
Mass (g)	52.6
Saturation Fluid	As Received
Bulk Density (g/cm^3)	2.69
Confining Pressure (psi)	2490
Pore Pressure (psi)	0
Static Young's Modulus (X10^6 psi)	7.96
Static Poisson's Ratio	0.17
Compressive Strength (psi)	49378

Core Laboratories

Results of Triaxial Test

Company: University of Wyoming
Well: RSU #1

Date: May, 2012
File: HOU-120536
Saturation Fluid: As Received



Sample	11V
Depth (ft)	10630.70
Diameter (in)	0.9683
Length (in)	1.1935
Mass (g)	40
Saturation Fluid	As Received
Bulk Density (g/cm^3)	2.78
Confining Pressure (psi)	2490
Pore Pressure (psi)	0
Static Young's Modulus (X10^6 psi)	6.11
Static Poisson's Ratio	0.20
Compressive Strength (psi)	38504

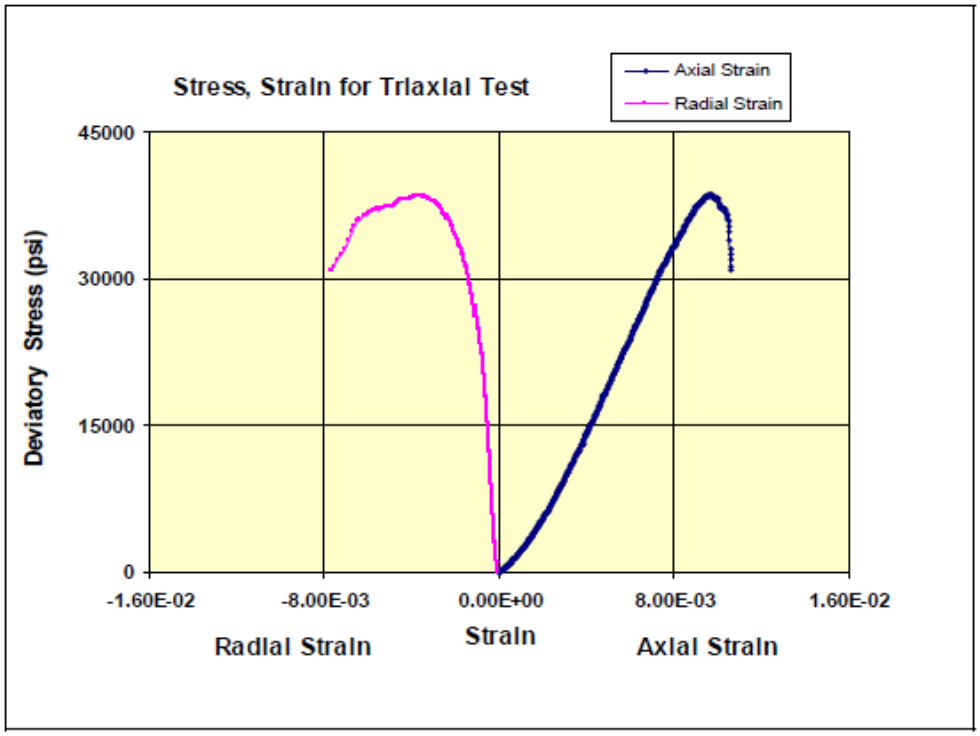
Core Laboratories

9

Results of Triaxial Test

Company: University of Wyoming
Well: RSU #1

Date: May, 2012
File: HOU-120536
Saturation Fluid: As Received



Sample	19V
Depth (ft)	10683.25
Diameter (in)	0.9735
Length (in)	0.6779
Mass (g)	21.88
Saturation Fluid	As Received
Bulk Density (g/cm^3)	2.65
Confining Pressure (psi)	2490
Pore Pressure (psi)	0
Static Young's Modulus (X10^6 psi)	5.04
Static Poisson's Ratio	0.19
Compressive Strength (psi)	41146

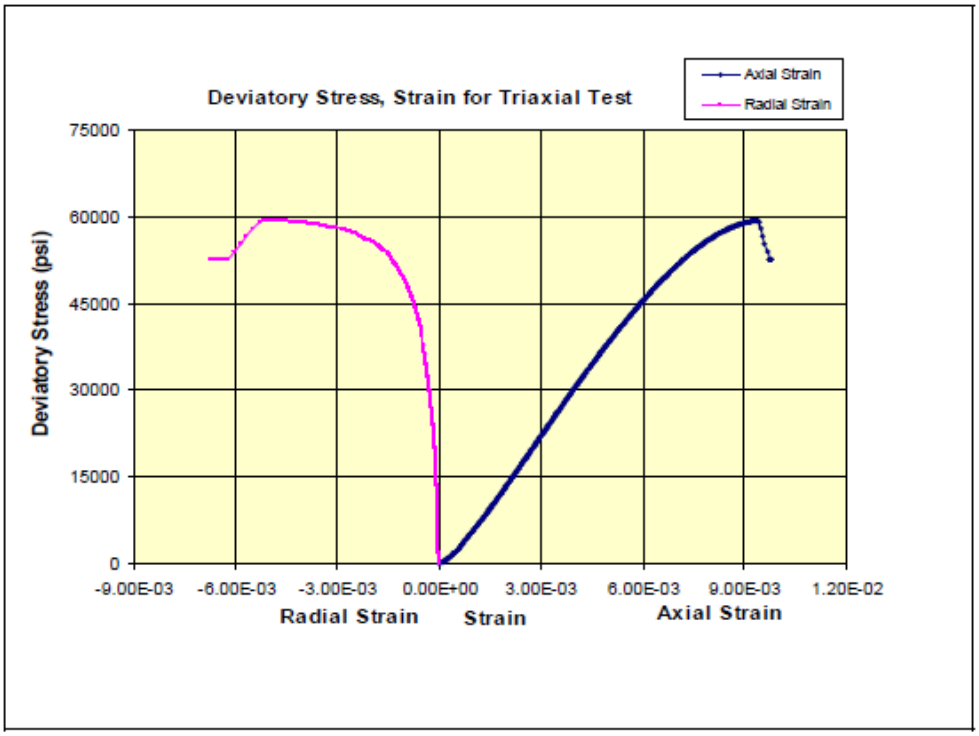
Core Laboratories

10

Results of Triaxial Test

Company: **University of Wyoming**
Well: **RSU #1**

Date: **May, 2012**
File: **HOU-120536**
Saturation Fluid: **As Received**



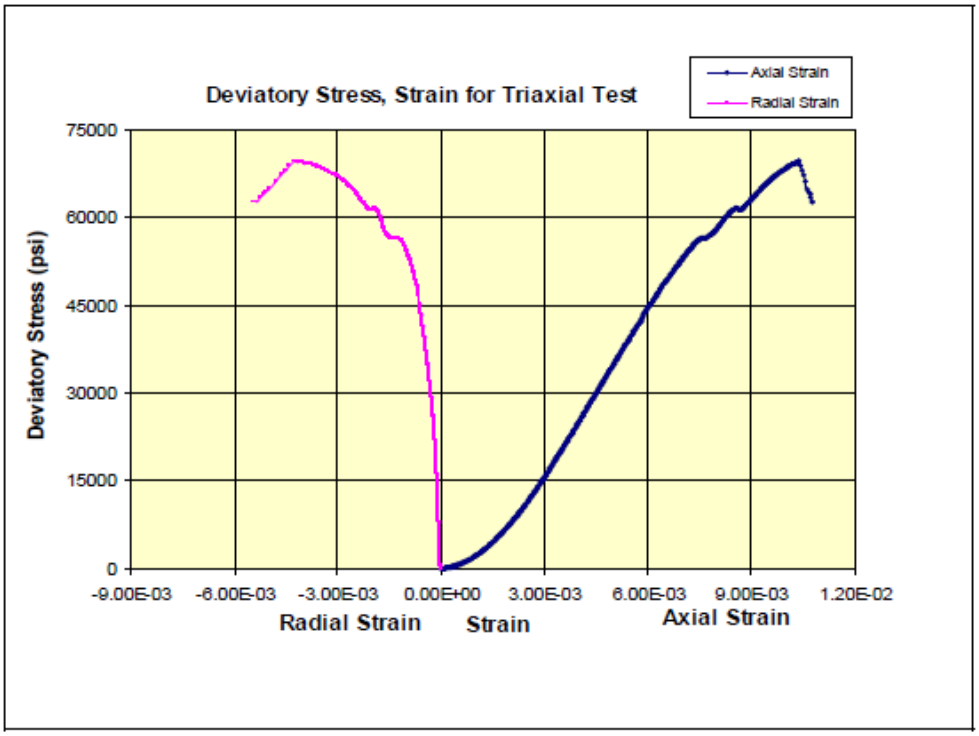
Sample	31V
Depth (ft)	11417.25
Diameter (in)	0.9717
Length (in)	1.7875
Mass (g)	53.86
Saturation Fluid	As Received
Bulk Density (g/cm^3)	2.48
Confining Pressure (psi)	2490
Pore Pressure (psi)	0
Static Young's Modulus (X10^6 psi)	8.23
Static Poisson's Ratio	0.16
Compressive Strength (psi)	61867

Core Laboratories

Results of Triaxial Test

Company: University of Wyoming
Well: RSU #1

Date: May, 2012
File: HOU-120536
Saturation Fluid: As Received

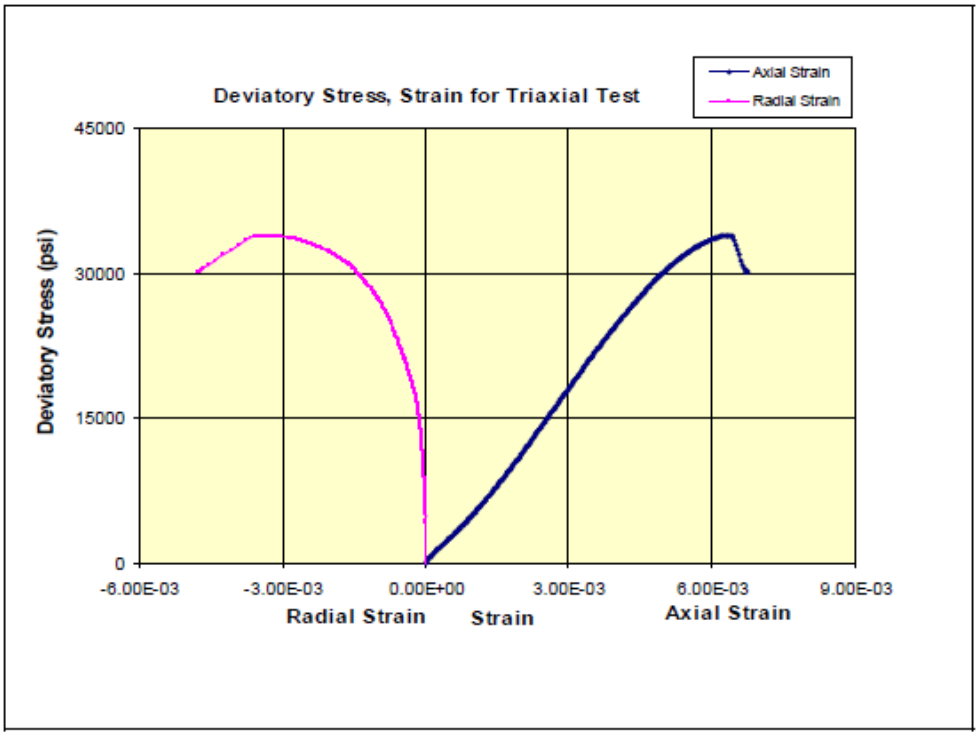


Sample	34V
Depth (ft)	11521.35
Diameter (in)	0.9618
Length (in)	1.7710
Mass (g)	53.95
Saturation Fluid	As Received
Bulk Density (g/cm^3)	2.56
Confining Pressure (psi)	2490
Pore Pressure (psi)	0
Static Young's Modulus (X10^6 psi)	9.56
Static Poisson's Ratio	0.19
Compressive Strength (psi)	72048

Results of Triaxial Test

Company: University of Wyoming
Well: RSU #1

Date: May, 2012
File: HOU-120536
Saturation Fluid: As Received



Sample	95V
Depth (ft)	12384.00
Diameter (in)	0.9661
Length (in)	1.8585
Mass (g)	56.55
Saturation Fluid	As Received
Bulk Density (g/cm^3)	2.53
Confining Pressure (psi)	2490
Pore Pressure (psi)	0
Static Young's Modulus (X10^6 psi)	6.91
Static Poisson's Ratio	0.26
Compressive Strength (psi)	36400

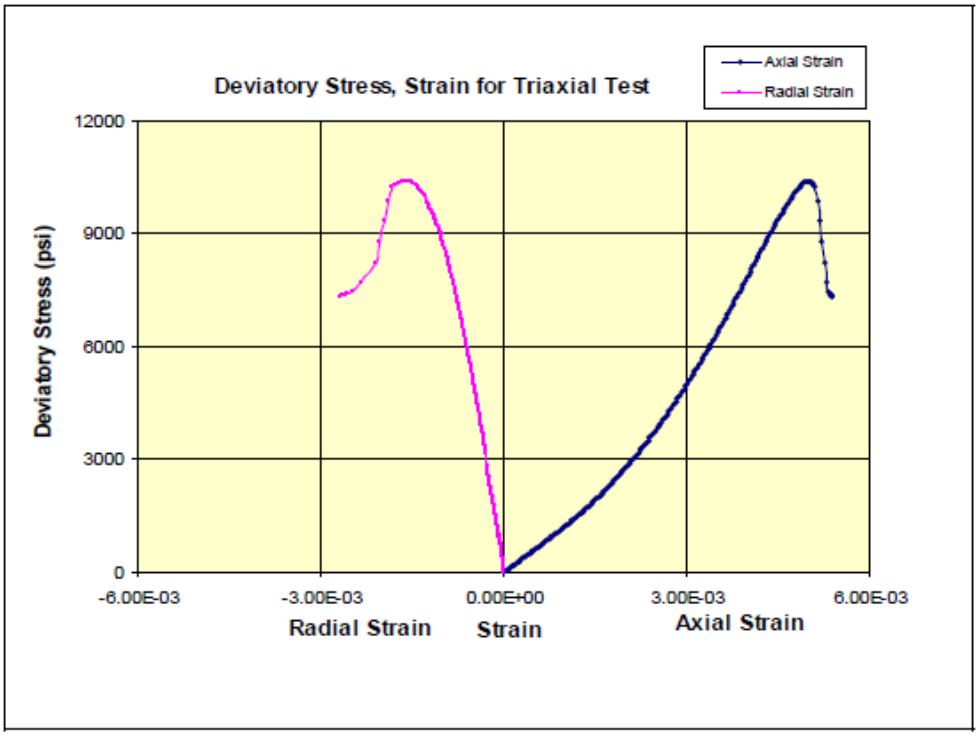
Core Laboratories

13

Results of Triaxial Test

Company: University of Wyoming
Well: RSU #1

Date: May, 2012
File: HOU-120536
Saturation Fluid: As Received



Sample	113V
Depth (ft)	12512.00
Diameter (in)	.9652
Length (in)	1.8425
Mass (g)	54.69
Saturation Fluid	As Received
Bulk Density (g/cm^3)	2.48
Confining Pressure (psi)	2490
Pore Pressure (psi)	0
Static Young's Modulus (X10^6 psi)	2.62
Static Poisson's Ratio	0.29
Compressive Strength (psi)	12870

Core Laboratories

14

TRIAXIAL COMPRESSIVE TEST RESULTS

Company:	**University of Wyoming**	Date:	**Feb. 2013**
Well:	**RSU #1**	File:	**HOU-120536**
Field:		Saturation Fluid:	**As Received**

Triaxial Static Young's Modulus, Poisson's Ratio and Compressive Strength

Sample Number	Depth (ft)	Confining Pressure (psi)	Bulk Density (g/cm^3)	Compressive Strength (psi)	Young's Modulus (10^6 psi)	Poisson's Ratio
1V	11536.50	3000	2.66	34122	7.08	0.24
3V	11540.90	5000	2.79	64990	8.80	0.25
4VB	11543.00	8000	2.79	79660	8.83	0.24
5V	12182.00	5500	2.75	97693	10.35	0.23
114V	12513.30	5000	2.45	23498	3.94	0.22
115V	12519.60	8000	2.62	30919	7.14	0.23

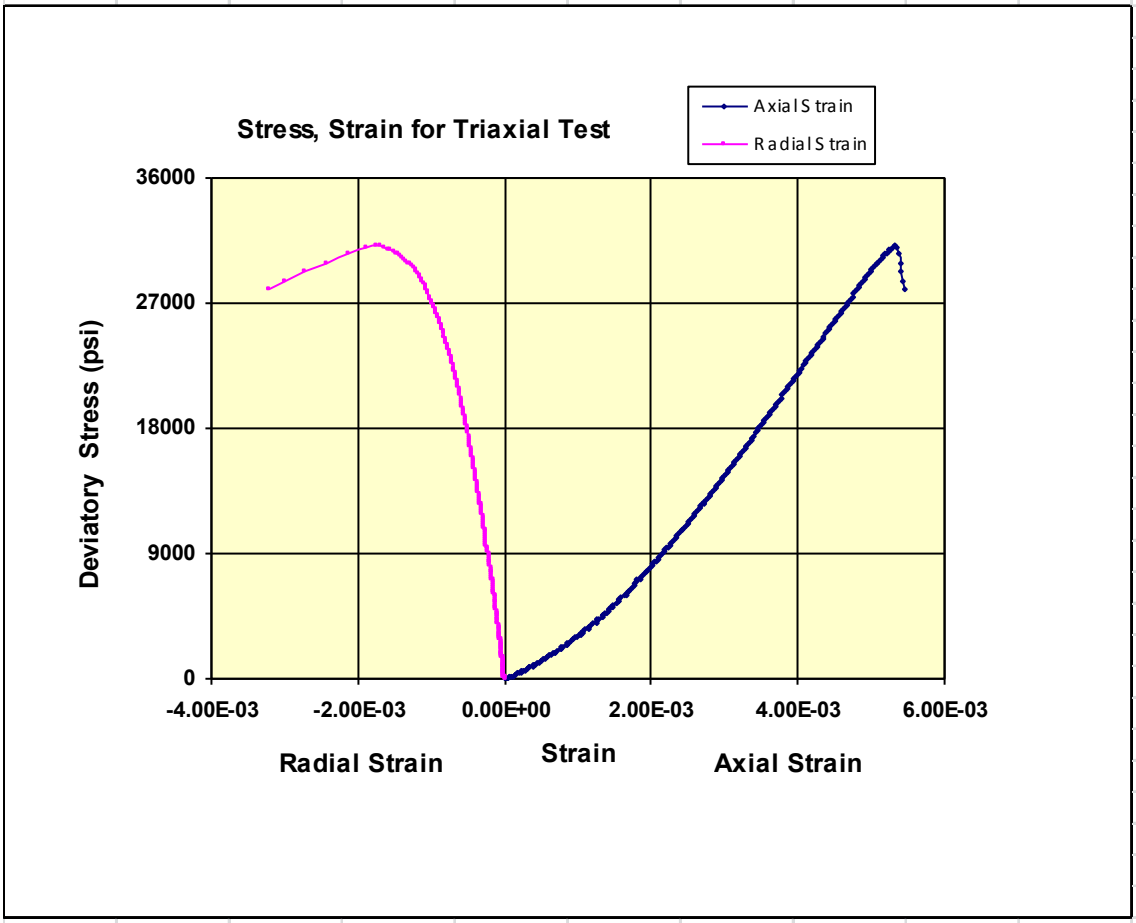
ACOUSTIC VELOCITIES AND DYNAMIC ELASTIC PARAMETERS

Company:	**University of Wyoming**	Date:	**Feb. 2013**
Well:	**RSU #1**	File:	**HOU-120536**
Field:		Saturation Fluid:	**As Received**

Acoustic Velocities and Dynamic Moduli at Triaxial Stress Conditions

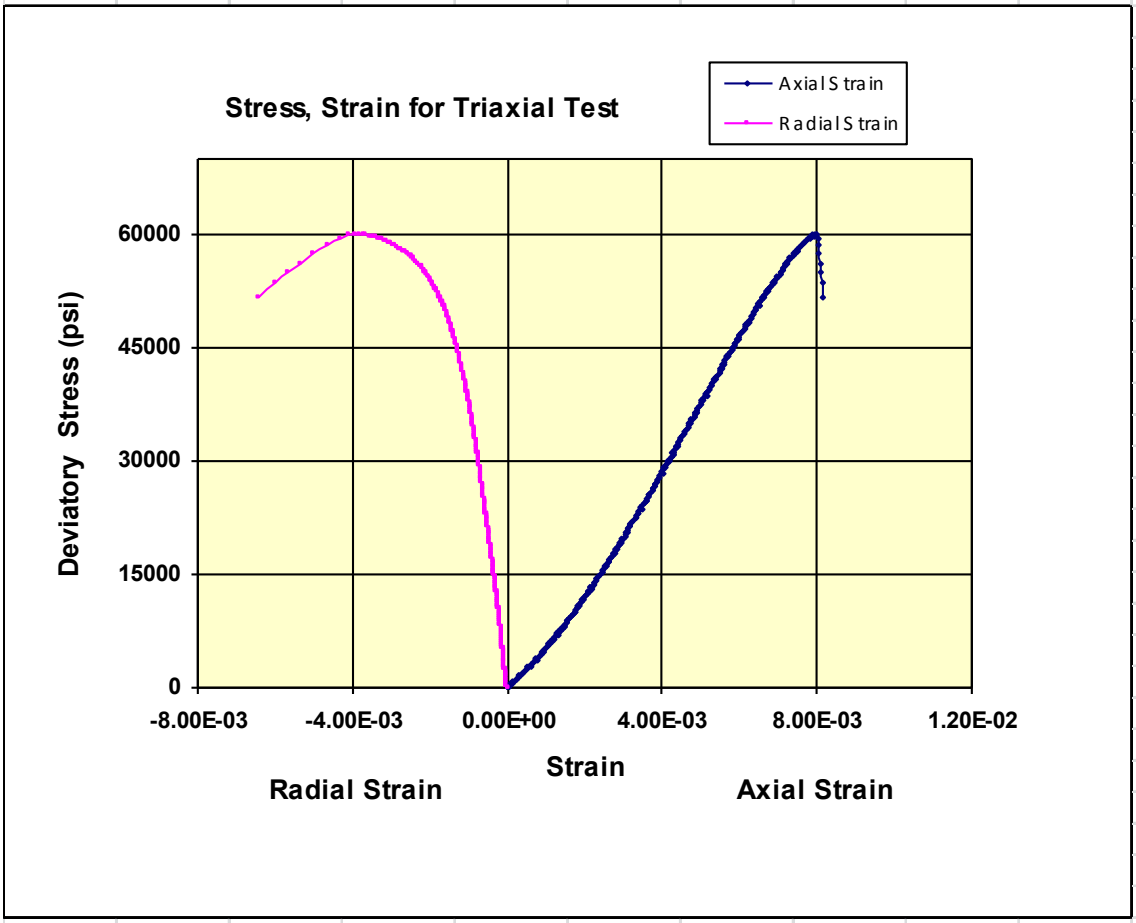
					Acoustic Velocity				Dynamic Elastic Parameters			
					Compressional		Shear					
Sample Number	Depth (ft)	Confining Pressure (psi)	Axial Pressure (psi)	Bulk Density (g/cm^3)	ft/sec	µs/ft	ft/sec	µs/ft	Bulk Modulus ($x10^6$ psi)	Young's Modulus ($x10^6$ psi)	Shear Modulus ($x10^6$ psi)	Poisson's Ratio
1V	11536.50	3000	3000	2.66	20318	49.2	11682	85.6	8.29	12.28	4.90	0.25
		3000	15000	2.66	20917	47.8	11878	84.2	8.96	12.79	5.07	0.26
3V	11540.90	5000	5000	2.79	21268	47.0	12268	81.5	9.48	14.18	5.67	0.25
		5000	32000	2.79	21992	45.5	12506	80.0	10.36	14.86	5.89	0.26
4VB	11543.00	8000	8000	2.79	20743	48.2	12097	82.7	8.86	13.69	5.51	0.24
		8000	40000	2.79	21415	46.7	12322	81.2	9.65	14.32	5.72	0.25
5V	12182.00	5500	5500	2.75	20847	48.0	12632	79.2	8.23	14.32	5.92	0.21
		5500	50000	2.75	21398	46.7	12832	77.9	8.84	14.89	6.11	0.22
114V	12513.30	5000	5000	2.45	18235	54.8	10695	93.5	5.95	9.36	3.78	0.24
		5000	12000	2.45	18655	53.6	10838	92.3	6.33	9.67	3.88	0.25
115V	15519.60	8000	8000	2.62	19598	51.02	11322	88.32	7.53	11.31	4.53	0.25
		8000	15000	2.62	20109	49.73	11491	87.03	8.06	11.73	4.66	0.26

Company:	**University of Wyoming**	Date:	**Feb. 2013**
Well:	**RSU #1**	File:	**HOU-120536**
Field:		Saturation Fluid:	**As Received**



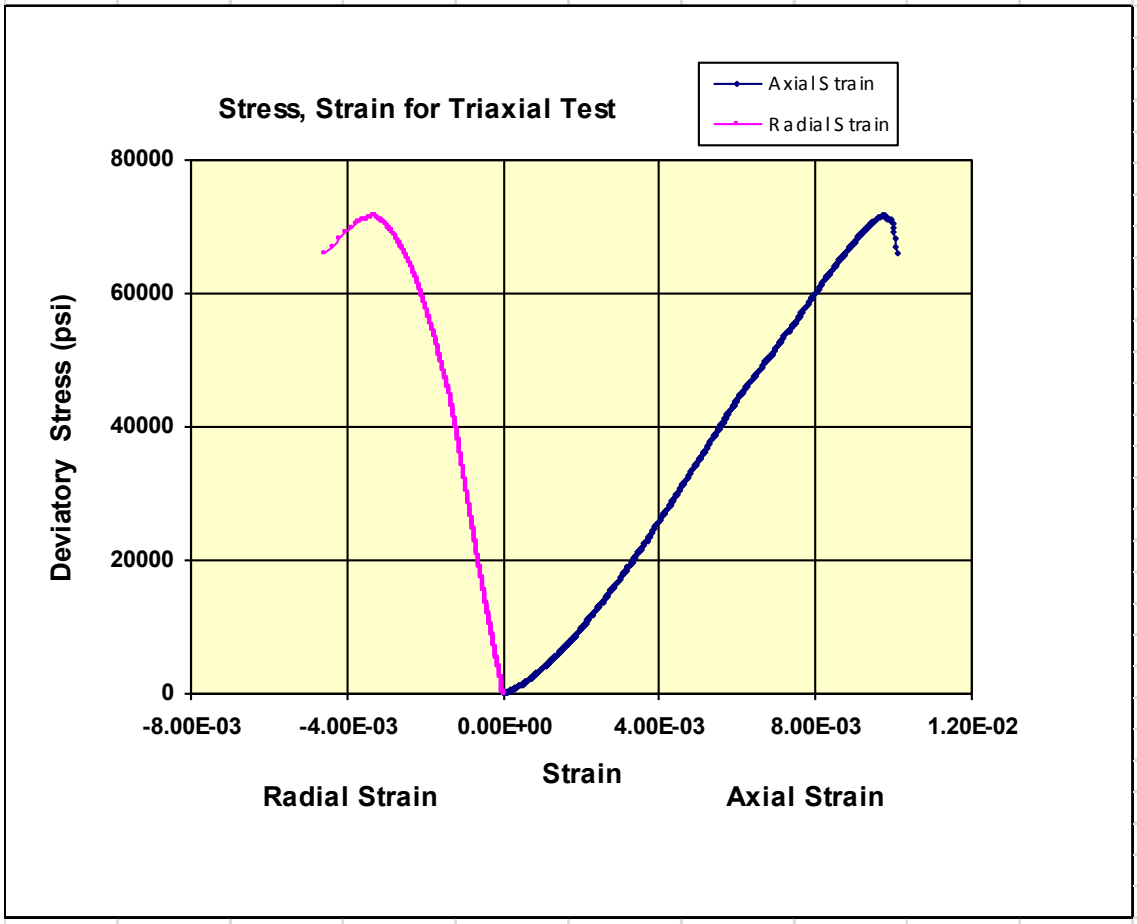
Sample	1V
Depth (ft)	11536.50
Diameter (in)	0.9612
Length (in)	1.7018
Mass (g)	53.9
Saturation Fluid	As Received
Bulk Density (g/cm^3)	2.66
Confining Pressure (psi)	3000
Pore Pressure (psi)	0
Static Young's Modulus (X10^6 psi)	7.08
Static Poisson's Ratio	0.24
Compressive Strength (psi)	34122

Company:	**University of Wyoming**	Date:	**Feb. 2013**
Well:	**RSU #1**	File:	**HOU-120536**
Field:		Saturation Fluid:	**As Received**



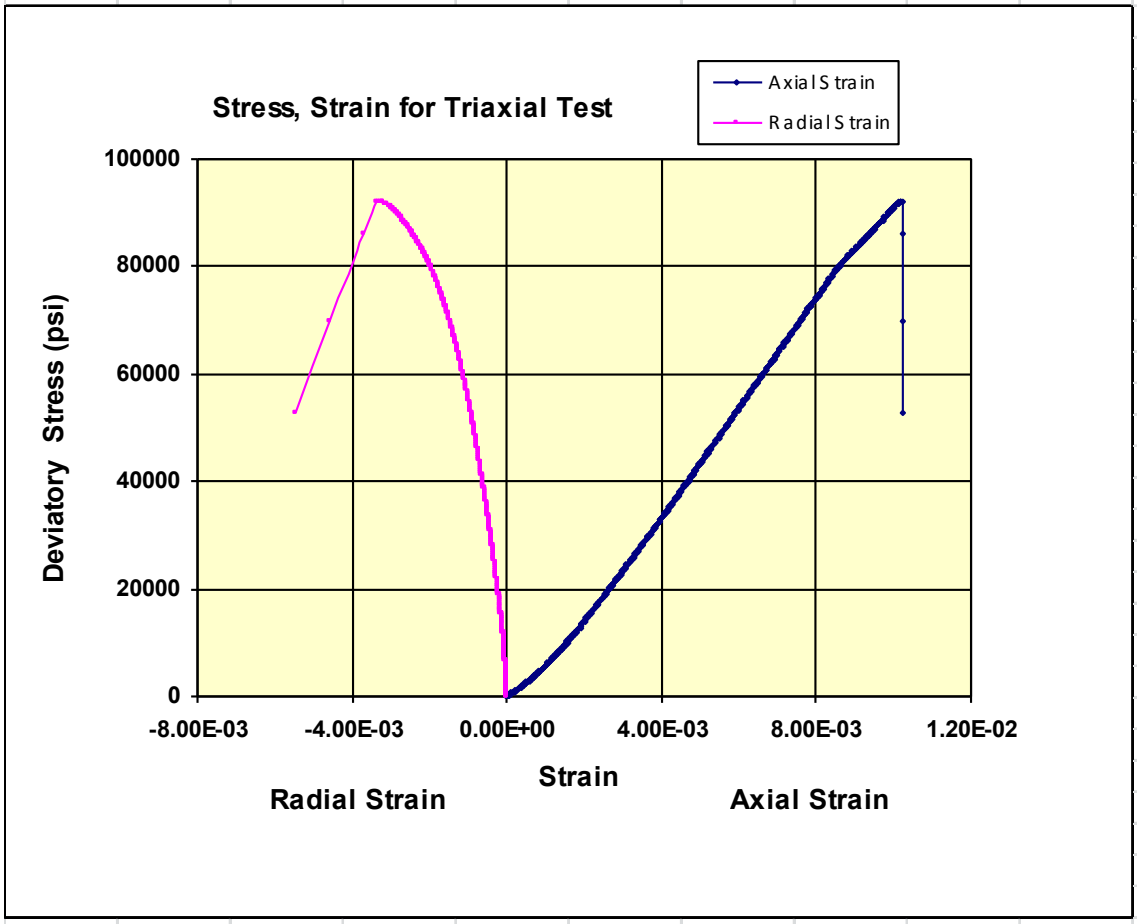
Sample	3V
Depth (ft)	11540.90
Diameter (in)	0.9615
Length (in)	1.5517
Mass (g)	51.6
Saturation Fluid	As Received
Bulk Density (g/cm^3)	2.79
Confining Pressure (psi)	5000
Pore Pressure (psi)	0
Static Young's Modulus (X10^6 psi)	8.80
Static Poisson's Ratio	0.25
Compressive Strength (psi)	64990

Company:	**University of Wyoming**	Date:	**Feb. 2013**
Well:	**RSU #1**	File:	**HOU-120536**
Field:		Saturation Fluid:	**As Received**



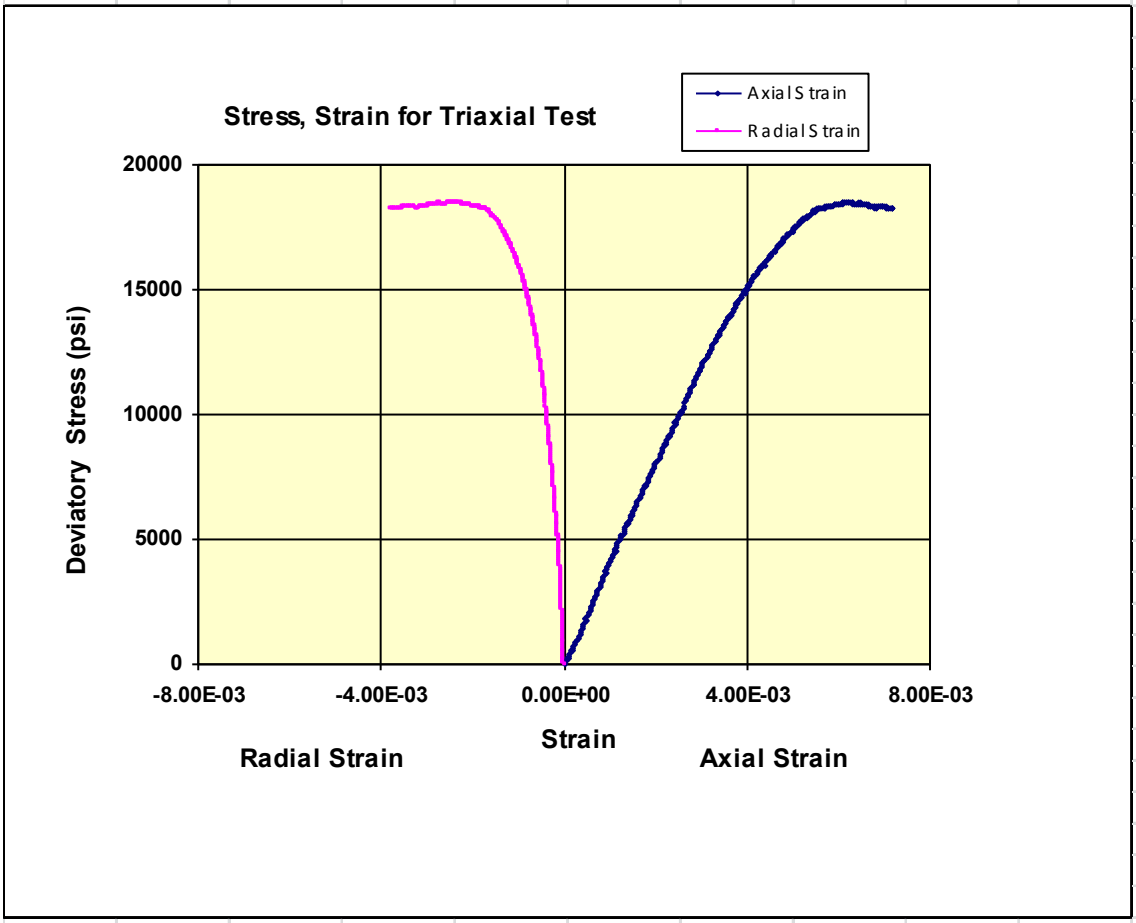
Sample	4VB
Depth (ft)	11543.00
Diameter (in)	0.9607
Length (in)	1.5881
Mass (g)	52.7
Saturation Fluid	As Received
Bulk Density (g/cm^3)	2.79
Confining Pressure (psi)	8000
Pore Pressure (psi)	0
Static Young's Modulus (X10^6 psi)	8.83
Static Poisson's Ratio	0.24
Compressive Strength (psi)	79660

Company:	**University of Wyoming**	Date:	**Feb. 2013**
Well:	**RSU #1**	File:	**HOU-120536**
Field:		Saturation Fluid:	**As Received**



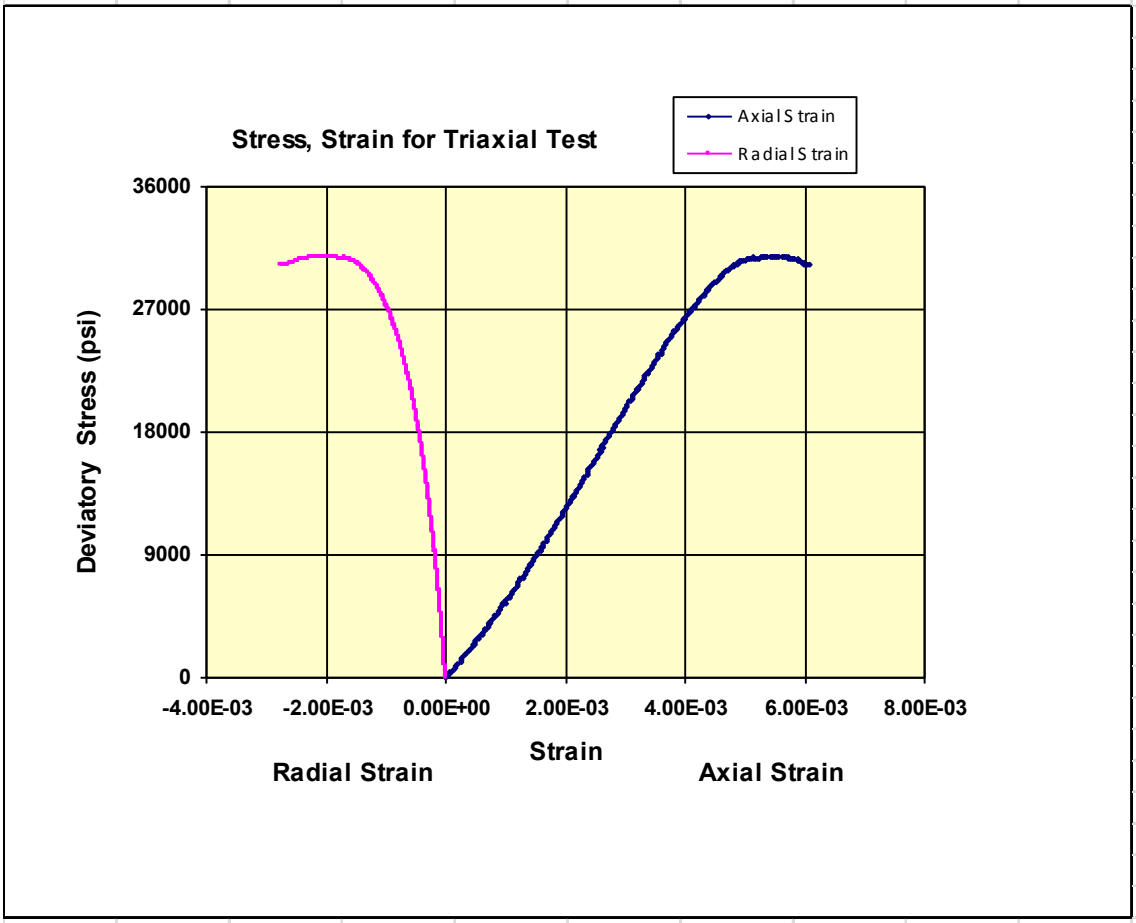
Sample	5V
Depth (ft)	12182.00
Diameter (in)	0.9608
Length (in)	1.9463
Mass (g)	63.61
Saturation Fluid	As Received
Bulk Density (g/cm^3)	2.75
Confining Pressure (psi)	5500
Pore Pressure (psi)	0
Static Young's Modulus (X10^6 psi)	10.35
Static Poisson's Ratio	0.23
Compressive Strength (psi)	97693

Company:	**University of Wyoming**	Date:	**Feb. 2013**
Well:	**RSU #1**	File:	**HOU-120536**
Field:		Saturation Fluid:	**As Received**



Sample	114V
Depth (ft)	12513.30
Diameter (in)	0.9684
Length (in)	1.9431
Mass (g)	57.5
Saturation Fluid	As Received
Bulk Density (g/cm^3)	2.45
Confining Pressure (psi)	5000
Pore Pressure (psi)	0
Static Young's Modulus (X10^6 psi)	3.94
Static Poisson's Ratio	0.22
Compressive Strength (psi)	23498

Company:	**University of Wyoming**	Date:	**Feb. 2013**
Well:	**RSU #1**	File:	**HOU-120536**
Field:		Saturation Fluid:	**As Received**



Sample	115V
Depth (ft)	12519.60
Diameter (in)	0.9718
Length (in)	1.8532
Mass (g)	59
Saturation Fluid	As Received
Bulk Density (g/cm^3)	2.62
Confining Pressure (psi)	8000
Pore Pressure (psi)	0
Static Young's Modulus (X10^6 psi)	7.14
Static Poisson's Ratio	0.23
Compressive Strength (psi)	30919

Appendix H: Weber Core Description

Facies		Bedding Continuity		G.S.	
0	Xlam	0	100% perfect bedding	0	clay
1	wavy-lam	1	mostly perfectly laminated, minor waves	1	mud
2	massive	2	somewhat wavy but can get bedding measurement	2	vfl
3	mottled	3	slightly beyong bedding measurement	3	vfu
4	vague bedding	4	wisps of bedding	4	fl
5	black shale	5	no bedding visible	5	fu
6	soft sed def.			6	ml
7	dolomite mudstone			7	mu
8	dolomite wackestone				
9	dolomitized sandstone				
10	limestone				
11	calcareous sandstone				

Top Depth	Facies	Continuity	Grain Size	log shift
11185	0	0	4	11178.5
11191.7	5	0	1	11185.2
11192.1	3	5	3	11185.6
11194.75	0	0	3	11188.25
11196.25	1	2	3	11189.75
11198	3	4	3	11191.5
11199.85	0	1	5	11193.35
11200.5	3	3	5	11194
11201.5	0	0	5	11195
11203.5	4	2	4	11197
11204.9	1	2	4	11198.4
11206.5	0	0	4	11200
11207	0	1	3	11200.5
11208	0	1	4	11201.5
11210.2	4	4	4	11203.7
11211.9	4	2	4	11205.4
11213.6	2	5	4	11207.1
11215.2	4	4	4	11208.7
11216.9	1	3	3	11210.4
11217.25	4	4	3	11210.75
11218.5	4	4	3	11212
11219.5	2	5	4	11213
11220	4	4	3	11213.5
11221.8	1	2	3	11215.3
11223.25	4	4	4	11216.75
11224.5	1	2	4	11218
11225.8	6	4	3	11219.3
11227.25	0	1	3	11220.75
11229	4	5	3	11222.5
11230	1	3	2	11223.5
11231.25	2	5	3	11224.75
11231.75	0	4	3	11225.25
11232	0	2	3	11225.5

Top Depth	Facies	Continuity	Grain Size	log shift
11232.4	4	3	2	11225.9
11233.4	0	2	2	11226.9
11235.6	0	4	2	11229.1
11236.3	0	0	3	11229.8
11236.8	2	3	3	11230.3
11238.5	0	3	3	11232
11246.5	4	4	7	11240
11247.5	2	5	2	11241
11248.1	2	5	2	11241.6
11249.8	2	5	2	11243.3
11252.4	0	2	3	11245.9
11253.4	0	1	3	11246.9
11255.4	0	2	3	11248.9
11255.6	0	1	3	11249.1
11260	0	2	3	11253.5
11261	0	0	3	11254.5
11262.75	4	4	3	11256.25
11264.6	4	3	3	11258.1
11264.8	4	4	3	11258.3
11266.2	0	0	3	11259.7
11266.4	1	3	3	11259.9
11267.5	4	5	3	11261
11268.2	0	3	2	11261.7
11268.4	4	3	2	11261.9
11268.7	4	3	3	11262.2
11271	1	4	3	11264.5
11271.2	2	5	3	11264.7
11271.8	0	2	4	11265.3
11272.4	4	4	3	11265.9
11273	2	2	3	11266.5
11274.3	0	0	3	11267.8
11275.5	0	4	3	11269
11281.7	0	4	3	11275.2
11282.2	0	4	3	11275.7
11286	4	4	3	11279.5
11286.3	0	3	3	11279.8
11286.6	4	3	3	11280.1
11289	0	2	3	11282.5
11289.6	0	4	3	11283.1
11295.5	0	1	2	11289
11296.5	2	5	3	11290
11297.5	0	3	3	11291
11298	1	4	2	11291.5
11299.7	4	4	3	11293.2

Top Depth	Facies	Continuity	Grain Size	log shift
11300.5	1	4	3	11294
11303	4	4	3	11296.5
11305.5	4	4	3	11299
11306	3	4	3	11299.5
11307.5	4	3	4	11301
11307.8	3	5	3	11301.3
11308.75	1	4	3	11302.25
11308.9	2	5	2	11302.4
11309.6	2	3	3	11303.1
11310.2	4	3	2	11303.7
11311.25	0	1	2	11304.75
11311.6	2	5	2	11305.1
11312.4	4	3	3	11305.9
11313.1	2	5	2	11306.6
11314.6	4	2	2	11308.1
11323.6	2	5	2	11317.1
11325.8	2	4	2	11319.3
11327.8	2	4	2	11321.3
11328.5	2	4	2	11322
11329.5	4	3	3	11323
11333.6	0	4	4	11327.1
11337	0	1	3	11330.5
11342	2	5	2	11335.5
11342.6	0	0	6	11336.1
11343.4	1	3	3	11336.9
11344.5				11338
11348	0	1	3	11341.5
11349.2	0	0	3	11342.7
11351.2	0	2	3	11344.7
11353.5	4	4	3	11347
11361	4	3	2	11354.5
11363	0	0	2	11356.5
11368.5	4	4	3	11362
11371.9	0	1	2	11365.4
11372.2	2	5	2	11365.7
11373	4	3	2	11366.5
11373.6	2	4	2	11367.1
11374.9	0	1	2	11368.4
11379.3	4	4	3	11372.8
11380.3	0	1	2	11373.8
11384.6	3	4	3	11378.1
11386	0	2	2	11379.5
11388.5	2	5	2	11382
11391.2	4	3	2	11384.7

Top Depth	Facies	Continuity	Grain Size	log shift
11392.8	3	4	2	11386.3
11394.6	2	4	3	11388.1
11398.5	4	3	3	11392
11399.5	0	1	3	11393
11400.4	2	5	3	11393.9
11401.2	4	3	2	11394.7
11402	4	4	3	11395.5
11403	2	5	2	11396.5
11404.2	0	1	2	11397.7
11404.8	4	4	3	11398.3
11405.9	0	0	3	11399.4
11406.2	3	4	2	11399.7
11415.8	1	3	2	11409.3
11417.8	2	5	3	11411.3
11419.9	2	5	3	11413.4
11421	4	4	2	11414.5
11423	0	2	3	11416.5
11425	6	4	3	11418.5
11426.6	0	1	3	11420.1
11428.4	4	3	2	11421.9
11429.5	0	1	2	11423
11431.5	2	2	2	11425
11433	0	1	3	11426.5
11434.6	4	4	5	11428.1
11436.7	0	0	2	11430.2
11438.1	0	0	2	11431.6
11438.5	0	3	3	11432
11441.6	0	0	3	11435.1
11444	4	3	3	11437.5
11445.6	0	2	5	11439.1
11447.2	2	2	4	11440.7
11450.4	0	0	4	11443.9
11452	2	4	4	11445.5
11453	0	3	3	11446.5
11460.5	0	1	2	11454
11463.4	4	3	4	11456.9
11464.6	0	0	3	11458.1
11471	2	5	3	11464.5
11473	0	1	3	11466.5
11475.9	2	2	2	11469.4
11476				11469.5
11490.12	2	5	4	11483.62
11492.3	3	3	4	11485.8
11494	0	1	4	11487.5

Top Depth	Facies	Continuity	Grain Size	log shift
11502.5	2	5	3	11496
11504.1	0	2	3	11497.6
11506.7	2	5	3	11500.2
11509.8	4	4	2	11503.3
11511.62				11505.12
11520	0	0	3	11513.5
11524.4	4	3	2	11517.9
11527.3	2	5	3	11520.8
11530	0	2	2	11523.5
11531	0	1	3	11524.5
11533	0	0	3	11526.5
11534.75	2	5	2	11528.25
11536.1	7	5	1	11529.6
11543.45	4	4	8	11536.95
11548.61	4	4	4	11542.11
11555	2	3	3	11548.5
11559.5	2	5	4	11553
11563	2	1	2	11556.5
11584	1	3	3	11577.5
11587.1	0	1	3	11580.6
11601.5	10	5	5	11595
11602.5	9	4	5	11596
11609	4	4	4	11602.5
11612	2	5	2	11605.5
11615	2	5	2	11608.5
11617.4	2	5	3	11610.9
11623.25	1	3	2	11616.75
11623.75	2	5	2	11617.25
11625				11618.5
11701	1	5	3	11694.5
11702.1	1	3	2	11695.6
11703.9	1	2	2	11697.4
11706	0	1	2	11699.5
11706.25	5	1	1	11699.75
11706.3	2	5	3	11699.8
11709	0	0	2	11702.5
11709.5	2	5	3	11703
11711	0	0	3	11704.5
11718.5	5	1	1	11712
11718.6	3	5	3	11712.1
11719.2				11712.7
11731	4	3	2	11724.5
11732.5	0	1	3	11726
11734.8	4	4	2	11728.3

Top Depth	Facies	Continuity	Grain Size	log shift
11739.5	3	3	2	11733
11740.8	1	2	2	11734.3
11746.2	2	3	3	11739.7
11749.3	0	2	2	11742.8
11754	2	5	2	11747.5
11757	1	2	3	11750.5
11760	10	5	1	11753.5
11764.7	3	4	2	11758.2
11768.9	4	2	3	11762.4
11775.2	11	5	1	11768.7
11778.1	11	4	2	11771.6
11780.4	11	3	3	11773.9
11783.6	2	5	2	11777.1
11787.2	4	2	3	11780.7
11789.4	0	1	4	11782.9

With Log Shift

Top Depth	Facies	Continuity	Grain Size
11178.5	0	0	4
11185.2	5	0	1
11185.6	3	5	3
11188.25	0	0	3
11189.75	1	2	3
11191.5	3	4	3
11193.35	0	1	5
11194	3	3	5
11195	0	0	5
11197	4	2	4
11198.4	1	2	4
11200	0	0	4
11200.5	0	1	3
11201.5	0	1	4
11203.7	4	4	4
11205.4	4	2	4
11207.1	2	5	4
11208.7	4	4	4
11210.4	1	3	3
11210.75	4	4	3
11212	4	4	3
11213	2	5	4
11213.5	4	4	3
11215.3	1	2	3
11216.75	4	4	4
11218	1	2	4
11219.3	6	4	3
11220.75	0	1	3
11222.5	4	5	3
11223.5	1	3	2
11224.75	2	5	3
11225.25	0	4	3
11225.5	0	2	3
11225.9	4	3	2
11226.9	0	2	2
11229.1	0	4	2
11229.8	0	0	3
11230.3	2	3	3
11232	0	3	3
11240	4	4	7
11241	2	5	2
11241.6	2	5	2

Top Depth	Facies	Continuity	Grain Size
11243.3	2	5	2
11245.9	0	2	3
11246.9	0	1	3
11248.9	0	2	3
11249.1	0	1	3
11253.5	0	2	3
11254.5	0	0	3
11256.25	4	4	3
11258.1	4	3	3
11258.3	4	4	3
11259.7	0	0	3
11259.9	1	3	3
11261	4	5	3
11261.7	0	3	2
11261.9	4	3	2
11262.2	4	3	3
11264.5	1	4	3
11264.7	2	5	3
11265.3	0	2	4
11265.9	4	4	3
11266.5	2	2	3
11267.8	0	0	3
11269	0	4	3
11275.2	0	4	3
11275.7	0	4	3
11279.5	4	4	3
11279.8	0	3	3
11280.1	4	3	3
11282.5	0	2	3
11283.1	0	4	3
11289	0	1	2
11290	2	5	3
11291	0	3	3
11291.5	1	4	2
11293.2	4	4	3
11294	1	4	3
11296.5	4	4	3
11299	4	4	3
11299.5	3	4	3
11301	4	3	4
11301.3	3	5	3
11302.25	1	4	3
11302.4	2	5	2
11303.1	2	3	3

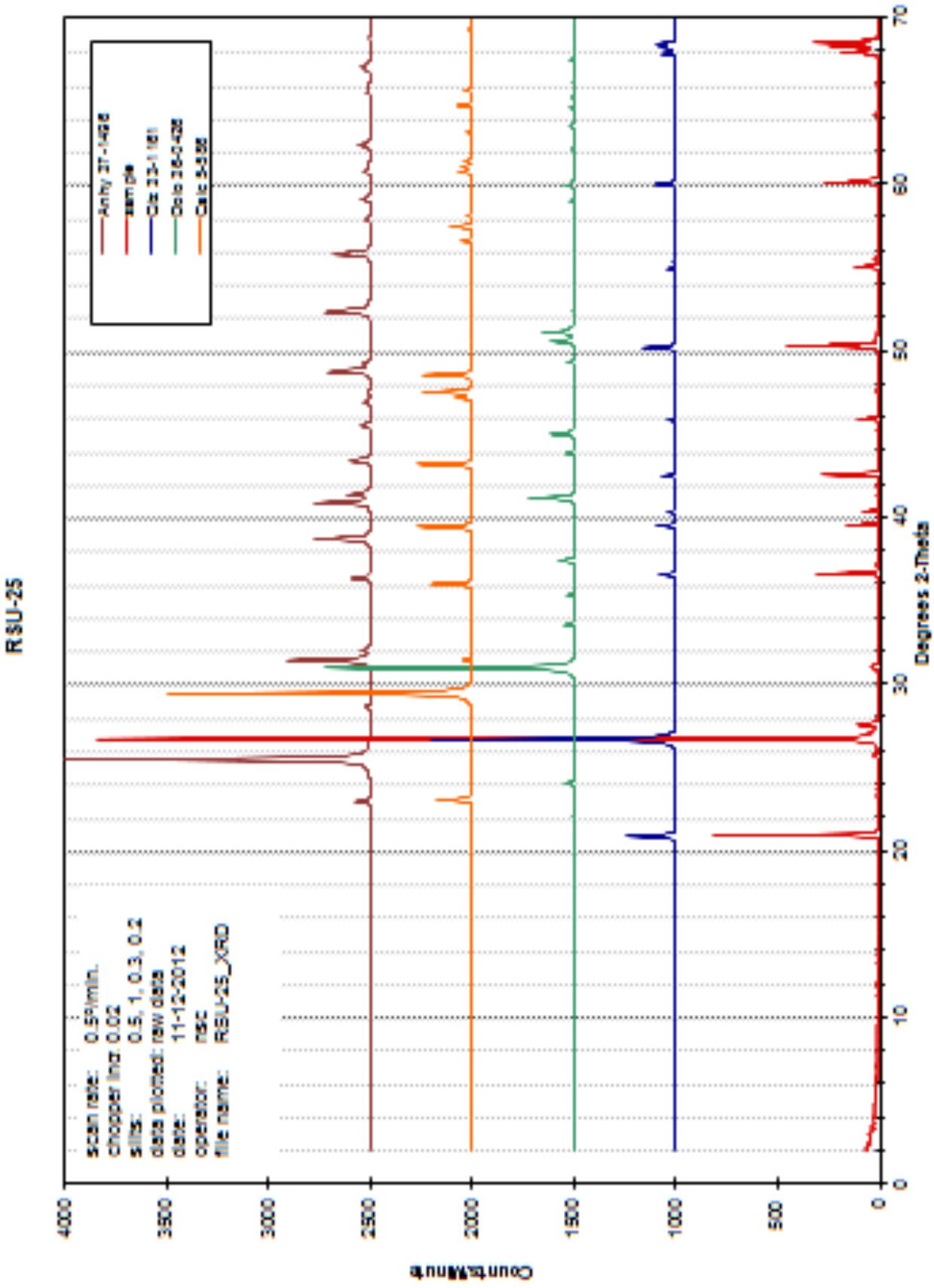
Top Depth	Facies	Continuity	Grain Size
11303.7	4	3	2
11304.75	0	1	2
11305.1	2	5	2
11305.9	4	3	3
11306.6	2	5	2
11308.1	4	2	2
11317.1	2	5	2
11319.3	2	4	2
11321.3	2	4	2
11322	2	4	2
11323	4	3	3
11327.1	0	4	4
11330.5	0	1	3
11335.5	2	5	2
11336.1	0	0	6
11336.9	1	3	3
11338			
11341.5	0	1	3
11342.7	0	0	3
11344.7	0	2	3
11347	4	4	3
11354.5	4	3	2
11356.5	0	0	2
11362	4	4	3
11365.4	0	1	2
11365.7	2	5	2
11366.5	4	3	2
11367.1	2	4	2
11368.4	0	1	2
11372.8	4	4	3
11373.8	0	1	2
11378.1	3	4	3
11379.5	0	2	2
11382	2	5	2
11384.7	4	3	2
11386.3	3	4	2
11388.1	2	4	3
11392	4	3	3
11393	0	1	3
11393.9	2	5	3
11394.7	4	3	2
11395.5	4	4	3
11396.5	2	5	2
11397.7	0	1	2

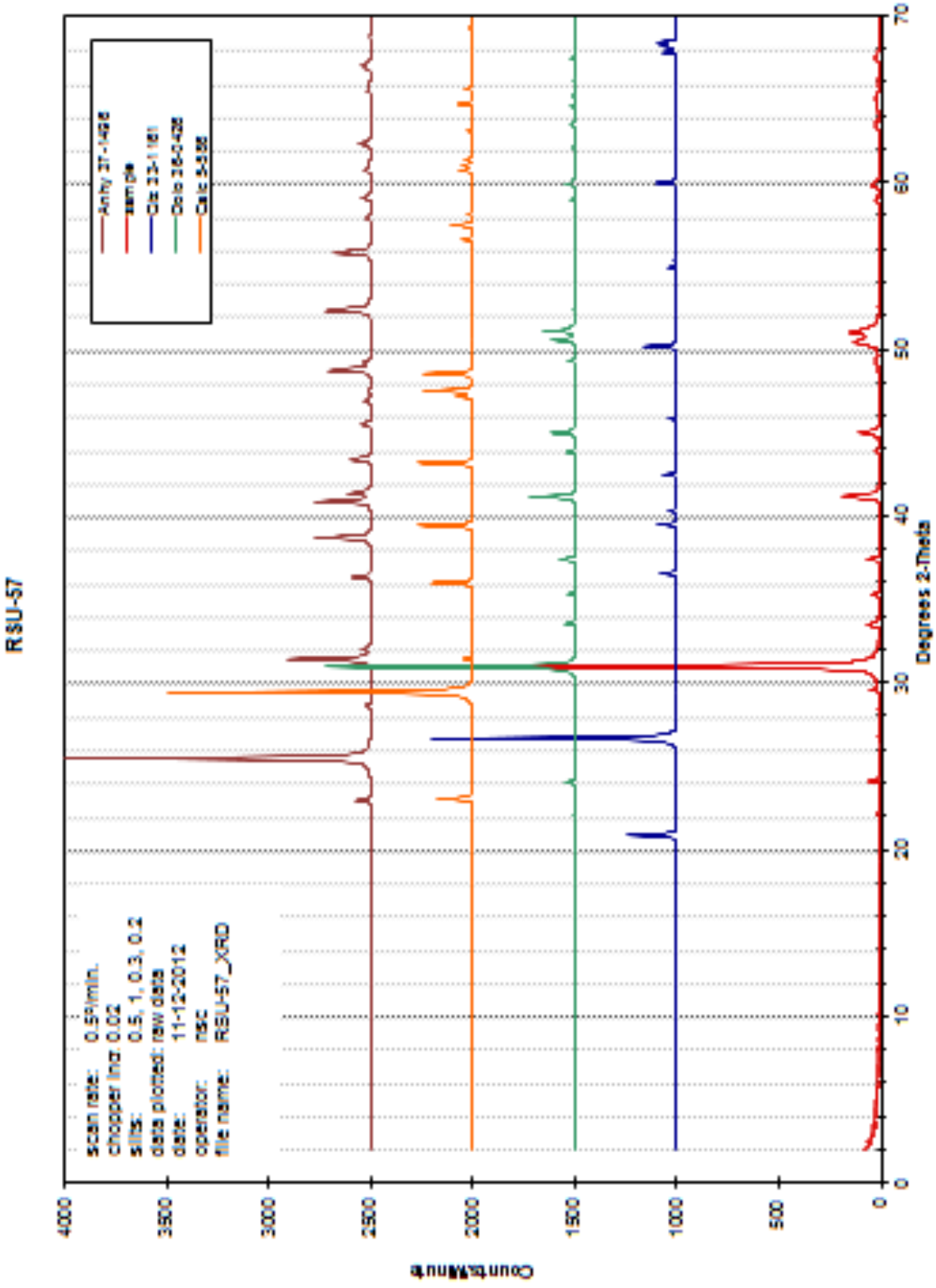
Top Depth	Facies	Continuity	Grain Size
11398.3	4	4	3
11399.4	0	0	3
11399.7	3	4	2
11409.3	1	3	2
11411.3	2	5	3
11413.4	2	5	3
11414.5	4	4	2
11416.5	0	2	3
11418.5	6	4	3
11420.1	0	1	3
11421.9	4	3	2
11423	0	1	2
11425	2	2	2
11426.5	0	1	3
11428.1	4	4	5
11430.2	0	0	2
11431.6	0	0	2
11432	0	3	3
11435.1	0	0	3
11437.5	4	3	3
11439.1	0	2	5
11440.7	2	2	4
11443.9	0	0	4
11445.5	2	4	4
11446.5	0	3	3
11454	0	1	2
11456.9	4	3	4
11458.1	0	0	3
11464.5	2	5	3
11466.5	0	1	3
11469.4	2	2	2
11469.5			
11483.62	2	5	4
11485.8	3	3	4
11487.5	0	1	4
11496	2	5	3
11497.6	0	2	3
11500.2	2	5	3
11503.3	4	4	2
11505.12			
11513.5	0	0	3
11517.9	4	3	2
11520.8	2	5	3
11523.5	0	2	2

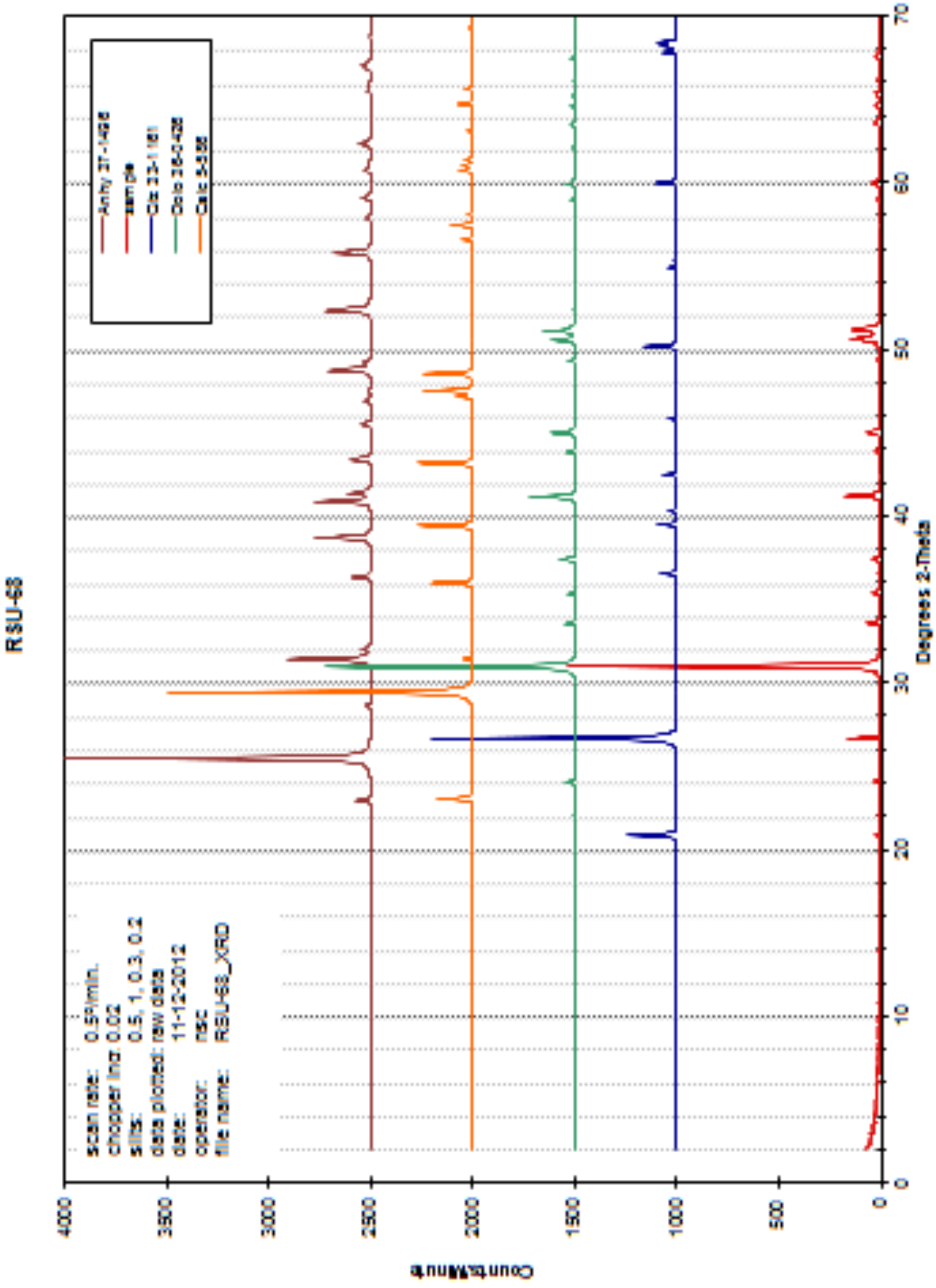
Top Depth	Facies	Continuity	Grain Size
11524.5	0	1	3
11526.5	0	0	3
11528.25	2	5	2
11529.6	7	5	1
11536.95	4	4	8
11542.11	4	4	4
11548.5	2	3	3
11553	2	5	4
11556.5	2	1	2
11577.5	1	3	3
11580.6	0	1	3
11595	10	5	5
11596	9	4	5
11602.5	4	4	4
11605.5	2	5	2
11608.5	2	5	2
11610.9	2	5	3
11616.75	1	3	2
11617.25	2	5	2
11618.5			
11694.5	1	5	3
11695.6	1	3	2
11697.4	1	2	2
11699.5	0	1	2
11699.75	5	1	1
11699.8	2	5	3
11702.5	0	0	2
11703	2	5	3
11704.5	0	0	3
11712	5	1	1
11712.1	3	5	3
11712.7			
11724.5	4	3	2
11726	0	1	3
11728.3	4	4	2
11733	3	3	2
11734.3	1	2	2
11739.7	2	3	3
11742.8	0	2	2
11747.5	2	5	2
11750.5	1	2	3
11753.5	10	5	1
11758.2	3	4	2
11762.4	4	2	3

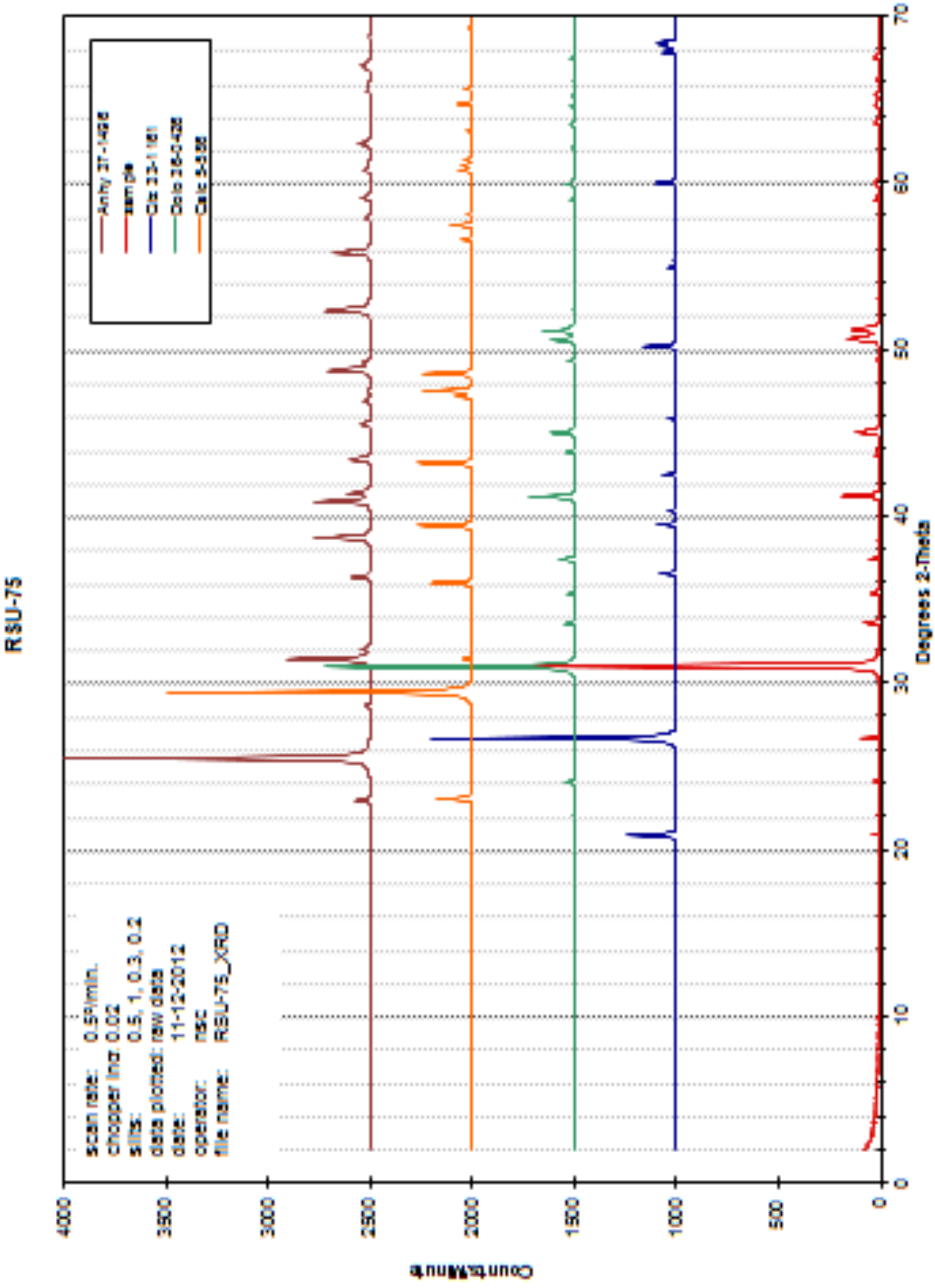
Top Depth	Facies	Continuity	Grain Size
11768.7	11	5	1
11771.6	11	4	2
11773.9	11	3	3
11777.1	2	5	2
11780.7	4	2	3
11782.9	0	1	4

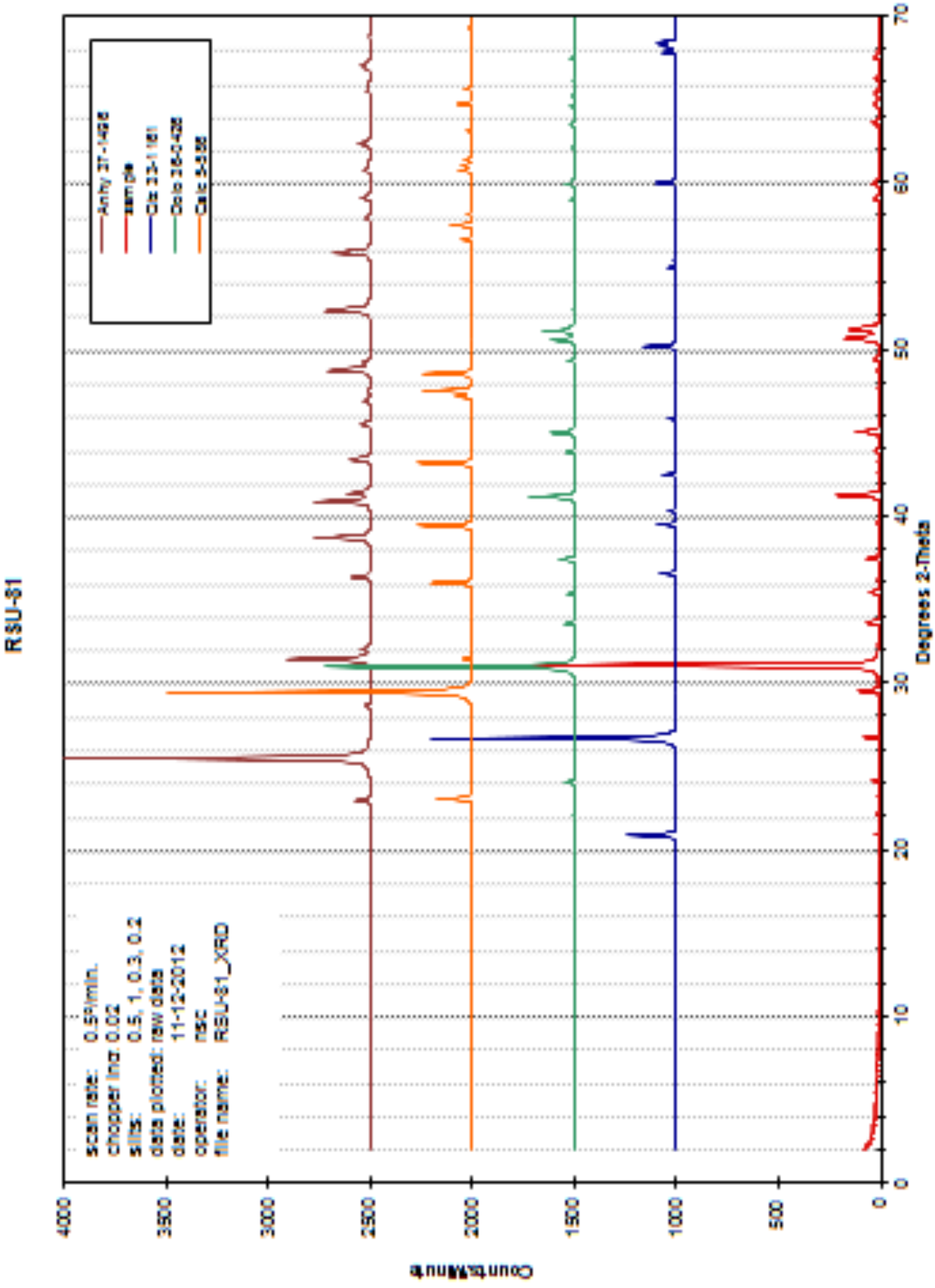
Appendix I: XRD Diagrams

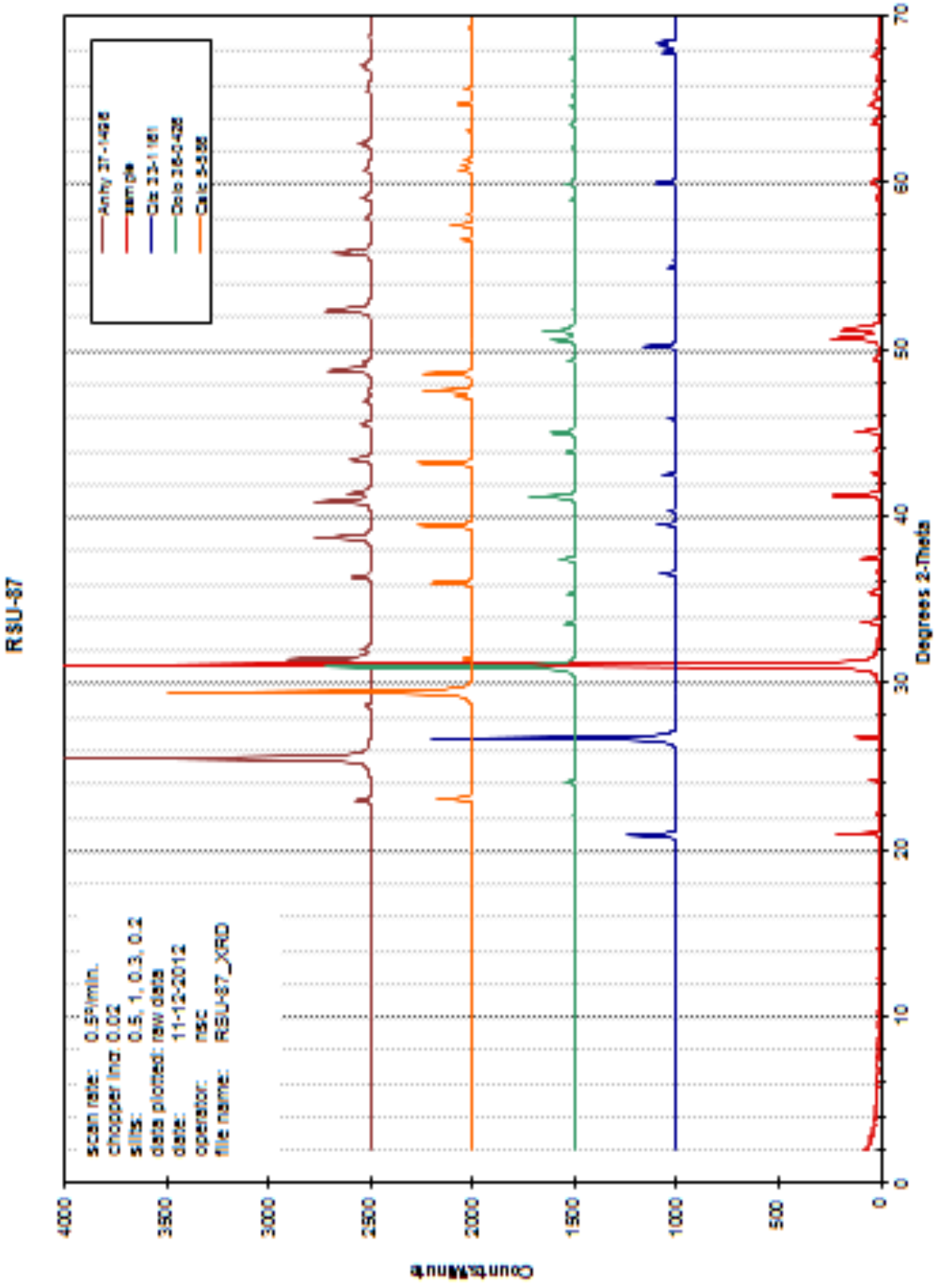

RSU-25
Anhy 37-1468
sample
Cc 33-1161
Dolo 36-0426
Calc 5-0586
scan rate: 0.5°/min.
chopper incr: 0.02
slits: 0.5, 1, 0.3, 0.2
data plotted: raw data
date: 11-12-2012
operator: rsc
file name: RSU-25_XRD
Counts/Minute
Degrees 2-Theta
0
500
1000
1500
2000
2500
3000
3500
4000
10
20
30
40
50
60
70

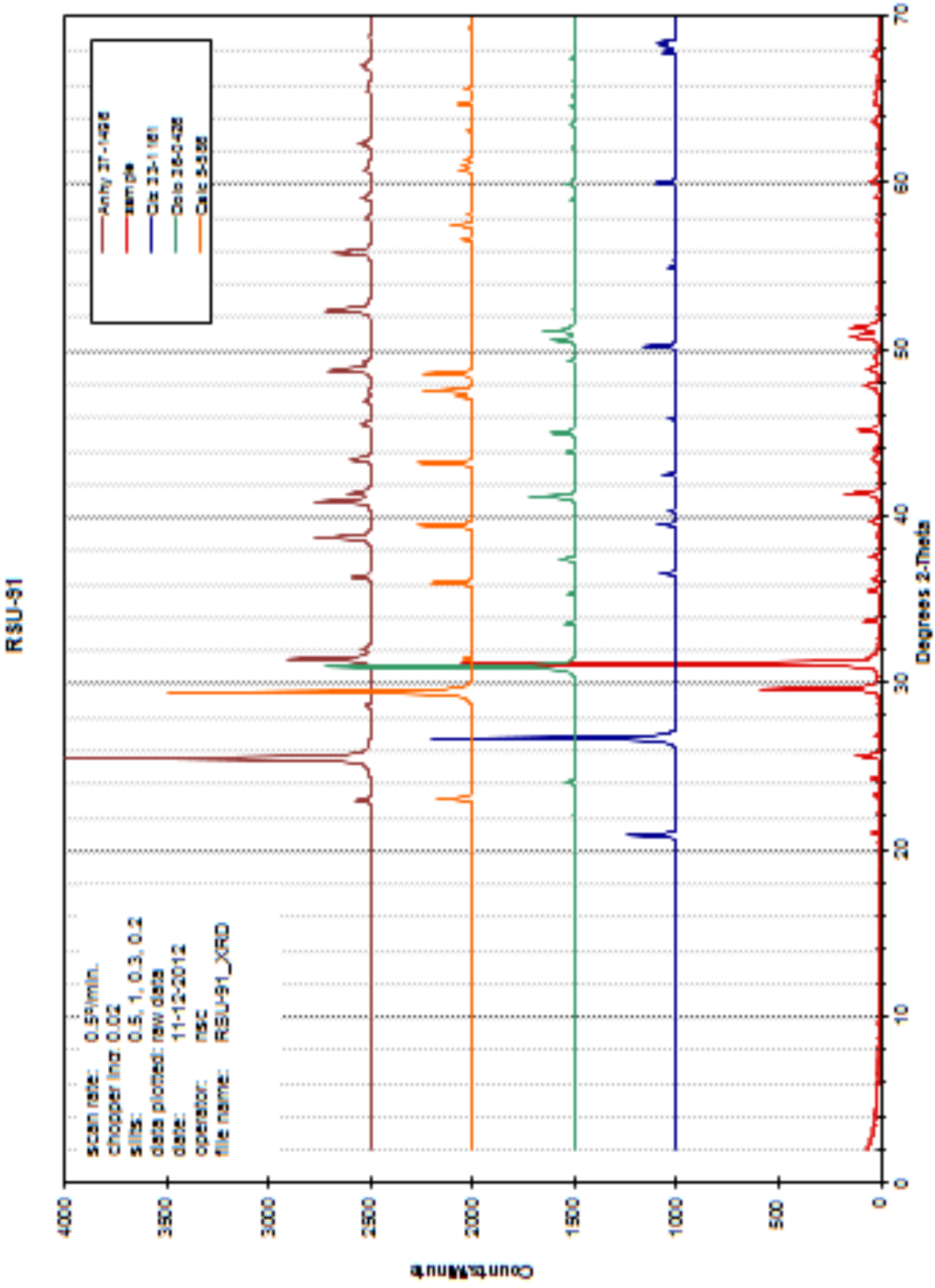

RSU-57
Anhy 37-1496
sample
Cla 33-1161
Dolo 36-0426
Calc 5-586
scan rate: 0.5°/min.
chopper Inc 0.02
slits: 0.5, 1, 0.3, 0.2
data plotted: raw data
date: 11-12-2012
operator: rsc
file name: RSU-57_XRD
Counts/Minute
Degrees 2-Theta
0
500
1000
1500
2000
2500
3000
3500
4000
10
20
30
40
50
60
70

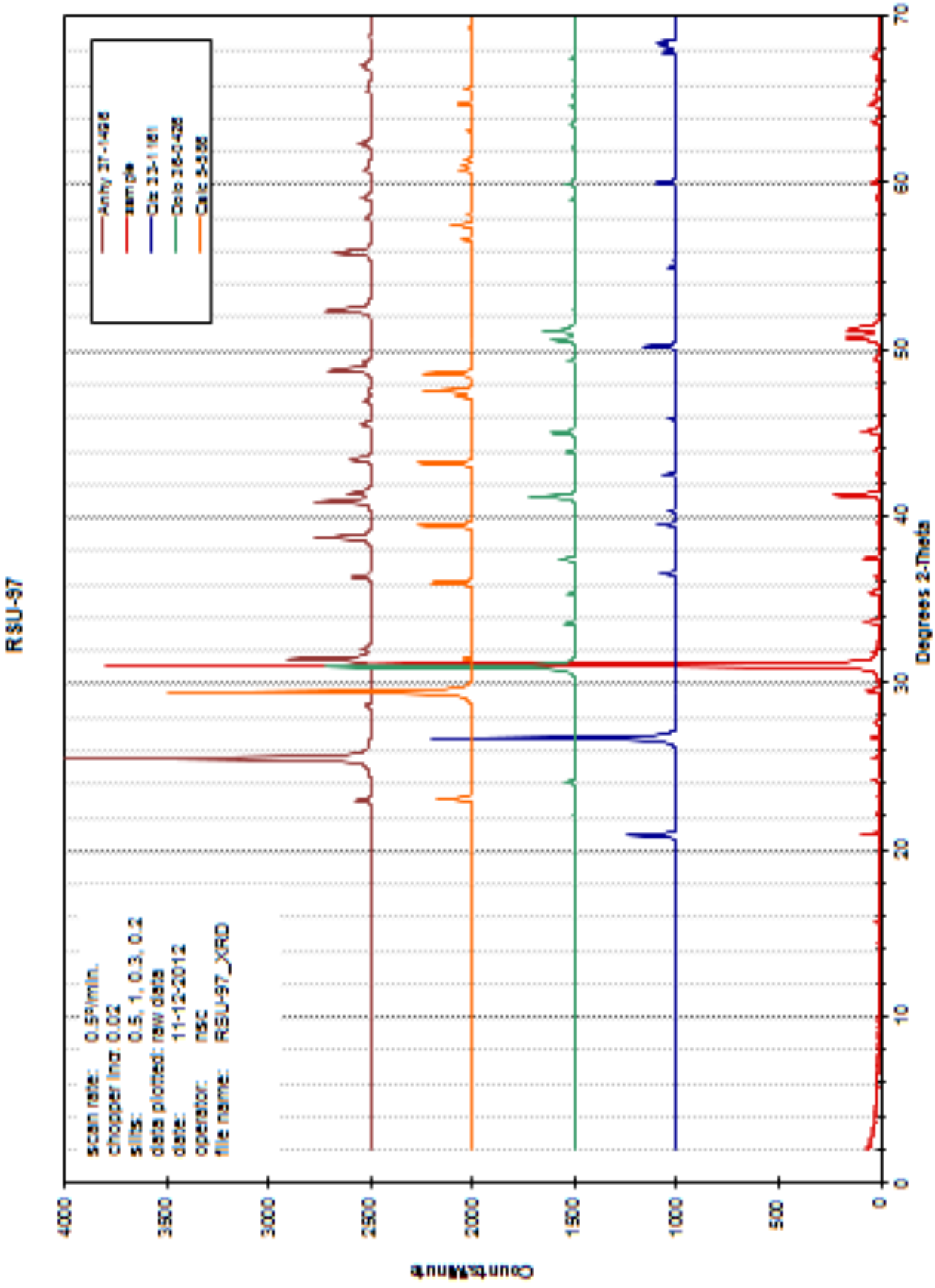

RSU-68
Anhy 37-1468
sample
Cla 33-1161
Dolo 36-0426
Calc 5-586
scan rate: 0.5°/min.
chopper Inc 0.02
slits: 0.5, 1, 0.3, 0.2
data plotted: raw data
date: 11-12-2012
operator: rsc
file name: RSU-68_XRD
Counts/Minute
Degrees 2-Theta
0
500
1000
1500
2000
2500
3000
3500
4000
10
20
30
40
50
60
70

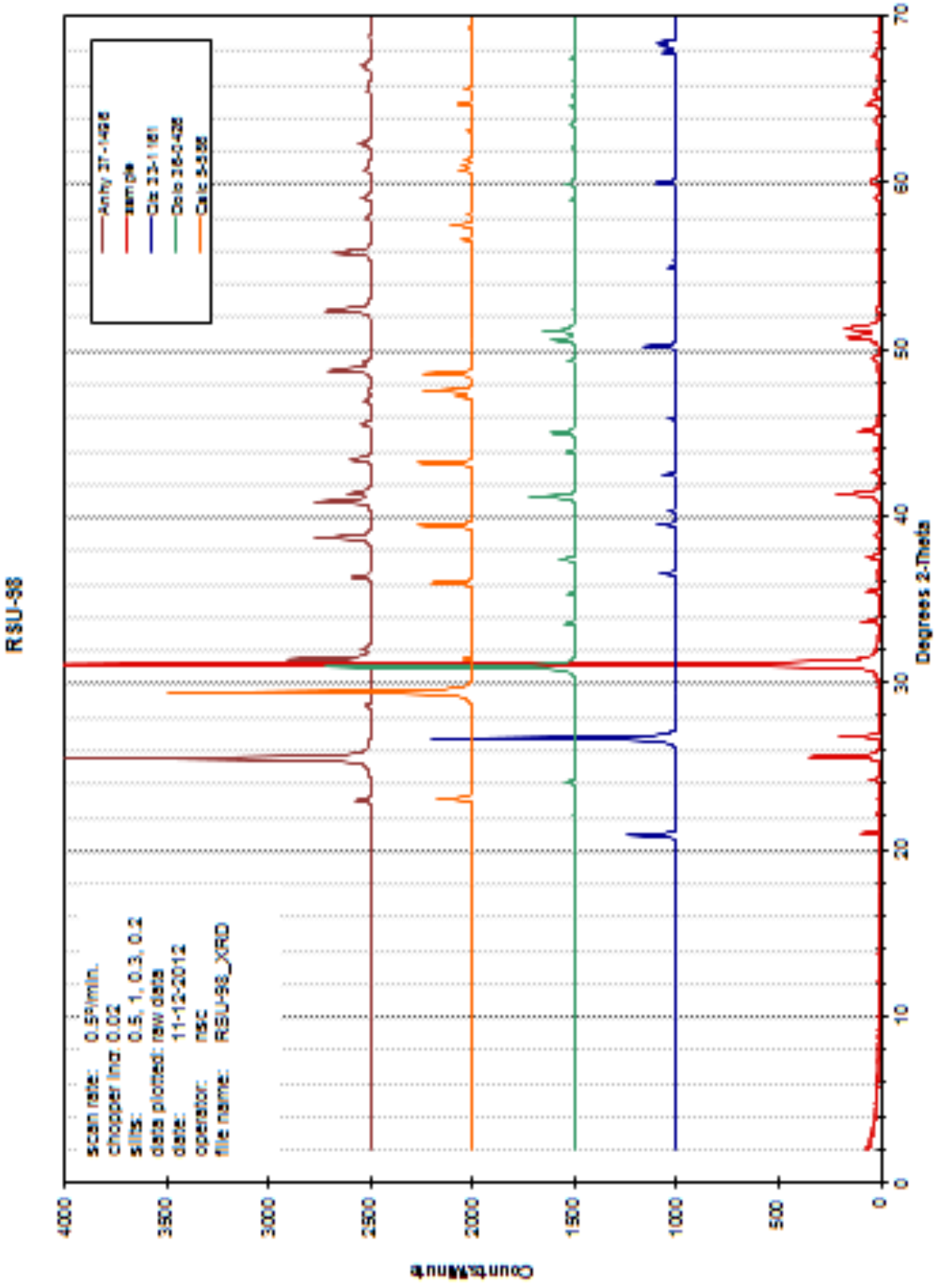

RSU-75
Anhy 37-1496
sample
Ca 33-1161
Dolo 36-0426
Calc 5-586
scan rate: 0.5°/min.
chopper Inc 0.02
slits: 0.5, 1, 0.3, 0.2
data plotted: raw data
date: 11-12-2012
operator: rsc
file name: RSU-75_XRD
Counts/Minute
Degrees 2-Theta
0
500
1000
1500
2000
2500
3000
3500
4000
10
20
30
40
50
60
70

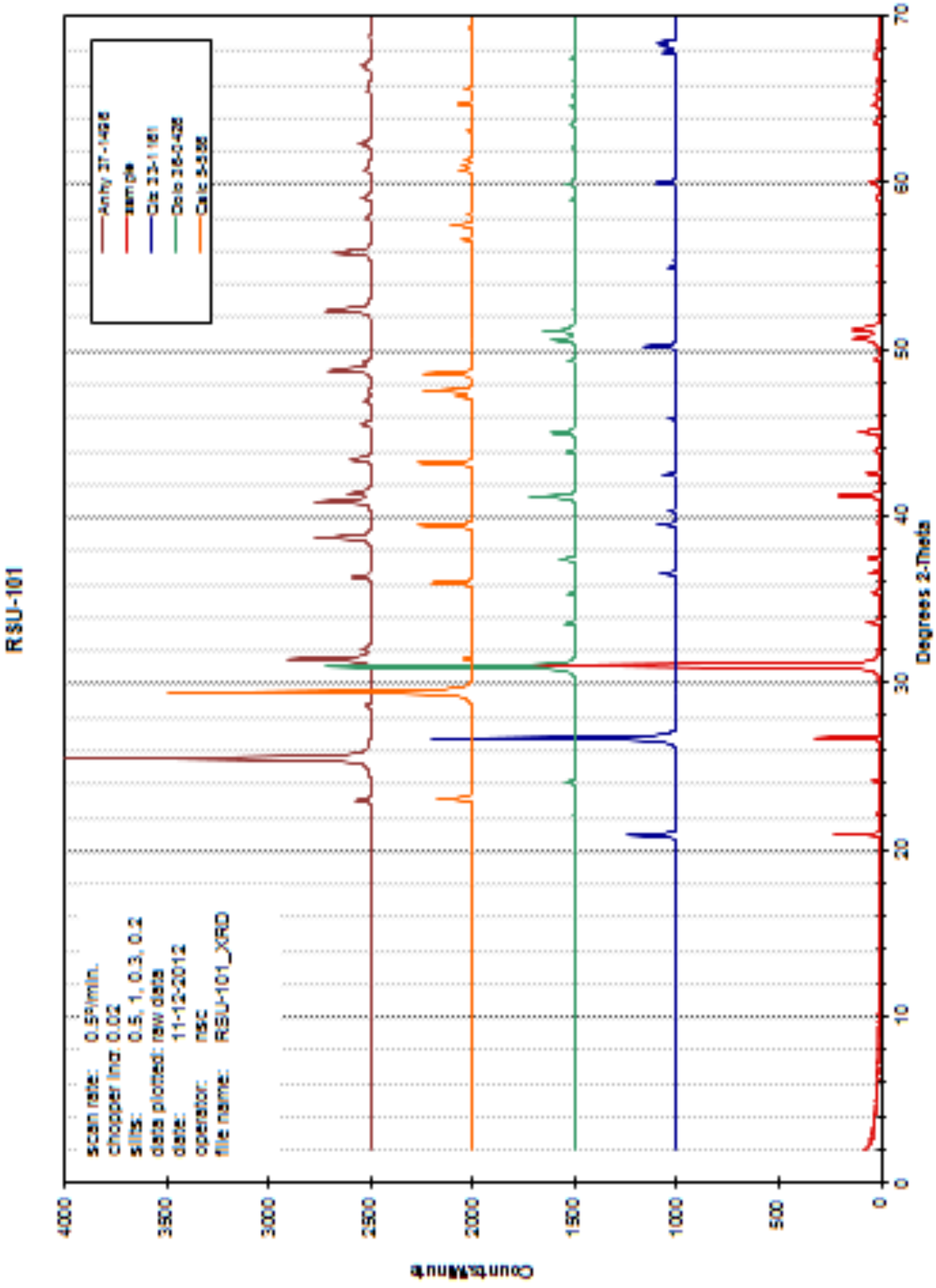

RSU-61
Anhy 37-1496
sample
Ca 33-1161
Dolo 36-0426
Calc 5-586
scan rate: 0.5°/min.
chopper Inc 0.02
slits: 0.5, 1, 0.3, 0.2
data plotted: raw data
date: 11-12-2012
operator: rsc
file name: RSU-61_XRD
Counts/Minute
Degrees 2-Theta
0
500
1000
1500
2000
2500
3000
3500
4000
10
20
30
40
50
60
70


RSU-87
Anhy 37-1496
sample
Cla 33-1161
Dolo 36-426
Calc 5-586
scan rate: 0.5°/min.
chopper Inc 0.02
slits: 0.5, 1, 0.3, 0.2
data plotted: raw data
date: 11-12-2012
operator: rsc
file name: RSU-87_XRD
Counts/Minute
Degrees 2-Theta
0
500
1000
1500
2000
2500
3000
3500
4000
10
20
30
40
50
60
70


RSU-91
Anhy 37-1496
sample
Cla 33-1161
Dolo 36-0426
Calc 5-586
scan rate: 0.5°/min.
chopper Inc: 0.02
slits: 0.5, 1, 0.3, 0.2
data plotted: raw data
date: 11-12-2012
operator: rsc
file name: RSU-91_XRD
Counts/Minute
Degrees 2-Theta
0
500
1000
1500
2000
2500
3000
3500
4000
10
20
30
40
50
60
70


RSU-97
Anhy 37-1496
sample
Cla 33-1161
Dolo 36-0426
Calc 5-586
scan rate: 0.5°/min.
chopper Inc 0.02
slits: 0.5, 1, 0.3, 0.2
data plotted: raw data
date: 11-12-2012
operator: rsc
file name: RSU-97_XRD
Counts/Minute
Degrees 2-Theta
0
500
1000
1500
2000
2500
3000
3500
4000
10
20
30
40
50
60
70


RSU-98
Anhy 37-1496
sample
Cla 33-1161
Dolo 36-426
Calc 5-586
scan rate: 0.5°/min.
chopper Inc 0.02
slits: 0.5, 1, 0.3, 0.2
data plotted: raw data
date: 11-12-2012
operator: rsc
file name: RSU-98_XRD
Counts/Minute
Degrees 2-Theta
0
500
1000
1500
2000
2500
3000
3500
4000
10
20
30
40
50
60
70


RSU-101
Anhy 37-1496
sample
Cla 33-1161
Dolo 36-426
Calc 5-586
scan rate: 0.5°/min.
chopper Inc 0.02
slits: 0.5, 1, 0.3, 0.2
data plotted: raw data
date: 11-12-2012
operator: rsc
file name: RSU-101_XRD
Counts/Minute
Degrees 2-Theta
0
500
1000
1500
2000
2500
3000
3500
4000
10
20
30
40
50
60
70

Appendix J: XRF Data

XRF results, based on loose powder measurements

	RSU-25	RSU-57	RSU-68	RSU-75	RSU-81	RSU-87	RSU-91	RSU-97	RSU-98	RSU-101
Weight %										
Sum:	100.0	100.0	100.0	100.0	100.0	100.0	100.0	100.0	100.0	100.0
Compound	Conc.	Conc.	Conc.	Conc.	Conc.	Conc.	Conc.	Conc.	Conc.	Conc.
Name	(%)	(%)	(%)	(%)	(%)	(%)	(%)	(%)	(%)	(%)
SiO2	84.6	0.8	6.5	2.9	2.5	5.3	1.5	2.3	7.7	13.3
Al2O3	3.5	0.1	0.1	0.2	0.1	0.2	0.1	0.1	0.1	0.1
CaCO3	3.5	62.1	53.8	56.1	61.0	56.8	69.8	60.0	54.7	50.2
MgCO3	2.9	35.2	38.4	39.3	35.1	35.3	23.9	35.6	28.4	35.4
Na2O	0.1	0.2				0.6				
K2O	2.0	0.03	0.03	0.1		0.2			0.04	0.1
SO3	1.0	0.1	0.2	0.0	0.2	0.1	3.8	1.1	8.0	0.0
P2O5	1.3	0.6	0.7	0.6	0.6	0.8	0.6	0.7	0.7	0.7
Cl	0.1	0.1	0.1	0.2	0.2	0.5	0.05	0.1	0.1	0.1
I				0.2						
TiO2	0.22				0.01	0.03				
Fe2O3	0.54	0.45	0.10	0.07	0.07	0.15	0.08	0.07	0.11	0.08
MnO		0.19	0.03	0.01	0.01	0.01	0.02	0.04	0.01	0.01
ZnO		0.01	0.01	0.00	0.00	0.00	0.00		0.00	0.00
BaO	0.05							0.01		
CuO		0.00								
NiO	0.01	0.01	0.01	0.00	0.01	0.01	0.01	0.00	0.00	0.00
PdO	0.01	0.02		0.00				0.00		
Rb2O	0.01			0.00	0.00	0.00	0.00	0.00		
SrO	0.01	0.02	0.01	0.01	0.01	0.01	0.11	0.04	0.11	0.00
ZrO2	0.05	0.00	0.00	0.00	0.00	0.00	0.02	0.01	0.02	0.00
Stoichiometry: (atomic ratios)										
	100.00	100.00	100.00	100.00	100.00	100.00	100.00	100.00	100.00	100.00
Compound	Mol	Mol	Mol	Mol	Mol	Mol	Mol	Mol	Mol	Mol
Name										
SiO2	89.8	1.2	9.7	4.4	3.9	8.0	2.3	3.5	11.4	19.1
Al2O3	2.2	0.1	0.1	0.2	0.1	0.2	0.1	0.1	0.1	0.1
CaCO3	2.2	57.9	48.3	51.3	56.3	51.2	65.7	55.3	48.6	43.5
MgCO3	2.2	39.0	40.9	42.6	38.5	37.8	26.7	38.9	30.0	36.4
Na2O	0.1	0.3				0.9				
K2O	1.3	0.03	0.03	0.1		0.1			0.04	0.1
SO3	0.8	0.2	0.3	0.0	0.3	0.1	4.5	1.3	8.9	0.03
P2O5	0.6	0.4	0.4	0.4	0.4	0.5	0.4	0.4	0.4	0.4
Cl	0.18	0.37	0.19	0.64	0.46	1.15	0.13	0.34	0.23	0.25
I				0.14						

TiO2	0.18				0.01	0.04				
Fe2O3	0.22	0.26	0.06	0.04	0.04	0.09	0.05	0.04	0.06	0.04
MnO		0.25	0.03	0.02	0.02	0.01	0.02	0.05	0.02	0.02
ZnO		0.01	0.01	0.00	0.00	0.00	0.01		0.00	0.00
BaO	0.02							0.01		
CuO		0.00								
NiO	0.01	0.01	0.01	0.01	0.01	0.01	0.01	0.01	0.01	0.01
PdO	0.00	0.01		0.00				0.00		
Rb2O	0.00			0.00	0.00	0.00	0.00	0.00		
SrO	0.00	0.02	0.01	0.01	0.01	0.01	0.10	0.03	0.10	0.00
ZrO2	0.03	0.00	0.00	0.00	0.00	0.00	0.01	0.00	0.01	0.00

Mineralogy by XRD

RSU-25	RSU-57	RSU-68	RSU-75	RSU-81	RSU-87	RSU-91	RSU-97	RSU-98	RSU-101

Peak intensity of main peak

NOT APPROPRIATE FOR CALCULATING MINERAL ABUNDANCES
ONLY FOR ROUGH COMPARISON BETWEEN
SAMPLES

Qu	4000	0	160	100	90	130	30	50	210	330
Calc	0	60	0	0	100	0	600	80	0	0
Dolo	50	2000	1600	2200	2300	5100	2100	3900	4400	2400
Anhy	10	0	0	0	0	0	130	50	350	0

Appendix K: Water Quality Data

	Weber Formation Energy Labs (08/27/2011)	Weber Foramtion Core Labs (08/27/2011)	Weber Formation Energy Labs (12/14/12)	Madison Limestone Energy Labs (08/27/2011)	Madison Limestone Core Labs (08/27/2011)	Madison Limestone Energy Labs (12/03/12)
Analyses						
Microbiological						
Heterotrophic (MPN/mL)	< 2	–	40	2	–	10
Major Ions						
Alkalinity, Total as $CaCO_3$ (mg/L)	509	–	3030	1170	–	2620
Carbonate as CO_3 (mg/L)	ND	0	ND	ND	0	ND
Bicarbonate as HCO_3 (mg/L)	621	720	3690	1420	1,610	3190
Calcium (mg/L)	734	705	539	1190	1,280	1630
Chloride (mg/L)	60,900	61,830	57,400	50,300	52,290	51,600
Flouride (mg/L)	11.5	8.4	6.1	3.5	13	2.8
Magnesium (mg/L)	37	40	45	158	170	195
Nitrogen, Ammonia as N (mg/L)	33.4	–	33.1	42	–	39
Nitrogen, Nitrate+Nitrite as N (mg/L)	0.1	ND	ND	ND	ND	0.1
Nitrogen, Nitrite as N (mg/L)	ND	ND	ND	ND	ND	ND
Phosphate	–	ND	–	–	ND	–
Potassium (mg/L)	–	1,940	1,910	–	4,210	3,780
Silicon (mg/L)	–	26	45.2	–	36	59.5
Sodium (mg/L)	40,700	43,250	36,500	29,000	32820	27,900
Strontium (mg/L)	–	26	14	–	67	51.1
Sulfate (mg/L)	11,600	10,320	6030	2,800	2,280	1,820
Non-Metals						
Dissolved inorganic carbon (mg/L)	144	–	786	355	–	724
Dissolved organic carbon (mg/L)	2.9	–	4.5	1	–	4.4
Total organic carbon (mg/L)	2.7	–	4.7	1	–	4.5
UV Absorbance at 254 nm (cm-1)	0.92	–	1.99	0.558	–	1.28
Total recoverable phenolics (mg/L)	0.61	–	0.16	0.05	–	0.7
Total cyanide (mg/L)	ND	–	0.098	ND	–	0.339
Sulfide (mg/L)	0.04		120	28	0	82
Sulfide as hydrogen sulfide (mg/L)	0.04	–	127	29	–	87
Physical properties						
Chemical oxygen demand (mg/L)	2420	–	9120	1940	–	3050
pH	7.54	7.11	6.46	7.36	6.01	6.43
Total dissolved solids @ 180 C (mg/L)	89,800	119,155	109,000	75,000	95,126	89,800
BOD (mg/L)	56.7	–	517	50.2	–	234
Sodium adsorption ratio	397	–	380	209	–	174

	Weber Formation Energy Labs (08/27/2011)	Weber Foramtion Core Labs (08/27/2011)	Weber Formation Energy Labs (12/14/12)	Madison Limestone Energy Labs (08/27/2011)	Madison Limestone Core Labs (08/27/2011)	Madison Limestone Energy Labs (12/03/12)
Metals						
Aluminum (mg/L)	ND	ND	3.5	ND	ND	1.9
Arsenic (mg/L)	0.095	–	0.444	1.76	–	0.376
Barium (mg/L)	ND	ND	14.3	1	ND	4.48
Beryllium (mg/L)	ND	–	0.007	ND	–	0.037
Bismuth (mg/L)	–	–	0.02	–	–	0.02
Boron (mg/L)	61.1	–	71.8	95.2	–	101
Borate (mg/L)	–	81		–	120	
Bromide (mg/L)	–	94	99	–	115	140
Cadmium (mg/L)	ND	ND	0.006	ND	ND	ND
Chromium (mg/L)	ND	ND	0.61	0.06	ND	0.576
Cobalt (mg/L)	0.02	ND	0.019	ND	ND	0.009
Copper (mg/L)	ND	ND	13.6	ND	ND	1.35
Iodide (mg/L)	–	ND	2	–	ND	ND
Iron (mg/L)	0.94	2.2	44.1	0.54	8.1	32.2
Lead (mg/L)	ND	ND	2.91	ND	ND	0.305
Lithium (mg/L)	92.8	100	90..5	91.9	105	91.6
Manganese (mg/L)	0.07	0.07	0.777	0.12	0.35	7.76
Mercury (mg/L)	ND	–	0.0006	ND	–	ND
Molybdenum (mg/L)	–	ND	–	–	ND	–
Nickel (mg/L)	ND	ND	0.093	ND	ND	0.03
Phosphorus	–	ND	–	–	ND	–
Selenium (mg/L)	0.0004	–	0.054	0.013	–	0.041
Silver (mg/L)	ND	–	ND	ND	–	0.001
Uranium (mg/L)	–	–	0.0187	–	–	0.0004
Vanadium (mg/L)	ND	–	0.26	ND	–	0.01
Zinc (mg/L)	0.26	–	4.58	0.4	–	2.1
Radionuclides						
Gross Alpha (pCi/L)	–	–	-400	–	–	157
Gross Beta (pCi/L)	–	–	1630	–	–	2990
Radium 226 (pCi/L)	–	–	24	–	–	39
Radium 228 (pCi/L)	–	–	14	–	–	1.2
Cesium 134 (pCi/L)	–	–	–	–	–	0
Cesium 137 (pCi/L)	–	–	–	–	–	0
Data Quality						
Anion/Cation Balance (± 5)	-3.15%	0.37%	-5.42%	-3.71%	2.61%	-4.57%

	Weber Formation Energy Labs (08/27/2011)	Weber Foramtion Core Labs (08/27/2011)	Weber Formation Energy Labs (12/14/12)	Madison Limestone Energy Labs (08/27/2011)	Madison Limestone Core Labs (08/27/2011)	Madison Limestone Energy Labs (12/03/12)
Organic Acids						
Acetate (mg/L)	–	5.5	–	–	0	–
Butyrate (mg/L)	–	0	–	–	0	–
Formate (mg/L)	–	5.4	–	–	1.7	–
Glycolate (mg/L)	–	0	–	–	0	–
Propionate (mg/L)	–	0	–	–	0	–
Valerate (mg/L)	–	0	–	–	0	–
Volatile organic compounds						
1,1,1,2-Tetrachloroethane (µg/L)	ND	–	ND	ND	–	ND
1,1,1-Trichloroethane (µg/L)	ND	–	ND	ND	–	ND
1,1,2,2-Tetrachloroethane (µg/L)	ND	–	ND	ND	–	ND
1,1,2-Trichloroethane (µg/L)	ND	–	ND	ND	–	ND
1,1-Dichloroethane (µg/L)	ND	–	ND	ND	–	ND
1,1-Dichloroethene (µg/L)	ND	–	ND	ND	–	ND
1,1-Dichloropropene (µg/L)	ND	–	ND	ND	–	ND
1,2,3-Trichlorobenzene (µg/L)	ND	–	ND	ND	–	ND
1,2,3-Trichloropropane (µg/L)	ND	–	ND	ND	–	ND
1,2,4-Trichlorobenzene (µg/L)	ND	–	ND	ND	–	ND
1,2,4-Trimethylbenzene (µg/L)	210	–	190	190	–	73
1,2-Dibromo-3-chloropropane (µg/L)	ND	–	ND	ND	–	ND
1,2-Dibromoethane (µg/L)	ND	–	ND	ND	–	ND
1,2-Dichlorobenzene (µg/L)	ND	–	ND	ND	–	ND
1,2-Dichloroethane (µg/L)	ND	–	ND	ND	–	ND
1,2-Dichloropropane (µg/L)	ND	–	ND	ND	–	ND
1,3,5-Trimethylbenzene (µg/L)	30	–	62	30	–	54
1,3-Dichlorobenzene (µg/L)	ND	–	ND	ND	–	ND
1,3-Dichloropropane (µg/L)	ND	–	ND	ND	–	ND
1,4-Dichlorobenzene (µg/L)	ND	–	ND	ND	–	ND
2,2-Dichloropropane (µg/L)	ND	–	ND	ND	–	ND
2-Chloroethyl vinyl ether (µg/L)	ND	–	ND	ND	–	ND
2-Chlorotoluene (µg/L)	ND	–	ND	ND	–	ND
4-Chlorotoluene (µg/L)	ND	–	ND	ND	–	ND
Benzene (µg/L)	ND	–	230	ND	–	13
Bromobenzene (µg/L)	ND	–	ND	ND	–	ND
Bromochloromethane (µg/L)	ND	–	ND	ND	–	ND
Bromodichloromethane (µg/L)	ND	–	ND	ND	–	ND
Bromoform (µg/L)	ND	–	ND	ND	–	ND
Bromomethane (µg/L)	ND	–	ND	ND	–	ND
Carbon tetrachloride (µg/L)	ND	–	ND	ND	–	ND
Chlorobenzene (µg/L)	ND	–	ND	ND	–	ND

	Weber Formation Energy Labs (08/27/2011)	Weber Foramtion Core Labs (08/27/2011)	Weber Formation Energy Labs (12/14/12)	Madison Limestone Energy Labs (08/27/2011)	Madison Limestone Core Labs (08/27/2011)	Madison Limestone Energy Labs (12/03/12)
Chlorodibromomethane (µg/L)	ND	–	ND	ND	–	ND
Chloroethane (µg/L)	ND	–	ND	ND	–	ND
Chloroform (µg/L)	ND	–	ND	ND	–	ND
Chloromethane (µg/L)	ND	–	ND	ND	–	ND
cis-1,2-Dichloroethene (µg/L)	ND	–	ND	ND	–	ND
cis-1,3-Dichloropropene (µg/L)	ND	–	ND	ND	–	ND
Dibromomethane (µg/L)	ND	–	ND	ND	–	ND
Dichlorodifluoromethane (µg/L)	ND	–	ND	ND	–	ND
Ethylbenzene (µg/L)	20	–	54	20	–	26
Hexachlorobutadiene (µg/L)	ND	–	ND	ND	–	ND
Isopropylbenzene (µg/L)	30	–	9	20	–	8.4
m+p-Xylenes (µg/L)	55	–	280	50	–	98
Methyl ethyl ketone (µg/L)	ND	–	280	ND	–	88
Methyl tert-butyl ether (MTBE) (µg/L)	ND	–	ND	ND	–	ND
Methylene chloride (µg/L)	ND	–	ND	ND	–	ND
n-Butylbenzene (µg/L)	57	–	44	40	–	53
n-Propylbenzene (µg/L)	ND	–	27	ND	–	28
Naphthalene (µg/L)	190	–	74	190	–	77
o-Xylene (µg/L)	ND	–	110	ND	–	66
p-Isopropyltoluene (µg/L)	ND	–	16	ND	–	15
sec-Butylbenzene (µg/L)	ND	–	15	ND	–	16
Styrene (µg/L)	ND	–	ND	ND	–	ND
tert-Butylbenzene (µg/L)	ND	–	ND	ND	–	ND
Tetrachloroethene (µg/L)	ND	–	ND	ND	–	ND
Toluene (µg/L)	ND	–	490	ND	–	86
trans-1,2-Dichloroethene (µg/L)	ND	–	ND	ND	–	ND
trans-1,3-Dichloropropene (µg/L)	ND	–	ND	ND	–	ND
Trichloroethene (µg/L)	ND	–	ND	ND	–	ND
Trichlorofluoromethane (µg/L)	ND	–	ND	ND	–	ND
Vinyl chloride (µg/L)	ND	–	ND	ND	–	ND
Xylenes (µg/L)		–	380		–	160
Organic Characteristics						
Oil and Grease (HEM) mg/L	270	–	1100	490	–	510
Compositional Analysis of Flash Gas						
Nitrogen (Mole %)	–	78.888	–	–	16.75	–
Carbon Dioxide (Mole %)	–	14.738	–	–	82.892	–
Hydrogen Sulfide (Mole %)	–	0	–	–	0	–
Methane (Mole %)	–	2.537	–	–	0.189	–
Ethane (Mole %)	–	0.297	–	–	0	–

	Weber Formation Energy Labs (08/27/2011)	Weber Foramtion Core Labs (08/27/2011)	Weber Formation Energy Labs (12/14/12)	Madison Limestone Energy Labs (08/27/2011)	Madison Limestone Core Labs (08/27/2011)	Madison Limestone Energy Labs (12/03/12)
Propane (Mole %)	–	0.213	–	–	0.021	–
Iso-Butane (Mole %)	–	0.043	–	–	0.004	–
N-Butane (Mole %)	–	0.071	–	–	0.011	–
Iso-Pentane (Mole %)	–	0.397	–	–	0.04	–
N-Pentane (Mole %)	–	0.02	–	–	0.004	–
Hexanes (Mole %)	–	2.119	–	–	0.006	–
Heptanes (Mole %)	–	0.244	–	–	0.015	–
Octanes (Mole %)	–	0.116	–	–	0.026	–
Nonanes (Mole %)	–	0.08	–	–	0.012	–
Decanes Plus (Mole %)	–	0.237	–	–	0.03	–

Appendix L: Microseismic Monitoring Report

RSU #1

Sweetwater County,

Wyoming

MICROSEISMIC MONITORING

Monitor Well: RSU #1

TABLE OF CONTENTS

Reservoir storage capacity .....Error! Bookmark not defined.
Methodology and approach 81
Establish reservoir heterogeneity through correlation seismic attributes with well log parameters and core observations 82
Core measured porosity 82
Export realistic 3-D petrophysical property models to numerical simulation 95
Perform a series of CO_2 injection-formation fluid production scenarios to optimize CO_2 storage capacity 97
Laboratory measurement of containment-mineralization and brine 99

Pressure management **116**

Evaluate a range of potential CO_2 injection/storage scenarios for targeted reservoir intervals using numerical simulation techniques **116**
Inject to the Weber Sandstone with homogeneous petrophysical properties 116
Inject to the Weber Sandstone with heterogeneous property 117
The Madison Limestone with homogeneous property 118
The Madison Limestone with heterogeneous property 119
Determine the CO_2 plume geometry, volume, and the rate of displaced fluid removal required to low storage risks for each CO_2 injection/storage scenario, ...**120**
The Weber Sandstone with homogeneous property 120
The Weber Sandstone with heterogeneous property 122
The Madison Limestone with homogeneous property 124
The Madison Limestone with heterogeneous petrophysical property 126

Introduction **429**

Executive summary **430**
Project Setup **430**
Tool Depths **431**
TOOL DEPTH 1: To monitor shales 5180-5210 ft **433**
TOOL DEPTH 2: To monitor shales 4150 -4200 ft **436**
TOOL DEPTH 3: To monitor sands 3020 - 3090 ft **441**
TOOL DEPTH 4: To monitor sands 2540 - 2610 ft **445**
Summary **448**
Appendix A: Recording Network Characteristics **449**
Sensor specifications 449
3C-sensor polarity 449
3C-sensor orientation 449
Appendix B: Velocity Model **451**
Standard velocity model 451
Inversion Velocity Model 452
Appendix C: Microseismic Event Selection **453**
Methodology 453
Automatic microseism detection 453
Validation of microseismic candidates 454
Appendix D: Microseismic Data Processing – Including SRV **455**
Appendix E: Sensor Orientation Method **466**
Measured polarization 466
Expected polarization 467
Inversion method 467
Appendix F: Event Location & Uncertainty **468**
Location method 468

Location uncertainty 468
Appendix G: Nomenclature & Conventions 470

Introduction

This report presents several sections on:

1. Results from microseismic data recording and review
2. Description of the data processing procedure available and background information

For this project, the specific objectives of the microseismic monitoring were, in priority order:

- To detect microseismic events
- If possible, locate those events.
- If there were sufficient events detected, characterize the nature of the microseismic data
- Establish the background noise level for the 4 levels montiors

Deliverables for this project include this report, and the raw data.

Executive summary

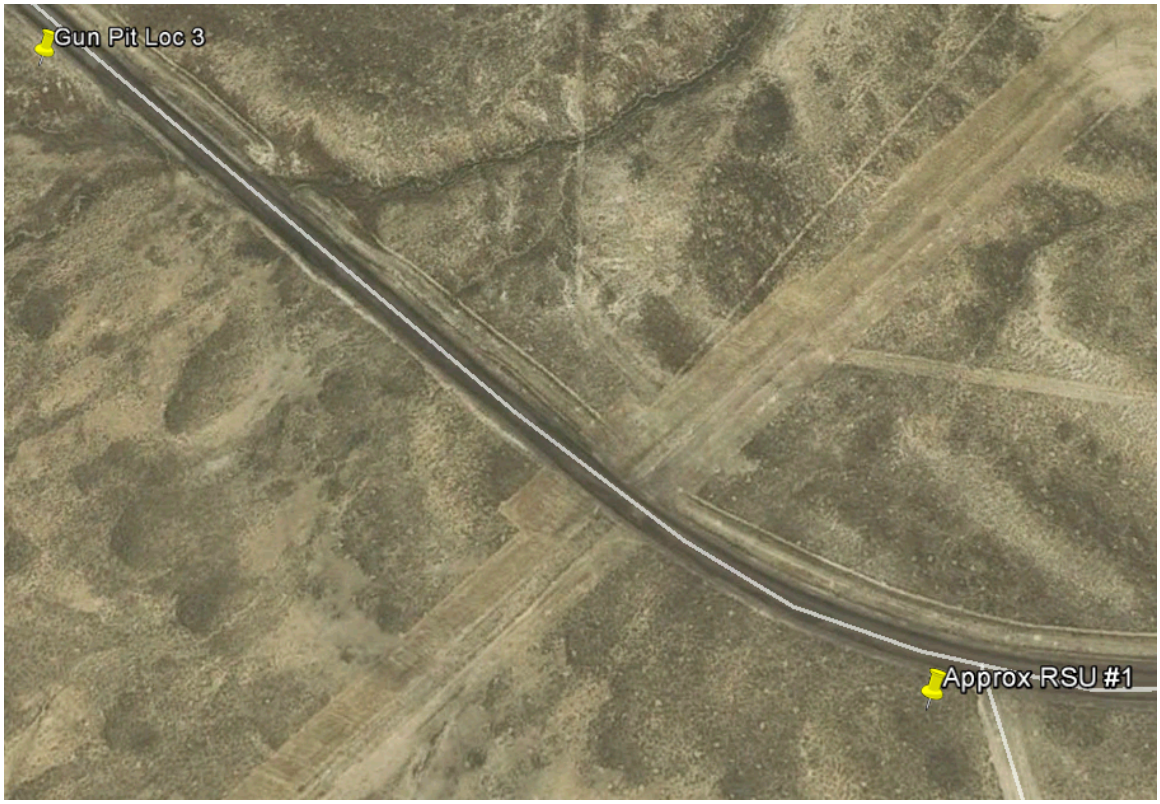
Microseismic monitoring was performed at four levels in the RSU #1 test well between September 22, 2013 and September 28, 2013. A velocity model was generated from the VSP previously run in this well. A vibrator was used to provide a source for orienting the tools at each level.

After the data was recorded, it was reviewed for potential events. These triggers were further analized to determine if they were siesmic or microseismic. All triggers were tube waves moving within the well bore itself.

At each level, Vrms noise levels were measured for all records.

Project Setup

The following map shows the approximate location of the RSU #1 well and the location utilized to orient the geophones for each of the four levels.



This location was chosen to ensure that we had at least 20 degrees angle of incidence on the horizontal geophones so we could determine orientation. Exact coordinates are in the following table. Latitude and Longitude are based upon the WGS 84 datum.

	Latitude	Longitude
RSU #1	41.7212614N	-108.794820W
Vibrator Location	41.7124400N	-108.795430W

Tool Depths

We deployed 15 Maxiwave tools at 4 different depths in order to monitor the following 4 horizons. The Maxiwave 3 component tools were spaced 15 m (49.2 ft) apart.

Sands

1. 2,540-2610’ below surface – Tool depth 1
2. 3,020-3,090’ below surface – Tool depth 2

Shales

1. 4,150-4200’ below surface – Tool depth 3
2. 5,180-5210’ below surface – Tool depth 4

Appendix B describes the maxiwave tools utilized. Appendix C is a diagram of tool assembly.

The following table describes the instruments, settings, and 4 tool locations to monitor the levels.

Company	**University of Wyoming**	**Tool**	MAXIWAVE	**Array Length**	688.8
Field	Rock Springs Uplift	**Levels**	15	**Ref. Point**	RKB
Engineers	JEWELL / MINTO / KLEB	**Sensor**	FIXED 15 HZ	**Depth Ref.**	6860
Crew	Ramirez	**Sensitivity (dB)**	40	**System**	SERCEL
Rig Site Loc.	Sweetwater County Wyoming	**Spacing**	49.2	**Format**	SEG-Y

Background Monitoring Shales

Depth 1: 5180 to 5210 Shales

Monitor Well Name-1			*RSU-1*
Depth	*5310*	***Date***	*22-Sep-13*
MONITORING DETAILS			
	Tme		**Record No.**
Start Recording	15:42		1
Stop Recording	3:45		904

Depth 2: 4150 to 4200 Shales

Monitor Well Name-1			*RSU-1*
Depth	*4300*	***Date***	*24-Sep-13*
MONITORING DETAILS			
Number	**Time**		**Record No.**
Start Recording	4:30		905
Stop Recording	16:30		3961

Background Monitoring Sands

Depth 1: 3020 to 3090 Sands

Monitor Well Name-1			*RSU-1*
Depth	*3190*	***Date***	*25-Sep-13*
MONITORING DETAILS			
	Tme		**Record No.**
Start Recording	17:21		3964
Stop Recording	5:22		1288

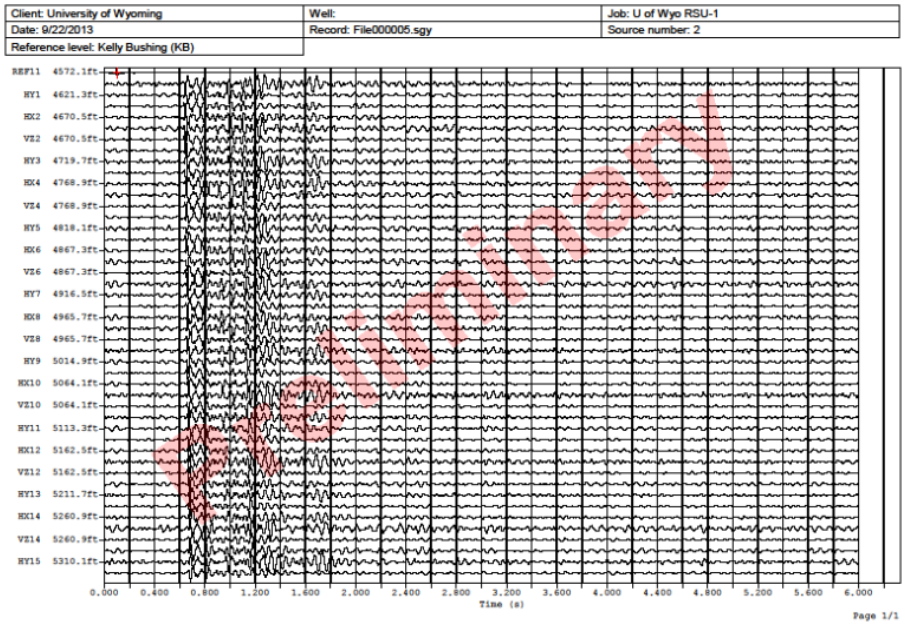
Depth 2: 2540 to 2610 Sands

Monitor Well Name-1			*RSU-1*
Depth	*2710*	***Date***	*27-Sep-13*
MONITORING DETAILS			
Number	**Time**		**Record No.**
Start Recording	5:51		1289
Stop Recording	17:51		4284

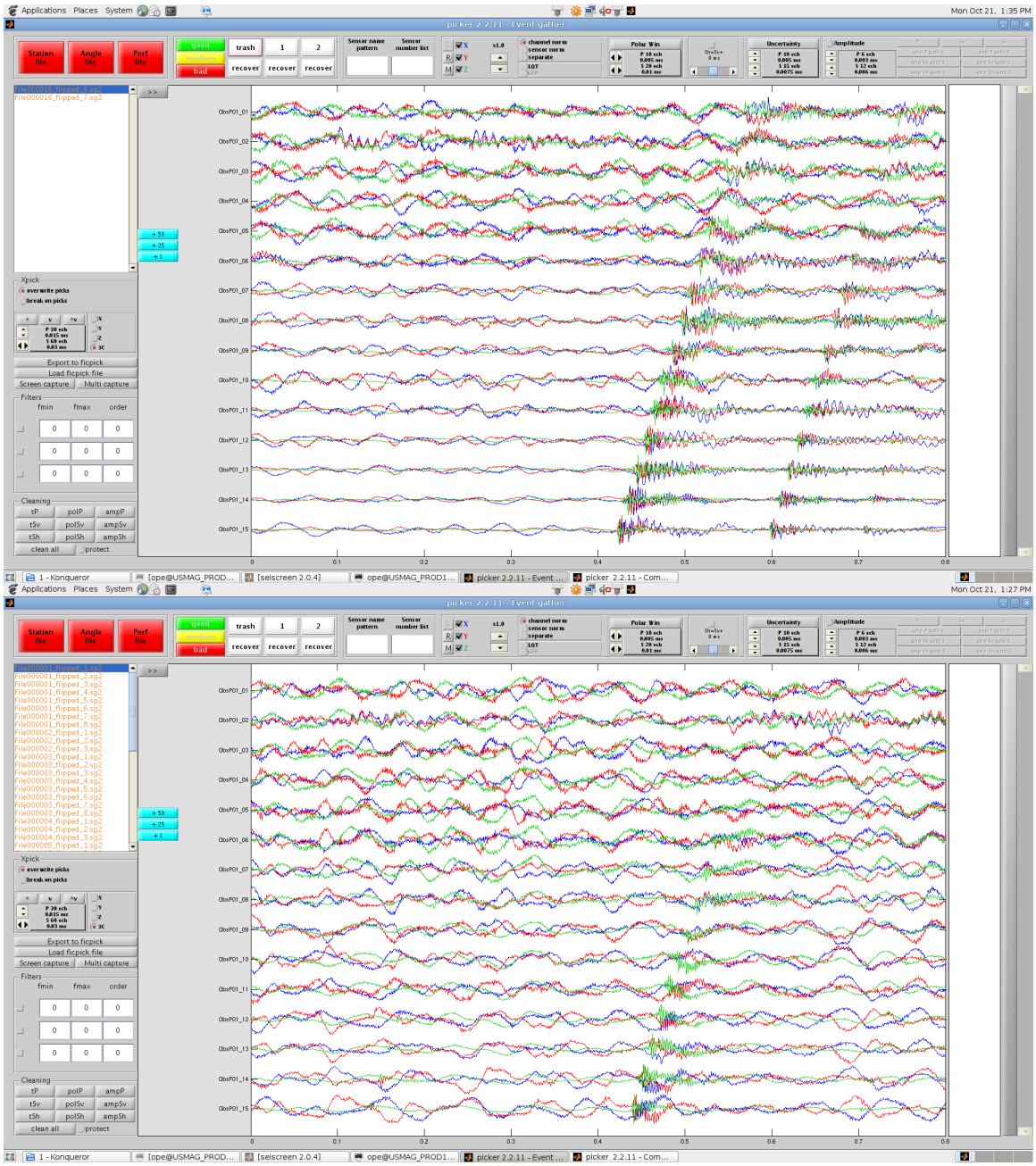
Please note that depth indicates the depth of the bottom tool. We chose to place two tools of the string below the interval of interest to increase sensitivity for any events below that particular interval.

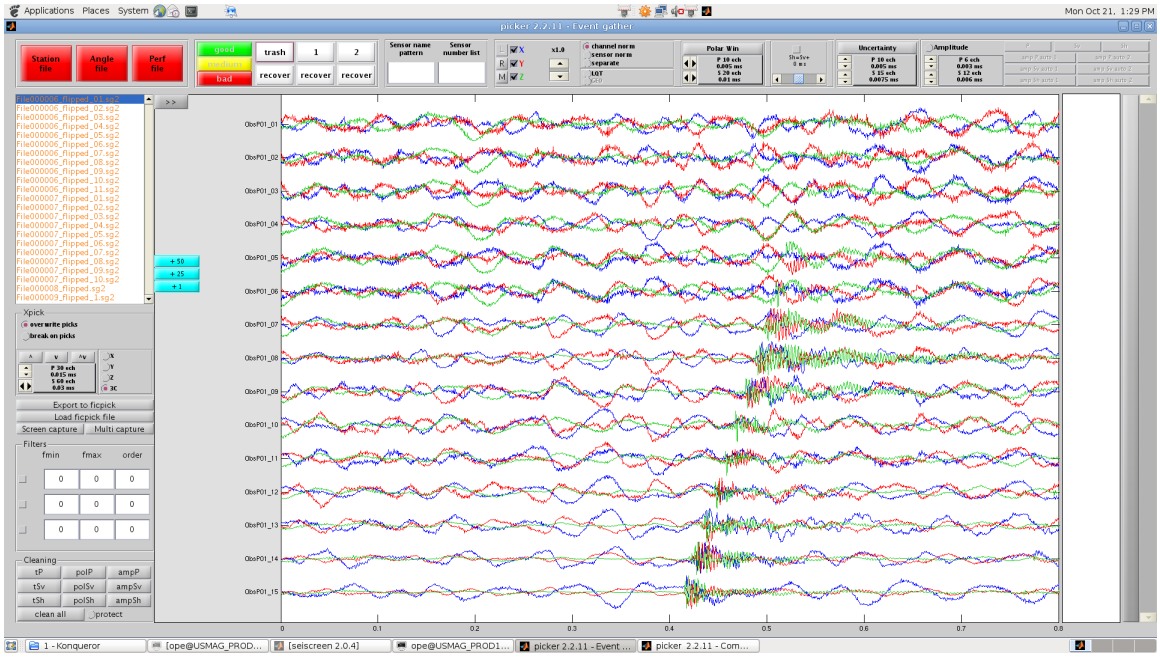
TOOL DEPTH 1: To monitor shales 5180-5210 ft

The folloiwng diagram is the vibe shot used to orient the tools at this level. Note there is clear energy on both of the H axes.

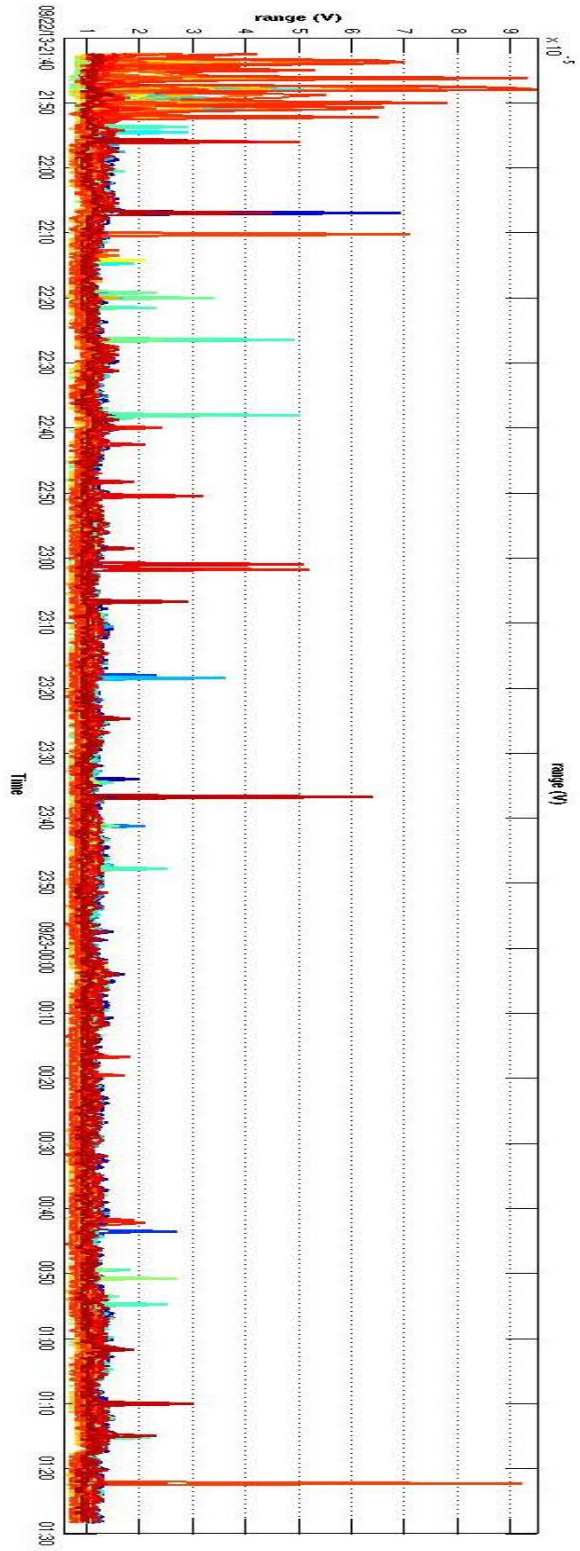


The following 3 examples are records from this level. In the images, all three axes are plotted for each tool (V, H1, H2). Note the linear moveout in each image. This is tube wave energy moving in the fluid of the well bore. We detected no microseismicity at this level.


Applications Places System
Mon Oct 21, 1:35 PM
picker 2.2.11 - Event gather
Station file
Angle file
Perf file
good
medium
bad
trash
recover
Sensor name pattern
Sensor number list
Polar Win
Uncertainty
Amplitude
Xpick
over write picks
break on picks
Export to ficpick
Load ficpick file
Screen capture
Multi capture
Filters
fmin
fmax
order
Cleaning
clean all
protect
Mon Oct 21, 1:27 PM

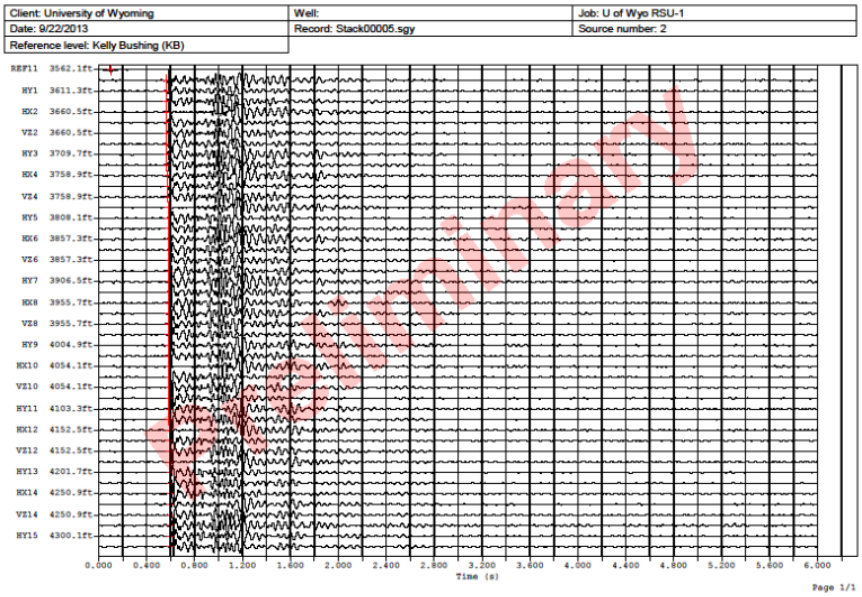


The following diagram is the RMS noise level for all records at this depth.

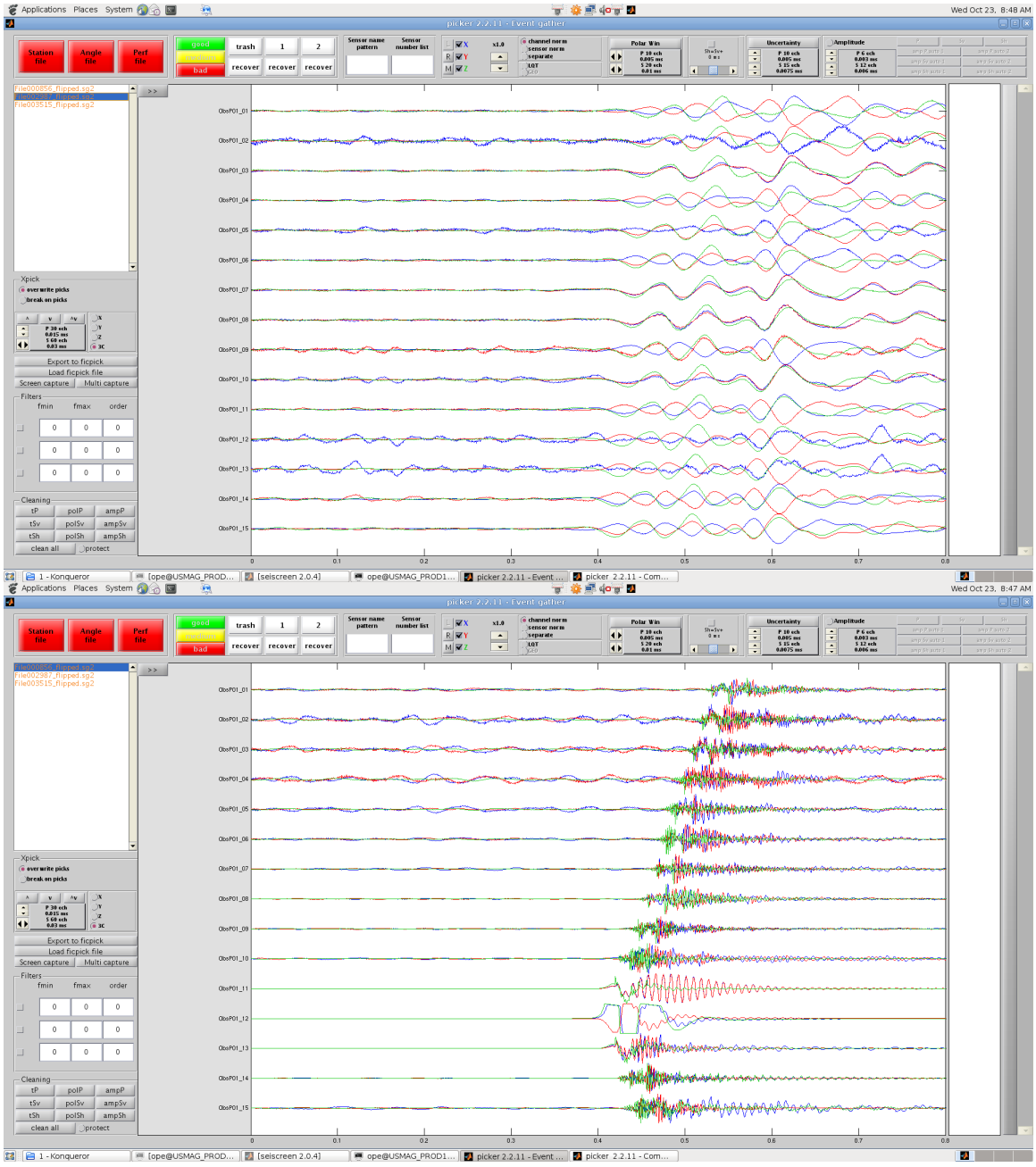


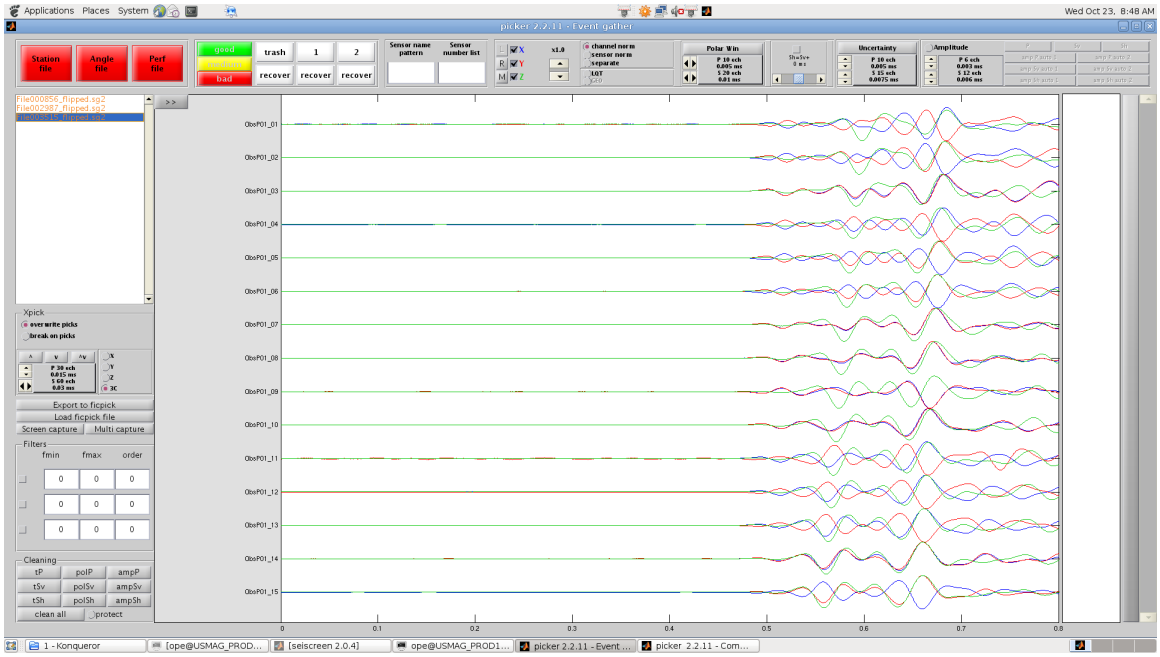
TOOL DEPTH 2: To monitor shales 4150 -4200 ft

The folloiwng diagram is the vibe shot used to orient the tools at this level. Note there is clear energy on both of the H axes.

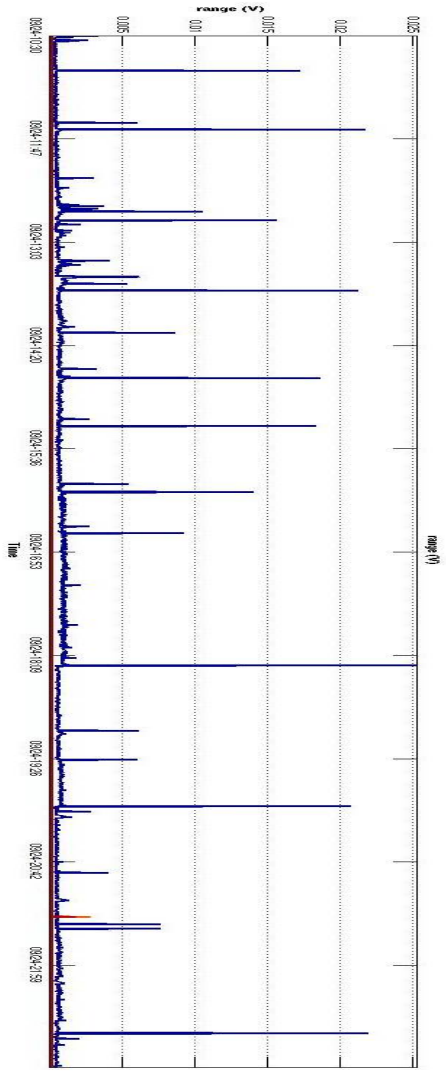


The following 3 examples are records from this level. In the first and third image there is some low frequency energy. This is not local microseismic energy. Note the linear moveout in the second image. That was something falling in the fluid column (e.g. bits of cement). It struck very near tool 12 and that noise propigated along the tool string. The other two records show back ground noise level.


Applications Places System
Wed Oct 23, 8:48 AM
picker 2.2.11 - Event gather
Station file
Angle file
Perf file
good
medium
bad
trash
recover
Xpick
over write picks
break on picks
Export to ficpick
Load ficpick file
Screen capture
Multi capture
Filters
fmin
fmax
order
Cleaning
clean all
protect
Wed Oct 23, 8:47 AM
picker 2.2.11 - Event gather



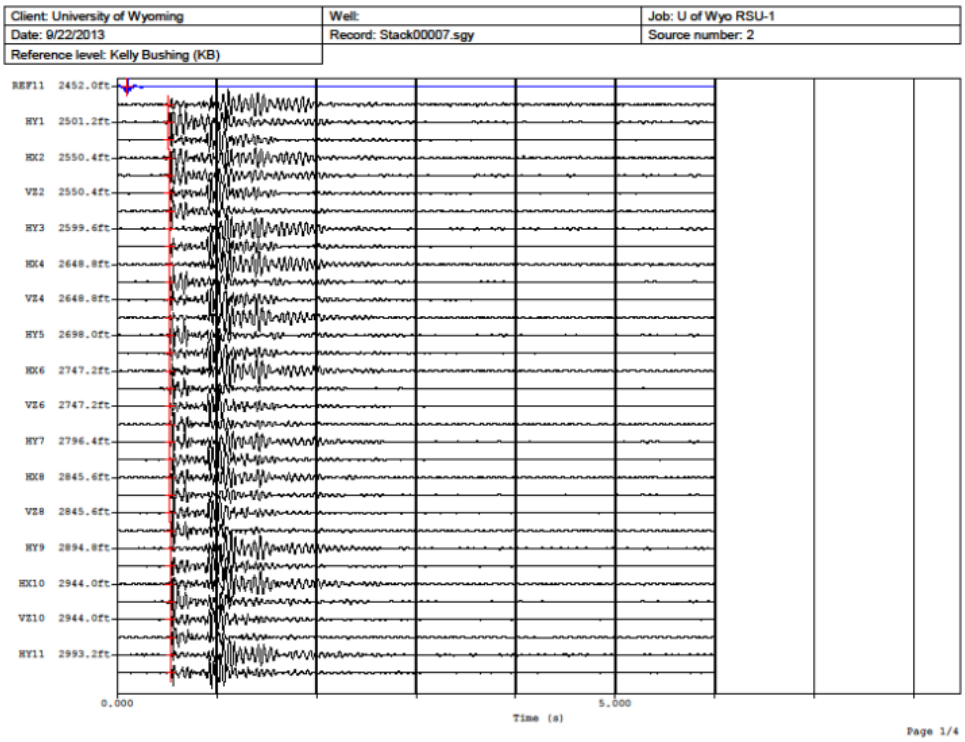
The following diagram is RMS noise levels for all records at this level


range (V)
0.005
0.01
0.015
0.02
0.025
09/24 10:00
09/24 11:47
09/24 13:33
09/24 15:20
09/24 17:06
09/24 18:53
09/24 20:39
09/24 22:26
09/25 00:12
09/25 01:59
Time
range (V)

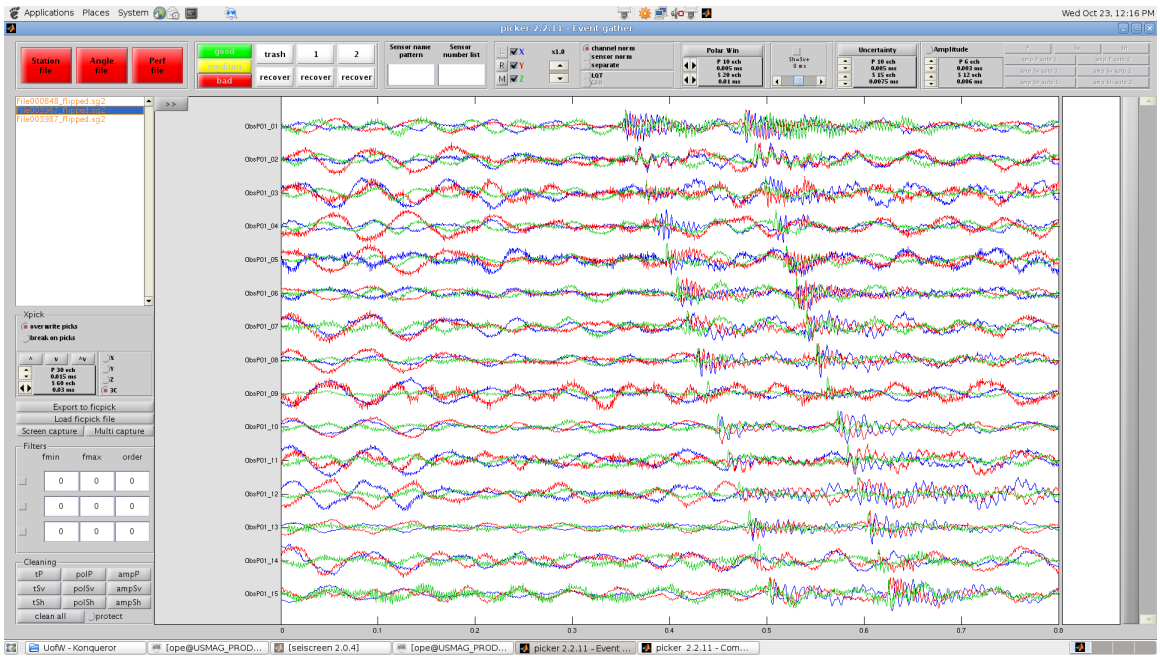
.

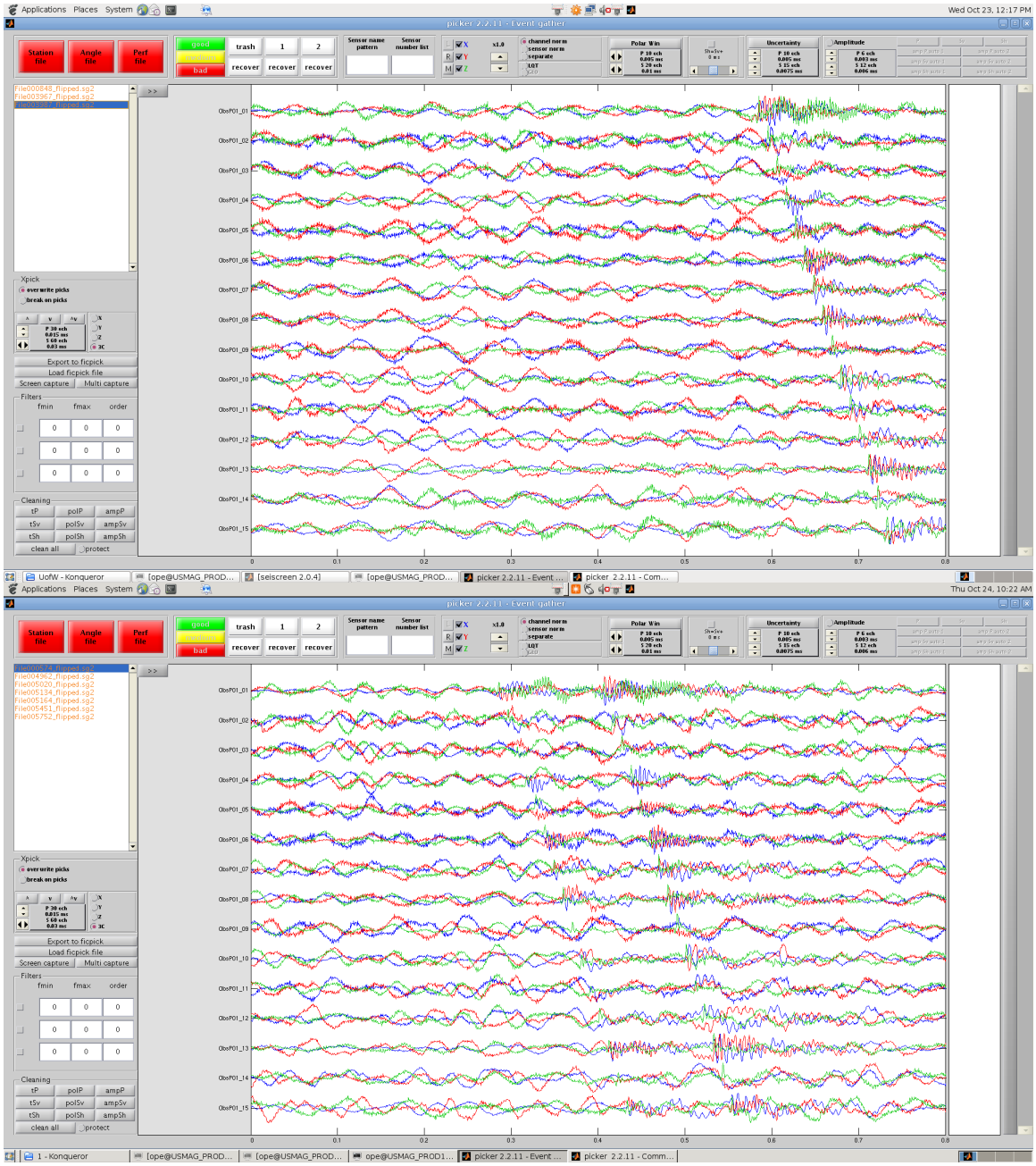
TOOL DEPTH 3: To monitor sands 3020 - 3090 ft

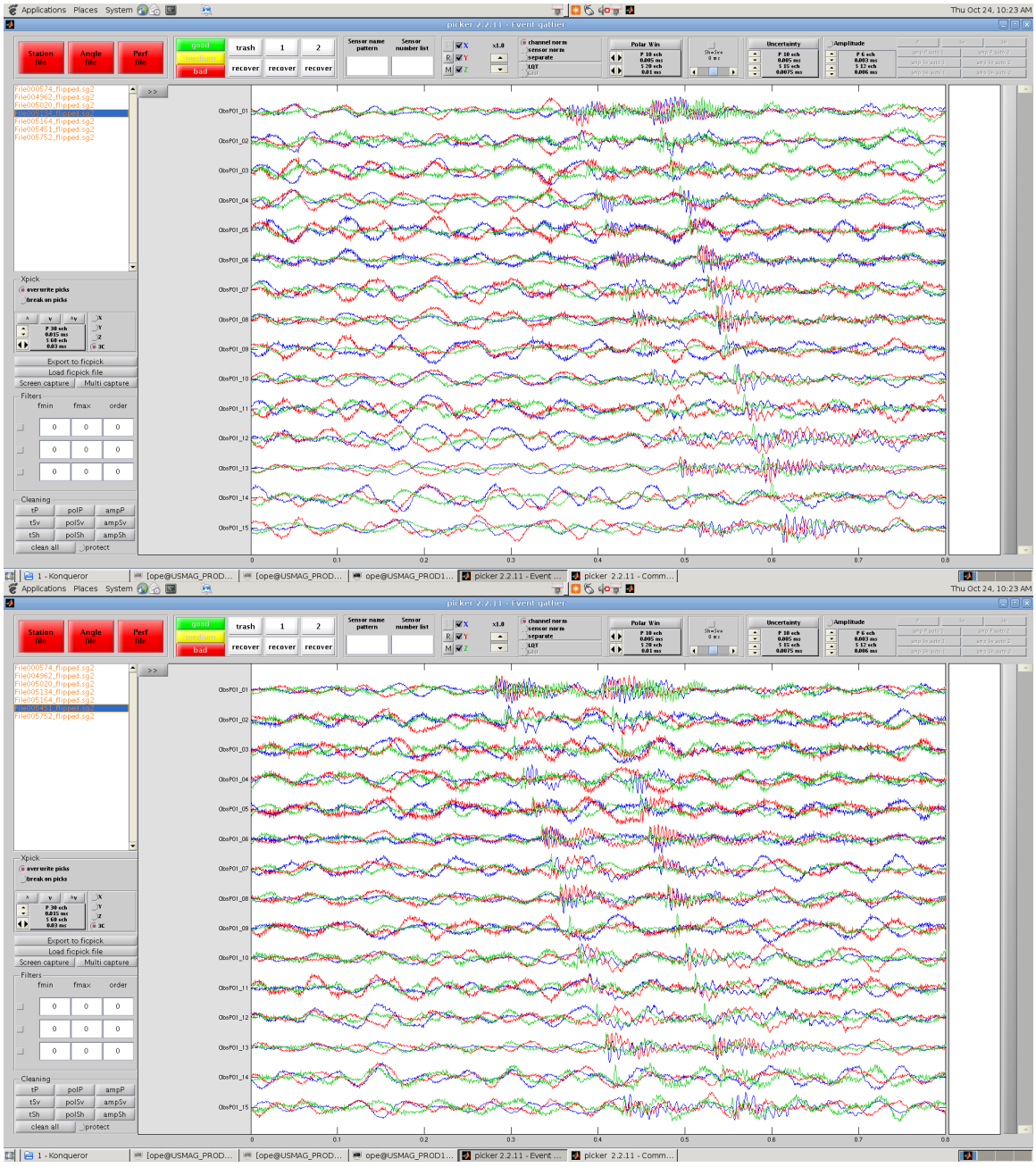
The following diagram is the vibe shot used to orient the tools at this level. Note there is clear energy on both of the H axes.



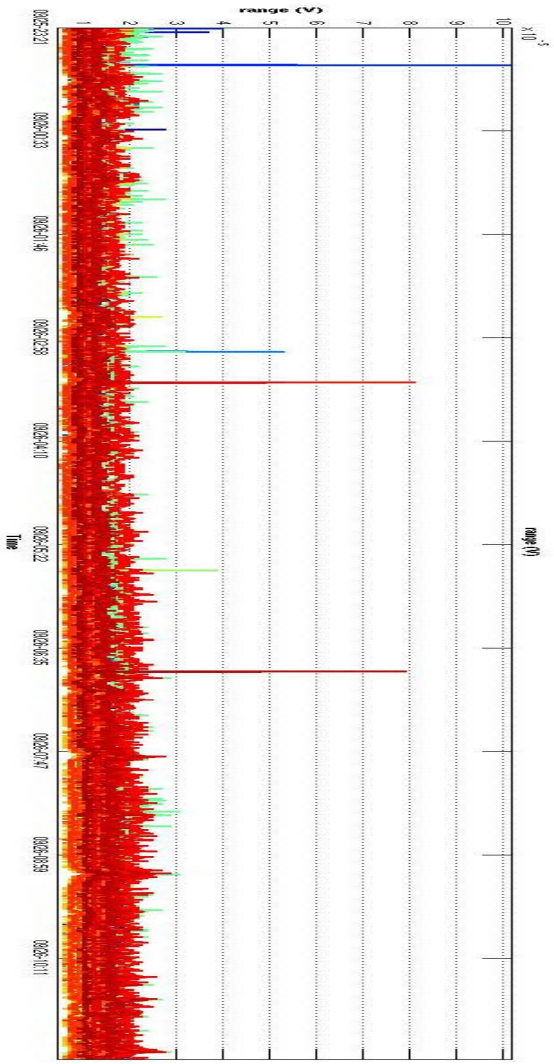
The following 5 examples are records from this level. In the images, all three axes are plotted for each tool (V, H1, H2). Note the linear moveout in each image. This is tube wave energy moving in the fluid of the well bore.




Applications Places System
Wed Oct 23, 12:17 PM
picker 2.2.11 - Event gather
Station file
Angle file
Perf file
good
medium
bad
trash
recover
Xpick
over write picks
break on picks
Export to ficpick
Load ficpick file
Screen capture
Multi capture
Filters
fmin
fmax
order
Cleaning
clean all
protect
Applications Places System
Thu Oct 24, 10:22 AM
picker 2.2.11 - Event gather

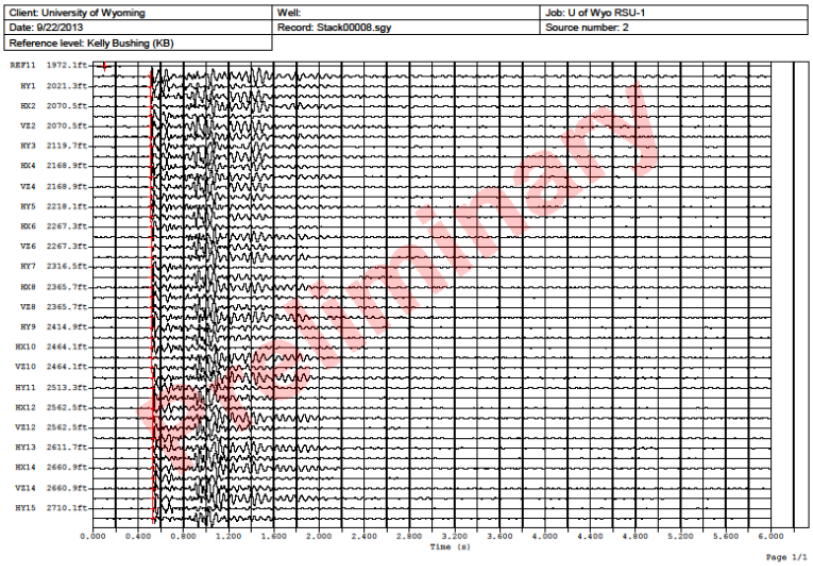


The following diagram is the RMS noise levels for all records of this depth.

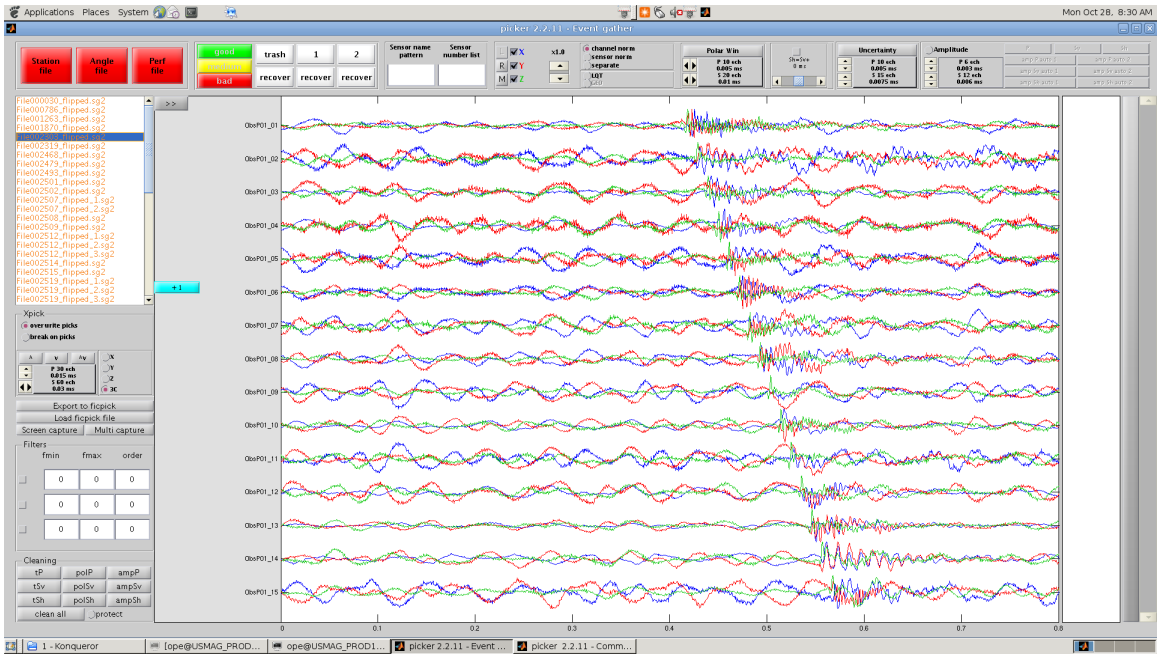

range (V)
Time
range (V)

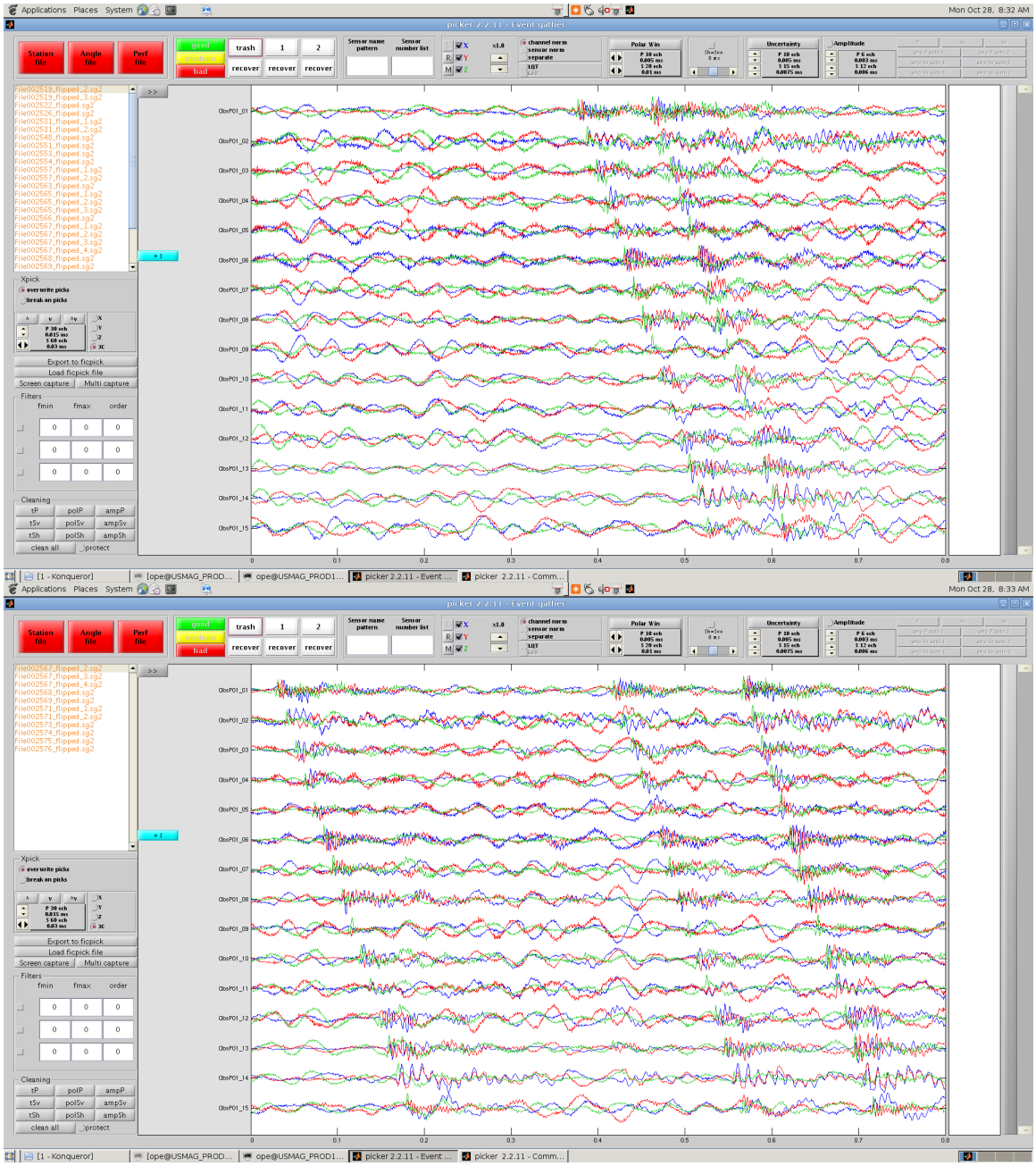
TOOL DEPTH 4: To monitor sands 2540 - 2610 ft

The folloiwng diagram is the vibe shot used to orient the tools at this level. Note there is clear energy on both of the H axes.

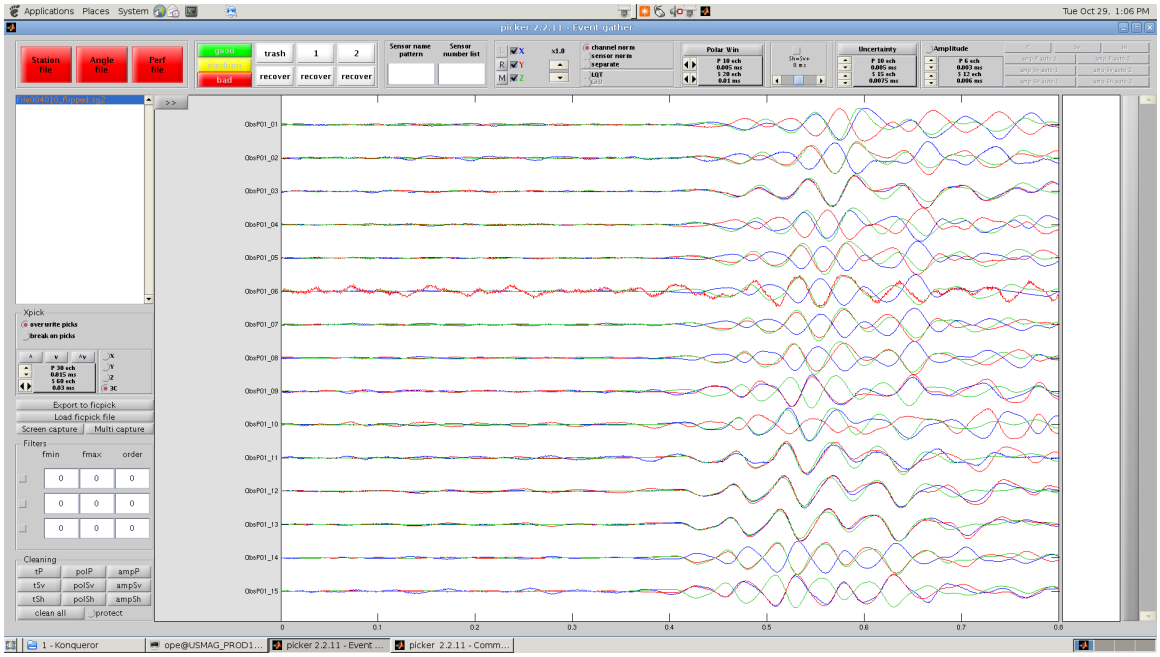


The following 3 examples are records from this level. Note the linear moveout in each image. This is tube wave energy moving in the fluid of the well bore. As before, linear moveout suggests noise traveling in well bore.

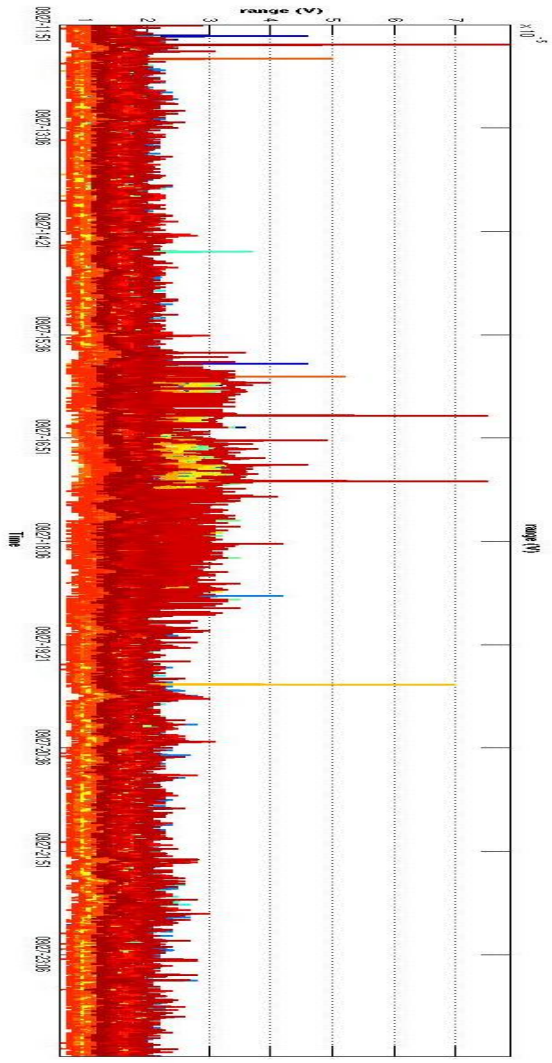




Note the low frequency noise in the folloiwng image. Again, not a microseism but an arrival nonetheless.



The following is the RMS noise for each file of this depth.



Summary

We monitored four levels in the RSU #1 well for microsiesmic activity over a seven-day period. While triggers – potential microseismic events – were detected at all levels, careful inspection demonstrated these were tube waves moving in the well bore fluid, which is common in microseismic monitoring. We also calculated Vrms noise levels for each record at each level. As expected, as we moved shallower in the well, noise levels grew larger.

Appendix A: Recording Network Characteristics

Sensor specifications

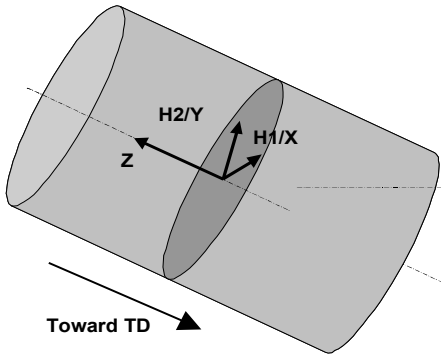
According to the specification sheets of the microseismic tool provider, all sensors of the microseismic array are:

Provider:	Sercel-Maxiwave
Type:	Omni 2400
Natural Frequency:	15 Hz
Sensitivity:	.52V/cm/sec

3C-sensor polarity

According to the tool provider, the three components of each satellite are as follows:

- Z (or HUp) = along hole, pointing upward,
- X (or H1) = perpendicular to Z,
- Y (or H2) = such as X, Y and Z form a right-normal basis.



Since the monitoring well is vertical, the Z component of each sensor is vertical.

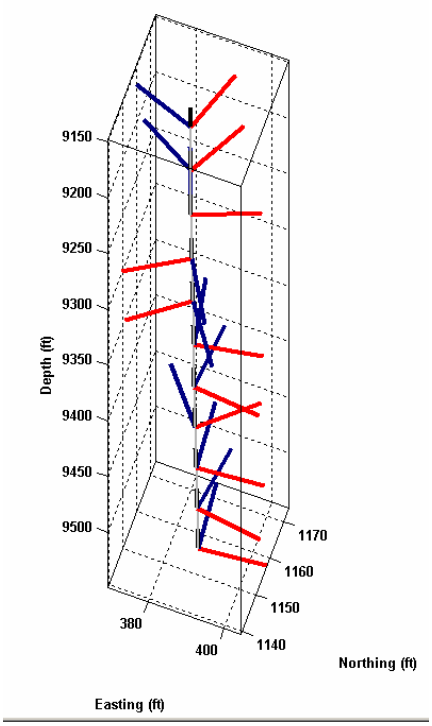
3C-sensor orientation

In order to orient the 3C-sensors deployed in observation well, the known locations of the perforation shots carried out in treatment well and recorded by the microseismic network are used. The orientation of the receivers was determined by:

1. Measurement of the polarization of the first arrival (P-wave) generated at the source point for one 3C-sensor and one shot (one seismogram);
2. For the same 3C-sensor/shot couple, compute the expected polarization of this wave using the velocity model; and
3. Minimize the differences between both polarization vectors by rotating the station. The final orientation angles represent the spatial orientation of X, Y and Z components of the station geophones.

In our context, the orientation of the 3C-sensors was performed jointly with the calibration of the velocity model.

Methodology example



Appendix B: Velocity Model

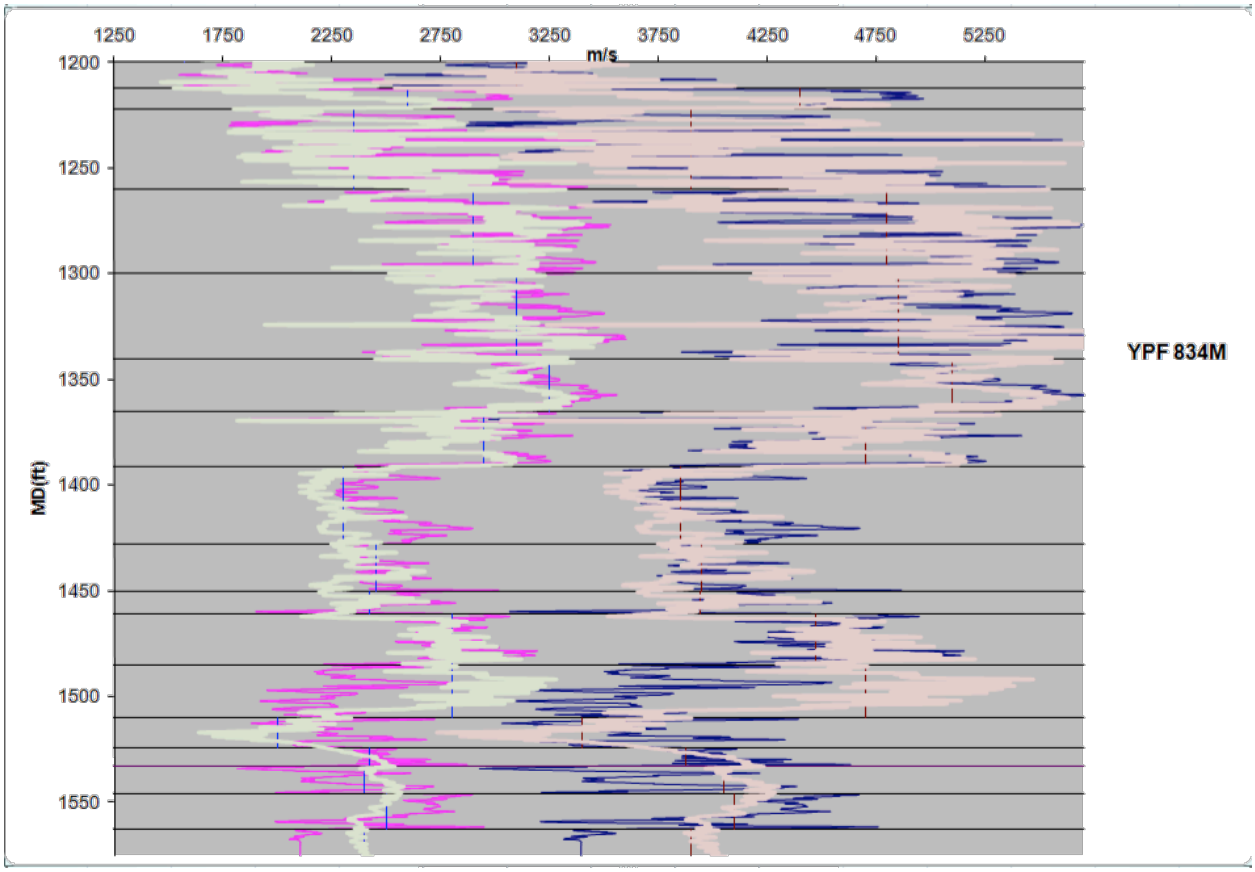
Standard velocity model

In general, 1D (or horizontal) layered media are considered for hydraulic fracture job processing.

Log smoothing

The velocities or slownesses of the acoustic logs were smoothed to create the velocity model. We used a median filter ranging between 100- and 300-Hz to smooth the acoustic logs (selected from the expected frequency content of the microseismic events).

For this project we used the perforation shot calibrate the velocity model. This source point was also used to orient the 3C-sensors (see previous section “3-C sensor orientation”).



Inversion Velocity Model

In order to correctly calibrate the “new” velocity model, we performed a joint inversion of both the velocity model, the orientation of the 3C-sensors and the perforation shots, using a simulated annealing technique. The method is based on the minimization of the perforation re-location errors.

The inputs to the inversion were the P- and S-wave perforation arrivals. The free variables were the sensor orientations (with Z-axes fixed along the wellbore), the P- and S-wave velocities for each layer (both P & S vary) and the layer interface depths. A solution minimizes the difference between the actual and the calculated perforation locations.

Appendix C: Microseismic Event Selection

Methodology

The objective of this section of the processing is to discriminate between seismic events and noise.

Magnitude's Screening Protocol is:

- Manual random screening of the complete dataset of records. During this phase, the seismologist screens the seismograms and learns to recognize microseisms as opposed to the different types of noises. For fracture monitoring, most events appear as shear-slip events exhibiting P- and S- wave arrivals;
- Subsequent to the random screening, automatic screening is carried out to pre-select microseism candidates and reject noise;
- Manual review of the screened events is performed to extract the actual microseisms;
- Manual picking of P- and S- arrival times are done, helped by the "multiplet" method, which uses spectral correlation with reference events.

Automatic microseism detection

To select events among a raw dataset, this is done by checking wave arrivals consistency on several geophones rather than classical channel-by-channel triggering. Indeed if a microseismic event occurs:

- It will be recorded by more than one geophone;
- Wave arrivals will be consistent from one channel to another one.

Automatic screening is based on the chirplet theory for the signal processing and on a STA/LTA algorithm for the detection itself. This is taking into account:

- The geophones network, in terms of expected wave arrivals delay;
- The kind of events expected, in terms of waveform and main frequency.

Figure 1 illustrates the general workflow for event screening.

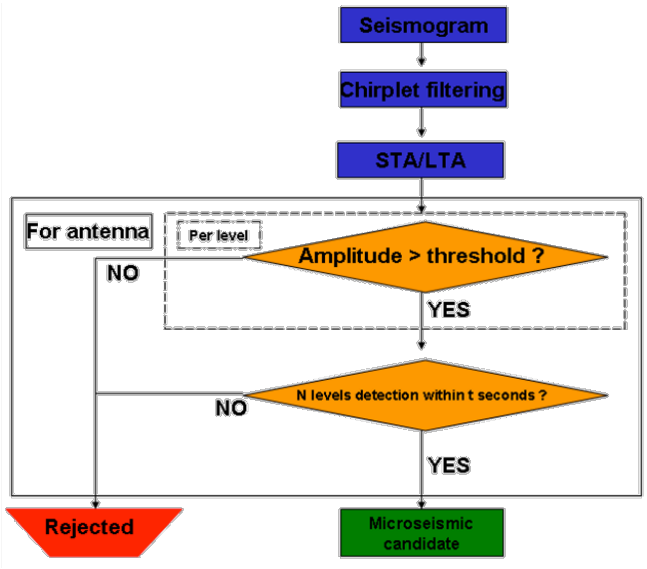


Figure 1: Flow chart of the automatic detection process

Validation of microseismic candidates

To confirm that the selected events correspond to a microseismic event, key characteristics are used to describe the signal of interest (SI). These characteristics answer the following questions:

- Does the SI reach all stations of the antenna (Answer should be yes for expected shear-slip events)?
- Is the polarization of the SI constant over all stations, in their own coordinate system (It must not be the case for shear-slip events)?
- Is the polarization of the SI constant in time, or is it function of time (It should not be constant for a shear-slip event since P- and S-waves have different polarizations)?
- Has the SI a wide frequency range or is it monochromatic (It should not be monochromatic for shear-slip events)?
- What is the main frequency of the SI?
- Is the SI longer than the recording window size? In other words, is it a finite or an infinite signal duration?
- Does the SI present an impulsive or an emergent onset?

These seven keys are used to rank the probability of an individual candidate event as a valid microseismic event.

Appendix D: Microseismic Data Processing – Including SRV

Background 3D Microseismic Processing Methodology

Introduction

The microseismic event locations remain challenging. It is mandatory to improve the accuracy and reliability of those locations since it is the base of any further processing and interpretation. Even if the velocity model is the main question mark, the reliability of the location methodologies needs to be improved. Location methods can be separated in two categories.

The first one is the conventional picking method, which is based on P & S waves detection and picking and on polarization measurement. This procedure requires to be fully performed by the geophysicist and is therefore time-consuming. In addition, it will only provide reliable results if the signal to noise ratio is good enough to pick arrival times and measure polarizations. Because of that, only a fraction of the detected events will be located and the polarization uncertainties result in inaccurate locations.

The second category consists of the automated methods based on the full waveforms. These methods have historically been developed for dense surface arrays monitoring. They are based on stacking traces shifted in time to perform the joint detection and location of events. But recently, these waveform based methods have been updated to be used even with sparse networks or geophones strings deployed in boreholes (Fuller et al. 2007, Gharti et al. 2010). These methods allow detecting and locating more events than the manual picking based ones, in a faster way. However, like every fully automated methods, the main drawback is the lack of accuracy and reliability of locations.

In this paper, we propose a new composite methodology, called assisted-migration method, based on a combination of automatic waveform-based and manual-picking-based methods. By doing this we expect to get the efficiency of waveform based methods, but also the reliability brought by human control and correction.

Method

Picking based method:
The reference picking method we use is a grid-search probabilistic method based on the P and S wave arrival times and P and/or S wave polarizations (Bardainne and Gaucher 2010). A likelihood location function is obtained by comparing the real measurements (picked arrival times and polarizations) with the theoretical ones at every node of the model.
Automatic migration:
The automatic method we developed is a 3C migration of P and S waves (Bardainne et al. 2009). Figure 1 summarizes the process, which consists in a 4D grid search (systematically or randomly explored) of a migration likelihood function. For each analyzed 4D "position" (t0, x, y and z), seismograms are first rotated along the theoretical wave coordinate system. They are then shifted in time according to P-wave (for L component) and S-wave (for R and T components) theoretical arrival times. Finally the seismograms are stacked. The likelihood function is based on the energy of this summation.
Thanks to the signal to noise ratio improvement due to the stack, the polarization (and time) "measurements" are generally more accurate and allow handling low signal-to-noise-ratio events.
Assisted Migration:
The Assisted-Migration consists in verifying and / or correcting the picking deduced from the automatic migration location. If the resulting pickings are modified, a new location combining migration, arrival time picking and polarization measurement is performed. Figure2 illustrates the results obtained with a full migration method (2/a) and with an assisted-migration method (2/b). The full-migration correctly identified and picked the first P-wave motion, but only identified the second motion of the S-wave, because of the S-wave splitting (due to an anisotropy effect). The geophysicist controlled and picked the first motion of the S-wave, allowing the assisted migration to correctly relocate the event during the second run. This method handles datasets obtained on sparse, string or multi-string networks. The weight ratio between the picking based likelihood function and the migration likelihood function is related to the ratio between the number of manual pickings and the total number of sensors.

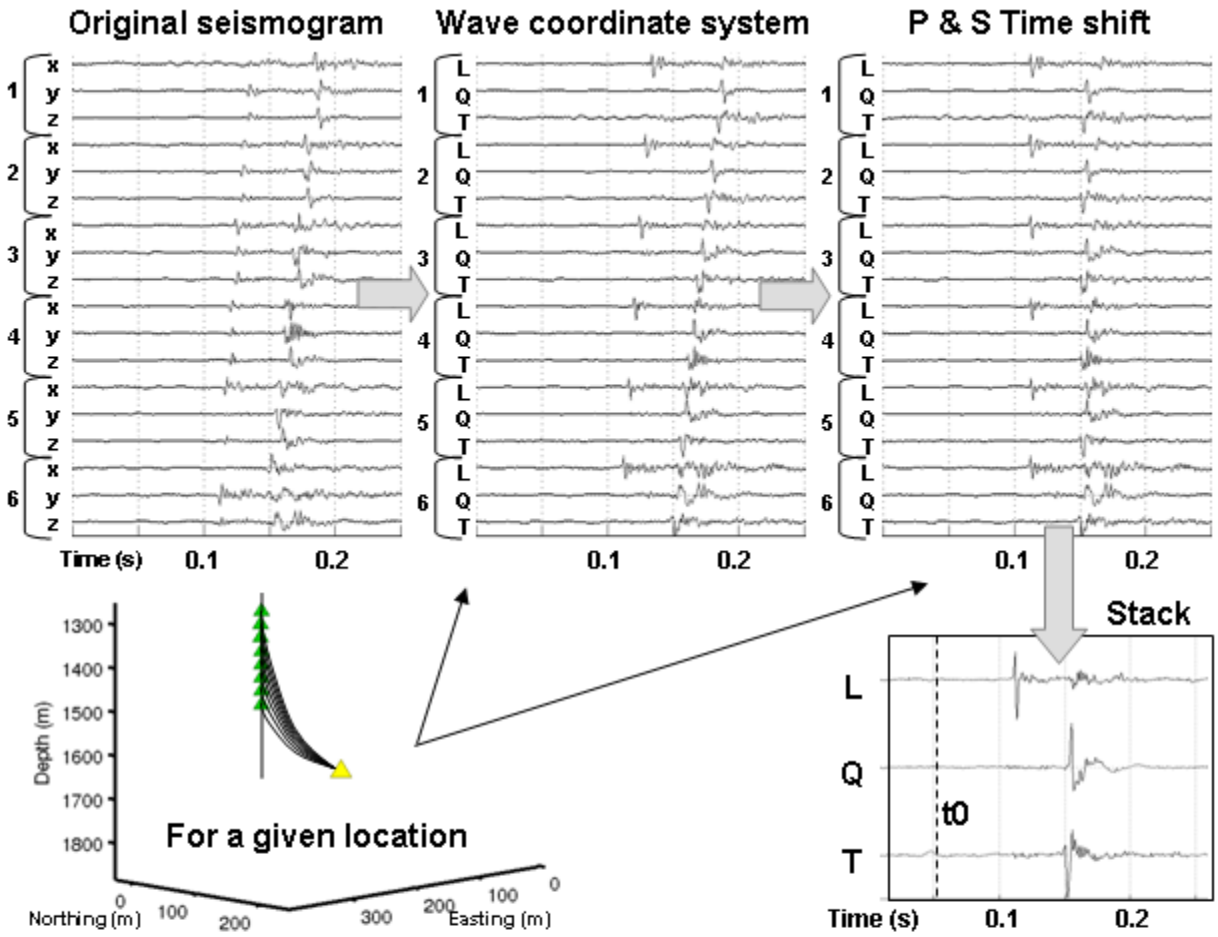


Figure 1 For a given position, the seismograms are (1) rotated in the theoretical wave referential, (2) shifted in time according to the P&S theoretical arrival times and (3) stacked.

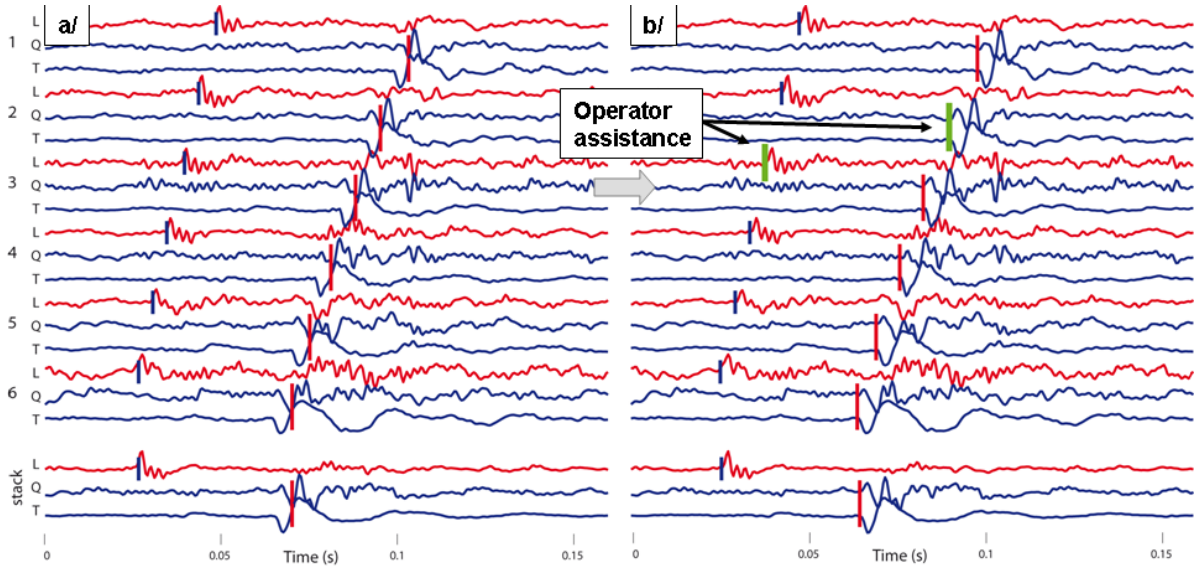


Figure 2 Resulting pickings from migration after a/ automatic migration and b/assisted migration. The result of the automatic process was not satisfying because of the anisotropy splitting that resulted in a late picking. Operator assistance consisted in correcting one of the bad S picking but also in improving the P-wave picking accuracy. It improved the resulting location.

Two main limitations exist. First, the migration techniques are velocity model dependent. Basically, a wrong velocity model induces wrong rotations and time shifts, resulting in a poor summation. In the same way, very complex waveforms can lead to miss the detection of the first wave motion. Then, it is very difficult to deliver and estimate of the location uncertainty. Indeed, the uncertainty volumes determination involves a very time-consuming systematic grid-search.

Example case study: a fracturing job microseismic monitoring

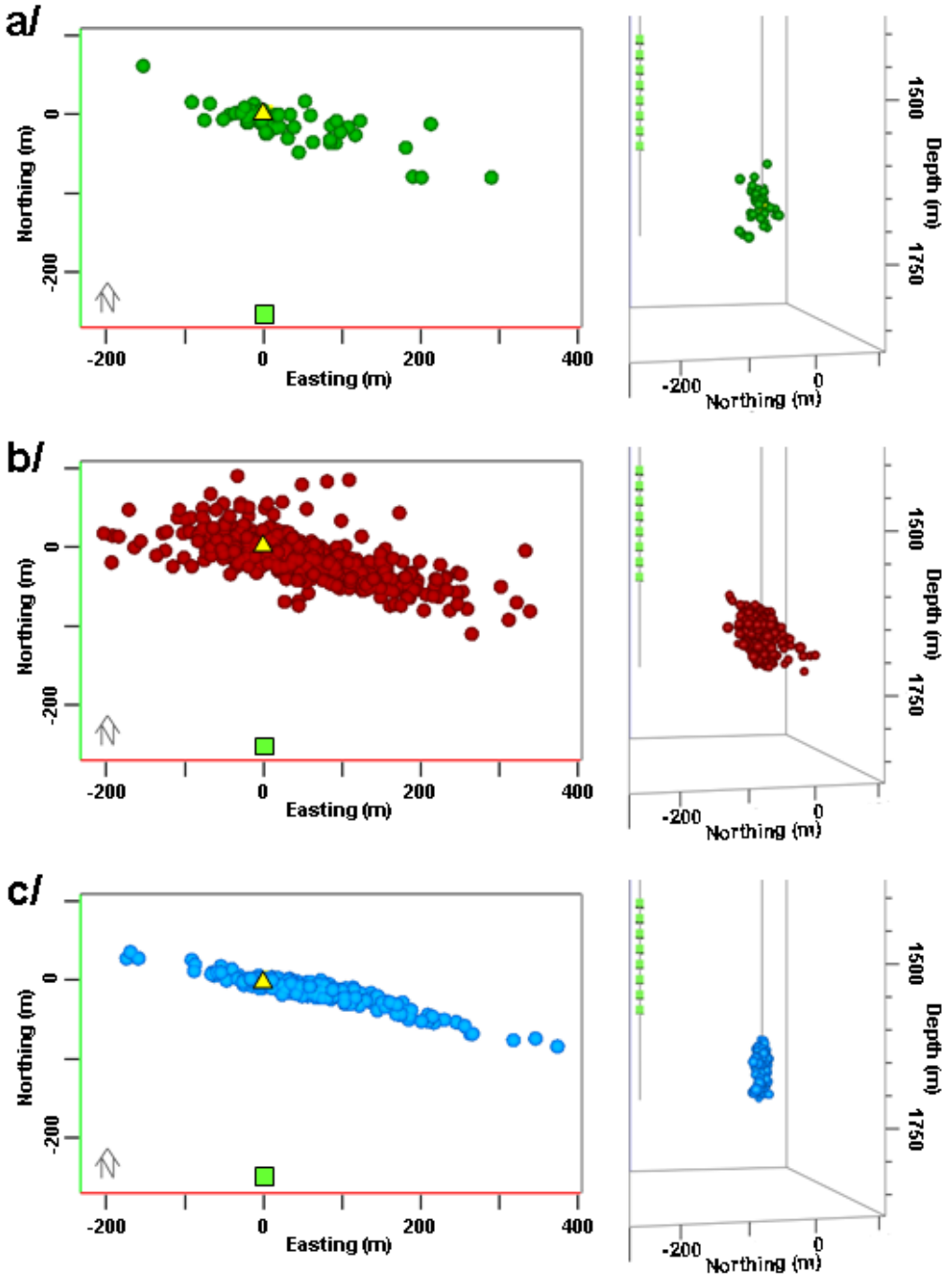


Figure 3 Microseismic events located during a hydraulic fracturing job using (a) conventional picking based method displayed in green, (b) automatic 3C P&S migration in red and (c) assisted 3C P&S migration in blue. Results are shown in a map view on the left and 102°N cross section view on the right. Sensors are displayed with green squares; injection point is displayed with a yellow square.

Stimulated Reservoir Volume (SRV) Estimation

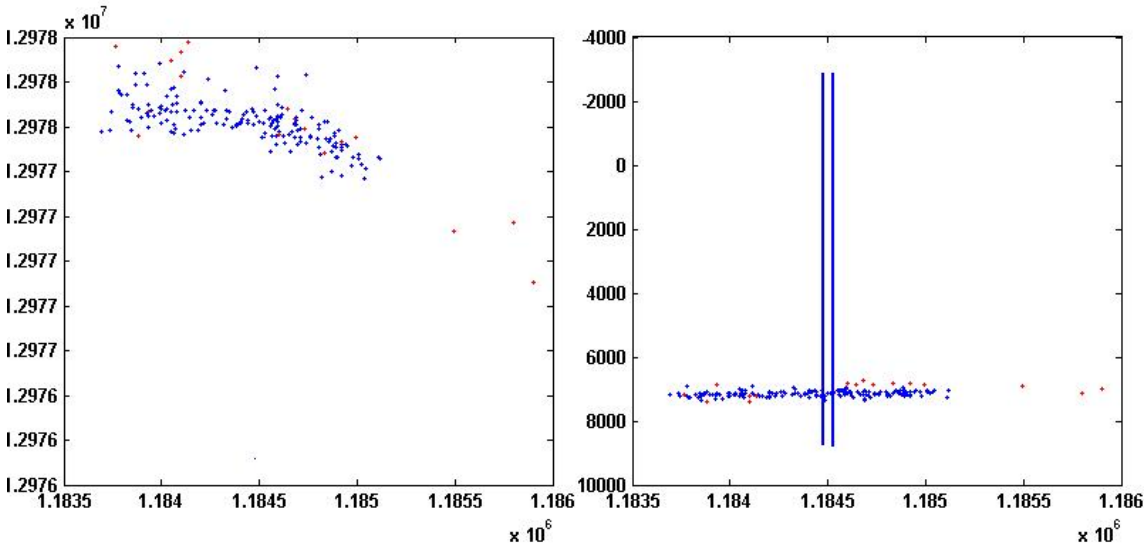
The SRV represents an estimate of the volume of earth over which there was sufficient stress release to induce microsiesmic activity. It is important to recognize that the SRV determined from microseismic analysis will always be larger than the volume of earth in contact with treatment fluids and propant. This is because microseisms are manifested when there is sufficient induced stress by the treatment to cause slippage in the formation. This stress release is believed to occur largely beyond the location of fluids and propant. Some authors have suggested this volume may be as much as 2 to 5 times larger than the actually contacted volume of rock.

Methods of Calculating SRV

Outlier Elimination – Chauvenet's Criterion

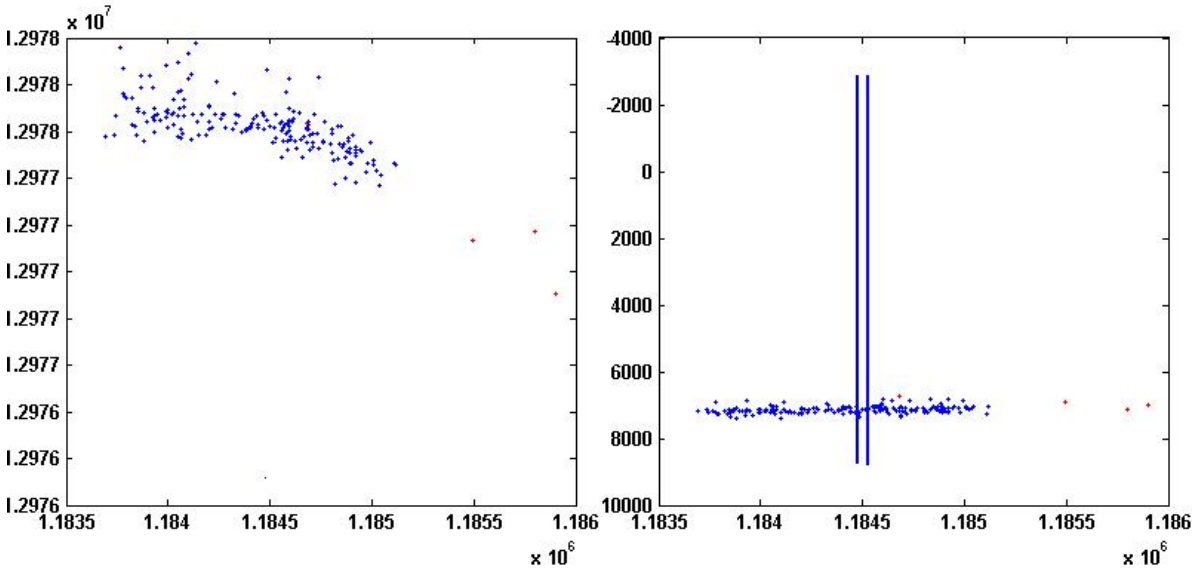
- This is the standard statistical criteria for outlier elimination in scientific datasets
- The *erfc* (complimentary error function) is calculated for each coordinate of each event.
- This is compared to a set value (0.5) and if it is less, the event is flagged as an outlier

This process is iterated until no outliers are found



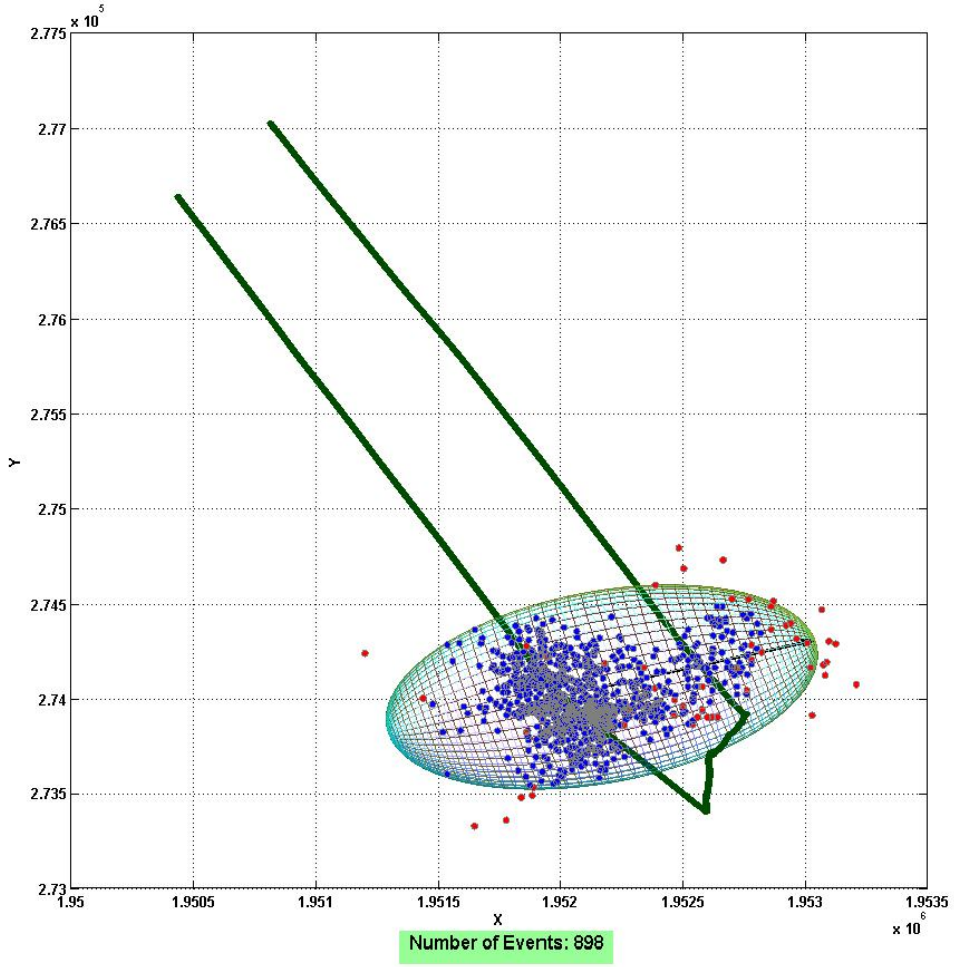
Outlier Elimination - 3σ Method

- The standard deviation for each coordinate set is computed
- For each event, the difference between its coordinates and the standard deviations are computed
- If this difference is greater than 3σ, the event is flagged as an outlier



MVE (Minimum Volume Ellipsoid)

- Calculate the Löwner MVE matrix
- Eigenvectors are the axes vectors of the ellipsoid
- Eigenvalues are the half-lengths of the axes.
- Plot the Ellipsoid

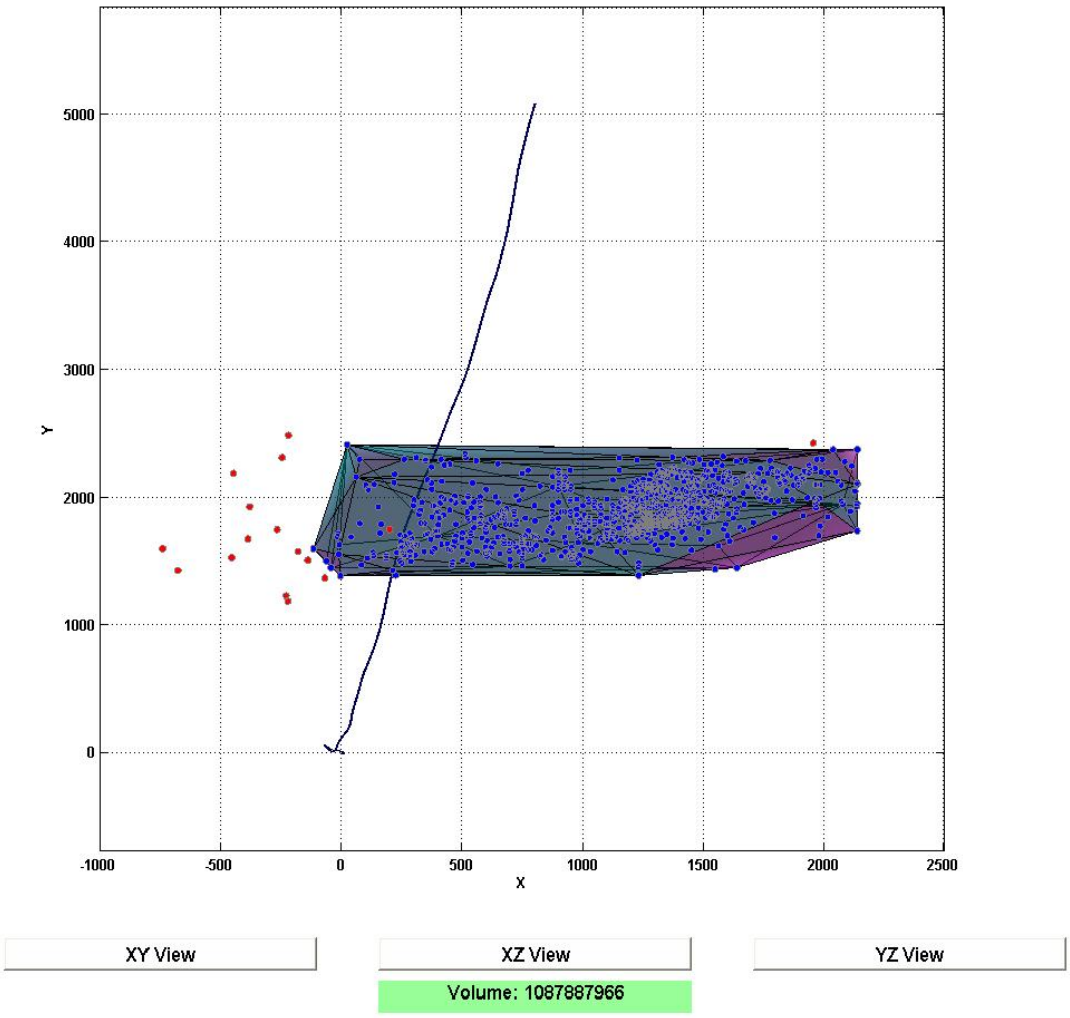


XY View | XZ View | YZ View

Half-Length: 906 | Volume: 656907753 | Major Axis Length: 1812 | Minor Axes Lengths: 1005, 689 | Azimuth: 16° N of E

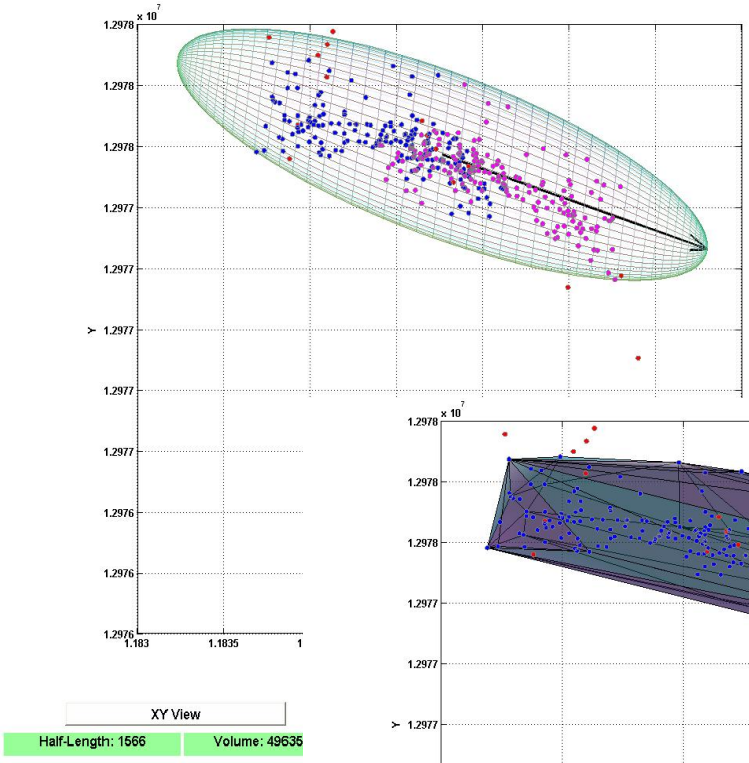
Arbitrary Polygonal Minimum Volume

- Convex hull method is used to identify boundary events
- A minimum polygonal surface is plotted between this subset of events
- Enclosed volume is calculated.

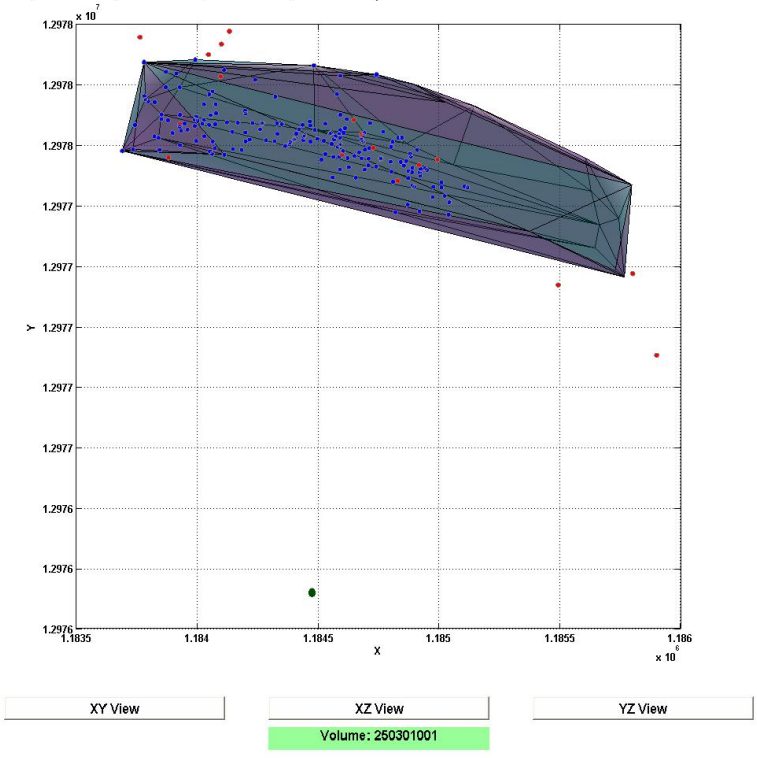


Assuming Symmetry

- If appropriate, symmetry about the wellbore can be assumed
- The plane of symmetry is computed
- Events are reflected across this plane
- New surface is calculated based on the set of real and reflected events
- The reflected events may be plotted in a different color, or suppressed



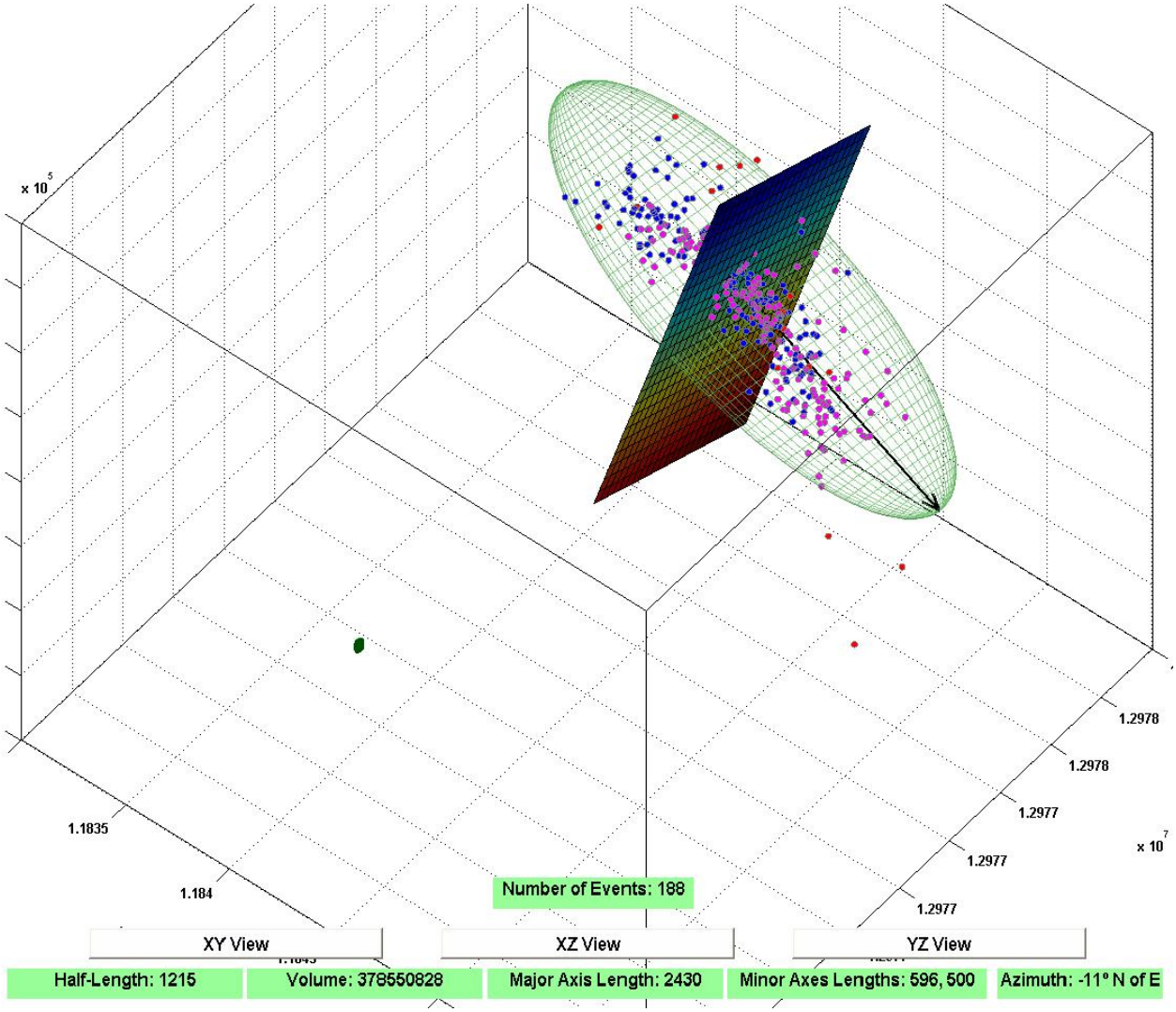
Outliers are plotted red,
Reflected events purple,
Normal events blue.



Calculating the Best Plane of Symmetry

- A dummy MVE is calculated
- The plane is assumed to be parallel to both minor axes and orthogonal to the major axis
- The plane is moved along the major axis until the intersection of the plane and the axis and the intersection of the plane and wellbore is minimized.
- This is considered the best plane of symmetry

The vector between each event and this plane is then calculated, and twice this vector is subtracted from the event to reflect the event.



Appendix E: Sensor Orientation Method

Measured polarization

For one 3C-sensor/shot couple:

To estimate the polarization of the first arrival, we compute the 3D space distribution of the signal energy around the P-wave. Mathematically, we compute the auto-covariance matrix of the X, Y and Z components around the P-wave arrival. The spatial distribution of the energy is then displayed as an ellipsoid (see Figure 2). Under the assumption that this ellipsoid is a straight line (l_2 and l_3 nearly null), which assumes the signal linearity is close to 1, the normalized vector $\mathbf{V_1}$, corresponding to the highest eigenvalue, will be the measured polarization vector and shows the direction from which most of the energy arrives.

If $\mathbf{X}_{ij}$ is the amplitude vector (on X, Y and Z components of the 3C-sensor) at sample *i* for the 3C-sensor number *j*, then the covariance matrix is defined by its coefficients:

$$\mathbf{C}_{jk} = \frac{1}{n-1}\sum_{i=1}^{n}\left[\mathbf{X}_{ij} - \text{mean}_i(\mathbf{X}_{ij})\right]\left[\mathbf{X}_{ik} - \text{mean}_i(\mathbf{X}_{ik})\right]^T$$

If $j=k$, only one 3C-sensor is involved and we compute an auto-covariance matrix,
If $j \neq k$, two 3C-sensors are involved and we compute a cross-covariance matrix.

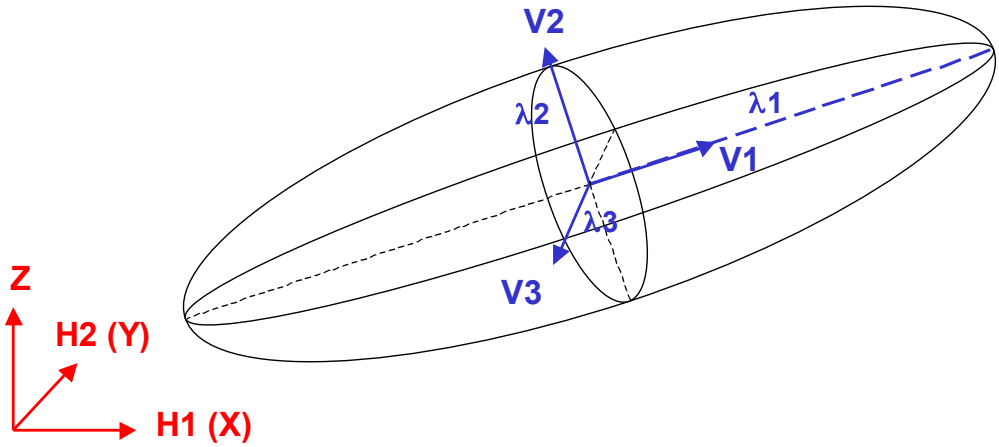


Figure 2. The 3D space distribution of the energy around the P-wave is compared to an ellipsoid. This ellipsoid has semi-axes of size l_1, l_2 and l_3 in the V_1, V_2 and V_3 (orthogonal) directions. Since $l_1 \geq l_2 \geq l_3$, most of the energy is oriented along V_1 direction. Mathematically speaking, V_1 is the eigenvector of the auto-covariance matrix which corresponds to the main eigenvalue, l_1. The polarization vector refers to V_1, but as shown, this makes sense only if l_2 and l_3 are small compare to l_1.

Expected polarization

For one 3C-sensor/shot couple:

Our task is to estimate the polarization the P-wave should have at the sensor, if induced at the source point *n* and after propagation in the earth. We assume the ray propagation theory. We compute the polarization vector from known sensor and source locations, as well as the details of the velocity medium. The possible cases are:
The velocity model is homogeneous: in this case, the expected seismic ray azimuth and inclination are modeled by the straight line between the sensor and the source locations,
The velocity model consists of horizontal, stacked layers: in this case, the expected seismic ray azimuth is modeled by a straight line between the sensor and the source locations; we use Snell's law to model the inclination,
The velocity is complex: in this case, we must compute the expected polarization by some ray-trace or inversion method.

Inversion method

For one 3C-sensor/shot couple, we measured the P-wave polarization and we know which one was expected. If the hypotheses supporting our expected polarizations are correct, there is only one 3D rotation which fits our assumptions, moreover, this rotation should remain the constant for each 3C-sensor for all source-points.

The problem can be formulated as:

Find $\gamma, \beta, \varphi,$ such that: $\left(\mathbf{R}_{\mathbf{Z3}}(\gamma)\mathbf{R}_{\mathbf{X2}}(\beta)\mathbf{R}_{\mathbf{Z1}}(\varphi)\mathbf{L}-\mathbf{P}\right)^{-1}\left(\mathbf{R}_{\mathbf{Z3}}(\gamma)\mathbf{R}_{\mathbf{X2}}(\beta)\mathbf{R}_{\mathbf{Z1}}(\varphi)\mathbf{L}-\mathbf{P}\right)$ is minimum.

With:

L: matrix of the expected polarization vectors,
P: matrix of the measured polarization vectors,
$\gamma, \beta, \varphi,$ the 3 rotation angles such that

$$\mathbf{R}_{\mathbf{Z}i}(\alpha)=\begin{pmatrix}\cos(\alpha) & \sin(\alpha) & 0\\ -\sin(\alpha) & \cos(\alpha) & 0\\ 0 & 0 & 1\end{pmatrix}$$ is a matrix defining a rotation orthogonal to axis Z

$$\mathbf{R}_{\mathbf{X}i}(\alpha)=\begin{pmatrix}1 & 0 & 0\\ 0 & \cos(\alpha) & \sin(\alpha)\\ 0 & -\sin(\alpha) & \cos(\alpha)\end{pmatrix}$$ is a matrix defining a rotation orthogonal to axis X

(X, Y and Z define the Cartesian basis)

The application of the 3 rotation matrices, one after the other, on a vector, can define any rotation in the 3D space.

For one 3C-sensor/shot couple, only one solution is possible and **L** and **P** are vectors. But, for one 3C-sensor and many shot points, we will minimize this cost function (in the least-squares sense), and **L** and **P** are matrices of vectors. In many cases, the Z component of all 3C-sensors is aligned with the well and for a vertical well, points upward. This allows us to fix two of the three angles to rotate (φ and β) and invert for the third one only (γ).

Appendix F: Event Location & Uncertainty

ONLY FOR P and S WAVE PICKING LOCATION METHOD. DOES NOT APPLY TO MIGRATION PROCESSING

The input data for event location determination are the P- and S-wave arrival times. Additionally, P-wave polarization may be used, either the azimuth or/and the inclination of the incoming ray at each sensor.

Location method

We typically use a grid search method.

The theoretical ray parameters are computed in a 3D velocity model using ray tracing based on the 3D Eikonal method and/or a wavefront propagation method. Solution parameters consist of 3D travel-time maps of seismic body waves and the 3D polarization maps of the P-wave arrival. The best fit between the measured or observed data and the theoretical arrival times determines the event location.

Location uncertainty

The uncertainty of the location is quantified by a probability density function (PDF). The shape and distribution of the PDF, which takes into account the uncertainties in the arrival picks and in the P-wave polarization, illustrates the location accuracy shape. The event hypocenter is defined as the maximum of the PDF.

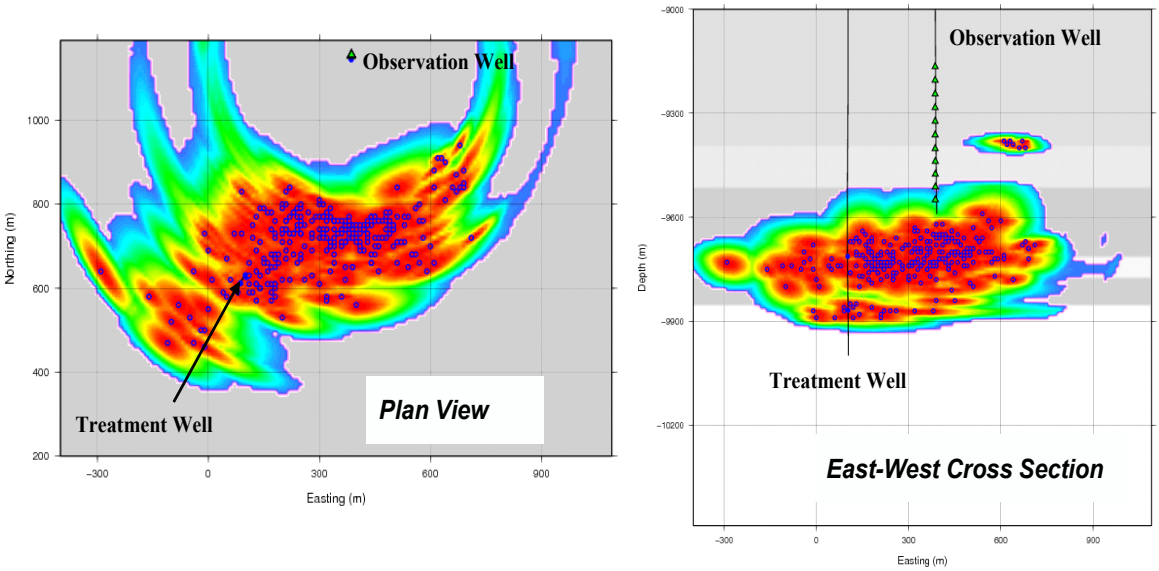


Figure 3. PDF plan view map of location uncertainties for Stages 1 & 2. Red contour encloses a probability of 68.3%.

The PDF represents a probability distribution that theoretically ranges from a maximum of 100% (no uncertainty) and 0 (no certainty). PDF distributions shown for the HH Gill wells are contoured at intervals of 1 σ. The area contoured in red represents a location uncertainty of 68.3% (1 σ).

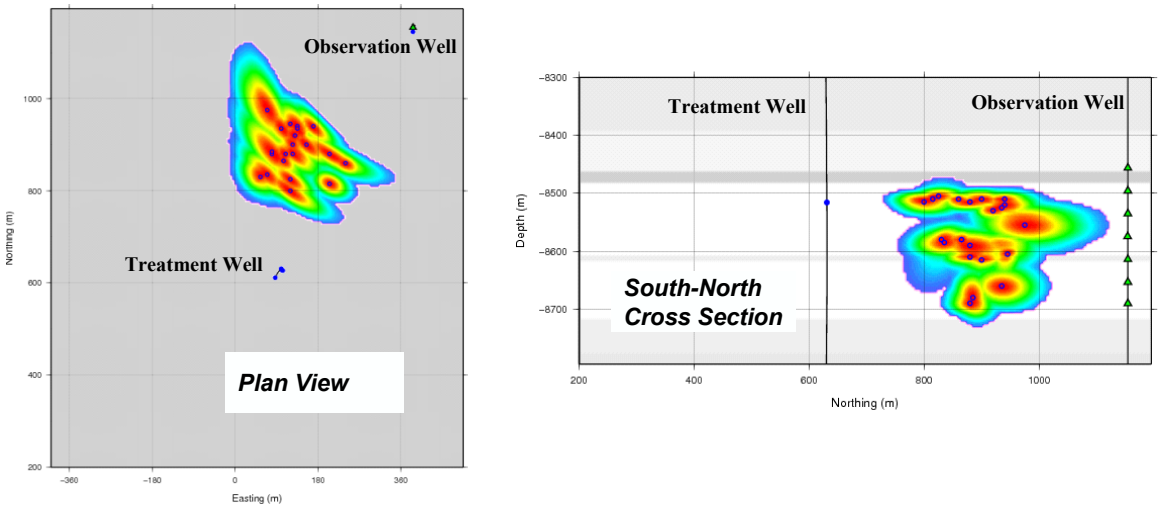
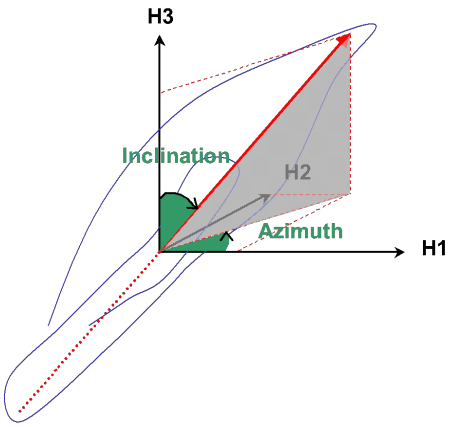


Figure 4. PDF plan view map of location uncertainties for Stage 4. Red contour encloses a probability of 68.3%.

Appendix G: Nomenclature & Conventions

Polarization analysis & angles

The polarization analysis consists in measuring the spatial distribution of a 3C (right-normal basis) signal over a time window using the covariance matrix. Most of the time, the results used are the "azimuth" and the inclination of the distribution main direction which is defined by a vector.



In that case, the azimuth means the anticlockwise and horizontal angle between the 1st axis or H1 component and the main direction. Units are degrees and measurement conventions usually specify H1 to H2 (°H1toH2).

The inclination is the angle between the 3rd axis or H3 (in general the "vertical" component) and the main direction. Units are degrees and measurement conventions usually specify H3 to Horizontal (°H3toH).
On the main direction vector, a ±1 factor can be applied. This allows us to rotate the azimuth and inclination accordingly.

Most of the time, it is assumed that the P-wave, or compression wave, of a double-couple seismic event is propagating collinearly to the seismic ray. Therefore its polarization, at the seismic tool, is indicating the arrival direction of the ray coming from the seismic source.

Seismic attributes

To compute the seismic attributes presented below, the source mechanism, which generated the seismic event, is assumed to be a double-couple mechanism.

Corner frequency & Plateau amplitude

The corner frequency (F_c, in Hz) and the plateau amplitude (W_0, in m.s) are computed using the formula from: Snoke, J.A. (1987). Stable determinations of (Brune) stress drops, *Bull. Seis. Soc. Am.*, **73**, 530—538.

Seismic moment

The seismic moment (M_0) is computed using the formula from: Lee, W. H. K & Stewart, S. W. (1981). Advances in Geophysics, Supp. 2, Principles and applications of microearthquake networks, *Academic Press*.

$$M_0 = \frac{4\pi\rho V_S^3 W_0 R}{0.85}$$

R is the source-receiver distance.
0.85 is the assumed radiation coefficient.

Moment magnitude

The local magnitude (M_L), Richter equivalent, is computed using the formula from: Lee, W. H. K & Stewart, S. W. (1981). Advances in Geophysics, Supp. 2, Principles and applications of microearthquake networks, *Academic Press.*

$$M_L = \frac{Log_{10}(M_0 - 16)}{1.5}$$

Please note that magnitudes below –3 are most likely not representative of the reality. So, we will write "magnitude" in brackets or talk about pseudo-magnitude. Actually, with such small values, it would be better to talk about seismic moments. However, the magnitude, which is calculated from the decimal logarithm of the seismic moment, remains a good *relative* scaling.

Duration magnitude

The duration magnitude (M_D) is computed by the Lee et al. (1972) formula used by the USGS – NCSN network (see also Lee, W. H. K & Stewart, S. W. (1981). Advances in Geophysics, Supp. 2, Principles and applications of microearthquake networks, *Academic Press*):

$$M_D = -0.87 + 2Log_{10}(\tau) + 0.0035\,\Delta$$

t = the time duration of the event, which is defined as the duration between the P-wave arrival and the moment the S-wave coda amplitude is twice the pre-P background noise amplitude. D the time duration of the event, which is

Using this formula we can estimate the event magnitude without an absolute measurement of the signal amplitude. Note that the epicentral distance must be greater than 28 km to increase the magnitude by 0.1. For hydraulic fracture monitoring, the distance effect may be neglected.

b-*value*

The *b*-value gives an indication of the relation between the "earthquake" size and its frequency of occurrence. Assuming a Gutenberg/Richter distribution law, the *b*-value can take values between 1 and 2.5. It is generally accepted that high *b*-values reflect higher density of small faults (or fractures) than small *b*-values. *b*-values around 1 are observed for "natural" (tectonic) earthquakes but get closer to 2.5 for volcanoes or mines.
The *b*-value appears in the formula:

$$Log_{10}N = A - bM_L$$

where N is the number of seismic events of local magnitude greater or equal to M_L.

Appendix B Sercel Maxiwave Tools

Contractor Experience Level

Baker Hughes has been acquiring microseismic data for several years. We have acquired, processed or reprocessed dozens of surveys. Our clients have included Apache, Williams, Chesapeake, Hillwood, DTE, EOG, Marathon, ConocoPhillips.

Equipment Description

Sercel Maxiwave Downhole Equipment.

Voltage Regulation Section
The primary function is as a voltage regulator, to establish the voltage required by the clamping arm motors in all of the tools above. It also serves as a weight to help guide the lighter tools down through thick mud or deviated boreholes. It is fitted with a sensitive motion sensor, so that hang-ups on the run-in can be quickly spotted.

Inter-Tool Cable
An inter tool cable is a 50 ft. length of 7-conductor wireline fitted at each end with our special compact cable heads. The lower inter tool cable head is fitted with weak-points. These must be selected carefully so that the weakest weak-point bolts are located at the bottom of the tool-string.

Seismic Receivers
The seismic receiver tools house a three-component seismic sensor package and is equipped with a motor-controlled clamping arm, which greatly improves the coupling between sensors and the formation. The sensors are orthogonal geophones which are mounted in a fixed package to be compatible with micro-seismic operations.

Telemetry Adapter Section
The telemetry adapter section serves to interface the Maxiwave tool-string to the main wireline cable. System power from the surface is distributed equally over six Wireline conductors. Transformers in the telemetry adapter section separate this power from the downlink and uplink data signals. The telemetry adapter section receives the data from the Maxiwave tool-string and re-transmits this to the surface, in a coded and modulated form.

Sercel Maxiwave Surface Equipment

Wireline Interface Box
The wireline interface box is the interface to the wireline at the surface. It is a passive device, a steel box containing transformers to isolate both the downlink command and uplink telemetry signals from the power supply.

Power Panel
The power panel supplies power to the Maxiwave tool-string (via a wireline interface box).

System Panel
The Maxiwave must be operated in conjunction with our surface recording system.
This comprises a unit connected, via a USB cable, to a suitable PC running the data acquisition program.

Telemetry and Equalization

Signal Clarity. A wireline cable presents a challenge for high-speed data transmission. The transmitted signal suffers frequency-dependant amplitude attenuation and phase distortion during its path through the wireline. The filtering imposed by the Wireline must be reversed. Specialized digital signal processors have made it possible to perform real-time inverse filtering in the digital domain. This process is performed automatically and transparently as required, only in one or two seconds.

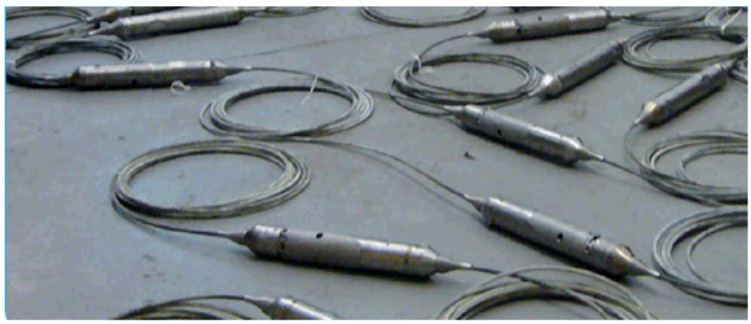
Operational Failures

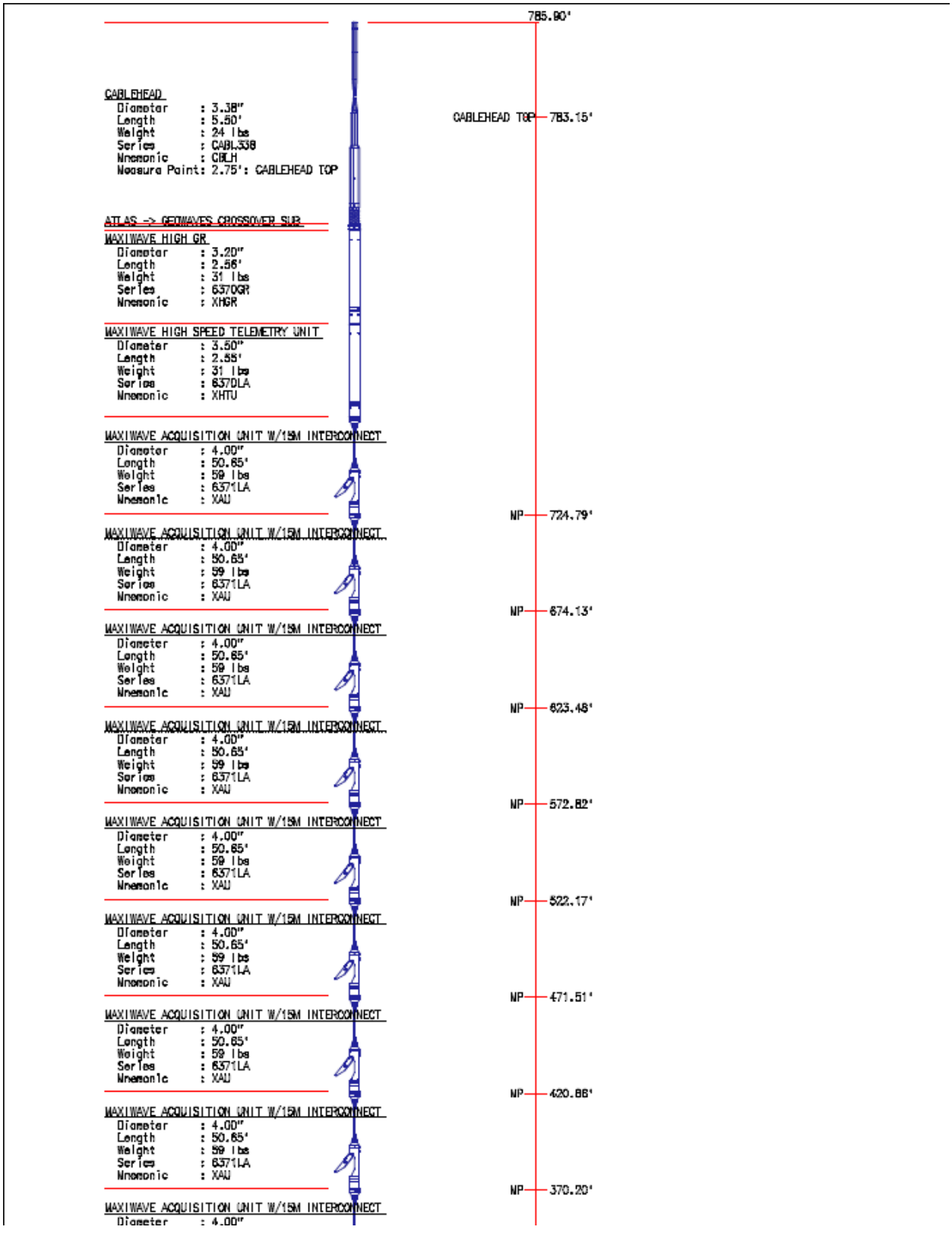
Most of the problems presented are related to down hole equipment (Telemetry and geophone tools). After being deployed for more than three days at average down hole temperatures of 250^{o} F the QC control flag reported 97% error or less in the recovered signal. This led to replacing the down hole equipment when fracing operations permitted.

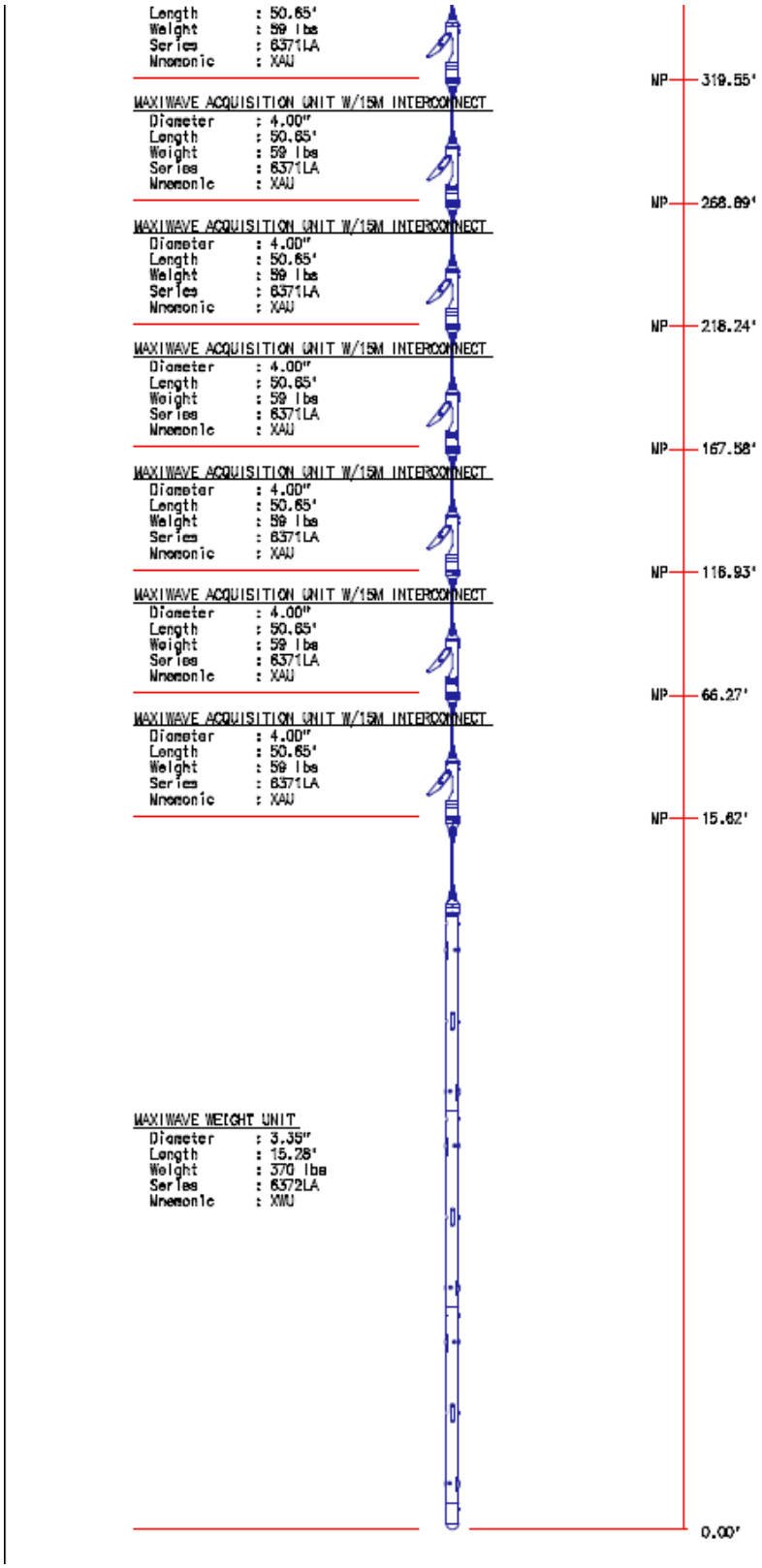
When faults were discovered, the engineer in charge completed the Service Repair Order procedure for the faulty equipment. A red tag was attached to the faulty or suspected equipment to prevent it from being used inadvertently. The faulty equipment was rectified by using backup equipment.

- Baker Atlas MaxiWave
  - 100 levels maximum
  - Superior telemetry
  - Superior transmission rates
  - 1 to 100 levels
  - ¼ to 1/2 msec, 25 levels
  - Motion Sensors
  - Downhole Digitization
  - Long Line communications
  - 135 Degrees C (275°F)
  - 14,400 psi
  - 3 5/8" diameter
- For large 3D VSP's






785.90'
CABLEHEAD
Diameter : 3.38"
Length : 5.50'
Weight : 24 lbs
Series : CABL338
Mnemonic : CBLH
Measure Point: 2.75': CABLEHEAD TOP
CABLEHEAD TOP 783.15'
ATLAS -> GEOWAVES CROSSOVER SUB
MAXIWAVE HIGH GR
Diameter : 3.20"
Length : 2.56'
Weight : 31 lbs
Series : 6370GR
Mnemonic : XHGR
MAXIWAVE HIGH SPEED TELEMETRY UNIT
Diameter : 3.50"
Length : 2.55'
Weight : 31 lbs
Series : 637DLA
Mnemonic : XHTU
MAXIWAVE ACQUISITION UNIT W/15M INTERCONNECT
Diameter : 4.00"
Length : 50.65'
Weight : 59 lbs
Series : 6371LA
Mnemonic : XAU
NP 724.79'
MAXIWAVE ACQUISITION UNIT W/15M INTERCONNECT
Diameter : 4.00"
Length : 50.65'
Weight : 59 lbs
Series : 6371LA
Mnemonic : XAU
NP 674.13'
MAXIWAVE ACQUISITION UNIT W/15M INTERCONNECT
Diameter : 4.00"
Length : 50.65'
Weight : 59 lbs
Series : 6371LA
Mnemonic : XAU
NP 623.48'
MAXIWAVE ACQUISITION UNIT W/15M INTERCONNECT
Diameter : 4.00"
Length : 50.65'
Weight : 59 lbs
Series : 6371LA
Mnemonic : XAU
NP 572.82'
MAXIWAVE ACQUISITION UNIT W/15M INTERCONNECT
Diameter : 4.00"
Length : 50.65'
Weight : 59 lbs
Series : 6371LA
Mnemonic : XAU
NP 522.17'
MAXIWAVE ACQUISITION UNIT W/15M INTERCONNECT
Diameter : 4.00"
Length : 50.65'
Weight : 59 lbs
Series : 6371LA
Mnemonic : XAU
NP 471.51'
MAXIWAVE ACQUISITION UNIT W/15M INTERCONNECT
Diameter : 4.00"
Length : 50.65'
Weight : 59 lbs
Series : 6371LA
Mnemonic : XAU
NP 420.86'
MAXIWAVE ACQUISITION UNIT W/15M INTERCONNECT
Diameter : 4.00"
Length : 50.65'
Weight : 59 lbs
Series : 6371LA
Mnemonic : XAU
NP 370.20'
MAXIWAVE ACQUISITION UNIT W/15M INTERCONNECT
Diameter : 4.00"


Length : 50.65'
Weight : 59 lbs
Series : 6371LA
Mnemonic : XAU
MAXIWAVE ACQUISITION UNIT W/15M INTERCONNECT
Diameter : 4.00"
Length : 50.65'
Weight : 59 lbs
Series : 6371LA
Mnemonic : XAU
MAXIWAVE ACQUISITION UNIT W/15M INTERCONNECT
Diameter : 4.00"
Length : 50.65'
Weight : 59 lbs
Series : 6371LA
Mnemonic : XAU
MAXIWAVE ACQUISITION UNIT W/15M INTERCONNECT
Diameter : 4.00"
Length : 50.65'
Weight : 59 lbs
Series : 6371LA
Mnemonic : XAU
MAXIWAVE ACQUISITION UNIT W/15M INTERCONNECT
Diameter : 4.00"
Length : 50.65'
Weight : 59 lbs
Series : 6371LA
Mnemonic : XAU
MAXIWAVE ACQUISITION UNIT W/15M INTERCONNECT
Diameter : 4.00"
Length : 50.65'
Weight : 59 lbs
Series : 6371LA
Mnemonic : XAU
MAXIWAVE WEIGHT UNIT
Diameter : 3.35"
Length : 15.28'
Weight : 370 lbs
Series : 6372LA
Mnemonic : XWU
WP 319.55'
WP 268.89'
WP 218.24'
WP 167.58'
WP 116.93'
WP 66.27'
WP 15.62'
0.00'

TOTAL LENGTH: 785.90'
TOTAL WEIGHT: 1352 lbs
MAX DIAMETER: 0'4.00"

Appendix M: Final Drilling Report

www.bakerhughes.com

WELL INTERVENTION END OF WELL REPORT
RSU #1







Prepared for University of Wyoming

November / 2013

BAKER HUGHES

© 2013 Baker Hughes Incorporated. All rights reserved

UNIVERSITY OF WYOMING

BAKER HUGHES

WELL INTERVENTION END OF WELL REPORT

FLUID SAMPLING, INJECTIVITY TEST, INSTALLATION AND REMOVAL OF SEISMIC MONITORING SYSTEM, AND PLUG & ABANDONMENT

WELL RSU # 1

Document:	Well Intervention RSU#1 end of well report	Revision Number:	0
Prepared by:	Catalina Leal / Stephen Lynn	Revision Date:	Nov 11-2013
Reviewed by:	Oscar Picon		
Approved by:	Kate Humphrey		

BHIO Engineering Disclaimer: -

Any interpretations, interpretational data, research, analysis, recommendations, opinions or advice (including but not limited to any engineering designs, geological studies or analyses, well programs, reservoir or other models and/or forecasts, or drilling or production optimization or management programs) ("interpretations and/or recommendations") furnished by BAKER HUGHES INTEGRATED OPERATIONS (BHIO) hereunder are opinions based upon inferences from measurements, empirical relationships, and assumptions, and industry practice, which are not infallible, and with respect to which professional geologists, engineers, and analysts may differ. Accordingly, BHIO does not warrant the accuracy, correctness, or completeness of any interpretations and/or recommendations, or that CUSTOMER'S reliance and/or any third party's reliance on such interpretations and/or recommendations will accomplish any particular results, and CUSTOMER assumes all responsibility for any use of, or reliance upon, interpretations and/or recommendations, and for all decisions based thereon, (including without limitation decisions based on any oil and gas evaluations, production forecasts and reserve estimates, furnished by BHIO to CUSTOMER hereunder), by any person, party, or entity, and CUSTOMER hereby releases, indemnifies and holds harmless BHIO from and against any and all claims, damages, costs, losses, and liabilities arising out of such use or reliance.

Amendment Summary

Revision No	Review Date	Summary description of changes	MOC Ref
0	November-2013	First Issue	

UNIVERSITY OF WYOMING

BAKER HUGHES

End of Well Report

Well Name: RSU #1
Field: Rock Springs Uplift
Rig : Key Energy # 6052

	Name	Date d/m/y	Signature
Prepared by DE BHIO	Catalina Leal / Stephen Lynn	14/11/2013	
Endorsed by Engineering Manager BHIO	Oscar Picon	14 Nov. 2013	
Endorsed by Project Manager BHIO	Kirk Broussard	14 NOV 2013	
Approved by VP of Engineering BHIO	Kate Humphrey	14 NOV 2013	

Revision History

Version	Description	Prepared by	Date d/m/y	Reviewed by
0	Original Issue	C. Leal (BHIO) / S. Lynn (BHIO)		

Distribution List

Distribution	Hardcopy	Electronic
University of Wyoming:		
Deputy Director	1	1
Baker Hughes Integrated Operations Office:		
Well File (Original)	1	1
Workspace UoW Project		1
Total Copies	**2**	**3**

TABLE OF CONTENTS

Executive Well Summary **7**
1 Well Overview **9**
1.1 Well Specific Data 9
1.2 Well Intervention Objectives 10
1.3 Location 11
1.4 Initial Well Schematic 12
1.5 Phase I Rig Equipment 13
1.6 BOP Stack 14
1.7 Phase I Well Schematic After Sampling and Injection Tests 22
1.8 Phase II Final Well Schematic After Setting Geophones 23
1.9 Phase III Final P&A Well Schematic 24
2 Operations Summary **25**
2.1 Well History 25
2.2 Health, Safety & Environment Summary 28
2.3 Environmental Report 29
2.4 Daily Operations Summary 30
3 Time Analysis **37**
3.1 Time Breakdown 37
3.2 NPT Analysis 40
4 Activities Summary **43**
4.1 Phase I of Planned Well Intervention 43
4.2 Phase II of Planned Well Intervention 55
4.3 Phase III of Planned Well Intervention 63
5 Recommendations and Lessons Learned **97**
6 Annexes **99**
6.1 Location images for records 99

Executive Well Summary

The University of Wyoming RSU #1 well was drilled during 2011 to investigate the feasibility of long term storage of CO_2 within the Madison and Weber formations of the Rock Springs Uplift. The objective of this CO_2 storage trial was to limit the CO_2 injection profile to prevent exceeding the rock formation breakdown gradient or fracture pressure.

Drilling the RSU #1 well, formed part of the initial stratigraphic test and proof of concept of CO_2 storage, and was managed/constructed by Baker Hughes for University of Wyoming. RSU #1 was spudded on June 13th, 2011 and the rig was released on August 30th, 2011 after drilling to TD / PBTD 12,810 ft. / 12,747 ft., final logging, and setting a liner across the zones of interest; the well was temporarily abandoned. Total operating time for the drilling process was 79 days.

The well intervention performed on RSU#1 had three phases. The first phase had the main objectives of perforating selected intervals and recovering formation fluid samples from the Madison and the Weber, and performing limited injection tests on both the Madison and Weber formations. This operation with workover rig Key #6052, started on November 13 /2012 and ended on December 21st/2012.

The second phase of the planned intervention had the objective of leaving the well with the capability of monitoring potential seismic activity due to future CO_2 injection in the vicinity of the well-bore by deploying a permanent geophone array (micro-seismic sonde) within the top part of the 3½" liner. Surface interface data recording equipment was intended to be installed and fenced adjacent to the well-head for the purposes of long term micro seismic monitoring, recording, and data collection. This operation using a coil tubing unit, started on December 27th/2012 and was suspended on December 29th/2012. While performing the operation it was observed that the array used to set the geophones would not test and no signals were detected at surface and it was decided to secure the well and send the array for repairs. It was determined that there was a manufacture defect on the geophones that allowed fluid to enter the main chamber. Once a detailed investigation of the array failure was finished, and repairs were done, the operation was planned for the first week of April 2013.

Operations for the second phase of the well intervention successfully started on April 3rd/2013 when clean-up and logging on the well was performed and the geophone array was lowered, set and cemented in place. Operations concluded on April 8th / 2013 when surface recording equipment was installed and the area was fenced. Total operating time of 6 days.

At the University of Wyoming's request, well intervention for RSU #1 entered a third phase where the previously cemented geophone array was requested to be removed, along with the 1 ½" coiled tubing the array was attached to. Along with this, the University requested 4 zones to be monitored for background seismicity with a wireline deployed geophone monitoring array. Each interval was planned for 36 hours of continual monitoring. The objective of this monitoring was to assess seismic noise levels at 4 different depths in the well and during the monitoring period, identify, locate and

characterize any detected seismicity. Once monitoring reached completion, the well was to be plugged and abandoned and the site reclaimed.

Because a third phase was not originally planned for, unique operations were needed to sever the uncemented portion of the tubing and Kevlar geophone cable and retrieve an adequate amount to allow for correct monitoring to take place.

The third phase of operations began on August 26th/2013 and ended on October 2nd/2013 with a total operating time of 23 days. During this phase of well intervention, the permanently deployed microseismic monitoring array and 1 ½" coiled tubing was removed from the well. Following removal of the geophone array and coiled tubing, a passive seismic monitoring array was deployed on wireline with 36 hours of monitoring in 4 zones each. After seismic monitoring reached completion, the RSU #1 well was permanently abandoned with 4 cement plugs. With the well abandoned, the existing fence was removed, an abandonment well monument was set in place, and the reclamation of the site was scheduled for spring, after the winter thaw.

1 Well Overview

1.1 Well Specific Data

Well Name :	RSU #1
Well Classification :	CO_2 Injection Test Well
API Number :	049-037-07154
County, State :	Sweet Water County, Wyoming
Operator :	University of Wyoming / BHIO
Regulatory :	Wyoming Oil & Gas Conservation Commission and Wyoming Department of Environmental Quality
Rig :	Key Energy # 6052
Rig Contractor :	Key Energy Services Inc.
Service Contractor:	Baker Hughes Integrated Operations (BHIO)
Type of Rig :	Workover Rig
Well Coordinates :	Lat. = 41.7212614 N Long =108.794820 W Coordinate Reference System : WGS 84/ UTM zone 38 North
Ground Elevation :	6841.2 ft
RT Elevation (MSL) :	10.8 ft.
Well TD :	PBTD 12,747 ft MD (Wiper Plug). Originally drilled to 12,810 ft MD
Perforation History: (4 SPF / Total Shots, holes)	**Weber**: 11,188-11,222 ft (136 holes), 11,268-11,294 ft (104 holes), 11,396-11,412 ft (64 holes), 11,424-11,432 ft (32 holes) **Madison**: 12,342-12,374 ft (128 holes), 12,395-12,429 ft (136 holes), 12,502-12,512 ft (40 holes)
Maximum Inclination:	Vertical well
BHST :	208 °F
Wellhead :	Seaboard International Inc. 5K PSI Wellhead & Tree Assembly 10-3/4" x 7" x 1-1/2" 7" casing hanger
Mud Weight :	8.34 ppg Fresh Water currently in hole
Final Abandonment Plug Depths :	50-250 ft. TVD 1,880-2,200 ft. TVD 4,091-4,200 ft. TVD 5,780-5,881 ft. TVD

1.2 Well Intervention Objectives

1. HSE objectives are:

- Zero Injuries.
- Zero environmental incidents.

2. The operational objectives of the 3 stages of well intervention were:

Stage 1:

- Obtain and recover fluid samples from Madison and Webber formation.
- Perform an injection test in Madison and Webber formation.

Stage 2:

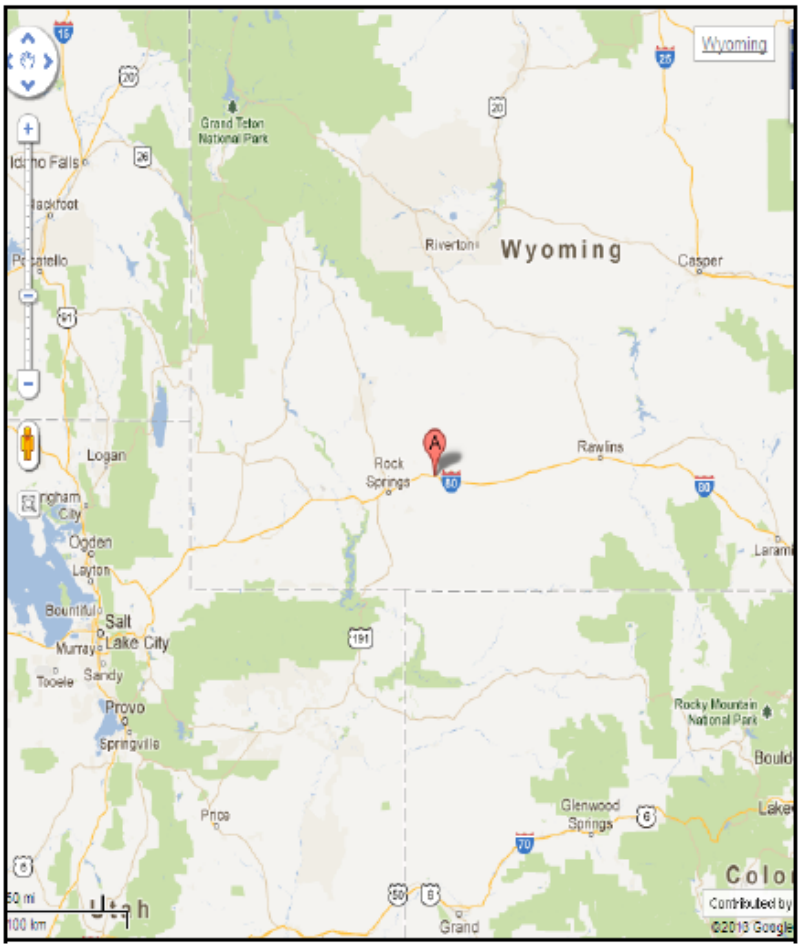
- Install a "Seismic Monitoring System" as per University of Wyoming specification.

Stage 3:

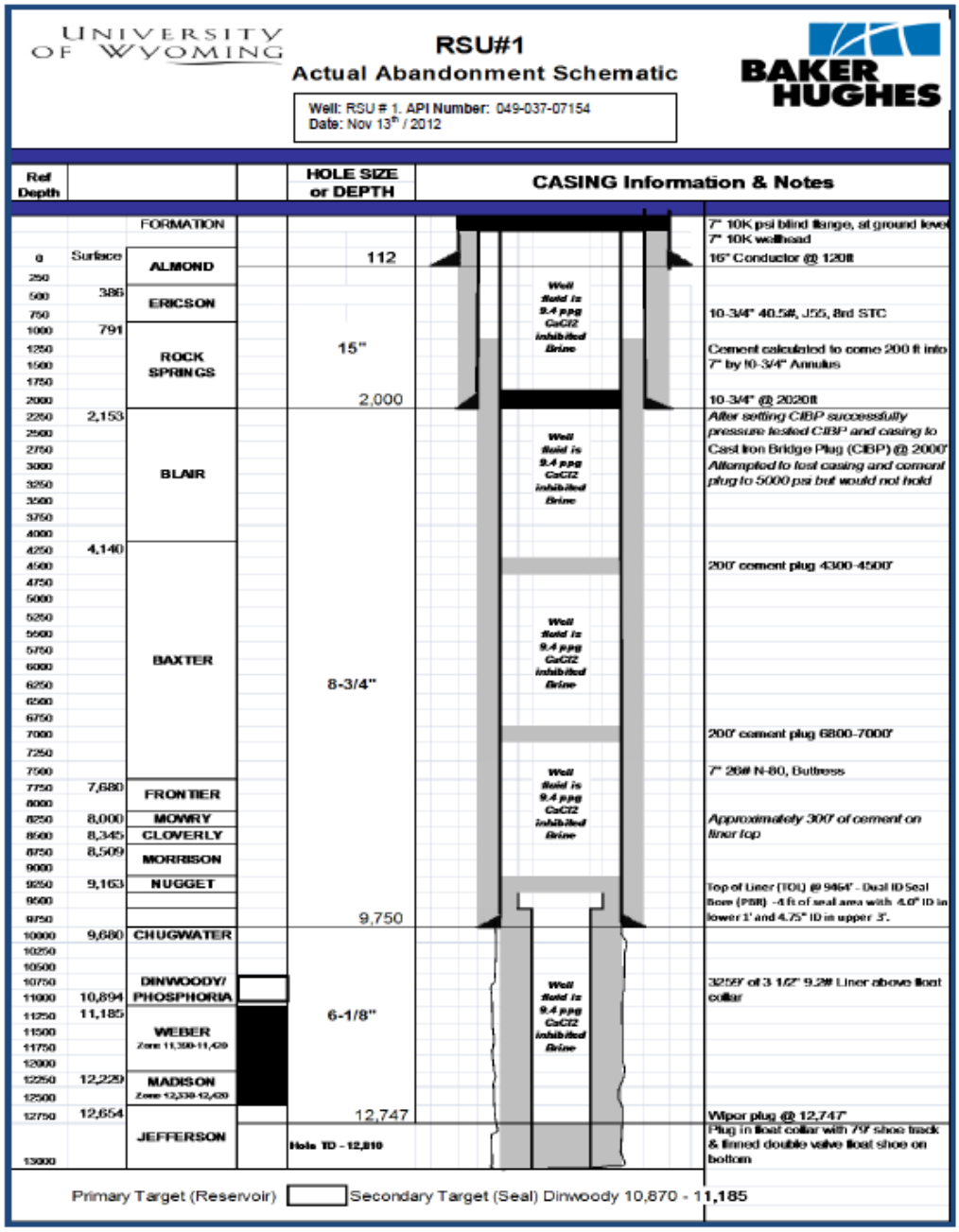
- Remove failed permanent seismic monitoring array.
- Perform passive seismic monitoring with wireline array in four formations specified by the University of Wyoming to detect background seismicity.
- Permanently plug and abandon RSU #1 well.

1.3 Location

The well RSU#1 is located in Sweetwater County, 24 miles east of Rock springs, Wyoming. The location is approximately 2090' South and 678' West of NE corner of Sector 16.



1.4 Initial Well Schematic



STRING	OD in	ID in	DRIFT in	WT #/FT	GRADE	DEPTH ft.	EST TOC Ft	CAPACITY BBL/FT	BURST PSI	COLLAPSE PSI
Surface	10 3/4	10.05	9.894	40.5	J-55, STC	2,000	0	NA	3,130	1580
Intermediate	7	6.276	6.151	26	N-80 Buttress	9,750	1,800	.03826	7,240	5,410
Liner	3 ½	2.992	2.867	9.20	L-80 FJ-150	12,747	9,264	.00876	10,160	10,530
PBR	NA	4 / 4.75	NA	NA	NA	9,464	NA	NA	NA	NA

1.5 Phase I Rig Equipment

Key Energy Rig #6052 was used for the first stage of the programmed well intervention operations.

Key Energy Rig #6052 is a self-propelled carrier, Key built "Cabot Type" rig with a national derrick. Scoping Mast rated up to 300,000 lbs., racks double joints of tubing and hangs triple rods.The mast height is 106 ft. and the rig floor can be elevated from ground level to 14 ft.

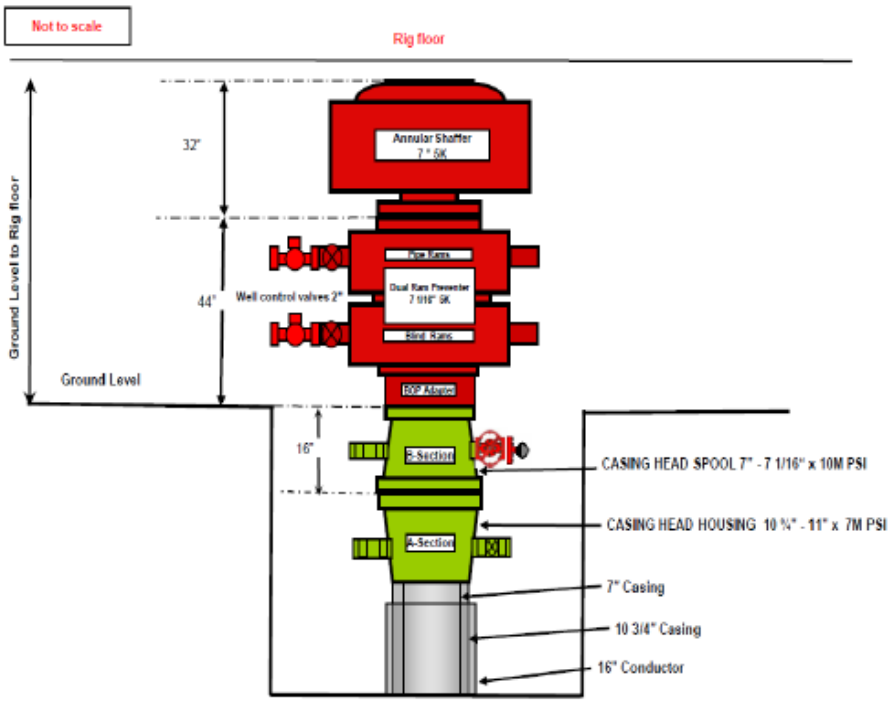


The rig comes with a 140 bbls open top work tank and a Garden-Denver 750 HP, series 60 motor (dressed with 4 ½" liner/6" stroke).

4ea - 500 bbls frac tank(s) will be spotted on the location (location footprint plan to be determined) in the immediate vicinity of the rig and well head.

1.6 BOP Stack

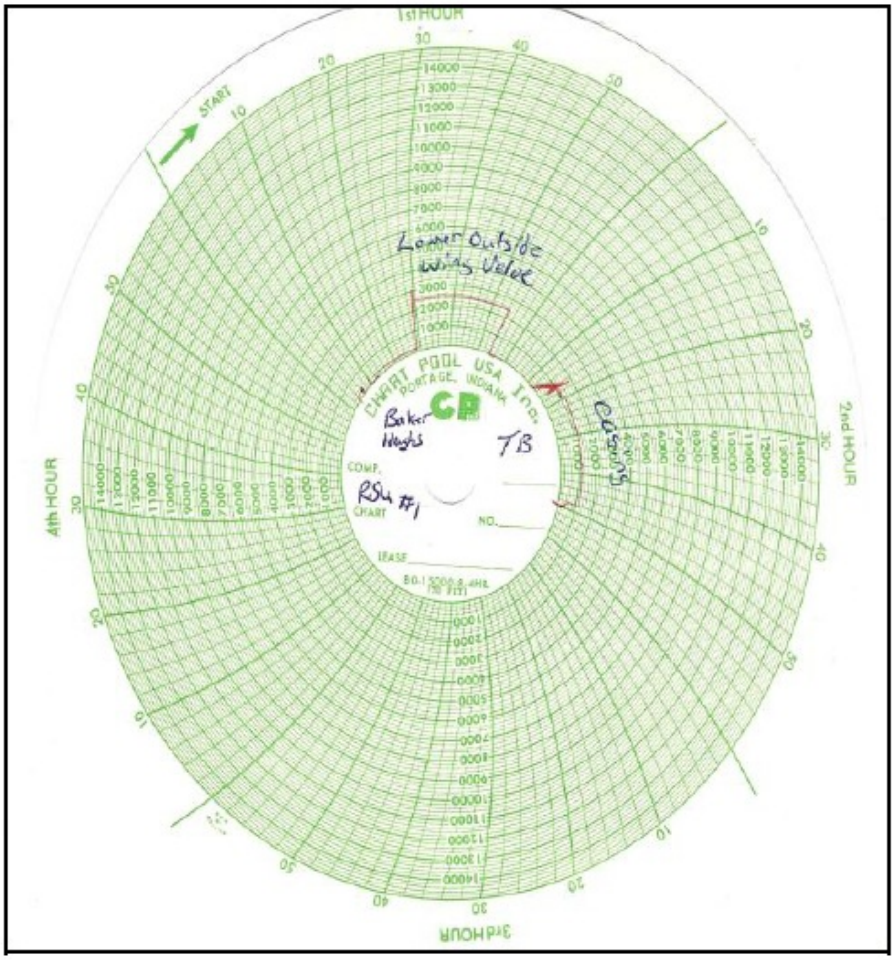
1.6.1 Phase I BOP Stack



Phase I BOP Stack

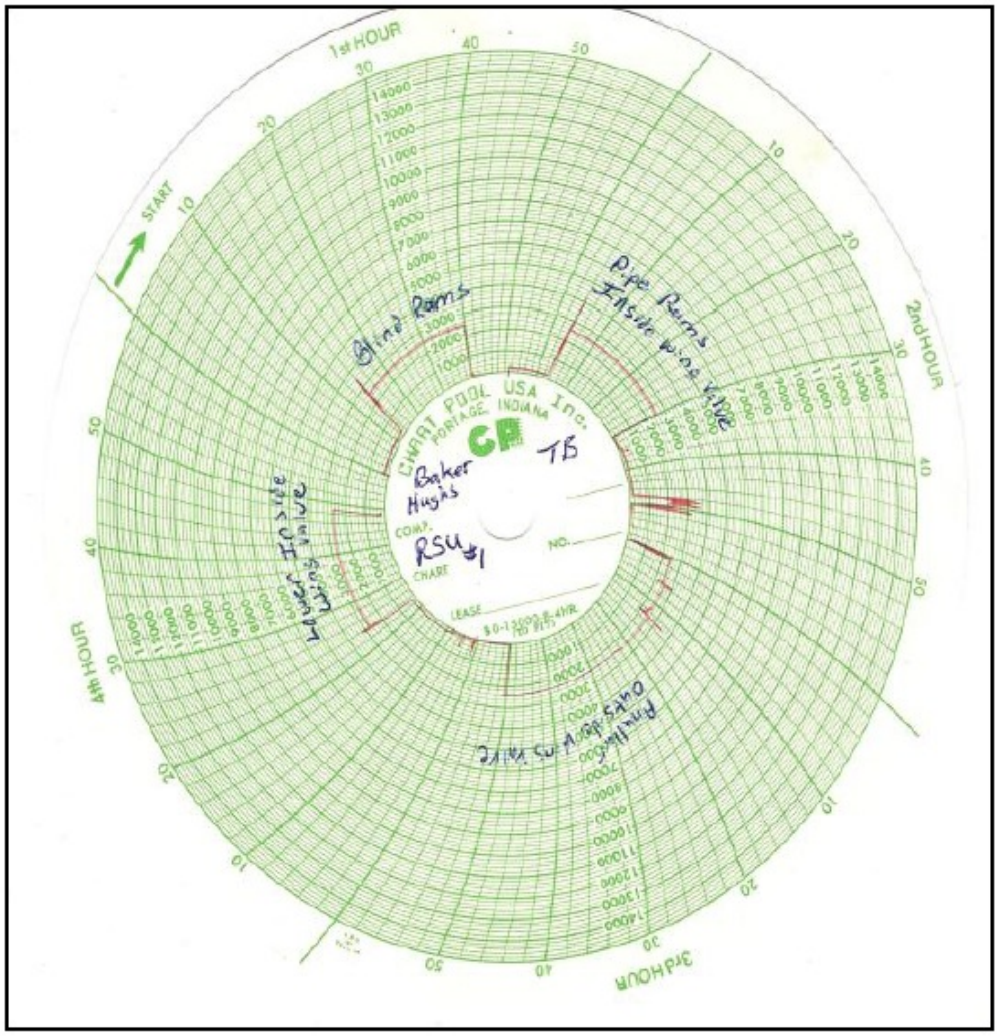
1.6.2 BOP Test Chart 1 (Phase I)

Nov. 13th/ 2012 14:30

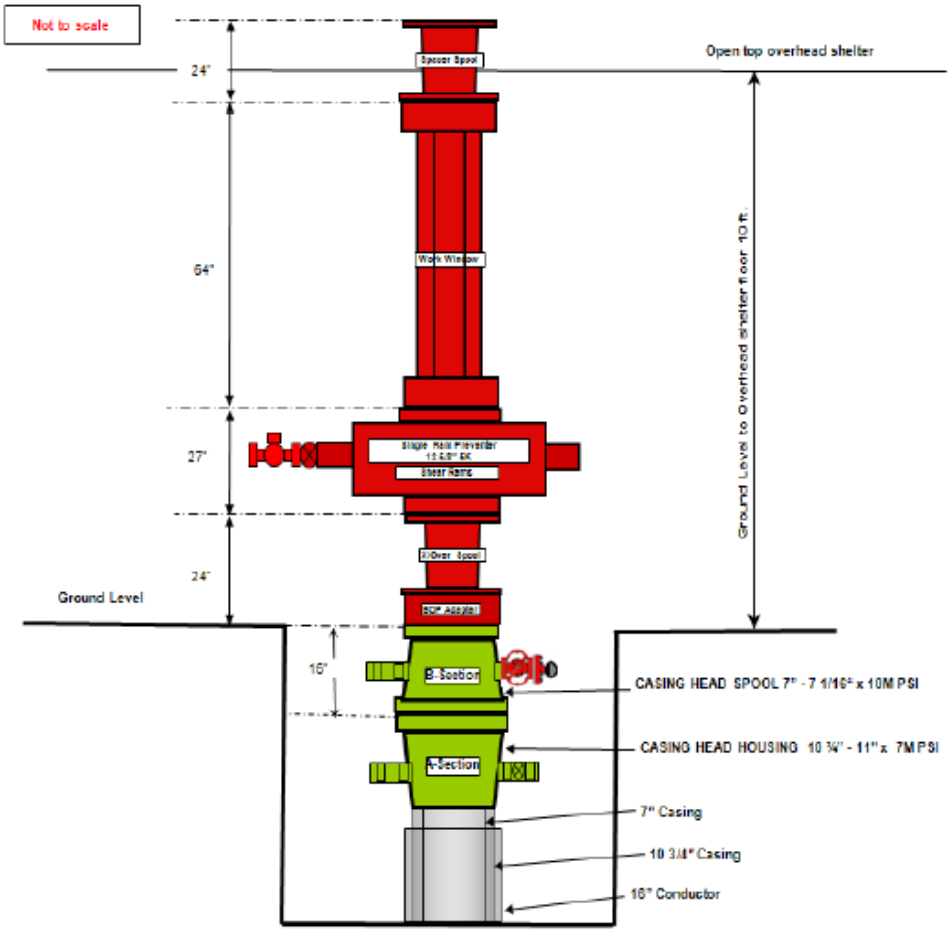


1.6.3 BOP Test Chart 2 (Phase I)

Nov. 13th/ 2012 14:30



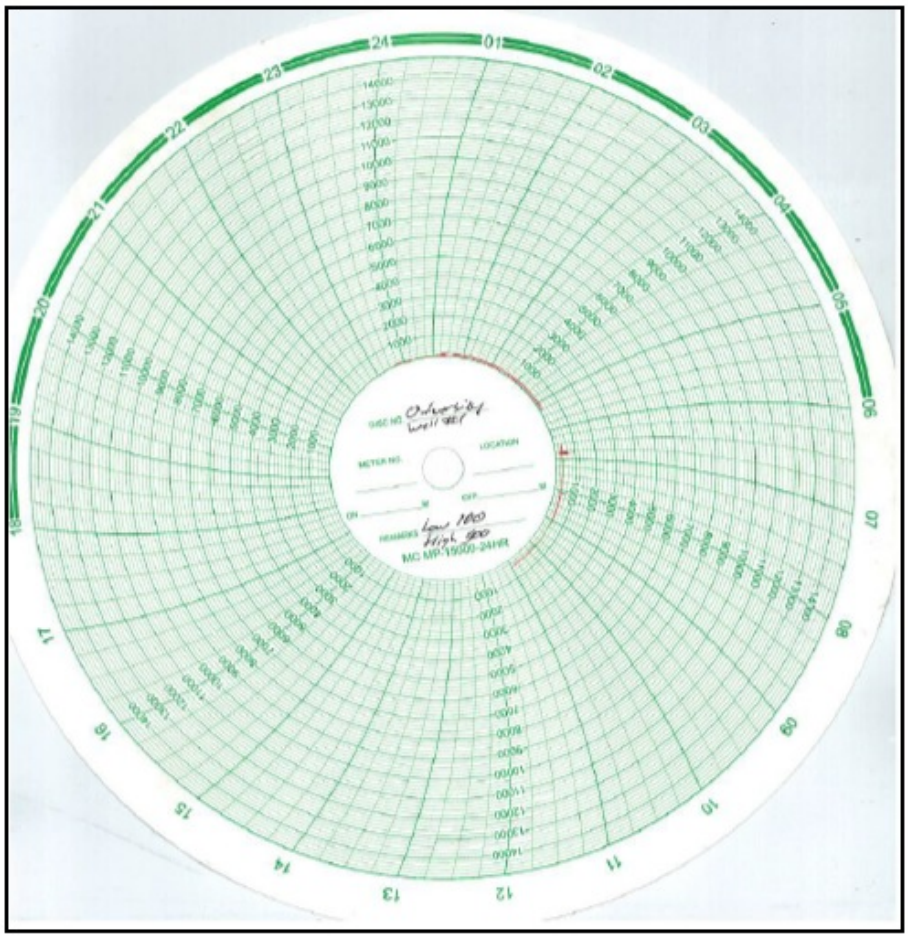
1.6.4 Phase II and III BOP Stack



Phase II and III BOP Stack

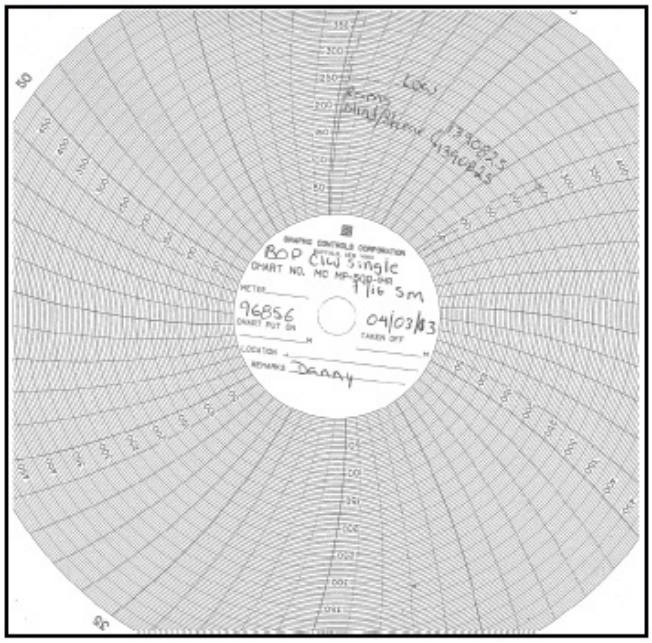
1.6.5 BOP Test Chart 1 (Phase II)

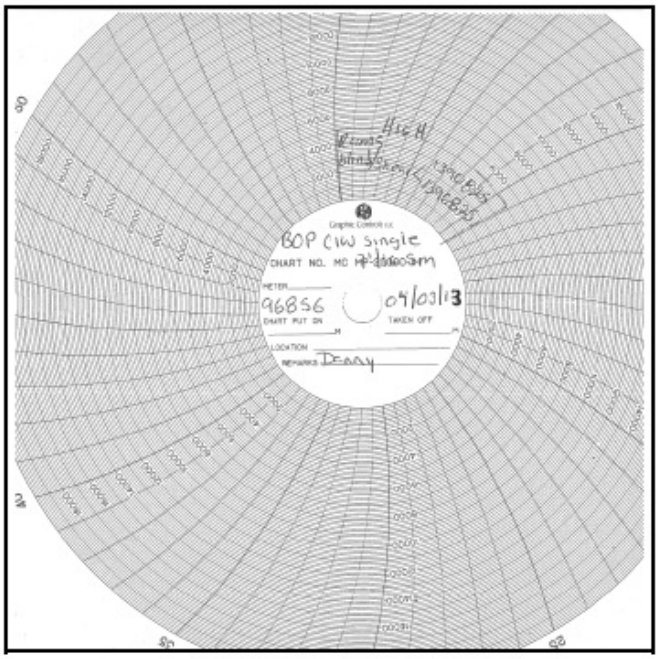
April. 6th/ 2012 14:45



1.6.6 BOP Test Chart 2 (Phase II)

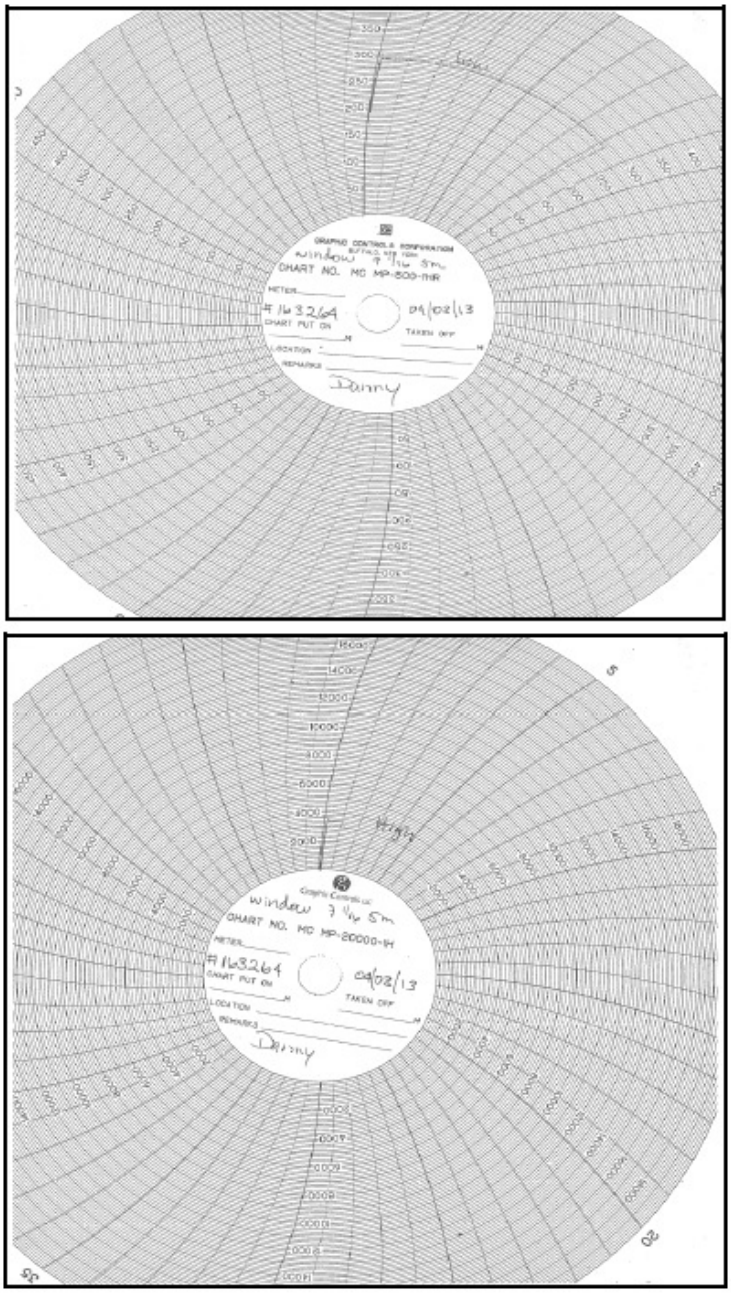
April. 6th/ 2012 14:45





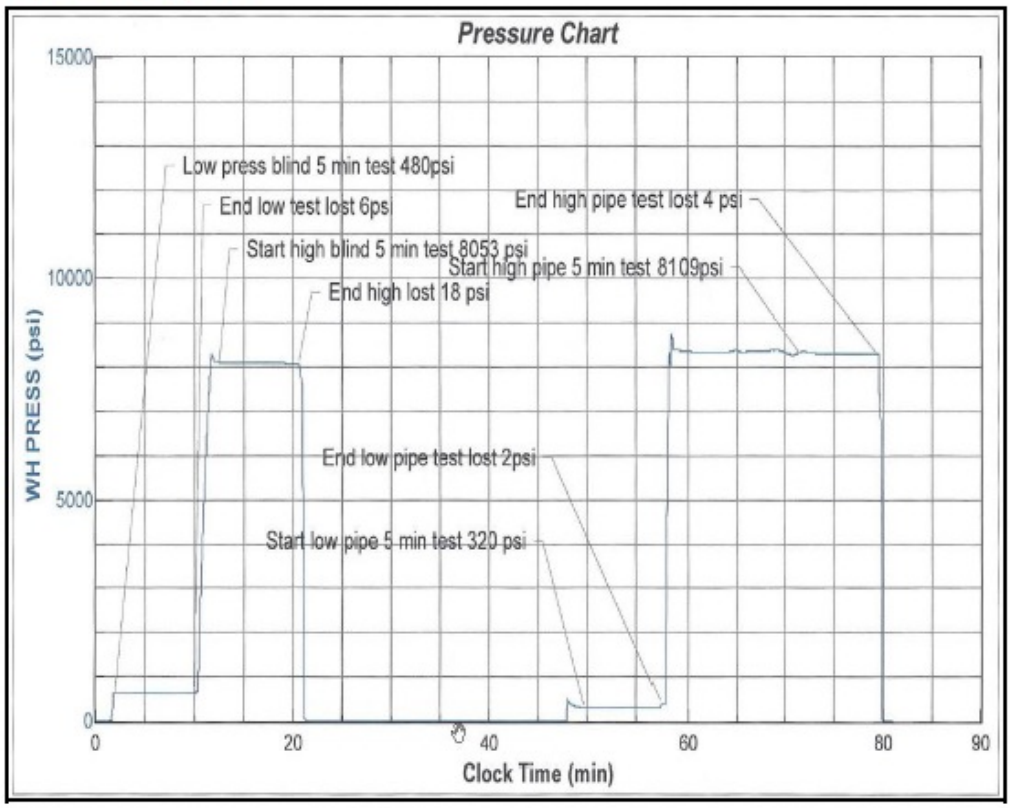
1.6.7 BOP Test Chart 3 (Phase II)

April. 6th/ 2012 14:45



1.6.8 BOP Test Chart (Phase III)

September 28th / 2013



1.7 Phase I Well Schematic After Sampling and Injection Tests

UNIVERSITY OF WYOMING

RSU#1

Actual Abandonment Schematic

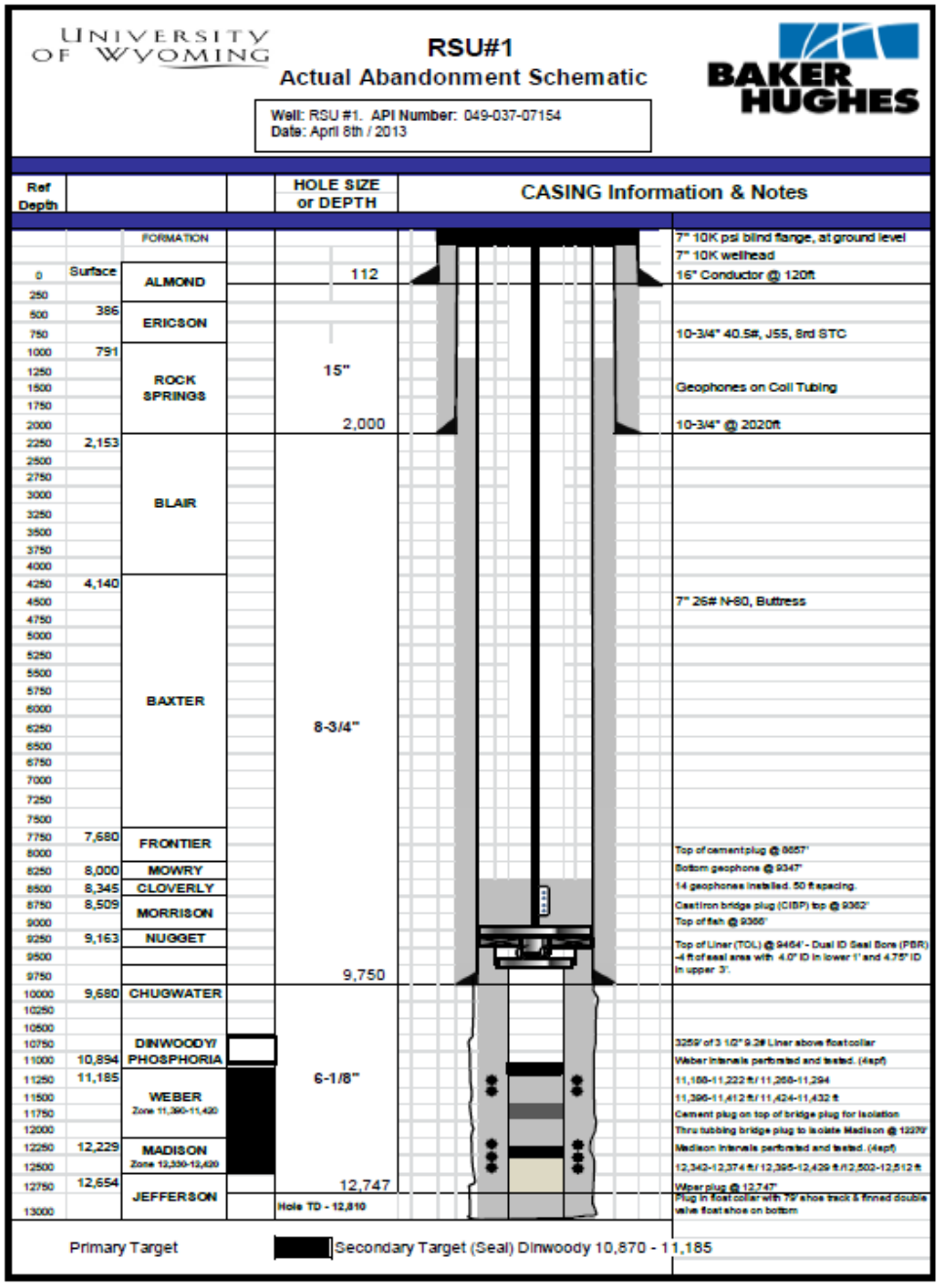
BAKER HUGHES

Well: RSU # 1. **API Number:** 049-037-07154
Date: Dec 27th / 2012
Remarks: Madison and Weber formation zones perforated and sampled. Injection tests done.

Ref Depth		FORMATION	HOLE SIZE or DEPTH	CASING Information & Notes
				7" 10K psi blind flange, at ground level
				7" 10K wellhead
0	Surface	ALMOND	112	16" Conductor @ 120ft
250				
500	386	ERICSON		
750				10-3/4" 40.5#, J55, 8rd STC
1000	791	ROCK SPRINGS	15"	
1250				
1500				
1750				
2000			2,000	10-3/4" @ 2020ft
2250	2,153	BLAIR		
2500				
2750				
3000				
3250				
3500				
3750				
4000				
4250	4,140	BAXTER		
4500				
4750				
5000				
5250				
5500				
5750				
6000			8-3/4"	
6250				
6500				
6750				
7000				
7250				
7500				7" 26# N-80, Buttress
7750	7,680	FRONTIER		
8000				
8250	8,000	MOWRY		
8500	8,345	CLOVERLY		
8750	8,509	MORRISON		
9000				
9250	9,163	NUGGET		Top of Liner (TOL) @ 9464' - Dual ID Seal Bore (PBR) -4 ft of seal area with 4.0" ID in lower 1' and 4.75" ID in upper 3'.
9500				
9750			9,750	
10000	9,680	CHUGWATER		
10250				
10500				
10750		DINWOODY/ PHOSPHORIA		3259' of 3 1/2" 9.2# Liner above float collar
11000	10,894			
11250	11,185	WEBER Zone 11,390-11,420	6-1/8"	
11500				
11750				
12000				
12250	12,229	MADISON Zone 12,330-12,420		
12500				
12750	12,654	JEFFERSON	12,747	Wiper plug @ 12,747'
13000			Hole TD - 12,810	Plug in float collar with 79' shoe track & finned double valve float shoe on bottom

Primary Target — Secondary Target (Seal) Dinwoody 10,870 - 11,185

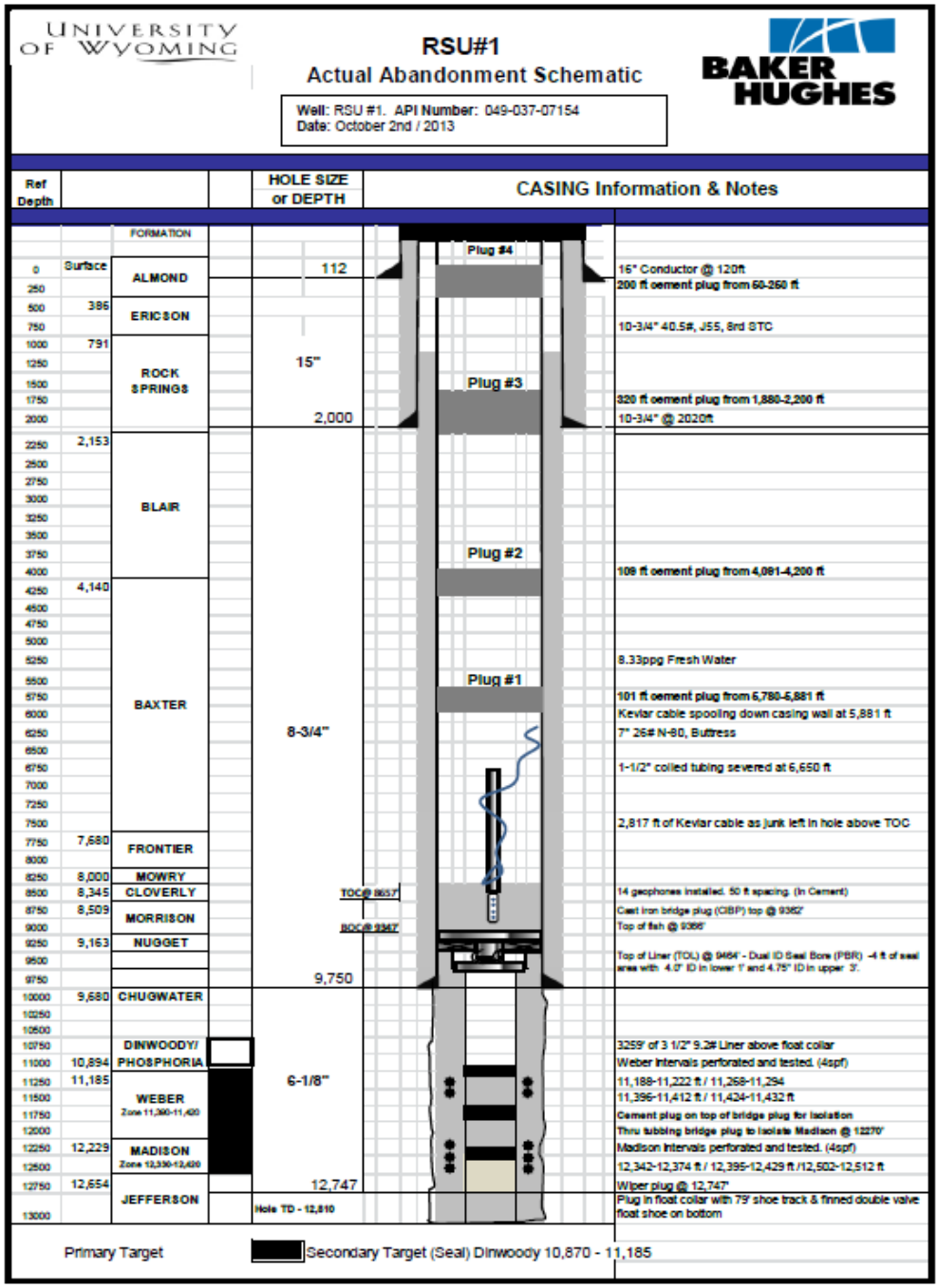
1.8 Phase II Final Well Schematic After Setting Geophones



14 Geophones were successfully installed with 50 feet spacing between them. Bottom geophone set at 9347 ft. Cemented in place. Top of the cement was located at 8657'

23

1.9 Phase III Final P&A Well Schematic



2 Operations Summary

2.1 Well History

Operations at RSU #1 were executed according to plan to meet the operational objectives. The fluid sampling and injection test planned for Madison and Weber formation were accomplished with minor issues and handled with mitigation plans that were discussed at the moment with the University of Wyoming representatives and the engineering manager.

The operation initially planned for 15 days on the first stage took 38 days as it was needed to overcome with problems along the way that will be identified in this document. Most of the issues had already been identified in the planning stage and mitigation plans were put in place to minimize falling behind schedule. The risk assessment considered that this well was not planned to be re-entered and for that reason it made the operation somewhat challenging.

The well intervention was divided into three main phases. In the work flow diagrams below the main operations are defined for each of the phases. The first one included operations such as cleaning out the wellbore, logging, perforating, obtaining fluid samples and performing the injection test. The second phase of the intervention covered the installation of the seismic monitoring array and the surface monitoring equipment. The third phase of intervention covered the removal of the monitoring array and coiled tubing, passive wireline seismic monitoring, and permanent plug and abandonment of the RSU #1 well.

Some remarks during the operation:

- Operation conference call was performed with the engineering team in Houston on a daily basis to discuss the progress on the operation
- Operation stopped completely for a holiday on November 22nd and on December 8th due to a weather storm.
- Multifinger caliper failure while doing the casing inspection log left a fish in the hole that required a fishing job to continue the operation.
- Tool failure of a cement bond log tool resulted in an additional trip to replace the tool.
- Round trip was needed to change the bit while drilling out the cement plugs.
- Completion assembly got stuck downhole, resulting into fishing operations that required the use of chemical cutters.
- Retrievable packer was left in hole as a fish.
- Partial signal of geophones after deployment.
- During Phase II well intervention, a permanent geophone array was cemented in place.
- A third phase had not originally been foreseen, however, a request from the University of Wyoming was made for monitoring four intervals. The objective of this monitoring was to assess seismic noise levels at 4 different depths in the well and during the monitoring period, identify, locate and characterize any detected seismicity.

- During Phase III, after cable cutting and fishing operations, 3,867 ft. of Kevlar cable was left as junk in the hole, 3,177 ft. of it being free above the TOC that the geophones were originally cemented in. A portion of the cable, starting at 5,881 ft., laid against the casing wall and did not permit wireline monitoring tools from reaching originally planned setting depths across the Cloverly, Mowry, or Frontier formations.
- A separate operations program was prepared, approved, and executed for each stage of well intervention.



Overall workflow of three phases of planned well intervention for RSU#1

2.2 Health, Safety and Environment Summary

During the course of the operations at RSU #1, HSE pre-job safety meetings were held daily and additional meetings were scheduled as necessary to ensure that the operation was carried out safely.

Below is a summary of good and mandatory practices of HSE that were carried out at RSU#1 to highlight:

- HSE representative on location reviewed rig and location conditions daily.
- Crisis Management plan and emergency response procedures were reviewed and maintained on location.
- Sign-in sheet was maintained on location to track personnel in and out of rig-site.
- It was insured that all personnel entering location received the Black Butte Mine company orientation.
- Drills were performed to insure proper procedures for evacuation of location in case on an emergency.
- Audit of the Rig and operational procedures according to Key Energy Services employee safety handbook.
- HSE related issues were reviewed between HSE representative and Co-man on site.

During the operations at RSU #1, only one injury type incident occurred without lost time.

Incident Description:

- The injured was on the floor of the rig helping to rig-up the power swivel when the operator picked up on the traveling block.
- Attached to the power swivel was a chain utilized to align the swivel vertically with the pipe. The chain has a hook on the end of it to allow adjustments.
- The hook momentarily snagged on the expanded metal of the floor when the block was lifted and then released striking the crew hand on the left forearm below the elbow.
- There was no bleeding, no broken skin - injured complaint of numbness, tingling in his arm and weakness in his grip. Injured denied any previous injury to the arm or any previous cervical injuries.
- Injured spoke with Keys supervisors and insurance representative.
- There was a follow-up with the injured and Key Energy management on the reporting and final outcome in the future.

Based on the incident on location, a safety stand down was also done to review what happened and the best practices to prevent it. Incident was reported to all parties involved and follow up was made to insure the well-being of the crew hand.

No HSE major incidents occurred which is a highlight of the operation. No additional costs were added due to any HSE related action.

2.3 Environmental Report

For the well intervention at RSU#1 no spills were reported and no cuttings were treated in surface or left on location. No environmental marks were left on site.

Waste water and cuttings from the cast iron and cement plugs were disposed through a third party waste management company that would clean the frac tanks as needed.

A trash dumpster was set on location for the length of the operation and was also serviced by WISE waste management company.

A portable restroom on location was serviced by Western relief every week for all, first, second and third phases of the well intervention.

Fresh water (1500 bbls) were hauled from Pacificorp pond (Jim Bridger power plant) with the permit 34749 from the State Engineer's office for the first stage of the well intervention as it was needed for the injection test underground. 240 bbls of potable water were hauled for the second stage as it was needed for circulation of the well and coil tubing run.

After operations of Phase II were finished and the surface equipment was fenced and secured a complete location clean-up was made as it can be seen in the below image.

During Phase III, the fence and surface monitoring site was removed and the location cleaned for surface reclamation. The cellar was dug out, removed, and backfilled, along with the mousehole. The casing was cut 4 ft. below surface and was welded over with a steel, flat-top plate. At the well location, an abandonment marker was set in place. Along with this, pit liners and rig anchors were removed. After the winter thaw, ploughing of topsoil and re-seeding of native sage grass is scheduled for spring.



Location cleaned and working area fenced and secured at end of Phase II

2.4 Daily Operations Summary

Day	Date	Main Activities	Issues detected	Mitigation actions	Unplanned operations
1	11/13/2012	Rigged up service rig equipment, BOP stack and BOP Test.			
2	11/14/2012	Finished rigging up equipment, pick up BHA and TIH and proceeded to drill out cast iron bridge plug.			
3	11/15/2012	Completed drilling cast iron bridge plug and performed casing integrity test to 4200 ft. (Top of 1st cement plug)	Pressure bled off 50 psi in 2.5 min during casing integrity test showing possible leak.	Proceeded to locate leak and prepare for repair.	
4	11/16/2012	Established condition of cement plug and evaluate pressure drop at 4000 ft., 3000 ft., 2500 ft. Located casing leak is between 2000 and 2500 ft.			
5	11/17/2012	Established exact depth of leak between 2103 and 2103.4 ft. and determined leak profile. Prepared for squeeze job.			
6	11/18/2012	Performed squeeze job, POOH with retrievable packer, P/U 6 1/8" clean out BHA and TIH 1542 ft.			
7	11/19/2012	Proceeded to clean out wellbore from squeeze job. Pressure tested successful to 1200 psi after clean out.			
8	11/20/2012	TIH to next cement plug and continue cleaning wellbore.			
9	11/21/2012	Round trip pipe to change bit and add additional drill collars and continue cleaning out wellbore.	Low ROP, small amount of returns observed at the shakers.	POOH to inspect bit, change bit and conditioned fluid system to improve hole cleaning.	
10	11/22/2012	Well secured. No operations on this day.			
11	11/23/2012	Drilled completely first cement plug, pressure tested casing and TIH to next cement plug.			
12	11/24/2012	Cleaned wellbore from 6625 to 8246ft.			

13	11/25/2012	Cleaned tanks, conditioned drilling fluid system, and continue cleaning the wellbore from 8246 to 9182.8 ft.			
14	11/26/2012	Cleaned wellbore to TOL at 9468 ft., tripped pipe to change BHA, cleaned PBR and polished it.			
15	11/27/2012	Trip out of hole, rig up coil tubing and clean out 3 1/2" liner to 12720 ft.	Malfunction of pump truck during coil tubing run.	Repaired and Replaced pump truck.	
16	11/28/2012	POOH and rig down coil tubing equipment. Attempted to run casing inspection log but malfunction of tool aborted attempt and left a piece of the tool in the hole requiring a fishing job.	Malfunction of logging tool.	Fish left in hole. Required fishing job to retrieve tool left in hole.	Fishing job was an unplanned event as a consequence of the malfunction of the logging tool.
17	11/29/2012	Perform fishing job and continue running casing and cement bond logs.			
18	11/30/2012	Finished logging. Run seal assembly and set packer.	Malfunction of logging tool.	POOH and changed logging tool to continue logging.	
19	12/01/2012	Run wireline to break ceramic disk, spent the rest of the day analyzing problem to getting logging tools to bottom.			
20	12/02/2012	Run temp log, perforate Madison formation from 12502-12512ft and from 12415 ft. to 12429ft, flow well.	Perforating gun would not go below 9400 ft. Tight spot located at this point.	P/U pup joint and 2ft of tubing to release weight on packer and correct issue with wellbore.	
21	12/03/2012	Confirmed well production for sampling (fluid level in well at 506), Continued perforating Madison(12405 - 12415 ft.) and (12395 - 12405 ft.). Collected 585 cc of pressurized samples and 10 liters of well fluids.			
22	12/04/2012	Finished sampling Madison formation, successfully perforated 4 runs in Madison from 12342 to 12374 ft.			
23	12/05/2012	Attempted step-rate injection test but reached max pressure (4500 psi) on second stage of seven stage test.			

24	12/06/2012	Completed step rate injection test. Confirmed that pipe is stuck by pulling 100k with no movement.	Pipe Stuck	Several attempts to identify stuck pipe	
25	12/07/2012	Completed all data collection on the Madison formation and developed a plan for the work on the Weber.			
26	12/08/2012	Waiting on thru-tubing plug to arrive from New Orleans & a winter storm made driving unsafe.			
27	12/09/2012	Isolated Madison zone with bridge plug & 10' of cement.			
28	12/10/2012	Pressure test failed on plug, tagged with sinker bar, ran an additional bailer of cement on top of plug.			
29	12/11/2012	Pressure test failed on plug, tagged with slickline bailer to dump sand mixture on top of cement plug but plug fell to bottom of well below Madison.			
30	12/12/2012	Evaluated plug back options and researched availability of equipment to isolate Madison. No operations at the rig site.			
31	12/13/2012	Braden-head a cement plug down to 11,640', squeezed to a pressure of 7000 psi and displaced tubing fluid with N_2.			
32	12/14/2012	Perforated the Weber zone and sampled the Weber formation fluid.			
33	12/15/2012	Completed step-rate injection test & 30 min shut-in bleed off test.			
34	12/16/2012	Completed data collection on Weber with temperature survey and equalized pressures.			
35	12/17/2012	Attempted to chemical cut below the packer and retrieve it. Did not have success.			
36	12/18/2012	Cut tubing above packer, ran overshot and tubing jars & jarred on completion assembly with no affect.			

37	12/19/2012	Continue jarring and evaluated contingencies.			
38	12/20/2012	Plug off the Weber formation, release over-shot and pump csg inhibitor in preparation to remove tubing.			
39	12/21/2012	Completed securing well and suspending operation until Dec 26th.			
40	12/27/2012	Completed Pressure Testing of Casing with a 30 min leak off test & rigged up equipment to install geophones.			
41	12/28/2012	Coil tubing run to install geophones.			
42	12/29/2012	Attempted to install geophones but equipment issues aborted plan. Evaluate problems and revised well completion. Operations at the well site completed until cable is repaired in shop and new attempt to set geophones array is scheduled.	Test system and line would not test. Cable failed test.	Cable sent to the shop for inspection and repairs. New date to be scheduled to deploy the geophone array.	
BEGIN PHASE II – April 3, 2013					
43	04/03/2013	Confirmed location clear, confirm no pressure on the well, casing integrity wireline runs (JB/GR/CLL/Caliper), set cast iron bridge plug successfully above fish at 9366'.			
44	04/04/2013	Rig up coiled tubing, flowback equipment, BOP, work window, prepare location for CT & geophone operations			
45	04/05/2013	RIH with CT and geophone array, cement geophones in hole, hang CT and phones from well head.			
46	04/06/2013	Install and test well head, prepare geophone data unit, begin soldering geophone cable back to data unit cable head.	Well head would not hold pressure.	Removed tubing head, re-set pack-off rubbers, and re-tightened tubing head - well head now holding pressure.	
47	04/07/2013	Continue wiring geophone cable.			

48	04/08/2013	Finish wiring geophone cable and perform final function test on array. Troubleshoot geophone system.	Geophone array showing abnormal response.	Checked resistivity readings for phones - readings within specification, however, a signal sent from surface to downhole could not be detected.	Ordered geophone tester with known transmitting frequency.
49	04/09/2013	Standby for geophone tester to arrive due to weather.			
50	04/10/2013	Test geophone array with geophone tester.	Phone array still not detecting signal properly.	Sent data files to manufacturer for analysis.	
51	04/11/2013	Fence-off and clean location. Standby for results of geophone data analysis.			
BEGIN PHASE III – August 26, 2013					
52	26/08/2013	Confirmed location clear, confirm no pressure on the well. Perform gauge runs thru tubing to check for obstruction in upcoming cutting operations.	Incorrect adapter flange for tree delivered to site.	Hot shot adapter from Rock Springs.	
53	27/08/2013	Rig up BOPE, and function test. Latch onto 1-1/2" CT stub with overshot and hoist with crane. RIH with E-line to tag cement plug inside 1-1/2" CT.			
54	28/08/2013	Cut 1-1/2" CT with jet cutter at 6,695'.			
55	29/08/2013	Begin pulling 1-1/2" CT out of well. Begin removing geophone cable.	Kevlar cable did not sever along with CT.	Attach spare crane to Kevlar cable while removing 1-1/2" CT to allow for smooth removal of tubing. Plan for 2nd cut of Kevlar cable.	
56	30/08/2013	Attempt 2nd jet cut of Kevlar cable and begin removing cable. Completely remove 1-1/2" CT from well.	While positioning cable on surface to attach to recovery reel, connection point from surface anchor line / Kevlar cable parted. Kevlar cable dropped down hole.	Plan for full gauge (1/10" under 7" casing drift) gauge run to detect obstruction by Kevlar cable in the 7" casing to verify if wireline monitoring array could reach 5,310'.	
57	31/08/2013	Perform gauge run.	Could not get beyond 197' with gauge tool. Cable sticking up at surface preventing wireline from going deeper.	Make arrangements for fishing operations to take place with 2" CT with circulation rotatable, fingered-spear extension to remove cable downhole.	

58	01/09/2013	Rig up CT unit with 2" tubing. RIH with rotatable spear fishing assembly. Perform 9 cable recovery runs, removing small sections of Kevlar cable.	Only small sections of cable being removed each run. On run 8, cable slipped off spear and fell back downhole. Larger sections too heavy to pull with recovery cable reel or crane.	Shorted fishing BHA to allow all CT on spear to be visible at window and allow clamping at surface, preventing loss of retrieved cable. Use forklift to help hoist cable out of hole.	
59	02/09/2013	Continue fishing operations. Recovered 3480' of cable over 13 runs.			
60	03/09/2013	Continue removing cable for a total of 5,480' cable removed. Perform gauge run to 5,550' to verify no obstruction. Able to reach 5,881' without obstruction. Begin rigging down CT equipment.			
61	04/09/2013	Purge CT with N2, complete rigging down CT equipment. Return CT equipment to yard.			
BREAK IN OPERATIONS - STANDBY FOR SEISMIC MONITORING CREW AVAILABILITY					
62	21/09/2013	Perform cleanout run with Gauge Ring, Junk Basket, and Collar Locator prior to passive monitoring run.			
63	22/09/2013	Rig up VSFusion passive monitoring array, function test, and RIH to begin monitoring deepest interval (tool position: Top = 4621', Bottom = 5310').	High winds and inclement weather.	Paused operations for 2 hours to ensure monitoring tools were not damaged.	
64	23/09/2013	Finish monitoring of first interval, move array up to second interval (tool position: Top = 3600', Bottom = 4300') and log.			
65	24/09/2013	Continue monitoring.			
66	25/09/2013	Move array to next interval (tool position: Top = 2452', Bottom = 3190'). Monitor 3rd interval.			
67	26/09/2013	Continue monitoring 3rd interval. Move up to 4th interval (Tool position: Top = 1972', Bottom = 2710'). Begin monitoring 4th interval.			
68	27/09/2013	Continue monitoring.			
69	28/09/2013	Complete 4th interval monitoring. Rig down VSFusion equipment.			

70	29/09/2013	Mobilize CT unit and rig up 2" CT equipment.			
71	30/09/2013	Standby for cement crew.	Cement crew maxed out on driving hours.	Post-pone operations to ensure protection of personnel and equipment.	
72	01/10/2013	Rig up cement equipment. RIH with CT and pump first plug. Wait on cement for 6 hours. Tag cement with wireline at 5780'. Pressure test plug. RIH with CT and pump 2nd plug. Wait on cement.			
73	02/10/2013	Rig up wireline and tag plug at 4091'. RIH with CT and pump plug 3. Wait on cement. Rig up wireline and tag plug at 1880'. Test plug. Pump 4th and final plug with top at 50'. Rig down cementers and CT.			
74	03/10/2013	Clean location, cut casing head, and remove cellar and mousehole. Erect P&A monument.			

3 Time Analysis

3.1 Time Breakdown

PHASE I Intervention

1. Time due to isolating depth of casing leak-off (11/15/12) – additional **unplanned** 19.25 hrs.
2. Squeeze job (11/18/12), drill out of cement, and additional pressure testing – additional **unplanned** 17.75 hrs.
3. Repair coiled tubing pumps (11/27/12), standby for new coiled tubing pump unit (11/28/13) – **equipment** repair 8.25 hrs.
4. Fish out wireline casing inspection logging tool (multi-finger caliper) (11/29/12) – additional **unplanned** 10.5 hrs.
5. POOH malfunctioned wireline tool to replace (11/30/12) – malfunctioning **equipment** 2.25 hrs.
6. Wait on thru-tubing bridge plug & wireline crew due to inability to travel (12/8/12) – **weather** related 12.0 hrs.
7. Wait on wireline equipment – sinker bar & cement bead dump bailer (12/10/12) – standby for **equipment** 2.0 hrs.
8. Attempt stuck tubing recovery (12/16-12/17/12) – additional **unplanned** 10.08 hrs.
9. Continue stuck pipe recovery attempts (12/19/12) – additional **unplanned** 17.95 hrs.

PHASE II Intervention

1. Due to much quicker operational time of coiled tubing being RIH, standby for cement equipment and water pump truck (4/5/13) – standby for **equipment** 1.75 hrs.
2. Final well head not holding pressure – breakdown stack and re-seat packoff rubbers, re-align tubing head bolts, and re-tighten tubing head to re-test (4/6/13) – additional **unplanned** 3.75 hrs.
3. Geophone array not testing after soldering the array cable back to the cable head – standby for shipment of specialized geophone tester equipment (4/8/13) – standby for **equipment** 8 hrs.

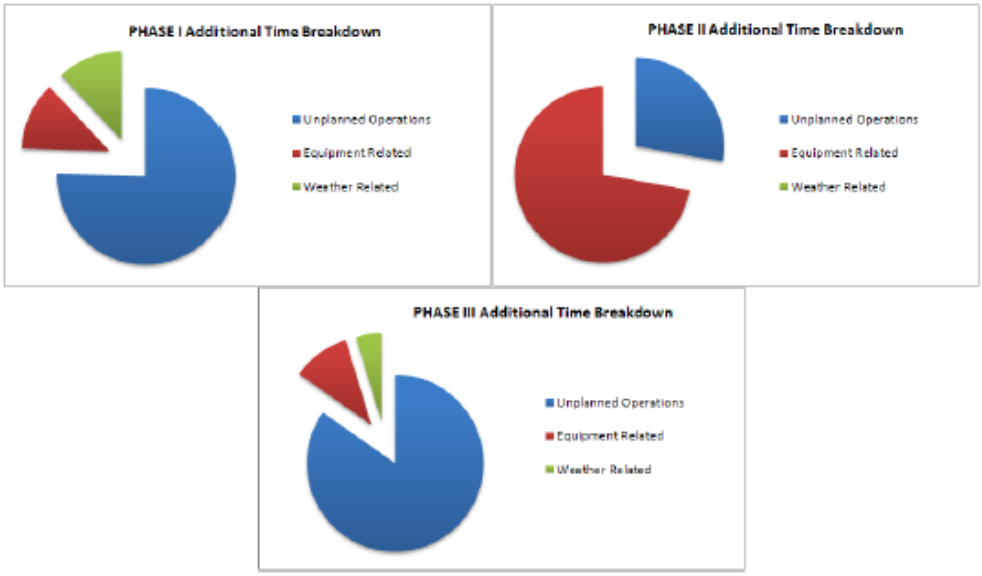
PHASE III Intervention

1. Incorrect adapter flange brought to location. Standby for hot shot with correct adapter (08/26/13) – standby for **equipment** 0.5 hrs.
2. Could not remove "doughnut" from casing head bowl. Forced to weld casing bowl doughnut, gland nut, and CT lightly together to allow all three to move as one. When pulling on CT, gland nut and doughnut came free together (08/29/13) – additional **unplanned** 6.0 hrs.
3. Crane breakdown (08/29/13) – **equipment** repair 2.0 hrs.

4. VSFusion recovery reel motor could not hoist cable (08/29/13) – added time due to **equipment** 1.0 hrs.
5. While securing Kevlar cable to anchor point on surface, cable fell downhole. Fingered-spear fishing operations were planned for contingency operations, but time was lost due to dropping the cable downhole (08/30/13) – additional **unplanned** 14.0 hrs.
6. During fishing run #8, cable slipped off spear and fell back downhole. (09/01/13) – Additional **unplanned** 4.0 hrs.
7. VSFusion surface software encryption issue (09/22/13) – **equipment** repair 1.0 hrs.
8. Standby for high winds and inclement weather (09/22/13) – **weather** related 2.0 hrs.
9. Standby for cement crew due to maxed out driving hours (09/30/13) – additional **unplanned** 12.0 hrs.

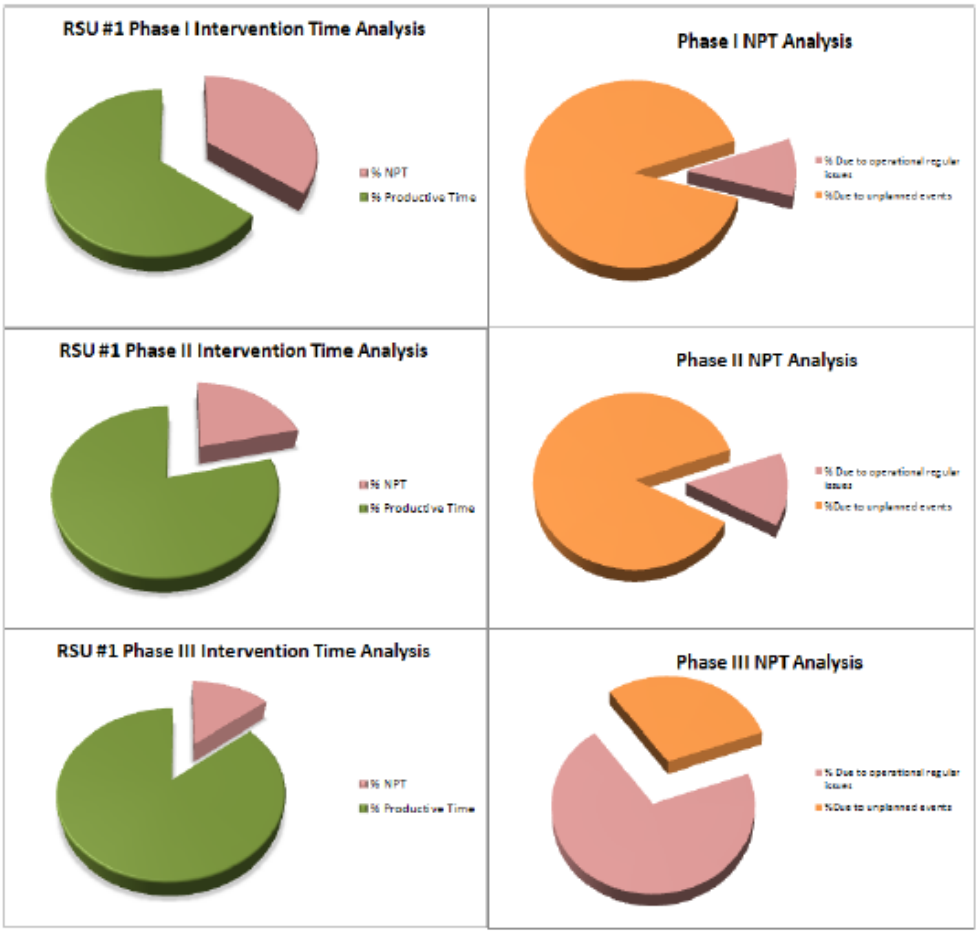
BREAKDOWN OF ADDITIONAL TIME OUTSIDE OF PLANNED OPERATIONAL TIMELINE

PHASE I		
Unplanned Operations	Equipment Related	Weather Related
75.53	12.5	12
% of total operational time		
16.9%	2.8%	2.7%
PHASE II		
Unplanned Operations	Equipment Related	Weather Related
3.75	9.75	0
% of total operational time		
6.1%	16.0%	0.0%
PHASE II		
Unplanned Operations	Equipment Related	Weather Related
36.00	4.50	2.00
% of total operational time		
11.7%	1.5%	0.6%



Breakdown of additional time outside of the planned operational timeline

3.2 NPT Analysis



NPT Breakdown from Phase I-III Well Intervention Operations

Because much of the well intervention operations throughout this project were unique to RSU #1, during each phase of intervention planning, multiple contigency scenarios outside of normal operations were assessed. The University was aprised of all of the risks and contingencies for each phase of well intervention. Due to the operational uniqueness, however, every contigency scenario could not be imagined. Those which were planned for and alotted time in the pre-planning scheduling of the project were considered NPT, but not as unplanned events. Likewise, those events that were not imagined during pre-planning were considered unplanned events.

Despite an operation being unplanned or not, the University was informed at all times of a change in operational procedure.

As can be seen by the above graphs, with each phase of well intervention, lessons were learned and applied, leading to increased percentages of contigency events being pre-

planned in the intervention programs and having contigency operations in place prior to the event ever occurring.

NPT Root Cause Analysis and Corrective Actions for Phases I-III

PHASE I - NPT ROOT CAUSE & CORRECTIVE ACTION		
NPT Event	**Root Cause**	**Corrective Action**
Casing leak	Had been identified in planning stage after reviewing drilling phase operations where a pressure drop was noticed during temporary abandonment that a possible casing integrity issue could arise as a result of corrosion, excessive casing wear, or connection failure could arise	Remedial procedure was undertaken following the decision tree which had been prepared in operations program - Performed squeeze job to repair casing leak
Waiting on equipment	Contingency operations led to immediate need for contingency equipment and crews that had not been scheduled in advance as part of normal operations	Quick notification to 3rd parties to limit downtime waiting for equipment, updated project schedule and notified all product lines and Univeristy of Wyoming of operation timing
Wireline tool became stuck	Third-party connection incorrectly torqued leading to tool disconnecting downhole. This connection was not to be serviced by BHI wireline shop workers during tool servicing	Fishing operations - fish recovered on first attempt. A full investigative report was followed up and notification to the 3rd party provider of the connection was made
Cement Bond Log (CBL) tool failure	Surface acquisition software incorrectly configured for CBL	Restart acquisition software in wireline truck, run spare tool in place for added risk mitigation
Completion string stuck downhole	Pup joint / cross-over below packer buckled under setdown force to set packer	Unset packer and pull string in to tension to relieve some of the buckling force to allow logging tools to pass beyond this depth and achieve operational goals. After fluid sampling and injection testing in both formations it was decided to cut below the packer, leaving fish in the hole.

PHASE II - NPT ROOT CAUSE & CORRECTIVE ACTION		
NPT Event	**Root Cause**	**Corrective Action**
Wait on Equipment (cement & pump truck)	Underestimating speed of CT/geophone running	Documented speed of operations, updated vendor to let them know of updated timeline
Wellhead not testing	Pack-off rubber and tubing head setting	Rather than continue to try to get a good test, recommended removing the tubing head, re-setting pack-off, and re-setting tubing head & re-tightening. Help pressure immediately after this.

PHASE III - NPT ROOT CAUSE & CORRECTIVE ACTION		
NPT Event	**Root Cause**	**Corrective Action**
Incorrect adapter flange delivered to well site	Miscommunication	Hotshot correct adapter to wellsite from Rock Springs.
Could not remove doughnut from casing bowl	Casing bowl doughnut deformation obstructing it from clearing casing head bowl.	Tack welding casing bowl doughnut, gland nut, and CT together to apply force on doughnut when hoisting CT. By hoisting up on CT, enough force was applied to free the doughnut.
Crane breakdown	Minor engine problems, engine idling improperly and backfiring.	Repairs made on-site.
VSFusion recovery reel was inadequate to hoist weight of Kevlar cable	Due to untraditional operations taking place, the first attempt to remove the Kevlar cable along with the CT was made by attempting to hoist the cable with the motorized spool it was originally deployed with. During hoisting attempt, it was discovered that the spool motor had inadequate power to hoist the weight of the Kevlar cable.	Cable was attached to crane rather than VSFusion recovery reel for hoisting.
Cable fell downhole while trying to anchor to VSFusion reel (acting as a fixed tie-point)	Cable had been crimped the day before. The following day, it was tied to the reel with the tie point near the crimp. The additional stress at this point created a weak point where the cable eventually parted.	Began contigency operations as planned in operations program with fingered-spear fishing runs on 2" CT to recover Kevlar cable.
During fishing, cable slipped off fingered-spear and fell back downhole	Not enough spear rotations to coil enough cable in spear fingers for a secure grab.	On following fishing run, extra rotations were performed to ensure cable spooled around spear fingers.
VSFusion surface software encryption error	Improperly configured software.	Contacted technical support to correct issue.
Inclement weather	High winds risked damage to passive monitoring array.	Delay operations to ensure integrity of monitoring tools.
Standby for cement crew due to maxed out driving hours	Scheduling conflict between operations at RSU #1 rig site and location cement crew was departing from.	Delay operations for HS&E compliance and to ensure safety of personnel.

4 Activities Summary

4.1 Phase I of Planned Well Intervention

4.1.1 Bit Record

Two bits were used to drill out the cast iron bridge plug and cement plugs left in the well when it was plugged and abandoned.

Bit No.	Bit Code	Length (ft.)	OD (in)	Connection
1	STX-1	0.61	6 1/8	3 ½ Reg Pin
2	MX-1	0.61	6 1/8	3 ½ Reg Pin

4.1.2 Bottom Hole Assemblies

BHA #1 Drill out — **Length:** 66.55'

Item	Length (ft.)	OD (in)		ID (in)	Connection	
		Blade / TJ	Body		Bottom	Top
Bit #1 STX-1 6 1/8"	0.61		6 1/8	1 5/8		3 ½ Reg Pin
Bit sub	3.22		4 3/4	2	3 ½ Reg Box	3 ½ IF Box
2 ea. Drill Collar	61.97		4 3/4	2 1/4	3 ½ IF Pin	3 ½ IF Box
XO Sub	0.72		4 11/16	2	3 ½ IF Pin	2 7/8 EUE 8rd Box

BHA #2 Packer Run to locate leak in the 7" casing — **Length:** 7.66'

Item	Length (ft.)	OD (in)		ID (in)	Connection	
		Blade / TJ	Body		Bottom	Top
Retrievable Packer	7.16		5.968	2.405		3 ½ IF Box
Test Sub	0.5		3.7	1.725	3 ½ IF Pin	2 7/8 EUE 8 RD Box

BHA #3 Drill out — **Length:** 127.54'

Item	Length (ft.)	OD (in)		ID (in)	Connection	
		Blade / TJ	Body		Bottom	Top
Bit #1 STX-1 6 1/8"	0.61		6 1/8	1 5/8		3 ½ Reg Pin
Bit sub	3.22		4 3/4	2	3 ½ Reg Box	3 ½ IF Box
4 ea. Drill Collar	122.99		4 3/4	2 1/4	3 ½ IF Pin	3 ½ IF Box
XO Sub	0.72		4 11/16	2	3 ½ IF Pin	2 7/8 EUE 8rd Box

BHA #4 Drill out / Bit change **Length:** 189.55'

Item	Length (ft.)	OD (in)		ID (in)	Connection	
		Blade / TJ	Body		Bottom	Top
Bit #2 MX-1 6 1/8"	0.61		6 1/8	1 5/8		3 ½ Reg Pin
Bit sub	3.22		4 3/4	2	3 ½ Reg Box	3 ½ IF Box
6 ea. Drill Collar	185		4 3/4	2 1/4	3 ½ IF Pin	3 ½ IF Box
XO Sub	0.72		4 11/16	2	3 ½ IF Pin	2 7/8 EUE 8rd Box

BHA # 5 PBR clean out **Length:** 13.75'

Item	Length (ft.)	OD (in)		ID (in)	Connection	
		Blade / TJ	Body		Bottom	Top
Polish Mill	1.55	4.680	4.132	2.0		2 7/8 IF Box
XO	1.09		4.071	1.09	2 7/8 IF Pin	2 7/8 8 Rd Box
4' Pup Joint	3.70		2.875	2.441	2 7/8 8Rd Pin	2 7/8 8 Rd PIN
XO	1.55		4.267	1.50	2 7/8 8Rd Box	3 ½ Reg Pin
Casing Scraper	3.89		3.89	1.30	3 ½ Reg Box	3 ½ Reg Pin
XO	1.97		4.223	1.50	3 ½ Reg Box	2 7/8 8 Rd EUE Box

BHA # 6. 3 ½" Liner clean out Coil Tubing run **Length:** 15.38'
Attached Drawing

Item	Length (ft.)	OD (in)		ID (in)
		Blade / TJ	Body	
2 7/8" 3-way insert blade mill	0.23		2.867	0.00
Bit Sub	0.22		2.010	0.850
2 1/8 VIP Motor	11.13		2.120	0.00
2 1/8 Drain Sub Bypass	0.83		2.130	0.970
2 1/8 Universal Hydraulic disconnect with 5/8 Ball seat	1.24		2.120	0.563
2 1/8 Dual Back pressure Valve	1.38		2.135	0.960
Weld-on connector for 1 ¾ Coil	0.35		2.120	1.00

Customer:	UNIVERSITY OF WYO
Well Name:	R.S.U. #1
Field:	WILDCAT
Lease:	
Tubing:	1 3/4 COIL
Casing:	7" 26#
Liner:	3 1/2" 9.3#
Job Type:	CTCO with Agitator and Jar

BAKER HUGHES

Baker Oil Tools

THRU-TUBING SERVICES – ROCK SPRINGS, WY – (307) 362-3050

Proposed BHA	Equipment Description	Serial Number	OD (Inches)	ID (Inches)	Length (Feet)	Total (Feet)
	WELD-ON CONNECTOR FOR 1 3/4 COIL		2.120	1.000	0.38	0.38
	2 1/8 DUAL BACK PRESSURE VALVE S/N - ZRR917		2.125	0.000	1.35	1.73
	2 1/8 UNIVERSAL HYDRAULIC DISCONNECT WITH 5/8" BALL SEAT SHEAR VALUE 2400PSI (3 BRASS) S/N - 10062097		2.120	0.563	1.24	2.97
	2 1/8 DRAIN SUB DRESSED TO 1 1/2 EDL BYPASS AT 35BL/MIN RATE S/N - ZRX00987		2.130	0.870	0.93	3.90
	2 1/8 VIP MUD MOTOR X 1 1/2" MT FLOW RATE 17-74 GAL/MIN 160-700RPM MAX OVER PULL - 29,000# S/N - ZMC20113		2.120	0.000	11.13	14.93
	BITSUB 1 1/2 MT PIN X 1 1/2 AROD BOX S/N - ZRT00149		2.010	0.000	0.22	15.15
	2 1/8 BLADE BIT		2.067	0.000	0.23	15.38

DATE:	BHA DRAWING PREPARED BY:		OVERALL LENGTH OF BHA:
11.27.12	PAUL GREEN		15.38

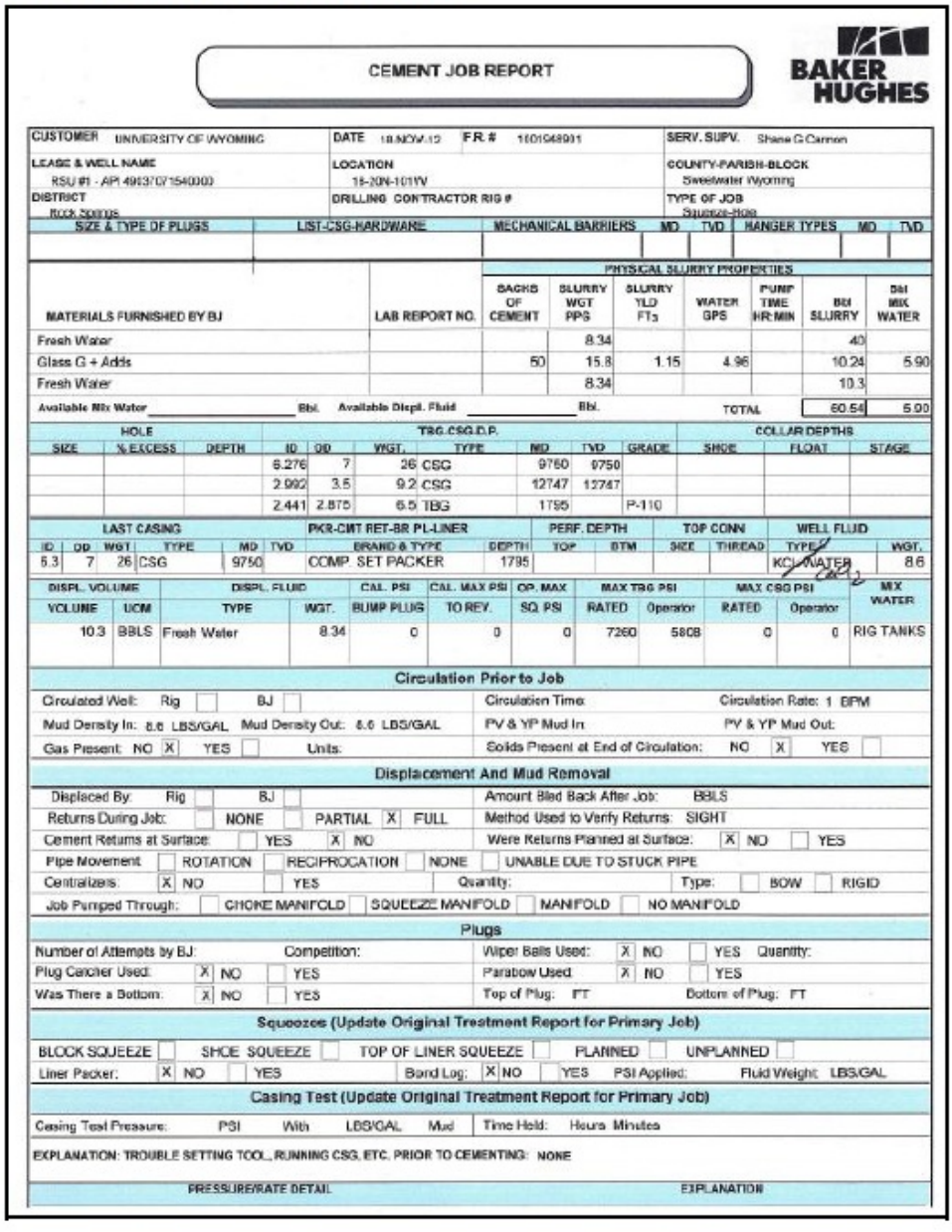
4.1.3 Drilling Fluid

For the well intervention on RSU #1 the primary drilling system used was fresh water. The well at the beginning had calcium chloride water of 9.4ppg. During the operations additives were added to the system to improve hole cleaning.

Stage	Mud Type	Density (PPG)	Volume used Fresh water	Comments
Abandoned well	Calcium chloride water	9.4	-	
Drill out cement plugs	Mix of fresh water and CaCl2	8.7	1002 bbls	Replaced system completely once and conditioned system twice.
PBR Polish	Fresh water	8.4	80 bbls	Additional barrels to condition system
Liner clean out	Fresh water +New drill	8.6	100 bbls	Additional 60 bbls of hot water for CT run.
Perforations and water sampling	Fresh water	8.4	50 bbls	Amount reflects additional water used.
Injection test	Fresh water	8.4	300 bbls	Amount reflects additional water used.

4.1.4 Cementing Operations

A squeeze job was required to fix a leak encountered at 2,103.4 ft. Below are detailed reports regarding the cementing operations.



CEMENT JOB REPORT

BAKER HUGHES

CUSTOMER: UNIVERSITY OF WYOMING	DATE: 18-NOV-13 F.R. #: 1601948931	SERV. SUPV.: Shane G Cannon
LEASE & WELL NAME: RSU #1 - API 49037071540000	LOCATION: 18-20N-101W	COUNTY-PARISH-BLOCK: Sweetwater Wyoming
DISTRICT: Rock Springs	DRILLING CONTRACTOR RIG #:	TYPE OF JOB: Squeeze-Hole

SIZE & TYPE OF PLUGS	LIST-CSG-HARDWARE	MECHANICAL BARRIERS	MD	TVD	HANGER TYPES	MD	TVD

MATERIALS FURNISHED BY BJ	LAB REPORT NO.	PHYSICAL SLURRY PROPERTIES: SACKS OF CEMENT	SLURRY WGT PPG	SLURRY YLD FT3	WATER GPS	PUMP TIME HR:MIN	Bbl SLURRY	Bbl MIX WATER
Fresh Water			8.34				40	
Glass G + Adds		50	15.8	1.15	4.96		10.24	5.90
Fresh Water			8.34				10.3	
						TOTAL	60.54	5.90

Available Mix Water _____ Bbl. Available Displ. Fluid _____ Bbl.

HOLE SIZE	% EXCESS	DEPTH	TBG.CSG.D.P. ID	OD	WGT.	TYPE	MD	TVD	GRADE	COLLAR DEPTHS SHOE	FLOAT	STAGE
			6.276	7	26	CSG	9750	9750				
			2.992	3.5	9.2	CSG	12747	12747				
			2.441	2.875	6.5	TBG	1795		P-110			

LAST CASING ID	OD	WGT.	TYPE	MD	TVD	PKR-CMT RET-BR PL-LINER BRAND & TYPE	DEPTH	PERF. DEPTH TOP	BTM	TOP CONN SIZE	THREAD	WELL FLUID TYPE	WGT.
5.3	7	26	CSG	9750		COMP. SET PACKER	1795					KCL WATER	8.6

DISPL. VOLUME VOLUME	UOM	DISPL. FLUID TYPE	WGT.	CAL. PSI BUMP PLUG	TO REV.	CAL. MAX PSI OP. MAX SQ. PSI	MAX TBG PSI RATED	Operator	MAX CSG PSI RATED	Operator	MIX WATER
10.3	BBLS	Fresh Water	8.34	0	0	0	7260	5808	0	0	RIG TANKS

Circulation Prior to Job

Circulated Well: Rig [ ] BJ [ ] | Circulation Time: | Circulation Rate: 1 BPM

Mud Density In: 8.6 LBS/GAL Mud Density Out: 8.6 LBS/GAL | PV & YP Mud In: | PV & YP Mud Out:

Gas Present: NO [X] YES [ ] Units: | Solids Present at End of Circulation: NO [X] YES [ ]

Displacement And Mud Removal

Displaced By: Rig [ ] BJ [ ] | Amount Bled Back After Job: BBLS

Returns During Job: [ ] NONE [ ] PARTIAL [X] FULL | Method Used to Verify Returns: SIGHT

Cement Returns at Surface: [ ] YES [X] NO | Were Returns Planned at Surface: [X] NO [ ] YES

Pipe Movement: [ ] ROTATION [ ] RECIPROCATION [ ] NONE [ ] UNABLE DUE TO STUCK PIPE

Centralizers: [X] NO [ ] YES Quantity: Type: [ ] BOW [ ] RIGID

Job Pumped Through: [ ] CHOKE MANIFOLD [ ] SQUEEZE MANIFOLD [ ] MANIFOLD [ ] NO MANIFOLD

Plugs

Number of Attempts by BJ: Competition: | Wiper Balls Used: [X] NO [ ] YES Quantity:

Plug Catcher Used: [X] NO [ ] YES | Parabow Used: [X] NO [ ] YES

Was There a Bottom: [X] NO [ ] YES | Top of Plug: FT Bottom of Plug: FT

Squeezes (Update Original Treatment Report for Primary Job)

BLOCK SQUEEZE [ ] SHOE SQUEEZE [ ] TOP OF LINER SQUEEZE [ ] PLANNED [ ] UNPLANNED [ ]

Liner Packer: [X] NO [ ] YES Bond Log: [X] NO [ ] YES PSI Applied: Fluid Weight: LBS/GAL

Casing Test (Update Original Treatment Report for Primary Job)

Casing Test Preasure: PSI With LBS/GAL Mud | Time Held: Hours Minutes

EXPLANATION: TROUBLE SETTING TOOL, RUNNING CSG, ETC. PRIOR TO CEMENTING: NONE

PRESSURE/RATE DETAIL EXPLANATION

CEMENT JOB REPORT

BAKER HUGHES

Shoe Test (Update Original Treatment Report for Primary Job)

Depth Drilled out of Shoe: FT	Target EMW: LBS/GAL Actual EMW: LBS/GAL
Number of Times Tests Conducted:	Mud Weight When Test was Conducted: LBS/GAL

Problems Before Job (I.E. Running Casing, Circulating Well, ETC)
NONE

Problems During Job (I.E. Lost Returns, Equipment Failure, Bulk Delivery, Foaming, ETC)
NONE

Problems After Job (I.E. Gas at Surface, Float Equipment Failed, ETC)
NONE

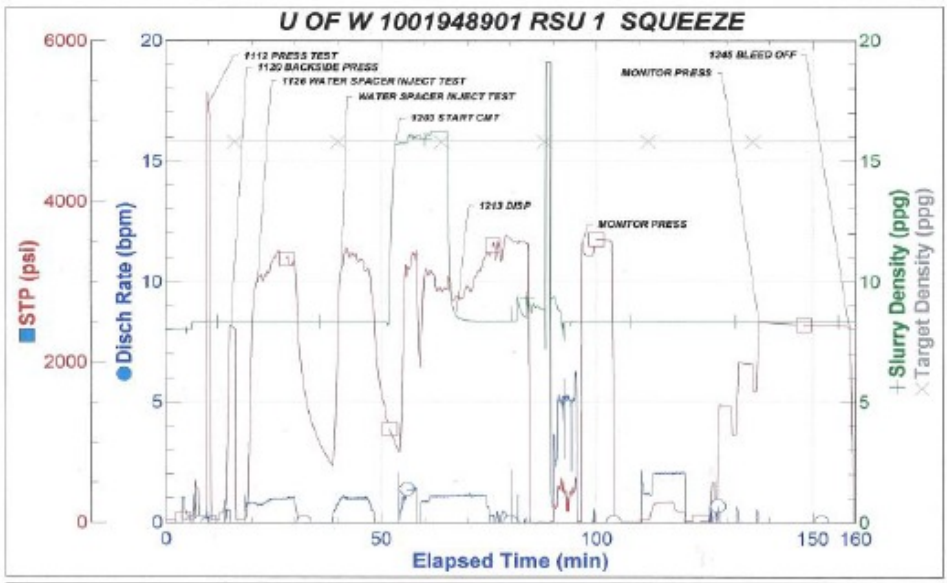
PRESSURE/RATE DETAIL

TIME HR:MIN.	PRESSURE - PSI PIPE	PRESSURE - PSI ANNULUS	RATE BPM	BBL FLUID PUMPED	FLUID TYPE	EXPLANATION
						SAFETY MEETING: BJ CREW [X] CO. REP. [X]
						TEST LINES 5335 PSI
						CIRCULATING WELL - RIG [ ] BJ [ ]
09:00					----------	ON LOCATION
09:30					----------	SAFETY MEETING WITH RIG CREW AND CO-REP.
11:12		5335			H2O	PRESS TEST PUMP AND LINES
11:26		3300	1	7	H2O	START WATER SPACER GET INJECTION RATE
11:38		3000			----------	SHUT DOWN MONITOR PRESS
11:47		3360	1	13	H2O	WATER SPACER
11:56					----------	BATCH CMT AT 15.8 PPG 50 SKS
12:03		3350	1	10.2	CMT	START CMT
12:13		2750	1		H2O	START DISP, SQUEEZE CMT
12:28		3550		12	H2O	SHUT DOWN MONITOR PRESS
12:58			2	17	H2O	REVERSE OUT 2 BBLS CMT BACK
13:15		2500			H2O	PRESS UP AND MONITOR
13:45					----------	BLEED OFF STOP JOB
					----------	THANKS SHANE AND CREW !!!!!

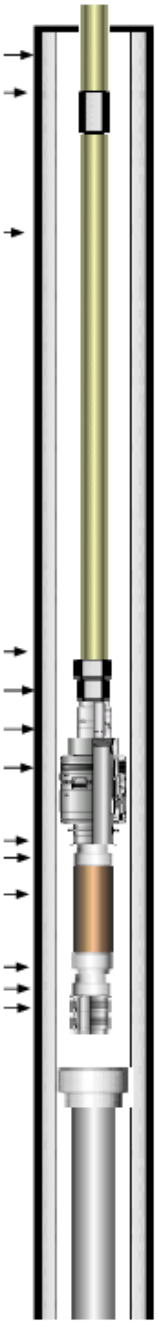
BUMPED PLUG	PSI TO BUMP PLUG	TEST FLOAT EQUIP.	BBL CMT RETURNS/ REVERSED	TOTAL BBL PUMPED	PSI LEFT ON CSG	SPOT TOP OUT CEMENT	Service Supervisor Signature:
Y [N]		Y [N]	2	190	0	Y [N]	

BAKER HUGHES

Baker Hughes JobMaster Program Version 3.60
Job Number: 1001948901
Customer: UNIVERSITY OF WYOMING
Well Name: RSU 1 15-20N-101W



4.1.5 Completion Assembly Sketch



SOUTHWEST
WYOMING
COMPLETIONS

BAKER HUGHES
Baker Oil Tools

COMPANY	UNIVERSITY OF WYOMING				DATE	11/30/12
LEASE	R.S.U. #1					
CASING	Size 7"	Weight 26	Grade N-80	Thread BTRSS	Depth 9468	
LINER	Size 3.5	Weight 9.2	Grade L-80	Thread	Depth 12747	
TUBING	First String	Size 2.875	Weight 6.5	Grade P110	Thread EU8RD	Depth
	Second String	Size	Weight	Grade	Thread	Depth
Prepared for: JIM GIVENS			Perforations:			

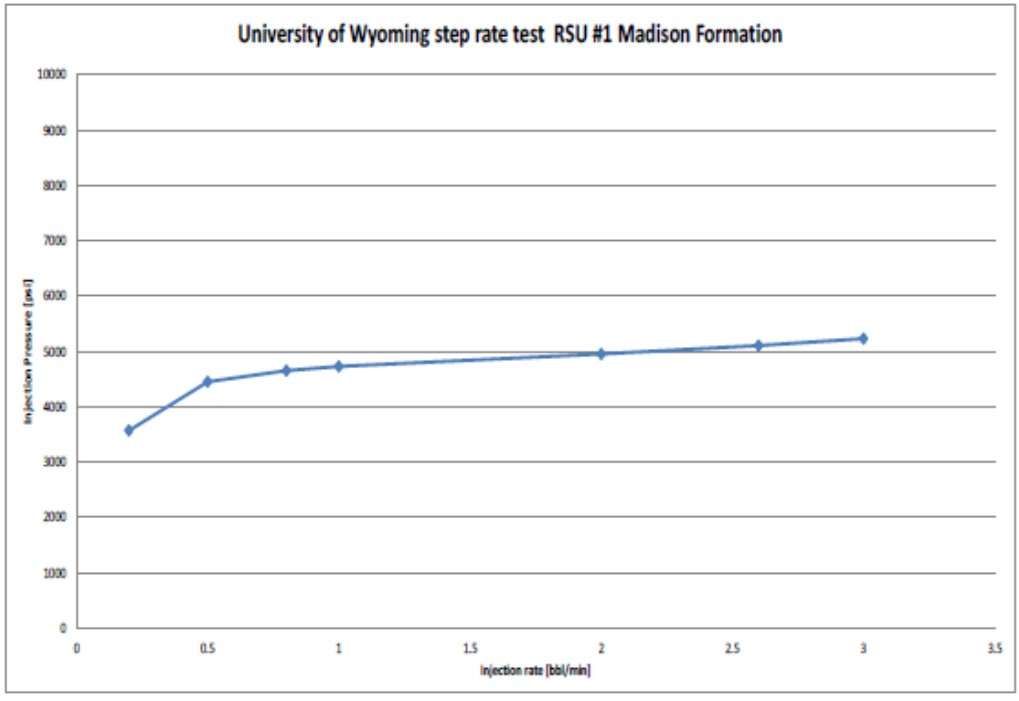
ITEM No#	Length	Description	ID	OD	Depth
		E.O.T.			9468.00
1	1.77	81FA47 LTSA WITH A-RYTE SEAL	3.875	5.18	9466.23
2	0.89	XOVER 2.875 EU8RD X 4.5 BUTRES	2.415	4.51	9465.34
3	1.39	XOVER 3.5 IF X 2.875 EU8RD S/N - ZW82-1934	2.308	4.75	9463.95
4	62.01	2 x 4 3/4" DRILL COLLARS x 3.5 IF (1 - 31.02 // 2 - 30.99)	2.25	4.75	9401.94
5	1.42	XOVER 3.5 IF x 2.875 EU8RD	2.25	4.75	9400.52
6	2.29	2' 2.875 EU8RD PUP JT	2.441	2.875	9398.23
7	6.14	47B2 AR-1 "SNAP-SET PKR	2.4	5.935	9392.09
8	3.81	R.H. EQUALIZING VALVE	2.4	4.5	9388.28
9	0.77	BURST DISK SUB (PORCELAIN) 10K BELOW // 1K ABOVE	2.4	3.685	9387.51
10	6.24	6' 2.875 N-80 EU8RD PUP JT	2.441	2.875	9381.27
11	9326.70	299 JTS 2.875 EU8RD P110 TBG	2.441	2.875	54.57
12	18.13	2 x 2.875 eu8rd n80 pup jts			36.44
13	31.15	1 JT 2.875 EU8RD P110 TBG			5.29
	4.20	pup jt (2.875 eu8rd n80)			1.09
	10.80	adjusted kb measurement			-9.71
		the 9.71 leftover is tool travel and compression			

4.1.6 Injection Test Results

4.1.6.1 Madison Formation. SRT Surface Chart

Injection pressure not to exceed:	8000 psi		ISIP (psi):4527
Maximum anticipated Injection rate:	3 bbl/min	Date:	12/06/2012
Formation tested:	Madison	Well:	RSU # 1

Step	Rate (bbl/min)	Pressure (psi)	Time (Min) 0	5	10	15	20	25	30
1	0.2		350	2791	3218	3394	3495	3495	3570
2	0.5		3570	3923	4049	4199	4376	4451	4451
3	0.8		4451	4678	4703	4678	4678	4678	4652
4	1		4652	4728	4728	4778	4728	4652	4728
5	2		4728	5055	5055	5005	5030	4954	4954
6	2.6		4954	5231	5281	5181	5206	5156	5105
7	3		5105	5332	5207	5307	5256	5281	5231



4.1.6.2 Madison Formation. SRT BHP

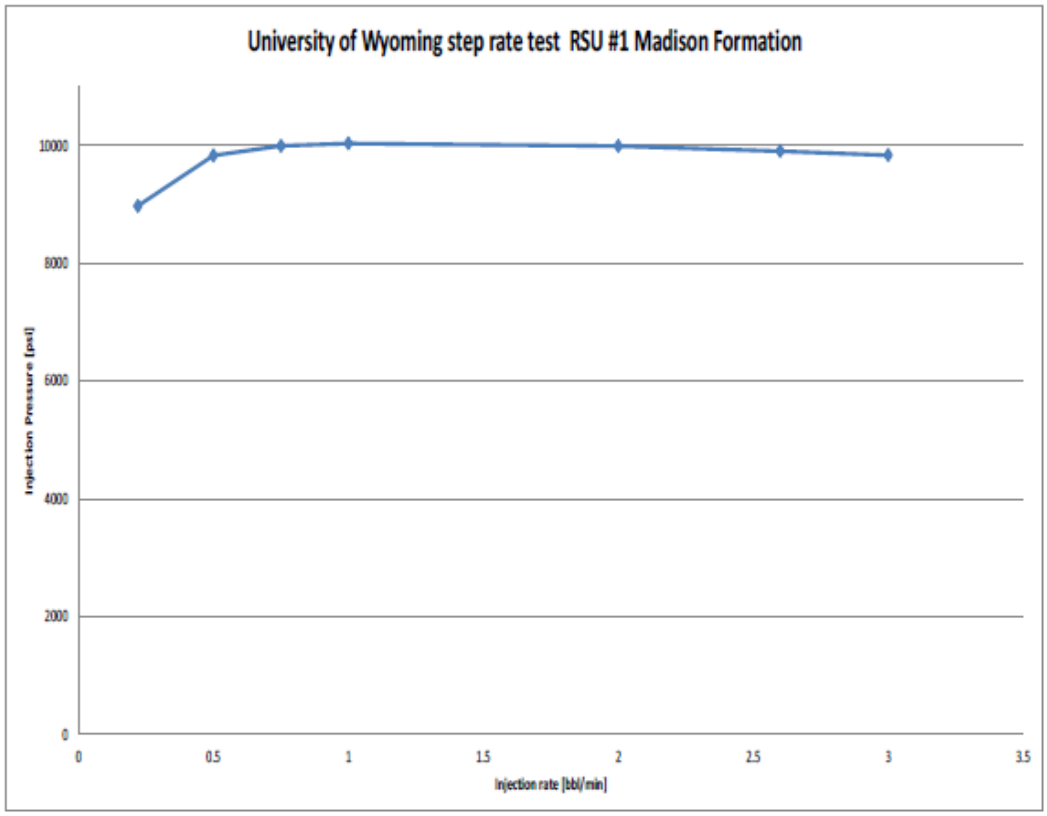
The bottom hole pressure had to be calculated from surface data and friction estimates because the down hole measurement tool failed during the job.

Step	Rate (bbl/min)	Pressure (psi)	Time (Min) 30
1	0.22		8973
2	0.5		9831
3	0.75		9994
4	1		10036
5	2		9992.6
6	2.6		9905
7	3		9837

Madison formation Bottom hole pressure estimations:

Rate (bbl/min)	Depth (ft)	Pressure on down hole tool (psi)	Pressure at Surface (psi)	Delta Pressure (psi)	Calculated Hydrostatic (psi)	P ref Friction Delta Pressure less Hydro (psi)	BHP less friction (psi)
0.3	12,470	8956	3272	5684	5352	332	8624
0.3	12,470	9489	3871	5618	5352	266	9223
0.3	12,470	9740	4196	5544	5352	192	9548
0.3	12,470	9864	4346	5518	5352	166	9698
0.3	12,470	10000	4546	5454	5352	102	9898
0.3	12,470	9977	4501	5476	5352	124	9853

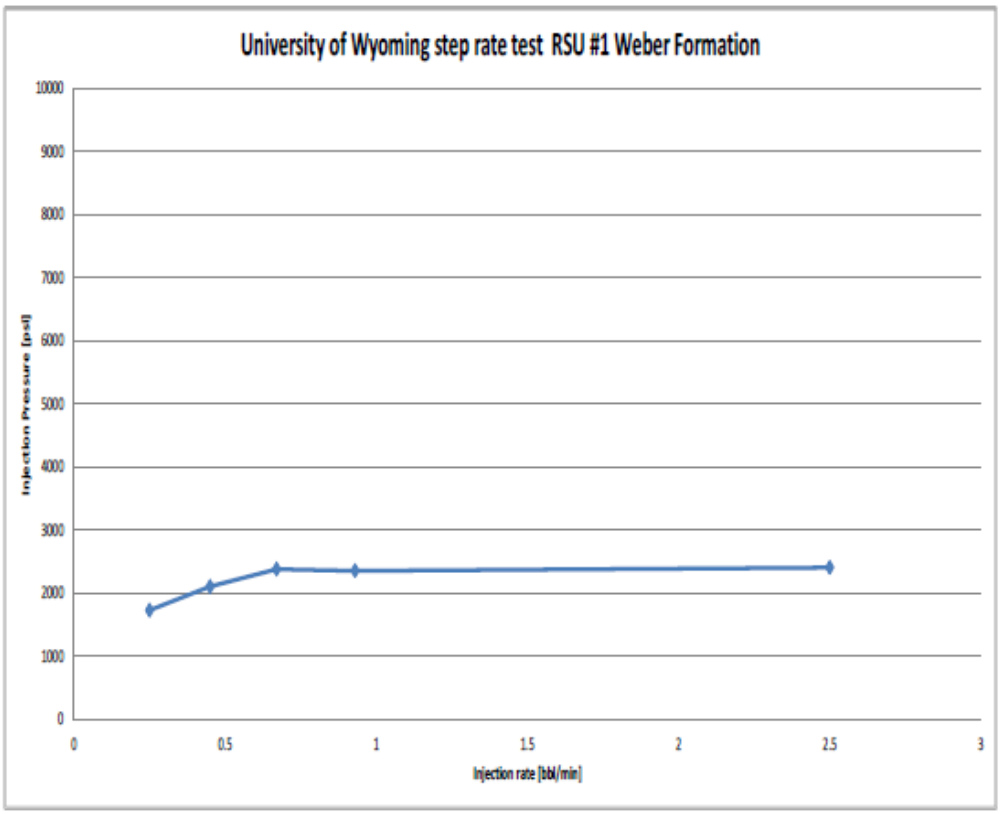
Rate (bbl/min)	Final Pressure at surface (psi)	Calculated Hydrostatic (psi)	Friction in tubing (psi)	Friction in liner (psi)	Total pipe friction (psi)	Estimated BHP (psi)
0.2	3570	5408	5		5	8973
0.5	4451	5408	26	2	28	9831
0.8	4652	5408	62	4	66	9994
1	4728	5408	93	7	100	10036
2	4954	5408	345.4	24	369.4	9992.6
2.6	5105	5408	568	40	608	9905
3	5231	5408	750	52	802	9837


University of Wyoming step rate test RSU #1 Madison Formation
Injection Pressure [psi]
10000
8000
6000
4000
2000
0
0
0.5
1
1.5
2
2.5
3
3.5
Injection rate [bbl/min]

4.1.6.3 Weber Formation. SRT Surface Chart

Injection pressure not to exceed:	8000 psi		ISIP (psi): 2329
Maximum anticipated Injection rate:	3 bbl/min	Date:	12/15/2012
Formation tested:	Weber	Well:	RSU # 1

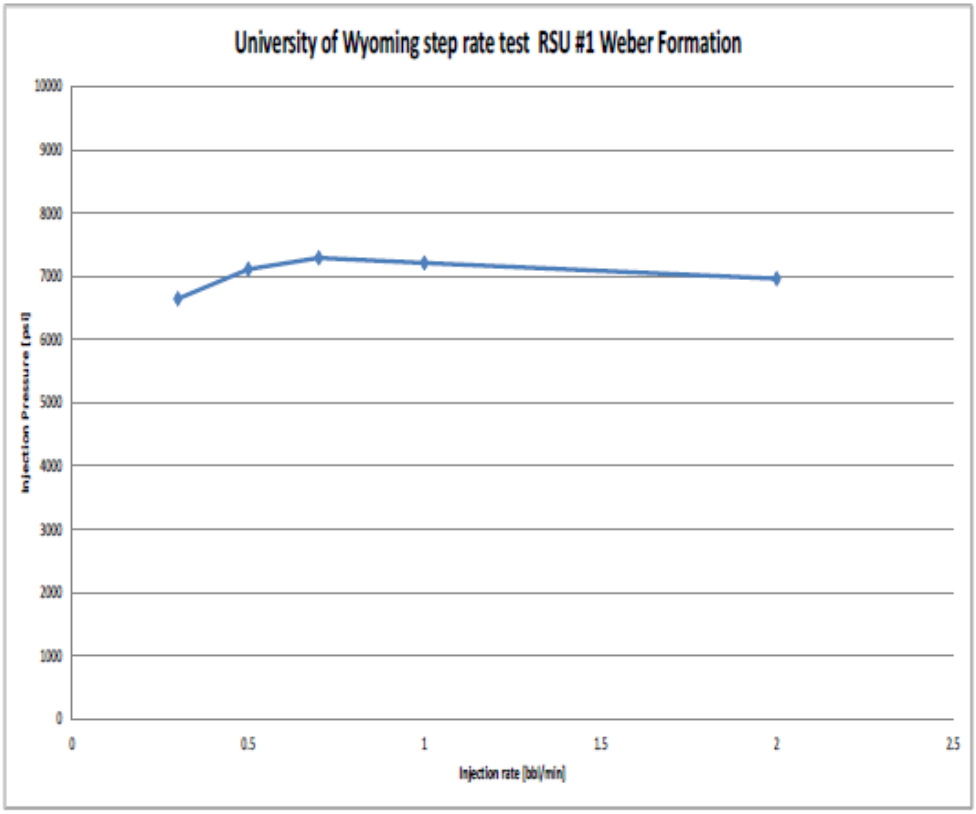
			Time (Min)						
Step	Rate (bbl/min)	Pressure (psi)	0	5	10	15	20	25	30
1	0.25		49	926	1578	1653	1678	1703	1728
2	0.45		1828	1954	2029	2054	2054	2079	2104
3	0.67		2014	2229	2229	2254	2379	2329	2380
4	0.93		2405	2430	2154	2179	2154	2254	2355
5	2.5		2530	2655	2254	2279	2304	2384	2405
7									



4.1.6.4 Weber Formation. SRT BHP

Injection pressure not to exceed:	8000 psi		ISIP (psi): 2329
Maximum anticipated Injection rate:	3 bbl/min	Date:	12/15/2012
Formation tested:	Weber	Well:	RSU#1

			Time (Min)						
Step	Rate (bbl/min)	Pressure (psi)	0	5	10	15	20	25	30
1	0.3		4928	4794	5880	6535	6586	6625	6642
2	0.5		6642	7000	7061	7069	7060	7080	7110
3	0.7		7110	7170	7170	7189	7213	7253	7288
4	1		7288	7295	7030	7035	7028	7067	7208
5	2		7208	7145	6998	6990	6964	6958	6960
7									



4.1.7 Performance

- Highlights
  - No major incidents or accidents were reported
  - Water sampling and injection test was done in both Madison and Weber formation.
- Lowlights
  - Longer operational time due to unplanned events and unexpected tool failure.
  - Weather affected operation times. Additional steps needed to drain lines and prevent from freezing.
- Deviation from plan
  - Additional trip to change bit was necessary to continue intervention plan.
  - Fishing job resulted from malfunction of logging tool.
  - Completion assembly stuck downhole required additional equipment to proceed with well testing.
  - Chemical cutter used to retrieve tubing.

4.2 Phase II of Planned Well Intervention

4.2.1 Description of Operations

- Operations spanned from April 3-10, 2013.
- A second attempt at running a geophone array in the hole for permanent deployment via 1-1/2 inch coiled tubing after setting a cast-iron bridge plug above the top of the fish left during remedial operations in December, 2012.
- After the geophone array was landed at depth, it was permanently cemented down hole to provide coupling with the surrounding 7 inch casing (705 ft cement plug)

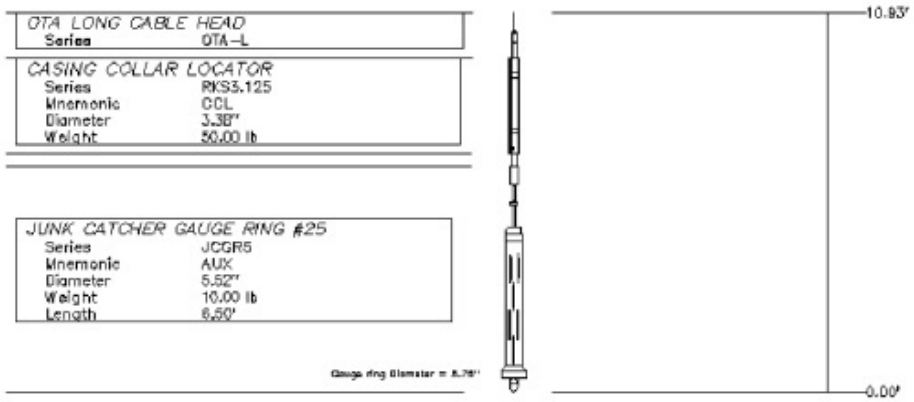
4.2.2 Drilling Fluid

For the second stage of the planned well intervention fresh water was used for circulating and clean-up of the wellbore. No additives used.

4.2.3 Casing Integrity Test, Wellbore Clean-up and Logging.

Prior to running coiled tubing and the geophone array in the hole, it was necessary to ensure the 7 inch casing was free of debris so the risk of damaging the geophone array/cable was reduced.

It was planned and executed a run with junk basket and a casing inspection log using the assemblies shown below.



Total Length: 10.93'
Total Weight: Not Available
Max Diameter: 0' 5.52"

4.2.4 Cast Iron Bridge Plug (CIBP) Information

A 4 ft. N-1, wireline set, cast-iron bridge plug (CIBP) was set directly on top of the fish left in the hole at 9366 ft. resulting in a PBTD of 9362 ft. isolating the tested areas and the fish on top of the PBR.

After applying voltage to the wireline, 43 seconds passed before the E-4 setting tool released 55,000 lb.-f of shearing force to shear the setting screws and result in the CIBP being set in place. The timing of the events agrees with manufactured design.

Below is an image of the CIBP and setting tool and the assembly used to set the tool.



CIBP and setting tool to cover fish left in hole during Phase I

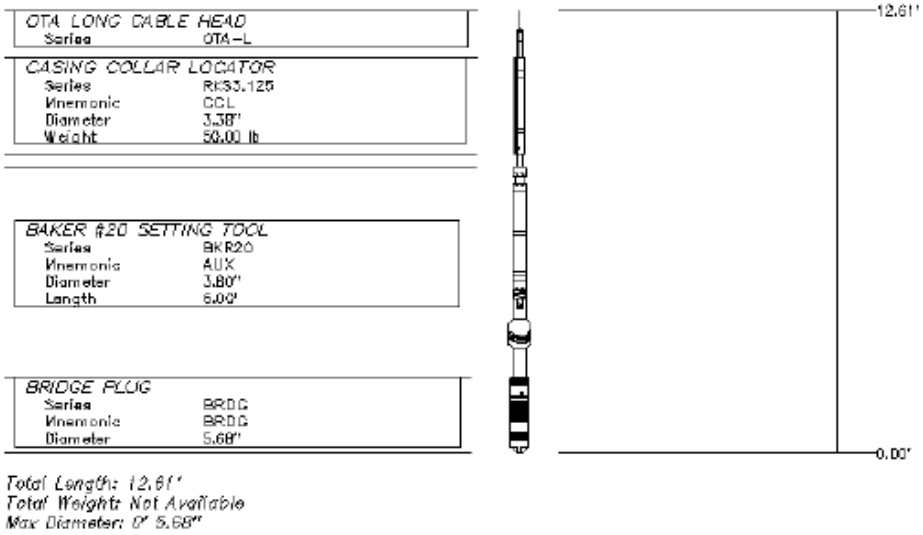


Diagram of CIBP, setting tool, and CCL used in Phase II

4.2.5 Geophone Specifications

The OMNI-2400 High Temperature Geophone has been tested at 200°C for more than 300 hours with no loss in performance specifications. Its design structure and strength magnetic field makes the output of this small geophone equal to or greater than the output of larger units.

Geophones have dual coil construction that should allow it to withstand severe shocks and rough handling. The patented PCB header provides easy and reliable electrical connections. Features of the geophones are summarised below.

- High output sensitivity (1.32 volt/in/sec)
- Sensors rated to 200°C
- Tri-axial and gimbal down hole operations
- Omni directional geophone design provides ideal vector fidelity response

The geophones were placed in a protective housing and connected to the surface unit through armoured cable (see images below).



OMNI-2400 geophone sensor




Protective casing surrounding geophone sensor (left) and the armoured cable linking the array (right).

4.2.6 Geophone Cable Specifications

The reinforced cable that was used to connect the sensors is approximately 0.68 inch in diameter. The cable had external protection which is abrasion resistant, and internal to this cable is Kevlar to carry the load.

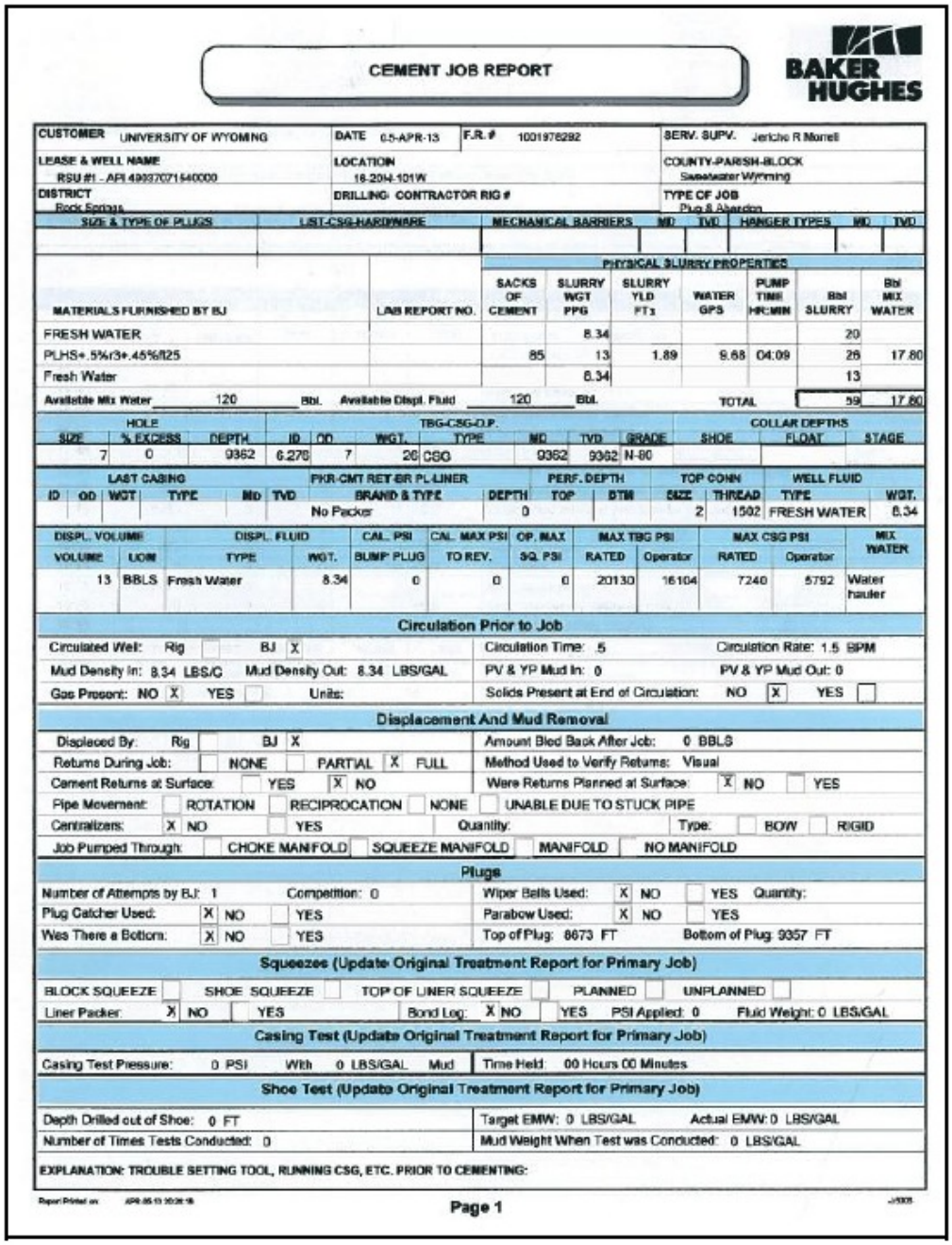
There is also a PVC protection inside for the paired conductors that connect to the sensor. The diameter of the PVC section of the cable is 0.65 – 0.66 inches. The first 650 ft. of the cable connected each of the 14 geophones.

The cable was successfully landed and cemented in place. Monitoring of data received from these devices will be provided on separate contract by VS Fusion.

4.2.7 Cementing Operations

The geophone array was cemented within the 7 inch intermediate casing for permanent geo-seismic monitoring. The array was cemented with 27 bbl of 13.0 ppg cement slurry resulting in 55 ft. of cement over the uppermost phone for a total of a 705 ft. balanced plug.

A detailed report of this activity can be found below.



CEMENT JOB REPORT

BAKER HUGHES

CUSTOMER: UNIVERSITY OF WYOMING	DATE: 05-APR-13	F.R. #: 1001976292	SERV. SUPV.: Jericho R Morrell
LEASE & WELL NAME: RSU #1 - API 49037071540000	LOCATION: 16-20N-101W		COUNTY-PARISH-BLOCK: Sweetwater Wyoming
DISTRICT: Rock Springs	DRILLING CONTRACTOR RIG #:		TYPE OF JOB: Plug & Abandon

SIZE & TYPE OF PLUGS	LIST-CSG-HARDWARE	MECHANICAL BARRIERS	MD	TVD	HANGER TYPES	MD	TVD

PHYSICAL SLURRY PROPERTIES

MATERIALS FURNISHED BY BJ	LAB REPORT NO.	SACKS OF CEMENT	SLURRY WGT PPG	SLURRY YLD FT3	WATER GPS	PUMP TIME HR:MIN	Bbl SLURRY	Bbl MIX WATER
FRESH WATER			8.34				20	
PLHS+.5%r3+.45%fl25		85	13	1.89	9.68	04:09	28	17.80
Fresh Water			8.34				13	
Available Mix Water: 120 Bbl. Available Displ. Fluid: 120 Bbl.						TOTAL	59	17.80

HOLE SIZE	HOLE % EXCESS	HOLE DEPTH	TBG-CSG-D.P. ID	OD	WGT.	TYPE	MD	TVD	GRADE	COLLAR DEPTHS SHOE	FLOAT	STAGE
7	0	9362	6.276	7	26	CSG	9362	9362	N-80			

LAST CASING ID	OD	WGT	TYPE	MD	PKR-CMT RET-BR PL-LINER TVD	BRAND & TYPE	PERF. DEPTH TOP	BTM	TOP CONN SIZE	THREAD	WELL FLUID TYPE	WGT.
						No Packer	0		2	1502	FRESH WATER	8.34

DISPL. VOLUME VOLUME	UOM	DISPL. FLUID TYPE	WGT.	CAL. PSI BUMP PLUG	CAL. MAX PSI TO REV.	OP. MAX SQ. PSI	MAX TBG PSI RATED	Operator	MAX CSG PSI RATED	Operator	MIX WATER
13	BBLS	Fresh Water	8.34	0	0	0	20130	16104	7240	5792	Water hauler

Circulation Prior to Job

Circulated Well: Rig [ ] BJ [X]	Circulation Time: 5 Circulation Rate: 1.5 BPM
Mud Density In: 8.34 LBS/G Mud Density Out: 8.34 LBS/GAL	PV & YP Mud In: 0 PV & YP Mud Out: 0
Gas Present: NO [X] YES [ ] Units:	Solids Present at End of Circulation: NO [X] YES [ ]

Displacement And Mud Removal

Displaced By: Rig [ ] BJ [X]	Amount Bled Back After Job: 0 BBLS
Returns During Job: [ ] NONE [ ] PARTIAL [X] FULL	Method Used to Verify Returns: Visual
Cement Returns at Surface: [ ] YES [X] NO	Were Returns Planned at Surface: [X] NO [ ] YES
Pipe Movement: [ ] ROTATION [ ] RECIPROCATION [ ] NONE [ ] UNABLE DUE TO STUCK PIPE	
Centralizers: [X] NO [ ] YES Quantity:	Type: [ ] BOW [ ] RIGID
Job Pumped Through: [ ] CHOKE MANIFOLD [ ] SQUEEZE MANIFOLD [ ] MANIFOLD [ ] NO MANIFOLD	

Plugs

Number of Attempts by BJ: 1 Competition: 0	Wiper Balls Used: [X] NO [ ] YES Quantity:
Plug Catcher Used: [X] NO [ ] YES	Parabow Used: [X] NO [ ] YES
Was There a Bottom: [X] NO [ ] YES	Top of Plug: 8673 FT Bottom of Plug: 9357 FT

Squeezes (Update Original Treatment Report for Primary Job)

BLOCK SQUEEZE [ ] SHOE SQUEEZE [ ] TOP OF LINER SQUEEZE [ ] PLANNED [ ] UNPLANNED [ ]

Liner Packer: [X] NO [ ] YES Bond Log: [X] NO [ ] YES PSI Applied: 0 Fluid Weight: 0 LBS/GAL

Casing Test (Update Original Treatment Report for Primary Job)

Casing Test Pressure: 0 PSI With 0 LBS/GAL Mud Time Held: 00 Hours 00 Minutes

Shoe Test (Update Original Treatment Report for Primary Job)

Depth Drilled out of Shoe: 0 FT	Target EMW: 0 LBS/GAL Actual EMW: 0 LBS/GAL
Number of Times Tests Conducted: 0	Mud Weight When Test was Conducted: 0 LBS/GAL

EXPLANATION: TROUBLE SETTING TOOL, RUNNING CSG, ETC. PRIOR TO CEMENTING:

Report Printed on: [illegible]

Page 1

J1005

CEMENT JOB REPORT

BAKER HUGHES

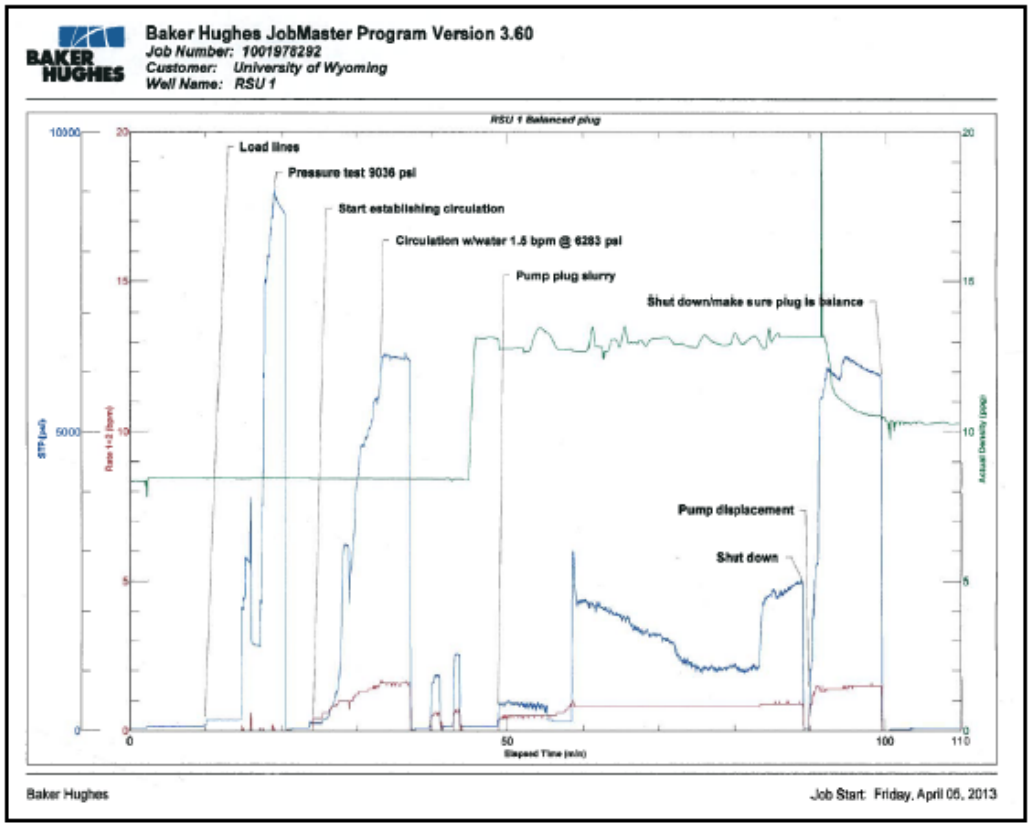
Problems Before Job (I.E. Running Casing, Circulating Well, ETC)

Problems During Job (I.E. Lost Returns, Equipment Failure, Bulk Delivery, Foaming, ETC)

Problems After Job (I.E. Gas at Surface, Float Equipment Failed, ETC)

PRESSURE/RATE DETAIL						EXPLANATION
TIME HR:MIN.	PRESSURE - PSI PIPE	PRESSURE - PSI ANNULUS	RATE BPM	BBL FLUID PUMPED	FLUID TYPE	SAFETY MEETING: BJ CREW [X] CO. REP. [X] TEST LINES 9036 PSI CIRCULATING WELL - RIG [ ] BJ [X]
15:10						Leave yard
15:50						Arrive on location
15:52						Spot equipment on location
15:57						Pre-rig up safety meeting
17:46	75	0	.5	.5	H2O	Load lines
18:04	9038	0	0	0	H2O	Pressure test/check lines for leaks and iron integrity
18:09	125	0	.5	.5	H2O	Start establishing circlation rate and pressure
18:19	6283	0	1.5	11	H2O	Established rate and pressure for circulation
18:28	0	0	0	21	H2O	Shut down/batch up cement slurry
18:34	475	0	.4	1	CMT	Pump plug slurry
19:15	0	0	0	26	CMT	Shut down
19:15	2778	0	1.5	1	H20	Start displacement
19:26	0	0	0	13	H20	Shut down/verify balanced plug
19:39						Pre-rig down safety meeting

BUMPED PLUG	PSI TO BUMP PLUG	TEST FLOAT EQUIP.	BBL.CMT RETURNS/ REVERSED	TOTAL BBL. PUMPED	PSI LEFT ON CSG	SPOT TOP OUT CEMENT	Service Supervisor Signature:
Y [N]	0	Y [N]	0	60	0	Y [N]	


Baker Hughes JobMaster Program Version 3.60
Job Number: 1001978292
Customer: University of Wyoming
Well Name: RSU 1
RSU 1 Balanced plug
Load lines
Pressure test 9036 psi
Start establishing circulation
Circulation w/water 1.5 bpm @ 6283 psi
Pump plug slurry
Shut down/make sure plug is balance
Pump displacement
Shut down
Elapsed Time (min)
Baker Hughes
Job Start: Friday, April 05, 2013

4.2.9 Performance

- Highlights
  - No major incidents or accidents were reported.
  - Geophones were successfully deployed to depth via coiled tubing.
- Lowlights
  - 30 of 42 geophone data channels (3 axes/channels for each of 14 phones) non-functional after cementing.
  - Weather affected operational times while attempting to further troubleshoot geophone system.
- Deviation from plan
  - None. Operations carried out on schedule.

4.3 Phase III of Planned Well Intervention

4.3.1 Description of Operations

- Operations spanned from August 26 – October 3, 2013 with 23 operational days.
- The existing geophone cable and 1 ½" coiled tubing cemented in the hole was removed. The first jet cut severed the tubing at 6,695 ft. A second jet cutter attempt was made to sever the Kevlar cable at the first cut depth, however, when hoisting the cable out of the hole, the Kevlar cable severed at the cable splice.
- While attempting to secure the Kevlar cable at surface, the cable parted and was dropped downhole. Following this, 13 fishing runs on 2" coiled tubing were performed to recover 5,480 ft. of cable from the well.
- After tubing and existing geophone cable had been removed and the hole gauged and cleaned, a passive seismic monitoring array was deployed on wireline, with four zones being monitored at 36 hours each.
- Once logging was completed, the well entered the plug and abandonment stage. The well was plugged with 4 cements plugs with located at 5,780-5,881 ft., 4,091-4,200 ft., 1,880-2,200 ft., and 50-250 ft. MD.
- After the well had been plugged, surface abandonment was commenced. The Location was cleaned, the casing head cut, the cellar and mouse hole removed, and a P&A monument erected. The location is scheduled to be reseeded in the spring.

4.3.2 Drilling Fluid

For the third stage of the planned well intervention, fresh water had been left in the hole from Phase II. During the P&A stage of Phase III, 8.34 ppg fresh water was also used as the displacement fluid during cementing operations. After pumping and displacing cement, a 9.0 ppg mud plug of poz ash and bentonite was circulated and displaced out of the well using fresh water. At abandonment, the well is full of 8.34 ppg fresh water.

4.3.3 Coil and Cable Cutting

Two jet cutting runs took place to ensure both the 1 ½" coil and the Kevlar geophone cable were parted downhole. The 1 ½" tubing was discovered to be buckled below 6,695 ft., yielding bend angles the jet cutting assembly could not pass beyond. Because of this obstruction, the coil was forced to be cut at 6,695 ft.

The coil was successfully parted with the first cut, signified by the drop in coil surface weight from, approximately, 35,000 lbs. to 16,000 lbs. After the first cut, the Kevlar cable would not come to surface while attempting to hoist with wireline crane, signifying the cable had not come free. A second cut was attempted at the same depth, and again the cable was hoisted, this time showing signs of the cable being free. When attempting to secure the cable to a fixed point on surface to begin recovery operations, the cable parted on surface and fell downhole.

Fishing operations with 2" coiled tubing were then carried out to retrieve as much cable as possible so as to ensure the upcoming monitoring array would not be compromised. Upon retrieving all of the free cable, it was discovered the Kevlar cable had severed at the cable splice, not the cut point.

Spectra Jet Cutter Specifications

Pipe O.D. (in)[mm]	Type	Cutter O.D. (in)[mm]	Max. Pressure (psi)[MPa]	Explosive Weight (g)	Explosive Type	Hazard Class
1.50 [38]	Coiled Tubing	1.00 [25]	18,000 [124]	3	HMX	1.4D

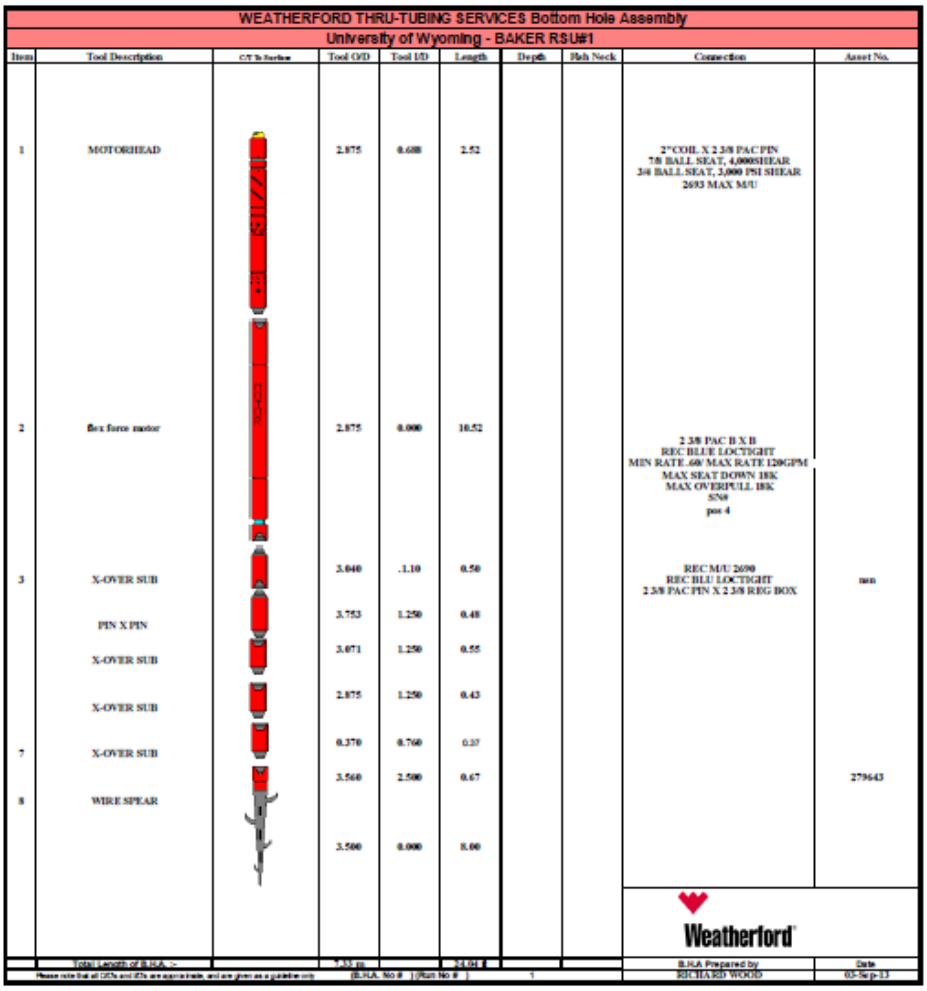


Example model of Titon Spectra® jet cutter used in cutting operations

4.3.4 Tubing Recovery and Fishing Operations

The well intervention program planned to latch on to the 1 ½" tubing using an overshot tool and remove the tubing and Kevlar cable simultaneously, however, due to the cable parting at surface while attempting to anchor it to a fixed surface point, the cable was lost downhole. This occurrence led to operations moving in to pre-planned contingency operations where the tubing was first removed separately via a coiled tubing unit and spooled on to a recovery reel. 6,650 ft. of tubing was recovered from the well.

After removing tubing from the well, 2" coil tubing fixed with a fingered-spear fishing tool was used to fish out the fallen Kevlar cable. Fishing operations were carried out to retrieve as much Kevlar cable as possible to minimize the risk of compromising or damaging the passive seismic monitoring array in Stage 2 monitoring operations. 5,480 ft. of Kevlar cable was able to be removed from the well over 13 fishing runs.



WEATHERFORD THRU-TUBING SERVICES Bottom Hole Assembly
University of Wyoming - BAKER RSU#1

Item	Tool Description	O/T To Surface	Tool O/D	Tool I/D	Length	Depth	Fish Neck	Connection	Asset No.
1	MOTORHEAD		2.875	0.688	2.52			2"COIL X 2 3/8 PAC PIN 7/8 BALL SEAT, 4,000SHEAR 3/4 BALL SEAT, 3,000 PSI SHEAR 2693 MAX M/U	
2	flex force motor		2.875	0.000	10.52			2 3/8 PAC B X B REC BLUE LOCTIGHT MIN RATE .60/ MAX RATE 120GPM MAX SEAT DOWN 18K MAX OVERPULL 18K S760 pos 4	
3	X-OVER SUB		3.640	.1.10	0.50			REC M/U 2690 REC BLU LOCTIGHT 2 3/8 PAC PIN X 2 3/8 REG BOX	nnn
	PIN X PIN		3.753	1.250	0.48				
	X-OVER SUB		3.071	1.250	0.55				
	X-OVER SUB		2.875	1.250	0.43				
7	X-OVER SUB		0.370	0.760	0.37				
8	WIRE SPEAR		3.560	2.500	0.67				279643
			3.500	0.000	8.00				
	Total Length of B.H.A. --				24.04 ft			Weatherford	
	Please note that all OD's and ID's are approximate, and are given as a guideline only			B.H.A. No #	Run No # 1			B.H.A Prepared by: RICHARD WOOD	Date: 03-Sep-13

Coiled tubing deployed rotating fishing-spear assembly used in Kevlar cable retrieval operations after 1-1/2" tubing had been removed from the well

4.3.5 Passive Seismic Monitoring

In Stage 2 of Phase III, monitoring was planned for the following intervals:

Dakota/Cloverly:	8,380 – 8,430 ft. TVD
Mowry:	8,200 – 8,250 ft. TVD
Frontier:	7,730 – 7,780 ft. TVD
Baxter:	4,150 – 4,200 ft. TVD

During Stage 1's cutting operations, it was discovered that the 1 ½" coiled tubing in the hole was buckled below 6,695 ft. and the jet cutting assembly could not pass below this depth. Because of this, the coil was forced to be cut 1,835 ft. shallower than originally planned. With the 1 ½" tubing being buckled, it is likely the Kevlar cable was not against the tubing body. This could have prevented the second cutter from severing the cable.

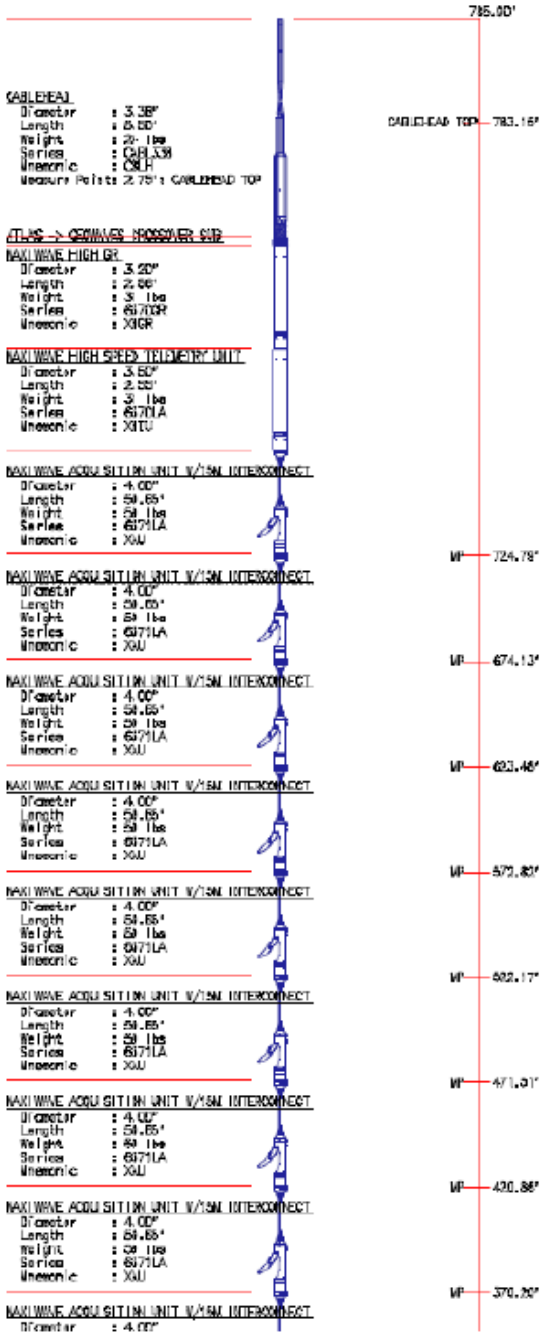
After fishing out as much cable as possible (5,480 ft. removed), a 5.89" OD gauge run was performed. During this run, the wireline could not progress beyond 5,881 ft. This led to the belief that the cable had begun spooling down the casing walls. Rather than compromising the upcoming monitoring stage, the monitored intervals had to be moved shallower.

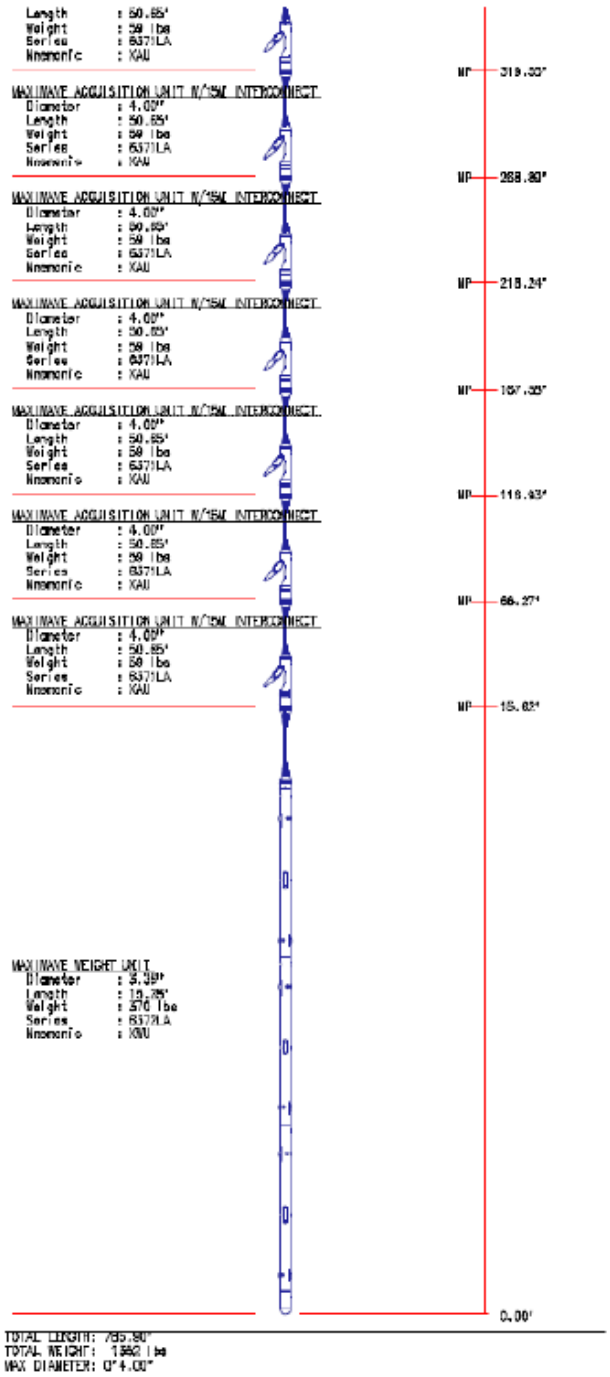
These shallower intervals for monitoring were as follows:

Baxter:	4,621 – 5,310 ft. TVD
Blair/Baxter:	3,600 – 4,300 ft. TVD
Blair:	2,452 – 3,190 ft. TVD
Rock Springs/Blair:	1,972 – 2,710 ft. TVD

36 hours of monitoring background seismicity were performed for each of the four intervals.

Below is the monitoring array diagram.

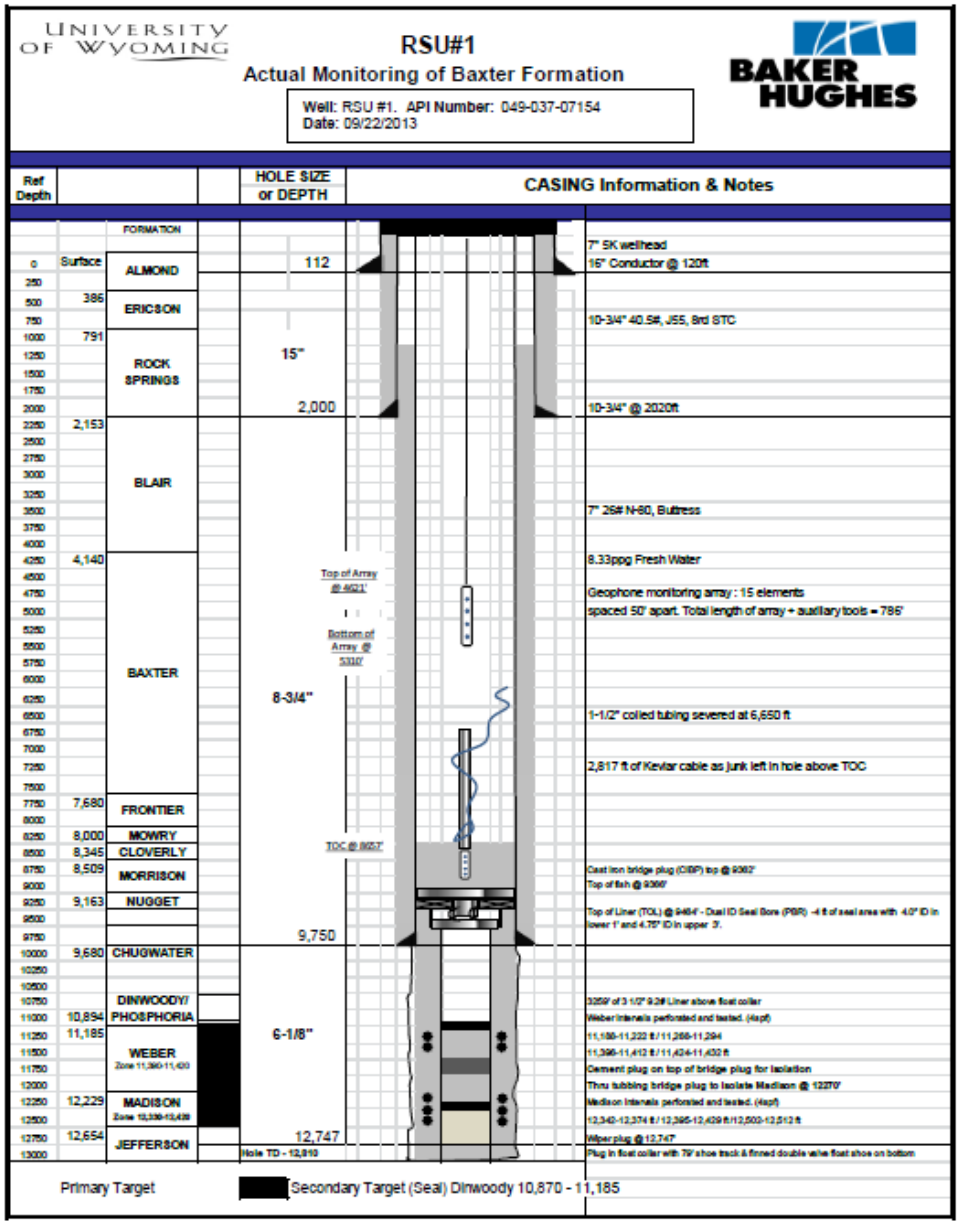

785.00'
CABLEHEAD
Diameter : 3.38"
Length : 6.00'
Weight : 20 lbs
Series : CABLXSW
Mnemonic : CBLH
Measure Points: 2.75': CABLEHEAD TOP
CABLEHEAD TOP 783.16'
ATLAS -> SCHLUMBERGER CROSSOVER SUB
NAXIWAVE HIGH GR
Diameter : 3.20"
Length : 2.00'
Weight : 3 lbs
Series : 6570GR
Mnemonic : XHGR
NAXIWAVE HIGH SPEED TELEMETRY UNIT
Diameter : 3.50"
Length : 2.55'
Weight : 3 lbs
Series : 6571A
Mnemonic : XHTU
NAXIWAVE ACQUISITION UNIT W/15M INTERCONNECT
Diameter : 4.00"
Length : 58.65'
Weight : 58 lbs
Series : 6571A
Mnemonic : XAU
MP 724.78'
NAXIWAVE ACQUISITION UNIT W/15M INTERCONNECT
Diameter : 4.00"
Length : 58.65'
Weight : 58 lbs
Series : 6571A
Mnemonic : XAU
MP 674.13'
NAXIWAVE ACQUISITION UNIT W/15M INTERCONNECT
Diameter : 4.00"
Length : 58.65'
Weight : 58 lbs
Series : 6571A
Mnemonic : XAU
MP 623.48'
NAXIWAVE ACQUISITION UNIT W/15M INTERCONNECT
Diameter : 4.00"
Length : 58.65'
Weight : 58 lbs
Series : 6571A
Mnemonic : XAU
MP 572.83'
NAXIWAVE ACQUISITION UNIT W/15M INTERCONNECT
Diameter : 4.00"
Length : 58.65'
Weight : 58 lbs
Series : 6571A
Mnemonic : XAU
MP 522.17'
NAXIWAVE ACQUISITION UNIT W/15M INTERCONNECT
Diameter : 4.00"
Length : 58.65'
Weight : 58 lbs
Series : 6571A
Mnemonic : XAU
MP 471.51'
NAXIWAVE ACQUISITION UNIT W/15M INTERCONNECT
Diameter : 4.00"
Length : 58.65'
Weight : 58 lbs
Series : 6571A
Mnemonic : XAU
MP 420.86'
NAXIWAVE ACQUISITION UNIT W/15M INTERCONNECT
Diameter : 4.00"
Length : 58.65'
Weight : 58 lbs
Series : 6571A
Mnemonic : XAU
MP 370.20'
NAXIWAVE ACQUISITION UNIT W/15M INTERCONNECT
Diameter : 4.00"



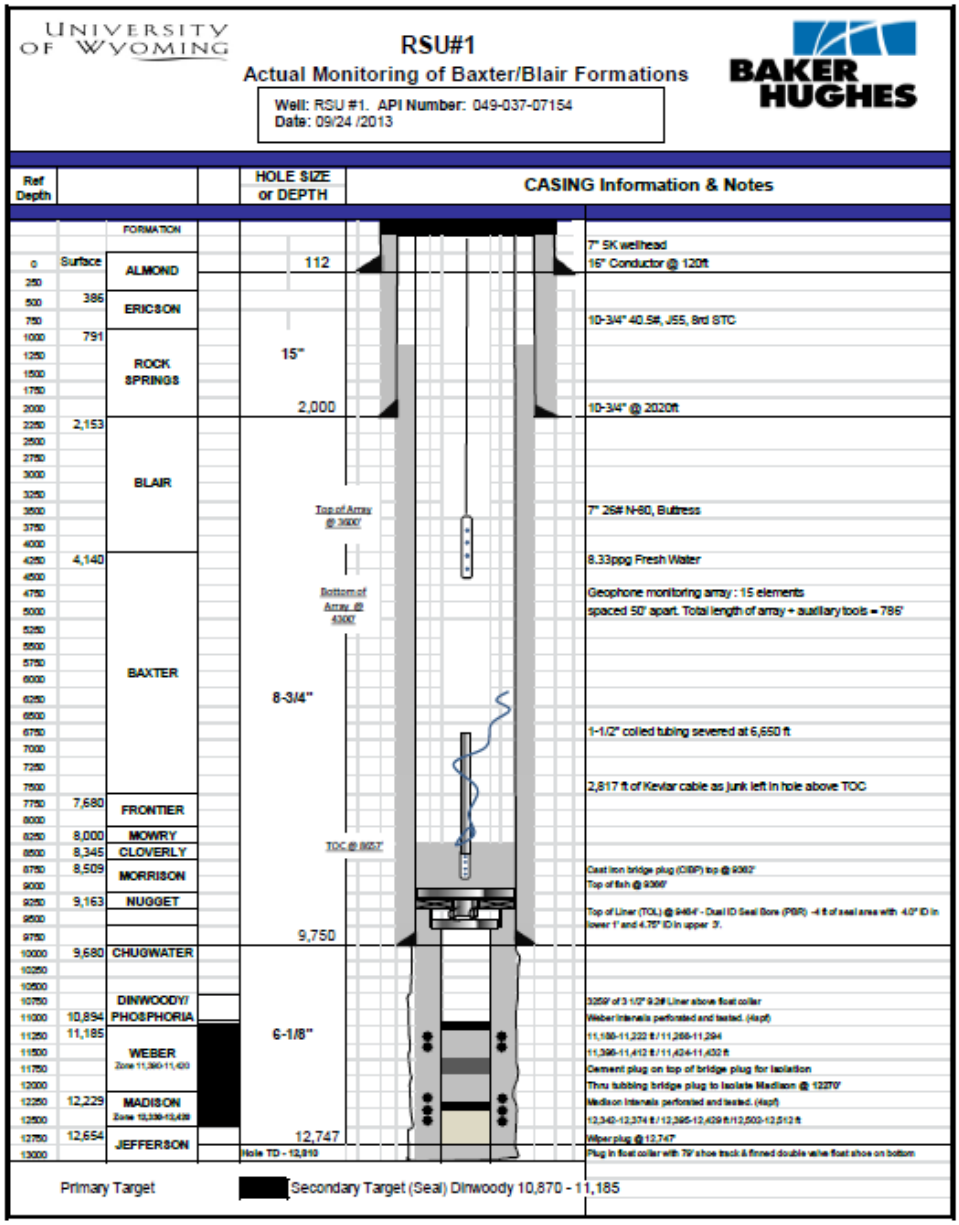
Passive monitoring array deployed on wireline for measuring seismicity during Phase III monitoring operations

Below are schematics of the array position for each monitoring interval.

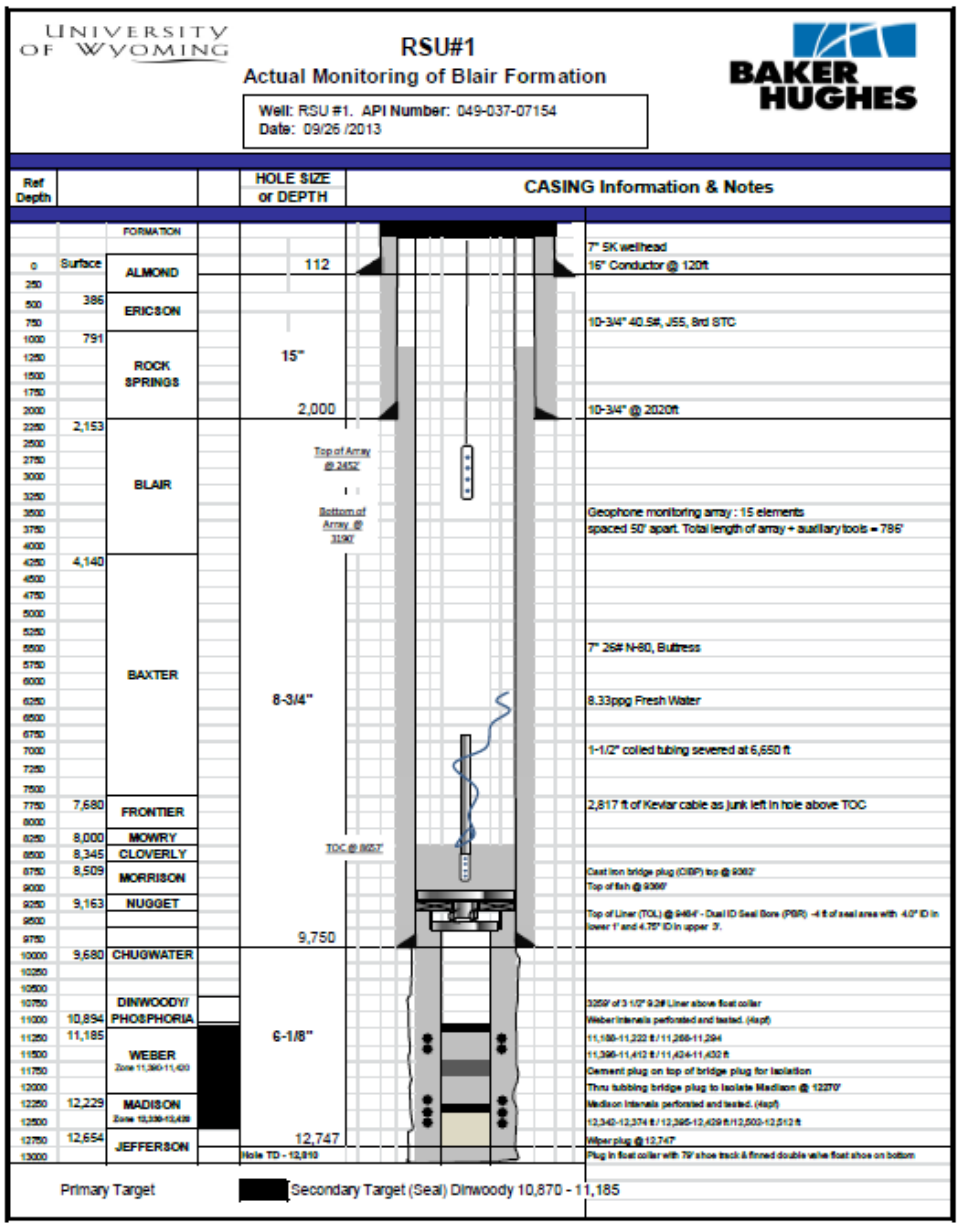
Interval #1 – Baxter Formation



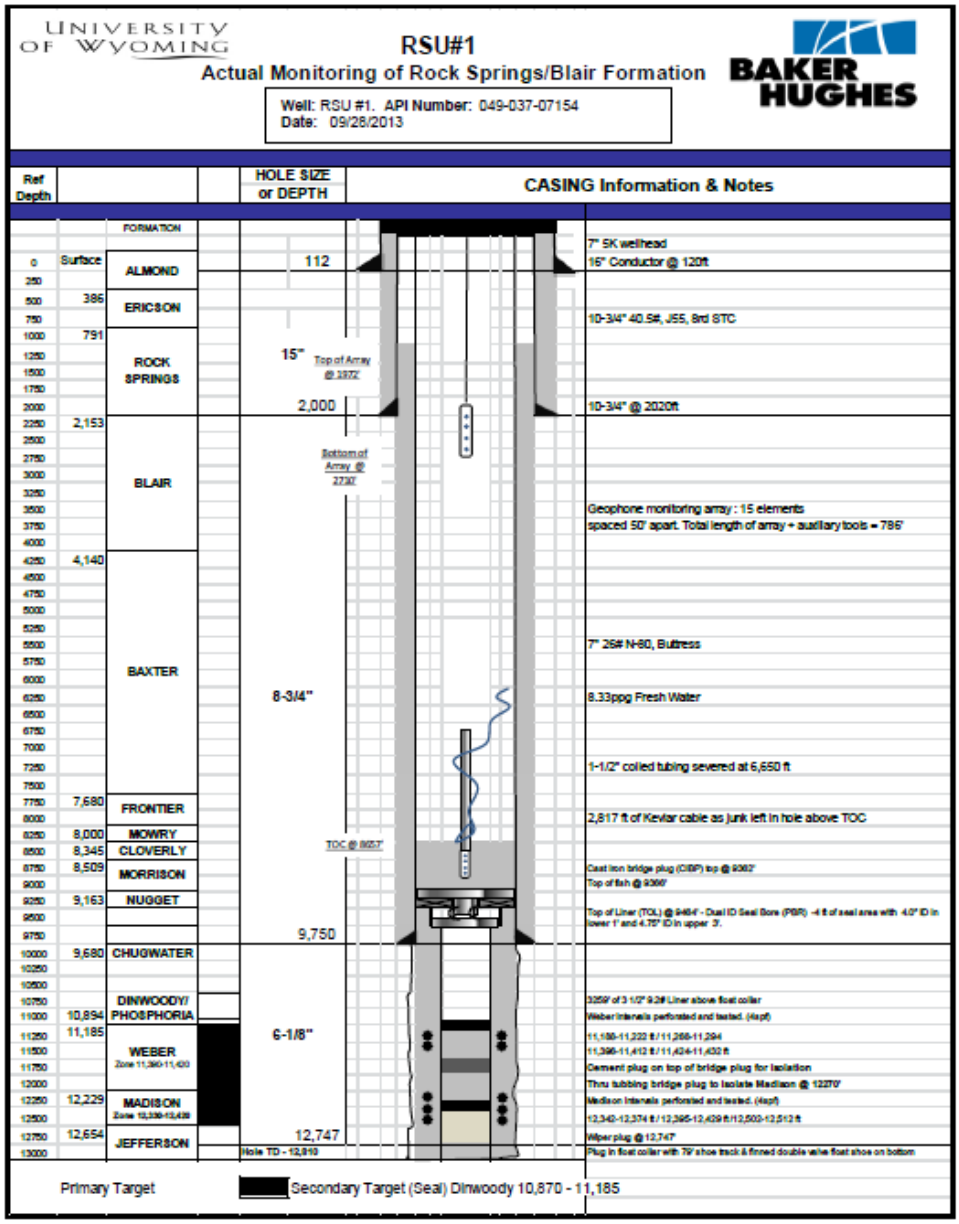
Interval #2 – Baxter/Blair Formations



Interval #3 – Blair Formation



Interval #4 – Rock Springs/Blair Formations



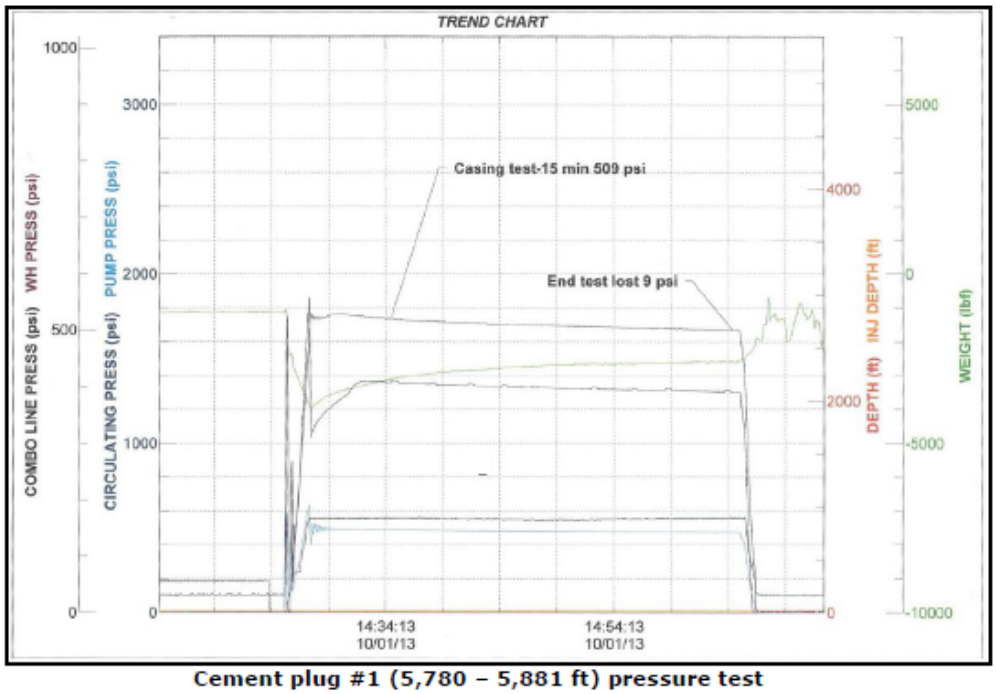
4.3.6 P&A Operations

After the monitoring stage, operations moved in to Phase III Stage 2 P&A operations. During this stage, the well was plugged with four Class G + Additive cement plugs pumped via 2" coiled tubing, totalling 134 sacks (27.4 bbl) of cement slurry used to plug the well.

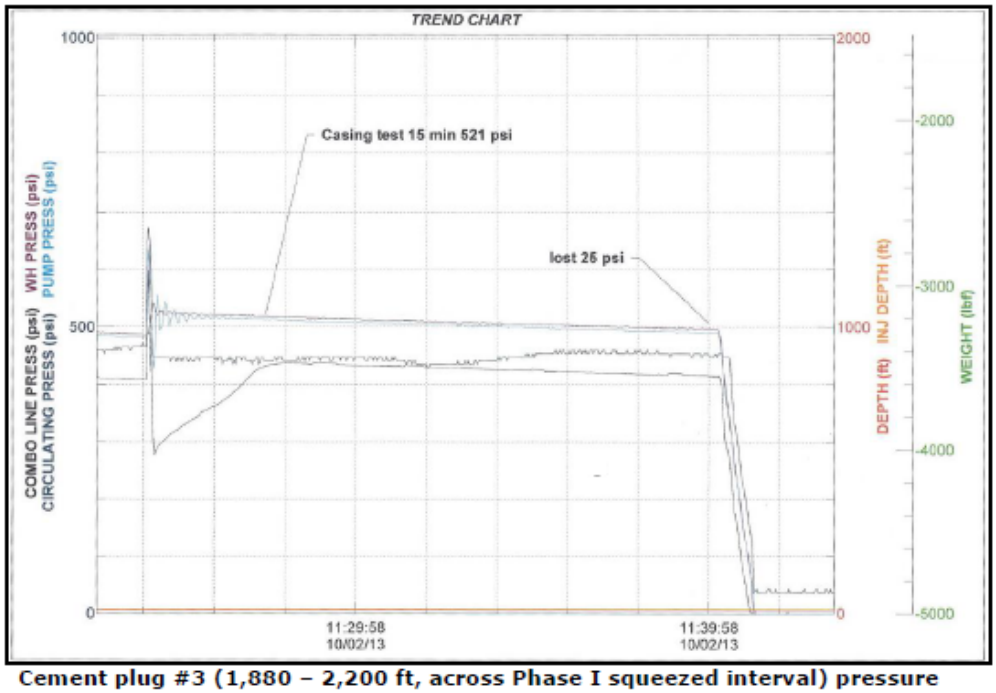
The cement plugs were located over the following depths:

Plug #1: 5,780 – 5,881 ft. TVD (101 ft.)
Plug #2: 4,091 – 4,200 ft. TVD (109 ft.)
Plug #3: 1,880 – 2,200 ft. TVD (320 ft.)
Plug #4: 50 – 250 ft. TVD (200 ft.)

Plugs number 1 and 2 were allowed to set for at least six hours each prior to tagging the plug with a wireline dummy bar. Plug numbers 3 and 4 were allowed to set for 1 hour. After each set time, all plugs were tagged. After tagging, plugs 1 and 3 were tested to 500 psig. The deepest plug, plug 1, was tested to ensure the deepest plug nearest the previously perforated (and subsequently sealed) Weber interval held pressure. Plug number 3 was tested to ensure the previously squeezed interval was isolated and the plug could hold pressure.



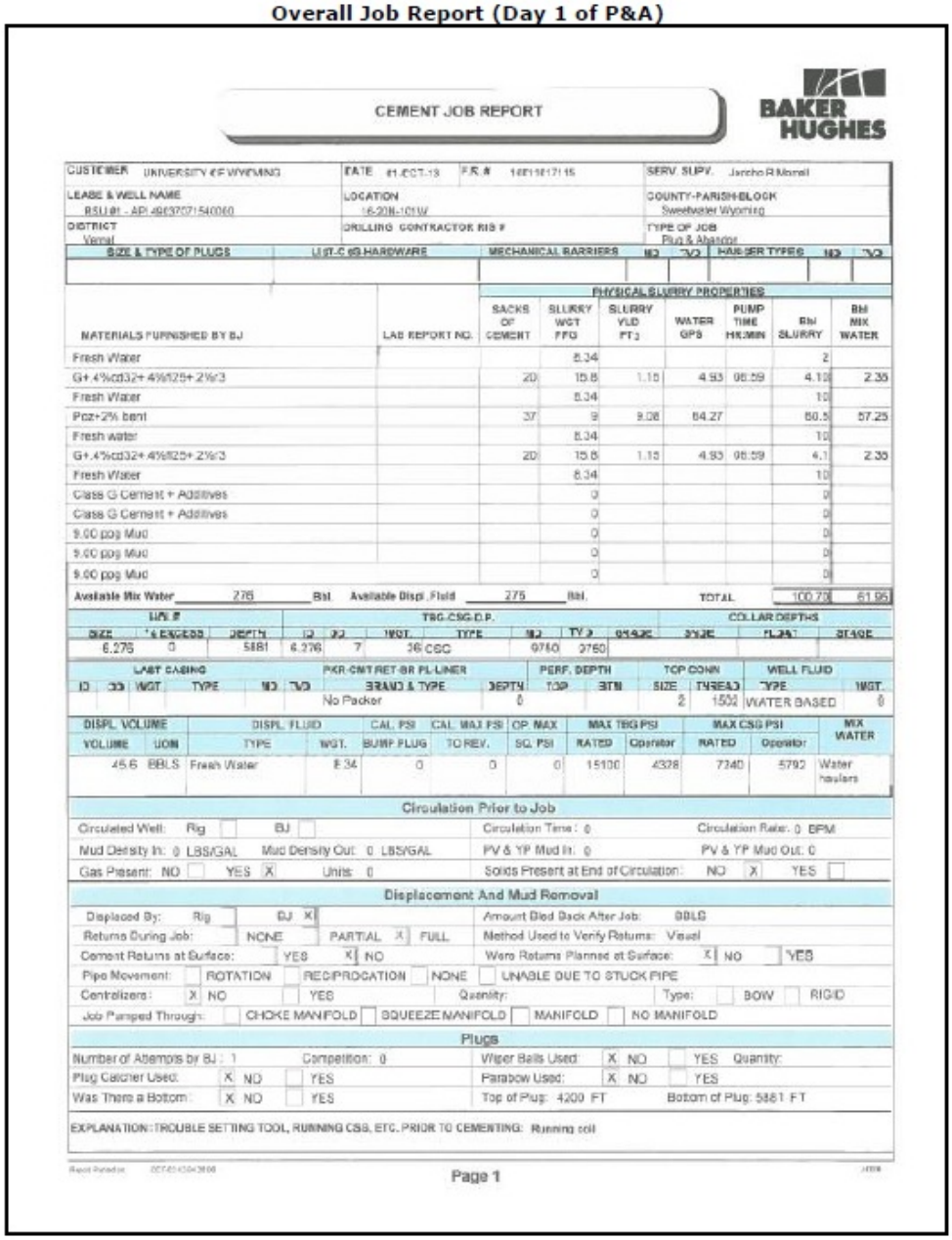
Cement plug #1 (5,780 – 5,881 ft) pressure test



Cement plug #3 (1,880 – 2,200 ft, across Phase I squeezed interval) pressure test

Below are detailed job logs of all cement and pumping operations which took place during the plug and abandonment stage of Phase III, separated by the cement plug number.

Overall Job Report (Day 1 of P&A)



CEMENT JOB REPORT

BAKER HUGHES

CUSTOMER: UNIVERSITY OF WYOMING	DATE: 01-OCT-18	SERV. SUPV.: Jaycho R Morrell
LEASE & WELL NAME: RSU #1 - API 49037071540000	LOCATION: 16-20N-101W	COUNTY-PARISH-BLOCK: Sweetwater Wyoming
DISTRICT: Vernal	DRILLING CONTRACTOR RIG #:	TYPE OF JOB: Plug & Abandon

SIZE & TYPE OF PLUGS	LIST-C eS HARDWARE	MECHANICAL BARRIERS	ID	TVD	HAS SER TYPES	ID	TVD

MATERIALS FURNISHED BY BJ	LAB REPORT NO.	SACKS OF CEMENT	SLURRY WGT PPG	SLURRY YLD FT3	WATER GPS	PUMP TIME HR:MIN	BH SLURRY	BH MIX WATER
Fresh Water			8.34				2	
G+.4%cd32+.4%fl25+.2%r3		20	15.8	1.15	4.93	00:59	4.1	2.35
Fresh Water			8.34				10	
Poz+2% bent		37	9	3.08	64.27		60.5	57.25
Fresh water			8.34				10	
G+.4%cd32+.4%fl25+.2%r3		20	15.8	1.15	4.93	00:59	4.1	2.35
Fresh Water			8.34				10	
Class G Cement + Additives			0				0	
Class G Cement + Additives			0				0	
9.00 ppg Mud			0				0	
9.00 ppg Mud			0				0	
9.00 ppg Mud			0				0	

Available Mix Water: 275 Bbl. Available Displ. Fluid: 275 Bbl. TOTAL: 100.75 61.95

HOLE			TBG-CSG-D.P.						COLLAR DEPTHS			
SIZE	% EXCESS	DEPTH	ID	OD	WGT.	TYPE	MD	TVD	SHOE	SIZE	FLOAT	STAGE
6.275	0	5881	6.276	7	36 CSG		9750	2750				

LAST CASING				PKR-CMT RET-BR PL LINER			PERF. DEPTH		TOP CONN		WELL FLUID	
ID	OD	WGT	TYPE	MD	TVD	BRAND & TYPE	DEPTH	TOP	BTM	SIZE	THREAD	TYPE	WGT.
						No Packer	0			2	1502	WATER BASED	0

DISPL. VOLUME		DISPL. FLUID		CAL. PSI	CAL. MAX PSI	OP. MAX	MAX TBG PSI		MAX CSG PSI		MIX WATER
VOLUME	UOM	TYPE	WGT.	BUMP PLUG	TO REV.	SQ. PSI	RATED	Operator	RATED	Operator	
45.6	BBLS	Fresh Water	8.34	0	0	0	15100	4328	7340	5792	Water haulers

Circulation Prior to Job

Circulated Well: Rig [ ] BJ [ ] Circulation Time: 0 Circulation Rate: 0 BPM

Mud Density In: 0 LBS/GAL Mud Density Out: 0 LBS/GAL PV & YP Mud In: 0 PV & YP Mud Out: 0

Gas Present: NO [ ] YES [X] Units: 0 Solids Present at End of Circulation: NO [X] YES [ ]

Displacement And Mud Removal

Displaced By: Rig [ ] BJ [X] Amount Bled Back After Job: BBLS

Returns During Job: NONE [ ] PARTIAL [X] FULL Method Used to Verify Returns: Visual

Cement Returns at Surface: YES [X] NO Were Returns Planned at Surface: [X] NO [ ] YES

Pipe Movement: [ ] ROTATION [ ] RECIPROCATION [ ] NONE [ ] UNABLE DUE TO STUCK PIPE

Centralizers: [X] NO [ ] YES Quantity: Type: [ ] BOW [ ] RIGID

Job Pumped Through: [ ] CHOKE MANIFOLD [ ] SQUEEZE MANIFOLD [ ] MANIFOLD [ ] NO MANIFOLD

Plugs

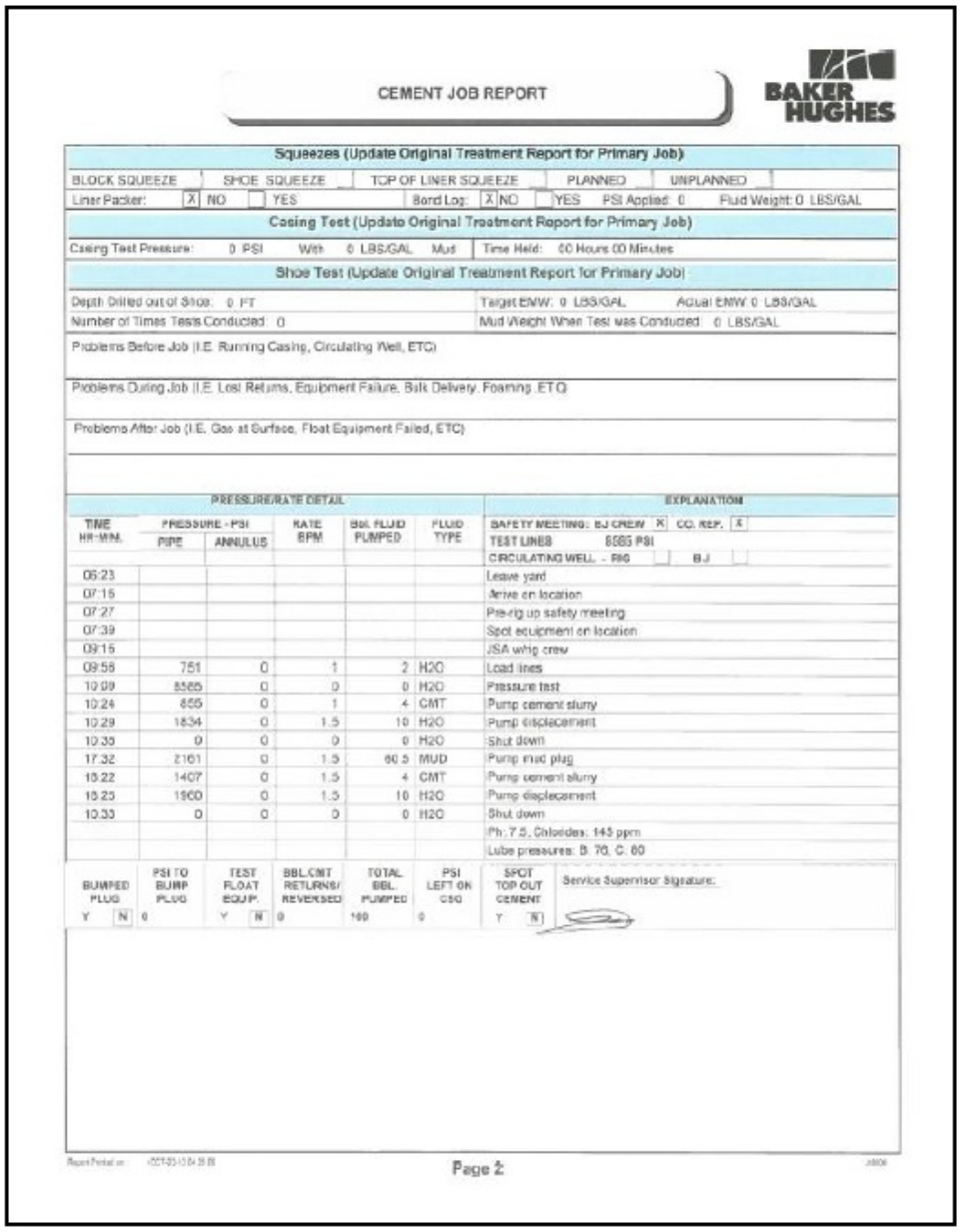
Number of Attempts by BJ: 1 Completion: 0 Wiper Balls Used: [X] NO [ ] YES Quantity:

Plug Catcher Used: [X] NO [ ] YES Parabow Used: [X] NO [ ] YES

Was There a Bottom: [X] NO [ ] YES Top of Plug: 4200 FT Bottom of Plug: 5881 FT

EXPLANATION: TROUBLE SETTING TOOL, RUNNING CSG, ETC. PRIOR TO CEMENTING: Running coil

Page 1



CEMENT JOB REPORT

BAKER HUGHES

Squeezes (Update Original Treatment Report for Primary Job)

BLOCK SQUEEZE | SHOE SQUEEZE | TOP OF LINER SQUEEZE | PLANNED | UNPLANNED

Liner Packer: [X] NO [ ] YES Bond Log: [X] NO [ ] YES PSI Applied: 0 Fluid Weight: 0 LBS/GAL

Casing Test (Update Original Treatment Report for Primary Job)

Casing Test Pressure: 0 PSI With 0 LBS/GAL Mud | Time Held: 00 Hours 00 Minutes

Shoe Test (Update Original Treatment Report for Primary Job)

Depth Drilled out of Shoe: 0 FT | Target EMW: 0 LBS/GAL | Actual EMW: 0 LBS/GAL

Number of Times Tests Conducted: 0 | Mud Weight When Test was Conducted: 0 LBS/GAL

Problems Before Job (I.E. Running Casing, Circulating Well, ETC)

Problems During Job (I.E. Lost Returns, Equipment Failure, Bulk Delivery, Foaming ,ETC)

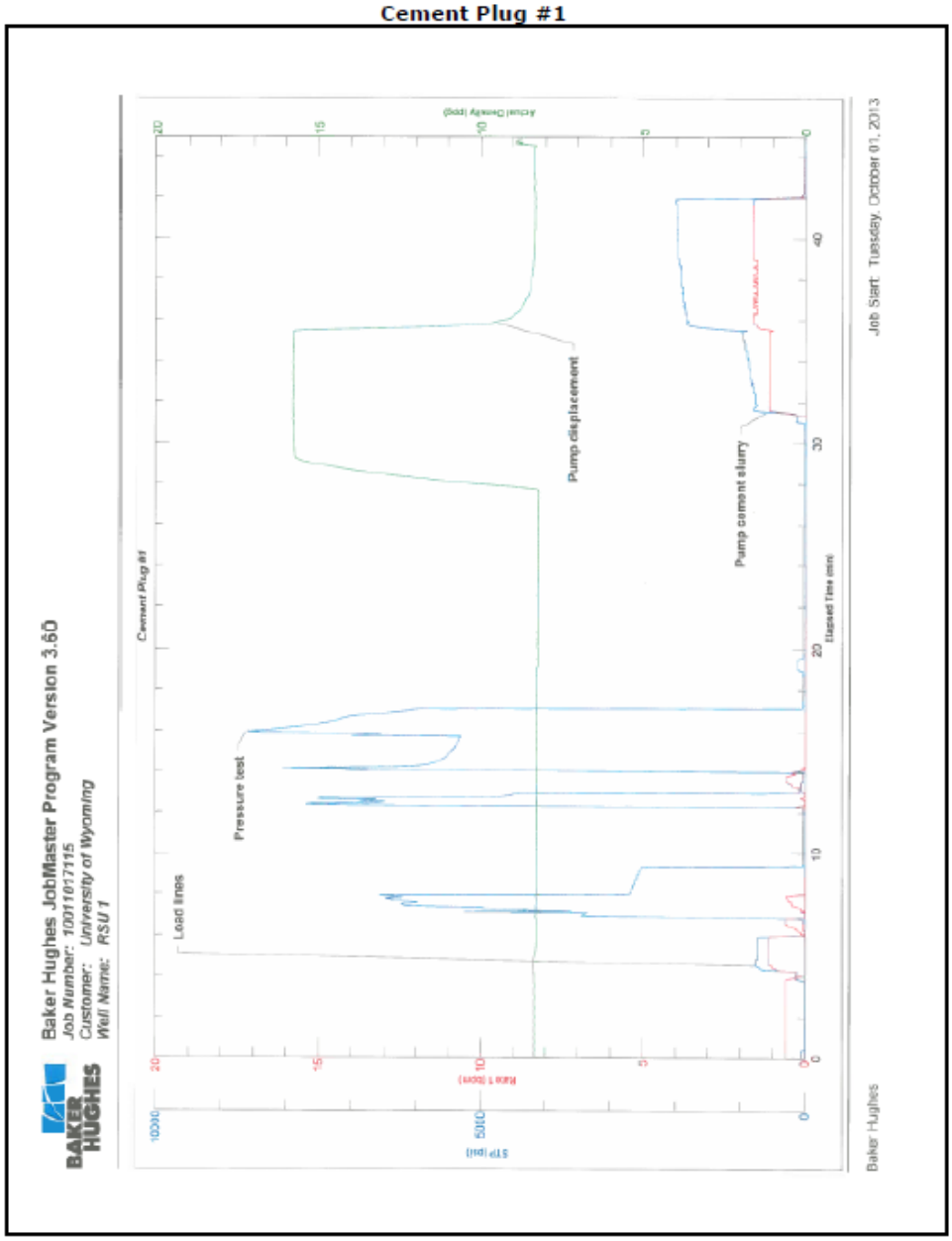
Problems After Job (I.E. Gas at Surface, Float Equipment Failed, ETC)

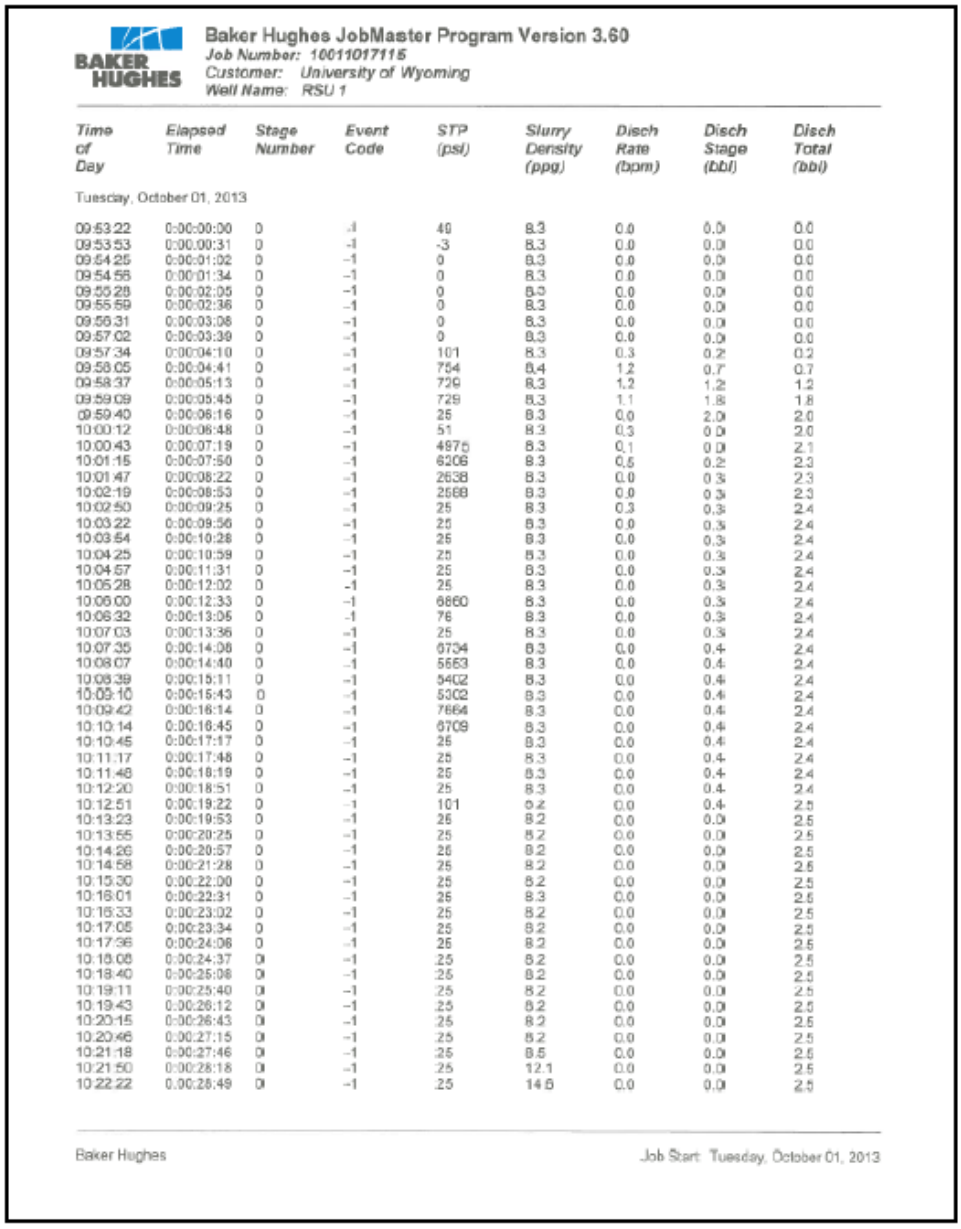
PRESSURE/RATE DETAIL						EXPLANATION
TIME HR-MIN.	PRESSURE - PSI PIPE	PRESSURE - PSI ANNULUS	RATE BPM	BBL FLUID PUMPED	FLUID TYPE	SAFETY MEETING: BJ CREW [X] CO. REP. [X]
						TEST LINES 8585 PSI
						CIRCULATING WELL - RIG [ ] BJ [ ]
05:23						Leave yard
07:15						Arrive on location
07:27						Pre-rig up safety meeting
07:39						Spot equipment on location
09:15						JSA whig crew
09:58	751	0	1	2	H2O	Load lines
10:09	8585	0	0	0	H2O	Pressure test
10:24	855	0	1	4	CMT	Pump cement slurry
10:29	1834	0	1.5	10	H2O	Pump displacement
10:39	0	0	0	0	H2O	Shut down
17:32	2161	0	1.5	60.5	MUD	Pump mud plug
18:22	1407	0	1.5	4	CMT	Pump cement slurry
18:23	1900	0	1.5	10	H2O	Pump displacement
10:33	0	0	0	0	H2O	Shut down
						Ph: 7.5, Chlorides: 143 ppm
						Lube pressures: B: 70, C: 60

BUMPED PLUG	PSI TO BUMP PLUG	TEST FLOAT EQUIP.	BBL/CMT RETURNS/ REVERSED	TOTAL BBL. PUMPED	PSI LEFT ON CSG	SPOT TOP OUT CEMENT	Service Supervisor Signature:
Y [N]	0	Y [N]	0	100	0	Y [N]	

Page 2

Cement Plug #1





Baker Hughes JobMaster Program Version 3.60
Job Number: 10011017115
Customer: University of Wyoming
Well Name: RSU 1

Time of Day	Elapsed Time	Stage Number	Event Code	STP (psi)	Slurry Density (ppg)	Disch Rate (bpm)	Disch Stage (bbl)	Disch Total (bbl)
Tuesday, October 01, 2013								
09:53:22	0:00:00:00	0	-1	40	8.3	0.0	0.0	0.0
09:53:53	0:00:00:31	0	-1	-3	8.3	0.0	0.0	0.0
09:54:25	0:00:01:02	0	-1	0	8.3	0.0	0.0	0.0
09:54:56	0:00:01:34	0	-1	0	8.3	0.0	0.0	0.0
09:55:28	0:00:02:05	0	-1	0	8.3	0.0	0.0	0.0
09:55:59	0:00:02:36	0	-1	0	8.3	0.0	0.0	0.0
09:56:31	0:00:03:08	0	-1	0	8.3	0.0	0.0	0.0
09:57:02	0:00:03:39	0	-1	0	8.3	0.0	0.0	0.0
09:57:34	0:00:04:10	0	-1	101	8.3	0.3	0.2	0.2
09:58:05	0:00:04:41	0	-1	754	8.4	1.2	0.7	0.7
09:58:37	0:00:05:13	0	-1	729	8.3	1.2	1.2	1.2
09:59:09	0:00:05:45	0	-1	729	8.3	1.1	1.8	1.8
09:59:40	0:00:06:16	0	-1	25	8.3	0.0	2.0	2.0
10:00:12	0:00:06:48	0	-1	51	8.3	0.3	0.0	2.0
10:00:43	0:00:07:19	0	-1	4975	8.3	0.1	0.0	2.1
10:01:15	0:00:07:50	0	-1	6206	8.3	0.5	0.2	2.3
10:01:47	0:00:08:22	0	-1	2638	8.3	0.0	0.3	2.3
10:02:19	0:00:08:53	0	-1	2588	8.3	0.0	0.3	2.3
10:02:50	0:00:09:25	0	-1	25	8.3	0.3	0.3	2.4
10:03:22	0:00:09:56	0	-1	25	8.3	0.0	0.3	2.4
10:03:54	0:00:10:28	0	-1	25	8.3	0.0	0.3	2.4
10:04:25	0:00:10:59	0	-1	25	8.3	0.0	0.3	2.4
10:04:57	0:00:11:31	0	-1	25	8.3	0.0	0.3	2.4
10:05:28	0:00:12:02	0	-1	25	8.3	0.0	0.3	2.4
10:06:00	0:00:12:33	0	-1	6860	8.3	0.0	0.3	2.4
10:06:32	0:00:13:05	0	-1	76	8.3	0.0	0.3	2.4
10:07:03	0:00:13:36	0	-1	25	8.3	0.0	0.3	2.4
10:07:35	0:00:14:08	0	-1	6704	8.3	0.0	0.4	2.4
10:08:07	0:00:14:40	0	-1	5563	8.3	0.0	0.4	2.4
10:08:39	0:00:15:11	0	-1	8402	8.3	0.0	0.4	2.4
10:09:10	0:00:15:43	0	-1	5302	8.3	0.0	0.4	2.4
10:09:42	0:00:16:14	0	-1	7664	8.3	0.0	0.4	2.4
10:10:14	0:00:16:45	0	-1	6709	8.3	0.0	0.4	2.4
10:10:45	0:00:17:17	0	-1	25	8.3	0.0	0.4	2.4
10:11:17	0:00:17:48	0	-1	25	8.3	0.0	0.4	2.4
10:11:48	0:00:18:19	0	-1	25	8.3	0.0	0.4	2.4
10:12:20	0:00:18:51	0	-1	25	8.3	0.0	0.4	2.4
10:12:51	0:00:19:22	0	-1	101	8.2	0.0	0.4	2.5
10:13:23	0:00:19:53	0	-1	25	8.2	0.0	0.0	2.5
10:13:55	0:00:20:25	0	-1	25	8.2	0.0	0.0	2.5
10:14:26	0:00:20:57	0	-1	25	8.2	0.0	0.0	2.5
10:14:58	0:00:21:28	0	-1	25	8.2	0.0	0.0	2.5
10:15:30	0:00:22:00	0	-1	25	8.2	0.0	0.0	2.5
10:16:01	0:00:22:31	0	-1	25	8.3	0.0	0.0	2.5
10:16:33	0:00:23:02	0	-1	25	8.2	0.0	0.0	2.5
10:17:05	0:00:23:34	0	-1	25	8.2	0.0	0.0	2.5
10:17:36	0:00:24:06	0	-1	25	8.2	0.0	0.0	2.5
10:18:08	0:00:24:37	0	-1	25	8.2	0.0	0.0	2.5
10:18:40	0:00:25:08	0	-1	25	8.2	0.0	0.0	2.5
10:19:11	0:00:25:40	0	-1	25	8.2	0.0	0.0	2.5
10:19:43	0:00:26:12	0	-1	25	8.2	0.0	0.0	2.5
10:20:15	0:00:26:43	0	-1	25	8.2	0.0	0.0	2.5
10:20:46	0:00:27:15	0	-1	25	8.2	0.0	0.0	2.5
10:21:18	0:00:27:46	0	-1	25	8.5	0.0	0.0	2.5
10:21:50	0:00:28:18	0	-1	25	12.1	0.0	0.0	2.5
10:22:22	0:00:28:49	0	-1	25	14.6	0.0	0.0	2.5

Baker Hughes — Job Start: Tuesday, October 01, 2013

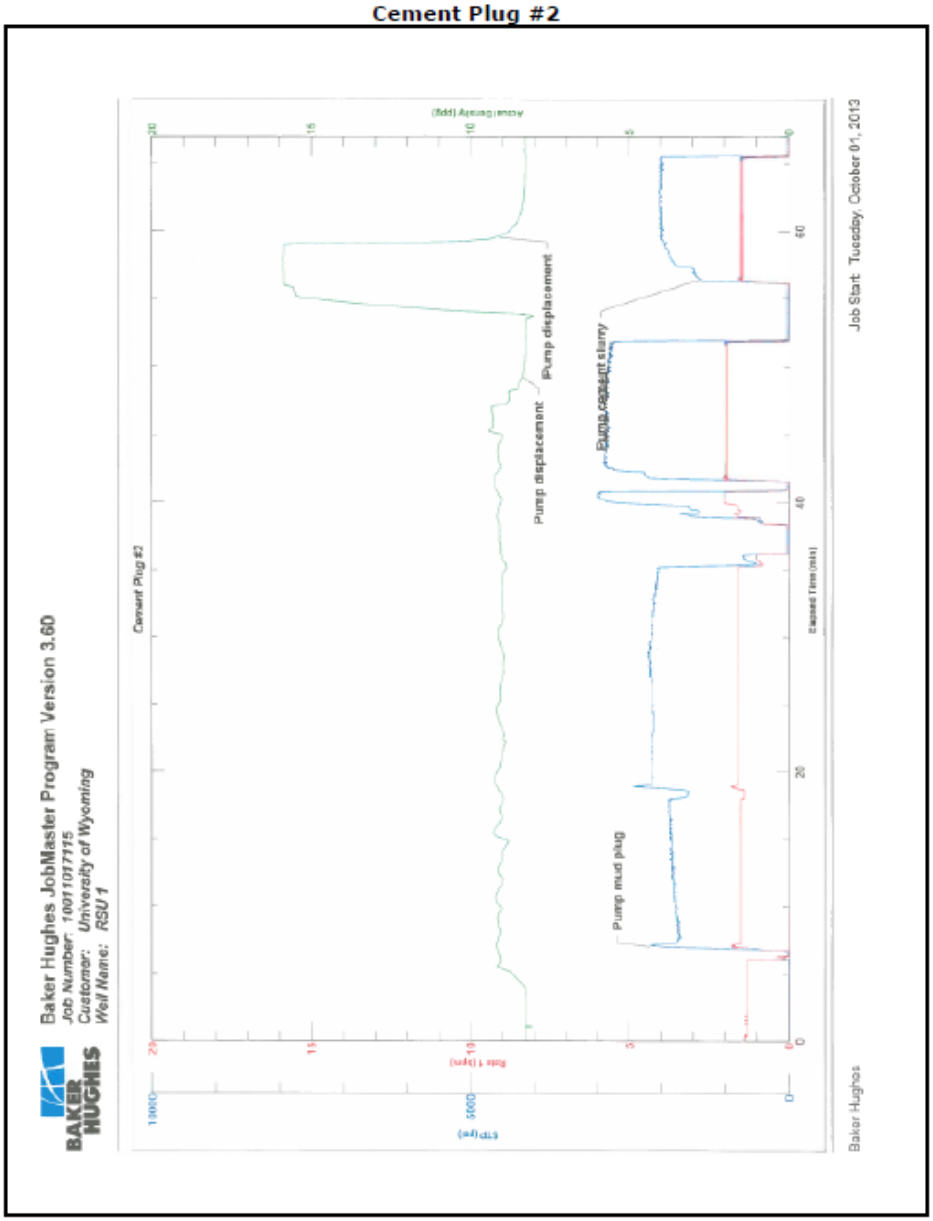
Baker Hughes JobMaster Program Version 3.60

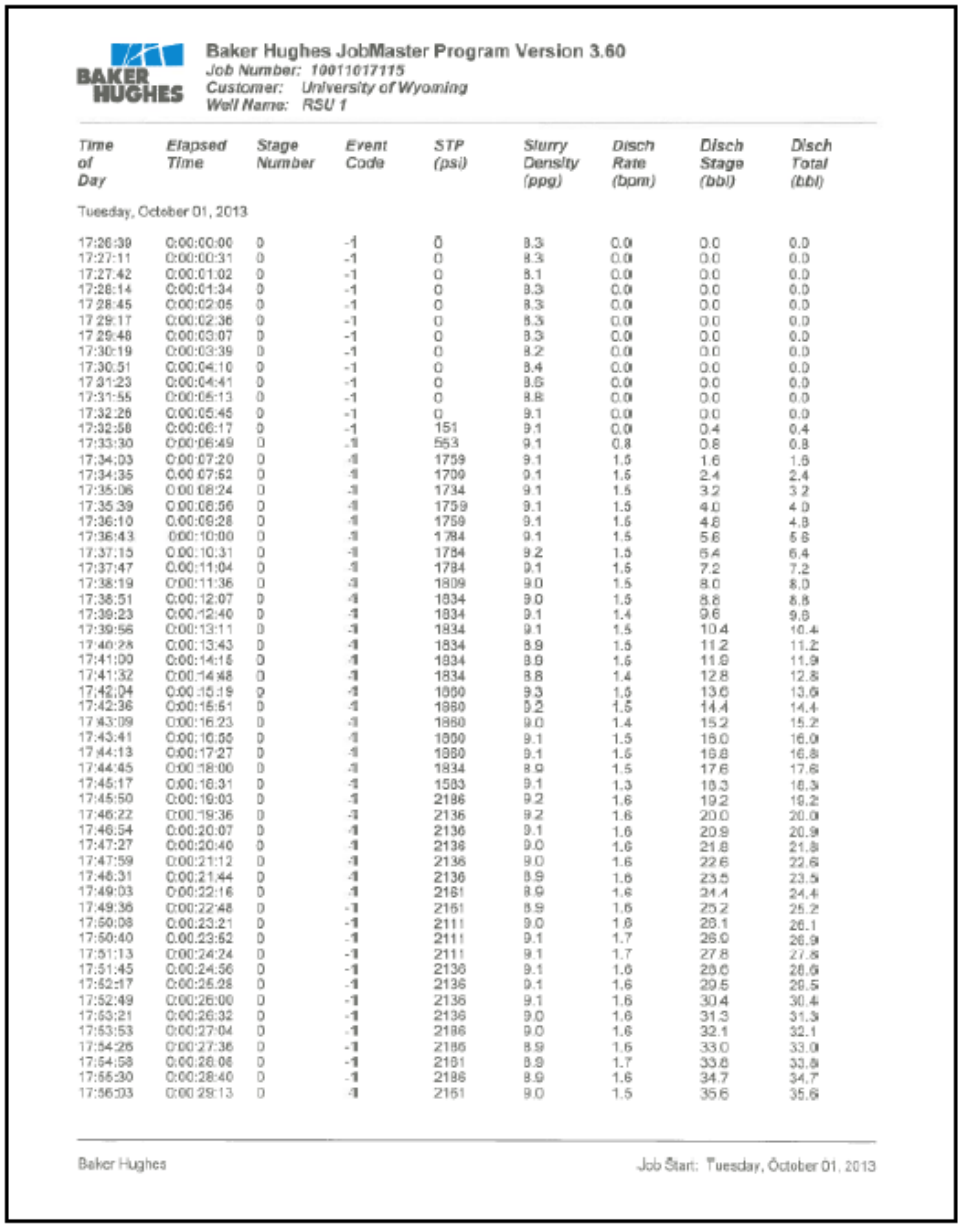
Job Number: 10011017115
Customer: University of Wyoming
Well Name: RSU 1

Time of Day	Elapsed Time	Stage Number	Event Code	STP (psi)	Slurry Density (ppg)	Disch Rate (bpm)	Disch Stage (bbl)	Disch Total (bbl)
Tuesday, October 01, 2013								
10:22:53	0:00:29:21	0	-1	25	15.7	0.0	0.0	2.5
10:23:25	0:00:29:53	0	-1	25	15.7	0.0	0.0	2.5
10:23:57	0:00:30:24	0	-1	25	15.8	0.0	0.0	2.5
10:24:28	0:00:30:56	0	-1	25	15.8	0.0	0.0	2.5
10:25:00	0:00:31:28	0	-1	201	15.8	0.5	0.2	2.6
10:26:32	0:00:31:50	0	-1	779	15.8	1.1	0.7	3.2
10:26:02	0:00:32:29	0	-1	804	15.8	1.1	1.3	3.7
10:26:33	0:00:33:00	0	-1	829	15.8	1.1	1.8	4.3
10:27:05	0:00:33:32	0	-1	855	15.8	1.0	2.4	4.8
10:27:37	0:00:34:04	0	-1	880	15.8	1.0	2.9	5.4
10:28:09	0:00:34:35	0	-1	930	15.8	1.0	3.5	5.9
10:28:40	0:00:35:07	0	-1	955	15.8	1.0	4.1	6.5
10:29:12	0:00:35:38	0	-1	1533	12.3	1.4	0.3	7.1
10:29:44	0:00:36:10	0	-1	1834	9.0	1.5	1.1	7.9
10:30:16	0:00:36:42	0	-1	1886	8.7	1.5	2.0	8.7
10:30:48	0:00:37:14	0	-1	1885	8.5	1.5	2.8	9.5
10:31:20	0:00:37:46	0	-1	1910	8.5	1.5	3.6	10.4
10:31:52	0:00:38:17	0	-1	1910	8.4	1.5	4.4	11.2
10:32:24	0:00:38:49	0	-1	1935	8.4	1.6	5.2	12.0
10:32:56	0:00:39:21	0	-1	1960	8.4	1.5	6.1	12.8
10:33:28	0:00:39:53	0	-1	1985	8.3	1.7	6.9	13.7
10:34:00	0:00:40:25	0	-1	1985	8.3	1.6	7.7	14.5
10:34:32	0:00:40:57	0	-1	1985	8.3	1.6	8.6	15.3
10:35:04	0:00:41:28	0	-1	1985	8.3	1.5	9.4	16.1
10:35:36	0:00:42:00	0	-1	377	8.3	0.1	10.1	16.9
10:36:08	0:00:42:31	0	-1	25	8.3	0.0	10.1	16.9
10:36:39	0:00:43:03	0	-1	25	8.3	0.0	10.1	16.9
10:37:11	0:00:43:35	0	-1	25	8.3	0.0	10.1	16.9
10:37:43	0:00:44:06	0	-1	25	8.3	0.0	10.1	16.9
10:38:15	0:00:44:38	0	-1	25	8.9	0.0	10.1	16.9
10:38:47	0:00:45:09	0	-1	25	8.7	0.0	10.1	16.9
10:39:19	0:00:45:41	0	-1	25	8.6	0.0	10.1	16.9
10:39:50	0:00:46:13	0	-1	25	8.6	0.0	10.1	16.9
10:40:22	0:00:46:45	0	-1	25	8.5	0.0	10.1	16.9
10:40:54	0:00:47:16	0	-1	25	8.5	0.0	10.1	16.9
10:41:26	0:00:47:47	0	-1	25	8.5	0.0	10.1	16.9
10:41:58	0:00:48:19	0	-1	25	8.9	4.5	10.9	17.7
10:42:30	0:00:48:51	0	-1	25	20.0	281.1	44.2	51.0
10:43:02	0:00:49:23	0	-1	25	7.7	2.4	86.4	73.2
10:43:34	0:00:49:55	0	-1	25	8.2	4.0	58.2	74.9
10:44:07	0:00:50:27	0	-1	25	8.3	4.7	77.5	84.2
10:44:39	0:00:50:59	0	-1	25	8.3	5.6	80.7	87.5
10:45:11	0:00:51:31	0	-1	25	8.3	3.5	83.7	90.5
10:45:43	0:00:52:02	0	-1	25	8.3	0.0	83.8	90.6
10:46:16	0:00:52:34	0	-1	25	8.3	0.0	83.8	90.6
10:46:48	0:00:53:06	0	-1	25	8.3	5.8	84.7	91.4
10:47:21	0:00:53:39	0	-1	25	8.2	6.5	87.9	94.7
10:47:53	0:00:54:10	0	-1	25	8.1	0.0	88.2	94.9

Baker Hughes — Job Start: Tuesday, October 01, 2013

Cement Plug #2



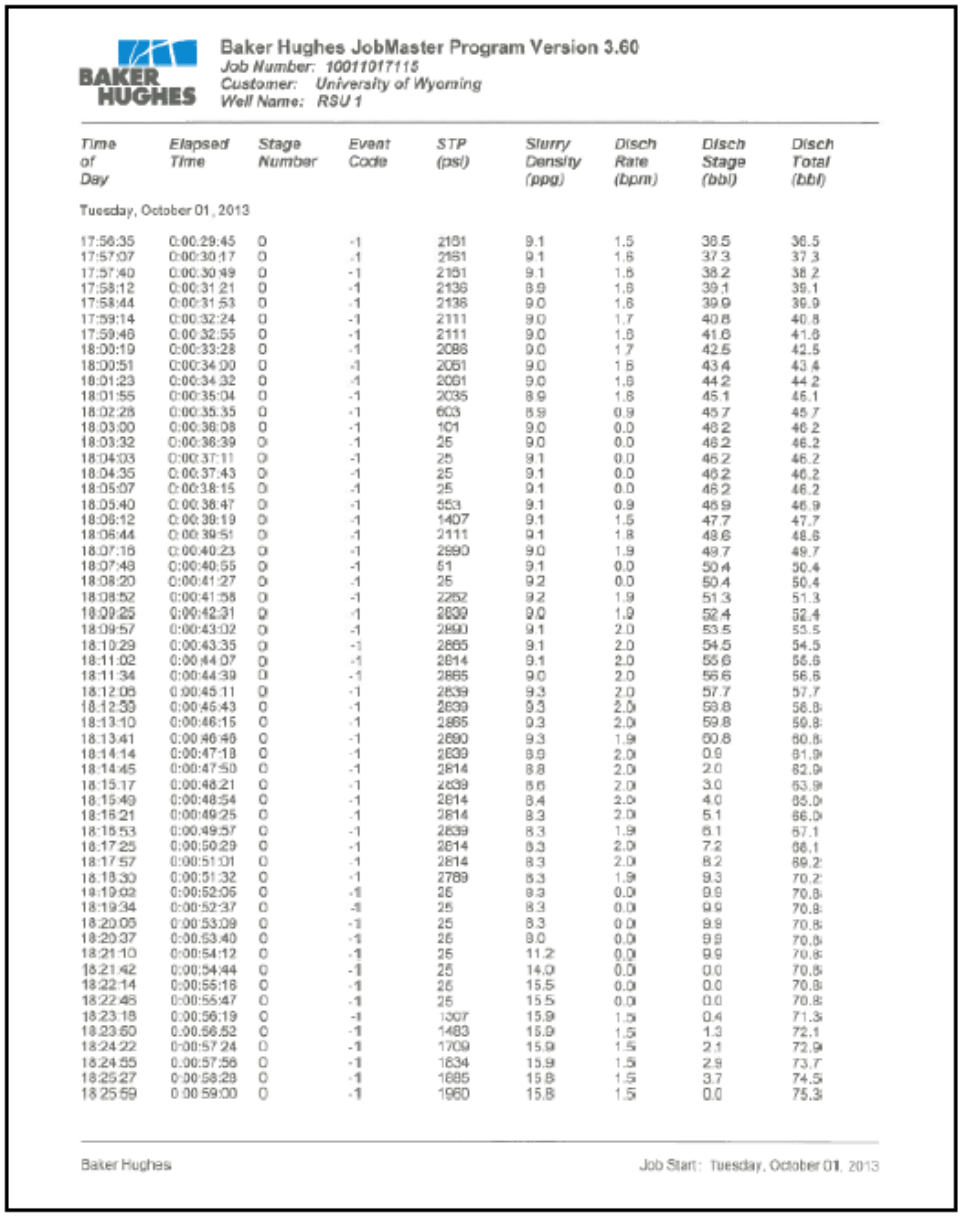


Baker Hughes JobMaster Program Version 3.60

Job Number: 10011017115
Customer: University of Wyoming
Well Name: RSU 1

Time of Day	Elapsed Time	Stage Number	Event Code	STP (psi)	Slurry Density (ppg)	Disch Rate (bpm)	Disch Stage (bbl)	Disch Total (bbl)
Tuesday, October 01, 2013								
17:26:39	0:00:00:00	0	-1	0	8.3	0.0	0.0	0.0
17:27:11	0:00:00:31	0	-1	0	8.3	0.0	0.0	0.0
17:27:42	0:00:01:02	0	-1	0	8.1	0.0	0.0	0.0
17:28:14	0:00:01:34	0	-1	0	8.3	0.0	0.0	0.0
17:28:45	0:00:02:05	0	-1	0	8.3	0.0	0.0	0.0
17:29:17	0:00:02:36	0	-1	0	8.3	0.0	0.0	0.0
17:29:48	0:00:03:07	0	-1	0	8.3	0.0	0.0	0.0
17:30:19	0:00:03:39	0	-1	0	8.2	0.0	0.0	0.0
17:30:51	0:00:04:10	0	-1	0	8.4	0.0	0.0	0.0
17:31:23	0:00:04:41	0	-1	0	8.6	0.0	0.0	0.0
17:31:55	0:00:05:13	0	-1	0	8.8	0.0	0.0	0.0
17:32:26	0:00:05:45	0	-1	0	9.1	0.0	0.0	0.0
17:32:58	0:00:06:17	0	-1	151	9.1	0.0	0.4	0.4
17:33:30	0:00:06:49	0	-1	553	9.1	0.8	0.8	0.8
17:34:03	0:00:07:20	0	-1	1759	9.1	1.5	1.6	1.6
17:34:35	0:00:07:52	0	-1	1709	9.1	1.5	2.4	2.4
17:35:06	0:00:08:24	0	-1	1734	9.1	1.5	3.2	3.2
17:35:39	0:00:08:56	0	-1	1759	9.1	1.5	4.0	4.0
17:36:10	0:00:09:28	0	-1	1759	9.1	1.5	4.8	4.8
17:36:43	0:00:10:00	0	-1	1784	9.1	1.5	5.6	5.6
17:37:15	0:00:10:31	0	-1	1784	9.2	1.5	6.4	6.4
17:37:47	0:00:11:04	0	-1	1784	9.1	1.5	7.2	7.2
17:38:19	0:00:11:36	0	-1	1809	9.0	1.5	8.0	8.0
17:38:51	0:00:12:07	0	-1	1834	9.0	1.5	8.8	8.8
17:39:23	0:00:12:40	0	-1	1834	9.1	1.4	9.6	9.6
17:39:56	0:00:13:11	0	-1	1834	9.1	1.5	10.4	10.4
17:40:28	0:00:13:43	0	-1	1834	8.9	1.5	11.2	11.2
17:41:00	0:00:14:15	0	-1	1834	8.9	1.5	11.9	11.9
17:41:32	0:00:14:48	0	-1	1834	8.8	1.4	12.8	12.8
17:42:04	0:00:15:19	0	-1	1860	9.3	1.5	13.6	13.6
17:42:36	0:00:15:51	0	-1	1860	9.2	1.5	14.4	14.4
17:43:09	0:00:16:23	0	-1	1860	9.0	1.4	15.2	15.2
17:43:41	0:00:16:55	0	-1	1860	9.1	1.5	16.0	16.0
17:44:13	0:00:17:27	0	-1	1860	9.1	1.5	16.8	16.8
17:44:45	0:00:18:00	0	-1	1834	8.9	1.5	17.6	17.6
17:45:17	0:00:18:31	0	-1	1583	9.1	1.3	18.3	18.3
17:45:50	0:00:19:03	0	-1	2186	9.2	1.6	19.2	19.2
17:46:22	0:00:19:36	0	-1	2136	9.2	1.6	20.0	20.0
17:46:54	0:00:20:07	0	-1	2136	9.1	1.6	20.9	20.9
17:47:27	0:00:20:40	0	-1	2136	9.0	1.6	21.8	21.8
17:47:59	0:00:21:12	0	-1	2136	9.0	1.6	22.6	22.6
17:48:31	0:00:21:44	0	-1	2136	8.9	1.6	23.5	23.5
17:49:03	0:00:22:16	0	-1	2161	8.9	1.6	24.4	24.4
17:49:36	0:00:22:48	0	-1	2161	8.9	1.6	25.2	25.2
17:50:08	0:00:23:21	0	-1	2111	9.0	1.6	26.1	26.1
17:50:40	0:00:23:52	0	-1	2111	9.1	1.7	26.9	26.9
17:51:13	0:00:24:24	0	-1	2111	9.1	1.7	27.8	27.8
17:51:45	0:00:24:56	0	-1	2136	9.1	1.6	28.6	28.6
17:52:17	0:00:25:28	0	-1	2136	9.1	1.6	29.5	29.5
17:52:49	0:00:26:00	0	-1	2136	9.1	1.6	30.4	30.4
17:53:21	0:00:26:32	0	-1	2136	9.0	1.6	31.3	31.3
17:53:53	0:00:27:04	0	-1	2186	9.0	1.6	32.1	32.1
17:54:26	0:00:27:36	0	-1	2186	8.9	1.6	33.0	33.0
17:54:58	0:00:28:08	0	-1	2161	8.9	1.7	33.8	33.8
17:55:30	0:00:28:40	0	-1	2186	8.9	1.6	34.7	34.7
17:56:03	0:00:29:13	0	-1	2151	9.0	1.5	35.6	35.6

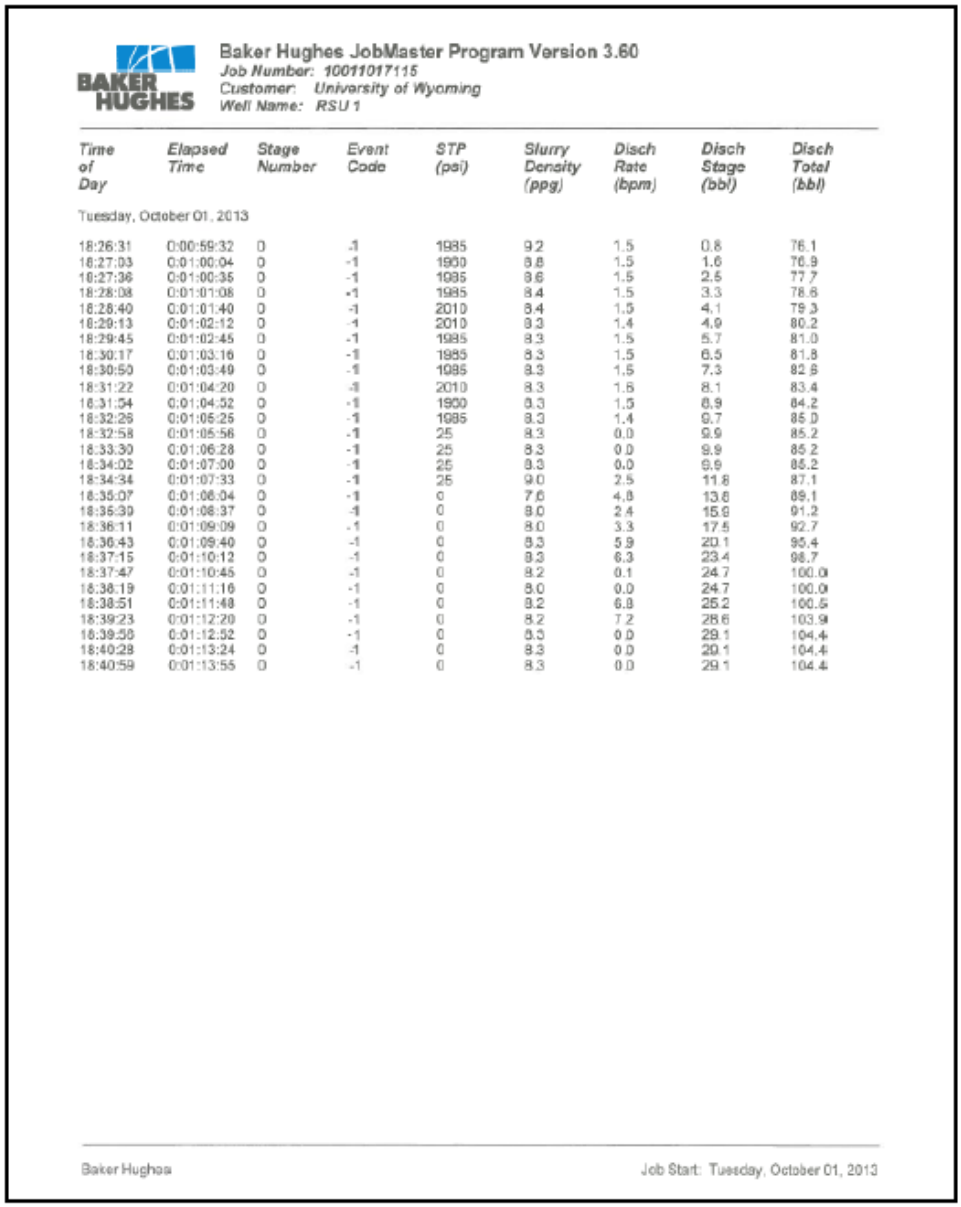
Baker Hughes — Job Start: Tuesday, October 01, 2013



Baker Hughes JobMaster Program Version 3.60
Job Number: 10011017115
Customer: University of Wyoming
Well Name: RSU 1

Time of Day	Elapsed Time	Stage Number	Event Code	STP (psi)	Slurry Density (ppg)	Disch Rate (bpm)	Disch Stage (bbl)	Disch Total (bbl)
Tuesday, October 01, 2013								
17:56:35	0:00:29:45	0	-1	2151	9.1	1.5	36.5	36.5
17:57:07	0:00:30:17	0	-1	2161	9.1	1.6	37.3	37.3
17:57:40	0:00:30:49	0	-1	2151	9.1	1.6	38.2	38.2
17:58:12	0:00:31:21	0	-1	2136	8.9	1.6	39.1	39.1
17:58:44	0:00:31:53	0	-1	2136	9.0	1.6	39.9	39.9
17:59:14	0:00:32:24	0	-1	2111	9.0	1.7	40.8	40.8
17:59:46	0:00:32:55	0	-1	2111	9.0	1.6	41.6	41.6
18:00:19	0:00:33:28	0	-1	2086	9.0	1.7	42.5	42.5
18:00:51	0:00:34:00	0	-1	2051	9.0	1.6	43.4	43.4
18:01:23	0:00:34:32	0	-1	2061	9.0	1.6	44.2	44.2
18:01:55	0:00:35:04	0	-1	2035	8.9	1.6	45.1	45.1
18:02:28	0:00:35:35	0	-1	603	8.9	0.9	45.7	45.7
18:03:00	0:00:36:08	0	-1	101	9.0	0.0	46.2	46.2
18:03:32	0:00:36:39	0	-1	25	9.0	0.0	46.2	46.2
18:04:03	0:00:37:11	0	-1	25	9.1	0.0	46.2	46.2
18:04:35	0:00:37:43	0	-1	25	9.1	0.0	46.2	46.2
18:05:07	0:00:38:15	0	-1	25	9.1	0.0	46.2	46.2
18:05:40	0:00:38:47	0	-1	553	9.1	0.9	46.9	46.9
18:06:12	0:00:39:19	0	-1	1407	9.1	1.5	47.7	47.7
18:06:44	0:00:39:51	0	-1	2111	9.1	1.8	48.6	48.6
18:07:16	0:00:40:23	0	-1	2990	9.0	1.9	49.7	49.7
18:07:48	0:00:40:55	0	-1	51	9.1	0.0	50.4	50.4
18:08:20	0:00:41:27	0	-1	25	9.2	0.0	50.4	50.4
18:08:52	0:00:41:58	0	-1	2252	9.2	1.9	51.3	51.3
18:09:25	0:00:42:31	0	-1	2839	9.0	1.9	52.4	52.4
18:09:57	0:00:43:02	0	-1	2890	9.1	2.0	53.5	53.5
18:10:29	0:00:43:35	0	-1	2865	9.1	2.0	54.5	54.5
18:11:02	0:00:44:07	0	-1	2814	9.1	2.0	55.6	55.6
18:11:34	0:00:44:39	0	-1	2865	9.0	2.0	56.6	56.6
18:12:05	0:00:45:11	0	-1	2839	9.3	2.0	57.7	57.7
18:12:38	0:00:45:43	0	-1	2839	9.3	2.0	58.8	58.8
18:13:10	0:00:46:15	0	-1	2865	9.3	2.0	59.8	59.8
18:13:41	0:00:46:46	0	-1	2890	9.3	1.9	60.8	60.8
18:14:14	0:00:47:18	0	-1	2839	8.9	2.0	0.9	61.9
18:14:45	0:00:47:50	0	-1	2814	8.8	2.0	2.0	62.9
18:15:17	0:00:48:21	0	-1	2839	8.6	2.0	3.0	63.9
18:15:49	0:00:48:54	0	-1	2814	8.4	2.0	4.0	65.0
18:16:21	0:00:49:25	0	-1	2814	8.3	2.0	5.1	66.0
18:16:53	0:00:49:57	0	-1	2839	8.3	1.9	6.1	67.1
18:17:25	0:00:50:29	0	-1	2814	8.3	2.0	7.2	68.1
18:17:57	0:00:51:01	0	-1	2814	8.3	2.0	8.2	69.2
18:18:30	0:00:51:32	0	-1	2789	8.3	1.9	9.3	70.2
18:19:02	0:00:52:05	0	-1	25	8.3	0.0	9.9	70.8
18:19:34	0:00:52:37	0	-1	25	8.3	0.0	9.9	70.8
18:20:05	0:00:53:09	0	-1	25	8.3	0.0	9.9	70.8
18:20:37	0:00:53:40	0	-1	25	8.0	0.0	9.9	70.8
18:21:10	0:00:54:12	0	-1	25	11.2	0.0	9.9	70.8
18:21:42	0:00:54:44	0	-1	25	14.0	0.0	0.0	70.8
18:22:14	0:00:55:16	0	-1	26	15.5	0.0	0.0	70.8
18:22:46	0:00:55:47	0	-1	25	15.5	0.0	0.0	70.8
18:23:18	0:00:56:19	0	-1	1307	15.9	1.5	0.4	71.3
18:23:50	0:00:56:52	0	-1	1483	15.9	1.5	1.3	72.1
18:24:22	0:00:57:24	0	-1	1709	15.9	1.5	2.1	72.9
18:24:55	0:00:57:56	0	-1	1634	15.9	1.5	2.9	73.7
18:25:27	0:00:58:28	0	-1	1685	15.8	1.5	3.7	74.5
18:25:59	0:00:59:00	0	-1	1960	15.8	1.5	0.0	75.3

Baker Hughes — Job Start: Tuesday, October 01, 2013



Baker Hughes JobMaster Program Version 3.60
Job Number: 10011017115
Customer: University of Wyoming
Well Name: RSU 1

Time of Day	Elapsed Time	Stage Number	Event Code	STP (psi)	Slurry Density (ppg)	Disch Rate (bpm)	Disch Stage (bbl)	Disch Total (bbl)
Tuesday, October 01, 2013								
18:26:31	0:00:59:32	0	-1	1985	9.2	1.5	0.8	76.1
18:27:03	0:01:00:04	0	-1	1950	8.8	1.5	1.6	76.9
18:27:36	0:01:00:35	0	-1	1985	8.6	1.5	2.5	77.7
18:28:08	0:01:01:08	0	-1	1985	8.4	1.5	3.3	78.6
18:28:40	0:01:01:40	0	-1	2010	8.4	1.5	4.1	79.3
18:29:13	0:01:02:12	0	-1	2010	8.3	1.4	4.9	80.2
18:29:45	0:01:02:45	0	-1	1985	8.3	1.5	5.7	81.0
18:30:17	0:01:03:16	0	-1	1985	8.3	1.5	6.5	81.8
18:30:50	0:01:03:49	0	-1	1985	8.3	1.5	7.3	82.6
18:31:22	0:01:04:20	0	-1	2010	8.3	1.5	8.1	83.4
18:31:54	0:01:04:52	0	-1	1900	8.3	1.5	8.9	84.2
18:32:26	0:01:05:25	0	-1	1985	8.3	1.4	9.7	85.0
18:32:58	0:01:05:56	0	-1	25	8.3	0.0	9.9	85.2
18:33:30	0:01:06:28	0	-1	25	8.3	0.0	9.9	85.2
18:34:02	0:01:07:00	0	-1	25	8.3	0.0	9.9	85.2
18:34:34	0:01:07:33	0	-1	25	9.0	2.5	11.8	87.1
18:35:07	0:01:08:04	0	-1	0	7.6	4.8	13.6	89.1
18:35:39	0:01:08:37	0	-1	0	8.0	2.4	15.9	91.2
18:36:11	0:01:09:09	0	-1	0	8.0	3.3	17.5	92.7
18:36:43	0:01:09:40	0	-1	0	8.3	5.9	20.1	95.4
18:37:15	0:01:10:12	0	-1	0	8.3	6.3	23.4	98.7
18:37:47	0:01:10:45	0	-1	0	8.2	0.1	24.7	100.0
18:38:19	0:01:11:16	0	-1	0	8.0	0.0	24.7	100.0
18:38:51	0:01:11:48	0	-1	0	8.2	6.8	25.2	100.5
18:39:23	0:01:12:20	0	-1	0	8.2	7.2	28.6	103.9
18:39:56	0:01:12:52	0	-1	0	8.5	0.0	29.1	104.4
18:40:28	0:01:13:24	0	-1	0	8.3	0.0	29.1	104.4
18:40:59	0:01:13:55	0	-1	0	8.3	0.0	29.1	104.4

Baker Hughes — Job Start: Tuesday, October 01, 2013

Overall Job Report (Day 2 of P&A)

CEMENT JOB REPORT

BAKER HUGHES

CUSTOMER: UNIVERSITY OF WYOMING	DATE: 02-OCT-13 F.R.# 3716101141	SERV. SUPV.: Jericho R Morrell
LEASE & WELL NAME: RSU #1 - API 49037071540000	LOCATION: 16-20N-101W	COUNTY-PARISH-BLOCK: Sweetwater Wyoming
DISTRICT: Vernal	DRILLING CONTRACTOR RIG#	TYPE OF JOB: Plug & Abandon

SIZE & TYPE OF PLUGS	LIST-CSG-HARDWARE	MECHANICAL BARRIERS	MD	TVD	HANGER TYPES	MD	TVD

PHYSICAL SLURRY PROPERTIES

MATERIALS FURNISHED BY BJ	LAB REPORT NO.	SACKS OF CEMENT	SLURRY WGT PPG	SLURRY YLD FT3	WATER GPS	PUMP TIME HR:MIN	Bbl SLURRY	Bbl MIX WATER
Poz+2% bent		45	9	9.08	84.27		72.7	68.79
G+.4%cd32+.4%fl25+.2%r3		96	15.8	1.15	4.93	05:59	11.5	6.59
Fresh Water			8.34				10	
Poz+2%bent		41	9	9.08	84.27		65	61.51
Fresh water			8.34				10	
G+.4%cd32+.4%fl25+.2%r3		38	15.8	1.15	4.93	05:59	7.7	4.41
Fresh water			8.34				10	
Class G Cement + Additives			0				0	
9.00 ppg Mud			0				0	
9.00 ppg Mud			0				0	
9.00 ppg Mud			0				0	

Available Mix Water: 500 Bbl. Available Displ. Fluid: 500 Bbl. TOTAL: 196.9 141.30

HOLE SIZE	% EXCESS	DEPTH	TBG-CSG-D.P. ID	OD	WGT.	TYPE	MD	TVD	GRADE	COLLAR DEPTHS SHOE	FLOAT	STAGE
6.276	0	4100	6.276	7		26 CSG	4100	4100	N-80			

LAST CASING ID	OD	WGT.	TYPE	MD	TVD	PKR-CMT RET-BR PL LINER BRAND & TYPE	DEPTH	PERF. DEPTH TOP	BTM	TOP CONN SIZE	THREAD	WELL FLUID TYPE	WGT.
						No Packer	0			2	1502	WATER BASED	9

SHEAL VOLUME VOLUME	UOM	DISPL. FLUID TYPE	WGT.	CAL. PSI BUMP PLUG	CAL. MAX PSI TO REV	OP. MAX SQ. PSI	MAX TBG PSI RATED	Operator	MAX CSG PSI RATED	Operator	MIX WATER
10	BBLS			0	0	0	15100	12090	7240	5792	

Circulation Prior to Job

Circulated Well: Rig [ ] BJ [ ]		Circulation Time: 0	Circulation Rate: 6 BPM
Mud Density In: 0 LBS/GAL	Mud Density Out: 0 LBS/CAL	PV & YP Mud In: 0	PV & YP Mud Out: 0
Gas Present: NO [ ] YES [X]	Units: 0	Solids Present at End of Circulation: NO [X] YES [ ]	

Displacement And Mud Removal

Displaced By: Rig [ ] BJ [X]		Amount Bled Back After Job: 0 BBLS	
Returns During Job: [ ] NONE	[ ] PARTIAL [X] FULL	Method Used to Verify Returns: Visual	
Cement Returns at Surface: [ ] YES	[X] NO	Were Returns Planned at Surface: [X] NO	[ ] YES
Pipe Movement: [ ] ROTATION	[ ] RECIPROCATION	[ ] NONE	[ ] UNABLE DUE TO STUCK PIPE
Centralizers: [X] NO	[ ] YES	Quantity:	Type: [ ] BOW [ ] RIGID
Job Pumped Through: [ ] CHOKE MANIFOLD	[ ] SQUEEZE MANIFOLD	[ ] MANIFOLD	[ ] NO MANIFOLD

Plugs

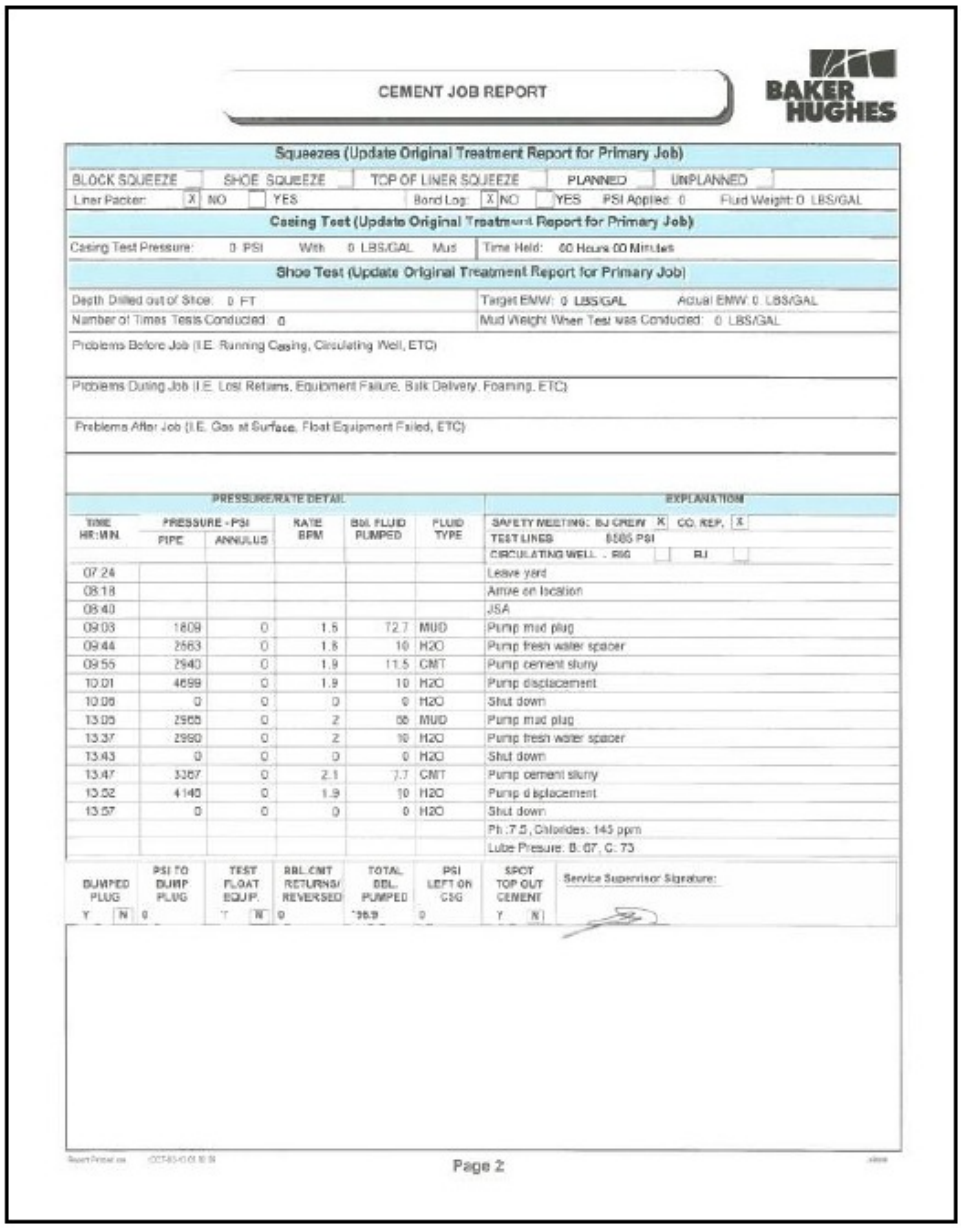
Number of Attempts by BJ: 1	Competition: 0	Wiper Balls Used: [X] NO	[ ] YES Quantity
Plug Catcher Used: [X] NO	[ ] YES	Parabow Used: [X] NO	[ ] YES
Was There a Bottom: [X] NO	[ ] YES	Top of Plug: 2200 FT	Bottom of Plug: 0 FT

EXPLANATION: TROUBLE SETTING TOOL, RUNNING CSG, ETC. PRIOR TO CEMENTING: Running coil

PRESSURE/RATE DETAIL	EXPLANATION

Report Formation: OCT-03-2013 0310

Page 1



CEMENT JOB REPORT

BAKER HUGHES

Squeezes (Update Original Treatment Report for Primary Job)

BLOCK SQUEEZE	SHOE SQUEEZE	TOP OF LINER SQUEEZE	PLANNED	UNPLANNED

Liner Packer: [X] NO [ ] YES Bond Log: [X] NO [ ] YES PSI Applied: 0 Fluid Weight: 0 LBS/GAL

Casing Test (Update Original Treatment Report for Primary Job)

Casing Test Pressure: 0 PSI With 0 LBS/GAL Mud | Time Held: 00 Hours 00 Minutes

Shoe Test (Update Original Treatment Report for Primary Job)

Depth Drilled out of Shoe: 0 FT | Target EMW: 0 LBS/GAL Actual EMW: 0 LBS/GAL

Number of Times Tests Conducted: 0 | Mud Weight When Test was Conducted: 0 LBS/GAL

Problems Before Job (I.E. Running Casing, Circulating Well, ETC)

Problems During Job (I.E. Lost Returns, Equipment Failure, Bulk Delivery, Foaming, ETC)

Problems After Job (I.E. Gas at Surface, Float Equipment Failed, ETC)

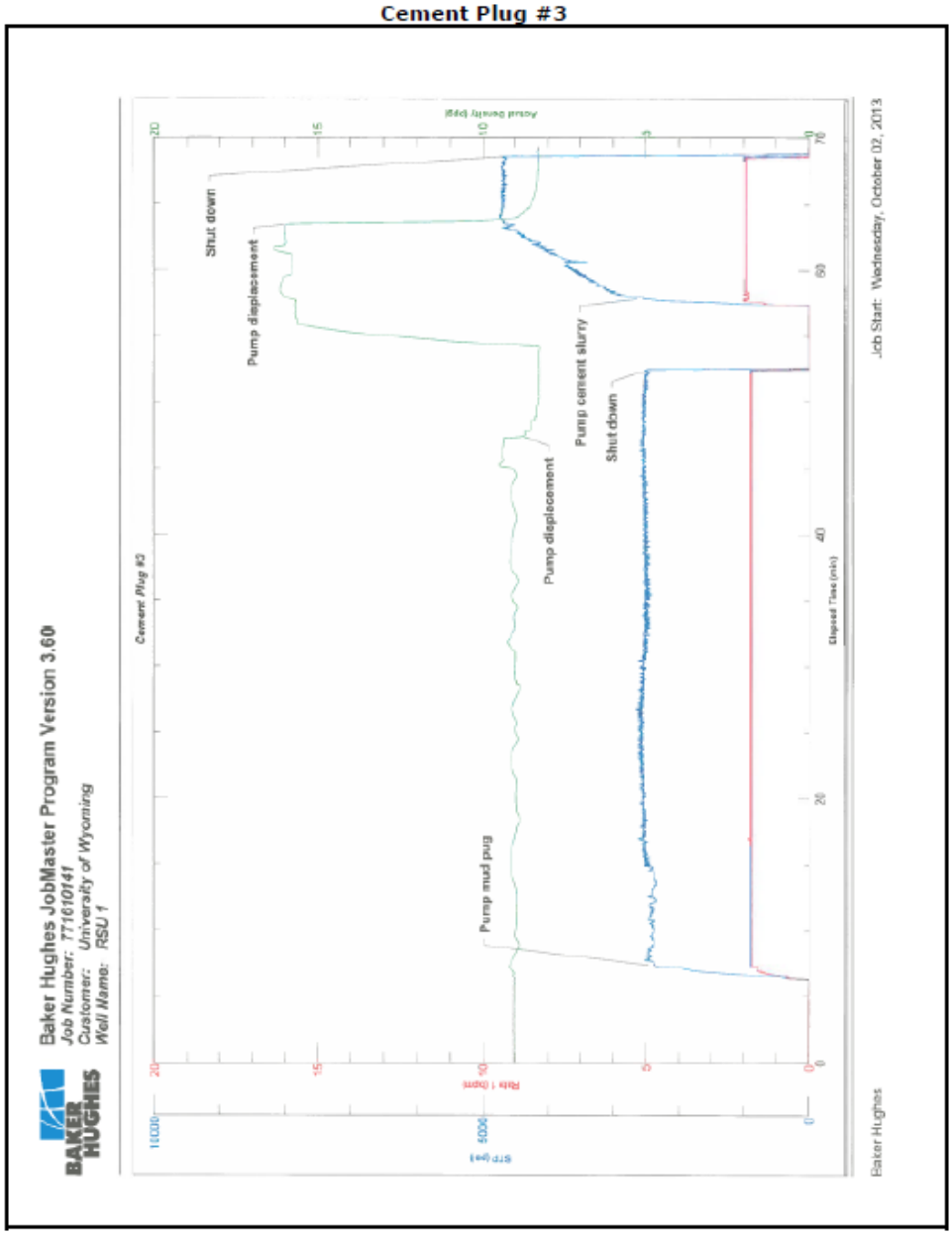
PRESSURE/RATE DETAIL

TIME HR:MIN	PRESSURE - PSI PIPE	PRESSURE - PSI ANNULUS	RATE BPM	BBL FLUID PUMPED	FLUID TYPE	EXPLANATION
						SAFETY MEETING: BJ CREW [X] CO. REP. [X]
						TEST LINES 8585 PSI
						CIRCULATING WELL - RIG [ ] BJ [ ]
07:24						Leave yard
08:18						Arrive on location
08:40						JSA
09:03	1809	0	1.5	72.7	MUD	Pump mud plug
09:44	2563	0	1.8	10	H2O	Pump fresh water spacer
09:55	2940	0	1.9	11.5	CMT	Pump cement slurry
10:01	4699	0	1.9	10	H2O	Pump displacement
10:08	0	0	0	0	H2O	Shut down
13:05	2565	0	2	68	MUD	Pump mud plug
13:37	2960	0	2	10	H2O	Pump fresh water spacer
13:43	0	0	0	0	H2O	Shut down
13:47	3267	0	2.1	7.7	CMT	Pump cement slurry
13:52	4140	0	1.9	10	H2O	Pump displacement
13:57	0	0	0	0	H2O	Shut down
						Ph :7.5 , Chlorides: 145 ppm
						Lube Presure: B. 67, C. 73

BUMPED PLUG	PSI TO BUMP PLUG	TEST FLOAT EQUIP.	BBL CMT RETURNS/ REVERSED	TOTAL BBL PUMPED	PSI LEFT ON CSG	SPOT TOP OUT CEMENT	Service Supervisor Signature:
Y [N]	0	Y [N]	0	156.9	0	Y [N]	

Page 2

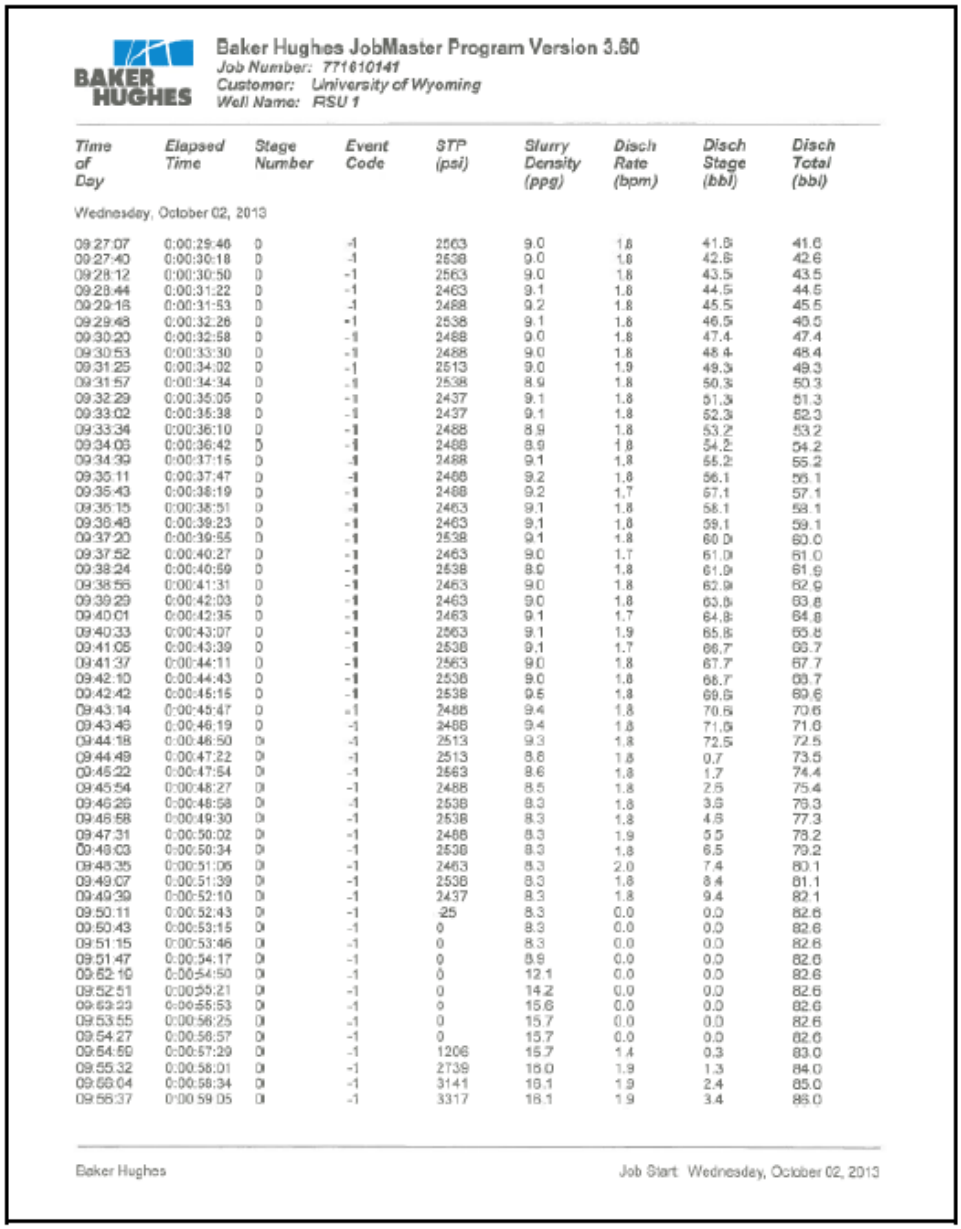
Cement Plug #3



Baker Hughes JobMaster Program Version 3.60
Job Number: 771610141
Customer: University of Wyoming
Well Name: RSU 1

Time of Day	Elapsed Time	Stage Number	Event Code	STP (psi)	Slurry Density (ppg)	Disch Rate (bpm)	Disch Stage (bbl)	Disch Total (bbl)
Wednesday, October 02, 2013								
08:57:13	0:00:00:02	0	-1	-25	9.0	0.0	0.0	0.0
08:57:44	0:00:00:33	0	-1	-25	9.0	0.0	0.0	0.0
08:58:16	0:00:01:05	0	-1	-25	9.0	0.0	0.0	0.0
08:58:47	0:00:01:36	0	-1	-25	9.0	0.0	0.0	0.0
08:59:19	0:00:02:07	0	-1	-25	9.0	0.0	0.0	0.0
08:59:51	0:00:02:39	0	-1	-25	9.0	0.0	0.0	0.0
09:00:22	0:00:03:10	0	-1	-25	9.0	0.0	0.0	0.0
09:00:53	0:00:03:42	0	-1	-25	9.0	0.0	0.0	0.0
09:01:26	0:00:04:13	0	-1	-25	9.0	0.0	0.0	0.0
09:01:57	0:00:04:45	0	-1	-25	9.0	0.0	0.0	0.0
09:02:28	0:00:05:16	0	-1	-25	9.0	0.0	0.0	0.0
09:03:00	0:00:05:47	0	-1	0	9.0	0.0	0.0	0.0
09:03:31	0:00:06:18	0	-1	-25	9.0	0.0	0.0	0.0
09:04:03	0:00:06:50	0	-1	1407	9.0	1.4	0.5	0.5
09:04:35	0:00:07:22	0	-1	2337	9.2	1.8	1.4	1.4
09:05:08	0:00:07:54	0	-1	2437	9.0	1.8	2.3	2.3
09:06:40	0:00:09:26	0	-1	2483	8.9	1.8	3.3	3.3
09:06:12	0:00:08:58	0	-1	2387	8.9	1.7	4.2	4.2
09:06:44	0:00:09:30	0	-1	2412	9.0	1.8	5.2	5.2
09:07:17	0:00:10:02	0	-1	2387	9.0	1.8	6.1	6.1
09:07:49	0:00:10:34	0	-1	2437	8.9	1.7	7.0	7.0
09:08:21	0:00:11:06	0	-1	2437	8.9	1.8	8.0	8.0
09:08:53	0:00:11:38	0	-1	2412	9.0	1.8	8.9	8.9
09:09:25	0:00:12:10	0	-1	2382	9.0	1.8	9.9	9.9
09:09:58	0:00:12:42	0	-1	2412	9.0	1.8	10.8	10.8
09:10:30	0:00:13:14	0	-1	2387	9.0	1.8	11.8	11.8
09:11:02	0:00:13:46	0	-1	2382	9.0	1.8	12.7	12.7
09:11:34	0:00:14:18	0	-1	2387	9.1	1.7	13.6	13.6
09:12:06	0:00:14:51	0	-1	2412	9.1	1.9	14.6	14.6
09:12:39	0:00:15:22	0	-1	2513	9.1	1.8	15.6	15.6
09:13:11	0:00:15:55	0	-1	2563	9.1	1.8	16.5	16.5
09:13:43	0:00:16:27	0	-1	2513	9.1	1.8	17.5	17.5
09:14:16	0:00:17:00	0	-1	2513	9.0	1.8	18.5	18.5
09:14:48	0:00:17:31	0	-1	2488	9.0	1.8	19.5	19.5
09:15:20	0:00:18:03	0	-1	2538	8.9	1.8	20.4	20.4
09:15:52	0:00:18:35	0	-1	2513	8.9	1.8	21.4	21.4
09:16:24	0:00:19:07	0	-1	2538	8.9	1.8	22.3	22.3
09:16:56	0:00:19:39	0	-1	2588	9.0	1.9	23.3	23.3
09:17:28	0:00:20:11	0	-1	2513	9.0	1.7	24.3	24.3
09:18:01	0:00:20:43	0	-1	2588	9.0	1.9	25.2	25.2
09:18:33	0:00:21:15	0	-1	2538	8.9	1.8	26.2	26.2
09:19:05	0:00:21:46	0	-1	2513	9.0	1.8	27.1	27.1
09:19:37	0:00:22:18	0	-1	2588	9.1	1.9	28.1	28.1
09:20:09	0:00:22:51	0	-1	2538	9.1	1.9	29.1	29.1
09:20:41	0:00:23:22	0	-1	2513	9.1	1.8	30.0	30.0
09:21:13	0:00:23:54	0	-1	2538	9.0	1.8	31.0	31.0
09:21:45	0:00:24:26	0	-1	2538	8.9	1.7	32.0	32.0
09:22:17	0:00:24:58	0	-1	2563	9.0	1.8	32.9	32.9
09:22:49	0:00:25:30	0	-1	2538	9.0	1.8	33.9	33.9
09:23:22	0:00:26:02	0	-1	2538	9.0	1.8	34.9	34.9
09:23:54	0:00:26:34	0	-1	2538	9.1	1.9	35.8	35.8
09:24:26	0:00:27:06	0	-1	2563	9.1	1.7	36.8	36.8
09:24:58	0:00:27:38	0	-1	2513	9.0	1.8	37.8	37.8
09:25:31	0:00:28:10	0	-1	2513	8.9	1.8	38.7	38.7
09:26:03	0:00:28:42	0	-1	2513	9.0	1.8	39.7	39.7
09:26:35	0:00:29:14	0	-1	2563	9.0	1.7	40.7	40.7

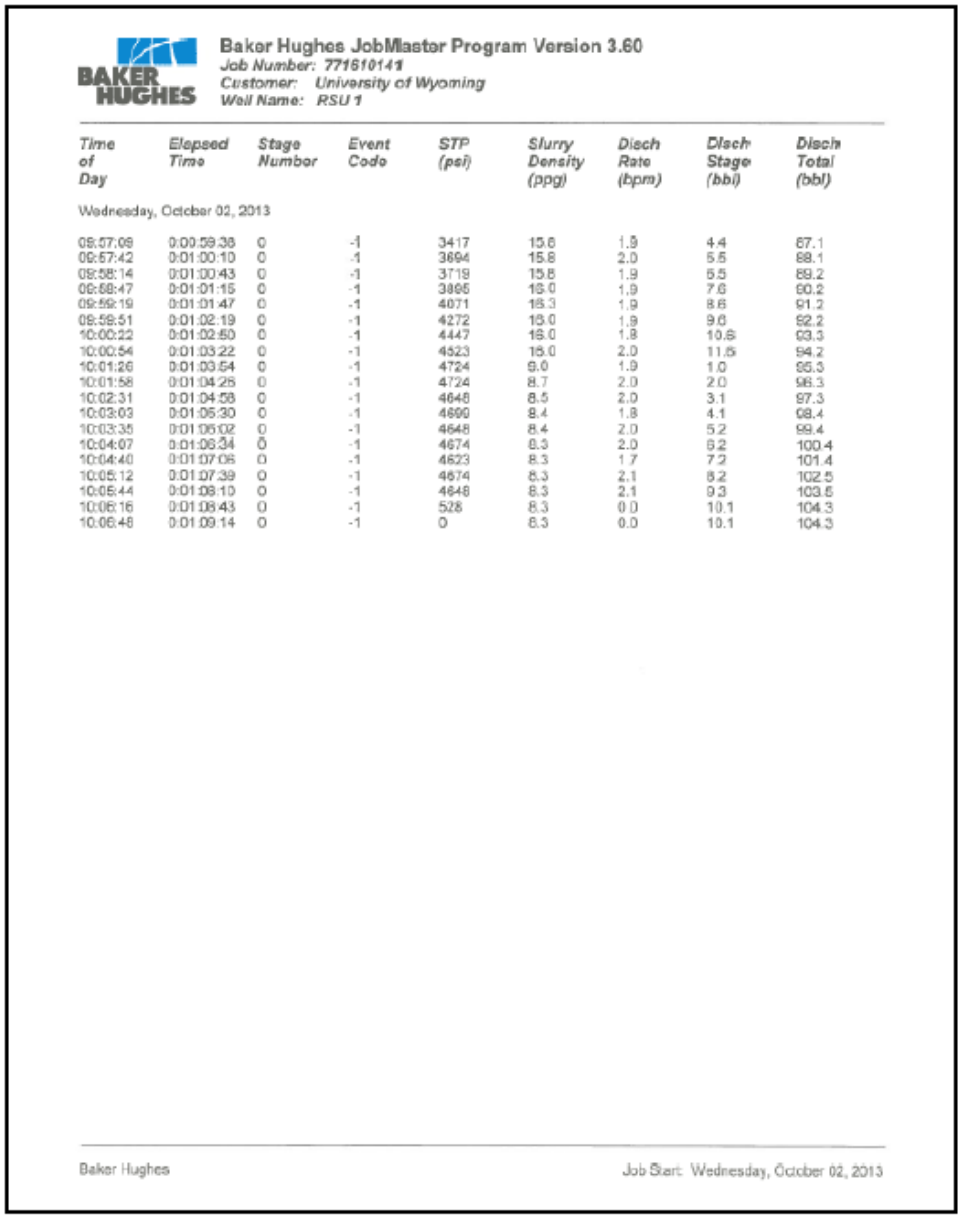
Baker Hughes — Job Start: Wednesday, October 02, 2013



Baker Hughes JobMaster Program Version 3.60
Job Number: 771610141
Customer: University of Wyoming
Well Name: RSU 1

Time of Day	Elapsed Time	Stage Number	Event Code	STP (psi)	Slurry Density (ppg)	Disch Rate (bpm)	Disch Stage (bbl)	Disch Total (bbl)
Wednesday, October 02, 2013								
09:27:07	0:00:29:46	0	-1	2563	9.0	1.8	41.6	41.6
09:27:40	0:00:30:18	0	-1	2538	9.0	1.8	42.6	42.6
09:28:12	0:00:30:50	0	-1	2563	9.0	1.8	43.5	43.5
09:28:44	0:00:31:22	0	-1	2463	9.1	1.8	44.5	44.5
09:29:16	0:00:31:53	0	-1	2488	9.2	1.8	45.5	45.5
09:29:48	0:00:32:26	0	-1	2538	9.1	1.8	46.5	46.5
09:30:20	0:00:32:58	0	-1	2488	9.0	1.8	47.4	47.4
09:30:53	0:00:33:30	0	-1	2488	9.0	1.8	48.4	48.4
09:31:25	0:00:34:02	0	-1	2513	9.0	1.9	49.3	49.3
09:31:57	0:00:34:34	0	-1	2538	8.9	1.8	50.3	50.3
09:32:29	0:00:35:05	0	-1	2437	9.1	1.8	51.3	51.3
09:33:02	0:00:35:38	0	-1	2437	9.1	1.8	52.3	52.3
09:33:34	0:00:36:10	0	-1	2488	8.9	1.8	53.2	53.2
09:34:03	0:00:36:42	0	-1	2488	8.9	1.8	54.2	54.2
09:34:39	0:00:37:15	0	-1	2488	9.1	1.8	55.2	55.2
09:35:11	0:00:37:47	0	-1	2488	9.2	1.8	56.1	56.1
09:35:43	0:00:38:19	0	-1	2488	9.2	1.7	57.1	57.1
09:36:15	0:00:38:51	0	-1	2463	9.1	1.8	58.1	58.1
09:36:48	0:00:39:23	0	-1	2463	9.1	1.8	59.1	59.1
09:37:20	0:00:39:55	0	-1	2538	9.1	1.8	60.0	60.0
09:37:52	0:00:40:27	0	-1	2463	9.0	1.7	61.0	61.0
09:38:24	0:00:40:59	0	-1	2538	8.9	1.8	61.9	61.9
09:38:56	0:00:41:31	0	-1	2463	9.0	1.8	62.9	62.9
09:39:29	0:00:42:03	0	-1	2463	9.0	1.8	63.8	63.8
09:40:01	0:00:42:35	0	-1	2463	9.1	1.7	64.8	64.8
09:40:33	0:00:43:07	0	-1	2563	9.1	1.9	65.8	65.8
09:41:05	0:00:43:39	0	-1	2538	9.1	1.7	66.7	66.7
09:41:37	0:00:44:11	0	-1	2563	9.0	1.8	67.7	67.7
09:42:10	0:00:44:43	0	-1	2538	9.0	1.8	68.7	68.7
09:42:42	0:00:45:15	0	-1	2538	9.5	1.8	69.6	69.6
09:43:14	0:00:45:47	0	-1	2488	9.4	1.8	70.6	70.6
09:43:46	0:00:46:19	0	-1	2488	9.4	1.8	71.6	71.6
09:44:18	0:00:46:50	0	-1	2513	9.3	1.8	72.5	72.5
09:44:49	0:00:47:22	0	-1	2513	8.6	1.8	0.7	73.5
09:45:22	0:00:47:54	0	-1	2563	8.6	1.8	1.7	74.4
09:45:54	0:00:48:27	0	-1	2488	8.5	1.8	2.5	75.4
09:46:26	0:00:48:58	0	-1	2538	8.3	1.8	3.3	76.3
09:46:58	0:00:49:30	0	-1	2538	8.3	1.8	4.0	77.3
09:47:31	0:00:50:02	0	-1	2488	8.3	1.9	5.5	78.2
09:48:03	0:00:50:34	0	-1	2538	8.3	1.8	6.5	79.2
09:48:35	0:00:51:06	0	-1	2463	8.3	2.0	7.4	80.1
09:49:07	0:00:51:39	0	-1	2538	8.3	1.8	8.4	81.1
09:49:39	0:00:52:10	0	-1	2437	8.3	1.8	9.4	82.1
09:50:11	0:00:52:43	0	-1	-25	8.3	0.0	0.0	82.6
09:50:43	0:00:53:15	0	-1	0	8.3	0.0	0.0	82.6
09:51:15	0:00:53:46	0	-1	0	8.3	0.0	0.0	82.6
09:51:47	0:00:54:17	0	-1	0	8.9	0.0	0.0	82.6
09:52:19	0:00:54:50	0	-1	0	12.1	0.0	0.0	82.6
09:52:51	0:00:55:21	0	-1	0	14.2	0.0	0.0	82.6
09:53:23	0:00:55:53	0	-1	0	15.6	0.0	0.0	82.6
09:53:55	0:00:56:25	0	-1	0	15.7	0.0	0.0	82.6
09:54:27	0:00:56:57	0	-1	0	15.7	0.0	0.0	82.6
09:54:59	0:00:57:29	0	-1	1206	15.7	1.4	0.3	83.0
09:55:32	0:00:58:01	0	-1	2739	16.0	1.9	1.3	84.0
09:56:04	0:00:58:34	0	-1	3141	16.1	1.9	2.4	85.0
09:56:37	0:00:59:05	0	-1	3317	16.1	1.9	3.4	86.0

Baker Hughes — Job Start: Wednesday, October 02, 2013

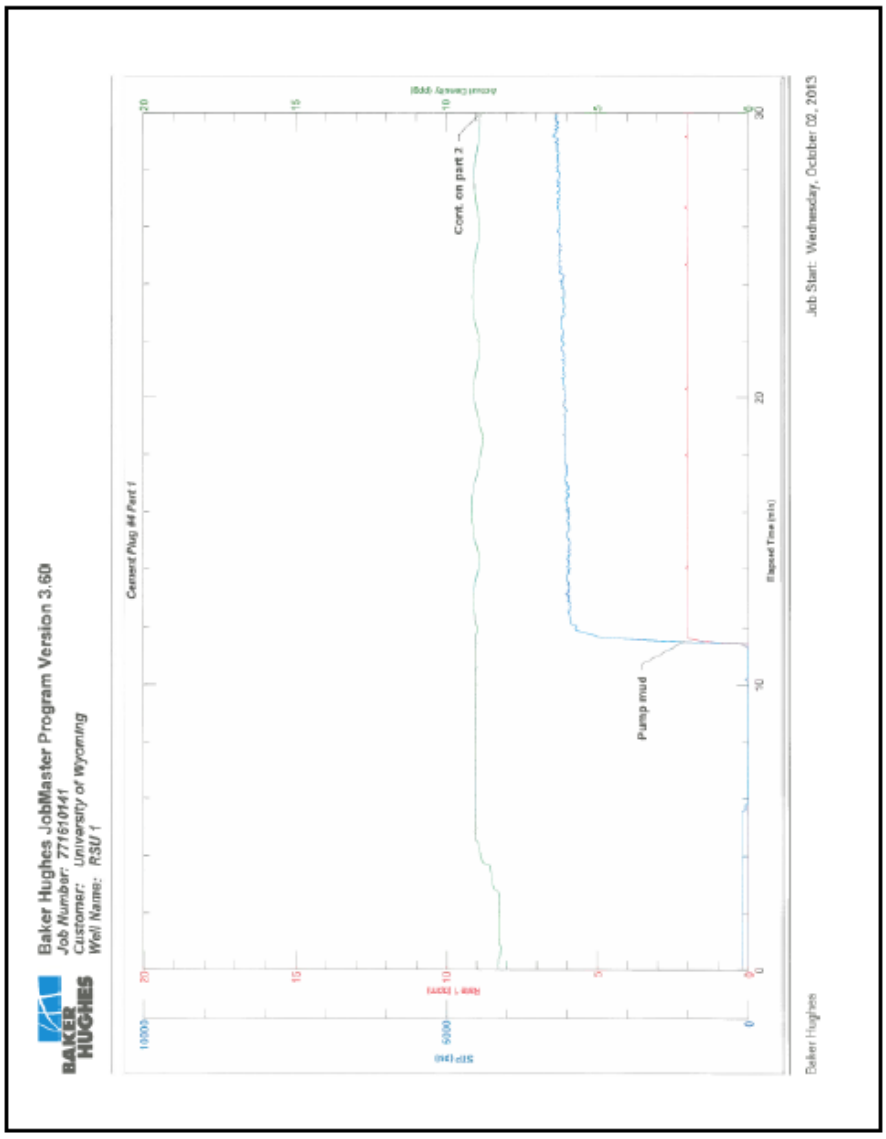


Baker Hughes JobMaster Program Version 3.60
Job Number: 771610141
Customer: University of Wyoming
Well Name: RSU 1

Time of Day	Elapsed Time	Stage Number	Event Code	STP (psi)	Slurry Density (ppg)	Disch Rate (bpm)	Disch Stage (bbl)	Disch Total (bbl)
Wednesday, October 02, 2013								
09:57:09	0:00:59:38	0	-1	3417	15.6	1.9	4.4	87.1
09:57:42	0:01:00:10	0	-1	3694	15.8	2.0	5.5	88.1
09:58:14	0:01:00:43	0	-1	3719	15.8	1.9	5.5	89.2
09:58:47	0:01:01:15	0	-1	3895	16.0	1.9	7.6	90.2
09:59:19	0:01:01:47	0	-1	4071	16.3	1.9	8.6	91.2
09:59:51	0:01:02:19	0	-1	4272	16.0	1.9	9.6	92.2
10:00:22	0:01:02:50	0	-1	4447	16.0	1.8	10.6	93.3
10:00:54	0:01:03:22	0	-1	4523	16.0	2.0	11.5	94.2
10:01:26	0:01:03:54	0	-1	4724	9.0	1.9	1.0	95.3
10:01:58	0:01:04:26	0	-1	4724	8.7	2.0	2.0	96.3
10:02:31	0:01:04:58	0	-1	4648	8.5	2.0	3.1	97.3
10:03:03	0:01:05:30	0	-1	4690	8.4	1.8	4.1	98.4
10:03:35	0:01:06:02	0	-1	4648	8.4	2.0	5.2	99.4
10:04:07	0:01:06:34	0	-1	4674	8.3	2.0	6.2	100.4
10:04:40	0:01:07:06	0	-1	4623	8.3	1.7	7.2	101.4
10:05:12	0:01:07:39	0	-1	4674	8.3	2.1	8.2	102.5
10:05:44	0:01:08:10	0	-1	4648	8.3	2.1	9.3	103.5
10:06:16	0:01:08:43	0	-1	528	8.3	0.0	10.1	104.3
10:06:48	0:01:09:14	0	-1	0	8.3	0.0	10.1	104.3

Baker Hughes — Job Start: Wednesday, October 02, 2013

Cement Plug #4



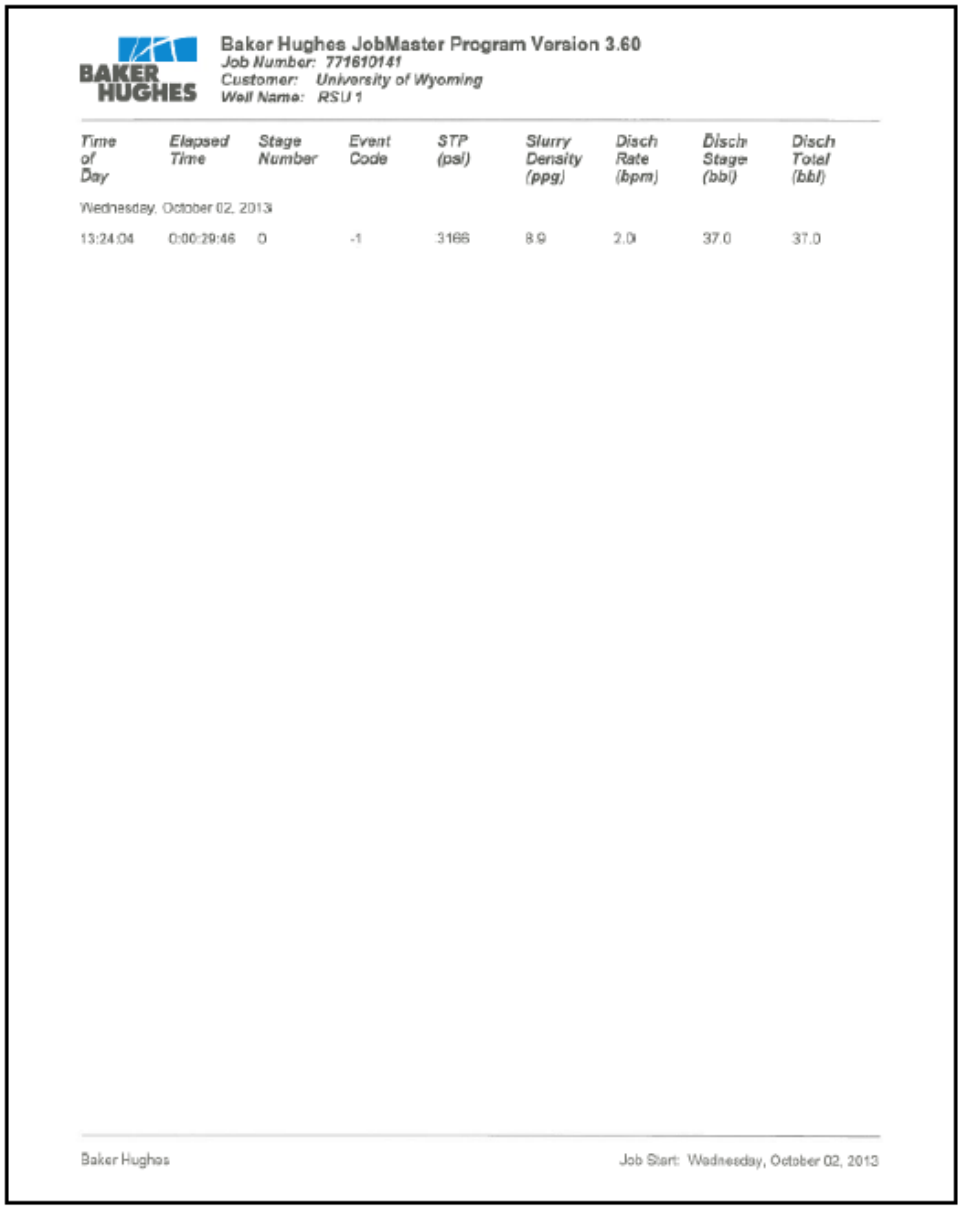
Baker Hughes JobMaster Program Version 3.60

Job Number: 771610141
Customer: University of Wyoming
Well Name: RSU 1

Time of Day	Elapsed Time	Stage Number	Event Code	STP (psi)	Slurry Density (ppg)	Disch Rate (bpm)	Disch Stage (bbl)	Disch Total (bbl)
Wednesday, October 02, 2013								
12:54:08	0:00:00:01	0	-1	101	8.3	0.0	0.0	0.0
12:54:40	0:00:00:33	0	-1	101	8.2	0.0	0.0	0.0
12:55:12	0:00:01:04	0	-1	101	8.2	0.0	0.0	0.0
12:55:44	0:00:01:36	0	-1	101	8.2	0.0	0.0	0.0
12:56:15	0:00:02:07	0	-1	101	8.2	0.0	0.0	0.0
12:56:47	0:00:02:39	0	-1	101	8.2	0.0	0.0	0.0
12:57:19	0:00:03:10	0	-1	101	8.5	0.0	0.0	0.0
12:57:51	0:00:03:42	0	-1	101	8.7	0.0	0.0	0.0
12:58:22	0:00:04:13	0	-1	101	8.9	0.0	0.0	0.0
12:58:54	0:00:04:45	0	-1	101	9.0	0.0	0.0	0.0
12:59:26	0:00:05:17	0	-1	101	9.0	0.0	0.0	0.0
12:59:58	0:00:05:48	0	-1	51	9.0	0.0	0.0	0.0
13:00:30	0:00:06:20	0	-1	25	9.0	0.0	0.0	0.0
13:01:01	0:00:06:51	0	-1	25	9.0	0.0	0.0	0.0
13:01:33	0:00:07:23	0	-1	25	9.0	0.0	0.0	0.0
13:02:05	0:00:07:55	0	-1	25	9.0	0.0	0.0	0.0
13:02:36	0:00:08:26	0	-1	25	9.0	0.0	0.0	0.0
13:03:08	0:00:08:58	0	-1	25	9.0	0.0	0.0	0.0
13:03:39	0:00:09:29	0	-1	25	9.0	0.0	0.0	0.0
13:04:11	0:00:10:00	0	-1	25	9.0	0.0	0.0	0.0
13:04:43	0:00:10:32	0	-1	25	9.0	0.0	0.0	0.0
13:05:14	0:00:11:03	0	-1	25	9.0	0.0	0.0	0.0
13:05:49	0:00:11:37	0	-1	2138	9.0	2.0	0.5	0.5
13:06:21	0:00:12:10	0	-1	2940	9.0	2.0	1.5	1.5
13:06:53	0:00:12:41	0	-1	2965	9.1	2.1	2.6	2.6
13:07:25	0:00:13:14	0	-1	2990	9.1	2.0	3.7	3.7
13:07:57	0:00:13:46	0	-1	2990	9.0	2.0	4.8	4.8
13:08:30	0:00:14:18	0	-1	2985	8.9	2.0	5.8	5.8
13:09:02	0:00:14:49	0	-1	2985	9.0	2.0	6.9	6.9
13:09:34	0:00:15:22	0	-1	2985	9.1	2.0	8.0	8.0
13:10:05	0:00:15:53	0	-1	2985	9.2	2.0	9.1	9.1
13:10:30	0:00:16:26	0	-1	2990	9.2	2.0	10.1	10.1
13:11:11	0:00:16:58	0	-1	3015	9.1	2.1	11.2	11.2
13:11:43	0:00:17:30	0	-1	2990	8.9	2.0	12.3	12.3
13:12:15	0:00:18:01	0	-1	3015	8.8	2.1	13.4	13.4
13:12:47	0:00:18:33	0	-1	3015	8.8	2.1	14.4	14.4
13:13:19	0:00:19:06	0	-1	3015	8.9	2.1	15.5	15.5
13:13:51	0:00:19:37	0	-1	3040	9.0	2.0	16.6	16.6
13:14:23	0:00:20:09	0	-1	3015	9.1	2.1	17.6	17.6
13:14:55	0:00:20:42	0	-1	3091	9.0	2.0	18.7	18.7
13:15:28	0:00:21:13	0	-1	3066	9.0	2.0	19.8	19.8
13:16:00	0:00:21:45	0	-1	3091	8.9	2.1	20.9	20.9
13:16:32	0:00:22:17	0	-1	3066	9.0	1.9	21.9	21.9
13:17:04	0:00:22:49	0	-1	3066	9.1	1.9	23.0	23.0
13:17:37	0:00:23:22	0	-1	3066	9.1	2.0	24.1	24.1
13:18:09	0:00:23:53	0	-1	3066	9.1	2.0	25.2	25.2
13:18:41	0:00:24:25	0	-1	3141	9.1	2.0	26.2	26.2
13:19:13	0:00:24:57	0	-1	3141	9.0	1.9	27.3	27.3
13:19:45	0:00:25:30	0	-1	3116	8.9	2.0	28.4	28.4
13:20:18	0:00:26:02	0	-1	3116	8.9	2.0	29.5	29.5
13:20:50	0:00:26:34	0	-1	3141	9.0	2.0	30.5	30.5
13:21:22	0:00:27:06	0	-1	3141	9.0	1.9	31.6	31.6
13:21:55	0:00:27:38	0	-1	3141	9.1	2.0	32.7	32.7
13:22:27	0:00:28:10	0	-1	3141	9.0	1.9	33.8	33.8
13:23:00	0:00:28:43	0	-1	3166	9.0	1.9	34.9	34.9
13:23:32	0:00:29:15	0	-1	3101	8.9	2.0	35.9	35.9

Baker Hughes

Job Start: Wednesday, October 02, 2013

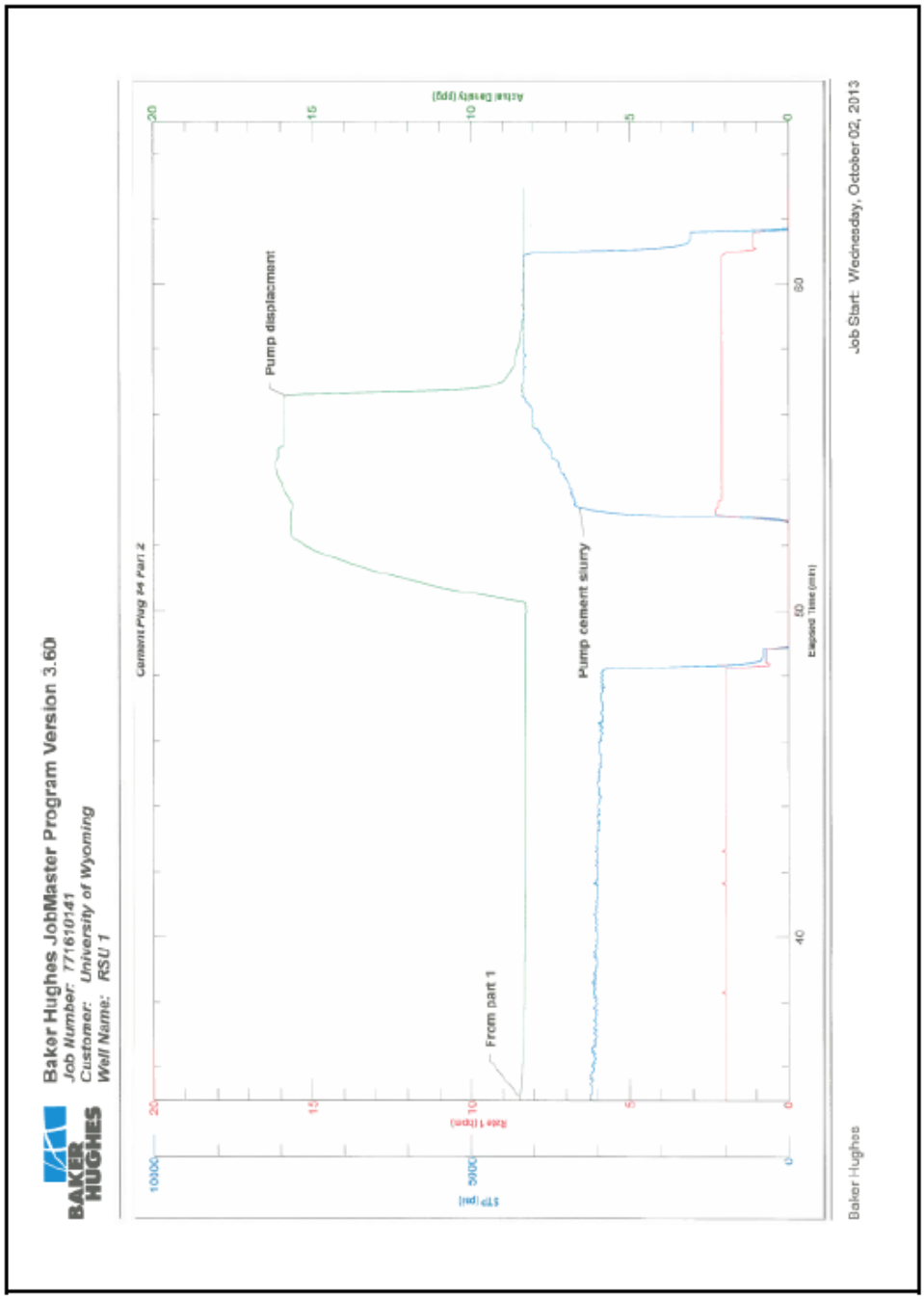


Baker Hughes JobMaster Program Version 3.60
Job Number: 771610141
Customer: University of Wyoming
Well Name: RSU 1

Time of Day	Elapsed Time	Stage Number	Event Code	STP (psi)	Slurry Density (ppg)	Disch Rate (bpm)	Disch Stage (bbl)	Disch Total (bbl)
Wednesday, October 02, 2013								
13:24:04	0:00:29:46	0	-1	3166	8.9	2.0	37.0	37.0

Baker Hughes

Job Start: Wednesday, October 02, 2013


Baker Hughes JobMaster Program Version 3.60
Job Number: 171610141
Customer: University of Wyoming
Well Name: RSU 1
Cement Plug #4 Part 2
Pump displacment
Pump cement slurry
From part 1
Rate 1 [bpm]
STP [psi]
Active Density [PPG]
Elapsed Time [min]
Job Start: Wednesday, October 02, 2013
Baker Hughes

Baker Hughes JobMaster Program Version 3.60
Job Number: 771610141
Customer: University of Wyoming
Well Name: RSU 1

Time of Day	Elapsed Time	Stage Number	Event Code	STP (psi)	Slurry Density (ppg)	Disch Rate (bpm)	Disch Stage (bbl)	Disch Total (bbl)
Wednesday, October 02, 2013								
12:54:17	0:00:34:09	0	-1	3141	8.6	2.0	45.8	45.8
12:54:49	0:00:34:40	0	-1	3116	8.5	1.9	46.9	46.9
12:55:21	0:00:35:13	0	-1	3091	8.4	2.1	47.9	47.9
12:55:54	0:00:35:45	0	-1	3116	8.4	2.0	49.0	49.0
12:56:26	0:00:36:17	0	-1	3040	8.4	1.9	50.1	50.1
12:56:59	0:00:36:49	0	-1	3066	8.3	2.0	51.3	51.3
12:57:31	0:00:37:22	0	-1	3040	8.3	1.9	52.3	52.3
12:58:04	0:00:37:54	0	-1	3040	8.3	1.8	53.4	53.4
12:58:36	0:00:38:26	0	-1	3040	8.3	2.2	54.5	54.5
12:59:09	0:00:38:58	0	-1	3040	8.3	2.0	55.6	55.6
12:59:41	0:00:39:30	0	-1	3066	8.3	2.0	56.7	56.7
13:00:13	0:00:40:02	0	-1	3015	8.3	2.2	57.8	57.8
13:00:45	0:00:40:33	0	-1	3040	8.3	1.9	58.8	58.8
13:01:16	0:00:41:04	0	-1	3040	8.3	1.9	59.9	59.9
13:01:48	0:00:41:35	0	-1	2990	8.3	2.0	60.9	60.9
13:02:20	0:00:42:07	0	-1	2990	8.3	1.9	62.0	62.0
13:02:51	0:00:42:38	0	-1	3040	8.3	1.7	63.0	63.0
13:03:23	0:00:43:10	0	-1	2990	8.3	2.4	64.1	64.1
13:03:55	0:00:43:41	0	-1	2990	8.3	1.9	0.2	65.2
13:04:27	0:00:44:13	0	-1	2965	8.3	2.0	1.3	66.2
13:05:00	0:00:44:45	0	-1	2965	8.3	2.1	2.3	67.3
13:05:32	0:00:45:17	0	-1	2965	8.3	2.0	3.4	68.4
13:06:04	0:00:45:49	0	-1	2965	8.3	2.0	4.5	69.4
13:06:36	0:00:46:22	0	-1	2940	8.3	2.0	5.6	70.5
13:07:09	0:00:46:54	0	-1	2940	8.3	1.9	6.6	71.6
13:07:42	0:00:47:25	0	-1	2940	8.3	2.0	7.7	72.7
13:08:14	0:00:47:58	0	-1	2940	8.3	2.0	8.8	73.8
13:08:47	0:00:48:30	0	-1	427	8.3	0.5	9.6	74.5
13:09:19	0:00:49:01	0	-1	-25	8.3	0.0	9.8	74.8
13:09:51	0:00:49:33	0	-1	0	8.3	0.0	9.8	74.8
13:10:23	0:00:50:05	0	-1	0	8.3	0.0	9.8	74.8
13:10:55	0:00:50:37	0	-1	0	10.5	0.0	0.0	74.8
13:11:27	0:00:51:09	0	-1	0	12.8	0.0	0.0	74.8
13:11:59	0:00:51:41	0	-1	0	14.5	0.0	0.0	74.8
13:12:31	0:00:52:13	0	-1	0	15.6	0.0	0.0	74.8
13:13:03	0:00:52:45	0	-1	51	15.7	5.5	0.1	74.8
13:13:36	0:00:53:17	0	-1	3342	15.6	2.1	1.2	76.0
13:14:08	0:00:53:49	0	-1	3442	15.9	2.1	2.3	77.1
13:14:41	0:00:54:22	0	-1	3593	16.1	2.1	3.5	78.2
13:15:13	0:00:54:54	0	-1	3744	16.1	2.1	4.6	79.4
13:15:46	0:00:55:27	0	-1	3920	15.9	2.1	5.7	80.5
13:16:18	0:00:55:58	0	-1	4020	15.9	2.1	6.8	81.6
13:16:49	0:00:56:30	0	-1	4121	15.9	2.0	7.9	82.7
13:17:21	0:00:57:02	0	-1	4171	8.0	2.0	1.0	83.8
13:17:54	0:00:57:34	0	-1	4146	8.6	2.1	2.1	84.9
13:18:26	0:00:58:06	0	-1	4171	8.5	2.1	3.2	86.0
13:18:58	0:00:58:38	0	-1	4146	8.4	2.1	4.3	87.1
13:19:31	0:00:59:10	0	-1	4171	8.3	2.0	5.4	88.2
13:20:03	0:00:59:42	0	-1	4146	8.3	2.1	6.5	89.3
13:20:35	0:01:00:15	0	-1	4171	8.3	2.2	7.6	90.4
13:21:08	0:01:00:47	0	-1	4171	8.3	2.0	8.8	91.5
13:21:41	0:01:01:19	0	-1	1558	8.3	1.1	9.6	92.3
13:22:13	0:01:01:52	0	-1	0	8.3	0.0	9.9	92.7
13:22:45	0:01:02:24	0	-1	0	8.3	0.0	9.9	92.7
13:23:16	0:01:02:55	0	-1	-25	8.3	0.0	9.9	92.7

4.3.7 Surface Abandonment

After plugging the well, operations moved in to Stage 4, surface abandonment. The earth around the casing was dug out and the casing cut 4 ft. below surface. After cutting the casing, a flat-top metal plate was welding across the casing and the cellar was dug out, removed, and back filled. The steel lining of the mouse hole was also dug out, removed, and back filled to surface. Rig anchors and pit liner were also removed from location.

A 10 ft. abandonment monument was placed over the well with 4 ft. buried beneath the earth and 6 ft. visible above surface. The API number, well name, well depth, township, operator name (UNofWY-BHIO) and range were welded in to the pole.

Plans have been arranged for location to be ploughed with top soil and be re-seeded with native sage grass in the spring after winter thaw.

4.3.8 Performance

- Highlights
  - No major incidents or accidents were reported.
  - Adequate lengths of 1 ½" CT and Kevlar cable were able to be removed from the wellbore to allow passive monitoring operations to commence, though not at planned depths.
  - When the cement crew was scheduled to be on location for plugging operations, they were maxed out on driving hours. The operations group handled this correctly by delaying operations to ensure the safety of human life.
  - The well was successfully plugged with four Class G cement plugs.
- Lowlights
  - Only 6,650 ft. of 1 ½" CT and 5,480 ft. of Kevlar cable could be recovered from the well.
  - During fishing operations, while attempting to anchor the Kevlar cable to a fixed surface point, the cable parted and was dropped down hole. This led to pre-planned contingency operations taking place to again retrieve the cable and allow it to be handled at surface.
    - During the fishing operations Run #8, the Kevlar cable slipped off of the fingered-spear adding a non-productive fishing run.
  - Coiled tubing was required to be on location 2.8 days longer than planned in contingency operation forecasts.
  - Cement crew driving hours were maxed out for the day they were scheduled to arrive for plugging operations. This delayed operations by one 12 working hour day.
- Deviation from plan
  - With 1 ½" CT being buckled beyond 6,695 ft., jet cutting assembly could not go beyond this depth. This forced the coil cut to be made 1,835 ft. shallower than planned.

- When it was discovered that the 5.89" OD gauge tool could not pass beyond 5,881 ft., it suggested that the Kevlar cable remaining in the hole rested along the casing wall, preventing wireline from progressing deeper. Because of this, 3 out of the 4 seismic monitoring intervals could not be reached and monitoring was forced to take place at shallower depths.

5 Recommendations and Lessons Learned

The well intervention carried out on RSU#1 had both low and highlights to remark on all first, second, and third phases that were noted in the performance section. It is important to mention that the operation was performed in a safely manner and all the operational objectives set, were achieved.

It is vital to communicate potential operational risks to all parties involved prior to the planning and start of operations so everyone is aware of possible contingency plans when operations do not go as planned and a healthy working relationship can be kept.

Fluid samples from Madison and Weber were successfully obtained and injection tests on both formations were executed as planned.

As stated on the well intervention program, one of the three potential hazards to the operation was detected as issues during deployment of microseismic array on coil tubing and cementing them on top of the liner. BHIO alongside with specialized subcontractors planned and identified the optimum operational sequence to deliver a successful outcome. Due to the nature of this unique operation on-the-fly changes were envisaged since the planning stage.

To our knowledge there was no offset information available where an equivalent operation / procedure had been carried out by the O&G industry. Therefore, this part of the operation was considered experimental due to multiple uncertainties and new procedures and tool configurations being deployed in this unique manner as was always stated on the intervention program.

To minimize the impact of this experimental procedure all involved parties discussed and agreed on the best possible procedures to will deliver a safe and successful outcome.

Procedures were followed carefully and the operation itself is considered a success. Below it is show some of the issues and lessons learned from the team:

1. It was concluded that a geophone array and electrical cable can be successfully deployed on coil tubing and function at depth over 9,300 ft.
2. Post-cementing, issues began to arise with geophone responses.
    a. Resistivity readings (~6000 ohms) signify connectivity of geophones (allowing to determine that the phones were connected from surface)
    b. Unable to receive signal from surface to downhole through casing or tubing
    c. A geophone tester, with a known signal frequency, was used to further test phones, however geophone responses do not indicate useful seismic responses.
    d. Data capturing seems to be getting worse over time (tested at 2, 3, and 5 days after being cemented) At this point it is being analyzed the effect of cement surrounding the phones attenuating the signal, or a matter of pressure and fluid seepage in to the geophone's protective housing.
3. After cutting the cable on surface, rather than spending 2 days to solder the 120 wires within the cable back to the cable head before testing, a "quick connect" (twisting the wires together) is recommended to allow for a quick test so that a benchmark of functionality can be made before, during, and after cement setting.

4. A study on the influence cement of varying hardnesses and thicknesses (radius of cement between geophone and casing - in this operation 2.676" of cement between phone OD and casing wall) has on geophone signal response is recommended to be conducted before another attempt of a similar operation.

5. For future cable deployments on coiled tubing, modeling tubing buckling forces during cementing operations and post-cementing could be a useful tool in assessing the risk of cutting operations and estimating the success of jet cutter impact severing the Kevlar cable hung outside the tubing. Determination that the tubing is buckled could provide insight as to whether the cable lays against the tubing or away from the tubing body, thus adjusting the estimate of success for severing the cable with the same cut as the tubing.

6. The unique operations in Phases II and III made contingency scenario planning difficult at times, however the integrated operations approach allowed cohesion between all Baker Hughes service lines. Subject matter experts from each division involved in the RSU #1 operations were able to take part in project planning, risk assessment, operational recommendations, and execution while providing feedback in each stage. Single focal points for each area of expertise provided a streamlined communication funnel between service lines and Integrated Operations engineering and project management, and in turn, between Integrated Operations and the University of Wyoming.

6 Annexes

6.1 Location images for records



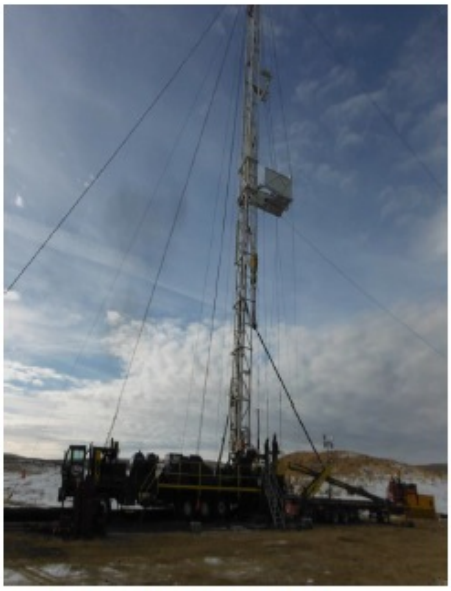
A. Abandoned well RSU#1. October 2012.



B. Anchors used to set workover rig on location.



C. BOP stack of Phase I of intervention



D. Workover equipment rigged up.



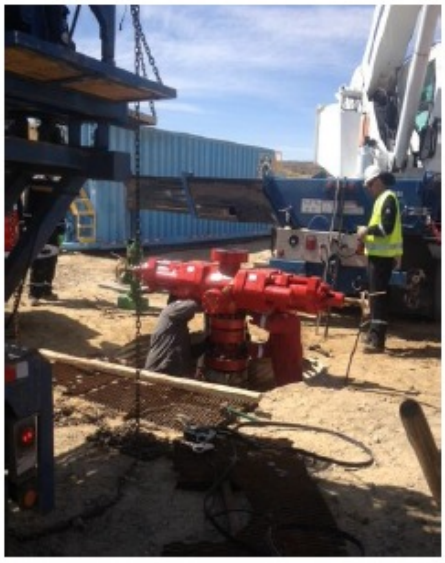
E.Multi-finger caliper wireline tool



F. Cast Iron Bridge Plug (CIBP) and setting tool



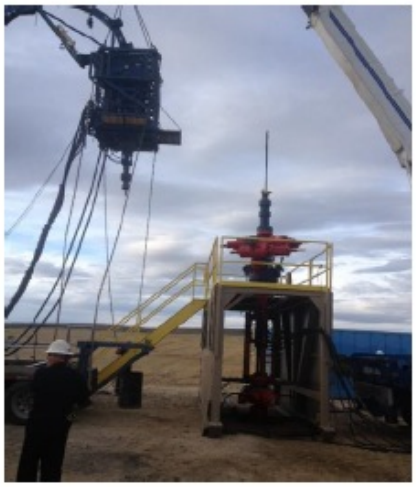
G. Geophone cable spool



H. BOP stack for Phase II



I. Work window, spacer spool, and overhead shelter



J. Positioning injector head over well



K. Injector head in position



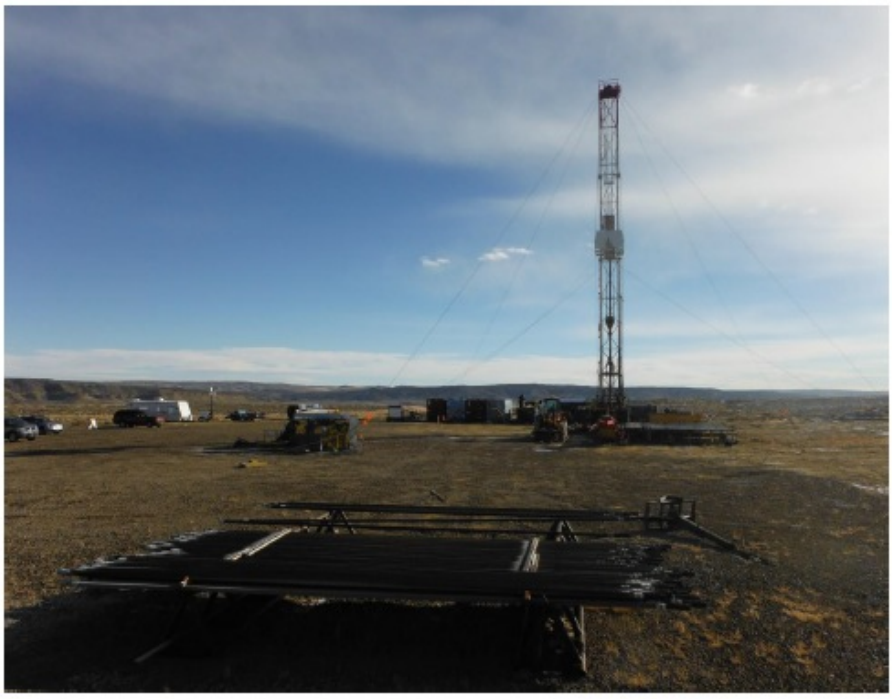
L. Securing cable to coiled tubing to be run in the hole



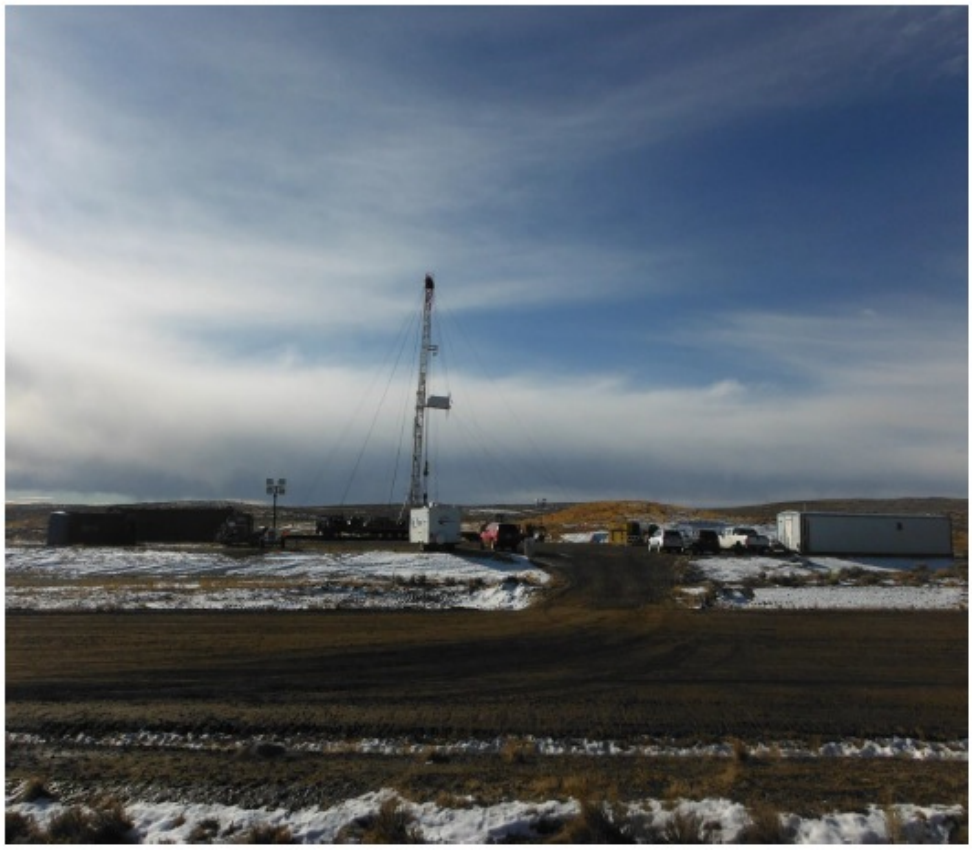
M. Final geophone function test prior to cementing



N. Location fenced and secured. April/ 2013



O. View of location during Phase I of well Intervention.



P. View of location during Phase I of well Intervention.

Appendix N: Mini-Drill Stem Test and Vertical Interference Test

THE UNIVERSITY OF WYOMING

ROCK SPRINGS UPLIFT NO.1

RESOLUTION

Reservoir Characterization Instrument (RCI)

Mini-DST/VIT Analysis

Report Status :	**Preliminary**
Author :	Ravi Manglani
Reviewers :	Elif Altinay
Date :	09/22/2011



17021 Aldine Westfield Road
Houston, Texas,USA, 77073-5101
Tel: +1 713-879-1370

IN MAKING INTERPRETATIONS OF LOGS OUR EMPLOYEES WILL GIVE THE CUSTOMER THE BENEFIT OF THEIR BEST JUDGMENT, BUT SINCE ALL INTERPRETATIONS ARE OPINIONS BASED ON INFERENCES FROM ELECTRICAL OR OTHER MEASUREMENTS WE CANNOT AND DO NOT GUARANTEE THE ACCURACY OR THE CORRECTNESS OF ANY INTERPRETATION. WE SHALL NOT BE LIABLE OR RESPONSIBLE FOR ANY LOSS, COST, DAMAGES, OR EXPENSES WHATSOEVER INCURRED OR SUSTAINED BY THE CUSTOMER RESULTING FROM ANY INTERPRETATION MADE BY ANY OF OUR EMPLOYEES.

1 EXECUTIVE SUMMARY

- The University of Wyoming deployed the Baker Atlas Reservoir Characterization Instrument (RCI) in the Rock Springs Uplift No.1 well on August 24th, 2011. RCI's straddle packer (SP) configuration was run in combination with an observation probe (OP).
- RCI's straddle packer acts as a source where the fluid production takes place and the probe acts as an observation point to measure the pressure disturbance due to fluid production in SP. The observation probe was placed 6.5 feet above the mid-point of the straddle packer.
- One VIT (vertical interference test) and one Mini-DST were conducted in the selected intervals. The straddle Packer's mid-point was placed at 12361.57 ft MD, and at 11398.53 ft MD for the VIT and Mini-DST, respectively.
- The objective of this study is to analyze the pressure transients from SP and OP for the calculation of the representative permeability values, radius of investigation, and the assessment of layer connectivity.
- Paradigm's Interpret-2010 is the well test analysis software package used to analyse the Mini-DST and VIT data.
- Porosity value used in the analysis was 0.2, while the viscosity of the flowing fluid was calculated as 0.3 cP (at the given reservoir pressure and temperature), and the total compressibility was 1E-006 1/psi.
- The thickness of the tested flow units is 60 ft for the VIT and 30 ft for the Mini-DST.
- In the VIT, during the pressure drawdown and build-up periods at the SP interval, corresponding pressure disturbances were observed at the OP. This indicates that there is good vertical communication between the SP and the OP within the 6.50 feet distance.
- In the Mini-DST interval, the pre-tests at several locations with the observation probe were tight indicating no reservoir communication at the probe depths. Consequently, the OP was not used and only a Mini-DST was conducted.
- In the analysis of the VIT, a partially penetrating wellbore model in a homogeneous infinite acting reservoir was used. The results indicate a horizontal permeability value of 13.63 mD, a vertical permeability of 13.00 mD, a radius of investigation of 74.00 ft and a model calculated initial pressure of 5312.47 psi.
- For the Mini-DST analysis, a partially penetrating wellbore model in a homogeneous infinite acting reservoir was used. The results indicate a horizontal permeability value of 1.73, a vertical permeability of 0.41 mD, a radius of investigation of 159.00 ft and a model calculated initial pressure of 4860.35 psi.

- The results of the analysis are summarized in the table below.

TEST	h	k_{xy}. h	k_{xy}	k_z	r_{inv}	P*	P_{wf}	PI
	ft	mD.ft	mD	mD	Ft	psia	psia	B/D/psi
VIT	60	249.6	4.16	0.48	74	5312.47	5264.80	0.090
Mini-DST	30	52.02	1.73	0.41	159	4860.35	4349.82	0.012

TABLE OF CONTENTS

1 EXECUTIVE SUMMARY I

2 INTRODUCTION 1
2.1 Tool Description and Configuration 1
2.2 Flow Models in Straddle Packer Test Configurations 2
2.3 Analysis Parameters 4

3 COMPOSITE PLOTS 5

4 PRESSURE TRANSIENT ANALYSIS OF VIT AT 12361.57 FT MD 6
4.2 Diagnostic Features 7
4.3 Reservoir Parameters 9

5 PRESSURE TRANSIENT ANALYSIS OF THE MINI-DST AT 11398.53 FT MD 13
5.2 Diagnostic Features 13
5.3 Reservoir Parameters 15

LIST OF TABLES

Table 2.1.1. Depth of SP and OP in each test 1
Table 2.3.1. Input reservoir and fluid parameters used in the analysis 4
Table 4.3.1. Analysis Results for the main build-up 12
Table 5.3.1. Analysis Results for the main build-up 17

LIST OF FIGURES

Figure 2.1.1. RCI Tool Configuration 2
Figure 2.2.1. Straddle Packer schematic and expected flow regimes 3
Figure 2.2.2. Expected Log-Log diagnostic plot from a straddle packer test 3
Figure 3.1.1. Composite plot for the VIT; SP midpoint at 12361.57 ft and the OP at 12355.07 ft 5
Figure 3.1.2. Composite plot for the Mini-DST; SP midpoint at 11398.53 ft. 6
Figure 4.1.1. Pressure Profile of SP data during the test period 7
Figure 4.1.2. Pressure Profiles from SP, and OP gauges during the test period 7
Figure 4.2.1. Diagnostic log-log plot for SP data in the 2nd (main) build up period. 8
Figure 4.2.2. Diagnostic log-log plots from the 1st (brown,) and 2nd (blue) pressure build-up periods (SP). 9
Figure 4.3.1. Model matching in Log-log plot for the main build-up period; Symbols are the measured data; lines are the calculated data by the model 10
Figure 4.3.2. Model matching in Log-log plot for the main build-up period for the SP (blue) and OP (green) 10

Figure 4.3.3. Model matching in Horner plot for the main build-up period in; Symbols are the measured data; lines are the calculated data by the model..... 11
Figure 4.3.4. Pressure history match for the entire test based on analysis results from the main build-up; blue symbols are the measured data; red line is the synthetic match..... 11
Figure 5.1.1. Pressure and flow rate profile of the Mini-DST. 13
Figure 5.2.1. Diagnostic log-log plot for SP data in the 2nd (main) build up period. 14
Figure 5.2.2. Diagnostic log-log plots from the 1st (black) and 2nd (blue) pressure build-up periods (SP). 14
Figure 5.3.1. Model matching in Log-log plot for the main build-up period; Symbols are the measured data; lines are the calculated data by the model..... 15
Figure 5.3.2. Model matching in Horner plot for the main build-up period in; Symbols are the measured data; lines are the calculated data by the model..... 16
Figure 5.3.3. Pressure history match for the entire test based on analysis results from the main build-up; blue symbols are the measured data; red line is the synthetic match..... 16

2 INTRODUCTION

One Mini-DST and a VIT were performed in the University of Wyoming - 2 well (OCS-G 20351 001 ST00 BP00) on August 24th, 2011. The objectives of the Mini-DST and VIT's were to obtain the representative permeability values, productivity index, radius of investigation, skin, and the connectivity with respect to the OP location in the VIT. The Mini-DSTs were conducted with the Baker Atlas Reservoir Characterisation Instrument (RCI). The single probe was located 6.50 ft above the mid-point of the straddle packer interval to observe vertical connectivity.

Mini-DST pressure data was imported into the analytical well test software "Interpret-2010" along with the fluid rate, fluid properties and reservoir/wellbore parameters to analyze the pressure transient data from the build-up tests.

2.1 Tool Description and Configuration

The 1970DB RCI Straddle Packer consists of two inflatable packers that are set in the borehole isolating the section of the formation to be tested. The distance between the packers is 3.28 ft. The fluid inlet port is placed approximately 2.19 feet from the bottom of the isolated section. The packer elements are inflated with filtered mud – the mud is filtered by drawing-in borehole mud through large area filters that are fitted in the six-tank carrier. The mud is filtered to prevent plugging of the sample lines within the tool. An observation probe (1970 MB) is included above the SP to assess connectivity and estimate the vertical permeability between the straddle packer and the location of the probe. The observation probe is located 6.50 feet above the center of the straddle packer. Table 2.1.1 illustrates the depth of the SP and OP in all tests. Both the straddle packer and the single probe modules have their own quartz pressure gauges and measure the pressure disturbance in the formation around the vicinity of their respective locations. Figure 2.1.1 below is the schematic representation of straddle packer and probe modules used during testing.

Table 2.1.1. Depth of SP and OP in each test

Test	SP-midpoint MD (ft)	OP MD (ft)
VIT	12361.57	12355.07
Mini-DST	11398.53	N/A

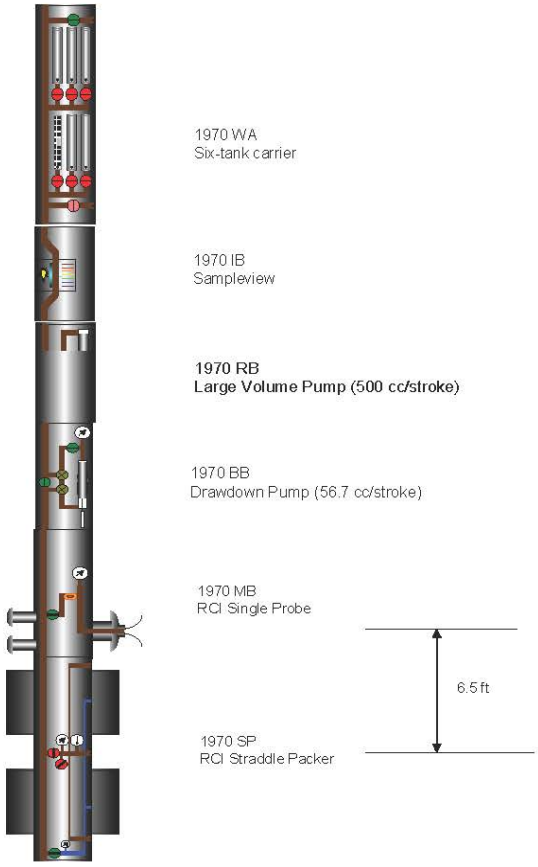


Figure 2.1.1. RCI Tool Configuration

2.2 Flow Models in Straddle Packer Test Configurations

To predict pressure and rate response during pressure testing, it is necessary to make assumptions as to the nature of the formation and the fluids therein. For the packer configuration, an analytical model for a partially completed well with storage and skin is used. The partially penetrating well model with homogenous reservoir behaviour assumes uniform reservoir thickness, h, and porosity,ϕ, with the well completed over a limited section, h_w, in the middle of the zone. The distance from the center of the isolated section to the bottom of the reservoir is designated as Z_w. Permeability anisotropy is included in the model as defined by the horizontal permeability, k_{xy}, and vertical permeability, k_z. A diagram of the tool and the flow model is shown below in Figure 2.2.1.

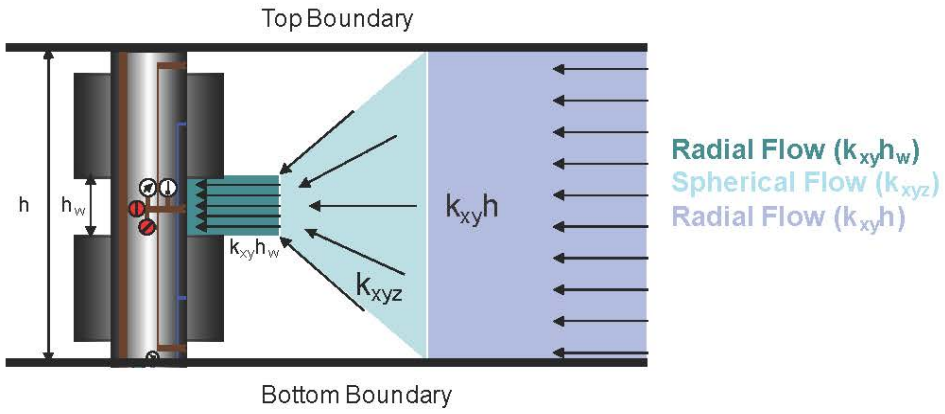


Figure 2.2.1. Straddle Packer schematic and expected flow regimes

For a very short time during the early fluid flow, it is expected to have radial flow due to thickness of the isolated zone ($k_{xy} \times h_w$). It is unlikely to observe this flow regime in most tests (except the ones in very low permeability formations) because it might be masked by the tool storage effect in early time. The spherical flow regime, which represents the geometric mean of three directional permeability (k_{xyz}), is the dominant flow regime in early time with straddle packer configuration. Flow regime becomes radial once the flow is restricted by top and bottom no-flow boundaries. The radial flow represents the product of horizontal permeability and reservoir thickness ($k_{xy} \times h$). Figure 2.2.2 shows an example of the expected log-log diagnostic plot from a straddle packer test.

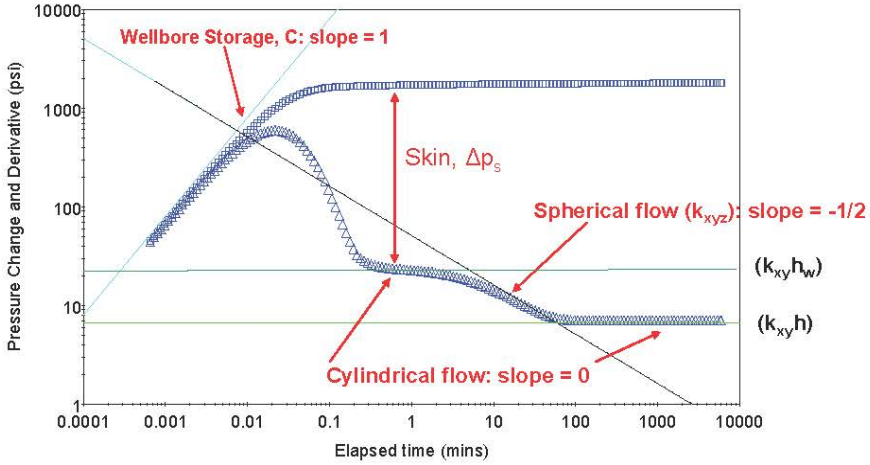


Figure 2.2.2. Expected Log-Log diagnostic plot from a straddle packer test

2.3 Analysis Parameters

Table 2.3.1 lists the parameters used in the analysis of pressure data. The measured pressure data from both source and observation pressure gauges were imported into the well test analysis software Interpret-2010 for data QC and analysis.

Table 2.3.1. Input reservoir and fluid parameters used in the analysis

Test	Matrix Porosity	Net Reservoir Thickness ft	Water Viscosity cP	Reservoir Temperature degF	Total Compressibility 1/psi
VIT	0.20	60	0.31	204.00	1E-006
Mini-DST	0.20	30	0.33	198.00	1E-006

3 COMPOSITE PLOTS

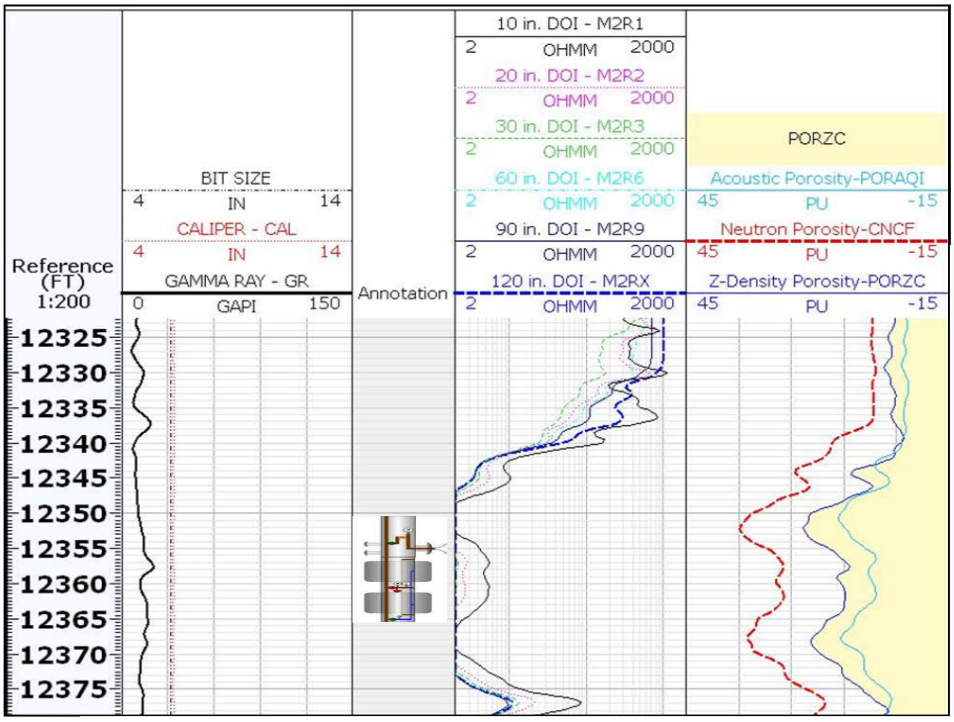


Figure 3.1.1. Composite plot for the VIT; SP midpoint at 12361.57 ft and the OP at 12355.07 ft

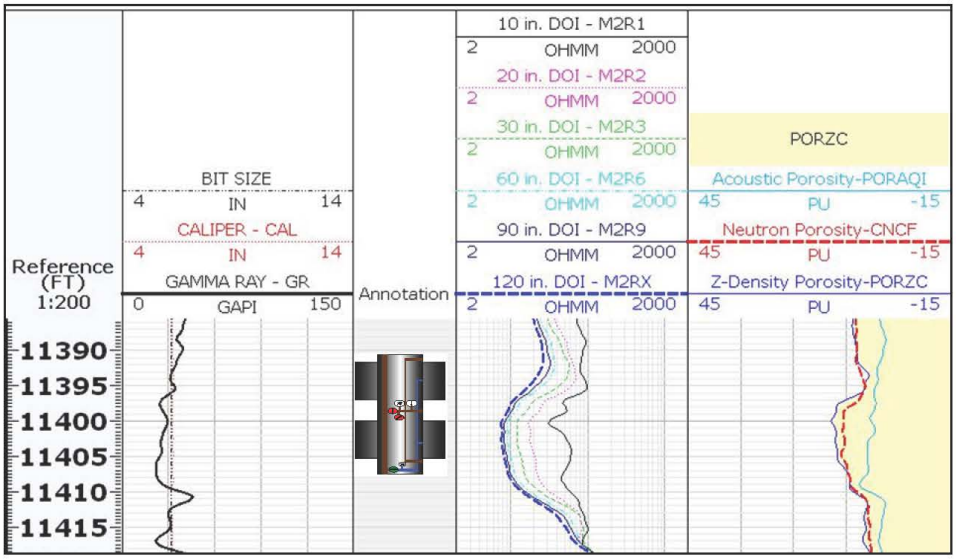


Figure 3.1.2. Composite plot for the Mini-DST; SP midpoint at 11398.53 ft.

4 PRESSURE TRANSIENT ANALYSIS OF VIT AT 12361.57 FT MD

A total of 163.61 liters of fluid was pumped using the large-volume pump (500 cc/stroke) during the VIT operation. This comprised of:

51.6 liters of fluid was pumped in 74.2 minutes prior to the packer re-inflation, which lasted 13.8 minutes. The packer re-inlaftion was conducted to confirm the seal between the packer elements and the borehole wall.

65.3 liters of fluid was pumped in 93.9 minutes prior to the 1st build-up, which lasted 23.2 minutes.

46.7 liters of fluid pumped in 53.5 minutes prior to the 2nd (main) build-up, which lasted 59.5 minutes.

A flow rate of 11.6 cc/s was obtained prior to the final shut-in. The maximum pressure drawdown at the SP probe during the final flow period was 82 psi [$(pav)_{i(calculated)}$-pwf].

Figure 4.1.1 shows the pressure profile of the SP data during the whole test period.

Figure 4.1.2 shows the pressure profile at the observation probe (OP) in green, with the SP probe data in blue. During the pressure drawdown and build-up periods at the SP interval, there was corresponding

pressure disturbances observed at the OP. This indicates that there is good vertical communication between the SP and the OP within the 6.50 feet distance.

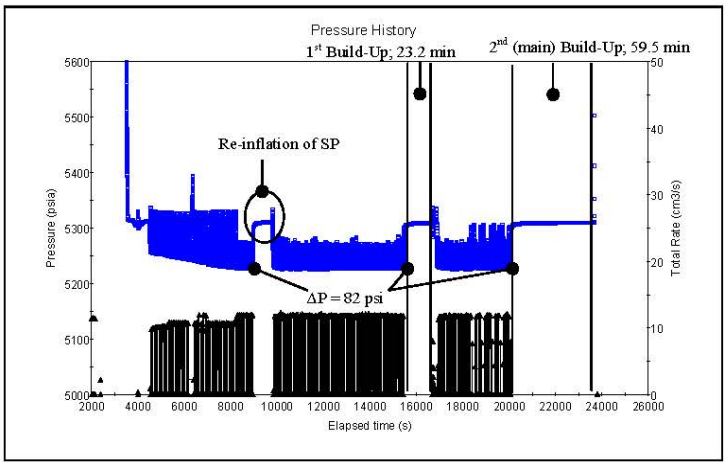


Figure 4.1.1. Pressure Profile of SP data during the test period

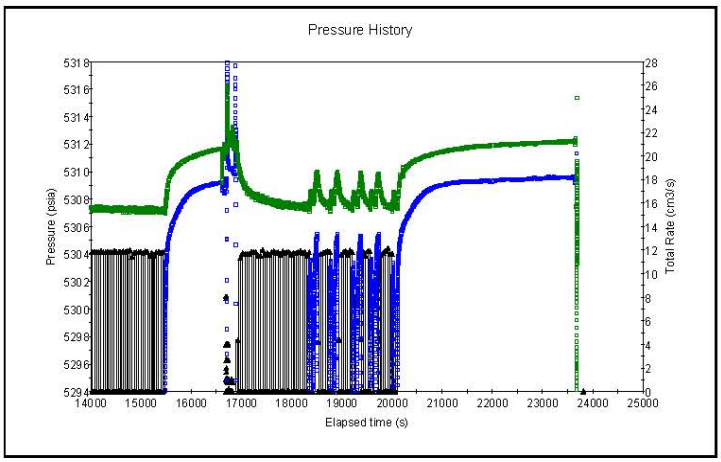


Figure 4.1.2. Pressure Profiles from SP, and OP gauges during the test period

4.2 Diagnostic Features

The diagnostic log-log plot for SP data is shown in Figure 4.2.1. The pressure build-up [Pd] and its derivative [Pd'] in SP data show that the early time pressure transient is dominated by the tool storage (20 seconds). After a period of tool storage, a transition to radial flow is observed (from 20 to 2000 seconds). The late time data indicates the start of radial flow regime.

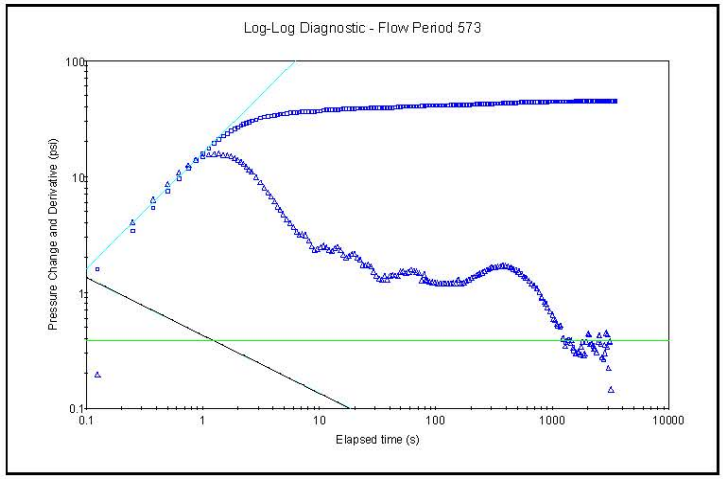


Figure 4.2.1. Diagnostic log-log plot for SP data in the 2nd (main) build up period.

From Figure 4.2.1 the data suggests that 20 seconds into the build-up a radial flow is reached. This behaviour could suggest that the response above might be due the straddled thickness of the formation itself. The thickness is the approximately 3.28 ft (the spacing of the straddle packer)

The pressure transients and analysis rates are validated by comparing the pressure response and its derivative from the two shut-in periods as shown in the log-log rate validation plot in Figure 4.2.2. Good repeatability of the derivates which indicates the same average k*H, valid formation response and accurate rate data. The differences observed are due to the decreased skin in the second (main) build-up.

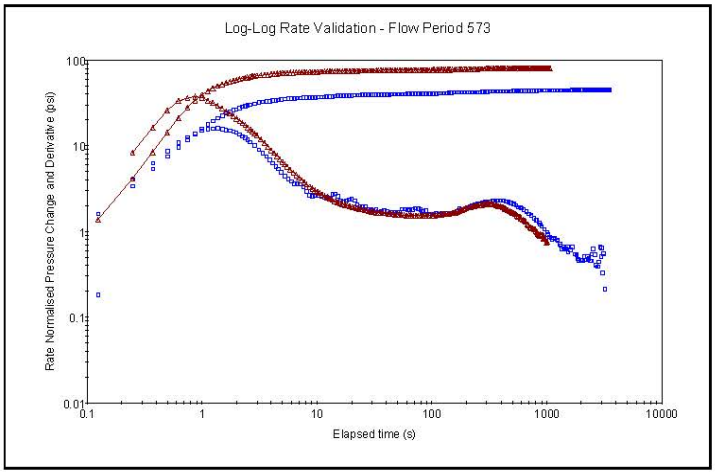


Figure 4.2.2. Diagnostic log-log plots from the 1st (brown,) and 2nd (blue) pressure build-up periods (SP).

4.3 Reservoir Parameters

The main pressure build-up data is analysed using the partially penetrating wellbore model in an infinitely acting homogeneous reservoir.

The log-log pressure derivative match, the semi-log Horner match and the pressure history match of the SP an OP data are presented in Figures 4.3.1 to 4.3.4. In the Figures, the blue coloured symbols are the actual data and red coloured lines are the calculated data by the model for SP data.

The pressure transient analysis results indicate 249.60 mD.ft of permeability thickness (K_{xy}.h). This gives a horizontal permeability (K_{xy}) of 4.16 mD, based on the 60 ft formation thickness.

The estimated vertical permeability is 0.48 mD, corresponding to a permeability anisotropy ratio (K_z/K_{xy}) of 0.11

The average pressure is calculated to be 5312.47 psia by the model.

The estimated radius of investigation for the main build-up period is 74.00 ft.

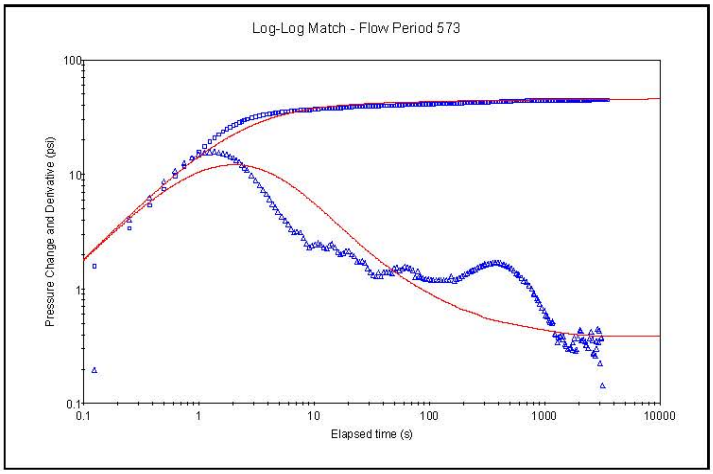


Figure 4.3.1. Model matching in Log-log plot for the main build-up period; Symbols are the measured data; lines are the calculated data by the model

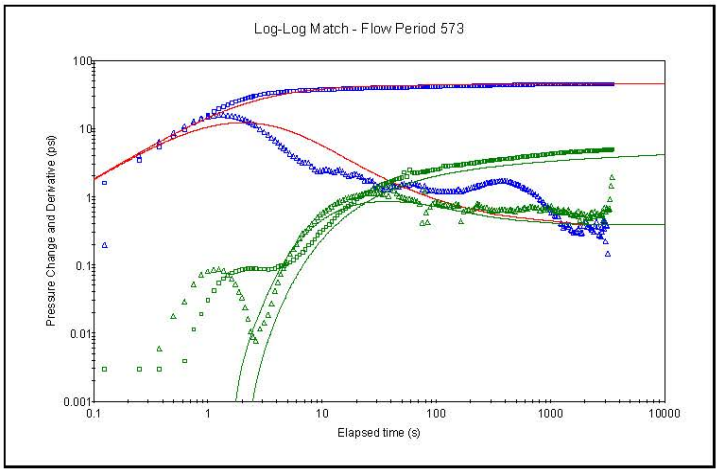


Figure 4.3.2. Model matching in Log-log plot for the main build-up period for the SP (blue) and OP (green)

Figure 4.3.2 shows the model match for the OP (green curves) and SP (red on blue). Only the timing of the cross-over of the OP's pressure change and its derivative was matched to be able to calculate the vertical permeability accurately. This gave a vertical permeability value of 0.48 mD. We can see in the late time responses from the OP and SP that they read almost the same horizontal permeability due to the fact the derivates of the OP and SP start merging.

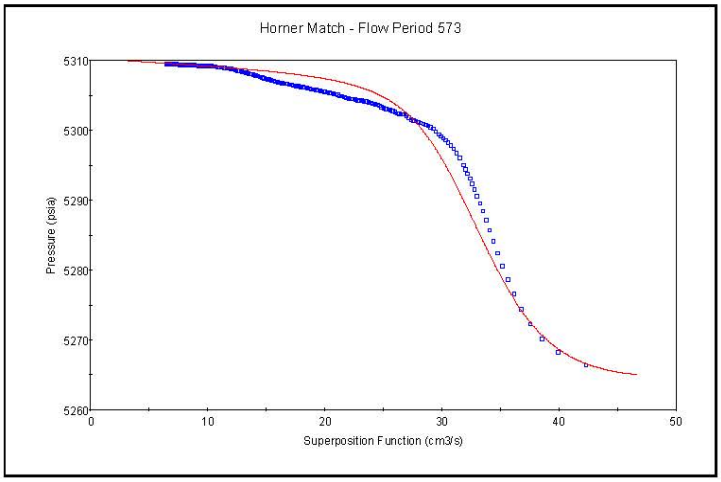


Figure 4.3.3. Model matching in Horner plot for the main build-up period in; Symbols are the measured data; lines are the calculated data by the model

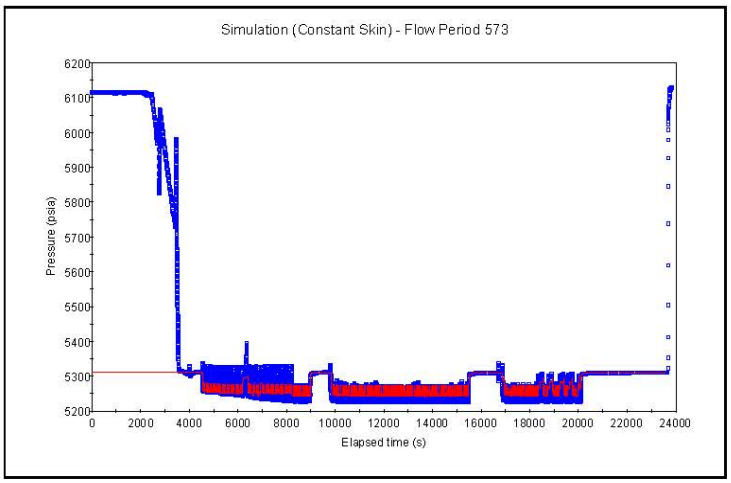


Figure 4.3.4. Pressure history match for the entire test based on analysis results from the main build-up; blue symbols are the measured data; red line is the synthetic match

The summary of the results based on the analysis of the test is presented in the Table 4.3.1 below.

Table 4.3.1. Analysis Results for the main build-up

Parameters		
Initial average reservoir pressure, (pav)i	5312.47	psia
Flowing pressure, pwf	5264.80	psia
Permeability Thickness, kh	249.6	mD.ft
Horizontal Permeability, k(xy)	4.16	mD
Vertical Permeability, k(z)	0.48	mD
Wellbore storage coefficient, C	2.5856E-006	Bbl/psi
Perforated Interval, Hw	3.28	ft
Wellbore skin factor, S(w)	-0.08	
Completion skin, S(c)	53.50	
Total Skin, S(t)	51.99	
Distance to Lower Boundary, Zw	20	ft
Type of top boundary	No Flow	
Type of bottom boundary	No Flow	
Radius of investigation (approx.), ri	159.00	ft
Measured Productivity Index, PI	0.094	B/D/psi
Flow Efficiency, FE	1.026	Fraction
Pressure drop due to skin, Δp(S)	-1.169	Psi

5 PRESSURE TRANSIENT ANALYSIS OF THE MINI-DST AT 11398.53 FT MD

A total of 213.00 liters of fluid was pumped using the large-volume pump (500cc/stroke) during the Mini-DST operation.

92.3 liters of fluid was pumped in 132.7 minutes prior to the 1st build-up, which lasted 33.5 minutes.

120.7 liters of fluid pumped in 202.0 minutes prior to the 2nd (main) build-up, which lasted 69.2 minutes.

A flow rate of 11.6 cc/s was obtained prior to the final shut-in. The maximum pressure drawdown at the SP during the final flow period was 507 psi [$(pav)_{i(calculated)}$-pwf].

Figure 5.1.1 illustrates the pressure and flow rate profiles during the Mini-DST pump out and build-ups.

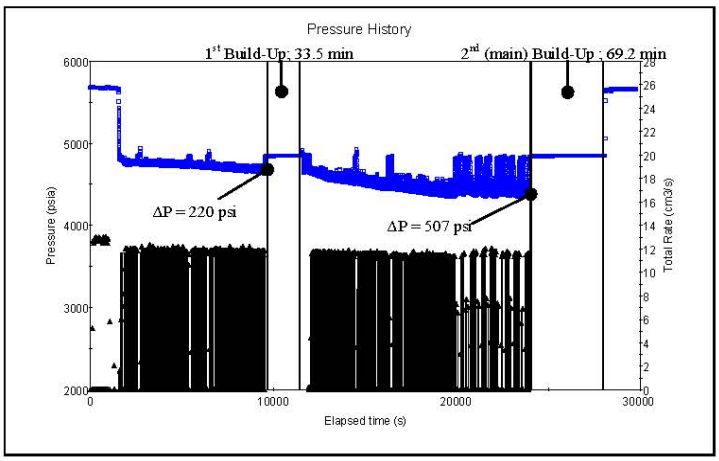


Figure 5.1.1. Pressure and flow rate profile of the Mini-DST.

In the Mini-DST interval, the pre-tests at several locations with the observation probe were tight indicating no reservoir communication at the probe depths. Consequently, the OP was not used and only a Mini-DST was conducted.

5.2 Diagnostic Features

The diagnostic log-log plot for SP data is shown in Figure 5.2.1. The pressure build-up [Pd] and its derivative [Pd'] show tool storage in the early time. After the tool storage effect, a transition into the spherical flow regime is observed. The late time data indicates radial flow regime.

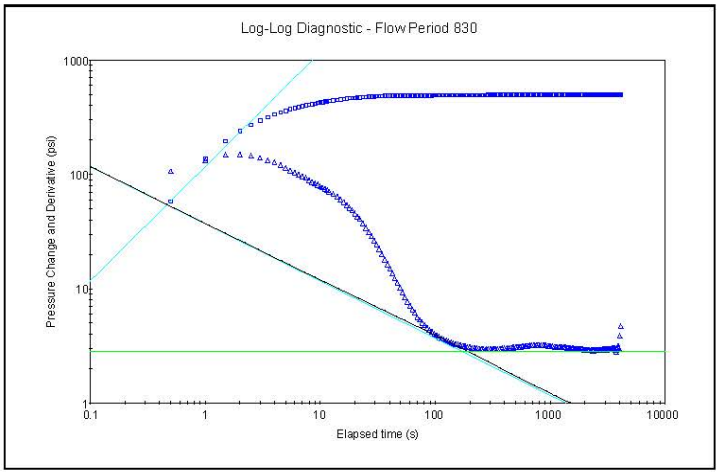


Figure 5.2.1. Diagnostic log-log plot for SP data in the 2nd (main) build up period.

The pressure transients and analysis rates are validated by comparing the pressure response and its derivative from the two shut-in periods as shown in the log-log rate validation plot in Figure 5.2.2. It is seen that the derivative curves from the first and second build-ups are overlaying in the late time confirming the radial flow regime. The differences observed are due to the increased skin in the second (main) build-up. In this Mini-DST, it is seen that the pressure drawdown increases with time while the rate is constant. As a result, the calculated skin values vary based on different flow periods.

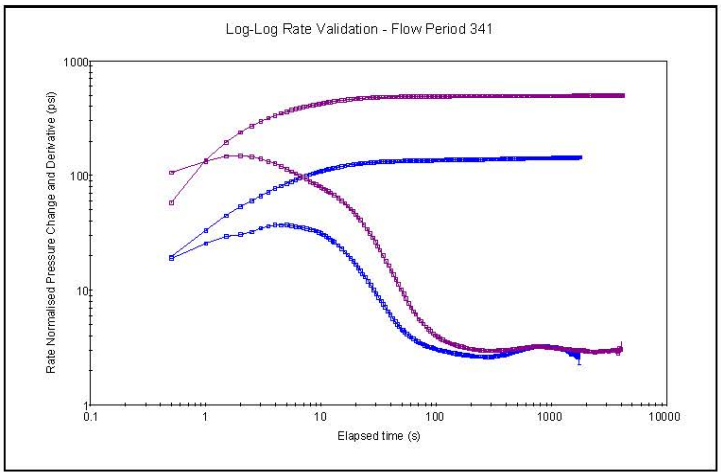


Figure 5.2.2. Diagnostic log-log plots from the 1st (black) and 2nd (blue) pressure build-up periods (SP).

5.3 Reservoir Parameters

The main pressure build-up data is analysed using the partially penetrating wellbore model in an infinitely acting radial composite reservoir.

The log-log pressure derivative match, the semi-log Horner match, and the pressure history match of the SP data are presented in Figures 5.3.1 to 5.3.3.

The pressure transient analysis results indicate 52.02 mD.ft of permeability thickness (K_{xy}.h). This gives a horizontal permeability (K_{xy}) of 1.73 mD, based on the 30 ft formation thickness.

The estimated vertical permeability is 0.41 mD, corresponding to a permeability anisotropy ratio (K_z/K_{xy}) of 0.24

The average pressure is calculated to be 4866.78 psia by the model.

The estimated radius of investigation for the main build-up period is 159.00 ft.

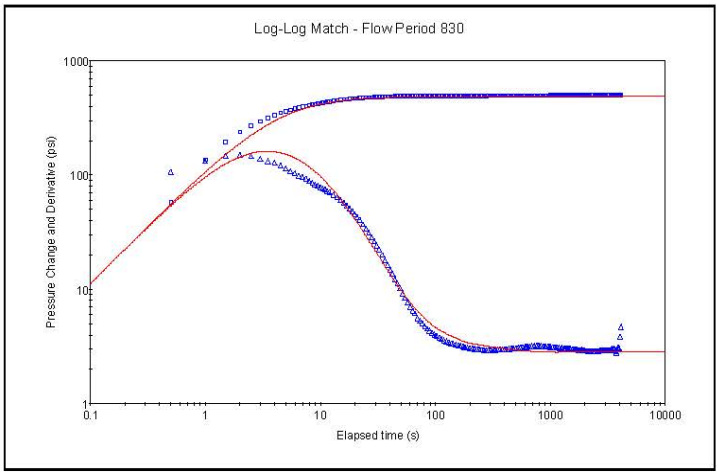


Figure 5.3.1. Model matching in Log-log plot for the main build-up period; Symbols are the measured data; lines are the calculated data by the model

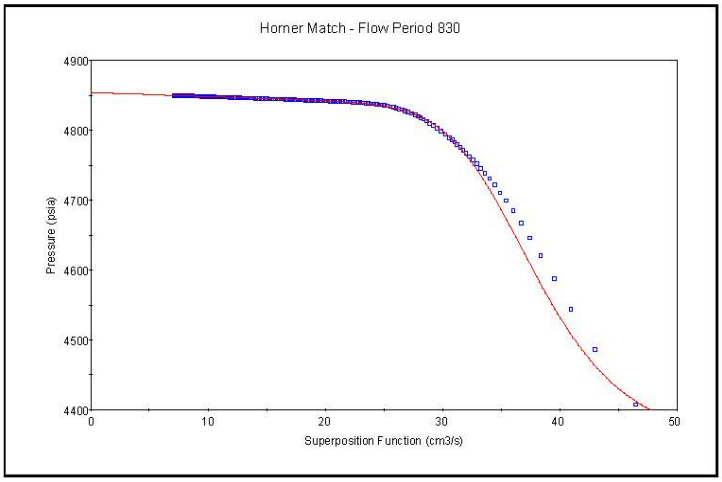


Figure 5.3.2. Model matching in Horner plot for the main build-up period in; Symbols are the measured data; lines are the calculated data by the model

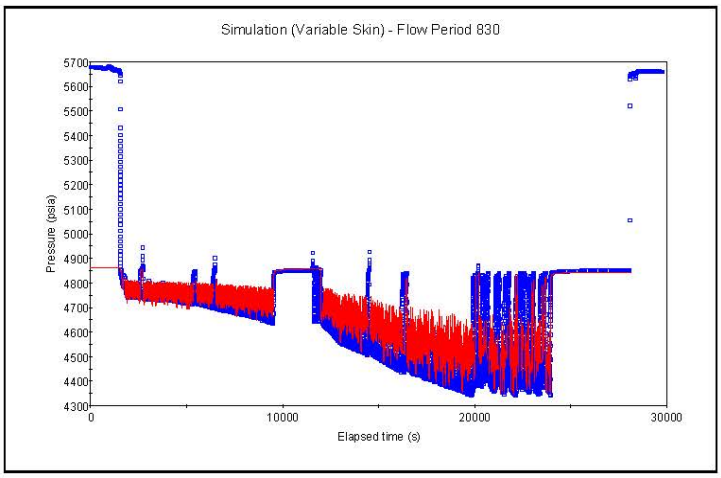


Figure 5.3.3. Pressure history match for the entire test based on analysis results from the main build-up; blue symbols are the measured data; red line is the synthetic match

The summary of the results based on the analysis of the test is presented in the Table 5.3.1 below.

Table 5.3.1. Analysis Results for the main build-up

Parameters		
Initial average reservoir pressure, (pav)i	4866.78	psia
Flowing pressure, pwf	4349.82	psia
Permeability Thickness, kh	52.02	mD.ft
Horizontal Permeability, k(xy)	1.73	mD
Vertical Permeability, k(z)	0.41	mD
Wellbore storage coefficient, C	6.3078E-007	Bbl/psi
Perforated Interval, Hw	3.28	ft
Wellbore skin factor, S(w)	2.47	
Completion skin, S(c)	36.45	
Total Skin, S(t)	81.62	
Distance to Lower Boundary, Zw	10	ft
Type of top boundary	No Flow	
Type of bottom boundary	No Flow	
Radius of investigation (approx.), ri	159.00	ft
Measured Productivity Index, PI	0.012	B/D/psi
Flow Efficiency, FE	0.504	Fraction
Pressure drop due to skin, Δp(S)	255.9	Psi